AD-A162 434 EXTENDED ABSTRACTS INTERNATIONAL SOCIETY OF ELECTROCHEMISTRY (36TH) HELD AT SALAMANCA SPAIN ON 23-28 SEPTEMBER 1985(U) INTERNATIONAL SOCIETY OF ELECTROCHEMISTRY 28 SEP 85 1/12

UNCLASSIFIED F/G 7/4 NL

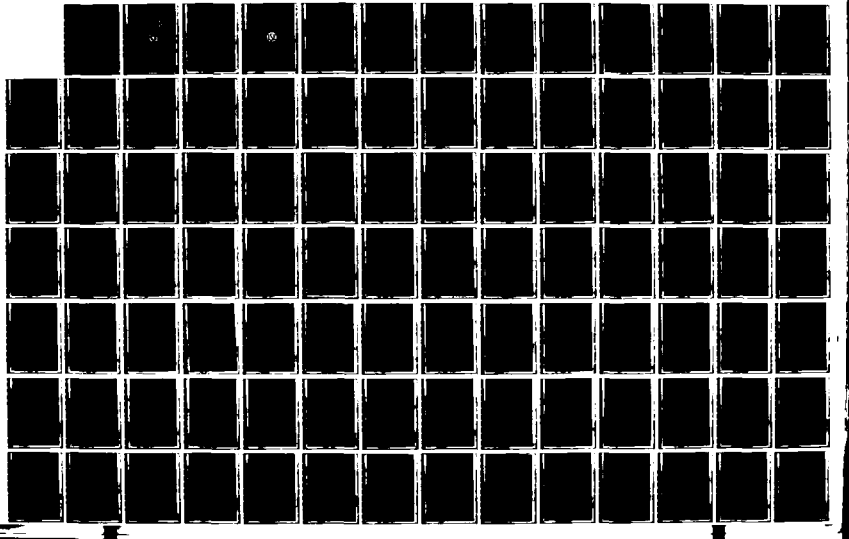

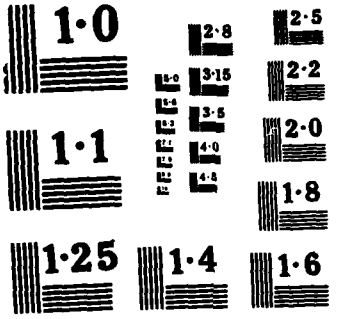

(2)

INTERNATIONAL SOCIETY OF ELECTROCHEMISTRY
36TH MEETING-SALAMANCA, SPAIN
SEPTEMBER 23-28, 1985

EXTENDED ABSTRACTS

INTERNATIONAL SOCIETY OF ELECTROCHEMISTRY
36TH MEETING-SALAMANCA, SPAIN
SEPTEMBER 23-28, 1985

INTERNATIONAL SOCIETY OF ELECTROCHEMISTRY
36TH MEETING-SALAMANCA, SPAIN
SEPTEMBER 23-28, 1985

EXTENDED ABSTRACTS

Mailing Address:

Dr. J. Alonso-López

Cea Bermudez, 51. 5ºB

28003-Madrid

SPAIN

Depósito Legal S. 539-1985
Imprime GRAFICAS VARONA
Río Mayor, 44. Telf. 923 23 33 08
37002 Salamanca, 1985.

ACKNOWLEDGMENTS

The expense of publishing the Extended Abstracts and the costs of the 36th ISE Meeting have been generously supported by the following institutions:

- Consejo Superior de Investigaciones Científicas.

- Comisión Asesora de Investigación Científica y Técnica. Ministerio de Educación y Ciencia.

- European Research Office, United States Army.

-Asociación Nacional de Químicos (Delegación Centro).

- Universidad de Salamanca.

- Diputación Provincial de Salamanca.

- Ayuntamiento de Salamanca.

CONTENTS

LIST OF LECTURES

LIST OF POSTERS

LIST OF LECTURES

TECHNICAL PROGRAMME

LIST OF PLENARY (P) AND DISCUSSION (D) LECTURES

1. Corrosion

1.1. (P) M. Keddam and C. Pallota, Paris
"New Data on the Dynamic Behaviour of the Passive Film on Iron"

1.2. (D) E. Heitz, Dechema
"Practical Significance of Electrochemical Methods for the Study of Corrosion Kinetics"

1.3. (D) J.R. Galvele, Buenos Aires
"Passivity Breakdown and Repassivation Processes in Pitting and Stress Corrosion Cracking of Metals and Alloys"

1.4. (D) E. Wendler-Kalsch, Erlangen
"Effect of Electrochemical Processes on the Initiation and Propagation of Stress Corrosion Cracks in Metals"

1.5. (D) M. Froment, Paris
"Intergranular Corrosion: Chemical and Structural Aspects"

1.6. (D) C. Gutiérrez, Madrid
"Characterization of Anodic Oxides by Modulated Specular Reflectance Spectroscopy"

2. Organic Electrochemistry

2.1. (P) D. Pletcher, S.R. Forsyth, Southampton

"The Chlorination of Napthalenes by two Phase Electrolysis"

2.2. (D) T. Shono, Kyoto

"Electroorganic Synthesis using Mediators"

2.3 (D) J. Simonet, Rennes

"Recent Aspects of Indirect Reductions and Mixed Electrolysis"

2.4. (D) D.H. Evans, Wisconsin

"Structural Changes Associated with Electrode Reactions of Highly Hindered Organic Compounds"

2.5. (D) E. Vianello, Padua

"Self Protonation Reactions in Organic Electrochemistry"

2.6. (D) H. Wendt, Darmstadt

"Electrode Kinetics and Selectivity of Organic Electrosynthesis Reactions"

3. Electrochemical Kinetics

3.1. (P) J.A. Arvía, La Plata

"Modifications of Electrocatalyst Surface by Electrochemical Procedures"

3.2. (D) L.D. Burke, Cork

"Electrochemical Formation and Reactivity of Hydrous Oxides of the Noble Metals"

3.3. (D) A. Despic, Beograd

"Surface Structure and Electrochemical Kinetics"

3.4. (D) R. Parsons, Southampton

"The Double Layer Effect of Electrochemical Reactions at Solid Electrodes"

3.5. (D) M. Costa and F. Chao, Paris

"Ellipsometry and Interfacial Electrochemistry"

3.6. (D) A. Bewick, Southampton

"In Situ Spectroscopy of Intermediates in Electrochemical Processes"

3.7. (D) E. Gileadi, Tel Aviv

"The Effect of Temperature on the Kinetic Parameters of Electrode Reactions"

3.8. (D) M. Sluyters-Rehbach, Utrecht

"Small Amplitude AC Methods and the Understanding of Simple Electrode Processes"

3.9. (D) W. Vielstich, Bonn

"New Results on the Electrocatalysis of Methanol and Formic Acid Oxidation"

3.10. (D) M. Enyo, A. Aramata, K. Machida, Hokkaido

"Electrocatalytic Properties of Alloys towards Oxidation of Simple Organics"

4. Bioelectrochemistry

4.1. (P) J.M. Saveant, Paris

"Molecular Environment Effects in the Electrochemistry of Superstructured Porphyrins"

4.2. (D) H.A.O. Hill and N.J. Walton, Oxford

"Surface-Modified Gold Electrodes for the Promotion of Direct Redox Protein Electrochemistry"

4.3. (D) J.O.M. Bockris, Texas

"Electron Charge Transfer at the Biological-Solution Interface"

4.4. (D) J. Koryta, Prague

"Sensors Based on Bioelectrochemical Principles"

4.5. (D) I. Taniguchi, Kumamoto

"Rapid Direct Electron-Transfer of Horse Heart Cytochrome C at Promoter Modified Electrodes"

5. Electroanalysis

5.1. (P) J. Osteryoung, Buffalo

"Determination of Biologically Interesting Molecules by Pulse Voltammetry"

5.2. (D) H.W. Nürnberg and P. Valenta, Jülich

"Applications of Advanced Voltammetry in the Environmental Chemistry of Ecotoxic Heavy Metals"

6. Electrochemical Thermodynamics

6.1. Zb. Koczorowski, Warsaw

"The Volta Potential Measurements and their Applications in Electrochemistry"

LIST OF POSTERS

01. Solid State Properties and Electrochemistry

02. Surface Properties and Electrochemistry

02010 J.I. Peña, M.A. Martínez, Mª Sánchez and C. Gutierrez
STUDY BY POTENTIAL MODULATED SPECULAR REFLECTANCE SPECTROSCOPY OF ANODIC IRIDIUM OXIDE FILMS.

02020 A. Visintin, A.C. Chialvo, W.E. Triaca and A.J. Arvia
ELECTROFORMATION OF ANODIC OXIDE FILMS ON NICKEL PRODUCED BY SQUARE-WAVE POTENTIAL SIGNALS

02030 R.M. Cerviño, W.E. Triaca and A.J. Arvia
VOLTAMMETRIC RESPONSES OF PLATINUM ELECTRODES SUBJECTED TO THERMAL, CHEMICAL AND ELECTROCHEMICAL TREATMENTS

02040 O.A. Albani, J.O. Zerbino, J.R. Vilche and A.J. Arvia
ELECTROCHEMICAL AND ELLIPSOMETRIC RESPONSES OF IRON ELECTRODES IN SATURATED CALCIUM HYDROXIDE SOLUTIONS

02050 B. Kosanović, S. Strabac, T. Grozdić and M.M. Jaksić
ELECTROCATALYTIC ACTIVITY OF THE BREWER INTERMETALLIC PHASES FOR THE HYDROGEN EVOLUTION REACTION

02060 Z. Bolanca, B. Lovrecek, O. Korelic
INFLUENCE OF SULPHATE IONS ON THE INTERPHASE OXIDIZED ALUMINIUM/ELECTROLYTE

02070 B. Lovrecek, M. Lovrecek, O. Korelic
A STUDY OF INTERNAL BEHAVIOUR OF Al/AQUEOUS SOLUTION SYSTEM

02080 M. Novák and J. Boa
ROLE OF THE ANODIC SURFACE LAYER IN ELECTROCHEMICAL FLUORINATION

02090 A.R. Despić, D.M. Drazić and Lj. Gajić-Krstajić
EFFECT OF ADDITION OF CHLORIDE ON THE PROPERTIES OF BARRIER-FILMS ON ALUMINIUM

02100 A. Tripković, R. Adzić, V. Vesović
THE ROLE OF STEPS IN THE OXIDATION OF FORMIC ACID ON SINGLE CRYSTAL SURFACES

02110 R. Adzić, N. Anastasijević and V. Vesović
OXYGEN REDUCTION ON GOLD SINGLE CRYSTAL STEPPED SURFACES

02120 E. Fatas and P. Herrasti,F. Arjona, E. García-Camarero
ELECTROCHEMICAL PREPARATION OF THIN FILMS PHOTOACTIVES OF CADMIUN SULFIDE ON DIFFERENT METALLIC SUSTRATES IN ORGANIC SOLVENTS

02130 D. Abercam, A. Nagib, R. Faure, F. El Omar, R. Durand
STUDY OF THE UPD OF HYDROGEN AND METALS ON Pt(111) AND Pt (110) ELECTRODES BY LEED-AES AND VOLTAMMETRY

02140 F. Hahn, B. Beden and C. Lary
INVESTIGATION OF THE NICKEL ELECTRODE-ALKALINE SOLUTION INTERFACE BY "IN SITU" UV-VISIBLE REFLECTANCE SPECTROSCOPY

02150 Z. Koczorowski and I. Zagorska
THE VOLTA POTENTIALS AND SURFACE POTENTIALS AT WATER-NITROBENZENE INTERFACES

02160 S. Biniak, M. Pakuła and A. Swiatkowski
ELECTROCHEMICAL INVESTIGATIONS OF CHEMICALLY MODIFIED ACTIVE CARBONS

02170 M. Fujihira, H. Muraki and S. Aoyagui
INDEPENDENT DETECTION OF H_2O_2 AND O_2 ON CHEMICALLY MODIFIED Au ELECTRODES

02180 F. Chao and M. Costa
ELLIPSOMETRY: ELECTRONS PROFILES AT THE Au-ELECTROLYTE INTERFACE

02190 A. Podobaev and K. Yanokova
THE PERMEATION OF HYDROGEN IN A STEEL AT ELEVATED TEMPERATURES BY AN ELECTROCHEMICAL METHOD

02200 S.M. Geraty, A.G. Ross and J.G. Vos
ELECTROCHEMICAL PROPERTIES OF ELECTRODE SURFACES MODIFIED WITH POLY-VINYLIMIDAZOLE BOUND RUTHENIUM COMPLEXES

02210 G. Pierre, M. El Kordi and G. Cauquis
THE USE OF ADATOMS IN THE ELECTROCHEMICAL SYNTEHSIS OF GLYOXYLIC ACID FROM GLYOXAL

02220 V.Z. Barsukov, N.R. Meshcherjakova, L.N. Sagcjan
ON THE MECHANISM OF THE EFFECT OF COBALT ADDITION ON THE PROPERTIES OF A NICKEL OXIDE ELECTRODE

02230 J. Haenen, W. Visscher and E. Barendrecht
CHARACTERIZATION OF $NiCo_2O_4$ SPINELS FOR O_2 EVOLUTION IN ALKALINE ELECTROLYTE

02240 F. Castaneda, E. Pezron and V.Plichon
ELECTROCHEMICAL OXIDATION OF SULPHIDE ION IN WATER CONTAINING SURFACTANTS

02250 M. Keddam and C. Pallotta
NEW DATA ON THE DYNAMIC BEHAVIOUR OF THE PASSIVE FILM ON IRON

02260 C. Deslouis, M. Keddam, M. Krarti and B. Tribollet
FREQUENCY RESPONSE TO A MODULATED FLOW AT PARTIALLY BLOCKED ELECTRODES

02270 C.Angelinetta, S.Trasatti, Lj.D.Atanasoska, R.T.Atanasoski, A.Zalar
SURFACE PROPERTIES OF MIXED IrO_2 + RuO_2 MIXED OXIDE ELECTRODES

02280 U. König, M.M. Lohrengel and J.W. Schultze
COMPUTER SUPPORTED PULSE MEASUREMENT OF CAPACITY DURING FAST OXIDE FORMATION REACTIONS

02290 M.M. Lohrengel, J.W. Schultze, H.D. Speckmann
THE EQUIVALENT CIRCUIT DIAGRAM OF OXIDE FILMS WITH A LIMITED POTENTIAL DROP

02300 K. Leitner, J.W. Schultze
PHOTOELECTROCHEMICAL INVESTIGATIONS OF PASSIVE FILMS ON TITANIUM ELECTRODES

02310 M.B.C. Roche and L.D. Burke
INVOLVEMENT OF ANIONIC OXIDE SPECIES IN REACTIONS AT THE METAL/SOLUTION INTERPHASE

02320 B. Savova-Stoynov, Z. Stoynov
STUDY OF THE INDUCTANCE INFLUENCE ON THE MEASURED ELECTROCHEMICAL IMPEDANCE

02330 Ph. Vermeiren, R. Leysen, R.W. King, C.G. Murphy and H. Vandenborre
OXYGEN EVOLUTION ON $La_{0.8}Sr_{0.2}Ni_{0.2}Co_{0.8}O_3$ ELECTROCATALYSTS

02340 M. Spichiger-Ulmann and J. Augustynski
CHARACTERIZATON OF TITANIUM DIOXIDE-SUPPORTED PLATINUM CATALYSTS

02350 A.I. Onuchukwu
HYDROGEN EMBRITTLEMENT OF STEEL UNDER APPLIED STRESS

02360 M.J. Armstrong and R.H. Muller
EFFECTS OF ION BOMBARDMENT ON THE MORPHOLOGY OF LEAD FILMS

02370 W. Kutner, T.J. Meyer and R.W. Murray
CARBON PASTE ELECTRODE CONTAINING CATION EXCHANGER BEADS LOADED WITH CATIONIC REAGENT FOR ELECTROCATALYSIS

02380 M. Janik-Czachor
APPLICATION OF SURFACE ENHANCED RAMAN SPECTROSCOPY TO IN-SITU CHARACTERIZATION OF METAL/SOLUTION AND SEMICONDUCTOR/SOLUTION INTERFACES

02390 M. Enyo, A. Aramata and K. Machida
ELECTROCATALYTIC PROPERTY OF ALLOYS BETWEEN GROUP VIII AND IB METALS TOWARDS OXIDATION OF SIMPLE ORGANICS

02400 J. Sobkowski and K. Franaszczuk
THE INFLUENCE OF TIN ON THE ELECTROOXIDATION OF CHEMISORPTION PRODUCTS DERIVED FROM METHANOL

02410 E.P.M. Leiva, E. Santos and T. Iwasita
THE HYDROGEN EVOLUTION REACTION ON PLATINUM IN THE PRESENCE OF ADSORBED CARBON MONOXIDE

03. Materials for Electrochemical Application

03010 R. Atanasoski, G. Perović, B.Nikolić, N.Blagojević, R.Reeves
ELECTROCHEMICAL CHARACTERISTICS OF TuO_2 CATALYZED SURFACE OF GLASSY CARBON

03020 Y. Yamamoto
THE INFLUENCE OF YTTRIUM, COPPER, ZINC, AND TIN ON A SILVER -SILVER OXIDE ELECTRODE IN KOH SOLUTION

03030 W. Schnurnberger
OXYGEN EVOLUTION REACTION ON PEROVSKITE COATED NICKEL ELECTRODES IN ALKALINE SOLUTION

03040 A. Pinkowski , K.P. Thiessen , K. Wiesener
THE INFLUENCE OF CONTINUOUS IMPACTING OF PASSIVATED IRON ELECTRODES ON THEIR SEMICONDUCTOR BEHAVIOR

03050 A.Pinkowski, K. Wiesener
A PIN JUNCTION MODEL OF THE PASSIVE FILM ON IRON

04. Electrochemical Engineering

04010 J. Legrand, J.M. Marracino and F. Coeuret
COPPER REMOVAL IN THE FALLING-FILM CELL

04020 L.J.J. Janssen, E. Barendrecht and S.J.D. van Stralen
EFFICIENCY OF GAS BUBBLE EVOLUTION AT A GAS-EVOLVING ELECTRODE

04030 D. Schmal, J. van Erkel, P.J. van Duin
MEASUREMENTS OF MASS TRANSFER AT FIBRE ELECTRODES

04040 J. van Erkel, D. Schmal, P.J. van Duin
ELECTROCHEMICAL DETOXIFICATION OF AQUEOUS WASTE SOLUTIONS

04050 F. Bravo de Nahui and A.A. Wragg
ESTIMATION OF MASS TRANSFER RATE FOR A PACKED BED COPPER CEMENTATION SYSTEM

04060 G. Nahui-Palomino and A.A. Wragg
A PARAMETRIC STUDY OF COPPER DEPOSITION IN A CIRCULATING BED ELECTRODE

04070 M. Spasojević, R. Stevanović, N. Krstajić and M.M. Jaksić
HYDRODYNAMIC OPTIMIZATION OF FARADAIC YIELDS IN THE CHLORATE CELL PROCESS

04080 V.D. Stanković
BATCH RECIRCULATING THREE-DIMENSIONAL ELECTROCHEMICAL CELL: OPERATIONAL MODES AND ENERGY CONSUMPTION

04090 J. Comiti and J. Legrand
ELECTROCHEMICAL DETERMINATION OF AXIAL DISPERSION IN FIXED BEDS OF FLAT PLATES BY THE RTD METHOD

04100 A. Mestrović-Markovinović, Dj. Matić
ELECTROCHEMICAL REACTOR WITH PARTIALLY IMMERSED ROTATING HORIZONTAL CYLINDER

05. Electrochemical Kinetics

05060 M. Ristić, S. Strbac, B.Kosanović, N. Krstajić, T. Grozdić and M.M. Jaksić
SYNERGETIC ELECTROCATALYTIC EFFECTS OF COMPOSITE d-METALS CATALYSTS FOR THE HIDROGEN EVOLUTION REACTION ON PLATINUM METAL SUBSTRATES

05070 M.V. Susić, S.V. Mentus and M.M. Dojcinović
CYCLIC VOLTAMMETRY OF $MnSO_4$ IN MOLTEN Li_2SO_4-K_2SO_4 EUTECTIC MIXTURE

05080 G. Barral J.P. Diard, B. Le Gorrec, C. Montella
DIAGRAMMES D'IMPEDANCE DE MODELES ELECTROCHIMIQUES EN COUCHE MINCE

05090 S. Roffia, C. Paradisi and V. Concialini
ELECTROCHEMICAL BEHAVIOUR OF SOME POLYPYRIDINE COMPLEXES OF COBALT (III) IN APROTIC SOLVENTS

05100 J.P. Diard, R. Durand, B. Le Gorrec, S. Maximovitch
COMPORTEMENT INDUCTIF DU MECANISME DE VOLMER-HEYROVSKY COMPARAISON AVEC LE SYSTEME H^+/H_2 SUR NICKEL

05110 M.S. Lorenzo, P. Cañas, C. Montemayor, J.M. Vara and E. Fatas
STUDY OF DIGITAL SIMULATION IN SECOND ORDER TECHNIQUES FOR ELECTROCHEMISTRY

05120 P. Cañas, M.S. Lorenzo, C. Montemayor, J.M. Vara and E. Fatas
APPLICATION OF THE DIGITAL SIMULATION METHOD TO THE STUDY OF THE IMPEDANCE OF ELECTRODIC SYSTEMS

05130 E. González-Fernan, C. Alonso and J. González-Velasco
INFLUENCE OF THE ACTIVATION OF A GOLD ELECTRODE ON THE OXIDATION MECHANISM OF METHANOL

05140 C. Alonso and J. González-Velasco
A STUDY OF THE OH COVERAGE ON GOLD IN BASIC SOLUTIONS

05150 A. Hubin, H. Terryn , B. van der Linden, J. Vereecken
ELECTROCHEMICAL REDUCTION OF SILVERCOMPLEXES IN PHOTOGRAPHIC SYSTEMS

05160 E. Bouhier-Charbonnier, B. Boden, J.M. Leger and C. Lamy
IDENTIFICATION BY FTIR AND HPLC OF THE PRODUCTS GENERATED DURING THE PROLONGED ELECTROLYSIS OF ETHYLENE GLYCOL ON NOBLE METAL ELECTRODES

05170 E. Guaus, F. Mas, J. Puy and F. Sanz
A FORMALISM FOR DEVELOPING CHRONOCOULMETRY AT A SPHERICAL ELECTRODE

05180 F. Mas, J. Puy and F. Sanz
THEORETICAL TREATMENT OF REVERSIBLE REACTIONS WITH ADSORPTION AT THE RDE. ATTEINMENT OF STATIONARY STATE

05190 S.I. Cordoba, R.E. Carbonio, M. López Teijelo and V.A. Macagno
OXYGEN EVOLUTION REACTION ON CHEMICALLY CO-PRECIPITATED NICKEL HYDROXIDE-IRON HYDROXIDE MIXTURE ELECTRODE

05200 R.M. Torresi, O.R. Camara and C.P. de Pauli
CATHODIC BEHAVIOUR OF THICK TITANIUM OXIDE FILMS

05210 L.M. Yudi, A.M. Baruzzi and V.M. Solis
INDIRECT ELECTROSYNTHESIS OF MONOBROMONORCARANE IN TWO PHASE SYSTEMS

05220 C.F.Darbyshire and O.R. Camara
ELECTROCHEMICAL BEHAVIOUR OF ACID AND NEUTRAL ZINC (II) SOLUTIONS ON THIN TITANIUM OXIDE FILM SUBSTRATES

05230 J. García-Domenech, J.L. Vázquez, J.M. Feliu, A. Aldaz and J. Clavilier
ELECTROCATALYSIS BY FOREIGN AD-ATOMS. REDUCTION OF NITRATE ON A GOLD ELECTRODE CATALYSED BY UPD OF CADMIUM

05240 E. Gomez, E. Valles, J.M. Feliu, A. Aldaz
CHLORIDE INHIBITION OF OXALIC ACID AT A GOLD ELECTRODE IN ACID MEDIA

05250 E. Valles, E. Gomez, J.M. Feliu, A. Aldaz
PYRUVATE OXIDATION ON GOLD ELECTRODES IN BASIC MEDIA

05260 J.M. Feliu, J. Claret, C. Muller, J.L. Vázquez, A. Aldaz
OXALIC ACID OXIDATION ON GOLD IN ACID MEDIUM

05270 M. Blazquez, L. Camacho, M. Jimenez and M. Domínguez
DIAGNOSTIC CRITERIA FOR CHARACTERIZATION OF MECHANISMS IN POLAROGRAPHY

05280 J.M. Rodríguez-Mellado, M. Blázquez, M. Domínguez and J.J. Ruiz
AN APPROXIMATE EXPLICIT EQUATION IN DIFFERENTIAL PULSE POLAROGRAPHY FOR FIRST-ORDER PROCESSES

05290 M. Barrera, M. Pérez Sánchez, M. Martin Artiles and A. Arevalo
POTENTIOSTATIC REDUCTION OF METAL COMPLEXES ON MERCURY ELECTRODE FOR ANY LIGAND/METAL RELATIONSHIP VALUE

05300 M. Barrera, M. Pérez Sánchez, M. Martin Artiles and A. Arevalo
GALVANOSTATIC REDUCTION OF METAL COMPLEXES ON MERCURY ELECTRODE FOR ANY LIGAND TO METAL RELATIONSHIP VALUE

05310 M. Barrera, M. Martin Artiles, M. Pérez Sánchez and A. Arevalo
POLROGRAPHIC REDUCTION OF METAL COMPLEXES TO A LOWER OXIDATION STATE FOR ANY VALUE OF ANALYTICAL LIGAND CONCENTRATION/ANALYTICAL METAL ION CONCENTRATION

05320 M. Pérez Sánchez, M. Barrera, B. Domínguez and A. Arevalo
A STUDY ON THE REDUCTION OF THE Zn(II)-SUCCINATE COORDINATE SYSTEM ON MERCURY ELECTRODE

05330 S. Jarek and J. Thonstad
VOLTAMMETRIC STUDY OF ANODIC ADSORPTION PHENOMENA ON GRAPHITE IN CRYOLITE MELTS WITH VARYING ALUMINA CONCENTRATION

05340 R.M. Souto, M. Sluyters-Rehbach and J.H. Sluyters
A FARADAIC IMPEDANCE STUDY OF THE CATALYTIC EFFECT OF THIOUREA ON THE ELECTROCHEMICAL REDUCTION OF Cd(II) IONS FROM 1 M KJ SOLUTIONS AT THE D.M.E.

05350 W. Visscher, J. Hendrikx and E. Barendrecht
IMPEDANCE MEASUREMENTS OF ZINC AND AMALGAMATED ZINC IN ALKALINE ELECTROLYTE

05360 A. van der Putten, A. Elzing, W. Visscher and E. Barendrecht
OXYGEN REDUCTION ON CARBON SUPPORTED METAL-PHTHALOCYANINES USING A ROTATING RING DISC ELECTRODE (RRDE)

05370 J. Garche, S. Petrovic, K. Wiesener and J. Mrha
ON THE OXYGEN REDUCTION RATE ON PLASTIC BONDED CADMIUM ELECTRODES

05380 U. Frese and U. Stimming
HYDROGEN EVOLUTION AT Cu AND Ag ELECTRODES IN A WIDE RANGE OF TEMPERATURES

05390 U. Frese, T. Iwasita, W. Schmickler and U. Stimming
INVESTIGATION OF HYDROGEN EVOLUTION AT PLATINUM ELECTRODES

05400 T.F. Otero and Y. Jiménez Jiménez
ANODIC ACTIVITY OF THE NO_3^- ON AN ACTIVATED IRIDIUM ELECTRODE

05410 I. Urbina, G. Barreiro and G. Poillerat
OXYGEN REDUCTION ON Ni, Cu AND Ni-Cu ALLOY IN MOLTEN CARBONATES

05420 C. Paliteiro , A. Hamnett and J.B. Goodenough
O_2 REDUCTION BY PLATINUM PHTHALOXYANINE IN ALKALINE SOLUTIONS

05430 M.J.B.V. Melo and M.I.S. Pereira
THE ELECTROCRYSTALLIZATION OF PbS ON Pb (Hg)

05440 D.H. Evans and M.R. Anderson
EVALUATION OF ELECTROCHEMICAL KINETIC PARAMETERS USING THE BOND-HENDERSON-OLDHAM "GLOBAL ANALYSIS"

05450 V.F.Vargalyuk,Y.M.Loshkaryev,V.S. Polonsky,N.V.Knoroshavkina
INVESTIGATION OF ELECTROCHEMICAL AND CHEMICAL STAGES OF THE Cu(II) ELECTROREDUCTION PROCESS IN THE PRESENCE OF ALLYL ALCOHOL

05460 V.V. Trofimenko, V.S. Kovalenko, Y.M. Loshkaryev
THE ADATOMS INFLUENCE ON THE OVERPOTENTIAL OF THE TRANSITION IN THE PROCESS OF METAL ELECTROCRYSTALLIZATION

05470 V.V. Trofimenko, V.P. Zhitnik. E.V. Isaenko, Y.M. Loshkaryev
THE DYNAMIC OF CONCENTRATION ADATOM CHANGE IN THE PROCESS OF POLYCRYSTALLINE DEPOSIT GROWTH OF COPPER

05480 J. Galvez, J. Zapata and M.L. Alcaraz
PULSE POLAROGRAPHY: CURRENT-POTENTIAL CURVES IN NORMAL PULSE POLAROGRAPHY; REVERSE PULSE POLAROGRAPHY AND DIFFERENTIAL PULSE POLAROGRAPHY FOR ELECTRODE PROCESSES WITH NON-NERNSTIAN BEHAVIOUR

05490 J. Galvez, J. Zapata, M.L. Alcaraz and F. Robles
CHRONOPOTENTIOMETRY WITH PROGRAMMED CURRENT AT A DROPPING MERCURY ELECTRODE: POTENCIAL-TIME CURVES FOR AN ECE MECHANISM

05500 J. Galvez, F. Robles, J. Zapata and M.L. Alcaraz
CHRONOPOTENTIOMETRY WITH PROGRAMMED CURRENT AT A DROPPING MERCURY ELECTRODE: THEORY FOR ELECTRODE PROCESSES WITH FIRST-ORDER REGENERATION MECHANISMS

05510 J. Galvez, M.L. Alcaraz and J. Zapata
THEORY OF THE EE MECHANISM WITH ADSORPTION OF THE INTERMEDIATE AT AN ELECTRODE EXPANDING WITH ANY POWER LAW

05520 O. Haas
KINETIC CHARACTERISATION OF $Ru(bipy)_2Cl$ poly(4-vinyl-pyridine) Cl COATED ELECTRODES

05530 G. Grampp, W. Harrer and W. Jaenicke
UNEXPECTED SOLVENT DEPENDENCE OF SOME HOMOGENEOUS ELECTRON EXCHANGE REACTIONS

05540 T.H. Birkeland, R. Tunold , R. Ødegård, T. Hurlen
KINETICS OF THE HYDROGEN EVOLUTION REACTION ON STEEL FROM AQUEOUS SOLUTIONS IN EQUILIBRIUM WITH CO_2

05550 J. Willsau and J. Heitbaum
ELEMENTARY STEPS OF THE ELECTROCHEMICAL REACTIONS OF ETHANOL ON PLATINUM A "DEMS" S[illegible]

05560 C.J. van Velzen, G.J. Brug, M. Sluyters-Rehbach, J.H. Sluyters
ELECTROCHEMICAL REDUCTION OF OXYGEN.KINETICS, MECHANISM AND CATALYSIS

05570 G. Horányi
SOME FEATURES IN THE ELECTROCATALYTIC REDUCTION OF NO_2^- AND NO_3^- IONS AT PLATINIZED PLATINUM ELECTRODES

05580 Qi-Xin Zhang, Ze-Shan Zhu, Jin-Ming Lian
A STUDY ON ELECTRODE KINETICS OF THE DEPOSITED ELECTROLYTIC MANGANESE DIOXIDE (EMD) PROCESS

05590 Qi-Xin Zhang, Ze-Shan Zhu, Jin-Ming Lian
A STUDY ON ELECTRODE KINETICS OF THE DEPOSITED EMD PROCESS

05600 J. Tarazaewska and A. Walega
KIENTICS OF Zn(II) REDUCTION AT THE Hg ELECTRODE FROM WATER + DIMETHYLFORMAMIDE MIXTURES

05610 G. Bech-Nielsen, C. Qvist Jessen and J.C. Reeve
CHEMICAL AND ELECTROCHEMICAL REACTIONS OF HYPOPHOSPHITE ON Ni AND Pd ELECTRODES

05620 R. Ødegard, A. Sterten and J. Thonstad
ON THE ELECTRODEPOSITION OF CARBON FROM NaF-AlF_3 MELTS SATURATED WITH ALUMINIUM CARBIDE

05630 R. Durand, F. El Omar and G. Jorge
ELECTROCATALYSIS AND PASSIVATION-DEPASSIVATION: MEANING OF THE INVERTED VOLTAMMETRIE PEAKS

05640 Mª.J. González Tejera
ANODIC REDUCTION OF THE PERCHLORATE ANION. INFLUENCE OF pH AND ANION CONCENTRATION

06. Corrosion

06010 I.F. Fishtik
THERMODYNAMIC AND STOICHIOMETRIC ASPECTS OF THE POURBAIX DIAGRAMS DERIVATION

06020 R.C. Salvarezza, V.D. Vasquez Moll and A.J. Arvia
NUCLEATION AND GROWTH MECHANISM APPLIED TO THE LOCALISED CORROSION OF METALS

06030 H. Avila Mendoza
ELECTROCHEMICAL MEASUREMENTS FOR STRESS CORROSION CRACKING OF A COMMERCIAL 5LX LOW ALLOY PIPELINE STEEL IN CARBONATE-BICARBONATE SOLUTIONS

06040 D.M. Drazić and V. Vasić
THE ANALYSIS OF THE REACTION STEPS CONTROLLING THE OXYGEN CORROSION OF IRON AND STEEL IN CHLORIDE SOLUTION

06050 Lj. Arsov, T. Grcev and A. Prusi
CORROSION STABILITY OF TITANIUM IN ACID MEDIA.ELECTROCHEMICAL AND OPTICAL STUDIES

06060 A. Prusi and Lj. Arsov
ELECTROCHEMICAL FORMATION AND CHARACTERISATION OF OXIDE FILMS ON TITANIUM IN ALCALINE SOLUTION

06070 T. Grcev and M. Cvetkovska
ELECTROCHEMICAL PASSIVATION OF IRON IN BORATE BUFFER SOLUTION AT THE PRESENCE OF POLYACRYLAMIDE

06080 J.R. Cullere
METHANOL CORROSION OF MAGNESIUM

06090 M.P. Mateo, M.D. Salvador, I. Barba
THE STUDY AND DETECTION OF INTERNAL DEFECTS OF NON-FERROUS ALLOYS BY OPTICAL AND ELECTROCHEMICAL METHODS

06100 I. Petrovich and J.C. Galvan
CORROSION PERFORMANCE OF PAINTED GALVANIZED STEEL BY ELECTROCHEMICAL METHODS

06110 P. Ll. Cabot, M. Crotes, F. Centellas, J.A. Ga[illegible] and E. Perez
POTENTIODYNAMIC BEHAVIUOR OF ZINC IN ALKALINE SOLUTIONS

06120 F.A. Centellas, J.A. Garrido, P. Ll. Cabot and E. Perez
TAFEL SLOPES FOR Cu(I) AND Cu(II) OXIDE FORMATION IN ALKALINE SOLUTIONS

06130 F.A. Centellas, P. Ll. Cabot, J.L. Fernandez, J.A. Garrido and E. Pérez
TREATMENT OF POTENTIOSTATIC CURVES IN ANODIC OXIDATION OF COPPER IN ALKALINE SOLUTIONS

06140 M. Cid, D. Desjardins, M.C. Petit, M. Pluggali
COMPARISON BETWEEN MECHANICAL AND ELECTRICAL DEPASSIVATION OF STAINLESS STEELS IN HOT CHLORIDE MEDIA

06150 H. di Nezio, C. Manfredi, S. Simison and S.R. de Sánchez
THE EFFECT OF SO_4Fe TREATMENT ON COPPER ALLOYS IN POLLUTED SEA WATER

06160 A. Molina, C. Andrade, M.C. Alonso and J.A. González
FACTOR CONTROLLING CORROSION RATE IN CONCRETE EMBEDDED REBARS

06170 J.J. Royuela
PITTING AND PROTECTION POTENTIAL OF 18/8 STAINLESS STEEL IN CHLORIDE SOLUTIONS. CATION ADN DILUTION EFFECT

06180 M. Ergun and S. Uneri
INVESTIGATION OF THE PROPERTIES OF OXIDE LAYERS FORMED ON ALUMINIUM AND ACTION OF CITRATE AND CHLORIDE IONS ON THE OXIDE BY THE POTENTIODYNAMIC METHOD

06190 I.T.E. Fonseca and A.C.S. Marin
THE EFFECT OF SO_4^{2-} ON THE KINETICS OF THE ANODIC OXIDATION OF COPPER

06200 K. Leitner, J.W. Schultze, U. Stimming
PHOTOELECTROCHEMICAL INVESTIGATIONS OF PASSIVE FILMS ON TITANIUM ELECTRODES

06210 J.M. Albella, I. Montero and O. Sánchez-Garrido
APPROXIMATE EQUATIONS FOR THE CONSTANT VOLTAGE STAGE OF THE ANODIC OXIDATION

06220 S. Raicheva, E. Sokolova, R. Gulamali
THE EFFECT OF THE FUNCTIONAL GROUPS IN THE INHIBITOR MOLECULE UPON ITS PROTECTIVE EFFICIENCY

06230 G. Rondelli, T. Pastore, B. Vicentini
ELECTROCHEMICAL EVALUATION OF THE DEGREE OF SENSITIZATION CAUSED BY HEAT TREATMENTS ON COLD ROLLED AISI 304L

06240 D.W. Shoesmith, S. Sudner, M.G. Bailey, G.J. Wallace and L.H. Johnson
CORROSION OF NUCLEAR FUEL (UO_2) UNDER WASTE DISPOSAL VAULT CONDITIONS

06250 C.M. Rangel, I.T. Fonseca, M.F. Reis
THE CORROSION OF MILD STEEL EVALUATED FROM DATA IN THE PRE-TAFEL AND TAFEL REGIONS

06260 F. Bellucci, L. Nicodemo, A. Bongiovanni, A. di Martino, G. Capobianco
GALVANIC CORROSION OF AL ALLOYS COUPLED TO ADVANCED COMPOSITE MATERIALS

06270 D. Zur Megede and E. Heitz
INTERGRANULAR CORROSION OF WC/Ni AND WC/Co METAL MATRIX COMPOSITES

06280 M. Metikos-Hukovic, M. Ceraj-Ceric
ACTIVE, PASSIVE AND TRANSPASSIVE CHROMIUM

06290 A. Rendić, M. Metikos-Huković, S. Ferina
PLATINIZED TITIANIUM ANODES IN CATHODIC PROTECTION

06300 M. Prazak
DUAL EFFECT OF ANIONS IN PITTING CORROSION

06310 R. Duran, J. Genesca
ELECTRODISSOLUTION KINETICS OF PALLADIUM IN ACIDIC CHLORIDE SOLUTIONS

06320 T. Tzvetkov
CORROSION OF IRON AND IRON OXIDES IN MOLTEN SODIUM HYDROXIDE

06330 T. Tzvetkov
CORROSION OF GOLD, SILVER AND PLATINUM IN A SODIUM HYDROXIDE MELT

06340 J. Przyluski, A. Krolikowski and J. Fulara
THE CORROSION BEHAVIOUR OF IRON -AND COBALT- BASE METALLIC GLASSES

06350 A. Krolikowski
THE CORROSION STUDY OF AMORPHOUS AND CRYSTALLIEN Co-P FILMS

06360 M.M. Musiani, G. Mengoli and M. Fleischmann
SURFACE ENHANCED RAMAN SCATTERING (SERS) INVESTIGATION OF CORROSION INHIBITION OF COPPER

06370 K. Carr, S. XU and C.A. Melendres
LASER RAMAN SPECTRO-ELECTROCHEMICAL STUDIES ON THE CORROSION AND PASSIVATION BEHAVIOR OF NICKEL IN AQUEOUS SOLUTIONS

06380 S.S. Abd el Rehim and A. el Sayed
EFFECT OF ADDITION OF HALIDE IONS ON THE ANODIC BEHAVIOUR OF TIN IN STANNATE PLATING SOLUTIONS

06390 C. Alonso, A. Macías, P. Santos, C. Andrade
SOME RESULTS OF A.C. AND D.C. TECHNIQUES USED TO MEASURE THE CORROSION RATE OF STEEL AND Zn EMBEDDED IN MORTAR

06400 P. Allongue, H. Cachet, P. Clecher, M. Froment, J.R. Martin and E. Verney
CORROSION AND STABILIZATION OF n-GaAs IN AQUEOUS IODIDE SOLUTIONS

06410 F. Huete and J.J. Royuela
APPLICABILITY OF THE ELECTROCHEMICAL METHODS TO THE STUDY OF THE EXTERNAL CORROSION OF METALLIC TUBES IN BUILDINGS

06420 S. Feliu, J.M. Bastidas and M. Morcillo
ELECTROCHEMICAL ESTIMATION OF CORROSION RATES ON PAINT COATED METAL SURFACES

06430 S. Feliu , J.A. González, C. Andrade, V. Feliu
ELECTRICAL MODEL FOR STUDYING THE CORRODING STEEL/CONCRETE SYSTEM

06440 G. Capobianco, G. Farnia, C.A. Farina, F. Bellucci
ANODIC BEHAVIOUR OF A.I.S.I. 446 STAINLESS STEEL IN METHANOLIC ENVIRONMENT

06450 J. Piroth and E. Brauer
ELECTRODE PROCESSES AT HAFNIUM IN VARIOUS ELECTROLYTES

06460 M.V. Susić
INVESTIGATION OF AMORPHOUS TITANIUM ALLOY IN 0.2 N H_2SO_4

06470 I.N. Ozeryanaya, T.I. Manukhina,V.I.Sannikov,A.I.Anfinogenov
CORROSION PROTECTION OF TITANIUM ALLOY AND STEELS IN MOLTEN ALKALI CARBONATES

06480 I.N. Ozeryanaya, N.T. Shardakov
INFLUENCE OF WATER VAPOR PRESSURE ON ALUMINIUM CORROSION IN MOLTEN LITHIUM AND KALIUM CHLORIDES

06490 G. Rocchini
A GENERALIZATION OF THREE POINT METHOD

06500 M. Koda, H. Takahashi and M. Nagayama
HOT-WATER HYDRATION OF POROUS ANODIC OXIDE FILMS ON ALUMINIUM-ANALYSIS OF FILM STRUCTURE BY ANODIC POLARIZATION

06510 M. Janik-Czachor
EFFECT OF METALLOID ELEMENTS ON THE CORROSION BEHAVIOUR OF Fe BASE GLASSY ALLOYS

06520 L. Graillot , R. Reich, C. Flaud
STAINLESS STEELS WITH ALUMINIUM AND SILICON ADDITIONS: PREPARATION, METALLOGRAPHY AND PITTING CORROSION STUDY

06530 R. Goetz, J. Laurent, D. Landolt
INFLUENCE OF MINOR ALLOYING ELEMENTS ON PASSIVATION BEHAVIOUR OF IRON-CHROMIUM ALLOYS IN HCl

06540 O. Lunder and K. Nisancioglu
ELECTROCHEMICAL BEHAVIOUR OF AlMnFe INTERMETALLICS IN ALKALINE SOLUTION

06550 P. Kirkov, T.Anovski, J.Arsovski, S.Pejovski, J.Naumovski, T. Grcez, Lj.Arsov, A. Prussi
THE EFFECT OF DRAG REDUCERS ON THE INHIBITOR EFFICIENCY AND CORROSION PROTECTION IN NON-AQUEOUS MEDIUM

07. Electrochemical Energy Conversion and Photoelectrochemistry

07010 J. Kankare, K. Haapakka, O. Puhakka and S. Kulmala
ELECTROGENERATED LUMINESCENCE OF TERBIUM COMPLEXES ON AN ALUMINIUM ELECTRODE

07020 K. Haapakka, J. Kankare and O. Puhakka
DETERMINATION OF FLUORESCENT COMPOUNDS BY ELECTROLUMINESCENCE

07030 P. Salvador and C. Gutierrez
ROTATING RING-DISK ELECTRODE STUDY OF THE COMPETITIVE PHOTOOXIDATION OF I^- AND H_2O AT n-TiO_2 ELECTRODE

07040 M. Maja, P. Spinelli, M.V. Ginatta and G. Orsello
KINETICS OF THE DISSOLUTION OF SPENT LEAD-BATTERIES WITH THE "G.S." ELECTROCHEMICAL PROCESS

07050 A.R. Despić, K. Krsmanović, A. Vorkapić, M. Dobrić and B. Vesić
SOME NEW EXPERIENCE IN THE OPERATION OF SALINE ALUMINIUM-AIR BATTERIES

07060 A. Anastasijević, Z. Dimitrijević and R. Adzić
OXYGEN REDUCTION ON RUTHENIUM ELECTRODE MODIFIED BY THALLIUM AND LEAD ADSORBATES

07070 F. Castaneda and V. Plichon
ELECTROCHROMISM OF LUTETIUM DIPHTHALOCYANINE THIN FILMS ELECTROCHEMICAL INVESTIGATION

07080 [illegible]. Bosch, P. Crouigneau, [illegible]nes and C. Lamy
"IN SITU" SPECTROSCOPIC STUDIES OF N,N'-DIBENZYL-VIOLOGEN RADICALS ADSORBED ON METALLIC (Pt,Au) OR SEMICONDUCTOR (TiO_2) SURFACES

07090 O. Enea and M. Grätzel
THE EFFECT OF Pt AND RuO_2 DEPOSITS ON THE PHOTOREDUCTION OF METHYLVIOLOGEN ON Ti/TiO_2 ELECTRODES AT OPEN CIRCUIT

07100 O. Enea and A.J. Bard
pH EFFECTS ON THE PHOTOOXIDATION OF SOME SUGARS BY THE IRRADIATED SUSPENSIONS OF TiO_2

07110 F. Trinidad, J. Alonso-López and M. Nebot
ELECTROCHEMICAL BEHAVIOUR OF POLYPYRROLE FILMS IN ClO_4Li/PC AS SECONDARY BATTERY ELECTRODES

07120 P. Garces, M.A. Climent, M. López Segura and A. Aldaz
REDOX FLOW BATERRY USING Fe^{3+}/Fe^{2+} AND Cr^{3+}/Cr^{2+} COUPLES

07130 M. Fujihira and K. Nishiyama
ELECTROCHEMICAL AND PHOTOELECTROCHEMICAL BEHAVIOUR OF LANGMUIR-BLODGETT MONOMOLECULAR ASSEMBLIES ON Au AND SnO_2 ELECTRODES

07140 M. Fujihira, K. Aoki, S. Inoue, H. Takemura and S. Aoyagui
DYE SENSITIZATION OF RHODAMINE B AND $Ru(bpy)_3^{2+}$ SURFACTANT DERIVATIVES ON Au AND SnO_2 OTE

07150 I.T.E. Fonseca and A.C.S.S. Marin
THE OXIDATION OF HCOOH AT A Pt ANODE PARTIALLY COVERED BY COPPER

07160 J.M. Hornut and A. Storck
DISCHARGE BEHAVIOUR OF A REDOX THERMOGALVANIC AND CONCENTRATION CELL

07170 D. Pavlov and E. Bashtavelova
EVOLUTION IN THE POROSITY OF THE LEAD DIOXIDE ACTIVE MASS DURING CYCLING AND PHENOMENA LEADING TO ITS DESTRUCTION

07180 O. Solorza and G. Poillerat
STUDY OF CdTe/ELECTROLYTE INTERFACE: FLAT-BAND POTENTIALS, PHOTOCURRENT AND PHOTOCORROSION

07190 S. Agachi and L. Oniciu
OPTIMIZATION OF THE ELECTROCHEMICAL PROCESS TAKING PLACE IN A METHANOL-HYDROGEN PEROXIDE FUEL CELL

07200 M. Biserni, P. Buttol, A. Marinnageli, M. Mastragostino
BROMINE DOPED POLYDITHIENOTHIOPHENE: CATHODE ACTIVE MATETERIAL IN AQUEOUS MEDIUM

07210 A. Felske, W.J. Plieth
PHOTOCHEMICAL INVESTIGATIONS OF THE METAL/ELECTROLYTE AND THE METAL/METALOXIDE/ELECTROLYTE INTERFACE USING HIGH POWER LASER PULSES

07220 R. Knödler
IMPEDANCE OF A SODIUMPOLYSULPHIDE ELECTRODE DURING THE PHASE TRANSITION MOLTEN/SOLID

07230 C. Rüssel, D. Krauss and K. Ledjeff
THE INFLUENCE OF THE ELECTROLYTE ON THE KINETICS OF Cr(III)-REDUCTION

07240 K. Kordesch, J. Gsellmann and M. Posch
THE BIPOLAR ZINC-BROMINE BATTERY: IMPROVED CARBON-BROMINE ELECTRODES

07250 W.J. Harer and K. Kordesch
ELECTROLYTIC MANGANESE DIOXIDE PRODUCTION IN A FLOWING ELECTROLYTE SYSTEM

07260 J.P. Roger, D. Fournier, A.C. Boccara, R. Noufi, D. Cahen
IN SITU MONITORING OF SEMICONDUCTOR/LIQUID JUNCTION BY SIMULTANEOUS PHOTOCURRENT AND PHOTOTHERMAL DEFLECTION SPECTROSCOPY

07270 L. Binder
ELECTRODEPOSITION OF ZINC USING PULSE-CURRENT

08050 G. Pierre, P. Chautemps and J.L. Pierre
A SYNTHETIC MODEL OF NADH WORKING CATALYTICALLY IN A BIPHASIC MEDIUM

09. Double Layer and Adsorption

09010 G. Barral, J.P. Diard, C. Montella
EFFETS DE LA DOUBLE COUCHE D'HELMOLTZ SUR LA DISTRIBUTION DU POTENTIEL ET LE COMPORTEMENT CAPACITIF DE L'INTERFACE SEMICONDUCTEUR OU SEMIMETAL/ELECTROLYTE

09020 M. Erceg and D. Suznjević
ADSORPTION OF THE ETHYLENEDITHIOLDIACETIC ACID AND THIOGLYCOLIC ACID AT THE MERCURY SOLUTION INTERFACE

09030 R.I. Tucceri and D. Posadas
DIFFERENTIAL CAPACITANCE AND SURFACE CONDUCTANCE OF GOLD IN THE PRESENCE OF ADSORBED AMYL ALCOHOL

09040 G.J. Gordillo and D. Posadas
IONIC COMPONENTS OF CHARGE AT THE MERCURY/KI + KCl AQUEOUS SOLUTION INTERPHASE

09050 J. Malina and B. Lovrecek
PROPERTIES OF THE INTERFACE STEEL-THERMALLY FORMED OXIDE/ELECTROLYTE

09060 J. Barbier, E. Lamy-Pitara
INVESTIGATION OF SULFUR ADSORPTION ON NOBLE METALS BY CYCLIC VOLTAMMETRY

09070 M^{a}.M. Gomez and E. Alda
ADSORPTION OF ASCORBATE IONS ON MERCURY ELECTRODE IN PRESENCE OF POTASSIUM PERCHLORATE

09080 M. Cid and M.C. Petit
STUDY AND COMPARISON OF ANOMALIES OBSERVED ON IMPEDANCE DIAGRAMS OF NICKEL IN THE PRESENCE OF F^- AND HSO_4^- ANIONS

09090 M. Pérez Sánchez, M. Barrera, S. González and A. Arévalo
STUDY ON THE ADSORPTION OF Zn(II) IN PYRIDINE-$NaClO_4$ MEDIA

09100 Z. Samec and V. Marecek
EVALUATION OF OHMIC POTENTIAL DROP AND DOUBLE LAYER CAPACITANCE OF THE INTERFACE BETWEEN TWO INMISCIBLE ELECTROLYTE SOLUTIONS FROM GALVANOSTATIC PULSE MEASUREMENTS

09110 A. Hamelin , L. Stoicoviciu, F.A. Silva, M.J. Sottomayor
TEMPERATURE EFFECT AT GOLD SINGLE CRYSTALS/AQUEOUS SOLUTION INTERFACES

09120 S. González, P. Carro and A. Arévalo
ADSORPTION OF Tl(II) ON MERCURY IN AZIDE MEDIA

09130 G.J. Hansen , W.N. Hansen, A.P. Andrew
OBSERVING THE COMPONENTS OF THE IDEALLY POLARIZABLE DOUBLE LAYER USING INFRARED SPECTROSCOPY

09140 L. Victori, W. Bek, L. Núñez, R. Fortuny
INTERFACE CONSTRUCTION TO INFORMATIZATION OF ELECTROCHEMICAL PROCESSES

09150 D. González-Arjona and M. Rueda
ADSORPTION OF α, β-UNSATURATED ALDEHYDES AT THE MERCURY-WATER INTERFACE

09160 H.D. Hurwitz, A. Jenard and B. Bicamumpaka
FLUORIDE AND BROMIDE COADSORPTION AT THE Hg ELECTRODE

09170 M. Bacchetta , S. Trasatti, A. Hamelin, L. Doubova
ADSORPTION ON DIFFERENT FACES OF Ag SINGLE CRYSTAL ELECTRODES

09180 A. Daghetti , S. Trasatti, I.Zagorska,Z. Koczorowski
ADSORPTION OF ETHERS OF ETHYLENE GLYCOL AT THE AIR/SOLUTION AND THE Hg/SOLUTION INTERFACE

09190 E. Dutkiewicz and P. Skoluda
IONIC ADSORPTION FROM MIXED ELECTROLYTE SOLUTION AT CONSTANT CATIONIC STRENGTH

09200 E. Dutkiewicz and J. Stoczynska
ADSORPTION OF SULFONATE IONS ON MERCURY ELECTRODE FROM SOLUTION AT CONSTANT IONIC STRENGTH

09210 Z. Borkowska
SOLVENT EFFECTS OF THE DOUBLE LAYER AT THE ELECTRODE/SOLUTION INTERFACE

10. Electroanalytical Chemistry

10010 J. Chevalet, N. Fatouros, R. Reeves
THEORETICAL ANALYSIS OF THE MEANS OF IMPROVING THE SENSITIVITY OF ELECTROANALYTICAL TECHNIQUES

10020 C. Locatelli, F. Façioli, C. Bighi
DETERMINATION OF METALS AT TRACE LEVEL BY SECOND HARMONIC ALTERNATING CURRENT ANODIC STRIPPING VOLTAMMETRY

10030 I.D. Grama, I.I. Vataman and Yu. M. Loshkarev
THE EFFECTS OF ADSORPTION OF THE ION ASSOCIATES IN ELECTROANALYSIS

10040 G. López Cueto and A.F. Cueto Rejón
POTENTIOMETRIC BEHAVIOUR OF THE Ce(IV)/Ce(III) COUPLE AT PLATINUM AND CARBON PASTE ELECTRODES

10050 A.M. Martínez, J.L. Polo and R. Guzmán
CONTRIBUTIONS TO THE ETCHING OF ABS PLASTICS FOR THE CHEMICAL COPPER PLATING

10060 J.M. López Fonseca, J.C. García Monteagudo, A. Riveiro and A. Otero
THE APPLICATION OF REVERSE NORMAL PULSE POLAROGRAPHY TO THE CATHODIC STRIPPING DETERMINATION OF SUBSTANCES OF BIOLOGICAL INTEREST

10070 M.J. García Gutierrez, P. Tuñon Blanco, A. Costa, S. Arribas
PHASE SELECTIVE ALTERNATING CUPRENT POLAROGRAPHIC BEHAVIOUR OF MESNA. ANALYTICAL APPLICATIONS

10080 A.J. Miranda Ordieres, P. Tuñon Blanco, A. Costa García, M.A. García Fernández, S. Arribas Jimeno
OXIDATIVE AMPEROMETRIC DETECTION IN HPLC DETERMINATION OF ANTICANCER DRUG METHOTREXATE

10090 A.J. Miranda Ordieres, P. Tuñoz Blanco, A. Costa, S. Arribas
PHASE SELECTIVE ALTERNATING CURRENT POLAROGRAPHIC DETERMINATION OF METHOTREXATE IN BIOLOGICAL MATRICES

10100 J.L Muñiz Alvarez, A.J. Miranda Ordieres, P. Tuñoz Blanco, A. Costa GArcía and S. Arribas Jimeno
VOLTAMMETRIC TECHNIQEUS APPLIED TO THE STUDY OF THE HYDROLISIS OF S-DENOSIL L-METHIONINE

10110 J. Osteryoung, M. Wojciechowski, A. Webber and E. Takeuchi
DETERMINATION OF BIOLOGICALLY INTERESTING MOLECULES BY PULSE VOLTAMMETRY

10120 E. Casassas, C. Ariño and M. Esteban
POLAROGRAPHIC AND VOLTAMMETRIC STUDY OF 2-MERCAPTOETHANOL AND ITS COMPLEXES WITH CADMIUM (II) ION

10130 E. Casassas, M. Esteban and C. Ariño
POLAROGRAPHIC STUDY OF THE ANODIC OXIDATION OF MERCURY IN THE PRESENCE OF THIOETHER CARBOXYLIC ACIDS

10140 Y. Castrillejo, E. Barrado, R. Pardo and P. Sánchez Batanero
POLAROGRAPHIC DETERMINATION OF TITANIUM AT TRACE LEVEL

10150 M. Barajas, E. del Real, R. Pardo, Y. Castrillejo, E. Barrado and P. Sánchez Batanero
DETERMINATION OF ARSENIC AND GERMANIUM BY MEANS OF AN INDIRECT POLAROGRAPHIC METHOD

10160 M. Eguren, M.L. Pascon, M.D. Vazquez and P. Sánchez Batanero
STUDY OF THE ELECTROCHEMICAL BEHAVIOUR OF MINERAL SOLID SUBSTANCES USING A HOME-MADE CARBON PASTE ELECTRODE

10170 U. Nickel, M.Schneider and W. Jaenicke
ANALYSIS OF THE OXIDATIVE SULFONATION OF AROMATIC COMPOUNDS

10180 L. Campanella, M. Mascini, G. Palleschi, M. Tomassetti
DETERMINATION OF PHOSPHOLIPIDIS IN DRUGS AND BIOLOGICAL LIQUIDS

10190 L. Hernández, J.M. Pinilla and J.R. Procopio
APPLICATION OF A FIA SYSTEM WITH AMPEROMETRIC DETECTION TO THE DETERMINATION OF FOLMALDEHYDE

10200 E. González Romero and L. Hernández Hernández
ANODIC STRIPPING VOLTAMMETRY ANALYSIS OF CLOZAPINE ON A GLASSY CARBON ELECTRODE

10210 L.I. de la Cruz Yaguez, J.M. Pingarron Carrazon and L.M. Polo Díez
POLAROGRAPHIC REDUCTION OF NAPHTHOL YELLOWS

10220 G. Tomaino Beltrami, J.M. Pingarron Carrazon and L.M. Polo Díez
APPLICATION OF SEVERAL REVERSIBILITY CRITERIA TO THE POLAROGRAPHIC REDUCTION OF METHYLENE BLUE IN A BRITTON-ROBINSON BUFFER

10230 M. Valcárcel, M.D. Luque de Castro and A. Fernández
AMPEROMETRIC DETERMINATION OF ETHANOL IN BLOOD BY FLOW INJECTION ANALYSIS

10240 J.Hernández Mendez, R. Carabias Martínez, J. Sánchez Martin
POLAROGRAPHIC DETERMINATION OF PARATHION AND PARAOXON. INDUCTION OF PARATHION HYDROLYSIS BY Pd(II)

10250 J. Hernández Mendez, C. González Pérez, M.I. González Martin and M.J. Arias Rodríguez
DETERMINATION OF CLOBAZAM AND NORCLOBAZAM BY DIFFERENTIAL PULSE POLAROGRAPHY

10260 J. Hernández Mendez, A. Sánchez Pérez and M. Delgado Zamarreño
POLAROGRAPHY OF CIMETIDINE AND RANITIDINE

10270 J. Hernández Mendez, R. Carabias Martínez and E. Rodríguez Gonzalo
ELECTROANALYTICAL STUDIES OF PESTICIDES. DETERMINATION OF GUTHION

11. Metal Deposition and Dissolution.

11010 J.N. Jovićević and V.D. Jović
ALUMINIUM ELECTRODEPOSITION FROM $AlCl_3$ -NaCl AND $AlCl_3$-KCl MELTS ON PLATINUM, GOLD AND VITREOUS CARBON ELECTRODES

11020 C. Moina and D. Posadas
SALT FORMATION DURING THE ANODIC DISSOLUTION OF IRON IN AQUEOUS $(NH_4)_2SO_4$ AT pH = 2

11030 C.R. Valentini, C.A. Moina, E.B. Castro, J.R. Vilche and A.J. Arvia
KINETICS OF THE POLYCRYSTALLINE IRON ELECTRODE IN CARBONATE-BICARBONATE SOLUTIONS IN THE 0-75°C RANGE

11040 B. Parajón Costa, M.C. Giordano and A.J. Arvia
THE ELECTRODEPOSITION OF SILVER AT THE SUBMONOLAYER AND MULTILAYER LEVELES ON POLYCRYSTALLINE RHODIUM IN ACID ELECTROLYTES

11050 R.E. Sioda
ELECTRODEPOSITION OF COPPER FROM SOLUTIONS CONTAINING NITRATES

11060 D. Suznjević, D. Spagnut, C. Lacnjevac and M. Jaksić
ELECTRODEPOSITION AND DISSOLUTION OF NICKEL ON AND FROM TRANSITION METALS SUBSTRATES WITH VACANT OR PARTLY FILLED d-ORBITALS

11070 M.G. Pavlović, V.D. Jović, J.N. Jovićević
TITANIUM ANODES FOR THE CHROMIUM PLATING

11080 M.A. Quiroz, I. González and Y. Meas
ELECTRODEPOSITION OF PLATINUM-RUTHENIUM ALLOYS

11090 B. Popov, D. Slavkov and D. Drazić
ELECTROCHEMICAL REDUCTION OF CHROMIUM (VI) IN PRESENCE OF FLUORINE COMPOUNDS

11100 B. Popov, D. Slavkov and H.A. Laitinen
ELECTROCHEMICAL REDUCTION OF INDIUM (III) IN MOLTEN LITHIUM CHLORIDE-POTASSIUM CHLORIDE MELT

11110 J. Hotlos and M. Jaskuła
APPLICATION OF CYLINDRIC SYSTEM WITH A ROTATING ELECTRODE FOR INVESTIGATION OF THE SILVER TRANSPORT PHENOMENA DURING COPPER ELECTROREFINING

11120 R. Ødegard, A. Sterten and J. Thonstad
ON THE ELECTRODEPOSITION OF CARBON FROM NaF-AlF_3 MELTS SATURATED WITH ALUMINIUM CARBIDE

11130 C. Fruhwirth, G.W. Herzog
A SIMPLE LINEAR THERMODYNAMIC MODEL OF ZINCOXIDE CHARGING AND DARK DISSOLUTION

11140 M. Fernández, J.M. Martínez-Duart and J.M. Albella
ELECTROLESS DEPOSITION OF Ni-P THIN FILMS ON CERAMICS SUBSTRATES

11150 E. Julve
THROWING POWER AND CATHODE EFFICIENCY STUDIES OF GOLD PLATING ELECTROLYTES USED IN PRINTED CIRCUITS AND ELECTRONICS

11160 Ya.M. Kolotyrkin, A.N. Chemodanov, I.I. Asheulova
INTERRELATION OF CORROSION, ELECTROCATALYTIC AND ADSOTPTION CHARACTERISTICS

11170 A.N. Baraboshkin, V.A. Isaev
KINETICS OF THE INITIAL STAGES OF GALVANOSTATIC ELECTRODEPOSITION

11180 M.Sarret, J. Claret and M. Müller
THE ANODIC FORMATION OF MERCUROUS OXALATE IN $CHlO_4$ AQUEOUS SOLUTIONS

11190 A. Molenaar and B.C.M. Meenderink
AUTOCATALYTIC TIN DEPOSITION

11200 A. Prieto, J. Doménech and C. Franco
EFFECT OF UV-ILLUMINATION ON THE DISSOLUTION OF ZnO POWDER AQUEOUS SOLUTIONS

11210 K. Nisancioglu and M. Metzger
INVESTIGATION OF THE ELECTROCHEMISTRY OF IRON ON IN-SITU GENERATED SURFACES IN ALKALINE SOLUTION

11220 R. Reich, S.M. Mayanna and M. Maldy
ANODIC DISSOLUTION OF GADOLINIUM IN PERCHLORATES AND CHLORIDES IN AQUEOUS AND NON AQUEOUS SOLVENTS

11230 J. Sabater and L. Victori
PREPASSIVE DISSOLUTION AND PASSIVATION OF Zn IN ALKALINE MEDIA

12. Ionics and Electrochemical Thermodynamics.

12010 M. Syrjämä and J. Kankare
POLYMER COATED SEMICONDUCTOR AS A CALCIUM SELECTIVE ELECTRODE

12020 E. Brillas, J. Doménech, J.A. Garrido and R.M. Rodríguez
POLAROGRAPHIC BEHAVIOUR OF Cd(II) CATION IN ETHYLENE GLYCOL-WATER MIXTURES WITH LITHIUM PERCHLORATE AS BACKGROUND ELECTROLYTE

12030 M.A. Esteso, M.M. Lobos, E.M. Grandoso, A.R. Bueno and O.M. González
ELECTROCHEMICAL MEASUREMENTS IN AQUEOUS-MIXTURES WITH HIGH CONTENTS OF ETHANOL. TRANSFERENCE NUMBERS FOR NaCl AT 25°C

12040 E. Forecz and T. Török
ON THE STRUCTURE OF AQUEOUS AND HYDROCHLORIC SOLUTIONS OF $MnCl_2$. THE EFFECT OF CHANGES IN THE COMPOSITION ON THE STRUCTURE

12050 M. Pourbaix
ELECTRODE-POTENTIAL/TEMPERATURE EQUILIBRIUM DIAGRAMS AND SOME OF THEIR APPLICATIONS

12060 G. Ruiz Cabrera, C. Quintana Perera, J.C. Rodríguez Placeres, A. Arevalo
POLAROGRAPHIC STUDY OF THE COORDINATED SYSTEM Cd(II)-LEUCINATE

12070 G. Ruiz Cabrera, G. Pastor, J.C. Rodríguez Placeres and A. Arevalo
POLAROGRAPHIC STUDY OF THE COORDINATED SYSTEM Cd(II)-OXALATE-NITRATE

12080 M.J. Isaacson, E.J. Cairns and F.R. McLarnon
ACTIVITY COEFFICENTS IN CONCENTRATED POTASSIUM HYDROXIDE-POTASSIUM ZINCATE ELECTROLYTES

12090 K.K. Choudhary, S.C. Baghel and J.N. Gaur
THERMODYNAMICS OF THE COMPLEXES OF Cd(II) AND Pb(II) WITH GLYOXYLATE IONS

13. Organic Electrochemistry.

13010 L. Oniciu, I.A. Silberg, I. Baldea, D. Cioinos, M. Jitaru, D.A. Lowy, O.H. Oprea and L. Radu
KINETICS OF COMPETING REACTIONS OF ACRYLONITRILE ELECTROREDUCTION TO ADIPONITRILE AND PROPIONITRILE

13020 L. Oniciu, I.A. Silberg, V. Danciu, M. Olea and S. Bran
KINETICS AND MECHANISM OF p,p'-DIAMINODIBENZYL ELECTROSYNTHESIS

13030 H. Wendt, V. Plzak, W. Jenseit
ADSORPTION OF ANODICALLY GENERATED RADICALS AT CARBON AND Pt-ELECTRODES AND ITS ROLE IN ELECTROORGANIC SYNTHESIS

13040 C. Amatore, C. Combellas, M.A. Oturan, J. Pinson, J.M. Saveant and A. Thiebault
CARBON-CARBON BOND FORMATION BY REACTION OF ELECTROCHEMICALLY GENERATED ARYL RADICALS WITH NUCLEOPHILES

13050 I. Carelli, A. Casini and F. Lombardo
ELECTROCHEMICAL BEHAVIOUR OF 1-METHYL-2,4-DICYANOPYRIDINIUM ION IN DIPOLAR APROTIC SOLVENTS

13060 A. Trazza, R. Andruzzi and G. Marrosu
ON THE OXIDATION MECHANISM OF NITROXIDE RADICALS IN APROTIC MEDIA

13070 C3. Visy and M. Novák
ANODIC CHLORINE EVOLUTION AND CHLORINATION OF c-HEXENE IN NITROMETHANE SOLUTION

13080 M. Cvetkovska, T. Grcev, Lj. Arsov
POLYMER FILM FORMATION OF A STEEL CATHODE BY ELECTROCHEMICALLY INITIATED COPOLYMERIZATION OF ACRYLONITRILE AND ACRYLAMIDE IN AQUEOUS SOLUTIONS

13090 Z. Ibrisagić and D. Pletcher
EFFECT OF CONTACTING PATTERNS ON SOME ELECTROLYSES IN TWO PHASE ELECTROLYTES

13100 P. Moran, E. Vianello, G. Cavicchioni and F. D'Angeli
ELECTROCHEMICAL REDUCTION OF 2-BROMO-CARBOXAMIDES. SELF-PROTONATION AND PARTICIPATION OF THE SOLVENT

13110 G. Filardo, S. Gambino, A. Gennaro, G. Silvestri, E.Vianello
ELECTROCHEMICAL CARBOXYLATION OF STYRENE

13120 A. Sánchez, P. Calle and C. Sieiro
ESR STUDY OF SEVERAL METHYLBENZOATES RADICAL ANIONS OBTAINED BY IN SITU ELECTROCHEMICAL METHOD

13130 J.M. Duprilot, F. Bedioui, J. Devynck, J.C. Folest and C. Bied-Charreton
ELECTROCHEMICAL STUDY OF ETHYLENE BIS SALICYLIDENEIMINATO COBALT COMPLEX. APPLICATION TO THE ELECTROCATALYSIS OF ORGANIC HALIDES REDUCTION

13140 M.C. Arevalo, G. Farnia, M.G. Severin, E. Vianello
KINETIC AND THERMODYNAMIC PARAMETERS IN THE REDUCTION OF ALKYLARYLSULPHIDES IN APROTIC MEDIUM

13150 L. Griggio and M.G. Severin
HOMOGENEOUS REDOX CATALYSIS OF ELECTROCHEMICAL REACTIONS. CATALYTIC REDUCTION OF SOME SULFILIMINE

13160 J.E. Cosano, J.L. Avila, L. Camacho, A.M. Heras and F. García-Blanco
ELECTROCHEMICAL REDUCTION OF CEFUROXIME

13170 M.A. Almiron, L. Camacho, A.M. Heras, J.L. Avila and F. García-Blanco
ELECTROCHEMICAL REDUCTION OF 4,4-DIMETHYL-1-PHENYL-1-PENTEN-3-ONE

13180 C.M.A. Brett and A.M.C.F. Oliveira Brett
REDOX PROPERTIES OF MESO-TETRAALKYL PORPHYRINS

13190 A. Inesi and E. Zeuli
HOMOGENEOUS REDOX CATALYSIS. COMPETITION BETWEEN ELECTRON EXCHANGE AND PROTON EXCHANGE

13200 F. Barba, M.D. Velasco, A. Guirado and N. Moreno
CATHODIC REDUCTION OF DIHALOKETONES IN DMF-$LiClO_4$

13210 F. Barba, M.D. Velasco, A. Guirado and N. Moreno
SYNTHESIS OF 3,6-DIARYLPYRIDAZINES FROM PHENACYL BROMIDES

13220 V. Montiel, M. López-Segura , A. Aldaz , F. Barba
ANODIC OXIDATION OF (-)-α-PINENE

13230 M. Blazquez, J.M. Rodríguez-Mellado and J.J. Ruiz
ELECTRODIMERIZATION OF BENZOPHENONE ON MERCURY ELECTRODE

13240 S. Arias, E. Brillas and J.M. Costa
A VOLTAMMETRIC STUDY ON THE OXIDATION OF 2,4-DIBROMO-6-METHYLANILINE IN ACID MEDIA

13250 E. Brillas, J.M. Costa and E. Pastor
ELECTRODE BEHAVIOUR OF 2,6-DIHALO-4-BROMOANILINES IN AQUEOUS SULPHURIC ACID SOLUTIONS

13260 E. Roldan, D. González-Arjona and M. Domínguez
REDUCTION MECHANISM OF PARABANIC ACID ON A DME

13270 T.F. Otero, Mª.A Mugarza and Y. Jimenez
ANODIC ELECTROPOLYMERIZATION OF THE ACRYLAMIDE IN $NaNO_3$ AQUEOUS SOLUTION: CONVERSION AND MOLECULAR WEIGHT MODIFICACATION

13280 T.F. Otero and Mª.A. Mugarza
KINETICS OF THE ACRYLAMIDE ELECTROPOLYMERIZATION IN NO_3^- AQUEOUS SOLUTION

13290 Z. Takehara and Z. Ogumi
PROGRESS OF THE SPE ELECTROLYZER TO ORGANIC ELECTROCHEMISTRY

13300 C.P. Andrieux, J. Badoz-Lambling, C. Combellas, D. Lacombe, J.M. Saveant, A. Thiebault, D. Zann
H ATOM TRANSFER REACTIONS FROM ALCOHOLS IN ORGANIC ELECTROCHEMISTRY

13310 C. Amatore, C. Combellas, M.A. Oturan, J.Pinson, J.M.Saveant, A. Thiebault
ELECTROCHEMICAL DETERMINATION OF ARYL RADICALS REACTIVITY VS NUCLEOPHILES IN AROMATIC NUCLEOPHILIC SUBSTITUTIONS $S_{RN}1$

13320 M. Lapkowski and I. Baranowska
VOLTAMMETRIC AND SPECTROELECTROCHEMICAL BEHAVIOR OF 2,2-DI-QUINOXALYL AND ITS DERIVATIVES

13330 G. Hambitzer and J. Heitbaum
MASS SPECTROMETRIC ANALYSIS OF ELECTROCHEMICAL REACTANTS BY ION FORMATION WITH THERMOSPRAY

13340 G. Farnia, F. Marcuzzi, G. Melloni and G. Sandona
MECHANISM AND STEREOCHEMISTRY OF THE ELECTROCHEMICAL REDUCTION OF PHENYL-SUBSTITUTED INDENES

13350 E. Saint-Aman and D. Serve
ETUDE CINETIQUE DES INTERACTIONS ENTRE UNE CYLCODEXTRINE ET LES ESPECES I^- ET I_2

13360 J. Casado and I. Gallardo
ELECTROLYSIS OF HALOBENZENES IN DIMETHYLFORMAMIDE

13370 J. Casado and I. Gallardo
POLAROGRAPHIC BEHAVIOUR OF o-DIBROMOBENZENE IN PSEUDOAPROTRIC MEDIA

13380 K. Zutshi, R. Rastogi and G. Dixit
SYNTHETIC APPLICATIONS OF INDIRECT ELECTRODE REACTIONS:ROLE OF ELECTROCHEMICAL GENERATED REAGENTS

13390 Miss Rajani, X.P.S. Chandel and C.M. Gupta
STUDIES ON MIXED LIGAND COMPLEXES OF CADMIUM WITH PYRIDOXINE (VITAMIN B_6) AND SOME AMINO ACIDS

13400 M. Opallo and A. Kapturkiewicz
THE SOLVENT EFFECT ON THE KINETICS OF THE ELECTROOXIDATION OF PHENOTHIAZINE

13410 E.M. Genies and J.M. Pernaut
SPECTROELECTROCHEMICAL STUDY OF POLARON AND BIPOLARON IN POLYPYRROLE STRUCTURAL CHANGES UPON CYCLING

13420 V. Surya Narayana Rao and D. Knittel
ELECTROCHEMICAL REDUCTION OF α-AZIDO CHALCONES

13430 D. Knittell
ELECTROREDUCTION OF α-AZIDOCINNAMIC ESTERS AND RELATED COMPOUNDS

AUTHOR INDEX

A

CONTENTS

L

LECTURES

NEW DATA ON THE DYNAMIC BEHAVIOUR OF THE PASSIVE FILM ON IRON

M. KEDDAM* and C. PALLOTTA**

* LP 15 CNRS "Physique des Liquides et Electrochimie", Université Pierre et Marie Curie, 4 place Jussieu, 75230 Paris Cedex 05, France.

** Departamento de Fisoco-Quimica, Facultad de Ciencias Exactas, Ciudad Universitaria, Pabellon II, 1428 Nunez Buenos Aires, Argentina.

Introduction

During the last ten years passivity studies have been performed mainly by means of *in-situ* optical techniques and non *in-situ* surface spectroscopies[1]. Most of these contributions dealt with neutral weakly agressive media (boric-borate buffered solutions). During the same period no serious advantage was taken from the advances in non steady state electrochemical techniques such as complex impedance measurement at very low frequencies by correlation or FFT signal processing. This lecture will report the results recently obtained in our group by applying these techniques to iron passivity in various acidic media. The use of impedance measurements was essentially aimed at separating the transport properties of the passive film, the charge transfer at the film boundaries and the growth kinetics. One of the main point being the identification of the process controlling the electrode polarization in the passive range. In addition to electrochemical impedance, electrohydrodynamical (EHD) impedances [2] were introduced for the first time in passivity studies.

Experimental

A Solartron equipment (TFA 1250 and electrochemical interface 1186) was used. FFT techniques (HP 5451C) was restricted to the very low frequency part of the spectrum ($f < 0.01$ Hz). Modulation of the angular velocity of the disc electrode (EHD) was performed with a fast response mechanical feed-back.

Results

A typical shape of the impedance diagram of passive iron is shown in Fig. 1.

Transport mechanism in the film sustaining the passive current I_p was analysed from the potential dependence of R_{HF}, resistance of the film with no relaxation of the film thickness. Results obtained for the transfer parameter $R_{HF}I_p$ are shown in Fig. 2, establishing a similarity of behaviour among all the electrolytes investigated. All the parallel straight lines would overlap perfectly if their potential scale were recalibrated on the Flade potential relative to each medium. From Fig. 2 it was inferred that R_{HF} consists of an interface component (R_{HF} at the Flade potential) plus a film bulk contribution (high field transport). A 3.5 nm V^{-1} film thickness is deduced in good agreement with literature data.

The occurrence of a pure capacitance Γ in the millihertz range is tightly connected with the infinite polarization resistance (passivity plateau) exhibited by the system. It rules out any diffusion controlled and reflects the relaxation of film thickness with the potential. However the Γ value (order of 30 $mF.cm^{-2}$) is by one order of magnitude greater than the value predicted from the faradaic charge stored in the passive film. This result is consistent with the existence of a notable dissolution component in the transient response of the passive film [3].

Classically, redox reactions provide information on the film ability to support electron transfer. The use of hydrodynamical perturbations gave a new insight into the control of redox kinetics in an outer region of the film, strongly influenced by the electrolyte composition. Fig. 3 shows the reciprocal Levich plot ($I^{-1}/\Omega^{-1/2}$) for the ferro to ferricyanide oxydation on a passive iron surface in the three acidic media investigated. A fast reaction with pure diffusion control is found in $HClO_4$, a mixed kinetics is observed in H_3PO_4, H_2SO_4 lying in the midrange. EHD data (Bode-plane) presented in Fig. 4 allowed to establish that the passive film in $HClO_4$ behaves classically as a platinum disc (diffusion layer in the liquid phase). In contrast, H_2SO_4 and even more clearly H_3PO_4 reveal a more complicated EHD pattern thus indicating the existence of a diffusion control in a surface region of the passive film undergoing a specific alteration by the modulation of the rotation speed [4].

Conclusion

The resulting picture of the passive film on iron in acidic media is that of a two-layer structure [5] : an inner region practically independent of the electrolyte composition in which the electric field is located, an outer part accomodating the composition effects in which most of the film interactions with the surrounding electrolyte take place. A serious similarity with the surface properties of iron oxides colloidal particles is emphasized. This idea is also strongly supported by the behavioural sequence: perchlorate-sulfate-phosphonate, found in the present work and the increasing adsorbability of these anions on iron oxides in their colloidal state.

References

1. "Passivity of Metals", R.P. Frankenthal and J. Kruger Ed., The Electrochemical Society, Corrosion Monograph Series, Princeton N.J. (1978). "Passivity of Metals and Semiconductors", M. Froment Ed., Elsevier (1983).
2. C. Deslouis, C. Gabrielli, P. Sainte-Rose Fanchine and B. Tribollet, J. Electrochem. Soc. 129, 107 (1982).
3. M. Keddam, J.F. Lizee, C. Pallotta and H. Takenouti, Ibid. 131, 2016 (1984).
4. M. Keddam and C. Pallotta, Ibid. 132, 781 (1985).
5. J.L. Ord and D.J. Desmer, Ibid. 113, 1258 (1966).

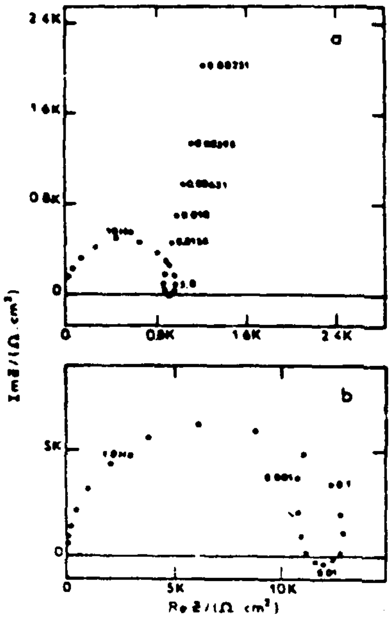

Fig.1 . Complex impedance diagrams: (a) Fe/1M H_3PO_4, 37°C, E = 0.65V; (b) Fe/1M H_2SO_4, 25°C, E = 0.35V.

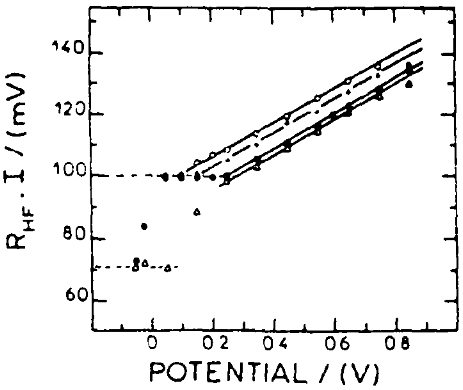

Fig.2 . Potential dependence of $R_{HF} \cdot I$ for iron in different solutions at 25°C. △: 1M H_2SO_4. ●: 1M H_3PO_4. +: 1M (H_3PO_4 + KH_2PO_4), pH = 2.2. ○: 1M (H_3PO_4 + KH_2PO_4), pH = 2.8.

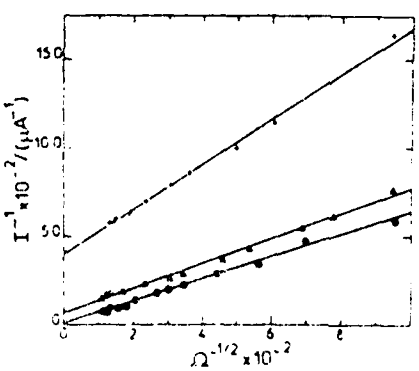

Fig.3. I^{-1} vs. $\Omega^{-1/2}$ plots for the ferrocyanide oxidation on passive iron for different electrolytes: + + + 1M H_3PO_4, E = 0.65V; ▲▲▲ 0.5M H_2SO_4, E = 0.6V; ●●● 1M $HClO_4$, E = 0.35V. 1 mM $Fe(CN)_6K_4$.

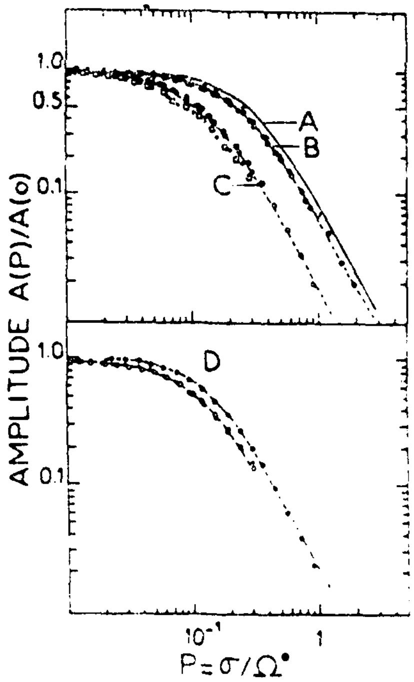

Fig.4. Reduced amplitude of the potentiostatic EHD impedance. Ferrocyanide concentration 1 mM. A: Theoretical curve. B: Fe/1M $HClO_4$, E = 0.65V. C: Fe/0.5M H_2SO_4, E = 0.4V. D: Fe/1M H_3PO_4, E = 0.65V. Ω = 200 (●), 500 (…), 1200 (+), 2000 (○).

1.2

PRACTICAL SIGNIFICANCE OF ELECTROCHEMICAL METHODS FOR THE STUDY OF CORROSION KINETICS

E. Heitz
Dechema-Institut, Frankfurt/M., Fed.-Rep. Germany

The objectives of corrosion testing and corrosion investigations are the production of data on the performance of material/medium systems, the study of corrosion mechanisms and the choice of appropriate corrosion protection methods. Since most corrosion processes are electrochemical in nature an increasing interest to apply such methods in corrosion testing and corrosion control has been experienced in recent times.

It is important for the discussion of the applicability of electrochemical methods to analyse the type and distribution of problems occurring in industrial practice and in everyday life. They are:

1. Corrosion case history evaluation and corrosion control measures
2. Determination of corrosion rates for given corrosion systems
3. Material selection for given corrosive media and corrosion conditions
4. Development of new electrochemical testing and monitoring methods
5. Accompanying research to enhance the application of new technologies and the development of new materials.

With regard to the relative importance of thermodynamic or kinetic methods, only in a few cases purely thermodynamic considerations of the kind: corrosion - yes or now? are relevant. By far the largest amount of problems is concerned with kinetic questions such as corrosion rates as function of aggressive agents concentrations, of critical conditions for the occurrence of certain corrosion mechanisms or the range of safe applicability of a corrosion protection method.

In addition the great variety of practical problems requires a great number of electrochemical methods to be analysed with regard to their use, significance and limitations. Since experimental methods in electrochemistry are becoming more diverse new techniques of electrochemical corrosion testing have to be considered /1/.

It is useful to classify the large field of electrochemical methods as follows:

a) Polarisation measurements - Stationary methods (corrosion rates; active-passive behaviour; critical potentials)
b) Polarisation measurements - Non-stationary methods (impedance spectroscopy, voltammetry a.s.o.)
c) Potential measurements (monitoring in the plant or in the field)
d) Current measurements (bimetallic corrosion; stray current corrosion)
e) Advances in measuring techniques (computer control and evaluation).

Prior to applying electrochemical methods one must realize the scale of the experiments with respect to the size of the specimen and the test apparatus and the choice of an appropriate test duration. It is only recently, that systematic considerations on the principles of scaling corrosion test have been made /2,3/.

For the illustration of the above statements a number of examples are given.

References

1) Electrochemical Corrosion Testing with special consideration of Practical Applications; Proc. of a workshop in Ferrara, Sept. 1985 (in preparation)

2) E. Heitz, Proc. 9th Intern. Congr. Met. Corrosion, Toronto, Vol. 3, p. 9 (1984)

3) L. Clerbois, E. Heitz, F. P. Ijsseling, J. C. Rowlands, J. P. Simpson; Brit. Corr. J. 1985 (in print)

PASSIVITY BREAKDOWN AND REPASSIVATION PROCESSES IN PITTING AND STRESS CORROSION CRACKING OF METALS AND ALLOYS.

José R. Galvele.

Departamento Materiales, Comisión Nacional de Energía Atómica,
Avda. Libertador 8250, Buenos Aires-1429, Argentina.

Passivity of metals and alloys is very important from an applied point of view, and its breakdown is usually a source of serious problems. Two aspects of passivity breakdown will be discussed in the present work. In the first one, as a result of environmental changes, passivity breaks down leading to pitting. In the second, passivity breakdown occurs as a result of the action of environment plus mechanical stresses in the metal, and stress corrosion cracking (SCC) is found. Our degree of understanding in these two areas is very different. While in some cases of pitting we have reached a reasonable degree of understanding, which allows us to predict new cases of pitting, as well as the conditions leading to pitting inhibition, we are still very far from such a degree of understanding in the case of stress corrosion cracking.

Three different types of pitting, presenting similar morphologies, but following different mechanisms, are to be distinguished (1):

1)-Electrochemical depassivation,
2)-Chemical depassivation,
and 3)-Etch pitting (or: Stainless steel-HCl type).

In the present work we are concerned only with the first type: Electrochemical depassivation. Under potentiostatic conditions this type of pitting starts only above a certain potential, called pitting potential (Ep). This potential was found to be function of the aggressive ion concentration, the alloy composition, the pH, the presence of buffers, etc.

Transport process analysis (2,3,4) has shown that electrochemical depassivation appears as a result of localized acidification (or more precisely, depletion of the OH^- ligand) at the metal-solution interface. This analysis shows that there is a critical parameter, $\underline{X}.i$, for passivity breakdown; where $\underline{X}$ is the ion diffusion path in incipient pits, and i, the anodic current density circulating through them. Usually the value of the critical parameter is low, typically $\underline{X}.i \approx 10^{-6}$ A.cm^{-1}, and it increases in the presence of buffers, or with the increase of pH of the environment. The existence of this parameter shows that pitting and crevice corrosion are mechanistically equivalent, the only difference being the size of the diffusion path, $\underline{X}$. The pitting potential is given by (2,3,4):

$$Ep = E_c^* + \eta + \phi \ ;$$

where E_c^* is the corrosion potential of the metal in the pit-like solution, η is the polarization necessary to reach the critical $\underline{X}.i$ value, and ϕ is the potential drop in the pit.

In the case of SCC the three most frequent mechanisms found are:

a)-liquid metal embrittlement,
b)-hydrogen embrittlement,
and c)-brittle film rupture plus anodic dissolution.

The third type of mechanism is frequent with ductile metals and alloys that are protected by a corrosion film and exposed to environments where electrochemical corrosion could take place. The intermediate strain rate technique (ISRT), used in our laboratory, has shown that there are numerous cases where SCC propagates under anodic control (5,6,7), anodic dissolution accounting for all the crack velocities found. The mechanism of this process, at an atomic level, is still unclear. Isotropic slip dissolution and slow repassivation were widely suggested, but have not been confirmed by recent experimental results. Cleavage of the metal, triggered by the cracking of an anodically formed film, has also been suggested, but does not fit with the electrochemical measurements. Alternative mechanisms, discussed in the present paper, are: 1) anisotropic slip step dissolution; and 2) cleavage of an anodically formed film, where the rate of crack propagation is given by the rate of formation of such a film. This type of mechanism could be operative with dealloyed films and with thick, anodically formed films. No cracking should be found in the presence of thin passive films. In this last situation only low aspect ratio cracks could theoretically be formed. In practice, as a result of the metallurgical properties of the metal, ductile failure will take place before any measurable crack is formed.

(1)-J.R.Galvele, Present State of Understanding of the Breakdown of Passivity and Repassivation, in: PASSIVITY OF METALS (R.P.Frankenthal and J. Kruger, ed.) The Electrochemical Society, New Jersey, 1978, p. 285.

(2)-J.R.Galvele, J. electrochem Soc., 123, 464 (1976).

(3)-J.R.Galvele, Corrosion Sci., 21, 551 (1981).

(4)-S.M.Gravano and J.R.Galvele, Corrosion Sci.,24, 517 (1984).

(5)-J.R.Galvele, Stress Corrosion Cracking-Plenary Lecture, Proceedings 7th International Congress on Metallic Corrosion, Rio de Janeiro, 1978, ABRACO, Vol. 1, p. 65.

(6)-M.G.Alvarez, C.Manfredi, M.Giordano and J.R.Galvele, Corrosion Sci., 24, 769 (1984).

(7)-I.A.Maier, C.Manfredi and J.R.Galvele, Corrosion Sci., 25, 15 (1985).

1.4

EFFECT OF ELECTROCHEMICAL PROCESSES ON THE INITIATION AND PROPAGATION OF STRESS CORROSION CRACKS IN METALS

E. WENDLER - KALSCH
Institute of Materials Science
University of Erlangen - Nürnberg (Germany)

The initiation of stress corrosion cracks on a metallic material occurs as the result of a preferred corrosion attack on localized microscopic surface sites. The condition can normally be observed following the formation of a protecting surface layer, which suffers a localized breakdown or rupture during mechanical stressing of the metal in a specific corrosion agent. The localized rupture of the oxide film can have various causes and is largely determined by the particular metal/agent corrosion system as shown below in using some typical examples.

In the System Cu70Zn30/ammoniacal solution, crack initiation is determined by the morphology, structure and thickness of the particular oxide surface layer (Cu_2O or CuO) and its possible effects on the dislocation motion in the surface areas of the oxide-coated material.

Based on these experimental findings, a mechanism of the stress corrosion cracking of brass in ammoniacal solutions is proposed, which assumes an accelerated electrochemical dissolution of the metal at those sites where high dislocation densities or dislocation pile-ups result in local rupture of the oxide film.

Unalloyed and low-alloy steels show active/passive response in alkaline solutions and also, for example, in carbonate solutions. At low anodic potentials, Fe_3O_4 is formed along with $FeCO_3$ which is subsequently oxidized to Fe_2O_3 at higher anodic potentials.

In the initial stages of film formation, individual Fe_3O_4 microcrystals form at several centers of nucleation along with $FeCO_3$ precipitates on the steel surface. The Fe_3O_4 crystal agglomerates then combine to procude continuous magnetite layers with increasing duration and degree of anodic polarization. A non-continous magnetite surface layer with $FeCO_3$ precipitates promotes a pitting-like corrosion and on simultaneous tensile loading of the steel specimens notch-like transgranular surface fissures appear.

In the potential range where a thick magnetite layer forms, Fe_3C precipitates in the steel retard the formation of oxide resulting in grooving at the grain boundaries and at carbide/ferrite interfaces within the pearlite constituent. A marked susceptibility to intergranular stress corrosion cracking is observed under simultaneous tensile loading of the steels, leading to a considerable reduction of ductility of the material (Fig. 1).

By further increasing the anodic polarization, however, a highly continuous, even and very thin passive film with good protective characteristics is formed. Analogous to investigations using the rotating ring-disc electrode, the oxide is converted in this case to γ-Fe_2O_3. This passive oxide not only protects the steels against uniform overall corrosion, but also against pitting, intergranular corrosion and even stress corrosion cracking.

According to our findings, the corrosion protection qualities are not only caused by the type of oxide film in question but also by the repassivation rate at which the surface film forms or at which any ruptures of the protective layer can repair again. Analyses of the current-time transients after mechanical activation of the steel surface have shown that the charge density Q_p, i.e. the area under the repassivation transient, can be used as a qualitative criterion for the metal dissolution between film fracture and its complete repair:

$$Q_p = \int_0^{t_p} i_s \, t^{-\alpha} \, dt$$

where i_s is the current density of the active steel electrode, α is the repassivation constant and t_p is the repassivation time. This charge density is dependent on the potential attaining maximum values in the potential range of stress corrosion cracking where magnetite surface layers form.

The ratio of the charge density Q_p and the repassivation time t_p can be used as a qualitative criterion for the SCC-susceptibility. A simple relationship between the crack velocity v and the ratio Q_p/t_p can be derived from Faraday's law:

$$v = \frac{M}{z \, F \, \rho} \, Q_p/t_p$$

where M is the equivalent weight of the metal with the density ρ, F is the Faraday constant and z is the number of electrons involved in the reaction.

As Figure 2 shows, the consistency of the measured critical potential range for SCC and the range predicted on the basis of such passivation data enables a correlation to be formed between the crack propagation rate and the modified faradaic equivalence. At the potential threshold between the formation of Fe_3O_4 and γ-FeOOH surface layers, the SCC susceptibility sharply decreases, eventually disappearing. This behaviour is caused by the high repassivation rate of the γ-FeOOH passive films. In comparison to magnetite surface layers, the γ-FeOOH passive films repassivate at

a high rate reaching passive current densities after several milliseconds. In this passive range, the charge density Q_p and the associated amount of iron dissolution between the fracture of the protective passive film and its complete repair attain very small values and this can prevent localized corrosion.

References:
E. Wendler-Kalsch, Z. Werkstofftech. 13 (1982) 129-137
E. Wendler-Kalsch, Proceedings of the 164th Meeting of the Electrochemical Society, Washington 1983, Vol. 83-2, p. 268

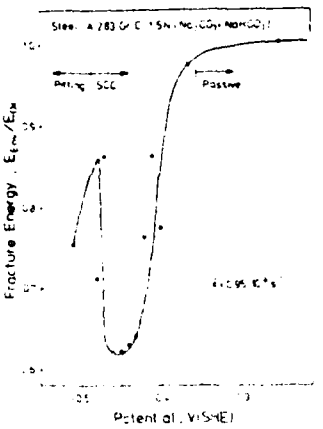

Fig. 1
Effect of electrode potential on corrosion behaviour and relative fracture energy of unalloyed steel in carbonate solution

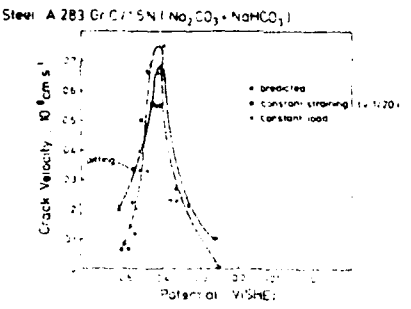

Fig.2
Correlation between experimental crack propagation rates and velocities predicted from passivation data for unalloyed steel in carbonate/bicarbonate solution
o predicted values
x velocities at 0.7 UTS
o velocities (factor 1/20 at an extension rate of 2.4 10^{-6}s

I.5

INTERGRANULAR CORROSION : CHEMICAL AND STRUCTURAL ASPECTS

M. FROMENT
Physique des Liquides et Electrochimie, LP 15 du CNRS,
associé à l'Université Pierre et Marie Curie,
4 place Jussieu, 75230 PARIS Cedex 05, FRANCE.

Intergranular attack of metals and alloys is a localized corrosion phenomenon induced by chemical or structural heterogeneities at the emergence of grain boundaries on the surface of materials. The high reactivity of these areas, compared with these of the bulk, gives rise to a preferential anodic dissolution.

In fact three types of heterogeneities can be identified. The first one concerns the intergranular precipitations which have been specially studied in the case of light and chromium, iron, nickel alloys[1]. Precipitation of chromium carbides at the grain boundaries of certain alloys (stainless steels, nickel base alloys...) is produced during welding operations and other thermal treatments between 450 and 870°C. Precipitations of these chromium carbides at the grain boundaries remove chromium from the matrix adjacent to the precipitations. Then the passivation of the chromium depleted area is no longer possible.

The investigation of sensitivity of steels to intergranular corrosion is based on the use of classical tests. Sensitized steels are immersed in standard solutions (Huey , Strauss...) and the intergranular corrosion is evaluated from weight losses[1]. Potentiodynamic reactivation of passivated steels was proposed some years ago as a test of detecting susceptibility to intergranular corrosion. One method[2] was based on the selection of experimental conditions in which differences in electrochemical behaviour of the chromium depleted grain boundaries, the precipitates of carbides and the grain themselves plays a role. The measurement of the number of coulombs passed through the cell in the active range of potentials is a quantitative evaluation of the sensibilization of the alloy to the intergranular corrosion. In an another test, called the double loop test[3], the surface is first polarized anodically through the active region before the reactivation scan in the opposite direction is conducted. In this test the degree of sensibilization is measured by determining the ratio of the maximum current generated by the reactivation scan to that of the anodic one. Some tests allowing a rapid identification of the potential range where the influence of intergranular corrosion or intergranular stress corrosion cracking can be avoided have been also proposed[4].

In spite of the development of alloys with low carbon or nitrogen contents the problem of intergranular corrosion induced by precipitations remains at importance specially in nuclear energy and some examples will be given. The disposal of nuclear wastes for long periods implies the suppression of localized corrosion phenomena. Intergranular attack requires little or no induction period and its importance can be tested. However during long times at relatively high temperatures and under intense irradiation the possibility of forming a new phase that could lead to intergranular attack cannot be overlooked.

Homogeneous water-quenched materials free from intergranular precipitations are also susceptible to a preferential attack of grain boundaries. Firstly because of the misorientation between to adjacent grains, atomic positions in the plane of the grain boundary are relaxed in new positions where energy is different of that in the perfect crystal. These new positions are the active sites of corrosion at the emergences of the grain boundary on the surface. Secondly the existence of relaxed atomic positions generally favour segregation of impurities in the grain boundaries which modifies the forces of the atomic bounds[5]. On the other hand solute segregation causes a major charge in the dislocation structure of the grain boundary[6]. These modifications of the grain boundary structure can increase the susceptibility to intergranular corrosion.

A dissolution model has been developped to interpret intergranular corrosion in ideal conditions of high dissolution rate and in absence of anisotropic phenomena[7]. This model allows to correlate the level of a intergranular corrosion evaluated thanks to the measurement of the geometrical characersitics of the grooves formed at the emergence of the grain boundaries. For a quantitative interpretation potentiostatic attacks and a control of the quantity of electricity passed threw the cell are necessary.

Unfortunately the relations between structure, segregation and intergranular corrosion phenomena are very complex. The use of bicrystals where level of impurities has been carefully controlled is very interesting to separate the effects of structure and segregation in intergranular corrosion. The study of stainless steel bicrystals with a < 100 > tilt axis shows a correlation between the importance of the intergranular attack and the atomic arrangement in the grain boundary[8].

Until now segregation phenomena have been studied with polycrystalline materials. It is well known that segregation of sulfur, silicon, phosphorus influences the intergranular corrosion and the intergranular hydrogen embrittlement of iron, nickel, chromium alloys. The dissolution model we have developped is able to follow the level of segregation and its effect on the preferential attack of the grain boundaries. Examples will be discussed in the case of sulfur and silicon segregation in nickel and phosphorus segregation in iron base alloys.

The effect of the grain boundary structure on segregation has been discussed in the litterature[9]. It seems that segregation occurs preferentially in high energy grain boundaries which energy can be more reduced than low ones. Nevertheless the determination of precise relations between segregation, structure an corrosion needs a direct determination, boundary by boundary of their structure, level of segregation and corrosion behaviour. Some results have been recently obtained in ultra pure nickel doped with 8 and 10 ppm of sulfur. The structure is determined by TEM observations and segregation is evaluated on the same thin foils by analytical STEM[10]. From these observations it can be concluded that general boundaries present a continuous segregation and are evenly microetched. The special grain boundaries which present a coïncidence site lattice (specially $\Sigma = 3$) dont present segregation nor preferential attack. This approach seems very promising for a systematical study of the relations between structure, segregation and intergranular corrosion.

1 V. CIHAL
Intergranular corrosion of steels and alloys, Elsevier 1984.

2 V. CIHAL, A. DESESTRET, M. FROMENT, P. GUIRALDENQ
5th European Congress of Corrosion 1973, Vol. of the Symposium, p 249.

3 A.P. MAJIDI, M.A. STREICHER
Corrosion NACE, 1984, 40, p 584.

4 J. WOODWARD
Corrosion NACE, 1984, 40, p 640.

5 P.P. MESSMER, C.L. BRIANT
Acta Metallurgica, 1982, 30, 457.

6 P. LAMARRE, F. SCHMÜCKLE, K. SICKAFUS, S.I. SASS
Ultramicroscopy, 1984, 14, p 11.

7 L. BEAUNIER, M. FROMENT, C. VIGNAUD
Electrochimica Acta, 1980, 25, p 1239.

8 L. BEAUNIER, M. FROMENT, C. VIGNAUD
J. Electroanal. Chem., 1981, 119, p 125.

9 H. HASHIMOTO, Y. ISHIDA, R. YAMAMOTO, M. DOYAMA
Acta Met. 1984, 32, p 1, 13, 21.

10 L. BEAUNIER, C. VIGNAUD, D. BOUCHET, C. COLLIEX, P. TREBBIA
J. Physique, in press.

1.6

CHARACTERIZATION OF ANODIC OXIDES BY MODULATED SPECULAR REFLECTANCE SPECTROSCOPY

C. Gutiérrez
Instituto de Química Física "Rocasolano", Madrid (Spain)

The technique of Pulse Modulated Specular Reflectance Spectroscopy (PMSRS) (1) measures the (mostly minute) changes, ΔR, in the reflectance, R, of a specular electrode produced by a (square-wave or sinusoidal) modulation of the potential of the electrode. As values of $\Delta R/R$ lie in the range 10^{-3}-10^{-6}, lock-in amplification and/or signal averaging are necessary. Many effects, both physical and chemical, can contribute to the observed $\Delta R/R$ signal. Our goal is to identify the valence state of anodic oxide films on metals, and especially noble metals. For that purpose, we measure the PMSR spectra of the said anodic oxides, and compare the structures that appear in them with known optical spectra of the metal, in order to try and assign a PMSR spectrum to a given oxide.

In the case of iron in 0.1M NaOH, the results have been rather good. At an electrode potential of +1.508 mV vs RME, we have been able to resolve a broad peak between 2.3 and 3.0 eV reported by Hara and Sugimoto (2) as two peaks at 2.2 and 2.95 eV. Peaks at these two energies had been observed in both acid and neutral media and at about the some potential vs RHE by Froelicher et al (3). The two transitions have been identified as spin-flip crystal field transitions, ($6A_1 \rightarrow 4E$) and ($3e_{g\uparrow} \rightarrow 3e_{g\downarrow}$), respectively, and have been observed in the absorption spectra of single crystals and thin crystalline films of α-Fe_2O_3 (4), and also in reflectance spectra of α-Fe_2O_3 single crystals (5). Therefore, it can be concluded that at +1.500 mV vs RHE an iron electrode is covered by hematite, probably in a hydrated form.

The PMSR spectrum at +8 mV vs RHE is more interesting. It only shows a maximum at 3.65 eV, which nearly coincides with the absorption edge of wüstite, FeO (6). It is interesting that it also coincides with the peak in PMSR spectra of passivated iron at pH 8.4 and +1050 mV vs NHE, calculated by extrapolation of data at lower energies by Wheeler et al. (7), assuming a Lorentzian oscillator. According to initial state molecular orbital cluster calculations (8), it is a charge transfer peak corresponding to ferrous ions. This is in agreement with the fact that we have found it at about the H^+/H_2 potential.

The result obtained with an iridium electrode, although encouraging, have not enabled us to identify the oxidation state of the different peaks found in cyclic voltammetry. Thick anodic iridium oxide films can be easily grown on iridium electrodes by potential cycling, as first reported by Buckley and Burke (9). The electrochromic effect concomitant with the oxidation and reduction of these films makes this system attractive as a possible display device. Modulation of the electrode potential changes the oxidation state of the anodic oxide; these changes involve movement of

protons and/or water molecules, and therefore the effect disappears at higher frequencies, at which the ionic and/or molecular entities can not follow the potential modulation.

We have found that there is a linear relationship between the wavelength of the main absorption maximum in the PMSR spectrum of a voltammetric peak and the corresponding peak potential. This is valid for the last three voltammetric peaks, in acid, neutral, and alkaline media. We have not been able to find an explanation for this behaviour. It is definitely not due to an interference effect, as the position of the absorption maxima was independent of the thickness of the anodic oxide film.

REFERENCES

1. A. Bewick and M. Tuxford, Symp. Faraday Soc. Nº 4, 114 (1970)
2. N. Hara and K. Sugimoto, J. Electrochem. Soc. 126, 1328 (1979)
3. M. Froelicher, A. Hugot-Le Goff and V. Jovancicevic, in "Passivity of Metals and Semiconductors", ed. M. Froment, Elsevier, 1983, p. 85
4. L.A. Marusak, R. Messier and J.B. White, J. Phys. Chem. Solids 41, 981 (1980)
5. P.C. Bailey, J. Appl. Phys. 31, 395 (1960)
6. M. Froelicher, A. Hugot-Le Goff and V. Jovancicevic, "Passivity of Metals and Semiconductors", ed. M. Froment, Elsevier, 1983, p. 491
7. D.J. Wheeler, B.D. Cahan, C.T. Chen and E. Yeager, "Passivity of Metals", eds. R.P. Frankenthal and J. Kruger, The Electrochemical Society, 1978, p. 546
8. N.C. Debnath and A.B. Anderson, J. Electrochem. Soc., 129, 2169(1982).
9. D.N. Buckley and L.D. Burke, J. Chem. Soc., Faraday Trans. I, 71, 1447 (1975)

2.1

THE CHLORINATION OF NAPHTHALENES BY TWO PHASE ELECTROLYSIS

S.R. FORSYTH and D. PLETCHER
Department of Chemistry, The University,
Southampton SO9 5NH, England

Since Eberson and Helgee[1] first demonstrated the anodic nucleophilic substitution of aromatic molecules by two phase electrolysis, these reactions have been somewhat of an enigma. In many cases, the yield of substituted product from an electrolysis in an CH_2Cl_2/H_2O emulsion (using phase transfer catalyst to supply nucleophile to the organic phase) far exceeds that from the corresponding reaction using a single phase, aprotic medium. Other reactions, in contrast, do not lead to the expected products in significant yields. Moreover, some aspects of the mechanism of these reactions remains unclear. Hence we believe that very detailed studies of two phase electrolyses are essential and in this paper we shall discuss an investigation of the chlorination of substituted naphthalenes.

It is certain that such two phase electrolyses can be used for cyanation[1,2], acetoxylation[3], acyloxylation in general[3], and chlorination[4] and when successful have many attractive features. Namely, (i) good selectivity (ii) simple product isolation (iii) clean counter electrode chemistry, H_2 evolution (iv) use of undivided cell (v) reasonable current densities, 50 —100 mA cm^{-2} (vi) buffering of organic phase by the aqueous solution (vii) use of nucleophile in cheap and readily available form (viii) relatively low cell voltage. The chemistry involved in these electrolyses may be understood from the sketch in figure 1. In practice, however, the electrolysis medium is an emulsion

Figure 1

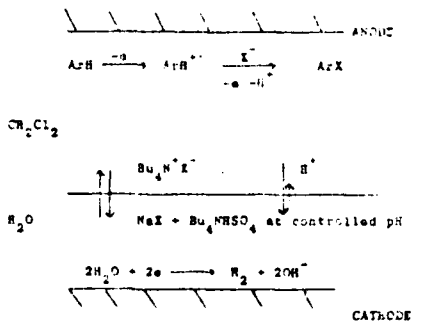

of CH_2Cl_2 in H_2O and it is likely that the oxidation occurs within a continuous film of CH_2Cl_2 on the anode surface. The rôle of the emulsion is to exchange material rapidly with the film; the CH_2Cl_2 supplies the reactant and extracts product and the H_2O replenishes the nucleophile and removes proton as well as acting as a low resistance pathway for current. Certainly in some re- cor

Table 1

Naphthalene	Preparative Electrolysis[a]			Cyclic Voltammetry[a]		
	Naphthalene consumed/%	Yield monochloro/%	Selectivity/%	E_p^{ox}/V vs $\frac{1}{2}H_2$	n_{app}	$\left(\frac{g^{ox}}{p}\right)_{product}$
unsubstituted	70	39	56	1.82	4	2.32
unsubstituted[d]	55	38	83			
1-F	44	36	81	2.00	2	2.27
1-CN	25	15	61	2.42	3	2.54
1-CH_3CO	39	19	50	-	-	-
1-CH_3O	70	12	15	1.52	2	1.96
1-C_2H_5O	68	21	30	1.54	2	1.95
1-CH_3	57	5	10	1.83	3	1.98
2-CH_3O	64	49	76	1.71	3	1.92
2-CH_3	62	28	45	1.85	3	2.10

a. electrolysis conditions: 10 mmol naphthalene in 100 cm^3 CH_2Cl_2 + 100 mmol NaCl, 10 mmol Bu_4NHSO_4 and 10g Na_2SO_4 in 100 cm^3 H_2O. I = 50 mA cm^{-2}. Charge passed 2F mol^{-1} naphthalene.

b. C.V. run on 5 mM naphthalene in CH_3CN/Bu_4NBF_4 (0.1M) at 0.1V s^{-1}.

c. n_{app} in the absence of Cl^- estimated by comparison of peak for Cp_2Fe oxidation (0.66V)

d. + 50 mmol $ZnCl_2$.

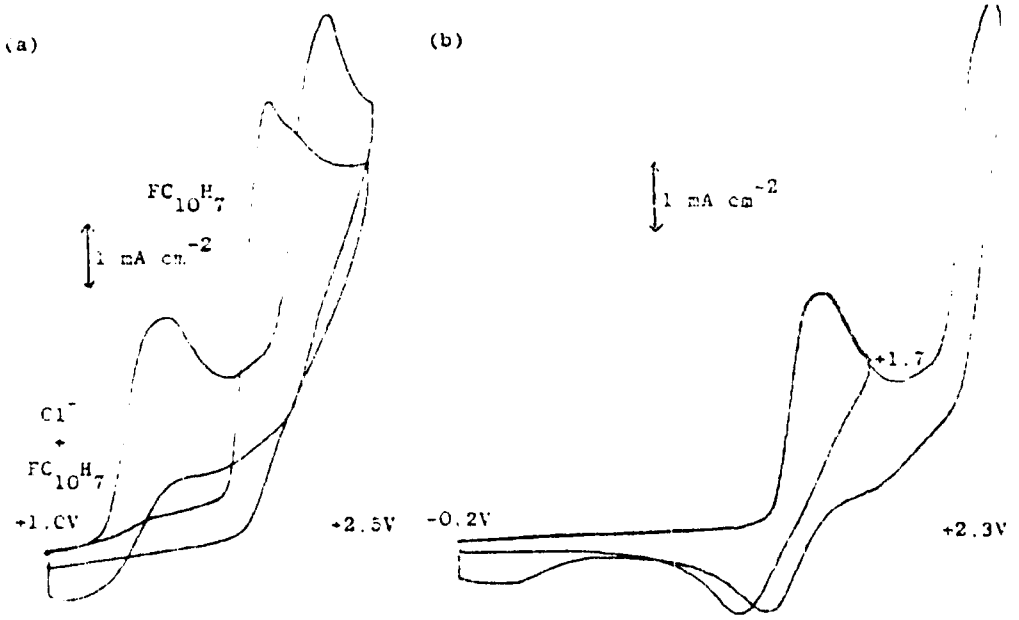

Figure 2 Cyclic voltammograms run at 0.1V s^{-1} for

(a) 5 mM 1-fluoronaphthalene in the presence and absence of 20 mM Cl^-

(b) 5 mM 1-fluoronaphthalene + 20 mM Cl^-

CH_3CN/Bu_4NBF_4. Pt electrode.

configurations such a pattern is enforced[5].

In chlorination reactions it should be noted that the nucleophile is more readily oxidised than the organic substrates. Hence the success of the reaction is dependent on the principle of flux balancing[6] to prevent Cl^- reaching the anode surface.

In this paper we shall discuss both preparative experiments and investigations of the mechanisms using cyclic voltammetry in CH_3CN. We feel that such experiments are relevant because of the anode film mechanism discussed above. The key data is reported in table 1.

The data from the preparative experiments, carried out at constant current density, show that reasonable selectivities to monochlorinated products can generally be achieved; the exceptions are the 1-methyl and 1-alkoxy derivatives. In these cases we believe that the chemistry of the cation radicals are different. It can also be seen that there is a correlation between the consumption of substrate after 2F mol^{-1} and its oxidation potential although more complete conversion can be achieved by continuing the electrolysis, see figure 1. Of course, at very high F mol^{-1}, the monochlorinated product undergoes further chlorination.

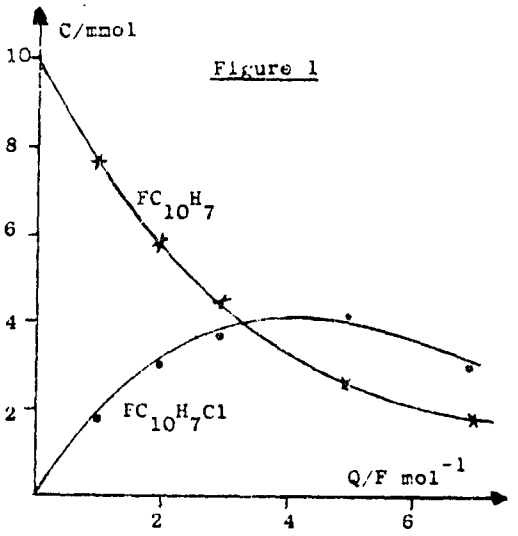

Figure 1

The peak potentials for the naphthalenes studied vary over a broad range and comparison of peak currents with that for ferrocene shows that multi-electron oxidation occurs in the absence of Cl^-. Figure 2 shows cyclic voltammograms for 1-fluoronaphthalene (5 mM) in the presence and absence of Cl^- (20 mM). Curve (a) shows the effect of Cl^- on the oxidation of the naphthalene. It can be seen that with a large excess of Cl^- the peak for 1-fluoronaphthalene is not observed but a product is oxidised at more positive potentials (the peak potentials for the oxidation are also reported in table 1). Curve (b) shows the influence of the positive potential limit on the Cl_2 reduction peak. Clearly Cl_2 does not react with the naphthalene but this peak is diminished by sweeping into the naphthalene oxidation process. This also produces a new peak at +0.1V presumably for the oxidation of a reaction intermediate.

References

1. L. Eberson and B. Helgee, Chem. Scripta, 5, (1974), 47.
2. D. Pletcher et al, J. Applied Electrochem., 12, (1982), 687.
3. D. Pletcher et al, J. Applied Electrochem., 12, (1982), 693.
4. M. Fleischmann et al, J. Applied Electrochem., 13, (1983), 593 and 603.
5. D. Pletcher et al, J. Applied Electrochem., 13, (1983), 799 and 15, (1985).
6. M. Fleischmann et al, J. Electroanal. Chem., 85, (1978), 455 and Electrochim. Acta, 18, (1974), 511.

2.2

ELECTROORGANIC SYNTHESIS USING MEDIATORS

TATSUYA SHONO
Kyoto University, Kyoto (Japan)

In the electroorganic reactions, the generation of active species by the direct electron transfer between electrode and substrates is highly controlled by the oxidation and reduction potentials of the substrates. When the oxidation and reduction potentials of a substrate are beyond the range accessible by the usual technique of electrochemical reaction, the direct electron transfer between the substrate and electrode is not expectable and hence it is necessary to devise some other method to oxidize or reduce the substrate. Also, even if the oxidation and reduction potentials of substrates are in the accessible range of the electrochemical method, it is more desirable to oxidize or reduce the substrates with using some indirect method at much lower potential than that applied in the direct method. The electroorganic synthesis using mediators has been devised to actualize these ideas. The oxidative reaction system using a mediator is schematically represented in Figure 1.

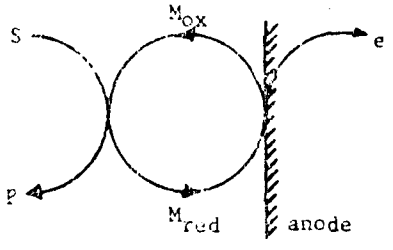

Fig. 1. Anodic Oxidation Using Mediators

S; Substrate, P; Product, M_{red} and M_{ox} ; Mediators

When the oxidation potential of a substrate S is beyond the range accessible by the electrochemical method, the direct electron transfer from S to anode hardly takes place. On the other hand, when M_{red} oxidizable at lower potential than S is added to the reaction system, the oxidation of M_{red} to M_{ox} takes place prior to the oxidation of S. Provided that M_{ox} is able to oxidize S to the product P and M_{ox} itself is reduced to M_{red} by the reaction with S, the oxidation of S will be achieved with a catalytic amount of M_{red} at lower potential than that necessary in the direct oxidation of S (Figure 1). M_{red} (or M_{ox}) is named a mediator. Our subject is to exploit new mediatory systems applicable to organic synthesis. This paper describes the following results.

Transformation of Hydroxy Group

1. The oxidation of secondary alcohols to ketones was effectively achieved by using KI as a mediator.[1]

$$R^1R^2CHOH \xrightarrow{\text{"}I^+\text{"}} R^1R^2C{=}O$$

2. Primary alcohols gave the corresponding esters.[1]

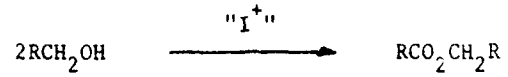

3. The mixture of aldehydes and primary alcohols yielded mixed esters.[2]

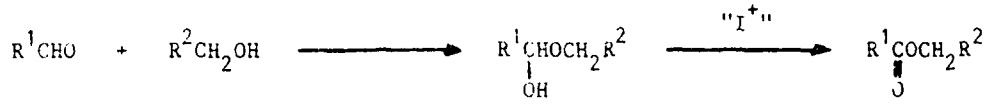

4. N-Hydroxyamines were transformed to nitrones through oxidation with iodonium cation electrogenerated from iodide ion.[3]

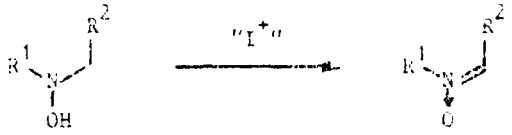

5. With using NaCl as a mediator, aldoximes were converted to the corresponding nitriles.[4]

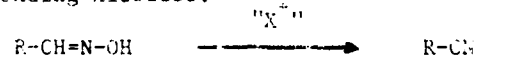

Transformation of Amines and Amides

1. Primary amines were converted to nitriles by using bromonium cation as the oxidizing agent.[5]

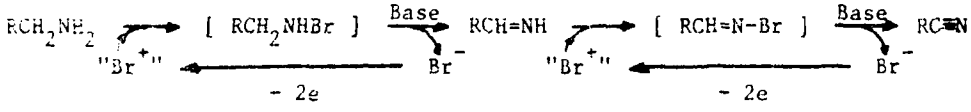

2. Nitriles were obtained from amino acids or amino esters by using bromine as a mediator.[5]

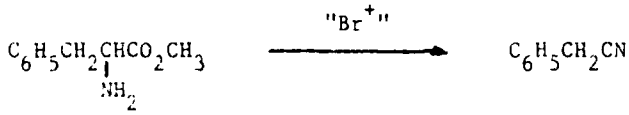

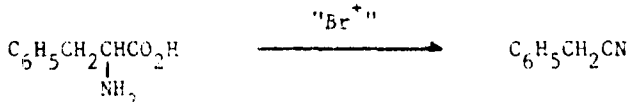

3. The methoxylation of carbamates at the position α to nitrogen could be achieved through the reaction with "Cl^+" in methanol.[6]

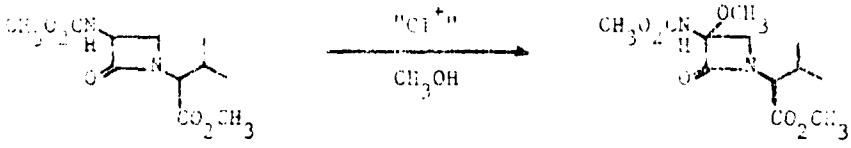

Transformation of Enolic Compounds

1. Enamines were converted to amino ketones through a reaction pathway involving rearrangement.[7]

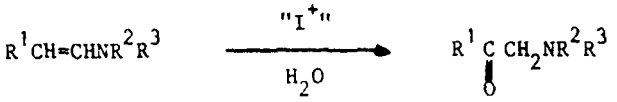

2. The hydroxylation of carbonyl compounds at the α-position could be carried out through oxidation with iodonium cation in methanol.[8]

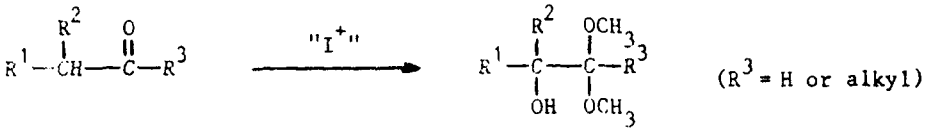

3. α-Amino aldehydes were obtained from enecarbamates by using iodonium cation as the oxidizing agent.[9]

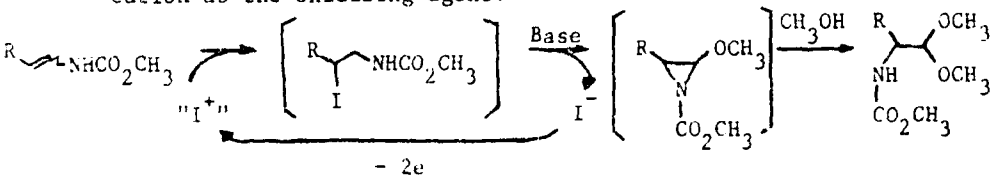

Anodic Oxidation Using Pb Salts as Mediators[10]

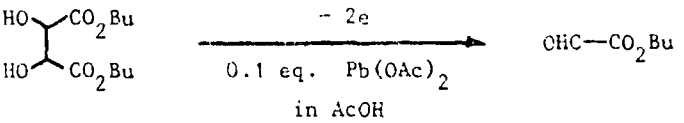

References

1. T. Shono, Y. Matsumura, J. Hayashi, and M. Mizoguchi, Tetrahedron Lett., **1979**, 165.

2. T. Shono, Y. Matsumura, K. Inoue, and F. Iwasaki, the Autumn Meeting of the Electrochemical Society of Japan, Abstr., C217, p. 140 (1983).

3. T. Shono, Y. Matsumura, K. Inoue, and A. Sakai, the 49th Annual Meeting of the Chemical Society of Japan, Abstr., 4F38, p. 848, Vol. II (1984).

4. T. Shono, K. Tsubata, Y. Nakamura, K. Rindo, the 49th Annual Meeting of the Chemical Society of Japan, Abstr., 4F37, p. 847, Vol. II (1984).

5. T. Shono, Y. Matsumura, and K. Inoue, J. Am. Chem. Soc., **106**, 6075 (1984).

6. T. Shono, Y. Matsumura, and K. Inoue, J. Org. Chem., **48**, 1388 (1983).

7. T. Shono, Y. Matsumura, J. Hayashi, M. Usui, S. Yamane, and K. Inoue, Acta Chem. Scand., **B37**, 491 (1983).

8. T. Shono, Y. Matsumura, K. Inoue, F. Iwasaki, and A. Sakai, the 1984 International Chemical Congress of Pacific Basin Societies, Abstr., 10I14 (1984).

9. T. Shono, Y. Matsumura, K. Inoue, and A. Sakai, the 49th Annual Meeting of the Chemical Society of Japan, Abstr., 4F39, p. 848, Vol. II (1984).

10. T. Shono, Y. Matsumura, S. Katoh, and S. Kashimura, the 49th Annual Meeting of the Chemical Society of Japan, Abstr., 4F36, p. 847, Vol. II (1984).

2.3

RECENT ASPECTS OF INDIRECT REDUCTIONS AND MIXED ELECTROLYSES.

Jacques SIMONET

Laboratoire d'Electrochimie, **U.A. CNRS n° 439,**
Université de Rennes I - Campus de Beaulieu
35042 - RENNES Cédex (France)

A general survey on the formation at the cathode of reducing reagents (anions radical, dianions) and/or nucleophiles of which the reactivity is discussed in terms of either electron transfers or nucleophilic displacements.

It is proposed to focus especially the attention on the following reactions :

- mixed electrolyses in the presence of O_2 and CO_2 (expected reactions and unusual results)
- reactivity of tosylates (indirect cleavage in specific deprotection reactions or use as electrophiles)
- redox catalysis of dienes and trienes (why a catalysis?)
- use of conductive sulphur solid electrodes for the introduction of a S element in organic molecules
- cathodic reactivity of tertiobutylhalides towards activated olefins and the selectivity of those new reactions
- spin trapping associated to redox catalysis.

The matter of the lecture corresponds essentially to the following references :

- J. SIMONET et G. LE GUILLANTON, Bull. Soc. Chim. Fr., 1985, 180.
- P. MARTIGNY and J. SIMONET, J. Electroanal. Chem., 1983, 148, 51.
- P. MARTIGNY, J. SIMONET, G. MOUSSET et J. SIMONET, Nouv. J. Chim., 1984, (8), 217.
- G. LE GUILLANTON, Q.T. DO and J. SIMONET, Chem. Comm., to be published
- K. BOUJLEL and J. SIMONET, Tetrahedron Lett., in press.

AD-A162 434 EXTENDED ABSTRACTS INTERNATIONAL SOCIETY OF ELECTROCHEMISTRY (36TH) HELD AT SALAMANCA SPAIN ON 23-28 SEPTEMBER 1985(U) INTERNATIONAL SOCIETY OF ELECTROCHEMISTRY 28 SEP 85 2/12

UNCLASSIFIED F/G 7/4 NL

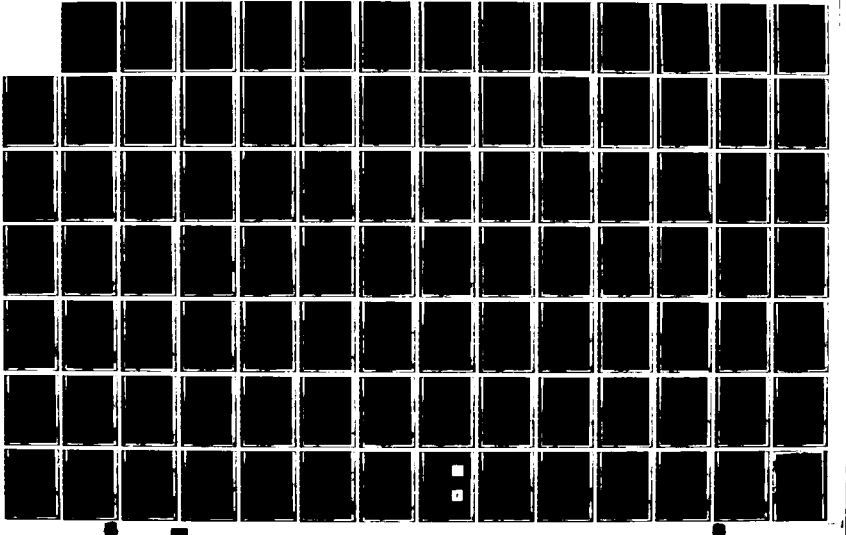

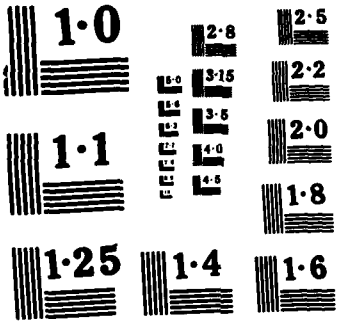

NATIONAL BUREAU OF STANDARDS
MICROCOPY RESOLUTION TEST CHART

2.4

STRUCTURAL CHANGES ASSOCIATED WITH THE ELECTRODE REACTIONS OF HIGHLY HINDERED ORGANIC COMPOUNDS

D. H. EVANS
Department of Chemistry, University of Wisconsin-Madison
Madison, Wisconsin 53706 (U.S.A.)

Different conformations of a molecule should possess different electrochemical properties. However, it is not immediately evident that the differences will be large enough to allow resolution of distinctly different electrode reactions for two or more different conformations. Thus, it is of considerable interest that a number of examples have been discovered in which separate electrode reactions of different conformations can be detected.

An early example was found during studies of the oxidation of cyclic tetraalkylhydrazines. These hydrazines can be electrochemically oxidized in a one electron process to the rather stable radical cation. When the oxidation was studied at low temperatures, two separate oxidation peaks were observed by cyclic voltammetry. These turned out to be the voltammetric peaks for the two dominant conformations of the six-membered ring tetraalkylhydrazines, one conformation with two equatorial alkyl groups and one with one axial and one equatorial alkyl group. Low temperatures were required to resolve the two reactions because the conformational interconversion was very rapid at room temperature so the process would proceed entirely by way of the more easily oxidizable conformation under such conditions.

For the tetraalkylhydrazines the factor which caused a measurable difference in oxidation potential to exist for the two different conformations was the large difference in their standard heterogeneous electron transfer rate constants. Thus the overpotential for oxidation of one conformation was significantly different than that of the other.

Kinetic factors of this type are at work in several other cases of conformational effects on electrode reactions. Frequently, however, the basis for the observed differences is of a thermodynamic origin, i.e., the standard potential for an electrode reaction of one conformation differs from that of the other. Thermodynamic factors are prevalent in the numerous organometallic systems which have been investigated. In these cases, one is dealing with isomers rather than conformations. Both conformational change and isomerization are examples of structural changes associated with electrode reactions.

Structural effects may be manifested prior to electron transfer, following electron transfer, concurrently with electron transfer or some combination of all three. In the case where structural change follows electron transfer, the process can be an electron-transfer-induced isomerization where the product is an isomerized reduced (or oxidized) form of the reactant. Electron-transfer-catalyzed isomerization can also occur. Here an unusual ordering of standard

potentials permits isomerization of the reactant with little net consumption of charge.

Some of the most interesting examples of the structural consequences of electron transfer reactions have been observed for a series of molecules which may be regarded as highly hindered ethylenes. The bianthrones and related compounds exist in two distinct structures whose free energies are similar enough to allow conversion from one form to the other by thermal means. Similar structural changes can be induced by reduction or oxidation of the compounds. The inherent simplicity of the structural changes and the felicitous reversibility of the electrode reactions have allowed a surprisingly complete thermodynamic and kinetic description of the processes to be developed.

Structural changes of various types are being discovered frequently in the investigation of electrode reactions and their full characterization is being increasingly recognized as an important element in detailed electrochemical kinetics.

SELF PROTONATION REACTIONS IN ORGANIC ELECTROCHEMICAL PROCESSES

E. Vianello

Dipartimento di Chimica Fisica, 35131 Padova (Italy)

In the course of the electrochemical reduction of organic molecules, charge transfer reactions are quite generally associated with proton transfer steps. Although in dipolar aprotic solvent the basic reaction intermediates (anion radicals, carbanions, dianions etc) are often relatively stable, residual water, acidic impurities, tetraalkylammonium cations and the solvent itself may act as proton donors towards them. An interesting situation arises when the starting (parent) molecule is the strongest acid present in the medium. In such a case an intermolecular proton transfer from the latter to the basic intermediates may occur, giving rise to a self-protonation mechanism. Several examples have been already reported of this type of father-son reaction, which is probably more frequent than it is generally recognized [1]. In fact self-protonation may be observed not only with organic molecules bearing relatively strong acidic moieties [2] but also with rather weak proton donors such as CH acids [3].

When self-protonation involves the primary anion radicals, the reaction sequence most frequently observed is the following:

$$AH + e \longrightarrow AH^{\cdot-}$$
$$AH^{\cdot-} + AH \longrightarrow AH_2^{\cdot} + A^-$$
$$AH_2^{\cdot} + e \longrightarrow AH_2^{-} \quad \text{and/or}$$
$$AH_2^{\cdot} + AH^{\cdot-} \longrightarrow AH_2^{-} + AH$$
$$AH_2^{-} + AH \longrightarrow AH_3 + A^-$$
$$\overline{AH + (2/3)e \longrightarrow (2/3)A^- + (1/3)AH_3}$$

The overall stoichiometry involves the exchange of 2/3 of electron per molecule, conversion of 1/3 of the parent compound into the dihydrogenerated product and 2/3 into its conjugate base. When the parent molecule bears a nucleofugic moiety, self-protonation leads to a slightly different stoichiometry [3]

$$AHX + e \longrightarrow AHX^{\cdot-}$$
$$AHX^{\cdot-} \longrightarrow AH^{\cdot} + X^-$$
$$AH^{\cdot} + e \longrightarrow AH^- \quad \text{and/or}$$
$$AH^{\cdot} + AHX^{\cdot-} \longrightarrow AH^- + AHX$$
$$AH^- + AHX \longrightarrow AH_2 + AHX^-$$
$$\overline{AHX + e \longrightarrow (1/2)AH_2 + (1/2)AHX^- + X^-}$$

the anion AHX^- being in some cases rather unstable [4].

Occurrence of self-protonation is thus evidenced by controlled potential macroscale electrolysis through: i) the presence of the conjugate base of the substrate among the products; ii) the apparent coulometric value being lower than that expected according to the charge transfer stoichiometry. However a detailed kinetic analysis is required for identifying the basic species which actually react with the parent molecule, for assigning the rate-controlling steps and for determining the pertinent rate constants. Such an analysis, carried out mainly in the conditions of cyclic voltammetry, is presented and the theoretical results utilised for the determination of the kinetic parameters of several electroorganic reactions undergoing self-protonation.

[1] C.Amatore, G.Capobianco, G.Farnia, G.Sandonà, J.M.Savéant, M.G.Severin, and E.Vianello
J.Am.Chem.Soc., 107, 1815 (1985) and references therein.

[2] E.Brillas, G.Farnia, M.G.Severin and E.Vianello, in the press.

[3] C.Arevalo, G.Farnia, M.G.Severin and E.Vianello, in the press.

[4] F.Maran, E.Vianello, G.Cavicchioni and F.D'Angeli
J.Chem.Soc., Chem.Commun. 660 (1985).

ELECTRODE KINETICS AND SELECTIVITY OF ORGANIC ELECTROSYNTHESIS REACTIONS [1]

Hartmut WENDT
Inst. f. Chem. Technologie, TH Darmstadt
Petersenstr. 20, D-6100 DARMSTADT/Fed.Rep.Ger.

Usually electroorganic synthesis reactions are inherently relatively unselective because initially generated radicals and radical ions are so reactive that they are able to react simultaneously with any reaction partner accessible to them at the electrode /electrolyte interface or close to the electrode-surface in the reaction layer.
The aim of the organic electrochemist and the electrochemical engineer is therefore to increase the selectivity by rationally altering the process parameters. This demands a knowledge of electrosorption effects and of relationships between mass transfer and chemical reaction rates of competitive reactions which procede either at the electrode-surface, provided at least one of the reactants is reacting in the adsorbed state, or in the reaction layer, where homogeneous reactions of reactive intermediates competes with diffusion.
If a reactive intermediate $^{\pm\cdot}$ (which as a radical ion is formed by a one-electron-charge transfer according to (1)

(1) $$S \overset{+}{-} e^- \longrightarrow S^{\pm\cdot}$$

reacts with three different reactants R_1, R_2, R_3 to form via three intermediates I_1, I_2 and I_3 eventually the three products P_1, P_2 and P_3:

(2 a) $$S^{\pm\cdot} + R_1 \xrightarrow{k_1} I_1 \longrightarrow P_1$$

(2 b) $$S^{\pm\cdot} + R_2 \xrightarrow{k_2} I_2 \longrightarrow P_2$$

(2 c) $$S^{\pm\cdot} + R_3 \xrightarrow{k_3} I_3 \longrightarrow P_3$$

then the selectivity γ_i of the ith product is given by:

(3) $$\gamma_i = \dot{N}(Pi) / \sum_{j=1}^{n} \dot{N}(Pj) = k_i \cdot c(R_1) / \sum_{j=1}^{n} k_j c(Rj)$$

so that $k_i \cdot c(R_i)$ for the relevant consecutive reaction following the first charge transfer is the most important factor determining the selectivity η_i. Since rate constants - especially if they are close to diffusion controlled can be changed only little, the most important issue for improving the selectivities is to find optimal process-parameters which increase the reactant concentration $c(R_i)$ of the desired reactant and to decrease the concentrations of all other competing reactants. As a well investigated example will serve the addition of anodically generated radicals to olefins [2,3,4,5,6].

(4) $X^- - e^- \longrightarrow X^\cdot$; (4 a) $2\,X^\cdot \xrightarrow{k_{dim}} X_2$

(5) $X^\cdot + {>}C = C{<} \xrightarrow{k_{add}} X - \overset{|}{\underset{|}{C}} - \overset{|}{\underset{|}{C}}^\cdot$; (5 a) $2(X - \overset{|}{\underset{|}{C}} - \overset{|}{\underset{|}{C}}^\cdot) \longrightarrow (X - \overset{|}{\underset{|}{C}} - \overset{|}{\underset{|}{C}})_2$

(5b) $X - \overset{|}{\underset{|}{C}} - \overset{|}{\underset{|}{C}} - + X^\cdot \longrightarrow X - \overset{|}{\underset{|}{C}} - \overset{|}{\underset{|}{C}} - X$

In order to avoid the undesired annihilation reaction (4 a) the stationary radical concentration $c(X^\cdot)$ must be lowered and the concentration of the scavenger-olefin c(olefin) must be increased as far as possible in the reaction layer. Both can be established by reducing the current density for $X^\cdot$-generation as far as technically sensible and to increase the bulk-concentration of the scavenger as far as technically feasible. For this type of reaction an adimensional quantity

$(k_{add.} \cdot c(\text{olef}))^{3/2}\, F \cdot D^{1/2} / (i \cdot k_{dim}) = (AD(\eta_{dim}))$ determines the selectivity in so far as selectivities of more than 90 % are obtained whenever this adimensional quantity is higher than 20.

(Fig. 1:)

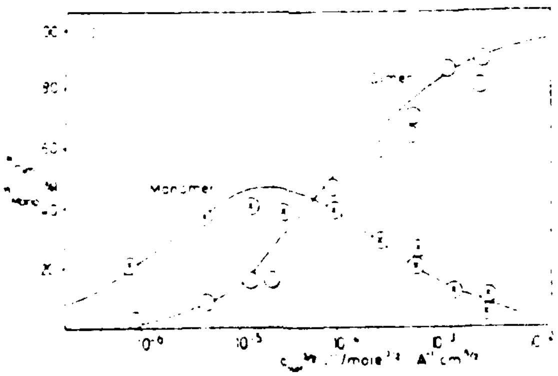

Fig. 1 Total current yield of compounds carrying azido groups dependent on [illegible] model curves calculated with k_{13} = 0.5, 1 and 2 × 10 [illegible] M^{-1} s [illegible], $k_1 = 10$ [illegible] M [illegible] s [illegible], diffusion coefficient of all species assumed to be equal $D(i) = 10^{-5}$ cm^2 s^{-1}, (b) ratio of dimer to monomer current yields dependent on total current efficiency [illegible] selected values 0.125, 0.18, 0.25 [illegible] experimental and calculated [illegible] current yields for monomer I and dimer II dependent on [illegible] M

A different situation prevails whenever the consecutive reactions following the initial charge transfer are true heterogeneous reactions which procede at the electrode surface and in which at least one reactant or both reactants are adsorbed species. In such cases the most effective means to increase the selectivity of a given reaction is to look for electrode/electrolyte combinations which offer optimal adsorption conditions for both reactants ($S^{\pm}$ and $R_{\cdot}$) and to establish for the optimal electrode/electrolyte combination optimal coverage conditions for $R_{\cdot}$, which usually means to establish highest stationary concentrations of $R_{\cdot}$ in the immediate neighbourhood of the electrode.

The anodic oxidation of olefins[8,9] which, if performed in alcohols, may yield - by a heterogeneous reaction - either 1-2 diolethers or dimeric 1-4 diolethers may be optimized either with respect to the dimer at electrodes like carbon where adsorption condition for the olefin are optimal.

(6) 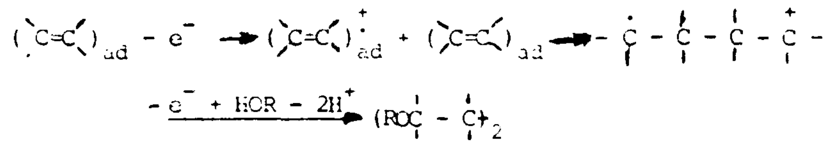

or with respect to the 1,2-diol at electrodes where the solvent-alcohol adsorbs more strongly than the olefin and/or where due to depletion of the olefin-concentration at the electrode surface its surface-concentration is much lower.

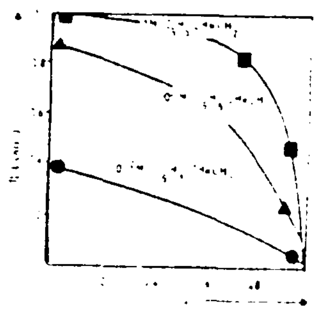

Fig. 2 The dependence of the selectivity [illegible] current yield [illegible] for the formation [illegible] dimer during the anodic oxidation of styrene at a carbon anode on [illegible] for [illegible] concentrations in [illegible] mol L methanolic NaClO₄. The [illegible] [illegible] correspond to the different surface concentrations of styrene at the anode

Table 3 The dependence of the relative yield of dimer in the oxidation of styrene on the anode material. [illegible] surface concentration of styrene. Electrolyte: methanolic [illegible] mol L NaClO₄ [illegible] mol L styrene, current density [illegible]

[illegible] material	Rel. yield of dimer	[illegible]
Graphite		
[illegible]	[illegible]	[illegible]
[illegible]		[illegible]
[illegible]		[illegible]

/1/ H.Wendt, Angew.Chem.Intern.Ed.Engl.21 (1982) 256; /2/ H.Schäfer, A.Alazrak, Angew.Chem. 80 (1968) 485; /3/ V.Plzák, H. Wendt, Ber. Bunsenges.physik.Chem. 83 (1979) 481; /4/ H.Wendt, V.Plzák, J. electroanal.Chem. 154 (1983) 13; /5/ V. Plzák, H. Wendt, J. electroanal.Chem. 154 (1983) 29; /6/ V. plzák, H. Wendt, J.electroanal. Chem. 180 (1984) 185; /7/C.Amatore, J.M. Saveant, J.electroanal.Chem. 123 (1981) 189; /8/ H.Schäfer, H. Steckhan, Angew.Chem. 81 (1969) 532; /9/ V.Plzák, H.Schneider, H.Wendt, Ber. Bunsenges.physik.Chem. 78 (1974) 1373.

MODIFICATIONS OF ELECTROCATALYST SURFACES BY ELECTROCHEMICAL PROCEDURES

A.J. Arvia
Instituto de Investigaciones Fisicoquímicas Teóricas y Aplicadas - (INIFTA)
Casilla de Correo 16, Sucursal 4, (1900) La Plata, ARGENTINA

Different non-electrochemical procedures produce changes in the surface structure of metals. Faceting effects on metal surfaces are accomplished by means of adsorption of molecules from the gas phase, by chemical etching, by thermal treatments and by surface ionic bombardment. Through chemical etching surface layers including those metal layers altered by a mechanical treatment such as polishing, can be removed; and through this procedure the enhancement of faceting of polycrystalline metals can be achieved. On the other hand, thermal treatments are used to eliminate the effects and residual tensions and to change grain size distribution.

Very recently various electrochemical procedures to change the surface structure of solid metal electrodes have been discovered. The first method consists in applying to the electrode fast electroadsorption/electrodesorption cycles by means of a periodic potential signal, which covers the potential range of water underpotential decomposition (procedure 1)[1,2].

A second method combines the electroadsorption/electrodesorption cycles with thermal treatments (procedure 2)[3].

The electrode surface can also be changed by means of fast electrooxidation and electroreduction cycles covering a potential range much greater than that corresponding to the oxygen monolayer formation (procedure 3)[4,5].

Finally, similar effects can be obtained by means of modulated electrodeposition of metals (procedure 4)[6].

In all these cases, the surface changes can be followed voltammetrically. Procedure 1 was used at room temperature in aqueous acid solution to change polycrystalline platinum either into a platinum surface with (100) crystallographic orientation or into a reconstructed (111) crystallographic orientation, depending on the characteristics of the potential perturbation (upper and lower potential limits and frequency). The same procedure was used to change the crystallographic orientation of gold, rhodium and nickel electrodes; the latter being applied in alkaline solution[6].

Procedure 2 was employed in molten potassium bisulphate and molten sodium potassium bisulphate mixtures in the 180-300°C range to obtain a reconstructed platinum (111) preferred crystallographic orientation from polycrystalline platinum[3].

Procedure 3 was applied in acid solution at room temperature to enhance the (111) preferred crystallographic orientation of platinum and to approach an equilibrium distribution of the crystallographic orientation of gold from polycrystalline gold[8].

Procedure 4 results useful to electrodeposit (111) and (100) preferred crystallographic oriented platinum from the polycrystalline metal by setting the electrodeposition conditions at a potential of net electrodeposition under a square was modulation of the order of 1 V at a frequency in the order of kHz[6].

The crystallographic orientation effect becomes very remarkable when the periodic potential perturbation in all the procedures is greater than 2,5 kHz. Under these circumstances additional effects such as surface roughness and sintering are appreciably diminished[9].

The preferred oriented electrodes were also used to electrooxidize different adsorbed residues resulting from different molecules (carbon monoxide, carbon dioxide, formic acid, methanol, etc.). The corresponding electrodesorption voltammograms are remarkably dependent on the metal substrate, solution composition, adsorption potential and adsorption time[10].

The present results suggest that the restructuring and faceting effects coming out from polycrystalline platinum are closely similar to the different states reported from single crystal platinum electrodes during restructuring. It is suggested that common surface structures under true crystallographic equilibrium can be obtained either from polycrystalline or single crystal platinum. This idea can be extended to the electrochemical behaviour of other metals used in electrocatalysis.

REFERENCES

1. R.M. Cerviño, W.E. Triaca and A.J. Arvia, J.Electrochem.Soc., 132, 266 (1985).
2. J.C. Canullo, W.E. Triaca and A.J. Arvia, J.Electroanal.Chem., 175, 337 (1984).
3. A.C. Chialvo, W.E. Triaca and A.J. Arvia, Anal.Asoc.Quím. Arg. (in press).
4. A.C. Chialvo, W.E. Triaca and A.J. Arvia, J.Electroanal.Chem., 146, 93 (1983).
5. A.C. Chialvo, W.E. Triaca and A.J. Arvia, J.Electroanal.Chem., 171, 303 (1934).
6. E. Custidiano, A.C. Chialvo and A.J. Arvia, J.Electroanal. Chem. (in press).
7. A. Visintín, W.E. Triaca and A.J. Arvia (in preparation).
8. M.C. Galindo, M.E. Martins and A.J. Arvia, Anal.Asoc.Quím. Arg. (in press).
9. R.M. Cerviño, W.E. Triaca and A.J. Arvia J.Electroanal.Chem., 182, 51 (1985).
10. E.P.M. Leiva, E. Santos, M.C. Giordano, R.M. Cerviño and A. J. Arvia, J.Electrochem.Soc. (in press).

ACKNOWLEDGEMENT

INIFTA is a Research Institute jointly established by the Universidad Nacional de La Plata, the Consejo Nacional de Investigaciones Científicas y Técnicas and the Comisión de Investigaciones Científicas de la Provincia de Buenos Aires.

3.2

ELECTROCHEMICAL FORMATION AND REACTIVITY OF HYDROUS OXIDES OF THE NOBLE METALS

L.D. BURKE

Department of Chemistry, University College, Cork, Ireland.

There appears at the present time to be a strong reluctance to accept the fact that redox processes involving only insoluble materials, such as metals, oxides or hydroxides, in an aqueous environment exist in other than a neutral state. Thus, some typical well known metal oxidation and oxide charge storage reactions are generally represented as follows:

$$Pt + H_2O = PtOH + H^+ + e^- \quad (1)$$

$$NiO.OH + H^+ + e^- = Ni(OH)_2 \quad (2)$$

$$MnO_2 + H^+ + e^- = MnOOH \quad (3)$$

In each case here, since the number of electrons and protons are equal, the reversible reduction potential should shift by the factor 2.303 RT/F V per unit change in solution pH (pH-independent scale) or show a zero shift in terms of the RHE scale. Such behaviour is observed with compact, non-hydrous, oxide electrode systems, e.g. the well known $Hg/HgO/OH^-$ reference electrode.

It is necessary, however, to distinguish between compact and micro-dispersed (or hyper-extended) oxide systems. The latter are low density materials, usually prepared by electrochemical or base precipitation techniques in an aqueous environment. They may be viewed as aggregates of hydroxy species, i.e. a loose, weakly cross-linked polymer, premiated by the aqueous phase in which reside the counterions. These materials can also be viewed as regular oxide lattice species, e.g. rutile, in which most of the bridging oxygen (M-O-M) linkages have become hydroxylated - the lattice dilating as the material imbibes water. While such a process is scarcely feasible in the case of a thermally prepared oxide, e.g. RuO_2, it probably plays a crucial role in metal dissolution reactions where the conversion of compact to hydrous oxide appears to be essential if passivation of the substrate is to be avoided or removed.

The difference in redox behaviour between anhydrous and hydrous oxides was first noted in cyclic voltammetry work with gold [1,2]. The potential required to reduce the hydrous deposit dropped by a value of ca. 3/2(2.303 RT/F) V per unit increase in solution pH and conventional electrochemical analysis (based on the assumption of a Au(III) cation and OH^- ligands) suggested that the hydroxy complex involved was $[Au_2(OH)_9]^{3-}$ or $[Au_2O_3(OH)_3.3H_2O]^{3-}$. A similar shift was noted by various authors - see ref. 3 for details - in the case of the hydrous iridium oxide system. The same analysis, based on the assumptions of an Ir(III)/Ir(IV) transition and the stoichiometry of the reduced state being the same as that for the Au(III) complex, suggested that the stoichiometry of the oxidized state is $[Ir(OH)_6]^{2-}$ or $[IrO_2(OH)_2.2H_2O]^{2-}$. In the absence of structural data for

these hydrous materials, it is significant that the above formula for the Ir(IV) compound is in agreement with well established acidic hydroxy species, e.g. platinic acid $H_2Pt(OH)_6$ - and it salts [4], and iridic acid, $H_2Ir(OH)_6$ [5].

If one examines the type of charge storage reaction proposed for iridium, viz.

$$2Ir(OH)_6^{2-} + 6H^+ + 4e^- = [Ir_2(OH)_9^{3-}] + 3H_2O \qquad (4)$$

the mean charge per cation, i.e. the number of excess coordinated hydroxide ions, is greater in the more oxidized state - a common observation in homogeneous hydrolysis processes. This raises the possibility that on reducing the oxidation state of the central metal ion a cationic polymer would eventually be obtained, i.e. the film would contain a deficiency of hydroxide ions - the positive charge being compensated for by adsorption of other anions, e.g. Cl^- or SO_4^{2-}. Indeed such seems to be the case with certain (M/M^+) transitions for the three Gp. 1(b) metals, Cu, Ag and Au. The shift in pH in this case is +2.303 RT/F V per pH unit (RHE scale) - zero shift on the S.H.E. scale; this confirms the absence of OH^- or H^+ involvement, the electrode reaction being of the following type

$$M^+(X^-) + e^- = M(+X^-) \qquad (5)$$

Marked SERS effects are also almost unique to the Gp. 1(b) metals and it is obviously possible that the cationic (M^+) species, solvent separated from their counterions, coordinate basic organic molecules such as pyridine (indeed to observe the Au/Au(1) transition in cyclic voltammetry experiments in aqueous media a basic species such as pyridine must be present to stabilize the Au^+ species). Assuming that these ligands separate univalent cations attached to the surface from their anionic counterions - and bearing in mind that the electric field between unit charges of opposite sign in vacuum, separated by a distance of 6Å, is ca. 3×10^{10} V m^{-1}, it is clear that this ligand-separated cation-anion model provides a simpler alternative to the usual surface plasmon view as to the origin of the large interphasial electromagnetic field which is fundamental to the interpretation of SERS phenomena.

The oxidation-reduction cycling (ORC pretreatment) - a necessary step in many cases in the study of SERS effects - plays essentially the same role as repetitive potential cycling in the generation of hydrous oxide films on metals such as Pt[6], the major difference being that pyridine replaces hydroxide ions as ligands when the charge on the central metal ion is low. In the absence of cycling, hydroxy or pyridine complex formation is inhibited as with the metal atoms partially imbedded in the lattice a full coordination state is impossible to attain. On cycling, the metal either dissolves and redeposits (Ag), or place-exchanges forming a higher compact oxide (e.g. some PtO_2 at the anodic limit of the sweep) which is then largely reduced at the lower limit of the sweep. In both cases the net result is adatom formation which facilitates formation of a more complete ligand coordination sphere: As pointed out in the case of platinum the stability of the complex is surprisingly high (usually more so than its adsorbed oxygen equivalent) - absence of a response for either the hydroxy or pyridine complex on the anodic sweep under normal conditions is due to the difficulty of adatom formation.

There appear to be certain circumstances where hydrous oxide formation preceeds conventional monolayer formation on noble metals. In recent years some very unusual voltammograms have been recorded for Pt single crystal electrodes by Clavilier and other authors. The highly reversible

peaks occur in the region where hydrous oxide reduction is observed. In a review of this topic Parsons [7] has stressed both the importance of high energy sites (possibly individual adatom species) and the high sensitivity of the adsorption to the nature of the anion. Scherson and Kolb [8] have recently postulated that rather than hydrogen desorption, the process involved here in the anodic cycle is anion adsorption. The sharp reversible peaks for Au[111] in acid at +0.72 V(SCE), ca. 1.0 V(RHE) [8], cannot be due to hydrogen. Since this potential virtually coincides with that for hydrous oxide reduction on gold at low pH [1,2], the peaks are most likely due to reversible hydrous oxide formation at individual adatom sites on an otherwise atomically flat surface. It is only when the surface restructures, when for instance the sweep is allowed to enter the oxygen adsorption region, that these adatom sites (and hence the sharp peaks due to reversible hydrous oxide formation) disappear. The anion sensitivity in the case of the platinum peaks may be due to the presence of such species in the coordination sphere (the latter would seem more probable if the metal ions were present in a low oxidation state). Further evidence that some hydrous oxide formation can preceed monolayer growth may be found in the report [9] that polycrystalline gold in highly purified base exhibits minor reversible peaks at ca. 0.6 V - this again is the region where the hydrous gold oxide films reduce in solutions of high pH [1,2].

Other areas where charged anionic oxide species may be involved include the initial stages of compact monolayer formation [10], electrocatalysis at oxide substrates[11], battery-type processes [12], etc. The basic idea of the charged oxide framework being permiated by its discrete counterion equivalents is in excellent agreement with the Porous Double Layer model of the oxide-solution interface (oxide colloids having high charge values combined with low electrophoretic velocities). The relevance of oxide hydration and acid-base behaviour to metal corrosion reactions has already been outlined [13].

REFERENCES

1. L.D. Burke and M. McRann, J. Electroanal. Chem., 125 (1981) 387.
2. L.D. Burke, M.E. Lyons and D.P. Whelan, ibid., 139 (1982) 131.
3. L.D. Burke and D.P. Whelan, ibid., 162 (1984) 121.
4. H.G. Scott, Acta Cryst. B, 35 (1979) 3014.
5. W.P. Griffith, The Chemistry of the Rarer Platinum Metals, John Wiley, New York, 1967, p. 248.
6. L.D. Burke and M.B.C. Roche, J. Electroanal. Chem., 164 (1984) 315.
7. R. Parsons, ibid., 118 (1981) 3.
8. D.A. Scherson and D.M. Kolb, ibid., 176 (1984) 353.
9. H. Angerstein-Kozlowska, B.E. Conway, B. Barnett and J. Mozota, ibid., 100 (1979) 417.
10. L.D. Burke and M.B.C. Roche, ibid., 159 (1983) 89.
11. L.D. Burke and J.F. Healy, ibid., 124 (1981) 327.
12. L.D. Burke and M.J.G. Aherne, ibid., 183 (1985) 183.
13. L.D. Burke and R.A. Scannell, Equilibrium Diagrams; Localized Corrosion (R.P. Frankenthal and J. Kruger, eds.), The Electrochem. Soc., Pennington, N.J., 1984, pp. 135-147.

3.5

ELLIPSOMETRY AND INTERFACIAL ELECTROCHEMISTRY

M. COSTA and F. CHAO
Laboratoire d'Electrochimie Interfaciale du C.N.R.S.
1 Place A. Briand, 92195 MEUDON Principal Cédex, France

The fields of application of ellipsometry in electrochemistry are very diversified : from the characterisation of semi-infinite medium or films considered as macroscopically homogeneous phases to characterisation of atoms or molecules adsorbed on a surface or the electronic distribution at the electrochemical interface.

The ellipsometric technics which have to be used depend of the studies which are considered.

During the lecture we shall make a screening of some kinds of ellipsometers which are in use in electrochemistry. This screening will be illustrated through experimental examples.

- Ellipsometer with rotating analysor (or polarisor) : growth of oxyde films.

- Ellipsometer with phase and azimuth modulation : initial processes in the grafting of polymers, adsorption metal on metal, electronic distribution at the interface.

- Spectroscopic ellipsometer : polymers doping, adsorption of organic molecules.

For each technic we shall analyse the possibilities and limits of the method.

SMALL AMPLITUDE AC METHODS AND THE UNDERSTANDING OF SIMPLE ELECTRODE REACTIONS

M. SLUYTERS-REHBACH
Van 't Hoff laboratory, State University of Utrecht, The Netherlands

Among the small amplitude relaxation methods the ac impedance method has found a wide application in several fields of electrochemistry. The reason for this is the relative simplicity of the mathematical formulation of the interfacial impedance or admittance as a function of frequency, compared with the response to e.g. pulse or step perturbations, that has to be expressed as a function of time. Theories are available for the interfacial admittance in many complex cases, e.g. of electrode reactions accompanied by reactant adsorption, homogeneous chemical reactions, and of processes involved in metal deposition, corrosion, etc.[1,2]

Recently in our laboratory the attention has been focussed again to the more simple electrode reactions, controlled only by diffusion and charge transfer, i.e. obeying the original Randles' circuit. However, in contrast with the tendency in literature to describe charge transfer in terms of the kinetic parameters k_{sh} (standard heterogeneous rate constant) and α (transfer coefficient), it was found preferable to determine the potential dependent rate constant k_f, being the essential parameter in the rate equation

$$-j_F = nFk_f[c_O - c_R\exp(\varphi)] \qquad (1)$$

where j_F = faradaic current, c_O, c_R = surface concentrations of oxidized and reduced form, and

$$\varphi = (nF/RT)(E-E^o) \qquad (2)$$

Using a high precision automatic network analyzer system[3] that provides compensation of systematic instrument errors, and choosing optimal concentrations of the electroactive species, it is possible to determine k_f in a very wide potential region. To this end the ac potential perturbation is superimposed on a dc-polarizing mean potential $\bar{E}$. The technique has been applied to electrode reactions at the dropping mercury electrode (DME), and at poly- and monocrystalline gold electrodes. In the latter case it is necessary to account for the fact that the double-layer charging process is not purely capacitive, but should be represented by the so-called "constant phase element" (CPE)[4].

In many cases, studied thus far, it is found that $\ln k_f$ is a non-linear function of $\bar{E}$, in other words the operational transfer coefficient α, defined by

$$\alpha = -\, d\ln k_f/d\varphi \qquad (3)$$

is potential dependent. Evidence is growing that this behaviour should be explained by the idea that the reaction $O+ne \rightleftarrows R$ proceeds via a sequence of elementary reactions, not only single electron transfers, but also heterogeneous "chemical" conversions preceding or following electron transfer steps. The underlying assumptions are that the individual rate constant of a

"chemical step" is independent of potential, whereas the rate constant of an "electrochemical step" obeys the Butler-Volmer relationship

$$k_i = k_{s,i}\exp[-\alpha_i(F/RT)(E-E^o)] \qquad (4)$$

with $\alpha_i \approx 0.5$.

An important conclusion from this approach is that all kinds of medium effects on the rate of electrode reactions, e.g. of complexing ligands, catalysis or inhibition by adsorbed species, and specific effects due to the nature of the electrode material, should be investigated considering their action upon the separate steps. Some examples (e.g. the rôle of pH in the reduction of O_2, or the rôle of adsorbed I^- in the reduction of Zn^{2+}) make this very clear.[9,10]

The nature of the "chemical step" is obvious in some cases, e.g. a protonation reaction or a dissociation. However, it is less obvious or even mysterious in other cases, as for example in the reaction tris-oxalato Fe(III)/Fe(II)[5,6].

The mechanistic studies as outlined above can be considerably extended and improved by application of a new method, called demodulation voltammetry, that was recently developed in our laboratory[7]. In this method an amplitude-modulated current, $j = j_A\sin\omega_H t\cos\omega_L t$, is forced through the cell, while simultaneously the mean potential $\bar{E}$ of the indicator electrode is controlled by a potentiostat. Typical values for the frequencies are $\omega_H = 10^5$ to 10^6 Hz, $\omega_L = 10^2$ to 10^3 Hz; the optimal values depend on the kinetic parameters of the electrode reaction. Due to the non-linear current-potential relationship, the cell response contains the demodulation voltage $\Delta E_{dem} = I_{LF}\cos 2\omega_L t + Q_{LF}\sin 2\omega_L t$, which originates from the second order terms in the Taylor-expansion of the rate equation. However, also the double-layer charging is a non-linear process, and contributes to I_{LF} and Q_{LF}. Analysis procedures have been developed to obtain the information about the charge transfer process.

The demodulation method is essentially a high-frequency method, being not seriously limitated by the ohmic resistance and the double layer capacity. Consequently it can be applied to very fast electrode reactions, with rate constants up to ca. 30 cm s^{-1}, as compared to ca. 1 cm s^{-1} in the impedance method. Moderately fast electrode reactions can be studied in a much wider potential range. In addition the response contains explicit information on both k_f and α, providing an internal check on the potential dependency of α.

Even more important is that the demodulation signal provides a check on the validity of the rate equation, given by eq. (1), that is derived on the assumption that the reaction mechanism is a linear sequence of (pseudo-) first order elementary reactions. However, also mechanisms can be conceived that involve second-order elementary reactions, e.g. a dismutation of an intermediate Y according to $2Y \rightleftarrows O+R$. Generally in such a case the rate equation is more complex; sometimes it is of the form

$$-j_F = nFk_{ff}[c_O^p c_R^q - c_O^r c_R^r \exp(t\varphi)], \qquad (4)$$

sometimes only an implicit expression can be derived, e.g. a quadratic equation of j_F. However, both the impedance and the demodulation parameters retain explicit formulations if the electrode reaction is dc reversible[7]. Then, in accordance with the arguments pointed out before by Reinmuth[8], it turns out that discrimination between linear and non-linear mechanisms is only possible if results from the two methods are combined.

In this lecture the theoretical and experimental principles of the two methods will be outlined, and both prospects and limitations will be indicated, especially with a view to mechanistic studies. Conclusions about systems studied thus far will be briefly reviewed and some quite recent results will

be presented.

1. I. Epelboin, C. Gabrielli, M. Keddam, in (E. Yeager, J.O'M. Bockris, B.E. Conway and S. Sarangapani, Eds.) Comprehensive Treatise of Electrochemistry, Vol. 9, Plenum Press, 1984, Ch. 3.
2. M. Sluyters-Rehbach, J.H. Sluyters, Ibid. Ch. 4.
3. C.P.M. Bongenaar, M. Sluyters-Rehbach, J.H. Sluyters, J. Electroanal. Chem. 109 (1980) 23.
4. G.J. Brug, A.L.G. van den Eeden, M. Sluyters-Rehbach, J.H. Sluyters, J. Electroanal. Chem. 176 (1984) 275.
5. J. Struijs, M. Sluyters-Rehbach, J.H. Sluyters, J. Electroanal. Chem. 146 (1983) 263.
6. G.J. Brug, M. Sluyters-Rehbach, J.H. Sluyters, J. Electroanal. Chem. 176 (1984) 297.
7. J. Struijs, M. Sluyters-Rehbach, J.H. Sluyters, J. Electroanal. Chem. 143 (1983) 37, 61; 171 (1984) 157.
8. W.H. Reinmuth, J. Electroanal. Chem. 34 (1972) 297.
9. C.J. van Velzen, M. Sluyters-Rehbach, A.G. Remijnse, G.J. Brug, J.H. Sluyters, J. Electroanal. Chem. 134 (1982) 87; 142 (1982) 229.
10. R. Andreu, M. Sluyters-Rehbach, J.H. Sluyters, J. Electroanal. Chem. 171 (1984) 139.

NEW RESULTS ON THE ELECTROCATALYSIS OF METHANOL AND FORMIC ACID OXIDATION

W. Vielstich

Institute for Physical Chemistry, University of Bonn, Wegelerstr. 12

D-5300 Bonn FRG

The efforts to develop a methanol/air-fuel cell of technical interest have not turned out to be a success yet, due to a too positive potential of the methanol electrode.

The first step in the methanol oxidation is the dissociative chemisorption on the metal surface forming a strongly adsorbed intermediate:

$$CH_3OH \longrightarrow -C\begin{matrix}H\\ \diagup\\ \diagdown\\ O\end{matrix} + 3\,H_{ad} \qquad \text{or}$$

$$CH_3OH \longrightarrow \begin{cases} -C \equiv O + 4\,H_{ad} \\ =C=O + 4\,H_{ad} \end{cases}$$

For a stationary current with HCO or CO the further oxidation of the adsorbate to CO_2 is necessary. The additional oxygen atom can only be made available by the water of the electrolyte

$$HCO + H_2O \longrightarrow CO_2 + 3H^+ + 3e^- \qquad \text{or}$$

$$CO + H_2O \longrightarrow CO_2 + 2H^+ + 2e^-$$

Partial steps assumed are:

$$M - H_2O \longrightarrow M - OH + H^+ + e^- \qquad \text{and}$$

$$HCO + OH \longrightarrow CO_2 + 2H^+ + 2e^-$$

The OH-forming reaction is obviously catalyzed at platinum above +450 mV only (see Fig.1). The search of a new type of catalyst is necessary.

In this investigation the effect of underpotential deposition of non-noble metals like Pb and Sn on noble metals is studied at smooth electrodes and at Teflon-bonded carbon substrates.

Basic questions have been studied by the application of formic acid as a model system. It is assumed that the same intermediate as with methanol blocks the further oxidation. The co-adsorption of lead and the strongly adsorbed intermediate was followed by a flux cell technique. A long time increase of activity through the use of upd lead on platinum could be shown for porous carbon substrate anodes (Fig.2). It follows from this study that the third-body-effect in the electrocatalysis of formic acid is of minor importance.

In order to study the nature of the adsorbed intermediate in-situ IRRAS is discussed together with the results of Electrochemical SIMS, Vacuum Transfer Desorption Mass Spectroscopy and on-line Mass Spectroscopy of the volatile oxidation products.

REFERENCES

1. W. Vielstich, "Fuel Cells", Interscience, New York 1970

2. J. Willsau, O. Wolter and J. Heitbaum, "On the Nature of the Adsorbate During Methanol Oxidation at Platinum" - A DEMS (Differential Electrochemical Mass Spectroscopy)-Study", J. Electroanal. Chem. 185 (1985)163

3. M. Beltowska-Brzezinska, J. Heitbaum and W. Vielstich, "The Influence of UPD-Lead on the Adsorption of Formaldehyde, Formic Acid and Methanol on Pt in Acid Solution", J. Electroanal. Chem., in press

4. A. Castro Luna, T. Iwasita and W. Vielstich, "UPD Metal Electrocatalysis of Formic Acid Oxidation at Teflon Bonded Carbon Substrate Electrodes", J. Electroanal. Chem., in press

5. M.M.P. Janssen and J. Moolhuysen, "Platinum-Tin Catalysts for Methanol Fuel Cells Prepared by a Novel Immersion Technique by Electrocodeposition and by Alloying" Electrochimica Acta 21 (1976) 861

6. A. Bewick, K. Kunimatsu, B.S. Pons and J.W. Russell, "Electrochemically Modulated Infrared Spectroscopy" J. Electroanal. Chem. 160 (1984) 47

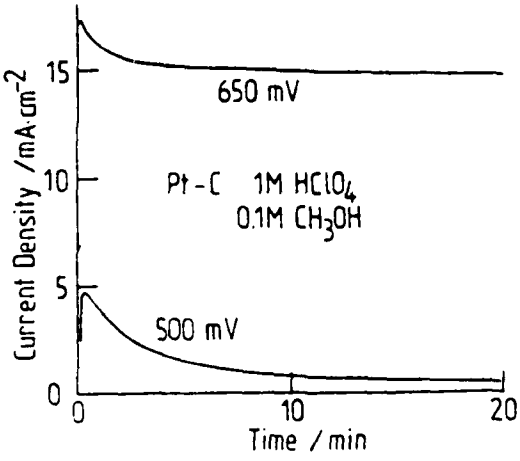

Fig.1 Oxidation of methanol in 1N $HClO_4$ at finely divided platinum on a Teflon bonded carbon substrate electrode at +500 and +650 mV vs RHE and 20°C

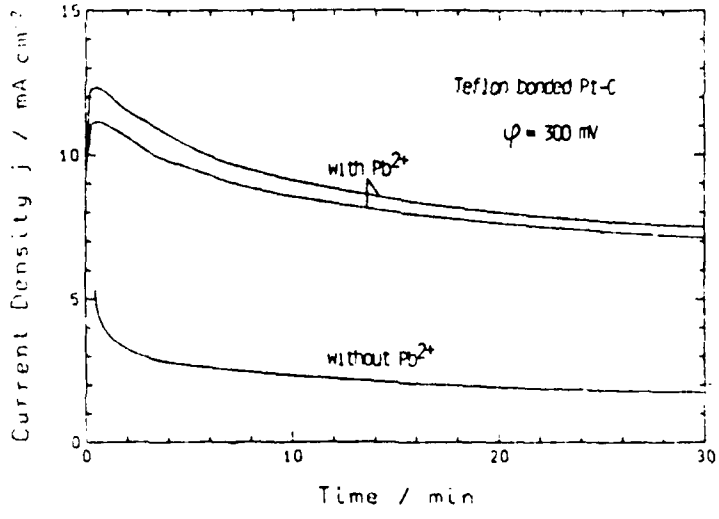

Fig. 2 Influence of upd lead on the long-term oxidation of 1N HCOOH in 1N $HClO_4$ on a Teflon bonded platinum carbon anode at +300 mV vs RHE and 20°C, upper line shows data for a stirred solution

3.10

ELECTROCATALYTIC PROPERTY OF ALLOYS TOWARDS OXIDATION OF SIMPLE ORGANICS

M. ENYO, A. ARAMATA AND K. MACHIDA
Research Institute for Catalysis, Hokkaido University,
Sapporo, 060, (Japan)

Realization of methanol fuel cells depends strongly upon the development of electrodes with high electrocatalytic activity. A large number of reports have been accumulated on advantagelus effects of surface modification of platinum metals with less noble metals. In particular, underpotential deposition (upd) of foreign metals, typically Sn, is known to give rise to a strong enhancement of the electrocatalytic activity towards electro-oxidation of various kind of fuels.

It is of some interest to see if alloy systems have in their electrocatalytic property any commonality with the surface modification by upd foreign metals. The present report contains electro-oxidation of CH_3OH, HCHO, and HCOOH on amorphous alloys of Pt-Zr-Sn or Pt-Zr-Ru, and on polycrystalline Pd-Au and Cu-Ni alloys.

Electro-oxidation of CH_3OH and related compounds on Pt-based amorphous alloys

Amorphous Pt-Zr alloys, prepared in the form of ribbons (thickness 0.02 mm) by a melt-quench technique, can be used to prepare porous Raney-type Pt electrodes by leaching Zr out with aq. HF[1]. In the present experiment, Sn or Ru was added further to this type of alloys as the third component. Electro-oxidation of CH_3OH in acidic solution was carried out and results in the case of modification with Sn are shown in Fig. 1. With comparable magnitudes of the surface roughness factor (RF), the electrocatalytic activity was raised by roughly one order of magnitude (or more in the case of HCHO and HCOOH) by the addition of Sn. However, the activity could not exceed the highest level reported in the literature[2], and also no indication was observed to believe that the amorphous structure has any advantage over ordinary polycrystalline samples.

Electro-oxidation of CH_3OH and related compounds on Pd-Au alloys

Electrocatalytic activity of Pd-Au alloys in acidic and alkaline solutions exhibited various levels of synergetic electrocatalytic effect, depending on the kind of compounds to be oxidized. More details of this series of investigation will be reported separately in this Meeting. The electrocatalytic activities are summarized schematically in Fig. 2 where relative activity levels are shown by the length of the arrows. Results on a Pt electrode are also shown for comparison.

Pd-rich Pd-Au alloy electrodes are reasonably active towards the CH_3OH electro-oxidation in alkaline solution, and an activity maximum appears at around 90 % Pd. In contrast with this behaviour, these alloys are entirely inactive in acidic solution.

Au is very active, higher than Pt, in the HCHO electro-oxidation in alkaline solution, whereas the activity decreases monotonically with increase of the content of Pd in the Pd-Au alloys. In acidic solution, an activity maximum appears at a Pd-rich alloy composition while Au is entirely inactive. The strong contrast between the behaviours in alkaline and acidic solutions on Au, but not on Pd-rich Pd-Au alloys, is not well understood.

Pronounced levels of synergetic effect are seen in the $HCOO^-$ electro-oxidation, but the composition which yields the maximum activity is likely to be different in alkaline and acidic solutions. The activity levels are, except for pure Au or Au-rich alloys, far more higher than Pt.

Electro-oxidation of HCHO on Cu-Ni alloy electrodes

Cu and Cu-rich Cu-Ni alloy electrodes are found to be very active in the HCHO electro-oxidation in alkaline solution (but not in any other fuels). The highest activity among the specimens employed, as judged from the most negative value of the rest potential, was on the $Cu_{89}Ni_{11}$ alloy, with the value of some -90 mV RHE in 0.2M HCHO, 1M NaOH, as shown in Fig. 3(A).

It is known[3,4] that electro-oxidation of HCHO on Cu, Ag, and Au in alkaline solution is accompanied with the co-production of H_2 but that is not the case on Pt, Ni, etc. The evolution of H_2 has therefore been followed in the present experiment on the Cu-Ni alloy electrodes and results are shown in Fig. 3(B). The efficiency of H_2 evolution on the alloy electrodes was on a smooth line connecting the constituent metals and no drastic change was observed at any particular composition.

In view of two extreme models of catalytic beha.iours of alloys, namely, the component metal atoms having a homogeneous electronic/catalytic property on the one hand (the collective model[5]) or maintaining their individualities on the other (the localized model[5]), the present investigations appear to support the latter model. In addition, a significant extent of synergetic effect was often observed at intermediate compositions in the case of alloys between group VIII and IB metals.

References

1. M. Enyo et al., Electrochim. Acta, **28**, 1573 (1983).
2. K. J. Cathro, J. Electrochem. Soc., **116**, 1608 (1969).
3. M. Saito, Kinzoku Hyomen Gijutsu (Metal Surf. Tech.), **16**, 22 (1965).
4. M. L. Avramov-Ivic and R. R. Adzic, Bull. Soc. Chim. Beograd, **48**, 357 (1983).

5. W. M. H. Sachtler and P. Van der Plank, Surface Sci., **18**, 62 (1969).

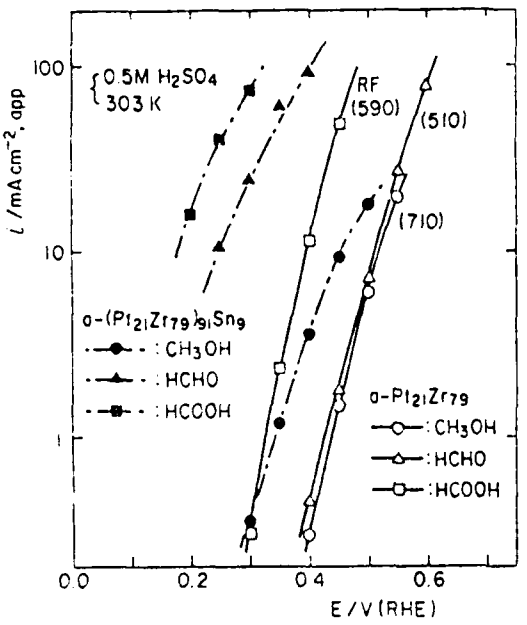

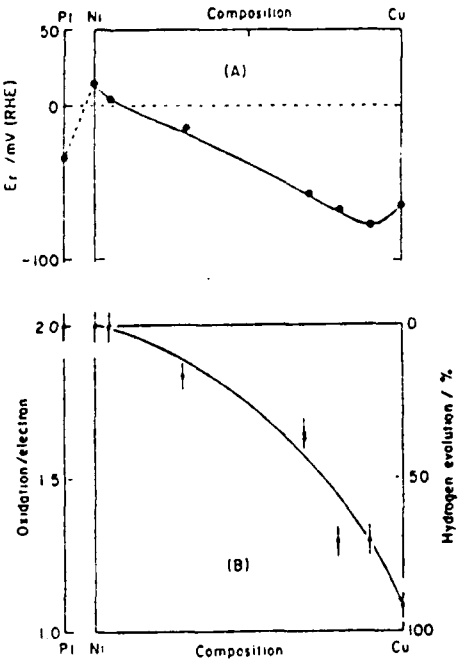

Fig. 1 (left). Electro-oxidation of CH_3OH, HCHO and HCOOH on Pt-Zr amorphous alloys without (open symbols) or with (filled symbols) the addition of Sn as the third component.

Fig. 3 (right). (A) Open-circuit rest potentials and (B) evolution of H_2 during the electro-oxidation of 0.2M HCHO in 1M NaOH on Cu, Ni and Cu-Ni alloy electrodes, 30°C.

Fig. 2. Schematic presentation of electrocatalytic activity of Pd, Au, and Pd-Au alloys towards electrooxidation of CH_3OH, HCHO, HCOOH and CO in acidic and alkaline media. The cases of Pt are also shown for comparison.

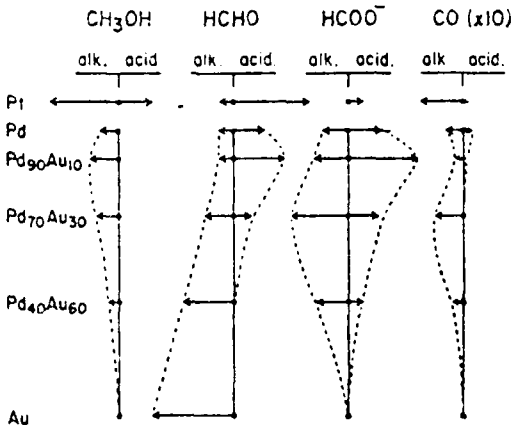

MOLECULAR ENVIRONMENT EFFECTS IN THE ELECTROCHEMISTRY OF SUPERSTRUCTURED PORPHYRINS.

J.M.SAVEANT
Laboratoire d'Electrochimie de l'Université de Paris VII
2, place Jussieu - 75 231 - Paris Cedex 05 - France -

The presence of hydrocarbon chains attached to the phenyl rings of the tetraphenylporphyrin macrocycle forming "basket-handle" or picket fence structures of the type shown below :

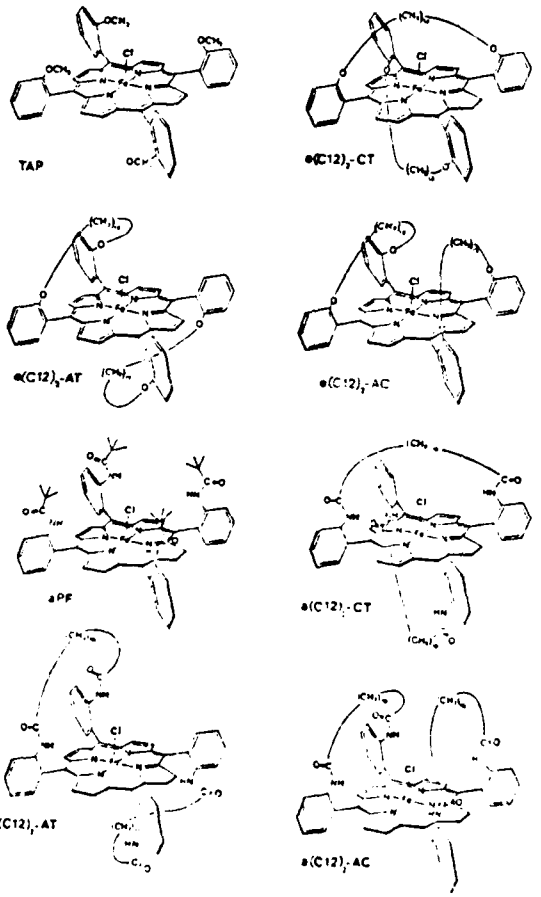

exerts a strong influence on the redox and coordination chemistry of the central porphyrin complex both from the thermodynamic and kinetic viewpoints.

The electrochemical investigation of the reduction of a large series of the corresponding iron complexes in various solvents showed that three types of effects can be identified : protection of the reactive center from interaction with the surrounding medium, local solvent effects resulting from

the presence of amide groups in the protecting chains, steric discrimination between the axial ligands of the iron atom. Variations as large as five orders of magnitude in terms of equilibrium constants are observed. These effects resemble certain functions of the protein surrounding the prosthetic group in metallo-proteins.

Spectacular effects are also observed in the oxidation of similar copper, zinc and magnesium complexes. While this usually involves the sucessive formation of the one and two electron products separated by several hundreds millivolts, the presence of amide groups in the superstructures lead to a reversible direct two-electron uptake. With the cofacial dimeric structure shown below :

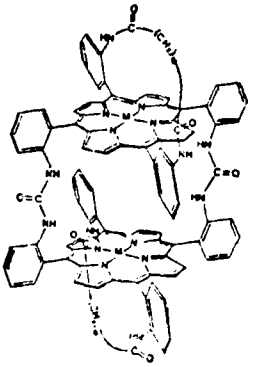

a four electron reversible pattern is observed.

Such modifications of the immediate molecular environment of the porphyrin complex by groups which influence but do not interfere directly into the chemistry of the reacting center, leading to integrated molecular systems, are also useful in the design of catalytic cycles in the electrochemical activation of small molecules.

4.2

SURFACE-MODIFIED GOLD ELECTRODES FOR THE PROMOTION OF DIRECT REDOX PROTEIN ELECTROCHEMISTRY

H.A.O. HILL, and N.J. WALTON
Inorganic Chemistry Laboratory, Oxford, (England)

It is well known that, in general, biological electron transfer molecules such as cytochrome C do not exhibit reversible electrochemistry at normal voltammetric electrodes. This is despite their role in vivo as efficient agents of electron transport. We have found, however, that the modification of a gold electrode-solution interface with many bifunctional organic (and some inorganic) molecules results in the realisation of well-behaved electrochemistry for such redox proteins. We believe that in order the surface-modifying species to act as a successful promoter of this electrochemistry that it should first bind to the electrode through one of its functional groups. An array of the second functional group will then be presented at the interface in contact with the solution. These functional groups should be of the correct chemistry to interact either electrostatically or through hydrogen bonding with amino acid side chains present at the surface of the protein in its electron transfer binding domain. Such binding and the associated dissociation process should both be rapid so as to constitute an efficient exchange of molecules on the electrode surface. This interaction of the physiological electron transfer binding domain on the redox protein with functional groups on the electrode will often lead to a concomitant orientation of the proteins prosthetic group towards the electrode. Together the above processes result in the observation of near diffusion-controlled electrochemistry.

The hypothesis outlined above has resulted largely from a survey of some 60 surface-modifying species as potential promoters of the electrochemistry of horse heart cytochrome C. The conclusions of the survey are summarized in the categories: nature of the group presented at the interface, delocalised vs. Aliphatic promoters, directionality, distance, and hydrophobic domain.

More sophisticated surface modification through adsorption can be achieved in two ways. Mixtures of surface modifiers on an electrode can be produced by allowing a surface substitution reaction to proceed. Alternatively the use of a bifunctional molecule can equally yield an electrode-solution interface containing two sorts of fuctional group. We have used a class of such molecules typified by the pyridine-aldehydethio-semicarbazones. We have begun to characterise the electrode reactions of horse heart cytochrome C, cytochrome C 551 and the blue copper protein azurin at electrodes modified by such molecules and their derivatives.

4.3

ELECTRON CHARGE TRANSFER AT BIOLOGICAL-SOLUTION INTERFACE

JOHN O'M. BOCKRIS
Dept. of Chemistry, Texas A&M University, College Station (USA)

In the experimental part of this work it was attempted to manifest electron transfer at a bio-surface in contact with an ionic solution. For this purpose, contact to the membrane (dipalmitoyl phosphatidylcholine containing gramicidin) was made by use of a Langmuir-Blodget trough. Three or five layers of lipid were thus formed on the metal substrate (gold, platinum, or tin dioxide); electronic connection was made to the latter; and aqueous solution containing redox ions (quinone-hydroquinone system) was brought into contact with the electrode in such a way that only the bimembrane was exposed to the solution.

Experiments were particularly oriented to guard against the possibility that electrons could reach the quinone via direct contact of the solutions to the metal through pinholes in the membrane or by diffusion through the membrane. Thus, experiments were made with the biolipid alone, and then with the biolipid-gramicidin mixture.

The behavior of these systems differed radically. The lipid alone showed time dependence in its behavior and finally behaved as though it simply covered the substrate while ions found access to the underlying metal. However, the gramicidin-containing membrane showed no time dependence. Underpotential deposition on it differed from that on the biolipid alone, the latter showing anodic stripping peaks equal to those of the substrate. Tafel line characteristics with the biolipid-gramicidin were radically different from those of the biolipid (which resembled those on the substrate).

It is concluded that inclusion of the protein in the membrane introduced sufficient electronic conductance so that the membrane surface was the source of the electron exchange with the redox system.

The main implication of such a conclusion is that energy conversion by living things may be explained in the framework of interfacial electrochemistry concepts. Thus, consideration of the high energy conversion efficiency of biological systems leads to the idea that mechanical energy may arise via a series of steps, of which a rate-determining one occurs in a fuel cell like element. The mitochondrion is suggested as the site of such entities. The observed efficiency would be consistent with a potential loss of about 0.5 V. The supposed biological fuel cells would be able to act as an electrical power source, driving chemical reactions against their spontaneous direction.

Consideration of electrical conductance in wet proteins shows that ohmic (i.e. non-interfacial) p. d.'s through mitochondrial membranes could be negligible. The cathodic reaction would be the reduction of oxygen, $O_2 + 4H^+ + 4e^- \rightarrow 2H_2O$ and the anodic reaction, $2NADH \rightarrow 2NAD^+ + 2H^+ + 4e^-$. The enzymes are suggested as being molecular, buried in the invaginations of the inner membrane forming the cristae. The cathodes are located on enzymes which are probably on the inner side of the membrane but could be, respectively, on the outer (cathodic), and inner (anodic) side. The elec-

tron transport occurs through proteins within each membrane. The relation of the so-called fuel cell potentials to potentially observable membrane potentials, and those measured by fluorescent probes, will be discussed.

The fuel cells produce electrical energy and this energy is transferred to ADP by an electrolytic route, using electric power from the cells to work the endergonic ATP synthesis. An exponential dependence of the rate of ATP synthesis upon applied potential has been observed.

Biological cells radiate electromagnetically in the 10^9 to 10^{12} c.p.s. region. Such phenomena support a fuel cell model of a biological cell because they demand the presence of mobile electrons.

Sensors based on bioelectrochemical principles

J.Koryta

J.Heyrovský Institute of Physical Chemistry
and Electrochemistry, Czechoslovak Academy of Sciences
Opletalova 25
CS-11000 Prague 1

In this kind of sensors the systems are included using either structural elements of biological entities and their models or processes taken from or modelled after those occuring in organisms.

The first group comprises enzyme, bacterial and tissue electrodes. The most sofisticated are immunoelectrodes.

In the second group particularly the sensors are included that are based on ionophore-facilitated membrane transport. The ion-selective electrodes with natural or synthetic ion-carriers are examples of these systems as well as alkaline earth cation and ionophore determination with electrolysis at the interface of two immiscible electrolyte solutions.

4.5

RAPID DIRECT ELECTRON-TRANSFER OF HORSE HEART CYTOCHROME c AT PROMOTER-MODIFIED ELECTRODES

ISAO TANIGUCHI
Department of Industrial Chemistry, Faculty of Engineering,
Kumamoto University, Kurokami, Kumamoto 860 (Japan)

Direct rapid electron-transfer between a solid electrode and a metalloprotein has recently received much attention. Until recently, metalloproteins have generally shown no voltammetric response at ordinary electrodes because of their slow kinetics, except some special cases[1,2]. However, in recent years, various functional electrodes, on which direct rapid electron-transfer of metalloproteins, especially of cytochrome c (cyt c), takes place, have been developed[2-13]. These electrodes made possible to apply conventional electrochemical techniques, such as cyclic voltammetry, to bioelectrochemical studies.

To accelerate the rate of electron-transfer of cyt c, for example, Eddowes and Hill[3] proposed at the first time that the addition of 4,4'-bipyridine (PyPy) into the solution is effective. Since then, various promoters, which themselves are electroinactive at the potentials of interest but can promote the rapid electron-transfer of cyt c, have been found; bipyridines[3-6,8], purines[9], and others[11].

We have found[5,6,9,12] that sulfur atom is effective to immobilize a promoter onto the surfaces of electrodes such as gold and silver. A bis(4-pyridyl)disulfide modified gold (PySSPy-Au) electrode is a typical example. 4-Mercaptopyridine (PySH) and 6-mercaptopurine (PuSH) modified electrodes were also prepared. These promoter immobilized electrodes, especially a PySSPy-Au electrode, acted as suitable electrodes for the rapid electron-transfer of cyt c in the absence of any promoter or mediator in the solution. At PySSPy-Au and PySH-Au electrodes, the heterogeneous electron-transfer rate constant of cyt c, k^0_{sh}, was estimated to be ca. 5×10^{-3} cm^2 s^{-1}, rapid enough to say reversible in an electrochemical sense. Moreover, a PySSPy-Au electrode has such advantages as easy fabrication, durable working and high stability at various temperatures; these properties encouraged us to apply this electrode for various electrochemical studies of cyt c as will be described later.

In addition to these promoters and promoter-modified electrodes, today, metal oxides[7,13], surface pretreated metals[2] and the edge plane of pyrolytic graphite[10] are known to provide the rapid electron-transfer of cyt c.

To understand better how the acceleration of the rate of the electron-transfer of cyt c originates, we need much knowledge about the surface of these functional electrodes. For this purpose, we examined[14,15] the promoter-modified surfaces by using the surface enhanced Raman scattering (SERS) technique. The SERS spectra of both PySSPy-Au and Ag electrodes showed that PySSPy adsorbed as PyS· through the S atoms with the S-S bond cleavage in the standing up orientation. This is because: (1) a signal at 550 cm^{-1} due to the S-S bond stretching was missing in the SERS spectrum, (2) the SERS signals of a PySSPy-modified electrode were very similar to those of a PySH-modified electrode, (3) the so-called X-sensitive band of

PySH at 1120 cm^{-1} shifted to 1100 cm^{-1} with an increase in intensity in the SERS spectra of the modified electrodes, whereas no appreciable difference in the Raman shift of the signal due to the pyridine ring breathing at 1010 cm^{-1} between a PySH solution and the SERS spectra of modified electrodes, was observed. Interestingly, furthermore, the rapid displacement of cyt c from the electrode surface by the promoter was monitored[14] in the SERS spectrum, by adding PySSPy into a cyt c solution, indicating that the rapid electron-transfer of cyt c takes place on the promoter adsorbed layer.

On the basis of this surface structure of a PySSPy modified electrode, a plausible mechanism for the rapid electron-transfer of cyt c at this electrode would be that the electrostatic interaction between the positively charged lysine residues near the heme of cyt c and the lone-pair electrons of the N atoms of the adsorbed promoter, which are faced out to the solution, gave an appropriate orientation of cyt c at the electrode. This model can explain steep decrease in current for the electron-transfer of cyt c at modified electrodes in acidic solutions; the critical pH value for each modified electrode to work depended on the pK_a value of the promoter (in adsorbed form) for the protonation at the N atom. Since no remarkable change in the SERS spectra of a PySSPy-Au electrode was observed by adding cyt c into the solution, the interaction between cyt c and the PySSPy-Au electrode is not so strong to affect the electronic structure and the orientation of the adsorbed species. Thus, weak hydrogen bonding between cyt c and the adsorbed promoter species is likely for the interaction.

Note, however, that the other types of mechanism for the rapid electron-transfer of cyt c at modified electrodes would also be possible, depending upon the promoter used; e.g., SERS spectra showed[9] that purine and cyt c adsorbed together on an Ag electrode, when purine was used as a promoter, where the rapid electron-transfer of cyt c was achieved.

At a PySSPy-Au electrode, the addition of poly-L-lysine did not affect significantly to the cyclic voltammogram of cyt c; a well-defined redox wave was still observed, unlike the case at an Au electrode in the presence of PyPy[10]. This indicates that poly-L-lysine does neither exclude the adsorbed promoter, because of strong chemisorptivity of PySSPy onto a gold electrode, nor interact with the promoter on the electrode surface. Also, since poly-L-lysine is expected to bind cyt c at negatively charged sites, giving rise to the change in the direction of dipole of cyt c, the dipole-dipole interaction between cyt c and the electrode does not play an important role for the rapid electron-transfer of cyt c at a PySSPy-Au electrode in a phosphate buffer solution (7.04 M NaH_2PO_4 + 0.026 M Na_2HPO_4) containing 0.1 M NaClO, (pH 7.0), although the dipole-dipole interaction is suggested[17] to be important for the reaction of cyt c in vivo.

Using a PySSPy-Au electrode, the formal redox potential of cyt c, $E^{0'}$ which can be easily estimated from the midpoint of the anodic and cathodic peak potentials of the cyclic voltammogram, was measured as a function of temperature (T) to obtain thermodynamic parameters in pH 7 phosphate buffer solutions (pH's 6-8)[12]. In an alkaline solution, the temperature dependence of $E^{0'}$ obtained in the temperature range of 0-55 °C showed biphasic behavior with an intersection point at ca. 40 °C, which would be attributable to a structural change in the protein moiety of cyt c from the similarity of the temperature dependence of $E^{0'}$ to that of the absorbance at 695 nm of ferricyt c. In acid and neutral solutions, a monotonous relationship between $E^{0'}$ and T was observed.

Also, no drastic biphasic dependence of $E^{0'}$ on T was observed in a neutral NaCl solution, when $E^{0'}$ values were measured at a PySSPy-Au electrode in the temperature range of 2-55 °C, although the specific effect of

Cl^- on the temperature dependence of $E^{0'}$ on T was previously reported by other workers[1B] using an OTTLE technique. The type of the supporting electrolyte used ($NaClO_4$, NaCl and NaF) did not affect significantly the temperature coefficient of $E^{0'}$ of cyt c, but changed the $E^{0'}$ values themselves; $E^{0'}$ values obtained in a phosphate buffer solution (pH 7.0) at 25 °C were, 0.021 ± 0.002 and 0.015 ± 0.002 V vs. SCE in the presence of 0.1 M NaCl (or NaF) and 0.1 M $NaClO_4$, respectively. In an alkaline solution with any supporting electrolyte, the biphasic behavior in the $E^{0'}$ vs. T plot was observed. The influences of the environmental conditions on the redox behavior of cyt c can thus be easily examined.

In summary, I would like to stress again the following points:
(1) Among various types of promoters and functional electrodes developed to date, a PySSPy-Au electrode is one of the most effective electrodes for the rapid electron-transfer of cyt c (and probably for related cytochromes). Sulfur atom is effective to immobilize a promoter onto the electrode.
(2) The mechanism for the rapid electron-transfer at functional electrodes has increasingly become clear; an electrostatic interaction (hydrogen bonding is likely) between cyt c and the N atoms of the adsorbed promoter on the electrode is important, although the other mechanism seems to be possible, depending upon the promoters used and other experimental conditions.
(3) Modified electrodes are promising as convenient probes for bioelectrochemical studies; e.g., using a PySSPy-Au electrode, the biphasic dependence of $E^{0'}$ on T was found to be a characteristic of cyt c in an alkaline solution, but neither in acid and neutral solutions nor the specific effect of chloride ion.
(4) Finally, such efforts as those described here, hopefully, provide not only much knowledge for better understanding of the electron-transfer reaction of metalloproteins in vivo and in vitro, but also a basis for the future development of artificial systems having functions of biomolecules.

References

1 K. Niki et al., J. Electrochem. Soc., 124 (1977) 1889.
2 B.F. Bowden et al., J. Electroanal. Chem., 161 (1984) 355.
3 M.J. Eddowes & H.A.O. Hill, J. Chem. Soc., Chem. Commun., (1977) 771.
4 I. Taniguchi et al., J. Electroanal. Chem., 131 (1982) 397.
5 I. Taniguchi et al., J. Chem. Soc., Chem. Commun., (1982) 1032.
6 I. Taniguchi et al., J. Electroanal. Chem., 140 (1982) 187.
7 B.F. Bowden et al., J. Am. Chem. Soc., 104 (1982) 7641.
8 J. Kalndrian et al., Electrochim. Acta, 28 (1983) 1823.
9 I. Taniguchi et al., J. Electroanal. Chem., 164 (1984) 385.
10 F.A. Armstrong et al., J. Chem. Soc., Chem. Commun., (1984) 976.
11 P.M. Allen et al., J. Electroanal. Chem., 178 (1984) 69.
12 I. Taniguchi et al., Bioelectrochem. Bioenerg., 13 (1985) in press.
13 M.A. Barmer & H.A.O. Hill, J. Electroanal. Chem., 170 (1984) 369.
14 I. Taniguchi et al., J. Electroanal. Chem., 175 (1984) 341.
15 I. Taniguchi et al., J. Electroanal. Chem., 186 (1985) 389.
16 M.J. Eddowes et al., J. Am. Chem. Soc., 101 (1979) 7113.
17 W.J. Koppenol & E. Margoliash, J. Biol. Chem., 257 (1982) 4426.
18 C.P. Freidman et al., Bioelectrochem. Bioenerg., 5 (1978) 156; Biochem. Biophys. Res. Commun., 76 (1977) 339.

5.1

DETERMINATION OF BIOLOGICALLY INTERESTING MOLECULES BY PULSE VOLTAMMETRY

J. OSTERYOUNG, M. WOJCIECHOWSKI, A. WEBBER AND E. TAKEUCHI
Department of Chemistry, State University of New York at Buffalo,
Buffalo, New York (U.S.A.)

Pulse voltammetry comprizes a suite of techniques based on current-sampled chronoamperometry, the most important of which are normal pulse, differential pulse, staircase, and square wave voltammetry. These techniques are described in Figure 1.[1] These techniques provide many possibilities for

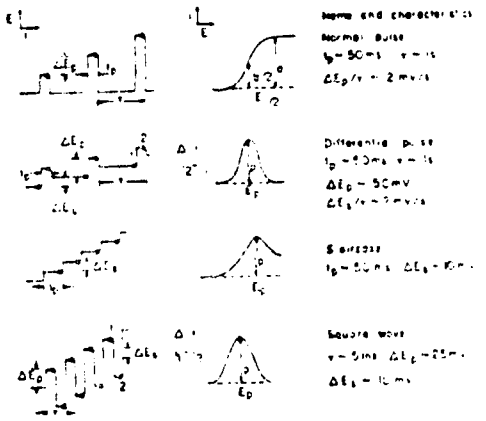

Fig. 1. Potential-time sequence and resulting current-time response in pulse voltammetry

analytical and mechanistic studies of biologically interesting molecules. The examples described here include mechanistic and analytical studies of an antibacterial agent, 1,2-dibromo-2,4-dicyanobutane (DBDCB),[2] of reduced nicotinamide adenine dinucleotide (NADH) and related compounds[3,4] and of a proposed intracellular intermediate in nitrate-induced vasodilatation, N-acetyl penicillamine thionitrite (RSNO).[5] These examples illustrate a range of mechanisms, compound types, techniques, and electrodes.

The Compound DBDCB.[2] In general organic halides undergo irreversible cathodic reduction with formation of halide ions and organic product on products. Vicinal dihalides usually loose halides in a single two-electron step which yields an olefin. Because the cyanide group is strongly electron-withdrawing, halogenated alkyl nitriles are reduced at more positive potentials than corresponding alkyl halides. It is widely observed that mercury electrodes participate chemically in the reduction process. Cyclic staircase voltammetry (Figure 2) shows the strong catalytic effect of the mercury

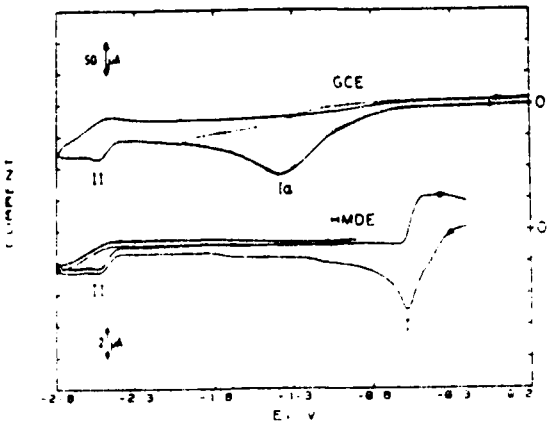

Figure 1. Cyclic voltammetry of DBDCB on glassy carbon electrode (GCE) and on hanging mercury dropping electrode (HMDE) in acetonitrile). The solution was 0.5 mM in DBDCB and 0.1 M in TEAP. The scan rate was 0.63 V s^{-1}.

electrode on the first reduction process which corresponds to the reaction

$$H_2C(Br)-C(CN)(Br)-CH_2CH_2CN + 2e^- \rightarrow C_6N_2H_6 + 2Br^- \quad (1)$$

in which $C_6N_2H_6$ is most probably 2,4-dicyano-1-butene. The solubility of DBDCB in water was determined by reverse pulse polarography[6] as 0.16±0.01%.

The compound NADH.[3] The compound NADH can be converted to and held for a period of hours in its hydrated form which results from adding water across the 5,6-double bond of the nicotinamide ring. This compound adsorbs on mercury surfaces under diffusion-control and gives rise to a cathodic stripping current proportional to concentration in solution. The technique of choice for determination is square wave voltammetry, although staircase voltammetry can be used as well. The detection limit is less than 7 nM, and the range of linear response covers 2-3 orders of magnitude change in concentration of NADH. Nicotinamide adenine dinucleotide (NAD+) and related compounds exhibit very similar electrochemical response, which is due to a 4H+-4e- totally irreversible reduction of the adsorbed adenine moiety.[4]

The compound RSNO.[5] Thionitrites are proposed intracellular intermediates in organic nitrate-induced mammalian vasodilatation. Although these intermediates have been demonstrated indirectly no sensitive quantitative methods for direct determination have been developed previously. On mercury electrodes a reversible pH-dependent wave appears which is the same as that for the parent penicillamine and probably corresponds to the reaction

$$RSNO + Hg + H_2O \rightarrow RSHg + HONO + H^+ + e^- \quad (2)$$

An irreversible wave appears at more negative potentials at both mercury and glassy carbon electrodes which appears to be due to the reaction

$$RSNO + H^+ + e^- \rightarrow RSH + NO \quad (3)$$

This reaction can be used for analytical purposes employing square wave voltammetry as shown in Figure 3 with resulting detection limits ca 40 μM and

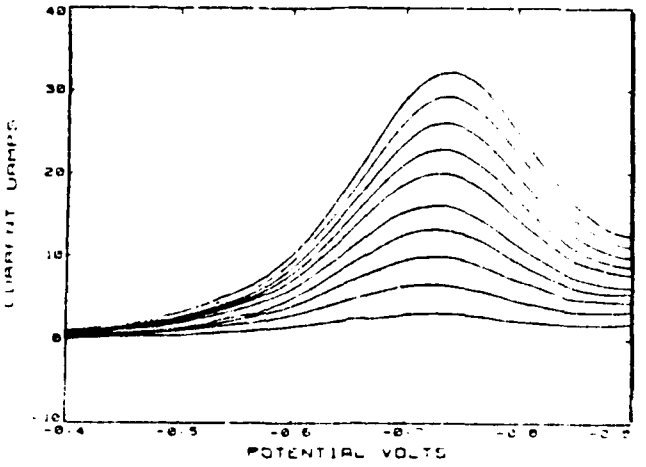

Figure 3. Square wave voltammetry of N-acetyl penicillamine thionitrite from 0.1 mM to 1 mM in steps of 0.1 mM. 0.1 M HCl/KCl, pH 2.0. Step height = 5 mV, amplitude = 25 mV, frequency = 10 Hz.

linear range up to 1.5 mM.

Acknowledgments.

The authors thank John O'Dea, Mumtaz Shah, and Ho-Leung Fung for their assistance. This work was supported by the National Science Foundation of the U.S.A. under Grant Numbers CHE-7917543 and CHE-8505748.

REFERENCES

1. Janet Osteryoung, J. Chem. Ed. 60, 296 (1983).

2. M. Wojciechowski and Janet Osteryoung, Anal. Chem. 57, 927 (1985).

3. A. Webber, M. Shah and Janet Osteryoung, Anal. Chim. Acta 157, 1 (1984).

4. A. Webber and Janet Osteryoung, Anal. Chim. Acta 157, 17 (1984).

5. E. S. Takeuchi, Janet Osteryoung and H.-L. Fung, Anal. Chim. Acta, in press.

6. Janet Osteryoung and E. Kirowa-Eisner, Anal. Chem. 52, 62 (1980).

APPLICATION OF ADVANCED VOLTAMMETRY IN THE ENVIRONMENTAL CHEMISTRY OF ECOTOXIC HEAVY METALS

P. VALENTA
Institute of Applied Physical Chemistry, Nuclear Research Center (KFA) Jülich, D-5170 Jülich (F.R.G.)

In Memoriam H.W. Nürnberg

INTRODUCTION

Efficient and comprehensive control and management of the environmental burden caused by hazardeous chemicals has become an issue of primary importance for man. In this context ecochemical research on the levels, fate and pathways of environmental chemicals have gained great significance. Many toxic chemicals, e.g. ecotoxic metals Cd, Pb, Hg, Cu, Cr and Ni are emitted in large quantities into the environment but afterwards they are rapidly dissipated and occur in most terrestrial and aquatic ecosystems at trace levels. Therefore, the methods of trace chemistry and trace analysis have a key function in ecochemistry and ecotoxicology in the detection and diagnosis of existing pollution and its hazards.

Trace analytical methods have to combine sufficient determination sensitivity with good precision and accuracy if reliable data on environmental pollution levels of hazardeous substances are needed. Among these methods voltammetry in its advanced modes has a wide applicability because it is essentially a substance specific and not just an element specific approach. It happens that nearly all of the metals of particular ecotoxicological significance are well determinable by voltammetry. This applies particularly to Cd, Co, Cr, Cu, Hg, Ni, Pb, Tl and Zn and to the metalloids As and Se. These methods have been successfully applied to the determination of levels of ecotoxic heavy metals in natural waters, body fluids and food and to the investigation of their speciation.

EXPERIMENTAL

Special sampling procedures have been developed to avoid contamination. Thus, for aqueous environmental samples (fresh water, sea water, rain, drinking water) manually sampling with polyethylene flasks fitted eventually to a telescopic fiber gear, Go-Flo-samplers fabricated completely from plastic material or CIT samplers mounted on a hydrowire for sampling at a predetermined depth and automated rain water sampler controlled with a humidity sensor have been developed. Sampling and partitioning of solid samples was performed using instruments of quartz or plastic under a clean bench to exclude contamination by dust from the ambient air. Aqueous samples were filtered through 0.45 µm pore size membrane filters in a closed device under slight N_2-pressure (1 bar).

Filters with the suspended matter were digested by low temperature ashing (LTA) in an oxygen plasma. Body fluids and food samples were subjected to wet digestion with a $HClO_4$-HNO_3 mixture before the

voltammetric analysis. The dissolved organic matter (DOM) was destroyed by photolysis (UV-irradiation) to decompose inert metal chelates.

Voltammetric determination was performed in the differential pulse or the square-wave mode. In-situ electrochemical preconcentration at a mercury or gold electrode under stirring or rotating of the electrode was used at low levels (lower than about 100 µg/l). For Ni, Co and Cr the adsorption of their chelates in a suitable potential range was used in the preconcentration step[6]. The evaluation of the concentration was performed by standard additions.

RESULTS AND DISCUSSION

As a contribution to chemical oceanography and limnology the distribution of ecotoxic trace metals Cd, Cu and Pb in the oceans, coastal waters[3] and in inland waters (rivers and lakes) has been determined voltammetrically. The remarkable accuracy even at the ultra trace level (< 1 µg/l) was established by interlaboratory comparison. A reliable basis for the detection of anthropogenic changes in the North Sea within the coming years has been established by the determination of the dissolved and total concentrations of Cd, Pb, Cu and Ni in the North Sea, Norwegian Sea, Barents Sea and the Eastern Arctic Ocean during several missions from 1975 to 1982. Depth profiles of the concentration of Cd, Pb and Cu in various parts of the oceans have been studied to elucidate the concentration regulation. The levels of the heavy metals Cd, Pb and Hg have been determined in water and sediments of the River Rhine and the main tributaries from Lake Constance to the Dutch/German border within a rather dense sequence of sampling stations[4].

For the input of ecotoxic heavy metals (Cd, Pb, Cu, Zn and Ni) from the atmosphere into terrestrial and aquatic ecosystems their wet deposition with rain and snow in the Federal Republic of Germany has been followed systematically since 1980 with a network of automated samplers of own construction distributed over the various regions of the country (rural areas, urban agglomerations, industrial zones and locations with metallurgical industry[5].

Voltammetry has also been used in the determination of the heavy metal levels in the most important liquid and solid components of the food basket[6] and in body fluids[7]. If the square-wave mode is used the voltammetry has in comparison with the usually used graphite furnace atomic absorption spectrometry the advantage of a simultaneous determination of several metals in one run and of the large linear concentration range.

Voltammetry offers - due to its substance specificity - particular potentialities for investigations on speciation[8,9]. Thus, the complexation capacity, i.e. the sum of the chelating components of the dissolved organic matter (DOM), has been determined in several water types (sea water, lake water, river water) using Cu or Pb as a test metal ion. The chelation of Cd, Pb and Zn in sea water and in lake water with the moderately strong chelator NTA was studied and compared with the natural chelator humic acid. Prognostic predictions on the required ligand concentrations as function of the

stability constant of the inert complex emerged. The rate constants of chelate formation of Cd, Pb and Zn with EDTA in sea water and in lake water have been determined voltammetrically and the mechanism of the complex formation has been elucidated.

REFERENCES

1. L. Mart, Tatanta 29 (1982) 1035-1040
2. B. Pihlar, P.Valenta and H.W. Nürnberg, Fresenius Z. Anal. Chem. 307 (1981) 337-346
3. L. Mart, H.Rützel, P.Klahre, L.Sipos, U.Platzek, P.Valenta and H.W.Nürnberg, Sci. Tot. Environm. 26 (1982) 1-17
4. P.Breder, H.W.Nürnberg, J.Golimowski and M.Stoeppler, in: Pollutants and Their Ecotoxicological Significance, Ed. H.W. Nürnberg, J.Wiley, New York, 1985, p. 205-225
5. H.W.Nürnberg, P.Valenta, V.D.Nguyen, M.Gödde and E.Urano de Carvalho, Fresenius Z. Anal. Chem. 317 (1984) 314-323
6. P.Valenta, P.H. Ostapczuk, B.Pihlar and H.W.Nürnberg, Proc. Int. Conf. Heavy Metals in the Environment, CEP Consult., Edinburgh 1981, p. 619-621
7. H.W. Nürnberg, in: Analytical Techniques for Heavy Metals in Biological Fluids, Ed. S. Facchetti, Elsevier, Amsterdam, 1983, p. 209-232
8. H.W.Nürnberg, Fresenius Z.Anal.Chem., 316 (1983) 557-565
9. P.Valenta, in: Trace Element Speciation in Surface Waters and its Ecological Implications, Ed. G.G. Leppard, Plenum Press, New York 1983, p. 49-69

THE VOLTA POTENTIAL MEASUREMENTS AND THEIR APPLICATIONS IN ELECTROCHEMISTRY

Z. KOCZOROWSKI
Department of Chemistry, University of Warsaw
ul. Pasteura 1, 02-093 Warsaw (Poland)

It is the aim of the lecture to remind the classical basis of the Volta potentials and to show the present state of study of them and their importance in various electrochemical systems.

The Volta potential $\Delta_\beta^\alpha \psi$ is the difference of outer potentials, i.e. of potentials in points situated just outside the phases α and β. Any two-phase electrochemical systems may be characterised by the commonly known relation:

$$\Delta_\beta^\alpha \psi = - z_i F (\alpha_i^\alpha - \alpha_i^\beta) \qquad (1)$$

where α_i^α and α_i^β are the real potentials of the charged species i, defined as the sum of its chemical potential and of the electrical term containing the surface potential of phase:

$$\alpha_i^\alpha = \mu_i^\alpha + z_i F \chi \qquad (2)$$

Relationships (1) and (2) together with

$$\Delta_\beta^\alpha \psi = \Delta_\beta^\alpha \varphi - \Delta_\beta^\alpha \chi \qquad (3)$$

where $\Delta_\beta^\alpha \varphi$ is the Galvani potential of two-phase system make it possible to find some important information from the electrochemical point of view. One should distinquish three basic groups of such information. The first concerns a possibility to measure the real potentials from the relationship (1) for such two-phase systems like metal - metal, metal - solid - electrolyte, metal - liquid solution of electrolyte, electrolyte solutions in two solvents or in the same solvent. This last enumerated system provides the basis for measuring the so-called real activities.

The second group of information originates from the Volta potential measurements of systems where conditions are created to allow measuring the changes in surface potential of one phase only. Such measurements are most popular and they are used in investigation of adsorption on solids and liquids.

The third group deals with measuring of changes in chemical potentials of species in a phase. They are applied for investigation of diffusion and partition potentials (look at the poster by Koczorowski and Zagórska).

The newest most characteristic and most important results of the Volta potential measurements belonging to the three groups are presented. Among them the importance of Volta potential of metal - electrolyte solution system is stressed. This magnitude together with work function of electrons in metal constitutes the absolute electrode potential as it was shown by Trasatti.

The principles are reminded of the Volta potential measurements, namely of the ionization method, the condenser method and jet method. The examples are given of recent experimental setups.

P

POSTERS

01010

1

ELECTROCHEMICAL INVESTIGATION OF SOME SOLID PROTON CONDUCTORS

D.M.Mimić and M.V.Sušić

Institute of Physical Chemistry, Faculty of Science, Belgrade, Studentski trg 16, Yugoslavia

It has been proved that a great number of both organic and inorganic substances in a solid state are characterized by a proton conductivity[1]. Some of these substances show a very good conductivity (a conductivity of liquid electrolytes order) at room temperature already, what proved to be the reason of ever increasing scientific and practical interes for these systems. A proton conductivity depends on the structure of a solid electrolyte, first and foremost on proton bounding energy and on some other energetic and steric barriers that influence on proton mobility. Therefore, investigation of structure, particularly of energetic and steric position of protons, as well as a correlation of these properties with electrochemical properties should be thoroughly carried out. Our research work of this type of electrolyte was directed to acidic phosphates LiH_2PO_4 (A), $UO_2HPO_4.3H_2O$(B) and crystallohydrates $SdBr_2.4H_2O$ (C), $K_2H_2Sb_2O_7.4H_2O$ (D).

The polycrystalline powder of these electrolytes samples was pressed under the pressure of 0.5 GPa in pellets thickness of 1-3mm and diameter of 8 mm. Electrochemical analyses were performed in three-electrode system (Pt being the working and Ag both reference and counter electrode) by electrocnemical system PAR 170 at several different temperatures.

It is evident from cyclovoltamograms, Fig.1(a-d) that both the cathodic and anodic decomposition of A,B,C and D electrolytes was carried out at room temperature.

The anodic decomposition of crystallohydrates corresponded to oxidation process of OH^- group: $2OH^- - 2e \longrightarrow 1/2O_2$, equilibrium potential E_r=0.5 V while oxidation of PO_4^{3-} group occured acidic phosphates: $PO_4^{3-} - 2e \longrightarrow 1/2O_2 + PO_3^-$, E_r=1.2V[3]. Decomposition voltage of the mentioned electrolytes are given in Table I.

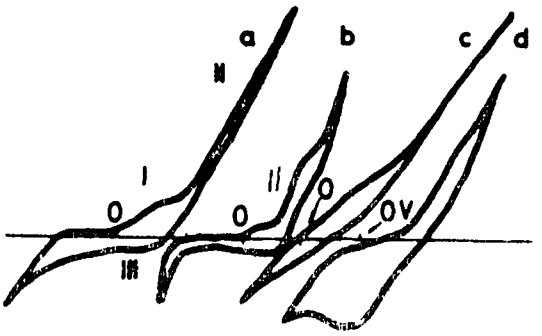

Fig.1 Cyclic voltammograms at room temperature: a) LiH_2PO_4 for E_i=2.0V i E_f=-2.0V; b) $UO_2HPO_4.3H_2O$,E_i=1.5V and E_f=-2.0V; c) $CdBr_2.4H_2O$,E_i=0.5V and E_f=-2.0V; d) $K_2H_2Sb_2O_7.4H_2O$, E_i=2.0V and E_f=-1.6V.

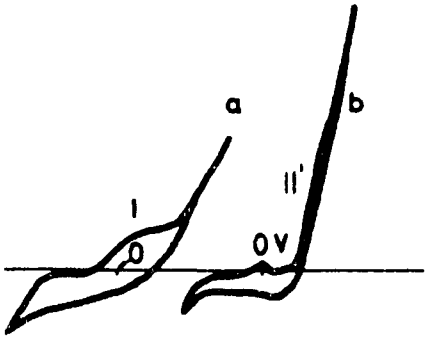

Fig.2 Cyclic voltammograms: a) LiH_2PO_4 at 365K for E_i=2.0V and E_f=-2.0V and b) $UO_2HPO_4.3H_2O$ at 345 K, E_i=1.4V and E_f-1.5V.

Anodically evoluted oxygen was partially deposited along the electrode, as well as near electrode layer and was reduced before hydrogen, during cathodic polarization, peak I. The increase in temperature and the prolongation of anodic polarization was followed by the rise in height of these peaks. Besides, the reduction of H^+ ions was evident in all the cases within the cathodic potential field $H^+ + e \rightarrow 1/2H_2$. It can be seen from the Figure that the evoluted hydrogen either of lower or greater quantity detained along the electrode or near electrode layer and was oxidized during recurrent polarization,peak III.

The equilibrium potential of this process and the exchange current were determind by application of the Tafel equataion on polarization

curves. At this, the correlation for ohm drop through electrolyte was made on the basis of measured resistance, Table I.

Table I. Decomposition voltage U_r, equilibrium potential E_r and exchange current i_o of cathodic evolution of hydrogen on Pt electrode.

Electrolyte	Temperatura K	U_r /V/	E_r /V/	i_o /mA/
LiH_2PO_4	293	2.1	-0.9	15.15
	355	2.0	-0.8	47.86
	398	1.9	-0.7	31.20
$UO_2HPO_4.3H_2O$	293	1.9	-0.7	1.10
	338	0.9	-0.4	69.18
$NdBr_2.4H_2O$	293	1.0	-0.4	3.16
$K_2H_2Sb_2O_7.4H_2O$	293	1.0	-0.44	0.41

Having considered the values in Table I we noticed that equilibrium potential of H^+ reduction depended on the bonding energy existing between H^+ ions which was -0.8V aproximately when acidic salts are concerned and -0.4V approximately when crystallohydrates are considered. The structural changes caused by dehydration due to heating of samples provoked the changes of electric properties, too. With the beginning of acid crystallohydrate dehydration at 323 K approximately, the cathodic reduction of acidic hydrogen at -0.8V approximately was proceeded by reduction of H^+ ions, peak Π', which originated from a crystal water, Fig.2.

Literature

1. L. Glasser, Chem. Rev. 75(1975) 21.
2. M. G. Shilton and A. T. Howe, Mater. Res. Bull. 12(1977) 701.
3. M. Pušić and D. Minić, Solid State Ionics 6(1982) 327.
4. M. Pušić and D. Minić, ibid 2(1981) 309.

01020

PHASE TRANSITIONS IN INSERTION COMPOUNDS

T. Jacobsen, K. West, B. Zachau-Christiansen and S. Atlung
Fysisk-Kemisk Institut , The Technical University of Denmark
DK 2800 , Lyngby , Denmark

In insertion compounds, relevant for secondary battery electrodes, metal ions can be incorporated into the host lattice according to the electrochemical reaction:

$$x\ M^{+} + x\ e^{-} + H \rightarrow M_xH \qquad (1)$$

Due to the finite number of sites, determined by structural and electronic properties of the host compound, the species inserted can be treated as a highly non-ideal lattice gas. In many cases strong attractive forces are present and phase separations inside the host lattice are often observed. This condensation phenomenon is illustrated by the linear sweep voltammograms in fig.1 indicating a phase transition at 2.55 V [1].

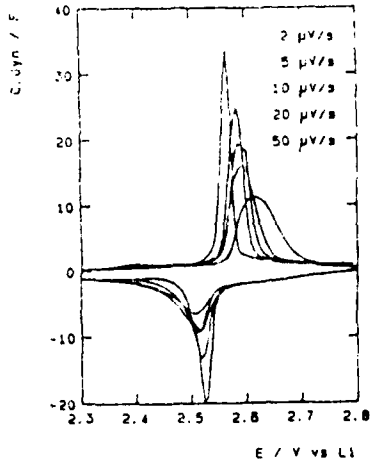

fig.1 Dynamic capacity for Li insertion in $VO_2(B)$.

The present work is a computer study of the phase transition reaction with emphasis on the solid state diffusion process. To treat diffusion in a non-ideal lattice gas the uni-dimensional transport equation is written as:

$$J = -bx(1-x)(\partial \mu_M / \partial z) \qquad (2)$$

where x is the propability of a site to be occupied by a guest ion and (1-x) the probability of finding an empty neighbouring site. Considering only first order deviations from ideality the chemical potential of inserted species is given by:

$$\mu_M = \mu^{\circ}_M + RT\ln[x/(1-x)] + f(x-0.5) \qquad (3)$$

where x-0.5 is taken as standard state and f is the interaction parameter. For values of f below -4 this expression is no longer a monotonic function of x and phase separation occurs. From eqs. (2), (3) and the condition of mass conservation the following analog to Fick's second law is obtained:

$$\frac{\partial x}{\partial t} = -\frac{\partial}{\partial z}(D_o[1 + fx(1-x)]\frac{\partial x}{\partial z}) \qquad (4)$$

This diffusion equation has an interesting feature. Below the critical value of the interaction parameter the enhancement factor (the square bracket) turns negative in the region where the μ-x relation has a negative slope. As consequence stable solutions contain a discontinuity and phase separation is an inherent property of the transport equation. Furthermore, since eq (4) has the form of the second Fick law with a diffusion coefficient depending on composition it can be solved numerically with a simple computer routine without the introduction of moving boundary conditions.

In the surface charge transfer reaction the metal ion is removed from the solvating electrolyte phase and inserted in the surface layer of the host lattice. Taking the interactions in the insertion phase into account and assuming these to have no influence on the transition state, the Volmer Butler equation is modified to:

$$i_+ = Fx^*k^o\exp[\frac{(1-\alpha)(\varepsilon-\varepsilon^o)F}{RT} + f(x^* - 0.5)] \qquad (5)$$

$$i_- = -F(1-x^*)c_M k^o\exp[\frac{-\alpha(\varepsilon-\varepsilon^o)F}{RT}] \qquad (6)$$

where k^o is the rate constant at the standard potential ε^o (x=0.5 and c_M=1 mol dm^{-3}) and x^* is the degree of insertion in the surface.

To investigate the phase transition, linear sweep voltammograms have been simulated for an insertion electrode of finite thickness L by a finite difference method. In this case the diffusion equation (4) is solved with the boundary conditions:

$$z = L \Rightarrow J = 0 \qquad (7)$$

$$z = 0 \Rightarrow J = -D_o(1+fx(1-x))\frac{\partial x}{\partial z} = F(i_+ + i_-) \qquad (8)$$

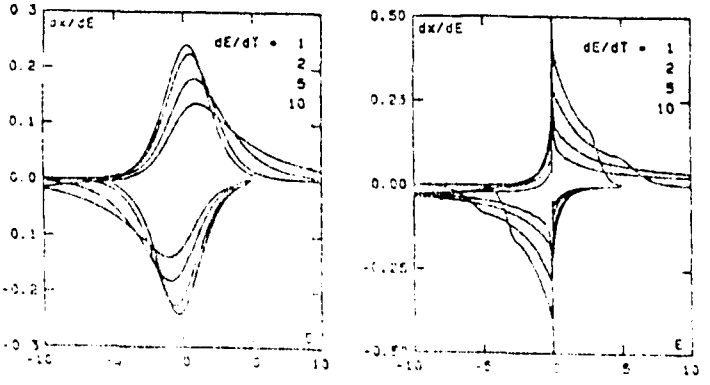

Fig.2
Simulated sweeps for f=0 and f=-4.2

In fig.2 simulations performed for f=0 (ideality) and f=-4.2 (miscibility gap : 0.31<x<0.69) are shown. In both cases equilibrium for the surface reaction was assumed. Whereas the ideal electrode exhibits an almost reversible behaviour, the phase transition introduces a pronounced hysteresis, even at very low sweep rates. Furthermore, the extremely narrow peak (in theory a delta function), when the phase transition occurs on the electrode surface, is noted.

To illustrate the formation and movement of the phase boundary concentration profiles are plotted in fig.3.

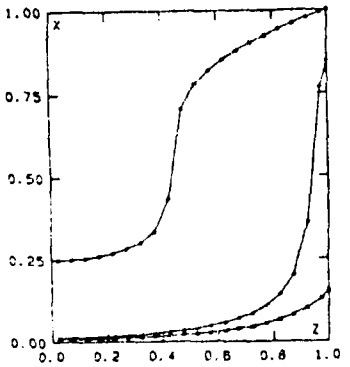

Fig.3 Concentration profiles for f=-4.2 and $\frac{d\xi}{dT}$=10

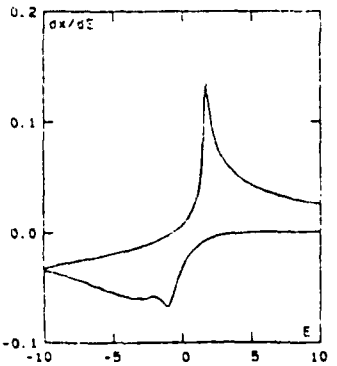

Fig.4 Simulated sweep for f=-4.2, $\frac{d\xi}{dT}$=10, K=1, α=0.5

Due to the presence of iR drops and surface kinetics linear sweep voltammograms do in practice not show the delta function behaviour of fig.2 [2]. In fig.4 the effect of surface kinetics is included and the broadening of the peaks is seen.

TABLE I Dimensionless quantities

Length	$Z = z/l$
Time	$T = tD_o/L^2$
Potential	$E = \varepsilon F/RT$
Rate constant	$K = k^oL/D_o$

REFERENCES

1. B. Zachau-Christiansen, K. West and T. Jacobsen, *Mat. Res. Bull.* 20 1985. In press.
2. J.R. Dahn and R.R. Haering, *Solid State Ionics* 2 19 (1981)

01030

AUTOMATED FOUR-PROBE MEASUREMENT OF THE TEMPERATURE DEPENDENCE OF THE CONDUCTIVITY OF POLYCRYSTALLINE SOLID ELECTROLYTES

P.Linhardt, M.Maly-Schreiber and M.W.Breiter
Institut für Technische Elektrochemie, TU Wien, 9 Getreidemarkt, A-1060 Wien, Austria

An automated set-up for the four-probe measurement of the conductivity of a solid electrolyte as a function of temperature was described in a previous communication[1]. Essentially, the AC voltage across a standard resistor is compared with that between the two inner contacts with respect to the absolute value and phase angle. Since the standard resistor and the amplification of the two signals remain constant, the accuracy of the measurement is good for comparable values of the resistor and of the said impedance. The accuracy decreases when the resistor and the impedance are vastly different. Satisfactory accuracy is only achievable in a limited temperature range. The overall accuracy was improved by a modified set-up which makes use of the logarithmic output of the gain phase meter (HP 3575A).

A schematic diagram of the new set-up is shown in Fig.1. The sample with the leads and inner contacts is held inside the alpha alumina tube of a small furnace surrounded by insulating material. The attachment of the leads and inner contacts was the same as in the previous work[2] of one of the authors. The furnace and the insulation are kept inside a glass vessel with a removable lid under an inert atmosphere. The furnace is heated by DC power from a programmable power supply (HP 6269B). The personal computer (HP 86B) controls the increase or decrease of the temperature with time. The heating rate is nearly a linear function of time and can be varied between 0.1 and 10 K/min. A thermocouple in close contact with the solid electrolyte cell measures the temperature.

At predetermined intervals the AC signals between the two inner contacts and across a standard resistor are amplified and recorded by the data acquisition unit (HP 3412A) under control of the PC. The AC current is supplied by a suitable potentiostat operating in the galvanostatic mode. The frequency can be varied between 1 and 10000 Hz. The data acquisition unit also records the output voltages of the gain phase meter and the voltage of the thermocouple. Since the inputs of the phase meter are grounded, they have to be connected to the outputs of the differential amplifiers of the same make in the amplification stage (see Fig.1). The acquisition unit transfers the data point by point to the PC. The processed data are available in the form of a disc and/or listings and different forms of plots produced by a printer (HP 82906).

To reduce the influence of a contact resistance at the two inner contacts the input impedance of the amplifier is made large ($9\ 10^9$ ohm). This reduces the AC current which flows through the contacts and the input impedance. A second possibility of an influence of the contacts on the measured conductivity arises when the good conductivity of the relatively wide contacts (brushed on silver paint) makes a part of the AC current enter at one side of each of the two contacts (transition from ionic to electronic conductivity) and leave at the other side (transition from electronic to ionic conduction). The phase angle which should be close to 0 in the absence of contact effects indicates when the influence of the second possibility has to be considered. The effect depends upon temperature and frequency.

The processed data of measurements on three isomorphs (Na, Ag and Pb beta" alumina), produced by ion exchange from polycrystalline material (about 85% beta" alumina and 15% beta alumina) from Brown, Bovery & Cie., are shown as (T) versus 1000/T in a semilogarithmic plot in Fig.2 as an example. The plots for Na and Ag beta" alumina are similar to those obtained[2] on the respective isomorphs made from Ceramatec Inc. material. The conductivity of Pb beta" alumina is much better than the values quoted in reference 3.

References.

1. P.Linhardt, M.Maly-Schreiber and M.W.Breiter, Proceedings of the Sixth RISO International Symposium on Materials Science, 1985, in print
2. M.W.Breiter and B.Dunn, Solid State Ionics 7 (1983) 227
3. E.E.Hellstrom, Extended Abstract A1-11, 35 th ISE Meeting, Berkeley, 1984

Acknowledgement.
Support of the project by the Austrian Fonds zur Förderung der wissenschaftlichen Forschung is gratefully acknowledged. The authors thank Brown, Bovery & Cie. for supplying the solid electrolyte material with which the ion exchanges were made.

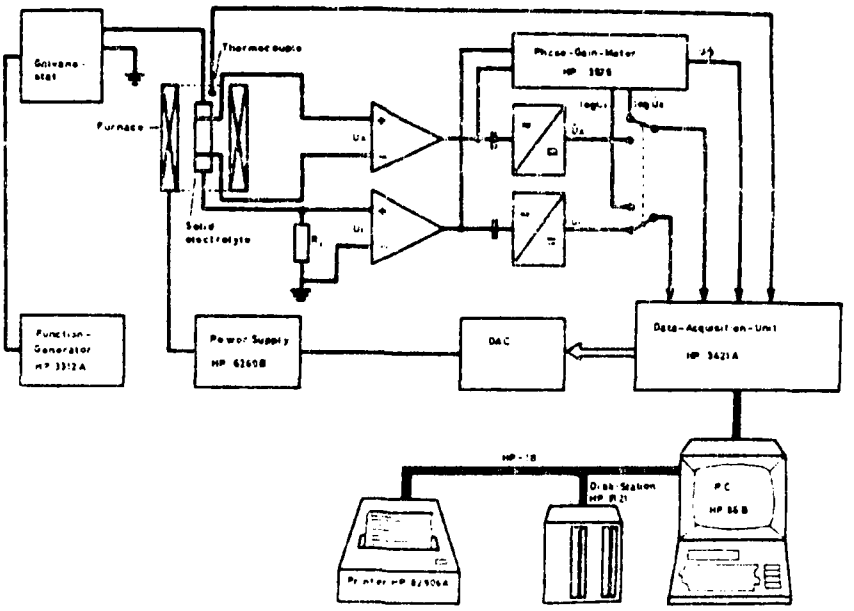

Fig.1. Schemetic diagram of the set-up.

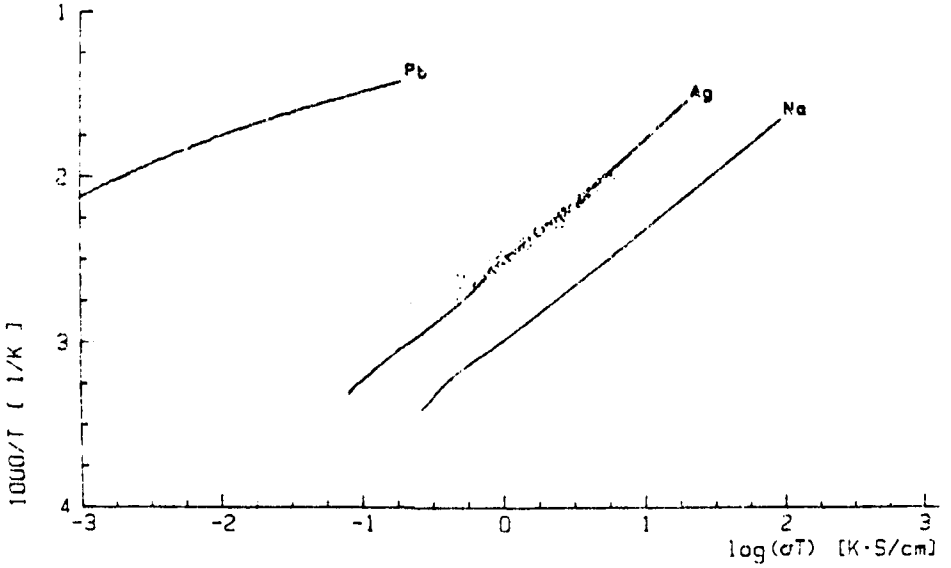

Fig.2. Plots of the product (σT) versus 1000/T for polycrystalline lead, silver and sodium beta" alumina.

01040

AN ELECTROCHEMICAL REDOX REACTION IN A SOLID MATRIX

Tsutomu Ohzuku and Keijiro Sawai
Electrochemistry and Inorganic Chemistry Laboratory,
Department of Synthetic Chemistry, Faculty of Engineering,
Okayama University, Okayama 700, Japan

Taketsugu Hirai
Industrial Inorganic Chemistry Laboratory,
Department of Applied Chemistry, Faculty of Engineering,
Osaka City University, Sugimoto 3-3-138, Sumiyoshi,
Osaka 558, Japan

Mixed valence compounds containing an element in two different oxidation states in a crystal lattice seem to be able to offer a class of electrode system unique in electrochemistry (1,2). In the previous paper(3), we have dealt with the expression on the electrode potential for Prussian blue(PB)/Everitt's salt(ES) system from a stastical thermodynamic consideration and the differences between a redox reaction in a solution and that in a solid matrix have been discussed.

The final equation which was derived in the paper was

$$E = E_0 + \frac{RT}{F}\ln(a_R) - \frac{RT}{F}\ln\frac{n_e}{(n_0 - n_e)} - \frac{RT}{F}\ln\frac{n_R}{(n_0 - n_R)} \quad (1)$$

where

$$E_0 = \frac{\mu_R^{\ominus El}}{F} - \frac{(\mu_e^{\ominus PB} + \mu_R^{\ominus PB})}{F} \quad (2)$$

According to eqs.(1) and (2), the 59 mV dependence at 25°C with respect to $\log(a_R)$ and the different E_0 values with different R ions would be expected. In order to understand the electrode potential of PB/ES system more in details, this series of experimental works were carried out.

Thin film of PB was electrochemically prepared on Pt. Electrodes were cathodically polarized at 40 $\mu A \cdot cm^{-2}$ for 120 sec in freshly prepared the mixed electrolyte (0.02M $FeCl_3$, 0.02M $K_3Fe(CN)_6$) at room temperature(4). Thin film of PB deposited on Pt-electrode was rinsed with distilled water to remove a part of undesirable chemical species from an electrode surface. The prepared electrode were soaked in the same concentrations of RCl solutions (R^+ = Cs^+, Rb^+, NH_4^+, K^+, Na^+ and Li^+) as those to be examined for about 3 hours before use. Cyclic voltammetry was performed using a potentiostat Model PGS-1525 (Kowa Electronics Works, Co.Ltd.,Japan) combined with a function generator Model FG-101 (Kowa Electronics Works) and the data were recorded on a Houston Model 100 X-Y recorder.

Figure 1 shows the shapes of voltammetric peaks for the reduction of PB and the oxidation of ES in RCl solution. The voltammetric reduction peak of PB and the oxidation of of ES were

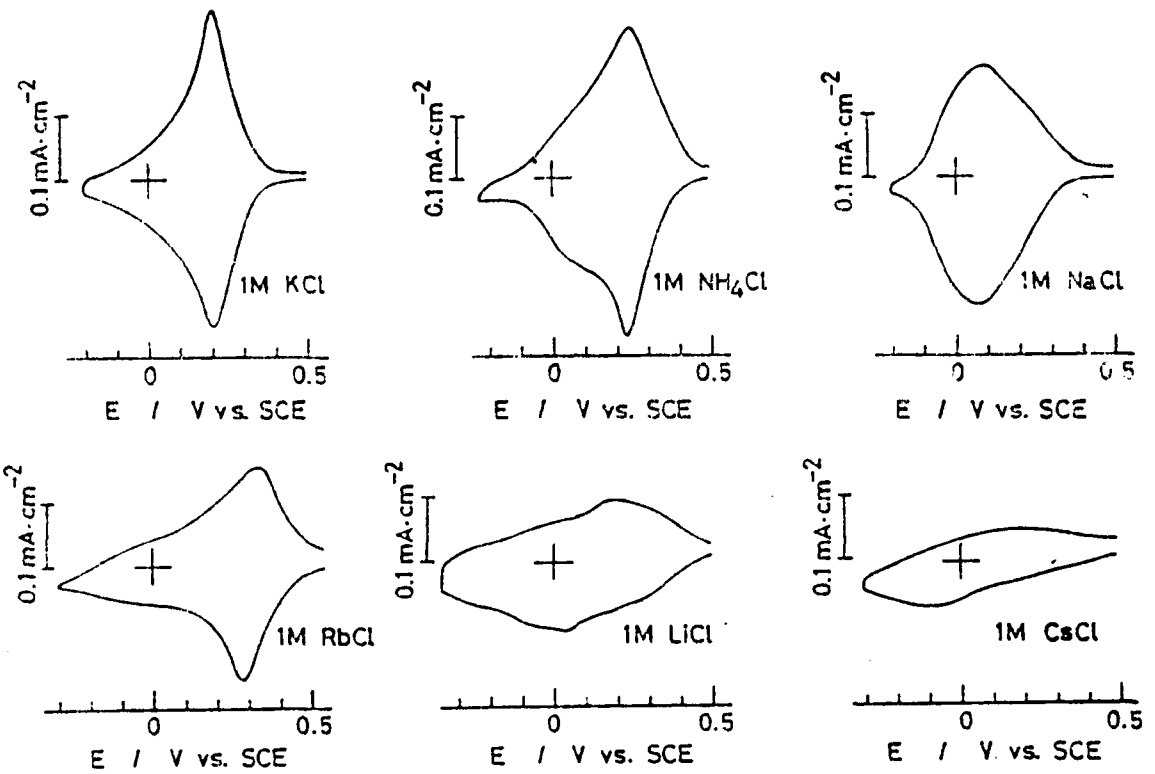

Fig.1 Voltammetric shapes of PB/ES electrode system in RCl solution (R^+ =Li^+, Na^+, K^+, Rb^+, Cs^+ and NH_4^+). Sweep rate : 0.01 V·sec^{-1}.

almost symmetrical up to the sweep rate of 100 mV·sec^{-1} in RbCl, NH_4Cl, KCl and NaCl solution. Well-defined voltammetric peaks, however, were not observed in LiCl and CsCl solution, suggesting that the dimentional limit with respect to ionic radius exist for the insertion of cation into the PB matrix.

The peak potentials and the mid-points of them were shifted toward the anodic direction with increasing in RCl (Rb^+, NH_4^+, K^+ and Na^+) concentrations as a function of $(RT/F)\ln(a_{R^+})$ as was shown in Fig.2. The mid-points of anodic and cathodic peaks (E^0) at a_{RCl} = 1 were summarized as the standard electrode potential (E_0) of PB/ES electrode system in Table 1. The E_0 values depended on the types of cations used as was expected from eq.(2),. From these experimental results, we will discuss on how to define the standard electrode potential of such an electrode system from a thermodynamic point of view.

References

(1) D.Ellis, M.Eckhoff and V.D.Neff, J.Phys.Chem.,85, 1225 (1981)
(2) L.M.Siperko and T.Kuwana, J.Electrochem.Soc.,130, 396

(3) T.Ohzuku, K.Sawai and T.Hirai,ibid.,submitted.
(4) K.Itaya, H.Akahoshi and S.Tosnima, ibid.,129, 1498(1982)

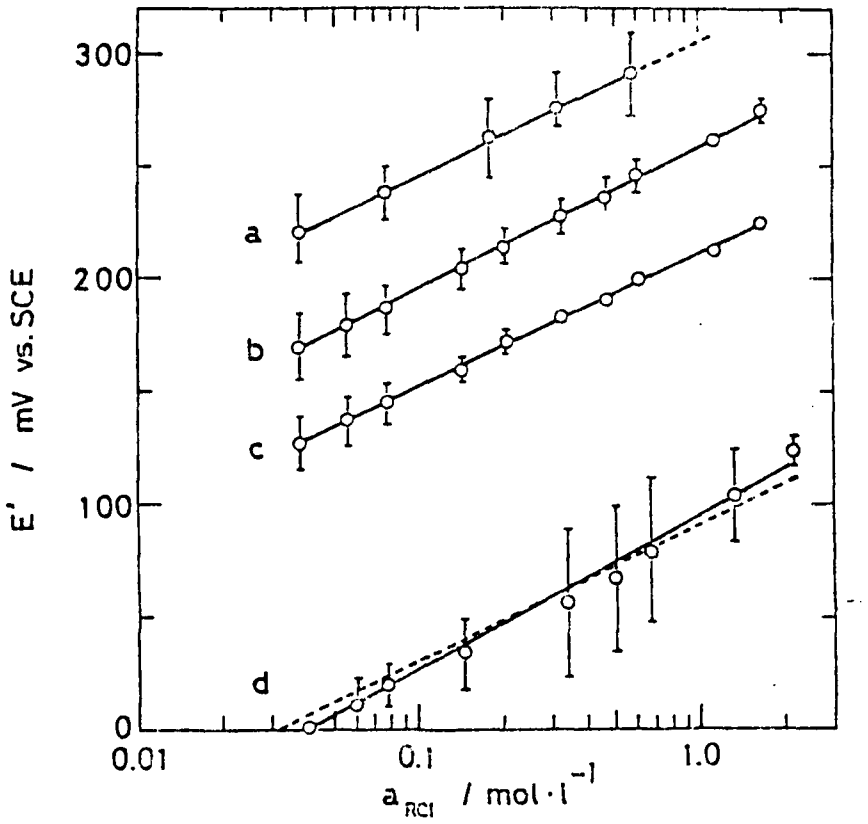

Fig.2 The mid-point of anodic and cathodic peak (E') vs. $\log(a_{RCl})$ plots for PB/ES electrode system. (a) RCl, (b) NH_4Cl, (c) KCl and (d) NaCl.

Table 1 The standard electrode potential of PB/ES electrode system in RCl solution.

R^+	E_0		ΔG^0
	mV vs.SCE	mV vs.SHE	kcal·mol^{-1}
Li^+	---	---	---
Na^+	94 ± 10	338 ± 10	- 7.794 ± 0.231
K^+	212 ± 2	456 ± 2	-10.515 ± 0.046
NH_4^+	258 ± 4	502 ± 4	-11.576 ± 0.092
Rb^+	306 ± 4	550 ± 4	-12.683 ± 0.092
Cs^+	---	---	---

01050

SEPARATION OF FARADAIC AND CAPACITIVE CURRENTS IN CONDUCTING POLYMER VOLTAMMETRY

E. VIEIL and J.F. OUDARD
Laboratoire d'Electrochimie Organique et Analytique (UA CNRS 321)
Laboratoires de Chimie, Département de Recherche Fondamentale,
Centre d'Etudes Nucléaires de Grenoble,
85 X, F-38041 GRENOBLE CEDEX, France.

Capacitive phenomena are very important perturbations in the electroanalysis of conducting polymers like polypyrrole, and are complicated by the dependence of the capacitance upon the oxidation state as shown by FELDBERG [1].

The approach presented here is based on deconvolution procedures allowing extraction of the pure faradaic response of a linear potential sweep voltammetry. Two distinct cases can be handled :

- The electrochemical mechanism is known (reversibility, semi-infinite or restricted diffusion or absence of mass transport, number and nature of the steps, ...) but not the dependence law of the capacitance versus the faradaic charge : This last law can be determined together with the evaluation of eventual resistive effects.

- The opposite case of a known variation law for the capacitance, measured by an impedance method for example, or by analysis of limiting cases in cyclic voltammetry, and an unknown electrochemical mechanism. This is the most interesting situation which can also be treated in presence of resistive effects.

Application of this method is illustrated with polypyrrole films voltammetry.

1. S.W. FELDBERG, J. Am. Chem. Soc., 106 (1984) 4671.

2

02010

STUDY BY POTENTIAL MODULATED SPECULAR REFLECTANCE SPECTROSCOPY OF ANODIC IRIDIUM OXIDE FILMS.

J.I. PEÑA, M.A. MARTINEZ, Ma SANCHEZ and C. GUTIERREZ
Instituto de Química Física "Rocasolano", C.S.I.C.
Madrid (Spain)

Since the discovery in 1975 of the electrochromic effect of thick anodic iridium oxide films by Buckley and Burke[1], many works have appeared on this system, due to its potential use as display. Much effort has been devoted to the identification of the changes in oxidation state of iridium corresponding to the four peaks which can be seen in cyclic voltammograms, such as that in 0.1M H_2SO_4 shown in Fig. 1. The main peak (designated as II) corresponds to the coloration-bleaching process occurring at more positive-more negative potentials, respectively. Most researchers agree[2] that it is due to a change in the oxidation state of iridium, from Ir(III) to Ir(IV).

The in-situ technique of Potential-Modulated Specular Reflectance Spectroscopy (PMSRS) knew a short-lived surge of interest in the early 70s, as it was then thought that this technique could throw light on many unsolved problems of Interfacial Electrochemistry[3]. PSMRS is inexpensive and experimentally simple. However, when used for identification of mono-or multilayers electrodeposited on the electrode, interpretation of the results is far from simple.

The technique was conventional: a 100 mV peak-to-peak sinusoidal modulation was applied to the electrode, and the change (ΔR) in the specularly reflected light (R) was detected with a lock-in amplifier.

The oxide films were grown by triangular potential cycling at 200 mV/s between 0 and 1500 mV vs reversible hydrogen electrode (RHE). The shape of the spectra was independent of the thickness of the oxide layer, which shows that the maxima observed are not due to interference effects. Typical PMSR spectra are shown in Fig. 2. They correspond to peak II in acid, neutral, and basic media (pH 0.9, 6.9 and 12.4, respectively). There is an absorption maximum at 360-380 nm, which shows that it corresponds to the same process. Apparently the different coordination spheres of the iridium ion , with different proportions of H_3O^+, H_2O and OH^- species, do not nearly change the absorption spectrum of the Ir ion. An extreme example of this constancy of the spectrum is that of the Cr^{3+} ion , which shows the same two maxima at ~ 430 and 600 nm, either in aqueous solution as $Cr(H_2O)_6^{3+}$ ion, or in the green, solid sesquioxide Cr_2O_3

It is to be noted that the spectrum obtained when stopping the potential sweep at the anodic peak exactly coincided with that obtained when stopping at the cathodic peak, i.e. reversibility seems to be perfect.

A very interesting fact is that the wavelength of the main absorption maximum increases linearly with peak potential (i.e. with increasing oxidation of the anodic film), as is shown in Fig. 3. We can offer no explanation for this relationship.

Finally, in Table I we present the absorption maxima observed in 0.1M H_2SO_4 at several potentials. It is clear that each peak has a typical absorption spectrum. The maximum at 280-300 nm constitutes an exception, as it appears over the whole potential range. This could be due to dismutation of the higher oxides, perhaps by a mechanism such as that proposed by Kötz et al[2]:

$$IrO_3 + H_2O \longrightarrow IrO(OH)_2 + 1/2\ O_2\uparrow$$

The absorption maxima at neutral and basic pH basically coincide with those observed for the same peaks at acid pH. As said before, this implies that the electronic levels of a given oxidation state of Ir are not altered much when OH^- is substituted for H_2O in the coordinations sphere of Ir.

Transmission spectra of KBr pellets of Ir oxides from Fluka showed the following absorption maxima

Ir_2O_3 : 430 nm, 525 nm, 640 nm (weak)
IrO_2 : 270 nm (weak), 440 nm (very broad), 640 nm (weak).

Unfortunately, these data do not allow us to assign oxidation states to the absorption maxima observed in the PMSR spectra.

Table I. Absorption maxima in PMSR spectra of an iridium electrode in 0.1M H_2SO_4, pH 0.9.

	Pot. vs RHE/mV	Absorption maximum/nm				
Peak II_a	950	280				580
	1060	260(sh)	320			580
	1100	290	330(sh)			
	1140	300(sh)	350			580
Peak III_a	1250			400		
	1280	270(w)		415		
Peak IV_a	1400	280(sh)			450	
	1480				440	
Assignment		see text	Peak II	Peak III	Peak IV	Peak II

References

1. D.N. Buckley and L.D. Burke, J. Chem. Soc., Faraday Trans. I, 71, 1447 (1975).
2. R. Kötz, H. Neff, and S. Stucki, J. Electrochem. Soc., 131, 72 (1984).
3. "Optical studies of adsorbed layers at interfaces", Faraday Symp. No. 4, The Faraday Society, London, 1970.

Fig. 1

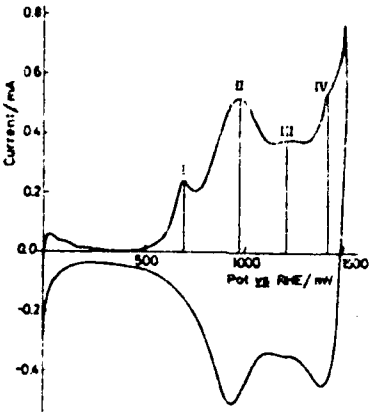

Fig.2

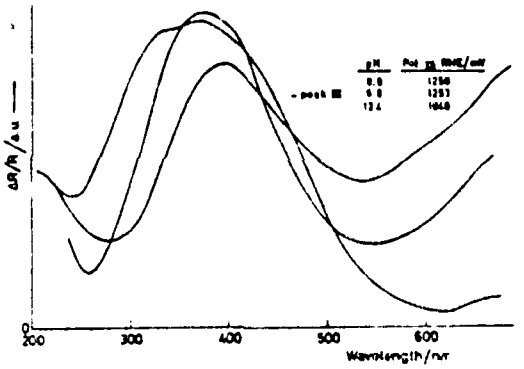

Fig.3

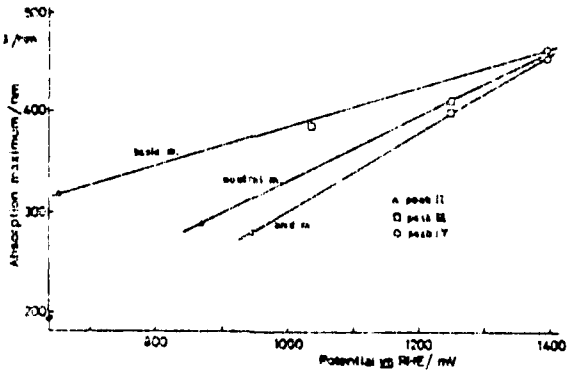

02020

ELECTROFORMATION OF ANODIC OXIDE FILMS ON NICKEL PRODUCED BY SQUARE-WAVE POTENTIAL SIGNALS

A. Visintin*, A.C. Chialvo**, W.E. Triaca* and A.J. Arvia*
* Instituto de Investigaciones Fisicoquímicas Teóricas y Aplicadas (INIFTA)
Casilla de Correo 16, Sucursal 4, (1900) La Plata, ARGENTINA

** Programa de Electroquímica Aplicada e Ingeniería Electroquímica (PRELINE)
Santa Fe, ARGENTINA

INTRODUCTION

Nickel oxide films are usually obtained either by chemical or electrochemical precipitation of nickel hydroxide on different substrates[1-4]. On the other hand, the direct anodic oxidation of nickel in alkaline solution seems to be not a suitable method to obtain thick oxide films[5].

The present work describes a square wave potential anodizing procedure which promotes the macroscopic growth of thick oxide films on nickel electrodes in alkaline solution.

EXPERIMENTAL

Runs were made in a three electrode compartment Pyrex glass cell. The working electrodes were nickel wires 1 cm long and 0,5 mm diameter. A large platinum counterelectrode was used. The counterelectrode compartment was connected directly to the rest of the cell to minimize the ohmic drop between electrodes. Runs were made in NaOH solutions at different concentrations between 0.1 M and 2 M at 30°C. A hydrogen reference electrode in the same electrolyte solution was employed.

The anodizing procedure consisted of applying a square wave potential signal (SWPS) to the working electrode between lower (E_ℓ) and upper (E_u) potential limits at a certain frequency (f) during a certain time (t).

RESULTS

When a nickel electrode is subjected to the SWPS under a proper set of potential perturbation conditions a thick anodic oxide film is formed. Voltammograms run at 0,1 V/s between 0,05 and 1.55 V show a remarkable increase in the electrooxidation/electroreduction charges associated with the presence of the nickel oxide film in the potential range of the Ni(II)/Ni(III) redox system.

The relative increase in charge (R) is evaluated through the relationship:

$$R = (Q_o)_a/(Q_o)_b$$

where Q_o denotes the electroreduction charge associated with the nickel oxide film before (b) and after (a) the SWPS treatment.

The dependence of R on the characteristics of the SWPS was determined in a 0.1 M NaOH solution. Thus, when E_ℓ = -1.3 V, f = 2.5 kHz and t = 1 min, the R vs E_u plot shows two maximum values of R close to 20 and 25 at 1.6 and 1.7 V, respectively. On the other hand, for constant E_ℓ, f and t (E_ℓ =

1.7 V, f = 2.5 kHz, t = 3 min) the dependence of R on E_ℓ presents a maximum at E_ℓ = -1.6 V.

The dependence of R on f was also determined. For E_u = 1.7 V, E_ℓ = -1.6 V and t = 3 min, there is an optimal frequency at ca. 2.5 kHz. The lower threshold frequency to obtain a remarkable increase in the value of R is ca. 0.5 kHz, a value previously reported for oxide films formation on platinum[6]. Furthermore, the value of R depends on the duration of the SWPS. For E_u = 1.7 V, E_ℓ = -1.1 V and f = 2.5 kHz, R initially increases linearly with t, attains a maximum value at t = 1 min and then decreases with t.

DISCUSSION

The present results demonstrate that the application of the SWPS to a nickel electrode in alkaline solution under carefully preset potential perturbation conditions promotes the macroscopic growth of a thick anodic oxide film and correspondingly a remarkable increase in the charge storage capacity. The preliminary results suggest that the growth of the anodic oxide film under SWPS follows a mechanism similar to that recently discussed for the oxide films on noble metals[6,7].

REFERENCES

1. P. Kelton, A.D. Sperrin and F.L. Tye, in "Power Sources", Vol. 4, D.H. Collins (Ed.), Oriel Press (1973).
2. M. Pazkiewicz, J.Appl.Electrochem., 11, 443 (1981).
3. J.L. Weininger in "Proc.Symp. of the Nickel Electrode", R.G. Gunther and S. Gross (Eds.), The Electrochemical Society, Pennington, New Jersey (1982).
4. R. Barnard, G.T. Crickmore, J.A. Lee and F.L. Tye, J.Appl.Electrochem., 10, 61 (1980).
5. C.K. Dyer, J.Electrochem.Soc., 132, 13 (1985).
6. A.C. Chialvo, W.E. Triaca and A.J. Arvia, J.Electroanal.Chem., 146, 93 (1983).
7. A.C. Chialvo, W.E. Triaca and A.J. Arvia, J.Electroanal.Chem., 171, 303 (1984).

ACKNOWLEDGEMENT

INIFTA is a Research Institute jointly established by the Universidad Nacional de La Plata, the Consejo Nacional de Investigaciones Científicas y Técnicas and the Comisión de Investigaciones Científicas de la Provincia de Buenos Aires.

02030

VOLTAMMETRIC RESPONSES OF PLATINUM ELECTRODES SUBJECTED TO THERMAL, CHEMICAL AND ELECTROCHEMICAL TREATMENTS

R.M. Cerviño, W.E. Triaca and A.J. Arvia
Instituto de Investigaciones Fisicoquímicas Teóricas y Aplicadas - (INIFTA)
Casilla de Correo 16, Sucursal 4, (1900) La Plata, ARGENTINA

INTRODUCTION

It has been shown recently that the voltammetric response of polycrystalline Pt electrodes in acid solutions in the H- and O-adatoms electrosorption/electrodesorption potential range can be modified by applying fast periodic potential perturbations under well defined potential perturbation conditions[1]. The final voltammetric response of the electrodes after the treatment approached closely to that accomplished from either Pt(111) or Pt(100) surfaces after they have been subjected to some cycles in the O-electrosorption potential range. It was also found that this treatment yielded surfaces with preferred orientation from the polycrystalline platinum electrode[2]. More recently, the structural changes of an atomically smooth Pt(111) surface induced by either the annealing and cooling procedure or the electrochemical adsorption of oxygen, has been followed by voltammetry in a sulphuric acid solution. The difference in the type of the voltammograms of H-adatoms on a Pt(111) surface was related to the difference in the cooling conditions[3].

Special attention should be paid to these modifications of the Pt electrode surfaces resulting from either an initial single crystal or a polycrystalline Pt as they probably imply common configurations of the electrode surface which are apparently achieved after applying preset potential perturbation conditions. The present work points out that most of the voltammetric responses of Pt electrodes obtained from "true" single crystal surfaces can be also approached from polycrystalline Pt when the latter is treated with a fast periodic potential perturbation under well defined potential limits and frequency conditions.

RESULTS

When a polycrystalline Pt electrode in 1 M H_2SO_4 at 25°C is subjected to a repetitive triangular potential sweep (RTPS) at 10^4 V/s during 12 hs between 0.42 V and 1.10 V (vs. RHE), the voltammogram run immediately afterwards at 0.1 V/s between 0.05 V and 0.60 V approaches to those reported in refs. 4a (Fig. 3) and 4b (Fig. 1b). The voltammogram reported in ref. 4b as corresponding to the "initial state" was obtained from a Pt(111) surface cleaned in UHV (Ar- and O-bombardment) and characterized by LEED and AES. After a single triangular potential sweep at 0.1 V/s between 0.05 V and 1.50 V, the resulting voltammogram becomes similar to that referred to as the voltammogram for the "standard state" of the Pt(111) surface (Fig. 1c in ref. 4b) and also to those obtained by several authors after the Pt(111) single crystal has been cycled in the O-electrosorption potential region[2]. Finally, after RTPS during 30 min between 0.05 V and 1.50 V at 0.1 V/s the resulting voltammogram becomes now similar to that reported as the "final state" of the Pt(111) surface[4b].

On the other hand, a Pt electrode surface with (100) preferred crystal orientation is achieved from a polycrystalline Pt electrode by means of a RTPS at 1.4×10^4 V/s applied between 0.06 V and 1.50 V during 12 hs in 1 M H_2SO_4. The voltammogram run at 0.1 V/s in the H-adatom potential range approaches closely to those reported by several authors for Pt(100) surfaces in sulfuric acid solutions[6]. When the polycrystalline electrode is treated with a RTPS between 0.002 V and 1.50 V at 1.4×10^4 V/s, the resulting voltammogram at 0.1 V/s approaches closely to those obtained with Pt(100) surfaces in 0.5 M H_2SO_4 (Fig. 2 in ref. 7a and Fig. 1 in ref. 7b). Furthermore, when the potential scan at 0.1 V/s covers the O-electrosorption potential range, the voltammogram is similar to those found from Pt(100) single crystals cycled in the same potential range[5c,7].

DISCUSSION

The present results demonstrate that structural changes of the Pt surfaces followed by voltammetry occur both in single crystal and polycrystalline Pt electrodes. In any case, from both materials it appears that common surface configurations are accomplished from either Pt(111) or Pt(100) single crystals and from polycrystalline Pt when the corresponding surfaces are disturbed by relatively drastic potential perturbations. These common preferred orientations of Pt which are well characterized by voltammetry in the H-adatom electrosorption/electrodesorption potential range, are closely representing the true characteristics of the metal surface in the absence of residual mechanical stresses.

Data reported at present can be successfully compared to the surface modifications of Pt single crystals induced either by bombardment with high energy particles, by thermal treatment or by O-adsorption. Thus, the different states of the Pt surfaces resulting from Pt(111) single crystals, as described in ref. 4b, can be also, in principle, approached from polycrystalline Pt after producing the preferred orientation through the application of fast potential perturbations.

As far as the thermal and chemical procedures are concerned, under certain conditions, surface modifications yielding restructuring and faceting are achieved[3,8], while in the electrochemical procedure, comparable results are obtained through the fast potential perturbation applied to the electrode and the formation of either OH- or O-electroadsorbed species from the underpotential oxidation of water in acid solutions. Therefore, the thermal, chemical and electrochemical procedures, in principle, correlate reasonably well and this suggests that the same type of interaction energies plays an important role in the surface restructuring effect.

REFERENCES

1. (a) J.C. Canullo, W.E. Triaca and A.J. Arvia, J.Electroanal.Chem., 175, 337 (1984).
   (b) R.M. Cerviño, W.E. Triaca and A.J. Arvia, J.Electrochem.Soc., 13, 266 (1985).
2. R.M. Cerviño, A.J. Arvia and W. Vielstich, Surf.Sci. (in press).
3. S. Motoo and N. Furuya, J.Electroanal.Chem., 172, 339 (1984).
4. (a) J. Clavilier, R. Faure, G. Guinet and R. Durand, J.Electroanal.Chem., 107, 205 (1980).
   (b) D. Aberdam, C. Corotte, D. Dufayard, R. Durand, R. Faure and G. Guinet, in "Proc. 4th Int.Conf. on Solid Surfaces", Cannes, Vol. 1, 622 (1980).

5. (a) F.G. Will, J.Electrochem.Soc., 112, 451 (1965).
(b) P.N. Ross, Jr., J.Electroanal.Chem., 76, 139 (1977).
(c) A.T. Hubbard, R.M. Ishikawa and J. Katekaru, J.Electroanal.Chem., 86, 271 (1978).

6. (a) E. Yeager, W.E. O'Grady, M.Y.C. Woo and P. Hagans, J.Electrochem.Soc., 125, 348 (1978).
(b) K. Yamamoto, D.M. Kolb, R. Kötz and G. Lehmpfuhl, J.Electroanal.Chem., 96, 233 (1979).
(c) P.N. Ross, Jr., Surf.Sci., 102, 463 (1981).

7. (a) J. Clavilier, R. Durand, G. Guinet and R. Faure, J.Electroanal.Chem., 127, 281 (1981).
(b) C.L. Scortichini and C.N. Reilley, J.Electroanal.Chem., 139, 233 (1982).

8. (a) J.W. May, Ind.Eng.Chem., 57, 19 (1965).
(b) T. Biegler, Aust.J.Chem., 76, 2571 (1973).
(c) A.T. Hubbard, J.L. Stickney, M.P. Soriaga, V.K.F. Chia, S.D. Rosasco, B.C. Schardt, T. Solomun, D. Song, J.H. White and A. Wieckowski, J.Electroanal.Chem., 168, 43 (1984).
(d) A.C. Chialvo, W.E. Triaca and A.J. Arvia, Anal.Asoc.Quím.Argentina, 73 (1), 23 (1985).

ACKNOWLEDGMENT

INIFTA is a Research Institute jointly established by the Universidad Nacional de La Plata, the Consejo Nacional de Investigaciones Científicas y Técnicas and the Comisión de Investigaciones Científicas de la Provincia de Buenos Aires.

02040

ELECTROCHEMICAL AND ELLIPSOMETRIC RESPONSES OF IRON ELECTRODES IN SATURATED CALCIUM HYDROXIDE SOLUTIONS

O.A. Albani, J.O. Zerbino, J.R. Vilche and A.J. Arvia
Instituto de Investigaciones Fisicoquímicas Teóricas y Aplicadas - (INIFTA)
Casilla de Correo 16, Sucursal 4, (1900) La Plata, ARGENTINA

INTRODUCTION

The electroformation and electroreduction of surface oxide layers on iron in alkaline media involve simultaneous charge transfer and chemical rearrangements of the film structure considerably dependent on the solution composition and temperature [1-4]. The present paper refers to the electrochemical and ellipsometric measurements of polycrystalline iron in saturated calcium hydroxide solutions as compared to measurements made in sodium hydroxide solutions at pH 12,6.

EXPERIMENTAL

Polished polycrystalline iron (Specpure, Johnson Matthey Chemicals Ltd.) mounted in teflon holder was used. The electrolyte consisted of either saturated $Ca(OH)_2$ or 0.04 M NaOH solutions, kept under purified nitrogen. The electrochemical cell was mounted in a Rudolph Research ellipsometer, type 437-02/200 S manual, provided with a 150 W tungsten lamp with filter (5461 Å). The incidence angle was 69° and that of the compensator was 135°. Runs were performed at 25°C. Potential in the text is referred to the NHE scale.

RESULTS AND DISCUSSION

Results obtained in 0,04 M NaOH are similar to those reported in strong alkaline solution (Fig. 1). The voltammograms run at $v = 0.04$ V/s between -1.26 V and 0.54 V exhibit three anodic current peaks during the positive going potential excursion, at ca. -0,78 V (peak I), -0.62 V (peak II), and -0,38 V (peak III), and the cathodic current peaks during the returning scans at ca. -0,76 V (peak IV) and -0.98 V (peak V), respectively. Measurements made by changing systematically both the anodic and cathodic switching potentials reveal that conjugated processes take place in the potential ranges of peaks III and IV (Fig. 2a).

Ellipsometric results obtained by varying both the anodic potential and the potential holding time suggest the initial formation of a barrier layer whose thickness increases proportionally to the electrode potential. The correlation between ellipsometric parameters (P and A) and the anodic charge required to form the barrier layer shows at times larger than 0.4 s a new current contribution which can be, in principle, assigned to the migration of metallic ions through the barrier layer. The electrochemical and ellipsometric characteristics of the barrier layer are quite similar both in saturated $Ca(OH)_2$ and NaOH solutions.

Figs. 1 and 2 show the application of repetitive triangular potential sweeps (RTPS) producing the growth of a second hydrated iron oxide layer of low refraction indixes, whose thickness increases during cycling. The growth of the second film also occurs by holding the potential at a preset value. The characteristics of the second film is different in saturated $Ca(OH)_2$ than in NaOH solution at the same pH.

The ellipsometric data in 0.04 M NaOH after different potential cycling times, measured either under open circuit or at the anodic or the cathodic switching potential are shown in the figs. 2a and 2b. The inner P vs A plot corresponds to an increasing thickness of the second layer in the reduced state while the outer one corresponds to both the barrier and the second film in the oxidized state. The change of the optical parameters corresponds to an increase of the charge of the redox couple related to peaks III-IV. This charge accumulation is greater in 0.04 M NaOH than in saturated $Ca(OH)_2$.

On the other hand, the optical data corresponding to RTPS in saturated $Ca(OH)_2$ cannot be explained by the growth of an optical film at constant indixes. This difference in behaviour appears already in the first scan and it is also found in the potentiostatic runs, starting from the polished electrode. Moreover, in both solutions the characteristics of the second layer depends also on the potential perturbation conditions. In 0.04 M NaOH when the thickness is greater than 2000 Å the optical indices decrease, suggesting a larger water containt of the passive layer. The accumulation of the charge participating in the conjugated couple III-IV is gerater in 0.04 M NaOH than in saturated $Ca(OH)_2$. For the latter the second layer grows gradually from a less compact layer to a more compact one.

These results demonstrate the remarkable influence of Ca^{2+} in solution in defining the characteristics of the anodic film formed on iron in base electrolyte.

REFERENCES

1. R.S. Schrebler Guzmán, J.R. Vilche and A.J. Arvia, J.Appl. Electrochem., 11, 551 (1981).

2. J.O. Zerbino, J.R. Vilche and A.J. Arvia, J.Appl.Electrochem., 11, 703 (1981).

3. H. Oranowska and Z. Szklarska-Smialowska, Corros.Sci., 21, 735 (1981).

4. N. Sato, T. Noda and K. Kudo, Electrochim.Acta, 19, 471 (1974).

ACKNOWLEDGEMENT

INIFTA is a Research Institute jointly established by the Universidad Nacional de La Plata, the Consejo Nacional de Investigaciones Científicas y Técnicas and the Comisión de Investigaciones Científicas de la Provincia de Buenos Aires.

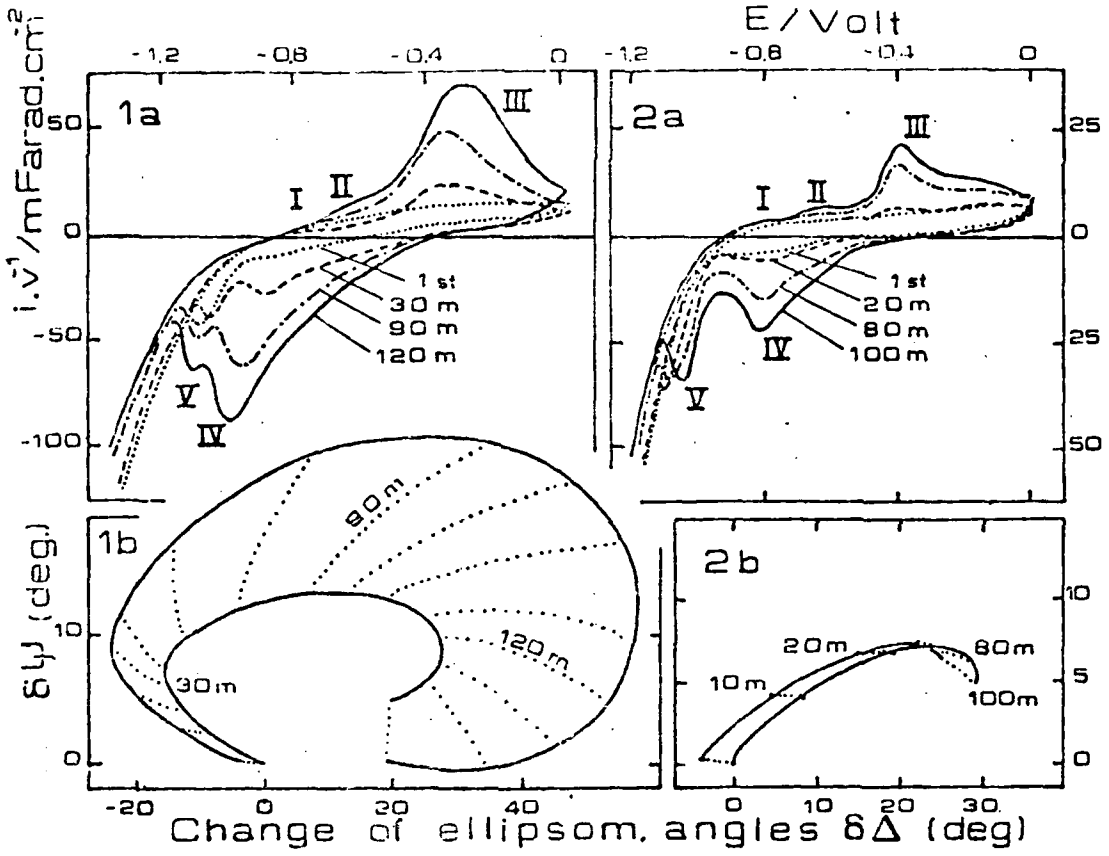

Comparison of potentiodynamic E/I contours and change of the ellipsometric parameters Δ and ψ during RTPS at v = 0.04 V/s. Switching potentials $E_{s,c}$ = -1.36 V, $E_{s,a}$ = 0.01 V. (1) 0.04 M NaOH and (2) saturated $Ca(OH)_2$ solutions.

02042

02050

ELECTROCATALYTIC ACTIVITY OF THE BREWER INTERMETALLIC PHASES FOR THE HYDROGEN EVOLUTION REACTION

B. Kosanović[1)], S. Štrbac[2)], T. Grozdić[1)] and M.M. Jakšić[2)]

University of Belgrade

1) Institute of Chemical Power Sources, Belgrade, Zemun Polje, Yugoslavia

2) Institute of Food Technology and Biochemistry, Faculty of Agriculture, Belgrade, Yugoslavia

Brewer[1] pointed out that the alloying of metals which are considerbly remote in the periodic table, proceeding with a definite charge transfer, provides the possibility of generalized Lewis acid–base reaction with the transfer in the opposite direction to that expected from the electronegativities with the stabilization through utilization of an otherwise non–bonding electron pair of electron donating metal and unused vacant orbitals of electron trapping element in their intermetallic interaction. For metals from the left side of the transition series reacting to produce intermetallic phases with element ranging from the seventh to the eleventh group, the stability of the compound is predicted to increase as the number of non–bonding internally paired d–electrons increases to reach a maximum and then decrease as the paired d–electrons become so stabilized with increasing nuclear charge that it would be difficult to transfer them. Likewise, for any metal from the right side, the variation from the sixth to third group on the left is predicted to produce an increase in stability of intermetallic phases as the number of vacant d–orbital is increased with subsequent decrease for smaller nuclear charges that could not hold donated d–electron pairs, the whole interaction increasing from 3d toward 5d level. Then, for fifth group d–metals (V, Nb, Ta) with only one vacant d–orbital, the interaction to form intermetallic phases would be small with rhenium, would increase substantially with osmium, would reach its maximum with iridium and would decrease with platinum and further with gold, while the whole interaction decreases from tantalum towards vanadium. For fourth group d–metals (Ti, Zr, Hf) with two vacant d–orbitals, the maximum in intermetallic interaction and stability is predicted to shift to the right and should be between the ninth (Ir, Rh, Co) and the tenth (Pt, Pd, Ni) group, whereas for the third group (Y, La) the maximum in interaction is predicted with Pt, Pd, or Ni decreasing downwards in the last order. On the basis of the generalized Lewis acid–base– and Brewer valence bond– theory for bonding in metals and intermetallic phases and alloys there has been pointed out[2] that whenever metals of the left–half of the transition series that have empty of half filled vacant d–orbitals are alloyed with metals of the right–half of the transition series that have internally paired d–electrons not available for bonding in the pure metal, there arises well pronounced synergism in electrocatalysis for the hydrogen evolution reaction (h.e.r.), which often exceeds individual effects of noble metals and each other (synergism condition) and approaches the reversible behaviour within the wide range of current density. The Brewer theory predicts that such intermetallic phases behave extraordinary stability features because of the improved bonding

properties. The actual question is why metals such as hafnium, zirconium, titanium or lanthanum with rather high individual hydrogen overvoltage and typical hydriding features advance the polarization properties of other d–metals, such as cobalt, nickel, palladium or iridium in their appropriate alloying compositions? In addition, what is the mutual point between the stability of Brewer intermetallic phases and their electrocatalytic activity?

There has been pointed out that whereas various physical features associated with electronic configuration of elements, such as melting and boiling point, the bonding effectivness[1], heat of fusion, sublimation and vaporization represent typical volcano curves as a function of the position in the periodic table with maximum at about d^5 – electrons, electrocatalytic features of transition metals for the h.e.r. shift the maximum of their volcano curves towards about d^8 – electrons. Quite similar relationship shows the bonding energy of zirconium or hafnium as a function of the position of the right–half transition metals in the periodic table[2]. The same dependence follows the electrocatalytic activity of composite catalysts: the best catalysts represent rather symmetric intermetallic Laves phases, such as $MoCo_3$, WNi_3, $LaNi_5$, $ZrNi_3$, $HfPd_3$, $ZrPt_3$, where the average electronic configuration approaches the same one characteristic for individual d–metals of highest electrocatalytic activity (about d^8, or rather hybridic arrangement between $d^7 - d^8$ electrons).

There has also been found that electrocatalytic activity of composite catalysts for the h.e.r. follows the so called Miedema[3] reversal stability law, which states that the higher the stability of some intermetallic phase, the lower the stability of its hydride, and the higher the capacity of hydrogen bonding. In other words, metals of the left–half of transition series induce hydridic features for the right–half of d–metals and the entire composite electrocatalyst improves its hydridic properties by increasing the stability of original intermetallic phase. Both features of the stability and electrocatalytic activity have also been associated[4] with the Cooper pairing effect of superconductivity: the most symmetric intermetallic phases are the best both for electrocatalytic activity and superconductivity.

The bonding energy of d–electrons increases very markedly with the nuclear charge from the first to the third transition series due to the deeper penetration of the p– and, particularly, the s– electrons towards the nucleus than for d–electrons of the same main shell. The effect of increased nuclear charge upon the strength of d–bond thereby appears due to contraction of the closed shells and increased exposure of the d–orbitals relative to the closed shells to allow better overlap of d–orbitals between atoms at the internuclear distances fixed by the balance of attractive bonding forces by the repulsive forces owing to interpenetration of the closed shells[1]. Therefore, the improved overlap of d–orbitals increases the cohesive bonding effectivness in going from 3d to 5d series and increased exposure of the d–orbitals with the proper pairing effect, apparently provides the higher electrocatalytic activity, and eventually improved superconductivity.

Some rather unusual intermetallic phases and alloys for electrochemical reactions that behave extraordinary stability in the light of the Brewer–Engel theory[1] have been employed for the h.e.r. as the electrocatalysts and their polarization properties were investigated in water electrolysis (Fig. 1 and 2). The promoting effect of some ionic species with rather filled d–orbitals have also been investigated and pointed out. The correlation between the stability of alloys and intermetallic phases and their electrocatalytic activity in the light of the Brewer–Engel theory has been con firmed. The hydridic feature of the Brewer electrocatalysts has been experimentally proved and pointed out as the main characteristics for such an advanced activity in the h.e.r.

References

1/ L. Brewer and P.R. Wengert, Metall. Trans., 4A, 83 /1973/;
L. Brewer, Science, 161, 115 /1968/

2/ J.K. Gibson, L. Brewer and K.A. Gingerich, Metall. Trans.,
15 A, 2075 /1984/

3/ K.H.J. Buschow, C.P.C. Bouten and A.R. Miedema,
Rep. Prog. Phys., 45, 937 /1982/

4/ M.M. Jakšić, Electrochim. Acta, 29, 1539 /1984/

Fig. 1. The activity of Zr–Ni intermetallic phases as a function of their atomic ratio in the composite catalysts presented as the increase of the current density at constant potential.

Fig. 2. Polarization characteristics of some Brewer intermetallic phases (2–Hf–Pd, 3 – Nb–Pd and 4 – Ta–Pd) for the h.e.r. in 40% NaOH as compared with nickel elcctrode (1) in the same solution.

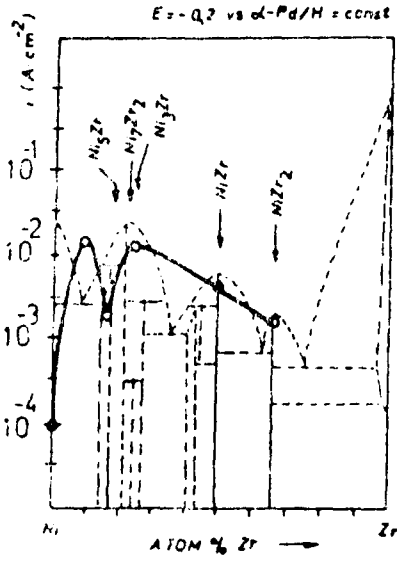

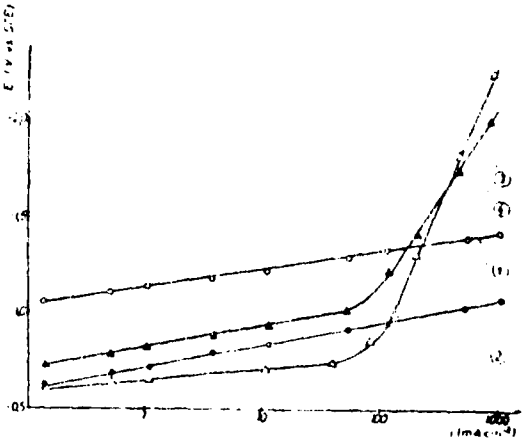

02060

INFLUENCE OF SULPHATE IONS ON THE INTERPHASE OXIDIZED ALUMINIUM/ELECTROLYTE

Z. BOLANČA, B. LOVREČEK[X], O. KORELIĆ
Higher School of Printing, University of Zagreb
Getaldićeva 2, Zagreb, Yugoslavia

[X]B. L. Nalješkovićeva 29, 41000 Zagreb, Yugoslavia

In our former work (e.g. ref. 1,2,3) we found that the charge density on the surface of the oxidized aluminium (evaluated from electrokinetic measurements) depends on the way of oxidizing, on possible aftertreatment of the oxidized layer, on composition and on pH of the solution in contact with this layer. The contact angles were measured also on the samples of the oxidized aluminium changing the mentioned parameters. It is found that there is a correlation between the charge density of the surface and the contact angle. The results of such investigations give possibilities for better understanding of the process in practical application of aluminium, particulary in the field of corrosion as well as in the fields of some specific applications of aluminium, such as lithography.

A part of broader investigation is presented in this paper concerning the surface charge and contact angle influenced by some anions in the solutions which are in contact with the oxidized aluminium. Measuring of the streaming potential and measuring of the contact angle were used as the experimental methods. The samples of aluminium of high purity were oxidized by boehmitizing in the boiling water. During the measuring of streaming potential and contact angle the samples were in contact with the solutions 10^{-4} M KCl of various pH values and with the same solutions with the addition of K_2SO_4 in various concentrations in the range from 2×10^{-5} to 5×10^{-4} M. From the values for streaming potential zeta potential and after that charge density were evaluated in the conventional way. The dependence of zeta potential on pH is linear but the slope and position of the straight lines change depending on concentration of added sulphate ions in the solution which is in contact with the oxidized aluminium (Fig. 1.). Fig. 2. shows the dependence of the charge density (q) and the contact angle (theta) with pH only for three solutions (10^{-4} M KCl, 10^{-4} M KCl + 10^{-4} M K_2SO_4 and 10^{-4} M KCl + 5×10^{-4} M K_2SO_4). The charge on the surface really denotes the charge of the immobile component of the system. There is obvious correlation between the values of the contact angle and the charge density on the surface of the oxidized aluminium as the function of pH. With the higher density of positive and negative charge the contribution of the charge to wetting is greater. The maxima on the curves theta - pH (10^{-4} M KCl and 10^{-4} M KCl + 10^{-4} M K_2SO_4) are close to the corresponding pH values where q = 0, i.e. to the isoelectric points.

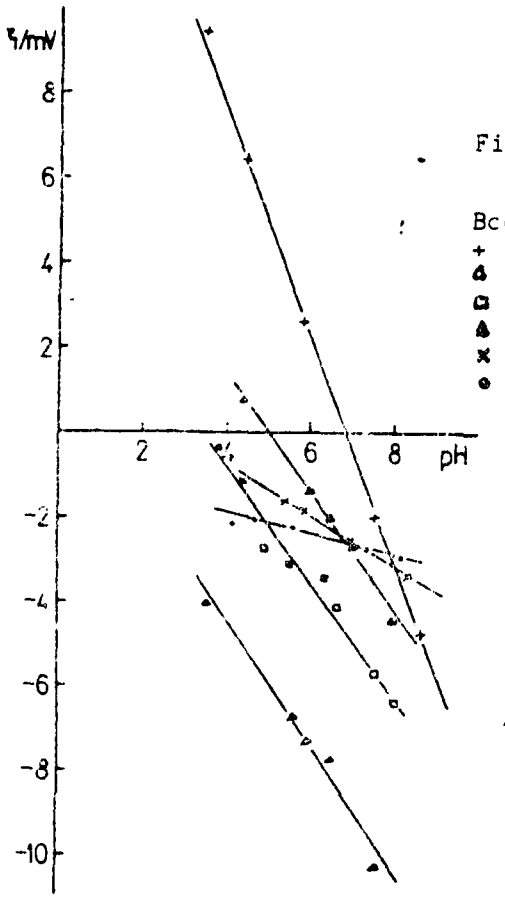

Fig. 1. Zeta potential vs. pH

Boehmitized Al in contact with:
+ 10^{-4} M KCl
▲ 10^{-4} M KCl + 5×10^{-4} M K_2SO_4
□ 10^{-4} M KCl + 2×10^{-4} M K_2SO_4
▲ 10^{-4} M KCl + 10^{-4} M K_2SO_4
× 10^{-4} M KCl + 5×10^{-5} M K_2SO_4
● 10^{-4} M KCl + 2×10^{-5} M K_2SO_4

The curve theta-pH shows no maximum but the curve q-pH also does not intersect the abscissa in case of 10^{-4} M KCl + 5×10^{-4} M K_2SO_4 solution.

These phenomena broaden our concept of the influence of the anions on the surface charge. The additional anions can influence the surface charge in various ways. Except anion adsorption it can come to their incorporation into the oxide layer e.g. by ion exchange[4], and all that can lead to the change in the charge density on the surface and to the shifting of isoelectric point. In some cases, we had investigated, such systems were analysed quantitatively, supposing that there is an algebraic addition of the surface charge of boehmite itself and the charge that brings a new anion added (an example is given in ref. 1.). However it obviously cannot always be used because in some occasions structural changes may occur and in connection with this, changes in the surface charge.

Mutal dependence of such influences on surface charge will be considered in our further work.

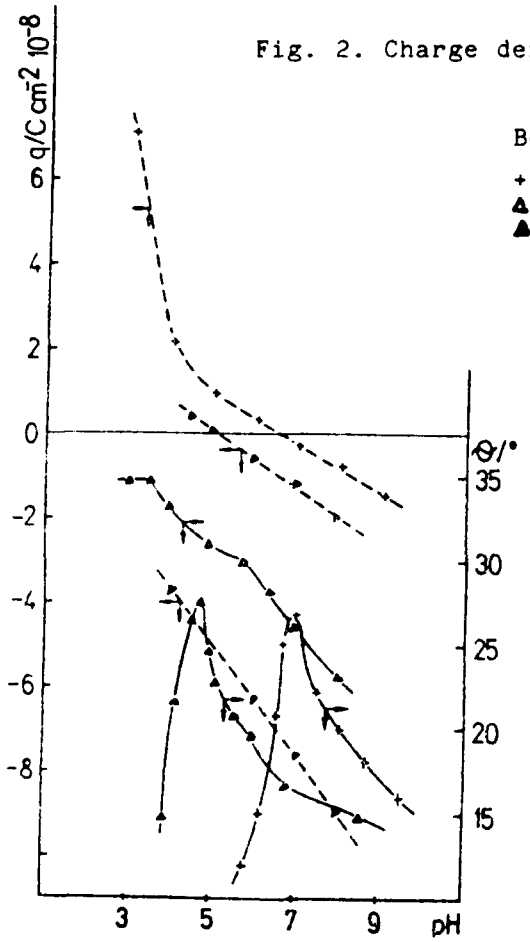

Fig. 2. Charge density and contact angle vs. pH

Boehmitized Al in contact with:
+ 10^{-4} M KCl
▲ 10^{-4} M KCl + 5×10^{-4} M K_2SO_4
▲ 10^{-4} M KCl + 10^{-4} M K_2SO_4

REFERENCES

1. Z. Bolanča, O. Korelić, B. Lovreček, Surf. Techn. 22 (1984) 323.

2. Z. Bolanča, O. Korelić, B. Lovreček, 5th International Symposium on Passivity, Bombannes-Bordeaux, France, 1983., Ext. Abstr. p. 313.

3. B. Lovreček, Z. Bolanča, O. Korelić, 35th Meeting of ISE, Berkley, USA, 1984., Ext. Abstr. p. 876.

4. S. Mattson and A.J. Pugh, Soil Sci., 38 (1934) 299.

02070

A STUDY OF INTERFACIAL BEHAVIOUR OF Al/AQUEOUS SOLUTION SYSTEM

B. Lovreček*, M. Lovreček, O. Korelić

Department of Printing Technology, University of Zagreb
YU-41000 Zagreb, Getaldićeva 2, Yugoslavia

The investigation of the interphase characteristics of the system Al/aqueous solution is of great theoretical and practical interest. As a rule, aluminium is even spontaneously covered by an oxide layer, and very often it is done intentionaly. The existence of these layers determines the specific physical, chemical and electrochemical states and processes and they are responsible for a group of phenomena very imortant for the practical application. One of the most important characteristics in that is corrosion stability of aluminium, but all of its aspects are not explained enough yet. The surface charge, resp. the interaction of the surface active groups with the solvent and/or the species from the solution on the corrosion processes[1-4] has been pointed at recently.

This work presents in the same sense a further contribution to the extension of such approach. Voltammetric method was used, as well as determination of the contact angle as a good indication of the interaction of the solid phase and solution. The investigations were performed in solutions with constant concentration of chloride ion of 10^{-3} M (except for the most acidic solution) and variable concentrations of hydrogen ion. In the part of the acid range it is also possible to keep constant the ionic strenght. The working electrode for voltammetric measurements is from superpurity Al of the cylindric shape, protected by synthetic resin, except on the active circular cross-section with the surface area of 3.0 cm^2. The counter electrode is of spiral platinum wire, and the reference is Ag/AgCl electrode in the same solution. The tests were performed at room temperature and in the air atmosphere. The working electrode was mechanicaly ground, degreased and treated in the hot NaOH, then washed and neutralzed in the nitric acid. This measurements were performed under constant stirring.

After stabilizing, the potential was changed for 50 mV from the resting potential, first in the cathodic direction up to -350 mV, and then back in steps of 100 mV, with direct reading of current after relative stabilization. After stabilization with the open circuit the procedure was repeated in the anodic direction up to +350 mV and then back towards the resting potential.

For determination of the contact angle (wetting angle respectively) the sample plates are from the superpurity Al in size 10 x 60 mm, treated in the way described above. The plates were vertically immersed up to about 1/3 of their lenght into a glass cuvette filled with electrolyte and oriented in the optical axis of the goniometer.

---

*B. Lovreček, YU-41000 Zagreb, Maršićkovićeva 29

Fig. 1 shows the results of voltammetric measurements on Al electrode immersed in the solution (a): 10^{-3} M Cl^-, 10^{-5} M H^+ and solution (b): 10^{-3} M Cl^-, 10^{-4} M H^+. The plot is given as the relation E vs. $E_{corr.}$ of the same electrode in the same solution. The measurements were done according to the procedure described before, after prepolarisation of the working electrode during 5 minutes at -1000 mV vs. Ag/AgCl electrode in the same electrolyce. The mean values from two measurements are shown, for forward polarisation only. The typical relations with relatively expressed linear parts are noticed in both cases and it is possible to determine the anodic and cathodic slope, as well as to estimate the corrosion current by extrapolation at $E_{corr.}$ The corresponding values differ significantly (see Fig. 1). The values of the cathodic and anodic slope indicate the presence of at least partial coverage with oxide layer. It can be noticed that the cathodic, as well as anodic slope in these two various solutions are not much different, in contrast to corrosion currents which differ considerably. It seems that the mechanism of the corrosion reactions does not change in this range, and the reason for various corrosion rates should be found in another factor.

The results of the contact angle determination are shown in Fig. 2. The contact angle is a very expressive function of H^+ resp. OH^- ion concentration. In fact, one gets steep increase and steep decrease around maximum in the solution with the addition of about 10^{-5} M H^+ ions. Similar reaction on the boehmitized Al has been found earlier and it is attributed to the interaction of the water dipole and solid phase, as a result of amphoteric surface dissociation of the surface species[4]. Analogous approach is possible because in the tested system Al is at least partly covered by species of the oxide character.

Voltammetric measurements, as presented, which left open the question of factor that can increase the corrosion rate, together with the results of the contact angle measurements, suggest the considerable influence of the surface charge. Namely, supposing that in the case when Al corrodes intermediary species appear, such surface has a given charge density as the result of before mentioned amphoteric surface reaction, which is, in the first place, the function of pH. It is logical to suppose, but this time on the basis of voltammetric measurements and determination of the contact angle on the corroding Al, that on step of its transition into solution will have the key role, which includes the interaction of surface species and water dipoles. This step of transition into the hydrated ion in the solution is surely favoured by the mentioned interaction. The system is complicated and demands further studying in the experimental and theoretical sense. It is interesting to mention that other relatively nonprecious metals can be treated in the same way.

REFERENCES

1. V. Vujičić, B. Lovreček, Surf. Technol. 17 (1982)29.

2. B. Lovreček, V. Vujičić, Surf. Technol. 19 (1983)59.

3. M. Lovreček, O. Korelić, B. Lovreček, 3rd Conference on Corrosion and Materials Protection, Dubrovnik, 1984. Proceedings p. 88.

4. V. Vujičić, B. Lovreček, Surf. Technol. (in print)

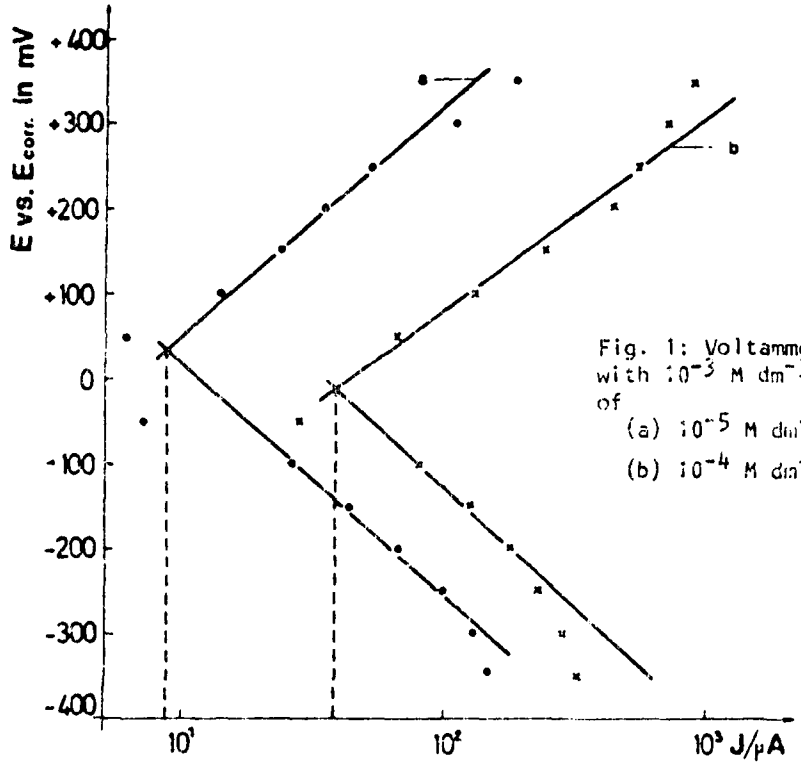

Fig. 1: Voltammetric measurements with 10^{-3} M dm^{-3} Cl^- and addition of
(a) 10^{-5} M dm^{-3} H^+
(b) 10^{-4} M dm^{-3} H^+

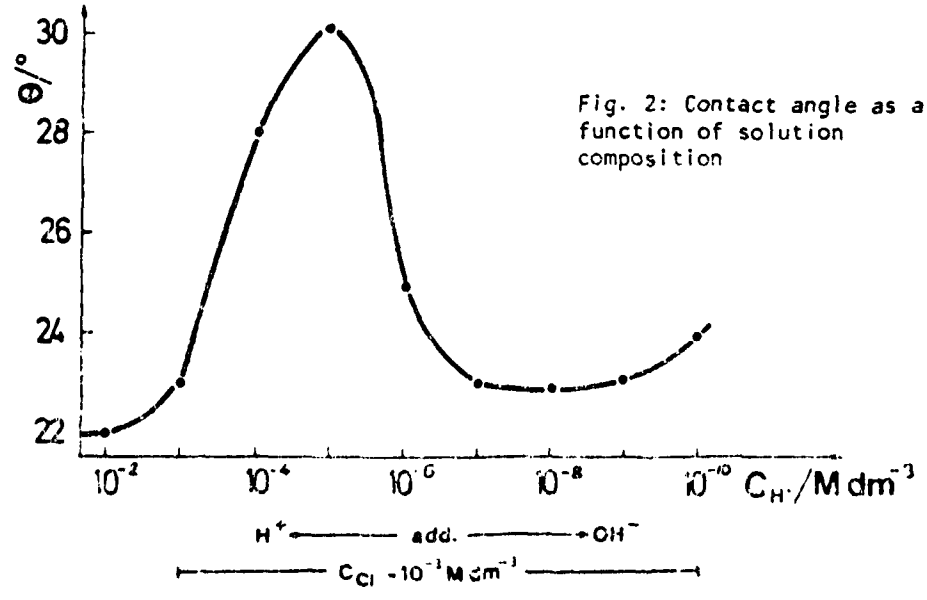

Fig. 2: Contact angle as a function of solution composition

02080

ROLE OF THE ANODIC SURFACE LAYER IN ELECTROCHEMICAL FLUORINATION

M.NOVÁK and J.BOA
Institute of General and Physical Chemistry,
University of Szeged,
H-6701 Szeged, P.O.Box 105, Hungary

Both chemical and surface analytical methods indicate that a Ni anode used in liquid HF for anodic fluorination is covered by a layer containing not only fluoride, but also oxide. Voltammetric features were interpreted as consequences of the formation of oxide and its behaviour.

Thus, under potentiostatic polarization the build-up of the layer and the subsequent change in its conductivity follow the pattern observed for other oxide systems. After an initial decrease, the current starts to increase, showing an increasing conductivity.

At open circuit, the relaxation of the potential follows the pattern indicating a structure in the layer mentioned in 1. The potential decay might be described by the presence of an inner oxide layer and an outer one. While the inner layer builds up in a very short time and is not influenced by the duration of polarization, the outer layer builds up slowly and is sensitive to the presence of fluorine and the organic substrate.

The change in the conduction behaviour might be followed by the formation of fluorine, detected with a ring-disc electrode[2], since the rate of fluorine formation increases in parallel with the increase in conductivity of the surface layer.

The addition of the organic substrate causes an elongation of the time necessary to overcome the current minimum, although the pattern of potential decay does not change. It is assumed that this is due to adsorption of the organic substrate, while the decay of the potential across the inner layer depends only on the conduction within the inner layer.

References:
1. N.Watanabe and M.Maruta
   Electrochim.Acta, 25, 461 (1980).
   Denki Kagaku, 43, 638 (1975).
2. M.Novák and J.Bóa
   J.Electroanal.Chem., 109, 179 (1980).

02090

EFFECT OF ADDITION OF CHLORIDE ON THE PROPERTIES OF BARRIER-FILMS ON ALUMINIUM

A.R. Despić, D.M. Dražić and Lj. Gajić-Krstajić
Institute of Technical Sciences of the Serbian Academy of Science and Arts, Belgrade, Yugoslavia

It was shown before that the active anodic dissolution of aluminium and some of its alloys in neutral chloride solutions is an advantageous behaviour for the use of aluminium and its alloys as the anode materials in batteries or as the sacrificial anodes, while it is a serious dissadvantage if aluminium is to be used as the material for metal construction work. Hence, the understanding of the influences that some anions, in particular chloride ions, have on the electrochemical behaviour of aluminium is of fundamental importance.

As a result of our previous studies of this problem, a hypothesis was forwarded that the activation of the oxide film covered aluminium in chloride solution is due to the adsorption (or absorption) of negatively charged chloride ions, so that the outer part of the oxide layer becomes negatively charged compared to the metal. Hence, the newly formed negative electric field inside the oxide layer accelerates the ionic transport through the oxide, and thereforethe overall metal disollution rate, as contrasted to the situation in the chloride free solutions (p.z.c. of Al is more negative than the corrosion potential).

The similar effect is known during anodization of aluminium when the presence of small amounts of chlorides prevents the growth of the barrier-film in the barrier-film forming electrolytes (e.g., borate, tartarate, etc.). This very fact was used in this work in an attempt to verify the previously mentioned hypothesis on the effect of adsorption of chloride ions on the activation of oxidized aluminium surface.

Experimental. The samples of Al foil were electropolished in a mixture of H_3PO_4, H_2SO_4, and CrO_3 at 80°C, with the subse-

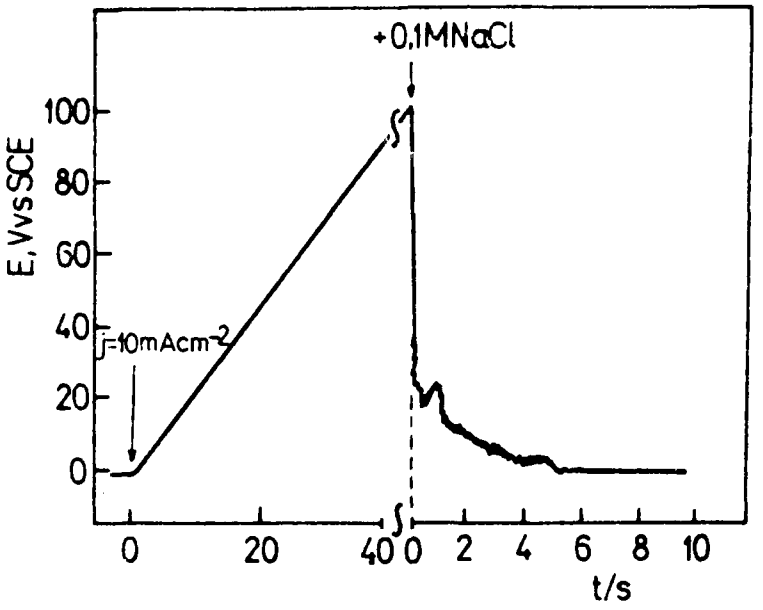

Fig. 1.

quent oxide removal in CrO_3 + H_3PO_4 solution at the same temperature (1 min). After washing the samples were used to form the barrier-films in 0.1 H_3BO_4 + 0.05 M $Na_2B_4O_7$ solution with 10 mA cm^{-2}. A good linearity of the voltage-time curve with the slope of 1.3 nm/V (Fig. 1) indicated the formation of the good barrier--type film. In most experiments the film growth was stopped at the film thickness of 130 nm (100 V), by the fast introduction of the NaCl solution, after which the electrode potential decayed suddenly, even though the anodic current is passing permenently. The amount of the NaCl solution used was such to provide the final concentrations in the range 10^{-3} - 1 M, while the potential changes were recorded on the Nicolet memory oscilloscope. The exponential decay of the potential was characterized by the time constant (for the 1/e of the potential change) in concentrated solutions being very small (50 ms). The results of the determination of the time constants for the decay as a function of chloride concentration and film thickness are shown in Figs.2a and 2b. As seen in Fig. 2a the concentration dependence of τ is showing

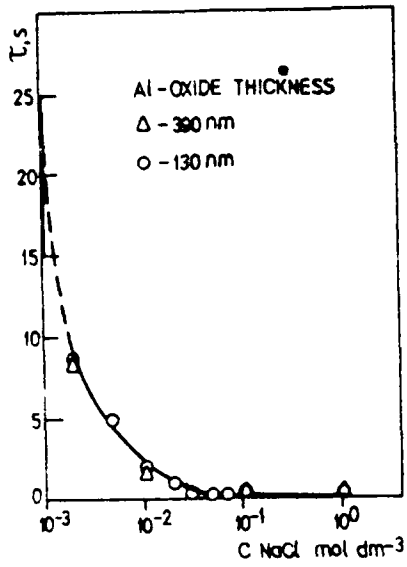

Fig. 2a.

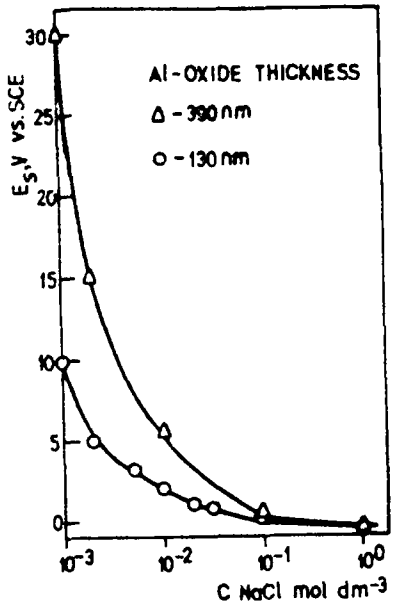

Fig. 2b.

an exponential increase in lower concentration region. Since the time constants for larger thicknesses follow the same experimental curve this indicates that the thickness of the layer is of no importance for the observed decay phenomenon, i.e. the penetration of the chloride ions inside the film is not the reason for the decay. Fig. 2b. presents the dependence of the steady state potential, E_s, of the electrode achieved after the decay, as a function of chloride concentration. The simillar dependence was obtained.

The observed experimental results, cannot be interpreted as to be the consequence of the slow diffusion of chloride to the oxide surface. Hence, the observed dependence of the time constant on concentration and independence on the film thickness could be interpreted as the consequence of the surface reaction, i.e., slow adsorption of chloride at the surface of oxide layer as known for chlorides. All this is in accord with the previously mentioned hypothesis. Further experimental work on the ESCA and Auger analysis of the studied films is in progress.

02100

THE ROLE OF STEPS IN THE OXIDATION OF FORMIC ACID ON SINGLE CRYSTAL SURFACES

A. Tripković, R. Adžić, V.Vešović •
Institute of Electrochemistry, ICTM Belgrade, Yugoslavia

Oxidation of HCOOH depends on the crystalographic structure of the electrode surface[1-3].

Considerably higher activity has been observed with the Pt(111) surface. This has been explained by the lack of formation of the strongly bound intermediate on this surface.

The strongly bond intermediate completly blocks the Pt(100) face and, to a lagre extend, the Pt(110) surface. We have recently shown that the introduction of steps of the same or different orientation on the Pt(100) and the Pt(111) surfaces causes a noticable change in the activity for the HCOOH oxidation (4). Preliminary studies have been performed with the surfaces with the following orientations: Pt-6(111)x(111), Pt-6(111)x(100) and Pt-4(100)x x(111). The introduction of the (111) step in the (100) surface caused an increase of the current in the positive going sweep, while the introduction of the (100) step in the (111) surface caused a decreased of the current in the same sweep and the appearence of the peak at ~0.9 V(4). The latter peak is usually ascribed to the oxidation of the strongly bound intermediate, which does not occur at the Pt(111) surface without the (100) step. Further information on the role of nature and density of steps has been obtained by examining the oxidation of HCOOH on the stepped single crystal electrodes with a higher step density.

The structure of all surfaces was determined by LEED before and after the electrochemical experiments. The characterization of surfaces has been performed ex-situ in ultra-high vacuum LEED/Auger apparatus. The electrodes were cleaned by sequential ion bombardment and annealing at 700°C, until Auger spectra showed less then 2% of impurities. LEED patterns were analyzed in the usual way for stepped surfaces. Taking into account the separation between double LEED spots and the overal pattern three surfaces were ascribed to have the following structures: Pt-2(111)x(100), Pt-3(111)x(100) and Pt-3(111)x(111).

Fig. 1. shows an anodic sweep of a cyclic voltammogram of HCOOH oxidation on the above surfaces. The step of (111) orientation on the (111) surface cause a sizable increase of the peak at 0.9V. It is considerably larger than the peak at the Pt-6(111)x(111) surface. This clearly shows that an increase of the number of steps on the (111) surface facilitates a formation of the strongly bound intermediate. Hence, it can be concluded that the introduction of steps with the (111) orientation on the Pt(111) surface leads to a

decrease of its activity for the HCOOH oxidation.

There is no much difference between the curves obtained for the Pt-2(111)x(100) and Pt-3(111)x(100) electrodes. Two peaks appear at both surfaces, one at ~0.9 V is probably due to the oxidation of the strongly bound intermediate. The activity of these electrodes is somewhat lower than that of the Pt(111), but not much different than that of the Pt-6(111)x(100).

Further work is needed in order to answer the question of the role of steps in the oxidation of HCOOH on the Pt single crystal electrodes. These data however suggest that the introduction of steps increases the surface activity for binding of strongly bound intermediate, thus decreasing its activity. This disturbs also the activity of the Pt(111) surface, which results from its inactivity for adsorption of intermediates (1, 2).

References:

1. R.R.Adžić, W.O´Grady and S.Srinivasan, Sufr. Sci., 94 (1980)1191.
2. R.R.Adžić, A.V.Tripković and W.O´Grady, Nature, London, 296,137(1982).
3. J.Clavillier, R.Parsons, R.Durand, C.Lamy and D.M.Leger, J.Electroanal.Chem.124, 321(1981).
4. R.Adžić, A.Tripković and V.Vešović, 35th I.S.E.Meeting, Berkeley Calif. Ext.abs. No. A7-28.

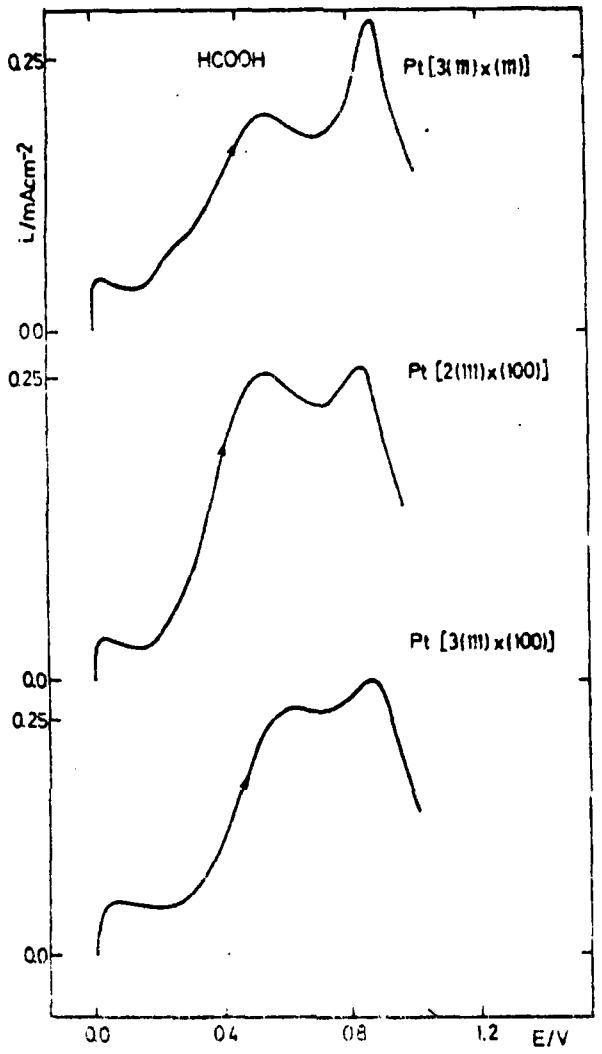

Fig. 1. Oxidation of HCOOH on the Pt - 3(111)x(111), - 2 (111)x(100) and -3 (111)x(100) surfaces in 1M $HClO_4$. Sweep rate 50 mV/sec.

02110

OXYGEN REDUCTION ON GOLD SINGLE CRYSTAL STEPPED SURFACES

R.Adžić, N.Anastasijević and V.Vešović
Institute of Electrochemistry, ICTM, Belgrade, P.O.B.815, Yugoslavia

Anomalous activity of the Au(100) surface for O_2 reduction in alkaline electrolyte has been recently analysed in some detail (1,2). Four--electron reduction of O_2 has been found in the potential region of the AuOh for--mation on Au(100), while only two-electron reduction is seen on the metallic gold surface. This surface is one of the best catalysts for HO_2^- reduction (2). In this work the effect of introduction of steps of monoatomic height on the Au(100) surface on its activity for O_2 reduction has been studied.

Experiments have been performed with the single crystal gold electrodes (Metal Crystals, Ltd, Cambridge) in the form of a rotating electrode. A preparation of electrode surface has been described elswere (2). The electrolyte was 0.1M NaOH prepared from the "carbonate free" Barker's NaOH.

The structure of all three surfaces was determined by LEED before and ofter electrochemical experiments. The characterization of surfaces has been performed ex-situ in ultrahighvacuum LEED/Auger apparatus. The electrodes were cleaned by sequential ion bombardment and annealing at 500°C, until Auger spectra showed only Au peaks, with only traces of impurities present. LEED patterns were analysed in the usual way. The clean Au(100) surfaces exibited a well-known (5x20) reconstruction, while the other two patterns were ascribed to stepped surfaces Au-6(100)x(100) and Au-2(100)x(100).

Figs 1 and 2 show the O_2 reduction on the Au-6(100)x(100) and Au-2(100)x(100) single crystal surfaces. It is seen that depending on the potential region there is a different activity of these surfaces. Similarly as in the case of the Au(100) surface it appears that four electrons are exchanged in the potential region -0.3 V< E< 0.0V. At more negative potentials only two electrons are exchanged. Table 1 gives calculated and experimental values for a diffusion constant $B = 0.62\, nFD^{2/3}\nu^{-1/6}\cdot C$ for two - and four-electron reduction.

E/V	B/mA (rad/s)$^{1/2}$cm^{-2}		
	Calc.	Exp.	
		Au-6(100)x(100)	Au-2(100)x(100)
-0.1	0.44	0.41(n=4)	0.43(n=4)
-0.5	0.22	0.20(n=2)	0.21(n=2)

Voltammograms for these two Au single crystal in the absence of O_2 differ considerably from that one obtained with the Au(100) surface. A similar behaviour with respect to the O_2 reduction indicate a role of steps in the

kinetics of this reaction. The adsorption of OH^-, leading to a formation of AuOH, is different for the two surfaces which is not similar to the same process on the Au(100) face.

It is interesting to note that with the Au-6(100)x(100) surface first sweeps show much lower activity than in the subsequent ones which indicates on the reconstruction of this surface. A sizable hysteresis between the sweeps in positive and negative directions (Fig. 1) also indicate on a possible role of reconstruction. These questions are being carefully investigated in the thin-layer cell which is coupled with the LEED-AES apparatus.

In the potential region of a four-electron reduction the Tafel slope is -125 mV/dek indicating a first electron exchange as a rate determining step (Fig.3). The reaction order with respect to a dissolved O_2 has been determined from the equation (3).

$$\log i = f \log \left(1 - \frac{i}{i_{DL}}\right)$$

It is given in Table 2.

-E/V	m	
	Au-6(100)x(100)	Au-2(100)x(100)
0.10	1.25	1.15
0.15	1.05	0.85

These data strongly suggest that the reaction order is 1 as found with the Au(100) surface.

Preliminary results with single crystal gold stepped surface indicate on a role of steps in the O_2 reduction. On the above two particular surfaces it appears, that under potential cycling applied in this work, the reaction kinetics and mechanism are similar to that one on the Au(100) surface.

The role of reconstruction on this reaction requires further study.

References

1. R.R.Adžić, N.M.Marković, J.Electroanal.Chem.138, 443(1982).
2. R.R.Adžić, N.M.Marković, V.B.Vešović, J.Electroanal.Chem. 165, 105 (1984).
3. B.B.Damaskin, Petrii, O.A., Introduction to Electrochemical Kinetics (russ.), V.S.Moscow (1983) p. 172.

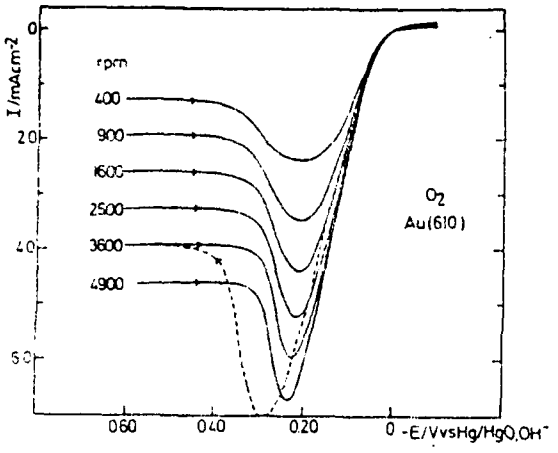

Fig.1. O_2 reduction on rotating Au-6(100)x(100) single crystal electrode in 0.1M NaOH

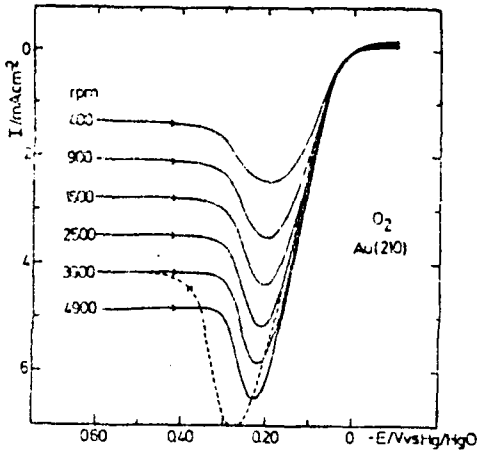

Fig.2. O_2 reduction on rotating Au-2(100)x(100) single crystal electrode in 0.1M NaOH

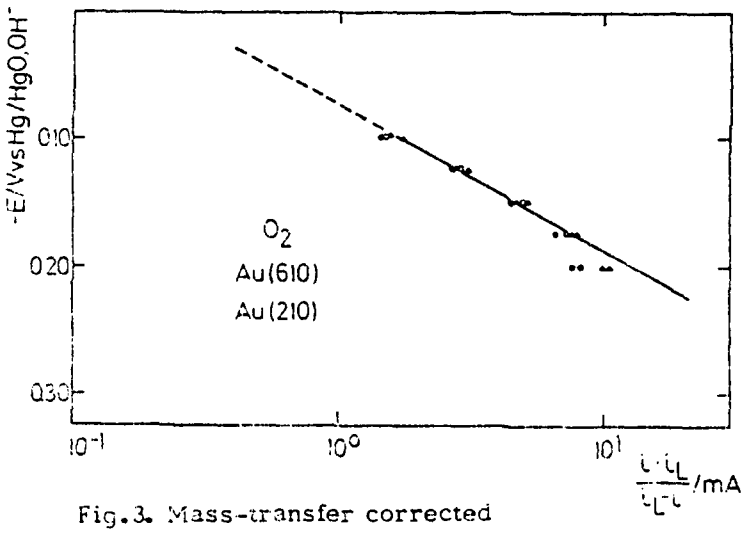

Fig.3. Mass-transfer corrected Tafel plot for O_2 reduction obtained from Figs. 1 and 2.

02120

ELECTROCHEMICAL PREPARATION OF THIN FILMS PHOTOACTIVES OF CADMIUM SULFIDE ON DIFFERENT METALLIC SUSTRATES IN ORGANIC SOLVENTS.

E. FATAS and P. HERRASTI
Dep. Electroquímica. Universidad Autónoma de Madrid. (Spain)

F. ARJONA and E. GARCIA-CAMARERO
Dep. Física Aplicada Universidad Autónoma de Madrid. (Spain)

INTRODUCTION

Cadmium sulfide is one of the semiconductor materials widely used in solar cells. Together with copper sulfide, in forms the well-known CdS/Cu_2S solar cell [1].

It is generally admitted that electrodeposition is an efficient method of film formation, allowing a more economical production and better control of properties and stoichiometry of the resulting layers than thermal evaporation, pyrolithic spraying, or sputtering [2].

Several thechniques have been developed to electrodeposit this sulfides, as anodic oxidation of the parent metal in a solution containing sulfide ions or by cathodic reduction from aqueous solutions containing soluble metal and sulfur compound. Recently, has been developed the cathodic electrodeposition of the metal sulfides in non-aquious solutions. The principle of the technique involves dissolving a salt containing the desired metal ion and the sulfur. In this case, ignoring the fact that the metal ion is often complexed with solvent moleculas or anions, and that the sulfur exists as plyatomic species in solution, the reaction for the formation of CdS may be [3].

$$Cd^{2+} + S + 2e^- \longrightarrow CdS$$

Since the sulfur is insoluble in water, reaction only can be carried out in disolutions non-aqueous.

We habe studied the formation of CdS films on steel and nickel by the for-mentioned method, using as solvents dimethyl-sulphoxide (DMSO) and diethylene glycol (DEG). The morphology, optical and structural properties of the films obtained in both solvents have been studied and compared.

RESULTS AND DISCUSSION

The CdS films have been obtained on stainless steel sustrates of composition: C=0.1%, S=0.006%, P=0.028%, Mn=0.8[illegible], Si=0.27%, Ni=7.34%, Cr=18.39%, Mo=0.17%, Cu=0.17% and Fe=73.72%. The sustrates of nickel were obtained electrochemically on a brass foil. The sustrates were carefully cleaned with doubly distilled water and then washing with acetone.

Two electrolytes were used. The first one electrolytic solution was made up in a mixture containing 1 part water and 10 parts DEG by volume sturated with elemental sulfur, in which, were solved 0.1 M NH_4Cl and 0.05 M $CdCl_2$ (I). The second one consisted of 0.055M

$CdCl_2$ and 0.19 M S in DMSO (II).

The electrodepositions were carried out galvanostatically. Several current values were applied and their influence on the morphology of the film was studied. At low current density the films shown rather low thickness about 4000 A, while at eigher current density, craks were developed on the surface. The developing of craks during deposition can be due to the presence of tensile stress in CdS crystal resulting from a piezo-electric effec[4]. This is because the electric field, applied for deposition, may result in the displacement of deposited ions along the axis which has no centre of symmetry. Another reason of craks formation can be the different thermal expansion coefficients of CdS ($4x10^{-6}/°C$) and stainless steel -- ($18x10^{-6}/°C$).

In order to verify this hypotesis, we have used tungsten as sustrate (thermal expansion coefficient $4.45x10^{-6}/°C$. The craks - about mencioned also appeared at high current density or long electrodeposition times, which seems to indicate that the piezo-electric effect is most important one for the craks formation.

The thickness of the electrodeposit can be computed from expresion:

$$d = \frac{jMt}{nF\rho}$$

where j is the current density, M the molecular weight of CdS 144.46 gr, ρ the density of CdS 4.82 gr/cm^3, t the time for which the current is passed, F the Faraday and n the number of electrons --- transferred, in this case 2.

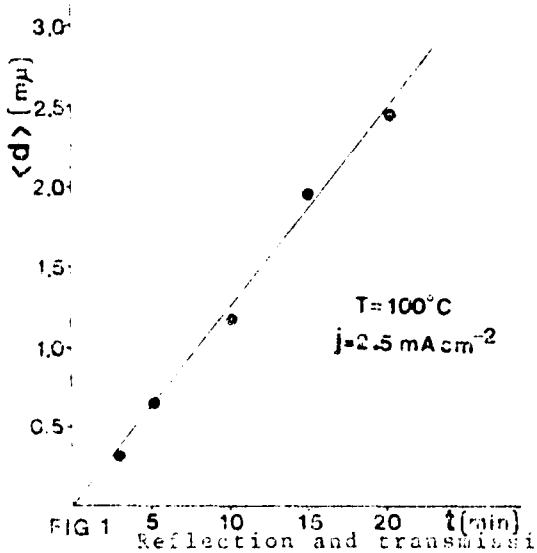

FIG 1

The most notable feature of the experimental data is the linear depencence of film thickness on time. Comparison of the slope observed in Fig. 1 with that precicted for reaction (1) according to Ec. (1) yields an efficiency of 90% for the deposition process. The discrepancy between the experimental and theoretical slopes may be attributed to the presence in solution of sulfur compounds with sulfur in a higher oxidation state. If sulfur in these -- form is involved in the deposition process, the effective number of electrons transferred during the process would be greater than that proposed by the simpler process involving sulfur.

Reflection and transmission measurements of the CdS films -- were carried out with a Cary 17 D spectrophotometer. With this dates was calculated the band gap of the semiconductor Fig. 2, their values were of 2.4 eV for both sustrates and solvents. These values are in good concordance with the Literature.

The structure of the CdS films was investigated using a Debye chamber of a Philips diffractometer and CuKα radiation. The XRD analysis of the various samples of the CdS obtained in both solvents

gave the results of some diffractograms similar appearance. The - interpretation of the diagram was made using the information in Table 1. With a detailed inspection of it we could observed, that all diffraction rings correspondede to the hexagonal phase.

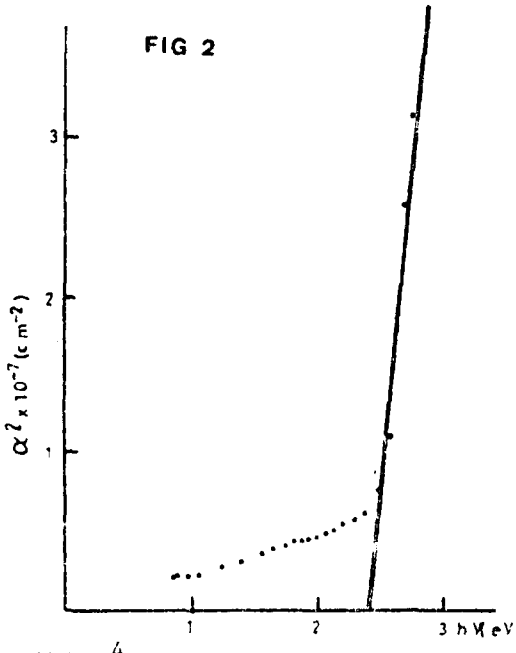

The specific resistivity of the CdS films were calculated using the expression

$$R_T = \frac{\rho}{d\pi} \text{ arc tag } \frac{4}{d/t} + \frac{4R_c}{\pi d^2} + R_0$$

where ρ is specific resistivity, d the contact diameter evaporated on the CdS film, t thickness of the - film, R_c specific contact resistance and R_0 residual resistances due to the sustrates. R_T vs $1/d\pi$arc tag $4t/d$ can be fitted with a value for the resistivity in the range of large diameters where the contact resistance contribution becomes negligible [4]. The values obtained are highe ($\sim$ KΩ).

Actualy, we have working to improve the electric properties of the films by means of two methods:

a) Introduction of dopant as Tl^{+} or In^{3+} in the lattice of the CdS
b) thermal treatment following the deposition process at temperatures about 200°C.

Table 1

I	d(ob.)	hkl
m	3.53	100
m	3.30	002
s	3.08	101
w	2.42	102
w	2.03	110
w	1.96	103
w	1.73	112
vw	1.71	201

REFERENCES

1.- A. G. Stanley, "Applied Solid State Science",Vol 5, p.251, Ac. Press, N.Y. (1975)
2.- R. Lorenz. Chem. Ber., 24, 1509 (1981)
3.- A. S. Baranski, M. S. Bennett and W. R. Fawcett. J. Appl. Phys. 54, 6390, (1983)
4.- Chopra K L, Thin film phenomenon (McGraw-Hill,New York)1969,266
5.-R. H. Cox and H. Strack. Solid-State Electronics., 10, 1213.1967

02130

STUDY OF THE UPD OF HYDROGEN AND METALS ON Pt(111) AND Pt(110) ELECTRODES BY LEED-AES AND VOLTAMMETRY

D. ABERDAM, A. NAGIB
L. A. CNRS 8, U. S. M. Grenoble, B. P. 87, 38402 Saint-Martin-d'Hères, France

R. FAURE, F. EL OMAR, R. DURAND
L. A. CNRS 265, E.N.S.E.E.G., B. P. 75, 38402 Saint-Martin-d'Hères, France

1. Introduction

The Ultra-High-Vacuum techniques provide electrochemists with a very powerful set of analytical tools for ex-situ study of structure and composition of single crystal electrodes (Low Energy Electron Diffraction, Auger Electron Spectroscopy ...). A few groups have performed experiments, especially on Platinum where the transfer in a protective environment[1-3] permits characterization of the electrode before and after the electrochemical experiment. In the present work, we also use a direct (i.e. without contact with air) transfer from the UHV chamber to the electrochemical cell and conversely. At the critical step of electrode emersion, we rinse the surface with 18 MΩxcm water, thus keeping on it only the strongly electrosorbed species. With this technique we have studied the structural aspects of the electrosorption of oxygen and hydrogen on Pt(110) and Pt(111), and the underpotential deposition (U. P. D.) of copper on Pt(110).

2. Structure of Pt(110) in aqueous solutions

The clean Pt(110) surface, in UHV, is reconstructed. The 2D periodicity is (2 x 1). It is believed to correspond to one [110] row missing every two rows (missing row model[4]). We observed that this structure remains stable under exposition to water vapour. However, water vapour hardly adsorbs on Pt(110) at room temperature, and thus we get no evidence of structural change under electrode immersion. Voltammetry, performed in sulfuric on perchloric solutions on the electrode transferred from the UHV chamber, leads to results for hydrogen or oxygen adsorption[5] similar to those obtained after annealing of the electrode in a H_2-O_2 flame[6]. Coulometry in the hydrogen range (220 μc x cm^{-2}) is compatible with a surface reconstructed according to the missing row model, since it corresponds to 3 adsorbed hydrogen atoms for each (2 x 1) surface mesh with 1 electron per hydrogen. This result supports the idea that the Pt(110) keeps its reconstructed structure in aqueous solutions.

3. Structural changes on Pt(111) upon cycling.

We have shown with J. CLAVILIER[6], voltammograms on Pt(111) are strongly dependent upon cycling in the oxygen range. After any cycling in that range, the initial curve shows specific peaks. In H_2SO_4 solutions (fig. 1a) these peaks are ascribed to strongly bonded hydroxyls. In $HClO_4$ or HF solutions, they are believed to be due to very strongly bonded hydrogen or to the reduction of $PtOH^2$. After UHV cleaning, we obtain the same type of voltammograms, and subsequent LEED examination still reveals a well ordered Pt(111) surface. Thus we associate these voltammograms with the well ordered, non reconstructed Pt(111) surface. Upon cycling in the oxygen range, an initially abrupt, then gradual change of the voltammogram occurs (60th cycle in fig. 1b).

Without any adequate transfer system, we had shown, five years ago[7], that this modified type of voltammogram was directly obtained on an electrode which had been previously argon-bombarded. This bombardment produces defects among which steps are easily detectable by LEED. With our new transfer system, we show that upon cycling in the oxygen range, an initially perfect Pt(111) surface exhibits a particular LEED pattern where some spots are changed into rings at some energies (fig. 2b). The analysis of these patterns leads to an surface containing monoatomic steps of random orientation, with terraces 15 Å wide on the average. The "cleaning" of electrodes by cycling in the oxygen range must then be considered with caution in view of the changes induced in the structure of the electrode. This drastic effect of oxygen adsorption may be related with the fact that one is able to adsorb much more oxygen in electrochemical than in gas phase experiments.

4. UPD deposition of Copper on Pt(110)

The under potential deposition of copper is performed on the Pt(110) surface in a 0.1 M $HClO_4$, 5 x 10^{-3}M $Cu(ClO_4)_2$ solution[8]. We find that working on a electrode prepared in UHV leads to voltammograms similar to those obtained with an electrode annealed in the H_2-O_2 flame.
After the electrosorption of about half a monolayer of copper the LEED pattern shows that the surface retains the (2x1) periodicity of the clean Pt(110) surface, but associated with streaks in the |001| direction. The periodicity remains perfect in the |110| direction. This is consistent with a simple model where the copper atoms fill at first the missing rows, thus smoothing the surface and keeping the (2x1) periodicity. At the same time, a few copper atoms form chains in the troughs of the smoothed surface, with a statistical distribution of the interchain distances. Quantitative Auger spectroscopy using calibration with clean platinum and copper single crystals correlates reasonnably well with the quantity of electricity corresponding to the amount of copper electrosorbed.

References

1. a) A. T. HUBBARD, R. M. ISHIKAWA and J. KATEKARU, J. Electroanal. Chem., 86 (1978) 271
   b) J. L. STICKNEY, S. D. ROSASCO and A. T. HUBBARD, J. Electrochem. Soc., 131 (1984) 260
2. a) F. T. WAGNER and P. N. ROSS, J. Electroanal. Chem., 150 (1983) 141
   b) P. C. ANDRICACOS and P.N. ROSS, J. Electroanal. Chem., 167 (1984) 301
3. D. M. KOLB, R. KOTZ and K. YAMAMOTO, Surf. Sci., 87 (1979) 20
4. H. NIEHUS, Surf. Sci., 145 (1984) 407
5. D. ABERDAM, R. DURAND, R. FAURE and F. EL OMAR, Proc. Ecoss 7 Surf. Sci. (in Press).
6. J. CLAVILIER , R. FAURE, G. GUINET and R. DURAND, J. Electroanal. Chem., 107 (1980) 205
7. D. ABERDAM, C. COROTTE, D. LUFAYARD, R. DURAND, R. FAURE and G. GUINET Proc. 4th, Int. Conference on Solid Surfaces, Cannes (1980) 622.

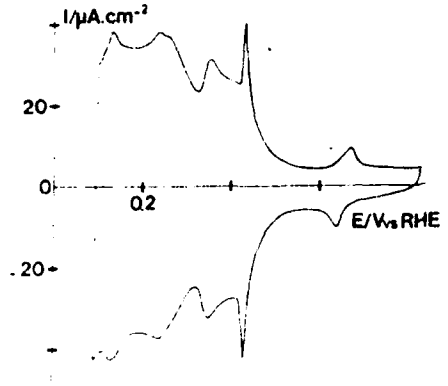

Fig. 1a : Voltammogram for the Pt(III) electrode in 1M H_2SO_4 solution. Sweep rate : 50 $mV.s^{-1}$

Fig. 2a : LEED pattern of clean Pt(III) E_p = 60.2 eV

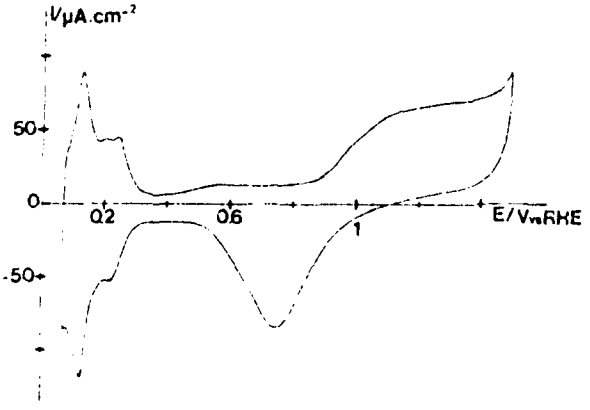

Fig. 1b : Voltammogram for the Pt(III) electrode in 1M H_2SO_4 after UHV cleaning and cycling in the oxygen range (60 cycles). Sweep rate : 50 $mV.s^{-1}$

Fig. 2b : LEED pattern of Pt(III) after 60 cycles in 1M H_2SO_4

E_p = 60.2 eV

02140

INVESTIGATION OF THE NICKEL ELECTRODE - ALKALINE SOLUTION INTERFACE by "IN SITU" UV-VISIBLE REFLECTANCE SPECTROSCOPY

by F. HAHN, B. BEDEN and C. LAMY
Laboratoire de Chimie I, Electrochimie et Interactions, U.A. au CNRS N° 350,
Université de Poitiers, 40, avenue du Recteur Pineau, 86022 POITIERS (France)

The formation of hydroxide or oxyhydroxide layers on the surface of a nickel electrode in contact with an alkaline solution has been investigated by UV-visible reflectance spectroscopy. This spectroscopic technique, coupled with cyclic voltammetry, is most interesting for such studies because not only it allows to control permanently the surface state of the electrode (by means of the potential which is applied), but also because it allows to investigate "in situ" the metal-solution interface, thus without causing any perturbation to the electrochemical reaction itself.

The formation of hydroxides and oxyhydroxides on the surface of nickel electrodes in alkaline solutions has been already widely studied in the literature, using classical electrochemical techniques, like cyclic voltammetry. Such an interest for the behaviour of nickel is explained by its important role either as positive electrodes in secondary batteries [1] or as negative electrodes in fuel cells [2, 3]. In both cases the electrochemical properties of the surface are mainly related to the formation of various crystallographic forms of hydroxide and oxyhydroxide layers, respectively α and β for $Ni(OH)_2$ and β and γ for NiOOH, as formely identified by BODE et al.[4] and more recently studied in details by LEDOVARIN et al.[5].

Due to the unstability of the nickel surface when in contact with alkaline solution and also due to the weakness of the optical signal (long acquisition times are thus necessary to obtain an "in situ" reflection-absorption spectrum), it was not possible to record direct reflectance spectra of any of the superficial layers. Furthermore, it is necessary to eliminate the background in order to cancel out any contribution from the species in aqueous solution. Two ways were then found to overcome these problems :

i) the first possibility consists in recording reflectogr[illegible]s (i.e. the change in relative reflectance of the surface $\frac{\Delta R}{R}$ versus the potential E at fixed wavelengths λ in order to draw a tridimensional diagram $\Delta = -\frac{\Delta R}{R} = f(E,\lambda)$ which, by a further section at a given E, and provided that the $\frac{\Delta R}{R}$ reference level of reflectivity is suitably chosen, gives the normal reflection-absorption spectra $\left|-\frac{\Delta R}{R},\lambda\right|_E$ of the superficial layers. This possibility was already described in details elsewhere [6] and is illustrated in Fig. 1a and Fig. 1b which give the final spectra respectively for $Ni(OH)_2$ and NiOOH.

ii) the second possibility, which is the aim of this work, is to record long accumulation series of spectra at two different potentials and to subtract them after averaging, in order to detect the changes in the surface layers which are due to the influence of potential, and to eliminate

the contribution from the solution. Comparatively to the first method, this second technique is theoretically much faster. However severe complications arise due to the unstability of the nickel surface. Many set of experiments were done. The best (i.e. the more reproducible) results were obtained by taking the reference spectrum on newly polished nickel surfaces when holding the potential at the onset of hydrogen evolution. It was found experimentally that even in such conditions the nickel surface tends to cover in hydroxide species within a few minutes ; but, using an Harrick UV-visible rapid scan spectrometer and a Nicolet signal averager, it is possible to store and process several hundred of scans in a few seconds.

Keeping then the reference spectrum in a memory of the averager, the potential of the electrode is stepped to more positive successive potential values at which several hundred scans are also stored and averaged. Subtracting them from the reference spectrum, leads to difference reflection-absorption spectra $[\Delta A, \lambda]_{(E - E\ ref)}$, such as those given in Fig. 2.

According to the potential, three kinds of spectra were obtained, corresponding to distinct regions of the voltammogram. It is tempting to identify the spectrum of fig. 2a to $\alpha Ni(OH)_2$, of fig. 2b to $\beta Ni(OH)_2$ and that of fig. 3a to NiOOH. Even by changing the reference spectrum it was not possible to detect any significant difference between the cristallographic forms of NiOOH. Such a spectroscopic technique is very useful to follow the growing of superficial layers. When holding the potential in the NiOOH region, successive difference spectra, like in fig. 3b, are obtained, in good correlation with the voltammetric results. No such a growing is observed for the hydroxide layers. Good similarities are obtained by both techniques for NiOOH (a wide peak with a maximum near 500-550 nm). The small differences for $\alpha Ni(OH)_2$ are probably due to the difference of techniques : some peaks may be eliminated by subtraction. On the other hand the long accumulation times necessary for the first technique may lead to a surface partially covered in the irreversible β hydroxide form, explaining that the spectrum of fig. 1a is intermediate to those of figs. 2a and 2b.

Finally, samples of $\alpha Ni(OH)_2$ and $\beta Ni(OH)_2$ were prepared chemically, according to the literature, and their transmission UV-visible spectra compared to the difference reflection-absorption spectra obtained here. It is to be concluded that the "chemical α" and "electrochemical α" hydroxides are almost identical, whilst the "chemical β" differs markedly from the "electrochemical β" hydroxide.

REFERENCES

1 - R.G. GUNTHER and S. GROSS (Eds), Proc. Symp. on the Nickel Electrode (The Electrochemical Society, Princeton, N.J. 1982).
2 - S. MAKSIMOVITCH and G. BRONOEL, Electrochim. Acta,26 (1981) 1331.
3 - H. ENE, E. JOSTI and M. PESDITSCHEK, Energy Conversion, Pergamon Press, 15 (1976) 9.
4 - H. BODE, K. DEHMELT and J. WITTE, Electrochim. Acta,11 (1966) 1079.
5 - R. OLIVA, J. LEONARDI, J-F. LAURENT, C. DELMAS, J.J. BRACONNIER, M. FIGLARZ, F. FIEVET and A. de GUIBERT, J. Power Sources,8 (1982) 229.
6 - F. HAHN, B. BEDEN, M-J. CROISSANT and C. LAMY, Electrochim. Acta, submitted.

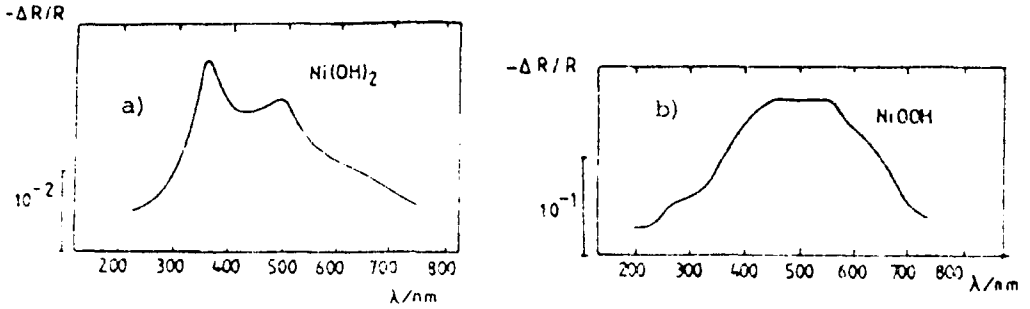

Fig. 1 - Reconstructed spectra for a) $Ni(OH)_2$ and b) NiOOH

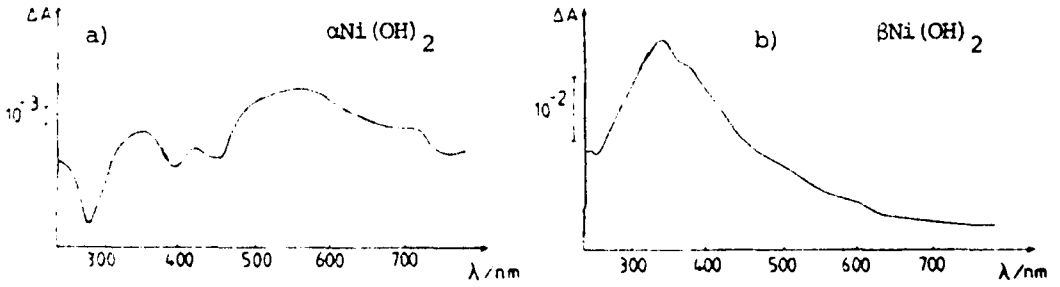

Fig. 2 - Difference spectra for a) $\alpha Ni(OH)_2$ and b) $\beta Ni(OH)_2$

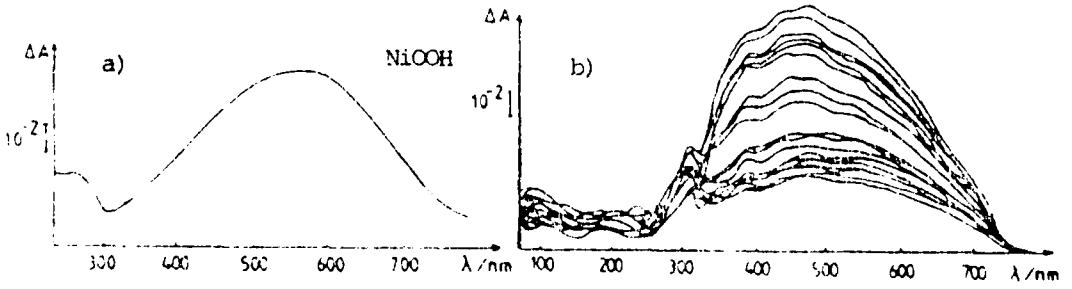

Fig. 3 - Difference spectra for NiOOH
a) first layers b) growing of the layers

02150

THE VOLTA POTENTIALS AND SURFACE POTENTIALS AT WATER - NITROBENZENE INTERFACES

Z. KOCZOROWSKI and I. ZAGÓRSKA
Department of Chemistry, University of Warsaw
ul. Pasteura 1, 02-093 Warsaw (Poland)

The widespread development of the electrochemistry of immiscible electrolyte solutions nowadays drew our attention to the Volta potential of these systems. We have chosen the often-investigated water-nitrobenzene distribution system as a model.

The Volta potential $\Delta_{nw}^{wn}\psi^{o}(MX)$ equals the difference between outer potentials of two immiscible, mutually saturated solutions of electrolyte MX, being in partition equilibrium. This Volta potential may be defined operationally as the compensation potential E_1 of the cell:

$$M \left| \begin{matrix} wn \\ MX \end{matrix} \right| N_2 \left| \begin{matrix} nw \\ MX \end{matrix} \right| \left| \begin{matrix} wn \\ MX \end{matrix} \right| M, \quad E_1 \qquad (I)$$

where wn and nw denote the aqueous and nitrobenzene phases respectively, mutually saturated, and N_2 means the chemically inert gaseous phase, e.g. nitrogen or clean air.

The value of $\Delta_{nw}^{wn}\psi^{o}(MX)$ may be measured as the difference between voltages compensating two cells:

$$M \left| \begin{matrix} \text{vibrating} \\ \text{plate} \end{matrix} \right| N_2 \left| \begin{matrix} nw \\ MX \end{matrix} \right| \left| \begin{matrix} wn \\ MX \end{matrix} \right| \left| \begin{matrix} \text{sat.} \\ \text{calomel} \\ \text{electrode} \end{matrix} \right| M, \quad E_2 \qquad (II)$$

and

$$M \left| \begin{matrix} \text{vibrating} \\ \text{plate} \end{matrix} \right| N_2 \left| \begin{matrix} wn \\ MX \end{matrix} \right| \left| \begin{matrix} \text{sat.} \\ \text{calomel} \\ \text{electrode} \end{matrix} \right| M, \quad E_3 \qquad (III)$$

The difference between compensation voltages (II) and (III) equals the Volta potential

$$\Delta_{nw}^{wn}\psi^{o}(MX) = E_1 = E_2 - E_3 \qquad (1)$$

provided the surface potentials of the vibrating plate as well as

wn and nw phases are kept constant.

Type (II) cells have been used earlier for the measurements of Volta-potential differences. The latter are, at the same time, identical with differences of partition potentials $\Delta^{M_1X_1}_{M_2X_2}\Delta^{wn}_{nw}\varphi^o$, i.e. are equal to changes of Galvani potentials at the water - nitrobenzene interface caused by the change of chemical composition:

$$\Delta^{M_1X_1}_{M_2X_2}\Delta^{wn}_{nw}\psi^o = \Delta^{M_1X_1}_{M_2X_2}\Delta^{wn}_{nw}\varphi^o \qquad (2)$$

An investigation of the following cell offers supplementary information on systems (II) and (III):

$$M \mid \text{vibrating plate} \mid N_2 \mid \begin{matrix} nw \\ MX \end{matrix} \Vert \begin{matrix} nw \\ TEAPi \end{matrix} \mid \begin{matrix} wn \\ TEAPi \end{matrix} \Vert \begin{matrix} \text{sat.} \\ \text{calomel} \\ \text{electrode} \end{matrix} \mid M, \quad E_4 \qquad (IV)$$

It has been shown that tetraethalammonium picrate (TEAPi) eliminates the diffusion potential on the interface of two nitrobenzene solutions and the partition potential of that electrolyte is cloze to zero. The difference of compensating voltages of cells (III) and (IV) type allows to estimate the difference between surface potentials of water, nitrobenzene saturated, and nitrobenzene saturated with water

$$\Delta^{wn}_{nw}\chi = E_3 - E_4 \qquad (3)$$

Operational values defined by eqns. (1) and (3) are related to Galvani potential by definition:

$$\Delta^{wn}_{nw}\varphi^o = \Delta^{wn}_{nw}\psi^o + \Delta^{wn}_{nw}\chi \qquad (4)$$

The $\Delta^{wn}_{nw}\psi^o$ values measured for several electrolytes have shown that the eqns. (1) - (4) are valid. The $\Delta^{w}_{n}\chi$ and $\Delta^{wn}_{nw}\chi$ values equal to 238 ± 10 and 105 ± 20 mV respectively, have been obtained. The influence of saturation of water with nitrobenzene and vice versa, on the surface potential of these solvents has been discussed.

In addition changes in the surface potential and the surface tension of water and water saturated with nitrobenzene have been studied as functions of tetrabutylammonium chloride and sodium tetraphenylborate concentrations for water and water saturated with nitrobenzene.

AD-A162 434 EXTENDED ABSTRACTS INTERNATIONAL SOCIETY OF ELECTROCHEMISTRY (36TH) HELD AT SALAMANCA SPAIN ON 23-28 SEPTEMBER 1985(U) INTERNATIONAL SOCIETY OF ELECTROCHEMISTRY 28 SEP 85 3/12

UNCLASSIFIED F/G 7/4 NL

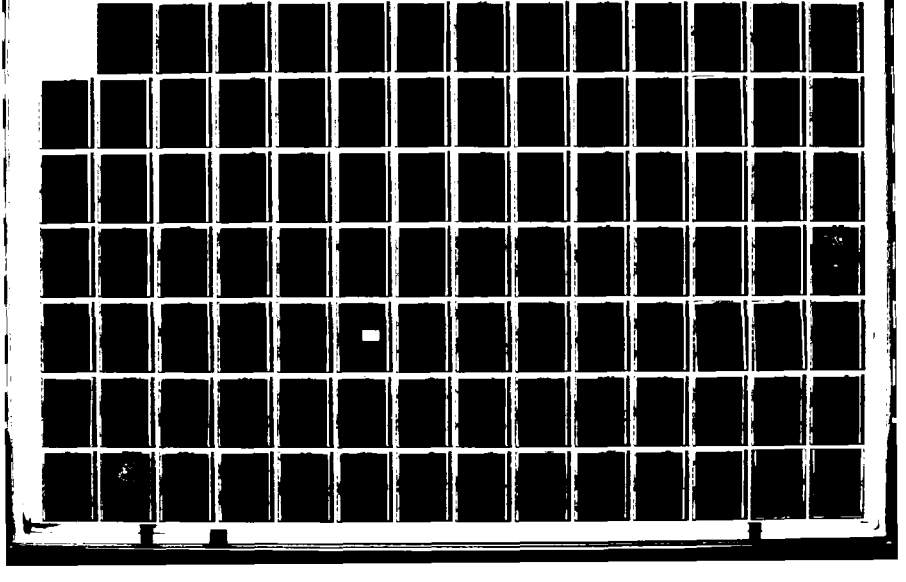

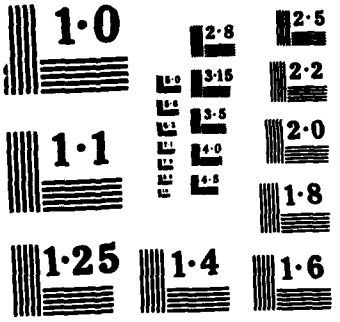

02160

ELECTROCHEMICAL INVESTIGATIONS OF CHEMICALLY MODIFIED ACTIVE CARBONS

S. BINIAK, M. PAKUŁA and A. ŚWIĄTKOWSKI

Institute of Chemistry, N. Copernicus University, 87-100 Toruń /Poland/,
Naval Academy, Gdynia 19 /Poland/,
Military Technical Academy, 00-908 Warszawa /Poland/

The chemisorptive, catalytic, ion-exchange and electrochemical properties of active carbons depend largely on the heteroatoms present on their surface and in particular on how and in what quantities is oxygen bound to their surface. This is the reason why much work is devoted to studies of the chemical character of the surface of active carbons as well as of that of other carbon materials. In the recent years attempts were made to use for this purpose chronovoltammetry to test among other things graphite[1], carbon black[2], glassy carbon[3] and active carbon[4]. However, many problems have not found so far full explanation.

In the present work the earlier described[5,6] active carbon CWN-2 was used for testing. It was preliminarily accurately demineralized with concentrated hydrochloric and hydrofluoric acids /what lowered the ash content to <0.1%/ upon which a part of it was exposed to oxidation with air oxygen at 673K during 6 hours in a fluidized bed.

In order to characterize the porous structure of both carbon preparations obtained, their benzene vapour adsorption and desorption isotherms at 293K were determined using a McBain-Bakr vacuum sorption balance. On this basis such porous structure parameters were calculated as: the volume, v_{mi}, of micropores and that, v_{me}, of mesopores, the specific surface area, S_{me}, of mesopores as well as the specific area, S_{BET}, by the BET method. The results are summarized in Table 1.

In order to characterize the chemical character of the surfaces of both carbon preparations the contents of acidic surface oxygen functional groups were determined by selective neutralization with bases of different strength. In the case of basic groups hydrochloric acid was used for neutralization. The quantities of all kinds of functional groups present on the surface, as well as the ratios of the total number of acidic groups to that of basic groups are given in Table 1. In the table the total contents of oxygen as determined directly are also given to allow evaluation of the effects of carbon modification.

The chronovoltammetric investigations of both carbon preparations were conducted with the use of a PLP 321 XY polarograph in four 0.1 N solutions of H_2SO_4 and NaOH mixed in such proportions as to obtain resulting pH values of 3.02, 6.00, 9.20 and 11.01. The measurements were carried out in an oxygen-free at-

Table 1. Physicochemical properties of unmodified and modified active carbon preparations

Physicochemical property		Active carbon preparation	
		unmodified	oxidized with air oxygen /6 h, 673K/
Content of surface oxygen functional groups, meq/g	-COOH	0.04	0.90
	-COO-	0.03	0.29
	-OH	0.11	0.78
	=CO	0.03	0.03
	basic	0.205	0.087
Σ acidic gr./Σ basic gr.		1.02	23.0
Total oxygen content, %		2.6	6.2
Parameters of porous structure	S_{me}, m^2/g	135	175
	v_{me}, cm^3/g	0.353	0.435
	v_{mi}, cm^3/g	0.291	0.391
	S_{BET}, m^2/g	845	1100

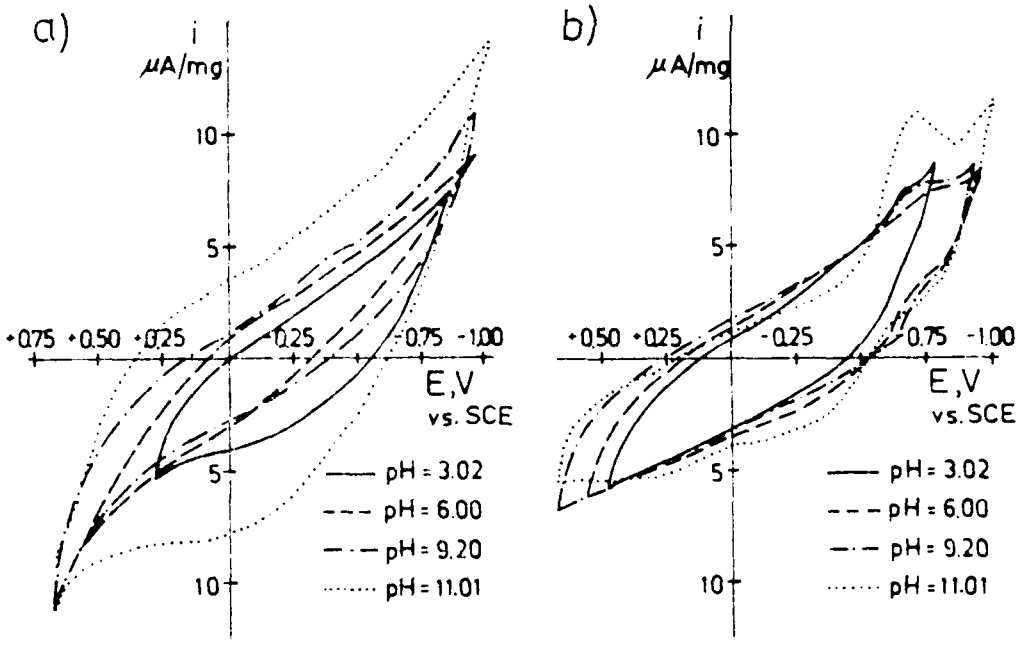

Fig. 1. Chronovoltammetric curves for CWN-2 active carbon preparations unmodified /a/ and oxidized /b/ in 0.1 N aqueous H_2SO_4-NaOH solutions of varying pH

mosphere at 298K and potential variation rate of 0.033 V/s, a saturated calomel electrode being used as reference. The size of the carbon samples /accurately determined in each measurement/ varied from 7 to 10 mg. The recorded chronovoltammetric curves are shown in Fig. 1.

The results obtained do not allow their full interpretation since the described investigations are only a preliminary stage of a more exhaustive work devoted to these problems. It can be indicated, however, that certain regularities exist which may find full explanation in the course of further studies.

First of all, for carbon with an oxidized surface we observe for growing pH values an increasing cathodic wave with a peak potential of about -0.7 V. This can be explained by a gradual hydrolysis of surface lactone systems which leads to the generation of carboxylic and phenolic groups[7]. The latter groups may take part in a redox reaction of the hydroquinone-quinone system. In the case of non-oxidized carbon no such effect is observed in view of the very low content of oxygen functional groups /Table 1/.

The results of chronovoltammetric studies of active carbons presented in this paper point to the necessity of continuing the investigations accompanied by parallel studies with the use of other techniques, e.g. IR spectroscopy.

REFERENCES

1. K.F. Blurton, Electrochim. Acta 18, 869 /1973/.
2. K. Kinoshita, J.A.S. Bett, Carbon 11, 403 /1973/.
3. D. Laser, M. Ariel, J. Electroanal. Chem. 52, 291 /1974/.
4. P. Żółtowski, J. Power Sources 1, 285 /1976/77/.
5. A. Świątkowski, Biul. WAT 31/6/, 81 /1982/.
6. H. Jankowska, A. Świątkowski, 33th Meeting of the International Society of Electrochemistry, Lyon 1982, Ext. Abstr. vol. I, p. 80.
7. J. Zawadzki, Polish J. Chem. 53, 2289 /1979/.

02170

INDEPENDENT DETECTION OF H_2O_2 AND O_2 ON CHEMICALLY MODIFIED Au ELECTRODES

M. FUJIHIRA, H. MURAKI, and S. AOYAGUI
Department of Chemical Engineering, Tokyo Institute of Technology, Ohokayama, Meguro-ku, Tokyo 152 (Japan)

In the last decade, chemical modification of electrode surfaces has been intensively investigated as a means for making various functional electrodes. In relation to electrocatalyses of the modified electrodes for fuel cells, most reserches have been intended for the persuit of novel molecular designs to accelerate electrochemical reactions. For mechanistic studies or analytical purposes, however, we very often require suppression of some undesirable electrode reactions to avoid overlapping of a wave of interest with these unwanted ones.

In the present paper, we will demonstrate that the surface catalytic reduction of H_2O_2 on a polycrystalline gold electrode in aqueous alkaline solutions can be greatly suppressed by the chemical modification of the electrode surface with n-dodecyltriethoxysilane while the reduction of O_2 and the oxidation of H_2O_2 are not affected appreciably. Such a chemical modification enables us to carry out the independent detection of H_2O_2 and O_2 in their mixture.

An unmodified gold plate and a chemically modified gold plate with n-dodecyltriethoxysilane were used as working electrodes. Electrochemical measurements were performed in a glass cell using a gold plate and a saturated calomel electrode (SCE) as a counter and a reference electrode, respectively. A deaerated 0.3 mM H_2O_2 and an air-saturated aqueous solution containing 10 mM NaOH and 0.1 M KCl were employed as sample solutions.

Figure 1a shows the cyclic voltammogram of the deaerated H_2O_2 solution on the unmodified gold electrode. On the negative sweep starting at -0.13 V, two cathodic waves were observed with the peak potentials of -0.2 V and -0.8 V, respectively. The first cathodic wave with the peak potential of -0.2 V has been ascribed to the surface catalytic reduction of H_2O_2 which proceeds via adsorption of H_2O_2 on the surface of gold in the form of OH:

$$HO_2^- + H_2O \longrightarrow 2OH(ads) + OH^- \quad (1)$$

$$2OH(ads) + 2e^- \longrightarrow 2OH^- \quad (2)$$

or the reduction of O_2 generated by the chemical decomposition of H_2O_2 on the surface:

$$2HO_2^- \longrightarrow O_2 + 2OH^- \quad (3)$$

$$O_2 + 2e^- + H_2O \longrightarrow HO_2^- + OH^- \quad (4)$$

However, the latter mechanism should be ruled out because the peak potential of the first cathodic wave of H_2O_2 reduction is ca.100 mV more positive than that of the O_2 reduction

as described below. The second cathodic wave with the peak potential of -0.8 V may be due to the direct reduction of H_2O_2 on the OH free surface:

$$HO_2^- + 2e^- + H_2O \longrightarrow 3OH^- \quad (5)$$

On the reversed scan, the cathodic current increased again in the potential region between -0.4 V and -0.2 V. This indicates that the reaction shown by the first cathodic wave is limited within the narrow potential region. Following the increase of cathodic current, an anodic wave started at -0.15 V. This wave can be assigned to the oxidation of H_2O_2:

$$HO_2^- + OH^- \longrightarrow O_2 + H_2O + 2e^- \quad (6)$$

Figure 1b shows the cyclic voltammogram of the deaerated H_2O_2 solution on the chemically modified gold electrode. In contrast with the current observed on the unmodified electrode, the only one cathodic wave with the peak potential of ca. -0.8 V was observed. This wave can be ascribed to the direct reduction of H_2O_2 described above. The pronounced suppression of the first wave on the modified surface may result from the blocking of catalytic sites which bind H_2O_2 in the form of OH. On the reversed scan, an anodic wave with the onset potential of -0.15 V was observed. This indicates that the oxidation of H_2O_2 to O_2 as well as the direct reduction of H_2O_2 to H_2O is not affected appreciably by alkylsilanization. On the second negative scan, a new wave starting at -0.1 V appeared. The peak potential of this new wave was -0.3 V which coincided with the peak potential of the first wave of the O_2 reduction as seen below. This wave, therefore, can be reasonably assigned to the reduction of O_2 which was generated on the preceeding positive sweep.

Figure 1c shows the cyclic voltammogram of the air-saturated solution on the chemically modified gold electrode which is similar to the one on the unmodified electrode. Two cathodic waves with the peak potentials of -0.3 V and -0.8 V were observed. The first wave corresponds to the reduction of O_2 :

$$O_2 + 2e^- + H_2O \longrightarrow HO_2^- + OH^- \quad (7)$$

Comparing the results shown in Figures 1a, b, c, we assigned the second wave to the direct reduction of H_2O_2 (eq. 5) which was generated by the O_2 reduction at the first cathodic wave (eq. 7). On the reversed scan, an anodic wave starting at -0.15 V was observed. This wave was not observed when the sweep started first to the positive direction. The comparison of Figures 1a, b, c reveals also that this anodic wave corresponds to the oxidation of H_2O_2.

On the unmodified electrode, the ratio of peak current of the first cathodic wave to that of the second cathodic wave, i_{p1}/i_{p2}, was slightly greater than the ratio obtained from Figure 1c. This indicates that H_2O_2 generated by the O_2 reduction in the first cathodic wave (eq. 7) was partially reduced further to H_2O by the succeeding reactions shown by the first cathodic wave in Figure 1a (eqs. 1, 2). On the other hand, since the further reactions were suppressed on the chemically modified electrode, the value of i_{p1}/i_{p2} became smaller than on the unmodified one.

These experimental findings described above lead to the conclusion that (i) the catalytic H_2O_2 reduction on gold proceeds mainly via the mechanism described eqs. 1 and 2 and

the catalytic sites can be blocked by alkylsilanization and (ii) on such an alkylsilanized gold electrode only oxygen can be reduced at around -0.3 V and therefore the independent electrochemical detection of H_2O_2 and O_2 in their mixture is possible. Namely the concentration of H_2O_2 can be determined by its anodic currents while that of O_2 by cathodic ones.

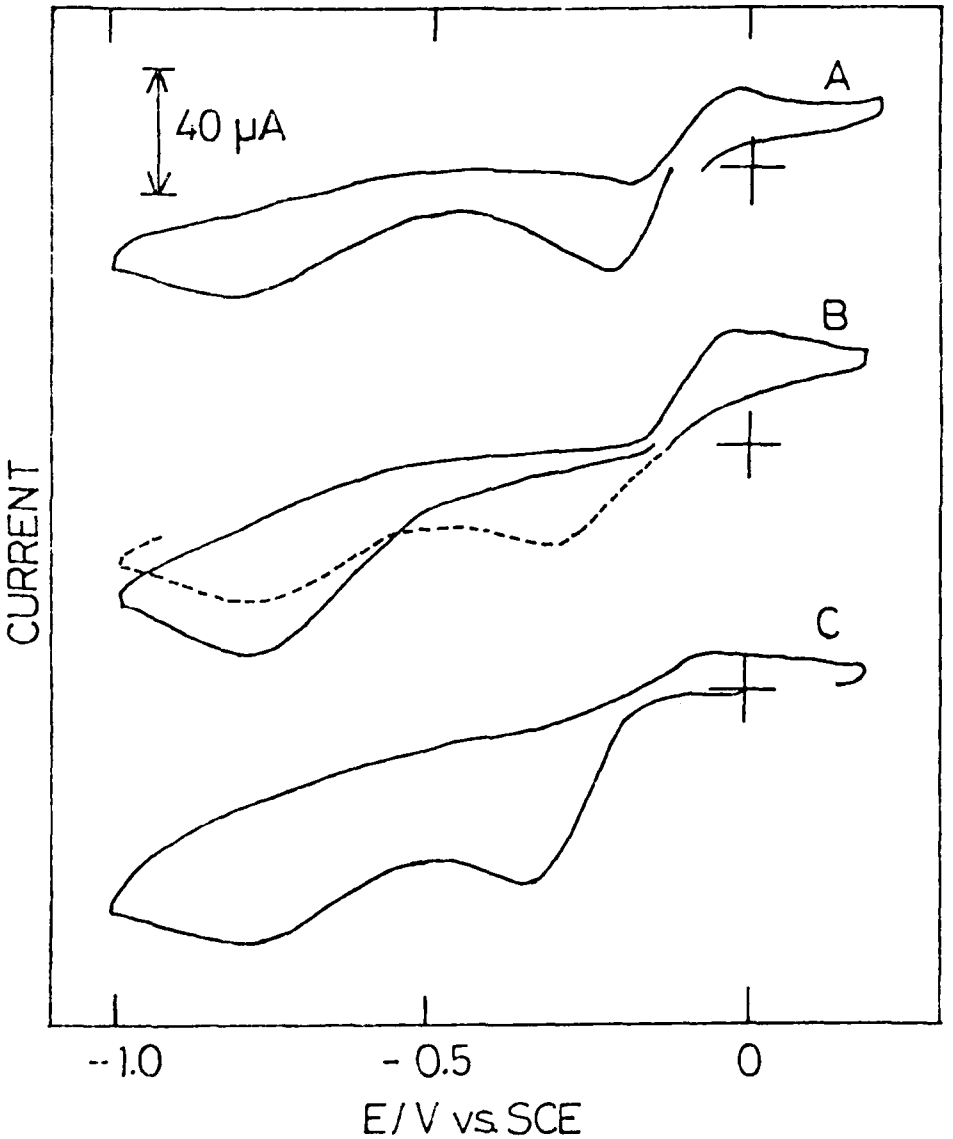

Fig. 1 Cyclic voltammograms of H_2O_2 and O_2 on unmodified and chemically modified gold electrodes
a. H_2O_2 on unmodified Au electrode
b. H_2O_2 on chemically modified Au electrode
c. O_2 on chemically modified Au electrode

02180

ELLIPSOMETRY : ELECTRONS PROFILES AT THE Au-ELECTROLYTE INTERFACE

F. CHAO and M. COSTA
Laboratoire d'Electrochimie Interfaciale du CNRS
1 Place A. Briand, 92195 MEUDON Principal Cédex, France

Numerous theoretical studies try to describe the free electrons distribution in the interfacial zone in absence of transfer reactions.

These studies are generally done with the electrode at the zero charge potential (see for example [1]). The electric charge metal effect on the deformation or displacement of these profiles has been the subject of some papers.

Recently Dzhavakhidze et al[2] calculated the characteristics of these profiles as a function of the electric charge for different metals, using the simple jellium model.

Ellipsometry with phase and azimuth modulation allows the measurement of very weak variations of Δ and Ψ (some minutes) corresponding to the charge variation of the electrode.

We propose a model of calculation of these variations starting from the integration of the dielectric function of the metal superficial layer modified by the electric field. The identification of calculated and experimental values of $\delta\Psi$ allows us to reach the parameters characteristic of the electronic distribution as a function of the charge. We shall compare these results to those calculated in ref.[2]

1. E. Fusco, C. Regnaut, J.P. Badiali, Extended Abstracts, 33rd Meeting ISE, Lyon, 1982, p.37.

2. P.G. Dzhavakhidze, A.A. Kornyshev, G.I. Tsitouashvili, Solid State Communications, 52 (1984) 401.

02190

THE PERMEATION OF HYDROGEN IN A STEEL AT ELEVATED TEMPERATURES BY AN ELECTROCHEMICAL METHOD

HARUSHIGE TSUBAKINO and KOJI YAMAKAWA
College of Engineering, University of Osaka Prefecture
Mozu-Umemachi, Sakai, Osaka 591, Japan

Steels exposed to high temperature and high pressure hydrogen result in a marked reduction in mechanical properties. This phenomenon is well known as hydrogen attack, which is caused primarily by a nucleation, growth and coalecence of methane bubbles[1].

All of studies on hydrogen attack have been performed by a usual gaseous method using pressure vessel or autoclave. But an electrochemical method has the following remarkable features[2)-4)]: a good detection limit for the measurement of hydrogen content in steel, a simpler measuring apparatus, suitability for successive measurement of the transport characteristics, and flexibility in variation of experimental conditions. However this electrochemical method has been restricted to temperatures below 373 K because an aqueous solution has been used as an electrolyte.

In this study, an electrochemical permeation method using molten sodium hydroxide at elevated temperatures (673-773 K) in the range of practical interest for hydrogen attack in steel is presented.

Procedure and Results

An electrochemical permeation method is based on the following concept: hydrogen is introduced into one side of a metallic specimen during cathodic polarization, while the other side of the specimen is held at an anodic potential sufficient to ionize any hydrogen arriving at the surface after passage through the metal. The resulting ionization current is a direct measre of the instantaneous rate of hydrogen permeated through the metal[2)-4)].

In this study, the cathodic charging and extraction of hydrogen are carried out by using molten salt electrolyte. The cathodic and anodic reactions are, respectively

$$H_2O + e^- \longrightarrow H_{ad} + OH^- \qquad (1)$$

and

$$H_{ad} + OH^- \longrightarrow H_2O + e^-. \qquad (2)$$

A schematic diagram of the experimental setup is shown in Fig.1. The specimen has a cylindrical geometry and its bottom is about three times thicker than the thickness of the side. The inner diameter is 25 mm and the thickness is varied from 2 to 6.5 mm. The specimen, into which a stainless steel tube is screwed, separates the entry side (A) and extraction side (B) of the hydrogen.

Entry Side (A): Sodium hydroxide (melting point=595 K) is

contained in an alumina crucible. Argon gas is bubbled through a water bath at 303 K with a gas flow rate of 1.7×10^{-6} m^3/s. The cathodic charging of hydrogen is carried out galvanostatically, using four graphite counter electrodes, located on the same circumference, and a current density of 50-200 A/m^2 [5].

Extraction Side (B): is also filled with sodium hydroxide [6]. The surface of the specimen is plated with a gold-coating of about 0.15 or 0.5 μm in thickness. Platinum-coated Magnesia-stabilized zirconia tube is used as the reference electrode. The electrolytic cell is filled with argon gas in a good airtight condition. The specimen is maintained at a constant potential in the range from -1.0 to -0.4 V vs Air/O^{2-}(ZrO_2).

When the anodic current density reached a steady state less than 0.5 A/m^2, without the cathodic hydrogen charging, the cathodic charging is started. The cathodic current density is increased (build up) and then decreased (decay). The permeated transient current during these build up and decay processes is recorded as a function of time.

The observed relationship between the permeation current and the extraction potential shows thet the most suitable potential to detect hydrogen is shown in the range of 200 mV from -800 to -600 mV vs Air /O^{2-}(ZrO_2). Typical build up and decay transients at 673 K are shown in Fig.2. The data agree fairly well with the theoretical curves. This result indicates that the extraction surface is held at an sufficient anodic potential to ionize the hydrogen. But the data tend to deviate from the theoretical curves as the thickness of the specimen decreases. This will be due to the effect of gold-plating on the hydrogen permeation rate.

The detection limit in this electrochemical method is less than 0.1 ppm, which is much less than the critical hydrogen contents for hydrogen attack in carbon steel (0.6 ppm) and in Cr-Mo steel (2.4-4.3 ppm)(Fig.3) [7]. The diffusivities obtained from several build up and decay runs at each temperature are in good agreement with the values obtained from the gaseous methods, i.e., gaseous permeation and evolution techniques. But a significant delay in the first transient is always observed (Fig.4). And the diffusivities tend to decrease gradually as the permeation run increases. These phenomena will be due to the hydrogen trapping in steels.

Therefore, this electrochemical permeation method using molten salt will be useful to study the hydrogen transport in metals at high temperatures and to predict the hydrogen attack of steels.

References

1) P.G.Shewmon: Metall.Trans., 7A(1976), p.279
2) J.McBreen, L.Nanis and W.Beck: J.Electrochem.Soc., 113(1966), p.1222
3) S.Yoshizawa, K.Tsuruta and K.Yamakawa: Boshoku Gijutsu (Corrosion Engineering), 24(1975), p.511
4) M.A.V.Devanathan and Z.Stachurski: Proc.Roy.Soc.London, A270(1962), p.90
5) H.Tsubakino, A.Ando, A.Masuda and K.Yamakawa: Trans.ISIJ, 25(1985), in press

6) H.Tsubakino, A.Ando and K.Yamakawa: Scripta Metall., 18(1984), p.1121
7) H.Tsubakino and K.Yamakawa: Boshoku Gijutsu (Corrosion Engineering), 24(1984), p.159

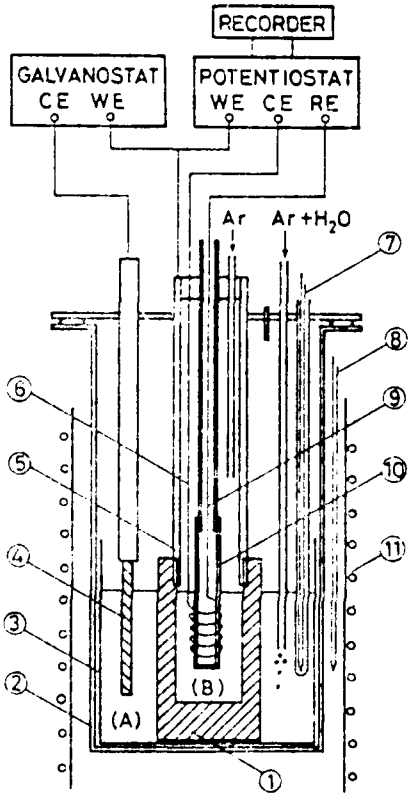

FIG.1 EXPERIMENTAL SET UP.

(A):Entry Side, (B):Extraction Side
1:Specimen, 2:Stainless steel tube,
3:Alumina crucible, 4:Graphite rod,
5:Stainless steel tube, 6:Nickel wire,
7,8:Thermocouple, 9:Stainless steel wire,
10:Stabilized zirconia tube, 11:Furnace

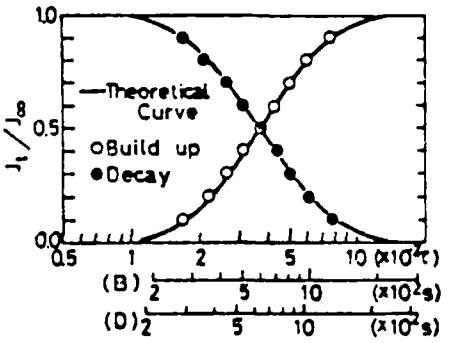

FIG.2 TYPICAL PERMEATION TRANSIENTS.

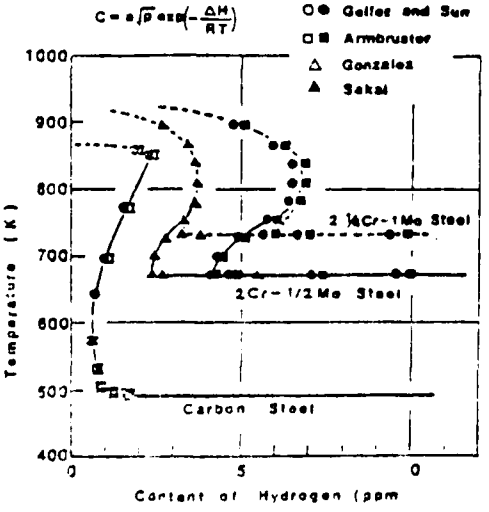

FIG.3 CRITICAL HYDROGEN CONTENT FOR HYDROGEN ATTACK.

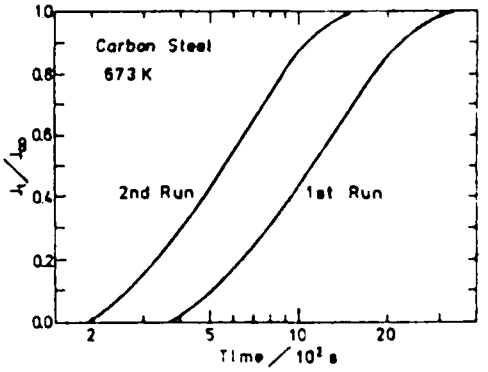

FIG.4 PERMEATION TRANSIENTS, FIRST AND SECOND RUN.

02200

ELECTROCHEMICAL PROPERTIES OF ELECTRODE SURFACES MODIFIED WITH POLY-VINYLIMIDAZOLE BOUND RUTHENIUM COMPLEXES.

S.M. GERATY, A.G. ROSS AND J.G. VOS
School of Chemical Sciences, National Institute for Higher Education, Dublin 9, Ireland.

Introduction.

Polymer bound ruthenium complexes are promising as new materials for electrochemical applications.[1] Such metallopolymers have been investigated both as thin films on electrode surfaces and in solution.[2,3] Areas of interest are energy conversion and catalysis. It is expected that both the nature of the ruthenium complex, and therefore its redox potential, and the charge transport through the polymer layer will be affected by the type of polymer backbone and the metal to polymer ratio.

We started a systematic investigation into the effect of the polymer backbone on the chemical properties of metallopolymers. In this contribution characterisation and electrochemical properties of electrodes modified with $Ru(bpy)_2$ - groupings bound to poly N-vinylimidazole (PNVI) and poly-4(5)-vinylimidazole are reported (PCVI).

Results and discussion

In contrast with earlier experiments using poly-4-vinylpyridine (PVP) as a polymer backbone[2], PNVI and PCVI often yield at least two types of bound ruthenium complexes when reacted with $Ru(bpy)_2Cl_2$. This is clearly shown by CV's of the polymer coated graphite electrodes (see fig.1). The data obtained suggests that reactions 1, 2 and 3 are taking place,

$$Ru(bpy)_2Cl_2 + PNVI \longrightarrow [Ru(bpy)_2(PNVI)\ Cl]^+ + Cl^- \qquad (1)$$

$$[Ru(bpy)_2(PNVI)\ Cl]^+ \longrightarrow [Ru(bpy)_2(PNVI)\ S]^{2+} + Cl^- \qquad (2)$$

$$[Ru(bpy)_2(PNVI)S]^{2+} + PNVI \longrightarrow [Ru(bpy)_2(PNVI)_2]^{2+} + Cl^- \qquad (3)$$

with the solvent complex $[Ru(bpy)_2(PNVI)\ S]^{2+}$ (S = H_2O, MeOH) possibly present as an intermediate. The nature of these complexes has been investigated by comparison of spectroscopic and electrochemical data of these materials with those obtained for analogous monomeric complexes. The composition of the metallopolymers obtained is influenced by the reaction conditions during the synthesis. In general addition of water will increase the amount of disubstituted complex obtained (see fig.1). Also the variation of the polymer, ruthenium ratio affects the product

distribution. In some cases an extra band at about 300 mV vs SCE is observed. The nature of this redox couple is not yet clear. The peak-to-peak separation and the stability of the polymer modified electrodes depends strongly on the nature of the electrolyte. Peak-to-peak separations are very small (< 20 mV) in HCl or H_2SO_4 and larger (> 50mV) in non acidic solutions and in $HClO_4$.

Both thermal and photochemical displacement of the Cl- ligand in the monosubstituted products are observed. The thermal exchange is faster than for the corresponding poly-4-vinylpyridine complex $[Ru(bpy)_2(PVP)Cl]^+$ [4]. Under irradiation (electrolyte, 1 M $HClO_4$) loss of Cl^- is very efficient, the product obtained from $[Ru(bpy)_2(PNVI)Cl]^+$ is most likely $[Ru(bpy)_2(PNVI)H_2O]^{2+}$. In sulfuric acid coordination of sulfate ions is also observed. Electrodes modified with ruthenium containing PNVI were used for oxidation of Fe^{2+}. It was found that the oxidation is mediated by the polymer coating. The limiting current depends on the Fe^{2+} concentration (see fig. 2). A Koutecky-Levich plot of this limiting current yields a straight line with an intercept that is dependent on the amount of the polymer used (fig. 3).

References

1. P.G. Pickup and W. Murray, J. Electrochem. Soc., 1984, 131, 833.

2. J. M. Clear, J. M. Kelly, C. M. O'Connell and J.G. Vos, J. Chem. Res., 1981, 3039 (M).

3. O. Haas and J.G. Vos, J. Electroanal. Chem., 1980, 113, 139.

4. O. Haas, H. R. Zumbrunnen and J.G. Vos, Electrochim. Acta, in print.

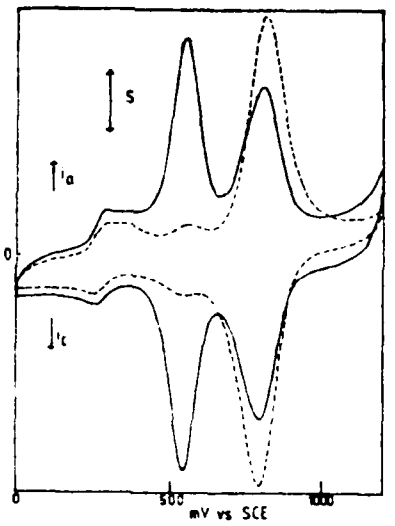

Fig. 1.
CV's of the materials obtained from the reaction of $Ru(bpy)_2Cl_2$ *with PNVI (Ru: PNVI ratio = 1 : 10) in;*
methanol (——)
methanol/water (– – –)
$S = 100\ \mu A$; *scan rate 50 mV/sec; electrolyte 1 M* H_2SO_4.

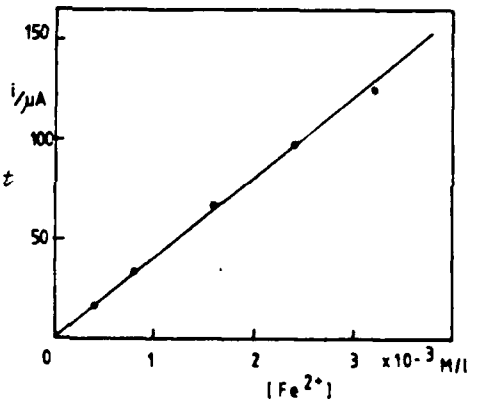

Fig. 2.
$[Fe^{2+}]$*dependency of the limiting current of the oxidation of this ion using a CG electrode coated with* $Ru(bpy)_2$ *containing PNVI.*

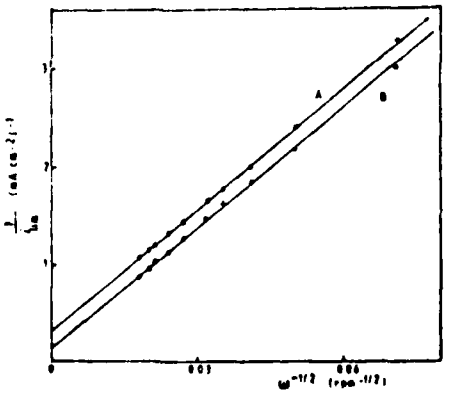

Fig. 3.
Koutecky-Levich plot of the oxidation of Fe^{2+} *using a CG electrode coated with* $[Ru(bpy)_2PNVI\ Cl]^+$
$[Ru] \simeq 2.5 \times 10^{-7}$ *M/cm*^{2} *(A)*
2.5×10^{-8} *M/cm*^{2} *(B)*
$[Fe^{2+}] = 2 \times 10^{-3}$ *M/l*

02210

THE USE OF ADATOMS IN THE ELECTROCHEMICAL SYNTHESIS OF GLYOXYLIC ACID FROM GLYOXAL

G. PIERRE, M. EL KORDI and G. CAUQUIS.
Laboratoire de Chimie Organique Analytique (U.A. C.N.R.S. 321)
B.P. n° 68 - Domaine Universitaire de Saint Martin d'Hères (France)

During the electrochemical synthesis of glyoxylic acid from oxidation of glyoxal, one of the main problem encountered was the total elimination of glyoxal itself. Indeed as three reactions are possible at the same potential on a platinum electrode,

$$CHOCHO - 2e + H_2O \rightarrow CHOCOOH + 2H^+ \quad (1)$$

$$CHOCOOH - 2e + H_2O \rightarrow (COOH)_2 + 2H^+ \quad (2)$$

$$(COOH)_2 - 2e \rightarrow 2CO_2 + 2H^+ \quad (3)$$

after complete electrolysis of solution containing 5% (0.86 M) of glyoxal, 0.9% (0,15 M) of this species remains in the solution after the passage of the quantity of electricity Qth corresponding to the reaction (1). A further oxidation beyond 1.2 Qth is of poor interest since glyoxylic acid vanishes quickly from the solution.

From the results of HORANYI et al[1,2] and FORNARO et al[3,4] we can deduce that glyoxal is adsorbed on Pt following two types of reaction. For high concentrated solution of glyoxal, the molecule is oxidized into glyoxylic acid after adsorption onto two activ sites of platinum, when for low concentrated solution it takes four activ sites and gives oxalic acid.

So a method which could promote the vanishing of glyoxal without an increase in oxalic acid, for example by blocking some activ sites of the metal of the anode, would be interesting. It was the role attributed to the adatoms added to the solution of the electrolysis.

The influence of the addition of 5.10^{-4} to 10^{-3} M of nine adatoms : Pd, Ru, Ag, Au, Tl, Pb, Bi, Sn, Cu on the ill defined oxidation curves of glyoxal, glyoxylic acid (about 0.2 M) and oxalic acid has been studied by cyclic voltammetry on platinum and in aqueous N $HClO_4$ solution which have a wide anodic domain. Three of them Tl, Ag, Au, gave a cathodic shift of the potential and an increase of the current of the peak corresponding to the oxidation of the organic species. An exemple is given below for Ag adatom. The addition of other adatoms lead generally to an opposite effect.

This effect is compared with the yields in glyoxylic acid and the concentrations of the different species after electrolysis in comparable conditions. The salt of the adatom is added at the beginning of the experiment, Sn is predeposit.

The results concerning the most interesting adatoms are compiled in the table.

Yields in glyoxylic acid. Anode Pt, θ = 50°C, Q = 1.2 Qth 1 N HCl solutions, starting concentration of glyoxal : ∿ 0.9 M. | adatoms | = 10^{-3} M.

Adatoms	none	Ag	Au	Sn	Pd
Glyoxal final M	0,095	0,034	0,052	0,034	0,37
Glyoxylic acid M	0,480	0,600	0,588	0,554	0,250
Oxalic acid M	0,089	0,080	0,083	0,064	0,067
Chemical yield %	62	69	69	63	51
Electrical yield %	46	54	53	52	24

Salts used : $AgNO_3$; $SnCl_2$; $KPdCl_4$; $HAuCl_4$, $3H_2O$.

It was observed that with adatoms making easier the oxidation of the organic product, *the yields are slightly increased*, but the main interest is a better elimination of glyoxal (concentration divided by about 3). With Ag a further oxidation (Q = 1,6 Qth) lead to almost a complete vanishing of glyoxal (0,007 M) with a still good chemical yield (52%), which has been impossible to obtain on bright platinum. Palladium adatom is a particular example where it is the peak of the adatom which is modified by addition of glyoxal or the other species. In this condition the main reaction is a CO_2 evolution. On vitreous carbon V 25 (le CARBONE LORRAINE), almost no variation are observed at 50°C by addition of adatoms studied up to now (Bi, Sn)

References :

1 G. INZELT and G. HORANYI, Acta Chim. Acad. Sci. Hung., 98, 403 (1978)

2. V.E. KAZARINOV, YU. B. VASSILIEV, V.N. ANDREEV and G. HORANYI, J. Electroanal. Chem., 147, 247 (1983)

3. L. FORNARO and S. TRASATTI, La Chimica et l'Industria, 48, 706 (1966)

4. L. FORNARO and G. CASTELLI, J. Electroanal. Chem., 28, 363 (1970).

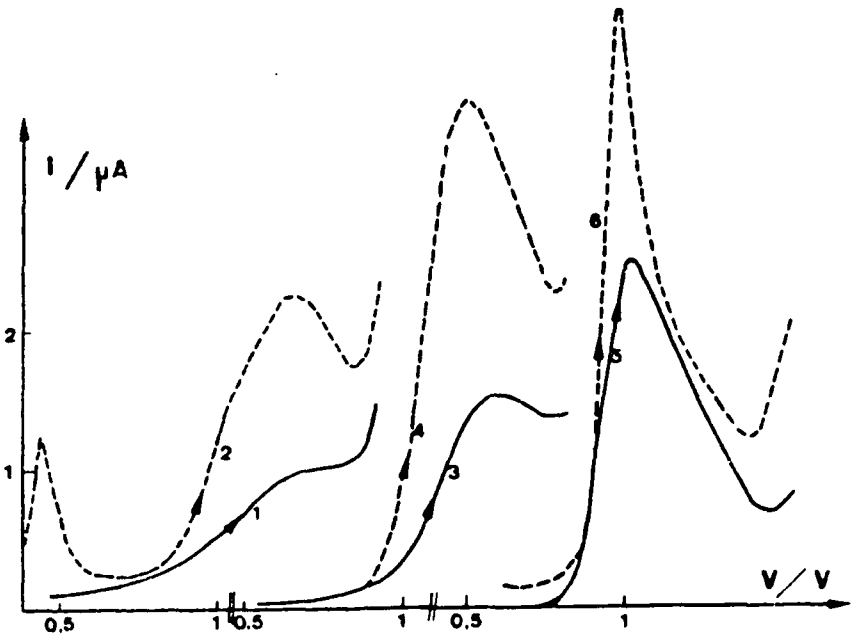

Influence of silver adatoms on the cyclic voltammetry of glyoxal and its oxidation products. All the concentrations are expressed in mol. l^{-1}

left side : |CHOCHO| = 0.17 ; 1 : $|Ag^+|$ = 0 ; 2 $|Ag^+|$ = $1.2.10^{-3}$

middle : |CHOCOOH| = 0.15 ; 3 : $|Ag^+|$ = 0 ; 4 $|Ag^+|$ = $1.2.10^{-3}$

right side : |COOHCOOH| = $3.2.10^{-2}$; 5 : $|Ag^+|$ = 0 ; 6 $|Ag^+|$ = $1.2.10^{-3}$

I scale = Curves 1-4 : 1 unit = 100 μA.
Curves 5,6 : 1 unit = 500 μA.

02220

ON THE MECHANISM OF THE EFFECT OF COBALT ADDITION ON THE PROPERTIES OF A NICKEL OXIDE ELECTRODE

V.Z.BARSUKOV, N.R.MESHCHERJAKOVA, L.N.SAGOJAN

Institute of Chemical Engineering, Dnepropetrovsk (USSR)

Cobalt is one of the most effective additives to nickel oxide electrodes (NOE)[1]. However, little evidence about the mechanism for the effect of such additions has been obtained up to now[2], this being to a considerable extent due to a lack of so far proved quantitative ideas as to the nature of the main current-forming process in the active material (AM) grain of NOE.

Authors of[3] on the basis of theoretical analysis of a dynamic model of an AM grain in NOE have shown that the cathodic process starts simultaneously within the whole volume of a grain, but the intensity of the process varies with depth considerably; it is defined by the distribution of electric field strength in the solid phase. The discharge process of the grain is decisively influenced by the change of the solid phase conductivity, which first drops gently and then abruptly with relationship of Ni^{3+}/Ni^{2+} ratio decrease. The cause of abrupt grain passivation during discharge is in faster exhaustion of electric conductivity of AM within the solid phase volumes adjacent to the areas of contact with the current lead. The parts of the grain that are inner and most remote from the contact of the three phases do not discharge completely, thus lowering the AM utilization factor.

In our opinion, cobalt introduction into the AM affects directly the grain passivation causes during discharge and results in smoothing down the non-uniform grain operation providing for more complete usage of the capacity of deeper parts of the solid phase remote from the areas of contact with the current lead.

The main prerequisites of the above effect are as follows: a practically complete isomorphism of crystal lattices of δ-$Co(OH)_2$ and β-$Ni(OH)_2$ facilitates easy implantation of Co ions into the crystal lattice of AM to replace Ni ions and to retain them in the lattice firmly during electrochemical transformations[4].

Co(II) transforms to its stable oxidized state Co(III) during the first charge cycle. From that moment on it does not change its degree of oxidation during mutual transformations $Ni(III) \rightleftharpoons Ni(II)$ within the normal range of NOE potential variations.

Cobalt implantation to the crystal lattice to form solid solution results in a definite type of interaction between Co(III) ion and nickel ions surrounding it. This type of solid solution can be regarded as a kind of solid-state complex compound of CoOOH·nNiOOH type in which Co(III) acts as a complexing agent. As known, ion reduction from a complex often is energetically more difficult and takes place at higher electrode polarizations. Therefore it might be supposed that in compounds of this type Co(III) will retain a part of the surrounding nickel ions in a higher degree of oxidation and that transformation of this part

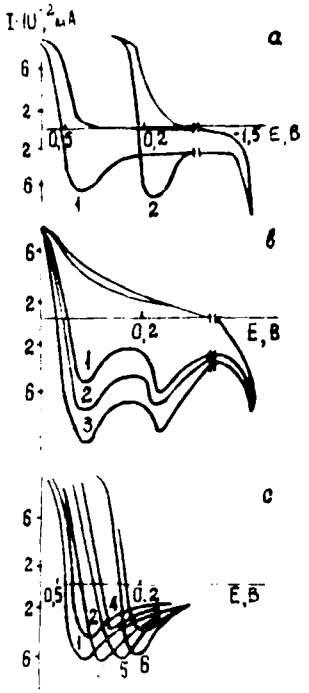

Fig.Cyclic I-E curves:
a)NiOOH(1), CoOOH(2)
b)mechanical mixtures:
CoOOH + NiOOH(1)
CoOOH + 2NiOOH(2)
CoOOH + 3NiOOH(3)
c)solid solutions:
CoOOH · 13NiOOH(1)
CoOOH · 12NiOOH(2)
CoOOH · 9NiOOH(3)
CoOOH · 6NiOOH(4)
CoOOH · 4NiOOH(5)
CoOOH · 3NiOOH(6)
CoOOH · 2NiOOH(7)

from Ni(III) to Ni(II) state will take place at somewhat lower potentials.

To obtain experimental evidence of these assumptions codeposition of hydroxides was accomplished. Compounds of CoOOH·nNiOOH (n=2,3,4,6,9,12 and 13) type were obtained as well as mechanical mixtures of CoOOH and NiOOH with the same n values. Individual phases of β-NiOOH and β-CoOOH were also obtained. Identification of phases and degrees of oxidation was carried out using electron diffractometry and electron paramagnetic resonance (EPR) spectroscopy techniques.

Using the derivatographic analysis techniques it was found that codeposition of substances results in obtaining solid substitution solutions rather than mechanical mixtures of initial components with additive features.

Cyclic voltage-current curves for CoOOH and NiOOH are shown in Fig.a. Transition of Ni^{3+} to Ni^{2+} takes place at potentials that are by about 285 mV more positive than those for Co^{3+} to Co^{2+} transition. Voltage-current curves for mechanical mixtures of CoOOH + nNiOOH (Fig.b) at cathodic polarization in the range of potentials from 0.1 to 0.5 V (normal hydrogen electrode) have two consecutive peaks corresponding, as can be seen from Figs.a and b, to independent reduction of Ni^{3+} to Ni^{2+} and then that of Co^{3+} to Co^{2+}.

Fig.b shows cyclic voltage-current curves for codeposited compounds CoOOH·nNiOOH In the range of potentials from 0 to 0.5 V a pair of peaks is observed on the curve of any substance; this pair of peaks is between voltage-current curves of initial NiOOH and CoOOH on the potential scale. The stationary potential and the position of the peaks depend on the ratio of cobalt and nickel in the lattice. Withincreasing n the stationary potential is shifted to a more positive region - up to the redox-potential of NOE.

It may be concluded that the presence of cobalt in the crystal lattice of NiOOH prevents Ni^{3+} from discharge up to a certain potential.

About the same conclusions as to the process of self-discharge of NOE can be drawn from the results of infra-red spectroscopic investigations of the substances.

Thus, the investigations provide for the conclusion that nickel ions surrounding cobalt in the crystal lattice are more firmly

retained in "3+" oxidation state in the presence of cobalt vs.its absence.

This results in the following: lower redox potential of Ni^{3+} Ni^{2+} transition, higher content of Ni^{3+} in the discharged AM, higher AM conductivity.

These circumstances has differently affect such vital parameters of NOE as self-discharge and AM utilization factor during discharge in dependence on the content and distribution of cobalt in the crystal lattice of hydroxide.

Uniform introduction of Co to AM (e.g., by codeposition of hydroxides) shall facilitate retardation of self-discharge of a NOE to the extent which is the greater the higher is Co content.

At the same time uniform distribution of cobalt in AM is of little effect on the AM utilization factor (η).

Uniform introduction of small amounts of cobalt may result in the increase of average AM conductivity due to a higher ratio of metal ions in "3+" state of oxidation. This is confirmed by experimental data given in[5].

It is obvious, that retaining part of nickel in Ni^{3+} state, cobalt prevents a certain amount of AM from taking part in the main current-forming process. Therefore, the increase of Co content in AM in excess of certain limits will result in reduction, η, and the relationship between the capacity of the electrode and Co content in it shall be of extreme type, what is evidenced by[6].

With regard to the above mechanism, non-uniform cobalt distribution on the surface and into the depth of the grain should be considered optimal. Cobalt content should be the highest in the area of contact with the current lead, as the process of exhaustion of electric conductivity is the fastest here. Cobalt content should decrease with grain depth according to the nearly-exponential law that expresses variation of field strength in a grain[3]. This type of cobalt distribution in the AM provides for compensation of unequal accessibility of different grain regions for electric field and for optimum usage of the stored electrochemical capacity. Cobalt consumption can be also minimized.

References

[1]. Bagotskij V.S., Skundin A.M. Khimicheskije Istochniki Toka,USSR, Energoizdat (1981). [2]. Novakovskij A.M., Shibajeva N.Yu., Gorleva L.K. - Tezisy Dokladov VI Vsesojuznoj Konferentsii po Electrokhimii, 124, (1982). [3]. Barsukov V.Z., Rogoza B.E., Sagoyan L.N. - 34-th ISE Meeting, Extended Abstracts, Erlangen, Germany, No.0112, (1983). [4]. Barsukov V.Z., Gerasimov A.G., Sagoyan L.N. - 32-th ISE Meeting, Extended Abstracts, Dubrovnik/Cavtat, Yugoslavia,2, 889, (1981). [5]. Appelt K. Electrochim.Acta,13, 1727, (1968). [6]. Dzhanushkevich S. XIII Jezhegodnaja Amerikanskaja Konf. po Khimicheskim Istochnikam Toka,2, 75, (1959).

02230

Characterization of $NiCo_2O_4$ spinels for O_2 evolution in alkaline electrolyte

J. Haenen, W. Visscher and E. Barendrecht

Laboratory for Electrochemistry, Department of Chemistry
Eindhoven University of Technology
P.O. Box 513, 5600 MB Eindhoven, The Netherlands.

$NiCo_2O_4$ spinel oxide, prepared by thermal decomposition of metal salts is a very promising anode material [1]. It was found that mainly the top surface of the $NiCo_2O_4$ electrode is electrochemically active. The surface morphology and composition of the freshly prepared $NiCo_2O_4$ layer were found to depend on the thermal treatment, particularly on the temperature of the final heat treatment T_F: the increase in activity with decreasing T_P was correlated with the increase in surface area and the change in surface composition. The kinetics of the oxygen evolution reaction were examined with galvanostatic steady-state measurements in the temperature range of 10 to 80°C, and in the electrolyte concentration range of 0.1 to 7.0 M KOH. The Tafel plots can be divided in two regions: one with a Tafel slope of 40 mV, i.e. 2 RT/3 F, for $\eta < 280$ mV and a range of Tafel slope values from 70 to 100 mV at higher overpotentials, i.e. $\eta > 280$ mV, which was assumed to be 2 RT/F. For the different potential regions, the kinetic behaviour can be explained by a reaction mechanism, by which either a shift in active site takes place from di- to trivalent sites, or by which the valence state (trivalent) does not change, but a shift from low coverages, i.e. $\theta_{TOH} \rightarrow 0$, to high coverages, i.e. $\theta_{TOH} \rightarrow 1$, occurs.

The $NiCo_2O_4$ catalyst was investigated with cyclic voltammetry in order to elucidate the electrocatalytic activity and the ageing phenomena.

In the potential range before oxygen evolution starts, the voltammogram of a freshly prepared $NiCo_2O_4$ electrode exhibits two anodic oxidation peaks, as shown in figure 1, representing one-electron-transfer surface redox reactions. The voltammetric response of a fresh $NiCo_2O_4$ electrode is not only influenced by the lower and upper switching potential of the scan range, but also in a different way by potentiostatic or potentiodynamic treatment. With prolonged oxidation a single peak voltammogram was obtained, as shown in figure 2. This is considered to be an ageing phenomenon which was interpreted

in terms of partial decomposition of the $NiCo_2O_4$ surface layer.
On the basis of the results of electrochemical and non-electrochemical techniques, the following general cation distribution was proposed:
$Co_x^{2+}Co_{1-x}^{3+}[Ni_y^{2+}N_{1-y}^{3+}Co_{1.0}^{3+}]O_{4+z}^{2-}$
with two valence states on the sublattices, and the possibility of excess oxygen to maintain the electroneutrality; x, y and z are related through $z = (x-y/2)$.
Furthermore, the electrochemical formation of oxides on nickel-cobalt alloys was investigated with cyclic voltammetry, kinetic analysis and ellipsometry. It was found that the electrocatalytic behaviour of the Ni_1Co_2-alloy changes with the pretreatment. At a freshly polished Ni_1Co_2-alloy, a Tafel slope of about 40 mV and a decrease of the overpotential is found after potentiodynamic cycling, whereas after preanodization a slope of 60 mV and an increase in η is found.
The optical behaviour of a Ni_1Co_2-alloy during a potential scan from -0.075 to 1.425 V is given in figure 3 in a Δ-ψ graph. With increasing anodic potential, up to about 1.25 V, the change of the ellipsometric parameters Δ and ψ is such that a linear Δ-ψ relation is obtained. This implies that in this potential range, an oxide layer is formed, which grows with a constant refraction index N. Beyond 1.25 V (at the maximum in the Δ-ψ curve), the optical properties change, the decrease in ψ coincides with the onset of a further oxidation process. From curve fitting, part a of figure 3 was found to correspond to a film layer with a refraction index $N = 2.3 - 0.1\ i$, and part b (beyond 1.25 V) pointed to the formation of a conductive oxide (high k-value) on the top of the first layer, for which the best fit corresponds to a layer with $N = 2.9 - 2.1\ i$.
The two different pretreatments lead optically to the same two-layer film model: only it appeared that with cycling the first film continuously grows, whereas with preanodization a limiting thickness of about 75 A is reached. The difference in kinetic behaviour was explained by assuming that either spinel-like oxides are formed on the Ni_1Co_2-alloy, or that, depending on the pretreatment, the alloy electrode behaves predominantly as a nickel or as a cobalt electrode.

[1] J.G.D. Haenen, W. Visscher and E. Barendrecht, J. Appl. Electrochem. 15, 29 (1985).

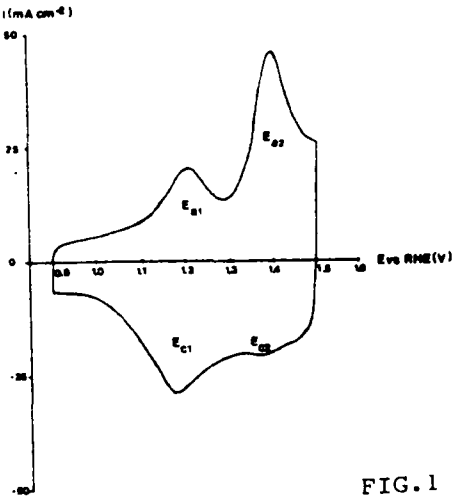

FIG.1

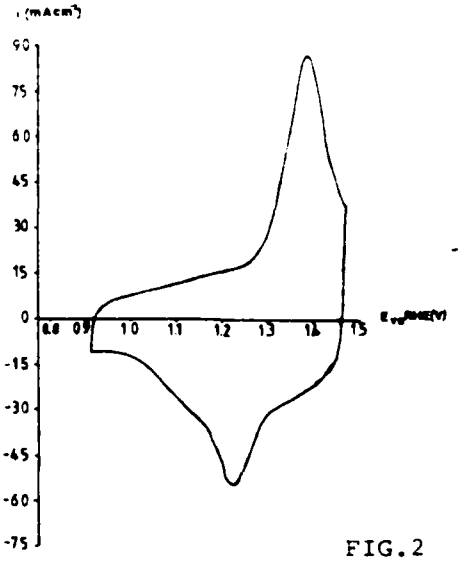

FIG.2

Figure 1: Cyclic voltammogram of a freshly prepared $NiCo_2O_4$ electrode in 5 M KOH, 25°C at a scan rate of 25 mV s^{-1}.

Figure 2: Cyclic voltammogram of a fresh $NiCo_2O_4$ electrode previously subjected to oxygen evolution; after 15 h 500 mA cm^{-2}; 5 M KOH, 25°C; scan rate 25 mV s^{-1}.

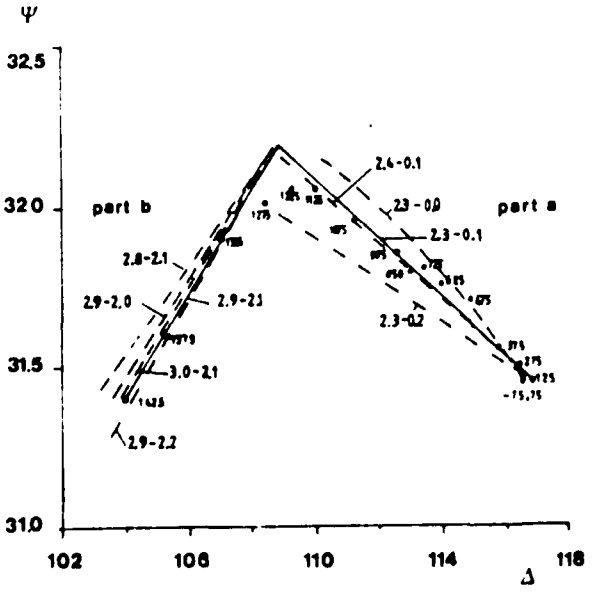

Figure 3:
Graph of ψ versus Δ of a Ni_1Co_2-alloy during a potential sweep from -0.075 to 1.425 V in 5 M KOH, 25°C; scan rate 20 mV s^{-1}, numbers along the curve refer to potential values. Solid and dashed curves: fitting curves.

02240

ELECTROCHEMICAL OXIDATION OF SULPHIDE ION IN WATER CONTAINING SURFACTANTS.

F. CASTANEDA*, E. PEZRON and V. PLICHON

Laboratoire de Chimie Inorganique et Electrochimie, ESPCI, 10 rue Vauquelin, 75231 PARIS CEDEX 05 (FRANCE).

Electrochemical oxidation of sodium sulphide in water at pH 8 is performed in the presence of cationic (CTAB, cetyl-trimethyl ammonium bromide), neutral (NP 10, NP 20 polyoxyethylene nonylphenylether), and anionic (SDS sodium dodecyl sulphate, sodium oleate) surfactants.

Voltammetric curves are improved but the electrode passivation by sulphur deposit gets suppressed only with combining the effect of the cationic surfactant and a temperature increase : diffusion limited plateaus are then obtained and molecular sulphur recovered by electrolysis (Table I).

TABLE I

Ratio of the voltammetric current i_p to the theorical diffusion value i_D of a 10^{-1} M sodium sulphide solution at pH 8 in the presence of surfactants (rotating glassy carbone electrode, 0.5 M potassium phosphate buffer).

Surfactant (C >> CMC)	i_p/i_D 22°C	80°C
none	0.03	0.12
"	0.12*	0.18*
oleate	*	0.06
SDS	0.02	0.06
NP 10	0.03	0.26
NP 20	0.09	0.50
CTAB	0.13	0.65

*1.6 10^{-2} M sodium sulphide solution normalized to 10^{-1} M.

EFFECT OF CTAB CONCENTRATION

The most effective surfactant, CTAB, was studied with more details. For CTAB < 6.10^{-5} M at room temperature, the sulphide peak is cathodically shifted and its height increased with the surfactant concentration (fig 1). Above 6.10^{-5} M, the peak current generally slightly decreases, then

* Scholarship of the Mexican Government (CONACYT)

remains alike with higher CTAB concentration.

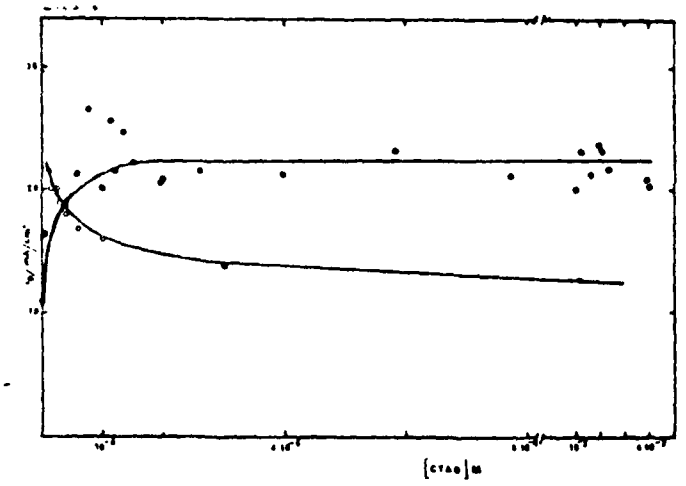

Fig .1. Variation of the peak current density i_p vs. CTAB concentration at 22°C (eeee) and 80°C (oooo).

Effect of CTAB is quite different at 80°C. For low concentration (typically 10^{-5} M), a peak or sometimes a pseudo-plateau is still present in 4 10^{-3} M sulphide solution, but its current almost reaches the diffusion current i_D for a two-electrons process.

At fairly high CTAB concentration (10^{-4}-5 10^{-3} M), one observes a genuine diffusion plateau (curve 4, fig. 2) decreases as the CTAB concentration is raised, with a slope of 46 mV for the E vs log (i/ie - i) plots. It appears that at the time scale of the voltammetry a polysulphide and not sulphur is obtained at high CTAB concentration. At the longer time scale of controlled-potential electrolysis however, 2 e^-/S^{2-} are easily consumed and colloidal sulphur is recovered by extraction by chloraform from the uncoloured solution.

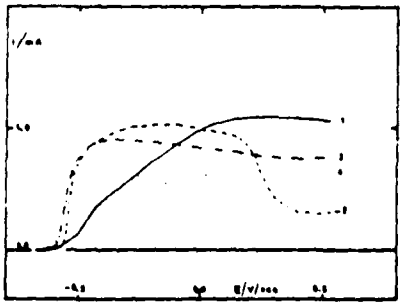

Fig .2. Current-potential curves of a 4×10^{-3} M Na_2S solution at pH 8 and 80°C in presence of CTAB.
C_{CTAB} = 0 (1); 1.2×10^{-5} M (2); 3×10^{-5} M (3); 1.1×10^{-3} M (4);
(rotating glassy carbone disk, potential scan rate 6mVs^{-1}).

DISCUSSION

Oxidation of sulphide has been explained (1,2,3) by a mechanism in which the primary step always leads to sulphur which may then react on the sulphide which diffuses towards the electrode to give a polysulphide :

$$S^{2-} - 2\,e^- \longrightarrow S \quad (1) \; ; \; S^{2-} + (x - 1)S \longrightarrow S_x^{2-} \quad (2)$$

If reaction (1) is slow and the sulphur insoluble, a layer of non conductive sulphur appears at the electrode surface and passivation occurs. This is observed in neutral water at room temperature.

Effect of surfactants will be discussed from several explanations. The first one supposes dissolution of sulphur into CTAB micelles which are certainly present in most of our solutions. A second one considers that adsorption at the electrode surface prevents sulphur deposit to be formed.

Effect of temperature is explained by an increase in the rate of reaction (2) which occurs whatever the surfactant and results in a partial depassivation of the electrode. Electrolysis can be performed up to the highest polysulphide stable in the medium, probably S_5^{2-} at pH 8. Then the electrolysis stops unless CTAB is present. When reaction (2) becomes fast at the voltammetry time scale, the electrode "sees" the total reaction $xS^{2-} - 2(x - 1)e^- \longrightarrow S_x^{2-}$ which corresponds to less than 2 e/S^{2-}.

REFERENCES

1. M. N. MOSCARDO-LEVELUT and V. PLICHON.
J. Electrochem. Soc. 131, 1538 (1984).

2. P. L. ALLEN and A. HICKLING.
Trans. Faraday Soc. 63 1626 (1957).

3. N. RAMASUBRAMANIAN.
J. Electroanal. Chem. 64 21 (1975).

02250

NEW DATA ON THE DYNAMIC BEHAVIOUR OF THE PASSIVE FILM ON IRON

M. KEDDAM* and C. PALLOTTA**

* LP 15 CNRS "Physique des Liquides et Electrochimie", Université Pierre et Marie Curie, 4 place Jussieu, 75230 Paris Cedex 05, France.

** Departamento de Fisoco-Quimica, Facultad de Ciencias Exactas, Ciudad Universitaria, Pabellon II, 1428 Nunez Buenos Aires, Argentina.

Introduction

During the last ten years passivity studies have been performed mainly by means of *in-situ* optical techniques and non *in-situ* surface spectroscopies[1]. Most of these contributions dealt with neutral weakly agressive media (boric-borate buffered solutions). During the same period no serious advantage was taken from the advances in non steady state electrochemical techniques such as complex impedance measurement at very low frequencies by correlation or FFT signal processing. This lecture will report the results recently obtained in our group by applying these techniques to iron passivity in various acidic media. The use of impedance measurements was essentially aimed at separating the transport properties of the passive film, the charge transfer at the film boundaries and the growth kinetics. One of the main point being the identification of the process controlling the electrode polarization in the passive range. In addition to electrochemical impedance, electrohydrodynamical (EHD) impedances [2] were introduced for the first time in passivity studies.

Experimental

A Solartron equipment (TFA 1250 and electrochemical interface 1186) was used. FFT techniques (HP 5451C) was restricted to the very low frequency part of the spectrum ($f < 0.01$ Hz). Modulation of the angular velocity of the disc electrode (EHD) was performed with a fast response mechanical feed-back.

Results

A typical shape of the impedance diagram of passive iron is shown in Fig. 1.

Transport mechanism in the film sustaining the passive current I_p was analysed from the potential dependence of R_{HF}, resistance of the film with no relaxation of the film thickness. Results obtained for the transfer parameter $R_{HF}I_p$ are shown in Fig. 2, establishing a similarity of behaviour among all the electrolytes investigated. All the parallel straight lines would overlap perfectly if their potential scale were recalibrated on the Flade potential relative to each medium. From Fig. 2 it was inferred that R_{HF} consists of an interface component (R_{HF} at the Flade potential) plus a film bulk contribution (high field transport). A 3.5 $nm.V^{-1}$ film thickness is deduced in good agreement with literature data.

The occurrence of a pure capacitance Γ in the millihertz range is tightly connected with the infinite polarization resistance (passivity plateau) exhibited by the system. It rules out any diffusion controlled and reflects the relaxation of film thickness with the potential. However the Γ value (order of 30 $mF.cm^{-2}$) is by one order of magnitude greater than the value predicted from the faradaic charge stored in the passive film. This result is consistent with the existence of a notable dissolution component in the transient response of the passive film [3].

Classically, redox reactions provide information on the film ability to support electron transfer. The use of hydrodynamical perturbations gave a new insight into the control of redox kinetics in an outer region of the film, strongly influenced by the electrolyte composition. Fig. 3 shows the reciprocal Levich plot ($I^{-1}/\Omega^{-1/2}$) for the ferro to ferricyanide oxydation on a passive iron surface in the three acidic media investigated. A fast reaction with pure diffusion control is found in $HClO_4$, a mixed kinetics is observed in H_3PO_4, H_2SO_4 lying in the midrange. EHD data (Bode-plane) presented in Fig. 4 allowed to establish that the passive film in $HClO_4$ behaves classically as a platinum disc (diffusion layer in the liquid phase). In contrast, H_2SO_4 and even more clearly H_3PO_4 reveal a more complicated EHD pattern thus indicating the existence of a diffusion control in a surface region of the passive film undergoing a specific alteration by the modulation of the rotation speed [4].

Conclusion

The resulting picture of the passive film on iron in acidic media is that of a two-layer structure [5] : an inner region practically independent of the electrolyte composition in which the electric field is located, an outer part accomodating the composition effects in which most of the film interactions with the surrounding electrolyte take place. A serious similarity with the surface properties of iron oxides colloidal particles is emphasized. This idea is also strongly supported by the behavioural sequence: perchlorate-sulfate-phosphonate, found in the present work and the increasing adsorbability of these anions on iron oxides in their colloidal state.

References

1. "Passivity of Metals", R.P. Frankenthal and J. Kruger Ed., The Electrochemical Society, Corrosion Monograph Series, Princeton N.J. (1978). "Passivity of Metals and Semiconductors", M. Froment Ed., Elsevier (1983).
2. C. Deslouis, C. Gabrielli, P. Sainte-Rose Fanchine and B. Tribollet, J. Electrochem. Soc. 129, 107 (1982).
3. M. Keddam, J.F. Lizee, C. Pallotta and H. Takenouti, Ibid. 131, 2016 (1984).
4. M. Keddam and C. Pallotta, Ibid. 132, 781 (1985).
5. J.L. Ord and D.J. Desmer, Ibid. 113, 1258 (1966).

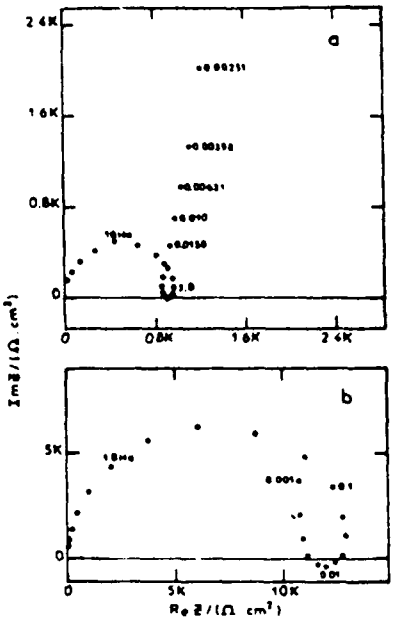

Fig.1 . Complex impedance diagrams: (a) Fe/1M H_3PO_4, 37°C, E = 0.65V, (b) Fe/1M H_2SO_4, 25°C, E = 0.35V.

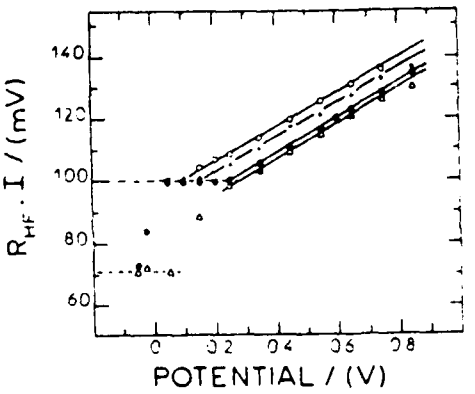

Fig 2 Potential dependence of $R_{HF} \cdot I$ for iron in different solutions at 25°C. △: 1M H_2SO_4 ● 1M H_3PO_4 + 1M (H_3PO_4 + KH_2PO_4), pH = 2.2. ○: 1M (H_3PO_4 + KH_2PO_4), pH = 2.8.

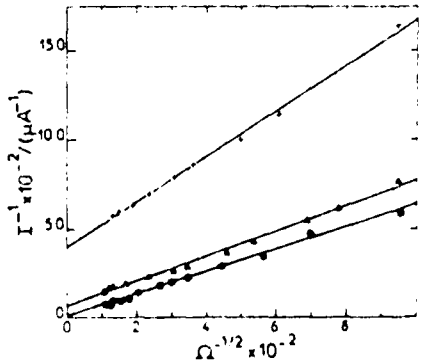

Fig 3 I^{-1} vs $\Omega^{-1/2}$ plots for the ferrocyanide oxidation on passive iron for different electrolytes + + + 1M H_3PO_4, E = 0.65V △△△ 0.5M H_2SO_4, E = 0.6V ●●● 1M $HClO_4$, E = 0.35V 1 mM $Fe(CN)_6^{4-}$.

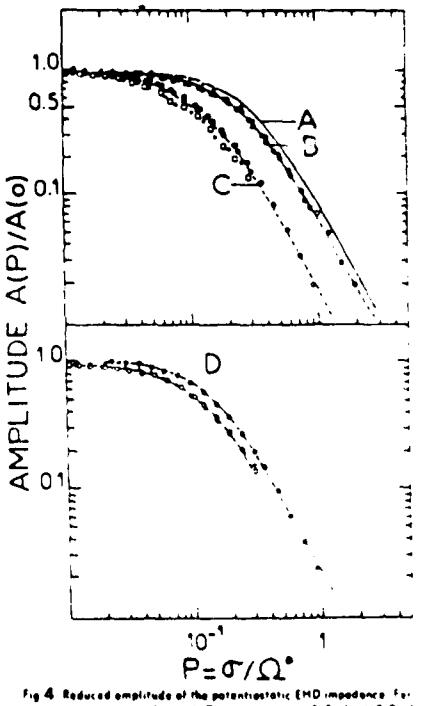

Fig 4 Reduced amplitude of the potentiostatic EHD impedance. Ferrocyanide concentration 1 mM. A Theoretical curve. B Fe/1M HClO, E = 0.65V. C Fe/0.5M H_2SO_4, E = 0.4V. D Fe/1M H_3PO_4, E = 0.65V. (○) = 200(●) 600( ) 1200(+) 2000(□)

02260

FREQUENCY RESPONSE TO A MODULATED FLOW AT PARTIALLY BLOCKED ELECTRODES

C. DESLOUIS, M. KEDDAM, M. KRARTI and B. TRIBOLLET
LP 15 du CNRS "Physique des Liquides et Electrochimie",
Université Pierre et Marie Curie, Tour 22,
4 Place Jussieu, 75230 PARIS Cedex 05, FRANCE

For a rapid redox system on an uniform accessible electrode, the frequency response to a sinusoidal speed modulation at a rotating disk electrode is well-known[1,2,3]. In this paper, we consider the case where the overall electrochemical behaviour of solid electrodes depends on the space -and possibly time- dependent distribution of the heterogeneous kinetics with, as a limit case, a set of active and blocked sites. This heterogeneous reactivity influences also the mass transport phenomena by the boundary conditions imposed to the wall fluxes and concentrations.

As a first step toward the partially blocked electrodes, we had considered theoretically the frequency response to a modulated flow for a single microelectrode of diameter d located at a distance R from the rotation axis[4]. All normalized impedance diagrams may be reduced by using the dimensionless frequency $p\ S_c^{1/3}\ (d/R)^{2/3}$. The transition between one active site to n active sites is not easy on the theoretical point of view (due to the mutal interactions), and so we cannot use the same procedure for the numerical calculation of the frequency response on n active sites.

If we consider the case of an heterogeneous reactivity where the overall steady state mass transfer is not very modified by comparison with that of an uniform accessible electrode, then the diffusion boundary layer thickness is not very modified, and the concentration field over one active site may be described as the concentration field over a microelectrode which is mounted flush with the disk electrode and insulated from it by a gap. This concentration is governed by the unsteady equation of convective diffusion :

$$\frac{\partial c}{\partial t} + v_z \frac{\partial c}{\partial z} + v_x \frac{\partial c}{\partial x} = D \left(\frac{\partial^2 c}{\partial z^2} + \frac{\partial^2 c}{\partial x^2}\right)$$

where v_z is the normal velocity component and v_x the tangential velocity component ($v_x = \sqrt{v_r^2 + v_\theta^2}$). This problem can be solved numerically by using the Newman's method (figure 1).

In the low frequency range, the frequency response corresponds to that of the rotating disk electrode and, in the high frequency range, the frequency response corresponds to that of an isolated microelectrode. The translation between the two HF asymptotes (disk and isolated microelectrode) is equal to $(0.8\ R/0.51\ d)^{2/3}$ and independant of the gap value (see figure 1). The gap value affects only the transition between the two limiting curves.

Experimental

. At first, a grid is used in order to modelize a partially blocked electrode. The relevant amplitude variation has been plotted on figure 2. The curve exhibits two clearly separated domains according to the frequency

range. The translation value between the HF asymptote and the HF theoretical disk asymptote provides therefore an estimate size of the active site ($d \simeq 40\,\mu$) which corresponds to the order of magnitude for the average value of the active part of the grid.

. The reduction of Fe^{+++} (0.5M) in H_2SO_4 (1M) on a rotating disk electrode made of carbon ($\emptyset$ = 0.3cm) has been taken as an example of heterogeneous kinetics. The amplitude variation shows the L.F. part and the beginning of the transition (figure 3A), and the phase shift variation exhibits the two domains (figure 3B) and from the translation between the two curves we can deduce the approximate value of d ($\simeq 6\,\mu m$).

References

-1- C. Deslouis, C. Gabrielli, Ph. Sainte-Rose Fanchine and B. Tribollet
J.E.C.S., vol. 129, n° 1, pp 107-118 (1982).

-2- B. Tribollet and J. Newman
J.E.C.S., vol. 130, n° 10, pp 2016-2026 (1983).

-3- C. Deslouis and B. Tribollet
J. Electroanal. Chem., vol. 185, pp 171-176 (1985).

-4- A. Ambari, C. Deslouis and B. Tribollet
I.J.H.M.T. (to be published).

-5- J. Newman
"Electrochemical Systems", Prentice Hall, Inc., Englewood Cliffs, N.J. (1973).

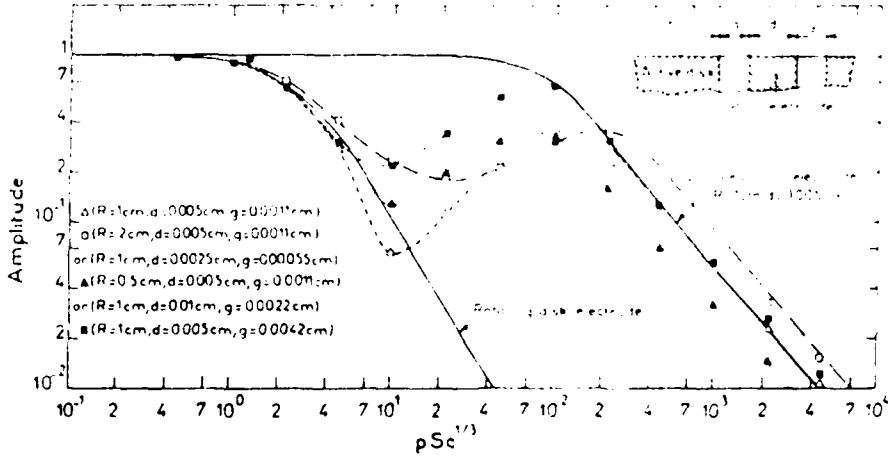

Figure 1 : Numerical calculation of the EHD impedance for a microelectrode inserted in an active disk. The two limiting cases : disk electrode and isolated microelectrode are in dashed line.

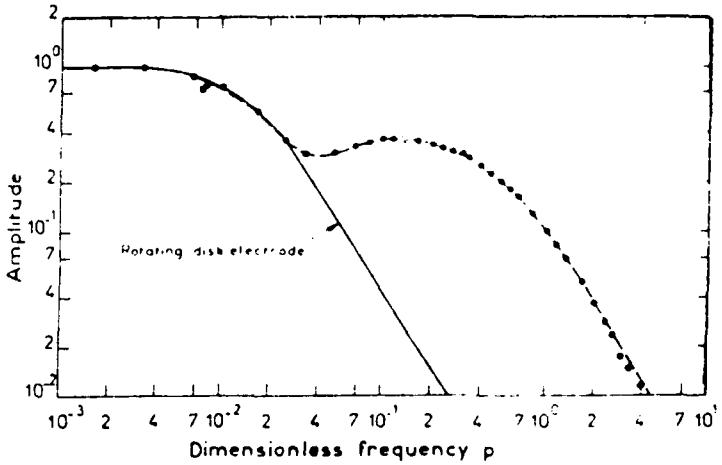

Figure 2 : Experimental EHD impedance on a grid electrode obtained in potentiostatic regulation for the reaction $Fe(CN_6)^{3-} + e \rightleftarrows Fe(CN_6)^{4-}$ in KCl(M), the viscosity is increasing by glycerol in order to obtain a response in low frequency.

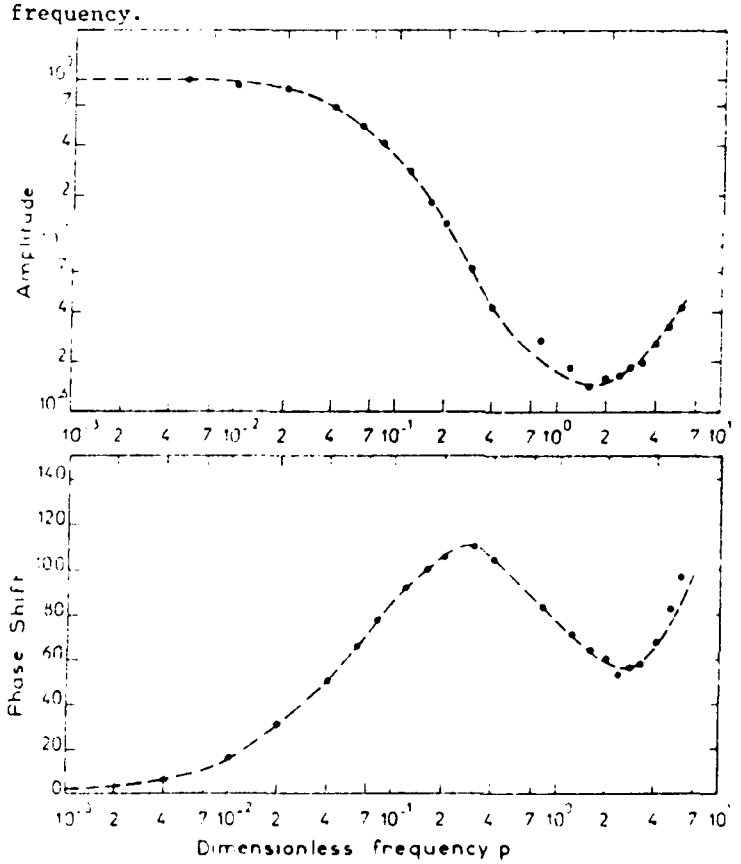

Figure 3 : Experimental EHD impedance obtained in galvanostatic regulation for the reduction of Fe^{3+}(0.5M) in H_2SO_4(M) on a carbon electrode (Ø3) at T = 25°C. (A) reduced amplitude, (B) phase shift.

02270

SURFACE PROPERTIES OF MIXED IrO_2 + RuO_2 MIXED OXIDE ELECTRODES

C. ANGELINETTA and S. TRASATTI
Department of Physical Chemistry and Electrochemistry,
University of Milan (Italy)

Lj. D. ATANASOSKA
Institute of Technical Sciences,
Serbian Academy of Sciences and Arts, Belgrade (Yugoslavia)

R. T. ATANASOSKI
Institute of Electrochemistry, ICTM,
University of Belgrade (Yugoslavia)

A. ZALAR
Institute of Electronics and Vacuum Techniques,
Ljubljana (Yugoslavia)

IrO_2 and RuO_2 are the most active components of industrial anodes (DSA = Dimensionally Stable Anodes) used for Cl_2 production, metal electrowinning, water and sea-water electrolysis etc[1]. More specifically, IrO_2 + RuO_2 mixed oxide electrodes have been used as anodes for oxygen evolution from acid media - for instance, SPE (= Solid Polymer Electrolyte) cells[2] - because of the higher stability compared to RuO_2 alone, or to mixed RuO_2 + TiO_2 oxides. Long-term performances are improved by the addition of SnO_2[3]. Despite the interest in these oxides, exhaustive investigations of the surface and electrocatalytic properties of mixed IrO_2 + RuO_2 oxides have not yet been carried out. Preliminary results of the measurement of the point of zero charge of RuO_2-rich samples have been published recently[4]. This work has been undertaken with the aim at filling this gap, more specifically the purpose has been to elucidate the surface behaviour as a function of composition.

RuO_2 + IrO_2 layers on Ti were prepared by thermal decomposition of aqueous solutions of $RuCl_3$ + $IrCl_3$ in the required mole ratio. The temperature of decomposition was 400 °C and the nominal thickness ca. 1 μm at any composition (from about 0.6 to 1.2 mg cm^{-2}). The support was a 1 × 1 cm thin plate of Ti. Electrodes were prepared at 10 mol% interval from pure RuO_2 to pure IrO_2 included. Three samples were prepared at the same time in the same furnace: two of them were used for in-situ electrochemical measurements and the other two for analysis by ex-situ vacuum techniques (AES and XPS).

The electrochemical characterization of the surface was carried out by means of voltammetric curves between 0.4 and 1.4 V(RHE) both in 0.5 mol dm^{-3} H_2SO_4 and 1 mol dm^{-3} KOH solutions at 20 mV s^{-1}. The charge (q*) obtained by integration of the voltammetric curves is plotted in Fig. 1 as a function of the nominal bulk composition. q* is low for the pure oxides and goes through a maximum at about 30 mol% RuO_2. This probably indicates that very fine crystallites are formed because RuO_2 and IrO_2 remain practically separated. There is evidence from the X-ray analysis for a possible phase mixture formation, although the low crystallinity of the layer prevents any more quantitative analysis to be carried out.

AES experiments showed that the surface is heavily contamined by carbon which could not be removed even after prolonged Ar ion bombardment. As a result no adequate symmetrical peak of Ru at 272 eV was obtainable. Therefore, the surface quantitative analysis was carried out by XPS. It is interesting that the symmetry factor of the 272 eV Ru Auger peak and the $d_{5/2}$ vs $d_{3/2}$ XPS ratio for Ru depends on the coating composition; they appear to approach the literature values as the IrO_2 content vanishes.

Fig. 2 shows a plot of the surface vs bulk composition of the coatings. It can be seen that the surface is enriched with Ir, which is in agreement with the result of Hutchings et al[5] despite the different preparation procedures. Evidence has also been found for the presence of a small amount of Ti at the surface which can come from the support during the preparation.

Surface analysis can also be attempted in-situ by resting on some features of the voltammetric curves which are associated with the pure oxides. Also this approach indicates that the surface is enriched with IrO_2. The XPS analysis has also shown that the Ir content increases after the electrodes have been used for oxygen evolution experiments. Therefore, Ru is probably selectively dissolved at the surface while the stability of IrO_2 towards anodic polarization is higher.

Voltammetric curves also show that these coatings are permeable to protons probably through a grain boundary diffusion mechanism as observed with pure RuO_2 layers.

REFERENCES

1. S. Trasatti (Editor), Electrodes of Conductive Metallic Oxides, Part A and B, Elsevier, Amsterdam, 1980 and 1981.
2. K. Müller, G. Scherer, S. Stucki, 32nd ISE Meeting, Dubrovnik, 1981, Extended Abstracts, p. 28.
3. R. Hutchings, K. Müller, R. Kötz, S. Stucki, J. Mater. Sci., 19(1984)3987.
4. R. Vigand, J. Taraszewska, A. Daghetti, S. Trasatti, J. Electroanal. Chem., 192(1985)203.
5. R. Hutchings, R. Kötz, K. Müller, S. Stucki, 34th ISE Meeting, Erlangen, 1984, Extended Abstracts, Abstr. 0305.

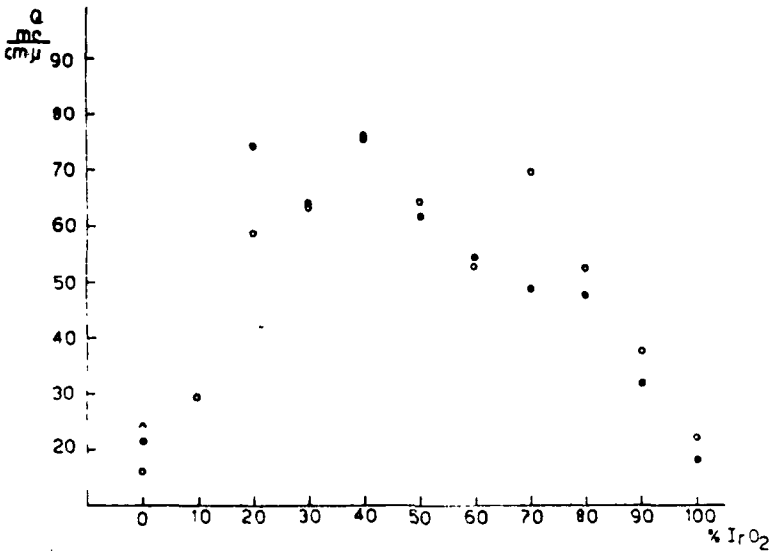

Fig. 1 - Dependence of the voltammetric charge between 0.4 V and 1.4 V(RHE) in 0.5 mol dm^{-3} H_2SO_4 solution on the bulk nominal composition of IrO_2 + RuO_2 mixed oxides.

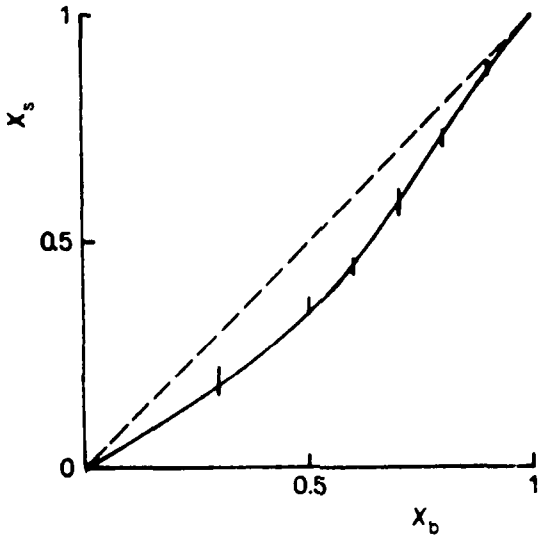

Fig. 2 - Relationship between the surface (x_s) and the bulk (x_b) nominal composition of fresh IrO_2 + RuO_2 mixed oxides. x = mole fraction of RuO_2.

02280

COMPUTER SUPPORTED PULSE MEASUREMENT OF CAPACITY DURING FAST OXIDE FORMATION REACTIONS

U. KÖNIG, M. M. LOHRENGEL, and J. W. SCHULTZE
Institut fuer Physikalische Chemie (II) der Universitaet Duesseldorf (Germany)

To analyse the problems of the passive layer formation and reduction kinetics, detailed knowledge of the semiconductor properties of these layers is necessary. A suitable method to evaluate kinetic models is the determination of the potential dependence of capacity followed by a Mott-Schottky analysis. The solid state properties of these layers change very fast during the initial steps of formation and during reduction because these layers are far from equilibrium state. Up till now, Mott-Schottky measurements could be carried out within some ten seconds only. The method presented here allows to shorten this time by up to 5 orders of magnitude. Moreover, the short pulse measurement corresponding to 50 kHz overcome the problems of the increase of C at low frequencies.

Convenient methods to measure the potential dependence of capacity in a time range starting at some microseconds are potentiostatic pulse measurements. Principles are shown in fig. 1. During potentiostatic or potentiodynamic polarisation short rectangular pulses with a small amplitude ΔU are superimposed. The capacitive charge Δq is obtained from simultaneous integration of the current i:

$$\frac{\Delta}{\Delta} = \frac{\int i\,dt}{\Delta U} \qquad (1)$$

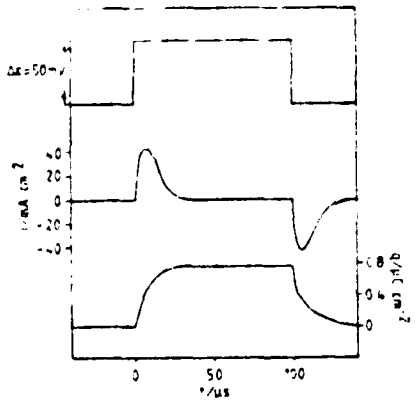

Fig. 1

Potential, current, and charge during a potentiostatic pulse.

Using a fast potentiostat a pulse length of 20 µs and pulse amplitudes of 20-50 mV are adequate. Such pulses do not influence formation and reduction kinetics and allow up to 10 measurements within 1 ms.

A block diagram of the circuit is shown in fig. 2. Integration was done by fast operational amplifiers because of the necessary bandwidth of 10 MHz. To avoid the interference with faradayic components of the current, a special active filter network was added. Pulse control, digitizing of the integral and the calculation of capacity data was done by a DEC LSI 11/23 laboratory computer.

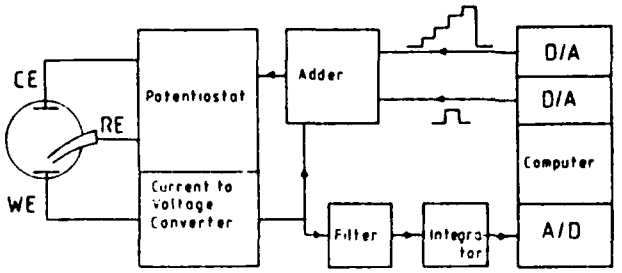

Fig. 2

Block diagram of circuit

Measurements of the potential dependence were realised by synthesis of a staircase pulse. Every step represents a measuring potential. The capacity was obtained by superimposing an additional pulse (fig. 3). To avoid distortions of the layer the duration of the whole pulse complex must be shorter than 1 ms. This allows experiments even at potentials where the layer is not stable, e.g. some hundred millivolts below the reduction potential.

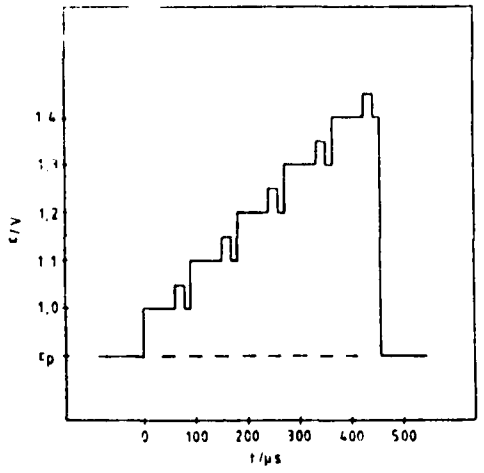

Fig. 3

Pulse complex to measure the potential dependence of capacity.

Some experimental results using this method are shown in fig. 4a. An iron electrode was potentiostatically polarised at 1.5 V vs. hydrogen electrode in same solution (HESS) with simultaneous capacity measurements at 1 ms, 10 ms, etc. up to 1000 s from .6 V to 1.5 V. During this period of time, the

oxide film grows continuously to about 3 nm (1 ks). Fig. 4b shows the results in a tentative Mott-Schottky-plot. For t_p = 1 ms, the capacity is very large and independent of potential which means a highly disordered oxide film with a large dielectric constant. With increasing polarization time the capacity decreases at high potentials. The potential dependence is typical for an n-type semiconductor. From fig. 4b, we would obtain a large donor concentration $N = 2 \cdot 10^{20}\ cm^{-3}$ for $t_p >= 1$ s. These measu ements demonstrate that the semiconducting properties of the passive film develop not immediately, but after 1 s only. Similar observations were made for the development of transpassivity.

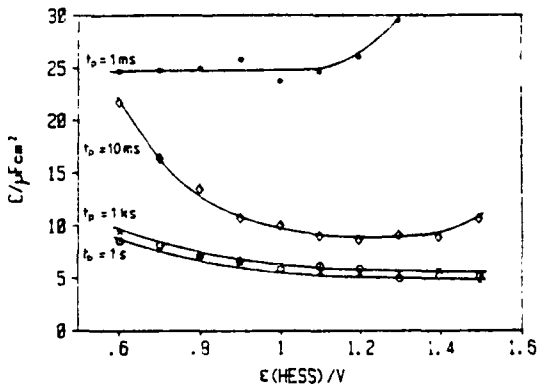

Fig. 4a

Potential and time dependent capacities measured during one potentiostatic pulse of 1.5 V (HESS) and 1000 s.

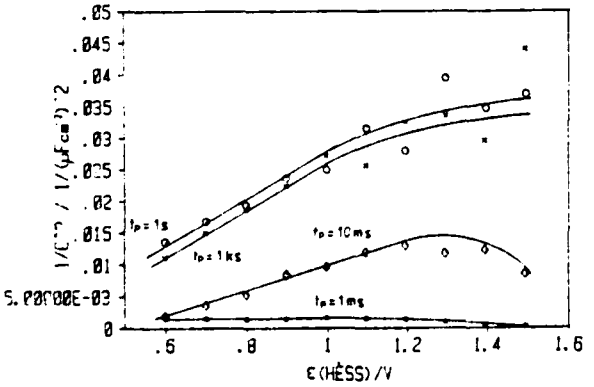

Fig. 4b

Mott-Schottky plot, values taken from fig. 4a.

02290

THE EQUIVALENT CIRCUIT DIAGRAM OF OXIDE FILMS WITH A LIMITED POTENTIAL DROP

M. M. LOHRENGEL, J. W. SCHULTZE, H. D. SPECKMANN
Institut für Physikalische Chemie II der Universität Düsseldorf
Universitätsstraße 1, 4000 Düsseldorf

Conventional equivalent circuit diagrams (fig. 1a) are insufficient for impedance analysis of semiconducting oxide films e. g. passive copper. Passive copper consists of semiconducting films of Cu_2O and CuO and shows a strong potential dependence of capacity (fig. 2, full line). The conventional equivalent circuit (fig. 1a) shows no potential dependence (fig. 2, dotted line). The rate determining process of oxide growth is a field dependent ionic migration. From experimental data we concluded [1] that the potential drops in the films increase with ε up to a limiting potential only. A corresponding potential drop / electrode potential diagram is qualitatively shown in fig. 3 by the dashed lines. The potential drops are limited for $\varepsilon > 0.8$ V in the Cu_2O film and for $\varepsilon > 1.3$ V in the CuO film. At higher potentials (transpassive region) an increasing number of holes is accumulated at the oxide surface and the potential drop at the Helmholtz layer increases.

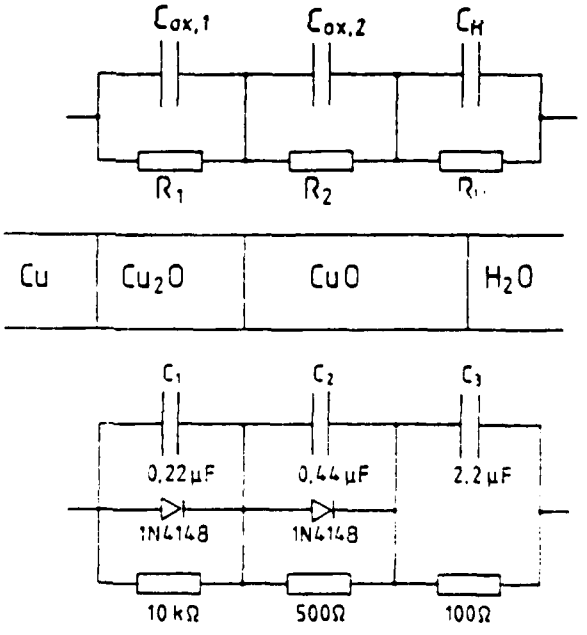

Fig. 1: Equivalent circuit diagrams of passive copper
a) conventional type
b) modified type using diodes to simulate the limited potential drops in the films.

The diode is a simple electronic component equivalent to the oxide film reaching the inversion region. At low potentials the resistance of the diode is high, but at higher voltages the voltage drop is limited to the threshold voltage. Therefore, an equivalent circuit diagram using diodes

(fig. 1b) should behave like oxide layers on copper[2]. The aim to design such a circuit is to show the validity of the model rather than to produce a perfect image of the electronic properties of a passive electrode.

Each of the oxide layers are represented by a capacitor, a diode, and, if necessary, a resistance in paralliel. The capacitor represents the capacity of the oxide film, taken as a pure dielectric medium. The diode and the resistance in parallel simulate the ionic and electronic conductivity of the oxide. To realise the different electronic properties of the oxide layers in duplex films, different resistors in parallel can be used.

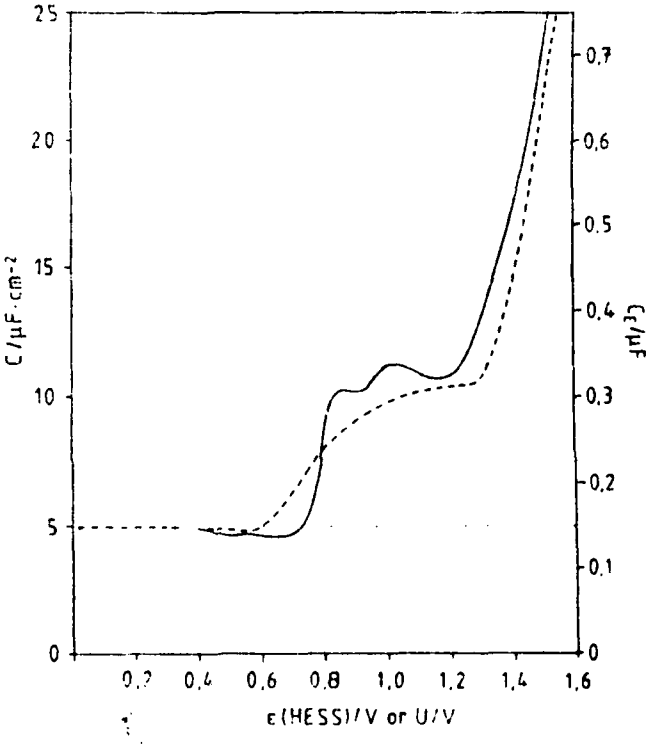

Fig. 2: The capacity of a passive copper electrode (full line) in dependence on the potential and of the conventional (dotted line) and the new equivalent circuit (dashed line) in dependence on the applied voltage.

The capacitors C1, C2 and C3 correspond to layers of Cu_2O, CuO, and the Helmholtz layer. The threshold voltage of the diodes (0.7 V) is similar to the limited potential drop of ≈0.4 V for Cu_2O and ≈0.5 V for CuO. The capacity of the equivalent circuit was measured with a frequency of 1 Hz. The resulting capacity in dependence on the overall potential drop is shown in Fig. 2 by the dashed line. It can be seen that the capacity at low potentials is very low. It increases at about 0.6 V and a further increase is observed at about 1.3 V.

The experimental capacity curve was measured at pH = 12 after a special pretreatment. Copper oxides were formed by a potentiodynamic sweep to 1.6 V and reduced to a single Cu-I-oxide layer by a cathodic sweep to 0.4 V. In the subsequent sweep to 1.6 V given in Fig. 2, parts of Cu-I-oxide are converted to Cu-II-oxide, but further oxide growth is almost negligible.

The curve of an equivalent circuit using diodes in parallel fits the electrochemical curve sufficiently, while the classical equivalent circuit (dotted line, fig. 2) fails definitely. The strong increase of capacity at potentials $\varepsilon > 1.3$ V is pronounced and even the step due to the oxidation of copper-I-oxide to copper-II-oxide at 0.7 V is seen.

The measured potential drops over the capacitors of the equivalent circuit are shown in fig. 3. It is seen that the potential drop in the inner layer U_1 increases up to the limited potential of about 0.5 V, then a further increase of the applied voltage causes a potential drop U_2 across C2, and at high potentials the increase of the potential drop occurs mainly across C3 and equals the potential distribution shown in fig. 3 derived from electrochemical measurements.

The model of limited potential drops in the oxide layers is consistent and the potential dependence of capacity of passive electrodes can be simulated by an equivalent circuit using diodes. Obvious contradictions between the classical equivalent circuit diagram and the experimental results are solved.

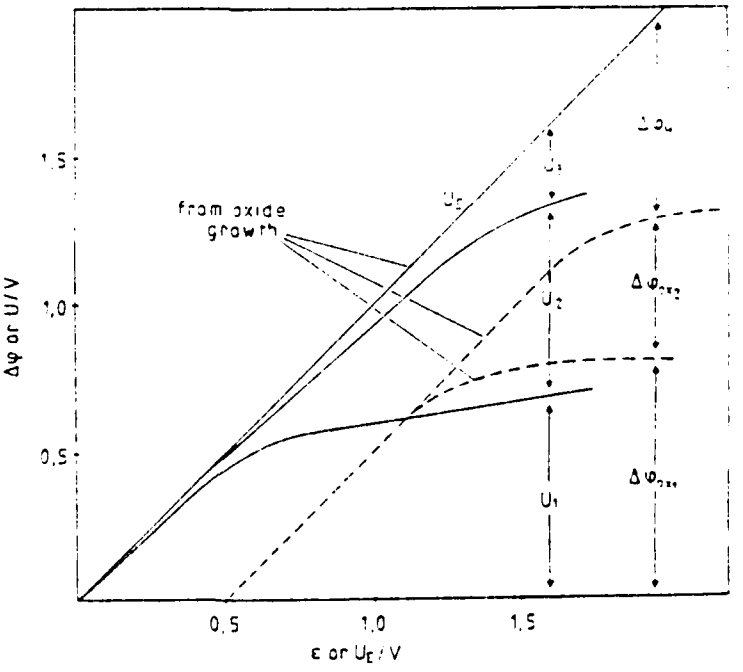

Fig. 3: The potential distribution of an oxide covered copper electrode derived from oxide growth measurements (dashed line) vs. the electrode potential and of various parts of the modified equivalent circuit vs. the applied voltage U_E.

References:
1 H. D. Speckmann, M. M. Lohrengel, J. W. Schultze, H. H. Strehblow, Ber. Bunsenges. Phys. Chem. 89 (1985) 392
2 M. M. Lohrengel, J. W. Schultze, H. D. Speckmann, Electrochim. Acta, submitted for publication

02300

PHOTOELECTROCHEMICAL INVESTIGATIONS OF PASSIVE FILMS ON TITANIUM ELECTRODES

K.Leitner, J.W.Schultze
Institute of Physical Chemistry (II)
University of Duesseldorf, 4000 Duesseldorf 1, F.R.G.
and
U.Stimming
Department of Chemical Engineering and Applied Chemistry,
Columbia University, New York, New York 10027, U.S.A.

Introduction

Passive films on metal electrodes are usually formed of the corresponding metal oxides which show semiconducting or insulating properties. For in-situ investigations of the passive film, photoelectrochemical techniques offer the possibility of characterizing the passive film with respect to its solid state properties. In particular, the observation of differences between the behavior of passive films and the corresponding bulk oxides allows for a more detailed analysis. Recent work with amorphous oxides /1/ and model calculations which were carried out for the photoinduced electron transfer in disordered materials /2/ demonstrate that the photoelectrochemical behavior of crystalline and amorphous compounds is quite different in various aspects. For passive films on titanium a change from the amorphous to crystalline state with formation potential of the film was found from electron diffraction /3/. So it seems interesting if such findings can be correlated with photoelectrochemical data. Previous work on photoelectrochemical behavior of passivated titanium electrodes /4,5/ demonstrated TiO_2 properties of thick films, however, breakdown phenomena of the film are also reflected in the results. For very thin films a strong influence of the electric field in the film and a band gap higher than in TiO_2 has been found /4/.

Experiments were carried with passive films of appr. 5-200 nm thickness. Photocurrents were measured as a function of the wavelength of the incident light and the electrode potential. Aging effects on photocurrent spectra and the potential dependence were carried out as well.

Experimental

Passive films were formed in 1M H_2SO_4 at various potentials U_{ox} = 4V to 105 V. The formation time was generally 5 min.; aging was performed at U_{ox}-1V for up to 21h. Photocurrent measurements were carried out in the same electrolyte with a monochromatic light source consisting of a 450 W Xe lamp and a monochromator. Spectra were recorded in the 200-800 nm range; the potential dependence of the photocurrent was measured between U = 0-1.8 V (SHE). Photocurrents were transformed into quantum efficiencies with respect to incident light.

Results and Discussion

Photocurrent spectra are shown in Fig.1 for various formation potentials, U_{ox}, of the passive film. At low U_{ox} a steady increase of the quantum efficiency with the photon energy, hν, is observed. For U_{ox} = 26V a shoulder develops at appr. 4eV which becomes a pronounced peak at 3.8eV for U_{ox} = 54V. For thick films which are represented by the film formed at 105 V this peak

disappears again. The four examples shown in Fig.1 are representative of four different types of behavior. Please note that the curves for 26 and 56 V are enhanced by a factor of five. Over a wide range of hν and especially at higher hν, the quantum efficiency, η, is higher for thin films compared to films of intermediate thickness.

Typical quantum efficiency-potential curves are given in Fig.2 for films formed at 13 and 105 V. Thick films show a limiting current for hν=5.2eV while for lower hν the quantum efficiency still increases with U up to 1.8V, although from U=0.8V on the potential influence is weaker than at low potentials. Thin films have a much stronger potential dependence. The shape for 5.2 eV is similar to that at thicker films for lower photon energies. At 3.2 eV, however, the potential dependence becomes exponential-like indicating a strong influence of the electric field in the passive film.

Aging of the film was done in the electrolyte under potentiostatic control. In general, photocurrents increased upon aging, for longer times also changes of spectral and potential characteristics are observed.

A detailed analysis of the absorption edge shows that band gap energies which were determined from $(\eta \cdot h\nu)^{1/2}$ vs. hν plots has a value of E_g^i of appr. 3.3 eV decreasing slightly to 3.2 eV for thick layers. This band gap value corresponds to indirect transitions in crystalline semiconductors; linearity is also observed with amorphous semiconductors, but reflects rather the density of state function close to the band edges. So-called direct band gaps which are obtained from $(\eta \cdot h\nu)^2$ vs. hν plots can not be observed for films formed at U_{ox}=20 V or less. For high U_{ox}, E_g^d first decreases from 3.7 eV to 3.5 (at U_{ox}=30 V) and then stays constant up to very thick films. This indicates that films formed below 20V are amorphous. This assumption is confirmed by an analysis of the potential dependence of the photocurrent. The strong potential influence found for low hν and thin films (see Fig.2) turns out to follow a Poole-Frenkel behavior which is typical for amorphous semiconductors, as well /1,2/.

The investigations demonstrate that photoelectrochemical measurements are able to determine important solid state properties of passive films under in-situ conditions. At the same time it allows for a distinction between the amorphous and crystalline state of the surface film.

References

/1/ B.Danzfuss and U.Stimming, J.Electroanal.Chem. 164 (1984) 89
/2/ U.Stimming and A.R.Newmark, Proceedings of TELAVI '84 Conference, Telavi U.S.S.R., in press
/3/ L.Arsov, M.Froelicher, M.Froment and A.Hugot-Le Goff, J.Chim.Phys. 72, (1975) 275
/4/ J.W.Schultze, U.Stimming and J.Weise, Ber.Bunsenges.Phys.Chem. 86 (1982) 276
/5/ see ref. 24-27 in /4/

02310

INVOLVEMENT OF ANIONIC OXIDE SPECIES IN REACTIONS AT THE METAL/SOLUTION INTERPHASE

M.B.C. ROCHE* and L.D. BURKE
University College Cork, Cork, Ireland

Equilibrium potential/pH diagrams - frequently referred to as Pourbaix diagrams - are widely used as a guide[1,2] in many areas of electrochemistry. However, it was recently[3] pointed out that a clear distinction must be made between the behaviour of anhydrous and hydrous oxides. For the latter it can no longer be assumed that the redox potential for a reversible transition will always vary with solution pH in the conventional manner of 59 mV, i.e. 2.303 RT/F volts per unit pH. As will be shown later, for these oxides a significantly higher value of about 88.5 mV, i.e. 3/2 (2.303 RT/F) volts, per unit pH was obtained. (Note: all values are quoted with respect to a pH-independent reference electrode, e.g. SHE or calomel). This is illustrated particularly well by the behaviour of hydrous iridium oxides films[4] produced by potential cycling. The reaction involved is an oxide/oxide transition which exhibits an unusually high degree of reversibility. It is now assumed to be of the form depicted in equation (1)

$$\{---[Ir(OH)_6]_2^{-2}---\} + 3H^+ + 2e^- = \{---[Ir_2(OH)_9]^{-3}---\} + 3H_2O \qquad (1)$$

these hydroxy complexes being part of a polymer chain or aggregate. Further details of other oxide/oxide transitions involving hydrous materials will be found in reference 3.

The slightly more complex case of hydrous oxide/metal transitions is considered in this extended abstract. Studies carried out with platinum and palladium (and to a lesser extent gold) have illustrated some important points with respect to metal surface oxidation processes. Thick hydrous oxide layers can be produced on platinum using either constant potential[5-7] or repetitive potential cycling[8] conditions, the latter having the distinct advantage that prior surface polishing is not required. Several hundred layers of platinum atoms at the surface of the metal lattice may be converted to oxide: alteration of the co-ordination state of the oxymetal complexes, associated with the evolution of oxygen gas (as has been outlined earlier for gold[9]), leads to the conversion of an anhydrous monolayer to a hydrous, multilayer film under d.c. conditions. With the potential cycling technique the anodic and cathodic limits are rather important. It was found that a value of ca. 2.2 V at $v = 100\ Vs^{-1}$ was optimum, this being sufficiently anodic to extend the compact oxide growth significantly beyond the single monolayer level. On the subsequent cathodic sweep much of this compact material is reduced; the optimum lower value is ca. 0.7 V at $v = 100\ Vs^{-1}$ this being adequate to reduce most of the monolayer material. This potential cycling between set limits presumably creates a high level of adatom species (designated Pt* see

* Present address: Billiton Research B.V., Arnhem, The Netherlands

below). On the next anodic sweep these are converted to hydrated species (e.g. $H_2Pt(OH)_6$) and compact monolayer growth occurs beneath the porous outer layer. This growth continues until eventually the thick film effectively excludes the metal from contact with its aqueous environment. Similar growth has also been found to occur with palladium, gold, etc. in both acid and base, although it is considerably less pronounced at intermediate pH values.

In acid media quantitative reduction of the thick hydrous oxide films takes place (the charge being independent of sweep-rate). A very sharp peak is obtained in the region of 0.2 to 0.5 V (with respect to a reversible hydrogen electrode in the same solution, RHE). This is well below the usual compact monolayer oxide peak which is also observed in the region of 0.6 to 0.8 V (RHE). The surface deposit is obviously duplex, with a compact, inner monolayer film on the metal surface, covered by a much thicker layer of dispersed platinum hydroxide now assumed to be an aggregate of platinic acid, $H_2Pt(OH)_6$. Hexahydroxyplatinc acid, $H_2Pt(OH)_6$ and its salts are established compounds of this metal and their structures are well known[10]. While the growth of this film is possible in base[8], it reduces readily only in solutions of low pH. This is understandable in terms of equation (2).

$$[Pt(OH)_6]^{-2} + 6H^+ + 4e^- = Pt + 6H_2O \qquad (2)$$

With a ratio of six protons to four electrons in the electrode reaction, the reversible potential for reductions must decrease by a factor of 3/2 (2.303 RT/F) V per unit increase in solution pH (pH-independent scale). If the hydrous material in acid (pH = 0) reduces at ca. 0.25 V (RHE), then in base (pH = 14) this reaction should require a potential of ca. -0.15 V (RHE). In view of the low hydrogen overpotential on platinum, large currents due to the latter reaction will overshadow the hydrous oxide reduction process. Indeed, at moderate hydrogen evolution currents the hydrous film in base appears relatively inert.

However, the situation with regard to oxide/metal transitions as outlined above is an oversimplification. The problem is that the reduction involves fast electron transfer (pseudo-reversible), e.g. it gives an unusually sharp peak with the peak current increasing linearly with sweep rate, but the reverse reaction, i.e. hydrous oxide growth on the reverse scan, is obviously highly inhibited. This inhibition is evidently related to the fact that the metal atom at the surface is partially imbedded in the metal lattice so that hydroxide ions do not have ready access to the six co-ordination sites required to form the complex $Pt(OH)_6^{-2}$. Such an entity can be readily produced only at metal atoms which are displaced from regular co-ordination sites, i.e. at adatoms (Pt*), such as are produced on repetitive cycling. The reduction process (equation (2)) can be viewed as a two-part reaction.

$$[Pt(OH)_6]^{-2} + 6H^+ + 4e^- = Pt^* + 6H_2O \qquad (3)$$

$$Pt^* = Pt_1 \qquad (4)$$

Equation (4) denotes the rearrangement of the initially discharged species (platinum adatoms, Pt*) to form bulk lattic species, Pt_1. Reaction (3) is highly reversible: applying the Nernst equation to this step yields the expression

$$E = E^0 - \frac{2.303\ RT}{4F} \log \frac{a_{Pt^*} \cdot a_{H_2O}^6}{a_{Pt(OH)_6}^{-2} \cdot a_{H^+}^6} \qquad (5)$$

The activity of the adatoms decays with time and this is an obvious explanation for the following observations: (a) that the peak potential drifts anodically with decreasing hydrous oxide reduction scan-rate, and (b) that the reduction profile for reaction (3) under potential sweep conditions shows an unusually sharp drop on the cathodic side of the hydrous oxide reduction sweep[8]. The formation of dispersed, platinum black-type deposits[8], rather than smooth platinum, on reduction of thick hydrous oxide layers further supports the above interpretation of this type of reaction. These aspects of transition metal/metal oxide electrochemistry would appear to be of widespread importance, extending well beyond the areas outlined here, e.g. in corrosion, battery, pH-monitoring and electrochromic systems.

From the above results it is clear that although potential values for peak maxima observed during the course of reduction of anodically produced oxide layers on platinum are influenced by sweep rate, the variation of such maxima potentials with change in solution pH is mainly of thermodynamic origin. From the values previously quoted a shift in the region of 30 mV per unit (RHE), or about 89 mV per unit pH with respect to SHE, is obtained. Such a shift (which has been described as 'super-Nernstian') is of widespread importance not only in the case of platinum but also for other hydrous oxide systems such as gold[11], iridium, iron and nickel.

In similar studies with palladium it was found that the behaviour of this metal is in many ways analogous to that of platinum. However, some significant differences were observed, specifically (a) base-grown hydrous palladium oxide layers are rather unstable in acid, and (b) both the ease of oxide growth and the susceptibility of the resulting layer to dissolution are significantly greater in the case of palladium.

1. POURBAIX, M. Atlas of Electrochemical Equilibria in Aqueous Solutions, Pergamon Press, Oxford, 1966.
2. FRANKENTHAL, R.P. and KRUGER, J. (Eds). Equilibrium Diagrams; Localised Corrosion. The Electrochem. Soc., Pennington, New Jersey, 1984.
3. BURKE, L.D. and SCANNELL, R.A., ref. 2, pp. 135 - 147.
4. BURKE, L.D. and WHELAN, D.P. J. Electroanal. Chem., 162, 1984, p. 121.
5. JAMES, S.D. J. Electrochem. Soc., 116, 1969, p. 1681.
6. BALEJ, J. and SPALEK, O. Collect. Czech. Chem. Commun., 37, 1972, p. 499.
7. SHIBATA, S. Electroanal. Chem., 89, 1978, p. 37.
8. BURKE, L.D. and ROCHE, M.B.C. Ibid, 164, 1984, p. 315.
9. BURKE, L.D. and McRANN, M. Ibid, 125, 1981, p. 387.
10. SCOTT, H.G. Acta. Cryst., B35, 1979, p. 3014.
11. BURKE, L.D., LYONS, M.E. and WHELAN, D.P. J. Electroanal. Chem., 139, 1982, p. 131.

02320

STUDY OF THE INDUCTANCE INFLUENCE ON THE MEASURED ELECTROCHEMICAL IMPEDANCE

B. SAVOVA-STOYNOV, Z. STOYNOV
Central Laboratory of Electrochemical Power Sources
Bulgarian Academy of Sciences, Sofia 1040, Bulgaria

The problem of the inductance influence on the measured impedance arises with the development of the high-frequency measurement instrumentation.

The inductance of the connecting wires and of the electrochemical cell itself deforms the impedance diagram especially of low-resistance systems even in the range of middle frequencies. Thetheoretical analysis and topology simulation show that the inductance limits the measurement frequency and on the other hand it can lead not only to parameter but also to structure deformations of the impedance diagram.

The own inductance of the cell is of a distributed parameter type but in a first approximation it can be treated as a lumped-parameter element, hence, the inductance influence can be treated as an additive term.

The aim of this paper is the study of the additive inductance influence in two aspects:

i) quantitative evaluation of the errors due to the inductance influence;

ii) analysis of the structural deformations on the impedance diagrams.

If the additive inductance influence is presented by a serial connected L element in the electrical equivalent circuit describing the measured impedance the relative error due to the inductance is estimated and the analytical dependence is

$$\varepsilon_L = -\omega^2 LC_M \qquad (1)$$

where ω is the measured frequency and C_M - the measured capacity.

It can be seen that this error is proportional to the frequency squared and depends on the value of the inductance as well as on the capacity C_M specific for the object.

For microobjects this error is small enough and appears at very high frequencies but for big real objects the error begins to play role even in the range of low (sound) frequencies.

If the acceptable inductance error is ε_L, then the limit frequency ω_L can be expressed by the relation:

$$\omega_L = \sqrt{\varepsilon_L / LC_M} \qquad (2)$$

respectively $$f_{max} = \frac{1}{2\pi}\sqrt{\varepsilon_L (LC_M)^{-1}} \qquad (3)$$

For large objects with an effective capacity of about 10 Farads the limit frequency is in the range of few cycles[1]. The simplified evaluation of the error ε_L and f_{max} (1) – (3) requires a

limitation of the measurement frequencies.

On the other hand, the inductance influence can lead to deformations of the ideal impedance shape and to a wrong structural identification. To analyze these effects a simulation is carried out and the results are presented later.

Topology studies have been performed over a set of typical electrochemical models using the simulation program "SIMA"[2] based on the method for a structural simulation of matrix models[2].

For the simplest electrochemical system, an ideal nonpolarized electrode, the impedance can be described as

$$Z = R + j\omega L, \tag{4}$$

hence, the behaviour of the imaginary impedance component is pure inductive.

The expressions for the complex inductance error are as follows:

$$\varepsilon^{L}_{A} = \frac{\omega^2 L^2 + R^2}{R} - 1 \tag{5}$$

$$\varepsilon^{L}_{\varphi} = \omega L/R \tag{6}$$

and the limit frequency:

$$f_{max} = \frac{\varepsilon^{L}_{A} \cdot R}{2\pi L} \tag{7}$$

The common impedance of an Ideal Polarized Electrode can be expressed as

$$Z = R_E + j\left(\omega L - \frac{1}{\omega C_D}\right) \tag{8}$$

With the frequency increase the capacitive impedance component decreases and tends to zero. At certain frequencies this term changes even its sign and begins to increase, i.e. the capacitive part even changes into an inductive one. For evaluation of the error and the maximal frequency, expressions (1), (3) are valid.

The topology analysis of One-Step Reaction was performed varying the factor φ which is a function of the model parameters L, R_p, C_D:

$$\varphi = L/R_p^2 C_D \tag{9}$$

in the frequency range ($\omega = 10^2 - 10^6$).

At low inductance values the impedance diagram is an approximately pure semicircle near to the case of an inductance-free impedance model and of one high-frequency inductive part.

When increasing the relative inductance value, at first the size and then the shape of the semicircle changes from a deformed semicircle to a sharp deformation tending to the value of $R_E + R_p$ for $\varphi = 1$. The 3-D plot (Re, Im, lg ω) is very important for a qualitative estimation of the model.

The errors of the R_E and R_p evaluation due to the inductance influence are obtained as follows:

$$\varepsilon^{L}_{R_E} = \varphi \frac{R_p}{R_E} \tag{10}$$

and respectively,

$$\varepsilon^{L}_{R_p} = -\varphi \qquad (11)$$

The dependence of the inductance on the electrode surface is also analysed. For real experiments the own cell inductance values depend on the cell size and configuration as well as on the electrode surface.

Following some assumptions and simplifications, the following dependence is obtained for the inductance error as a function of the electrode surface:

$$\varepsilon^{L} \approx K_1 \frac{1}{\tau r_s} \cdot S^2 , \qquad (12)$$

where K_1 is a coefficient of the shape, $\tau = r_p C_p$ and r_s - the specific resistances (r_{S_E} , r_{S_p}) represent the electrochemical parameters; S - the electrode surface.

As a result of the analysis, an evaluation of the error due to the inductance influence on the electrochemical impedance has been performed as well as the maximal frequency for a given inductance error has been estimated beyond which the impedance measurement becomes unreliable. Especially for low-impedance systems f_{max} goes to the range of low and middle frequencies.

From the calculations it follows that the limit measurement frequency can be increased by decreasing either the wire length or the object surface.

The topology analysis has shown that the presence of inductance leads to typical deformations of the main impedance shapes very often practically observed.

References

1. M.Keddam, Z.Stoynov, H.Takenoutti, J.Appl.Electrochemistry, 7 (1977) 539.
2. Z.Stoynov, B.Savova-Stoynov, J.Electroanal.Chem.,170 (1984) 63.

02330

OXYGEN EVOLUTION ON $La_{0.8}Sr_{0.2}Ni_{0.2}Co_{0.8}O_3$ ELECTROCATALYSTS IN ALKALINE MEDIUM

Ph. VERMEIREN*, R. LEYSEN*, H.W. KING**, G.G. MURPHY***, and H. VANDENBORRE*

* Studiecentrum voor Kernenergie, SCK/CEN, Boeretang 200, 2400 MOL Belgium

** Technical University of Nova Scotia, Canada

*** Atlantic Industrial Research, Canada

1. INTRODUCTION

Commercial electrolysers normally use nickel or nickel plated steel as anode material. This material is resistant to corrosion in hot concentrated caustic solutions and has one of the lowest oxygen evolution overvoltages of the non-noble metals. However, the overvoltage increases with time[1]. This phenomenon has been attributed to the gradual conversion of the Ni^{3+} to stable Ni^{4+} at the oxide surface.

The search for improvements has mainly been directed towards the development of catalytic semi-conducting oxides. Most of the oxides which have been studied for oxygen evolution in alkaline medium fall essentially into two major classes, according to their crystallographic structure ; spinel-type (e.g. $NiCo_2O_4$ and Co_3O_4) and perovskite-type (e.g. $LaCoO_3$) oxides.

Perovskite-type oxides exhibit interesting features for the oxygen evolution as shown recently in a review paper by S. Trasatti and G. Lodi[2].

In this paper we are going to discuss the properties of the perovskite-material $La_{0.8}Sr_{0.2}Ni_{0.2}Co_{0.8}O_3$ for oxygen evolution in alkaline medium.

2. EXPERIMENTAL

The perovskite type of ceramic electrocatalyst was made using a plasma spraying technique, and the catalyst was deposited onto a nickel expanded metal grid. Plasma spray deposition had been chosen as the preferred method for preparing catalytic electrodes as a result of work completed in earlier phases of this research. The formation of the perovskite phase has been followed by X-ray analysis and it was found that the perovskite phase was completely formed at 1000 °C.

Further characterisation of the electrodes was done by Scanning Electron Microscopy (SEM) , Energy Dispersive Analysis of X-rays (EDAX) and Microprobe Analysis.

The electrochemical experiments were mostly performed in a 30 wt % KOH solution. The reference electrode was a Hg/HgO using the same electrolyte. Long lasting and short-circuit experiments were performed under intentiostatic conditions and under forced electrolyte convection, the geometric area of the anodes was kept 4 cm^2. Cyclic voltammetry and polarisation curves were taken in an H-type cell and here the electrodes had a geometric surface area of 1 cm^2.

3. EXPERIMENTAL RESULTS AND DISCUSSIONS

3.1. Chemical stability testing

Chemical stability tests have been performed in a pressure vessel at a temperature of 200 °C and a pressure of 3.0 MPa. The cell was filled with a 45 wt % KOH solution and was maintained at pressure for 100 hours. Stability tests were done on two solid disc samples of $La_{0.8}Sr_{0.2}Ni_{0.2}Co_{0.8}O_3$ and the KOH solutions were analysed for all four components. Experimental results indicate that the strontium and lanthanum are stable. Cobalt leaches out an amount that corresponds to approximately 1-3 % of the cobalt content of the (10 gram) samples in the first 50 hours. After the initial 50 hour tests, the samples are essentially stable.
The same stability tests have been performed with plasma sprayed $La_{0.8}Sr_{0.2}Ni_{0.2}Co_{0.8}O_3$-electrodes, confirming their chemical stability.

3.2. Polarisation curves

Polarisation plots for the OER (Oxygen Evolution Reaction) on test electrodes were determined using steady state potentiostatic methods. Each electrode was preanodized at constant current density of 100 Am^{-2} for 1 hour. Three temperatures were investigated : 25 °C, 45 °C and 65 °C and the results are shown in Table I.

Table I

Temperature (°K)	b (V decade^{-1})	a (V at 1 Am^{-2})	x	i_o (Am^{-2})
298	0.045	0.17	1.3	$1.8\ 10^{-4}$
318	0.046	0.15	1.4	$5.5\ 10^{-4}$
338	0.049	0.13	1.4	$2.4\ 10^{-3}$

At low overpotentials, the Tafel slope is about 0.045-0.050 V . A Tafel slope of 0.04 V for a perovskite-type oxide has been reported by S. Trasatti and G. Lodi [2] . The proposed mechanism is a second electron transfer from adsorbed OH radicals as the rate determining step :

$$S - OH + OH^- \rightarrow SO + H_2O + e^-$$

where S is a surface site.
This mechanism predicts a Tafel slope of 0.04 V and a reaction order with respect to OH^- of 2. However, in our investigations the reaction order can not uniquely be defined since the Tafel slopes changes as a function of electrolyte concentration. More detailed analyses involving polarisation experiments and reaction order studies are needed to gain more insight in the complicated reaction mechanism.

From the experimental data, especially the observed current density as a function of the temperature, an apparent activation energy at zero overpotential $\Delta H(\eta = o)$ can be calculated and equals 50 kJ mole^{-1}.
Long lasting experiments have been performed with several electrodes at 10,000 Am^{-2} in a 30 wt % KOH solution. The electrode overvoltages for three electrodes have been measured as a function of time. The initial mean overvoltage equals 0.35 V and increases as a function of time at a rate of 1.3 mV day^{-1}.
However, after each current interruption the initial overvoltage value was restored. No explanation has yet been found for this phenomenon.

3.3. Short-circuiting experiments

Since it is envisaged to use these anodes in bipolar filter press type water electrolysers, the stability of the perovskite anodes against current interruptions has to be checked. This is important since it is known that a reduction of the anode oxide material can occur at current interruptions, especially when using in a bipolar configuration, highly active cathodes e.g. Raney-nickel, nickel sulphide.
To check the stability, the perovskite-electrodes were tested as follows : after some time of electrolysis at 10,000 Am^{-2} and 90 °C, the anode in a single cell configuration was short-circuited to a nickel sulphide type of cathode. After that the anode and cathode potentials were equalized at about -0.75 V vs Hg/HgO, the electrolysis was restarted. This sequence has been repeated for ten times. After each interruption, the anode potential reached its initial value, indicating the stability of this type of perovskite.
Voltammetric measurements also indicate the stability of these anodes since no corrosion peaks can be observed in a broad potential range between -0.85 V vs Hg/HgO and the OER. Similar measurements with PTFE-bonded $La_{0.9}Sr_{0.1}CoO_3$-electrodes performed by T. Kudo and co-workers [3] showed the reduction of the electrode oxide at negative potentials.

REFERENCES

1. P.W.T. Lu and S. Srinivasan, "Electrochemical-Ellipsometric Studies of Oxide Films formed on Nickel during oxygen evolution", Proceedings of Symposium on "Electrode materials and Processes for Energy Conversion and Storage". The Electrochemical Society , Princeton,N.J. p.396 (1977)
2. S. Trasatti and G. Lodi, "Oxygen and Chlorine Evolution at Conductive Metallic Oxides" (part B), Ed. by S. Trasatti, Elsevier Sci.Pub.Comp. Amsterdam (1980)
3. T. Kudo et al, J. of the Electrochemical Soc., vol. 124 no. 3, 321 (1977)

02340

CHARACTERIZATION OF TITANIUM DIOXIDE-SUPPORTED PLATINUM CATALYSTS

M. SPICHIGER-ULMANN and J. AUGUSTYNSKI
Département de Chimie Minérale, Analytique et Appliquée
30, quai E. Ansermet, 1211 Geneva 4, Switzerland

TiO_2-supported noble metals and/or noble metal oxides have in last years received special attention both as efficient photocatalysts (for the photodecomposition of water, for example) and as a new class of potential catalysts for CO-H_2 Fischer-Tropsch synthesis[1].

Thus, the photodecomposition of water into H_2 and O_2 has been demonstrated both using a suspension of platinized TiO_2 particles irradiated with the UV light[2], and also in a more complex system, consisting of Pt and RuO_2 catalysts supported on colloidal TiO_2, in the presence of a sensitizer (e.g., $Ru(bipy)_3^{2+}$) capable of absorbing the visible light[3]. Recently, carbon dioxide has been shown to undergo strong reductive adsorption at Pt/TiO_2 film electrodes[4]. In order to evaluate the modification of the adsorption properties, due to the dispersion and to the presence of (or the interaction with) the TiO_2 support, the electrochemical behaviour of different Pt/TiO_2 deposits was examined, particularly in the hydrogen adsorption-desorption region, using cyclic voltammetry.

The platinum catalysts investigated in this study were supported on 10 to 15um thick anatase TiO_2 films. These films were prepared by a layer-by-layer hydrolytic decomposition of an alcoholic $TiCl_4$ solution applied onto metallic Ti substrates[5]. After annealing in air at 450°C, all samples were reduced by heating in argon at 550°C. This mode of reduction confers on the TiO_2 films good electrical conductivity, associated with the presence of lower titanium oxides, including TiO and Ti_2O_3, close to the interface with Ti metal[6].

Platinum deposits were performed cathodically, according to ref. 7. Fig. 2 shows a typical scanning electron micrograph of such a Pt/TiO_2 surface (platinum appears as irregular white spheres). X-ray photoelectron spectroscopic measurements revealed that the Pt4f(7/2) binding energy of the dispersed platinum was identical, within 0.1 eV, to that of smooth Pt.

Amongst features of electrochemical behaviour of these Pt/TiO_2 film electrodes, the characteristic enhancement of the amount of strongly adsorbed hydrogen (with respect to a smooth polycrystalline Pt electrode) is visible in Fig. 1 for three different electrodes containing increasing amounts of Pt.

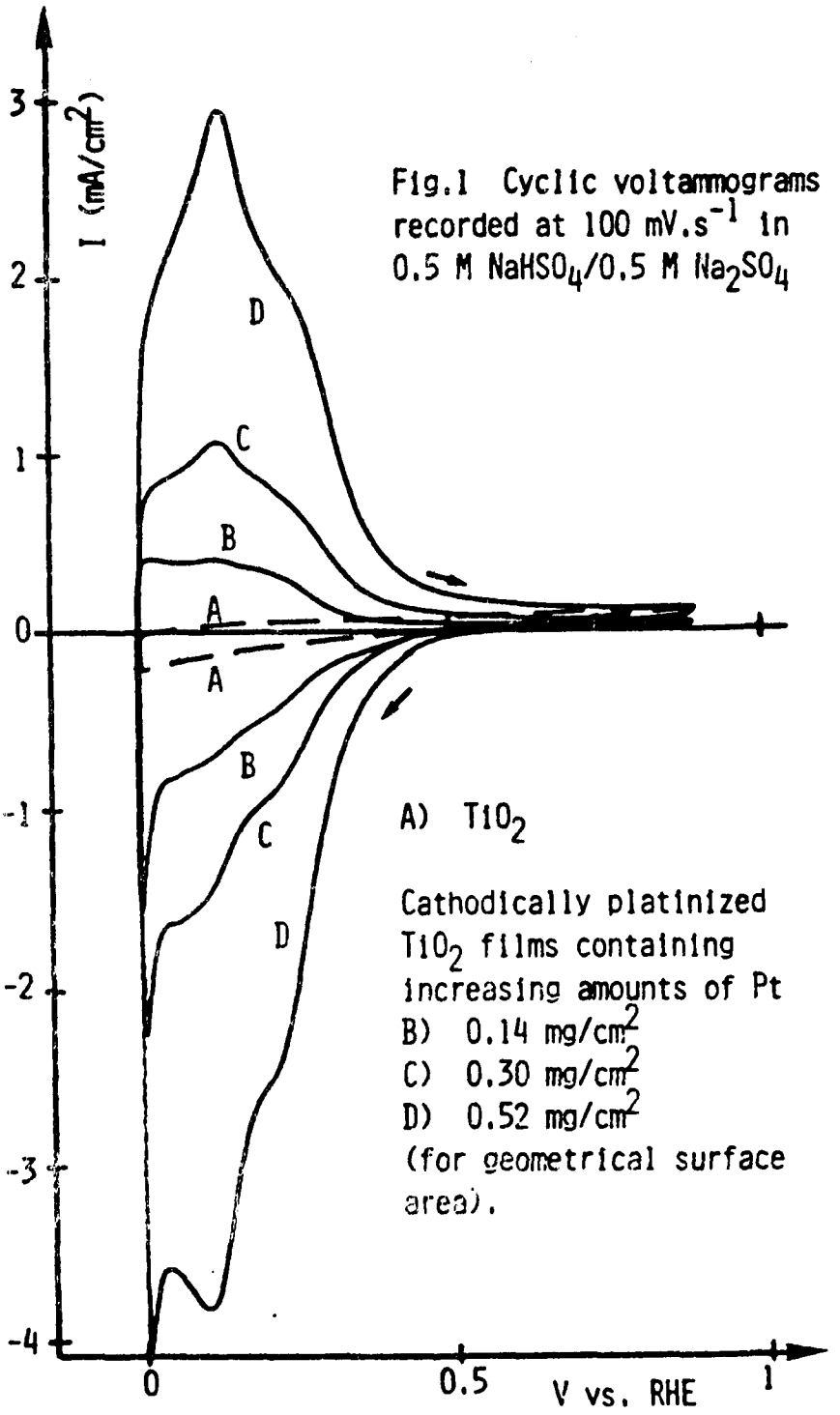

Fig.1 Cyclic voltammograms recorded at 100 $mV.s^{-1}$ in 0.5 M $NaHSO_4$/0.5 M Na_2SO_4

A) TiO_2

Cathodically platinized TiO_2 films containing increasing amounts of Pt

B) 0.14 mg/cm^2

C) 0.30 mg/cm^2

D) 0.52 mg/cm^2

(for geometrical surface area).

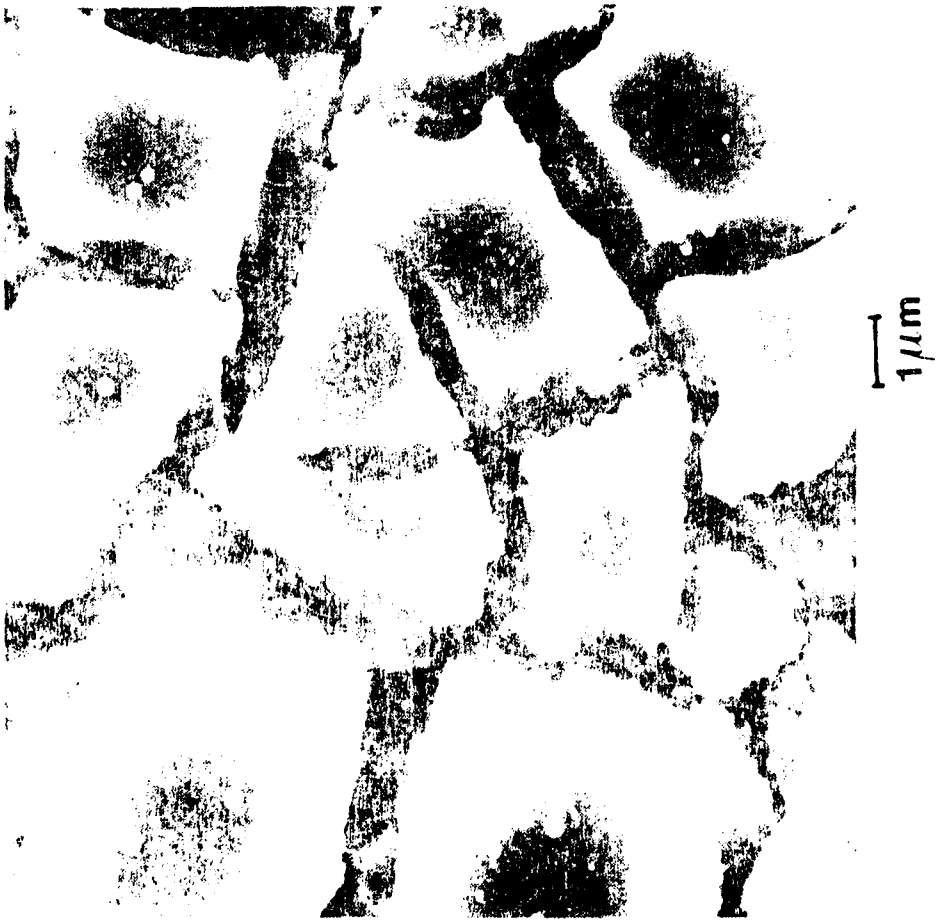

Fig. 2 Scanning electron micrograph of a cathodically platinized (0.25 mg of Pt/cm^2 of geometrical area) prereduced TiO_2 film surface.

References

1. S.J. Tauster, S.C. Fung, R.T.K. Baker and J.A. Horsley, Science, 211, 1121 (1981).
2. A.V. Bulatov and M.L. Khidekel, Izv.Akad.Nauk SSSR, Ser.Khim, 8, 1902 (1976).
3. E. Borgarello, J. Kiwi, E. Pelizzetti, M. Visca and M. Grätzel, Nature (London), 289, 158 (1981).
4. M. Koudelka, A. Monnier and J. Augustynski, J.Electrochem.Soc., 131, 745 (1984).
5. G. Stalder and J. Augustynski, J.Electrochem.Soc., 126, 2007 (1979).
6. M. Koudelka, A. Monnier, J. Sanchez and J. Augustynski, J.Mol.Catal., 25, 295 (1984).
7. O.A. Khazova, Yu.B. Vasil'ev and V.S. Bagotskii, Elektrokhimiya, 6, 1367 (1970).

02350

HYDROGEN EMBRITTLEMENT ON STEEL UNDER APPLIED STRESS.

A. I. ONUCHUKWU
Department of Chemistry
Bayero University,
P. M. B. 3011, Kano, Nigeria.

INTRODUCTION

Hydrogen atom dissolution and permeation in steel are often associated with composition and points of stress concentration in the material. These stress raisers may be flaws inadvertedly present in the material (e.g flaws in welds), sites of damage caused by use of the structure or caused by discontinuities in the geometry of the member. These structural defect paths for H permeation are enlarged in size or number by these stress raisers. It has been shown that H entry into steel grain boundaries is further enhanced by applied tensile stress (1).

In the previous paper (2, 3), it has been demonstrated that in the sour environment (i.e H_2S), the cathodic evolution of hydrogen on a corroding material is reduced, consequently, the amount of Had by Steel is enhanced. As the effect of applied stress on Had by steel in the absence of chemical agents has not adequately been established possibly due to experimental assembly difficulties, this paper proposes to investigate the relation between applied stress on H permeation in steel.

EXPERIMENTAL:

The En42 Steel membrane (thickness = 2.74 mm) was mechanically press-cut into standard tensil specimen according to ASTM. This was annealed, polished and degreased with acetone prior to introduction of strain guage. This specimen was made to fit the glassware flanges at the joints while projecting above and below this joint of the two compartment cell of Davanathan et al. (4). These projections of the specimen were clamped firmly to the provisions made for them on the Mosanto Type Tensometer which was held vertically while the flanges are horizontal.

The tensile steel diffusion membrane was initially at zero stress while cathodic compartment was maintained galvanostically at 10 mA/cm^2 H_2 charging.

The anode compartment is held at potentiostatic H_2 oxidation potential in 3.5% NaCl electrolyte. The H permeation current is recorded at this anodic mode by the Xt pen recorder. At the steady state of H - permeation current, the stress was increased from zero to 180 $N\text{-}mm^{-2}$. The H permeation current for this stress level was recorded. Thereafter, the stress level was once more increased from 180 $N\ mm^{-2}$ to 240, 370, 430 and 550 Nmm^{-2}. The limiting H permeation currents for each of these stress levels were recorded.

RESULT AND DISCUSSION:

The elastic modulus specification of the tensile specimen was confirmed (235 KN mm^{-2}) and the H permeation current within the elastic region to respond with increase in stress. This is consistent with the suggestion of Phalen et al, that the number of H paths is related to the magnitude of stress raisers. This observation in this work suggests that a preferential H diffusion path or acceleration of M-H reaction in a stress steel specimen.

However, the inability to detect a hydride phase (M - H) in steel supports the earlier view that H does enter the lattice of the stressed steel, diffuses into and concentrates in the region of highest tensile stress. This fact could hold an explanation for the rapid increase in H permeation current observed when the steel membrane was contracting as the steel was suddenly relieved (i.e to zero) of the applied stress. The observed increase in H, fig.1 permeation current could be due to a squeeze out of the dissolved H at high stress that could not be accommodated at the limited sites available at zero stress. Therefore, it is possible to conclude that in suitable hydrogen environment, hydrogen embrittlement is plausible in the presence of stress raisers.

REFERENCES.

1. Vaughan, D. A. and Phalen, D. I., Metal Eng., 3(5), 39, 1965.

2. Onuchukwu, A. I.; H. C. Chan and A. C. C. Tseung, Electrochem. Soc. Meeting Miss., U. S. A., Extended Abst. Vol. 79-1, 140, 1979.

3. Onuchukwu, A. I. and J. A. Lori, Corr. Sci., 24, 833, 1984.

4. Davanathan, M. A. V. and Stachurski, Z., J. Electrochem. Soc., 111, 619, 1964.

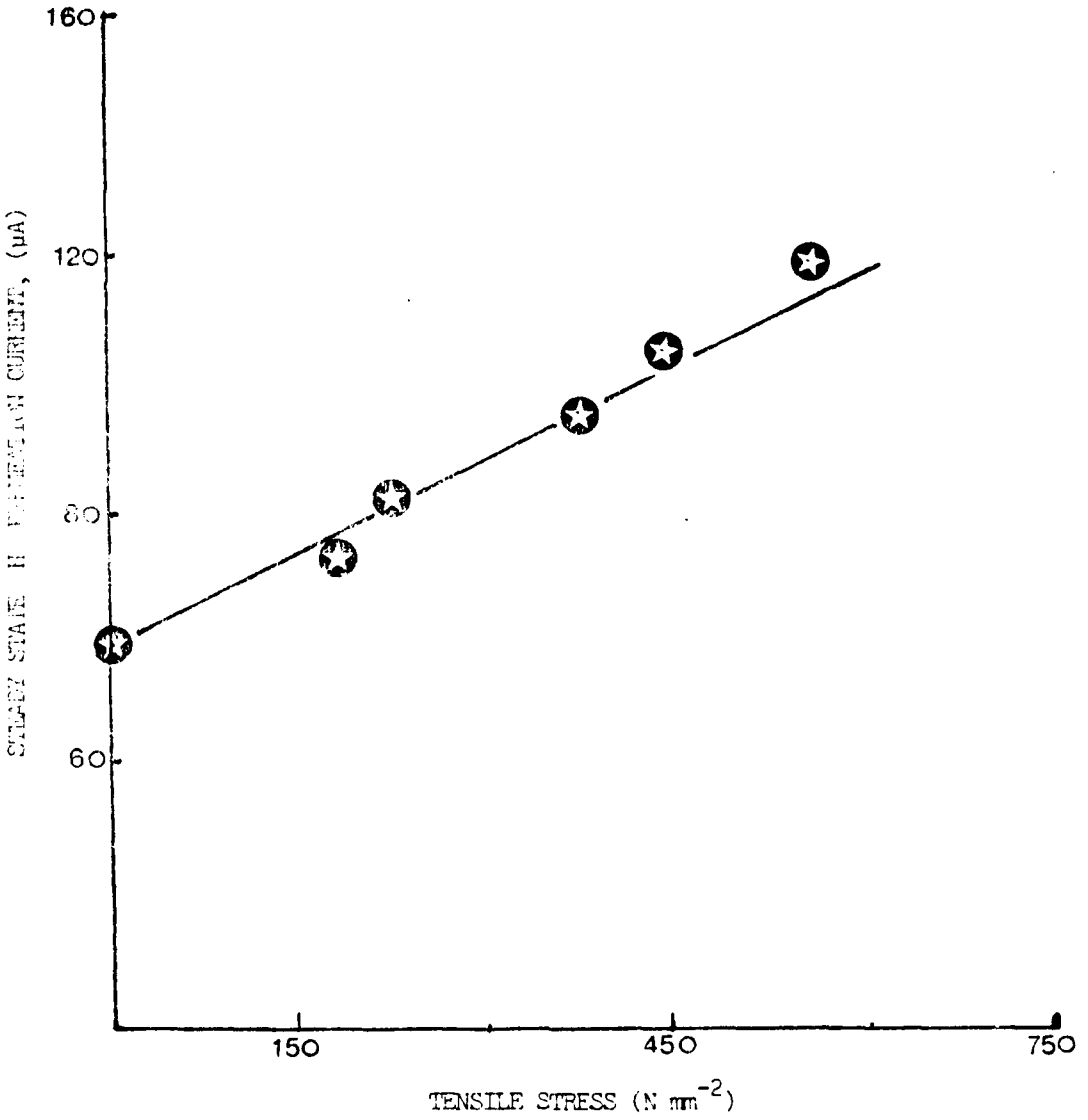

Figure 1. Effect of applied tensile stress (N mm^{-2}) on the steady state H paramcation current (μA) @ 30° C.

02360

EFFECTS OF ION BOMBARDMENT ON THE MORPHOLOGY OF LEAD FILMS

Michael J. Armstrong and Rolf H. Muller
Lawrence Berkeley Laboratory and Department of Chemical Engineering
University of California
Berkeley, CA 94720 USA

Ion bombardment is extensively used for determining composition profiles of surface layers by Auger electron spectroscopy [1]. For thin films on the order of a few tens of nm thickness, surface roughening is thought to be minor and a uniform removal of surface layers is expected. The present work concerns a case where these assumptions do not apply and composition profiles have to be interpreted differently.

This work was undertaken in connection with a previous effort on the effect of organic adsorbates on the initial stage of electrolytic metal deposition, where the presence of Rhodamine-B had been found to greatly reduce the microporosity of very thin layers of electrodeposited lead [2]. Ion bombardment in combination with Auger electron spectroscopy and spectroscopic ellipsometry were to be used to determine the porosity and composition profiles of the lead deposits.

The lead films used in this study were deposited by electrochemical and evaporation methods upon 12.3 mm diameter oxygen-free copper disks. These methods produced films that covered the surface uniformly. The copper substrates were mechanically polished with a final step using 0.05 μm alumina powder in water. An electrolyte consisting of 1.0M $NaClO_4$, 0.005M $Pb(NO_3)_2$, and 10 μM Rhodamine-B chloride at a pH of 2.4 was used for electrodeposition. After deposition, the samples were rinsed quickly with distilled water with excess water being removed by compressed Freon. Vapor deposition of lead films was performed under vacuum, both in the UHV chamber used for AES, and in a commercial evaporator. Both depositions were made by evaporating high purity lead (99.999%) from a tungsten basket. During vapor deposition, the background pressure in the commercial apparatus was 10^{-4} torr, in the UHV chamber it rose to 10^{-7} torr. The deposits prepared within the commercial apparatus were exposed to air for approximately 10 min. during transfer to the UHV chamber. The deposits made within the UHV chamber were not exposed to air before ion bombardment.

The UHV chamber was equipped with windows which were oriented to allow ellipsometry of the sample with a 75° angle of incidence. The electron gun for AES, and the ion bombardment gun were also oriented for a 75° angle of incidence of their respective beams but at azmuthal positions of 30° and 60° respectively from the plane of incidence of the ellipsometer beam. Ion bombardment was performed with argon ions at an energy of 1100 eV in 5×10^{-5} torr of Argon. The ion beam was rastered across the surface for an even bombardment. Optical properties of the film-covered surfaces were measured with a spectral-scanning ellipsometer. Its construction and use have been described elsewhere [3].

The optical response of the samples following ion bombardment was modeled in two successive stages. Early in the bombardment process, the film was modeled with a compact PbO layer upon a continuous, porous lead film. Following the removal of the oxide layer, the surface was modeled with a pitted, porous lead film (Fig. 1). Models of the surface that consisted of one or two layers of continuous films did not reproduce the measurements satisfactorily even when the films were assumed to be porous and contain lead and copper. The optical response of the pitted film was interpreted

with the coherent superposition of the reflection coefficients from the bottom of the pit and on the film [4]. The parameters of the surface model, porosity, thickness and surface coverage for the film, were determined with a routine which minimized the deviation between the prediction of the optical model and the spectroscopic ellipsometer measurements [2].

The ion bombardment of a lead film is represented in Fig. 2 by the results from a 0.039 C/cm^2 (36.9 nm compact) electrodeposit in which virtually all the lead was removed from the copper substrate after 125 min. of ion bombardment. Up to 5 min. of ion bombardment, the surface was modeled with a continuous oxide layer upon a continuous lead film of 20% porosity. The oxide layer was determined from ellipsometer measurements to be 3 nm thick initially and to be removed uniformly. Between 15 and 35 min. of ion bombardment the surface was modeled with a pitted lead film in which the pits did not reach the copper substrate. After 45 min. the ellipsometric data were modeled with a pitted lead film in which the copper substrate was exposed in the pits. Throughout the ion bombardment the porosity was found to remain constant at 20%. The fraction of the copper substrate covered by lead was also determined from Auger spectroscopy by an interpretation in which one assumed that all the lead is present in the area between the pits. Figure 2 shows the agreement of lead coverage determined by ellipsometry and Auger spectroscopy.

The formation of pits in lead films under the influence of Ar ion bombardment, derived from the spectroscopic ellipsometer measurements, has been confirmed at the later stages by scanning electron microscopy of films generated by evaporation or electrochemical deposition. Figure 3 shows pits of 1 μm diameter in a 75 nm deposit after 65 min. of bombardment.

Two possible causes of pitting were investigated, the presence of oxide or carbon on the surface, however, no firm correlations could be found.

It has been found that thin uniform lead films on copper are not uniformly removed by ion bombardment. The films become pitted following bombardment by 1100 eV argon ions. It appears that the pitting is a result of the sputtering process and not of a protective layer upon the lead film. The results of this study demonstrate the problems associated with using ion bombardment to obtain composition profiles of thin films. The interpretation of spectroscopic ellipsometer measurements on the basis of an optical island model agrees with that of Auger spectra with the same model.

Acknowledgment

This work was supported by the Director, Office of Energy Research, Office of Basic Energy Sciences, Materials Sciences Division of the U.S. Department of Energy under Contract No. DE-AC03-76SF00098.

References

1. G.K. Wehner, "Two Aspects of Sputtering in Surface Analysis Methods," in METHODS OF SURFACE ANALYSIS, A.W. Czanderna ed., Elsevier, Amsterdam, 1975, p. 9.
2. J.C. Farmer and R.H. Muller, J. Electrochem. Soc., 132, 313-319 (1985).
3. R.H. Muller and J.C. Farmer, Rev. Sci. Instrum., 55, 371-374 (1984).
4. R.H. Muller and J.C. Farmer, Surf. Sci., 135, 521-534 (1983).

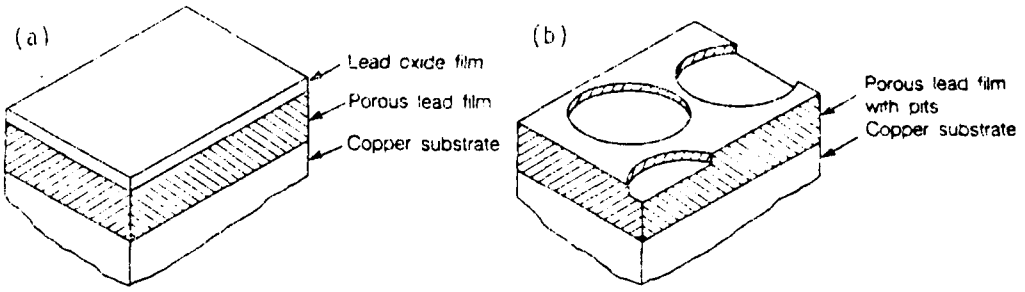

Fig. 1. Model surfaces used for interpreting spectroscopic ellipsometer measurements: a) oxide covered porous-lead film; b) pitted porous-lead film.

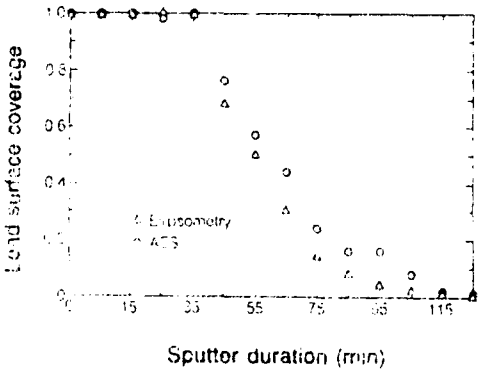

Fig. 2. Lead surface coverage derived from ellipsometer and AES measurements during ion bombardment of a 36.9 nm thick Pb film on Cu.

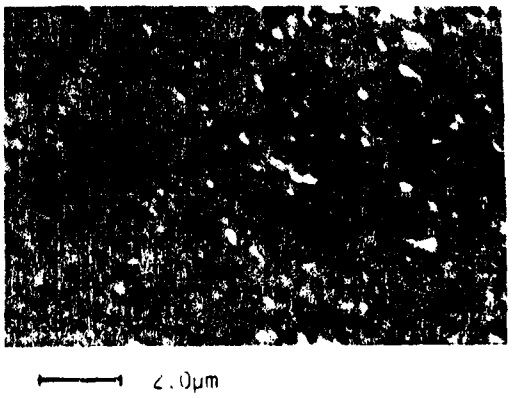

Fig. 3. Pitting in a electrodeposited lead film, 75 nm thick, after 55 min of ion bombardment.

CARBON PASTE ELECTRODE CONTAINING CATION EXCHANGER BEADS LOADED WITH CATIONIC REAGENT FOR ELECTROCATALYSIS

Wlodzimierz KUTNER, Thomas J. MEYER and Royce W. MURRAY
Kenan Laboratories of Chemistry, University of North Carolina, Chapel Hill, North Carolina 27514 (U.S.A.)

An ion exchange polymer and carbon paste electrode (CPE) are combined to immobilize an aquo ruthenium(II/IV)poly-pyridyl complex, $[Ru(trpy)(phen)(OH_2)](ClO_4)_2$ (where trpy = 2,2',2''-terpyridine, phen = 1,10-phenanthroline), as oxidative electron transfer mediator — a catalyst in basic solutions. The ionic complex is loaded into microparticulate sulfonated polystyrene (cat)ion exchange beads (Dowex 50Wx8), to which carbon powder and Nujol are admixed to form the modified carbon paste electrode.

At pH $\geq$ 13 the acid dissociation equilibrium of the complex is totally shifted towards the monoprotonated form since[1] pK_{a1} = 9.35.

$$[Ru^{II}(trpy)(phen)(OH_2)]^{2+} \rightleftharpoons [Ru^{II}(trpy)(phen)(OH)]^{+} + H^{+} \quad (1)$$

At pH = 13 $\underset{\sim}{I}$ is reversibly electrooxidized in a one, two-electron one-protone step with $E^{0\prime}$ = 0.285 V vs SSCE[1] (Fig. 1a). The resulting Ru(IV)complex oxidizes many organic substrates. We investigated oxidation of benzyl alcohol (BA) to benzaldehyde in detail and a number of other substrates in lesser detail.

$$[Ru^{II}(trpy)(phen)(OH)]^{+} \underset{\underset{I}{\sim}}{\rightleftharpoons} [Ru^{IV}(trpy)(phen)O]^{2+} + 2e^{-} + H^{+} \quad (2)$$
$$\underset{ox\ \underset{\sim}{I}}{}$$

$$[Ru^{IV}(trpy)(phen)O]^{2+} + C_6H_5CH_2OH \xrightarrow{k_1} [Ru^{II}(trpy)(phen)(OH)]^{+} + C_6H_5CHO + H^{+} \quad (3)$$

Basic solutions containing $\underset{\sim}{I}$ and BA show in cyclic voltammetry (CV) electrocatalytic currents at glassy carbon electrode and at CPE not containing catalyst (Fig. 1b). We compared the rates of electrocatalytic reactions of the homogeneous solutions and the modified CPE. In contrast to ox $\underset{\sim}{I}$ the reduced complex, $\underset{\sim}{I}$, is quite stable in 0.1 M NaOH. Thus, in situ the electrochemical oxidation of $\underset{\sim}{I}$ to generate ox $\underset{\sim}{I}$ was a promising electrocatalytic application of the Ru(IV/II) redox system for selective oxidation of redox species.

As the potential scan rate $\underline{v}$ or electrode rotation rate $\underline{f}$,

---

[+]On leave from the Institute of Physical Chemistry, Kasprzaka 44, 01-224 Warsaw (Poland).

is decreased, the oxidation currents in CV and rotated disc electrode (RDE) experiments become nearly independent of v and f. Such a behavior is typical of an electrocatalytic "EC" reaction where $E^{0'}$ of the irreversibly electrooxidized substrate is less positive than $E^{0'}$ of the reversibly electrooxidized catalyst. At small v or f values the catalytic reaction rate

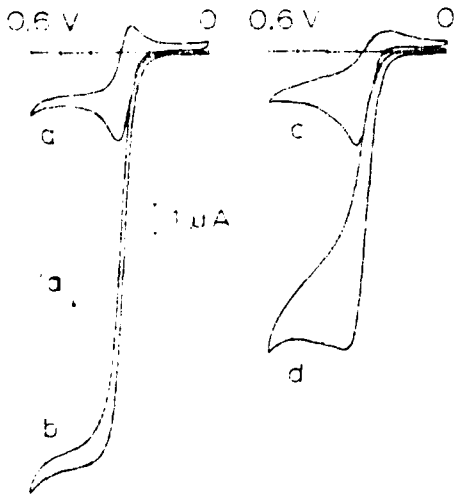

Fig. 1. Cyclic voltammograms at 0.01 V/s in 0.1 M NaOH for carbon paste electrodes in the absence (a,c) and presence (b,d) of 0.1 M benzyl alcohol. Solutions in a and b contain 0.2 mM I; paste electrodes contain $[I]/[SO_3^-] = 4.59 \times 10^{-2}$. Electrodes in a-d contain 60, 60, 52, and 52% of carbon, respectively; electrode surface area 0.091 cm^2.

constant, k_1, is calculated[2] (Table 1) by using v- and f- independent catalytic currents, i_{cat}, both in CV and RDE techniques

$$k_1 = i_{cat}^2 / (n F A C_R)^2 D_R C_S \qquad 4)$$

where: D_R and C_R are the diffusion coefficient and concentration of I, C_S is the substrate concentration and A_2 is the electrode surface area. The value $D_R = 4.6 \times 10^{-6}$ cm^2/s was found from the slope of the RDE Levich plot.

Cyclic voltammograms of I immobilized in CPE (denoted as CPE/PS-SO_3^-,I) are shown in Fig. 1c and 1d. In the absence of BA the oxidation peak current, i_{pa}, at CPE/PS-SO_3^-,I is directly proportional to v, to the effective electrode surface area A_{eff}, and at low loading to the concentration of I in the ion exchanger. In the presence of BA in a solution free of I i_{pa} at CPE/PS-SO_3^-,I tends to be independent of v at slow scan rates. For calculating k_1 we used the same procedure as that applied when both the catalyst and substrate were in solution, since the natures of catalysis and transport phenomena are the same. To avoid the use of estimated parameters such as

Table 1
Catalytic reaction rate constants, k_1, calculated from rotation rate independent i_{cat} data at rotated glassy carbon electrode for oxidation of different substrates by $\underset{\sim}{I}$ in 0.1 M NaOH.

Substrate	k_1, $M^{-1}s^{-1}$
Benzyl alcohol	30.8 ± 1.6(a) ; 28.2 ± 1.5(c)
Methanol	0.030 ± 0.006(a)
Ethanol	0.063 ± 0.011(a)
1-Propanol	0.074 ± 0.004(a)
2-Propanol	0.046 ± 0.008(a)
Ethylene glycol	0.043(b)
Acetone	0.21 ± 0.04(a)
D-Glucose	0.0084(b)
D-Maltose	0.012(b)
D-Lactose	0.82(b)
D-Mannitol	0.17(b)
Arginine	0.28(b)

(a) Reaction order verified to be first order in $\underset{\sim}{I}$ and pseudo-first order in substrate.
(b) Calculated from results at one substrate concentration.
(c) Calculated from results at carbon paste electrode.

$C_{PS-SO_3^-,\underset{\sim}{I}} = P\,C_S$, $D_{PS-SO_3^-,\underset{\sim}{I}}$ and A_{eff} which are necessary for the calculation of k_1, ^{3}eq.(4) was normalized to oxidation peak currents, i_{pa}, ^{1}expressed by the Randles-Sevcik equation for oxidation of $\underset{\sim}{I}$ in the absence of substrate, so at 25°C

$$k_1 = 7.77\ n\ v\ i_{cat}^2 / C_S\ P\ i_{pa}^2 \qquad (5)$$

where P is partition coefficient of S between the ion exchanger and solution. The calculated $k_1 = 10.8 \pm 4\ M^{-1}s^{-1}$ is within a factor of three the same as the corresponding homogeneous k_1 for electrocatalysis when both $\underset{\sim}{I}$ and BA are in solution. In 0.1 M NaOH P was found to be close to unity. At low loadings $D_{PS-SO_3^-,\underset{\sim}{I}} = 1.7 \times 10^{-10}\ cm^2/s$. The results of electrocatalysis at CPE/$PS-SO_3^-,\underset{\sim}{I}$ are interpreted as taking place entirely inside the ion exchange phase.

References
1. L. Roecker, W. Kutner, J. A. Gilbert, M. Simmons, R. W. Murray and T. J. Meyer, submitted.
2. Z. Galus, "Fundamentals of Electrochemical Analysis", Hasted Press, New York, 1976, Chap. 10.

02380

APPLICATION OF SURFACE ENHANCED RAMAN SPECTROSCOPY TO IN-SITU CHARACTERIZATION OF METAL/SOLUTION AND SEMICONDUCTOR/SOLUTION INTERFACES

M.JANIK-CZACHOR

INSTITUTE OF PHYSICAL CHEMISTRY,POLISH ACADEMY OF SCIENCES,WARSAW,POLAND

Surface Enhanced Raman Spectroscopy (SERS) is becoming a popular in situ technique of surface analysis in electrochemical systems. The technique provides a molecular specific characterization of the metal/solution interface, a goal long sought by electrochemists. SERS has a possibility of giving an insight into such important problems as: (I) what is the chemical identity of the atomic or molecular species, (II) what is orientation of these species with respect to the substrate surface, and (III) what is nature of the chemisorption bonding/1,2/. The following aspects of the method are briefly outlined:

- the characteristic features of the surface spectra
- the molecular generality of SERS
- determination of the orientation of the adsorbed species
- effect of surface roughness

Additional increase of the Raman scattering efficiency through application of Resonance Raman technique (SERRS) is discussed. A possibility of the investigations of surface processes on iron is demonstrated on an example of the active dissolution of iron in 1,10 phenanthroline containing solution. 1,10 phenanthroline is an inhibitor

of this reaction. There have been speculations in the literature that the metal dissolution goes via surface complexes with phenanthroline. With the aid of SERRS it was possible to identify the complexes as $Fe(phen)_3^{+2}$ and to show that that they are indeed present at the iron surface during its anodic dissolution, Fig.1 /3/.

Regarding the semiconductive character of the passive film on transition metals various aspects of SERRS of some adsorbates on semiconductor electrodes with a discontinuous Ag overlayers are examined. This method has been introduced by Van Duyne et al. /4/ in order to study adsorbates on GaAs and Si. Fig.2. shows an example of SERRS spectrum for a $Fe(phen)_2^{+3}$ treated n-GaAs electrode with an electrochemically deposited Ag overlayer. Since the above mentioned complexes have an absorption maximum at ca. 510 nm, an estimate of the resonance enhancement contribution to the signal in this case can be obtained from a comparison of the spectra A and B taken at 457.9 nm and at 514.5 nm, respectively.

A possibility of application of this method to studies of adsorbates on passive metals is discussed.

1. R.P.Van Duyne, in "Chemical and Biological Applications of Lasers", vol.4., Academic Press, N.York 1979, p.101
2. L.R .Burke et al.,Adv. in Chemistry 201, 69 (1982)
3. R.P.Van Duyne, M.Janik-Czachor, JECS 130,2320 (1983)
4. R.P.Van Duyne,J.P.Haushalter,M.Janik-Czachor,N.Levinger, J.phys. Chem.,in press

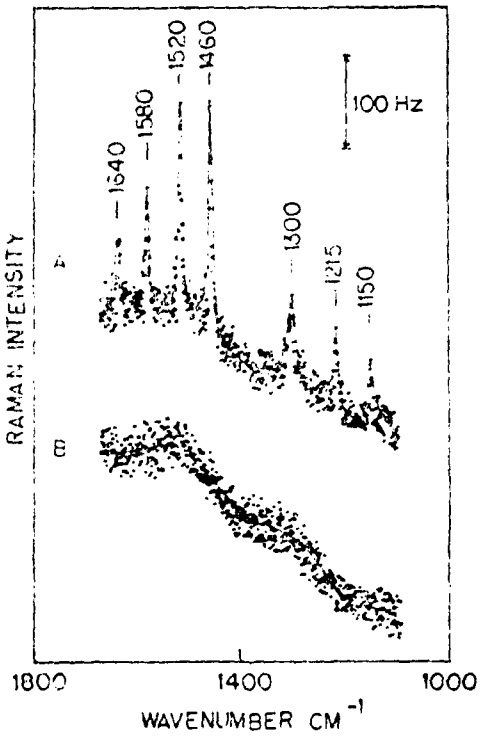

Fig.1.Effect of potential on the SERRS spectrum of $Fe(phen)_3^{+2}$ on iron electrode, in $5x10^{-3}$M, 1.10 phenanthroline solution. (a) -0.5 V, (b) +1V. Laser power 200 mW, slits 2cm^{-1}, exciting wavelength 514.5 nm.

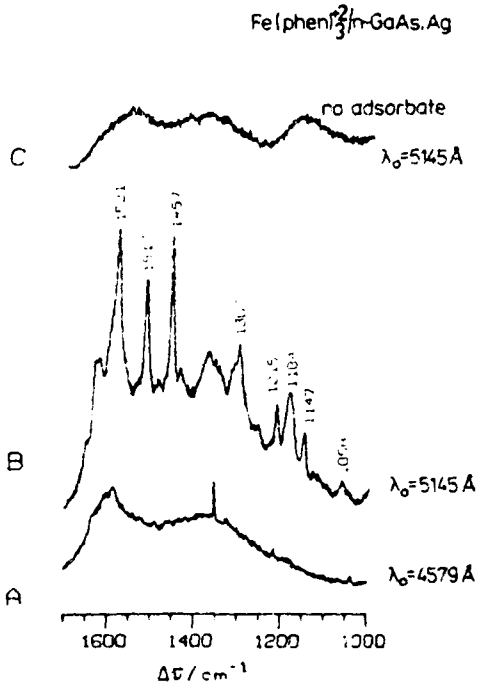

Fig.2. SERRS spectrum of $Fe(phen)_3^{+2}$ treated n-GaAs/Ag electrode (with a discontinuous Ag overlayer, A and B). C: n-GaAs/Ag with no adsorbate. Laser power 100 mW, slits 4cm^{-1}.

02390

ELECTROCATALYTIC PROPERTY OF ALLOYS BETWEEN GROUP VIII AND IB METALS TOWARDS OXIDATION OF SIMPLE ORGANICS

M. ENYO, A. ARAMATA, and K. MACHIDA
Research Institute for Catalysis, Hokkaido Unversity,
Sapporo, 060, (Japan)

A synergetic effect of appreciable extent was seen in the electrocatalytic activity of Pd-Au alloys in the $HCOOH/HCOO^-$ oxidation in acidic and alkaline solutions, as well as of Ni-Cu alloys in the HCHO oxidation in alkaline solution.

Elecro-oxidation of CH_3OH is sluggish and hence realization of methanol fuel cells awaits strongly the developement of electrodes of high electrocatalytic activity. The situation is rather different in the case of electro-oxidation of methanol-related compounds, HCHO and HCOOH. As is known, electrto-oxidation of HCHO in acidic media is not much different from that of CH_3OH, but it is far more facile in basic media such that the oxidation starts at potentials as negative as 0V RHE. Further, Pt is no longer the best electrode material and Cu or Pd may instead be used in the HCHC or HCOOH electro-oxidation, respectively. An interesting task that follows is the use of alloys, particularly those between group VIII and IB metals: These alloy systems have long been the subject of researches in catalysis in connection with the topic on the d-band electronic factor. Furthermore, it is known that electro-oxidation of alkaline HCHO on group IB metals was accompanied with the co-production of H_2, whereas the hydrogen was simultaneously oxidized on group VIII metals. Results observed on the electrodes of Pd-Au and Ni-Cu alloys are described in this report.

Foils of Pd-Au alloys or plates of Ni-Cu alloys of various composition were used. The surface compositions at various stages were examined by means of XPS or of electrochemical adsorption behaviours revealed in potential sweep curves: Some of them will be presented later, but otherwise the electrocatalytic activity data are presented below in terms of nominal bulk compositions as, whatever is the surface composition, the main interest at present may be grasped on the bulk composition basis. True surface areas of the electrodes needed to compare specific levels of the electrocatalytic activity were evaluated mainly from the d.l. capacitance data.

Electro-oxidation of CH_3OH on Pd-Au alloys

The Pd-Au alloys, as well as the pure components, are practically inactive towards the CH_3OH electro-oxidation in acidic media, but have appreciable activity in alkaline media. Typical potential sweep curves in 1M NaOH are shown in Fig. 1:

Pd and $Pd_{90}Au_{10}$ alloy are the most active whereas the activity rapidly decreases with decrease of the Pd content. Closer investigations have indicated a minor degree of synergetic effect in the electrocatalytic activity with the maximum activity around the $Pd_{90}Au_{10}$ composition.

Surface analysis by means of an XPS technique indicated, in agreement with some reports in the literature[1,2] that the surface composition in these alloys is approximately the same with the bulk composition. Nevertheless, in view of various inaccurate factors involved in this technique, and of some differences indicated between these data and those from electrochemical adsorption experiments[3], further investigations may be required in order to specify precisely the surface composition of the maximum activity.

Electro-oxidation of HCHO on Pd-Au alloy electrodes

The reaction in acidic solution as a whole is not very rapid. Nevertheless, the maximum oxidation current was observed on the $Pd_{90}Au_{10}$ alloy[4]. The reaction was exceedingly rapid in alkaline solution and, in that case, Au was the most active, followed by Au-rich Pd-Au alloys. These have been reported elsewhere[4].

Electro-oxidation of $HCOO^-$ on Pd-Au alloy electrodes

Potential sweep curves obtained during the $HCOO^-$ electro-oxidation in alkaline solutions are shown in Fig. 2. While Au and Pt are inactive towards this reaction, Pd and in particular Pd-Au alloys of intermediate composition are highly active. Synergetic effect is thus significant in this case.

Electro-oxidation of HCHO on Ni-Cu alloy electrodes

Open-circuit rest potential data on the Cu-Ni alloy electrodes indicated that the electrocatalytic activity towards the alkaline HCHO oxidation was the highest on the $Cu_{89}Ni_{11}$ alloy, as shown in Fig. 3. This was substantiated by the oxidation current data read arbitrarily at 0.10V RHE on the potential sweep curves but not quite by those on the Tafel lines.

Co-production of H_2 during the HCHO electro-oxidation, measured by a volumetric technique, was absent on the Ni (and Pt) electrode, close to equimolar with the amount of electro-oxidation of HCHO on the Cu electrode, and distributed on a smooth curve connecting these component metals on the Ni-Cu alloy electrodes. The alloy electrodes thus behaved, roughly speaking, as if they are mixtures of the component metals.

References

1) D. D. Eley and P. B. Moore, JCS Faraday I, 76, 1388 (1980).
2) L. Hilaire, et al., Surface Sci., 103, 125 (1981).
3) D. A. J. Rand and R. Woods, J. Electroanal. Chem., 31, 29 (1971).
4) M. Enyo, J. Electroanal. Chem., **186**, 155 (1985).
5) K. Machida and M. Enyo, Chem. Lett., 75 (1985).

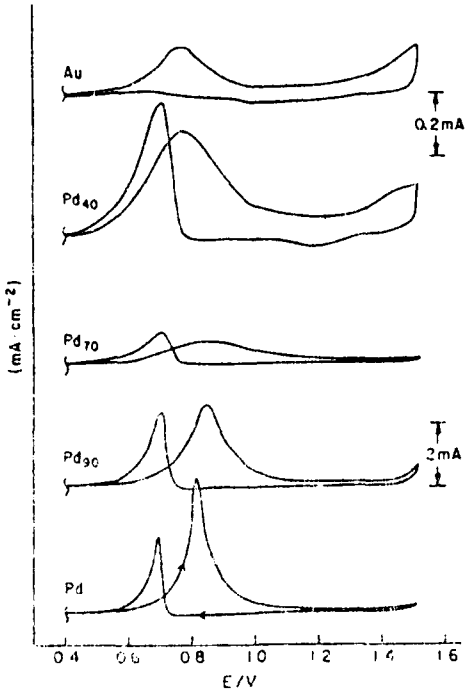

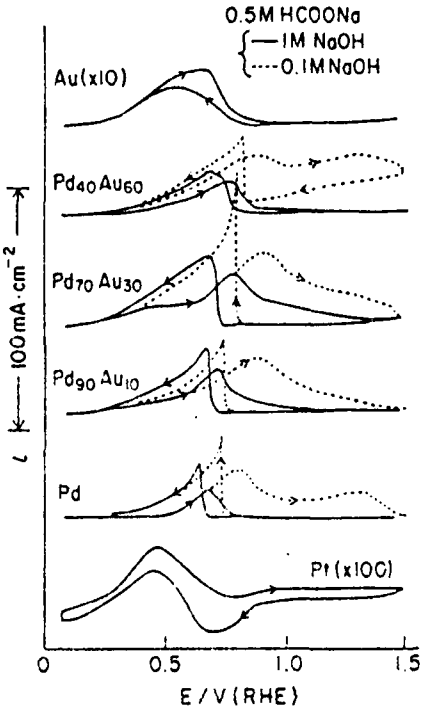

Fig. 1(left). Potential sweep curves during electro-oxidation of 1M CH_3OH, 1M NaOH on Pd-Au alloy electrodes at 30°C. Sweep rate; 50 mV sec^{-1}.

Fig. 2(right). Potential sweep curves during electro-oxidation of 0.5M $HCOO^-$ in 1M or 0.1M NaOH on Pt and Pd-Au alloy electrodes at 30°C. Sweep rate; 50 mV sec^{-1}.

Fig. 3. Rest potentials E_r and anodic oxidation current i at 0.1V RHE in 0.2M HCHO,1M NaOH as a function of composition of the Ni-Cu alloy electrodes. i(solid curve) is read from potential sweep curves and i(dotted curve) from the Tafel lines.

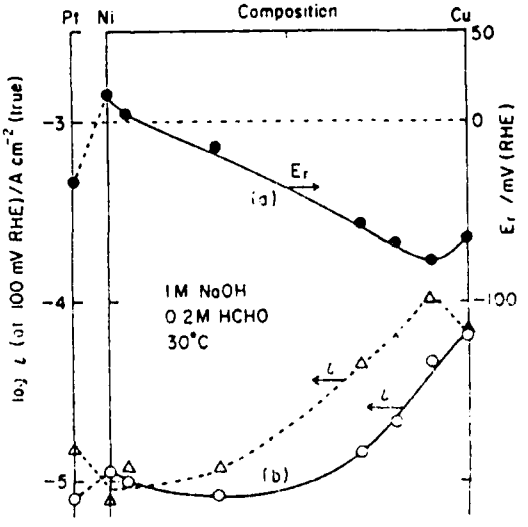

0240C

THE INFLUENCE OF TIN ON THE ELECTROOXIDATION OF CHEMISORPTION PRODUCTS DERIVED FROM METHANOL

JERZY SOBKOWSKI and KRZYSZTOF FRANASZCZUK
Department of Chemistry, Warsaw University, Warszawa (Poland)

The electrocatalysis of the oxidation processes of many organic compounds by the foreign metals adsorbed on platinum electrode was studied by many authors. However, the role of the electrodeposited metal is not clear yet.

In the so called "third body effect" mechanism it is believed that ad-atoms hinder the formation of the strongly bounded intermediates and prevent poisoning of the electrode surface[1-3], so the specific properties of the deposited layer play only a secondary role. In other works[4-6] it is assumed that the deposited metal - which is oxidized easier than platinum - can serve as an oxidant for organic species adsorbed on platinum sites. Hence, the oxidation of organic substances can be observed in the less positive range of potentials than that on the pure platinum electrode.

The electrocatalytic effects of ad-layers are mainly studied with voltammetric method. However, as was found recently[3], the interpretation of current-potential data is ambiguous because the underpotential deposition of ad-atoms alter the double layer capacitance and the charge on the metal surface. Moreover, the equilibrium of ad-atoms on the electrode surface may not be attained quickly enough and the competition with anions adsorption from the bulk of the solution may occur. Hence, the kinetics of underpotential deposition of ad-atoms can be controlled by various processes which influence the shape of potentiodynamic curves. Therefore, the independent method of surface concentration determination of electrodeposited metal is needed to recognize the mechanism of upd process.

In this work, the influence of adsorbed tin and tin (IV) ions on the oxidation of methanol chemisorbed species as well as the methanol from the bulk of the solution were studied on platinum electrode. Voltammetric and radiometric methods were used. The latter method directly monitors the mass flux during the upd of tin-121 as well as electrode coverage by methanol C-14 chemisorbed species.

The measurements have been carried out in 0.5 and 5 M H_2SO_4 solutions at ambient temperature. The polycrystalline platinum was used.

From the values of the number of sites occupied by one adsorbed tin species and from the number of electrons required for oxidation of adsorbate follows that tin is deposited as tin (II) species e.g. hydroxy or sulphate complexes. The kinetics of adsorption as well as desorption are rather slow processes. The desorption of tin from the electrode surface is easier in concentrated (5 M) than in diluted (0.5 M) solution of sulphuric acid. This process is accelerated by cyclic polarisation of the electrode.

The coverage of platinum electrode surface by tin species decreases the coverage by chemisorbed species of methanol. The surface coverage by methanol chemisorbed species on the electrode modified by tin is lower than that in the absence of tin on the platinum surface.

The promotion effect of methanol chemisorbed species oxidation by tin is limited to the narrow range of potentials. Below 0.4 V tin has no effect on the oxidation process and above 0.8 V the inhibition of this process is observed.

In the presence of methanol and tin ions in the solution the decrease of the oxidation peaks of methanol is observed. Only in the potential range of 0.4 - 0.6 V in anodic scan the oxidation current is higher in the presence of tin. The similar effect was obtained when tin was first adsorbed and then removed from the solution by washing procedure. It is an evidence that the enhancement of the oxidation current of me-

thanol on platinum is due to the presence of tin on the electrode surface.

The obtained results are only in moderate agreement with the data of other authors. The reason is that there are many factors which influence the electrocatalytic processes, namely: the state of the electrode surface (smooth or rough with various roughness factor, polycrystalline or monocrystals), the kind of supporting electrolyte (different energies of ad-atoms adsorption on platinum owing to the competition with anions adsorption and complex formation in the bulk of the solution), the concentration of adsorbed substance (selfinhibition) the sequence of addition of the fuel and promotor to the supporting electrolyte (preadsorption of one component influences the adsorption of the second one), the range of polarization potentials etc. Hence, the results could be hardly reproduced. Recently the structural effects on the electrooxidation of methanol was clearly demonstrated[7,8]. Because the polycrystalline electrode after prolonged cyclic polarization exhibits the reproducible voltammograms, it seems to be still suitable object for the study of electrocatalysis and promotion effects of ad-atoms and other species.

1. H.A.Angerstein-Kozlowska,B.McDoughall and B.E.Conway, J.Electrochem.Soc., 120 (1973) 756
2. D.M.Kolb in H.Gerischer and C.W.Tobias (Eds.), Advances Electrochem.Eng., Vol.11,p.125, Wiley Interscience, 1978
3. R.R.Adžić, D.N.Simić, D.M.Dražić and A.R.Despić, J.Electroanal.Chem., 61 (1975) 117
4. M.Watanabe and S.Motoo, J.Electroanal.Chem., 60 (1975) 259, 267, 275
5. S.Motoo, M.Shibata and M.Watanabe, J.Electroanal.Chem., 110 (1980) 105
6. A.R.Despić, R.R.Adžić and A.V.Tripković, Elektrokhimiya, 5 (1977) 660
7. J.Clavilier, C.Lamy and J.M.Leger, J.Electroanal.Chem., 125 (1981) 249
8. R.R.Adžić, A.V.Tripković and W.E.O'Grady, Nature, 296 (1982) 137

02410

THE HYDROGEN EVOLUTION REACTION ON PLATINUM IN THE PRESENCE OF ADSORBED CARBON MONOXIDE

E. P. M. LEIVA, E. SANTOS and T. IWASITA

Institute for Physical Chemistry, University of Bonn,
D-5300 Bonn, Germany

Introduction

The hydrogen evolution reaction (HER) on platinum in the presence of different adsorbates has been the subject of several investigations (1-4).

Early measurements in the presence of submonolayers of CO showed a dramatic inhibition while As adatoms and reduced CO_2 let the HER practically unaffected /1/. In the case of Cu submonolayers /2/ the decrease of the rate of hydrogen evolution was correlated with a diminution of the number of pairs of Pt-sites free from adatoms. Similar experiments carried out with Pb, Cd and Tl adatoms also showed an inhibition of the recombination reaction at low coverage of adatoms. At high values of θ a change in the rate controlling step was reported /3/.

More recent results /4/ show that low coverages of CO (up to $\theta = 0.6$) produce a relatively small decrease of the current density at constant overvoltage. For larger CO coverages a rapid decrease of the reaction rate was observed. However a mechanistic interpretation of these facts was difficult to assert.

In order to control the surface structure of the metal the use of single crystals would be desirable in these investigations. An electrochemical procedure recently developed by Arvia and co-workers /5/, makes possible to produce preferred oriented (PO) polycrystalline Pt electrodes, which exhibit an stabilized electrochemical behaviour close to that of single crystal surfaces.

We have applied this technique to get the (PO 111 Pt) and (PO 100 Pt) surface used in the present work.

Experimental technique and results

The hydrogen evolution reaction on preferred oriented Pt surfaces was studied at low current densities in the presence of adsorbed CO. The working electrode was a rotating Pt cylinder. The potentials were measured against a hydrogen electrode in 1M $HClO_4$.

After setting a monolayer of adsorbed CO, a flux cell technique was employed to change the CO saturated solution by fresh electrolyte. The coverage was reduced to the desired value by means of an anodic sweep and the hydrogen coverage was monitored. The solution was then saturated with hydrogen and a set of stationary galvanostatic measurements was taken. Finally the solution was replaced again by the supporting electrolyte and the hydrogen coverage was verified for a second time. This procedure was repeated for each coverage. The degree of coverage, θ, is reported here as the surface fraction blocked for hydrogen adsorption.

Semilogarithmic current-potential curves are shown in Fig. 1 for the (PO 100 Pt) and (PO 111 Pt) surfaces.

It can be observed that for $\theta \rightarrow 0$ both PO electrodes show the same behaviour. For large CO coverages the HER is strongly inhibited at the (PO 100 Pt) surface. There is a close similarity between our result for (PO 100 Pt) and that for polycrystalline platinum /4/ .

Conclusions

It is difficult at the present stage of the investigation to give a unique explanation to the above experimental findings. Adsorbed CO on PO surfaces shows distinctive oxidative behaviour /6/. It is therefore not surprising to observe also a different effect on the HER.

It could be possible that the the existence of different degrees of order for the adsorbed CO monolayer causes an effect similar to that observed for Cu adatoms /2/ . According to this, ordered arrangements of adatoms are more effective to inhibit the recombination of H atoms. However, as pointed out in Ref. /4/ the decrease of catalytic activity with increasing CO coverage between 0 and 0.5 is smaller than expected if we assume H-H recombination as the rate determining step.

A second possibility could be fomulated by assuming a modification of the free Pt site by the adsorbed CO. It is well known that CO adsorbes at the Pt-solution interface in at least two forms /7/ (linear and multibonded) which posess different electronic properties /8/. The ratio of this adsorbed species should depend on the kind of PO surface , thus creating different conditions for the hydrogen evolution reaction.

References

1. P. Stonehart and G. Kohlmayr, Electrochim. Acta 17 (1972) 369
2. N. Furuya and S. Motoo, J. Electroanal. Chem. 72 (1976) 165
3. R. Adzić, M. Spasojević and A. Despić, Electrochim. Acta 24 (1978) 569
4. M. W. Breiter, J. Electroanal. Chem., 115 (1980) 45
5. R. M. Cerviño, W. E. Triaca and A.J. Arvía, J. Electroanal. Chem. 182 (1985) 51
6. E. P. M. Leiva, E. Santos, R. M. Cerviño, M. C. Giordano and A. J. Arvía, (submited to the J. Electrochem. Soc.)
7. B. Beden, A. Bewick, K. Kunimatsu and C. Lamy, J. Electroanal. Chem. 142 (1982) 345
8. P. R. Norton, J. W. Goodale and E. B. Selkirk, Surf. Sci. 93 (1973) 189

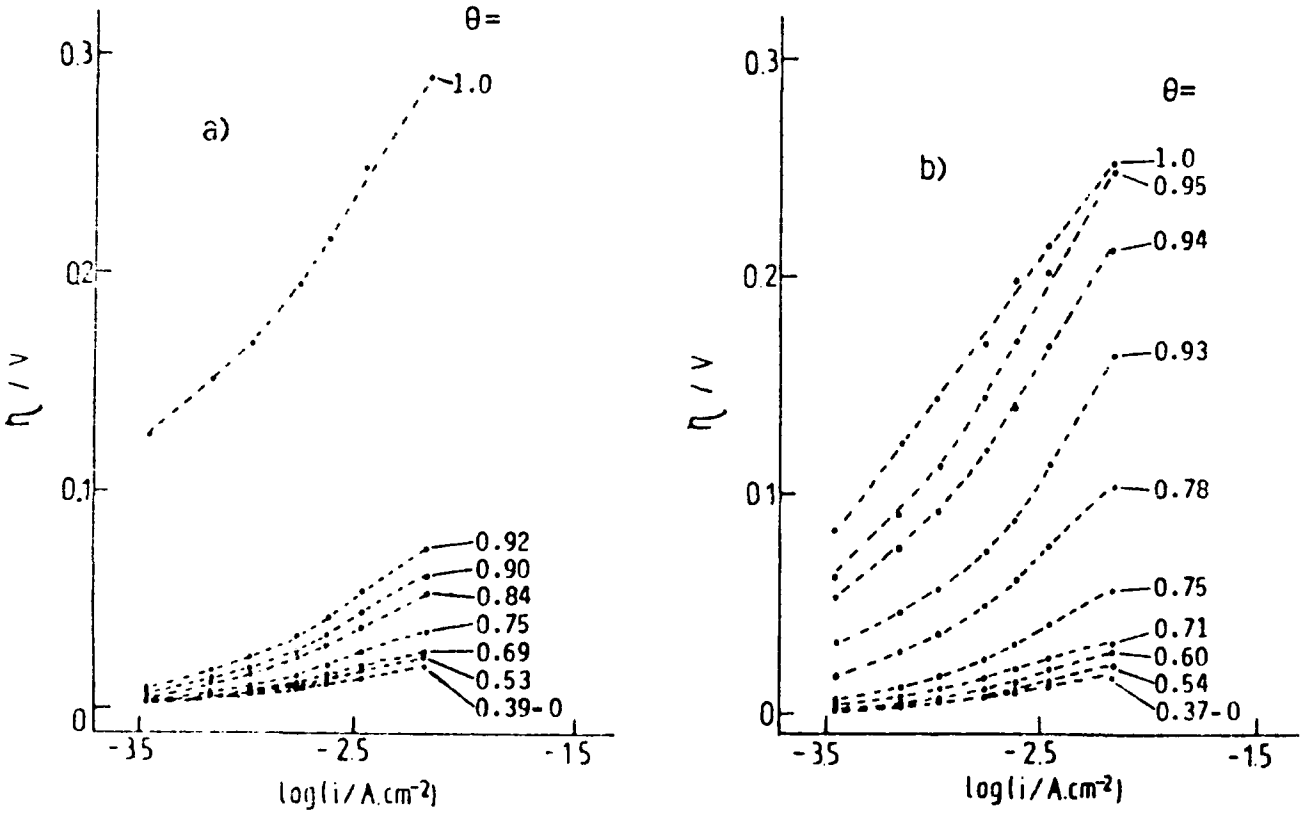

02412

Fig. 1 Stationary η-log i curves obtained at different CO coverages for H_2-evolution on a) (PO 111 Pt) and b) (PO 100 Pt) surfaces

03010

3

ELECTROCHEMICAL CHARACTERISTICS OF RuO_2 CATALYZED SURFACE OF GLASSY CARBON

Radoslav Atanasoski, Gordana Perović
ICTM Institute of Electrochemistry and Center for Multidisciplinary Studies, University of Belgrade, P.O.Box 815, Belgrade, Yugoslavia

Branislav Nikolić, Nikola Blagojević
Faculty of Technology and Metallurgy, University of Belgrade, P.O.Box 494, Belgrade, Yugoslavia

Robert Reeves
Laboratoire d'Electrochimie Interfaciale de C.N.R.S., Meudon, France

Glassy carbon as an electrode material is of interest in electroanalytical research due to the innert behaviour in the electrochemical environment. Glassy carbon shows a good conductivity and relatively poor catalytic activity. Hence, in this work glassy carbon has been used as a support for catalytic coating made on the basis of RuO_2, which is well known as an electrocatalist for gas evolving reactions.

Experimental. Two types of glassy carbon were examined ("Sigradur" - Sigri, Germany: L - low temperature (1000 °C) and H-high temperature (2500 °C) annealed). The cristalinity of the samples was checked by X-ray. As expected much higher diffraction peaks of the high temperature sample were obtained Fig. 1.

Cyclic voltammetry was used for surface characterisation. The base of glassy carbon rods (0.1 cm^2) was brought in contact with the electrolyte by touching their surfaces. The surface tension kept the contact through the experiment.

The base was subsequently activated with RuO_2 via standard thermal route. $RuCl_3$ solution in isopropyl alcohol was applied at the carbon surface. After the evaporation of the solvent the samples were heated at 400 °C in air. The activated samples were examined by cyclic voltammetry also, after each RuO_2 layer. The content of Ru in a layer was estimated to be 2.5×10^{-3} mmol cm^2.

Results and discussion. The cyclic voltammograms (in three different electrolytes) in the potential range in which the gas evolution reactions on RuO_2 are absent were taken prior to the activation of the surface. The charge associated with the cycle (Fig. 2) when a steady state was achieved is presented in table 1. Two obvious tendences of the charge changes can be distinguished. First of all, the charge increases with the pH value of the electrolyte. Secondly, the charge is larger electrode annealed at higher temperature.

In the presence of RuO_2 at the surface a rather unexpected dependance of the charge on the numer of applied layers was found (Fig. 3). Normally, a steady increase of the charge with the quantity of RuO_2 on the substrate is found. However, here a maximum at the second layer was observed, while the steady increase started only after a third layer was applied. The only resonable correlation at this point could be made with the crystal formation and growth of RuO_2 layer. In order to clarify the roles of the substrate and the solvent (from which the layers of RuO_2 are formed) experiments have been undertaken with the following parameters changed:

- solvent concentration
- solvents other than alcohol
- salts yielding similar layer structure to RuO_2
- the roughness of the substrate.

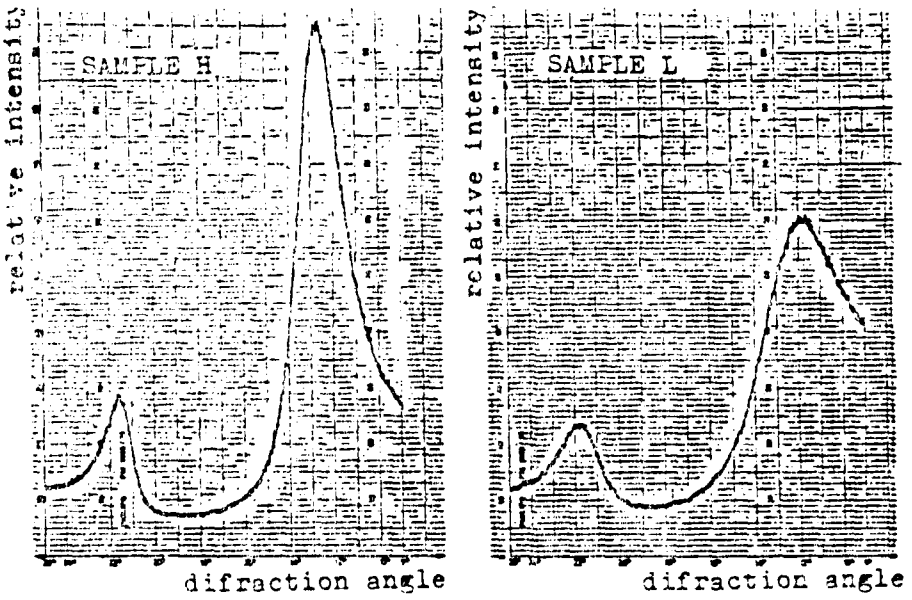

Fig.1. X-ray difraction for law (L-1000°C) and high(H-2500°C) temperature annealed glassy carbon.

	Q ($\mu C cm^{-2}$)		
	1M $HClO_4$	1M $NaClO_4$	1M NaOH
L	8.43	10.85	35.07
H	33.08	57.08	60.48

Table 1. Charge derived from the cyclic voltammograms of polished samples

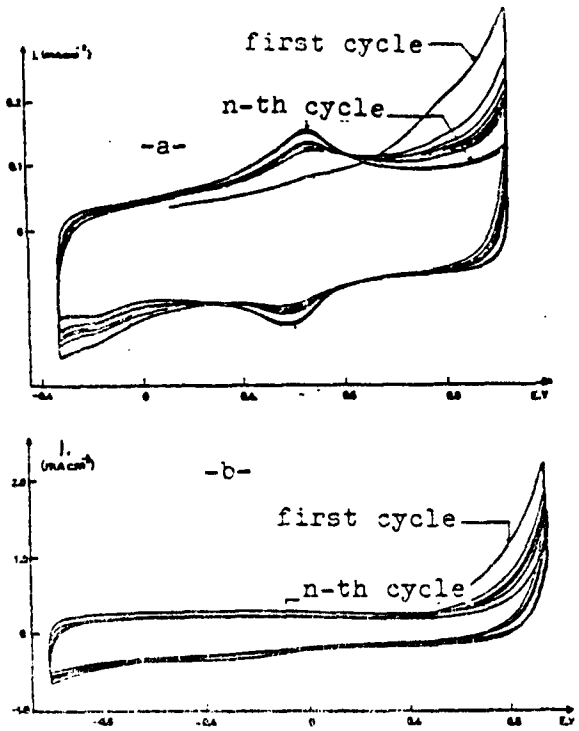

Fig.2. Cyclic voltammograms of polished glassy carbon (sample H)

a) 1M $HClO_3$

b) 1M NaOH

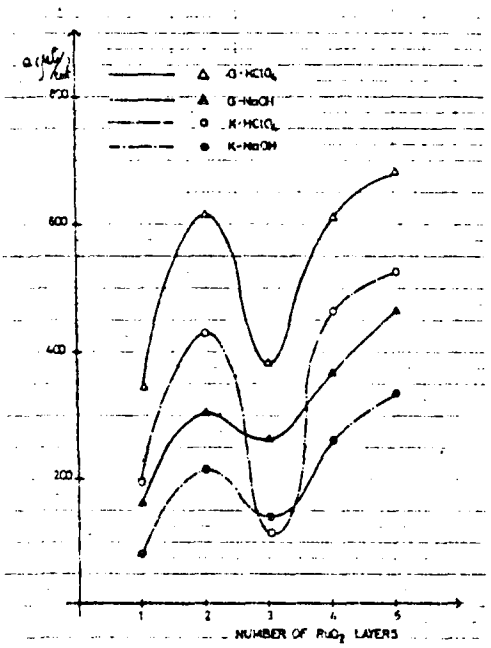

Fig. 3. Charge from the cyclic voltammograms as a function of quantity of RuO_2

03020

THE INFLUENCE OF YTTRIUM, COPPER, ZINC, AND TIN ON A SILVER - SILVER OXIDE ELECTRODE IN KOH SOLUTION

Yoshifumi YAMAMOTO

Department of Chemistry, Faculty of Science and Engineering,
Ritsumeikan University, Tojiin Kitamachi, Kita-ku,
Kyoto F 603 JAPAN

Polarization behaviours of the silver - silver oxide electrode in KOH solution containing a small amount of yttrium (III) chloride, copper (II) chloride, zinc (II) acetate, or tin (IV) chloride were investigated by potentiostatic and galvanostatic polarization methods. It is another purpose to increase the capacity of a silver - silver oxide electrode. The coulombic areas under all peaks on cyclic voltammograms which correspond to the capacity were increased by the addition of the these metal salt. The capacities of positive electrodes formed on silver plates measured by galvanostatic discharge were increased by the addition of these compounds in accordance with the observations. Especially, the addition of yttrium salt, copper salt, or zinc salt was effective in increasing the capacity.

The active materials of the electrode grew into big crystals at the absence of the these metal salts, while the addition of metal salts led to the formation of fine crystals which were observed by SEM. The increase in electrode capacity caused by the addition of these compounds seems to be assured of the formation of such finely crystalline.

It has been concluded that this behaviour of the electrode can be explained by the adsorption and the desorption of colloidal species produsedfrom the added yttrium (III) chloride during charge and discharg, and by the adsorption of ionized species produsedfrom the added copper (II) chloride, zinc (II) acetate, or tin (IV) chloride during charge.

Experimental

The experiments were carried out in a H-type glass cell at 298.15 K. The working electrode was a silver plate of 1cm^2 of geometrical area which was polished with abrasive paper, ref. 1000, and coated with epoxy resin on its back side. The counter electrode was a platinum plate of 2.85 cm^2. The electrode potential were measured against Hg/HgO/4.7M-KOH reference electrode. An aqueous 4.7M-KOH solution was used as a standard solution. $YCl_3 \cdot 6H_2O$, $CuCl_2 \cdot 2H_2O$, $Zn(CH_3COO)_2 \cdot 2H_2O$, or $SnCl_4 \cdot H_2O$ was added into the standard solution to prepare a 1×10^{-3} mol/l(4.7M-KOH) solution.

All voltammograms were obtained at a sweeping rate of 41.7 mV/sec. All potential - time transient curves were obtained under the constant current density of 1 mA/cm^2.

Results and Discussion

The potential - time transient curves under anodic and cathodic polarization on a silver - silver oxide electrode in a 4.7M-KOH standard solution were shown by the solid lines in Fig. 1,2,3, and 4. Next, only electrolyte was converted to the solutions containing the metal salts. The other conditions were kept unchanged, and the curves were shown by the dotted lines in Fig. 1,2,3, and 4. In Fig. 1·2·3·4, all curves were obtained after the steady conditions were achieved. The cyclic voltammograms in a standard solution were shown by the solid lines in Fig. 5, and the curves obtained in the solutions containing metal salts were shown by the dotted lines in Fig.5.

From these results and the observations with SEM, the following mechanism are proposed. It is considered that the yttrium salt added into the standard solution is reacted as follows.

$$YCl_3 + 3\ KOH \longrightarrow Y(OH)_3 + 3\ KCl \qquad (1)$$

Further, yttrium (III) hydroxide is influenced by alkaline ion, and leads to soluble colloidal species. It is presumed that crystal growth of Ag in the active point on Ag plate is controlled by adsorption of this colloidal species and is probably forced to deposit in other points during cathodic process. As a result of this presumption the fine crystals of the active materials were observed by SEM. Besides, the conditions of the distribution of crystal depositions on Ag plate were extremely satisfactory as well as ease of the addition of undermentioned copper salt.

In the case of copper salt,

$$CuCl_2 + 2\ KOH \longrightarrow Cu(OH)_2 + 2\ KCl \qquad (2)$$

$$Cu(OH)_2 + 2\ KOH \longrightarrow K_2CuO_2 + 2\ H_2O \qquad (3)$$

$$K_2CuO_2 \rightleftharpoons 2\ K^+ + CuO_2^{2-} \qquad (4)$$

or,

$$Cu(OH)_2 \rightleftharpoons Cu^{2+} + 2\ OH^- \qquad (5)$$

In the case of zinc salt,

$$Zn(CH_3COO)_2 + 2\ KOH \longrightarrow Zn(OH)_2 + 2\ CH_3COOK \qquad (6)$$

$$Zn(OH)_2 + 2\ KOH \longrightarrow K_2ZnO_2 + 2\ H_2O \qquad (7)$$

$$K_2ZnO_2 \rightleftharpoons 2\ K^+ + ZnO_2^{2-} \qquad (8)$$

In the case of tin salt,

$$SnCl_4 + 4\ KOH \longrightarrow Sn(OH)_4 + 4\ KCl \qquad (9)$$

$$Sn(OH)_4 + 2\ KOH \longrightarrow K_2SnO_3 + 3\ H_2O \qquad (10)$$

$$K_2SnO_3 \rightleftharpoons 2\ K^+ + SnO_3^{2-} \qquad (11)$$

It is presumed that these ionized CuO_2^{2-}, ZnO_2^{2-}, or SnO_3^{2-} are adsorbed on Ag formed on Ag plate during an anodic polarization process, and copper may be faintly codeposit with Ag during cathodic process.

Therefore, it has been concluded that the active materials on the silver - silver oxide electrodes were formed as the fine crystals by the actions of added metal salts.

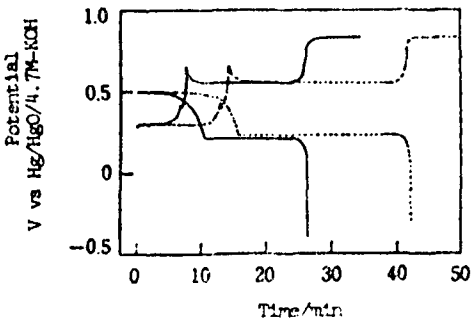

Fig.1 Potential - time transient curves for a silver - silver oxide electrode
—— : 4.7M-KOH solution
- - - : $YCl_3 \cdot 6H_2O$ 1X10^{-3}mol/l(4.7M-KOH) solution

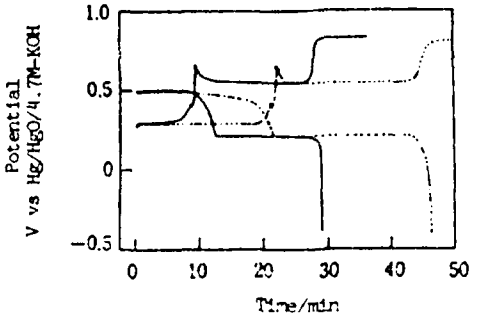

Fig.2 Potential - time transient curves for a silver - silver oxide electrode
—— : 4.7M-KOH solution
- - - : $CuCl_2 \cdot 2H_2O$ 1X10^{-3}mol/l(4.7M-KOH) solution

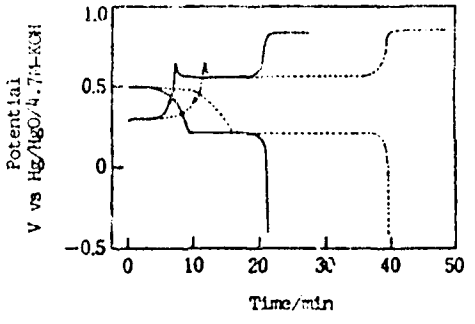

Fig.3 Potential - time transient curves for a silver - silver oxide electrode
—— : 4.7M-KOH solution
- - - : $Zn(CH_3COO)_2 \cdot 2H_2O$ 1X10^{-3}mol/l(4.7M-KOH) solution

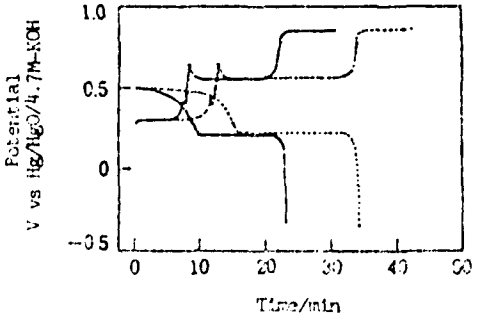

Fig.4 Potential - time transient curves for a silver - silver oxide electrode
—— : 4.7M-KOH solution
- - - : $SnCl_4 \cdot H_2O$ 1X10^{-3}mol/l(4.7M-KOH) solution

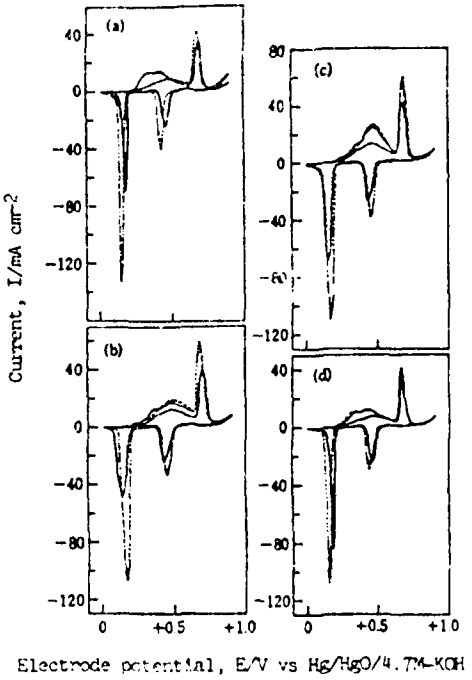

Fig.5 Cyclic voltammograms for the silver - silver oxide electrodes
—— : Steady curves in 4.7M-KOH solution
- - - : The first cycle in 4.7M-KOH solution containing each metallic salt
- - - - : Steady curves in 4.7M-KOH solution containing each metallic salt
(a) : Copper, (b) : Zinc, (c) : Yttrium, (d) : Tin

03030

OXYGEN EVOLUTION REACTION ON PEROVSKITE COATED NICKEL ELECTRODES IN ALKALINE SOLUTION

W. SCHNURNBERGER
DFVLR Institut für Technische Thermodynamik
D-7000 Stuttgart-80 (Germany)

The electrocatalytic properties of various Perovskites $Me_xCo_yO_3$ (Me = Lanthanide, Transition Metal) are very promising with respect to oxygen evolution in alkaline solution. For technical application, metal electrodes have to be coated with Perovskites. By means of Low-Pressure-Plasma-Spraying (LPPS), Perovskite powders have been applied on nickel electrodes.

In Fig.1 the Scanning Electrode Micrograph of a plasma-sprayed $LaCoO_3$ surface is given. The oxygen evolution reaction has been studied in 25wt% KOH solution at various potential sweep rates and temperatures up to about 80°C.

Cyclic voltammograms of the $LaCoO_3$/Ni-electrode are given in Fig.2, indicating a surface redox-reaction prior to the oxygen evolution. From the dependence of the peak current density on potential sweep rate for both anodic and cathodic reaction, Fig.3, a reversible redox-reaction (Co-II/Co-III) can be suggested at 22°C and 78°C.

With increasing potential the oxygen evolution reaction is observed. In Fig.4 the Tafel-plots for a plasma-sprayed $(La_xSr_{1-x})(Co_yNi_{1-y})O_3$/Ni-electrode are given. At low current densities, Tafel slopes about 60 mV/decade have been observed, independent from temperature in the range 22°C to 78°C.

These results indicate the suitability of Low-Pressure-Plasma-Spraying for application of oxide-catalysts on electrodes for alkaline water electrolysis.

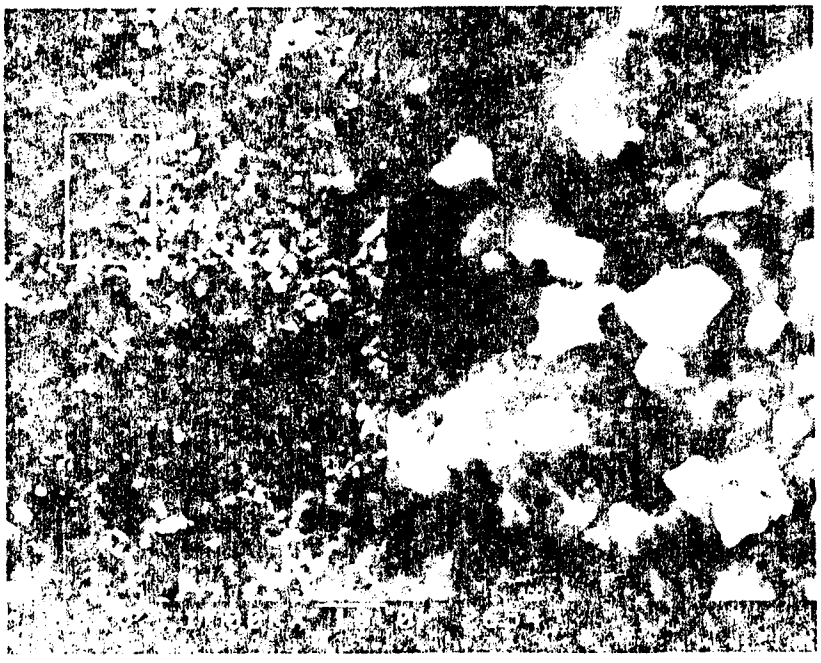

Fig. 1: Plasma-sprayed $LaCoO_3$ Ni-electrode surface. Catalyst load: 8 mg/cm^2. SE-micrograph.

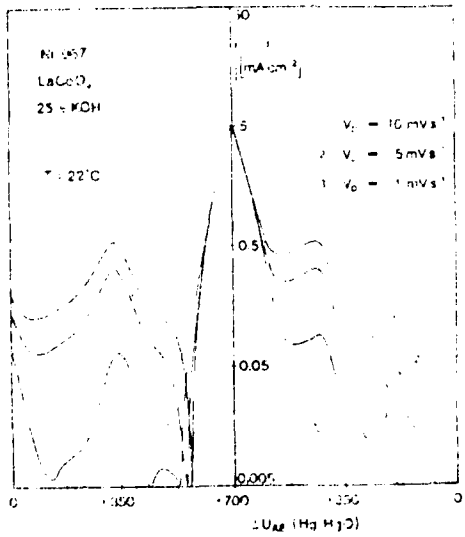

Fig. 2: $LaCoO_3$/Ni-electrode: current density at 0 to 700 mV (Hg/HgO) at different potential sweep rates.

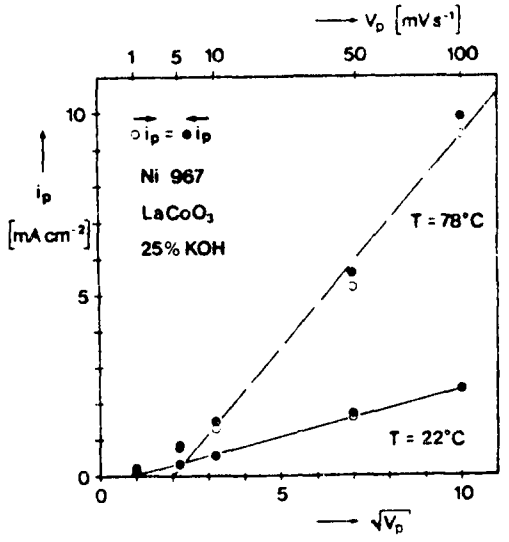

Fig. 3: $LaCoO_3$/Ni-electrode: peak current density of the surface redoxreaction as function of the potential sweep rate.

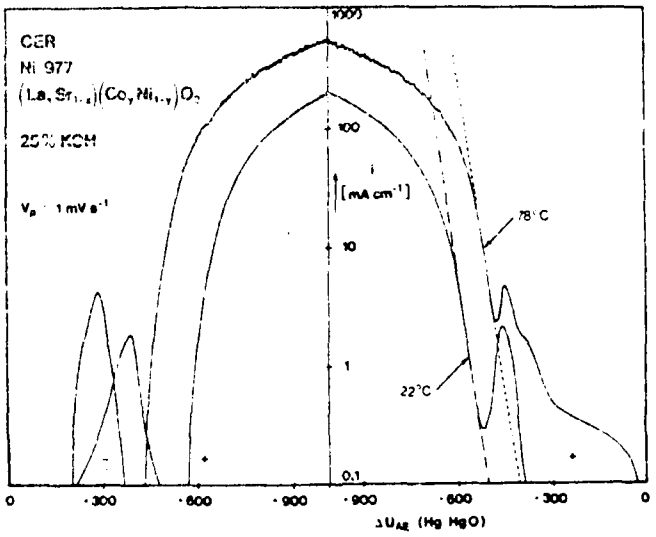

Fig. 4: $(La_xSr_{1-x})(Co_yNi_{1-y})O_3$/Ni-electrode: Tafel plot of the oxygen evolution reaction at 22°C and 78°C. (potential not IR-corrected).

03040

THE INFLUENCE OF CONTINUOUS IMPACTING OF PASSIVATED IRON ELECTRODES ON THEIR SEMICONDUCTOR BEHAVIOR

A. PINKOWSKI and K.P. THIESSEN, Academy of Sciences of the GDR, Central Institute of Physical Chemistry, Berlin (GDR)
K. WIESENER, Technical University of Dresden, Department of Chemistry, Dresden (GDR)

1. Introduction: The aim of the present work is the determination of changes in the electronic properties of continually impacted passivated iron electrodes by means of capacitance (C) measurements in dependence on the potential (V) for a constant thickness of the passive layer. The simulation of an erosion-like mechanical treatment (MT) was realized by applying a rotating disk electrode immersing in a bed of glass beads of diameter 0.6-0.8 mm suspended in the electrolyte. In the experiments with MT both the passivation process as well as the C measurement were carried out under MT.

2. Experimental: Iron rods (diameter 6 mm) of purity 99.97% and a deaerated 1 N $NaNO_3$ solution, borate buffered to pH 8.4 were used. The electrodes were prepared by polishing and electropolishing. The passivation potential was 0.84 V (all potentials vs. she) yielding a layer thickness of 3 nm for both without and with MT. Thus, the steady state layer thickness is determined by the applied potential and not by MT. The C values were corrected by a roughness factor r = 2.

3. Results: Typical C(V) lines show from cathodic toward anodic biasing three regions[1,2]: I - decreasing of C, II - nearly constancy of C, and III - increasing of C. The most striking feature from the experiments is that the C(V) lines under MT are shifted to higher C values in all three regions. Further features are the increased under MT slopes of the Mott-Schottky plots in regions I and III. Finally, independent of MT closer inspection of region II showed instead of constancy

of C two small however distinguishable C minima. This interesting detail is discussed elsewhere[1,3].

4. Discussion: The discussion will be based on the assumptions made by[2] considering the passive layer as n-type semiconductor with Fe^{2+} selfinterstitials as donor centers (cf. however the PIN junction approach by[3,4]). Following the evaluation procedure by[2] the semiconductor data of table 1 are obtained. As can be seen the product DN is enhanced under MT by a factor 2.6. Since D of the iron oxids strongly increases with increasing Fe^{2+} content[2], the enhancement of DN can be due to a change in both N and D. D can be obtained from the simple condenser relation applied to region II[2], thus we can calculate N (cf. table 1). Obviously the enhancement of DN is caused by an increase of D as well as of N by about the same factor 1.6. Since d_{SC} was not significantly altered by MT it follows that the increased under MT space charge has to be stored in a space charge layer of the same volume. This can be understood assuming new states in the gap created by MT allowing for more charge carriers to be stored.

Having in mind that our kind of MT creates fresh surfaces and dislocations[1] and that a mechanical damage of semiconductor surface layers produces centers for radiationless electron-hole recombination[5] and further that on mechanically polished silicon samples selfinterstitials occured[6], our increased under MT donor concentration and dielectric constant are not surprisingly.

The flatband potential is shifted under MT only slightly, nevertheless, the shift direction is in accord with findings on mechanically strained passivated iron[7] corresponding to a change from n- to p-type behavior.

In region III all experimental C values lie below the theoretical curves for nondegenerate semiconductor. It follows that no surface states can supposed to be existent even under MT, since surface states should cause the experimental points lying above the calculated lines[1].

Considering the degeneracy of the valence band in region III, well fitting between experimental and calculated lines

is achieved for the values given in table 1. Thus, the effective hole mass is increased under MT by a factor 4, the gap width is lowered by 0.1 eV, and the degeneracy starts at a lowered by 0.1 V anodic potential. These latter findings qualitatively agree with previous results on alteration of semiconductor properties under energy input[8] (for detailed discussion cf.[1]).

Table 1: Semiconductor data of passivated iron under MT

	without MT	with MT	notation
DN/cm^{-3}	$4.3 \cdot 10^{20}$	$1.1 \cdot 10^{21}$	D = dielectric constant
D	10.5	16.5	N = donor concentration
N/cm^{-3}	$4.1 \cdot 10^{19}$	$6.8 \cdot 10^{19}$	d_{SC} = Debye length
d_{SC}/nm	0.9	0.8	V_{FB} = flatband potential
V_{FB}/V	-0.06	-0.04	V_{deg} = degeneracy start
V_{deg}/V	1.1	1.0	potential
E_g/eV	1.5	1.4	E_g = gap width
m_{eff}	0.5	2.1	m_{eff} = effective hole mass

References

1 Pinkowski, A. and K.P. Thiessen: Z. Phys. Chem. (Leipzig) in press

2 Stimming, U. and J.W. Schultze: Ber. Bunsenges. physikal. Chem. 80(1976) 1297

3 Pinkowski, A.: Z. Phys. Chem. (Leipzig) 266(1985)2, 340

4 Pinkowski, A.: ibid., in press

5 Yamase, T. and H. Gerischer: Ber. Bunsenges. physikal. Chem. 87(1983) 349

6 Reichel, J.: phys. stat. sol. (a) 75(1983) 459

7 Oshe, E.K., V. Yu. Vasilev, V.B. Yakovlev, I.L. Rosenfeld and N.I. Isaev: Zasc. metallov

8 Gatos, H.C. (ed.): The Surface Chemistry of Metals and Semiconductors, John Wiley, New York, 1960

03050

A PIN JUNCTION MODEL OF THE PASSIVE FILM ON IRON

A. PINKOWSKI, Academy of Sciences of the GDR, Central Institute of Physical Chemistry, Berlin (GDR)
K. WIESENER, Technical University of Dresden, Department of Chemistry, Dresden (GDR)

1. Introduction: The capacitance of passivated iron is determined by the outer ferrite layer of the passive film. Here only this layer will be considered. Generally, the capacitance of passivated iron in neutral electrolytes from cathodic toward anodic biasing first exponentially decreases, then remains nearly potential independent, and finally rises. This course could be described quantitatively about donor exhaustion, condenser behavior, and inversion layer contribution[1]. This model however, basing on the assumption of ferrite being an n-type semiconductor, does not account for the spatial nonstoichiometry within the passive film. Considering the nonstoichiometry as doping a heavy doped three layered PIN junction results consisting of a middle stoichiometric i-type layer sandwiched by an adjacent to the underlying metal n-type layer, and an outer p-type layer, facing the electrolyte. In the following we treat first the capacitance potential dependence of a graded PIN junction and consider then in addition the possibility of degeneracy of the semiconducting passive film. Such PIN junction structures were already considered for the passive films on Al and Ta, however not for describing the capacitance potential dependence.

2. The Model[2]: In a first step the capacitance is assumed to be composed by series connection of the capacitances of the p-, i-, and n-type regions resp. acc. to (1)

$$C_{abr}^{-1} = C_p^{-1} + C_i^{-1} + C_n^{-1} \qquad (1)$$

with C_{abr} = capacitance of the abrupt PIN junction, and $C_{p,i,n}$ = capacitances of the p-, i-, and n-type regions.

Typical of naturally (anodic or thermal) grown oxide films are rather graded junctions, differing from abrupt junctions by diffusion regions between the p- and i-type, and the i- and n-type parts of the junction. Those diffusion regions are characterized by diffusion capacitances. Therefore, in a second step two diffusion capacitances of the PI and IN diffusion regions are taken into account acc. to (2)

$$C_{grad}^{-1} = C_{abr}^{-1} + C_{d,PI}^{-1} + C_{d,IN}^{-1} \qquad (2)$$

with C_{grad} = capacitance of the graded PIN junction, and $C_{d,PI}$ and $C_{d,IN}$ = diffusion capacitances.

For the calculation of the single capacitances C_p, C_i, and C_n in (1) the well-known theoretical capacitance potential relations[2] can be applied. For C_d Eq (3) holds

$$C_d = \left(\frac{\varepsilon D^2 D_o^2 K}{12(V_d - V)} \right)^{1/3} \qquad (3)$$

with D = dielectric constant of the semiconductor, D_o = permittivity of free space, K = impurity gradient, V_d = diffusion voltage, and V = electrode potential. Thus, suitable choosen parameters give straight lines in a $C_d^{-3}(V)$ plot[2].

Now the probability of the onset of degeneracy for the passive film on iron shall be considered. Degeneracy can be attained by heavy doping, high injection rates, carrier generation about energy input, and by voltage induced band bending. The obtained from Mott-Schottky plots[1] or from fitting between experimental and calculated C(V) lines[2] carrier densities for passivated iron (about 10^{20} cm^{-3}) lie above the theoretical degeneracy concentrations (about $2.5 \cdot 10^{19}$ cm^{-3}). Nevertheless in practice the limit for the onset of degeneracy is about one order of magnitude higher. For reasons outlined elsewhere in detail[3] we will consider here only the possibility of degeneracy by voltage induced band bending. Although on principle degeneracy can start in accumulation and in inversion,

with passive films on iron only degeneracy in accumulation seems to be likely[3]. Thus, the C(V) lines of the p-, i-, and n-type layers shall be composed of a degenerate in accumulation branch and a nondegenerate inversion branch. The essential feature of the present degeneracy approach is the assumption that any deviation (lowering) from exponential C(V) dependence is caused by the onset of degeneracy necessitating the application of the well-known C(V) relation for degenerate semiconductor[1,3].

3. Results: The approach of a graded PIN junction[2] as well as the degeneracy approach[3] allow quantitative fitting between experimental and calculated C(V) lines yielding the semiconductor data of table 1. Treating the PIN junction as diode the main DC results obtained in the literature under injection conditions can easy be explained[2]. As proof of the degeneracy approach the transfer and partition coefficients can be used[3].

Table 1: Semiconductor data of the passive film on iron

	ref. 2	ref. 3	notation
$D_p \cdot N_A \cdot 10^{21}/cm^{-3}$	1.0	-	$D_{p,i,n}$ = dielectric constants of the p-, i, and n-type regions resp.; N_A, n_i, N_D = acceptor, intrinsic and donor density; $m_{eff(n,p)}$ = effective electron and hole masses
$D_i \cdot n_i \cdot 10^{21}/cm^{-3}$	0.14	-	
$D_n \cdot N_D \cdot 10^{21}/cm^{-3}$	1.5	-	
K / cm^{-4}	about 10^{28}	-	
D	-	10	
$m_{eff(n,p)}$	-	0.5	

References

[1] Stimming, U. and J.W. Schultze: Ber. Bunsenges. physikal. Chem. 80(1976) 1297

[2] Pinkowski, A.: Z. Phys. Chem. (Leipzig) 266(1985)2, 340

[3] Pinkowski, A.: ibid., in press

4

04010

COPPER REMOVAL IN THE FALLING-FILM CELL

J. LEGRAND[+], J.M. MARRACINO[++] and F. COEURET
CNRS/ENSCR - Av. Général Leclerc 35000 RENNES-BEAULIEU (France)

One interesting field of application of the Falling-Film cell[1,2] is the electrolytic recovery of metals from dilute solutions. The inclined plane plate is the cathode (Figure 1) and the electrolyte is flowing as a film (three regimes are possible) through the small interelectrode distance. The metal deposited on the plate may be recovered mechanically. The cell could be particularly interesting when precious metals have to be recovered and also when the electrical conductivity of the solutions is small.

Copper has been removed from artificial solutions containing copper ; $CuSO_4$ is dissolved in pure water, without any addition of supporting electrolyte. The copper concentration is varied between 0.2 and 1 g/l. Thus the solutions may simulate rinsing baths as those existing in the printed circuits industry. They are solutions having small electrical conductivities.

The experiments are made at the room temperature in a cell 100 cm_3 long, 24 cm wide and with a tilted angle of 10°. The flow rate is of 83 cm^3/s. The regime is the capillarity flow regime.

The copper concentration in the system (batch operation) varies with the time t according to Figure 2 in which C_0 is the initial concentration. The time t_s is the overall residence time of each fluid element in the electrical field. At a current density of $4,3.10^{-3}$ A/cm^2 the concentration is reduced from 1 g Cu/l to 0,0001 gCu/l after a residence time t_s = 5 minutes. In the same experiments, the average faradaic yield remains higher than 40 %.

More results and details will be given in a further paper[3], but the conclusions of the work can be summarized as follows :

- industrial low conducting solutions containing copper at concentrations of about some grams per liter may be treated in the Falling-Film-Cell and the depletion of copper is very satisfactory.

- the final copper concentration is smaller than the maximum allowable value in effluents.

- the copper is deposited as a thin sheet which is separated from the catnode after the experiment.

[+] I.U.T. de Génie Chimique - 44606 SAINT-NAZAIRE (France)

[++] Universidad Nacional del Litoral, Facultad de Ingenieria Quimica - 3000 SANTA FE (Argentina).

- copper has been chosen as a useful and cheep example but many other industrial cases of metal recovery could be solved using the Falling-Film Cell (gold, silver, mercury, etc...), especially in batch operations.

1 - F. COEURET and J. LEGRAND. Frech Patent n° 81 19115.

2 - F. COEURET and J. LEGRAND, J. Appl. Electrochem., 15, 181 (1985).

3 - J. LEGRAND, J.M. MARRACINO and F. COEURET, submitted for publication.

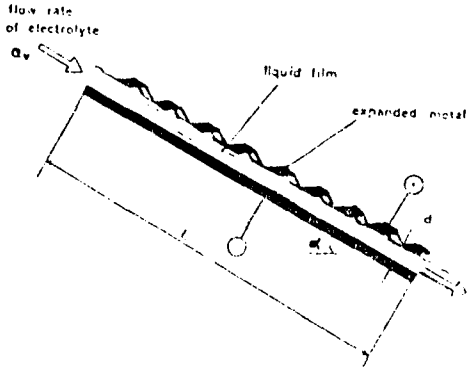

Figure 1

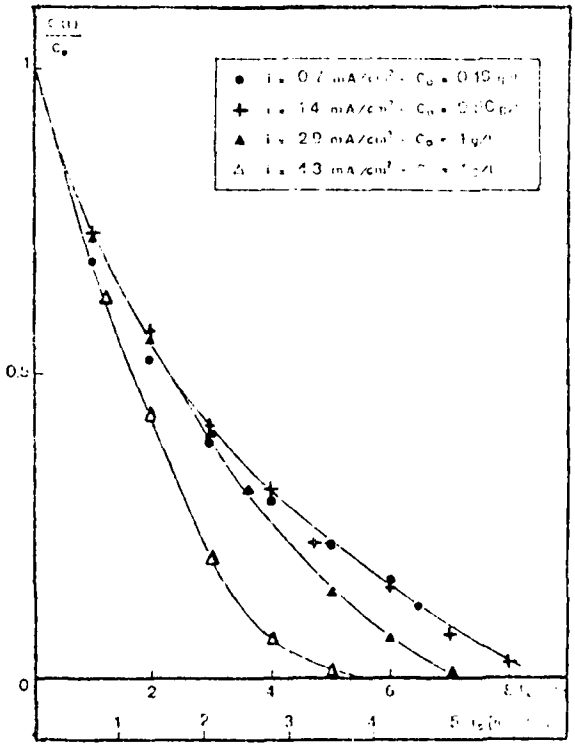

Figure 2

04020

EFFICIENCY OF GAS BUBBLE EVOLUTION AT A GAS-EVOLVING ELECTRODE

L.J.J. Janssen, E. Barendrecht and S.J.D. van Stralen
Laboratory for Electrochemistry, Department of Chemistry
Eindhoven University of Technology
P.O. Box 513, 5600 MB Eindhoven, The Netherlands

Bubbles are formed at a gas-evolving electrode which has been studied extensively over the last twenty years. The gaseous product formed by electrolysis is only partly taken up by bubbles evolved at the electrode on which the gaseous product is formed [1,2]. Some experimental results on efficiency of gas evolution have been published [1,2]. Additional results are given.

The experimental details have been described in [1]. Results for a hydrogen and an oxygen evolving nickel electrode (diameter 0.5 mm and height 3 mm) in 1 M KOH at 298 K and a solution flow rate of 0.12 m/s are shown in Fig. 1. This figure shows also results for a chlorine evolving RuO_2/Pt electrode (diameter 0.5 mm and height 2 mm) in 4 M NaCl + 0.1 M HCl solution at 298 K and a solution flow rate of 0.05 m/s and saturated with chlorine gas.

It has been found that for hydrogen-, oxygen- and chlorine-evolving electrodes the efficiency of gas bubble evolution is practically independent on temperature in the temperature range from 310 to 355 K, and decreases linearly with increasing rate of solution flow in the solution flow rate smaller than 2 m/s.

To obtain the supersaturation concentration of gas at the electrode surface, experiments have been carried out to determine the mass transfer coefficient for ferrocyanide ions at a oxygen-evolving electrode and the one for ferricyanide ions at a hydrogen-evolving electrode.

Taking into account the mass transfer coefficient k_i is proportional to $D_i^{2/3}$ where D_i is the diffusion coefficient of species i, k for dissolved oxygen can be calculated from k for ferrocyanide ions and k for dissolved hydrogen can be calculated from k for ferricyanide ions. The quantity of gas which is not taken up by the bubbles at the electrode surface is transported to the bulk of solution. The rate of this transport is $(1 - f_g)i_g/nF$ where nF is the charge used for the production of 1 mol gas.

Assuming $(1 - f_g)i_g/nF = k_g(c_g^\sigma - c_g^s)$ where k_g is the mass transfer coefficient for the dissolved gas, c_g^σ is the concentration of dissolved

gas at the electrode surface and c_g^s is the saturation concentration of dissolved gas in the bulk of solution at atmospheric pressure.
Since the behaviour of chlorine bubbles is similar to that of oxygen bubbles in alkaline solution, it is assumed that for both gas-evolving electrodes the mass transfer coefficient for a species i is equal at the same volumetric rate of gas bubble evolution.
The supersaturation factor S_g given by $(c_g^\sigma - c_g^s)/c_g^s$ is plotted in Fig. 2 as a function of current density for a hydrogen-, an oxygen- and a chlorine-evolving electrode. The electrolytic conditions are the same as for Fig. 1. Fig. 2 shows that log S increases linearly with log i_g for the various gas-evolving electrodes.

Literature

1. L.J.J. Janssen and E. Barendrecht, Electrochim. Acta 29, 1207, 1984.
2. L.J.J. Janssen and E. Barendrecht, Electrochim. Acta, to be published.

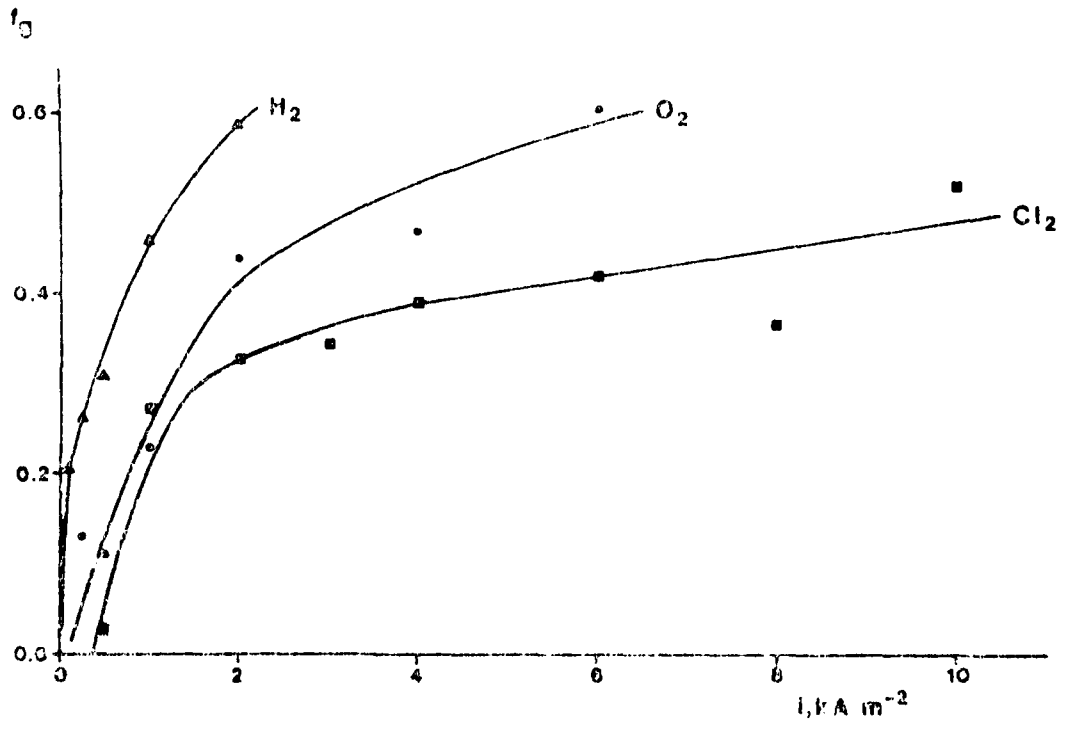

Fig. 2 Efficiency of gas bubble evolution as a function of current density for a hydrogen-, oxygen- and a chlorine-evolving electrode.

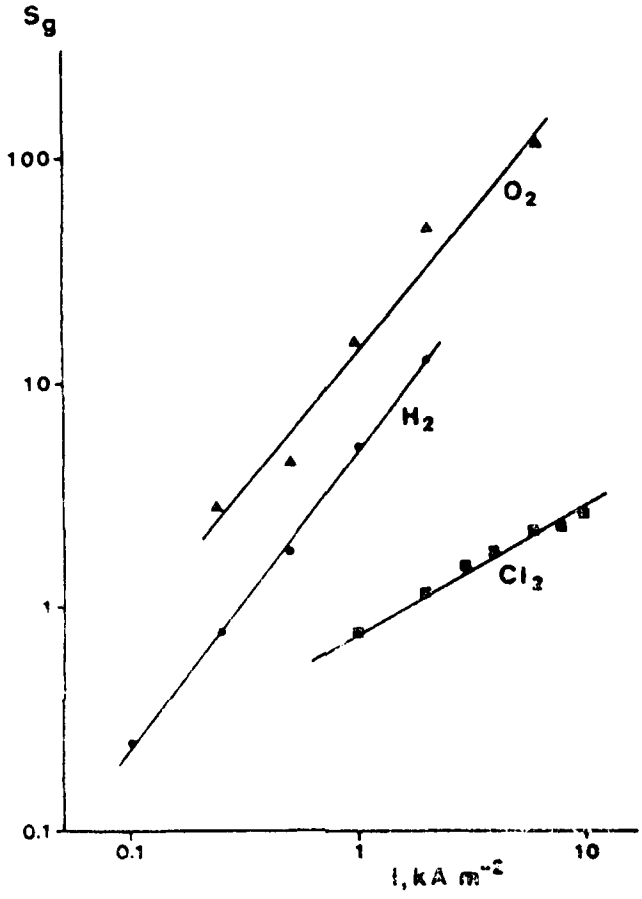

Fig. 2 Supersaturation factor as a function of current density for a hydrogen-, oxygen- and a chlorine-evolving electrode.

AD-A162 434 EXTENDED ABSTRACTS INTERNATIONAL SOCIETY OF 4/12
ELECTROCHEMISTRY (36TH) HELD AT SALAMANCA SPAIN ON
23-28 SEPTEMBER 1985(U) INTERNATIONAL SOCIETY OF
UNCLASSIFIED ELECTROCHEMISTRY 28 SEP 85 F/G 7/4 NL

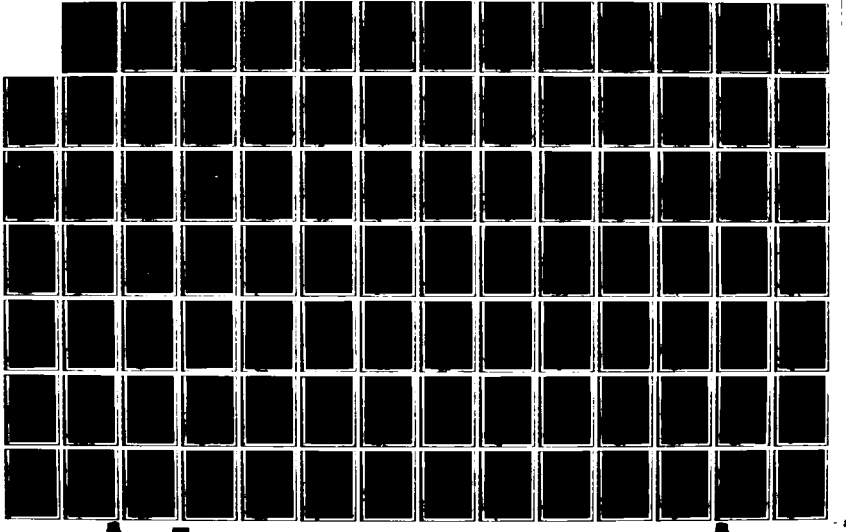

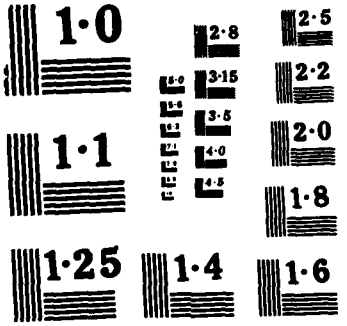

NATIONAL BUREAU OF STANDARDS
MICROCOPY RESOLUTION TEST CHART

MEASUREMENTS ON MASS TRANSFER AT FIBRE ELECTRODES

D. SCHMAL, J. VAN ERKEL, P.J. VAN DUIN
TNO Division of Technology for Society, Department of Chemistry,
PO Box 217, 2600 AE Delft, The Netherlands

INTRODUCTION

The electrochemical treatment of waste waters containing small amounts of toxic compounds (e.g. heavy metals, organohalogens) requires the use of eletrodes with a high surface-to-volume ratio. For this reason we have chosen carbon/graphite fibres as the electrode material.
For scaling-up purposes we have studied the mass transfer of various graphite fibre configurations, using the mass-transfer controlled reduction of potassium hexacyanoferrate (III) to -(II) in 1 M KOH.
For purposes of comparison, we also conducted measurements on single-fibre electrodes.

EXPERIMENTAL

For the single fibre experiments, fibres (of about 10 μm diameter) were fixed in a drawn-out glass capillary with epoxy resin. Electrical contact with the fibre was made via a mercury drop.
The multi-fibre cell is shown in Fig. 1. The various fibre configurations (bundles, cloth, felt) were clamped in the cell with a strip of platinum connected to the power source. Maximum electrode dimensions were 2×10×0.5 cm.
For the separator Nafion 425 was used.
All experiments were conducted in a single pass mode.
Conversions were calculated from the concentration of potassium hexacyanoferrate(II), as determined by potentiometric titration with cerium(IV) sulphate.

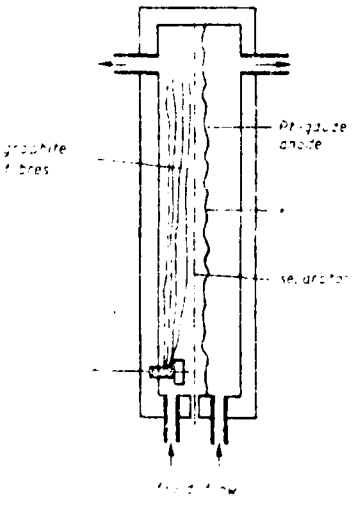

Fig. 1 Multi-fibre cell.

RESULTS AND DISCUSSION

Figure 2 shows the polarization curves obtained in the single-fibre experiments. They exhibit a mass-transfer controlled potential region from about 0 V to -1.6 V vs. SCE. Fluctations in the current at higher velocities are due to transition from laminar to turbulent flow in the cell (tube Reynolds number 1000 to 2000). The Sherwood-Reynolds relation calculated from the experiments at velocities up to 0.02 m/s reads[1]:

$$Sh = 7.0\ Re^{0.42} \qquad (0.04 < Re < 0.2) \qquad (1)$$

where Sh = kd/D (k mass transfer coefficient, d fibre diameter, D diffusion coefficient) and Re = vd/ν (v velocity, ν kinematic viscosity). This relation agrees with that calculated from heat transfer on wires[2] (Chilton-Colburn analogy for heat and mass transfer), and also with a Sh-Re relation calculated from measurements by Bek and Zamyatin[3] on a single fibre in a non-conducting felt.

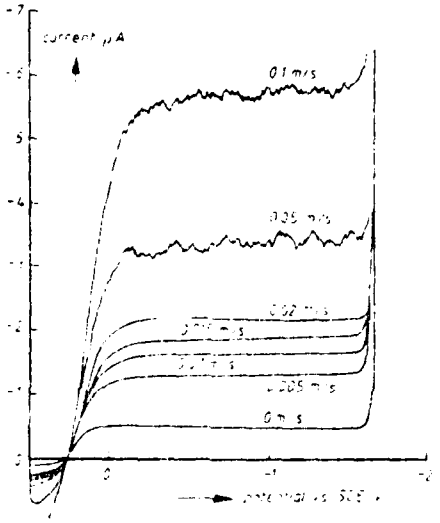

Fig. 2 Polarization curves of a single fibre electrode at different flow velocities (10^{-3} M $K_3Fe(CN)_6$ in 1 M KOH, L = 0.5 cm).

Some polarization curves of a bundle of 200,000 fibres use in flow-by mode are given in Fig. 3. Although at high flow rates the current is not truly constant, the figure reveals that most of the electrode is operating under limiting current conditions. By comparing the results for the various fibre configurations with those calculated from the relation for a single fibre, one arrives at the utilization factor η. In our case η is defined as the ratio of kS found experimentally for the configuration investigated to kS calculated from eq. 1, it being assumed that all fibres take part in the reaction (S is the surface-to-volume ratio of the electrode). Values of η are listed in Table 1, which shows that, (as might be expected) the total surface ara of a felt is available for the electrochemical reaction, whereas in bundles and cloth (in the flow-by mode) only a relatively small part of the surface area is utilized. This loss of efficiency is due to channelling effects and/or to masking of part of the electrode sureface.

Methodes of improving the efficiency, particulary that of bundle electrodes in a flow-by mode, are being further investigated, because these can be expected to be suitable for treating particle-laden waste streams without becoming clogged

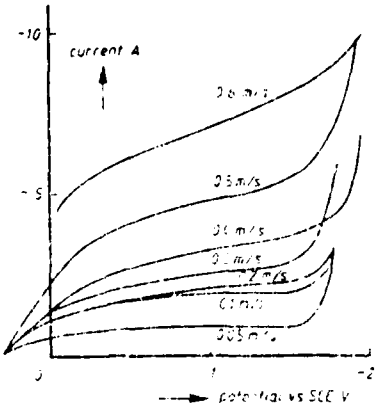

Fig. 3 Polarization curves for a bundle of 200,000 fibres at different velocities (10^{-2} M $K_3Fe(CN)_6$ in 1 M KOH, L = 8.3 cm).

Table 1 Utilization factors for various electrode geometries at 0.05 m/s.

Configuration	Number or quantity of fibres	Specific surface area (m^{-1})	Porosity (%)	η (%)
Parallel bundles	10,000	2,500	99.5	8.0
	50,000	12,600	98	1.6
	200,000	50,400	90	0.6
	500,000	126,000	75	0.6
Cloth	7 layers	82,500	83	0.9
Felt	1 layer	11,300	96	90

REFERENCES
1. Schmal D., Van Erkel J., Van Duin P.J., J. Appl. Electr., Submitted for publication.
2. Jacob M., Heat Transfer, Joh. Wiley and Sons, New York, 1962.
3. Bek M.Y., Zamyatin A.P., Sov. Electr. 14(1978)8, 1034-1039.

04040

ELECTROCHEMICAL DETOXIFICATION OF AQUEOUS WASTE SOLUTIONS.

J. VAN ERKEL, D. SCHMAL, P.J. VAN DUIN.
TNO Division of Technology for Society, Department of Chemistry,
PO Box 217, 2600 AE Delft, The Netherlands.

INTRODUCTION

The chemical process industry produces large amounts of waste waters containing toxic or non-biodegradable organic compounds (*e.g. halogenated organics*). For the removal of these undesirable substances, electrochemical treatment may be feasible.
One advantage of electrolysis over other methods of chemical treatment is that additional chemicals are not normally required. Electrolysis with electrodes of a large specific area such as those composed of very thin fibres, can reduce the concentration of toxic compounds to a very low level.

We have studied the method using the cathodic dehalogenation of pentachlorophenol (PCP) in aqueous solution as a model reaction. PCP has been chosen because it is a representative constituent of the type of waste waters in question, and because it has strong carbon-chlorine bonds and a relatively good solubility in (alkaline) aqueous solutions.

EXPERIMENTAL PART

The experiments were conducted in a batch-type recycle mode with aqueous solutions of 50 ppm of PCP in 0.1 M sodium sulphate / 0.1 M sodium hydroxide. Figure 1 shows a diagram of the electrochemical reactor. The cathode consisted of 240,000 carbon fibres with a diameter of about 7μm, clamped in the reactor with a platinum strip connected to a power-source. The dimensions of the cathode compartment were 2×10×0.5 cm. A Nafion 425 membrane was used as a seperator. An aqueous solution of 0.1 M sodium sulphate was circulated through the anode compartment, which was equipped with a Pt-gauze electrode. The experiments were performed under galvanostatic conditions (10 A). The superficial flow velocity in the cathode compartment was 0.1 m/s.

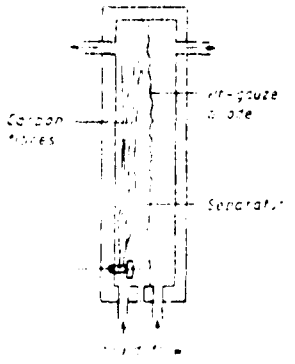

Fig. 1 Electrochemical reactor

Concentrations of the phenols were determined by high pressure liquid chromatography (HPLC). Cloride concentrations were determined by potentiometric titration with silver nitrate with a Metrohm 636 Titroprocessor and a silver indicator electrode.
Aquatic toxicity was determined by an instrumental method based on the bioluminescence of certain bacteria (Microtox method, Beckman). The toxicity was expressed as an EC 50 value, representing the concentration of neutralized electrolyte causing 50% reduction of light emission.

RESULTS AND DISCUSSION
Electrolysis of 1 litre of 50 ppm PCP solution caused the PCP concentration to decrease as shown in Fig. 2.

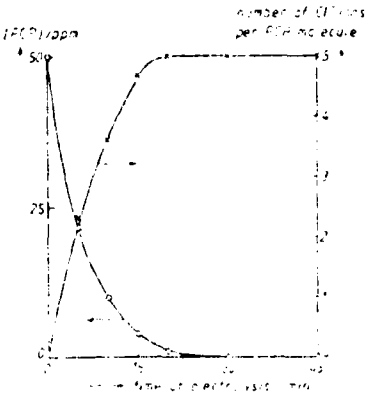

Fig. 2 Decay of PCP and yield of Cl^- ions per PCP molecule during electrolysis of 1 litre of 50 ppm PCP solution (10 A).

After 30 minutes of electrolysis the PCP concentration was below the detection limit of 0.5 ppm. Concurrently, the chloride content of the solution showed that five chlorine atoms per molecule of PCP were removed. The current efficiency for complete dehalogenation was 1%. Adding small quantities of certain surface active agents, improves the efficiency[1].
During electrolysis the toxicity of the solution fell from an initial EC 50 = 2% to a final 40%, indicating almost complete detoxification.

An experiment with two litres of the test solution was performed for the purpose of determining the intermediates and product(s) formed. Figure 3 shows the formation and decay of tetra-, tri-, di- and monochlorophenols, finally resulting in the formation of phenol and, possibly, monochlorophenols. The experiment shows that the total molar concentration of the phenols remains constant in time.
Experiments with other organohalogens and industrial waste waters are in progress.

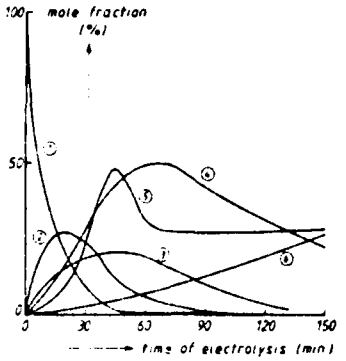

Fig. 3 Mole fraction of the phenols during electrolysis of 2 l of 50 ppm PCP solution (10 A)

1. PCP
2. tetrachlorophenols
3. trichlorophenols
4. dichlorophenols
5. monochlorophenols
6. phenol

REFERENCES

1. European Patent No. 0052907 (1980, TNO).

04050

ESTIMATION OF MASS TRANSFER RATE FOR A PACKED BED COPPER CEMENTATION SYSTEM

FLORA BRAVO de NAIUI * and A.A. WRAGG
Dept. of Chemical Engineering, University of Exeter,
Exeter, EX4 4QF (England)

INTRODUCTION

Hydrometallurgical processes for recovering metals are gaining an increasing importance in the non-ferrous metals industry largely due to environmental constraints on sulphur dioxide emissions and the depletion of high grade ore deposits. One of the most ancient, yet most effective, hydrometallurgical process for the recovery of dissolved metal values from aqueous solution is cementation.

Although there have been many previous studies of cementation kinetics and thermodynamics, most of these have been carried out under unsatisfactory hydrodynamic and geometric conditions so that the results given cannot be interpreted easily and cannot be scaled up to a practical size. In the present work a packed bed geometry has been used to estimate the mass transfer rate under different flow rates. The apparatus and some early results have been the subject of a previous publication [1], which particularly described the effect of pH on experimental performance.

EXPERIMENTAL PROCEDURE

The solution used in this study was of copper sulphate and sulphuric acid, the characteristics of which are given in Table I.

Table I - Solution characteristics

Copper Concentration	= 1080 ppm
Initial pH	= 3.02
Density, ρ	= 998.2 kg m^{-3}
Kinematic Viscosity, ν	= $1.0038 \times 10^{-6} m^2 s^{-1}$
Diffusion Coefficient, D	= $7.3 \times 10^{-10} m^2 s^{-1}$
Schmidt Number, Sc	= 1375

The experiments were carried out at room temperature (23°C) and at constant initial pH. Seven different flow rates were chosen and all other experimental parameters were kept constant. The experiments reported here were carried out with batch recirculation of the solution. The bed depth and mean particle diameter of the iron particles were 9 cm and 3.35 mm respectively and the volume of solution used in each experiment was 16 dm^3. Concentrations of Cu^{++} and Fe ions were monitored by sampling from the re-

* Permanent Address: Universidade Federal Da Paraiba, Departamento de Mineracao e Geologia, Campina Grande, Brasil.

servoir and determining by atomic absorption spectrophotometry. The pH value of 3.02 was selected in order to give minimum iron consumption and produce good quality copper powder [2].

RESULTS

A set of concentration-time curves for the copper deposition and iron dissolution at different flow rates is shown as Figures 1 and 2. Evidently, the depletion of Cu^{++} ions becomes more rapid with higher recirculation rate, Q, over most of the tested range. Flow rates of 1 to 7 dm^3/min were used although it was evident that at 7 dm^3/min the bed was fluidised and as a consequence the cementation performance decreased as observed in Fig. 1. This is due to a complex interaction between volumetric flow rate, increased exposed surface area, change of hydrodynamic regime and associated change in mass transfer behaviour. Fig. 2 shows the amount of iron consumption under the same conditions described above.

An approximate model, assuming mass transfer control and plug flow throughout the bed, which predicts an exponential relationship for the decrease of the concentration with time was used to estimate the overall mass transfer coefficient and is given by

$$C_t = C_o \exp\left[\frac{-t}{\tau}\left(1 - \exp\left(-\frac{kAaL}{Q}\right)\right)\right] \qquad (1)$$

It is important to note that k values were based only on the exponential portions of the concentration-time curves.

The specific surface area of the iron spheres, a, was calculated on the basis of the particles being smooth and spherical

$$a = 1/D_p\,(1 - \epsilon) \qquad (2)$$

However, microscopic observations [4] indicated that Equation (2) represents only a very rough approximation in view of the irregular form and the surface roughness of the iron spheres so that the effective surface area becomes greater than that assumed in the model. The mass transfer coefficient calculated with this model was incorporated into an empirical correlation of the form

$$Sh = 2.55\ Re^{0.57}\ Sc^{1/3} \qquad (3)$$

$$\text{for } 37 < Re < 550 \quad \text{and} \quad Sc = 1375$$

which predicts higher than other literature correlations for mass transfer in packed beds. Fig. 3 shows the variation in Sh/Sc with Re. Finally, Fig. 4 shows the present results together with other correlations of the authors indicated [3,4]. The mass transfer coefficient (here expressed as J_m) is almost four times higher than would be expected for spherical particles thus indicating the combined effect of enhanced surface area and micro-turbulence promotion due to the growing copper deposit on the irregular shaped particles. SEM's of the surfaces have demonstrated the powdery and dendritic nature of the copper deposit. High mass transfer coefficients are also consistent with the findings of Kubo et al [5] who also used a packed bed system.

ACKNOWLEDGMENT

Financial support from the Conselho Nacional de Desenvolvimento Cientifico e Tecnmologico (CNPq-Brasil) for the support of tnis work is gratefully acknowledge.

REFERENCES

1. Wragg A.A., Extended Abstracts, 34th Meeting-ISE, Erlangen, Germany, Sept. (1983) 18.
2. Bravo de Nahui F.N., Ph.D. Thesis, University of Exeter (1986)
3. Storck A., Vergnes F and Le Goff P., Powder Technology, 12, (1975) 215.
4. Upadhyay S.N. and Tripathi G., J. Chem.Eng.Data, 20 (1975) 20.
5. Kubo K., Mishina A., Aratani T. and Yano T., J. Chem. Eng. Japan, 12 (1979) 495.

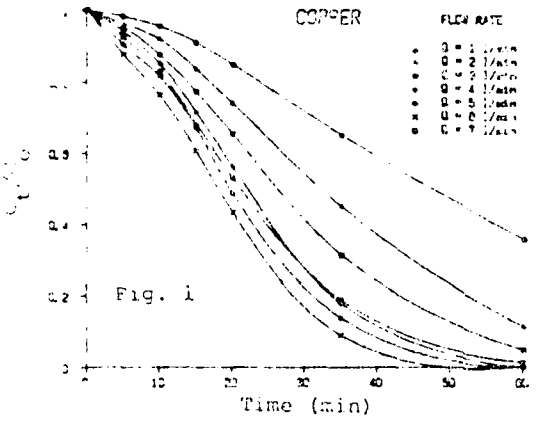

Fig. 1

Concentration-time plot for varying Q

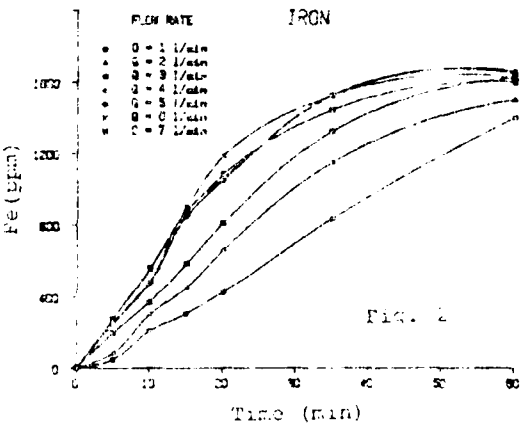

Fig. 2

Concentration-time plot for Fe consumption

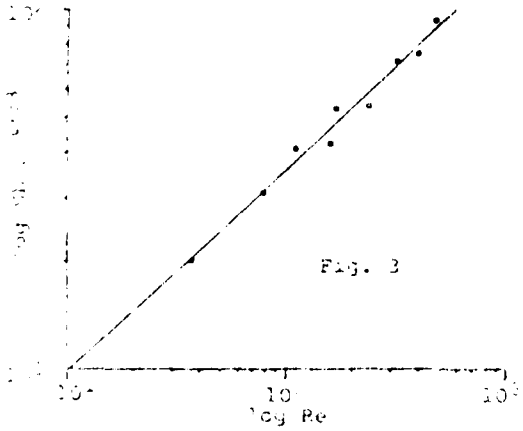

Fig. 3

Experimental mass transfer data

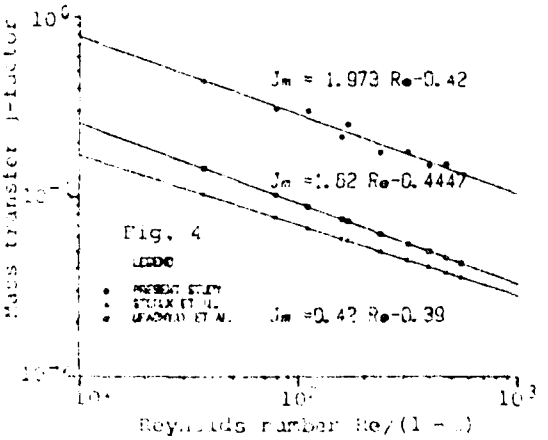

Fig. 4

Comparison with literature data

04060

A PARAMETRIC STUDY OF COPPER DEPOSITION IN A CIRCULATING BED ELECTRODE

G. NAHUI-PALOMINO * and A.A. WRAGG
Dept. of Chemical Engineering, University of Exeter,
Exeter, EX4 4QF (England)

INTRODUCTION

One of the drawbacks of using a uniformly fluidised bed electrode for metal winning arises from the fact that on running the cell over long periods, metal will accumulate on the feeder electrode. This can be avoided by tilting the cell away from the vertical and producing what is known as a circulating bed [1]. In this work some results for a circulating bed cell carrying out copper deposition are presented.

EXPERIMENTAL PROCEDURE

Experiments have been carried out using a cell of rectangular geometry and of the 'side-by-side' type; that is, the current flow is perpendicular to the direction of electrolyte flow. Most of the experiments were carried out with a cathode compartment width of 0.02 m in the current flow direction and this was separated from the anode compartment by an anionic semi-permeable membrane (Ionac type MA 3475) supported by a sheet of Vyon F. porous pvc diaphragm. The feeder electrode was a copper plate, 0.05 m wide and 0.3 m high in contact with the wall of the cathode chamber, the counter electrode was a sheet of lead placed in the anode chamber. The bed material consisted of copper particles, classified into mean diameters of 0.25, 0.38, 0.50, 0.65 and 0.77 mm. The cell was mounted in such a way that it could be inclined to the vertical and the inclination was adjusted between 0^{o} and 30^{o}.

The cell was operated at constant electrode potential using a potentiostat (Thompson Electrochem Ltd type Ministat 28V-7A). The current was measured by a shunt resistance attached across a digital voltmeter (Solartron 7055). Controlled electrode potentials (E) were measured between the input or the cathodic current and a mercury/mercurous sulphate reference electrode.

As electrolyte a solution of copper sulphate (100 ppm) was used with addition of sulphuric acid (1.5 M) as supporting electrolyte. All experiments were performed in a batchwise manner, the electrolyte being continuously recirculated through the cell. Current efficiency data for copper deposition were obtained by monitoring the reservoir catholyte copper concentration using A.A. Spectrophotometry and the amount of electricity passed during the course of a run.

* Permanent address: Departamento de Engenharia Quimica, Universidade Federal da Paraiba, Campina Grande, Brasil.

RESULTS

The gradual depletion of the instantaneous copper concentration C_t with time for six values of the working potential E and for identical hydrodynamic ($Q = 4.08 \times 10^{-5} m^3 s^{-1}$) and geometric conditions is shown in Fig. 1. It is noted that increasingly cathode potentials increase the speed of copper deposition up to - 0.95V, beyond which the rate of deposition does not change significantly. Fig. 2 shows trends in current efficiency over a range of cathode potentials. Current efficiency is seen to pass through a maximum and then decline with increasingly cathodic potential. This is largely due to the increasing proportion of current being consumed by the hydrogen evolution secondary reaction, which becomes more prominent at large cathode polarizations. The influence of circulation rate of the electrolyte in the cathodic compartment is shown in Fig. 3 for a fixed potential, E = - 0.95V, and total particle surface area A_p. The effect of the flow rate variation on the rate of copper depletion is small and not discernably systematic; this is discussed in more detail elsewhere [2]. Finally, Fig. 4 shows the variation of concentration with time for four values of cell inclination angle and identical hydrodynamic and geometric conditions. This clearly shows a decrease in the rate of depletion of concentration as the angle increases, there being an optimum value for a circulating bed in the range 50 - 150.

ACKNOWLEDGEMENT

Support by Conselho Nacional de Desenvolvimento Cientifico e Tecnologico (CNPq), Brasil, is gratefully acknowledged.

REFERENCES

1. Goodridge F. and Vance C.J., Electrochim. Acta, 22, 1073-1076, (1977).
2. Nahui-Palomino G., PhD Thesis, University of Exeter, (1986).

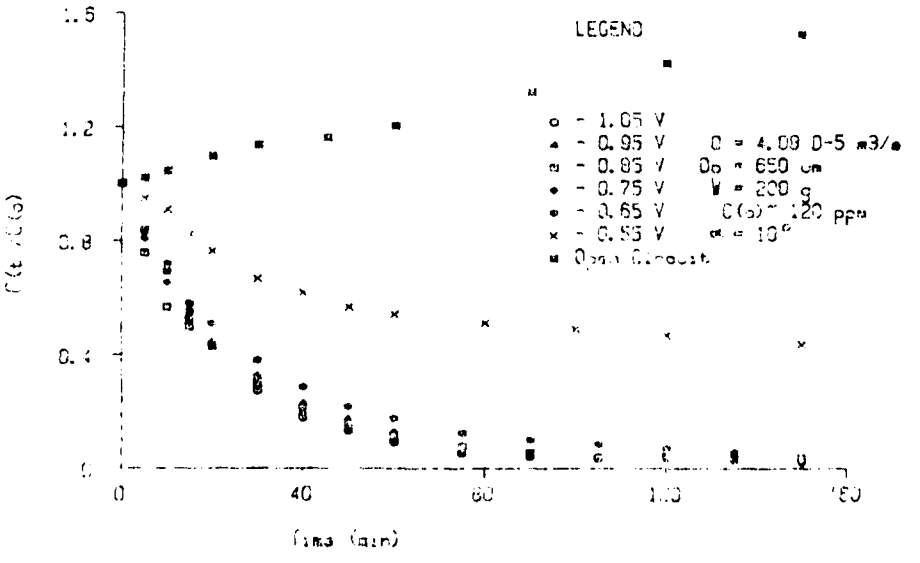

Fig. 1 Normalised Concentration-Time Curves for Various Control Potentials

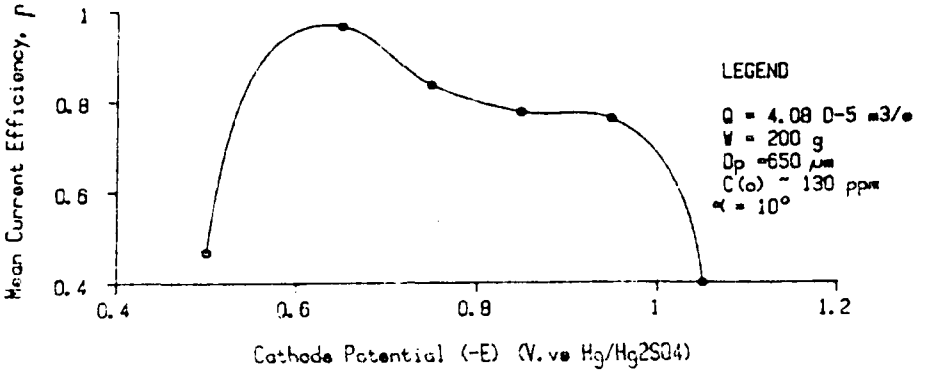

Fig. 2 Experimental Variations of the Current Efficiency

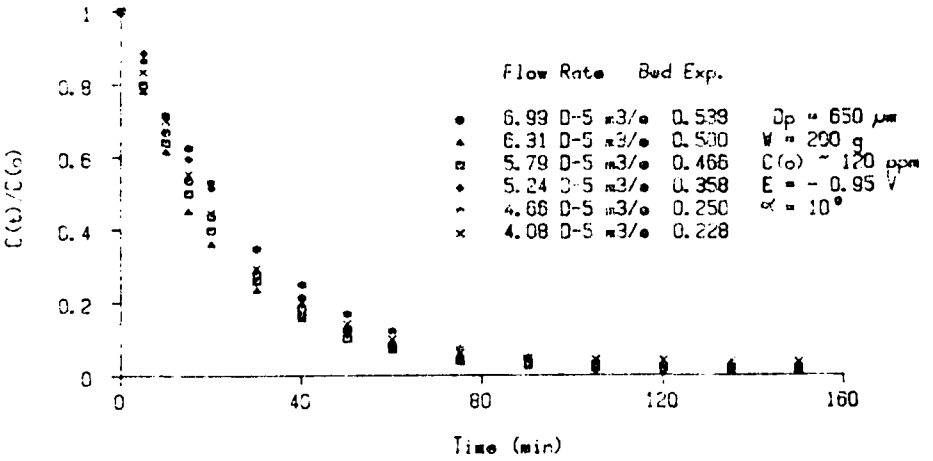

Fig. 3 Normalised Concentration-Time Curves for Various Flow Rates

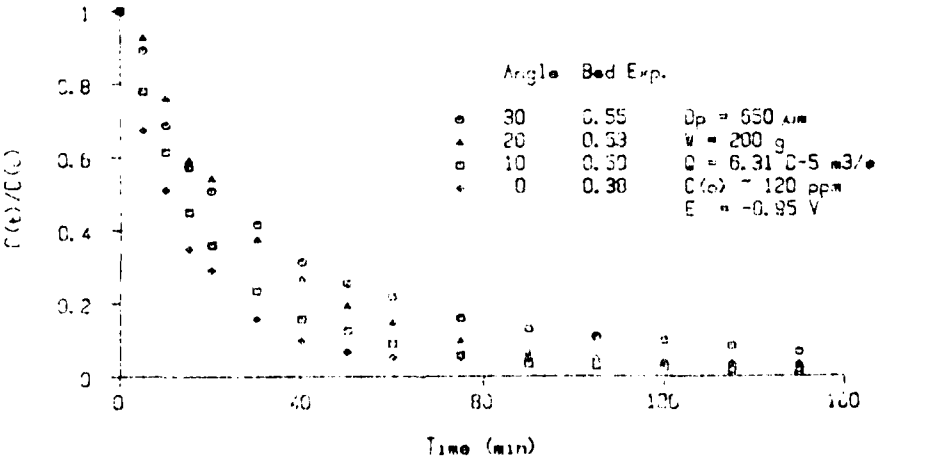

Fig. 4 Normalised Concentration-Time for Various Inclination Angles

04070

HYDRODYNAMIC OPTIMIZATION OF FARADAIC YIELDS IN THE CHLORATE CELL PROCESS

M. SPASOJEVIĆ[1)], R. STEVANOVIĆ[2)], N. KRSTAJIĆ[3)] and M.M. JAKŠIĆ[4)]

University of Belgrade, Yugoslavia

1) Faculy of Agriculture, Čačak
2) Institute "Boris Kidrič", Belgrade
3) Faculty of Technology and Metallurgy, Belgrade
4) Faculty of Agriculture, Belgrade

A theoretical approach to the hydrodynamic optimization of current yields in the chlorate cell process has been obtained by the consequent mathematical analysis of Faradaic balance and mass transfer of electroactive species within the anodic diffusion layer. For a rather "stagnant diffusion layer" it leads to a transcendental equation for the current efficiency[1] (t_1)

$$t_1 = \frac{1 - \frac{D_2 C_0 F}{i\delta}}{\frac{3}{2} - \frac{1}{2}\,\frac{\mathrm{tgh}(\sqrt{k_1/D_1}\,\delta)}{\sqrt{k_1/D_1}\,\delta}} \qquad (1)$$

where i is the current density, k_1 - rate constant for chlorine hydrolysis, δ - the diffusion layer thickness, C_0 - available chlorine bulk concentration, D_1 and D_2 - diffusion constants for elemental and total available chlorine, respectively. However, diffusion and hydrolysis of elemental chlorine, as well as diffusion mass transport of available chlorine could also be described by the Dunckwerts model[2,3] of "surface renewal", which assumes that elements of liquid are brought in contact with gas by turbulent mixing within the diffusion layer. The model implies such a gas diffusion through liquid "elements", which mass transport can be described by the equation for nonsteady state diffusion, and continuous renewal of liquid elements at the interface with gas phase. The probability of renewal of liquid elements with fresh liquid does not depend on its time contact with gas. At the steady state the fraction of surface being in contact with gas within the element of time (τ) between τ and $\tau + d\tau$ is supposed to be $S \cdot \exp(-S\tau)$, where S - means the fraction of surface replaced by fresh liquid in the unit time. If $C(x,\tau)$ represents gas content at distance x from the liquid surface at time τ after the beginning of their mutual contact, the average gas concentration at the same space coordinate follows from inte-

gration for all elements of the surface:

$$\bar{C}(x) = S \int_0^\infty C(x,\tau)e^{-S\tau}d\tau \tag{2}$$

that in mathematical interpretation means the application of Laplace-Karson transformation for the function $C(x,\tau)$.

The equation for nonsteady state diffusion describes the diffusion accompanied by hydrolysis for elemental- and available- chlorine, respectively:

$$\frac{\partial C_1}{\partial \tau} = D_1 \frac{\partial^2 C_1}{\partial x^2} - k_1 C_1 \tag{3}$$

and

$$\frac{\partial C_2}{\partial \tau} = D_2 \frac{\partial^2 C_2}{\partial x^2} + k_1 C_1 \tag{4}$$

Application of Laplace-Karson transforms upon Equations (3) and (4) with the boundary conditions:

a) for elemental chlorine (C_1)

$$\text{at } \tau = 0, \quad C_1 = 0 \tag{5}$$

$$x = 0, \quad -D_1 \frac{d\bar{C}_1}{dx} = \frac{it_1}{2F} \tag{6}$$

$$x \longrightarrow \infty, \quad C_1 \longrightarrow 0 \tag{7}$$

b) for available chlorine (C_2)

$$\text{at } \tau = 0, \quad C_2 = C_0 \text{ for } x > 0 \tag{8}$$

$$\tau > 0, \quad C_2 = 0 \text{ for } x = 0 \tag{9}$$

$$\tau > 0, \quad C_2 = C_0 \text{ for } x \longrightarrow \infty \tag{10}$$

leads to the new mass transport relations:

a) for elemental chlorine

$$D_1 \frac{d^2\bar{C}_1}{dx^2} - (k_1 + S)\,\bar{C}_1 = 0 \tag{11}$$

with interchanged boundary conditions

$$\text{at } x = \delta, \quad \bar{C}_1 = 0 \tag{12}$$

$$x = 0, \quad -D_1 \frac{d\bar{C}_1}{dx} = \frac{it_1}{2F} \tag{13}$$

and b) for available chlorine

$$\frac{d^2\bar{C}_2}{dx^2} - \frac{S}{D_2}\bar{C}_2 = -\frac{C_o}{D_2}S - \frac{k_1\bar{C}_1}{D_2} \tag{14}$$

$$\text{for } x \longrightarrow \infty, \quad \bar{C}_2 = C_o, \tag{15}$$

$$\text{at } x = 0, \quad \bar{C}_2 = 0 \tag{16}$$

where $\bar{C}_1$ and $\bar{C}_2$ are defined by Equation (2). Simultaneous solution of Equations (13) and (14) leads to the concentration profile of available chlorine within the diffusion layer, while the relation

$$\frac{(1-t_1)i}{F} = D_2 \left.\frac{dC_2}{dx}\right|_{x=0} \tag{17}$$

gives the current efficiency for chlorate cells

$$t_1 = \frac{1 - \frac{D_2 C_o F}{i\delta}}{\frac{3}{2} - \frac{1}{2}\frac{1}{\sqrt{1+(k_1/D_1)\delta^2}}} \tag{18}$$

where $S = D_1/\delta^2$, and which fairly well describes faradaic yields and agrees with formerly obtained[1] similar relationship (Equation (1)). However, at higher current densities ($i > 10$ A dm^{-2}), that are characteristic for modern trend in chlorate cells design, rather large fraction of chlorine escapes hydrolysis within the diffusion layer. Thus, to assess the real current yields, one has to consider and encompass the total mass balance of available chlorine in the entire volume of electrolyte[4]. Then the events at the anode surface described by Equation (18) appear incorporated in the whole mass balance for the entire producing system.

REFERENCES

1. M.M. Jakšić, Electrochim. Acta, 21, 1127 (1976)
2. P.W. Danckwerts, Ind. Eng. Chem., 43, 1460 (1951)
3. P.W. Danckwerts, Gas-Liquid Reactions, McGraw Hill, New York, 1970
4. I. Rousar, V. Cezner, V. Mejta, M.M. Jakšić, Č.M. Lačnjevac, M.D. Spasojević and N.V. Krstajić, Hydrodynamic Optimization of Energy in the Chlorate Cell Process, pape presented at 35. ISE-Meeting, Berkeley, 1984

04080

BATCH RECIRCULATING THREE-DIMENSIONAL ELECTROCHEMICAL CELL: OPERATIONAL MODES AND ENERGY CONSUMPTION

V. D. STANKOVIĆ
Department of Metallurgy, Technical Faculty Bor
University of Belgrade; 19210 Bor (Yugoslavia)

Many papers, published or presented on meetings, in the last decade, have been dedicated to three-dimensional electrode cell. This electrode has been object of considerable academic and some industrial interest.

In present article, the behaviour of a batch recirculating three-dimensional electrochemical cell has been analysed using a simple model. This model consists of depletion of metal ions from diluted solutions in a three-dimensional electrode under mass transfer controled reaction.

During removal of ions, not only concentration depends on time but also limiting current density, current efficiency, cell voltage, specific energy consumption and the other relative characteristics of the cell which determine possibilities of every electrochemical reactor per se.

In concrete analysis of a three-dimensional electrode cell, the reaction of electrodeposition of copper ions from acidic coppersulphate solution has been used in such a concentration which ensure diffusion controlled process. Sulphuric acid served as a supporting electrolyte. Bed of copper particles in contact with the current feeder is acted as a three-dimensional cathode. On the counter electrode, reaction of oxygen evolution occured. Cathodic and anodic compartments were separated by diaphragme which served to prevent oxygen passing through diaphragme into cathodic space and to prevent short circuit between anode and the bed of particles.

Plug flow conditions are assumed in the cathodic compartment of the cell and the reservoir is considered as a perfectly sti-

rred tank[1]. All hydrodynamical conditions are assumed to be constant during electrowinning process. The analysis has been made for the cases of constant operating current and constant potential of the three-dimensional cathode.

For the case of constant operating current the value of which is below the initial limiting current for the given concentration and hydrodynamical conditions, i. e. $I = \alpha \cdot I_L(C)$ for $t = 0$; process of metall winning passes through two periods[1,2]. During the first period, when the operating current is below the limiting one ($I < I_L(t)$), cell productivity is below its maximum possible. Current efficiency is on a high value and independant of time. Concentration of reacting ions decreases with time as well as limiting current does. The second period starts when operating current reachs the value of limiting current for a given conditions. Parallel reaction of hydrogen evolution starts up and operating current may be expressed by equation[2]

$$I = I_L(t) + I_H(t) \qquad \text{for} \quad t > t_c$$

In this period of the process winning, current efficiency decreases with time, cell voltage increases slowly, concentration of ions depletes following an exponential function, and specific energy consumption increases. Required time to reach a certain extraction degree depends on the ratio $I/I_L(0)$. In the second part of the process, current efficiency decreases with time, cell voltage increases as well as energy consumption.

For the potentiostatic mode of operation, with decreasing of reacting ions decreases operating current and cell voltage. Current efficiency remains on a high value (close to unit), for almost whole time of depletion of reacting ions, because reaction of hydrogen evolution is avoided.

Energy consumption is lower than in the first case, but required time to reach a given value of metal winning is much higher.

In both cases, pumping energy was for two order of magnitude lower than energy spended for the electrochemical reactions.

Analysis has showed that potentiostatic operational mode of metal winning, using the three-dimensional electrode cell,

is more attractive in a view of saving energy but rate of the process decreases with time. An optimisation was derived for both analysed modes of operation.

Used symbols

I - Operating current /A/

$I_L(0)$, $I_L(t)$ - Initial and instantaneous limiting current respectively /A/

$I_H(t)$ - Current spended for hydrogen evolution reaction /A/

t, t_c - time and critical time at which operating current is equal to the limiting current

References

1. L. F. Mustoe and A. A. Wragg; J. Appl. Electrochem., 13(1983)
2. V. D. Stanković and A. A. Wragg; J. Appl. Electrochem., 14 (1984)

04090

ELECTROCHEMICAL DETERMINATION OF AXIAL DISPERSION IN FIXED BEDS OF FLAT PLATES BY THE RTD METHOD

J. COMITI and J. LEGRAND
I.U.T., Département Génie Chimique, B.P. 420, 44606 SAINT-NAZAIRE (FRANCE)

The problem of longitudinal mixing in packed beds, using both gases and liquids as the fluid media, has been largely studied during the last thirty years. The mixing phenomenon is important because of its influence on the performance of packed bed reactors, mixers and extractors. The aim of most of these works[1] was to determine the axial dispersion of fluid flowing through isotropic fixed beds, constituted principally by spherical particles and Rashig rings. The present work concerns the study of the liquid flow through beds of flat plates, which are anisotropic media. The axial dispersion coefficients are determined by a polarographic method[2].

The experimental apparatus (Fig.1) consists of a packed column (internal diameter Φ_C = 6.0 cm and length 55 cm), a tank, a constant level reservoir and a pump. The polarographic liquid is a solution of 0.001 M potassium ferricyanide, 0.013 M potassium ferrocyanide and 1 M sodium hydroxyde. The tracer (solution of potassium ferricyanide) is detected by a polarographic method (reduction of the ferricyanide ions) at two identical cathodes located in the fixed bed (Fig.1) ; the anode is a knit of nickel wire.

When the tracer is injected uniformly over the cross-section of the bed of non-porous particles so that there are no radial concentration gradients, its concentration C is given as a function of time t and axial position x by (dispersed plug flow model) :

$$\frac{\partial C}{\partial t} + u \frac{\partial C}{\partial x} = Dax \frac{\partial^2 C}{\partial x^2} \qquad (1)$$

Where u is the mean axial interstitial velocity and Dax is the axial dispersion coefficient (assumed constant). The transfer function of the bed of L length (here, L = 15 cm) is given by[3] :

$$f(t) = \frac{1}{2\bar{t}_s \left[\pi N_d \left(\frac{t}{\bar{t}_s}\right)^3\right]^{1/2}} \exp\left[-\frac{1-(t/\bar{t}_s)^2}{4 N_d \frac{t}{\bar{t}_s}}\right] \qquad (2)$$

Where $\bar{t}_s = \frac{L}{u}$ is the mean residence time and $N_d = \frac{Dax}{Lu}$ the mass dispersion number. The two parameters $\bar{t}_s$ and N_d, characterizing the flow through the packed bed, are determined by the "Curve Fitting in the Time Domain" method[3]. The experimental curves C_{in} and C_{out} obtained at the two cathodes (Fig.1) are expressed by Fourier series. From the transfer function f(t) and C_{in} (t), we can calculate the response signal

C_{out}^{calc} (t) by a convolution integral. The computed response signal C_{out}^{calc} is compared with the measured signal C_{out} in the form of a criterion E :

$$E = \frac{\int_0^{2T} \left(C_{out} - C_{out}^{calc} \right) dt}{\int_0^{2T} C_{out}^2 \, dt} \qquad (3)$$

The parameters $\bar{t}_s$ and N_d (or Dax) are determined when E is minimum (<5%).

Figure 2 gives the evolution of the dimensionless diffusivity ratio $\frac{Dax}{\nu}$ (ν is the kinematic viscosity) with the Reynolds number, defined by $Re = \frac{u.d_h}{\nu}$, where $d_h = \frac{4}{4/\phi c \quad + a_g(1-\varepsilon)}$ is the hydraulic diameter. For the flat plates (a_g = 48 cm^{-1}; ε = 0.47), the data can be correlated by the equation :

$$\frac{Dax}{\nu} = 17.73 \, Re^{0.88} \qquad (4)$$

For the spherical particles (ε = 0.4 ; $d_h = d_p$), the data are well represented by the correlation obtained by MALL *et al*[4] . The comparison between the two types of beds shows that the dispersion coefficients are more important (a factor of 10) in the bed of flat plates.

In figure 3, we give a plot of Peclet number $Pe = \frac{u_o d_h}{Dax}$ versus $Re = \frac{u_o d_h}{\nu}$ (u_o = superficial velocity) for fixed beds data of many authors reported by CHUNG and WEN[1] . The data obtained with the bed of glass beads are in keeping with the data of the literature. It can be noted, as in Figure 2, that the axial dispersion is greater with the bed of flat plates, compared with all other beds (constituted by spheres, Rashig rings, saddles, pellets). This result is important, and an explanation can lie in the anisotropy of the bed of flat plates.

REFERENCES

1 - S.F. CHUNG and C.Y. YEN, A.I.Ch.E.J., 14, 857 (1968)
2 - M. FLEISCHMANN, J. GHOROGHCHIAN and R.E.W. JANSSON, J. Appl. Elect., 9, 437 (1979)
3 - N.WAKAO and S. KAGUEI, Heat and Mass Transfer in Packed beds, Gordon and Breach Science Publishers, 1982.
4 - I.D. MALL, M. SINGH, P.C. SINGH and V.K. MATHUR, Ind. J. of Tech., 14, 607 (1976).

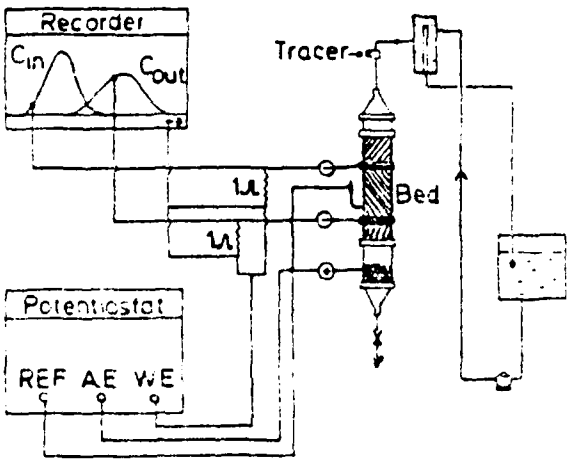

FIGURE 1 :

Flow and electric circuit.

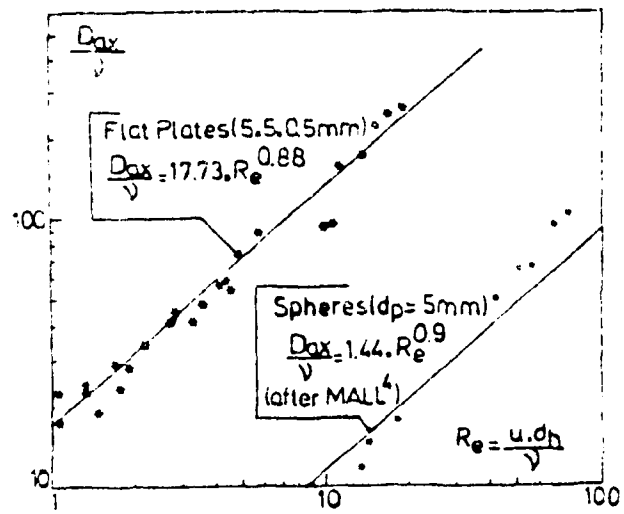

FIGURE 2 :

Experimental variation of the diffusivity ratio $\frac{D_{ax}}{\nu}$ with Reynolds number for fixed beds of flat plates and glass beads.

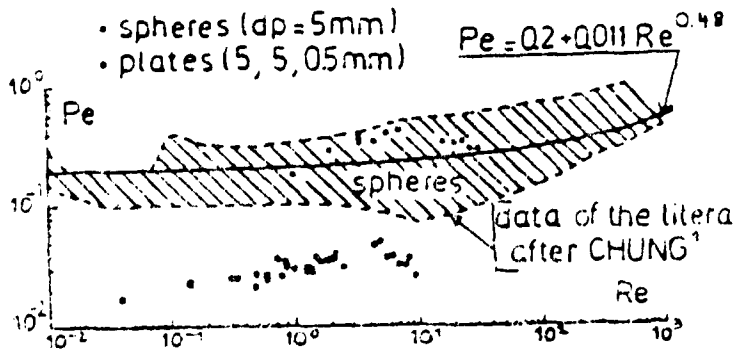

FIGURE 3 :

Comparison of our results with the literature in form of Pe versus Re.

04100

ELECTROCHEMICAL REACTOR WITH PARTIALLY IMMERSED ROTATING HORIZONTAL CYLINDER

A. Meštrović-Markovinović, Dj. Matić
Institute of Electrochemistry, Faculty of Technology,
University of Zagreb, Zagreb, Yugoslavia

This work is a continuation of investigations on horizontal rotating cylinder[1,2]. Mass transfer to a partially immersed rotating horizontal cylinder was investigated. Measurements were performed by observing the cathodic reduction of ferricyanide ion in a solution 1×10^{-2} mol dm^{-3} ferri-ferro-cyanide in 0,5 mol dm^{-3} KOH. Carbon paste electrode served as working electrode, and measurements were taken for different degrees of the cylinder immersion (2/3; 1/2; 1/3; 1/6) with in the rotation rate range $v = 0,2 - 6,5$ cm s^{-1}.

Regular oscillations of limiting currents which appear already at low rotation rates of the partially immersed horizontal cylinder were studied. It is found that the regularity of oscillations is influenced neither by a degree of immersion nor by the rotation rate of the cylinder. However micro deffects like non-uniformity of the carbon-paste electrode surface cause significant changes in limiting currents during the act of immersioning the cylinder. This was confirmed by intentional controled production of surface deffects. Thus it is posible to draw a conclusion that regular oscillations of limiting currents are caused by irregularities of the carbon-paste electrode surface.

On the basis of the results obtained, mass transfer to a partially immersed cylinder under the condition of forced convection can be discribed in the same way as the case of flat plate in free stream[3]. All experimental results fit to equation

$$Sh = (2/\sqrt{\pi}) \, Re_x^{1/2} \, Sc^{1/2}$$

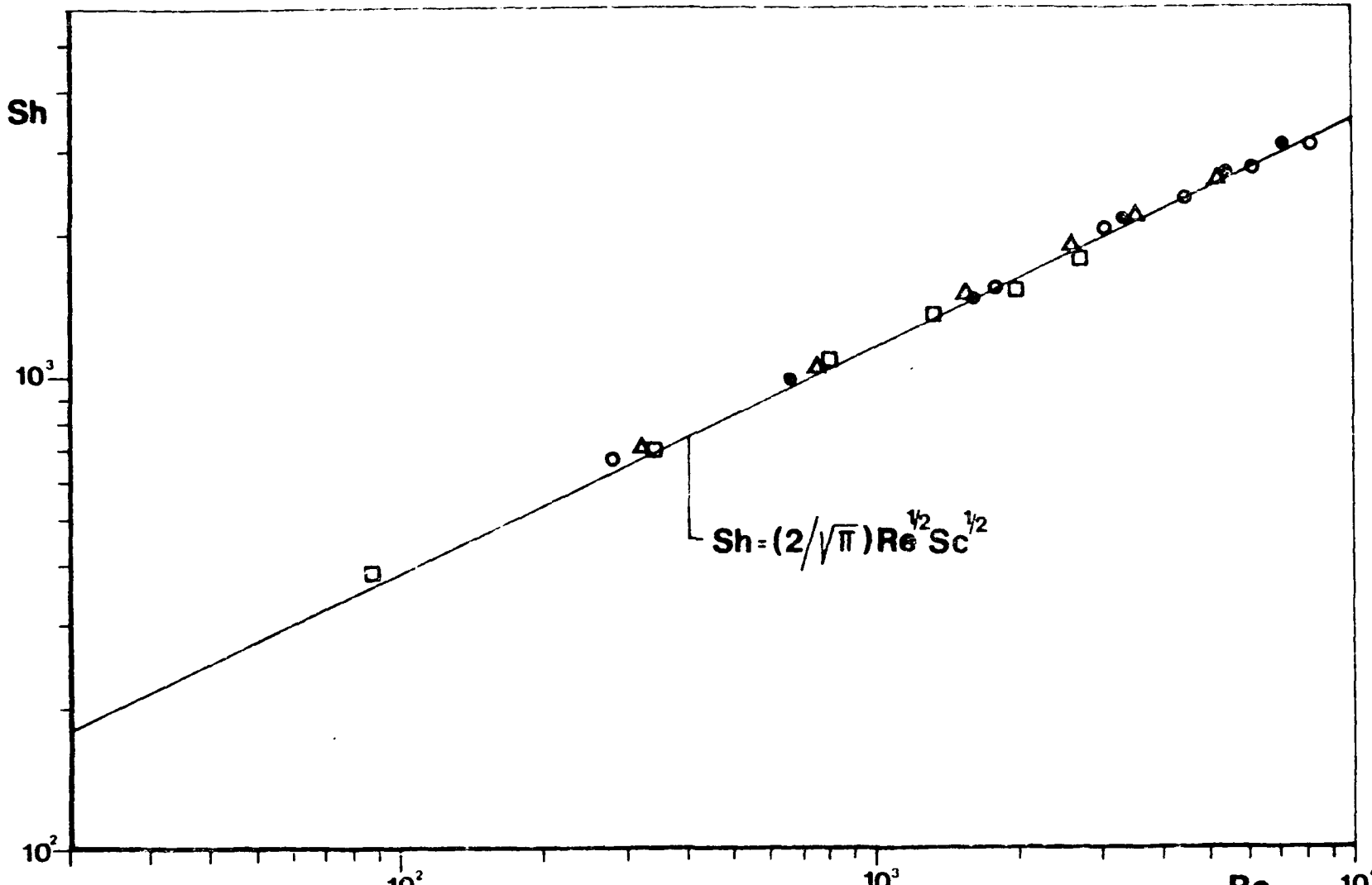

figure - 1

for the mass transfer on flat plate with uniform velocity, figure 1.

It is interesting to observe that the limiting current density increase with decrease of immersion degree. This offer one more possibility to run production capacity of such reactor type.

References:

1. A. Meštrović-Markovinović, Dj. Matić, 31 st Meeting ISE, Venice 1980, Extended Abstracts, 900

2. A. Meštrović-Markovinović, Dj. Matić, J. Appl. Electrochem. 14 (1984) 675

3. D. J. Pickett, Electrochemical Reactor Design, Elsevier N. Y. (1977)

04110

POTENTIAL AND CURRENT DISTRIBUTION IN A FLUIDIZED BED ELECTRODE

G. VALENTIN and A. STORCK

Laboratoire des Sciences du Génie Chimique - CNRS-ENSIC
1, rue Grandville - 54042 NANCY Cedex, France

The present work reports an experimental investigation of copper deposition in a laboratory scale fluidized bed electrode and attemps to describe the macroscopic behaviour of the electrode, taking into account the experimental conditions : bed porosity, operating current intensity, mass transfer rates, solution conductivity and equivalent electrical conductibility of the bed particles.

Figure 1 illustrates the cell configuration and the potential measurements within the bed using a microcomputer. Such a device allows the local time variations of the solution potential Φ_s and the metal potential Φ_b of a fixed particle at a same location to be deduced. For a given bed porosity ($\varepsilon = 0.55$) and current intensity ($I = 2.5$ A), figure 2 presents an example of such variations, showing clearly that Φ_b varies between two levels : one corresponding to the thermodynamic equilibrium and the other to a potential very close to the feeder potential. The communication will discuss the effect of most important parameters on the potential and overpotential profiles inside the bed.

Furthermore, theoretical analyses of the characteristics of the particulate electrode will be presented with combinations of the general equation of electrode reaction and the operating fluidization parameters. The model is based on the one dimensional two-phase approximation of the porous electrode[1](with the equivalent electrical resistivities ρ_m for metal and ρ_s for solution).

For a single electrode cathodic reaction (involving ν_e Faradays), the main equations governing the overpotential and potential distributions are :

- the charge balance equation :

$$\frac{d^2E}{dx^2} = (\rho_m + \rho_s).a.i$$

associated with the electrochemical reaction rate given by the Butler-Volmer equation[2]including mass transfer limitations.

- the mass balance equation for the reacting species[3]:

$$\nu_e.F.u.(C_o - C(x)) = - \int_o^x a.i.dx$$

(Concentration change along the electrode may therefore be taken into consideration).

by computer treatment of the previous equations with appropriate boundary conditions, the spatial distributions of E and also Φ_m and Φ_s (potential of the metal and solution respectively) are deduced assuming that the faradaic yield is 100 %. Comparison between the experimental and calculated profiles of Φ_s allows the unknown model parameter ρ_m to be obtained. For copper removal from a sulphuric acid solution within a fluidized bed electrode (particle diameter : 670 µm ; density : 8.9 g/cm^3)

operated at different current intensities I, there is a good agreement as shown by the results of figure 3 (best fit obtained for $\rho_m = 1.10^{-3}$ Ω.m). For the same conditions figure 4 gives the variations of the current distribution is largely non uniform and an important fraction of the bed operates near the thermodynamic equilibrium (where $i \sim 0$). More over an increase of the fluid velocity or bed porosity and consequently of the metal resistivity ρ_m results in the appearance of a second electrochemically active zone at the down part near the current feeder. Finally, the comparison between calculated and experimental overpotential distributions (taking also into account the time variation of Φ_b mentioned in figure 2) is reported in figures 5 and 6 : in both cases (I is different), the agreement is excellent if one considers the upper part of the experimental range of variations. The existence of packed bed clusters already mentioned in the literature seems therefore to be clearly demonstrated.

From these results, it appears that the advantage of avoiding the clogging of particles during the treatment of metal-bearing industrial effluent is counterbalanced by a bad current distribution (or selectivity). Due to this, the electrochemical fluidized bed technology is loosing its interest.

NOMENCLATURE

- a : specific surface area
- C_0 : inlet copper concentration
- $C(x)$: local bulk copper concentration
- $E = \Phi_m - \Phi_s$: electrode potential
- i : local current density
- u : fluid velocity
- x : axial coordinate along the bed

REFERENCES

1 J.S. NEWMAN and C.W.TOBIAS
J. Electrochem. Soc., 109 (1962) 1183

2 J. NEWMAN
Electrochemical Systems, Prentice Hall,Inc. 1973, p. 171

3 A. STORCK and F. COEURET
Eléments de Génie Electrochimique - Technique et Documentation (Lavoisier), Paris 1984

4 G. KREYSA
Electrochim. Acta, 25 (1980) 813

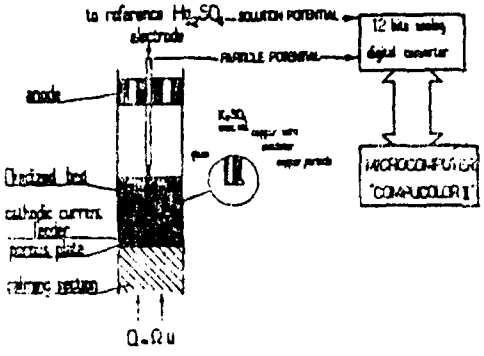

Figure 1

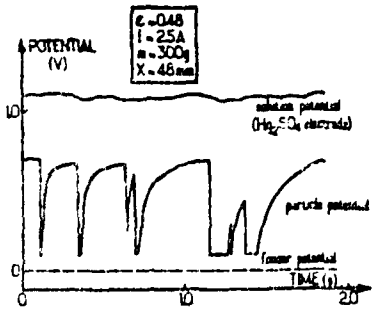

Figure 2

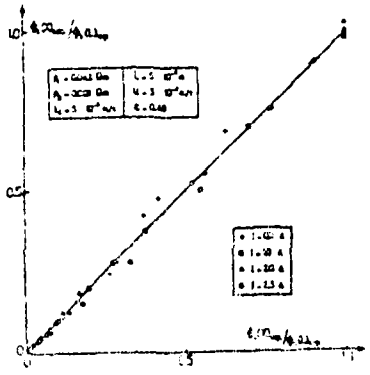

Figure 3

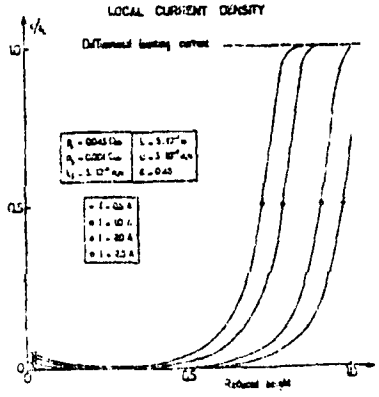

Figure 4

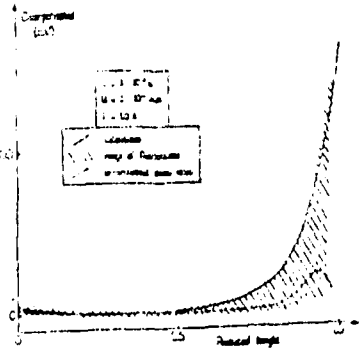

Figure 5

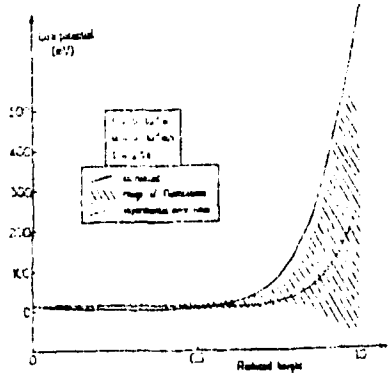

Figure 6

04120

MASS TRANSFER ENHANCEMENT IN EMULSION SYSTEMS

C. FURIET, G. VALENTIN and A. STORCK
Laboratoire des Sciences du Génie Chimique
CNRS-ENSIC, 1 rue Grandville
54042 NANCY CEDEX (FRANCE)

Electrochemical treatment of two-phase liquid systems has aroused interest in pilot and industrial scale organic electrosynthesis [1], especially for slightly soluble compounds. Although such processes show outstanding advantages (low-resistance electrolyte with respect to a non aqueous medium, high selectivity, improved current densities), little work has been reported on phenomena involved in these emulsions. At the present time, through lack of data and correlations, scale up requires substantial support in electrochemical engineering.

Turbulent mass transfer to an expanded metal electrode has been investigated in a new design of electrolyser with two immiscible liquid electrolytes. A spinning device, provided with four metal blades, was made suitable for both electrolysis and liquid dispersion. Operating parameters investigated were stirring rate (N), volume fraction (ε) and density (ρ) of the disperse organic phase. Mass transfer rates to the working electrode were obtained with the customary limiting current method by means of a rapid redox system (either ferri-/ferrocyanide or iodine/iodide, whether the electroactive species is present only in the aqueous phase or in both liquids). Organic phase was kept in contact with the aqueous electrolyte in a storage reservoir until just before suspended in the cell, so that liquid-liquid equilibrium was achieved.

Trial runs carried out for one-phase flow show attractive mass transfer rates k_d, over 10^{-4} m/s (Fig. 1), with regard to technical electrolysis cells.

In heterogeneous liquid systems, it was found that the limiting current densities were: (i) nearly the same in the case of an inert organic phase (toluene) lighter than the aqueous electrolyte (Fig. 2) (ii) at most 25% greater with emulsions of carbon tetrachloride (ρ=1.6) (Fig. 3). Something very similar was reported for turbulent and laminar flows in previous investigations [2,3,4,5]. Energetic heterogeneities induced by droplets in the vicinity of the hydrodynamic layer near the electrode may subsequently compress the underlying diffusion layer, that is, improved mass transfer is observed. Nevertheless, sufficient disturbance enhances mass transfer rates only if the dispersed phase possesses a higher density than the aqueous electrolyte. For such emulsions the enhancement factor is defined as the ratio of the diffusion limited current in two-phase electrolyte to the same quantity in droplet-free liquid. In Fig. 4 this factor, called E_j, is plotted vs carbon tetrachloride volume fraction. On log-log coordinates (Fig. 3), experimental data of k_d against N fall on a straight line whose slope does not change within more than 5% throughout the range of CCl_4 loads.

The constancy of slope implies that the impinging mechanism (through enhancement factor Ei) depends on the stirring rate only to a minor extent. It therefore seems that kinetic energy plays a relatively minute part in the former mechanism.

Whereas sole inert toluene drops have no great effect in homogeneous mass transfer (Fig. 2),electrochemically active iodine as a solute in the organic phase allows current densities to be increased some 3 times (Fig. 5). In terms of enhancement factor E_a *vs* volume fraction ε, the data suggested that E_a rises to a maximum for small ε values (Fig. 6). Such results are attributed to a "boundary layer replenishment": droplets supply the Nernstian diffusion layer where liquid-liquid equilibrium is shifted through aqueous iodine depletion at the electrode. Both lower liquid-liquid mass transfer and interfacial area (from droplet coalescence) and an electrode screening effect might account for the steadily decreasing values of E_a with increasing volumic fractions. It is worth mention that a "replenishment mechanism" may be assumed to occur if the droplets of the organic phase are able to penetrate through the hydrodynamic boundary layer to the Nernstian sublayer. Thus the latter mechanism cannot depend on the former, that is, compression of boundary layers.

References

1- H. Feess and H. Wendt. "Performance of two-phase electrolyte electrolysis" in "Technique of electroorganic synthesis", part III, ed. by N.L. Weinberg and B.V. Tilak. Technique of Chemistry, Vol. 5, Wiley & Sons Pub.,N.Y. (1982).
2- H. Feess, H. Wendt,J. Chem. Tech. Biotechnol.,1980, 30, 297-312.
3- R. Dworak, H. Wendt, Ber. Bunsenges. Phys. Chem.,1977, 81, 728-732.
4- H. Feess, H. Wendt, id., 1981, 85, 914-919.
5- P.Y. Lu, R.C. Alkire, J. Electrochem. Soc., 1984, 131 (5),1059-1067.

Figures caption

Fig. 1,2,3 and 5 : Mass transfer coefficients versus stirring rate
Fig. 4 and 6 : Enhancement factor versus dispersed volume fraction

Figure	Liquid system	Dispersed phase	Parameter
1	single phase	none	none
2	two-phase	inactive toluene	ε
3	two-phase	inactive CCl_4	ε
4	two-phase	inactive CCl_4	N
5	two-phase	active(tol.+I_2)	ε
6	two-phase	active(tol.+I_2)	N

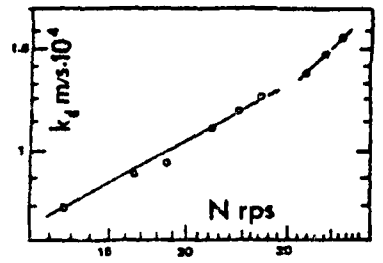

Figure 1.

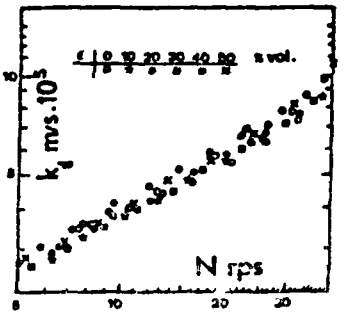

Figure 2.

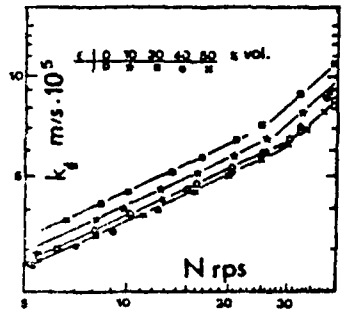

Figure 3.

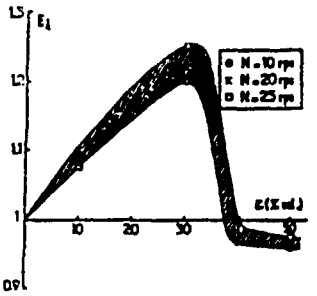

Figure 4.

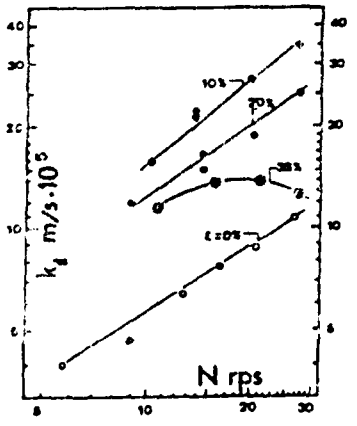

Figure 5.

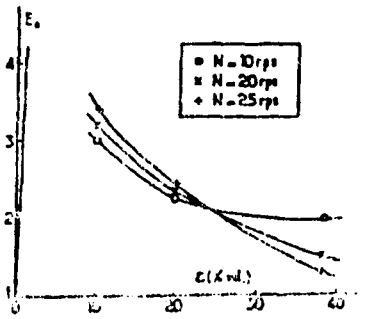

Figure 6.

04130

HYPOCHLORITE AND CHLORATE FORMATION

L.J.J. Janssen and E. Barendrecht
Laboratory for Electrochemistry, Department of Chemistry
Eindhoven University of Technology
P.O. Box 513, 5600 MB Eindhoven, The Netherlands

Little attention has been paid to chlorine generation at the anode in dilute NaCl solutions at a pH where hypochlorite and chlorate are produced industrially. The current efficiency for chlorine evolution strongly depends on the nature of anode material [1,2,3] and the effect of mass transfer for Cl^- ions. A divided electrolysis cell with a cation exchange membrane was used to reduce to a minimum the complexity of the investigation into the effect of various parameters on the hypochlorite and chlorate process. Experimental details are extensively given in [3].

The rate of the hypochlorite formation, n_3, and that of the chlorate formation, n_4, are determined as a function of electrolysis time, t_e, for a NaCl electrolysis at a platinum electrode (15.6 cm^2) in a NaCl solution with an initial chloride concentration, $c_{1,0}$. The pH of the bulk solution, the current density i, the flow rate of solution v, and the temperature of solution were kept constant during the electrolysis. From the rate of hypochlorite formation at $t_e = 0$ obtained by extrapolation, the efficiency of hypochlorite formation at $t_e = 0$, $\eta_{3,0}$ was determined. In Fig. 1 $\eta_{3,0}$ is plotted versus current density i. The efficiency of chlorate formation at $t_e = 0$, $\eta_{4,0}$, was practically zero. During the first periods of electrolysis, where the hypochlorite concentration c_3 was less than 40 mM, η_4 was proportional to c_3 and the chemical chlorate formation can be neglected.

From the slope of n_4/c_3 curve at low c_3 and mass transfer measurements where hypochlorite was reduced, it has been concluded that for the electrolytic conditions, given in the subscription of Fig. 1, the electrochemical formation of chlorate, n_4^e, is determined at $i > 1.5$ kA/m^2 by diffusion of hypochlorite only and at $i < 1.5$ kA/m^2 by both diffusion of hypochlorite and electrode kinetics of chloride oxidation.

It has been concluded that even at the highest $i = 4.5$ kA/m^2 the rate of chloride oxidation n_1 and so also the rate of chlorine formation n_2 and

the rate of hypochlorite formation n_3, where $n_1 = 2\ n_2 = 2\ n_3$, are determined by diffusion of chloride as well as electrode kinetics of chloride oxidation.

The effect of pH has been investigated in the pH range from 8 to 11.2. It has been found that at a low current density, viz. 0.39 kA/m^2, both the rate of hypochlorite formation and the rate of electrochemical chlorate formation are independent of pH.

The effect of NaCl concentration has been investigated in the concentration range from 17 to 1026 mol/m^3 at i = 4.09 and 0.64 kA/m^2. Deviating from the usual procedure for the series of experiments at i = 4.09 kA/m^2, after each period of electrolysis, the current was switched off for 5 minutes to homogenize the anolyte.

For both series of experiments $\eta_{3,0_2}$ increases with log $c_{1,0}$. The rate of chlorate formation at i = 0.64 kA/m^2 is practically zero and that at i = 4.09 kA/m^2 strongly depends on $c_{1,0}$, viz. 17 and 40 mol/m^3, the current efficiency for chlorate formation η_4 is practically independent on c_3 and $\eta_{4,0}$ is about 0.1.

At $c_{1,0}$ > 50 mol/m^3 η_4 decreases with increasing $c_{1,0}$ and becomes zero for $c_{1,0}$ higher than about 300 mol/m^3. At $c_{1,0}$ > 500 mol/m^3 η_4 is zero up to a fixed c_3 and thereafter η_4 increases with increasing c_3. In Fig. 2 η_3 and η_4 are plotted versus the average concentration of hypochlorite in a period, $c_{3,a}$. Moreover, in this figure the anode potential E_a, corrected for ohmic potential drop, is also given as a function of $c_{3,a}$. From Fig. 2 it follows evidently that the formation of chlorate and the decrease in the anode potential occur simultaneously. Consequently, the nature of the electrode surface has to be changed during the decrease in anode potential. To explain this change additional research is necessary.

References

1. A.T. Kuhn and C.J. Mortimer, J. of Applied Electrochemistry 2, 283 (1972).
2. M. Spasojevic, N. Krstajic and M. Jaksic, Surface Technology 21, 19 (1984).
3. L.J.J. Janssen and E. Barendrecht, to be published.

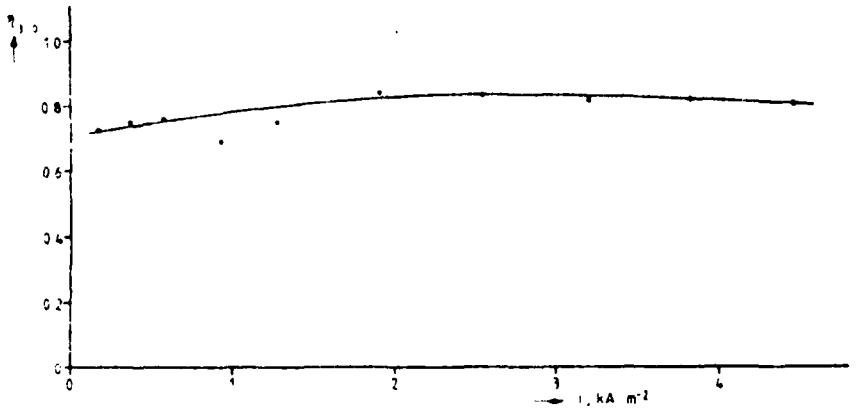

Fig. 1 The current efficiency of hypochlorite formation at the start of electrolysis is given as a function of current density.
Electrolysis conditions: anode: platinum sheet of 15.6×10^{-4} m^2; initial concentration of NaCl in anolyte: 513 mol/m^3; initial volume of anolyte: 1.15×10^{-3} m^3; pH: 8.5; temperature: 323 K; velocity of anolyte flow: 0.07 m/s.

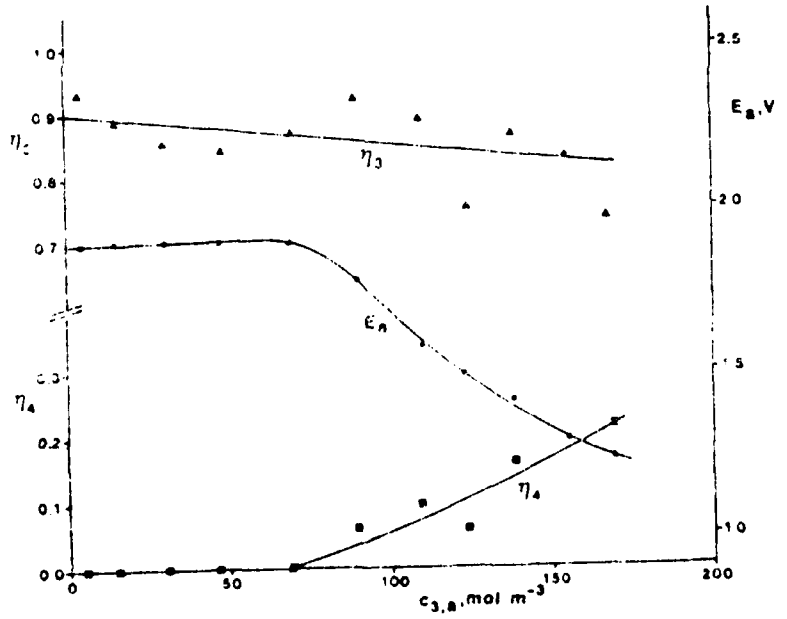

Fig. 2 The current efficiency for hypochlorite formation, η_3, and for chlorate formation, η_4, and the anode potential E_a vs. SCE are given as a function of the average concentration of hypochlorite during subsequent periods of electrolysis.
Electrolysis conditions: initial concentration of NaCl in anolyte: 1026 mol/m^3 and the other conditions as given at Fig. 1.

05010

THE KRAMERS - KRONIG RELATIONS AND EVALUATION OF IMPEDANCE FOR A DISK ELECTRODE

M.M. JAKŠIĆ and J. NEWMAN
Department of Chemical Engineering, University of California, Berkeley

To meet the original impedance function

$$Z(\omega) = Z_r(\omega) + i\, Z_i(\omega) = Z_\infty + z(\omega) + \frac{i\sigma}{\omega} \tag{1}$$

connected with the Kramers-Kronig (K-K) relations, where $z(\omega)$ represents an auxiliary function well behaved at $\omega = 0$ and vanishing as $\omega \to \infty$, and σ the constant strength of pole in impedance at zero frequency, the impedance can be considered as the Laplace transform,

$$z(s) = Z(s) - Z_\infty = \int_c^\infty e^{-st} f(t)\, dt \tag{2}$$

where

$$s = s_r + i\omega \tag{3}$$

a) There are no poles in the right half plane for passive (insulating) systems. b) There could be a simple pole at $s = 0$, and it is subtracted out (Fig. 1). c) $z(s)$ is analytic in the right half plane and thus subject to Cauchy integral formula,

$$\oint \frac{z(s)}{s - i\omega_0}\, ds = 0 \tag{4}$$

so that integration around the entire contour C (Fig. 1) leads to (whit ω and ω_0 interchanged).

$$\int_{-\infty}^{\infty} \frac{Z(\omega_0) - Z_\infty - \frac{i\sigma}{\omega_0}}{\omega_0 - \omega}\, d\omega_0 + \pi i \left| Z(\omega) - Z_\infty - \frac{i\sigma}{\omega} \right| = 0 \tag{5}$$

where $\int$ denotes the Cauchy principal value of the integral. Taking the real and imaginary parts separately, and suppressing i in argument, there follow the K-K relations for the disk electrode impedance[1,2]

$$Z_r(\omega) - Z_\infty = -\frac{1}{\pi} \int_{-\infty}^{\infty} \frac{Z_i(\omega_0) - \frac{\sigma}{\omega_0}}{\omega_0 - \omega}\, d\omega_0 \tag{6}$$

and

$$Z_i(\omega) = \frac{1}{\pi} \int_{-\infty}^{\infty} \frac{Z_r(\omega_o) - Z_\infty}{\omega_o - \omega} d\omega_o + \frac{\sigma}{\omega} \tag{7}$$

Taking the advantage of symmetry | $Z_r(\omega)$ is even in ω, and $Z_i(\omega)$ is odd in ω | and evaluating for positive frequencies, there further follows,

$$Z_r(\omega) - Z_\omega = -\frac{2}{\pi} \int_{o}^{\infty} \frac{\omega_o Z_i(\omega_o)}{\omega_o^2 - \omega^2} d\omega_o \tag{8}$$

and

$$Z_i(\omega) = \frac{2\omega}{\pi} \int_{o}^{\infty} \frac{Z_r(\omega_o) - Z_\infty}{\omega_o^2 - \omega^2} d\omega_o + \frac{\sigma}{\omega} \tag{9}$$

Notice that $\int_{o}^{\infty} d\omega_o/(\omega_o^2 - \omega^2) = 0$. According to the equivalent circuit (Fig.1), real and imaginary parts of the impedance can be related to the effective resistance and capacitance as follows

$$Z_r(\omega) = R_{eff}(\omega); \qquad Z_i(\omega) = -\frac{1}{\pi r_o^2 \omega C_{eff}(\omega)} \tag{10}$$

For an ideally polarizable electrode, where faradaic reactions cannot occur

$(J = (\alpha_a + \alpha_c)\, i_o F r_o / RT\kappa = 0)$

$$\sigma = -\frac{1}{\pi C r_o^2} \tag{11}$$

and at high frequencies[3], $Z_\infty = 1/4\kappa r_o$, so that with dimensionless frequency ($\Omega = \omega C r_o/\kappa$), tne K-K relations take on a more suitable form for the impedance at a disk electrode:

$$4\kappa r_o R_{eff}(\Omega) - 1 = \frac{8}{\pi^2} \int_{o}^{\infty} \frac{\frac{C}{C_{eff}(\Omega_o)} - \frac{C}{C_{eff}(\Omega)}}{\Omega_o^2 - \Omega^2} d\Omega_o \tag{12}$$

and

$$\frac{C}{C_{eff}(\Omega)} + \pi r_o^2 C\sigma = -\frac{\Omega^2}{2} \int_{o}^{\infty} \frac{4\kappa r_o R_{eff}(\Omega_o) - 4\kappa r_c R_{eff}(\Omega)}{\Omega_o^2 - \Omega^2} d\Omega_o \tag{13}$$

These allow the calculations of the effective resistance from the effective double-layer capacity, and vice versa, and any singularity at $\Omega_o = \Omega$ is effectively avoided. Thus no longer need for the Cauchy principal values. Two relations for capacitance and effective resistance,

$$\frac{C}{C_{eff(\Omega)}} = 1 + \frac{1}{8} \ln (1 + 0.646^8\ \Omega^2) \qquad (14)$$

and

$$4\kappa r_o\ R_{eff}(\Omega) - 1 = \frac{1}{\frac{1}{0.08076} + 2\Omega} = f(\Omega) \qquad (15)$$

were employed to approximate calculated values in the previous paper[3] to check the K-K relations for evaluation of impedance of the r.d.e. These relations brought in very good approximation the K-K relations for evaluation of capacitance from effective resistance, and vice versa. However, with residual function integrals for capacitance and effective resistance, the two relationships were brought into an ideal agreement (Fig. 2 and 3).

The present paper has shown that the impedance values from the disk electrode perfectly obey the K-K relations. One of the main benefits of the K-K relations is the ability to calculate the values of the effective resistance from the capacitance, and vice versa. The interpretarion of impedance by the K-K relations depends on the functions used for the capacitance and effective resistance: the higher the accuracy, the better the agreement. However, to calculate any individual value of the capacitance, or the effective resistance, from the K-K relations, one has to calculate the integrals for the entire range of frequency from zero to infinity. Normally, such calculations, as in the paper, have to proceed through the approximate relations, including the residual function integrals.

REFERENCES

1. H.A. Kramers, Phys. Z., 30, 522 (1929)
2. R. de L. Kronig, J. Opt. Soc. Am., 12, 547 (1926)
3. J. Newman, J. Electrochem. Soc., 117, 198 (1970)

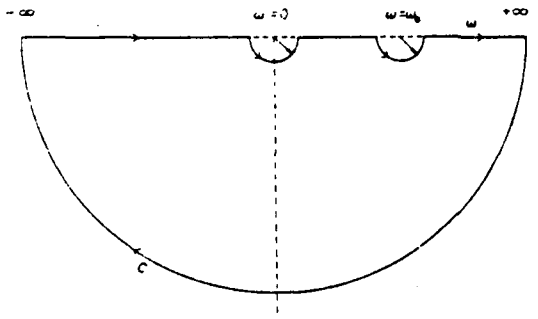

XBL 683-996

Figure 1a. Complex impedance diagram with the real and imaginary components and simple poles

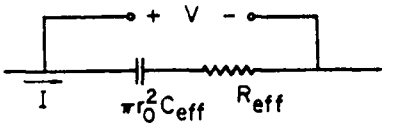

XBL594-2406

Figure 1b. Defining equivalent circuit of the disk system, where C_{eff} and R_{eff} can be regarded as the effective double-layer capacity and the effective resistance of the electrolytic solution, respectively, if faradaic reactions are of negligible importance. More generally, R_{eff} and C_{eff} are merely alternative ways of referring to the real and imaginary parts of the impedance.

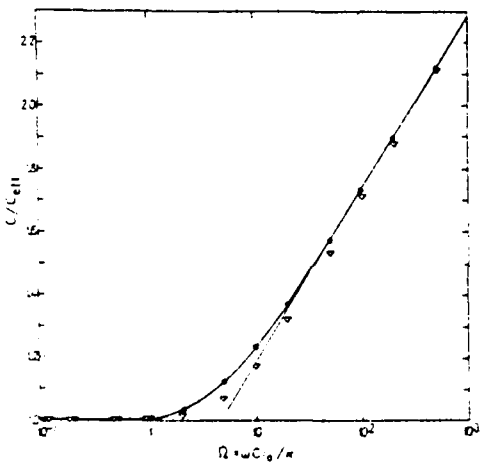

Figure 2. Frequency dependence of the effective capacity on a smooth disk
- the absence of faradaic reactions ($J = 0$)
-- values from reference 3,
▽ - values calculated from equation (34),
——— high-frequency asymptote

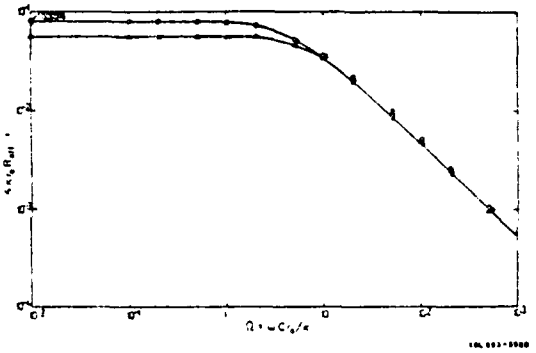

XBL 683-9980

Figure 3. Frequency dependence of the effective resistance for $J = 0$
-- values from reference 3,
Δ - first approximation from the K-K relation,
○ - values calculated from the K-K relation including the residual function integration

05020

ELECTROCHEMICAL BEHAVIOUR OF HYDROUS IRON HYDROXIDE FILMS IN ALKALINE SOLUTION

M.E. Vela, J.R. Vilche and A.J. Arvia
Instituto de Investigaciones Fisicoquímicas Teóricas y Aplicadas
INIFTA. C.C. 16, Suc. 4, 1900 La Plata, ARGENTINA

INTRODUCTION

Most of the conclusions related to the time-dependent structures of the oxi-hydroxide surface layer on iron, were obtained from massive iron electrodes where the electrodissolution contribution of the base metal interferes[1-5]. This interference can be overcame by using platinum electrode covered with a precipitated hydrous iron hydroxide layer. In this way, the influence of any structural change of the iron hydroxide layer on the kinetics of the different electrochemical reactions can be voltammetrically followed.

EXPERIMENTAL

The experimental set-up and electrode preparation procedure are the same already described in previous publications[6,7]. The precipitation of iron hydroxide on the clean platinum electrode was made by alternate and repetitive immersing the substrate in z M $FeSO_4.7\ H_2O$ (solution I), $0.002 \leq z \leq 0.2$, and in x M KOH + y M K_2SO_4 (solution II), $0.01 \leq x \leq 1$ and $0 \leq y \leq 0.33$. The number of immersions (n) in each solution was $5 \leq n \leq 100$ and the immersion time was set at 5 s. The average thickness of the iron hydroxide layer was varied accordingly to both n and the concentration of the precipitating solutions. Voltammetric runs at 25°C were performed in the following electrolyte solutions: 0.01 M KOH + 0.33 M K_2SO_4 (solution A); 1 M KOH (solution B); borate-boric acid buffers (solution C). Potentials in the text are referred to the NHE scale.

RESULTS

The voltammetric response of the precipitated iron hydroxide electrode in base solutions depends on the precipitation conditions, on the parameters defining the electrical perturbation, and on the number of potential cycles. The charge decrease in the negative potential region of the voltammograms during repetitive potential sweeps can be associated with the HER taking place on Pt in the presence of the hydrous iron hydroxide layer. As the cathodic switching potential ($E_{s,c}$) becomes more negative the HER contribution increases and the voltammograms become more complex.

When the perturbation programme includes a potential holding at $E_{s,c}$ during the time τ before continuing the potential cycle, the stabilized voltammogram obtained in solution A is attained faster as τ increases. This time, however, depends on

the amount of active material on the electrode. Therefore, a certain cathodization is required to achieve the complete electro reduction of the surface layer at the fixed $E_{s,c}$ values.

The composition of the precipitating solutions influences the electrochemical characteristics of the thin iron hydroxide layers. For a constant n, the amount of active material increases with the concentration z of Fe^{+2} ion in the precipitating solution. Consequently the voltammetric peaks become broader and the voltammograms approach those resulting with massive iron. For different values of n the accumulation of the anodic (Q_a) and the cathodic (Q_c) charge vs z plots, exhibit a maximum. For a constant z the voltammetric charge increases linearly with n, the slope of the straightline being proportional to log $c_{Fe^{2+}}$. As z decreases this relationship extends over a greater range of n. On the other hand, beyond a certain value of either n or z the accumulation of charge decreases.

The voltammetric response of thick iron hydroxide layer (n=100) depends to a great extent on v, and eventually on $E_{s,c}$ and $E_{s,a}$.

The voltammogram covering from 0.24 V to -1.16 V approaches that already described for massive iron electrodes under comparable condition[3].

The increase in pH probably favours a lower water content in the iron hydroxide layer, which turns its electroreduction at a constant potential more difficult, and for this purpose, the presence of water within the layer is required.

DISCUSSION

The voltammetric behaviour of thin precipitated iron hydroxide electrodes in solution A in the -0.6 V to -0.4 V range is influenced by the extent of the contribution of the HER at Pt, depending on the cathodization conditions and on the amount of iron hydroxide. The kinetic characteristics of the anodic peak related to the electrooxidation of hydrogen depend whether a thin or thick iron hydroxide electrode is considered. For thin layer electrodes (n=5) the voltammogram implies only the surface H-adatom electroreduction reaction, while for thick layer electrodes (n=100) the molecular hydrogen electrooxidation is to a large extent controlled by diffusion of the reactant from the solution side.

The voltammetric conjugated peaks at ca -0.4 V corresponds to the overall reaction Fe(II) ⇌ Fe(III) + e which is also influenced by the local decrease in pH produced by the preceding reaction at -0.6 V.

As $E_{s,c}$ is made more negative a greater degree of electroreduction of the iron hydroxide layer is accomplished and under certain conditions, the relative contribution of the HER decreases. Hence, a better definition of both anodic and cathodic peaks is observed. The cathodization at $E_{s,c}$ causes the formation of a poorly hydrous Fe_3O_4 film which is rather difficult to reduce further. On the other hand, as $E_{s,a}$ is gradually fixed at increasingly positive potentials the contribution of the O-electroadsorption/electrodesorption reactions on Pt becomes more important.

The results from thick iron hydroxide layers suggest that the pH in the iron hydroxide precipitation reaction becomes largely determined by the hydrolysis and the ionic equilibria involving ferrous and ferric species in solution.

Both total charge vs. $p[Fe^{2+}]$ and peak charge vs. n plots can be explained by admitting that two competing reactions take place, namely the formation and dissolution of the hydrated hydroxide layer. The counterbalance of these reactions should depend considerably on the local precipitation pH at the iron hydroxide layer. For small $p[Fe^{+2}]$ the local precipitating pH is apparently determined by the KOH concentration in solution II. For large $p[Fe^{+2}]$ values, it should be influenced by the concentration of $FeSO_4$ in solution I.

Thick iron hydroxide layers (n=100) probably consist of a double structure made of an inner layer which is mainly responsible of the ageing effects and an outer layer, which is associated with the diffusional resistance appearing in the overall electrochemical reaction.

In conclusion, the results obtained with the precipitated iron hydroxide electrodes show that the voltammetric response of the hydrous iron hydroxide layer remains practically the same whether it is formed on Fe or previously precipitated on Pt. The layer structure, particularly the outer part, depends on the solution pH, which to same extent is determined by the ionic species present in the solution including OH^- and Fe^{+2} ions and their insertion into the hydrous iron hydroxide film.

REFERENCES

1. D.D. Macdonald and D. Owen, J.Electrochem.Soc., 120, 317 (1973).
2. D. Geana, A.A. Miligy and W.J. Lorenz, J.Appl.Electrochem., 4, 337 (1974).
3. R.S. Schrebler Guzmán, J.R. Vilche and A.J. Arvia, Electrochimica Acta, 24, 395 (1979); J.Appl.Electrochem., 11, 551 (1981).
4. L.D. Burke and O.J. Murphy, J.Electroanal.Chem., 109, 379 (1980).
5. D.M. Drazic and Chen Shen Hao, Electrochim.Acta, 27, 1409 (1982).
6. V.A. Macagno, J.R. Vilche and A.J. Arvia, J.Appl.Electrochem., 11, 417 (1981).
7. M.E. Vela, J.R. Vilche and A.J. Arvia, in Passivity of Metals and Semiconductors (M. Froment, ed.), Elsevier, Amsterdam, pp. 59-65 (1983).

ACKNOWLEDGEMENT

INIFTA is a Research Institute jointly established by the Universidad Nacional de La Plata, the Consejo Nacional de Investigaciones Fisicoquímicas Teóricas y Aplicadas and the Comisión de Investigaciones Científicas de la Provincia de Buenos Aires.

05030

RECENT DEVELOPEMENT OF CASIDIE PROGRAM FOR CALCULATION AND SIMULATION OF ELECTROCHEMICAL IMPEDANCE DIAGRAMS

J.P. DIARD , B. LE GORREC , C. MONTELLA

Laboratoire d'Energétique Electrochimique L.A. CNRS n° 265.
Ecole Nationale Supérieure d'Electrochimie et d'Electrométallurgie
Domaine Universitaire B.P. 75, 38402 SAINT MARTIN d'HERES - FRANCE -

This program has been designed for Hewlett-Packard items HP 9816, HP 9826 and HP 9836 . It is written in Basic 2. The diagrams and comments can be edited on HP 7470 A plotter. It is available from SOLEA-TACUSSEL company.

With that program, for a selection of memorized electrochemical reactions mechanisms, one can now :

-study the evolution of the steady state current with potential electrode

-study the evolution of impedance diagrams as a function of the electrode polarisation ;

-study the elementary impedances of which the electrode impedance is constitued ;

-compare between themselves elementary impedances : transfert resistances, concentration impedances, etc.....;

-study the influence of the different kinetic parameters of the studied mechanisms (transfert coefficient, kinetic constant, electroactive species concentration) on the impedance diagram shape and on the importance of its different loops.

-study the evolution of the modulation of electroactive species with frequency.

The memorized library include several mechanisms : redox mechanism, redox mechanism EC/CE, electrosorption mechanism, cathodic reduction mechanism (Heyrovsky mechanism), cathodic reduction mechanism, (Volmer-Tafel mechanism), metal dissolution-passivation mechanism, two metal corrosion mechanisms, electrointercalation mechanism.

After entering of the program and selection of a mechanism, one proceed using a conversational mode. Starting from a set of typical values of the mechanism various parameters, the user can modify one or several values of the kinetic parameters : transfert coefficient, kinetic constant, electroactive species concentration as well as the calculation conditions of the impedance diagrams, electrode potential, studied frequency range , etc...

The study of the evolution of the impedance diagrams as a function of the electrode potential is made easier using an ortho-scaled display of the standardized electrode impedance. The frequency notation of 3-D diagrams is optional. The study of the elementary impedances can be effected in the Nyquist or in the Bode plane. Some examples of edited results are given by Figs 1,2.

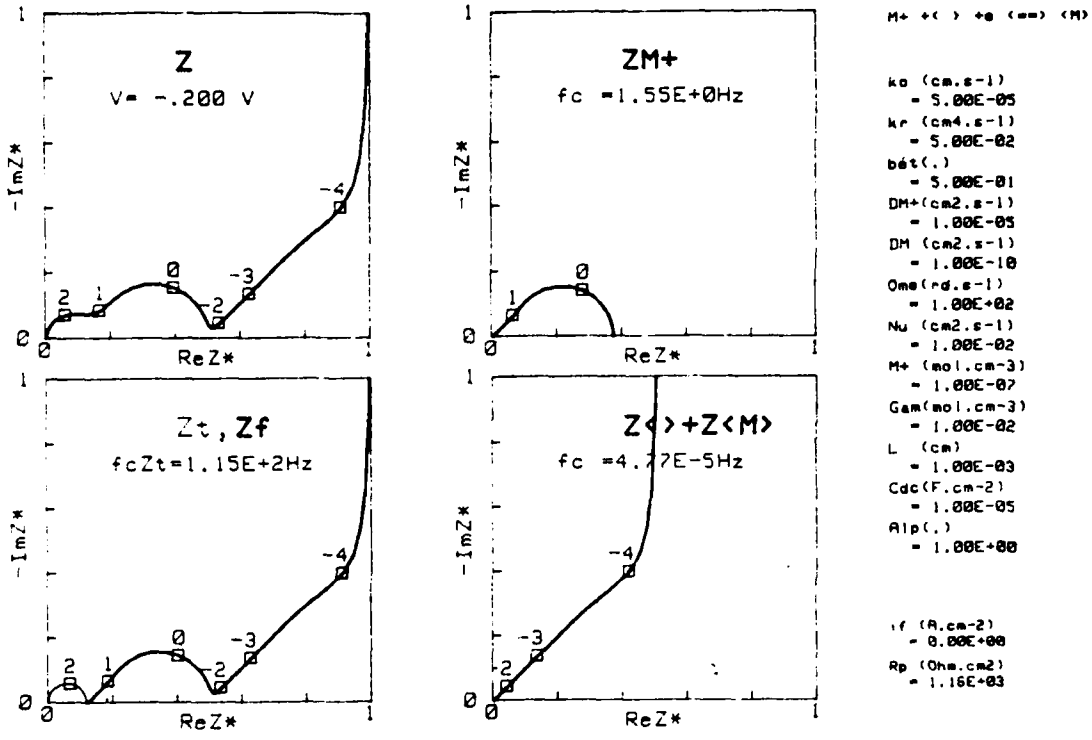

Fig. 1 : Impedance diagrams for an intercalation mechanism.

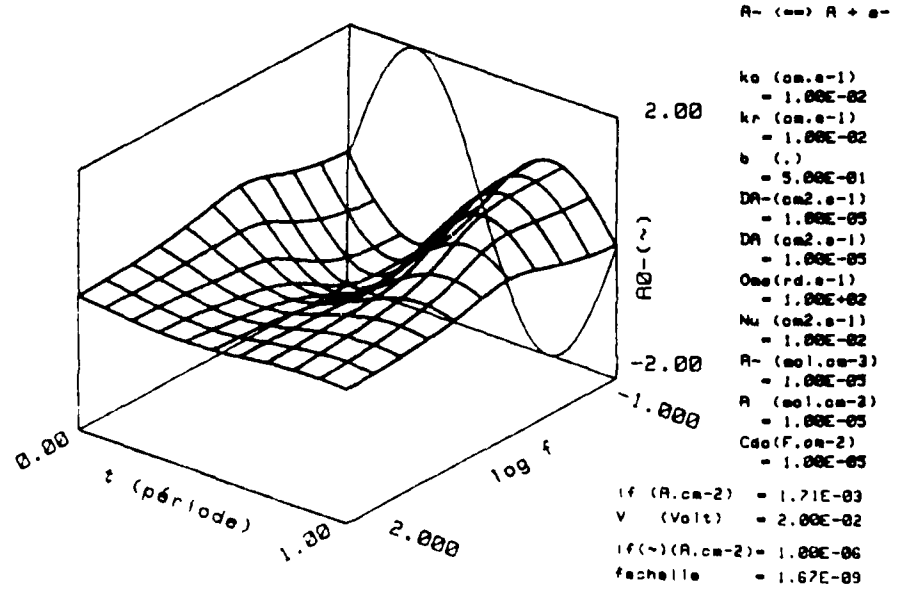

Fig. 2 : Evolution of the modulation of the interfacial A^- concentration for a redox mechanism.

05040

KINETICS OF THE MANGANESE DIOXIDE ELECTRODE STUDIED WITH ROTATING RING DISC ELECTRODES

A. Grzegorzewski and K. E. Heusler
Abteilung Korrosion und Korrosionsschutz
Institut für Metallkunde und Metallphysik
Technische Universität Clausthal
D 3392 Clausthal-Zellerfeld, Federal Republic of Germany

The electrodeposited γ-phase of manganese dioxide exists in a wide range of compositions /1/. The main components are manganese, oxygen and hydrogen. If one describes the composition by $MnO_x.yH_2O$, it appears that there is some coupling between the degrees x of oxidation and y of hydration. Therefore, the less general formula $MnOOH_z$ is sometimes used. As a logical consequence of the variability of the composition of phases containing more than one component, there must be at least as many parallel currents between the phase and a neighbouring phase as there are components. In principle, each of the component currents must involve the transfer of complexes containing the components in different ratios /2 /. At γ-manganese dioxide in an aqueous solution of some manganese(II) salt the component currents are of an electrochemical nature. In the simplest case one expects the transfer of manganese ions, oxygen ions and hydrogen ions. In addition there may be neutral currents in which e.g. water is transferred.

A manganese dioxide film on an "inert" metal like Pt or Au is considered. The oxide exchanges only electrons with the metal. In complete equilibrium the electrochemical potential of the ions is the same at both sides of the oxide/solution interface. Electronic equilibrium within the oxide and across the metal/oxide interface defines the chemical potentials of the components. One may consider the oxide electrode as a manganese electrode exchanging manganese ions, as an oxygen electrode exchanging oxygen ions or as a hydrogen electrode exchanging hydrogen ions. If one applies e.g. a positive overpotential, all the component currents become anodic, i.e. manganese ions and hydrogen ions dissolve from the oxide and oxygen ions enter it. The composition of the oxide changes towards a higher degree of oxidation and the chemical potentials of the components as well as the respective equilibrium potentials change accordingly. For an oxide in which the metal ions are in a higher state of oxidation than in the neighbouring electrolyte, the shift of the equilibrium potential between metal in the oxide and metal ions in the electrolyte is larger than the shift of the equilibrium potential between oxygen in the oxide and water /2, 3/. Consequently, there is a potential region where an anodic current can flow for one component and a cathodic current for another component. Although the degree of oxidation can be changed by any of the 3 component ion currents,

steady state deposition or dissolution of the oxide is possible only by transfer of oxygen and manganese. The steady state electrode potential is in between the oxygen and manganese equilibrium potentials, respectively, as determined by a ratio of the component currents necessary to deposit or dissolve an oxide of a specific composition at the applied total current:

$$ {}_3Mn^{2+} + 2\ {}_2e^- = {}_2Mn \qquad (1) $$

$$ x\ ({}_3H_2O = {}_2O + 2\ {}_3H^+ + 2\ {}_2e^-) \qquad (2) $$

$$ Mn^{2+} + x\ H_2O = MnO_x + 2x\ H^+ + 2(x-1)\ e^- \qquad (3) $$

The lower indices in front of the symbols indicate the oxide (2) and the electrolyte (3), respectively. In principle, for any total curent density the degree x of oxidation and the equilibrium potentials with respect to the components are different. Therefore, useful information on the kinetics and the mechanism of the component reactions can only be obtained by separating the total currents into the component currents.

Experimental

A rotating ring-disc electrode was used to separate the hydrogen ion current from the manganese ion current the sum of which is the total current. The hydrogen ion current results from reaction (2) and from proton transfer. Separation of the latter component currents was achieved by mass measurements with a quartz frequency balance, but results will be reported elsewhere. A manganese dioxide film was deposited onto the Pt disc at 0.2 mA/cm² from the electrolyte used for later experiments. Usually the film thickness was about 70 nm corresponding to a charge of 50 mC. The base electrolyte was a 1 M sodium sulfate solution. The pH-value was adjusted with sulfuric acid or sodium acetate/acetic acid buffer, and $MnSO_4$ was added. Most measurements refer to pH 4 and a manganese sulfate concentration c = 0.05 M. The temperature was always kept at 40°C. At the Au ring electrode changes of the diffusion limited current of hydrogen evolution due to the disc current were measured.

Results

Even for thin manganese dioxide films the equilibrium potential was established only after several hours. The two processes occuring are a decrease of the degree of oxidation and structural relaxation. The equilibrium potentials changed with pH and c as expected from theory /4/, i.e. $dE/d\,pH = (x/(x-1)) \cdot (RT/F)(\ln 10)$ or about 140 mV/pH at constant c and $dE/d\,\lg c = (1/2(x-1))(RT/F)(\ln 10)$ or about 39 mV/decade at constant pH. The electrode capacitance obtained from galvanostatic or from potentiostatic pulse measurements was between 30 and 40 µF/cm² which is close to the expected double layer capacitance at a fairly smooth surface. The Ohmic resistance of about 1 Ohm cm² was located in the electrolyte and not in the oxide. The transient polarization curves obtained immediately after charging the capacitance yielded exchange current densities of the order 0.1 mA/ cm² increasing with the concentration of manganese sulfate.

steady state deposition or dissolution of the oxide is possible only by transfer of oxygen and manganese. The steady state electrode potential is in between the oxygen and manganese equilibrium potentials, respectively, as determined by a ratio of the component currents necessary to deposit or dissolve an oxide of a specific composition at the applied total current:

$$ {}_3Mn^{2+} + 2\ {}_2e^- = {}_2Mn \qquad (1) $$

$$ x\ ({}_3H_2O = {}_2O + 2\ {}_3H^+ + 2\ {}_2e^-) \qquad (2) $$

$$ Mn^{2+} + x\ H_2O = MnO_x + 2x\ H^+ + 2(x-1)\ e^- \qquad (3) $$

The lower indices in front of the symbols indicate the oxide (2) and the electrolyte (3), respectively. In principle, for any total curent density the degree x of oxidation and the equilibrium potentials with respect to the components are different. Therefore, useful information on the kinetics and the mechanism of the component reactions can only be obtained by separating the total currents into the component currents.

Experimental

A rotating ring-disc electrode was used to separate the hydrogen ion current from the manganese ion current the sum of which is the total current. The hydrogen ion current results from reaction (2) and from proton transfer. Separation of the latter component currents was achieved by mass measurements with a quartz frequency balance, but results will be reported elsewhere. A manganese dioxide film was deposited onto the Pt disc at 0.2 mA/cm² from the electrolyte used for later experiments. Usually the film thickness was about 70 nm corresponding to a charge of 50 mC. The base electrolyte was a 1 M sodium sulfate solution. The pH-value was adjusted with sulfuric acid or sodium acetate/acetic acid buffer, and $MnSO_4$ was added. Most measurements refer to pH 4 and a manganese sulfate concentration c = 0.05 M. The temperature was always kept at 40°C. At the Au ring electrode changes of the diffusion limited current of hydrogen evolution due to the disc current were measured.

Results

Even for thin manganese dioxide films the equilibrium potential was established only after several hours. The two processes occuring are a decrease of the degree of oxidation and structural relaxation. The equilibrium potentials changed with pH and c as expected from theory /4/, i.e. $dE/d\,pH = (x/(x-1)) \cdot (RT/F)(\ln 10)$ or about 140 mV/pH at constant c and $dE/d\lg c = (1/2(x-1))(RT/F)(\ln 10)$ or about 39 mV/decade at constant pH. The electrode capacitance obtained from galvanostatic or from potentiostatic pulse measurements was between 30 and 40 µF/cm² which is close to the expected double layer capacitance at a fairly smooth surface. The Ohmic resistance of about 1 Ohm cm² was located in the electrolyte and not in the oxide. The transient polarization curves obtained immediately after charging the capacitance yielded exchange current densities of the order 0.1 mA/ cm² increasing with the concentration of manganese sulfate.

05050

OXYGEN REDUCTION ON IRON IN NEUTRAL SOLUTION

D.M. Dražić and S.K. Zečević
Faculty of Technology and Metallurgy, University of Belgrade, P.O.Box 494, and Institute of Electrochemistry ICTM, 11001 Belgrade, Yugoslavia

The reduction of oxygen on iron is the cathodic process occuring during the corrosion of steel in aerated media and the understanding of the reduction mechanism is of great practical importance for corrosion studies.

In this work, the O_2 reduction has been studied on pure iron (Puratronic) in neutral and near neutral buffered solutions of pH ranging from 4 to 10, containing various anions (Cl^-, SO_4^{2-}, PO_4^{3-}, borate, citrate, bicarbonate and phthalate). A rotating disk electrode has been employed. The rotation rate varied from 400 to 4900 rpm.

Prior to each experiment the electrode surface was grinded with 120 emery paper, washed in ethanol by using an ultrasonic cleaner, then rinsed with triply distilled water and left for 1 hour in the cell to stabilize the corrosion potential. Cathodic polarization curves were then recorded by a linear potential sweep technique with the scan rate of 10 mV/min.

In Fig. 1. are presented cathodic polarization curves for O_2 reduction in 0.5M NaCl buffered solution pH 10 at two rotation rates. The well defined S-shaped curves and the dependence of the reduction current on rotation rate indicate that the process is under mixed activation-diffusion control at all rotation rates examined. After the diffusion correction had been made, the Tafel like plots, as those in Fig. 2., were obtained. The Tafel slopes varied between -80 and -110 mV/dec, showing no dependence on rotation rate. At potentials in the limiting current region the system obeys Lewich equation $i - w^{1/2}$, indicating pure diffusion control (see Fig.3.). The number of trans-

fered electrons was calculated to be 4. The necessary data were taken from ref. 1. This means that O_2 is reduced completly to OH^- ions. The reaction order of O_2 was found to be about 0.7 (see Fig. 4.)

In thecase of 0.5M Na_2SO_4 buffered solution pH 10, the situation is quite different than that of chloride solution. At lower rotation rates and near corrosion potentials the i-E curves are rather steep and almost linear indicating the dominant influence of the diffusion control. At more cathodic potentials the current increases but with significant polarization. At higher rotation rates the mixed activation-diffusion kinetics is observed over the entire potential region and the polarization curves are taking the S shape. However, even at very negative potentials near to that for H_2 evolution, the kinetics for O_2 reduction is very slugish and a well defined plateau of the limiting current is not observed. The limiting currents could be only estimated and they are found to be about 3/4 of those observed in chloride solution of the same pH. Further more, the system shows a deviation from the Lewich mass-transfer equation being larger at higher rotation rates. The number of transfered electrons was estimated to be between 3 and 4. This means that the O_2 reduction in sulfate solution is not complete giving a significant amount of H_2O_2 as the final product of the electrochemical reduction.

At pH 4-6 (citrate and phthalate buffers) O_2 reduction is under pure diffusion control irrespective of the presence of Cl^- or SO_4^{2-} ions, whereas in phosphate buffered solutions the O_2 reduction is almost completly inhibited.

References:

1. K.E. Gubbins and R.D. Walker, Jr., J. Electrochem. Soc., 112 (1965) 469.

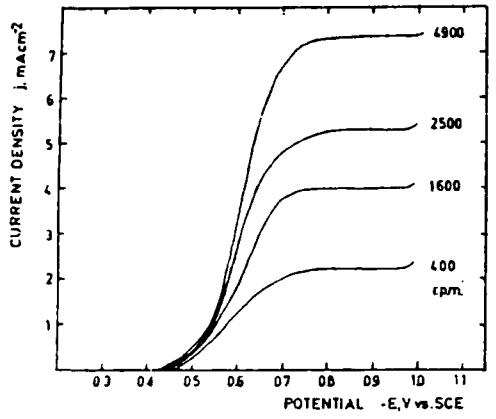

Fig. 1.

Cathodic polarization curves for O_2 reduction on iron in 0.5M NaCl buffered solution pH 10 (0.025M bicarbonate buffer, oxygen saturated). Sweep rate 10 mV/min. Rotation rate is indicated.

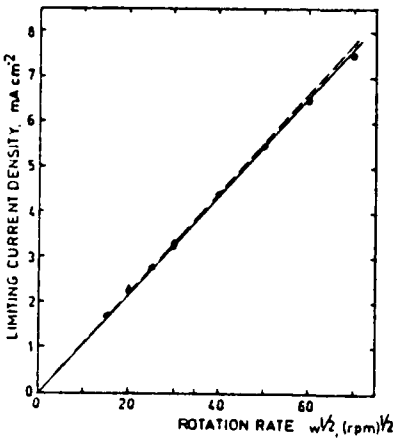

Fig. 3.

Dependence of limiting current of O_2 reduction on rotation rate in 0.5M NaCl buffered solution pH 10; solid line-experimental, dashed line-calculated for n=4.

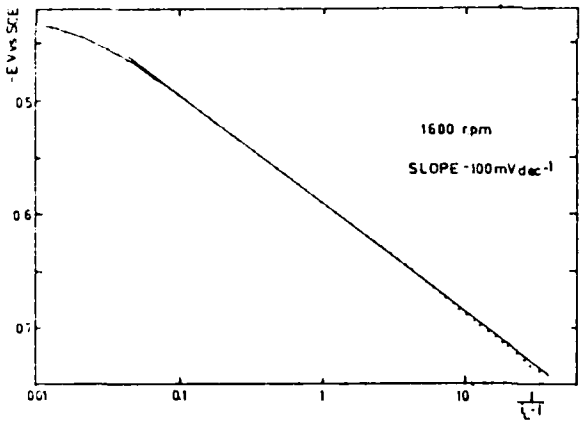

Fig. 2.

Tafel plots of data from Fig. 1. corrected for diffusion.

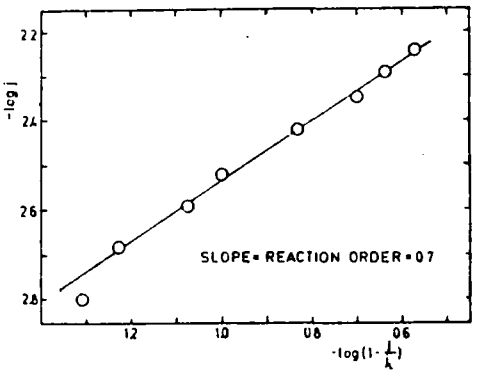

Fig. 4.

Dependence log i - log(1-i/i_L) for O_2 reduction in 0.5M NaCl buffered solution pH 10, at -0.6 V vs. SCE.

05060

SYNERGETIC ELECTROCATALYTIC EFFECTS OF COMPOSITE d-METALS CATALYSTS FOR THE HIDROGEN EVOLUTION REACTION ON PLATINUM METAL SUBSTRATES

M.RISTIĆ[1)], S.ŠTRBAC[1)], B.KOSANOVIĆ[2)], N.KRSTAJIĆ[3)], T.GROZDIĆ[1)], and M.M.JAKŠIĆ[2)]

University of Belgrade

1) Institute of Food Techology and Biochemistry, Faculty of Agriculture, Belgrade, Yugoslavia

2) Institute of Chemical Power Sources Belgrade, Zemun Polje, Yugoslavia

3) Faculty of Techology and Metallurgy, Belgrade, Yugoslavia

On the basis of the Brewer valence bond theory for bonding in metals and intermetallic phases there has been pointed out[1] that whenever metals of the left-half of the transition series that have empty or half filled vacant d-orbitals are alloyed with metals of the right-half of the transition series that have internally paired d-electrons not available for bonding in the pure metal, there arises well pronounced synergism in electrocatalysis for the hydrogen evolution reaction (h.e.r.), which often exceeds individual effects of precious metals and each other (the synergism condition) and approaches the reversible behaviour within the wide range of current density. There has been pointed out[1] the parallelism between the stability of Brewer intermetallic phases and the activity for the h.e.r., and thence the predictions between Brewer's multiphase diagrams and electrocatalytic effects resulting from such composite catalysts. In such a context there would be of interest to point out that recent measurements[2] of excess partial molal free energies for bonding of zirconium with d-metals of the right-half of the transition series at infinite dilution show the same type of curve, the same positions of maximum and the same trend as the individual d-metal activities for the h.e.r. in H.Kita[3] interpretation when related to the position in the Periodic

Table, or in other words to the electronic configuration. Such a syllogism in alloy stability and electrocatalytic activity testifies that the same average electron configuration provides in both issues the same trend and behaviour.

It has now been shown that the Brewer combinations of d-metals in the composite electrocatalysts not only exceed noble metals in their activity for the h.e. r., but dramatically improve electrocatalytic properties of all platinum metals employed as the substrate. There has been pointed out the most particularly electrocatalytic properties of the Mo-Co and Mo-Ni pairs upon all precious metal substrates as deposited in situ during the electrolytic process of hydrogen evolution. Molybdenum was added as 10^{-2}M molybdate solution, whereas nickel and cobalt were employed as tris-complexes of ethylenediamine three-chloride salts in amounts of 10^{-3}M solutions. The electrocatalytic effect has been dramatically pronounced even on palladium substrate (Fig.1) which is otherwise extremly emphasized amongst individual transition metals for the h.e.r. The peak of the composite catalyst deposition which is clearly delineated follows a dramatic jump in the activity for the h.e.r. that exceeds all so far scanned features for hydrogen evolution.

There has also been shown the promoting effect of some cations with rather filled d-orbitals (Cd, Tl, Ag). Substrates were only shortly immersed in corresponding solutions of low concentration (10^{-4}M) and then rinsed with water stream providing therefore only adsorbed amount of promoting species. The effect has been well pronounced on non-precious metal substrates (Fig. 2 and 3), but ceased to appear upon noble metals, or has been shadowed there. It perhaps could help to explain the promoting effect of d-metals with filled d-orbitals. Brewer[4] recently also pointed out such a promoting effect of lead for production of some most specific intermetallic phases of composite transition metal alloys. It seems that an optimal d-electron configuration of palladium and platinum when employed as substrates is enough to induce the promoting effect similar to the effect of cations with filled d-orbitals in an adsorbed amount upon other transition metal substrates for develepment of an extremly active electrocatalytic coating of the Mo-Co and Mo-Ni pairs (cf.(5,6)).

Polarization characteristics as obtained this way by in situ addition of rather common and cheap d-metal ionic species in rather low amounts exceed any so far scanned electrocatalytic effect for the h.e.r. Such catalytic features are provided for rather long life-time of about 120 days, or more, with simple reactivation by identical in situ addition of small amount of activating species.

R e f e r e n c e s

1) M.M. Jakšić, Electrochim.Acta, 29, 1539 (1984)

2) J.K.Gibson, L. Brewer and K.A. Gingerich, Metal.Trans., 15A, 2075 (1984)

3) H.Kita, J.Res.Inst.Catalysis, 21, 200 (1973)

4) L. Brewer, J.Chem.Educ., 61, 101 (1984)

5) N.V. Korovin, N.I. Kozlova, O.N. Savel'eva, T.V.Lapshina and M.V. Kumenko, J.Res.Inst.Catalysis, 29, 17 (1981)

6) B.E. Conway, H.Angerstein-Kozlovska, M.A. Sattar and B.V. Tilak, J.Electrochem.Soc. 130, 1825 (1983).

Fig. 1. Individual and synergetic electrocatalytic effects obtained upon palladium substrate: 1 - the substrate features, 2- the effect of tris-Co-complex and 3 - - dual Co-Mo composite effect upon palladium.

Fig. 2. Synergetic and promating effect obtained upon nickel substrate: 1 - synergetic Mo-Co effect, 2 - synergetic (Mo-Co) and promoting (Cd) effect for the h.e.r.

Fig. 3. Individual, synergetic and promoting electrocatalytic effects obtained on nickel substrate (downwards)

1 - Polarization characteristics of niskel in 40% NaOH,

2 - Individual electrocatalytic effect of tris-Co-complex upon nickel for the h.e.r.

3 - Mutial synergetic (Mo-Co) and promoting (Cd) electrocatalytic effecrt.

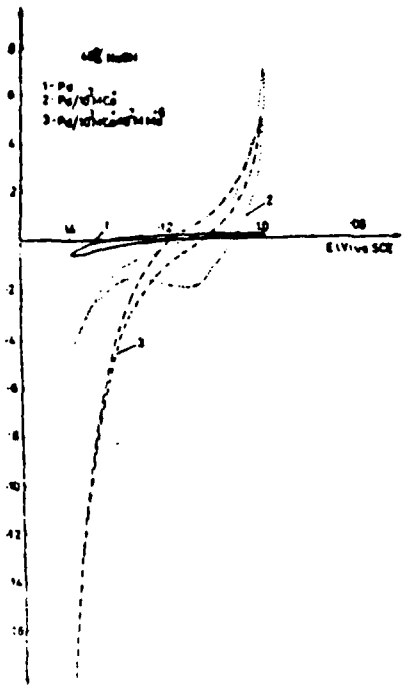

Fig. 1

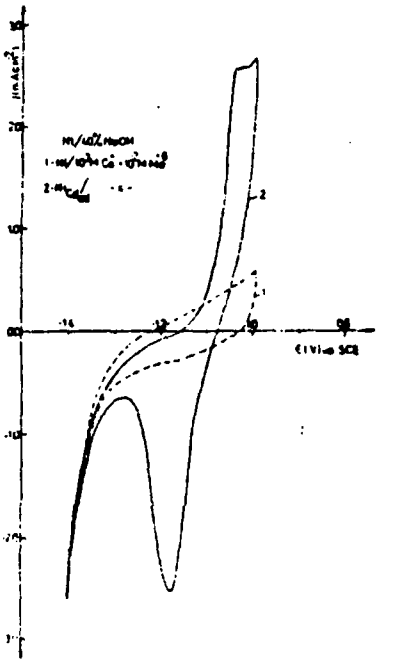

Fig. 2

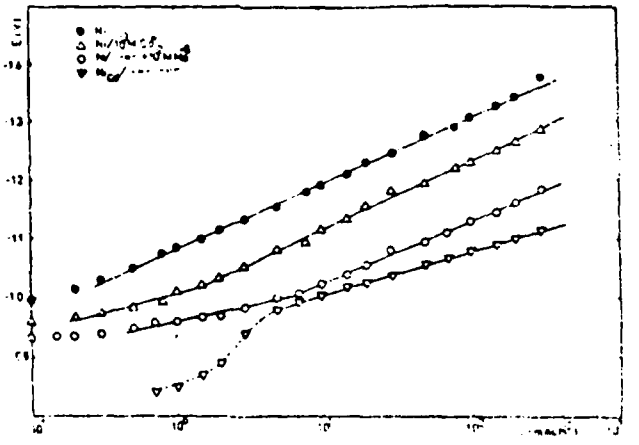

Fig. 3

05070

CYCLIC VOLTAMMETRY OF $MnSO_4$ IN MOLTEN Li_2SO_4-K_2SO_4 EUTECTIC MIXTURE

M.V.Šušić, S.V.Mentus and M.M.Dojčinović

Institute of Physical Chemistry, Faculty of Science, Belgrade, and Department of Catalysis, Institute of Chemistry, Technology and Metallurgy, Belgrade, Yugoslavia

Molten alkali sulphates are interesting as ionic solvents thanks to their excellent thermal stability. Their electrochemical properties have been examined by many authors[1-5]. It was accepted that the oxidation of SO_4^{2-} group, according to the reaction:

$$SO_4^{2-} - 2e^- = SO_3 + \tfrac{1}{2}O_2$$

limits the anodic polarization of platinum electrode [2,4,5] in these melts. According to Liu[2], cathodic reactions are complicated, and cathodic products are mainly alkali sulphites and sulphides.

From Fig.1a (dashed line) one sees that cathodic products hold some time on the cathode and can be oxidized in the course of reverse polarization at -1.8 V.

$MnSO_4$ dissolved in molten Li_2SO_4-K_2SO_4 eutectic mixture gives a well defined reduction wawe, starting at -1.76V.Cathodically deposited manganese dissolves in the course of reverse polarization, with zero current potential at -1.84 V. The cathodic deposition of manganese is accompanied with the appearance of the green colour in the melt. By approximate chemical analysis of the melt after cathodic polarization limited to -1.9 V, the sulphides were detected. That means that metallic manganese reduces the melt; the proposed reaction may be as follows:

$$3Mn + SO_4^{2-} = MnS + 2Mn^{2+} + 4O^{2-}$$

Significant cathodic current which starts considerably before the potential of manganese deposition is probable due to catalytic reduction of the melt:

$$SO_4^{2-} + 2e^- = SO_3^{2-} + O^{2-}$$
$$SO_3^{2-} + 4e^- = S + 3O^{2-}$$

Anodic peak starting at -0.8 V which appears in the presence of SO_3^{2-} ions (Fig.1b) becomes stronger in the presence of Mn^{2+} ions, but its appearance depends on no previous deposition of metallic manganese. That means that Mn^{2+} ions enable the increased concentration of reduction products appeared otherwise in the presence of SO_3^{2-} ions.

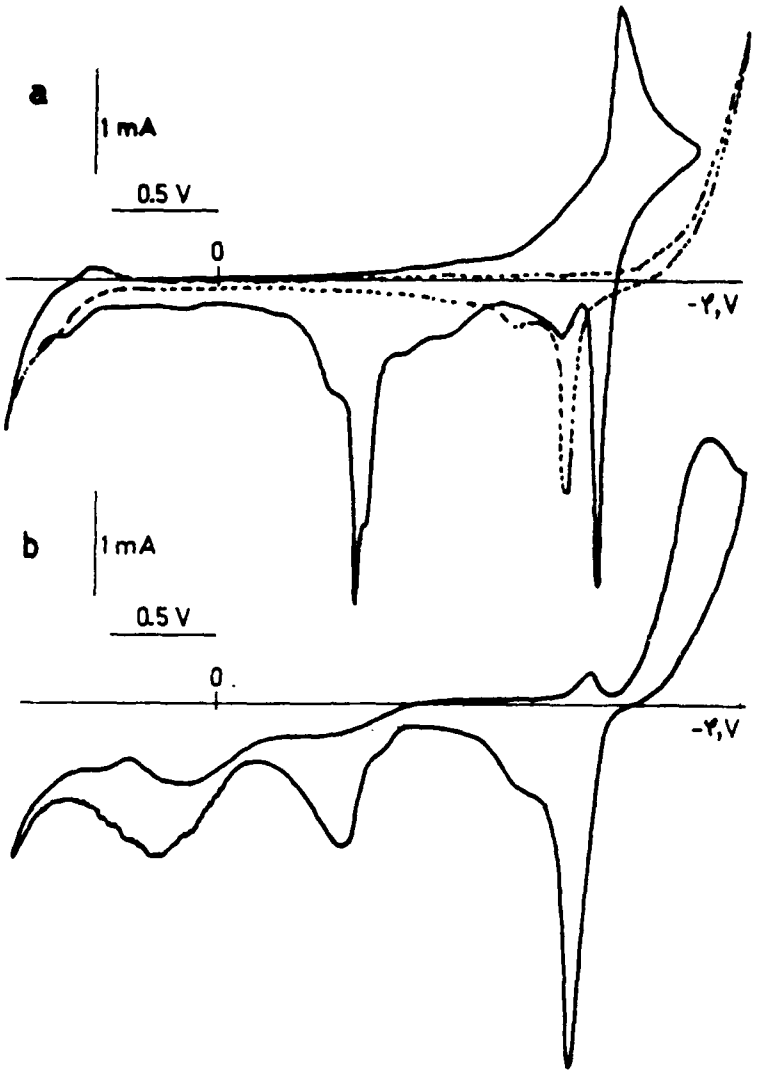

Fig.1. Cyclovoltammograms in molten Li_2SO_4-K_2SO_4 eutectic mixture at 540 °C on Pt working electrode, with polarization rate of 100 mV/s with respect to 1M Ag/Ag^+ reference electrode. a) ground melt (dashed line) and 1M solution of $MnSO_4$ (full line); b) 0.5 M solution of K_2SO_3.

Catalytic activity of Mn^{2+} ions in sulphate melts was confirmed recently in course of the investigation of $SO_2 \rightarrow SO_3$ conversion[6].

REFERENCES:

1. H. vom Hove and F.Müller, Z.anorg.Chem., 253,251(1947)
2. C.H.Liu, J.Phys.Chem., 66,164(1962)
3. K.E.Johnson and H.A.Laitinen, J.Electrochem.Soc., 110,314(1963)
4. B.W.Burrows and G.J.Hills, Electrochim.Acta, 15,445(1970)
5. C.A.C.Sequeira and M.G.Hocking, Electrochim.Acta, 23,381(1978)
6. M.V.Šušić, M.M.Dojčinović and S.V.Mentus, Bull.l'Acad.Serbe Sci.Arts, Classe Sci. nat. et mathem., LXXXII, 37(1982)

05080

DIAGRAMMES D'IMPEDANCE DE MODELES ELECTROCHIMIQUES EN COUCHE MINCE

G. BARRAL, J.P. DIARD, B. LE GORREC, C. MONTELLA

Laboratoire d'Energétique Electrochimique L.A. CNRS n° 265
Ecole Nationale Supérieure d'Electrochimie et d'Electrométallurgie
Domaine Universitaire B.P. 75, 38402 SAINT MARTIN D'HERES FRANCE

Les perspectives d'application de l'électrochimichromisme, de l'électro-insertion et de l'électrocatalyse redox dans les domaines de la visualisation électrooptique, des générateurs électrochimiques, du stockage de l'hydrogène et de l'électrosynthèse organique expliquent l'intérêt porté à l'étude des matériaux d'électrode en couche mince.

Des modèles diffusionnels simples sont généralement utilisés pour décrire le comportement des systèmes physiques précédents [1-5]. Leurs réponses à une commande potentiostatique étant identiquement nulles quelle que soit la tension imposée à l'électrode, il est nécessaire pour obtenir des informations complémentaires d'utiliser des méthodes d'étude transitoire, par exemple les méthodes de mesure d'impédance [6-8].

Le comportement des modèles étant linéaire pour une perturbation de faible amplitude autour d'un point de fonctionnement statique, l'expression de l'impédance faradique Z_f^* peut être établie selon la méthode introduite par Gerischer et Mehl [9] puis développée par Schuhmann [10] et Epelboin et coll. [11] et l'impédance d'électrode Z^* est calculée en supposant la capacité de double couche C_{dc}^* placée en parallèle avec l'impédance faradique.

Les impédances faradiques peuvent être décomposées en impédances élémentaires de transfert de charges et de concentration des espèces électroactives [12]. La comparaison des résistances limites en basse fréquence de ces impédances élémentaires et de l'impédance globale d'électrode mène à la construction de diagrammes de zones d'observation des formes limites de diagrammes d'impédance [13] et permet ainsi de préciser les conditions de mesure des paramètres cinétiques de systèmes supposés correctement décrits par les modèles étudiés.

Deux exemples sont donnés sur les figure 1 et 2. Le premier (fig.1) est relatif à l'étude d'un modèle de transfert électronique dans un film polymère greffé plan ou celle d'un modèle redox dans une cellule dissymétrique à couche mince d'électrolyte. Le deuxième (fig. 2) est tiré de l'étude d'un modèle d'électroinsertion cationique dans un film mince de matériau à conduction mixte. D'autres modèles, tel le mécanisme d'absorption de l'hydrogène, peuvent donner lieu à des études semblables.

1 - E. LAVIRON, J. Electroanal. Chem., 112 (1980) 1.

2 - C.P. ANDRIEUX et J.M. SAVEANT, J. Electroanal. Chem., 111 (1980) 377.

3 - M. ARMAND, Thèse, Grenoble (1978).

4 - S. ATLUNG, K. WEST et T. JACOBSEN, J. Electrochem. Soc., 126 (1979) 1311.

5 - G. BARRAL, J.P. DIARD et C. MONTELLA, Electrochim. Acta, 30 (1985) 585.

6 - C. HO, I.D. RAISTRICK et R.A. HUGGINS, J. Electrochem. Soc.,127 (1980)343.

7 - D.R. FRANCESCHETTI et J.R. MAC DONALD, J. Electrochem. Soc.,129 (1982)1754.

8 - G. BARRAL, J.P. DIARD et C. MONTELLA, Electrochim. Acta, 29 (1984) 239.

9 - H. GERISCHER et W. MEHL, Z. Elecktrochem., 59 (1955) 1049.

10 - D. SCHUHMANN, Thèse, Paris (1965).

11 - I. EPELBOIN et M. KEDDAM, J. Electrochem. Soc., 117 (1970) 1052.

12 - J.P. DIARD,B. LE GORREC et C. MONTELLA, J. de Chimie Physique (à paraître).

13 - J.P. DIARD,B. LE GORREC et C. MONTELLA, J. Electroanal. Chem.,161 (1984)235.

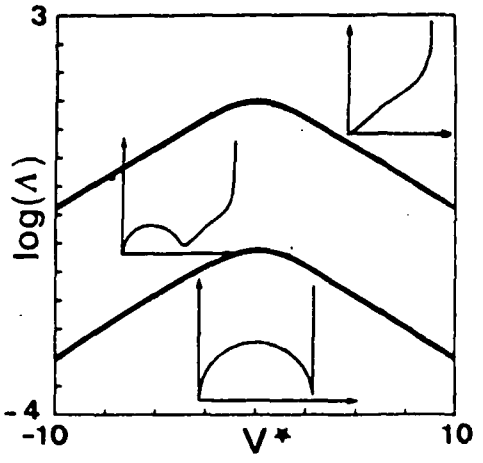

Figure 1

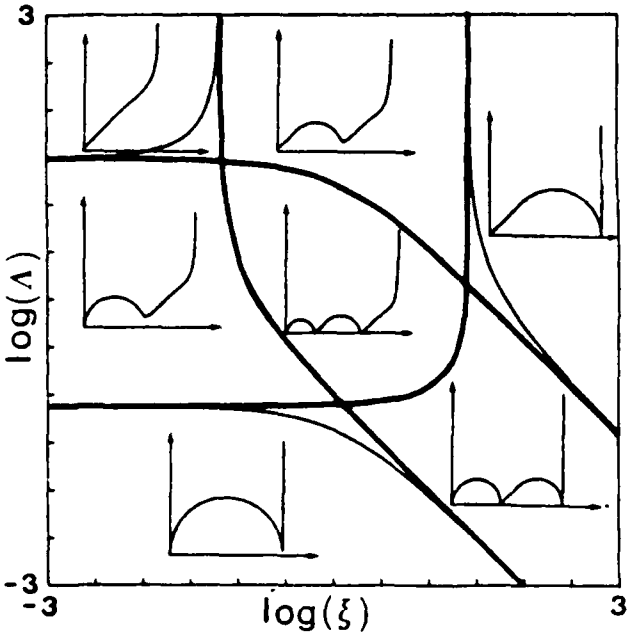

Figure 2

Diagrammes de zones d'observation des formes limites de diagrammes d'impédance tracés dans le plan de Nyquist des électrochimistes lorsque les impédances élémentaires sont totalement découplées en fréquence pour :

- un modèle de transfert électronique dans un film polymère greffé (fig. 1),

- un modèle d'électroinsertion cationique dans un matériau à conduction mixte (fig. 2) (coupe pour V* = 0).

ELECTROCHEMICAL BEHAVIOUR OF SOME POLYPYRIDINE COMPLEXES OF COBALT(III) IN APROTIC SOLVENTS

S.ROFFIA,C.PARADISI and V.CONCIALINI
Istituto Chimico "G.Ciamician",University of Bologna,Bologna, Italy.

The diffuse interest in the spectroscopic and electrochemical behaviour of metal polypyridine complexes is motivated primarily by the proven utility of several of these complexes in photochemical water cleavage[1-3].

Along this line of research, a few years ago an electrochemical study of the behaviour of several diimine complexes has been undertaken[4-7]. As a continuation of these investigations, the present work concerns the electrochemical behaviour of the following polypyridine complexes of Co(III) in acetonitrile(ACN) and dimethylformamide (DMF): $|Co(AA)_2(Cl)_2|^+$ and $|Co(AA)_2(CN)_2|^+$, where AA is 2,2'-bipyridine(bpy) and 1,10-phenantroline(phen).

In polarography at 20°C in ACN the complexes $|Co(AA)_2(Cl)_2|^+$ present a first combined anodic-cathodic wave, followed by other four reduction waves. In particular fig.1 shows the polarogram recorded on bpy complex(solid line). In the same figure the voltammetric curve recorded with a platinum electrode with periodical renewal of the diffusion layer in the potential range +0.5- - 0.5 V (vs SCE aq.) is also reported(dotted line).

As far as process I is concerned, the strong difference between the voltammetric curves recorded on different electrode materials indicates that the electrode material itself is involved in the process. In particular, the similarity between the anodic-cathodic wave of the complex and the anodic dissolution wave of mercury in the presence of Cl^-, along with the reducibility of the complex on platinum in the potential range bracketing the anodic-cathodic wave, suggest that process I is ascribable to a parallel ECE mechanism, in which the complex, reduced through a one-electron process, liberates two molecules of chloride ions, which are in turn responsible for the anodic dissolution of mercury. The presence of chloride ions in solutions electrolyzed at controlled potentials corresponding to the cathodic plateau of wave I and the coulometric results are in agreement with the above mechanism. Processes II and III should be due respectively to the reduction of bis and tri bpy complexes formed in the first and second waves, in line with results previously reported for these complexes in the same medium[8]. Finally, process IV can confidently attributed to the reduction

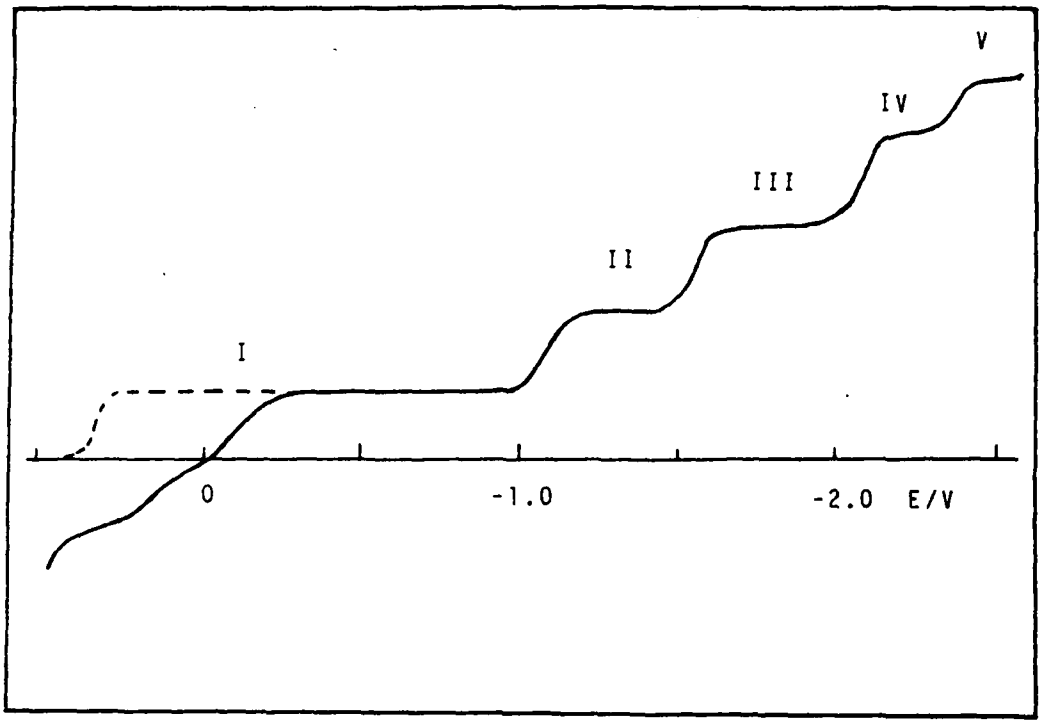

Fig.1- Polarograms of $5 \cdot 10^{-4}$ M $[Co(bpy)_2(Cl)_2]^+$ solution of 0.1 M $(C_2H_5)_4ClO_4$. Working electrodes: (——) dropping mercury electrode; (-----) Pt electrode with periodical renewal of the diffusion layer. Temperature: 20°C.

of bpy liberated in the preceding wave, while the last process seems to be attributable to a bis complex of Co(-I). The use of DMF istead of ACN gives rise to a more complicated pattern since the solvent itself apparently becomes involved in the electrode process.

As far as the electrochemical behaviour of the $[Co(AA)_2(CN)_2]^+$ complexes are concerned, in the two solvents utilized at 20°C, three reduction processes ascribable to the formal reduction of cobalt down to zero oxidation state are observed, after which multielectron waves, possibly due to the reduction of free bpy, appear.

For these species the three reduction processes of cobalt considered are not under normal conditions(ambient temperature and moderate sweep rate in cyclic voltammetry) one-electron re-

versible processes, since both the involvement of the solvent in the electrode mechanism, and the presence of adsorption phenomena concur in making the overall picture more complicated.

References

1.V.Balzani,F.Bolletta,M.T.Gandolfi and M.Maestri, Top.Curr.Chem. 75,1(1978).
2.J.S.Connolly,Ed.,"Photochemical Conversion and Storage of Solar Energy",Academic Press,New York,1981; J.Rabani,Ed.,"Photochemical Conversion and Storage of Solar Energy",Weizman, Jerusalem,1982;M.Grätzel,Ed.,Energy Resources through Photochemistry and Catalysis, Academic Press,New York,1983.
3.K.Kalyanasundaram, Coord.Chem.Rev.,46,159(1982).
4.S.Roffia and M.Ciano,J.Electroanal.Chem.,(a)77,349(1977);(b) 87,267(1978);(c)100,809(1979).
5.S.Roffia,M.Ciano and M.A.Raggi, J.Electroanal.Chem.,108,69(1980)
6 S.Roffia,V.Concialini,C.Paradisi and M.Ciano,J.Electroanal. Chem., 161,305(1984).
7.C.A.Bignozzi,S.Roffia and F.Scandola,J.Am.Chem.Soc.,107,1644 (1985).
8.B.C.Willett and F.C.Anson,J.Electroachem.Soc.,129,1260(1982).

05100

COMPORTEMENT INDUCTIF DU MECANISME DE VOLMER-HEYROVSKY COMPARAISON AVEC LE SYSTEME H^+/H_2 SUR NICKEL

J.P. DIARD , R. DURAND , B. LEGORREC , S. MAXIMOVITCH

Laboratoire d'Energétique Electrochimique L.A. CNRS n° 265
Ecole Nationale Supérieure d'Electrochimie et d'Electrométallurgie
Domaine Universitaire B.P. 75, 38402 SAINT-MARTIN d'HERES FRANCE

La réaction de Volmer-Heyrovsky est un cas particulier de réaction de transfert de deux électrons en deux étapes monoélectroniques. Elle s'écrit pour le cation A^+ :

$$A^+ + s + e \rightarrow A,s$$

$$A^+ + A,s + e \rightarrow A_2 + s$$

Les calculs cinétiques d'impédance montrent l'influence des deux constantes retour k_{o1} et k_{o2} des deux étapes électrochimiques. Il est nécessaire de supposer que les valeurs des deux facteurs de symétrie sont différentes pour que les diagammes d'impédance présentent un caractère inductif si l'on considère que les deux réactions électrochimiques sont irrenversables ($k_{o1} = k_{o2} = 0$). On peut observer successivement lorsque l'électrode est polarisée vers les surtensions cathodiques des diagrammes inductifs puis capacitifs. Ce comportement inductif s'observe (figure 1) pour des tensions d'électrodes supérieures à :

$$V = \frac{RT}{F(b_2-b_1)} \quad \text{Log} \frac{k_{r1}}{k_{r2}}$$

L'évolution des diagrammes d'impédance avec la tension d'électrode peut être plus compliquée lorsque les deux étapes électrochimiques sont renversables (figure 2). On peut observer successivement lorsque l'électrode est polarisée vers les surtensions cathodiques des diagrammes capacitifs, puis inductifs, puis de nouveau capacitifs.

Les figures 1 et 2 ont été réalisées à l'aide du logiciel de calcul et de simulation d'impédances électrochimiques CASIDIE 1.

Le comportement expérimental de la réaction de dégagement de l'hydrogène sur une électrode de Nickel polie préoxydée est présenté sur la figure 3. L'évolution des diagrammes d'impédance avec la tension d'électrode est incompatible avec l'hypothèse d'irrenversabilité des deux réactions électrochmiques. Un comportement capacitif doit être expérimentalement observable à des tensions d'électrode plus négatives en accord avec les prévisions théoriques du mécanisme de Volmer-Heyrovsky.

1 J.P. DIARD , B. LE GORREC , C. MONTELLA
soumis à J. de Chimie Physique

2 S. MAXIMOVITCH
Thèse Grenoble 1983

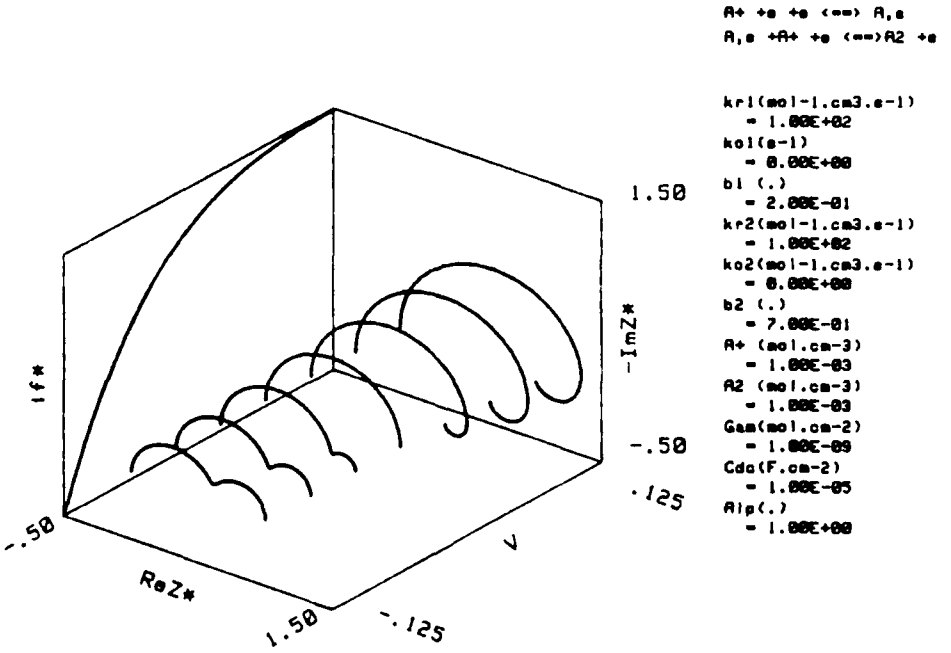

Fig. 1 : Evolution des impédances avec la tension d'électrode cas des réactions irrenversables

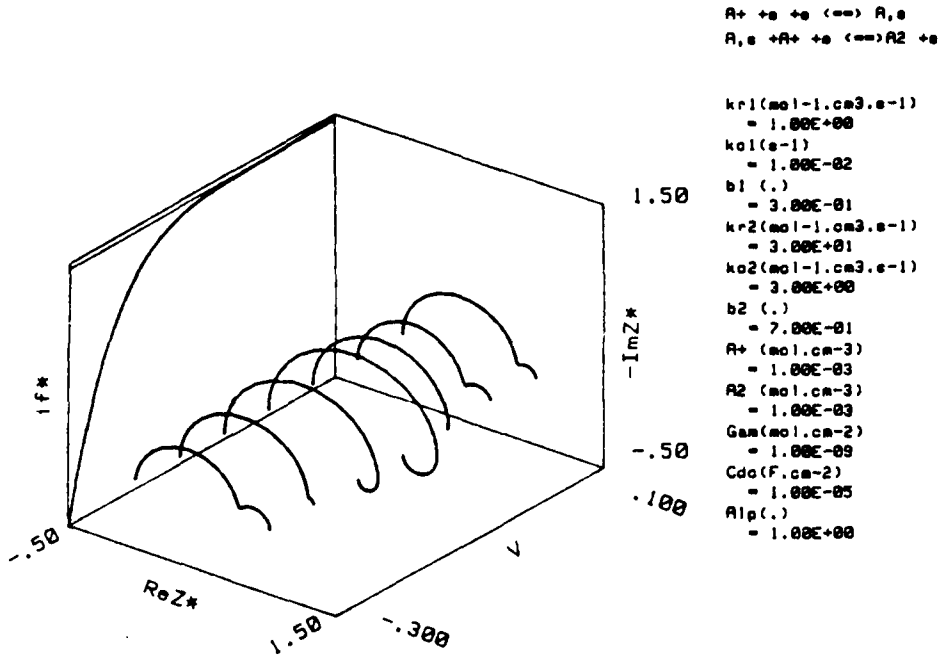

Fig. 2 : Evolution des impédances avec la tension d'électrode cas des réactions renversables

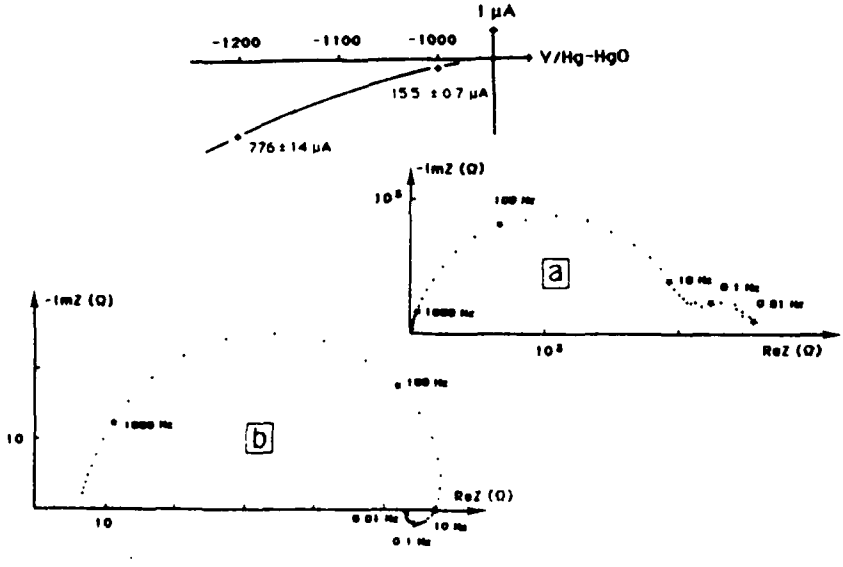

Fig.3 : Réaction de dégagement de l'hydrogène
Diagramme d'impédance de NYQUIST à diverses tensions . Electrode de nickel pré-oxydée 5 mn à V= 400 mV/Hg-HgO : T=20 °C: KOH 1M: S=0.125 cm^2
a- V= -1000 mV/Hg-HgO = 70 mV/ERH
b- V= -1200 mV/Hg-HgO = -270 mV/ERH

05110

STUDY OF DIGITAL SIMULATION IN SECOND ORDER TECHNIQUES FOR ELECTROCHEMISTRY

M.S. LORENZO, P.CAÑAS, C.MONTEMAYOR, J.M.VARA and E.FATAS
Departamento de Electroquímica. Facultad de Ciencias. Universidad Autónoma de Madrid. 28049 MADRID. Spain.

INTRODUCTION

The so-called second order techniques are reaching, during the last years, an increasing importance, either to investigate the fundamentals of electrode processes or for analytical purposes[1]. These techniques are based on the rectifying properties of the electrode-electrolyte interface. Despite of the recent progress, it never became very popular, probably because of the theoretically treatments are rather difficult. The numerical methods used in digital simulation seems to be an adequate tool for the study of complex electrode processes by means of second order techniques.

This paper intents the digital simulation of the ouput of an electrodic system, responding to a modulated input. Among the differents kinds of modulation we have studied the so-called D.B.S.,[2] which seems to offer most potentialities. We have considered the simple case (diffusion followed by charge transfer), and the mechanismes EC and CE.

RESULTS AND DISCUSSION

Among the differents algorithms used in digital simulation of electrode processes, we have make use of the explicit method, which despite to be one of the simplest, it leads to rather good results[3]. Along the calculations, a semi-infinite plane electrode has been considered.

Because of the non-linearity of the electrodic system[4], the response to a input modulated signal will be composed of several harmonics, being the most interesting one, the corresponding to a frequency double of the low frequency of the modulated input signal. We have obtained the response to the different frequencies by fitting the numerical flux obtained in the simulation, to a Fourier serie by the least-square method.

Figure 1 shows the representation of the amplitude of the ouput flux corresponding to the low frequency $(\Delta E_m=(I_{LF}^2+Q_{LF}^2)^{1/2}$, vs. d.c. polarization potential, for a simple electrode reaction (diffusion and charge transfer). The values of the parameters used in the simulation are: $\alpha=0.5$, $A_1=0.02$ V., $D_O/D_R=4/5$ $w_H/w_L=100$, $k°=0.1$, 1 and 10 $cm^2.s^{-1}$ for curves 1,2 and 3 resp.

It can be seen that all the curves show a minimum at potentials very near to E_o, and the higher the standard rate constant is, sharper is the shape of the minimum. Also it can be seen that the value of the amplitude at $2w_L$ depend strongly of the value of the standard rate constant for all the d.c. potentials. Generally, this results are in good agreement with the experimentally obtained ones, especially in the galvanostatic case[2].

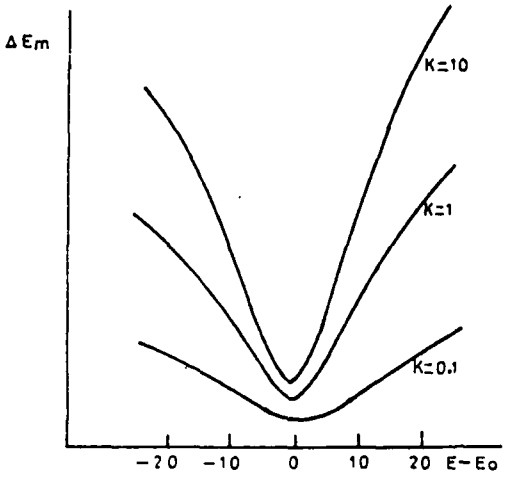

Fig. 1

Fig. 2 shows the representation of ΔE_m, calculated by digital simulation, vs. the d.c.potential for the simple case and for the mechanismes CE and EC.Remarkable diferences has been observed between the three cases. The minimun of the amplitude respect to E_o for EC mechanism, and at negative potentials for CE mechanism. Also the shape of the curves is quite different for the three cases.

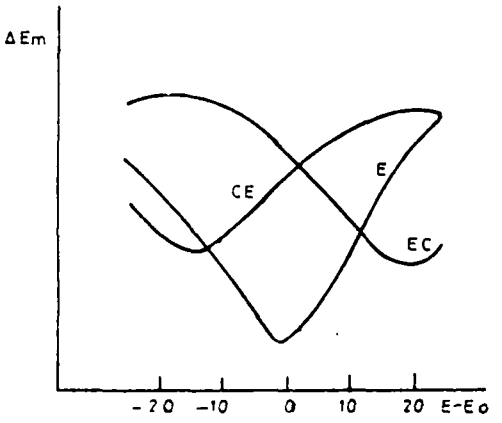

Fig. 2

From these facts it can be deduced that the digital simulation method in combination with demodulation polarography could be a technique specially suitable and sensible, for elucidation of mechanismes and determination of parameters of rather complex electrode processes.

LITERATURE

1. F.Van der Pol, M.Sluyters-Rehbach and J.H.Sluyters, J.Electroanal. Chem., 62(1975)281.
2. M.Sluyters-Rehbach, J.Struys and J.H.Sluyters,J.Electroanal. Chem., 143(1983)61.
3. Digital Simulation in Electrochemistry. Dieter Britz Ed.S.Verlag. S.W.Feldberg in A.J.Bard(Ed.)Electroanl.Chem. Vol.3. M.Dekker Ed.
4. M.Ichise, H.Yamagishi and T.Kojima, J.Electroanal.Chem.94(1978)187.

05120

APPLICATION OF THE DIGITAL SIMULATION METHOD TO THE STUDY OF THE IMPEDANCE OF ELECTRODIC SYSTEMS

P.CAÑAS, M.S. LORENZO, C.MONTEMAYOR, J.M.VARA and E.FATAS
Departamento de Electroquímica. Universidad Autónoma de Madrid.
28049 MADRID. Spain.

INTRODUCTION

The analytical solution of the equations describing electrode processes shows increasing difficulties with the complexity of the reaction that takes place on the electrode. This fact, make specially adequate digital simulation methods for the study of such systems[1], particularly in the analysis of the electrode ouput to a sine wave input.

In this work, the study of the response of an electrode perturbed by a sine wave signal is carried out by means of the digital simulation technique. The simple cases (diffusion followed by charge transfer), and then electrode processes with adsorption of electroactive specie have been studied, and the corresponding impedance diagrams have been calculated.

RESULTS AND DISCUSSION

We have used the equation

$$\frac{C(x_i,t_{i+1})-C(x_i,t_i)}{\Delta t} = D\,\frac{C(x_{i-1},t_i)-2C(x_i,t_i)+C(x_{i+1},t_i)\,\theta+}{\Delta x^2}$$

$$\frac{+(C(x_{i-1},t_{i+1}) - 2C(x_i,t_{i+1})+C(s_{i+1},t_{i+1}))\,(1-\theta)}{\Delta x^2}$$

where all the symbols have their usual meaning. We have try values of $\theta=0$ (explicit equation), $\theta=1/2$ (Crank, Nicholson's algorithm[2], and $\theta=1$ (Laasonen's implicit equation). It has been also performed calculations with the Hopscoth's algorithm[3], and the variable space-grid algorithm[4]. In all the cases the results have been very similars, so we have mainly used the explicit method ($\theta=0$). In all the calculations the electrode has been considered as one of semi-infinite plane geometry.

The digitalization of the input sine wave signal has been solved aplying the sampling theorem of Shannon. It five us the least number of samples that is necessary to take from an analogic signal, in order to rebuilt it without loss of the contained information.

Figure 1 shows the impedance diagram corresponding to the

simple case (diffusion and charge transfer), obtained by digital simulation. The values of the parameters used in the simulation are $k°=10^{-2}cm.s^{-1}$, $\alpha=0.5$, $C_O=C_R$, $D_O=D_R$, $C_d=10\ \mu F.cm^{-2}$, $E_{d.c.}=E°$ and $V_{a.c}=0.01$ sin wt V. This impedance plot is similar to those experimentally obtained. The classical half-circle at high frequencies, and the straigh line, slope of 45°, corresponding to the diffusion impedance, appear clearly in figure. This seems to confirm our correct application of the method.

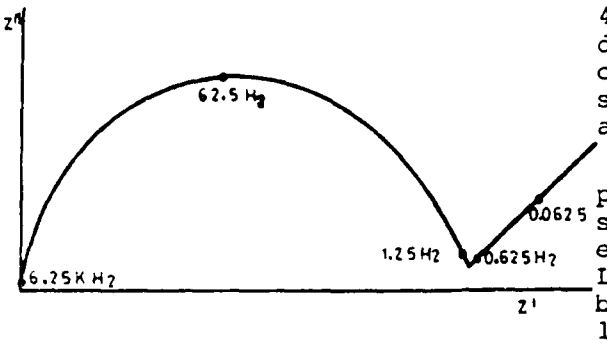

Fig. 1

Figure 2 shows the complex plane plot for several systems with adsorption of electroactive specie. A Langmuirian behaviour has been supposed, and the values of the parameters used in the simulation are:

$C_O=C_R$, $D_O=D_R$, $C_d=10$ uF.cm^{-2}, (surface excess at saturation coverage)$=10^{-5}$mol.cm^{-2} and adsorption coefficients$=10^4$, 1 and 10^{-2} $mol^{-1}.cm^3$ (curves 1,2 and 3 resp.). An inductive loop has been observed in all the cases. The influence of the adsorption coefficient on the shape of the curves, also can be seen in Fig. 2.

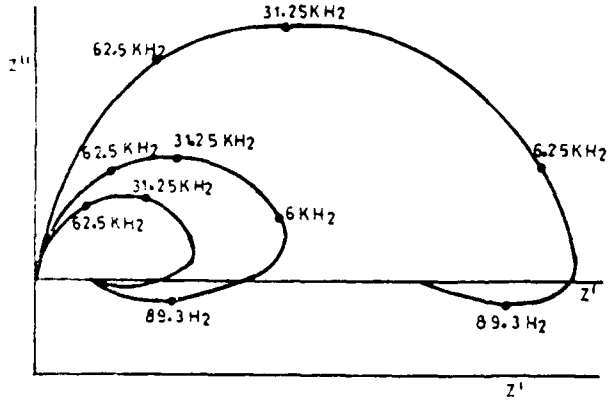

Fig. 2

The comparation between this digital simulated impedance diagrams and experimental data, using pattern recognition thecniques, give us a medium to identify parameters of complex electrode processes, which are difficult to solve analytically.

LITERATURE

1. S.W.Feldbergin A.J.Bard(Ed.). Electroanalytical Chemistry. A Series of Advances Vol.3. Marcel-Dekker Ed.

2. J.Crank and P.Nicholson, Proc.Cambridge Phil.Soc. 43(1947)50.

3. A.R.Gourlay, J.Inst.Math. Appl., 6(1970)375.

4. D.Shoup and A.Szabo. J. Electroanl.Chem., 160(1984)1.

5. P.Conti, R.Marassi and L.Misici, J.Electroanal. Chem., 184(1985)77.

INFLUENCE OF THE ACTIVATION OF A GOLD ELECTRODE ON THE OXIDATION MECHANISM OF METHANOL

by E.GONZALEZ-HERNAN, C.ALONSO and J.GONZALEZ-VELASCO
Departamento de Electroquímica. Facultad de Ciencias. Universidad Autónoma de Madrid. 28049 MADRID. Spain.

I.- INTRODUCTION

It has been reported the importance of the nature, structure and crystal orientation of the electrode material[1] in relation with the oxidation of organic compounds on noble metals. Likewise, studies on the methanol oxidation on platinum single crystal[2] and OH polycrystalline Pt show that the voltammogram obtained on the last kind of electrode can be approximately obtained as a combination of the voltammograms for the methanol oxidation on the (100), (110) and (111) faces of Pt.

On the other hand, Arvia and Co.[3] have obtained changes in the pollycrystalline gold electrode surface by means of the application of square wave potential programms.

We have studied the changes induced in the electroanalytical activity of polycristalline gold in relation with the methanol oxidation and the OH^- coverage formation in basic medium.

It can be seen that the region of the OH coverage presents a different voltammogram after than before the activation (see Fig. 1 and 2). There is an increase in the area attributed to the on coverage formation on the (111) face of gold in relation to the (110) and (100), changing in this way the mechanism for the methanol oxidation in basic medium.

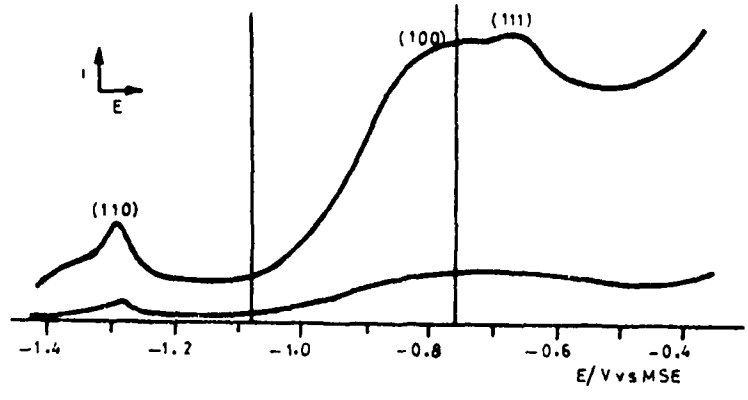

Fig. 1. Potentiodynamic E/I profiles run with 1M KOH at 25°C.-Gold electrode after repetitive triangular potential sweeps (RTPS) at 0.02 V/C. y=1mA cm^{-1}.

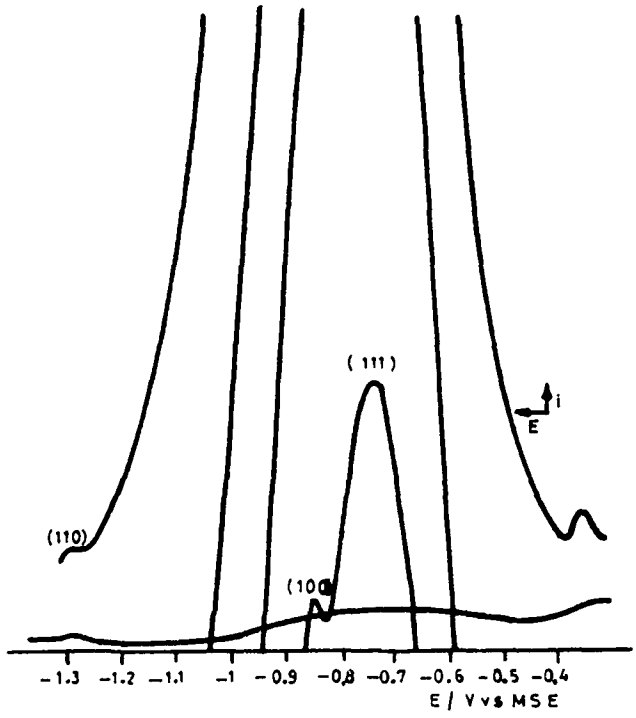

Fig. 2. Potentiodynamic E/I profil run with 1M KOH at 25°C at 0.02 V/s. y=5μA cm^{-1}.
Electropolished gold electrode after the square wave potential cycling treatment (t=305) and electroreduced at 0.01 V/s.

LITERATURE

1. C.Lamy, Electrochimica Acta, 29(1984)1581.

2. C.Lamy, J.M.Leger, J.Clavilier and R.Parsons, J.Electroanal.Chem. 150(1983)71.

3. A.C.Chialvo, W.E.Triaca and A.J.Arvía, J.Electroanal.Chem. 171(1984) 303.

05140

A STUDY OF THE OH COVERAGE ON GOLD IN BASIC SOLUTIONS

C. ALONSO and J.-GONZALEZ-VELASCO
Departamento de Electroquímica. Facultad de Ciencias. Universidad Autónoma de Madrid. 28049 MADRID. Spain.

I.- INTRODUCTION

Allthough the behaviour of Au electrodes has been studied in numerous ocassions, these does not exist an unambiguous explanation for the different experimental data. In basic solutions, the voltammetrie scan starts with a double layer current followed by a region in wich the current remains apparently constant before reaching the potential range in which the gold oxides are supposed to be formed.

The second mentioned range can be recorded under a high stability and, in this way, big variations in the current can be detected (Fig. 1).

In this work we have analized the I vs.E curves and found an adsorption modell for the OH coverage on gold. Likewise, we studied the mechanism of formation of the OH coverage by application of potential pulses.

The results show that the OH coverage takes place beginning with a charge transfer from one OH^- ion to the gold electrode, followed by a instantaneous bidimensional nucleation, and finishing with a bidimensional nucleation to the whole gold surface. After wards, the nucleation continue to the bulk, by formation of hydrogen bridges between the OH^- ions.

II.-RESULTS AND DISCUSSION

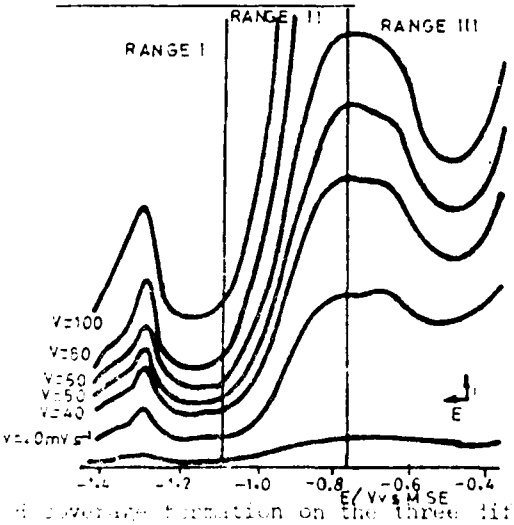

Cathodic scan almost reproduces the same features in the same potential values and the plot of Ip vs. v gives a straight line whose slope gives a value for the capacity. Since this current is attributed to the formation of the OH coverage according to the Eq:

$$Au+OH^- \rightarrow AuOH + 1e^- \qquad (1)$$

the value obtained would represent a pseudocapacity of adsorption. The capacity values which are a function of the potential can be used in order to deduce values for the coverage. On the other hand, Fig. 1, shows three different ranges, which were associated[1] to the OH coverage formation on the three different faces of the pollycrystalline gold electrode.

With the θ and the pseudocapacity values attributed to the (110),(100)and (111) orientations of the microcrystals it is possible to find a model for the adsorption isotherm we have found, that the OH coverage on each of the three mentioned faces can be described by means of a Temkin isotherm in which the interaction coefficient g results to be a linear function of the potential. Fig. 2 shows the variation of the calculated g

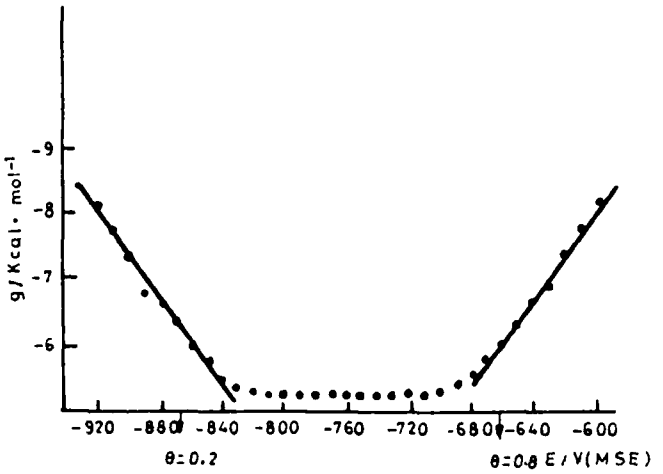

with the potential value for the second range of Fig. 1 (supossed to be the OH coverage on the (100) face of gold). This linear variation has been interpreted as a consequence of the OH bond polarization induced by the increasing anodic potential applied.

By means of the application of potentiostatic pulses, I-t curves were recorded for the three different ranges of Fig.1. Fig. 3 shows one of these

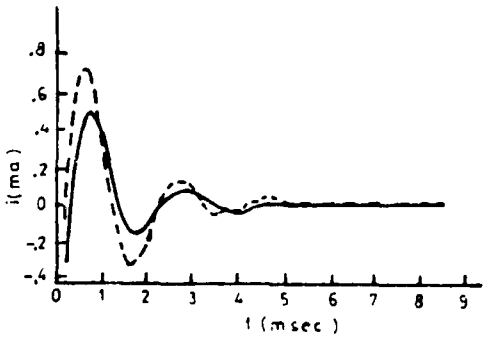

I-t characteristics. They were interpreted as the consequence of an initial electron transfer from an OH^- ion in the OHP to one active site on one concrete gold face according to the value fo the potential pulse applied followed by an instantaneous bidimensional nucleation and a posterior progressive bidimensional nucleation.

Finally, for positive potential values in relation with the zcp or the concrete face, the polarization of the whole "OH tissue" on the gold surface,

would influence the strength of the hydrogen bonds that unit the first OH layer with other layers in the bulk, giving rise to a tridimensional mechanism.

LITERATURE

1. D.W.KIRK, F.R.FOULKES and W.F.GRAYDON, J. Electrochem. Soc.,127(1980)1069.

2. B.E.CONWAY and H.ANGERSTEIN-KOZLOWSKA, Proc.Works. Electrocatalysis on Non-Metallic Surfaces, Nov. 1976.

05150

ELECTROCHEMICAL REDUCTION OF SILVERCOMPLEXES IN PHOTOGRAPHIC SYSTEMS

A. HUBIN, H. TERRYN, B. VAN DER LINDEN, J. VEREECKEN
Vrije Universiteit Brussel
Dept. Metallurgy, Electrochemistry and Materials Science
Pleinlaan 2, 1050 BRUSSELS, Belgium

Silver diffusion transfer development is a photographic process in which complexed silver ions are reduced to metallic silver to form an image.

The mechanism and the kinetic parameters of the reduction of silver thiosulphate and thiocyanate complexes are studied with stationary and non-stationary methods on a silver electrode.

For the thiosulphate complexes the following conclusions can be drawn from the stationary polarization curves :

> Charge transfer at low overpotentials (< 150 mV) and diffusion at high overpotentials are the rate determining steps. The complexes are the electroactive species and no influence of the decomplexation on the overall reaction rate is found. From the Tafel plots an average transfer coefficient of 0.58 is calculated. The rate constant depends on the free thiosulphate concentration. This means that the reduction doesn't proceed via a simple charge transfer mechanism.

The cyclic voltammograms for the reduction of thiosulphate complexes, showing a prewave, indicate that an adsorption of product, in this case thiosulphate, occurs. Assuming a Langmuir adsorption isotherm, a rate constant independent of the concentration can be calculated with an average value of $3.5\ 10^{-5}$ m/s.

For the thiocyanate complexes the same steps are rate determining in the different potential ranges, but the rate constant is 100 x greater. Thiocyanate doesn't adsorb on the electrode.

The following mechanism and rate equation can be proposed :

$$Ag\ L_m^{(1-mn)} \rightleftharpoons Ag^+ + m\ L^{n-}$$

$$Ag\ L_m^{(1-mn)} + e \rightleftharpoons Ag + m\ L^{n-}$$

$$L^{n-} \rightleftharpoons (L^{n-})_{ads}$$

$$\frac{1}{J} = \frac{1}{J_d} + \frac{1}{J_k}$$

J is the current density.

$$J_d = 6.2\ F\ D^{2/3}\ v^{1/2}\ [Ag\ L_m^{(1-mn)}]$$

v is the rotation speed of the electrode,

$$J_k = \frac{k_R\ [Ag\ L_m^{(1-mn)}]\ e^{-\frac{(1-\alpha)\ FE}{RT}}}{K_{ads}\ [L^{n-}] + 1}$$

E is the galvanic potential,

with :

		$L^{n-} = S_2O_3^{2-}$	$L^{n-} = SCN^-$
Diffusion coefficient D	(m^2/s)	$0.45\ 10^{-9}$	$0.75\ 10^{-9}$
Transfer coefficient α		0.58	0.74
Rate constant k_R	(m/s)	$3.50\ 10^{-5}$	$2.50\ 10^{-5}$
Adsorption constant K_{ads}	(l/mol)	3.5	-

Impedance measurements are performed, in order to study the influence of electrocrystallization on the reaction.

In accordance with the results of the polarization curves, a model that takes account of the influence of charge and mass transfer is proposed. As well for the thiosulphate as for the thiocyanate complexes, the same values for α and k_R can be determined as from the polarization curves, but it is impossible to fit the complete impedance curve.

A more complex model, including a surface diffusion of adions is proposed :

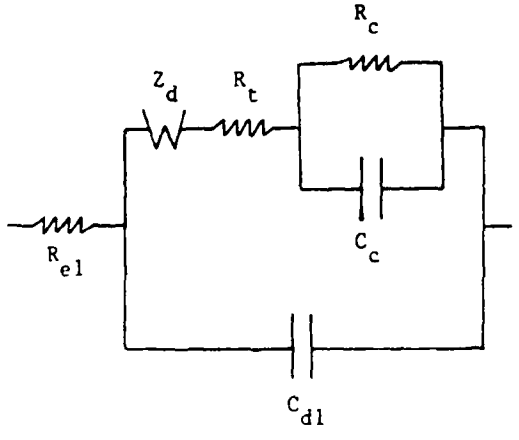

R_{el} = electrolyte resistance
Z_d = Warburg impedance
R_t = charge transfer resistance occuring at double layer transition
C_{dl} = double layer capacitance
R_c = crystallization resistance
C_c = crystallization capacitance

For the thiocyanate complexes, this model allows to calculate the rate constant of charge transfer from R_t.

The average value is $5\ 10^{-5}$ m/s. The effect of electrocrystallization is characterized by R_c and C_c.

ACKNOWLEDGEMENT

The authors gratefully acknowledge the financial support provided by Agfa Gevaert N.V.

05160

IDENTIFICATION BY FTIR AND HPLC OF THE PRODUCTS GENERATED DURING THE PROLONGED ELECTROLYSIS OF ETHYLENE GLYCOL ON NOBLE METAL ELECTRODES

E. BOUHIER-CHARBONNIER, B. BEDEN, J-M. LEGER and C. LAMY,
Laboratoire de Chimie I, Electrochimie et Interactions, U.A. CNRS N° 350,
Université de Poitiers, 40 avenue du Recteur Pineau, 86022 POITIERS (France)

The identification of the products and byproducts, which are formed during the prolonged electrolysis of a given small organic molecule, is of fundamental importance before writting any detailed electrochemichal mechanism. However such identifications are not trivial at all, especially when diluted aqueous solutions are concerned. Not only there is a lack of experimental technique of investigation, but some of the intermediates may be not stable in the electrolytic medium, which makes their identification much more complex.

It is the aim of this work to investigate the products formed during the electrocatalytic oxidation of ethylene glycol (EG) on noble metal electrodes in aqueous medium by means of two different analytical techniques, respectively the Fourier Transform Infrared spectroscopy, FTIR, and the High Performance Liquid Chromatography, HPLC.

Previous studies [1,2] have postulated that ethylene glycol could be oxidized in acid medium up to CO_2 , involving 10 electrons per molecule (e.p.m.) . However in alkaline medium the oxidation process stops at the oxalate stage, involving 8 e.p.m.. The generally accepted scheme in the literature is the following :

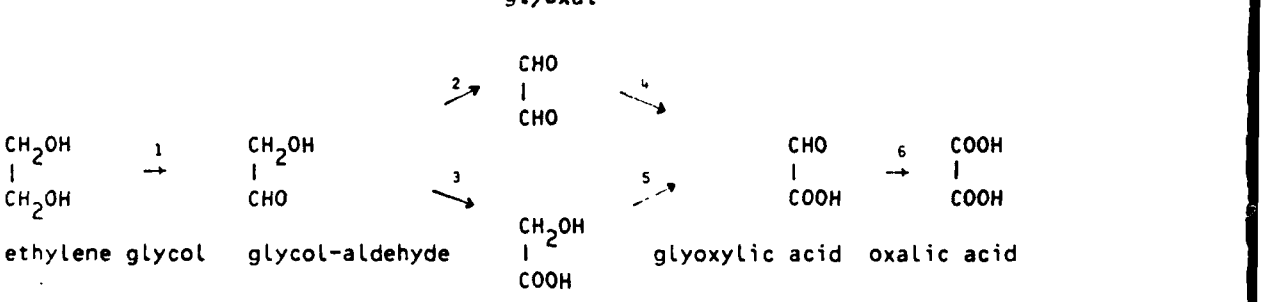

in which two different paths are supposed, either through glyoxal or through glycolic acid intermediates. Further oxidation may lead to carbon dioxide evolution in acid medium or carbonatation of the solution in alkaline medium. Secondary reactions are also to be considered, particularly in alkaline medium for the aldehydic groups : for instance the CANNIZZARO reaction, which transforms glyoxal in glycolate, and glyoxylate in both oxalate and glycolate, or the so-called aldolisation which affects the glycolaldehyde.

Long duration electrolysis were performed under potentiostatic control [using a mercurous sulphate electrode (MSE) as a reference] either with gold or platinum electrodes, in both acid and alkaline electrolytes. Due to the rapid blocage of the active surface by poisoning species, it appeared to be impossible to keep the current constant more than several tenth of seconds at a

suitable potential value E_e for the electrolysis to take place. To sustain the process it is thus necessary to clean periodically the surface of the electrode by a fast voltammetric pulse between two limits E_a and E_c and to hold the potential at a plateau E_e during a time τ until the current decreases by about one half of its initial value. All the parameters E_c , E_a , E_e and τ depend on the system under investigation and are determined by preliminary voltammetric experiments. Once these conditions are chosen, it is possible to carry out electrolysis during several days.

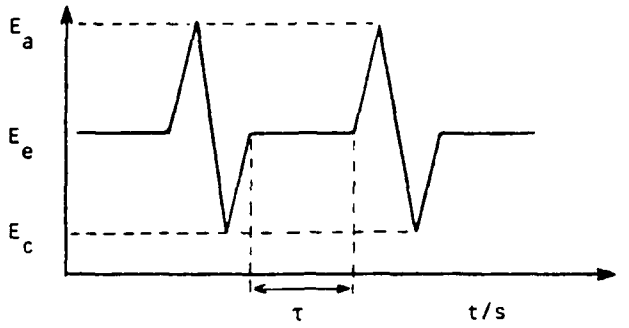

All the experiments were realized at 25°C with 0.1 M of the electroactive species in 0.1 M $HClO_4$ or 0.1 M NaOH electrolytic solutions.

During the electrolysis, voltammetric curves, (i,E), are periodically recorded, using the voltammetric pulses between E_a and E_c , in order to follow the evolution of the system and to check the activity of the electrodes. Samples of the electrolytic solution are taken out and immediately analyzed by HPLC (using both UV and refractive index detectors) and FTIR (a drop of solution is put between two AgCl or CaF_2 windows). All the chromatograms and spectra are compared with those of 10^{-1}, 10^{-2}, 10^{-3} M standard reference aqueous solutions of the expected products. It is thus possible to follow the decrease of concentration in ethylene glycol and the increase of that in products with respect to the time of electrolysis. The results are given in the following table, where the percentages are calculated with reference to the initial ethylene glycol content.

Electrolyte	NaOH		$HClO_4$	
Electrode	Pt	Au	Pt	Au
Potential of the plateau (E/V vs. MSE)	-0.62	-0.3	0.06	0.57
Time of electrolysis (hours)	29	92	96	29
Ethylene glycol	45 %	37.3 %	54 %	71.7 %
Glycolaldehyde	yes	-	7 %	-
Glyoxal	-	-	-	-
Glycolic acid	8.3 %	27.2 %	2.8 %	-
Glyoxylic acid	-	-	-	-
Oxalic acid	0.2 %	0.2 %	-	-
Formaldehyde	-	-	2.7 %	-
Formic acid	2.2 %	3.7 %	1.5 %	-
Carbonate	yes	31.6 %	-	-
CO_2	-	-	32 %	28.3 %

Interpretation of the results

Whatever the nature of the electrolyte or of the electrode, the presence of glyoxal or glyoxylic acid has never been detected. Glycolaldehyde is only formed with platinum electrodes.

Furthermore, conversely to the literature, oxalic acid was not accumulated even after several days as a final product (except as traces of oxalate in alkaline medium). The main interesting information is the presence of formic acid and formaldehyde in appreciable amounts, which demonstrates the breaking of the C-C bond during the oxidation process.

In order to give more precise informations, electrolysis were also performed on 0.1 M solutions of all the expected intermediate products. The most significant results were obtained in acid medium where there is practically no secondary reactions. Formation of formic acid is especially detected during the electrolysis of glycolaldehyde, but mainly during the oxidation of glyoxal (leading to a yield reaching 90 %) and of glyoxylic acid, on the contrary to glycolic acid during the oxidation of which it is not detected. However at the potentials, where the oxidation of EG takes place on a platinum electrode, glycolic acid and above all glyoxal are nearly not electrolyzed. Therefore the reaction path does not follow the usual scheme, and involved the breaking of the C-C bond, presumably at the glycolaldehyde stage, leading to CO_2 through formaldehyde and formic acid.

At higher potentials it is however possible to pass through the glyoxal stage, with further oxidation to glyoxylic acid leading then to oxalic acid and formic acid. This may corroborate the observation previously made by other authors [1,2].

At the present state of our investigation, including some studies on the electrochemical reactivity of the different expected products [3], it is thus possible to write the following reaction path for the oxidation of EG in acid medium on a Pt electrode held at 0.06 V/MSE :

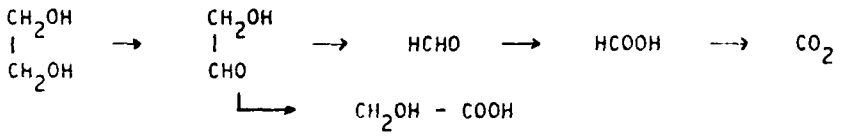

References

1 - W. HAUFFE and J. HEITBAUM, Electrochim. Acta, 23 (1978) 299.

2 - G. INZELT and G. HORANYI, Acta Chim. Acad. Sci. Hung., 101(3) (1979) 229.

3 - B. BEDEN, I. ÇETIN and C. LAMY, I.S.E. Extended Abstracts, 34 (1983) 1007.

A FORMALISM FOR DEVELOPING CHRONOCOULMETRY AT A SPHERICAL ELECTRODE

E. Guaus, F. Mas, J. Puy and F. Sanz.
Departament de Química-Física. Universitat de barcelona.
Av. Diagonal, 647 - 08028-BARCELONA.

Up today chronocoulometry has become the most useful technique for studying adscrption when a faradic process takes place. Anson and co. [1] have developped both the single and the double step techniques [2] . His treatment is focussed on the use of Cottrell's expression for a plane electrode.

Due to the crescent interest on the use of spherical stationary mercury electrodes (SDME or SME), and following a recently developed treatment for the pulse polarography in the DME [3] , a theoretical equation has been obtained for single step chronocoulometry at a spherical electrode when both reactant and product are adsorbed.

Let us consider a simple redox system $R \pm n e^- \rightleftharpoons P$. When at $t = t_o$ a pulse potential is applied driving the system from a base potential without reaction ($\delta = 0$) to another potential ($\delta = \delta$) with faradaic current, the intensity through the system at $t > t_o$ can be written as:

$$\eta_{pp}(\tau>\tau_o) = \eta_{dc}(\tau;\delta) + \frac{\delta}{1+\delta}\frac{f(\tau-\tau_o)}{\sqrt{\tau-\tau_o}} - \frac{\delta}{1+\delta}\int_0^{\tau-\tau_o} f(z)/\sqrt{\tau-z}\,dz \qquad (1)$$

where

$$\eta_{dc}(\tau;\delta) = \frac{\delta}{1+\delta}\tau^{-1/2} + \frac{2}{1+\delta}\theta_p'(\tau) - \frac{2\delta}{1+\delta}\theta_R'(\tau) + \frac{2}{\rho_o}\frac{\delta}{1+\delta}\left[1-(1-\sqrt{D_P/D_R})\,f(\tau)\right] \qquad (2)$$

The following simbols have been used

$\delta(t) = \frac{1}{\rho(t)}\sqrt{D_P/D_R}$ $\qquad$ $\tau = t/t_m$

$\rho(t) = \exp\left\{\frac{nF}{RT}[E(t)-E_o]\right\}$ $\qquad$ $t_m = n\Gamma_m^2/(4c^{o2}D_R)$

$f(t) = C_R(r_o,t)/C^o$ $\qquad$ $\theta_i(t) = \Gamma_i(t)/\Gamma_m$

$\varphi(t) = [1+\delta(t)]\,f(t)$ $\qquad$ $\eta(\tau) = i(\tau)/i_d(t_m)$

$i_d(t_m) = nFA\,c^o D_R^{1/2}/\pi^{1/2}t_m^{1/2}$ $\qquad$ $\rho_o = r_o/\Gamma_m = r_o/(n\Gamma_m/4c^o)$

The fuctions $\theta_i(\tau)$, $\varphi(\tau)$ or $f(\tau)$ are defined as:

$$\theta_i(\tau) - \theta_i(0) = \tau^{1/2} - \frac{1}{2}\int_0^{\tau}(1+\delta(z))\,\frac{f(z)}{\sqrt{\tau-z}}\,dz + \frac{1}{\varphi_0}\tau + \frac{1}{\varphi_0}\int_0^{\tau}\left(1+\sqrt{\frac{D_P}{D_R}}\,\delta(z)\right)f(z)\,dz \qquad (3)$$

together with the reversibility and the isotherm.

The charge involved in the whole process (O,t) can be simple found as $Q(t) = \int_0^t i(t')\,dt'$

Then

$$\Omega(\tau) = \Omega_{dc}(\tau) + \frac{\delta}{1+\delta}\,f(\tau_0)\sqrt{\tau-\tau_0} - \frac{\delta}{2(1+\delta)}\int_{\tau_0}^{\tau}\int_0^{\tau_0^-}\frac{f'(z)}{\sqrt{y-z}}\,dz\,dy + \Omega(\tau_0^+) \qquad (4)$$

with

$$\Omega_{dc}(\tau) = \frac{\delta}{1+\delta}\left[\tau^{1/2} - \tau_0^{1/2}\right] + \frac{1}{1+\delta}\left(\theta_P(\tau) - \theta_P(\tau_0^+)\right) - \frac{\delta}{1+\delta}\left[\theta_R(\tau) - \theta_R(\tau_0^+)\right] + \frac{1}{\varphi_0}\frac{\delta}{1+\delta}\left[\tau - \tau_0 - \left(1-\sqrt{\frac{D_P}{D_R}}\right)\int_{\tau_0}^{\tau} f(\tau')\,d\tau'\right] \qquad (5)$$

and $\Omega(\tau)$, $\Omega(\tau_0^+)$ stand respectively for the dimensionless charge defined by means of

$$\Omega(\tau) = \frac{Q(t)}{2\,i_d(t_m)\cdot t_m}$$

and for the instantaneous transformation $R \rightarrow P$ just at $\tau = \tau_0$, the moment when the pulse potential is applied. (nF AΓ_0).

For the limiting case $\delta \rightarrow \infty$, (5) becomes

$$\Omega(\tau)_{\delta\to\infty} = \sqrt{\tau}-\sqrt{\tau_0} + \frac{1}{\varphi_0}(\tau-\tau_0) - \frac{1}{2}\int_0^{\tau_0^-}\frac{f(z)}{\sqrt{\tau-z}}\,dz + \frac{1}{2}\int_0^{\tau_0^-}\frac{f(z)}{\sqrt{\tau_0-z}}\,dz + \Omega(\tau_0^+) \qquad (6)$$

If we take $\tau_0 = 0$, we have

$$\Omega(\tau)_{\delta\to\infty} = \sqrt{\tau} + \frac{1}{\varphi_0}\tau + \Omega(\tau_0^+) \qquad (7)$$

where the second term comes from the spherical correction. Therefore, we will obtain a linear representation for Q(t) vs. $\tau^{1/2} + 1/\varphi_0\,\tau$.

If we consider a plane electrode, $\varphi_0 \rightarrow \infty$, then (6) transforms into

$$\Omega(\tau)_{\delta\to\infty} = \sqrt{\tau}-\sqrt{\tau_0} - \frac{1}{2}\int_0^{\tau_0^-}\frac{f(z)}{\sqrt{\tau-z}}\,dz + \frac{1}{2}\int_0^{\tau_0^-}\frac{f(z)}{\sqrt{\tau_0-z}}\,dz + \Omega(\tau_0^+) \qquad (8)$$

where the third and fourth term corresponds then to the correction to the Cottrell espression due to the fact that in $\tau = \tau_0$ a inhomogeneity has appeared in the solution as a consequence of the adsorption.

References

1.- F. C. Anson, Anal. Chem. 38,54(1966)
2.- J. H. Christie, R. A. Osteryoung, F.C. Anson, J. Electroanal. Chem. , 13,236(1967).
3.- J. Puy, F. Mas, F. Sanz, J. Virgili, J. Electroanal. Chem. 183(1985) 27

THEORETICAL TREATMENT OF REVERSIBLE REACTIONS WITH ADSORPTION AT THE RDE. ATTEINMENT OF STATIONARY STATE.

F.MAS, J.PUY and F.SANZ
Departament de Química-Física. Universitat de Barcelona.
Av. Diagonal, 647 - 08028-BARCELONA.

When an electrodic transport controlled process with boundary conditions including adsorption processes is studied using an arbitrary time controlled potencial, the response functions (i(t), Q(t),....) depend on the concentrations of the species around the electrode and on the coverage concentration, wich makes necessary to solve the transport equations.

Following a treatment similar to that made for the DME[1], we have studied the equations that, with the usual hypothesis[2], describe the diffusion-convection transport that takes place in the RDE when reversible process $R \pm ne^- \rightleftharpoons P$ is considered. This treatment is based on the transformation of the transport differential equations into an integral equation, which in this case is:

$$\theta_t(\lambda) - \theta_t(0) = B \int_0^\lambda \{1 - \varphi(\mu)\} \frac{A(\lambda-\mu)}{\sqrt{\lambda-\mu}}\, d\mu \qquad (1)$$

being

$\lambda \equiv D_R t / \delta_d^2$ $\qquad$ $\delta(t) \equiv \sqrt{D_P/D_R}\, f(t)$

$\delta_d \equiv 1'61\, D_R^{1/3}\, \nu^{1/6}\, \omega^{-1/2}$ $\qquad$ $f(t) = \exp\{\pm \frac{nF}{RT}[E(t) - E_0]\}$

$\varphi(t) = (1 + \delta(t))\, f(t)$ $\qquad$ $\theta_i(t) = \Gamma_i(t)/\Gamma_m$

$f(t) = c_R(r=r_s, t)/c_R^*$ $\qquad$ $B = c_R^* \delta_d \propto \omega^{-1/2}/\Gamma_m$

and the function $A(\lambda)$ is defined by:

$$A(\lambda) = \left\{ e^{-3'10\lambda}/\sqrt{\pi} + 0'94\sqrt{\lambda}\ \mathrm{erf}(\sqrt{3.10\,\lambda}) \right\} \qquad (2)$$

The response functions i(t), Q(t) take, for the potentiostatic case, the form:

$$\eta(\lambda) = \frac{1}{1+\delta}\left\{\delta\,\frac{A(\lambda)}{\sqrt{\lambda}} + \frac{1}{B}\left[\theta_P'(\lambda) - \delta\,\theta_R'(\lambda)\right]\right\} \qquad (3)$$

$$\Omega(\lambda) - \Omega(0) = \int_0^\lambda [1 - f(\mu)]\,\frac{A(\lambda-\mu)}{\sqrt{\lambda-\mu}}\, d\mu - \frac{1}{B}\left[\theta_R(\lambda) - \theta_R(0)\right] \qquad (4)$$

where $\eta(\lambda)$ and $\Omega(\lambda)$ are dimensionless expressions of i(t) and Q(t):

$\eta(\lambda) \equiv i(\lambda)/i_d(\lambda)$ $\qquad$ $\Omega(\lambda) = Q(t)/(i_d(t)\cdot \delta_d^2/D_R)$

$i_d(\lambda)$ is the limit diffusion current obtanied by Levich[3] considering the diffusion layer hypothesis of Nernst (stationary state), and δ_d is the thickness of that layer.

Because of the general complexity of $A(\lambda)$, it is interesting to consider its assymptotic behaviour in order to solve equation (1):

$$A(\lambda) \sim \begin{cases} 1/\sqrt{\pi} & \lambda \ll 1 \\ 0.94\sqrt{\lambda} & \lambda \gg 1 \end{cases} \qquad (5)$$

Analysing the flux values, a critic value of λ can be determined for wich those assymptotic behaviours can be used. (λ_c)

Thus, in the absence of adsorption, it is found[3]

$$\lambda_c = 1/3.10$$

and then, for $\lambda > \lambda_c$, $A(\lambda) \sim 0.94\sqrt{\lambda}$.

In those conditions, the integral equation (1) can be solved exactly:

$$\varphi(\lambda) = 1 \qquad (6)$$

Due to this fact it is said that the stationary state is reached quickly when the RDE is used.

The results obtained when the langmuirian adsorption is assumed for the reaction components, show that the λ_c value is strongly dependent on both, the dimensionless parameter B (proportional to the rotation speed of the disc ($w^{1/2}$)) and the adsorption coefficients. Then the stationary state hypothesis does not hold when strong adsorption is considered.

References:

1. J.Puy, F.Mas, F.Sanz and J.Virgili, J. Electroanal. Chem, 183 (1985) 27.
2. Yu. V. Pleshov and V.Yu.Filinovskii, "The Rotationg Disk Electrode", Consultants Bureau, New York, 1976.
3. V.G.Levich, "Physicochemical hydrodinamics", Prentice Hall, New Yersey, 1962.

05190

OXYGEN EVOLUTION REACTION ON CHEMICALLY CO-PRECIPITATED NICKEL HYDROXIDE-IRON HYDROXIDE MIXTURE ELECTRODE

S. I. CORDOBA, R. E. CARBONIO, M. LOPEZ TEIJELO and V. A. MACAGNO
Instituto de Investigaciones en Fisicoquímica de Córdoba (INFIQC), Departamento de Físico Química, Facultad de Ciencias Químicas, Universidad Nacional de Córdoba. Suc. 16, C. C. 61, 5016 Córdoba, ARGENTINA.

Oxide anodes can be prepared by thermal decomposition depending their electrocatalytic properties on temperature and preparation procedure. The same (hydrous) oxides can be obtained by electrolytic growth or by chemical precipitation on a suitable substrate although in these cases corrosion is more pronounced. The present work deals with the electrochemical response of nickel hydroxide-iron hydroxide mixtures of different composition chemically co-precipitated on a conductive substrate (platinum or vitreous carbon) with particular reference to the electrocatalytic activity for the oxygen evolution reaction (OER). The films were chemically co-precipitated by alternative immersions of the substrate in $NiSO_4$ + $FeSO_4$ and NaOH solutions of different concentration following a procedure previously described to prepare colloidal electrodes[1,2].

Figure 1 shows the E/i potentiodynamic response for the $Pt/Ni(OH)_2$ and $Pt/Fe(OH)_2$ single interphases and the $Pt/Ni(OH)_2 + Fe(OH)_2$ mixed interphase at 25°C. The $Pt/Ni(OH)_2$ electrode shows the anodic and cathodic current peaks related to the H-electrosorption/electrodesorption (-0.90 to -0.50 V vs Hg/OHg/0.01 M NaOH) and to the O-electrosorption/electrodesorption (-0.50 to 0.30 V). At more positive potentials, the current peaks related to the Ni(II)/Ni(III) redox couple and the start of the OER are observed. The current peaks located at c.a. 0.55 V in the anodic potential scan and at 0.47 V in the cathodic scan correspond to the reaction[3]

$$Ni(OH)_2 + OH^- \rightleftharpoons NiOOH + H_2O + e \qquad (1)$$

The electrochemical response of a $Pt/Fe(OH)_2$ electrode shows two clearly defined redox couples. The first one appears at more negative potentials with the anodic and cathodic peaks located at c.a. -0.74 V and -0.89 V respectively, and the second one, which exhibits a greater reversibility, at c.a. -0.53 V and -0.63 V respectively. The comparison of the redox couple potentials with thermodynamic data and the results obtained on platinum and vitreous carbon for different pH values of the electrolytic and alkaline precipitating solutions as well as the effect of the cation employed (Na^+ or K^+)[4], allow us to postulate that the redox couple observed at more negative potentials, corresponds to the reaction [5]

$$3\,Fe(OH)_2 + 2\,OH^- \rightleftharpoons Fe_3O_4.4H_2O + 2\,e\,, \quad (E_o = -0.758\ V) \qquad (2)$$

while the second redox couple corresponds to the reaction

$$Fe(OH)_2 + OH^- \rightleftharpoons \delta\text{-}FeOOH + H_2O + e \quad (E^\circ = -0.653\ V) \qquad (3)$$

according to a bilayer model[6].

The $Pt/Ni(OH)_2 + Fe(OH)_2$ electrode shows the redox processes corresponding to the Fe(II)/Fe(III) couple at practically the same potentials as those obtained with the $Pt/Fe(OH)_2$ interphase, while there is a pronounced shift of the $Ni(OH)_2$ oxidation towards positive potentials as compared with the single interphase. Simultaneously, the $Ni(OH)_2$ oxidation peak is totally masked by the OER due to the considerable decrease in the overpotential for this reaction. The effect can be clearly seen in Fig. 2, where the potential scan includes the anodic current peak corresponding to the OER. In this case, the oxygen reduction current peak at -0.30 V can also be seen during the negative potential scan. The shift of the Ni(II)/Ni(III) current peaks measured through the NiOOH reduction peak potential decreases as the $Ni(OH)_2$ content in the mixture increases. The catalytic activity for the OER is maximum in a mixture with 20-25% of $Fe(OH)_2$.

Other important features shown by the mixed electrode is a greater stability of the E/i profile for the Fe(II)/Fe(III) redox couple than that of the individual components and a noticeable charge increase of the more reversible redox couple ($Fe(OH)_2/FeOOH$) as compared with that of the $Fe(OH)_2/Fe_3O_4.4H_2O$ redox couple. These facts indicate that the addition of $Ni(OH)_2$ to $Fe(OH)_2$ electrodes would stabilize the charge during successive charge/discharge cycles of the $Fe(OH)_2$ electrode.

Stationary polarization curves show values of the Tafel slope for oxygen evolution of 0.06 V for $Pt/Ni(OH)_2$ and 0.05 V for $Pt/Fe(OH)_2$. Mixed electrodes show a lower overpotential than either $Ni(OH)_2$ or $Fe(OH)_2$ single electrodes with a Tafel slope of 0.03 V and a reaction order with respect to the OH^- ions concentration of about 2. The experimental Tafel slope and the reaction order parameters for the mixed electrode are in reasonable agreement with the theoretically predicted values for the mechanism known as "oxide path"[7].

The performance of the electrode at 0.61 V in a 1 M NaOH electrolytic solution decreases from 8 mA/cm^2 to 4 mA/cm^2 over a period of 72 h. The voltammogram recorded after this time shows a decrease in the charge corresponding to the Fe(II)/Fe(III) redox couples and a shift of the current peaks related to the Ni(II)/Ni(III) process towards less positive potentials. These results could be an indication of the existence of a selective dissolution process of $Fe(OH)_2$ in the electrolytic solution.

References

1- R. E. Carbonio, V. A. Macagno, M. C. Giordano, J. R. Vilche and A. J. Arvía, J. Electrochem. Soc. 129, 983 (1982).
2- M. E. Folquer, J. R. Vilche and A. J. Arvía, J. Electroanal. Chem. 172, 235 (1984).
3- V. A. Macagno, J. R. Vilche and A. J. Arvía, J. Electrochem. Soc. 129, 301 (1982).
4- I. A. Dibrov, S. M. Chervyak-Voronich, T. V. Grigor'eva and G. M. Kozlova, Elektrokhimiya 16, 786 (1980).
5- S. I. Córdoba, R. E. Carbonio, M. López Teijelo and V. A. Macagno, to be published.
6- K. Ogura, A. Fujishima and K. Onda, J. Electrochem. Soc. 131, 344 (1984).
7- S. Trasatti and G. Lodi in Electrodes of conductive metallic oxides, Part B, p. 531. Ed. S. Trasatti, Elsevier Scientific Publishing Company, N. York (1981).

Financial support from CONICET and CONICOR is acknowledged.

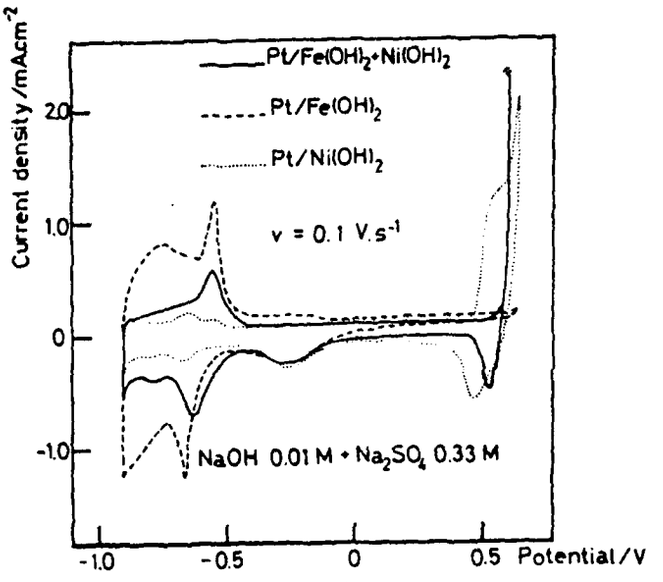

Fig. 1

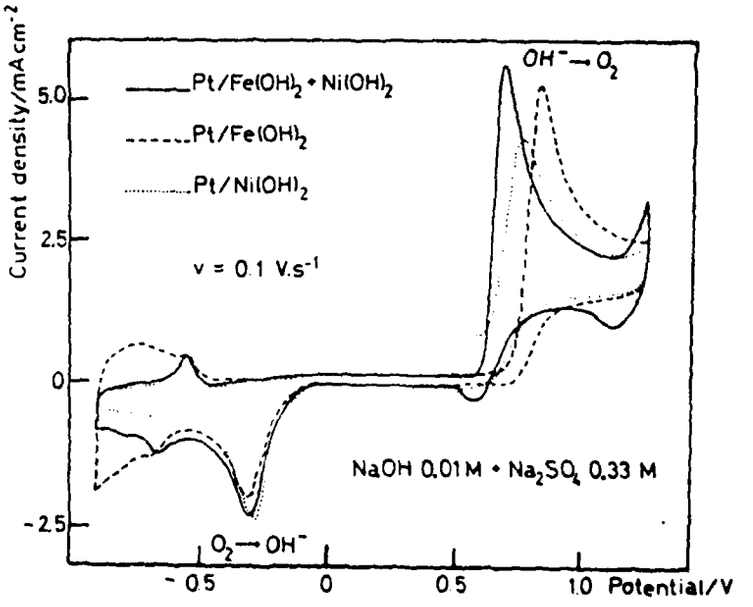

Fig. 2

Potentiodynamic E/i profiles of electrodes prepared by 5 alternative immersions in 1M NaOH and ---- 0.025M Fe^{2+}; .... 0.025M Ni^{2+}; —— 0.0125M Ni^{2+} + 0.0125M Fe^{2+}.

05200

CATHODIC BEHAVIOR OF THICK TITANIUM OXIDE FILMS

R. M. TORRESI, O. R. CAMARA and C. P. DE PAULI
INFIQC, Departamento de Físico Química, Facultad de Ciencias Químicas, Universidad Nacional de Córdoba. Sucursal 16, C. C. 61, 5016 Córdoba, ARGENTINA

Introduction:

The hydrogen evolution reaction (HER) which accompanies corrosion of the oxide films of titanium has been reported by different authors although results are not in agreement.[1]

At cathodic potential region, the oxide films lose their corrosion resistivity which could be explained by hydride formation at the surface.[2-3]

The behavior of the anodic oxide films of titanium electroformed in sulfuric acid 0,5 M under different experimental conditions is studied in the cathodic branch by linear voltammetry rotatory disc electrode (RDE) and impedance measurements.

Experimental:

The specimen was a titanium rod of 99,99% purity, fixed in a teflon holder. The exposed area was about 0,5 cm^2. After degreasing, it was chemically polished in a solution 1:4:5 parts by volume of 48% HF, 65% HNO_3 and water respectively.[4]

The oxide film was formed by linear sweep voltammetry using different final anodic potential and then it was carefully removed by chemical polishing. A saturated calomel electrode (SCE) was used as reference electrode. All the potentials are referred to the standard hydrogen electrode (SHE).

Results and discussion:

The hydrogen evolution reaction (HER) in perchloric and sulfuric acid solutions at different pH values, keeping ionic strength constant, was studied on electroformed thick oxide films.

The thickness and properties of the oxide films were evaluated by impedance measurements.[5]

The typical i/E curves obtained with a RDE showed a limit current between -1.8 and -2.0 V. A linear relationship between limit current density values and rotation rate square root was found as predicted by Levich equation for controlled processes for mass transport solution at different pH values (figure 1). From these results the diffusion coefficient for hydrogen ions was calculated and its value was in agreement with the literature for perchloric acid solutions. However, in sulfuric acid solutions it was necessary to correct the hydrogen ion concentration due to the presence of acid sulfate ions.[6]

The cathodic Tafel slope obtained from E-log i max representations was about -120 mV/dec, and the reaction order with respect to hydrogen ion was quite close to 1.

Figure 2 shows the simultaneous potentiodynamic measurements of current density (lower part) and capacity (upper part) as a function of potential. The potential electrode was swept anodically from 0 V up to 3,2 V, then reversed to -2,0 V, followed by a second sweep back to 3,2 V before returning to the starting potential. When the potential was reversed at the

cathodic limit the current density was higher than the values obtained in the negative sweep. This effect could indicate that changes in the hydrogen evolution reaction occurred.

During the second anodic sweep the current density profile between 0 V and 2.3 V shows negligible values although after 2.3 V it increases again up to the first cycle value which indicates that oxide film growth is occurring.

It can also be seen from figure 2 that electrode capacity decreases continuously with the increase of oxide films thickness which is well known for thicker oxide films. In the negative sweep the capacity remained almost constant up to 2.3 V, and then increased again for less positive potentials. During the second positive sweep, the capacity values are lower than those obtained in the first cycle up to 2.3 V. After it, similar capacity values were obtained in both cycles.

The capacity values obtained at lower potentials during both negative sweeps were plotted according to Schottky-Mott equation from which similar donor concentrations were found.

The C^{-1} vs d (oxide thickness) plot shows the same slope for both positive sweeps with a greater initial thickness (do) for the second one. This fact can be interpreted as a thinning of the oxide film occurring simultaneously with the hydrogen evolution reaction.

Acknowledgement:

This work was supported by the Consejo Nacional de Investigaciones Científicas y Técnicas (CONICET) and the Consejo de Investigaciones de la Provincia de Córdoba (CONICOR). R. M. T. thanks CONICET for the fellowship granted.

References:

1- E. J. Kelly and H. R. Bronstein. J. Electrochem. Soc. 131, 2343 (1984).
2- I. V. Riskin, V. B. Torshin, Ya B. Skuratnik and M. A. Dembrosky. Corrosion NACE 40, 266 (1984).
3- N. Sato and T. Ontsuka. 35th ISE Meeting. Berkeley, U.S.A. August 5-10, 1984.
4- W. J. Tegart "The electrolytic and chemical polishing of metals". Pergamon Press London (1956).
5- V. A. Macagno and J. W. Schultze. J. Electroanal. Chem. 180, 157 (1984).
6- N. I. Savitkin and N. I. Podobaev. Soviet Electrochem. 10, 558 (1974).

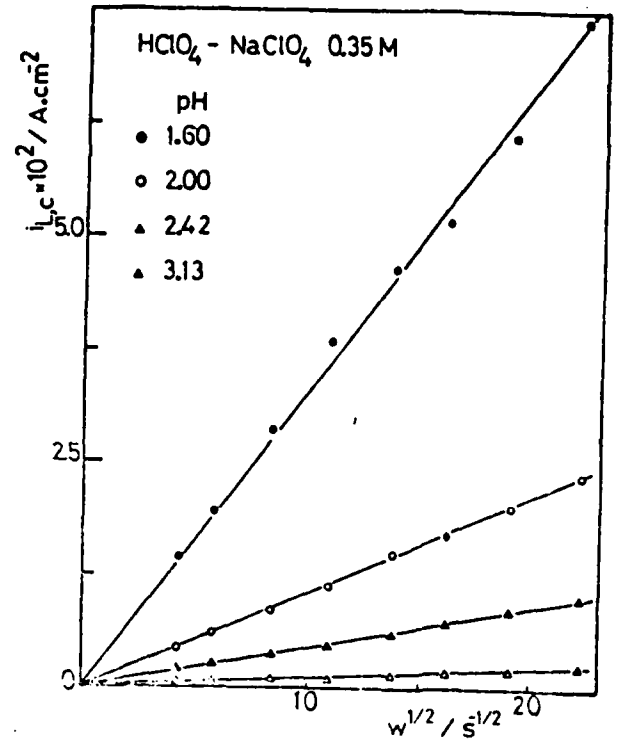

Figure 1

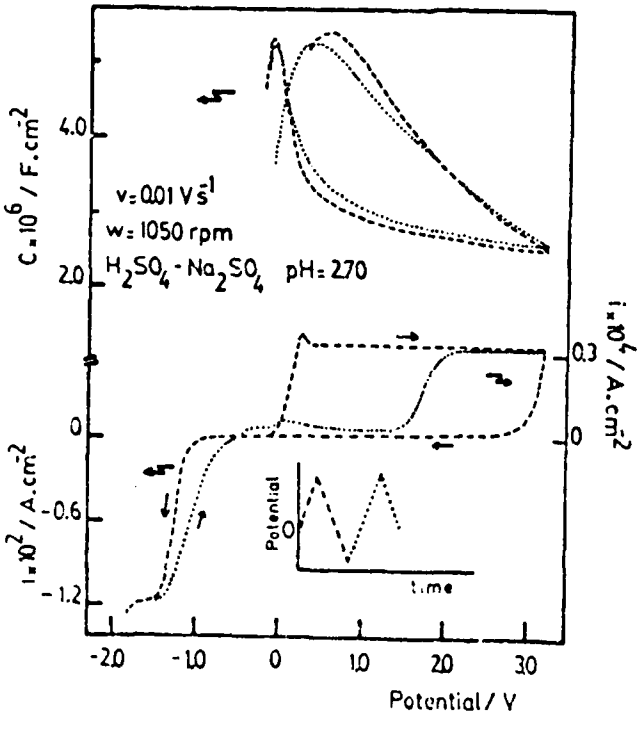

Figure 2

05210

INDIRECT ELECTROSYNTHESIS OF MONOBROMONORCARANE IN TWO PHASE SYSTEMS

L.M.YUDI, A.M.BARUZZI and V.M.SOLIS
Instituto de Investigaciones en Fisicoquímica de Córdoba (INFIQC)
Departamento de Físico Química, Facultad de Ciencias Químicas,
Universidad Nacional de Córdoba. Sucursal 16, C.C.61, 5016 Córdoba,
ARGENTINA

Introduction

In the present communication, the study of the electro-reduction of dibromonorcarane to the corresponding monobromo derivative carried out in a two-phase electrolytic system, assisted by mediating redox couple, is reported. The chemical synthesis of the same compound, although well characterized, is not satisfactory, due principally to the high temperature and long time required, as well as to the low specificity and yield. Electrosynthetic methods are more promising, but if a conventional monophasic electrolyte system is employed, very high negative potentials are required[2].

The electrosynthesis performed in an aqueous/non-aqueous heterogeneous system with a water soluble redox agent electrochemically regenerated has been successfully applied to other organic electrosynthesis[3], and we hope this procedure, if properly applied to the synthesis of monobromonorcarane, will help to overcome in a significant way the difficulties already mentioned.

Experimental

The electrolytic cell employed was of conventional design with three electrodes and separated anodic and cathodic compartments.

The silver working electrode was either a foil of 12 cm^2 of geometric area or a wire of 2,3 cm^2, depending on the type of experiments. The first one was employed in controlled potential electrolysis for preparative purposes, while the second, was suitable for the non-stationary voltammetric techniques. The counter electrode was a platinized platinum foil, and a saturated calomel electrode was employed as reference.

All reagents were of analytical grade, used without further purification except dibromonorcarane which was chemically synthesized from bromoform and cyclohexene[4]. Sodium perchlorate-perchloric acid and tetrabutyl ammonium perchlorate were employed as inert electrolytes. The biphasic emulsion, methylenechloride-water was maintained by mechanical agitation. The mediating reducing agent was the Cr(II)/Cr(III) redox couple.

The experiments were performed at $0 \pm 0,1°C$ and desoxygenated with N_2 bubbled through the emulsion.

Characterization and quantification of electrolysis products were performed by gas chromatography, using SE 30 as stationary phase.

Results and Discussion

Stationary and potentiodynamic current-potential curves for aqueous chromic chloride solutions at different pH, were performed. Two processes, the reduction of Cr(III) and the evolution of hydrogen, were well

characterized in stationary polarograms, whose middle wave potential difference was dependent upon pH. The voltammograms presented a well defined peak system due to the Cr(II)/Cr(III) redox couple.

The system water-methylene chloride emulsion-inert electrolytes, analyzed by cyclic voltammetry proved to be stable and electrochemically inert under the experimental conditions employed. From these results, proper parameters of pH and potential for the preparative electrolysis were chosen.

Table I summarizes the experimental conditions and results obtained in controlled potential electrolysis for the electrosynthesis of monobromonorcarane. Only in the case of electrolysis n°5, where both Cr(II)/Cr(III) and the biphasic solvent system were present, good yields (more than 50%) were obtained. It is clear form these results that aqueous Cr(II) electrochemically generated, is the reducing agent for dibromonorcarane present in the organic phase.

The biphasic electrolysis technique would help to solve problems such as the low conductivity of organic media and the insufficient solubility of organic substrates and products in the aqueous phase. Furthermore, the use of mediating water soluble redox systems allows lower electrolysis potential to be employed.

Optimization of operative conditions, such as the use of better emulsifying methods, minimization of resistive losses by meands of properly selected anolyte-catholyte separators and so on, would render the electrosynthetic method a proper one for the obtention of monohalogenocyclopropanic compounds.

References

1- T.Ando, T.Muranaka and T.Ishihara, Bull.Chem.Soc.Jpn., 54, 3227,(1981).
2- A.Fry and R.Moore, J.Org.Chem., 33, 1283 (1968).
3- H.Fees, H.Wendt, "Perfomance of Two-Phase-Electrolyte Electrolysis" in N.Weinber, B.Tilak (ed), Technique of Electroorganic Synthesis.Part III.
4- L.Skattebol, G.Aziz Abskharoun and T.Greibrokk, Tettrahedron Letters, 16, 1367 (1973).

Electrolysis n°	EMULSION		Potential (vs SCE)	Results
	Aqueous phase	Organic phase		
1	$NaClO_4$ 0,1 M $HClO_4$ 0,01 M $CrCl_3$ 7 mM	 2% V/V in Cl_2CH_2	-600 mV	The product was not obtained.
2	$NaClO_4$ 0,1 M $HClO_4$ 0,01 M	"	"	"
3	$NaClO_4$ 0,1 M $HClO_4$ 0,01 M $CrCl_3$ 7 mM	 2% V/V $ClO_4(C_4H_9)_4N$ 0,05M in Cl_2CH_2.	"	"
4	$NaClO_4$ 0,1 M $HClO_4$ 0,01 M	"	"	"
5	$NaClO_4$ 0,1 M $HClO_4$ 0,01 M $CrCl_3$ 7 mM	"	-800 mV	The product was obtained
6	$NaClO_4$ 0,1 M $HClO_4$ 0,01 M	"	"	The product was not obt.
7		"	"	"
8		"	-400 mV	"

TABLE I

05220

ELECTROCHEMICAL BEHAVIOUR OF ACID AND NEUTRAL ZINC (II) SOLUTIONS ON THIN TITANIUM OXIDE FILM SUBSTRATES

G.F.DARBYSHIRE and O.R.CAMARA
INFIQC, Departamento de Físico Química, Facultad de Ciencias Químicas
Universidad Nacional de Córdoba, C.C.61,Suc.16, 5016 Córdoba
ARGENTINA

Introduction

The electrocrystallization of zinc has been extensively studied in alkaline solutions, although in acid media fewer publications have appeared[1]. More recently, studies refered to the initial stages of deposition of zinc using foreign substrates such as silver[2], platinum, gold and graphite[3], or glassy carbon[4] have been published. There have been no reports on the use of titanium for zinc electrocrystallization and this metal is being used increasingly as a stable substrate in industrial electrochemistry[5].

The results presented here are related to zinc electrodeposition on titanium electrodes that are polished mechanically or chemically, and the effect of electrochemically grown thin titanium oxide films on the reduction process.

Experimental

The working solutions were prepared with de-ionized and purified water (Milli-Q system), using zinc oxide powder and ammonium chloride or zinc sulfate and sodium sulfate, and degassed using purified nitrogen. The pH was adjusted at desired values adding sulfuric acid or sodium hydroxide solutions. All measurements were done at 25°C.

The working electrode was an 8 mm titanium disk (Alfa 99.9%) polished mechanically with a 0.05 um alumina-water suspention to specular surface,or chemically by 10 to 15 second dip in a (1:4:5) fluorhydric acid-nitric acid-water mixture. The counter electrode was a large platinum foil and a saturated calomel reference electrode was used, to which all potentials in the text are refered.

The electrochemical measurements consisted of single or repetitive linear sweep voltammetry or pulse potential steps.

Results and Discussion

The i/E profile obtained with linear potential sweep voltammetry using a mechanically polished titanium electrode in slightly acid (pH=6.9) NH_4Cl 0.2M and ZnO $1x10^{-2}$ M solutions is shown in figure 1 (curve a). The repetitive potential cycling of the electrode produces a shift in the cathodic current peak towards more positive values (curve b), thus decreasing the current loop observed in the first cycle. (The cathodic current on reversal of the sweep is higher than that found on going in the cathodic direction in the initial stages of deposition). In the positive sweep a decrease in current values at potentials more negative than -0.9V, whilst an increase in current at potentials more positive than -0.9V can be seen. This last effect is enhanced, and another anodic current peak can be

observed, when the cathodic potential limit is changed to values where hydrogen evolution occurs (curve c) or when a chemically polished electrode is used.

When mechanically polished electrodes are previously oxidized, either potentiodynamically of galvanostatically, up to potentials between 0 and 1.0V, the zinc reduction processes are practically not affected, although higher currents are obtained in the positive sweep at potentials more positive than -0.09V.

The cathodic current loop observed in the zinc deposition process, together with the linear variations of peak current, peak potential and half-peak width with the square root of potential sweep rate are indicative of nucleation and growth phenomena[6]. The charges involved in the cathodic process point to multilayer deposition.

Results obtained with repetitive potential cycling of the electrode in the zinc reduction and oxidation potential region, in solutions with lower pH show a rapid decrease in the current related to the zinc processes in favour of an increase in current due to the hydrogen evolution reaction. This effect makes the analysis of the data rather difficult.

The i/t profiles obtained with pulse potential jumps (figure 2) show an initial charging current decay followed by an increase in current which goes through a maximum (I_m) at a time t_m and then falls to values corresponding to linear diffusion. The current maximum values increase as the final potential of the double pulse is made more negative. These features are common to the titanium substrate independently of the surface treatment applied.

For mechanically polished electrodes the product $I_m^2 . t_m$ remains constant, independently of the final potential applied, as required by theory of three dimensional nucleation with diffusion controlled growth.

The transients were compared with the non-dimensional equations obtained from theory[7] by plotting I^2/I_m^2 vs t/t_m, for which a reasonably good fit was obtained when compared with progressive nucleation equations.

When mechanichally polished electrodes were oxidized previous to the pulse potential jump, similar results were obtained showing a progressive nucleation, although there appears to be a change towards a predominance of instantaneous nucleation when a chemically polished electrode with or without previous oxidation is used. Dispersion of experimental results increased when the chemical polishing is used.

Some measurements were performed in the potential region of titanium oxide growth after the electrode was cycled repeatedly in zinc reduction and oxidation potentials (between -1.5 and 0 V). The currents related to the oxide growth were almost twice those obtained without the activation at cathodic potentials indicating an enhancement of oxide growth. This is probable related to zinc atoms incorporated into the zinc oxide formed on the surface which increases the electrodes electrical conductivity[1].

References

1- J.McBreen and E.J.Cairns in " Advances in Electrochemistry and Electrochemical Engineering". Vol II. H.Gerischer and C.W.Tobias Editors. J.Wiley and Sons, New York (1978).

2- M.Y.Abyaneh, J.Hendrikx, W.Visscher and E.Barendrecht, J.Electrochem. Soc. 129, 2654 (1982).

3- A.R.Despic and M.G.Pavlovic, Electrochim.Acta, 27, 1539 (1982).

4- J.McBreen and E.Gannon, J.Electrochem.Soc., 130, 1667 (1983).

5- S.Trasatti and G.Lodi, in " Electrodes of conductive Metal Oxides",Ed. S.Trasatti Vol.B, Elsevier 1981.

6) E.Bosco and S.K.Rangarajan, J.Electroanal. Chem. 129, 25 (1981).
7) B.Scharifker and G.Hills, Electrochim.Acta. 28, 879 (1983).

Acknowledgement

This work was supported by the Consejo Nacional de Investigaciones Científicas y Técnicas (CONICET) and the Consejo de Investigaciones de la Provincia de Córdoba (CONICOR).

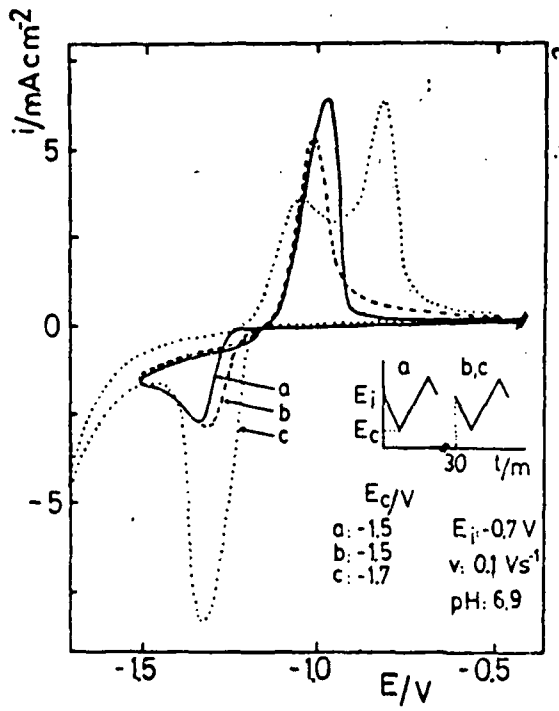

Fig.1 i/E profiles in NH_4Cl 0.2M+ZnO 0,01 M solutions.

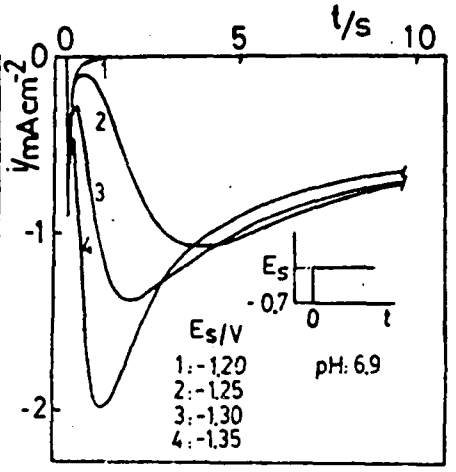

Fig. 2 Current transients in NH_4Cl 0.2M+ ZnO 0,01M solutions.

AD-A162 434 EXTENDED ABSTRACTS INTERNATIONAL SOCIETY OF 5/12
ELECTROCHEMISTRY (36TH) HELD AT SALAMANCA SPAIN ON
23-28 SEPTEMBER 1985(U) INTERNATIONAL SOCIETY OF
UNCLASSIFIED ELECTROCHEMISTRY 28 SEP 85 F/G 7/4 NL

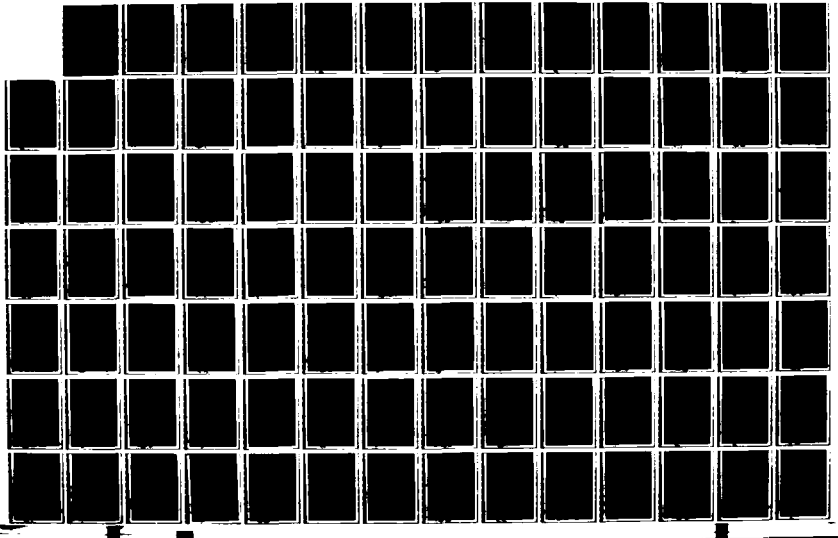

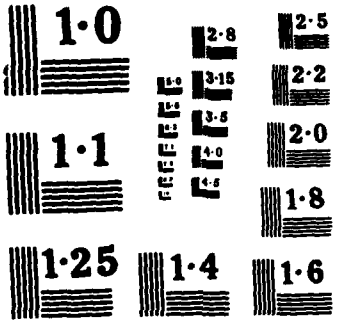

ELECTROCATALYSIS BY FOREIGN AD-ATOMS. REDUCTION OF NITRATE ON A GOLD ELECTRODE CATALYSED BY UPD OF CADMIUM.

J.García-Domenech, J.L.Vázquez, J.M.Feliu, A.Aldaz and J.Clavilier.*
Departamento de Química-Física. Universidad de Alicante. Alicante. Spain.
* Laboratoire d'Electrochimie Interfaciale. C.N.R.S. 92195 Meudon. France.

The underpotential deposition of Pb on polycrystalline gold electrocatalyzes the reduction of nitrate ion in an acid medium(1). Also, the electroreduction of nitrate ions on polycrystalline gold electrodes modified by underdeposited cadmium submonolayers, shows a significant electrocatalytic effect. So, the UPD of cadmium on gold shifts the reduction wave of nitrate 300 mv towards positive values with respect to that obtained on gold or cadmium electrodes.

Figure 1 shows the voltammetric curve for adsorption-desorption of cadmium on gold and its effect over nitrate ion reduction to nitrite ion.
The anion of the supporting electrolyte plays a significant role on the reduction process, figure 2. This type of behaviour can be attributed to same competitive adsorption between nitrate and the anion species present in the supporting electrolyte, essentially HSO_4^-. These facts are in agreement with the specific adsorption of nitrate ions on gold and their specific adsorption on the deposited Cd adatomos(2).

Quantitative analysis reveals that the current is diffusion controlled ($i \sim v^{1/2}$; $i \sim t^{-1/2}$). In non-buffered solutions and at constant pH, 2.4, the peak current increases with nitrate concentration until a value of 5.10^{-3}M is reached. At higher concentrations, the current remains constant, figure 3. This fact would suggest that the surface was saturated by a layer of adsorbed nitrate ions (3). However, at higher H_3O^+ concentration (for NO_3^- 5.10^{-3}M) the current increases clearly. This mean that H_3O^+ diffusion can play a determinant role on the reduction of nitrate ion in our experimental conditions.

In buffered solutions of a fixed pH higher than before, the peak current

increases as NO_3^- increases, figure 4. Also, at a constant nitrate concentration, 10^{-3}M, the peak current remains constar. at all pH values investigated, pH interval : 3.7 to 5.5.

Thus, the rate of the process is governed by H_3O^+ diffusion in non-buffered solutions and not by the saturation of the electrode surface by adsorbed nitrate ions.

Bibliography.

(1) J.García-Domenech, M.A.Climent, A.Aldaz, J.L.Vázquez and J.Clavilier. J.Electroanal.Chem. 159(1983)223.

(2) G.Horanyi, E.M.Rizmayer and P.Joo. J.Electroanal. Chem. 152(1983)211.

(3) N.M.Trepak, L.K.Il'ina, A.L.L'ov and Y.V.Seryanov. Electrokhimiya 12, nº11,(1976)1725..

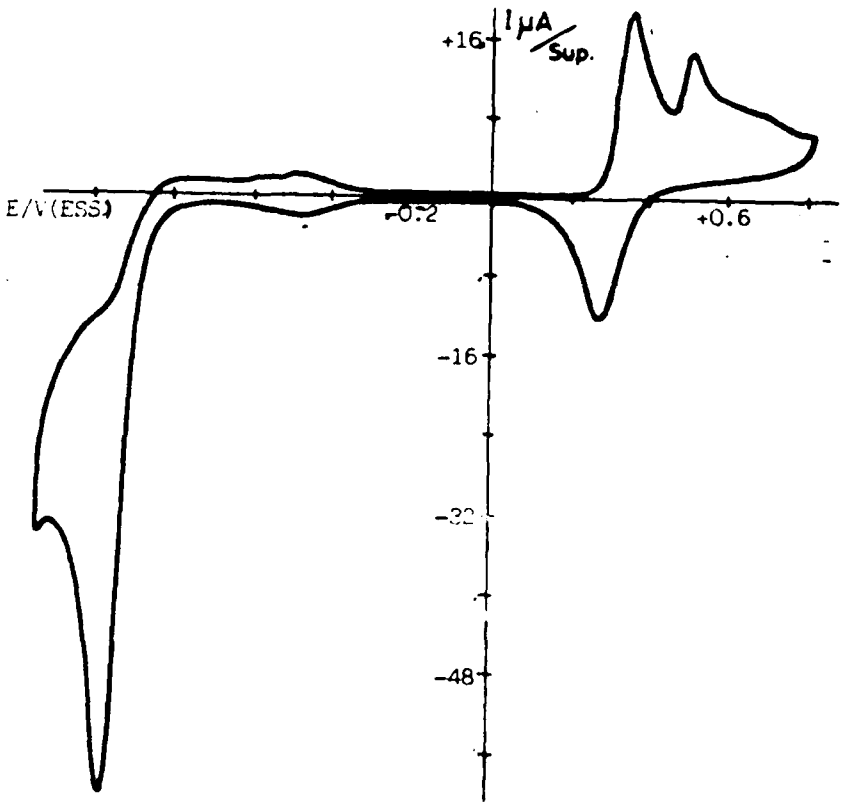

Figure 1. Au/Na_2SO_4 0.5M; $CdSO_4$ 5.10^{-3}M;$NaNO_3$ 2.10^{-2}M. pH = 3.45; v = 50 mv/s.

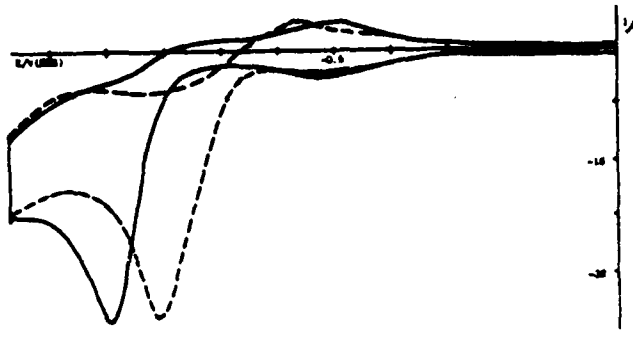

Fig.2. (——)$NaClO_4$ 1.5M + $Cd(ClO_4)_2$ 5.10^{-4}M + $NaNO_3$ 7.10^{-4}. pH=2.4
(——) as before + Na_2SO_4 5.10^{-2}M
v= 50 mv/s.

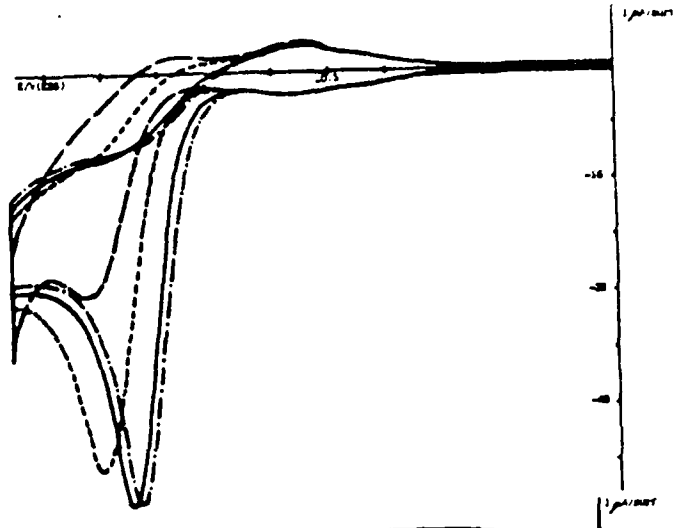

Fig.3 . $NaClO_4$ 1.5M + $CdSO_4$ 5.10^{-4}M; pH=2.40,
v = 50 mv/s.
$NaNO_3$: (— —) 5.10^{-4}M
( )(- - - - -) 1.10^{-3}M.
(———) 5.10^{-3}M.
(—·—·—) 2.10^{-2}M.

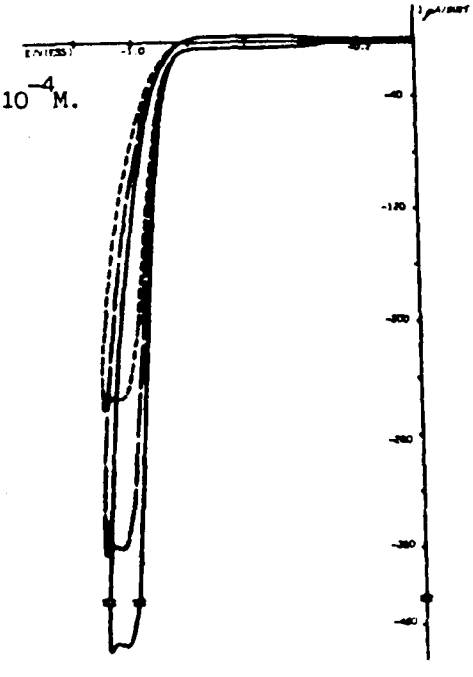

Fig.4. $NaClO_4$ 1.3M HAc/NaAc 0.2M. $CdSO_4$.5.10^{-4}M.
pH = 3.70; v= 50 mv/s.
$NaNO_3$: (- - - - -). 5.10^{-3}M.
(— —). 7,5.10^{-3}M.
(———). 1.10^{-2}M.

05240

CHLORIDE INHIBITION OF OXALIC ACID AT A GOLD ELECTRODE IN ACID MEDIA

E. GOMEZ[a], E. VALLES[a], J.M. FELIU[b], A. ALDAZ[b].
a) Dpto. Química Física, Fac. Química, Universidad de Barcelona.
b) Dpto. Química Física, Universidad de Alicante.

Oxalic acid oxidation usually takes place on bare gold surfaces in an acid (0.5 M H_2SO_4) medium. The process is diffusion controlled ($i\text{-}v^{1/2}$, $i\text{-}c$, $i\text{-}t^{-1/2}$, $i\text{-}w^{1/2}$ linear) and involves two electrons per oxalic acid molecule. The presence of chloride ion inhibits the oxalic acid oxidation progressively and causes the increase of its Tafel slope. At higher Cl^- concentrations ($> 10^{-4}$ M) the normal oxalic peak dissapears and the reaction takes place at more positive potentials.

The voltammetric behaviour of oxalic acid/gold system in 0.5 M H_2SO_4 in presence of different amounts of Cl^- has been studied. The chloride concentration ranges from 7.10^{-7} M (0.5 H_2SO_4 Merk suprapur in MilliQ water) to 10^{-2} M. The Cl^- effect on the oxidation of oxalic acid is clearly observed at concentrations higher than 4.10^{-6} M. Solution stirring (N_2 bubbling) gives smaller currents than quiet solutions at the foot of the wave. The Tafel slope increases from its initial value, accordingly to the following results:

$[Cl^-]$/mol/l	Tafel slope/mV
$7\ 10^{-7}$ (from H_2SO_4 Merk suprapur)	60.1
$1.1\ 10^{-6}$ (from H_2SO_4 Merk p.a.)	62
$4.3\ 10^{-6}$ (added NaCl Merk suprapur)	66.5
$1.1\ 10^{-5}$ (" " " ")	73
$2.2\ 10^{-5}$ (" " " ")	81
$4.3\ 10^{-5}$ (" " " ")	93.5

The later slope is similar to the obtained in a parallel experience after 5 min. immersion into the solution of a K401 Radiometer saturated calomel reference electrode (90 mV/decade).

Peak currents however, give the same current in these experiences. The diminution of the peak current starts for Cl^- concentrations higher than $4.3\ 10^{-5}$ M. From that concentration (Fig. 1) the usual oxalic peak drops quickly as Cl^- increases, and definitly disappears at chloride concentrations higher than $6\ 10^{-5}$ M. N_2 bubbling in this range of concentrations originates the shift of the oxalic peak that moves to more positive values (Fig. 2).

The different adsorption times (Fig. 3) have a strong influence in the voltammetric response at these low concentrations of chloride ion in which Cl^-

adsorption must be governed by difussion. So, the voltammogram varies with detention time at different potentials before the start of the sweep. Detentions at -300 mV vs MSE show an increase of the normal wave of oxalic acid with time. Moreover, detentions at the peak potential cause the inhibition of the oxalic oxidation reaction. So, the current drops to zero in 8 seconds when chloride concentration is 10^{-5} M.
At chloride concentrations higher than 10^{-4} M the normal oxalic peak disappears. The oxidation takes place simultaneously with the tetrachloro aurate complex formation[1]. The simultaneous oxidation of oxalic acid seems to affect the gold corrosion in these conditions (Fig. 4). The charge involved in the reduction peaks is greater in presence of oxalic than in a blank solution of the same chloride concentration.

REFERENCES

(1) J.N. Gaur, G.M. Schmid, J. Electroanal.Chem. 24 (1970) 279
S.H. Caddle, S. Bruckenstein J. Electroanal. Chem. 48 (1973) 325
J. Herrera, C.E. Castellano, A.J. Calandra, A.J. Arvía, J. Electroanal. Chem. 66 (1975) 207.

CAPTIONS

Fig. 1.- Current peak ratio vs log Cl^- . Oxalic acid 4 10^{-4} M in H_2SO_4 0.5 M; i_o is the current without Cl^- addition. 50 mV/s.
Fig. 2.- a) I-E curves of gold at 50 mV/s without agitation. (——) 0.5 M sulfuric acid, (- - -) + 10^{-5} NaCl.
b) I-E curves of 4 10^{-3} M oxalic acid oxidation in 0.5 M H_2SO_4 in presence of 10^{-5} M NaCl. (——) N_2 bubbling through the solution. (- - -) quiet solution. As before, v= 50 mV/s.
Fig. 3.- Effect of a detention at -300 mV vs MSE. Detention time 1-5: 0, 5, 10, 45 and 90 sec.;same conditions as fig. 2 but NaCl was 2 10^{-2} M.
Fig. 4.- I-E curve for 4 10^{-3} oxalic acid oxidation inpresence of 10^{-2} M NaCl (——); (- - -) without oxalic acid. Other conditions as Fig. 2.

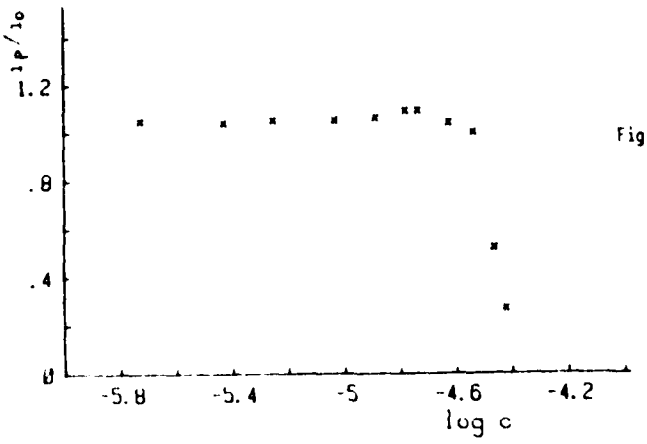

Fig 1

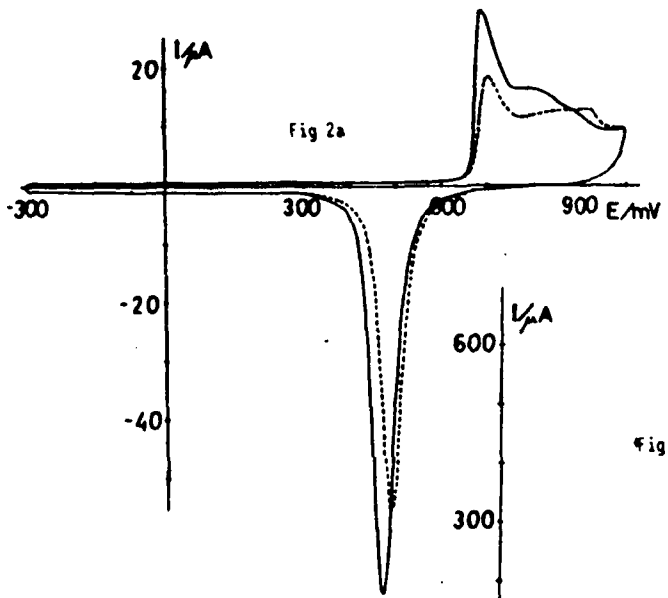

Fig 2a

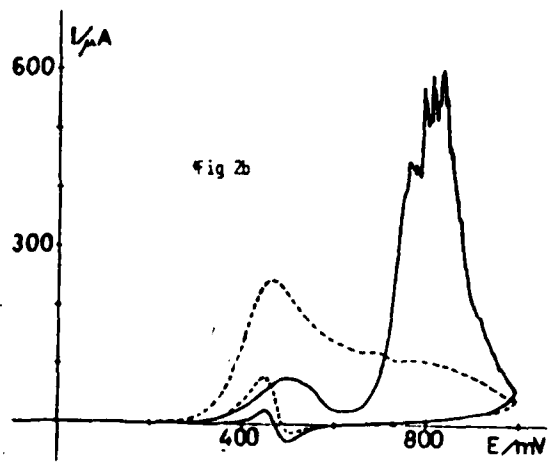

Fig 2b

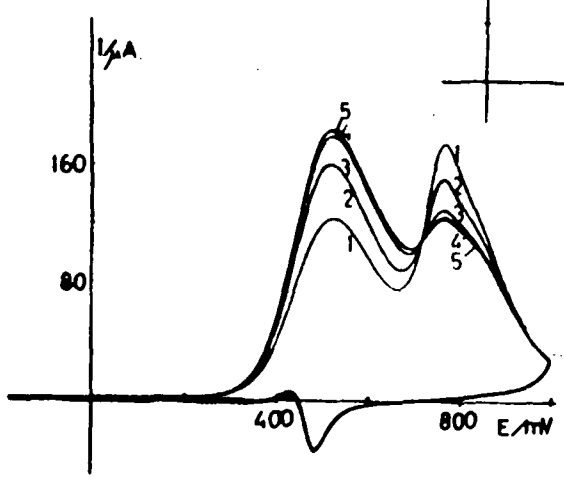

Fig 3

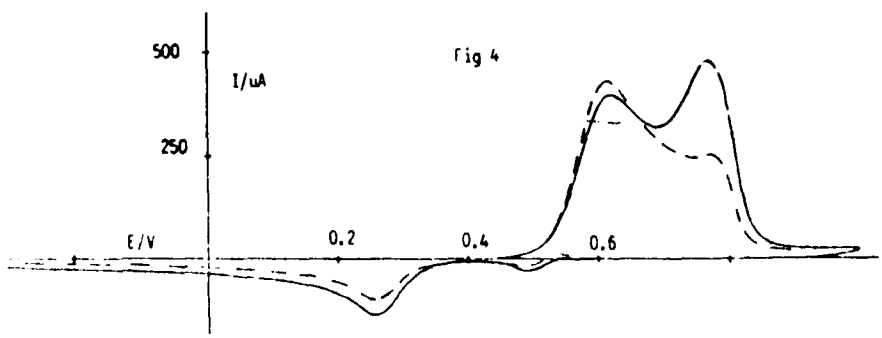

Fig 4

05250

PYRUVATE OXIDATION ON GOLD ELECTRODES IN BASIC MEDIA

E. VALLES[a], E. GOMEZ[a], J.M. FELIU[b], A. ALDAZ[b].
a) Dpto. Química Física, Fac. Química, Universidad de Barcelona.
b) Dpto. Química Física, Universidad de Alicante.

Pyruvate oxidizes on gold electrodes in 0.1 M NaOH through an irreversible two electron reaction. The oxidation process takes place in the OH adsorption zone, before the main gold surface oxidation (Fig. 1), showing a strong inhibition after the peak potential. The peak current is not totally diffusion controlled (the plots $i-v^{1/2}$, i-c and $i-w^{1/2}$ are not linear). The wave is strongly influenced by the presence of Br^- or I^- in solution (Fig. 2). If a positive going sweep is stopped before the peak potential (before the main gold surface oxidation) the current diminishes more quickly as the stirring of the solution increases (rotating disk electrode).

All these facts point to the existence of a heterogeneous process in the oxidation of pyruvate, together with a self-inhibition of the reaction.

Moreover, the reaction is completely blocked when the main surface oxides are formed and this inhibition disapears when the oxides are reduced. An anodic current during the negative going sweep is observed, related to that inhibition process.

The self-inhibition causes that the electrolysis for the obtention of the reaction products to be a very time consuming task because it is impossible to electrolyzer at constant potential. It is necessary to activate the electrode after a few seconds of electrolysis[1]. The overall process can be represented by:

$$C_3H_3O_3^- + 4\ OH^- \longrightarrow CO_3^= + C_2H_3O_2^- + 2\ H_2O + 2\ e$$

As kinetic parameters, Tafel slopes of 90 mV/decade were measured. Orders with respect to pyruvate and OH^- concentration were 0.5 and -0.5 respectively. The influence of solution equilibria have to be taken into account in order to fit these data in a datailed mechanism[2].

If the electrode is cycled in a non-stirred solution forming the same quantity of oxides in the positive going sweep and we alter the scan rate in the negative going sweep, the charge for the reduction of the gold oxides decreases as the same time as the scan rate. This fact siggests the existence of a chemical reaction between pyruvate anion and gold oxides, as in acid medium[3], but open circuit experiments with the system gold

oxides-pyruvate show that when the potential is allowed to reach the stationary state its value implies the existence of gold oxide. This fact shows that there is no direct interaction between gold oxides and pyruvate anion. This behaviour is different from that of oxalic and mesoxalic acids and suggests that slow adsorption of pyruvate on the bare gold formed by oxides reduction may be taking place and causing the difference in reduction charge with the negative scan rate (Fig 4).

REFERENCES

1.- J.M. Feliu, J. Claret, C. Muller, J.L. Vázquez, A. Aldaz, J. Electroanal. Chem. 178 (1984) 271.
2.- M. Ohmori, M. Takagi, Bull. Chem. Soc. Japan 50 (1977) 77.
3.- P. Gonzalo, A. Aldaz, J.L. Vázquez, J. Electroanal. Chem. 130 (1981) 209.

CAPTIONS

Gold electrodes of 0.16 cm^2 were used except in RDE experiments (0.2 cm. diameter). All potentials are referred to MSE.

Fig. 1.- 0.1 M NaOH (- - -) + 1.5 10^{-3} pyruvate (——); v= 50 mV/s.

Fig. 2.- 0.1 M NaOH + 1.25 10^{-3} M pyruvate (——) + 2 10^{-4} M NaCl (- - -) and + 5 10^{-6} M NaBr (-·-·-); v= 50 mV/s.

Fig. 3.- 0.1 M NaOH + 1.7 10^{-3} M pyruvate; v= 50 mV/s, w= 1500 rpm. Arrow indicates the effect of a potential hold on current.

Fig. 4.- 0.1 M NaOH + 10^{-3} M pyruvate; v_+ = 50 mV/s, v_- = 40 (——), 60 (- - -) and 80 (·····) mV/s.

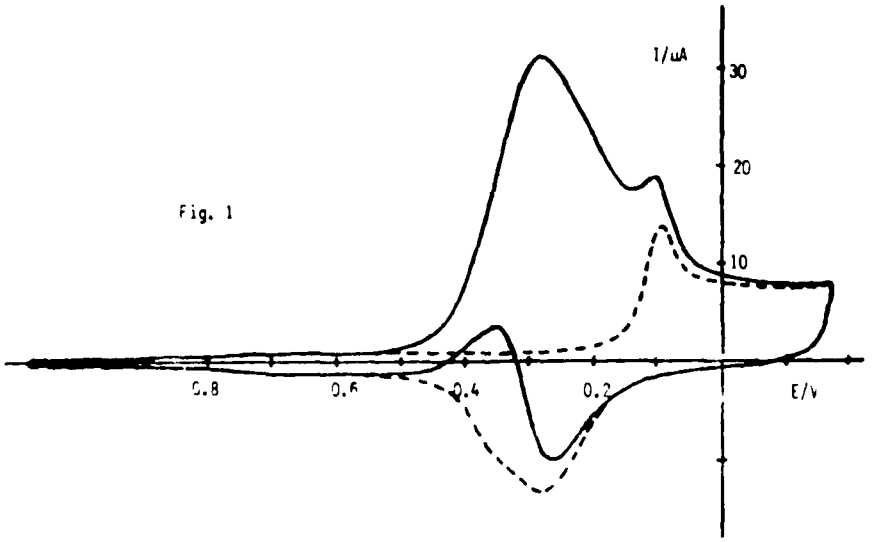

Fig. 1

Fig 2

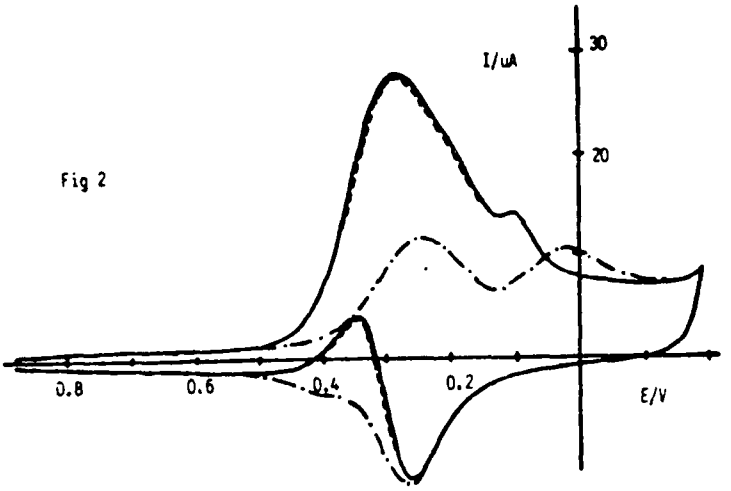

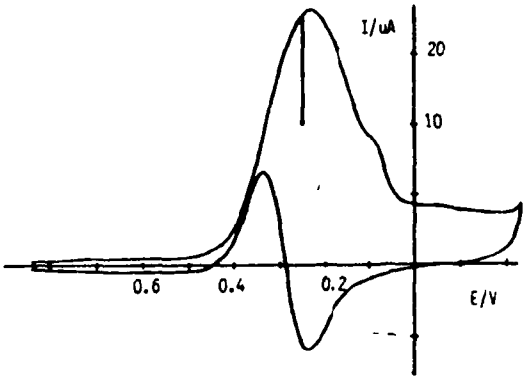

Fig 3

Fig 4

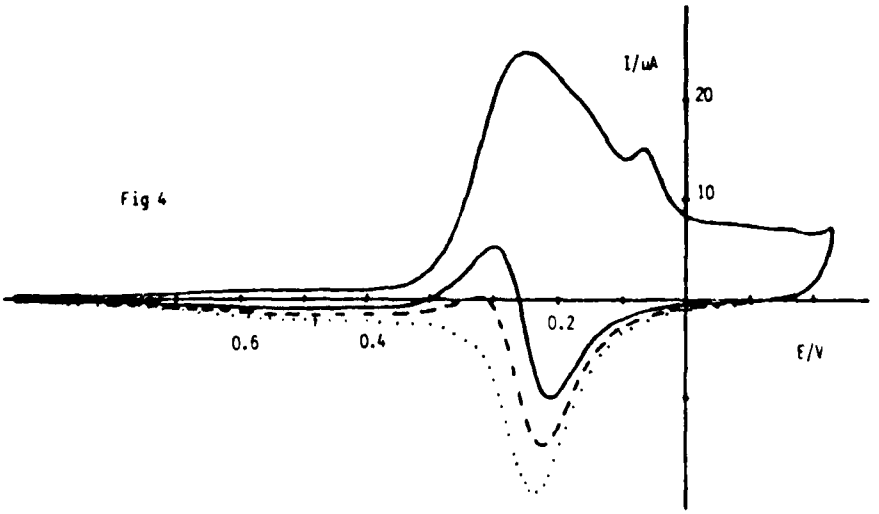

05260

OXALIC ACID OXIDATION ON GOLD IN ACID MEDIUM

J.M. FELIU[a], J. CLARET[b], C. MULLER[b], J.L. VAZQUEZ[a], A. ALDAZ[a]
a) Dpto. Química Física, Universidad de Alicante.
b) Dpto. Química Física, Fac. Química, Universidad de Barcelona.

Oxalic acid oxidation on policrystalline gold electrodes in an acid medium (H_2SO_4 0.5 M) takes place at potentials more negative than the surface oxidation of the metal. The voltammetric, diffusion controlled peak involves two electrons per oxalic acid molecule. Products are CO_2 and protons, in accordance with the general reaction[1]:

$$C_2O_4H_2 \longrightarrow 2CO_2 + 2H^+ + 2e$$

On bare gold surfaces Tafel slopes are 60 mV/decade. Orders with respect to oxalic acid concentration and pH are one in both cases. A mechanism according to this would be:

$$C_2O_4H_2 + M \rightleftharpoons MC_2O_4H + H^+ + e \qquad (K_1)$$

$$MC_2O_4H \longrightarrow MCO_2H + CO_2 \quad \text{rds} \qquad (k_2)$$

$$MCO_2H \rightleftharpoons M + CO_2 + H^+ + e$$

$$i = 2F\, K_1 k_2\, C_{ox}\, C_{H^+}^{-1} \exp fE$$

No Tafel slopes of 120 mV/decade were obtained[2].

In rotating disk experiments a potential hold at limiting current shows no significant diminution of the oxidation current with time, so there is no self-inhibition on bare gold surfaces (fig. 1). However, the current diminishes when metal surface oxidation takes place. This latter fact points to the heterogeneous character of the oxalic acid oxidation and shows the partial inhibition of this reaction due to the oxide formation.

When a hold was made in the negative going sweep after the metal oxidation, the current increases progressively and oxalic acid is accummulated near the surface (fig. 2). Moreover, the surface oxides reduction peak involves a charge which is lesser than the one obtained in absence of oxalic acid. These results show that the oxalic acid oxidation continues at a lower rate, on oxidized surfaces, and there is associated with a chemical reaction between oxalic acid and gold surface oxides. Open circuit experiments also support these explanations.

Different behaviour is observed when the positive oxidation limit is increased to sufficiently high values (1.5-1.7 V vs SSE). As in other cases[3] the oxalic acid oxidation is totally inhibited (fig. 3). When the negative going sweep is re-started, after the hold, the outer oxide peak diminishes in the presence of oxalic acid, but the surface oxides peak is unaffected. This This diminution is due probably to the existence of an electrochemical mechanism in the reaction of oxalic acid with the outer oxide. The reaction would start only when surface gold oxides are electrochemically eliminated.

After bulk oxides have been reduced an oxidation current in the negative going sweep is observed. This current is higher than the corresponding one obtained in the positive going sweep. This excess of current is observed in the usual potential controlled region, an has the aspect of a decay current. The new peak is unaffected by the agitation and it is influenced by pH and oxalic acid concentration. At constant potential the current of this new peak varies with time. These facts can be explained on the basis of a supposed re-organization of a higly active surface after the bulk oxide reduction.

REFERENCES

1.- J.W. Johnson, S.C. Mueller, W.J. James, Trans. Faraday Soc. 67 (1971) 2167.
2.- S.A. Sargisyan, Yu.B. Vasil'ev, Elektrokhimiya 18 (1982) 845.
3.- U. Oesch, J. Janata, Electrochim. Acta 28 (1983) 1237, 1247.

CAPTIONS

Fig. 1: 10^{-3} M oxalic acid in 0.5 M H_2SO_4. (——) v= 50 mV/s, w=0. (- - -) v= 50 mV/s, w= 1000 rpm.

Fig. 2: 10^{-2} M oxalic acid in 0.5 M H_2SO_4. Effect of 1 min. hold at 780 mV vs SSE during the negative going sweep (- - -). Normal sweep (——), v= 50 mV/s.

Fig. 3: 5.4 10^{-3} M oxalic acid in H_2SO_4 0.5 M. E_+ = 1.75 V vs SSE. v= 50 mV/s, w= 1000 rpm.

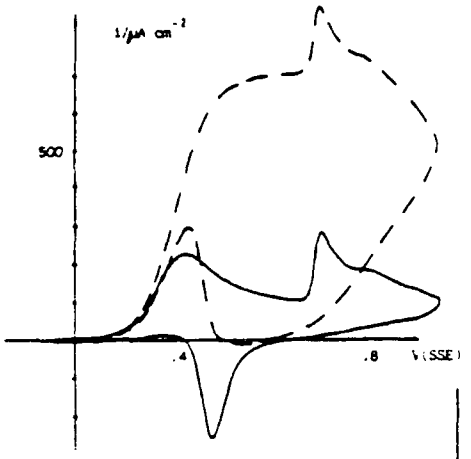

Fig. 1

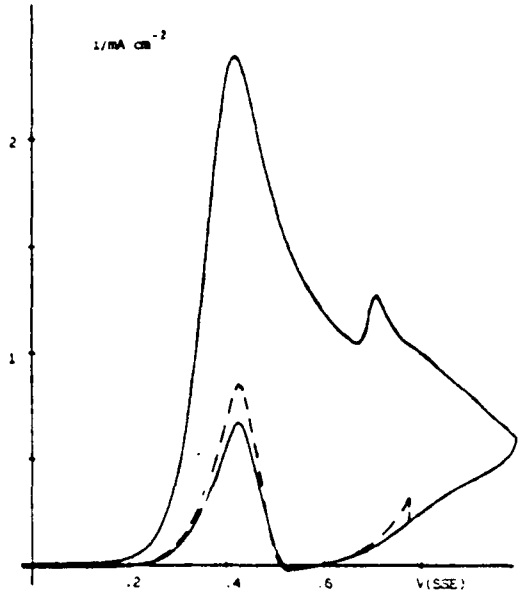

Fig.2

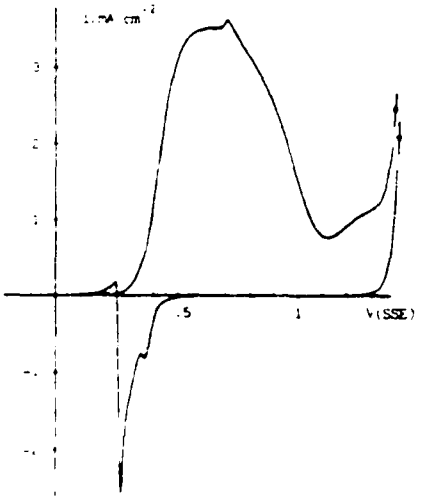

Fig.3

DIAGNOSTIC CRITERIA FOR CHARACTERIZATION OF MECHANISMS IN POLAROGRAPHY

M. BLAZQUEZ, L. CAMACHO, M. JIMENEZ and M. DOMINGUEZ
Departamento de Quimica Fisica, Facultad de Ciencias,
Universidad de Cordoba, 14005 Cordoba (Spain)

INTRODUCTION

In a previous paper[1] diagnostic criteria for characterization of CE and CEC mechanisms by polarography were presented. They were based in the calculation of i-E functions for such mechanisms using the reaction layer theory. The application to the first wave of pyridine-4-aldehyde reduction was discussed therein. However, pyridine-4-aldehyde, like other aromatic carbonyl compounds, yields two one-electron polarographic waves in acidic medium. Pyridinium carboxaldehydes give rise to a second wave whose behaviour is rather different to that corresponding to other carbonyl compounds. Thus, the half wave potential is not pH-independent, but shifts to more negative potentials as the pH increases[2-4]. This behaviour had been explained for 1-methylpyridinium carboxaldehydes assuming a protonation of the radical formed in the first wave prior to the second irreversible reaction transfer[3].

The aim of this study is the calculation of the i-E functions corresponding to the second reduction wave under different conditions for mechanisms corresponding both to diffusion processes and to kinetic ones in the limiting zone of the polarographic wave.

THEORETICAL

We shall consider the following reactions:

$$A \rightleftharpoons B \qquad (1)$$

$$B + e \rightleftharpoons C \quad \text{1st wave} \qquad (2)$$

$$2C \xrightarrow{k_3} D \qquad (3)$$

$$C + e \underset{k_{-4}}{\overset{k_4}{\rightleftharpoons}} E \quad \text{2nd wave} \qquad (4)$$

$$E \xrightarrow{k_5} F \qquad (5)$$

We have assumed the diffusion coefficient to be the same for all the species involved and B to be the only species existing in solution for diffusion-controlled processes. A mixture of species A and B in a ratio depending on the

equilibrium constant will exist in solution for kinetic processes.

Expresions have been obtained either by the reaction layer[5] approach or from the asumption that the reaction are rapid enough to take place at the surface of the electrode.[6] Diagnostic criteria for characterizing several processes have been obtained and their application to the pyridine-4-aldehyde will be discussed in the following section.

RESULTS AND DISCUSSION

Laviron[2] states that the limiting current of the second wave occurring above pH 4 is kinetically-controlled, the chemical reaction involving the dehydration of the carbonyl group. The abnormal behaviour with respect to a classic mechanism, (E shifts with the pH) can be explained by assuming an increase of the free radical reduction rate. formed in the first stage, with respect to the protonation rate, due to the strongly electronegative influence of heterocyclic nitrogen. However, no direct experimental evidence is presented herein.

Our results indicate that in acidic medium (pH 0-6) pyridine-4-aldehyde yields two polarographic waves with the same limiting current and kinetically-controlled in the limiting zone.

Owing to the proximity of both waves the logarithmic analyses perfomed for the second wave do not provide unequivocal results. Thus, E vs $\log(i^{3/2}/(i_L - i))$ plots give rise to straight lines with slopes close to -40 mV/dec, whilst E vs $\log(i^2/(i_L - i))$ plots also yield linear segments with slopes of about -30 mV/dec. The regression analysis of the graphs does not permit us to dicern between the mechanisms corresponding to both representations although they are in favour of a reversible transfer reaction.

The table shows theoretical and experimental values of $dE_{\frac{1}{4}}/d\log t$ for two possible mechanisms.

pH	$dE_{\frac{1}{4}}/d\log t$ (mV)	$d\ln i_L/d\ln t$	i_L/i_D	theoretical $dE_{\frac{1}{4}}/d\log t$ (mV)	
				mechanism a	mechanism b
2.14	0	0.62	0.1	1	1.5
4.15	8	0.50	0.38	3.7	5.6

The experimental results are in agreement with a mechanism involving a reversible transfer reaction followed by a first or pseudo-first order chemical reaction, the limiting current being controlled by a prior chemical reaction. One further evidence in favour of such mechanisms and which also permits us to account for the shift of the wave brought about by an

increase in pH, is the value of the slope of $E_{\frac{1}{2}}$ vs. pH plot, -60 mV/dec, which coincides with that reported for 1-methyl-pyridine-4-aldehyde[3], thus indicating the occurence of a protonation step prior to (mechanism a) or following the transfer reaction (mechanism b). In principle the latter alternative is considered to be more feasible and will be discussed first. For such a mechanism and assuming that $k = k|H^+|$, i.e., reaction (5) corresponds to the protonation of the product of the second one-electron transfer as for other cabonyl compounds occurs[7-9], the theoretical values of the slope of the $E_{\frac{1}{2}}$ vs. pH plot is -60 mV/dec, in agreement with our experimental results. The $dE_{\frac{1}{2}}/d\log C$ values, -30 mV/dec, is consistent with such mechanism.

However, if a quasi-equilibrium protonation step prior to the transfer is postulated, the theoretical value of the slope of the $E_{\frac{1}{2}}$ vs pH plot is also -60 mV for reversible mechanisms, although it would be necessary to postulate a further chemical reaction following the transfer in order to account for influence of the drop time on the half-wave potentials.

REFERENCES

1. L. Camacho, M. Blazquez, M. Jimenez and M. Dominguez, J. Electroanal. Chem., 172(1984)173.
2. E. Laviron, Bull. Soc. Chim. France, 2323(1961)
3. J. F. Rusling, J. P. Segretario and P. Zuman, J. Electroanal. Chem., 143(1983)291
4. R. Izquierdo, M. Blazquez, M. Dominguez and F. Garcia-Blanco, Bioelectrochem. and Bioenergetics, 12(1984)25.
5. R. Bridcka and K. Wiesner, Naturwiss 31(1943)247
6. R. Bonaterre and G. Cauquis, J. Electroanal. Chem., 32(1971)183.
7. P. Zuman, D. Barnes and A. Rivolova-Kejharova, Discuss. Faraday Soc., 45(1968)202.
8. P. Zuman, Coll. Czech. Chem. Comm., 33(1968)2548.
9. M. Blazquez, J.M. Rodriguez-Mellado and J.J. Ruiz, An. Quim., 79(1983)42.

05280

AN APPROXIMATE EXPLICIT EQUATION IN DIFFERENTIAL PULSE POLAROGRAPHY FOR FIRST-ORDER PROCESSES

J.M. RODRIGUEZ-MELLADO, M. BLAZQUEZ, M. DOMINGUEZ and J.J. RUIZ
Departamento de Quimica Fisica, Facultad de Ciencias,
Universidad de Cordoba. 14005 Cordoba (Spain).

The aim of this work is to propose an approximate method applicable to electrochemical processes either coupled or not to first-order chemical reactions. The method can be extended to those cases in which two or more electroactive species are discharged at relatively close potentials.

THEORETICAL

Explicit i-E functions for d.c. polarography have been derived in the literature and, particularly, by assuming that the reaction layer theory is satisfied for kinetic processes. These functions can be written in general forms as:

$$E = E_{\frac{1}{2}}' - \frac{RT}{\alpha nF} \ln \frac{i}{i_L - i} \qquad (1)$$

where $\alpha=1$ for reversible transfers and i_L is the limiting current.

The E_p values for each mechanism have been obtained when both the τ value, the potential-application time instead of drop time, and for prekinetic processes the known expressions for i_L/i_D are used.

From eqn. 1 and assuming that $di/de=\Delta i/\Delta E=I$, the approximate equation for DPP can be expressed as:

$$I = 4I_p \frac{L}{(1+L)^2} \qquad (2)$$

I_p being the peak intensity.

The validity of the approximation chosen for prekinetic cases, has been checked by comparing the theoretical values obtained from eqn. 2 with those found from a more sophisticated treatment recently derived[1], as shown in figure 1.

Eqn. 2 can be easily extended to two or more waves in DPP assuming that the mass transports of electroactive species are independent. In this case, for n waves:

$$I = \Sigma 4I_{p,i} \frac{L_i}{(1+L_i)^2} \qquad (3)$$

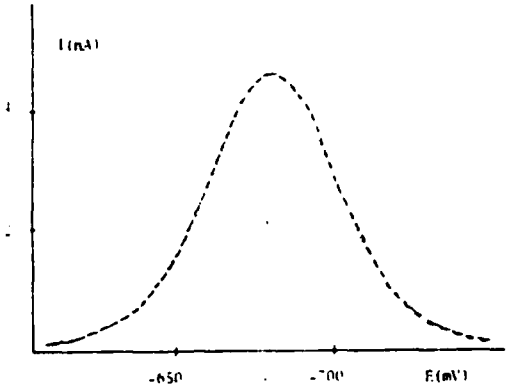

Fig.1 Dotted line: Theoretical values found with $1/K = 1.37.10^{-5}$, $k_1 = 15.8\ s^{-1}$ from ref. 1. Dashed line: Theoretical values obtained from eqn. 2.

RESULTS AND DISCUSSION

In order to check the validity of above theoretical expressions, an optimization BASIC program has been developed. This program accepts a series of potential and intensity experimental data, previously stored in a data file, the intensities being normalized by dividing each datum by the maximun value of this variable. From approximate values of peak intensities, peak potentials and logarithmic analysis slopes, an optimization of these parameters is carried out by minimizing the standard deviation of the residuals.

The method has been tested with the aid of well-known oxidation and reduction processes (reduction of Cd(II) ion, benzophenone in a neutral medium, diacetil and alloxan, and oxidation of ascorbic acid). In all cases, the parameters obtained, Ep, Ip and peak half-widths are in agreement with the experimental data. Logarithmic analysis slopes obtained with this method are consistent with those obtained by DC polarography.

On the other hand, the possibility of qualitative and quantitative determination of two electroactive species with close discharge potentials by DPP has been extensively analyzed recently by Bobrowski and applied to the reduction of In(III) and Cd(II) mixtures.

The curve-fitting method proposed herein has been applied to the analysis of the same mixtures. In figure 2 is shown a typical DPP polarogram together with the corresponding theoretical curve.

In the Table are shown the calculated and experimental errors for each quantitative determination. The results obtained by Bobrowski have also been included for comparison. As can be seen, the proposed method improves peak resolution, especially in those cases in which a shoulder appears.

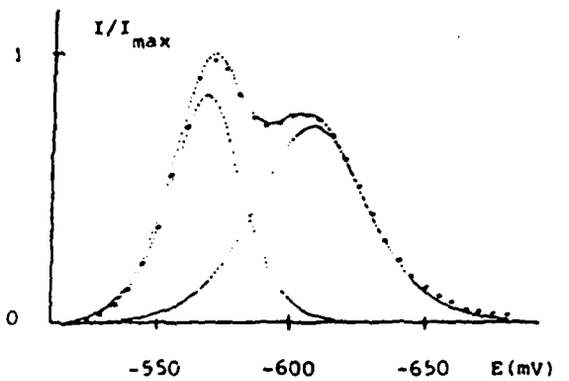

Fig.2 DP polarograms for 2.10^{-4}M Cd(II) and 1.10^{-4}M In(III) mixture in 0.2 M HCl.

Solutions		Experimental error (%)		Calculated error (%) (ref 2)		Calculated error	
In(III)	Cd(II)	In	Cd	In	Cd	In	Cd
$2 \cdot 10^{-5}$	$4 \cdot 10^{-5}$	15.0	18.8	17.7	4.0	0.0	9.8
10^{-4}	$2 \cdot 10^{-4}$	10.1	11.0	18.1	3.9	2.4	2.5
10^{-4}	$4 \cdot 10^{-4}$	31.9	9.3	*	2.2	0.4	5.8
10^{-3}	$4 \cdot 10^{-5}$	2.0	*	2.1	*	1.1	46.0
$2 \cdot 10^{-5}$	$2 \cdot 10^{-4}$	*	6.0	--	--	0.5	3.5

* Shoulder

Theoretical and experimental errors in the determination of In and Cd mixtures.

REFERENCES
1. M. H. Kim and R. L. Birke, Anal. Chem. 55 (1983) 1735
2. A. Bobrowski, Chem. Anal. 28 (1983) 557

POTENTIOSTATIC REDUCTION OF METAL COMPLEXES ON MERCURY ELECTRODE FOR ANY LIGAND/METAL RELATIONSHIP VALUE.

M. BARRERA, M. PEREZ SANCHEZ, M. MARTIN ARTILES and A. AREVALO.
Department of Physical Chemistry.Faculty of Chemistry.University of La Laguna.Canary Islands.Spain.

In this communication, the reduction wave on a mercury electrode of area $A(t) = a\ t^b$ is analized, where a and b are positive constants.The general pattern of the charge transfer process is :

$$^{n+}MX_j + (n-m)\ e^- \ (k_s, \alpha, E^o_{j/i}) = {}^{m+}MX_i + (j-i)\ X \qquad (1)$$

where j = 0 or j = p if the cation or $^{n+}MX_p$ complex is the electroactive species; likewise i = 0 or i = q if the reaction product is M^{m+} or $^{m+}MX_q$ coordinate species.

The difussion of all components to (from) the interface from (to) the bulk solution is described by the expanding-plane model.According to K. B. Oldham[1], we can write for the species M^{n+} and $^{n+}MX_p$:

$$\frac{\partial C_M n+(r,t)}{\partial t} = \frac{br}{t}\frac{\partial C_M n+(r,t)}{\partial r} + D\frac{\partial^2 C_M n+(r,t)}{\partial r^2}$$

$$\frac{\partial Cn+_{MX_p}(r,t)}{\partial t} = \frac{br}{t}\frac{\partial Cn+_{MX_p}(r,t)}{\partial r} + D\frac{\partial^2 Cn+_{MX_p}(r,t)}{\partial r^2} \qquad (2)$$

For mathematical simplicity the difussion coefficients of all species are assumed to be equal to D.

The homogeneity's and microelectrolysis's conditions can be expressed by the equations :

$$M^{n+} : C_M n+(r,0) + C_{n+_{MX_p}}(r,0) = C^t_M n+ = C_M n+(\infty,t) + C_{n+_{MX_p}}(\infty,t)$$

$$M^{m+} : C_M m+(r,0) + C_{m+_{MX_q}}(r,0) = 0 = C_M m+(\infty,t) + C_{m+_{MX_q}}(\infty,t)$$

$$X : C_X(r,0) + p\,C_{n+MX_p}(r,0) = C_X^t = C_X(\infty,t) + p\,C_{n+MX_p}(\infty,t) \qquad (3)$$

where $C_M^t{}^{n+}$ and C_X^t are the analytical concentrations of M^{n+} and X.

The surface concentration gradient, of the possible electroactive species M^{n+} and $^{n+}MX_p$, is related to the cathodic faradaic current by :

$$\left[\frac{\partial C_M{}^{n+}(r,t)}{r}\right]_{r=0} + \left[\frac{\partial C_{n+MX_p}(r,t)}{r}\right]_{r=0} = \frac{I(t)}{(n-m)FDA(t)} \qquad (4)$$

which follows from the requirements of Fick's and Faraday's laws.

The absolute rate reaction theory applied to pattern (1) gives :

$$\frac{I(t)}{(n-m)FA(t)} = k_s\left[C_{n+MX_j}(0,t)\,\varepsilon(t)^{-\alpha} - C_{m+MX_i}(0,t)\,C_X^{j-i}\,\varepsilon(t)^{1-\alpha}\right] \qquad (5)$$

where $\varepsilon(t) = \exp\left[\frac{(n-m)F}{RT}\left[E(t) - E^o_{j/i}\right]\right]$ and k_s is the standard heterogeneous rate constants (cm s^{-1}).

To solve the differential equations (2) the new independent variables x and y, according to ref. 1, are defined.By using the Laplace transformation with respect to y, the general equation is obtained :

$$\mathcal{L}\left[\frac{\left[i(y)\,y^{\omega-1/2}\,\varepsilon(y)^{\alpha}\,C_X^{-j}(0,y) + \varepsilon(y)\,\frac{\beta_i}{1+\beta_q C_X^q(0,y)}\right]\left[1+\beta_p C_X^p(0,y)\right]}{\beta_j + \varepsilon(y)\,\frac{\beta_i}{1+\beta_q C_X^q(0,y)}\left[1+\beta_p C_X^p(0,y)\right]}\right]$$

$$= (1/s) - (1/s^{1/2})\,\mathcal{L}\left[i(y)\,y^{2\omega-1}\right] \qquad (6)$$

where $\omega = 1/4b+2$, β_p and β_q are the overall stability constants of MX_p and MX_q.

As pointed out by K. B. Oldham[1] and N.G. Elenkova— T.K. Nedelcheva[2], this equation involves all degrees of reversibility and may be solved under different specific electrolysis regimes.

We think the equation (6) is more general than that obtained by N.G. Elenkova— T.K. Nedelcheva[2] because under the conditions : $m = 0$, $\beta_i = 1$ and $\beta_q = 0$, the equation (6) becomes identical to that given in ref. 2.

The equation (6) has been applied to the "order 0" and "order 2" electrolysis.In the latter, the "Levich-Guidelli aproximation"[3,4,5] has been used.The mean currents can be easily obtained by applying the procedure

given by R. Guidelli[4].

At the present we are carrying out a similar study to that of N.G. Elenkova— T.K. Nedelcheva[6,7], with the equation obtained by us in order to determine the mechanism of electrode process (i, j, k_s, α) and the overall stability constants of complex species.

REFERENCES

1. K.B. Oldham, Anal. Chem., 41,936 (1969).
2. N.G. Elenkova and T.K. Nedelcheva, J. Electroanal. Chem., 69,385 (1976).
3. V.G. Levich, B.I. Khainin and E.D. Belokolos, Elektrokhimiya,1,1273 (1965).
4. R. Guidelli, J. Electroanal. Chem., 33,291 (1971).
5. R. Guidelli, J. Electroanal. Chem., 33,303 (1971).
6. N.G. Elenkova and T.K. Nedelcheva, J. Electroanal. Chem., 69,395 (1976).
7. N.G. Elenkova and T.K. Nedelcheva, J. Electroanal. Chem., 108,239 (1980).

GALVANOSTATIC REDUCTION OF METAL COMPLEXES ON MERCURY ELECTRODE FOR ANY LIGAND TO METAL RELATIONSHIP VALUE.

M. BARRERA, M. PEREZ SANCHEZ, M. MARTIN ARTILES and A. AREVALO.
Department of Physical Chemistry.Faculty of Chemistry.University of La Laguna.Canary Islands.Spain.

From the equation given by N.G. Elenkova and T.K. Nedelcheva[1] the galvanostatic reduction of metal complexes on a mercury electrode whose area is expressed by $A(t) = a\ t^b$, is analized.The general scheme of reduction is :

$$MX_p + n\ e^- + Hg \quad (k_s, \alpha, E_p^s) = M(Hg) + p\ X \qquad (1)$$

where p = 0 or p = q when M(n+) or the complex MX_q are respectively reduced.

By using the expanded plane electrode model and assuming the difussion coefficients for all the complex species are equal and by using the independent variables defined in a previous paper of K.B. Oldham[2], the next expression has been obtained(ref. 1) :

$$\mathcal{L}\left[\frac{\left[i(y)\ y^{\omega-1/2}\ \mathcal{E}^{\alpha}(y)\ C_X^{-p}(0,y) + \mathcal{E}(y)\right]\ \left[1 + \beta_q\ C_X^q(0,y)\right]}{\beta_p + \mathcal{E}(y)\ \left[1 + \beta_q C_X^q(0,y)\right]}\right] = (1/s) - (1/s^{1/2})\,\mathcal{L}\left[i(y)\ y^{2\omega-1}\right] \qquad (2)$$

where $\omega = 1/4b+2$, β_q is the overall stability constants of MX_q and C_X is the free ligand concentration.This equation invclves all the degrees of reversibility and may be solved under the different specific electrolysis regimes.

The above equation will be studied in galvanostatic conditions, that is, i(y) do not depend on y, this condition leads to a simplification of equation (2).According to the identity :

$$(1/s) - (i/s^{1/2})\ \mathcal{L}\left[y^{2\omega-1}\right] = \mathcal{L}\left[1 - \frac{i\,\Gamma(2\omega)}{\Gamma(2\omega+1/2)}\ y^{2\omega-1/2}\right],$$

after application of the $\mathcal{L}^{-1}$ operator, the equation (2) is transformed

in the next way :

$$\frac{\left[i\, y^{\omega-1/2}\varepsilon^{q}(y)\; C_X^{-p}(0,y) + \varepsilon(y)\right]\left[1+\beta_q C_X^q(0,y)\right]}{\beta_p + \varepsilon(y)\left[1 + \beta_q C_X^q(0,y)\right]} = 1 - \frac{i\,\Gamma(2\omega)}{\Gamma(2\omega+1/2)}\, y^{2\omega-1/2} \qquad (3)$$

If the galvanostatic experience is carried out on a HMDE, the condition b = 0 and therefore A = a and $\omega = 1/2$ is introduced; by using the change of variables proposed by K.B. Oldham[2] and introducing the concept of "transition time", the equation (3) can be rewritten like :

$$(\pi D/\tau)^{1/2}\, \frac{\left[1 + \beta_q C_X^q(0,t)\right]}{2k_s \beta_p C_X^p(0,t)}\, \exp\left[\frac{nF}{RT}\left[E(t) - E_p^s\right]\right] +$$

$$+ (t/\tau)^{1/2}\, \frac{\left[1+\beta_q C_X^q(0,t)\right]}{\beta_p}\, \exp\left[\frac{nF}{RT}\left[E(t) - E_p^s\right]\right] = 1-(t/\tau)^{1/2} \qquad (4)$$

being : D = difussion coefficient ; τ = transition time; k_s = standard heterogeneous rate constant ; α = cathodic transfer coefficient and E_p^s = standard potential of the reaction (1).

The equation (4) is of the great generality, it is aplicable to all reversibility degrees.Furthermore, no simplifying assumpticns were made concerning either the stability of complex or the initial concentration C_M^t and C_X^t .

An early test of the validity of equation (4) is shown by the possibility to reach from it, already existing equations in the literature.Indeed, by following the terminology of R. Bennes[3], and by making the next substitutions :

$$\frac{nFAC_M^t k_s}{I}\, \exp\left[\frac{\alpha nF}{RT} E_p^s\right] = \exp\left[\frac{\alpha nF}{RT}\,(E_p^i)\right] \quad , \text{ and}$$

$$\frac{\left[1 + \beta_q C_X^q(0,t)\right]}{\beta_p}\, \exp\left[-\frac{nF}{RT} E_p^s\right] = \exp\left[-\frac{nF}{RT}\,(E_e^o)_C\right]$$

the equation (4) is inmediatly transformed to the equation proposed by R. Bennes if it is $C_X^t \gg C_M^t$, which implies $C_X(0,t) = C_X^t$.

In the analysis of equation (4) it is a fundamental condition that an expression of $C_X(0,t)$ as function of experimental variables and of previously established parameters is available.With this aim, the next

expression has been obtained :

$$C_X(0,t) = C_X^t - q\, C_M^t \frac{\beta_q\, C_X^t(\infty,t)}{\left[1 + \beta_q C_X^t(\infty,t)\right]} \left[1 - (t/\tau)^{1/2}\right] \qquad (5)$$

which let us to calculate by an experimental way the value of $C_X(0,t)$ at any time, whenever in a previous experience the free ligand bulk concentration is determined.This a measurement would not be necessary in the case of the very stable complexes, since the next expression

$$C_X(0,t) = C_X^t - q\, C_M^t \left[1 - (t/\tau)^{1/2}\right]$$

would be hold.

At the present we are carrying out an analysis of equation (4) which let us to obtain some experimental methods for determining the charge transfer mechanism(p, k_s, α), stability constants of complexes(very stable) and after all the experimental verification of equation (4).

REFERENCES

1. N.G. Elenkova and T.K. Nedelcheva, J. Electroanal. Chem., 69,385 (1976).
2. K.B. Oldham, Anal. Chem., 41,936 (1969).
3. R. Bennes, These, Montpellier, 1973.

POLAROGRAPHIC REDUCTION OF METAL COMPLEXES TO A LOWER OXIDATION STATE FOR ANY VALUE OF ANALYTICAL LIGAND CONCENTRATION/ANALYTICAL METAL ION CONCENTRATION.

M. BARRERA, M. MARTIN ARTILES, M. PEREZ SANCHEZ and A. AREVALO.
Department of Physical Chemistry.Faculty of Chemistry.University of La Laguna.Canary Islands.Spain.

The reversible polarographic reduction of a type of systems in which a metal ion and a series of its complexes are in fast equilibria is studied.The electrode process is represented by :

$$^{n+}MX_p + (n-m)\, e^- = {}^{m+}MX_q + (p-q)\, X \qquad (1)$$

The ratio C_X^t/C_M^t can have any value; being C_M^t and C_X^t, the analytical concentrations of cation and ligand.Initially there are neither M^{m+} nor its complexes in dissolution.

For thermodynamical suitabilities the process can be represented by the scheme :

$$^{n+}MX_p = M^{n+} + p\, X \; ; \; M^{n+} + (n-m)\, e^- = M^{m+} \; ;$$
$$M^{m+} + q\, X = {}^{m+}MX_q \qquad (2)$$

If the process shows a reversible polarographic behaviour, the interface concentrations and the electrode potential follow the Nernst equation. According the traditional methods of analysis for this type of systems , the next equation is obtained :

$$\exp\left[-\frac{(n-m)F}{R\,T}\left(E-E^{M^{n+}/M^{m+}}_{1/2}\right)\right]\frac{\bar{i}d_C'}{\bar{i}d_{M^{m+}}}\,\frac{\bar{i}d_{M^{n+}}}{\bar{i}d_C}\,\frac{\bar{i}d_C-\bar{i}}{\bar{i}} = \frac{\sum_{p=0}^{p=N}\beta_p\,(C_X^o)^p}{\sum_{q=0}^{q=N}\beta_q\,(C_X^o)^q} \qquad (3)$$

where : $\bar{i}d_{M^{m+}}$ = limiting difussion current for the charge transfer $M^{m+} + m\, e^- = M(Hg)$ in a similar experimental conditions to those of the scheme (2); $\bar{i}d_C'$ = limiting difussion current for the previous reduction but in

presence of the complexing agent X; $\bar{i}d_{M^{n+}}$, $\bar{i}d_C$ = limiting difussion currents according the scheme (2) respectively in absence and presence of ligand; C_X^o = complexing agent concentration in the interface.

In the studies where the ligand X is in a great excess to the metal ion , that is, for great values of C_X^t/C_M^t , the value of C_X^o can be identified with C_X^t and the equation (3) can be rewritten like known equations of the literature[1].

However, in this occasion a more general case is treated, and the C_X^o is expressed by :

$$C_X^o = C_X^t - \bar{p}\, C_{M^{n+}}^t + \left[(\bar{p}/K_X) - (\bar{q}^o/\bar{K}_{MX_q})\right] \bar{i} \qquad (4)$$

where : $\bar{p}$ = average number of ligands in the dissolution(refered to cation M^{n+}); $\bar{q}^o$ = average number of ligands in the interface (refered to cation M^{m+}); K_X and $\bar{K}_{MX_q}$ are the constants of Ilkovic for the ligand and the MX_q complexes.

In this way, the equation of the $\bar{i}$-E curve for the reduction according to the scheme (2) for any value of the ratio $C_X^t/C_{M^{n+}}^t$ in a determined medium and a supporting electrolyte at a suitable concentration is given by :

$$\exp\left[-\frac{(n-m)F}{RT}\left(E - E^{M^{n+}/M^{m+}}_{1/2}\right)\right] \frac{\bar{i}d_C'}{\bar{i}d_{M^{m+}}} \frac{\bar{i}d_{M^{n+}}}{\bar{i}d_C} \frac{\bar{i}d_C - \bar{i}}{\bar{i}} =$$

$$= \frac{\sum_{p=0}^{p=N_p} \beta_p \left[C_X^t - \bar{p}C_{M^{n+}}^t + \left[(\bar{p}/K_X) - (\bar{q}^o/\bar{K}MX_q)\right]\bar{i}\right]^p}{\sum_{q=0}^{q=N_q} \beta_q \left[C_X^t - \bar{p}C_{M^{n+}}^t + \left[(\bar{p}/K_X) - (\bar{q}^o/\bar{K}MX_q)\right]\bar{i}\right]^q} \qquad (5)$$

β_p and β_q being the overall and apparent stability constants of the MX_p and MX_q complexes; N_p and N_q being respectively coordination numbers of M^{n+} and M^{m+}.

The equation (5) is of the general validity, since it comprises to all processes of reversible polarographic reduction for the cases of change of oxidation state and for the amalgam formation; and it is possible to obtain the various and already known equations existing in the literature[1,2]. This can be assumed like an initial test of the validity of the equation (5).At present, the experimental verification of (5) by methods deduced from its algebraical expression.

REFERENCES

1. J. Heyrovský, J. Kuta : Principles of Polarography, Academic Press, New York, 1966.
2. M. Martín Artiles,: Tesina Licenciatura (1983).Department of Physical Chemistry.University of La Laguna.Canary Islands.Spain.

05320

A STUDY ON THE REDUCTION OF THE Zn(II)-SUCCINATE COORDINATE SYSTEM ON MERCURY ELECTRODE.

M. PEREZ SANCHEZ, M. BARRERA, B. DOMINGUEZ and A. AREVALO.
Department of Physical Chemistry.Faculty of Chemistry.
University of La Laguna.Canary Islands.Spain.

This communication presents a study on the electrode process of the Zn(II)-succinate coordinate system on mercury electrode.It has been carried out on basis of data arising from DC polarographic, chronoamperometric curves in the potential range corresponding to the polarographic limiting current and chronopotentiometric curves.The polarographic curves have been carried out with a DME whose capillary characteristics were m = 0.66 mg/s and controlled drop time at 3.5 s,in a set of dissolutions varying the succinate concentration from 0 to 0.32 M; the ionic strength was maintained at 1.0 and the pH was adjusted at 7.2 to assure the dissociation of the succinate salt present in each dissolution according to the dissociation constants of succinic acid existing in the literature[1].

The chronoamperometric recordings were made using the above capillary and also with a Smoler's horizontal capillary; no fundamental differences were found in both recordings for the studied succinate concentrations (0.1, 0.2 and 0.3M).

The chronopotentiometric curves have been carried out on a HMDE which area was 0.032 cm^2 in a current intensity range between 2.5 to 17.0 μA.

The i_l vs $h_{cor.}^{2/3}$ and i_l vs $C_{Zn(II)}$ dependencies showed the fundamentally diffusing character of polarographic limiting current in the -1.2 to -1.5 V vs SSCE potential range. At this potential range the log i vs log t relations arising from chronoamperometric data showed the mentioned diffusion control character.

The behaviour of $i\tau^{1/2}$ vs i relations obtained from chronopotentiometric curves showed the constancy of the $i\tau^{1/2}$ values characteristic of the processes which are diffusion controlled.A little deviation of this behaviour that was found at the lower intensity currents (2.5 to 4.0 μA) is probably due to the charge of the double layer effects.At the higher succinate concentrations (> 0.3 M) the observed behaviour can be probably attributed to a preceding ki-

netic complication.

The diffusion coefficients obtained from the limiting currents corresponding to the studied succinate concentrations are between 6.3 to 4.5 x 10^{-6} cm^2 s^{-1} after Matsuda's version[2] and between 5.7 to 4.2 x 10^{-6} cm^2 s^{-1} after Koutecky's version.[3] These results are in good agreement with those determined from constant value of $i\tau^{1/2}$ of the chronopotentiometric curves.

In the analysis of the polarographic curves, the characteristic parameters of a quasi-reversible process ($E^r_{1/2}$, $E^{ir}_{1/4}$, α and k^o) has been determined by using the Ruzic's method[4] for the various succinate concentrations.The calculations have been carried out by using an iterative fitting procedure, by means of a FORTRAN program, of the experimental data to the expression given by the mentioned author.In a further FORTRAN program, the $(\bar{i}_d - \bar{i})/\bar{i}$ vs E data from the Tomes and from the "reversible" and " irreversible" asymptotes corresponding to them have been determined for other calculations.

In order to determine the specific characteristics of the coordinate species $Zn(Succ)_p^{2-2p}$ which are reduced on the DME, the Matsuda's method[5] and the "simplified" Bennes' method[6] have been used.

In the Matsuda's method, the calculations of L_o functions have been carried out from the data obtained by the above mentioned program for the various potential and succinate concentrations which have been studied.The linear character of the polynomial expression of L_o vs /$succ^{2-}$/ has been showed.This fact gives rise to the detection of two electroactive species throughout the studied succinate concentration and potential ranges.The log M_p vs E dependencies let us to determine directly the α_p values and by means of various eqs. contained in Matsuda's work, the different rate constants were calculated. These are collected in Table I.

The method of Bennes makes use of a reordered expression from the eq. of the "irreversible" asymptote to Tomes curves. The H_o functions have been calculated from the $(\bar{i})/(\bar{i}_d - \bar{i})$ data for the studied potential and succinate concentration ranges, by means of the above mentioned FORTRAN program and from the F_o values at the different succinate concentrations which were calculated by using the De Ford's method[7].The fitting of the F_o vs /$succ^{2-}$/ curves gave rise to a second order polynomial expression; its coefficients were β_1 =28.1 $\pm$ 1.4 , β_2 = 67.9 $\pm$ 21.3 and β_3 = 718.3 $\pm$ 60.2 .

Likewise that in the Matsuda's method, the fitting of the H_o vs /$succ^{2-}$/ dependencies showed the existence of the two electroactive species which were already mentioned.The potential dependent coefficients Z_p in the polynomial expression of H_o were fitted to a straight line (log Z_p vs E) and from

its slope the α_p values were directly determined. In further calculations, the various rate constants were calculated from the intercept data. These rate constants were summarized in Table I.

The observed differences in some of the results obtained by both methods arise probably from the different data sources of the $(\bar{i}_d - \bar{i})/\bar{i}$ expression, viz , data from Tomes curves in the Matsuda's method and data from "irreversible" asymptote to the Tomes curves in the "simplified" Bennes' method.

Table I

Method	α_0	α_1	$\log k_0^0$	$\log k_1^0$	$\log {}^0k_f^0$	$\log {}^1k_f^0$
Matsuda	0.38	0.55	-2.36	-2.38	-15.34	-21.81
Bennes	0.38	0.57	-2.44	-2.40	-15.35	-22.45

The following scheme satisfies the found characteristics of the studied electrode process.

$$\begin{array}{ccccccc} Zn(II) & \rightleftharpoons & ZnSucc & \rightleftharpoons & Zn(Succ)_2^{2-} & \rightleftharpoons & Zn(Succ)_3^{4-} \\ \downarrow\uparrow 2e^-, k_0^\circ & & \downarrow\uparrow 2e^-, k_1^\circ & & & & \\ Zn(Hg) & & Zn(II) & & & & \end{array}$$

REFERENCES

1. H. J. Bruin, D. Kaitis and R. B. Temple, Austral. J. Chem., 15, 457 (1962).
2. H. Matsuda, Bull. Chem. Soc. Japan, 26, 342 (1953).
3. J. Koutecky, Czech. Cas. Fys. , 2, 50 (1953); J. Koutecky and M. v. Stackelberg, "Progress in Polarography", Vol. 1, P. Zuman and I.M. Kolthoff Eds., Willey Interscience, New York, 1962.
4. I.Ruzic, A. Baric and M. Branica, J. Electroanal. Chem.,29, 342 (1970).
5. H. Matsuda, Govt. Chem. Ind. Res. Inst., Tokyo, 61, 315 (1966).
6. E. Verdier, R. Bennes and B. J. Balette, J. Electroanal. Chem., 3, 463 (1971).
7. D.D. DeFord and D. N. Hume, J.Amer. Chem. Soc.,73, 5321 (1951).

05330

VOLTAMMETRIC STUDY OF ANODIC ADSORPTION PHENOMENA ON GRAPHITE IN CRYOLITE MELTS WITH VARYING ALUMINA CONCENTRATION.

S. JAREK and J. THONSTAD
Laboratories of Industrial Electrochemistry,
University of Trondheim, The Norwegian Institute of Technology
7034 Trondheim-NTH, Norway

Voltammetry measurements carried out at very high sweep rates (> 5 V/s) on graphite electrodes in cryolite-alumina melts (Na_3AlF_6-Al_2O_3) show the existence of a peak prior to CO_2 evolution. Frazer and Welch[1] attributed this peak to CO formation, suggesting a surface coverage close to a monolayer, while Damianacos et al.[2] ascribed it to either oxidation of a species of dissolved metal or a parasitic effect of the boron nitride crucible.

In order to elucidate this problem voltammetry studies were performed on graphite in cryolite with alumina contents ranging from 0.25 wt% to saturation (14 wt%) at 1020°C. The sweep rate was varied in the range 1 V/s - 1000 v/s and potentials 0.7V - 1.7V vs. an aluminium reference electrode.

No peak was visible in pure cryolite within the investigated potential range. Addition of alumina led to a peak preceding that of CO_2 formation. The potential of the peak was around 1.03V at 5V/s which agrees very well with the reversible thermodynamic potential for CO formation,

$$\frac{1}{3}Al_2O_3 + C = \frac{2}{3}Al + CO$$

A gradual increase of the anodic potential span from the potential of zero current was accompanied by an increase in cathodic current during the reverse scan. When the anodic potential approached the value of the first peak a reduction peak was observed in the cathodic region as shown in Fig. 1. The process was not reversible. The peak potential and the separation between the anodic and cathodic peaks increased significantly with sweep rate as illustrated in Fig. 2.

Apparently a carbon-oxygen surface complex (C_xO) is formed during oxidation of the surface, and it is being reduced again during the reverse scan. The C_xO complex is readily reduced since the ratio of anodic to cathodic peak currents was not far from unity. The anodic peak was hardly affected when the reverse scan was extended to a potential 0.5V below that of zero current.

The ratio of charges of the anodic and cathodic regions of the voltammograms at high sweep rates (> 100 V/s) was not far above unity, which implies that the oxidized species involved in the process largely remained on the electrode surface. In that case the attainment of surface coverage is responsible for the peak, and the charge should be constant[1]. It was observed that the calculated charge values decreased with increasing sweep rate and approached a constant level at sweep rates above 50 V/s. At lower sweep rates the cathodic charge was smaller than the anodic, which suggests that a part of the complex had been transformed to CO and escaped from the electrode surface. The surface coverage appeared to be of the order of a monolayer when assuming that two electrons were involved in the charge transfer step.

The effect of alumina is demonstrated in Fig. 3. The dashed area contains rather scattered results for alumina concentrations within the range from 1% to 5%. The upper limit of this area is set by peak current values found for 5% Al_2O_3. At alumina concentrations above 5% the peak was not detectable due to a very fast rise of current associated with the formation of CO_2. The influence of the alumina concentration on the current of the peak is not well defined. This behaviour could be explained in terms of already existing stable adsorption of oxygen-containing species at the anode surface.

References:

1. E.J.Frazer, B.J. Welch, Aus. I.M.&M.Proceedings, 260, 17 (1976)

2. D. Damianacos, F. Lantelme, M. Chemla, C.R. Acad.Sci. Paris Ser. C, 290, 149 (1980)

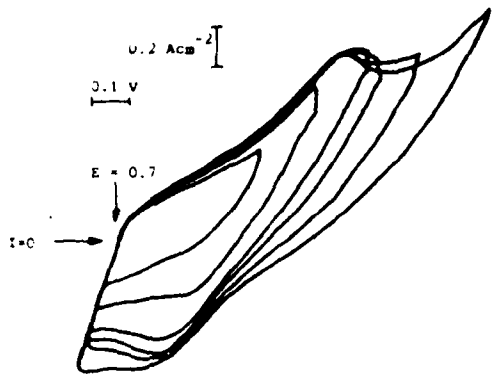

Fig. 1. Cyclic voltammograms with gradually increasing swiching potential; sweep rate 100 V/s; $c_{Al_2O_3}$ = 2 wt%.

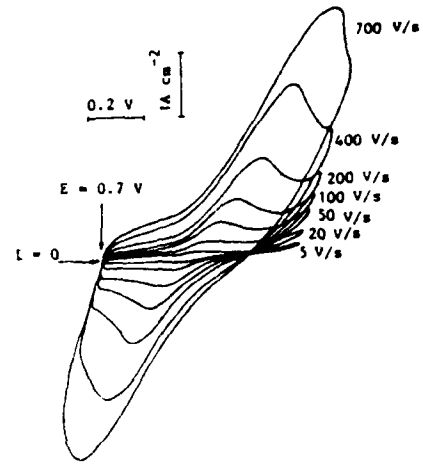

Fig. 2. Cyclic voltammogram run at different sweep rates; $c_{Al_2O_3}$ = 2 wt%.

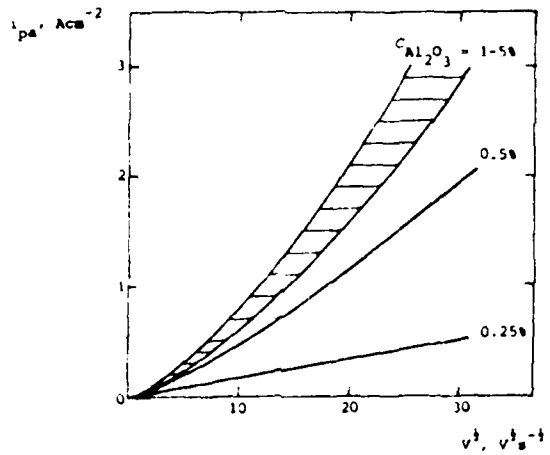

Fig. 3. Dependence of the first peak cd on the potential sweep rate for different alumina concentrations.

A FARADAIC IMPEDANCE STUDY OF THE CATALYTIC EFFECT OF THIOUREA ON THE ELECTROCHEMICAL REDUCTION OF Cd(II) IONS FROM 1 M KF SOLUTIONS AT THE D.M.E.

R.M. Souto*, M. Sluyters-Rehbach and J.H. Sluyters
Van 't Hoff Laboratory, State University, Utrecht, The Netherlands.

It is well known that electrode reactions are influenced by the structure of the electrical double layer and by the presence of substances that are adsorbed at the electrode/solution interface. A part from the so-called non-specific electrostatic effect (the Frumkin effect), frequently specific effects have been observed, e.g. catalysis of the reduction of the heavy metal ions by specifically adsorbed halide and thiocyanate anions [1-4].

The adsorption of thiourea (Tu) is comparable to the adsorption of these ions in many aspects and appears to enhance the reduction rate of metal ions in a similar way[5-7]. In this work a study has been made of the influence of the presence of thiourea on the rate and the mechanism of the reaction $Cd(II) + 2e \rightleftharpoons Cd(Hg)$ in 1 M KF solution. It has been concluded that in the pure KF solution this reaction proceeds via a three-step mechanism, consisting of a chemical reaction followed by two electrontransfer steps (CEE)[8-9]:

$$\begin{aligned} O &\rightleftharpoons O' \quad [R_c] \\ O' + e &\rightleftharpoons Y \quad [R_1] \\ Y + e &\rightleftharpoons R \quad [R_2] \end{aligned} \tag{1}$$

This conclusion was based on the potential dependence of the forward rate constant K_f, that is mathematically expressed by

$$\frac{1}{K_f} = \frac{1}{K_c} + \frac{\exp(\frac{1}{2}\alpha_1\zeta)}{K_{s,1}} + \frac{\exp(\frac{1}{2}(1+\alpha_2)\zeta)}{K_{s,2}} \tag{2}$$

with

$$\zeta = (2F/RT)\,(E-E^{o}) \tag{3}$$

In the presence of thiourea it is found that eqn (2) remains valid, as follows from Fig. 1 where $\ln K_f$ is plotted vs potential, at constant amount of adsorbed Tu. It turns out that at any potential a remarkable relationship exists between K_f and the surface excess Γ_{Tu}:

$$K_f(E) = K_f^{o}(E)\,(1 + A\,\Gamma_{Tu}) \tag{4}$$

in which $K_f^{o}(E)$ is the rate constant measured in the absence of Tu, and the proportionality constant A is independent of potential. This result means that the three terms in eqn. (1) all are affected by Tu in the same way, i.e. each of them is proportional to $(1 + A\,\Gamma_{Tu})^{-1}$. The magnitude of the effect is far beyond the non-specific Frumkin effect, since the potential of the Outer Helmholtz Plane varies only slightly going from 0 to 10 mM Tu. [illegible] the rate constants. Also complex formation between Cd(II) and Tu in the solution is of minor or no importance.

* On leave from Departamento de Química Física, University of La Laguna, Canary Islands, Spain.

The results summarized here strongly suggest that there is a fast equilibrium between the adsorbed Tu and the Cd(II), preceding the first step R_c in the mechanism (1). This can be considered as a special type of the so-called bridging model[1,10-11].

REFERENCES:

1. L. Pospíšil and R. de Levie, J. Electroanal. Chem., 25 (1970) 245.
2. H.A. Laitinen, A.J. Frank and P. Kivalo, J. Am. Chem. Soc., 75 (1953) 2865.
3. J.E.B. Randles and K.W. Somerton, Trans. Faraday Soc., 48 (1952) 951.
4. E.D. Moorhead and G.M. Frame, Anal. Chem., 40 (1968) 280.
5. Ya.I. Tur'yan and O.E. Ruvinskii, J. Electroanal. Chem., 23 (1969) 61.
6. O. Ireda, K. Watanabe, Y. Taniguchi and H. Tamura, Bull. Chem. Soc. Jpn., 57 (1984) 3363.
7. K. Sykut, J. Saba, B. Maczewska and G. Dalmata, J. Electroanal. Chem., 178 (1984) 295.
8. C.P.M. Bongenaar, A.G. Remijnse, M. Sluyters-Rehbach and J.H. Sluyters, J. Electroanal. Chem., 111 (1980) 139, 155.
9. J. Struijs, M. Sluyters-Rehbach and J.H. Sluyters, J. Electroanal. Chem., 171 (1984) 177.
10. R. Tamamushi, K. Ishibashi and N. Tanaka, Z. Phys. Chem. N.F., 35 (1962) 209.
11. R. de Levie, J. Electrochem. Soc., 118 (1971) 185C.
12. F.C. Anson, J. Electroanal. Chem., 47 (1973) 279.

Fig.1. Plot of ln k_f vs. potential for the Cd(II) reduction at several surface excesses of thiourea ($\times 10^{-12}$ mol cm^{-2}).

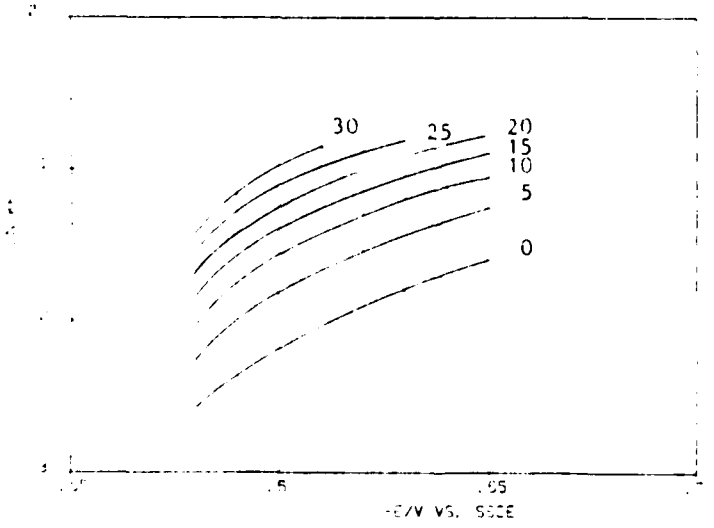

05350

Impedance measurements of zinc and amalgamated zinc in alkaline electrolyte

W. Visscher, J. Hendrikx and E. Barendrecht

Laboratory for Electrochemistry, Department of Chemistry
Eindhoven University of Technology
P.O. Box 513, 5600 MB Eindhoven, The Netherlands.

The behaviour of zinc and amalgamated zinc electrodes was investigated with the impedance technique in alkaline zincate solutions with concentrations ranging from 1.5 to 10 M KOH and 0.01 to 0.1 M ZnO. There is a striking difference between Zn and amalgamated Zn:

The impedance spectrum of an amalgamated zinc electrode at its rest potential in 7 M KOH + 0.1 M ZnO is shown in Fig. 1a for a quiescent solution and in Fig. 1b at a rotation frequency of 2000 rpm. Diagram a is typical for a simple charge transfer and diffusion controlled reaction. From the plot the exchange current density (i_o), the capacity of the double layer and the diffusion coefficient (D) of zincate can be calculated; this gave: i_o = 16 - 25 mA cm^{-2}, D = 2.4 10^{-6} cm^2 s^{-1}. D was found to increase with decreasing KOH concentration. The amalgamated electrodes were made from proprietary zinc containing mercury and from zinc, amalgamated with $HgCl_2$. All electrodes gave the same results.

The diagram of the rotated electrode (Fig. 1b) can likewise be described with the Randles circuit, in which now the Warburg impedance is corrected for convective transport.

The behaviour of a pure zinc electrode at its rest potential is given in Fig. 2a in quiescent solution and in Fig. 2b at the rotation frequency of 2000 rpm. The different impedance spectrum of zinc indicates that at zinc, surface processes play a more important role. The plots can adequately be described with a circuitry in which surface adsorption, surface diffusion and lattice formation are included. Calculation of the kinetic parameters from this diagram gives i_o = 20 - 75 mA cm^{-2} in 7 M KOH + 0.1 M ZnO. The i_o-values obtained with the impedance technique are in agreement with the i_o-data measured with the galvanostatic pulse method (1), both at Zn and Zn(Hg) electrodes.

The impedance spectrum with imposed d.c. current results for the amalgamated electrode in similar diagrams as in Fig. 1. At the zinc electrode the impedance spectrum is drastically changed: Fig. 3 shows that now an inductive and

an additional capacitive loop are observed, indicating the presence of two intermediates zinc species at the electrode surface.

The impedance of Teflon-bonded zinc-oxide electrodes was investigated in a nickeloxide-zinc cell (2); Fig. 4 gives the impedance spectrum for an uncharged zinc-oxide electrode and at various states of charge. Measurement of the impedance was carried out as a function of the cycle number in the charged and discharged state for cells containing respectively zinc-oxide electrodes with and without PbO or HgO additives. Though shape change occurred, it was not possible to detect the onset of shape change from the impedance data.

(1) J. Hendrikx, A. van der Putten, W. Visscher and E. Barendrecht, Electrochim. Acta 29 (1984) 81.

(2) J. Hendrikx, Thesis Eindhoven, 1984.

Legends to the figures

Fig. 1 Measured impedance plot (•) of Zn(Hg)-electrode in 7 M KOH/0.1 M ZnO at the rest potential (E_r = -1.382 V vs. Hg/HgO); a: at 0 rpm, b: at 2000 rpm. Simulated impedance plot (——). Frequency range: 0.01 Hz to 65 kHz (multiplication factor: 2).

Fig. 2 Measured impedance spectrum of the zinc electrode in 7 M KOH/0.1 M ZnO (•); a: at 0 rpm; b: at 2000 rpm. Simulated impedance plot (——); numbers indicate frequency.

Fig. 3 Impedance spectra of a zinc electrode in 7 M KOH/0.1 M ZnO at 2000 rpm with anodic cd = 35 mA cm^{-2}; numbers indicate frequency.

Fig. 4 Effect of the 1st discharge on the impedance spectrum of the zinc electrode.

□ uncharged (SOC 0%) start frequency 1 kHz
+ 0.015 Ah (SOC 3%) 4 Hz
o 0.075 Ah (SOC 14%) 0.01 Hz
• 0.50 Ah (SOC 100%) 0.01 Hz

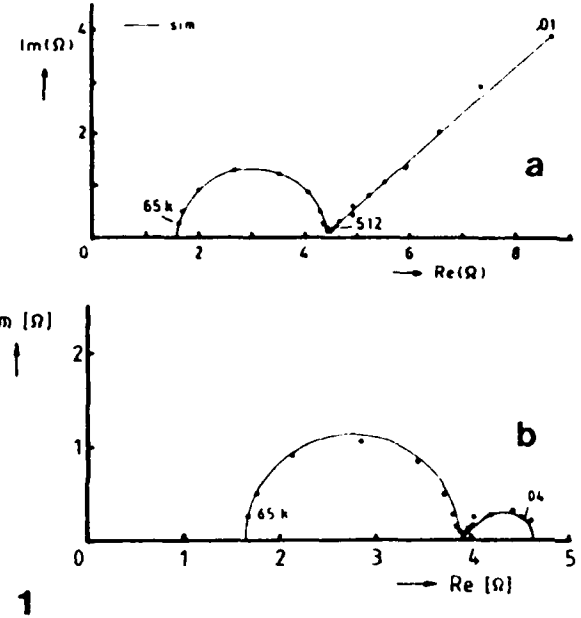

fig 1

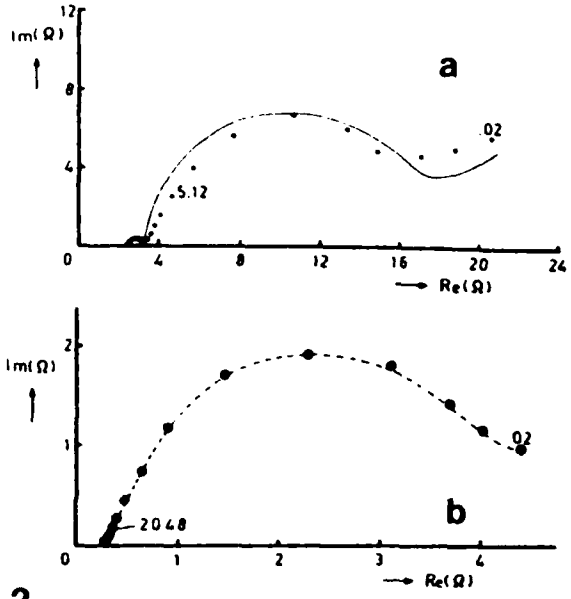

fig 2

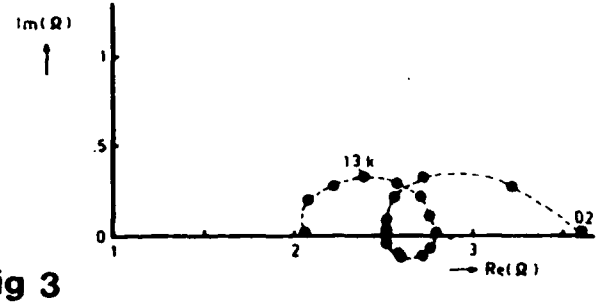

fig 3

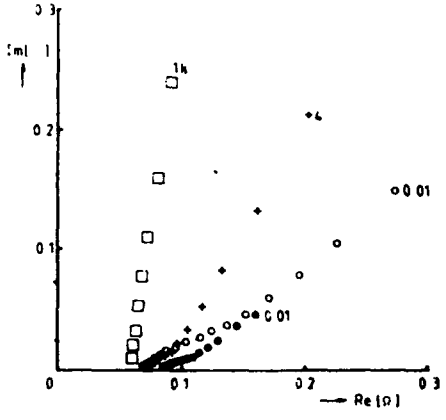

fig 4

05360

Oxygen reduction on carbon supported metal-phthalocyanines using a rotating ring disc electrode (RRDE)

A. van der Putten, A. Elzing, W. Visscher and E. Barendrecht

Laboratory for Electrochemistry, Department of Chemistry
Eindhoven University of Technology
P.O. Box 513, 5600 MB Eindhoven, The Netherlands.

In practical fuel cell electrodes, suitable catalysts are dispersed on carbon, mixed with a binder and pressed onto a metal screen. These gas diffusion electrodes are not very well suited for kinetic research since their voltammetric behaviour is determined not only by the electrocatalytic but also by the microgeometric properties of the carbon, determining the transport of reactants to the electrode. Moreover no information about the selectivity can be obtained. These problems can be solved using more sophisticated hydrodynamic methods such as the RRDE. In order to study carbon supported catalysts a RRDE was constructed via incorporation of the carbon particles into a polypyrrole film. This polymer is conducting and very porous enabling the transport of both electrons and oxygen to the catalyst. The experimental conditions for the electrode preparation are given in fig. 1. On top of a Pt-Au-RRDE (0.5 cm^2, N = 0.27) a KEL F hood was placed. The cilindrical hole in this hood was filled with 500 µl of carbon suspension (0.5 mg Norit BRX/ml). As electrolyte a 0.1 M $LiClO_4$ solution in CH_3CN was used, containing 0.5 vol % pyrrole. The suspension had been agitated in an ultrasonic bath for 5 minutes. A Pt counter electrode was placed in the convex meniscus. When the current is switched on (1 mA during 10 minutes) polymer chains will start to grow from the surface due to the oxidation of the pyrrole. At the same time the carbon particles coagulate and precipitate on the Au disc. The result of these processes is a three-dimensional network which attaches the carbon to the disc. A study of the hydrodynamic behaviour in 0.05 M $K_3Fe(CN)_6$ solution showed that it is undisturbed up to a frequency of 16 s^{-1}. At higher frequencies the disc current deviates in the positive direction due to the surface roughness.

With this new preparation method, O_2 reduction was studied in 1 N H_2SO_4 (O_2 saturated) at 4 different systems (fig. 2): Norit BRX and Norit BRX impregnated with 20 weight % metalfree-, cobalt- and ironphthalocyanine

(H_2Pc, CoPc and FePc). All currents were corrected for the high capacitive background current of the PP. At the platinized ring the hydrogen peroxide production was monitored. Similar to the results at gas diffusion electrodes[1], both CoPc and FePc significantly increase the activity: CoPc/BRX reduces oxygen to H_2O_2; at FePc/BRX the reduction proceeds partly to H_2O. Compared to the results of vacuum deposited CoPc and FePc films, the activity is surprisingly high. At a FePc film of 2000 Å the reduction in 1 M H_2SO_4 starts at only 0.2 V vs. RHE. The reason for this improvement is a vast increment in the number of available active sites. It appears that in vacuum deposited films only a very small fraction of the material present is electrochemically active.

Also the effect of pyrolysis was studied: the carbon supported catalysts were heated in N_2 for 4 hours at temperatures between 400 and 1200°C. The results (figs. 3 and 4) indicate that the activity of CoPc/BRX is increased due to the heat treatment up to 600°C. This increase is accompanied by a lower H_2O_2 production. The activity of FePc/BRX hardly changes up to 600°C. At higher temperatures the catalyst is destroyed. The activity of H_2Pc could not be increased, not even at very high temperatures. This is in contrast with results of Wiesener et al.[2] obtained with H_2TAA under somewhat different pyrolysis conditions. Our results indicate that the metal-ion remains the active center, not only at room temperature but also after pyrolysis.

References:

1. J.A.R. van Veen, C. Visser, Electrochimica Acta 24 (1979) 921.

2. G. Gruenig et al., J. Electroanal. Chem. 159 (1983) 1.

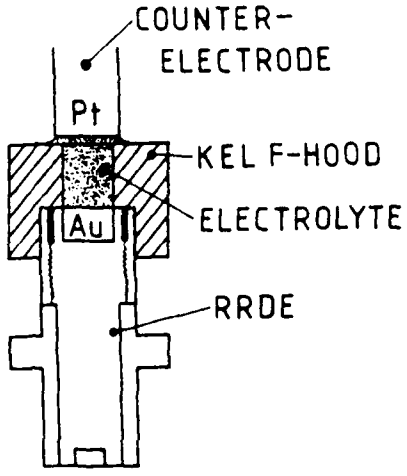

Fig. 1: The electrochemical cell

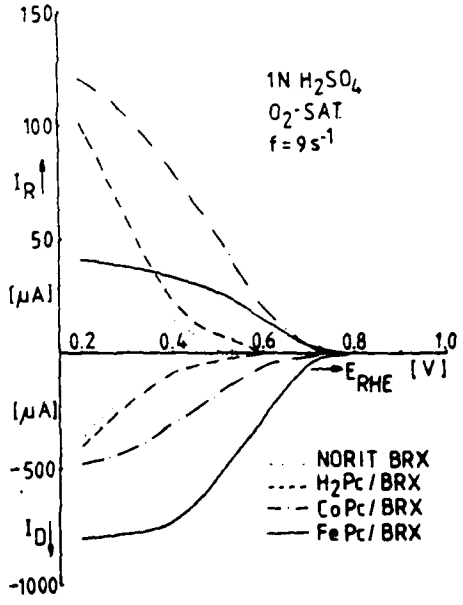

Fig. 2: O_2-reduction on Norit BRX and Norit BRX impregnated with 20% H_2Pc, CoPc and FePc respectively.

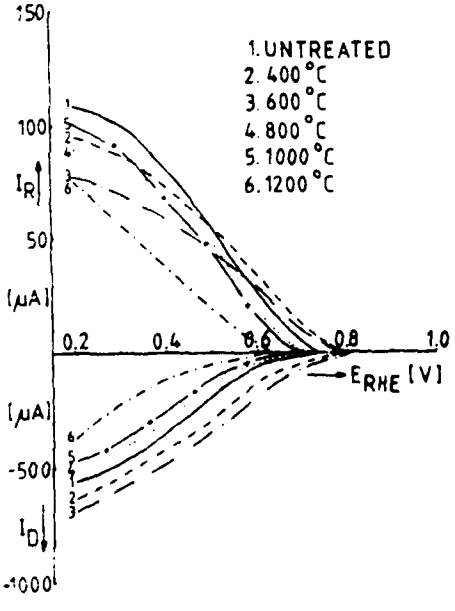

Fig. 3: O_2-reduction on CoPc/BRX as a function of pyrolysis temperature.

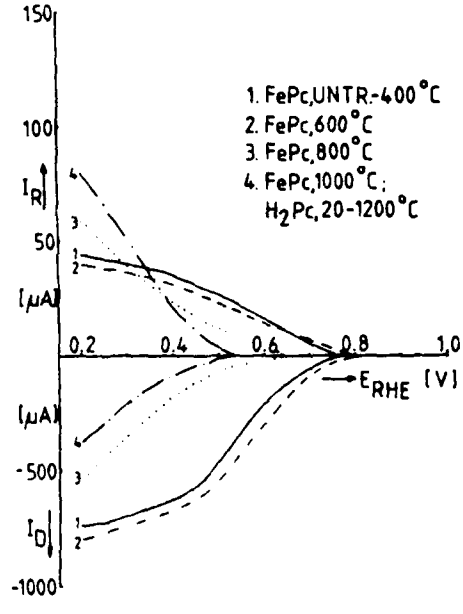

Fig. 4: O_2-reduction on 20% H_2Pc and 20% FePc/BRX as a function of pyrolysis temperature.

05370

ON THE OXYGEN REDUCTION RATE ON PLASTIC BONDED CADMIUM ELECTRODES

J. GARCHE, S. PETROVIĆ, K. WIESENER and J. MRHA[+]
Dresden University of Technology, Dresden (GDR)
[+]J. Heyrovsky Institute, Prague-Hostivař (Czechoslovakia)

Introduction

By adding teflon to the cadmium active mass and subsequent rolling this mixture in a current collector the so-called plastic bonded Cd electrodes can, if compared to the conventional pocket electrodes or sinter electrodes, be easily produced[1]. Unfortunately, these plastic bonded Cd electrodes that have stood the test in the unsealed Ni-Cd accumulator can not be used in sealed Ni-Cd systems, unless special measures are taken, since the oxygen reduction rate is greetly reduced. This behaviour is thought to be caused by a lack of reaction area stimulating oxygen reduction which is formed by the metallic components in the case of the pocket and sinter electrodes.

The aim of our work was, therefore, to increase the oxygen reduction rate by modifying the electrode in order to enable plastic bonded Cd electrodes to be used in sealed Ni-Cd accumulators.

Measuring method

Models of 2 Ah Ni-Cd cells were investigated which consisted of two plastic bonded Cd electrodes and a pocket nickel electrode between them. The internal pressure of these cells without free electrolyte could be continually recorded. Its course during overcharging and the following pause is shown in Fig. 1.

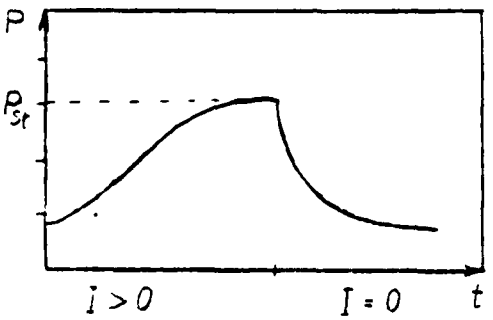

Fig. 1: Internal cell pressure (p) as function of the time during the overloading phase (I 0) and the following pause (I=0)

At $p=p_{st}$ a stationary state is attained which is characterized by the equality of the rate of oxygen formation at the positive electrode ($v^f_{O_2} = dn_{O_2}/dt$) and the rate of oxygen reduction at the negative electrode ($v^r_{O_2} = -dn_{O_2}/dt$):

$$v^f_{O_2} = v^r_{O_2} \tag{1}$$

As the rate of oxygen formation during the overloading phase is given by the charging current (I) according to FARADAY's law:

$$v_{O_2} = I/(z \cdot F) \tag{2}$$

the oxygen reduction rate at the pressure p_{st} can be obtained using equation (1). As shown by the following figures the function $v^r_{O_2} = f(p)$ may be obtained by measurements at different I.

Results and discussion

It was tried to create a sufficently large "reaction area" for oxygen by attaching secondary electrodes onto the Cd electrode and by modification of the active mass. The results are shown in Fig. 2.

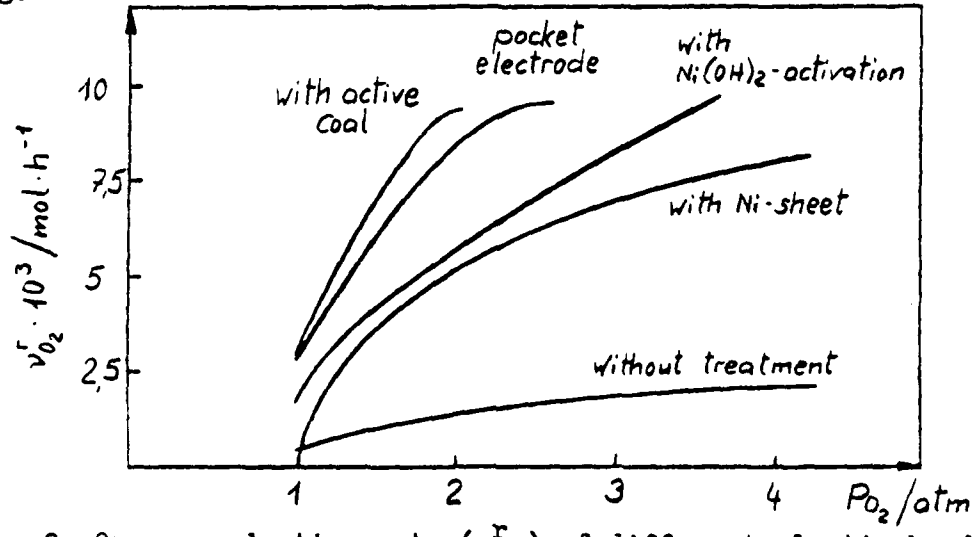

Fig. 2: Oxygen reduction rate ($v^r_{O_2}$) of different plastic bonded Cd electrodes and the pocket cadmium electrode as function of the pressure (p)

As may be seen from Fig. 2, the forcing on of metal nets (here: a nickel net), the rolling on of hydrophob layers of active

carbon and the $Ni(OH)_2$ activation of the cadmium mass (1^{th} step: addition of $NiSO_4$, 2^{nd} step: addition of NaOH) have proved to be hopeful.

Oxygen reduction is a electrochemical process according to:

$$O_2 + 2\,H_2O + 4e^- \quad 4\,OH^- \qquad (3)$$

which is said to be diffusion-controlled[3,4,5], i. e., according to FICK's first law and HENRY's law it holds:

$$v^r_{O_2} = D \cdot L_k \cdot p \cdot A/$$

D: diffusion constant
L_k: solubility coefficient
A: reaction area
: diffusion layer thickness

According to this equation $v^r_{O_2}/p$ should be constant. Deviations from this relation which occured in the experiments are obviously to be attributed to a change in the electrolyt distribution in the starved Ni-Cd system that results in a change of the reaction area A of the Cd electrode in dependence of the pressure.

References

1. J. JINDRA, J. MRHA, K. MICKA, Z. ZABRANSKY, V. KOUDELKA, J. MALIK; J. Power Sources 4(1970), 227
2. H. BODE, K. DEHMELT, H. v. DÖHREN; Proc. Int. Symp. on Batteries 1958, Christchurch, Paper yy
3. K. DEHMELT, H. v. DÖHREN; Proc. Ann. Power Sources Conf., 13th, Ft. Monmouth 1959, pp. 85-89
4. U.B. THOMAS; Batteries II (Ed.: D.H. COLLINS) Pergamon Press 1963, p. 117

05380

Hydrogen Evolution at Cu and Ag Electrodes in a Wide Range of Temperatures

U.FRESE and U.STIMMING
Electrochemistry Laboratory, Department of Chemical Engineering and Applied Chemistry, Columbia University, New York, N.Y.10027

Introduction

The analysis of kinetic data obtained in aqueous electrolytes is usually confined to a fairly small temperature range of about 80 K. This puts a severe limitation on any conclusion since the temperature change is usually only 30% with respect to the absolute temperature scale. Recently it has been shown /1-3/ that the electrochemistry of platinum electrodes takes place in frozen aqueous solutions in as much the same way as it does in liquid electrolytes. So far measurements could be performed down to appr. 140 K. This opens up new possibilities to investigate electrochemical kinetics in a wide range of temperatures.

In contrast to hydrogen evolution at platinum electrodes, at copper and silver electrodes this reaction is supposed to be charge transfer controlled /4/. This makes these systems especially attractive for studying the influence of temperature on kinetic parameter such as transfer coeffiecient and activation energy.

Results

Experiments were carried out in aqueous perchloric acid of the composition $HClO_4 * 5.5H_2O$. This electrolyte is a one phase system in the liquid as well as the frozen state; the freezing point is at 228 K. Fig.1 shows cyclic voltammograms of silver for typical temperatures; at room temperature, at temperatures close to the freezing point of the electrolyte in the liquid state and the frozen state, and at a low temperature. The anodic reaction is silver dissolution while the cathodic one is hydrogen evolution. The principal shape of the cyclic voltammograms in the frozen electrolyte is the same as in the liquid electrolyte; the overpotential, however, is higher at lower temperatures.

A critical point in passing the freezing point of the electrolyte is the quality of the electrode/electrolyte contact. Measurements of hydrogen adsorption on platinum showed that the area is maintained upon freezing. In the case of copper and silver capacity measurements were performed. Minima of the obtained capacity-potential curves were plotted as a function of temperature. The result is shown in Fig.2. A continous straight line is obtained for both, copper and silver, with no break at the freezing point of the electrolyte. This clearly demonstrates that the double layer remains intact also in the

frozen electrolyte.

Current-potential curves for the hydrogen evolution reaction were obtained from cyclic voltammetry curves (sweep rate 5 mV/s) in the temperature range 138 to 300 K. Corrections were made for the ohmic drop; ohmic resistances were determined from galvanostatic pulse measurements. In the whole temperature range straight lines were obtained in $\ln|i|$ vs. U plots. The slope is hardly affected by the temperature except for very low temperatures where it gradually decreases. This kind of behavior it true for copper as well as silver. In Fig.3 the Tafel plots of the results at copper electrodes are shown. The overpotential for the hydrogen evolution gradually increases with decreasing temperature. Just below the freezing point the current is higher than at a temperature slightly above freezing. This can be seen from Fig.3 by comparing the results for T = 231 K (liquid) and T = 214 K (frozen). A similar behavior has been found for the exchange current density of the redox reaction Fe(II)/Fe(III) /5/.

Discussion

Under the common assumption that the transfer coeffient in the Butler-Volmer equation is fairly insensitive to temperature, the Tafel slope should be temperature dependent according to /6/

$$b = RT/\alpha zF \qquad (1)$$

The results in Fig.3 suggest however, that α is strongly temperature dependent. This effect is even more pronounced at low temperatures. Transfer coefficients were calculated from the slopes in Fig.3 using Eq.(1). The result is plotted versus the temperature in Fig.4 for copper and silver electrodes. If the transfer coefficient is considered to be composed of two contributions /6/

$$\alpha = \alpha_H + \alpha_S \qquad (2)$$

with $\alpha_H = \frac{1}{F}\left(\frac{\partial \Delta H^*}{\partial U}\right)_T$ and $\alpha_S = -\frac{1}{F}\left(\frac{\partial \Delta S^*}{\partial U}\right)_T \cdot T$

A temperature dependent transfer coefficient suggests a major influence from the potential dependence of the entropy of the activated complex. Extrapolation from higher temperatures to T=0 yields an almost neglible α_H . At lower temperatures the temperature influence on α is obviously even stronger.

It seems too early to draw general conclusions from these results. It seems however, that some doubts are cast on the usual picture that in a charge transfer controlled reaction the potential influence is due to a change of activation energy with potential. An influence of the potential on the conformation of the activated complex has to be considered, as well, as a major source for the potential dependence of the hydrogen evolution reaction.

References

/1/ U.Stimming and W.Schmickler, J.Electroanal.Chem. 150 (1983) 125

/2/ U.Frese, T.Iwasita, W.Schmickler and U.Stimming, J.Phys.Chem. 89 (1985) 1059

/3/ U.Frese, T.Iwasita, W.Schmickler and U.Stimming, Extended Abstracts, I.S.E. Meeting in Salamanca, Spain, 1985

/4/ K.J.Vetter, Electrochemical Kinetics, Academic Press, New York 1967

/5/ T.Dinan and U.Stimming, unpublished results

/6/ B.E.Conway, D.J.MacKinnon and B.V.Tilak, Trans.Faraday Soc. 66 (1970) 1203

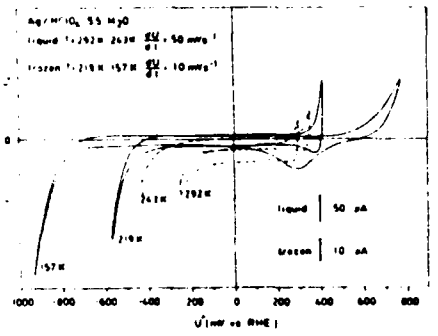

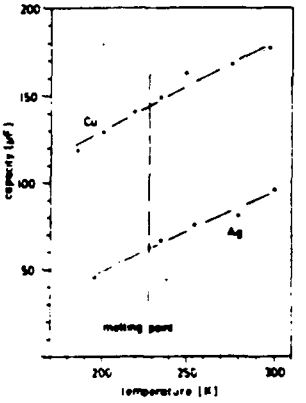

Fig.1 Cyclic voltammograms of Ag electrodes at various temperatures
Fig.2 Capacity of Cu and Ag electrodes as a function of temperature

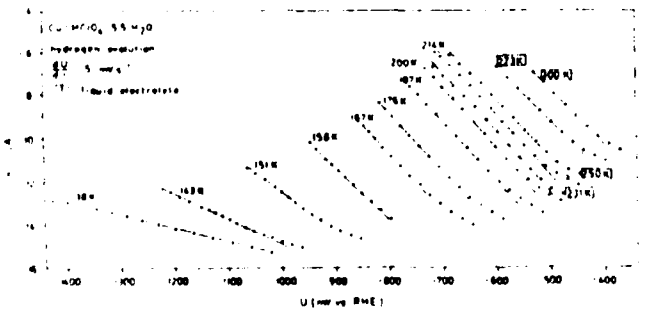

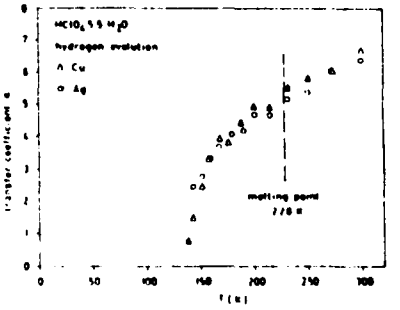

Fig.3 Tafel plots for the hydrogen evolution on Cu
Fig.4 Transfer coefficient as a function of temperature

05390

Investigation of Hydrogen Evolution at Platinum Electrodes in Liquid and Frozen Electrolytes

U.FRESE*, T.IWASITA**, W.SCHMICKLER** and U.STIMMING*
*Department of Chemical Engineering and Applied Chemistry, Columbia University, New York, N.Y. 10027, U.S.A.
**Institute of Physical Chemistry, University of Bonn, Bonn, F.R.G.

Introduction

It has been shown recently /1/ that typical reactions at platinum electrodes which are observed at room temperature such as hydrogen adsorption, oxide formation, hydrogen and oxygen evolution and double layer charging can be measured as well in frozen electrolytes. This enables the study of electrochemical behavior in a wide range of temperature. Here, results for the hydrogen evolution reaction at platinum together with the general electrochemical behavior using $HClO_4*5.5H_2O$ will be presented.

Results

In Fig.1 cyclic voltammograms of platinum in $HClO_4*5.5H_2O$ are shown, Fig.1a in the liquid and Fig.1b in the frozen electrolyte. Except for temperature related shifts, all typical reactions at platinum can be observed. A critical aspect is the quality of the electrode-electrolyte contact. In order to verify this, the hydrogen desorption charge was determined at various temperatures. A plot of the charge, Q_{des}, versus the temperature (Fig.2) shows no break at the freezing point of the electrolyte. This indicates that the contact with the double layer remains intact upon freezing.

The hydrogen evolution reaction was measured using potentiodynamic sweeps. At low overpotentials the current for hydrogen adsorption is superimposed, while at higher current densities effects from the ohmic resistance became noticable. The adsorption was corrected on the basis of the knowledge of the adsorption charge and the sweep rate. The ohmic drop correction was done using results from galvanostatic pulse measurements. The current-potential curves obtained after these corrections are shown as Tafel plots in Fig.3 for the liquid and the frozen electrolyte. Straight lines are obtained with a slope increasing with temperature. At low temperatures and high overpotentials a marked deviation from that behavior can be observed.

Discussion

For the hydrogen evolution at platinum generally a transfer coefficient of two is observed which is found as well in this study. The transfer coefficient does not seem to be markedly dependent on temperature. While several authors make a rate determining Tafel reaction, i.e. the recombination of atomic

hydrogen to molecular hydrogen, responsible for the transfer coefficient of two, Yeager et.al./ / found from rotating disk electrode experiments that a combined recombination-diffusion control of the molecular hydrogen is rate determining.

If the recombination reaction alone is made responsible than at high overpotentials a limiting current should be observed. The deviation from limearity observed at lower temperature may be an indication for such an effect. More experimental evidence, however, is necessary before the finding of such an effect would be claimed.

References

/1/ U.Frese, T.Iwasita, W.Schmickler and U.Stimming, J.Phys.Chem. 89 (1985) 1059
/2/ F.Ludwig, R.K.Sen and E.Yeager, Elektrokhim. 13 (1977) 847

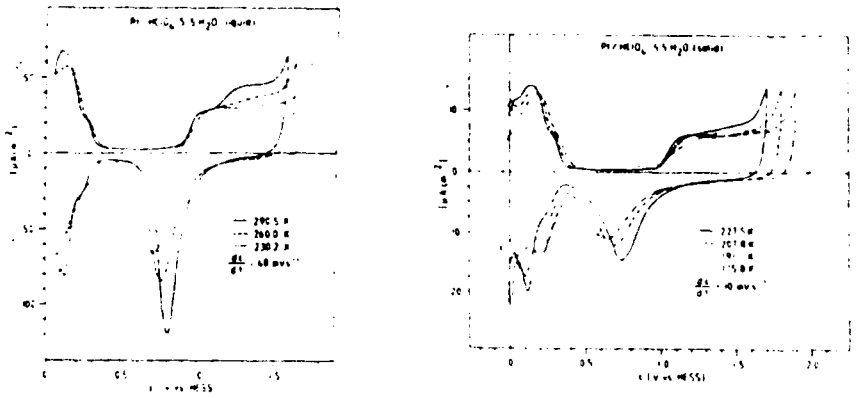

a b

Fig.1 Cyclic voltammograms of Pt-electrodes in the liquid (a) and the frozen electrolyte

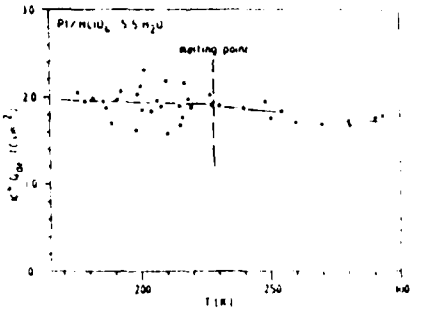

Fig.2 Hydrogen desorption charge as a function of temperature

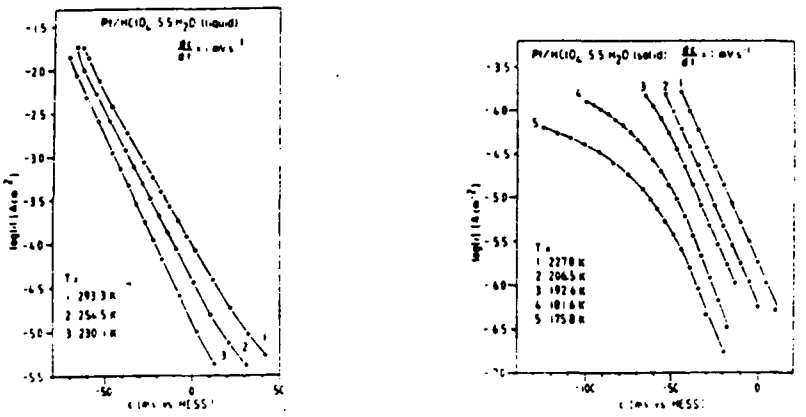

a b

Fig.2 Tafel-plots for the hydrogen evolution reaction at Pt-electrodes
(a) liquid electrolyte (b) frozen electrolyte

05400

ANODIC ACTIVITY OF THE NO_3^- ON AN ACTIVATED IRIDIUM ELECTRODE

T.F.Otero and Y.Jiménez Jiménez.
Facultad de Ciencias Químicas. Universidad del País Vasco.
Apdo. 1072. San Sebastián. Spain.

When an anodic current density goes through a $NaNO_3$ aqueous solution, using an Ir sheet of 0,5 cm^2 apparent area as anode, the acidification of the solution was as promoted. This fact was proved by titration of the anolyte with a NaOH solution, once the current was swithed off. The acid concentration obtained was proportional to the current density, for the same flow time.

The experimental results were obtained using a two compartment cell with a sintered glass wall in the middle. A Pt sheet was used as counter electrode. The S.C.E. was used as reference electrode when we did potentiostatic or potentiodynamic mesurements. We worked at constant temperature. The electrode was previously actived in 0,5M H_2SO_4.

The anolyte acidification was obtained, so, by anodic polarization of the electrode. Table 1 shows the H^+ mols obtained when an Ir electrode, with similar activations, was polarised at constant potentials for 30 minutes.

Table 1. $[H^+]$ $mol.l^{-1}$ obtained by anodic polarization of a 1M $NaNO_3$ solution. T=30ºC, t_{pol} = 30 min.

$E/_{mV}$ (S.C.E.)	1000	1100	1200	1300	1400
$[H^+]10^{-3}.mol.l^{-1}$	0,02	0,05	0,09	0,13	0,16

The acidification of the working compartment solution was attained, as well, when the working electrode was submitted to consecutive sweeps of potential, whenever the anodic limit for the potential sweeps was more anodic than 950 mV (S.C.E.). When the consecutive voltammograms were re-

corded, the acid concentration modification promotes the voltammogram transformation from the $NaNO_3$ characteristic shape to the dilute HNO_3 usual shape (fig 1).

There are a direct proportionality between the acid production and the time of current flow, when the current density throwing the electrode was kept constant.

The acid production, in the anodic compartment, was proportional to the current density, when the flow time was constant. This fact promotes the slope increase of the conversion/time curves when the current density grows.

At constant potential (1200 mV) the acid production was not modified when the $NaNO_3$ concentration was varied, and rose when the temperature and the electrode activation increased. This fact points toward an electrocatalytic efect.

Those variations were not observed at constant potentials higher than 1250 mV or current densities higher than 10 $mA.cm^{-2}$. This fact could be explained by the coexistence of the oxygen production on the electrode.

When the electrode was polarised at potentials higher than 1300 mV it loses its activation, such as was showed with a voltammogram in 0,5M H_2SO_4 after polarization in 1M $NaNO_3$.

The acid production seems related with a charge transfer between the NO_3^- ions and the electrode, such as was subgested with electroorganic process:

$$NO_3^- \longrightarrow NO_3^{\cdot} + e^- \qquad (1)$$

Following the same way of the electroorganic process, the radical could be capable to take a proton from a water molecule becaming nitric acid:

$$NO_3^{\cdot} + H_2O \longrightarrow HNO_3 + OH^{\cdot} \qquad (2)$$

Reaction (1) was electrocatalysed by the iridium oxides present on the electrode, such as we observed by increasing of the acid production when the electrode activation increased. This reaction was under control of the current flowing through the electrode surface when the oxygen release was not attained, existing a perfect correlation between the Coulombs crossing over the electrode and the acid production.

Fig.- (1) Reference voltammogram (-230/+1230 mV vs. S.C.E.) obtained in 0,5M H_2SO_4 to an Ir electrode activated in the same medium. (2) First voltammogram (-900/+1230 mV) obtained using this electrode in 1M $NaNO_3$, and consecutive voltammograms in the same medium. V_B=30 mV.s^{-1}, T=25ºC.

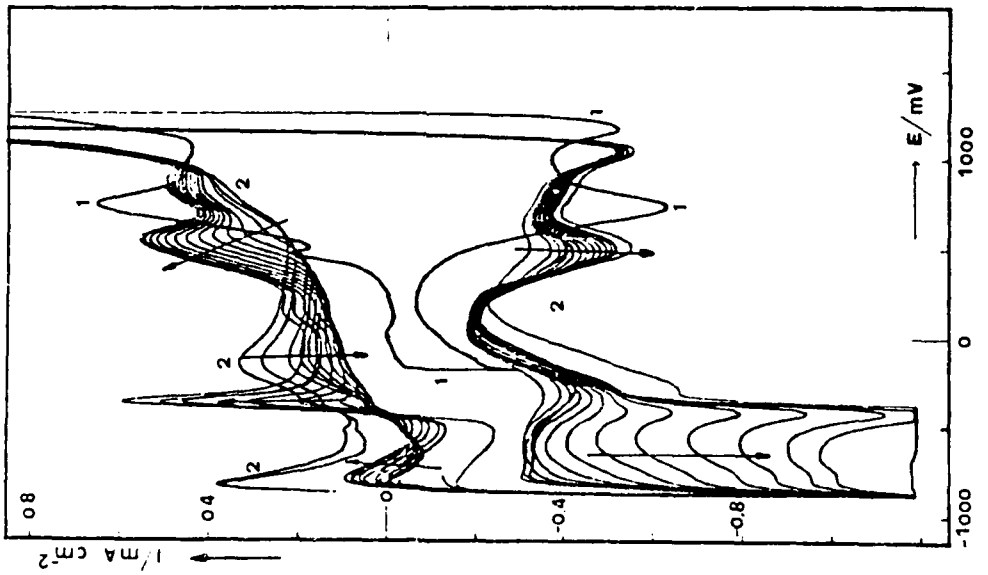

05410

OXYGEN REDUCTION ON Ni , Cu AND Ni-Cu ALLOY IN MOLTEN CARBONATES

I. URBINA*, G. BARREIRO and G. POILLERAT**

Laboratorio de Energetica Electroquimica
CINVESTAV, AP 14-740 , 07000 Mexico DF (Mexico)

During the last twenty years the molten carbonates fuel cells have been largly studied. The nickel cathode seem to have focused the interest during a long time. Recently, some works have been published on Cu electrode (1). In this work we have compared some metals as Au and Pt with Ni and Cu and a Cu Ni Zn alloy (a common alloy used for coin making) as a cathode for oxygen reduction in a molten carbonates fuel cell.

EXPERIMENTAL

The electrolyte was the ternary eutectic mixture of lithium, sodium and potassium carbonates which were carefully dried. As a reference electrode, we used a $Pt/CO_2,O_2$ system in the same eutectic mixture. The gas mixture was 33 % oxygen and 67 % carbon dioxide, dried on molecular sieves. This reference electrode was in a small quartz tube connected to the cell's electrolyte by a very small hole. As the working electrode we used Au, Pt, Ni, Cu and a Cu (62 %) Zn (23 %) Ni (14,5 %).

EXPERIMENTAL RESULTS

The cyclic voltammograms for each metal at 650°C are shown on figure 1 to 5 . Gold have been studied for comparison. Appleby et al have published (2) results on a slightly different system with Li_2CO_3 as electrolyte, 0.1 atm CO_2 and 0.9 atm O_2 as gas mixture and at 850°C . Nevertheless the potential for oxygen reduction that we have found (- 0.1 V) is near from that of these authors (- 0.1 V to - 0.22 V). The current densities are also coherent if we take into account the different temperatures. By addition of Na_2O_2 to the electrolyte (figure 1-c) we are abble to identify the peak with peroxyde ion reduction (3). Platinum and Copper (figures 2 and 3) give a higher current density. For the nickel working electrode the potential of the peak is more negative and the current density is much higher (about 30 times that of gold). The two others peaks could be related to NiO reduction and to CO production from CO_2 or $CO_3^=$ (4) . The Ni Cu Zn alloy shows (figure 5) and even better current density than nickel.

Present adresses :
* Univ. Guanajuato, Inst. de Inv. Cientif.
L. de Retana 5, Guanajuato, Gto, Mexico.

**Lab. Electrochimie, U.L.P., B.P. 296, F - 67008 Strasbourg Cédex.

CONCLUSION

This comparative study of different metals and alloy for oxygen reduction in molten carbonates shows that a Ni Cu Zn alloy give a higher current density than nickel alone and consequently could be interesting as a molten carbonates fuel cells cathode.

ACKNOWLEDGMENTS. We thank :

- Lab. Electrochimie, U.L.P., Strasbourg (Prof. P. Chartier) for support to attend the 36th ISE Meeting.
- Inst. Invest. Cientif., Univ. Guanajuato (Ing. A. Garcia), Mexico for a grant (I.C.).
- CONACYT, Mexico which support this research (contrat PCCBBCNA-001830).

BIBLIOGRAPHY

1. Selman J.R., Proceed 161th Meeting Electrochem. Soc., Montreal, Vol. 82-1, (1982)
2. Appleby A.J. and Nicholson S, J. Electroanal. Chem.
   a - 53, 105 (1974)
   b - 83, 309 (1977)
   c - 112, 71 (1980).
3. Appleby A.J. and Nicholson S., J. Electroanal. Chem., 38, 13 (1972).
4. Winnick J. and Ross P.N. Jr, J. Electrochem. Soc., 128, 991 (1981).

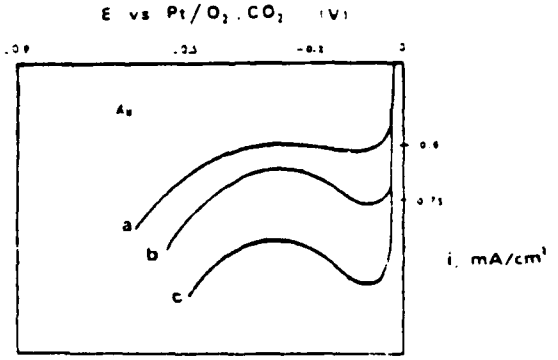

Figure 1 : Cyclic Voltammetry on Au electrode in Li, Na, K CO_3 at 650°C. Gas for reference electrode and cathode is 0.33 atm O_2 and 0.66 atm CO_2
a - 10 mV s^{-1} b - 100 mV s^{-1} c - 100 mV s^{-1} addition of Na_2O_2

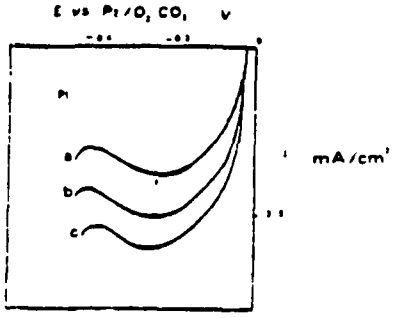

Figure 2 : Cyclic voltammetry on Pt electrode (same conditions as before) a - 50 mV s^{-1} b - 100 mV s^{-1} c - 150 mV s^{-1}.

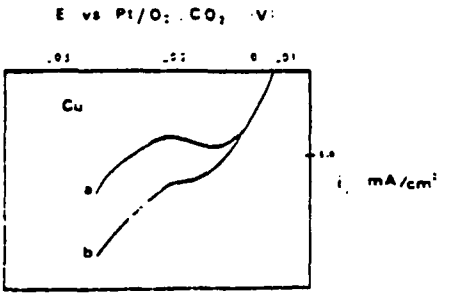

Figure 3 : Cyclic voltmametry on Cu electrode (same conditions as before) a - 100 mV s^{-1} b - 10 mV s^{-1}, Na_2O_2 addition.

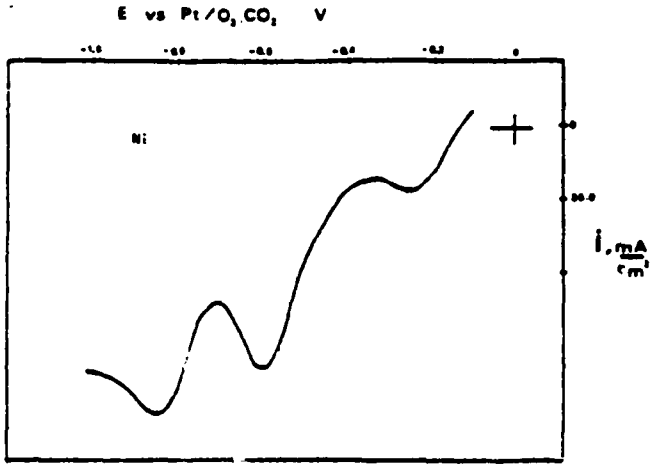

Figure 4 : Cyclic voltammetry on Ni electrode (same conditions) 100 mV s^{-1}.

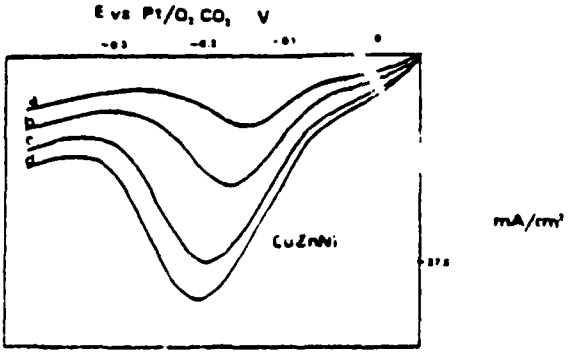

Figure 5 : Cyclic voltammetry on Cu (62 %) Zn (23 %) Ni (14,5 %) alloy electrode (same conditions)
a - 30 mV s^{-1} b - 50 mV s^{-1} c - 100 mV s^{-1} d - 130 mV s^{-1}

05420

O_2 REDUCTION BY PLATINUM PHTHALOCYANINE IN ALKALINE SOLUTIONS

C. PALITEIRO
University of Coimbra, Coimbra (Portugal)
A. HAMNETT and J.B. GOODENOUGH
Inorganic Chemistry Laboratory, Oxford (England)

When pure platinum phthalocyanine (PtPc) is mixed with an especially treated coconut-shell charcoal and formed into practical porous electrodes, high current densities are obtained. The performance of these PtPc electrodes is superior to that of porous electrodes made by incorporation of pure Pt and active metal phthalocyanines (FePc and CoPc) into the same type of carbon[1].

The mechanism of O_2 reduction by PtPc in alkaline solutions was studied by applying several electrochemical, structural and spectroscopic techniques to PtPc thin films vacuum sublimed on carbon, gold and platinum. The catalytic activity of PtPc on carbon is minimum. However, if a thin film of gold is deposited on carbon before PtPc is evaporated, a $4e^-$ reduction is approached. In this case a gradual increase of the RDE current with time is noticed. Electrochemical, Ressonance Raman and XPS experiments show that this aging is not due to film chemical change or the incorporation of an active impurity into the film; its role is to increase the rate of a step that is activation-controled in the fresh film.

The activity of aged films on gold substrates was studied in greater detail. RDE polarization curves have two Tafel slopes: 40 mV/dec and 120 mV/dec at low and high polarizations, respectively. The rate law for O_2 reduction was found to be

$$I \cong 4 F A K C_{O_2} C_{OH^-}^{m} \exp\left(-\frac{\alpha F E}{RT}\right)$$

where A is the electrode area, K is the reaction rate constant measured at 0 V in a pH-independent scale to which the potential E is referred, α is the transfer coefficiente, $m = -0.5$ and $\alpha = 1.5$ in the low-polarization region (950 to 850 mV/HE) and $m = 0.15$ ard $\alpha = 0.5$ in the high-polarization region (850 to 600 mV/HE).

HO_2^- was detected in RRDE collection experiments over the entire poten-

tial range explored, but only in small amounts. However, HO_2^- is not reduced by PtPc films. Since $n \cong 4$, this means that O_2 is predominantly reduced to OH^-; a parallel reaction produces a small amount of HO^-, which is not reduced further. This fact simplifies the calculation of the parcial rate constants (K_1: $O_2 \longrightarrow \longrightarrow OH^-$; K_2: $O_2 \longrightarrow HO_2^-$; K_3: $HO_2^- \longrightarrow HO^-$) of the overall reduction from the RRDE data. Their potential dependence is shown in Fig. 1. This parallel mechanism was confirmed by sampled-current voltammetry experiments.

Cyclic voltammetry and Raman spectroscopy show that PtPc molecules do not ionize over the potential range of O_2 reduction. Therefore, a redox mechanism cannot explain the electrocatalysis of O_2 by PtPc thin films. The following mechanism is suggested:

1. $O_2 + e^- \rightleftharpoons O_2^-$

2. $M + O_2^- \rightleftharpoons MO_2^-$

3. $MO_2^- + M + e^- \rightleftharpoons M - O - O - M$

4. $M - O - O - M + H_2O + e^- \rightleftharpoons MO^- + M + 2OH^-$

5. $MO_2^- + H_2O + e^- \longrightarrow M + 2OH^-$

3'. $MO_2^- + H_2O \rightleftharpoons MOOH^- + OH^-$

4'. $MOOH^- \longrightarrow M + H_2O$

Where M indicates a PtPc molecule. This mechanism, with step 3 as the rds in the low-polarization and step 1 as the rds in the high-polarization region, is consistent with the experimental rate low. The first step is an electron transfer to an O_2 molecule on the substrate surface; it is followed by end-on O_2^- adsorption on the film. We found the separation between Pt ions of close PtPc molecules in the film to be $\simeq 3.8$ Å. This separation is accepted as the most favourable for O_2 electroreduction by dimeric metal porphyrins[2]. Hence, adsorbed O^- can bridge two PtPc molecules to give a bridged-oxo species (step 3); this promotes the reductive split of the O - O bond (step 4). Electron transfer to the bridged - O_2^- ion likely to occur by ressonance-enchanced tunneling from the underlying gold. Therefore, reduction of O_2 only occurs very close to the Au surface (within 50 to 100 Å). The pzc of gold was found to be close to the PtPc flatband; this provides a better electron transfer to the bridged - O_2^- species

since it minimizes potential drops likely to impede tunneling.

Aging can result from the increase in the number of active sites close to Au surface due to film electrostriction. However, a slow uptake of O_2 by PtPc crystallites increases the number of trap sites; tunneling probability and, therefore, electron transfer to bridged - O_2 species is thus enhanced with time.

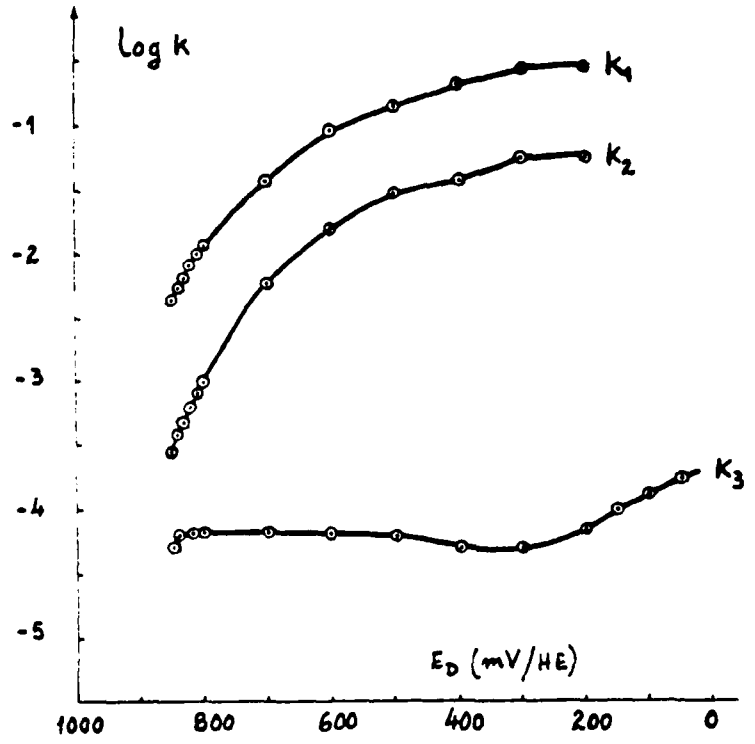

Fig. 1 - Potential dependence of the rate constants for the reduction of O_2 on an aged (PGb+400 Å Au) + 2000 Å PtPc film.

ACKNOWLEDGEMENTS

C P is very indebted to INIC, Portugal, for a scholarship.

REFERENCES

1. C. Paliteiro, A.K. Shukla, A. Hamnett and J.B. Goodenough, to be published.
2. R.R. Durand, Jr., C. Susana Bencosme, J.P. Collman and F.C. Anson, J. Am. Chem. Soc., 105 (1983) 2710.

05430

THE ELECTROCRYSTALLIZATION OF PbS ON Pb(Hg)

M.J.B.V. MELO and M.I.S. PEREIRA
CECUL - Faculdade de Ciências - 1294 LISBOA CODEX - PORTUGAL

In recent years there has been an increasing interest in the electrochemical properties of metal sulphides. Most of them are semiconductors and their resistivities are sufficient low to allow the application of sulphides in the development of photovoltaic converters for solar energy, and high energy batteries.

In this work the deposition of PbS on Pb(Hg) is studied, under potentiodynamic and potentiostatic conditions.

A cyclic voltammogram for the deposition of PbS on Pb(Hg)1 at % from 0.1M Na_2S + 1.0M $NaHCO_3$ solution is shown in fig. 1.

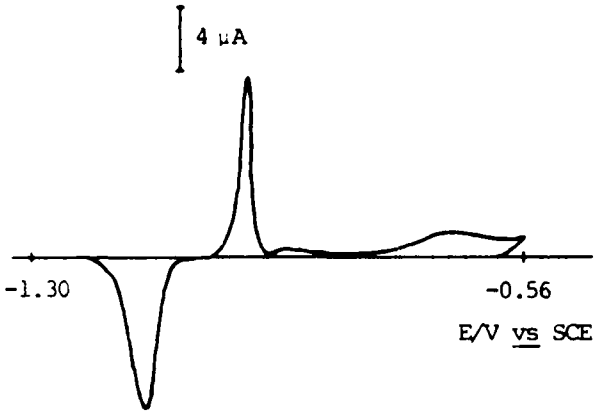

Fig. 1. Cyclic voltammogram (ν = 50mV s^{-1}) showing the deposition and reduction of PbS film on 1 at % Pb(Hg) from 0.1M Na_2S + 1.0M $NaHCO_3$ solution. Area = $1.39 \times 10^{-2} cm^2$.

According to the value for the reaction[1]

$$Pb + S^{2-} \rightleftarrows PbS + 2e^- \qquad E^0 = -1.179V \text{ vs S.C.E.}$$

the three anodic peaks were attributed to the PbS formation, and the cathodic one, to the reduction of the deposited film. Integration of the anodic peaks gave the charges of 373 ∓ 9 μC cm^{-2}, 130 ∓ 4 μC cm^{-2} and 288 ∓ 9 μC cm^{-2} for the first, sencond and third peaks respectively.

Potentiostatic transients are presented in fig. 2, for two different values of growth potential.

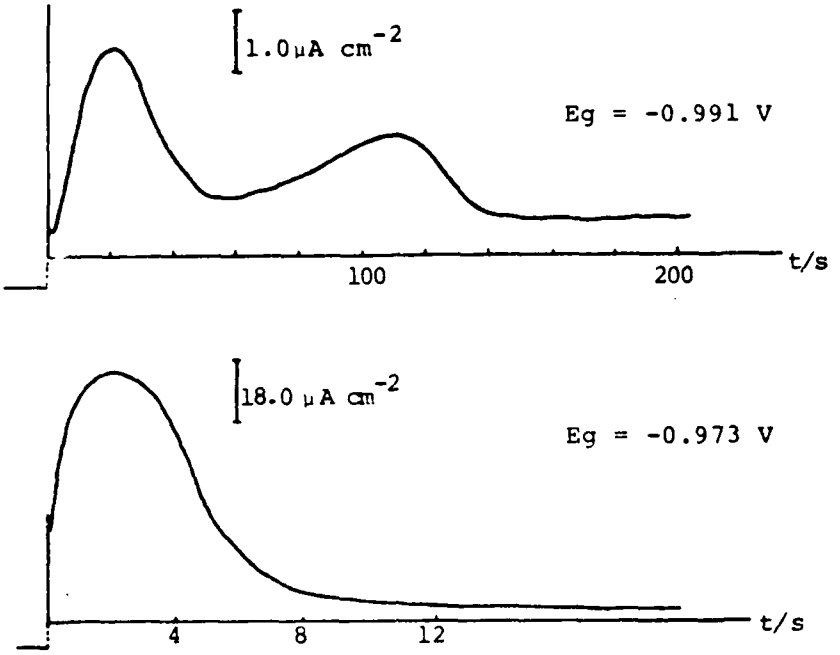

Fig. 2. Potentiostatic deposition transients for PbS on 1 At % Pb(Hg) from 0.1M Na_2S + 1.0M $NaHCO_3$ at two different growth potentials.

It can be seen that both transients show rising current in the initial stages, indicating that a process of nucleation and growth is occurring. However the mechanism is apparently different and depending on the value of the growth potential.

A particularly interesting feature of the results is that the transients obtained at very low values of potential are on a time scale of several minutes, and present two peaks, which the charges are 205 ∓ 20 μC cm^{-2} and 186 ∓ 18 μC cm^{-2} respectively. A comparision of these values with the calculated charges from the crystallographic data of lead sulphide[2], allowed us to interpret the growth of PbS in terms of the deposition of one layer, followed by the formation of another one, both with the (001) orientation parallel to the substrate.

The results at higher values of potential are quite different; the process is much faster and only a peak occurs, which the charge is 398 ∓ 40 μC cm^{-2}. This value is virtually identical with the sum of the charge of the two peaks formed at lower potentials. It seems that the peak formed at higher values of potential appears deconvoluted in two at lower potentials, what can be explained on the basis of the variation with potential of the overall growth constants β_1 and β_2, for the growth of the first and second layers respectively[3].

The number of peaks formed depends on the relation between β_1 and β_2. Only when $\beta_1 >> \beta_2$ do two peaks develop, otherwise only one peak is formed[4].

The results seem to point out that at low potentials β_1 should be bigger than β_2 and so two well developped peaks are formed. At higher potentials the two peaks occur convoluted, what can be attributed for instance to an increase of the constant β_2 in relation to β_1.

REFERENCES

1. W.M. Latimier,
Oxidation states of the elements and their potentials in aqueous solutions.
Prentice-Hall Inc. 1952.

2. B. Wasserstein,
Am. Mineral, 35, 337 (1950); 36, 102 (1951).

3. R.D. Armstrong and J.A. Harrison,
J. Electrochem. Soc., 116, 328 (1960).

4. M.I. da Silva Pereira and L.M. Peter,
J. Electroanal. Chem., 140, 103 (1982).

ACKNOWLEDGEMENTS

This work was partially supported by Junta Nacional de Investigação Científica e Tecnológica, under research contract No.319.81.63.

M.J.B.V. Melo acknowledges to the Instituto Nacional de Investigação Científica de Portugal for assistance in the form of scholarship.

05440

EVALUATION OF ELECTROCHEMICAL KINETIC PARAMETERS USING THE BOND-HENDERSON-OLDHAM "GLOBAL ANALYSIS"

D. H. EVANS and M. R. ANDERSON
Department of Chemistry, University of Wisconsin-Madison
Madison, Wisconsin 53706 (U.S.A.)

Bond, Henderson and Oldham[1] have developed an efficient procedure for analyzing cyclic voltammetric data to obtain the standard heterogeneous electron transfer rate constant, the electron transfer coefficient, the reversible half-wave potential and the diffusion coefficient of the reactant. The analysis involves the original current-potential data (corrected for background current) and the semiintegral (convolutive transform) of the current. At each potential on the voltammogram there are two values of the current and two values of the semiintegral, one from the forward and one from the reverse scan. If the two current-semiintegral-potential points at each potential are plotted, it can be shown that the linear extrapolation in the current-semiintegral plane to the current-potential plane where the semiintegral is zero will give an intercept current directly proportional to the forward heterogeneous electron transfer rate constant at that potential. Similarly the linear extrapolation in the current-semiintegral plane to the semiintegral-potential plane where the current is zero will give an intercept semiintegral, $m(t)_O$, related to the diffusion coefficient of the reactant, D_O, and the reversible half-wave potential, $E_{\frac{1}{2}}$, by equations (1) and (2)

$$m(t)_{lim}/m(t)_O = 1 + \exp[(nF/RT)(E - E_{\frac{1}{2}})] \quad (1)$$

$$m(t)_{lim} = nFAD_O^{\frac{1}{2}} C_O^* \quad (2)$$

where E is the potential, A is the electrode area, C_O^* is the bulk concentration of reactant and the other symbols have their normal meanings.

The extrapolations carried out at various potentials produce a set of forward heterogeneous rate constant-potential data and a set of $m(t)_O$-potential data. The former are readily analyzed to yield the standard heterogeneous electron transfer rate constant, k_S, and the transfer coefficient, α. The latter yield values of $E_{\frac{1}{2}}$ and D_O (knowing A and C_O^*).

The procedure is valid for semi-infinite linear diffusion in cases where there is no convection, migration or coupled chemical reactions.

In a separate study[2] a large collection of background-corrected cyclic voltammograms in digital form had been collected. These data had been analyzed by laborious trial-and-error comparison with digital simulations to obtain $E_{\frac{1}{2}}$, k_S, α and, in certain cases, the potential-dependence of α, $d\alpha/dE$.

Programs were written to analyze these data according to the Bond-Henderson-Oldham "Global Analysis" technique and the results were compared with those obtained by comparison with digital simulation.

In cases where potential dependence of α could be detected, a curved plot of the logarithm of the forward rate constant vs. potential was obtained. The plot was fit to a quadratic equation by linear regression to obtain $d\alpha/dE$.

Analysis of each voltammogram, including the calculation of all semi-integrals, required about 10 seconds on a Harris/7 computer. The results are summarized in the Table where it can be seen that good agreement is found between the two procedures.

1. A. M. Bond, T. L. E. Henderson and K. B. Oldham (in press).
2. R. A. Petersen, Ph.D. thesis, University of Wisconsin, 1983.

Table. Comparison of Results obtained by the Bond-Henderson-Oldham (BHO) "Global Analysis" With Those Obtained by Digital Simulation (DS)[a].

	k_s, cm/s		α		$E_{\frac{1}{2}}$, V[d]	
Compound	DS	BHO	DS	BHO	DS	BHO
4,4'-dimethoxybenzil[b]	0.35	0.29	0.43	0.40	-1.591	-1.589
2,3-butanedione[a]	0.65	0.56	0.50	0.50	-1.178	-1.718
2,3-butanedione[b,e]	0.021	0.022	0.43	0.40	-1.708	-1.704
nitromesitylene[b]	0.10	0.093	0.43	0.42	-1.773	-1.776
1,4-dicyanobenzene[b]	0.26	0.21	0.42	0.43	-1.927	-1.927
nitromethane[a]	0.36	0.28	0.55	0.53	-1.926	-1.912
nitroethane[a]	0.28	0.26	0.50	0.42	-1.956	-1.947
2-nitropropane[a,f]	0.11	0.12	0.43	0.42	-2.000	-1.996
trans-1-phenyl-4,4-dimethyl-1-pentene-3-one[b]	0.35	0.26	0.45	0.50	-2.060	-2.061
benzophenone[b]	0.79	0.59	0.50	0.47	-2.127	-2.119

[a] 0.10 M electrolyte, acetonitrile solvent, mercury electrode, 25°C, 100 V/s scan rate.
[b] Tetraethylammonium perchlorate electrolyte.
[c] Tetra-n-heptylammonium perchlorate electrolyte.
[d] vs. $Ag/AgNO_3$ (0.01 M) in acetonitrile.
[e] $d\alpha/dE$: 0.37 V^{-1} (DS), 0.28 V^{-1} (BHO)
[f] $d\alpha/dE$: 0.30 V^{-1} (DS), 0.37 V^{-1} (BHO)

05450

INVESTIGATION OF ELECTROCHEMICAL AND CHEMICAL STAGES OF THE Cu(II) ELECTROREDUCTION PROCESS IN THE PRESENCE OF ALLYL ALCOHOL

V.F. VARGALYUK, Y.M. LOSHKARYOV, V.A. POLONSKY, N.V. KHOROSHAVKINA
Department of Physical Chemistry, Dniepropetrovsk State University, Pr. Gagarin 72, Dniepropetrovsk, GSP 320625,USSR

Olefine compounds (acrylic acid, allyl alcohol and others) are recommended to be used as an addition to electrolytes to improve the structure of the cathode deposition of copper. We have established that Cu(II) electroreduction in the presence of Olefine compounds (OC) proceeds along the ECE mechanizm with an intermediate chemical reaction formation of univalent copper π - complexes. The properties of such complexes with ions of transitional metals were considered in a number of monographs, however, their role in the process of electroreduction of metal ions have not been studied.

A typical feature of allyl alcohol (AA) action during Cu(II) electroreduction on a mercury electrode is the appearance of anode currents during cathode polarization of the electrode (Figure). As seen in the figure, with the growth of the AA content the height of the polargraphic wave decreases, and at sufficiently high concentrations the cathode current changes to that of the anode. It should be noted that the magnitude of the anode current grows not only with the increase of the AA concentration, but also with copper sulfate.

The described effect is specific for a mercury electrode and is not observed at Cu(II) electroreduction on copper, platinum and glass-carbon electrodes. Here not only is the anode current not fixed, but there is also no decrease in the limiting current even at a high (1M) AA content in the solution.

A comparison of the polarograms with the dependencies of the double layer differential capacity from the potential shows that the decrease of the limiting current occurs in the AA adsorption area. However, the assumption about the inhibition of the copper ion discharge by the adsorbed AA layer does not explain the appearance of the anode current. Thus, it can be confirmed that the discussed effect depends on the interaction of allyl alcohol molecules or its complexes with Cu(I) with surface mercury atoms (according to data in literature AA complexes with Cu(II) are not formed). This is confirmed by the results of the analyses of the solutions on Hg(II) ions. After a prolonged (0.5 hour) electrolysis at a potential -0.5 V (saturated calomel electrode) on a stationary mercury electrode the Hg(II) ions are detected even at an AA concentration in the electrolyte equal to 0.1 M, i.e. under

conditions when the total cathode current is recorded on the polarograms.

Taking the possibility of forming Hg(II) complexes with AA into account, it was natural to associate the appearance of the anode current with the potential shift of the anode dissolution of the mercury to the negative side. But this assuption was also not confirmed experimentally. In the absence of Cu(II) allyl alcohol, even at high concentrations, does not practically influence the I,E-curve in I M sulfuric acid. Hence it follows that Cu(II) complexes with AA occur in the mercury ionization process in the considered system.

Proceeding from the above-mentioned we can write down the following reaction (scheme) of the electrode process:

$$Cu(II) + e = Cu(I) \quad (1)$$
$$Cu(I) + AA = [Cu(AA)]^{+} \quad (2)$$

A substitution of Cu(I) further occurs either in the $[Cu(AA)]^{+}$ complex by the Hg(II) ion according to equation

$$[Cu(AA)]^{+} + Hg = [Hg(AA)]^{+} + Cu(I) + 2e \quad (3a)$$

or the formation of a binuclear complex

$$[Cu(AA)]^{+} + Hg = [Hg.Cu(AA)]^{3+} + 2e \quad (3b)$$

Irrespective of the possible way of the process, according to equation (3a) or (3b) an anode current should occur at the expense of the different amount of electrons participating in the first and third stages.

In this interval of potentials an electroreduction of Cu(I) and $[Cu(AA)]^{+}$ ions with the formation of amalgams occurs.

$$Cu(I) + e = Cu^{o}(Hg) \quad (4)$$

$$[Cu(AA)]^{+} + e = Cu^{o}(Hg) + AA \quad (5)$$

The magnitude and sign of the resulting current are determined by the correlation process rates (3) and (4) - (5). If the reaction rate (3) is greater than the sum of those in (4) and (5), the anode current is fixed, and at a reversed relation of these rates - the cathode current is fixed.

The choice between the reactions presented in equations (3a) and (3b) require additional investigations. All the same the more probable seems the process mechanism including the stage of forming the binuclear complex, since the discussed effect distinctly appears precisely in the presence of allyl alcohol. Probably, here we should take into account the specificity of the AA molecular structure, similar to diolafine compounds for which the formation of binuclear complexes is typical.

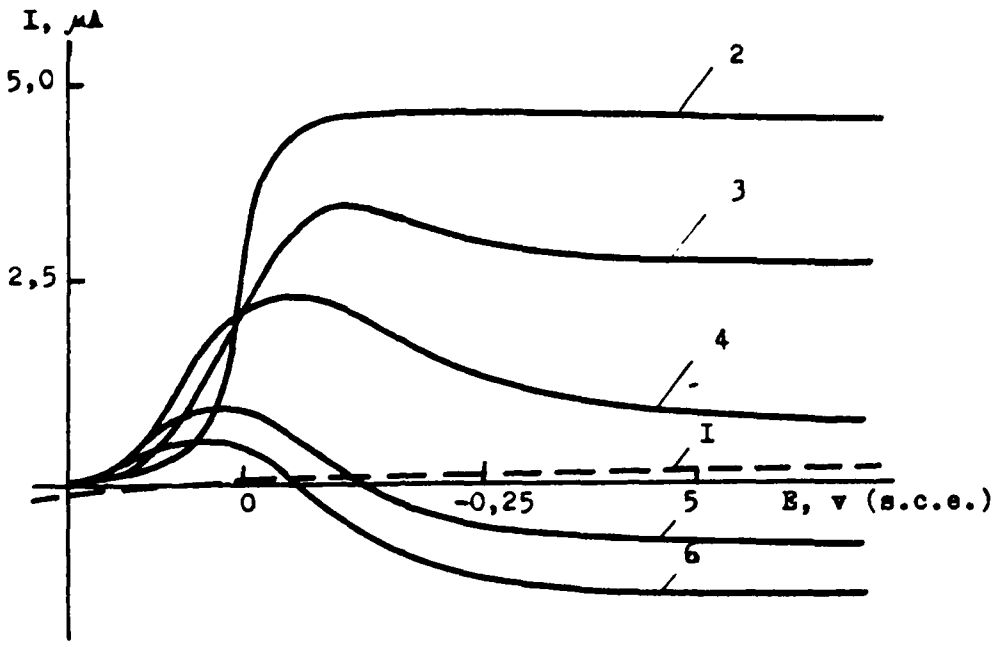

Fig. Polarograms obtained in solutions:
(I) 1M H_2SO_4; (2) I + 0,005M $CuSO_4$; (3) 2 + 0,1M AA;
(4) 2 + 0,2M AA; (5) 2 + 0,5M AA; (6) I + 0,01M $CuSO_4$ +
+ 0,5M AA.

05460

THE ADATOMS INFLUENCE ON THE OVERPOTENTIAL OF THE TRANSITION IN THE PROCESS OF METAL ELECTROCRISTALLIZATION

V.V. TROFIMENKO, V.S. KOVALENKO, Y.M.LOSHKARYEV
Dniepropetrovsk State University (USSR)

The inhibition of any crystallization stage during metal electrodeposition gives rise to an increase of adatom C concentration in comparison with the thermodynamically equilibrium value of C_o . The supersaturation C/C_o arising from this can influence the reaction of the electron transition directly which follows from the analysis of the known kinetic equation

$$i = i_o [exp(\alpha n F \eta_{n(\infty)}/RT - exp(-\beta n F \eta_{n(\infty)}/RT)] \qquad (1)$$

where the current exchange is

$$i_o = nF k_s^* C_R^{\alpha} C_{ox}^{\beta} exp[(\beta g_{ox} + \alpha g_R)/RT] \qquad (2)$$

In eguations (I) and (2) $\eta_{n(\infty)}$ is the transfer potential in the system without supersaturation, k_s^* is the absolute heterogeneous constant of the discharge rate, C_{ox} and C_R are the concentration of the oxidized and reduced form of the electroactive particles, g_{ox} and g_R are their specific standard adsorption energies (without taking into account the electrostatical component of the adsorption energy).

In a system with supersaturation eguation (I) takes the following form

$$i = i_o (C/C_o)^{\alpha} [exp(\alpha n F \eta_{n(r)}/RT) - exp(-\beta n F \eta_{n(r)}/RT)] \qquad (3)$$

as seen, the appearance of supersaturation in the cathode process ($C/C_o > 1$) gives rise to a decrease of $\eta_{n(\infty)}$ to the value $\eta_{n(r)}$ (Fig.I), curves I and 2 . An analogaus equation (3) expression was obtained when solving the problem about the influence of the electrode curvature on $\eta_{n(\infty)}$ [2] . BOth approaches are connected taking into account only the influence of supersaturation on the anodic component current through the concentration of adatoms.

Equation (3) can be written in another form through the total owervoltage $\eta = \eta_{n(r)} + \eta_k$ (η_k is the crystallization overpotential determined by the expression $\eta_k = (RT/nF) Ln(C/C_o)$

$$i = i_o [exp(\alpha n F \eta/RT) - (C/C_o) exp(-\beta n F \eta/RT)] \qquad (4)$$

If we ignore the influence of supersaturation on $\eta_{n(\infty)}$, then we can come to the erroneous method of determining η_k by the difference of values η and $\eta_{n(\infty)}$ (Fig.I, curves I and 3). Precisely due to this a wrong conclusion was drawn in paper [3] about the decrease of η_k with the growth of i , and the absence of the inhibiting stage of crystallization during metal electrodeposition with large current of exchange. Numerous experimental data contradict such conclusions.

Another aspect is the influence of supersaturation on the

overpotential $\eta_{n(\infty)}$ associated with the possibility of the discharge leaking onto the surface areas of the similar electrode with a large currature r (prenucleation cluster, growing nuclei, rough surface deposition area). SUch elements are conjugated with a definite supersaturation and a shift of the electronic therms of atoms, forming a distorted surface. Whith this the adsorption energy of the metal adatoms decreases in conformance with the Tompson equation at a magnitude of $2\sigma V/r$ (σ is the function of the surface tension of the electrode element with the r curvature, taking the two layer charge into account, V is the molar volume of the metal). This according to equation (2), results in a decrease of the current exchange in $(C/C_o)^{\alpha}$ times, and the growth of $\eta_{n(\infty)}$ to the $\eta_{n(r)}$ value (Fig.I, curve 4):

$$i = i_o (C/C_o)^{-\alpha} [\exp(\alpha n F \eta_{n(r)}/RT) - \exp(-\beta n F \eta_{n(r)}/RT)] \quad (5)$$

Homever, i_o increases to the same degree due to the heightened adatom concentration on the distorted surface. As a result of the action of both factors a full compensation of the supersaturation influence occurs at the exchange current, and appears to be independent on the electrode surface curvature from the similar metal, i.e. $\eta_{n(r)} = \eta_{n(\infty)}$. The total overpotential in such a system is described as follows:

$$i = i_o (C/C_o)^{-\alpha} [\exp(\alpha n F \eta/RT) - (C/C_o)\exp(-\beta n F \eta/RT)] \quad (6)$$

an adequate kinetic equation, written in a somewhat different form is given in the papers [4,5]

$$i = i_o \{\exp[\alpha n F(\eta - \eta_x)/RT] - \exp[-\beta n F(\eta - \eta_x)/RT]\} \quad (7)$$

a comparison of the kinetic curves corresponding to equations (I) and (6) (Fig.I) indicate the additivity of the magnitudes $\eta_{n(r)}$ and η_x .

According to equation (3) the effect of the supersaturation influence on η_n cannot exceed the magnitude η_x (approximately 20 - I00 mV), whereas for some processes the phaseformation, depending on the nature of the dissimilar electrode, the experimentally determined change of $\eta_{n(r)}$ reaches 200-500 mV, [6] and despite equation (3) is [7] associated with the growth C/C_o (Fig.2). As shown in paper [7], such significant changes of $\eta_{n(r)}$ can explain the difference in the adsorption energy of metal adatoms (adions) on different dissimilar electrodes.

Literature

I. K.Fetter - Elektrokhimicheskaya Kinetika,M.,Khimia, I967.
2. R.Kaishev, D.Kashchiev - 28-th Meeting ISE, Electrocrystallisation. Extended abstracts, Varna, I977, p.I22.
3. V.Klapka - Collection Chech.Chem.Commun., I970, v.35,p.I22.
4. A.I.Danilov, Yu.M.Polukarov - Electrokhimiya, I98I,v.I7, p. I883.
5. V.A.Isaev, V.N.Chebotin - IOnniye rasplavy i tverdie elektrolity, Sverdlovsk,I978, v.27, p.46.
6. V.V.Trofimenko, Yu.M.Loshkaryev, V.S.Kovalenko - Dokl. AN SSSR, I976, v.227, p. II8I.
7. V.V.Trofimenko, V.S.Kovalenko, Yu.M.Loshkaryev - Dokl. AN SSSR, I977, v.233, p. II42.

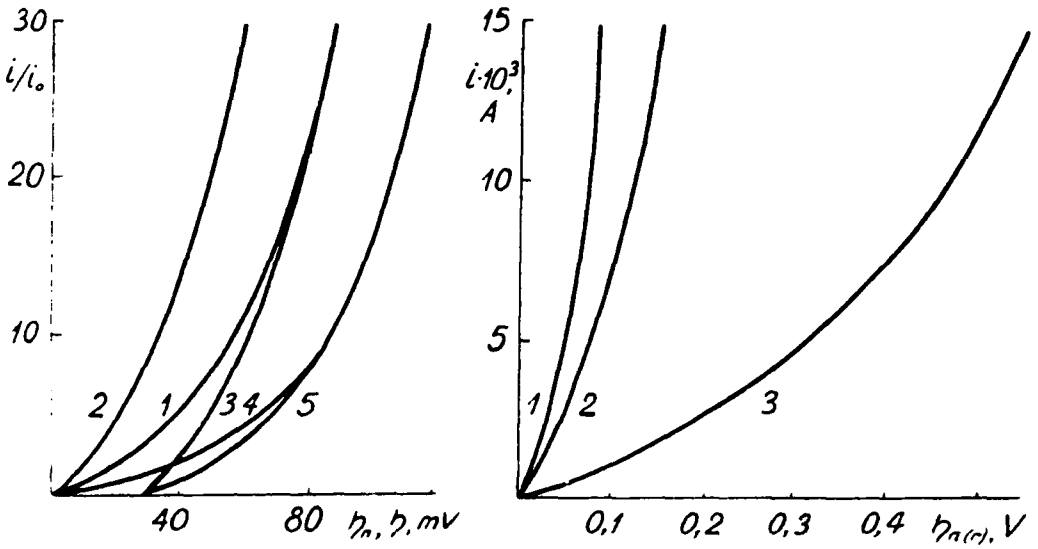

Fig.I. Cathode kinetic curves corresponding to equations I - (I), 2 - (3), 3 - (4), 4 - (5), 5 - (7). The culculation are made for $C/C_0 = 10$, $\alpha = 0,5$, $n = 2$, $T = 298$ K°.

Fig.2. The influence of the electrode nature on $\eta_{n(г)}$ in the process of galvanostatical formation of the nuclei Cu. I - copper, 2 - "basis" orientation of pyrographite, 3 - "edge" orientation of pyrographite. The electrolyte composition (mole/l): $CuSO_4$ - 0,8, H_2SO_4 - I.

25-b

05470

THE DYNAMICS OF CONCENTRATION ADATOM CHANGE IN THE PROCESS OF POLYCRYSTALLINE DEPOSIT GROWTH OF COPPER

V.V. TROPIMENKO, V.P. ZHITNIK, E.V. ISAENKO, Y.M. LOSHKARYEV
Dniepropetrovsk State University (USSR)

The validity of the conclusions, when studying the stages of crystallization processes of electrodeposition of metals, is better substantiated if the experimental determination of the adatom concentration (equilibrium C_0 and non-equilibrium C_i), or a supersaturation of C_i/C_0 (crystallization overpotential $\eta_к$) is possible. One of the most authentie is the two-impulse potentiostatic method for determining $\eta_к$, suggested in paper [1] , which was used in the present investigation.

The change of $\eta_к$ in its early stages of copper electrodeposition, and also the dependence $\eta_к$ on the current density i have been studied. An electrolyte containing I M $CuSO_4$ and 0,5 M H_2SO_4 was used, the cathode was a mechanically polished polycrystalline copper face microelectrode I mm diameter.

A typical feature of the change of the magnitudes $\eta_к$ and i in the process of the potentiostatic growth of the copper deposit is shown in Fig.I. As seen, the region of the pvorly reproducing changes of these magnitudes precede the stationary values $\eta_к$ and i . Irrespective of the stationary values i , the value $\eta_к$ stabilized after depositing a copper l yer 700 - 800 Å. Apparently, the period of the non-stationary values $\eta_к$ is determined by the transitional process of the conditions of epitaxical influence of the electrode to the conditions of growth, depending only on the electrochemical parameters of the system. Precisely that is why the deviation, appearing statistically in the structure of the initial electrode surface during its preparation, gives rise to various dynamics in changing the values $\eta_к$ and i .

The growth of the stationary values $\eta_к$ during the rate increase of the crystallization (Fig.2) is determined by the forced transition of the crystal nucleation on the deposition area with less electrocatalytic activity. With this in a number of active centres of crystallization, more and more screw dislocations, which appear morphologically as pyramidal projections of the growing surface, are included [2] .

The region of the limiting values $\eta_к$ during the i increase is determined by reaching the conditions at which the nuclei, the epitaxially non-associated dislocation appearing in the transition period are formed.

The transition overpotential $\eta_п$ was determined on the basis of the additive approach, with this the rated corrections on the ohmic component and the overpotential diffusion (Fig.2) were inserted. The analysis showed that the value $\eta_п$ does not obey the classical equation of the slow discharge. This is explained by the influence on i supersaturation, realized in the system. It showd be noted that with the i

increase the determining influence of the electron transition stage grows, but the value η_k remains high. The latter indicates the important part under such conditions of the proper crystallization stages in the process of forming structures and the properties of copper deposition.

Literature

I. Z.A.Tkachik, K.M.Gorbunova - V kn."Elektrokhimicheskiye protsessi pri elektroosazhdenii i anodnom rastvorenii metallov", M., Nauka, I969, str. 88.
2. K.Fetter - Elektrokhimicheskaya Kinetika, M., Khimia, I967.

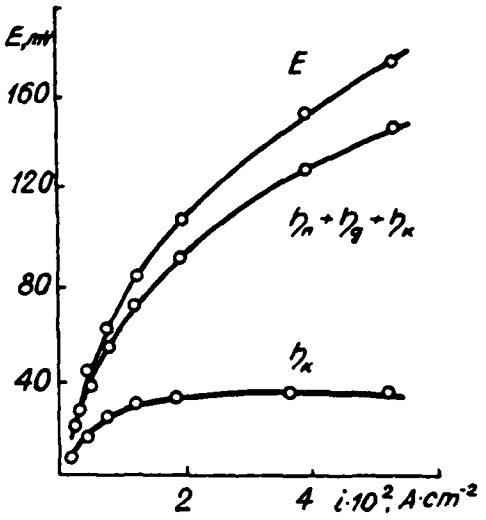

Fig.I.
(Explanation in the text)

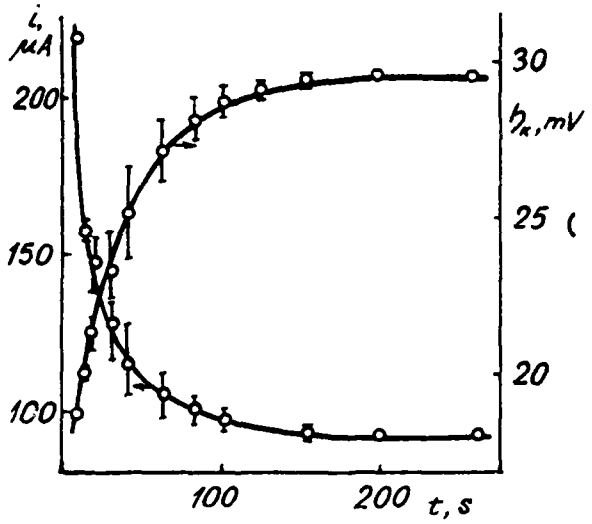

Fig. 2.
(Explanation in the text)

PULSE POLAROGRAPHY: CURRENT-POTENTIAL CURVES IN NORMAL PULSE POLAROGRAPHY, REVERSE PULSE POLAROGRAPHY AND DIFFERENTIAL PULSE POLAROGRAPHY FOR ELECTRODE PROCESSES WITH NON-NERNSTIAN BEHAVIOUR

J. GALVEZ, J. ZAPATA AND M.L. ALCARAZ
Laboratory of Physical Chemistry, Faculty of Science, Murcia (Spain)

Pulse polarography(NPP, RPP, DPP) is one of the most powerful electroanalytical techniques both for chemical analysis and for the study of electrode processes[1-2]. Theoretical studies for reversible processes have been made extensively[3,4,5]. In this context, we have obtained recently[6] the rigorous solution for the case where the reduction product dissolves in the electrode by adopting for the dme the expanding sphere electrode model. However, the corresponding theory for pulse polarography with slow charge-transfer steps contains some simplifying assumptions which are not well justified[3]. In turn, Matsuda[1] has derived theoretical expressions for the current response in NPP, RPP and DPP although, the restriction $t'/t \ll 1$(being t' the duration of the imposed pulse) was used. Finally, Aoki and Osteryoung[2] have also obtained expressions for the corresponding response in DPP but their final equations are very cumbersome.

In this work, expressions for Pulse polarography(DPP, NPP, RPP) are derived for charge-transfer processes with non-Nernstian behaviour by adopting for the dme the expanding sphere electrode model. We have used the derivational pattern based on the dimensionless parameter method described in reference(6). This allows then solving the problem through concentration profiles for any value of x and t so that the use of linearized profiles[3] is not neccesary. We have considered the process

$$A + ne- \underset{k_b}{\overset{k_f}{\rightleftharpoons}} B$$

where for simplicity the assumption $D_A=D_B=D$ has been made. In addition, we shall suppose that the potential is set on a constant value E_1 from t=0(beginning of the drop growth)to $t=t_1$ and at $t=t_1$ it is stepped up from E_1 to the other constant value E_2. Under these conditions the solution of the corresponding boundary value problem after the pulse is applied is given by

$$i(t)=i_{dc}(t)\left\{1+\beta\frac{i_{NPP}}{nFA(t)k_s C_A^*}\right\}+\left(\frac{K_1-K_2}{1+K_1}\right)i_{NPP} \qquad (1)$$

where

$$i_{dc}(t)=nFA(t)(7D/3\pi t)^{1/2}\frac{C_A^* F(\chi)}{1+K_1} \qquad (2)$$

$$i_{NPP}=nFA(t)(D/\pi t')^{1/2}C_A^* \frac{G(\tau,y)}{1+K_2} \quad (3)$$

$$\beta=(1+K_2)\left(\frac{K_1^\alpha}{1+K_1}-\frac{K_2^\alpha}{1+K_2}\right) \quad (4)$$

$$K_i=\exp\left((nF/RT)(E_i-E^\circ)\right) \quad (5)$$

$$\chi=(12t/7D)^{1/2}k_s\,(1+K_1)\exp\,(-\alpha nF/RT)(E_1-E^\circ) \quad (6)$$

$$y=(4t'/D)^{1/2}k_s(1+K_2)\exp(-\alpha nF/RT)(E_2-E^\circ) \quad (7)$$

$$\tau=t'/(t_1+t') \quad (8)$$

Note that i(t) is a function of the corresponding current response in dc polarography(equation (1))and in NPP(equation (3)). In any case, it is interesting to show that in equation (1) only are involved the Koutecky function[7], $F(\chi)$ (which is related to the dc polarographic response) and the Galvez function $G(\tau,y)$[8](which is involved with the NPP response)whose properties have been described in the literature(7-9).

From equation (1) we may easily obtain the expressions for the different modes of pulse polarography and so, we have:

a) $E_2=E_1$. In this case $K_2=K_1$, $\beta=0$ and as expected, equation (1) gives $i(t)=i_{dc}(t)$.

b) NPP. In NPP, E_1 is maintained at an initial value at which no current flows. Inserting the condition $K_1\to\infty$ in equation (1) we obtain $i(t)=i_{NPP}$.

c) RPP. In RPP, E_1 is set on the cathodic diffusion current plateau and the potential E_2 is scanned anodically. Inserting the condition $E_1\to-\infty(K_1\to 0)$ in equation (1) we have

$$i_{RPP}=i_{dc}\left\{1-\frac{i_{NPP}}{nFA(t)k_sC_A^*}\exp\left((\alpha nF/RT)(E_2-E^\circ)\right)\right\}-K_2i_{NPP} \quad (9)$$

d) DPP. In DPP E_1 and E_2 are scanned simultaneously toward the cathodic direction so that $E_1-E_2=\Delta E$ is kept constant. In addition, i_{DPP} is normally measured as a difference between i(t) at $t=t_1+t'$ and i(t) at $t=t_1$. Hence, we obtain

$$\left.\begin{aligned}\frac{i_{DPP}}{i_{d,p}}&=\frac{\tau^{1/2}F(\chi)}{1+K_1}\left\{1+\beta\frac{i_{NPP}}{nFA(t)k_sC_A^*}-(1-\tau)^{1/6}\frac{F(\chi)}{F(\chi_1)}\right\}+\\&+(3/7)^{1/2}\left((1/(1+K_2))-(1/(1+K_1))\right)G(\tau,y)\\ i_{d,p}&=(7D/3\pi t')^{1/2}nFA(t)C_A^*\end{aligned}\right\} \quad (10)$$

where $\chi_1=(1-\tau)^{1/2}\chi$. Examples of I/E curves computed from equations (3), (9) and (10) are shown in figures 1-3.

e) Reversible process: Under there conditions $k_s >> 1$ and equation (1) gives

$$i(t) = i_{dc}(t) + \frac{K_1 - K_2}{1 + K_1} i_{NPP} \qquad (11)$$

From this equation the different modes of pulse polarography for Nernstian behaviour are easily obtained as described previously.

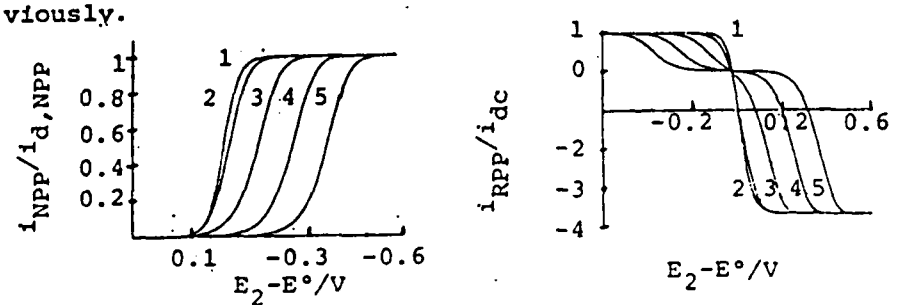

Fig.1.- NPP. Current-Potential curves for n=1, $D=10^{-5} cm^2.s^{-1}$, T=298K, α=0.5, and different values of $k_s (cm.s^{-1})$: (1) 1; (2) 10^{-2}; (3) 10^{-3}, (4) 10^{-4}, (5) 10^{-5}. $i_{d,NPP} = nFA(t)(D/\pi t)^{1/2}(1 + \frac{1}{3}\tau + ...)$. t=1s; t'=0.02s.

Fig.2.- RPP. Current-Potential curves computed from equation (1). Conditions as Fig.1

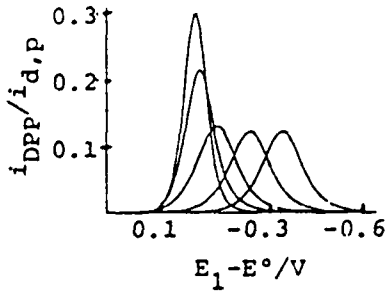

Fig.3.- DPP. Current-Potential curves for t=1s., t'=0.05s., ΔE=0.05V and different values of $k_s (cm.s^{-1})$: (1) 1; (2) $5x10^{-3}$; (3) 10^{-3}; (4) 10^{-4}; (5) 10^{-5}. Other conditions as Fig.1.

REFERENCES

1) H.Matsuda, Bull.Chem.Soc.Jpn.,53(1980)3439
2) K.Aoki and J.Osteryoung, J.Electroanal.Chem.,110(1980)19
3) R.L.Birke, Anal.Chem.,50(1978)1489
4) J.H.Christie and R.A.Osteryoung, J.Electroanal.Chem., 49(1974)301
5) G.J.M.Heigne, W.E. van de Linden, Anal.Chim.Acta,99(1978) 183
6) J.Galvez, Anal.Chem.,57(1985)585
7) J.Koutecky, Collect.Czech.Chem.Commun.,18(1953)597
8) J.Galvez and A.Serna, J.Electroanal.Chem.,69(1976)145
9) L.Camacho, J.L.Avila, A.M.Heras and F.Garcia-Blanco, J.Electroanal.Chem.,182(1985)173

CHRONOPOTENTIOMETRY WITH PROGRAMMED CURRENT AT A DROPPING MERCURY ELECTRODE: POTENTIAL-TIME CURVES FOR AN ECE MECHANISM

J. GALVEZ, J. ZAPATA, M. L. ALCARAZ AND F. ROBLES
Laboratory of Physical Chemistry, Faculty of Science, Murcia (Spain)

In a series of recent papers[1-6] we have shown that dme chronopotentiometry is a very appropiate technique for the study of electrode processes when a current-time function of the form $I(t)=I_0 t^{w+1/6}$ $(w \geq 0)$ is used. In the present work we have obtained the theoretical relationships, which show the behavior of the E/t curves, for the ECE mechanism. If the charge transfer reactions are reversible, this mechanism is described by the scheme

$$A + n_1 e^- \rightleftharpoons B;\ B \underset{k_2}{\overset{k_1}{\rightleftharpoons}} C;\ C + n_2 e^- \rightleftharpoons D$$

If we adopt for the dme the expanding sphere electrode model, the transition time, τ_e, is given by

$$\left(\frac{\tau_e}{\tau_{d,e}}\right)^w = \frac{g_w(0,\tau_{d,e})}{g_w(0,\tau_e)} \frac{1}{1+KG_{w,e}(\chi_{\tau_e})} \left\{1 + f - (f-K)\left[G_{w,e}(\chi_{\tau_e}) g_w(0,\tau_e) + H_w(\chi_{\tau_e})(1-g_w(0,\tau_e))\right]\right\} \quad (1)$$

where

$$\left.\begin{aligned} &\chi=(k_1+k_2)t \\ &g_w(0,t)= 1-f_w(0)\xi_0 t^{1/6} \\ &\tau^w_{d,e} = \sqrt{\frac{7D}{12}} \frac{p_{6w/7} n_1 F A_0 C^*_A}{I_0 g_w(0,\tau_{d,e})} \\ &f=n_2/n_1;\ \xi_0=\sqrt{12D/7a^2};\ a=(3m/4\pi d)^{1/3} \end{aligned}\right\} \quad (2)$$

$$f_w(j)= \frac{1}{22}\left\{7(3(w+j)+2)p_{\frac{6w+j}{7}} - \frac{12(w+j)(3(w+j)+4)}{p_{\frac{6(w+j)+1}{7}}}\right\} \quad (3)$$

$$G_{w,e}(\chi)= \frac{e^{-\chi} p_{6w/7}}{g_w(0,t)} \sum_{j=0} \frac{\chi^j}{j!} \frac{g_w(0,t)}{p_{\frac{6(w+j)}{7}}} \quad (4)$$

$$H_w(\chi)= p_{\frac{6w+1}{7}} e^{-\chi} \sum_{j=0} \frac{\chi^j}{j!} \frac{1}{p_{\frac{6(w+j)+1}{7}}} \quad (5)$$

and being $\tau_{d,e}$ the transition time which would be observed in

the absence of the chemical reaction. In turn, the potential-time function is

$$E(t) = E_1^0 + \frac{RT}{n_1 F} \ln \frac{C_A(0,t)}{C_B(0,t)} \tag{6}$$

with

$$C_A(0,t) = C_A^*(1-g_w(0,t)\varepsilon_e(t)) \tag{7}$$

$$C_B(0,t) = \frac{C_A^*}{1+K} \Big| ((1-K)\varepsilon_e(t)+KN(w,t))G_{w,e}(X)g_w(0,t) + \\ +(2\varepsilon_e(t)-N(w,t))Kg_w(0,t) - \\ -(1-K)(G_{w,e}(X)-H_w(X))g_w(0,t)(\varepsilon_e(t)-\varepsilon_p(t))\Big| \tag{8}$$

$$\varepsilon_e(t) = \varepsilon_p(t) + \frac{\xi_0 t^{1/6} \chi^w \sigma'_{1,1}(0)}{C_T P_{(6w+1)/7} g_w(0,t)} \tag{9}$$

$$\varepsilon_p(t) = -\frac{a_1 \chi^w}{C_T} \tag{10}$$

$$N(w,t) = \sqrt{\frac{12}{7D}} \frac{I_0 t^w}{n_1 F A_0 C_A^* P_{6w/7}} \tag{11}$$

In Fig.1 we have plotted E/t curves computed from eqn.(6) for different values of ξ_0. Note that the influence exerted by the sphericity of the electrode is very significant and so, there is a shift of E(t) towards positive potentials as ξ_0 is increased. In addition, the values of τ_e are also larger than those obtained with the expanding plane electrode model ($\xi_0=0$).

In Fig.2 we have represented $(\tau_e/\tau_{d,e})^w$ vs. χ_{τ_e} for w=1/2 and different values of K. Note that these curves allow us to obtain in a direct way the values of k_1 and k_2 if the equilibrium constant is known. In those cases where K is unknown a fitting procedure similar to that described in reference (6) can be applied.

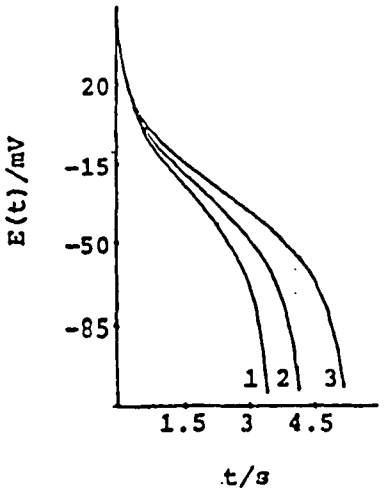

Fig.1.- Potential-time curves for w=1/2, $N_0=1.12s^{-1/2}$, K=0, $k_1=1s^{-1}$, $f=n_1=n_2=1$, $A_1=1$, D=1, T=298K. $\xi_0(s^{-1/6})$: (1) 0.0; (2) 0.1; (3) 0.2.

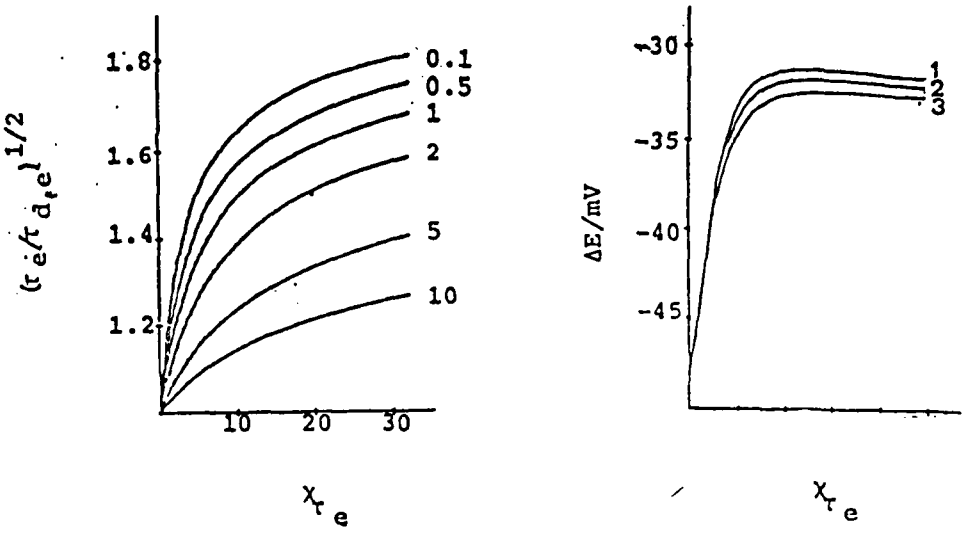

Fig.2.- Dependence of $(\tau_e/\tau_{d,e})^w$ vs. χ_{τ_e} for w=1/2 (eqn.(1)) and ξ=0.15. K-values shown on the curves.

Fig.3.- Dependence of ΔE vs. χ_{τ_e} for $\Omega \to \infty$. $\xi_0 (s^{-1/6})$: (1) 0.0; (2) 0.1; (3) 0.2.

Finally, in Fig.3 we show working curves of $E(3\tau_e/4)-E(\tau_e/4)$ vs. χ_{τ_e}. Note that these plots may be also used to determine k_1 and k_2 although, in this case, it is not necessary to know previously the value of $\tau_{d,e}$.

REFERENCES

1) J.Gálvez, J.Electroanal.Chem.,132(1982)15

2) J.Gálvez and A.Molina, J.Electroanal.Chem.,146(1983)221

3) J.Gálvez and R.Saura, J.Electroanal.Chem.,146(1983)223

4) J.Gálvez, T.Fuente, A.Molina and R.Saura, J.Electroanal. Chem.,146(1983)243

5) J.Gálvez, A.Molina, T.Pérez and M.H.Córdoba, Anal.Chem. 56(1984)887

6) J.Gálvez, M.L.Alcaraz, T. Pérez and M.H.Córdoba, Anal.Chem. (in press)

CHRONOPOTENTIOMETRY WITH PROGRAMMED CURRENT AT A DROPPING MERCURY ELECTRODE: THEORY FOR ELECTRODE PROCESSES WITH FIRST-ORDER REGENERATION MECHANISMS

J. GALVEZ, F. ROBLES, J. ZAPATA AND M. L. ALCARAZ
Laboratory of Physical Chemistry, Faculty of Science, Murcia (Spain)

The theory of regeneration mechanisms has been already proposed for different electrochemical techniques[1-4]; although, in dme chronopotentiometry this theory has not as yet been developed.

Consider the reaction scheme,

$$aA + ane^- \rightleftharpoons bB$$

$$B \xrightarrow{k} hA + \text{other products}$$

where n is the number of electrons transferred per molecule of A, k is a first-order rate constant and h may take on any positive value. Note that if a and b take on the values 1 and 2 we have the case of a dimerization on the electrode surface. If we used a current-time function of the form $I(t)=I_o t^{w+1/6}$ $(w \geq 0)$ and we follow the derivational pattern described in references (5,6) we find that the E/t curves are given by

$$(\theta(w,t))^{-1/2} N(w,t) 10^{an(t)} = C_A^{*\,a-1} \left\{ 1 + \left[(p-1) - pG_w(\chi) \right] \cdot g_w(0,t) N(w,t) \right\}^a - C_A^{*b-1} \left\{ p g_w(0,t) G_{w,e}(\chi) N(w,t) / h \right\}^b 10^{n(t)} \quad (1)$$

where

$$p = h \frac{b}{a} \quad (2)$$

$$\theta(w,t) = \theta_0 t / p_{6w/7}^2 \quad (3)$$

$$\theta_0 = 12 k_s^2 / 7D \quad (4)$$

$$n(t) = nF(E(t)-E^\circ)/RT\ln 10 \quad (5)$$

$$G_{w,e}(\chi) = \frac{e^{-\chi} p_{6w/7}}{g_w(0,t)} \sum_{j=0} \frac{\chi^j}{j!} \frac{g_w(j,t)}{p_{6(w+j)/7}} \quad (6)$$

$$g_w(j,t) = 1 - f_w(j) \xi_0 t^{1/6} \quad (7)$$

$$f_w(j) = \frac{1}{22} \left\{ 7\left[3(w+j)+2\right] p_{6(w+j)/7} - \frac{12(w+j)\ 3(w+j)+4}{p_{6(w+j)+1/7}} \right\} \quad j \geq 0 \quad (8)$$

In turn, the transition time, τ_e, is given by

$$\left(\frac{\tau_e}{\tau_{d,e}}\right)^w = \frac{1-f_w(0)\xi_0\tau_{d,e}^{1/6}}{1-f_w(0)\xi_0\tau_e^{1/6}} \frac{1}{1+p\left[G_{w,e}(\chi_{\tau_e})-1\right]} \quad (9)$$

with

$$\tau_{d,e}^w = (7/12D)^{1/2} \frac{nFA_0C_A^* P_{6w/7}}{I_0 g_w(0,\tau_{d,e})} \quad (11)$$

$$\chi_{\tau_e} = k\tau_e \quad (12)$$

Note that in equations (1) and (9) p is the regeneration fraction so that we may consider three different cases:

a) $p < 1$. In this case the regeneration of A is only partial and so, if $p=1/2$ we have the one-half regeneration mechanism and for $p=0$ the equations given above are simplified to that obtained for an EC mechanism[7].

b) $p=1$. Under these conditions we have a catalytic mechanism and equations (1) and (9) become identical to those previously derived for this mechanims.

c) $p > 1$. In this case, the regeneration of A is more than total.

In Fig.1 we show E/t curves for p=1/2(one-half regeneration mechanism), p=5/4 and different values of the spherical correction parameter(ξ_0). Note that for a given value of k, τ_e increases as ξ_0 becomes greater and this effect is similar to that found for other electrode processes[5-6].

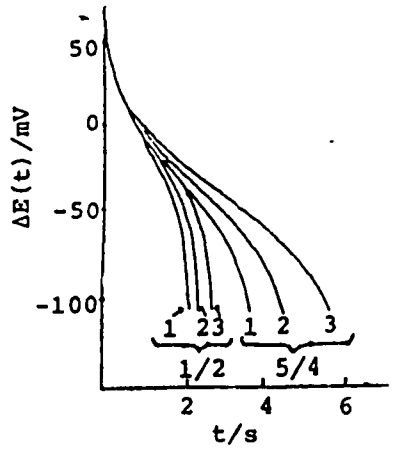

In addition, in Fig.2 we have obtained working curves of $(\tau_e/\tau_{d,e})^w$ vs. χ_{τ_e} which are useful to determine k. Note the different behavior of these plots for $p < 1$ and $p \geq 1$. Thus, if $p < 1$, $(\tau_e/\tau_{d,e})^w$ increases toward a maximum value which is equal to 1/1-p (see equation (9)). For p=1, $(\tau_e/\tau_{d,e})^w$ increases linearly with $\chi^{1/2}$ for values of χ sufficiently

Fig.1.- Potential-time curves for w=2/3, $N_0=1s^{-2/3}$, $k=0.5s^{-1}$, T=298K, $\theta_0 \to \infty$(reversible process). $\xi_0(s^{-1/6})$: (1) 0.0; (2) 0.1; (3) 0.2. p-values shown on the curves.

large. Finally, for p >1, $(\tau_e/\tau_{d,e})^w$ increases continuosly with χ, although, if the condition $G_{w,e}(\chi) \leq 1-1/p$ holds there is no transition time. An example of this is shown in Fig.3 .

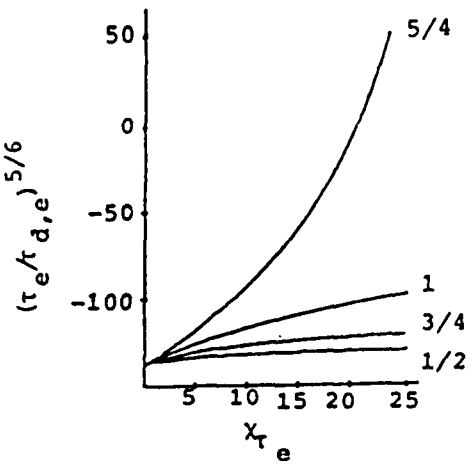

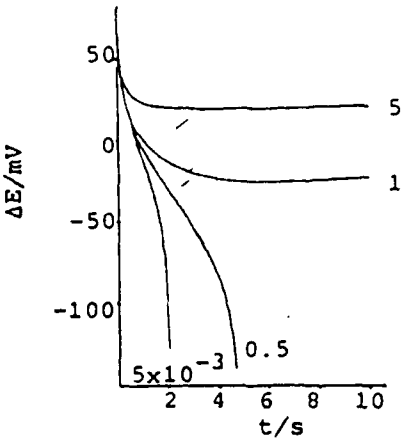

Fig.2.- Dependence of $(\tau_e/\tau_{d,e})^w$ vs. χ_{τ_e} for w=5/6 (eqn.(9)) and ξ=0. p-values shown on the curves.

Fig.3.- Potential-time curves for w=2/3, I_0=0.6 $\mu As^{1/2}$, $\theta_0 \to \infty$(reversible process),p=5/4, a=b=1, ξ_0=0.0 $s^{-1/6}$, T=298K. ^{0}k-values shown on the curves.

REFERENCES

1) T.H.Ridgway, R.P.Van Duyne and C.N.Reilley, J.Electroanal. Chem.,67(1976)1

2) E.Laviron, J.Electroanal.Chem.,87(1978)31

3) A.Vallat, M.Person and E.Lanviron, Electrochim.Acta,24(1979) 1125

4) J.Gálvez, A.Molina and C.Serna., J.Electroanal.Chem.,121(1981) 85 and references therein.

5) J.Gálvez, A.Molina, T.Pérez and M.H.Córdoba, Anal.Chem., 56(1984)887

6) J.Gálvez, M.L.Alcaraz, T.Pérez and M.H.Cordoba, Anal.Chem. (in press)

7) J.Gálvez and R.Saura, J.Electroanal.Chem.,146(1983)223

8) J.Gálvez, T.Fuente, A.Molina and R.Saura, J.Electroanal.Chem. 146(1983)243

THEORY OF THE EE MECHANISM WITH ADSORPTION OF THE INTERMEDIATE AT AN ELECTRODE EXPANDING WITH ANY POWER LAW

J. GALVEZ, M. L. ALCARAZ AND J. ZAPATA
Laboratory of Physical Chemistry, Faculty of Science, Murcia (Spain)

As it is well known, the electrochemical response for an electrode process can be significant influenced by the adsorption of one or more of the species involved in the charge transfer steps[1-3]. In these cases, the solution of the boundary value problem is more complicated than if only there are involved dissolved species, because one must consider an adsorption isotherm, and this involves the introduction of additional parameters. Regarding the EE mechanism, Lovrić[3-4] has developed recently the theory for this mechanism with adsorption of the intermediate which follows Henry's or Langmuir's isotherm. However, this theory is only valid for the stationary electrode and so, his results can not be applied quantitatively to the dropping mercury electrode. Hence, the aim of the present paper is to obtain explicit equations for an EE mechanism with adsorption of the intermediate which are valid for an electrode expanding with any power law. Under these conditions, the solutions for a stationary plane electrode and for a dme are only special cases of this general solution.

Consider the electrode process represented by

$$A + e^- \underset{}{\overset{i_1}{\rightleftharpoons}} B + e^- \overset{i_2}{\rightleftharpoons} C$$

$$B \underset{\Gamma}{\overset{K}{\rightleftharpoons}}$$

If the adsorption of B follows Henry's isotherm the boundary value problem for this mechanism is given by

$$\hat{D}C_A = \hat{D}C_B = \hat{D}C_C = 0 \tag{1}$$

$$t=0,\ x \geq 0: \quad C_A = C_A^*,\ C_B = 0,\ C_C = 0,\ \Gamma = 0 \tag{2}$$

$$t>0,\ x \to \infty: \quad C_A = C_A^*,\ C_B \to 0,\ C_C \to 0 \tag{3}$$

$$t>0,\ x=0: \quad D\left(\frac{\partial C_A}{\partial x}\right)_0 = \frac{i_1}{Fq(t)} \tag{4}$$

$$D\left(\frac{\partial C_B}{\partial x}\right)_0 = \frac{d\Gamma}{dt} + \frac{1}{q(t)}\frac{dq(t)}{dt}\Gamma + \frac{i_2}{Fq(t)} - \frac{i_1}{Fq(t)} \tag{5}$$

$$D\left(\frac{\partial C_C}{\partial x}\right)_0 = -\frac{i_2}{Fq(t)} \tag{6}$$

$$C_A(0,t) = C_B(0,t)K_1 \tag{7}$$

$$C_B(0,t) = C_C(0,t)K_2 \tag{8}$$

$$C_B(0,t) = K\Gamma(t) \tag{9}$$

$$K_i = \exp\left\{(E-E_i^0)F/RT\right\}\ ,\ i=1,2 \tag{10}$$

where $\hat{D}$ is the operator

$$\hat{D} = \frac{\partial}{\partial t} - \left(D\frac{\partial^2}{\partial x^2} + \frac{zx}{t}\frac{\partial}{\partial x}\right)$$

and q(t) the electrode area given by the general law $q(t)=q_0t^z$.

The solution of equations (1)-(9) is accomplished by using the dimensionless parameters method previously described (see for example reference (5)). Thus, using the transformations

$$\left.\begin{aligned} s &= \sqrt{\frac{2z+1}{4Dt}}\ x \\ X &= KA_0\sqrt{D(2z+1)t} \end{aligned}\right\} \tag{11}$$

where

$$A_0 = 1+K_1+1/K_2 \tag{12}$$

and the new variable

$$\psi = C_A+C_B+C_C \tag{13}$$

we find,

$$i_1 = Fq(t)\sqrt{\frac{D(2z+1)}{\pi t}}\ C_A^*\left\{1 - \frac{K_1}{A_0}F(z,X)\right\} \tag{14}$$

$$i_2 = Fq(t)\sqrt{\frac{D(2z+1)}{\pi t}}\ C_A^*\frac{F(z,X)}{A_0K_2} \tag{15}$$

$$i_{total} = Fq(t)\sqrt{\frac{D(2z+1)}{\pi t}}\ C_A^*\left\{1 - \frac{K_1-1/K_2}{A_0}F(z,X)\right\} \tag{16}$$

where the F(z,X) function is defined by

$$F(z,X) = \sum_{j=1} \frac{(-1)^{j+1}p_1(z)\ldots p_j(z)}{\prod_{i=1}^{j}(i+2z)} \tag{17}$$

with

$$p_j(z) = \frac{2\Gamma\left(1+\frac{j}{4z+2}\right)}{\Gamma\left(\frac{1}{2}+\frac{j}{4z+2}\right)} \tag{18}$$

being Γ the Euler γ function.

In Figs. 1-2 we have plotted I/E curves computed from equation (16) for z=2/3 (dme), z=0 (stationary plane electrode) and different values of $\Delta(=E_2^0-E_1^0)$ and $KD^{1/2}$. As expected, a bigger splitting of the curves is found as Δ and $KD^{1/2}$ become lower.

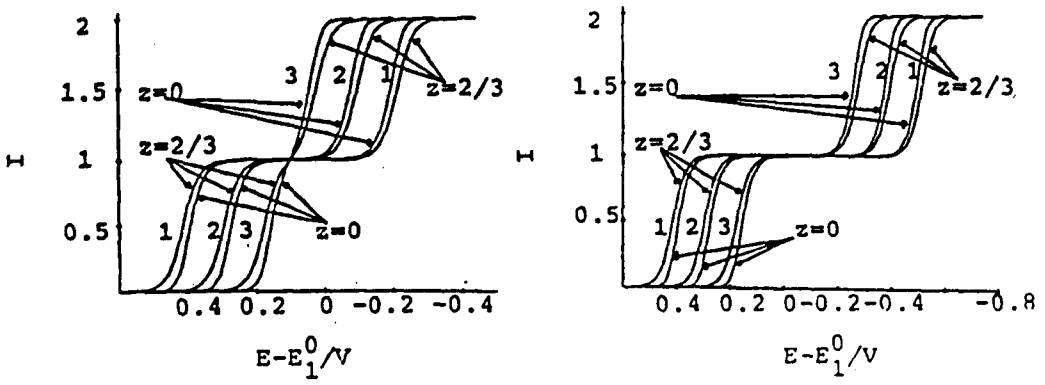

Fig.1.- Current-potential curves computed from equation (16) for Δ=0.2V, t=1s, $I=i_{total}/Fq(t)\sqrt{\frac{D(2z+1)}{\pi t}}\,C_A^*$. $KD^{1/2}(s^{-1/2})$: (1) 10^{-7}; (2) 10^{-5}; (3) 10^{-3}. z-values shown on the curves.

Fig.2.- Dependence of I on $KD^{1/2}$ for Δ=-0.1V. Other conditions as Fig.1.

In addition, these curves show an inflexion point, which from equation (16) is placed at the potential $E_{i.p.}=(E_2^0-E_1^0)/2$. In any case, it is interesting to show that the behavior of these curves are cualitatively similar for z=2/3 and z=0. However, from a quantitative point of view the differences between them are very significant. Thus, on the left of $E_{i.p.}$ we have I(z=2/3) > I(z=0). Conversely, on the right of $E_{i.p.}$ we find I(z=2/3) < I(z=0). Hence, it is clear that in this case the stationary plane electrode is not a good model for the dme even if we introduce the factor $(7/3)^{1/2}$.

REFERENCES

1) J. Heyrovský and J. Kùta, "Principles of Polarography"; Academic Press, New York,1966

2) A. J. Bard and J. R. Faulkner, "Electrochemical Methods", Wiley, New York,1980

3) M. Lovrić, J. Electroanal. Chem., 153(1983)1

4) M. Lovrić, J. Electroanal. Chem., 144(1983)45

5) J. Gálvez and A. Serna, J. Electroanal. Chem., 69(1976)145

05520

KINETIC CHARACTERISATION OF [Ru(bipy)$_2$Cl poly(4-vinylpyridine)]Cl COATED ELECTRODES

O. Haas
Swiss Federal Institute for Reactor Research, Würenlingen (Switzerland)

[Ru(bipy)$_2$Cl poly(4-vinylpyridine)]Cl: (I) coated electrodes have some interesting catalytic properties[1]. Savéant et al[2] showed that the mediation of electrochemical reactions by such redox polymer films may be described with four characteristic currents.

(1) $i_A = FSC_A^o D/\delta$: Substrate diffusion from the solution to the film.

(2) $i_S = FSC_A^o \kappa D_S/\Phi$: Substrate diffusion in the film.

(3) $i_E = FSC_p^o D_E/\Phi$: Electron transfer between different redox sites in the film.

(4) $i_k = FSC_A^o \kappa k \Gamma^o$: cross-exchange reaction between the redox center and the substrate in the film.

Where: F: Faraday's constant, S: electrode surface area, C_A^o: bulk concentration of the redox substrate, C_p^o: concentration of the redox sites in the film, Γ^o: surface concentration of the redox sites, D: diffusion coefficient of substrate in the solution, D_E: "diffusion" coefficient for the diffusion-like propagation of electrons in the film, D_S: diffusion of substrate in the film, κ: partition coefficient of the substrate between the film and the solution, k: second order rate constant of the reaction between the substrate and the active form of the redox sites, δ: diffusion layer thickness, Φ: film thickness.

Using Fe^{2+} and Fe^{3+} as a substrate in 1M HCl, we were able to evaluate these characteristic currents for electrodes coated with (I). For that purpose we used Koutecky Levich plots (Fig. 1) where slope and intercept might be used to determine i_A and i_k[3]. i_E was evaluated from chronoamperometric experiments with electrodes coated with (I) in 1M HCl. The results of these experiments are presented as Cotterell plots in Fig. 2. It can be shown that i_E is related to the slope p of these plots by the following relationship:

$$(5)\quad i_E = \frac{\pi p^2}{F \cdot \Gamma^o}$$

I_S was evaluated using Fe^{3+} as a substrate which because of its thermodynamic unfavourable reaction does hardly react with the RuII sites in polymere (I).

But the FeIII might be reduced at the electrode underneath the film. For such a system the relationship (6) might be used to find i_S:

$$(6)\quad \frac{1}{i_L} = \frac{1}{i_A} + \frac{1}{i_S}$$

Here i_L stands for the diffusion limited current obtained with the coated electrode. Unfortunately the electrodes underneath a polymere film tend to be very inactiv. To overcome this difficulty, the electrode was first coated with 1 hydroxiphenazin[5](II). With such a double coated electrode we were able to get good estimates for i_S (Fig. 3).

The results of our investigations are summarized in Table 1 for an electrode rotation speed of 1000 rpm and a substrate concentration of 10^{-6} mole/cm^3 calculated for a surface concentration of $2.6 \cdot 10^{-8}$ mole/cm^2. The results show that the catalytic process at this electrode is mainly limited by i_S and i_E.

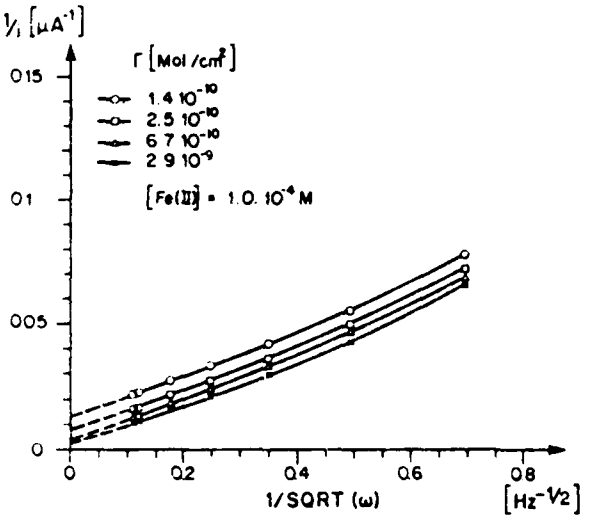

Fig. 1: Koutecky Levich plots of four electrodes with different surface concentration of (I)

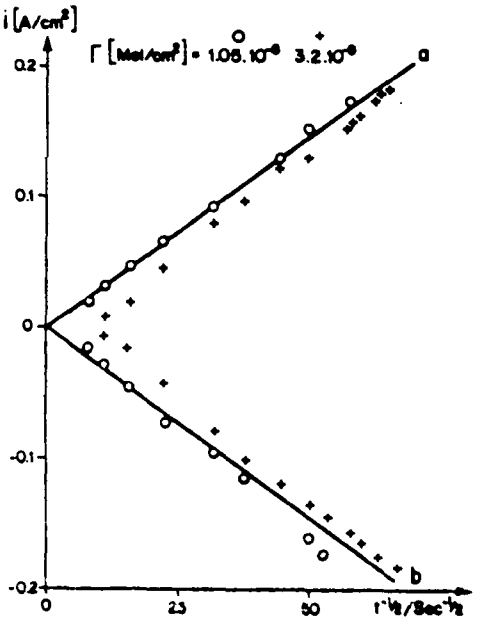

Fig. 2: Cotterell plots obtained from two electrodes coated with (I) in 1M HCl. a) anodic potential jump b) cathodic potential jump

i_A	0.45 mA/cm^2
i_S	0.4 mA/cm^2
i_E	7.9 mA/cm^2
i_k	180 mA/cm^2

Table 1

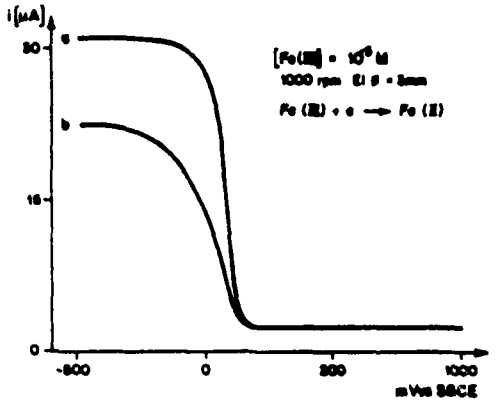

Fig. 3: Current potential curves
a) coated with (II) $\Gamma^o = 6 \cdot 10^{-9}$ mole/cm^2
b) coated with (II) and (I)
$\Gamma^o_{(II)} = 6.0 \cdot 10^{-9}$ mole/cm^2
$\Gamma^o_{(I)} = 1.0 \cdot 10^{-8}$ mole/cm^2

References

1 O. Haas and J.G. Vos
J. Electroanal Chem., 113 (1980) 139

2 C.P. Andrieux, J.M. Savéant
J. Electroanal. Chem., 134 (1982) 163

3 N. Oyama and F.C. Anson
Anal. Chem., 52 (1980) 1192

4 R.W. Murray et al.
J. Am. Chem. Soc., 104 (1982) 2683

5 O. Haas and H.R. Zumbrunnen
Helv. 64 (1981) 854

UNEXPECTED SOLVENT DEPENDENCE OF SOME HOMOGENEOUS ELECTRON EXCHANGE REACTIONS[1]

G.Grampp, W.Harrer and W.Jaenicke
Institut für physikalische und theoretische Chemie der Universität Erlangen
Egerlandstraße 3, D 8520 Erlangen

1.Introduction

For simple self exchange reactions of the form $Q + Q^r \rightleftharpoons Q^r + Q$ with $\Delta G^0 = 0$ a simple expression for the rate constant assuming weak overlap and an electron transmission coefficient $\kappa \approx 1$ was derived by Marcus[2]:

$$k = A \exp(-(\lambda_i + \lambda_o)/4RT) \quad (1)$$

the free energy of activation being given by the inner (λ_i) and the outer (λ_o) reorganization energies. λ_i is a function of force constants and differences in bond lengths of Q and Q^r, λ_o can be expressed by

$$\lambda_o = (e_o^2 L/4\pi\varepsilon_o)\cdot g\cdot\gamma \quad (2)$$

where e_o is the unit charge, L is Avogadro's constant, g is a distance parameter

$$g = (1/\bar{r}) - (1/d) \quad (3)$$

depending on a mean radius, $\bar{r}$, of the reactants and their distance in the transition state, d. The solvent parameter γ is given by

$$\gamma = (1/n^2) - (1/\varepsilon) \quad (4)$$

with n = refractive index, ε = dielectric constant.

The preexponential term is controversial[3]. It may be expressed by a precursor equilibrium with the constant K (a function of the reaction cage) and a frequency term ν. Especially the meaning of ν is open. Either a weighted mean value of orientation frequencies of the solvent and valence frequencies of the reactants is assumed or solvent relaxation phenomena are discussed which may be slower than the system's stay in the transition region. In this case the Debye relaxation time $\tau_D = 3 V_M\eta/RT$ (V_M = molar volume, η = viscosity) or the longitudinal relaxation time $\tau_L = \tau_D(\varepsilon(\nu\to\infty)/\varepsilon(\nu\to 0))$ is introduced.
To examine the factors influencing k the functions $\ln(\gamma)$ and $\ln(T^{-1})$ can be used. The former gives g and consequently λ_o, the latter $\lambda_i + \lambda_o$ and the preexponential term. (If relaxation processes are effective, an additional activation process has to be considered).

2.Experimental

The electron exchange was studied between tetracyanoquinonedimethane (TCNQ) and tetracyanoethylene (TCNE) and their radical anions in form of their tetrabutylammonium salts. It was possible to extend the experiments up to solvents with smaller dielectric constants as ever before ($2{,}2 < \varepsilon < 65.1$), the resulting γ-range being $0.05 < \gamma < 0.53$. The exchange rate constants were measured in the temperature range $220 < T/K < 320$, using ESR line broadening (slow exchange approximation) as a function of the concentration of the neutral substance.

3.Results

In Fig.1 the observed rate constants $\ln k_{obs}$ for both substances at T = 297K (crosses x...x) are given as a function of γ. Since they are not far from the diffusion limit a correction is necessary, using $1/k_{obs}=1/k_{diff} + 1/k$.

4.Discussion

4.1 The dependence of k on .

As it is shown in Fig.1, the measured rate constants cannot be correlated with γ. However, if $\ln(k\cdot\eta)$ or $\ln(k/k_{diff})$ is plotted against γ, straight lines are found (dots ●——● in Fig.1). The correlation is scarcely worse if τ_D is used instead of η. With τ_L , however, the linear dependence is less marked.

4.2 The slope of $\ln(k\cdot\eta)$ as a function of γ (Fig.1)

Since the preexponential term was found to be proportional to η^{-1}, g was obtained not from the slope of $\ln(\gamma)$ (see eqn(1) and (2)) but from the dependence of $\ln(k/k_{diff})$ on γ. In this case a straight line is found. The observed negative slope for TCNE results in a positive g, the positive slope for TCNQ in a negative g. In both cases g is much smaller than 1/2r as expected from two touching spheres (g = 1/r - 1/2 r).

This is possible for ellipsoidal molecules[4] with semiaxes $a \geq b > c$ if they react in a distance of about 2c. In table 1 the semiaxes of both molecules are compiled, as obtained from crystallographic data, also the resulting $\bar{r}$, and d calculated from g and $\bar{r}$. For both molecules c is equal. Therefore the same d is found. For TCNQ $\bar{r}$ is somewhat greater than d, for TCNE it is smaller than d. With the observed g λ_o (eqn(2)) and λ_i can be calculated, the latter from

$$\lambda_i = - 4R(d\ln k/dT^{-1}) - 4E_\eta - (e_o^2 L/4\pi\varepsilon_o)\cdot g\cdot m \qquad (5)$$

(Tab.2) E_η is the viscosity energy, m is a constant in the empirical equation[4] for $\gamma(T)$: $\gamma = m + nT$. The method of evaluation is confirmed by the result that λ_i is independent of the solvent. It is much greater than $|\lambda_o|$. In Tab.2 also ΔH^* and ΔS^* are included, calculated from the observed activation energy E according to $\Delta H^* = E - E_\eta$ and $\Delta G^* = \Delta H^* - T\Delta S^* = (\lambda_i + \lambda_o)/4$. ΔS^* is small.

References

1) see W.Harrer, G.Grampp, and W.Jaenicke, Chem.Phys.Lett. 112 (1984) 263.
2) R.A.Marcus, J.Chem.Phys. 24 (1956) 976, 979; 43 (1965) 679.
3) M.J.Weaver, T.Gennett, Chem.Phys.Lett. 113 (1985) 213, I.V.Alexandrov and V.I.Goldanskii, Chem.Phys. 87 (1984) 455.
D. F.Calef and P.G.Wolynes, J.Phys.Chem. 87(1983) 3387; J.Chem.Phys. 78 (1983) 470.
4) G.Grampp and W.Jaenicke, Ber.Bunsenges.Physik.Chem. 88 (1984) 325

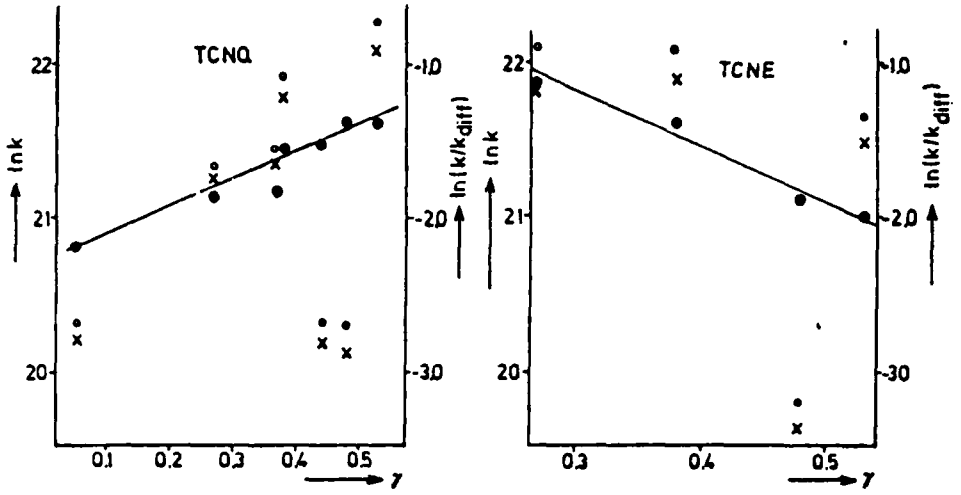

Fig.1 Rate constants as a function of γ.
Left hand scale: x...x: $\ln k_{obs}$; o...o: $\ln k$;
right hand scale: ●——● $\ln k/k_{diff}$.

Table 1 The parameter g and its components (for the calculction of $\bar{r}$ see[4])

Substance	Semiaxes (Å)	g_{obs} ($10^8 m^{-1}$)	$\bar{r}$ (10^{-10} m)	d (10^{-10} m)
TCNQ	a = 6.95 b = 4.85 c = 1.7	-1.19	4.4	4.3
TCNE	a = b = 4.7 c = 1.7	+2.35	3.7	4.2

Table 2 Activation parameters of TCNQ in different solvents

Solvent	m[a]	E (kJ mol^{-1})	λ_i[b] (kJ mol^{-1})	λ_o[c] (kJ mol^{-1})	ΔH^* (kJ mol^{-1})	ΔS^* (J mol^{-1}K^{-1})
dioxane	0.0152	12.2	27.8	-0.9	6.9	+1.3
$CHCl_3$	0.381	6.8	28.8	-4.5	5.7	+0.7
THF	0.435	8	28.2	-6.1	5.2	-1.0
PC[d]	0.321	14.4	27.7	-7.9	5.2	-1.3
CH_3CN	0.442	6.8	26.8	-8.7	4.9	+0.7
		calculated:	19.9	(297 K)		(297 K)

a) $\gamma = m + nT$ b) from eqn.(5) c) obs. d) propylene carbonate

05540

KINETICS OF THE HYDROGEN EVOLUTION REACTION ON STEEL FROM AQUEOUS SOLUTIONS IN EQUILIBRIUM WITH CO_2

T. H. BIRKELAND, R. TUNOLD and R. ØDEGÅRD,
Institutt for teknisk elektrokjemi, NTH
Universitetet i Trondheim, Trondheim Norway
and
T. HURLEN, Kjemisk Institutt
Universitetet i Oslo, Oslo Norway

The rate of corrosion of active metals in weak acids like carbonic acids is substantially higher than the rate in a strong acid at corresponding pH due to increased rate of hydrogen evolution.

The hydrogen evolution in the system: H_2O-$NaHSO_4$-$NaHCO_3$-CO_2 has been studied using a rotating iron disk electrode. The effect of angular velocity and of the chemical environment has been evaluated.

The cathodic polarization curve on pure iron is shown in Fig. 1 in 0.5 M Na_2SO_4 electrolyte with nitrogen atmosphere (broken line) and with 1 bar CO_2 atmosphere (solid line). The curve in nitrogen shows the typical behaviour of hydrogen evolution from water molecules. The curve describing hydrogen evolution from the solution saturated with CO_2 exhibits a limiting current at low negative potentials (in the vicinity of the corrosion potential), a subsequent tafelline and then a second limiting current at high negative potentials. Ultimately the two curves coincides. This behaviour has been reported earlier by Hurlen et al. /1/.

The effect of rotation speed on the first limiting current is shown in Fig. 2. The triangular points are measured values, whereas the straight lines represent calculated contributions. Line (1) is the calculated contribution from the reduction of protons whereas line (2) represents the calculated hydrogen evolution from HSO_4^--ions. Both currents are diffusion controlled. The measured curve however, seem to be made up of diffusion controlled contributions and one contribution independent of rotation speed. This last contribution seems to have the characteristics of a reaction limiting current. As shown by Hurlen et al. /1/ the magnitude of this limiting current might be calculated based on the assumption that hydration of dissolved CO_2 is the rate controlling reaction in the overall cathodic process. Line (3) represents such a calculation showing very good agreement with the experimental results. Line 4 then shows the total sum of the calculated contributions.

Additions of $NaHCO_3$ to the electrolyte seem to retard the reduction rate in the area of the first wave (Fig. 3). The current in the tafelregion and the second limiting current however, seem to increase with increasing amount of HCO_3^--ions. This could mean that the HCO_3^--ion is reduced directly according to the reaction:

$$HCO_3^- + e \rightarrow 1/2\ H_2\ (g) + CO_3^{--} \qquad (1)$$

The combined effect of additions of $NaHCO_3$ and rotation speed is shown in Fig. 4. The value of the first limiting current increase with increasing angular velocity as is shown in Fig. 2. At higher negative potentials however, the polarization curve seems to move towards lower current values, both in the tafel area and in the range of the second limiting current. It seems that convection transports away from the electrode surface a species giving some catalytic effect. This species could be CO_3^{--} which probably hydrolyze very quickly due to reaction with water:

$$CO_3^{--} + H_2O \rightarrow HCO_3^- + OH^- \qquad (2)$$

The first limiting current is conciderably higher than the corrosion current meaning that the effect of convection on the corrosion rate is minor under the prevailing conditions.

Reference:

/1/ T. Hurlen et al.
J. Electroanal. Chem. 180(1984) 511-526

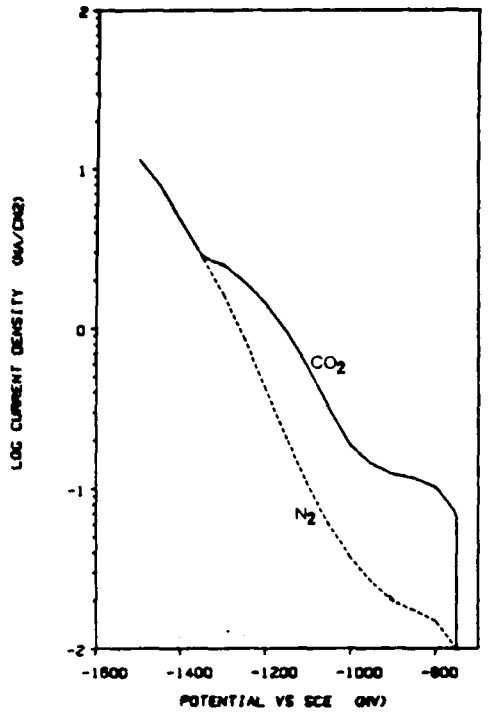

Fig.1. Cathodic polarization curve on pure iron in 0.5 M Na_2SO_4 electrolyte with nitrogen (·····) and CO_2 (——) atmosphere.

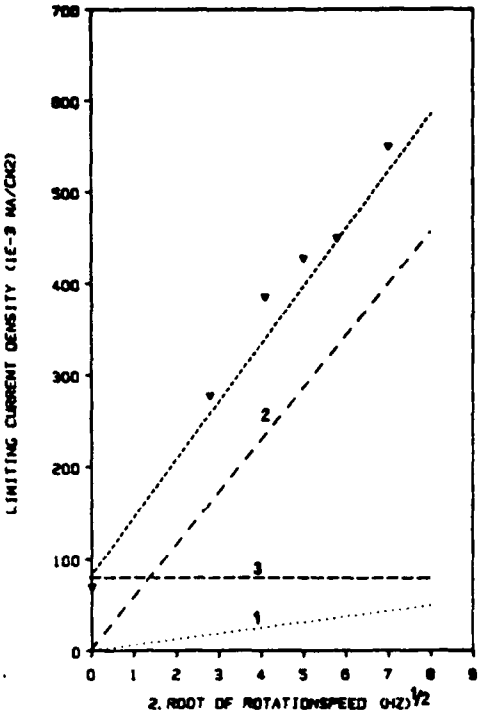

Fig.2. Effect of rotation speed on the first limiting current. (▼) Experimental values. 1, 2 and 3 are calculated contributions.

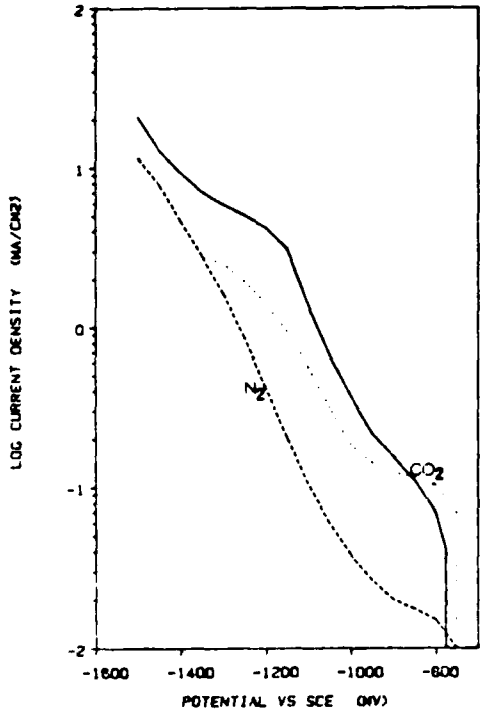

Fig.3. Effect of added $NaHCO_3$ on cathodic polarization curve of iron in 0.5 M Na_2SO_4 exposed to CO_2. (·····) 0.5 M Na_2SO_4. (——) same + 0.3 M $NaHCO_3$.

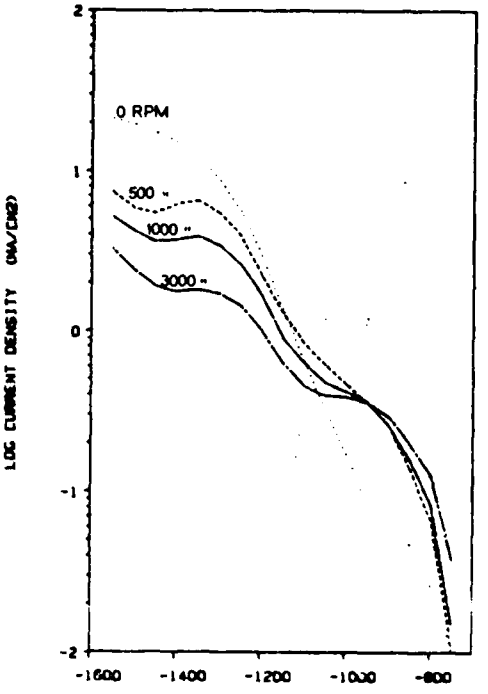

Fig.4. Combined effect of additions of $NaHCO_3$ and rotation speed in CO_2-exposed solution of 0.5 M Na_2SO_4 + 0.3 M $NaHCO_3$.

05550

ELEMENTARY STEPS OF THE ELECTROCHEMICAL REACTIONS OF ETHANOL ON PLATINUM A "DEMS" STUDY

J. WILLSAU AND J. HEITBAUM
Institute of Physical Chemistry, Wegelerstrasse 12, D-5300 Bonn 1, FRG

1. INTRODUCTION

The electrochemical oxidation of ethanol on Pt in sulfuric acid has been subject to numerous investigations /1,2,3,4/. The different proposed reaction mechanisms and reaction products made it necessary to reexamine this system by means of Differential Electrochemical Mass Spectroscopy (DEMS) in combination with deuterium and ^{18}O labelling. The experimental set up of DEMS, an on line technique which allows the qualitative and quantitative detection of electrogenerated products with a time constant of less than 0.5 s, is described in detail elsewhere /5,6/.

Ethanol can serve as a model system for the electrooxidation of an organic species containing two C-atoms, thereby extending the overall understanding of the electrochemical behavior of small organic molecules /7,8,9/.

2. OXIDATION IN THE PRESENCE OF BULK ETHANOL

Fig.1 shows the anodic scan of the mass spectroscopic cyclic voltammogram (MSCV) /9/ for m/e=43,44 and 45. The potential depenc' of m/e=45, the (M-1) signal of ethanol, is due to the shielding of ethanol when it is oxidized at the electrode. Mass 44 suggests CO_2 to be the major oxidation product, but parallel to m/e=44 mass 43 is recorded which clearly indicates an (additional(?)) H-containing species to be formed, eventually having a m/e= 44 peak too, which might hold for acetaldehyde.

Carbondioxid and acetaldehyde can easily be distinguished by using deuterium labelled ethanol: Fig.2 shows the formation of CD_3CDO (m/e=48) besides CO_2 evolution (m/e=44).

3. EVIDENCE FOR A PARALLEL PATH MECHANISM

The two observed reaction products seem to indicate a parallel reaction mechanism. Adsorption of ethanol-D_6, removal of all excess fuel by electrolyte exchange under strict potential control /7/, and subsequent electrode-

sorption leads exclusively to the formation of CO_2 (m/e=44) (Fig.3).

4. NATURE OF THE ADSORBED INTERMEDIATE

Adsorption of ^{18}O-ethanol in $H_2SO_4/H_2{}^{18}O$, replacement of the ^{18}-containing electrolyte by $H_2SO_4/H_2{}^{16}O$, and electrodesorption results in a MSCV whose anodic scan is shown in fig.4. Two different kinds of CO_2 ($C^{16}O^{16}O$, $C^{18}O^{16}O$) are detected which both appear exactly at the same potential.

5. CONCLUSIONS

On the basis of the results described above we can clearly state that the electrooxidation of ethanol exhibits a parallel reaction mechanism. Both, the direct oxidation of bulk ethanol and the formation and electrodesorption of a strongly bound intermediate are observed.

The product of the direct oxidation is acetaldehyde, whereas oxidation via the adsorbate delivers two ("different") CO_2 molecules, one originating from the α-C-atom, still containing the alcoholic O and receiving one O-atom from the elctrolyte, the other from the methyl group, obtaining both O-atoms from the electrolyte. The fact that both CO_2 appear at the same potential suggests that ethanol adsobs on Pt having the C-C-bond still intact. Splitting occurs during the electrodesorption process.

6. ADDITIONAL RESULTS

Similar experiments on the electrochemistry of propanol and isopropanol will also be presented.

7. ACKNOLEDGEMENTS

Financial support of this work by DFG is gratefully acknoleaged.

8. REFERENCES

/1/ E.Sokolova; Electrochim. Acta, 20, 323 (1975)

/2/ W.Vielstich; Fuel Cells, Wiley-Interscience, New York, 100 (1970)

/3/ V.D.Parker et al. in Encyclopedia of Electrochemistry of the Elements, A.J.Bard ed., Marcel Dekker, New York, 208 (1973)

/4/ O.A.Petrii in Progress in Electrochemistry of Organic Compounds, A.N. Frumkin, A.B.Evshler eds., Vol.1, Plenum Press, London, 319 (1971)

/5/ O.Wolter, J.Heitbaum; Ber. Bunsenges. Phys. Chem., 88, ? (1984)

/6/ J.Willsau, J.Heitbaum; Angew. Chem., in prep.

AD-A162 434 EXTENDED ABSTRACTS INTERNATIONAL SOCIETY OF ELECTROCHEMISTRY (36TH) HELD AT SALAMANCA SPAIN ON 23-28 SEPTEMBER 1985(U) INTERNATIONAL SOCIETY OF ELECTROCHEMISTRY 28 SEP 85 6/12

UNCLASSIFIED F/G 7/4 NL

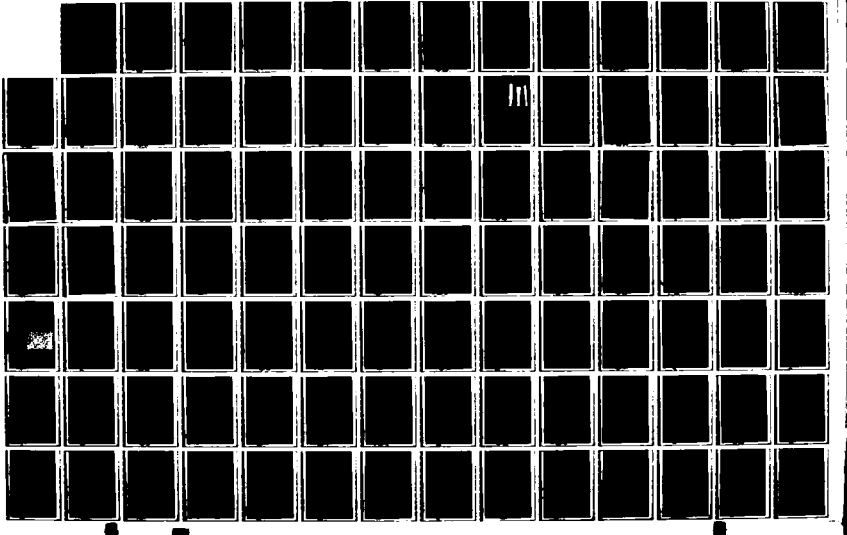

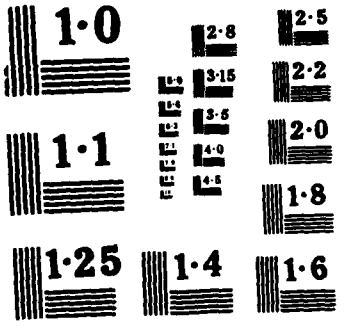

/7/ J.Willsau, O.Wolter, J.Heitbaum; J. Electroanal. Chem., 185, 163 (1985)
/8/ J.Willsau, J.Heitbaum; J. Electroanal. Chem.; 185, 181 (1985)
/9/ O.Wolter, J.Willsau, J.Heitbaum; J. Electrochem. Soc., 132, 1635 (1985)

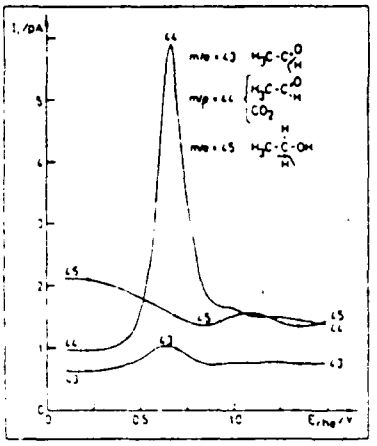

Fig.1.: Anodic scan of the MSCV in 10^{-2}M EtOH/0.5M H_2SO_4/H_2O on Pt

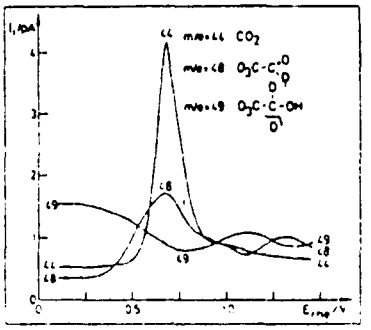

Fig.2.: Anodic scan of the MSCV in 10^{-2}M ethanol-D_6/0.5M H_2SO_4/H_2O

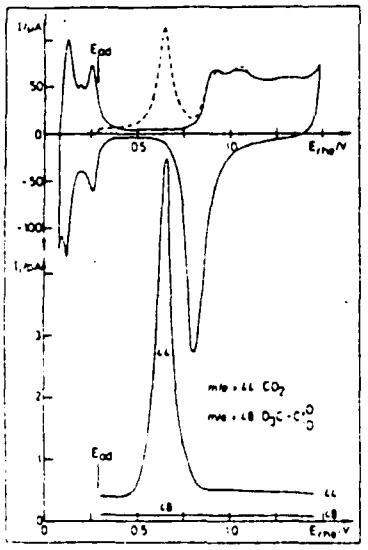

Fig.3.: Electrodesorption of pre-adsorbed ethanol-D_6 in 0.5M H_2SO_4/H_2O on Pt (above: I/E, below: I_i/E)

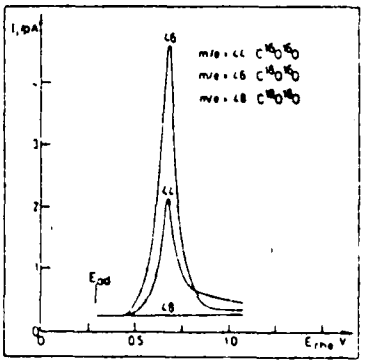

Fig.4.: Electrodesorption of pre-adsobed $Et^{18}OH$ in 0.5M $H_2SO_4/H_2{}^{16}O$ on Pt (only I_i/E is shown)

05560

ELECTROCHEMICAL REDUCTION OF OXYGEN KINETICS, MECHANISMS AND CATALYSIS

C.J. VAN VELZEN, G.J. BRUG, M. SLUYTERS-REHBACH, J.H. SLUYTERS
Van 't Hoff laboratory, State University of Utrecht, The Netherlands

The electrochemistry of oxygen has received and still receives considerable attention, due to both its scientific importance and its rôle in energy problems, corrosion, biological processes, etc. Nevertheless there is still much ambiguity and uncertainty about rather elementary questions such as kinetics, reaction mechanisms and the nature of catalytic effects of several kinds. A study of the electrochemical oxygen reduction under academic conditions is justified therefore, as this can deliver fundamental information that can help to understand observations concerning more complex systems.

Mercury and gold electrodes are suitable model electrodes for studying the electroreduction of oxygen, as they can be prepared in a reproducible way, reasonably free of surface contamination, and without oxide films. At mercury the reductions of O_2 to H_2O_2 and of H_2O_2 to H_2O proceed in well-separated potential regions, i.e. they give rise to two distinct waves in the dc polarogram. At gold the two waves are separated, though less than at mercury, at low pH, but these waves merge at pH $\approx$ 6, while at pH $\geq$ 12 only one four-electron wave is observed in the dc voltammogram (see Fig. 1). At mercury a similar situation can be created by adding a catalyst acting upon the rate of the H_2O_2 reduction, thus shifting its wave to more positive potentials. Since long it is known that some simple metal ions in neutral or alkaline medium are such catalysts[1], the most effective one being Pb(II) [2] (see Fig. 2). In addition it is known that some lead-hydroxo complexes are specifically adsorbed at the mercury solution interface[3].

In the present study dc voltammetry, admittance and demodulation voltammetry, and chronocoulometry have been employed to extend our knowledge and understanding of the oxygen reduction at mercury and gold. The results obtained are briefly summarized in the following.

(i) Reduction of oxygen to hydrogen peroxide. This electrode reaction obeys the linear rate equation describing the faradaic current j_F by

$$-j_F = 2Fk_f[c_{O_2} - c_{H_2O_2}c_{OH^-}^2 K_4 \exp(\varphi)] \qquad (1)$$

with

$$\varphi = (2F/RT)(E-E^\circ) \qquad (2)$$

where E° is the formal standard potential of the redox couple $O_2/(HO_2^-)(OH^-)$ (E° = -0.216 V vs SCE) and K_4 is the equilibrium constant of the association equilibrium $HO_2^- + H_2O \rightleftarrows H_2O_2 + OH^-$. The potential dependent rate constant k_f obeys the relationship

$$\frac{1}{k_f} = \frac{\exp(\frac{1}{2}\alpha_1\varphi)}{k_{s1}} + \frac{\exp(\varphi)}{k_c} \qquad (3)$$

At the mercury electrode in solutions of pH 0.4 to 12.5 the parameters in eq. (3) are equal to $\alpha_1 = 0.39 \pm 0.03$; $k_{s1} = 0.10 \pm 0.005$ cm s^{-1}; $k_c = 4 + 1 + (0.75 \pm 0.05)10^6\, a_{H^+}$. This behaviour is in very good agreement with the following reduction mechanism[4]:

R1 $O_2 + e \rightleftarrows O_2^-$ rate-determining

R2 $O_2^- + H_2O \rightleftarrows HO_2^\cdot + OH^-$ } rate-determining

R2' $O_2^- + H^+ \rightleftarrows HO_2^\cdot$ }

R3 $HO_2^\cdot + e \rightleftarrows HO_2^-$ fast

Two alternatives for the fast reaction R3, viz. $2HO_2^\cdot \rightleftarrows O_2 + H_2O_2$ and $HO_2^\cdot + O_2^- \rightleftarrows O_2 + HO_2^-$, cannot be ruled out on the basis of dc and admittance measurements alone. However, the demodulation voltammogram sharply rejects these dismutation reactions.

The hydrogen isotope and temperature effect on the mechanism above have been studied also[5]. In D_2O it is found that k_c is lower than in H_2O by a factor 2; the other parameters remain the same.

(ii) Reduction of hydrogen peroxide to water. The higher reactivity of the gold electrode, as compared to mercury, suggests that the rate-determining step is catalyzed by reactive sites that are more likely at a solid electrode surface. At both electrodes the rate constant k_f obeys the relationship

$$k_f = k_s \exp[-\alpha\varphi] \qquad (4)$$

with $\alpha = 0.11$. This low, but potential independent value should indicate a single asymmetric energy barrier. At mercury it is found that k_s is a function of pH in the region $10.5 < pH < 13.5$. This can clearly be related to the dissociation equilibrium H_2O_2/HO_2^- and the conclusion is that both the acid and the anion are reducible, but the latter with a smaller rate constant. [$k_s(H_2O_2) \approx 100\ k_s(HO_2^-)$]. This effect was not observed before.

(iii) Catalysis by Pb(II). The mathematical description of the dc voltammogram and the admittance voltammograms in the case of overlapping dc waves, applies quite well to the data obtained at the gold electrode and those at mercury in the presence of Pb(II). It is shown that $Pb(OH)_2$ is the active species, and the rate constant of the catalyzed H_2O_2 reduction could be determined as a function of the Pb(II) concentration. Surprisingly, however, the mechanism cannot be correlated to the degree of adsorption of Pb(II). The most probable mechanism involves a chemical oxidation of $Pb(OH)_2$ by H_2O_2 to a polynuclear species that is rapidly reduced electrochemically.

1. F. Strnad, Coll. Czech. Chem. Comm. 11 (1939) 391.
2. A. Arevalo, A. Bazo, Polarography 1964, G.J. Hills, ed. MacMillan, London, p. 457-471.
3. M.M.J. Pieterse, M. Sluyters-Rehbach, J.H. Sluyters, J. Electroanal. Chem. 109 (1980) 41.
4. C.J. van Velzen, M. Sluyters-Rehbach, A.G. Remijnse, G.J. Brug, J.H. Sluyters, J. Electroanal. Chem. 134 (1982) 87; 142 (1982) 229.
5. C.J. van Velzen, M. Sluyters-Rehbach, J.H. Sluyters, J. Electroanal. Chem., in press.

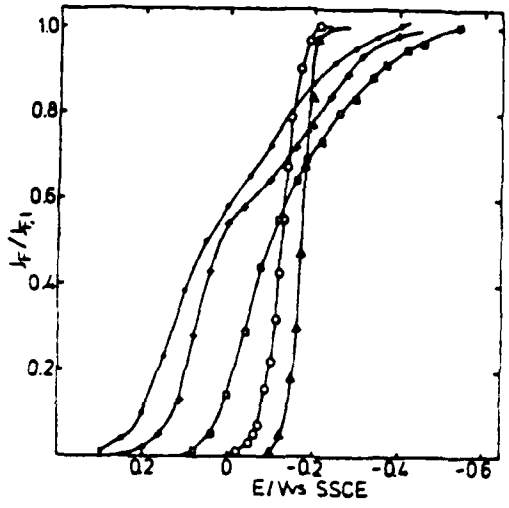

Fig. 1. Dc current vs potential for the oxygen reduction at polycrystalline goldin 1 M $NaClO_4$.
pH values: (●) 0.1, (+) 2.0, (□) 6.5, (o) 12.6, (Δ) 14.

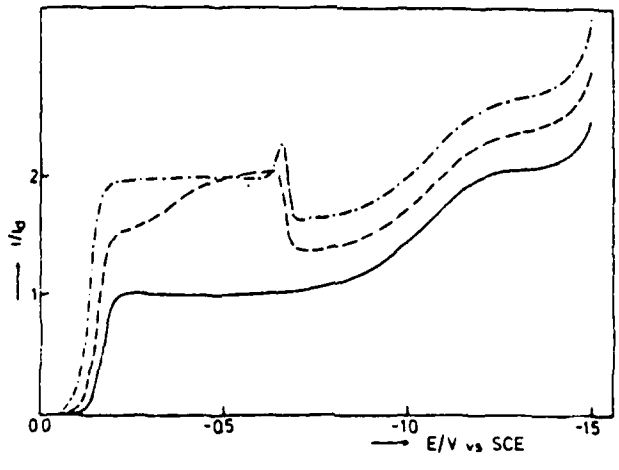

Fig. 2. Dc current vs potential for the oxygen reduction at the dropping mercury electrode in 1 M KNO_3 + 0.042 M KOH, with (——) 0, (---) 0.5 and (-·-·-) 1.1 mM Pb(II) added.

05570

SOME FEATURES IN THE ELECTROCATALYTIC REDUCTION OF NO_2^- AND NO_3^- IONS AT PLATINIZED PLATINUM ELECTRODES

G. HORÁNYI

Central Research Institute for Chemistry of the Hungarian Academy of Sciences, H-1525, Budapest (Hungary)

Electroreduction of nitric and nitrous acids has been the subject of several studies[1]. Relatively less information is available concerning the electrochemistry of NO_2^- and NO_3^- ions in neutral and alkaline media. It is assumed that the electrochemical reduction of NO_2^- and NO_3^- ions in alkaline solution differs from that in acid media due to the lack of various chemical equilibria between the higher oxidation states and the numerous possible intermediates. According to ref. 1 reduction in alkaline medium has to be considered as direct anion reduction. However, a number of experimental evidences may be found which suggest that there are some common features characterizing the polarization behaviour of NO_3^- and NO_2^- ions in both, alkaline and acid, media.

In order to gain more information about the role of the medium in the electrocatalytic behaviour of these ions a comparative steady state polarization study may be proposed in alkaline and acid media. Simultaneously an attempt should be made for the study of the adsorption phenomena occurring in the course of the reduction processes. To this end an indirect radiotracer method described elsewhere[2] may be used.

Experimental. The polarization measurements were carried out using the cell and apparatus described in previous electrocatalytic studies[3]. The indirect radiotracer adsorption study was carried out using P-32 labelled H_3PO_4. All potentials quoted in this paper are given on the RHE scale.

Results. The electrocatalytic reduction of NO_3^- ions was studied at a platinized platinum electrode in acidic media in the presence of different supporting electrolytes. It has been found that at low HNO_3 concentrations ($c \sim 10^{-2}$ mol dm^{-3}) the polarization behaviour, the shape of the polarization curves and the reduction rate depend significantly upon the nature of the supporting

electrolyte. (Fig. 1) These phenomena may be explained by the competitive adsorption of the reacting species and the anions of the supporting electrolyte. For instance, Fig. 2 shows the potential dependence of the adsorption of H_3PO_4 at different NO_3^- concentrations. However, independently from the nature of the supporting electrolyte, a common feature was observed. In all cases studied, a sharp decrease of the reduction rate was observed at potentials where the adsorption of hydrogen attains a significant value. Similar phenomena occur in alkaline medium in the case of NO_3^- and NO_2^- ions as shown by Figs 3 and 4.

Discussion. The behaviour observed, maxima on the polarization curves, can presumably be ascribed to the adsorption competition between reacting species and the species present in the system (ions of the supporting electrolyte) or formed under the experimental conditions studied (for instance adsorption of hydrogen). The decrease of the reduction rate at low potentials may be explained by the hydrogen adsorption which may result in a decrease of the adsorption of reacting species. Acceptance of this view involves the assumption that the reduction process, takes place, at least partly, via adsorbed species.

In the case of the electrocatalytic reduction of nitric acid in acid medium an attempt was made[4] to interpret the pecularities of the polarization curves in terms of competitive adsorption. In principle the same approach may be followed in the case of alkaline medium. There is, however, a fundamental problem. In the case of acidic medium there was a possibility of showing that a measurable adsorption of anions occurs on the electrode surface and the potential dependence of the adsorption observed experimentally by radiotracer method may be used for the explanation of the polarization phenomena. All our efforts to observe the specific adsorption of anions (Cl^-, PO_4^{3-} and SO_4^{2-} ions) in strong alkaline medium failed. This means that the extent of the adsorption of the anions, if occurs, is less than the experimental error of the method. It may be suggested that the low reactivity observed in alkaline medium may be connected with the low adsorption values with respect to NO_3^- ions.

References

1. A.J.Bard (Ed) Encyclopedia of Electrochemistry of the Elements, Vol. 8. Marcel Dekker, New York, 1978.
2. G.Horányi, V.E.Kazarinov, V.N.Andreev: J. Electroanal. Chem. 133 (1982) 333.
3. G.Horányi, E.M.Rizmayer, G.Inzelt: J. Electroanal. Chem. 92 (1978) 183.
4. G.Horányi, E.M.Rizmayer: J. Electroanal. Chem. 140 (1982) 347.

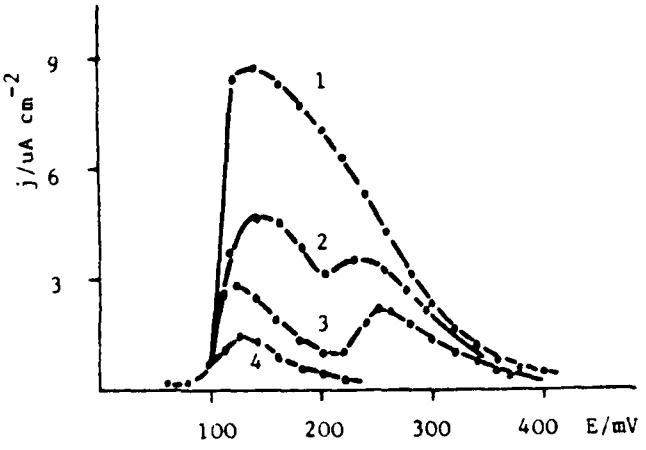

Fig. 1

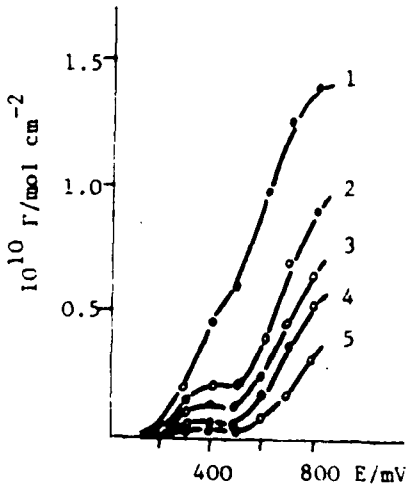

Fig. 2

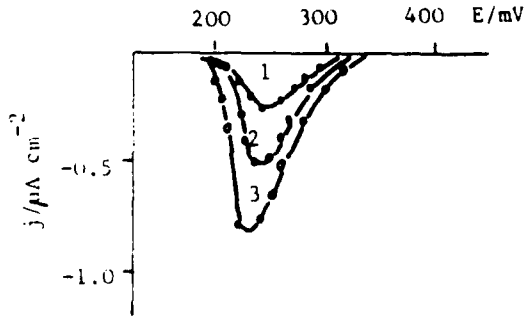

Fig. 3

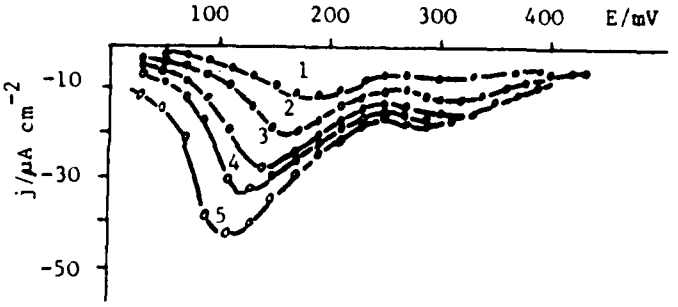

Fig. 4

1. Polarization curve of nitric acid (c=1.5x10^{-2} mol dm^{-3}) in: (1) 1 mol dm^{-3} $HClO_4$; (2) 1 mol dm^{-3} $HClO_4$ + 1x10^{-1} mol dm^{-3} H_3PO_4; (3) 1 mol dm^{-3} H_2SO_4; (4) 1 mol dm^{-3} $HClO_4$ + 1x10^{-3} mol dm^{-3} HCl.
2. Potential dependence of the adsorption of H_3PO_4 at different NO_3^- concentrations. $c_{H_3PO_4}$ = 8x10^{-4} mol dm^{-3}; $c_{NO_3^-}$ = (1) 0; (2) 4x10^{-4}: (3) 8x10^{-4}: (4)1.6x10^{-3}; (5) 3.2x10^{-3} mol dm^{-3}.
3. Polarization curves at differenc NO_3^- ion concentrations in 1 mol dm^{-3} NaOH supporting electrolyte. $c_{NO_3^-}$ = (1) 3.5x10^{-3}; (2) 7x10^{-3}; (3) 1.4x10^{-2} mol dm^{-3}.
4. Polarization curves obtained at different NO_2^- concentrations in 1 mol dm^{-3} NaOH supporting electrolyte. $c_{NO_2^-}$ = (1) 1x10^{-2}; (2) 3x10^{-2}; (3) 6x10^{-2}; (4) 1.2x10^{-1}; (5) 2.4x10^{-1} mol dm^{-3}.

05580

A STUDY ON ELECTRODE KINETICS OF THE DEPOSITED ELECTROLYTIC MANGANESE DIOXIDE(EMD) PROCESS

Qi-Xin Zhang, Ze-Shan Zhu, Jin-Ming Lian

Dept. of Chem. Fujian Normal University
Fuzhou, Fujian, China

Abstract

In the $MnSO_4$—H_2SO_4 solution there is probably existence of $(Mn_2(SO_4)_3)^{2-}$ complex ion. It is determined out both by ultraviolet spectrometric method and by using RDE method. Identification the potassium salt to be $K_2Mn_2(SO_4)_3$ by X-ray diffraction supports the possibility.

A set of regular equations, expressed by matrix form $GG^T\bar{C}=G\bar{D}m$ which could satisfy the "most probable value" of various ion species in solutions has been deduced by using least square principle. As G, the absorbance of standard solutions and $\bar{D}m$, that of electrolytic solutions are known values, $\bar{C}$ can be calculated by a computer. As a result, the concentrations of Mn^{3+} and MnO_4^- amount to 1.0×10^{-4}M respectively.

The electrode kinetics of EMD: first, $(Mn_2(SO_4)_3)^{2-}=2Mn^{3+}+3SO_4^{2-}$ and then two series of reactions simultaneous: (1) $Mn^{2+}\rightarrow Mn^{3+}$, $2Mn^{3+}+2H_2O=MnO_2+4H^+$, and (2) $4Mn^{2+}+MnO_4^-+8H^+ = 5Mn^{3+}+4H_2O$, $2Mn^{3+}+2H_2O = MnO_2 + Mn^{2+}+4H^+$.

05590

A STUDY ON ELECTRODE KINETICS OF THE DEPOSIDED EMD PROCESS

Qi-xin Zhang, Ze-shan Zhu, Jin-ming Lian

Dept. of Chem. Fujian Normal University
Fuzhou, Fujian, China

1. Introduction

Although the production of EMD from $MnSO_4$-H_2SO_4 solution has been carried out for twenty years, the electrode kinetics of the deposided EMD have not been studied carefully. Vetter K.J(1)(1961), M.Fleischman et al(2)(1962), Masatosh Sugimori and Taro Sekine(3,4)(1969), G.Ya.Slaidin and A.A.Spritsis(5)(1978) have proposed many approaches to the study of electrodeposited EMD, nevertheless they have not paid enough attention to industrial condition but to research of EMD deposited at pt-electrode within short time, at lower temperature(25°-50°C), in solution of lower concentration $MnSO_4$(0.01-0.1M) and higher concentrated H_2SO_4(1-15N). Perhaps the kinetics of electrodeposition at this condition should be somewhat different from that in industrial condition (i.e. 95°C, 0.6-1.2M $MnSO_4$, 0.2-1.0M H_2SO_4). The researches of Gentaro Kano(6)(1969) and A. Bartwright(7) have more or less taken into consideration the industril conditions. Gentaro Kano approacned the subject from thermodynamic standard electrode potentials point of view, and the latter emphasized the Mn^{2+} ions penetrating into intermediate product MnOOH layer. In general, they all overleaped the existence and the function of Mn^{2+} complex anion in solution during electrolysis. In this paper, some results of the investigation of Mn^{2+} complex anion existence and the concentration distribution of species such as MnO_4^- and $MnCl_4^{2-}$ are reported. And then the possible a part of electrode reaction mechanisms have been suggested.

2. Experimental

2.1 Instruments

(1) UV-300 Scanning Spectrophotometers, made in Japan.

(2) R_4X-10 X-ray diffractometer, made in Japan.

(3) Rotating Disc Electrods Set, made in China.

2.2 Chemical Reagents

All chemical reagents used were AR grade.

2.3 Procedures for estimation of the existence and composition of Mn^{2+} complex anion in H_2SO_4-$MnSO_4$ solution

(1) Job's optical absorbance vs mol-ration (at constant mol concentration) plot method.

First, from the scanning of absorption vs UV wave length curve, the maximum absorbance with its corresponding wave length (i.e. peak wave length) of $MnSO_4$, H_2SO_4 and $MnSO_4$-H_2SO_4 solutions was measured.

Second, a series of various mol ratio $MnSO_4$-H_2SO_4 solutions at a defined total mol concentration were prepared and their absorbances curves were measured at peak wave length. The so called Job's plots mol ratio of $MnSO_4$: H_2SO_4 (at a constant total mol concentration, e.g. $[MnSO_4]+[H_2SO_4]=0.06M$, or 1.2M and 1.4M) vs absorbances were plotted. Fig1 is a typical example. The mol ratio corresponding to curve maximum absorbance may usually be considered the composition of complex ion.

(2) By using rotating disc electrode method to determine the magnitude of limiting—current in $MnSO_4$-H_2SO_4 solution from i-ϕ curves, the rotating electrodes used were pt(0.12 cm^2) and pb-sb alloy(0.12 cm^2).

(3) X-ray analysis of potassium salt. the $MnSO_4$:H_2SO_4 solution(2:1mol) was neutralized by KOH, its salt has been analyzed by X-ray.

2.4 Procedures for determination of the concentration of various species such as Mn^{3+}, MnO_4^- and other ions in $MnSO_4$-H_2SO_4 solution during electrolysis

Standard (reference) solutions of $KMnO_4$(8.00×10^{-5}M), Mn^{3+}(7.4×10^{-4}M) and $MnSO_4$-H_2SO_4 mix solutions were prepared. The UV absorption curves in the range 200-300 um were determined.

EMD was electrodeposited from No1 cell (4 liter, containing 1.13M $MnSO_4$+0.16M H_2SO_4) and No2 cell (4 liter, containing 0.8M $MnSO_4$+0.5MH_2SO_4) at 95°C, anodic current density 1A/dm^2, pb-sb alloy rod as anode. After electrolysis for several hours, an aliquot solution was taken out every fifteen minutes lasting 4-6 hrs. It was let to cool rapidly and was scanned from 200-300um to get absorption curves immediately.

Owing to partly overleap of absorption curves of Mn^{2+}, Mn^{3+} and MnO_4^- solution, it is difficult to solve equations using the usual method to get concentrations of various species. However, a series of wave lengths (e.g. 20-40) with its corresponding absorbances can be taken through optimal calculation. The fundamental priciples are briefly as follows. If a system has n components species, there is a relation between wave length n, absorbance and molal extinction coefficient, $L=\sum_{(i=1)}^{n}\xi C_i$. L is a constant, let it equals to unity. If n wave lengths j (j=1,2,$\cdots$,n) are taken, concentration of n components can be obtained through a set of n linear equations,

$$\sum_{i=1}^{n}(\sum_{ij})C_i=D_j \qquad (j=1,2,\cdots,n)$$

By solving these equations,n components values $C_i(i=1,2,\cdots,n)$ can be obtained.However,for the sake of accuracy,k ($k>n$) wave lengths should be taken to determine absorbance,so k absorbance values can be obtained.By using the least square principle,the " most probable values" of various species can be calculated.The "most probable values" satisfy the so called set of positive definite equations,in matrix form:

$$GG^T\bar{C}=G\cdot\bar{D}_m$$

where G is the absorbance matrix of standard (reference) solutions,and $\bar{D}_m$ is the absorbance vector of $MnSO_4$-H_2SO_4 solutions.When measuring value G and $\bar{D}_m$ are known,the matrix coefficient GG^T and free term vetor $G\bar{D}m$ can be calculated by computer.In the set of equations $GG^T\bar{C}=G\bar{D}_m$,the matrix coefficient generally is positive definite symmtric matrix.Thus by using main element elimination method,the concentrations C_i of various component can be solved with the aid of computer.

3. Results and Discussion

3.1 The absorbance of $MnSO_4$-H_2SO_4 solutions exhibit marked decrease in comparison with $MnSO_4$ solution at peak wave length 208um.It shows possible existence of Mn^{2+} complex ion.

In Fig1,there are two maxima on the curve where $MnSO_4$:H_2SO_4 mol ratio are 2:1 and 1:1 respectively.The only (2:1) ratio will be considered because it is the condition of industrial importance.As shown in Fig2, the limiting-current is increased with the increasing of mol ratio of $MnSO_4$:H_2SO_4,and it should be constant when mol ratio of $MnSO_4$:H_2SO_4 is larger than 2:1.The potassium salt(prepared from $2MnSO_4$:$1H_2SO_4$ solution) identificated by X-ray belongs to $K_2[Mn_2(SO_4)_3]$.From these experimental facts,the possible existence of $[Mn_2(SO_4)_3]^{2-}$ complex anion in $MnSO_4$-H_2SO_4 solution can be suggested.

3.2 As shown in Table1,the concentration of Mn^{3+} and MnO_4^- are estimated to be 1×10^{-4}M in $MnSO_4$-H_2SO_4 system during electrolysis.The result is contrary to the literature which indicated no MnO_4^- formation at $0.5MH_2SO_4$ and $[Mn^{2+}]>0.1M$.

3.3 In the electrolytic $MnSO_4$-H_2SO_4 solution as the H_2SO_4 increases, the $[MnO_4^-]$ decreases and $[Mn^{3+}]$ increases.

3.4 From Fig.2,the limiting-current I_l reaches maximum when mol ratio of $MnSO_4$:H_2SO_4 is equal to or larger than 2:1.And further experiments

show that I_1 does not depend on rotation velocity of electrode. These facts indicate that the existence of complex ion is possible and I_1 is related to $[Mn_2(SO_4)_3]^{2-}$ concentration and not to Mn^{2+}body concentration. Therefore, a part of the electrode kinetics may be considered as follows:

First, the dissociation reaction proceeds

$$[Mn_2(SO_4)_3]^{2-} \rightleftharpoons 2Mn^{2+} + 3SO_4^{2-} \text{ ; and then}$$

the following two series electrode reaction simultaneously occur:

a) $Mn^{2+} - e \longrightarrow Mn^{3+}$, $2Mn^{3+} + H_2O \rightleftharpoons MnO_2 + Mn^{2+} + H^+$

b) $4Mn^{2+} + 8MnO_4^- + 8H^+ \rightleftharpoons 5Mn^{3+} + 4H_2O$,

$2Mn^{3+} + H_2O \rightleftharpoons MnO_2 + Mn^{2+} + H^+$

3.5 The fact that the current efficiency of EMD by electrolyzing nearly neutral $MnSO_4$ solution is not lower than in acidic solution (approximate equal concentration of $MnSO_4$) can be explained by the presence of more MnO_4^- during electrolysis.

4. Conclusions

4.1 In $MnSO_4$-H_2SO_4 solutions, there is possibly the presence of $[Mn_2(SO_4)_3]^{2-}$ complex anion.

4.2 During electrolyzing of industrial conditions, the concentrations of MnO_4^- and Mn^{3+} have estimated to be 1×10^{-4}M order of magnitude.

4.3 Two series of electrode reactions as shown above must be considered.

References

(1) Vetter K.J., Trans of Symposium on Electrode Process p47 (1961).
(2) M. Fleischman et al., Trans of Faraday Soc. 58, 1865(1962).
(3) Masatoshi Sugimori and Taro Sekine, Electrochemistry Japan, Vol 37, 63-69(1969).
(4) Masatoshi Sugimori and Taro Sekine, ibid 380-384(1969).
(5) G. Ya. Slaidin and A.A. Spritsis, Elektrokhimya, 14, 926(1978).
(6) Gentaro Kano, Electrochemistry Japan Vol 37, 356-361(1969).
(7) A.Cartwright and R.L. Pauli, 2nd Int. Symposium on MnO_2, 129(1980), Tokyo.

Table 1. The concentrations of various species in $MnSO_4$-H_2SO_4 solution during electrolysis at 95°C, anodic current density 1A/dm², pb-sb alloy rod as anode.

concentration (M) / electrolying time	ion species	$Mn^{2+}(free)$ + $(Mn_2(SO_4)_3)^{2-}$	MnO_4^-	Mn^{3+}
No.1 cell (4 liter, 1.13M $MnSO_4$+0.16M H_2SO_4)	4hr	0.713	1.47×10^{-4}	0.64×10^{-4}
	6hr	0.712	1.76×10^{-4}	0.71×10^{-4}
No.2 cell (4 liter, 0.8M $MnSO_4$+0.50M H_2SO_4)	4hr	0.667	0.64×10^{-4}	1.41×10^{-4}
	6hr	0.660	0.64×10^{-4}	1.38×10^{-4}

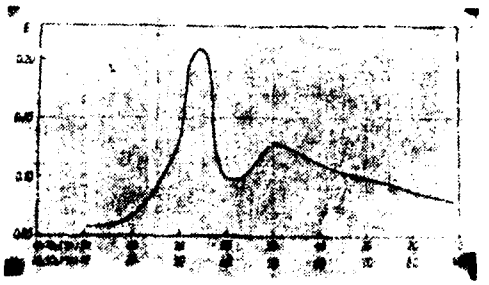

Fig.1 Job's absorbance vs mol ratio of $MnSO_4$:H_2SO_4 plot, $[MnSO_4]+[H_2SO_4]$=0.06M, at 208um.

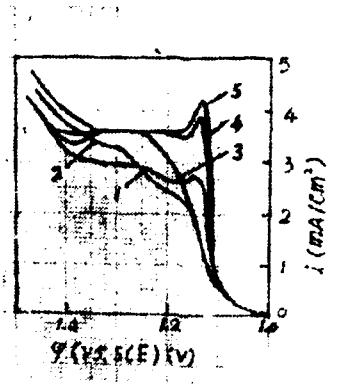

Fig.2 The i-φ curves of rotating [illegible] pt-electrode (anodic polarization) in $MnSO_4$-H_2SO_4 solution ($0.5MH_2SO_4$) at 12°C and 3000 rpm, mol ratio of $MnSO_4$:H_2SO_4 : curve 1-1:1; 2-3:2; 3-2:1; 4-3:1; 5-4:1.

KINETICS OF Zn(II) REDUCTION AT THE Hg ELECTRODE FROM WATER + DIMETHYLFORMAMIDE MIXTURES

J. TARASZEWSKA and A. WAŁĘGA
Institute of Physical Chemistry, Polish Academy of Sciences, Warsaw (Poland)

In the course of our studies concerning the electroreduction of cations from non-aqueous and mixed solvents [1-4] we were interested in reduction of Zn(II) from H_2O + dimethylformamide (DMF) + 0.9 M $NaClO_4$ in the entire composition range of the mixture as well as to check which factors are mainly responsible for the course of the rate constant vs. solvent composition.

The kinetic parameters were determined polarographically, by impedance bridge and by cyclic voltammetry. The dependence of the standard rate constant of Zn(II) electroreduction on the DMF content is shown in Fig.1 together with the literature data [5] for Mn(II). The rate constant of Zn(II) electroreduction passes through a maximum at small % vol.DMF and through a minimum at high concentration of this solvent in the mixture.

The kinetic parameters of the electrode reactions in H_2O+ organic solvent mixtures depend on the adsorption of the organic solvent which modifies the structure of the double layer at the electrode surface as well as on the properties of the bulk of solution. Therefore, the study of adsorption of the organic component of the mixture at the electrode as well as the information about the solvation of the reactant in the bulk of solution and in the surface phase are important.

The differential capacitance-potential curves and the potentials of zero charge (pzc) were measured. The potentials of Zn(II) electroreduction from H_2O + DMF mixtures are very near to the potentials of maximum adsorption of DMF from those mixtures. Using the capacitance data the degree of electrode surface coverage θ by DMF was calculated.

The values of pzc were used to determine the charge-potential curves what allowed to calculate the ψ_2 potentials at the formal potentials of Zn(II) electroreduction. Taking into account Frumkin's correction there was no change in the shape of the plot of the rate constant vs. solvent composition.

The equilibrium potentials of the Zn(II)/Zn(Hg) system were measured vs. aq NCE and then they were related to the solvent - independent redox reference systems: BCr, Fc and Cic. This allowed to estimate the free energies of transfer, ΔG_{tr}, of Zn(II) ions from aq. 0.9 M $NaClO_4$ to H_2O + DMF + 0.9 M $NaClO_4$ mixtures. The results are shown in Fig.2.

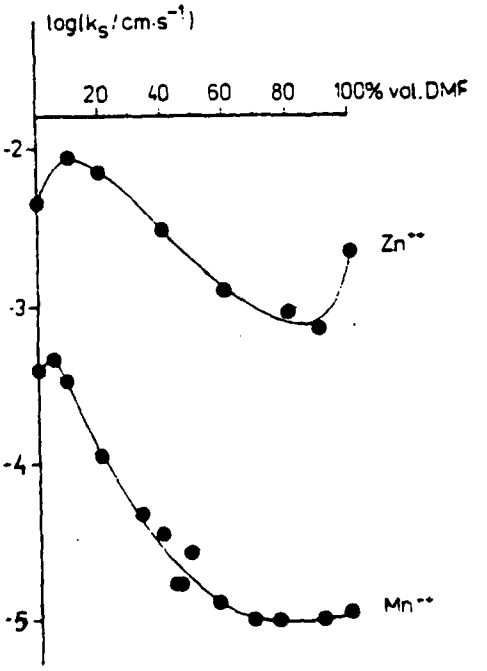

Fig.1. Standard rate constants of the Zn(II)/ Zn(Hg) and Mn(II)/ Mn(Hg) systems vs. DMF content in the mixture.

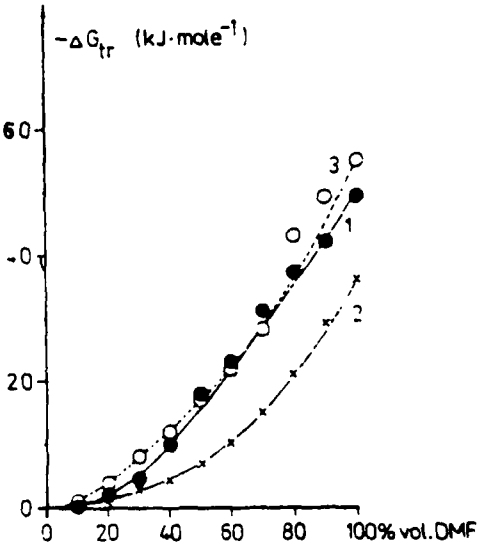

Fig.2. Changes in the transfer energies of Zn(II) ions from aqueous solutions of 0.9M $NaClO_4$ to H_2O + DMF + 0.9M $NaClO_4$ mixtures referred : to the Cic redox system (curve 1), to the BCr redox system (curve 2) and to the Fc redox system (curve 3).

In the entire composition range of the H_2O + DMF mixture ΔG_{tr} of Zn(II) are negative, however up to 30% vol.DMF the values are small and do not allow the unambigous conclusions concerning the preferential solvation of Zn(II) to be made. At higher DMF contents the preferential solvation of Zn(II) in H_2O + DMF mixtures and especially in pure DMF, compared to pure H_2O is found. However, the observed effects are smaller than in dimethylsulfoxide (DMSO) and H_2O + DMSO mixtures studied by us previously [3]. We consider the values of ΔG_{tr} expressed in the Fc and Cic potential scales too high and in the interpretation of the influence of the selective solvation of Zn(II) ions on the kinetics of the electrode process we used the values of ΔG_{tr} of Zn(II) expressed vs. BCr system.

From among numerous factors which are responsible for the changes in kinetics of cations electroreduction from mixed solvent the most important, independently on the basisity of the organic solvent, we consider: 1) the correction for the concentration of the reactant in the surface phase, introduced by Behr et al. [1] and 2) the activation energy of the electrode process. Both these factors were taken into account in the interpretation of the results of Zn(II) electroreduction from H_2O + DMF mixtures.

REFERENCES

1. B. Behr, J. Taraszewska and J. Stroka, J. Electroanal. Chem., 58 (1975) 71.
2. J. Taraszewska and A. Broda, J. Electroanal. Chem., 153 (1983) 243.
3. J. Taraszewska and A. Wałęga, J. Electroanal. Chem., 171 (1984) 243.
4. J. Taraszewska and A. Wałęga, J. Electroanal. Chem., in press.
5. J. Broda and Z. Galus, J. Electroanal. Chem., 130 (1981) 229.

05610

CHEMICAL AND ELECTROCHEMICAL REACTIONS OF HYPOPHOSPHITE ON Ni AND Pd ELECTRODES.

G. BECH-NIELSEN, C. QVIST JESSEN AND J.C. REEVE

Chemistry Department A, Building 207

The Technical University of Denmark

DK-2800 Lyngby, Denmark

In one of the technically important chemical nickel plating processes nickel ions are reduced specifically on a Ni or Pd surface by hypophosphite, which is oxidized to phosphite. However, some hypophosphite reacts differently yielding phosphorus, so that a Ni-P "alloy" containing some 7-12 % of P (w/w) results.

Electrochemical examinations at 90°C, pH ca. 7, using rotating disc electrodes of Ni and Pd in solutions containing chloride, citrate and varying amounts of hypophosphite showed some change of the cathodic portion of the polarization diagram (hydrogen evolution), and an anodic Tafel region, which near to plating conditions changes into a limiting cd (independent of speed of rotation of the electrode, but concentration dependent).

Among many features two will be emphasized: i) The high anodic Tafel mV-law combines with a low, fractional reaction order wrt hypophosphite to suggest a Freundlich adsorption

isotherm. ii) A reduction of hypophosphite to phosphorus in the potential region of plating is thermodynamically unfavoured. However, disproportionation of hypophosphite into phosphite and phosphorus may take place, conditioned by adsorption on the electrode, but independent of potential. If so, the occurrence of an anodic peak (at low potentials) can be ascribed to oxidation of a surplus of phosphorus deposited during a preceding cathodic process.

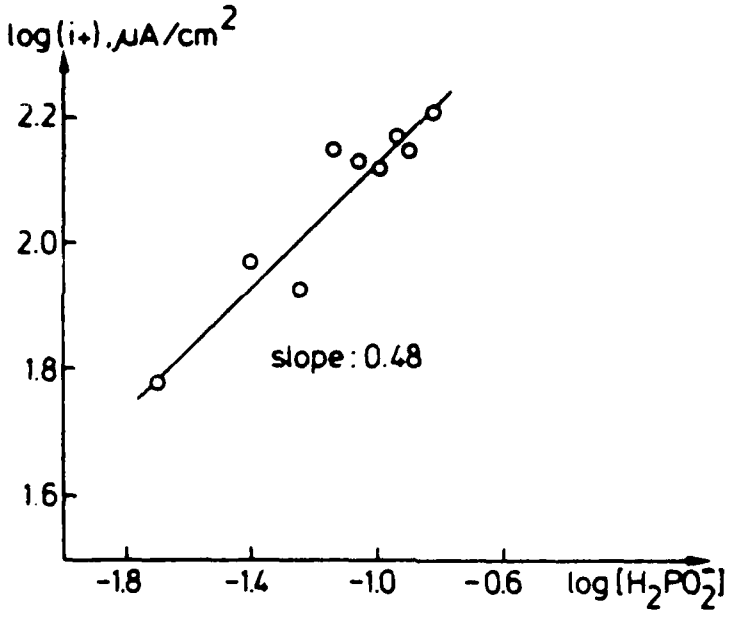

Fig. 1. Reaction order plot of the anodic oxidation of hypophosphite on a smooth Pd-electrode.
Solution: 0.5 M Na-citrate, 0.5 M NaCl, pH = 6.8. 90°C.
Values of cd obtained by extrapolation of Tafel lines (slopes: 224 to 299 mV) to -100 mV nhe.

05620

ON THE ELECTRODEPOSITION OF CARBON FROM $NaF-AlF_3$ MELTS SATURATED WITH ALUMINIUM CARBIDE.

R. ØDEGARD, A. STERTEN AND J. THONSTAD

Laboratories of Industrial Electrochemistry, and SINTEF,
The Foundation of Scientific and Industrial Research
at the Norwegian Institute of Technology,
N-7034 Trondheim-NTH, Norway.

Two subjects related to solutions of aluminium carbide in $NaF-AlF_3$ melts were studied:

1) The equilibrium concentration of dissolved aluminium carbide in $NaF-AlF_3$ melts.

2) The electrodeposition of carbon from aluminium carbide saturated melts.

Solubility. In the solubility experiments a graphite crucible with a close fitting graphite lid, containing 140g of molten salt and 25g of aluminium, was placed in the isothermal zone of a vertical Kanthal furnace with argon atmosphere. During a holding time of 5-6 hrs at temperature, aluminium carbide was formed by reaction between aluminium and the graphite crucible, saturating the melt. After removal of the lid a melt sample (3g) was taken with a steel ladle that was lowered from the cold part of the furnace. The aluminium carbide content of the sample was determined from the volume of $CH_4(g)$ evolved by treatment with a 10% HCl solution. The hydrolysis apparatus was similar to that described by Rogers et al.[1].

Fig. 1. shows the concentration of dissolved aluminium carbide as a function of the NaF/AlF_3 molar ratio (CR) at 1020°C. The full line represents the best fit for a model based on the equation

$$Al_4C_3(s) + 5AlF_3(diss) + 9NaF(l) = 3Al_3CF_8^{3-} + 9Na^+ \quad (1)$$

Activity data for AlF_3 and NaF given by Sterten and Mæland[2] were used in the calculations.

Dewing[3] has previously measured the solubility of aluminium carbide in $NaF-AlF_3$ melts for $1.6<CR<4.5$, as shown in Fig.1. The present data, although higher in carbide concentration, are in fair agreement with those of Dewing. Because Dewing's measurements were not extended to low CR's, the concentration peak shown in Fig.1 was not detected. The broken line in the figure is our representation of Dewing's data.

Electrodeposition of carbon. It was found that carbon could be electrodeposited by electrochemical oxidation of dissolved aluminium carbide. Voluminous deposits were obtained on electrodes made of graphite, vitreous carbon, iron, tungsten and platinum. The carbon deposit was found to be amorphous by x-ray diffraction analysis. Based on the weight loss when burning the carbon deposite the number of electrons exchanged pr mole of deposit was calculated to be ≈4 when assuming 100% current efficiency for the deposition reactions.

Fig. 2 depicts carbon deposits on iron, vitreous carbon and tungsten electrodes. Similar anodic deposits were obtained by Morris and Harry[4] in $LiCl-CaCl_2$ melts containing dissolved CaC_2.

In Fig.3 is shown an example of potential decay curves recorded in carbon deposition experiments. A constant current of 5A (≈0.5 A/cm^2) was disconneted at time zero. The potential difference between an aluminium electrode and a vitreous carbon electrode with carbon deposits on it was recorded. The potential plateau which is clearly visible in the figure, corresponds to an aluminium carbide formation cell. The semi-stable potential was +127 mV versus the aluminium electrode. This gives $\Delta G^o(Al_4C_3)$ = - 35.108 kcal/mol at the temperature of the experiment (1013°C). The interpolated JANAF[5] data is $\Delta G^o(Al_4C_3)$ = - 34.166 kcal/mol at that temperature. The difference is within the limits of error indicated in JANAF.

References:

1: Rogers, P.S., Bevan, D.J.M. and Tomlinson, J.W., Microchim. Acta 12, 1839 (1956).

2: Sterten, A. and Mæland, I., Acta Chem. Scand., A39 (1985). In print.

3: Dewing, E.W., Trans. Met.Soc. AIME 245, 2181 (1969).

4: Morris, D.R. and Harry, J.R., Proceeding of the Int. Conf. Ind. Carbon and Graphite (Society of Chemical Industry) London, 1965, p.36.

5: JANAF Thermochemical Tables, 2.ed., Dow Chemical Co., Midland, Michigan, 1971.

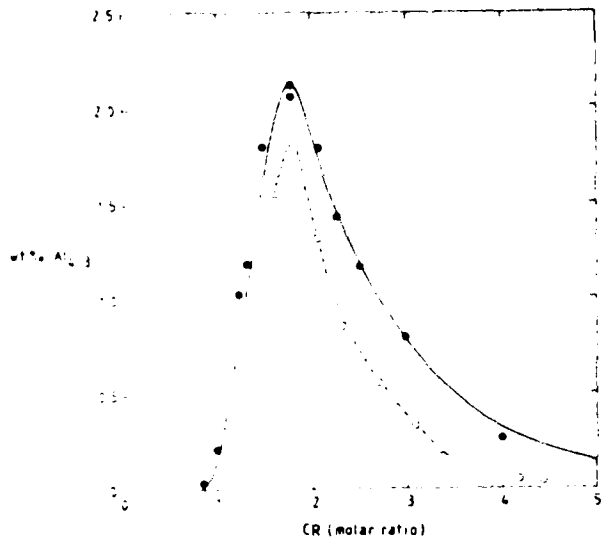

Fig.1.
Concentration of dissolved aluminium carbide as a function of the NaF/AlF_3 molar ratio (CR) at 1020°C.
● - present work;
o - Dewing[3]. The full line represents the model given by equation (1).

Fig.2.
Electrodeposited carbon on electrodes of:
1: iron, 2: vitreous carbon and 3: tungsten.
Melt composition:
CR = 1.50,
temperature: 1000°C,
total current: 1-5 A.

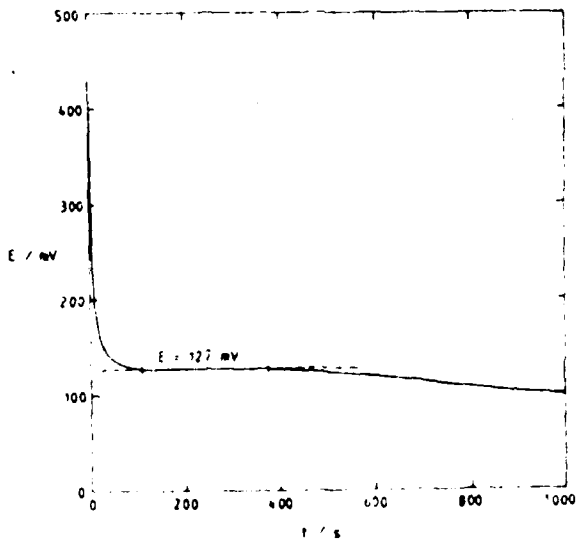

Fig.3.
Potential decay curve in a carbon deposition experiment. The potential of a vitreous carbon electrode with carbon deposit was measured versus an aluminium electrode. At t<0, I = 5A (0.5 A/cm²).
Temperature: 1013°C, CR = 1.50.

05640

ANODIC REDUCTION OF THE PERCHLORATE ANION. INFLUENCE OF pH AND ANION CONCENTRATION.

Ma J. González Tejera
Institute of Physical Chemistry, C.S.I.C., Serrano, 119
28006 Madrid, (Spain)

The slow cyclic voltammetry of electrodeposited ruthenium electrodes (Ru/Pt) in ClO_4^- solutions exhibits a current reversal during the positive sweep of the hydrogen region (1). This has been shown to be due to the electrocatalytic reduction of perchlorate anion to chloride ion. This phenomenon was also observed on black Pt, Os (1), Rh (2) and bright Ir (3) electrodes and depends markedly on the solution temperature and concentration.

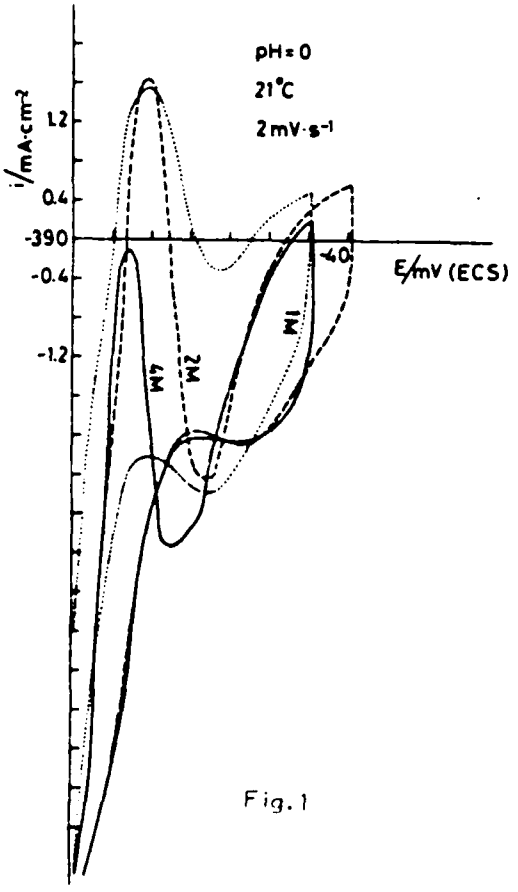

Fig. 1

The results suggest that ClO_4^- reduction on Ru electrodes proceeds very slowly by interaction of the anion and hydrogen adsorbed on the electrode. Thus, this work attempts to study the influence of the solution pH and ClO_4^- concentration on this reduction.

Cyclic voltammetry of Ru/Pt electrodes in perchlorate solutions at constant pH shows an increase of current reversal and a shift of the maximum current potential to more negative values with anion concentration (Fig. 1). Both effects are enhanced by the solution temperature. The potential region in which the ClO_4^- reduction occurs is also widened by increasing the perchlorate concentration.

The raising of the solution pH, at constant anion concentration, produces a decrease of the current reversal until its total suppresion at pH = 1

(Fig. 2), although this limit depends on ClO_4^- concentration and temperature. It seems that the anion reduction to Cl^- is favoured at a certain pH which value raties with ClO_4^- concentration.

The voltammetric ClO_4^- reduction appears as a very complex reaction but some considerations about its kinetics can be made from the results obtained.

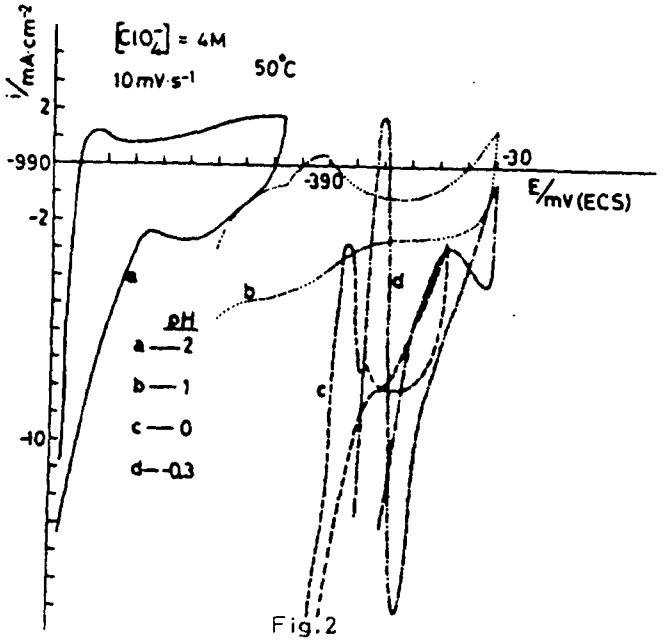

Fig. 2

REFERENCES

(1) F. Colom and Ma J. González Tejera, J. Electroanal. Chem. (to be published).
(2) S. Ya. Vasina and O.A. Petrii, Elektrokhimiya, 6, 242 (1970).
(3) M. Sánchez-Cruz, M.J. González Tejera and Ma C. Villamañan Giner, Electrochim. Acta (to be published).

06010

6 THERMODYNAMIC AND STOICHIOMETRIC ASPECTS OF THE POURBAIX DIAGRAMS DERIVATION

ILIE F.FISHTIK
Institute for Chemistry of the Academy of Sciences of the M.S.S.R.,277028,Kishinev,ul.Grosula,3, (U.S.S.R)

Potential-pH diagrams are of great importance in many fields of science.Pourbaix was the first who derived a lot of such diagrams and emphasizes their utility in the field of corrosion.In order to make the further discussion more concretely,let us consider the pH dependence of the redox potential of the system where both the oxidizing - Ox, and reducing - Red forms,undergoes hydrolysis as pH is changed to give hydroxo complexes $Ox_i(OH)_j$ and $Red_i(OH)_j$ .The formation of hydroxides (oxides) precipitates $Ox(OH)_{q(s)}$ and $Red(OH)_{m(s)}$ is also included here.Hence,the equilibrium in such a system may be described by the following set of equations:

$$Ox + ze = Red \qquad (1)$$

$$i\,Ox + jH_2O = Ox_i(OH)_j + jH \qquad \beta_{ij} \qquad (2)$$

$$p\,Red + qH_2O = Red_p(OH)_q + qH \qquad \beta_{pq} \qquad (3)$$

Here β_{ij} and β_{pq} are the equilibrium constants of the corresponding hydrolysis reactions.

The potential dependence on pH in such a system within the traditional way of Pourbaix diagrams derivation is represented by a linear-step system of functions.The latters correspond to the set of equations of the form:

$$Ox_i(OH)_j + (q-j)H_2O + ze = Red_p(OH)_q + (q-j)H \qquad (4)$$

$$E_{ijpq} = E^{\circ}_{Ox/Red} + \frac{RT}{zF}\ln\frac{\beta_{pq}}{\beta_{ij}} + \frac{RT}{zF}\ln[H]^{j-q} + \frac{RT}{zF}\ln\frac{C_{Ox}}{C_{Red}} \qquad (5)$$

where C_{Ox} and C_{Red} are the total concentrations of the oxidizing and reducing forms correspondingly.However,this calculation method of the potential-pH diagrams is not entirely regorous at least for two reasons.First,the electrochemical set of equations (4) is usualy linear-dependent.For example,in the case of chrom-water system Pourbaix wrote 57 equations,while only 11 are linear-dependent.Second,the potential-pH dependen-

ce as was stated above, is represented by a set of linear functions while this dependence must be represented by a continuous function.

In the present work these inadequaces are eliminated in the following way. A set of linear-independent equations which entirely describe the equilibrium in the system is selected using the linear algebra methods. In our case, the analysis shows, that the most convenient are the equations (1)-(3). To derive a continuously potential-pH function the generalized interaction equation of all the species presented in the system is introduced. The latter has the form:

$$\sum_i \sum_j f_{ij}\, Ox_i (OH)_j + \left(\sum_p \sum_q q f_{pq} - \sum_i \sum_j j f_{ij}\right) H_2O + ze = \tag{6}$$

$$= \sum_p \sum_q f_{pq}\, Red_p (OH)_q + \left(\sum_p \sum_q q f_{pq} - \sum_i \sum_j j f_{ij}\right) H$$

Here f_{ij} and f_{pq} represents the partial molar fractions of the corresponding species:

$$f_{ij} = \frac{\beta_{ij} [Ox]^{i-1} [H]^{-j}}{1 + \sum_i \sum_j i \beta_{ij} [Ox]^{i-1} [H]^{-j}} \tag{7}$$

$$f_{pq} = \frac{\beta_{pq} [Red]^{p-1} [H]^{-q}}{1 + \sum_p \sum_q p \beta_{pq} [Red]^{p-1} [H]^{-q}} \tag{8}$$

The sums in brackets in equation (6) as one can be easily convinced, represents the Bjerrum functions:

$$\bar{n} = \sum_i \sum_j j f_{ij}\,, \quad \bar{m} = \sum_p \sum_q q f_{pq} \tag{9}$$

Equation (6) was derived under the assumption that the species reacts or are formed as a result of the reaction in proportion to their partial molar fractions f_{ij} and f_{pq}. Such an assumption is necessary to take into account the mass balance in equation (6).

The regorous thermodynamic analysis of the equation (6) leads us to the following expression for the redox potential:

$$E = E^\circ_{Ox/Red} - \frac{RT}{zF} \ln \frac{\prod_i \prod_j \beta_{ij}^{f_{ij}}}{\prod_i \prod_j f_{ij}^{f_{ij}}} + \frac{RT}{zF} \ln \frac{\prod_p \prod_q \beta_{pq}^{f_{pq}}}{\prod_p \prod_q f_{pq}^{f_{pq}}} + \tag{10}$$

$$+ \frac{RT}{zF} \ln [H]^{\bar{m}-\bar{n}} + \frac{RT}{zF} \ln \frac{C_{Ox} \sum_i \sum_j f_{ij}}{C_{Red} \sum_p \sum_q f_{pq}}$$

The generalized character of equations (6) and (10) as compared with equations (4)-(5) consists in the fact, that the latters are a special case of the first. Indeed, one can easily be convinced, that when and and therefor n and m are integers, the equation (6) takes the form of equation (4). In the same conditions the equation (9) takes the form (5).

Hence, the following sequence of the Pourbaix diagram derivation is proposed. First, the thermodynamic characteristics of the set of equations (1)-(3) are determined:

$$\mu^{\circ}_{Red} - \mu^{\circ}_{Ox} = -zFE^{\circ}_{Ox/Red}$$

$$\mu^{\circ}_{Ox_i(OH)_j} + j\mu^{\circ}_{H} - j\mu^{\circ}_{H_2O} - i\mu^{\circ}_{Ox} = -RT\ln\beta_{ij}$$

$$\mu^{\circ}_{Red_p(OH)_q} + q\mu^{\circ}_{H} - q\mu^{\circ}_{H_2O} - p\mu^{\circ}_{Red} = -RT\ln\beta_{pq}$$

Further, the partial molar fractions f_{ij} and f_{pq} as well as the Bjerrum functions n and m are calculated. As the polynuclear hydroxo complexes are present in the system, it is necessary to solve tne mass balance equations:

$$C_{Ox} = \sum_i \sum_j i\,[Ox_i(OH)_j] = [Ox]\,\alpha_{Ox} \qquad (11)$$

$$C_{Red} = \sum_p \sum_q p\,[Red_p(OH)_q] = [Red]\,\alpha_{Red} \qquad (12)$$

where

$$\alpha_{Ox} = 1 + \sum_i \sum_j i\beta_{ij}\,[Ox]^{i-1}\,[H]^{-j}$$

$$\alpha_{Red} = 1 + \sum_p \sum_q p\beta_{pq}\,[Red]^{p-1}\,[H]^{-q}$$

The equations (11)-(12) are solved relative to [Ox] and [Red] at various pH. The substitution of the Ox and Red in equations (7) and (8) permits the calculation of f_{ij}, f_{pq}, $\bar{n}$ and $\bar{m}$. Simultaneously one can determine the stability field of the hydroxo species (the vertical lines on the diagram). The potential-pH dependence is represented by a single continuous function (10).

The present calculation method can be easily generalized for systems where many other complexation reactions occur. Some examples of concrete calculations are given.

06020

NUCLEATION AND GROWTH MECHANISM APPLIED TO THE LOCALIZED CORROSION OF METALS

R.C. Salvarezza, V.D. Vasquez Moll and A.J. Arvia
Instituto de Investigaciones Fisicoquímicas Teóricas y Aplicadas - (INIFTA)
Casilla de Correo 16, Sucursal 4, (1900) La Plata, ARGENTINA

INTRODUCTION

Localized corrosion involves the passive film breakdown locally as a result of the attack of the corrosive environment. This process requires the presence of aggressive anions acting on the passive layer. It starts when the applied potential (E_s) exceeds a critical value (E_b). The overall localized corrosion process involves film breakdown and pit propagation. Film breakdown is strongly dependent on both, thickness, composition and degree of perfection of the passive film and pH, type and concentration of the aggressive anion. Film breakdown implies an induction time (t_i) and terminates with the appearance of a sudden rise in the current density associated with pit growth. Frequently, two different types of pits are observed. Small crystallographic pits (etch pits) detected in early stages of pitting and hemispherical pits which appear later. In this case, dissolution at the pit bottom resemble anodic brightening where a non protective salt film is present. However, there is some evidence that the degeneration of the metal surface occurs prior to the appearance of the pits and it is related to the contamination of the passive film by a salt layer of the aggressive anion.

In this study an attempt is made to describe the kinetics of tne overall process under potentiostatic conditions on the basis of the nucleation and growth theories considering a serie of stages where at least two different phases are involved.

1. Film breakdown

Under a constant potential step at $E_s < E_b$, the instantaneous average anodic current density (j_t) can be associated with two main contributions namely the passive layer growth (j_p) and the corrosion current density through the passive layer (j_c). Thus,

$$j_t = j_p + j_c \qquad (1)$$

It is assumed that both processes are controlled by diffusion of cations and oxygen containing species through the passive layer. In this case the instantaneous value of j_p can be related to an instantaneous nucleation and circular bidimensional growth under diffusion control. The corresponding expression is:

$$j_p = P_1 \exp(-P_2 t) \qquad (2)$$

where $P_1 = q_{mon} K_e D N_0$ and $P_2 = K_e D N_0$, D is the diffusion coefficient of the reacting species, q_{mon} is the charge density required for the constant full coverage of the metal surface by the

passive layer, K_e is a proportionality constant and N_o is the number of sites available for nucleation.

On the other hand, the rate of metal corrosion through either the prepassive or passive layer appears as the dissolution of tridimensional nuclei under diffusion control following the rate equation:

$$j_c = \frac{P_3}{\sqrt{t}} |1.0 - \exp(-P_4 t)| \qquad (3)$$

where $P_3 = zFD^{1/2}\Delta c/\pi^{1/2}$ and $P_4 = \pi N_o' K_e D'$, Δc is the concentration difference of the diffusing species, N_o' is the number of sites available for the dissolution process, D' is the diffusion coefficient of the species involved in the process and K_e is a proportionality constant.

The oxide growth can be assigned to the diffusion of oxygen containing species while the corrosion current can be related to the cation diffusion through the passive film. Using equation (2) and (3) the characteristic decreasing current transients recorded for $E_s < E_b$ or in the absence of aggressive anions can be reproduced and P_1, P_2, P_3 and P_4 estimated. P_1/P_2 gives the charge density required to complete the passive film (q_{mon}) and from it the film thickness (h) is calculated using

$$h = \frac{M}{zF\rho} q_{mon}$$

where M is the molecular weight and ρ is the density of the layer component. On the other hand, from P_3 and P_4, it is possible to obtain Δc and N_o, respectively. For different systems reasonable values for h, Δc and N_o are estimated. Now, suppose that at $E_s > E_b$ the nucleation and growth of a salt of an aggressive anion competes with the passive film formation (stage 1). According to nucleation and growth theories the nuclei stability depends on its radius. The nucleous starts to grow when the radius (r) exceeds a critical value (r*) and it disappears when r is smaller than r*. When r > r* nuclei grow into the passive film (stage 2) and j_c becomes more complex because the current flowing at the film/salt nuclei interphase. The latter can be assigned to an instantaneous nucleation and growth of conical nuclei into the film under charge transfer control. Thus, equation (3) becomes

$$j_c = \frac{P_3}{\sqrt{t}} |1.0 - \exp(-P_4 t)| + P_5 |1.0 - \exp(-P_6 t^2)| \qquad (4)$$

$P_5 = zFK_{3c}'$, $P_6 = \pi M_s^2 K_{3c}^2 N_{os}/\rho_s^2$. K_{3c} and K_{3c}' are the rate constants for the layer growth in the directions parallel and perpendicular to the metal plane, respectively, ρ_s is the salt density whose molecular weight is M_s, and N_{os} is the number of sites available for the dissolution process. The right hand side of equation (4) corresponds to the apparent corrosion current density which flows at the salt/passive film interphase. Considering that the latter is larger than the corrosion current density through the oxide layer, from (4) it results:

$$j_c \quad P_5 |1.0 - \exp(-P_6 t^2)| \qquad (5)$$

Finally, at certain points of attack the passive film can be totally removed and the metal surface exposed to the electrolyte.

Processes related to stage 1 and 2 involves a time which corresponds to t_i.

2. Pit Growth

In the uncovered regions salt nuclei growth into the metal. This process can be described as a new nucleation and growth process which concentrates at defective sites of the metal surface such as the termination points of dislocations or grain boundaries leading to "etch" pits (stage 3). The growth of salt nuclei into the metal can be assigned to an instantaneous nucleation and conical growth under charge transfer control. The apparent current density (j_s) related to this process becomes:

$$j_s = P_7\{1.0 - \exp|\ P_8(t-t_i)^2|\} \qquad (6)$$

where P_7 and P_8 have the same significance than P_5 and P_6 respectively. Using equations (2), (5) and (6) the initial part of the current transient at $E_s > E_b$ is reproduced and P_7 and P_8 are obtained. The slope $dE/d(\log P_7)$ and $dE/d(\log P_8)$ gives reasonable values for different systems. This dependence is comparable to that of the pit current density on potential already reported in the literature. Evaluation of the pitted area (A_p) leads to the penetration rate (P_7/A_p) which is comprised between 0.01 A/cm^2 to 10 A/cm^2 for different systems studied.

During metal dissolution, corrosion products accumulate inside the pits changing the kinetic of pit growth from a charge transfer to a diffusional control. This change is closely related to the transition from "etch" to "hemispherical" shaped pits. The metal dissolution at the pit bottom becomes similar to transpassive dissolution controlled by diffusion (stage 4). In this case equation (6) is not longer valid. The growth of salt nuclei at this stage can be represented by an instantaneous nucleation and tridimensional growth under diffusion control. Thus,

$$j_s' = \frac{P_9}{\sqrt{t}}\{1.0 - \exp|-P_{10}(t-t_t)|\} \qquad (7)$$

where $P_9 = zFD_+^{1/2}\,\Delta c_+/\pi^{1/2}$ and $P_{10} = -N_{os}'K_sD_+N_{os}'$, N_{os} denotes the number of sites available for the precipitation of a thick salt layer, K_s is a proportionality constant, D_+ and Δc_+ are the diffusion coefficient and the concentration difference of the reacting species and t_t is the transition time required for the precipitation of the corrosion products.

The present model is used to interpret pitting data from potentiostatic current transients complemented with optical and other electrochemical techniques of nickel, copper and mild steel in the presence of different aggressive anions and through the physical meaning of the different adjusting parameters a reasonable understanding of the pitting phenomena is accomplished.

ACKNOWLEDGEMENT

INIFTA is a Research Institute jointly established by the Universidad Nacional de La Plata, the Consejo Nacional de Investigaciones Científicas y Técnicas and the Comisión de Investigaciones Científicas de la Provincia de Buenos Aires.

06030

ELECTROCHEMICAL MEASUREMENTS FOR STRESS CORROSION CRACKING OF A COMMERCIAL 5LX LOW ALLOY PIPELINE STEEL IN CARBONATE-BICARBONATE SOLUTIONS.

By
Javier Avila Mendoza
Dpto. de Metalurgia
Facultad de Química
Universidad Nacional Autónoma de México.

The anodic behaviour of X60 steel in 1N Na_2CO_3-$NaHCO_3$ solutions has been investigated by current decay and potentiodynamic measurements.

It has been shown that current decay curves are only useful as comparative data [1,2]. To try to recognize the existence of an intermediate range of current decay between the faster and slower rates, for which the system may be susceptible to stress corrosion cracking (SCC) is a very subjetive task. The current decay for -650mV, a potential value which lies whithin the experimentally determined cracking potential range -640 $\pm$ 60mV, shows a linear semilogaritmic functional realtionship in the decay throughout the whole test period (80 minutes), Figure 1. This behaviour is fundamental in relation to the necessary balance between an active electrode and a passive one. It was also observed that the correlation between crack velocity and the initial disolution current measured from current decay curves, is very poor; this fact suggests therefore, a strong filming tendency of the bare metal produced at the crack tip when exposed to the solution.

Potentiodynamic polarization curves overcame the lack of definition present in the current decay measurements and provided us with an accurate prediction of the electrochemical requirements for cracking, as well as the involved kinetic parameters. An inspection of the anodic behaviour of X60 steel contained in these curves, and the use of the empirical condition of the largest difference in current density between fast and slow curves, showed that the potential value for cracking lies around -640mV; Figure 2. Indeed, it is an experimental fact that X60 steel is most susceptible to SCC within a narrow range around the experimental value.

The anodic polarization curve showed two well defined oxidation peaks. The predicted SCC range lies within the thermodynamically stable zone of $FeCO_3$. As a consequence of these results, the non-protecting character allegedly conferred by $FeCO_3$ to the system requires further revision[3].

The existence of the stable iron complex $Fe(CO_3)_2^{2-}$ in Fe-CO_2-H_2O systems, has been studied and supported on thermodynamic grounds, Figure 3. The mechanism describes adequately the behaviour for iron in the present system and its concentration for the conditions under study.

Work on the effect of cathodic pre-tratment on X60 steels has been done by using different cathodic potentials and assessing their effect on - current maxima and current decay at a fixed anodic value of potential - during identical periods of time (Figure 4). It was shown that the behaviour of potentiodinamic and current decay curves vary proportionally - as a function of the cathodic value of potential used to activate the - surface of the electrode. It was concluded that the reduction of solvated protons is the major cathodic reactions at those potentials.

But this primary product, which is the monoatomic hydrogen, may either combine to form H_2 and evolve or be absrobed in the metal. When the -- electrode potential becomes more noble than tha reversible potential - for hydrogen the resultant current density is made up of the sum of the metal dissolution and the hydrogen oxidation rates. The value of potential at which this effect begins to have a measurable effect is around -860mV, very near the equilibrium potential for hydrogen evolution -- (-840mV vs. SCE).

Even when the details of the above described observations are difficult to explain solely on the basis of variations of only one parameter, to a first approximation the decesive influence of such parameter on the - behaviour of the system is clear.

REFERENCES.

1.- R.N. Parkins
Corrosion Science 20, 147, (1980).

2.- R.N. Parkins, N.J.H. Holroyd, R.R. Fessler
Corrosion, 34, 253, (1978).

3.- J.G.N. Thomas, T.J. Nurse, R. Walker
Br. Corrosion J., 5, 87 (1970).

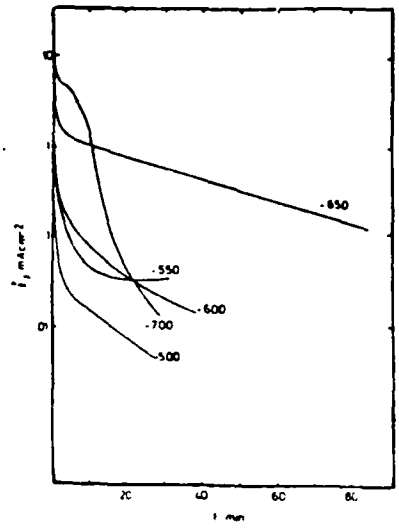

Figure 1

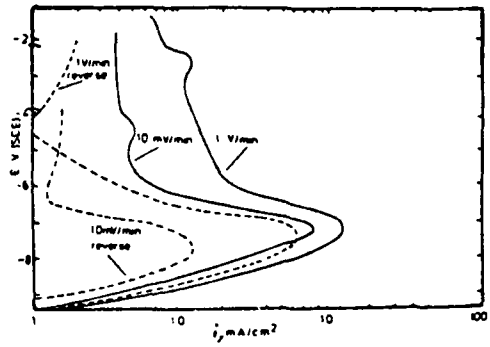

Figure 2

Figure 3

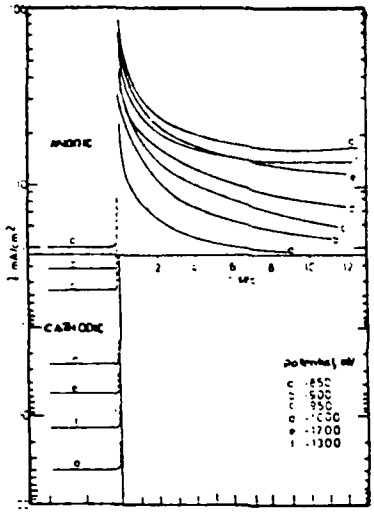

Figure 4

06040

THE ANALYSIS OF THE REACTION STEPS CONTROLLING THE OXYGEN COROSION OF IRON AND STEEL IN CHLORIDE SOLUTION

D.M. Dražić and V. Vaščić
Faculty of Technology and Metallurgy, University of Belgrade
Karnegijeva 4, P.O.Box 494, 11001 Belgrade, Yugoslavia

The oxygen corrosion of iron and steels in neutral chloride solutions is usually considered to be controlled by the diffusion of oxygen dissolved in the electrolyte. Hence, if that would be true, the better supply of oxygen would mean the higher corrosion rate of the metal (if the metal does not passivate, as expected for the chloride containing solutions). In this work we shall show that the above assumption is not always a correct one and that one can observe the inverse effect, which should be taken into consideration when one has the so called differential aeration, often encountered in the real corrosion situations.

Experimental. The cathodic and anodic steady state polarization measurements were carried out in a closed glass cell with a rotating disk electrode in 3% NaCl solution,the solution being purged all the time with air. Some of the experiments were carried out in a specially designed cell for the "in situ" electrochemical measurements in the salt chamber while the electrode was sprayed by the salt mist, as assumed by the salt chamber standard test. The cell corresponded to the cell used by Tomashov for the atmospheric corrosion measurements, except that it was placed so that a thin layer of solution formed by the mist all the time keeps the glass and metal surface under a thin layer of liquid. Potentiostatic steady state measurements with the IR drop corrections were carried out with the adequate instrumentation. In all the measurements steel Č4734(British equivalent En40B) was used as the electrode material. For the independent determination of the corrosion rates by the weight loss measurements the coupons of the same material were put in the same conditions as the measuring electrodes, and the results expressed as the corrosion current densities.

Results and discussion. In Fig. 1 cathodic and anodic polarization curves for the still electrode in the electrolytic cell and in the salt chamber are presented. As seen, the cathodic polarization curve for the sample in the cell showed a well defined oxygen diffusion current at ca. 0.7 $mAcm^{-2}$ and the anodic Tafel line with the slope of ca. 100 $mV.dec^{-1}$. The extrapolated anodic line to E_{cor} gave j_{cor} = 0.25 $mAcm^{-2}$, which was much smaller than the oxygen diffusion current. In many similar experiments the electrochemically determined j_{cor} by extrapolation of anodic Tafel line were smaller than the oxygen diffusion current. A separate weight loss measurements for the sam experiment gave exactly the same corrosion rate (0.25 $mAcm^{-2}$) indicating that the metal in the electrolytic cell corrodes under a mixed activation - diffusion control of oxygen reduction.

A more detail analysis of the partial currents for a still and rotating electrode (4500 rpm) is presented in Fig. 2. The full lines represent the experimentally determined cathodic and anodic polarization curves for two hydrodynamic conditions, while the dotted curves are the partial oxygen reduction currents calculated from the limiting diffusion curents and the experimentally obtained cathodic and anodic curves. The anodic Tafel line

did not depend on the change of the hydrodynamics, while the cathodic partial current density depended not only in the concentration polarization region, as expected, but also in the activation controlled part, showing an increase of the apparent exchange current density with the increased rate of oxygen supply. The experimentally observed shift of the corrosion potential of about 25 mV is in very good accord with the shift of the intersection points of the extrapolated anodic Tafel line and the calculated partial cathodic polarization curves (point a and b). The slope of ca. 120 mV dec^{-1} for the cathodic Tafel line indicates that first electron exchange is the probable rate determining step, but a good explanation for the increase of the exchange current density with the increase of the speed of rotation cannot be offered at this moment.

However, the fact that one can evaluate the cathodic Tafel lines for oxygen reduction on iron, and hence, measure the kinetic cathodic current offers a valuable possibility for the analysis of the mechanism of the oxygen reduction reaction on iron in a proper way as used in electrochemical kinetics. This possibility will be exploited in a separate communication.

Even more interesting were the polarization curves obtained in the "in situ" measurements in the salt chamber after 48 h. As shown in Fig. 1, again the anodic Tafel line with the approximatelly the same slope as in the electrolytic cell was obtained, but the process was somewhat inhibited. The extrapolation to E_{cor} gave j_{cor} = 67 μAcm^{-2}, what is somewhat larger than obtained from the weight loss (53 μAcm^{-2}). This shows clearly that the corrosion rate in a salt chamber is smaller than in an electrolytic cell.

The cathodic polarization curve in salt chamber experiment showed, contrary to that in the electrochemical cell, a straight Tafel like part at lower current densities with slope values ranging between 180 and 340 mVdec^{-1} in different experiments. Extrapolation of the linear portions intersected the anodic extrapolated lines exactly at the E_{cor}. This is a good confirmation that the corrosion of iron in a salt chamber is occuring so that both, anodic and cathodic reactions are under activation control, the anodic reaction proceeding somewhat slower than in the electrolytic cell. The inhibition of anodic and cathodic charge transfer processes in the salt chamber experiments are probably due to the formation of a layer of the reaction products accumulating at the surface during the 48 h of corrosion while the sample was inside the salt chamber (standard testing time).

We have shown recently (1) that, if the corrosion process is activation controlled by both reactions, the cathodic polarization curve in the range of small polarization must have an inflection point. The slope at the inflection point serves to calculate the corrosion current. Indeed, the corresponding plot showed the inflection point, and the calculated corrosion current was 53 μAcm^{-2}, even in better agreement with the weight loss result.

1) D.M. Dražić, V. Vaščić, J.Electroanal.Chem., 185 (1985) 229.

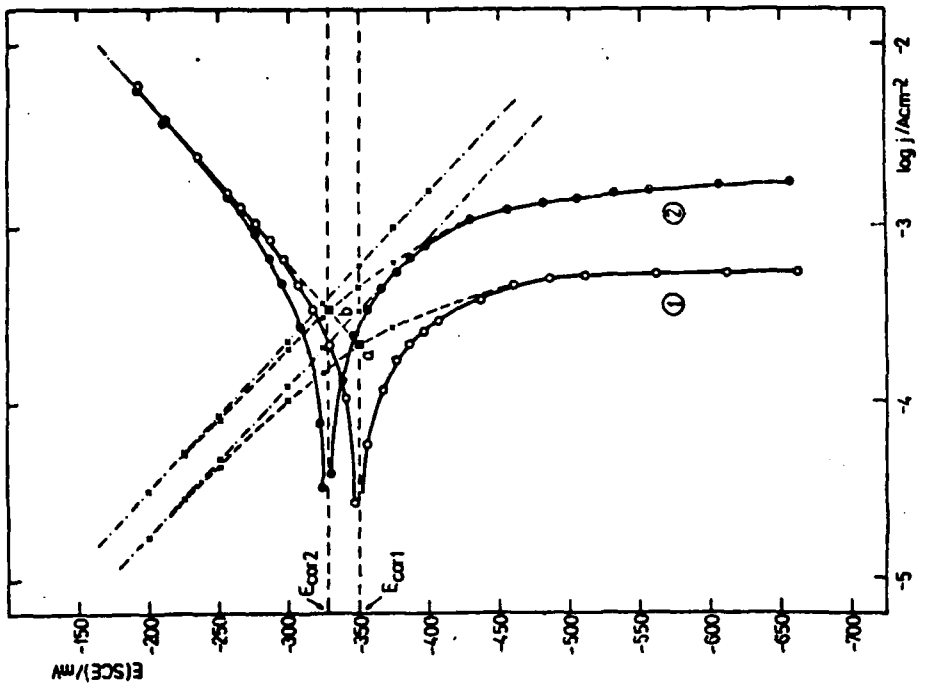
E(SCE)/mV
log j/Acm⁻²
E_cor2
E_cor1
a
b
①
②

Fig. 2.

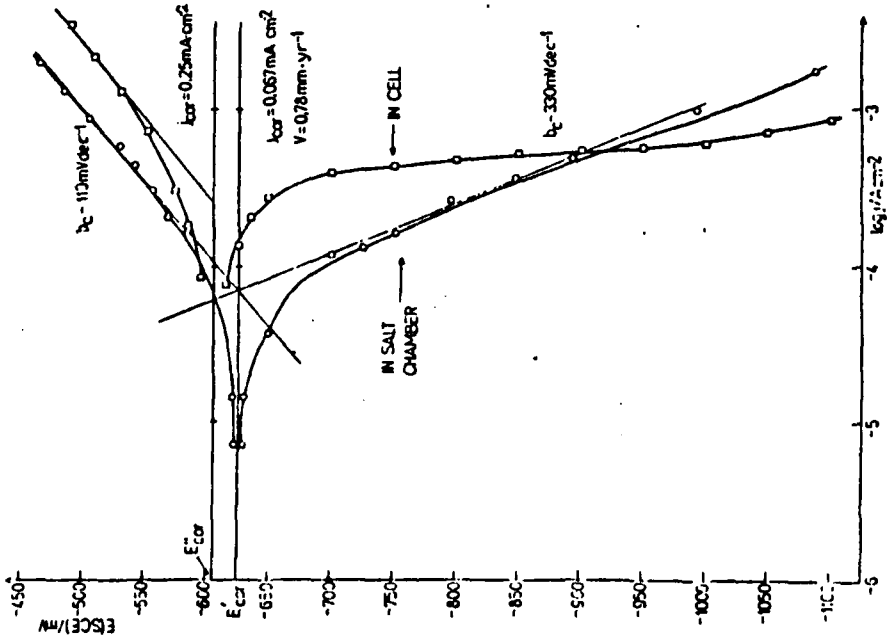
E(SCE)/mV
log j/Acm⁻²
b_c = 113mVdec⁻¹
i_cor = 0.25mA cm⁻²
i_cor = 0.067mA cm⁻²
V = 0.78mm·yr⁻¹
IN CELL
b_c = 330mVdec⁻¹
IN SALT CHAMBER
E'_cor
E_cor

Fig. 1.

06050

CORROSION STABILITY OF TITANIUM IN ACID MEDIA ELECTROCHEMICAL AND OPTICAL STUDIES

Lj.Arsov, T.Grčev and A.Prusi

Faculty of Technology and Metallurgy, Cyril and Methodius University
91000 Skopje, Yugoslavia

Introduction

It is well known fact that corrosion stability of many metals depend on the state of their surface, i.e. clean metal surface, presence of natural oxide or passive films, etc. Some metals such as titanium and aluminium, when exposed to atmospheric conditions form a natural oxide film that protects the base metal from corrosion. The thickness of this film can electrochemically be increased by means of anodic oxidation /1,2/. In case of titanium, using anodic oxidation can be form oxide films on its surface, and the thickness (a linear function of applied voltage) is around 2.5 nm/V /3/. Corrosion stability of these films differ from that of clean titanium surface. There is not sufficient data in the available literature on corrosion stability of titanium surface coated with anodic oxide films.

The objective of this paper is a study of the corrosion stability of a clean titanium surface, titanium surface coated with a natural oxide or passive film, and titanium surface coated with anodic film of various thickness.

Experimental

Corrosion stability of titanium surfaces in various concentrations of H_2SO_4 was studied by means of potentiostatic, potentiodynamic, metallographic and ellipsometric methodes. An optical electrolytic cell was adapted for simultaneous ellipsometric and electrochemical measurement of oxide layers during their formation on the titanium surface and their dissolutions at various cathodic potentials.

Electrochemical polishing proved to be most convenient methode for preparation of surfaces for electrochemical-optical measurements.

Anodic oxidation was carried in a 0.5 mol/dm^3 H_2SO_4 in a voltage range from 0 to 100 V /4/.

Results and disscusion

Natural oxide film formed on titanium surface builds up parabolically with passing of time and its thickness is around 3.5 nm /5/. Chemical dissolution of this film in a 0.5 mol/dm³ H_2SO_4 is a very slow process, while the electrochemical dissolution at a cathodic polarization of potential of -0.6 V (s.c.e.) is much faster and enables a complete dissolution of the natural oxide film, i.e. obtaining a clean metal surface.

The passive oxide film on titanium surface in a 0.5 mol/dm³ H_2SO_4 is formed at a potential range of -0.3 to +3 V(s.c.e.) This film consists oxide of Ti_2O_3 and TiO_2 /6/, dissolves much faster in more concentrated solutions of H_2SO_4. Its complete dissolution is possible only electrochemically at cathodic potentials of -0.692 and -0.764 V(s.c.e.) and then as a side product is TiH_2.

When compared to natural and passive oxide films, the anodic oxide film dissolves much more slowely both chemically and electrochemically. Fig.1. presents chemical dissolution of an anodic oxide film which was monitored ellipsometrically through the change of the positions of polarizer P and analyzer A. It may be seen from fig.1. that chemical dissolution lasts for about 1500 min. and it is not complete because P for titanium surface without anodic oxide film is 10.6 and A is 27.25. Fig.2. presents the changes of ellipsometric parameters P and A for anodic oxide films obtained at a voltage ranging from 0 to 100 V. As can be seen from fig.2., the curve is discontinued and for $\Delta = 90^\circ$ and $\Delta = 270^\circ$ it has no end values. Beside this, the curve is symetrical to the axis X and at any change of azimuth of Δ for 360° it returns to its original value. The symetricalness of the curve and its cyclic repetition at each 360° Δ value indicates formation of a barrier oxide film having a very low attenuation coefficient k.

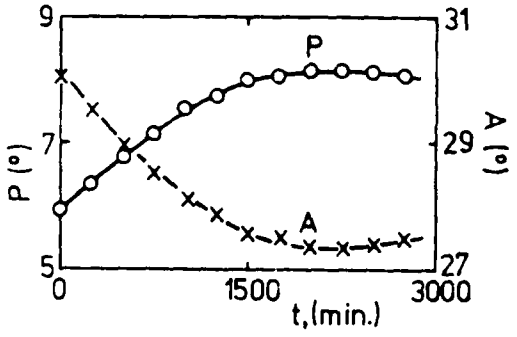

Fig.1. Change of P and A during chemical dissolution of anodic oxide film (with thickness of 2.5 nm) in a 0.5 mol/dm³ H_2SO_4

Based on above it can be said that the oxides present on titanium surface essentially contribute for increase of its corrosion stability, so that they act as protective coatings. Their dissolution is possible only by electrochemical reduction. The process of electrochemical dissolution can be monitored ellipsometrically by position of the analyzer.

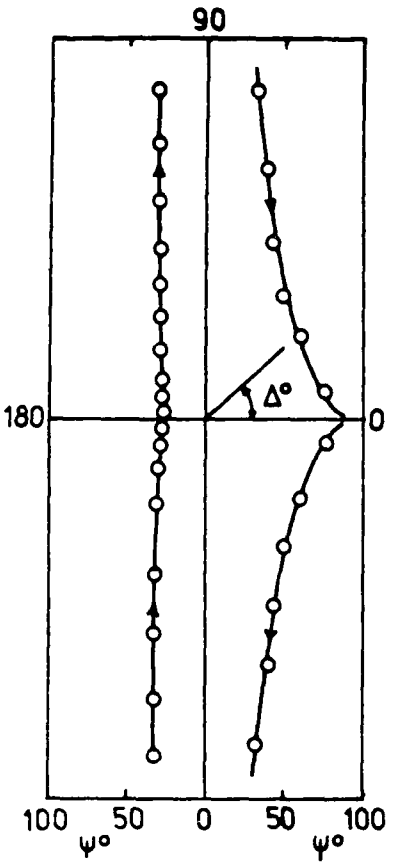

Fig.2. Experimentally determined ellipsometric curves plotted on polar coordinates for the growth of anodic oxide films on Ti surface in 0.5 mol/dm³ H_2SO_4

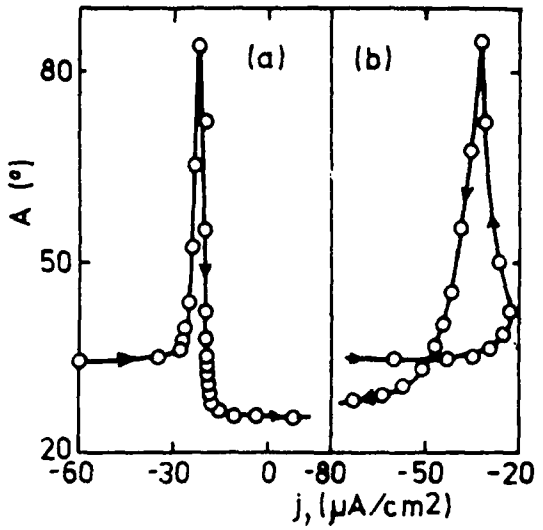

Fig.3. Dissolution of anodic oxide film with a thickness of 75 nm in 0.5 mol/dm³ H_2SO_4.
(a) Uniforme dissolution
(b) Nonuniforme dissolution

Fig.3.(a) presents curve of uniforme dissolution, and it can be seen that by the end of dissolution this curve shifts to anodic direction. Fig.3.(b) presents the same curve for a nonuniforme dissolution when during reaction TiH_2 is formed.

R e f e r e n c e s

1. Lj.Arsov, M.Froelicher, M.Froment et A.Hugot Le-Goff - Compt.rend.Acad. Sc.Paris 279, 485, (1974)

2. Lj.Arsov - Electrochim.Acta 27, 663, (1982)

3. Lj.Arsov, M.Froelicher, M.Froment et A.Hugot Le-Goff - J. Chim.Phys. 3, 275, (1975)

4. Lj.Arsov - Electrochim.Acta (in press)

5. Lj.Arsov - J.engin.Phys. 20, 5, (1979)

6. N.Tomashov - Corrosion Sc. 4, 315, (1964)

06060

ELECTROCHEMICAL FORMATION AND CHARACTERISATION OF OXIDE FILMS ON TITANIUM IN ALCALINE SOLUTION

A.Prusi and Lj. Arsov

Faculty of technology and metallurgy, Cyril and Methodius University
91000 Skopje, Yugoslavia

Introduction

The process of oxide film formation by anodic oxidation, when metal surface does not reakt chemically with the medium, can easily be monitored by use of clasic electrochemical methods. However, the procedure of these experiments is very complex when media that react to the metal are used.

Exept in media having a low pH, titanium shows a higher instability in media having a higher pH values, especially, higher than 12. The mechanism of anodic oxide film formation is studied rather frequently so for in acid solutions. Their formation runs, then, in accordance with a well controlled process, i.e. film thickness proportionally depends on the use potential[1]. At very strong acidic solutions, however, oxide films obtained are poorly adherent, and there is a present tendency of their dissolution after some time.[2]

As for experiments with titanium in strong alkaline media, the procedure of monitoring of formation and dissolution of these films is very complex owing to the chemical reaction of titanium with the alcaline media. At this, precipitates of titanium oxides and oxi-hydroxides are obtained, composition of which can very hardly be determined. Therefore, ellipsometric methode proved to be the best methode to indicate the changes that take place on titanium surface. Changes that occur on titanium surface in strong alcaline solution of potassium hydroxide were then monitored ex and in situ. We believe that results obtained will contribute for clarification of the mechanism of chemical and electrochemical reactions, and will provide a means for control of resulting oxide films.

Experimental

For this experiment were used titanium electrodes in form of a cilindar having a diameter of 25 mm. They were electropolished in a solution containing

$HClO_4$, CH_3OH and $C_6H_{14}O_2$ in a given ratio. Ellipsometric measurements were carried out at a 546,1 nm wavelength and an angle of incidence of 70^o.

Results and discussion

Titanium surface in alcaline solutions, in contrast to its reaction in acid solution, is less corrosion stable as a result of an intensive chemical reaction of formation of various surface products in form of films. The electrochemical measuring of steady-state potential in 1M KOH show that even after 1500 minutes stationary conditions of potential are not established in the metal-solution interface.

Potentiostatic and potentiodinamic measurements show that at higher pH values of the solution, titanium electrode does not indicate occurence of an active region which means that there is not a potential region whwre an intensive dissolution of titanium surface takes place and a diffusion of Ti^{+3} ions in the solution.[3] Figure 1 gives some obtained potentiostatic curves for titanium in 1M KOH and 4 M HCl. In 4M HCl, there is a very active region for potential range -0.65 to -0.3 v(s.c.e.). Owing to chemically formed film, having a considerable thickness, there is not an active region in 1M KOH.

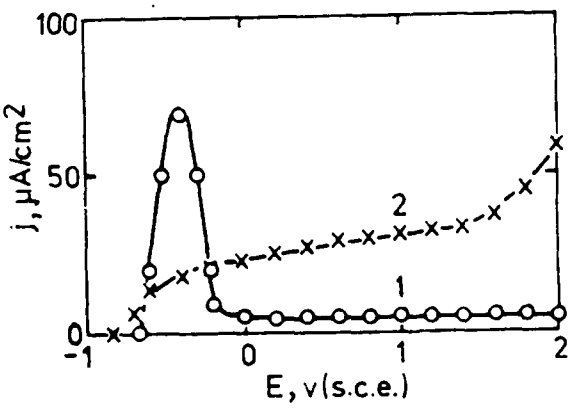

Figure 1.- I - E potentiostatic curves, 1- 4M HCl, 2- 1M KOH

By anodic oxidation of titanium in KOH, various colours of oxide films are formed and their colour depends on the film thickness and structure.

Ex-situ and in-situ ellipsometric measurings showed that there is a great reproducibity of results obtained and, thus, a possibility of determination of optical constants. Figure 2 and 3 presents changes of ellipsometric parameters $d\Delta$ and $d\Psi$ depending on voltage used ex-situ and in-situ. As can be seen on figure 2 and 3, $d\Delta$ and $d\Psi$ increase with potential increasing. tnese changes

are, however, much more evident are develop faster ex-situ. This shows that oxide film obtained by anodic oxidation is not quite stable in atmospheric conditions and that, in a short time, a reaction with atmospheric oxygen follows, so that, after some time thickness of the film is increased. We can conclude that more valid results are obtained with in-situ measurings where influence on anodic oxide film thickness is avoided.

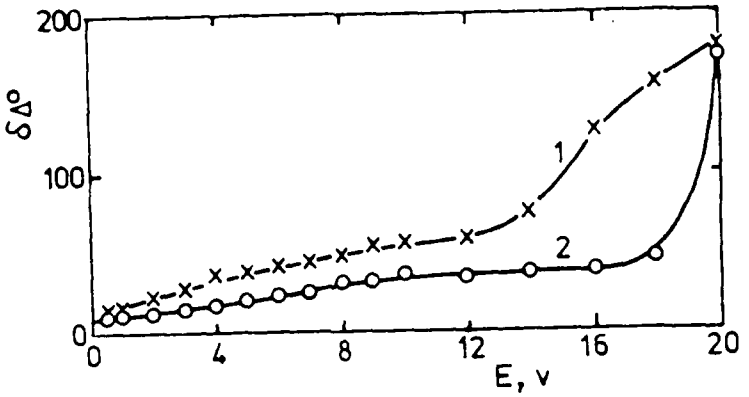

Figure 2.- Change of ellipsometric parameter d Δ versus applied voltage, 1- in-situ, 2- ex-situ

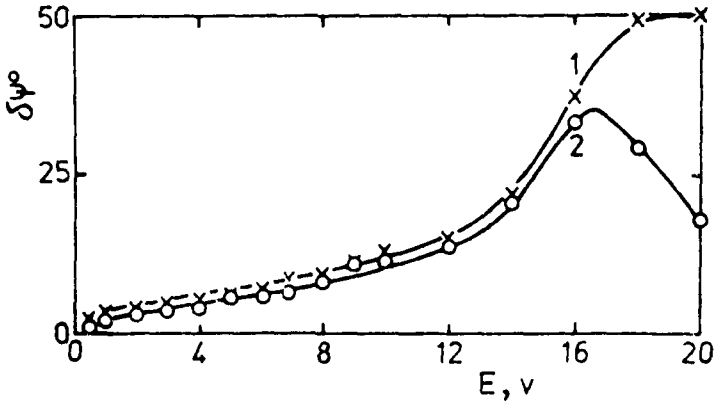

Figure 3.- Change of ellipsometric parameter d Ψ versus voltage 1- in situ, 2- ex situ

References

Lj.Arsov and T.Grčev, Maced.Acad. fo Sc. , 43, 1983 /-1-/

Lj.Arsov, Electroch. Acta, in press /-2-/

F.Nishimura and K.Kudo, Corrosion Science, 637, 1982 /-3-/

06070

ELECTROCHEMICAL PASSIVATION OF IRON IN BORATE BUFFER SOLUTION AT THE PRESENCE OF POLYACRYLAMIDE

T.Grčev, M.Cvetkovska
Cyril and Methodius University, Faculty of Technology and Metallurgy, Skopje, Yu

Introduction: Electrochemical passivation of iron in neutral and weak alkaline solution and particularly processes which take place in the active region, even today arouse great interest (1-3). It is of exceptional significance the question whether formation of primary film (most probably $Fe(OH)_2$) with a thickness of 0,8-1,5 nm is carried out by so called "dissolution-precipitation" mechanism or two parallel processes take place independently in this potential region:elegrochemical dissolution and film formation($Fe-Fe^{2+}$ and $Fe - Fe(OH)_2$).

For clarification of this question, the electrochemical passivation of iron in buffer borate solution, pH 8,45, was carried out at the presence of polyacrylamide (PAA)with Mn=60 000 which belongs to the group of iron inhibitors for prevention of corrosion in natural weters (4).

Our previous ellipsometric studies (5) indicated a significant adsorption of PAA on metallic surfaces.

Experimental: Electrochemical passivation of iron has been studied on rotational disk and ring-disk electrodes (Fe-disk,99,995% Fe and platinum ring) using cyclic voltammetry (v=10 mV/sec). PAA used, with Mn=60 000, was obtained by redox initiated polymerization of acrylamide with the system $Na_2S_2O_5$-Fe(III)-IDA(Fe(III)-salt of iminodiacetic acid).

The polymer was added as a 4% asolution of PAA and its concentration in buffer solution ranged from 0,01-0,25%. The voltamograms were recorded 30 minutes after polymer addition, i.e.after adsorbtion equilibrium was established.

Results and duscussion: Charcteristical current-potential dependence for passivation of iron in buffer borate solution (0,15N H_3BO_3+0,15N $Na_2B_4O_7$) pH 8,45 (curve 1,Fig.1.) points out the known regions: AB-active; BC-active to passive CD(CE)-passive region as well as regions EF and FG (FA) for reduction of passive film formed. It is obvious that the presence of PAA (0,01-0,165%) leads to a significant decrease in anodic current maximum which is proportional to the concentration of polymer added. At same time, ring current (at-1,1V/sce) shows a significant decrease in corresponding cathodic maximum which clearly indicates a reduction of the dissolution current of iron in this region.
On the other hand, its influence, both on the value of passive current and reduction current, is negligent.

The influence of PAA present in solution on the anodic current maximum j_β, as well as electricity quantities Q_s, in the region AC(Fig.2.), indicate most probably for a significant coverage of electrode surface by PAA.

Ring-disk experiments provide a quantitative resolution of the experimentally measured current in this region (AC in Fig.1.) on the dissolution current and current of film formation.

$$I_s = I_{dis} + I_{ff} \text{ or } Q_s = Q_{dis} + Q_{ff}$$

There was an assumption that the dissolution current (I_{dis}) dependes a both: the rate of polarization and the rate of rotation, while the current for film formation depends only on the rate of polirazation.

On this assumption, results presented on fig.2 and calculated values of dissolution current, that is, calculated value of I_{ff} or Q_{ff} of around 2 mC/cm^2, the decrease of I_{dis} or Q_{dis} is interpreted as an effect of PAA adsorbtion on metal suriace.

So, it can be obtained the dependence of degree of coverage of metal surface (θ) with polymer as a function of polumer concentration in the solution (fig.3.)

$$\theta = \frac{Q^o_{dis} - Q^c_{dis}}{Q^o_{dis}}$$

where $Q^o_{dis} = Q^o_s - Q_{ff}$ and $Q^c_{dis} = Q^c_s - Q_{ff}$; Q^o_{dis} and Q^c_{dis} - electricity quantities for dissolution of iron in absence or presence of polymer respectively.

Limiting values of θ(Fig.3) are reached at concentration of PAA 0,1 to 0,12% and are in good agreement with those for which is found greatest thickness of adsorbed PAA film on metalic surfaces (5).

Literature:

1. K.Ogura, K.Sato, Electrochim. Acta, 25,857,1980
2. M.Seo, N.Sato, Corrosion Sci., 18,577,1978
3. P.Lorbeer, W.J.Lorenz, ibid, 21,79,1981
4. Patent office - London, Pat.Specif. 1,133 382,28 feb. 1966, No 8607-66
5. Lj.Arsov, T.Grčev, M.Cvetkovska, Dj.Petrov, Bull.Soc. Chim., Beograd, 48 (7), 417, 1983

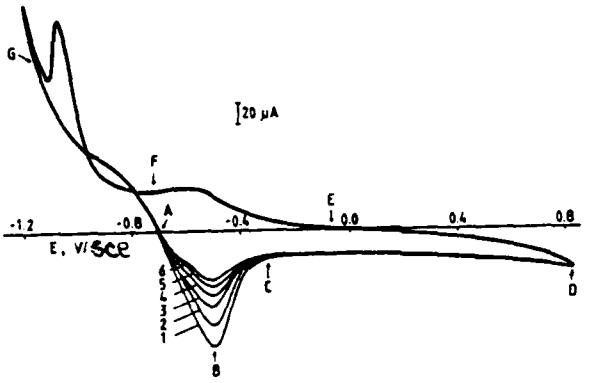

Figure 1: Voltammograms for passivation of iron in borate buffer solution, pH 8,45, in the presence of polyacrylamide, Mn=60 000;,1)0;2)0,33;3) 0,55;4)0,99;5)1,25 and 6)1,65 gPAA/dm^3. Disk area (Fe)0,20 sm^2; w=600 rpm; v=10mV/s.

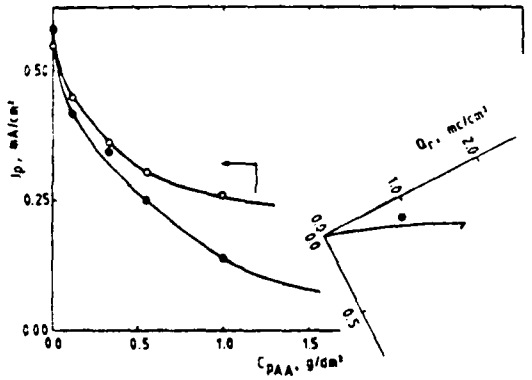

Figure 2: Dependence of anodic current peak and total quantity of electricity, Q_s, (region AC, Fig.1) on the concentration of PAA.

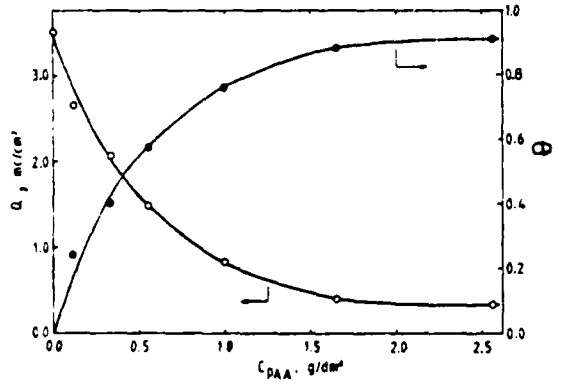

Figure 3: Dependence of Q_{diss} (for dissolution of iron in the active region) and θ-degree of coverage of electrode surface, on the concentration of PAA.

06080

METHANOL CORROSION OF MAGNESIUM

J. R. CULLERE
Departamento Química física
Universidad Autónoma de Barcelona
Bellaterra
(Spain)

Introduction. In a previous study about the anodic behaviour of magnesium in methanol [1], it was constated that the chemical reaction rate between magnesium and methanol producing magnesium methanolate and hydrogen is very appreciable using high purity methanol, but with methanol not dehydrated, the reaction rate fall drastically. In this communication is discussed the influence of water in the corrosion of magnesium by methanol and the results of weight loss and electrochemical experiments are compared.

Methodology. The corrosion rate was determined by weight loss of magnesium specimens sugmerged in methanol with variable amounts of water. The magnesium was 99,5 % purity, forming a rod of 10 mm diameter and approximatly 5 mm lenght. In each case the exact geometric surface was determined with a micrometer. The methanol was reactive quality and previous to their utilization was treated with magnesium methanolate and distilled.

In the electrochemical determinations, sodium bromide dryed 24 hours at 150° C was used as electrolyte. The methodology has been similar to the described in previous works.

Results. The FIG. 1 represent the corrosion rate of 24 hours duration experiments, of magnesium in methanol with variable amounts of water, determined by weight loss.

It is to note that water presence produce a strong inhibitor effect on the corrosion rate of magnesium by methanol and the presence of only 1% of water disminishes 10 times the corrosion rate. These values can be expressed analytically by the fitted expresion:

$$v\ (\mu g.cm^{-2}.s^{-1}) = (0,67 + 4,6c + 4,6c^2)^{-1}$$

where c is the water concentration in % weigt.

In these experiments were constated two facts:

a) As is frequent in metals corrosion [2], the corrosion rate of magnesium by methanol is function of time the metal is in contact with the solution. This is show in FIG. 2 where the corrosion rate of different specimens, in the same solution but with different atac time, is represented.

b) If a specimen is withdraw of the solution, as to weight and after is newly introduced in the solution, its corrosion rate is drastically reduced. To say, the contact

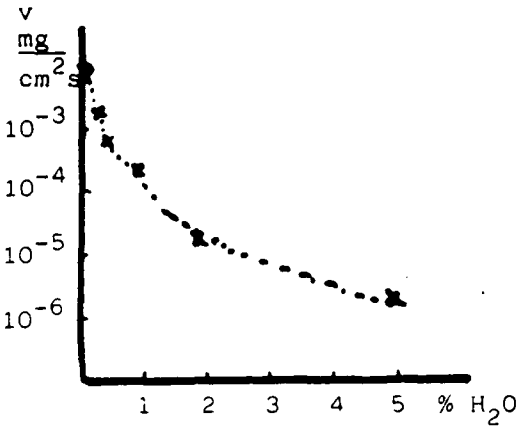

Fig. 1 Corrosion rate of Mg in CH_3OH containing H_2O.

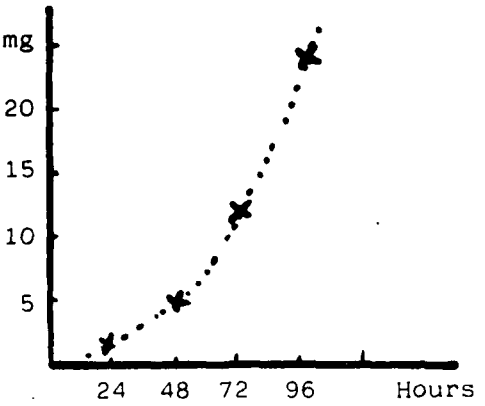

Fig. 2 Weigt loss of Mg in function of attack time

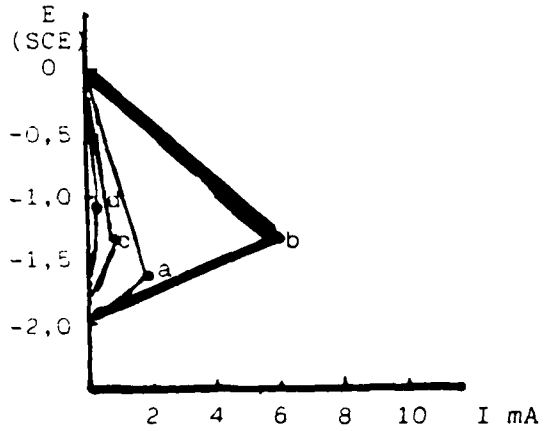

Fig. 3 Polarization diagram couple Mg/pt with different amounts of water:
a) 0,3% b) 1%
c) 2% d) 5%

with the atmosphere produce a strong passivation of magnesium.

The fact of corrosion rate acceleration with time can be explained considering that reaction of magnesium with methanol follow the equation: $Mg + HOCH_3 \longrightarrow Mg(OCH_3)_2 + H$ and the magnesium methanolate formed, reacts inmediatly with the water of the solution: $Mg(OCH_3)_2 + H_2O \rightarrow Mg(OH)_2 + HOCH_3$ and as the magnesium hydroxide produced is insoluble, form a gelatinous precipitate around the metal. The ultimate result is the creation around the metal of a zone without water, filled only with anhydrous methanol and according to FIG. 1 the corrosion rate increse exponentially.

The magnesium passivation when is withdraw of the solution and enter in contact with the atmosphere, can be attributed to a reaction of surface compounds with the

air humidity and formation of a passivating film, probably of different character as the habitual oxide film on magnesium surface and containing hydroxil groups. It is to notethat meanwhile the relation Volum (MgO) / Volum (Mg) is equal to 0,80 the relation Volum ($Mg(OH)_2$) / Volum (Mg) is equal to ,7 , to say, a more compact film.

Other experiments has been realicized to determine the influence of electrolytes in the corrosion rate of magnesium by methanol containing variables amounts of water. The corrosion rate is not influenced by the presence of NaBr 1 M, so in the electrochemical experiments sodium bromide in concentration 1 M was used as electrolyte.

For eacch solution the polarization resistence of Mg has been determined and the corrosion rate calculated. The value are in full agreement with the value obtained by weight loss.

The effect of water in the corrosion of magnesium by methanol is clearly put in evidence in polarization diagrams obtained when magnesium form a galvanic pair with platinum. The FIG. 3 show the initial and final potentials of Mg and Pt in NaBr 1M solution in methanol with differents amounts of water, and the intensity when te celle is shorted with a 10 ohm resistor. The process pass from cathodic control to a mix control with increasing amounts of water, showing the passivating action of water.

References.

1. Comportamiento anódico del magnesio en medio metanólico J. R. Culleré. En prensa
2. Theory of Corrosion and Protection of metals. N. D. Tomashov. MacMillan, New York 196

06090

THE STUDY AND DETECTION OF INTERNAL DEFECTS OF NON-FERROUS ALLOYS FOR OPTICALS AND ELECTROCHEMICAL METHODS

M.P.Mateo[1], M.D.Salvador[2], I.Barba[3]

1,2. Sección Técnica de Corrosión y Protección metálica de Valencia (España)

3. Sección Técnica de Corrosión y Protección metálica de Alicante (España)

Some of the most important problems produced in non-ferrous alloys,are corrosión and the formation of internal pores limiting oweself to copper alloys, in the case of brass to be more precise, these problems arise in the process of smelting or in other processes like welding or soldering.

In industries dedicated to the fabrication of illumination apparatus and artistic bronzes for example, these types of problems become much more important.[1]

In the bibliography[2,3], similar process have been described but emphasising only certain aspects.

The present work consists of two clearly different stages: a prior study by optical microscope[4,5], followed by another,electrochemical[6].

First, a macrographic study reveals the superficial defects, of great importance in subsequent treatments. Second. a metalographic examination is proposed to study the nature, size, and distribution of the internal pores, to determine the influence of these in possible subsequent corrosion processes.

Finally, an electrochemical study of different types of organic protection coatings [7], applied to these materials completes this work, taking into account the results previously aitained.

BIBLIOGRAPHY

1. M.P.Mateo,R.Guillen "Comportamiento de barnices en las lámparas". Jornadas Tecnicas Internacionales.Valen.

2. Herbert H. Uhlig. "Corrosión y control de corrosión" Ed.Urmo (1979)

3. C.E.N.I.M. Teoría y practica de la lucha contra la corrosión.

4. Metals Handbook. Vol.7. Atlas of Microstructures. American Society for Metals.

5. A.R. Bailey, L.E.Samuels. "Foundry Metallography". Metallurgical Servicies Laboratories Limited.Surrey, England (1976)

6. J.O'M. Bockris,A.K.N. Reddy. Electroquímica Moderna. Ed. Reverté (Tomo 2)

7. IB.F/02.269. Norma Interna de INESBA (Industria Española de Barnices y Pinturas). Valencia.

06100

CORROSION PERFORMANCE OF PAINTED GALVANIZED STEEL BY ELECTROCHEMICAL METHODS

I. PETROVICH and J.C. GALVAN
Centro Nacional de Investigaciones Metalúrgicas (ESPAÑA)

SUMMARY

A study has been carried out on the protectiveness of a zinc chromate alkyd paint applied on galvanized steel specimens having 300 g/m^2 zinc coats. Some of them had previously been subjected to a conversion treatment consisting of a dip in a $CrO_7Na_2 \cdot 2H_2O$ (200 g/l) and H_2SO_4 (5 ml, d = 1.84) bath. Various electrochemical methods were employed for the purpose, namely: impedance measurements by means of an analogic Hewlett-Packard 4800 impedance meter; potentiodynamic plotting of polarization curves performed by the use of a Corroscript Tacussel potentiostat; the measurement of linear polarization resistance and the plotting of potentiometric curves, both of which used a Corrovit Tacussel potentiostat.

All these techniques were sensitive to the system's degradation process thus proving the remarkable influence of the chromate coating as an additional protective agent. The aggressiveness was also revealed of the various electrolytes used: 3% NaCl and distilled water, simulating up to a certain extent a marine atmosphere and a pollution-free rural one, respectively.

RESULTS AND DISCUSSION

Impedance Diagrams

All the systems showed in an initial period a capacitive behaviour which may be attributed to the unaltered condition of the paint. At longer time intervals, the impedance diagrams tend to differentiate themselves and describe semicircumferences which, as a rule, become smaller as the test time increases (fig. 1a). A second semicircumference is finally obtained (fig. 1b) for long immersion times and low frequencies in the case of systems in contact with sodium chloride solutions. Such behaviour agrees with the equivalent circuit proposed by several authors (fig. 2).

Figure 1b also shows a reversal in the development of the first semicircumference, wherein the diameter has increased with immersion time. This is a rather frequent phenomenon in these systems which will be discussed later.

Resistance due to Electrolyte Penetration, Through Pores, R, and Linear Polarization Resistance, Rp.

The variation of R with time is shown in fig. 3. It has been observed that, as a rule, R decreases gradually while at the same time the paint coat undergoes degradation. This tendency is more marked in the case of systems in contact with sodium chloride.

The variation in polarization resistance, Rp, as measured by d.c. are also given in Fig. 3. Rp development is similar to that for R, although it always provides higher values. This is not surprising if one bears in mind that what is really being measured by this technique is the sum of all the resistances inherent to the system (fig. 2).

Variation of Corrosion Potential. Polarization Curves. Effect of Chromating

The development of the paint degradation process can also be followed apart from the use of the techniques described by means of polarization curves and by tracking the corrosion potential with time, at least qualitatively. A rapid decrease of E_{corr} values during the first hours of immersion has been observed in those systems with chromating treatment. This means an accelerated permeation of the electrolyte towards the substrate due to osmotic effect. The potential then becomes stabilized up to the end of test due to the protective action of the chromate coating (fig. 4).

From Fig. 5 it can be seen that a reduction in slopes of the anodic branches takes place, as a rule, depending on immersion times. For a 500 mV polarization, the response intensity is increasingly higher and this could be related to the degradation process in paint. However, in the absence of a chromate film, this tendency is reversed sporadically due to the fact that the reaction between the electrolyte and the metal substrate is unhibited. On this account, corrosion products are formed which temporarily block up the pores of the paint coat. This effect has also been detected with the occasional increases of Rp, R (fig. 3) and E_{corr} (fig. 4).

REFERENCE

1. PETROVICH e J.C. CALVAR: GALVANOTECNICA ; 26, 2, 29-34 (1995).

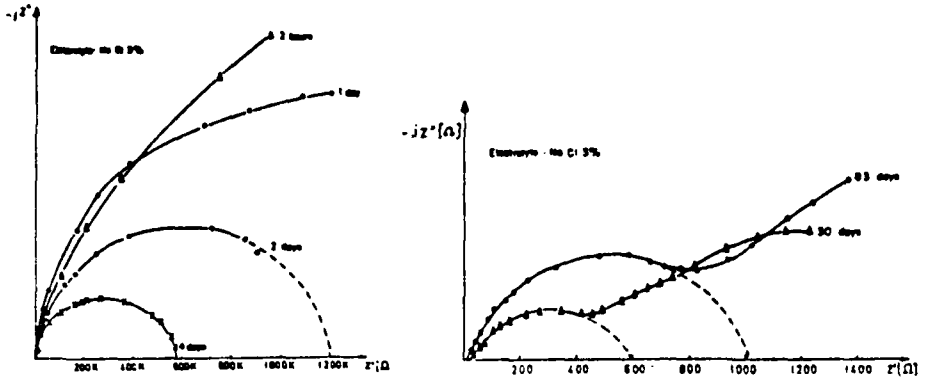

Fig. 1.- Development of impedance diagrams for a system without chromating

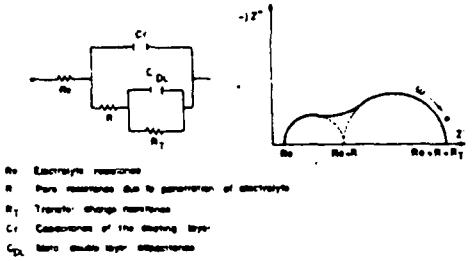

Fig. 2.- A model of the metal-paint couple.

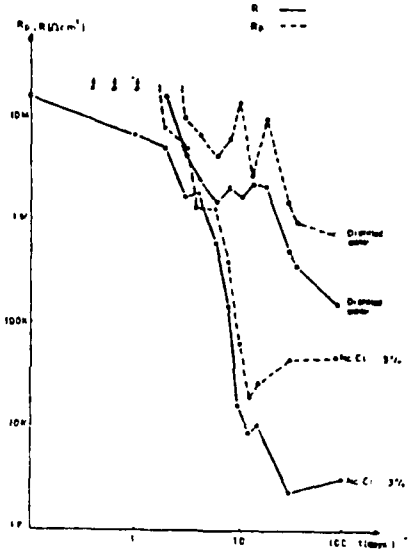

Fig. 3.- Development of R_T and R in non-chromated systems.

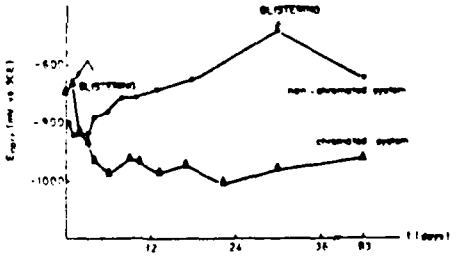

Fig. 4.- Variation of corrosion potential with time. Electrolyte: distilled water.

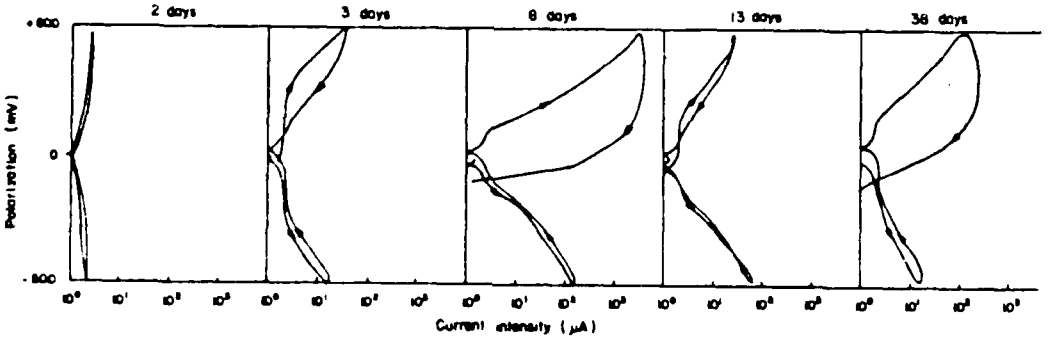

Fig. 5.- Polarization curves for a non-chromated system in contact with distilled water.

06110

POTENTIODYNAMIC BEHAVIOUR OF ZINC IN ALKALINE SOLUTIONS

P.Ll. CABOT, M. CORTES, F. CENTELLAS,
J.A. GARRIDO and E. PEREZ
Departament de Química Física. Facultat de Química.
Universitat de Barcelona. Spain.

INTRODUCTION

Zinc has been intensively studied because of its usefulness in cathodic protection of certain technologically important metals such as Fe and in the fabrication of many commercially important batteries. Several different mechanisms for the anodic oxidation of zinc in alkaline media can be found in the literature[1-4]. However, although the total reaction is fairly understood, the mechanism is not fully elucidated.

In this work, results concerning an extensive potentiodynamic study of a zinc electrode (99.9 %) in six deareated KOH solutions at concentrations in the range 0.40-5.00 M and sweep rates between 0.2 and 100 $mV.s^{-1}$ are presented. In order to interpret the experimental results, electrochemical, optical and electronoptical methods have been applied. The previous treatment of the electrode comprised mechanical polishing, potentiodynamic polarization, as Hendrikx et al[5] suggested, and cathodic reduction. Subsequently, the electrode was let free for 5 min in order to attain the rest potential. The working solutions were prepared with Merck p.a. KOH and water which was deionized, doubly distilled and purified by means of a Millipore Milli-Q system.

RESULTS AND DISCUSSION

The experimental curves obtained are of the type shown in Fig.1. Starting the potentiodynamic cycle at -1.425 V vs. Hg/HgO, an exponential increase of the current density with the potential is found (region T). Tafel plots for this region, similar to that shown in Fig.2, were always circa 40 $mV.dec^{-1}$, in agreement with previous potentiodynamic work of Armstrong and Bulman[6]. Also for the same region, reaction orders with respect to OH^- have been obtained, being of 2.8 and 3.4 for sweep rates of 2 and 5 $mV.s^{-1}$ (Fig.3).

The existence of the first anodic peak (A in Fig.1) has been considered to be the consequence of the precipitation of $Zn(OH)_4^{2-}$ (denoted by Breiter and Powers[7] as oxide of type I). Af-[7-9]

ter this peak, the current density decreases and at the passivation potential (P in Fig.1), a protective layer of ZnO is formed (type II oxide of Breiter and Powers). Starting at the same potential and the electrode being in the same conditions, several potentiodynamic cycles of different potential ranges have been carried out. The anodic sweep has been reversed before the first anodic peak and between this peak and the passivation potential. As shown inf Fig.1, a new cathodic wave (N) appears if the previous anodic sweep ends after the passivation potential. This result implies the formation of two different reducible species during the anodic sweep, being consistent with previous optical data.

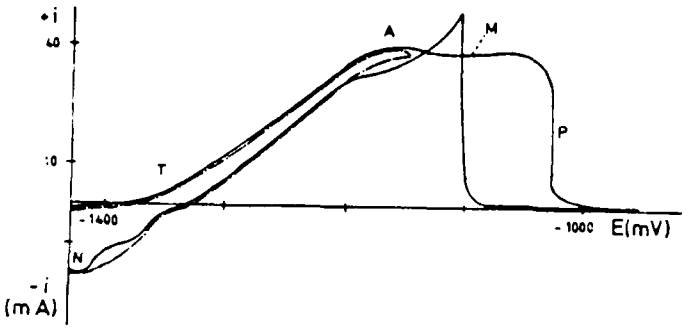

Fig.1.-Potentiodynamic curves, 2.00 M KOH and sweep rate of 5 mV.s^{-1}.

Fig.2-4.00 M KOH, 2 mV.s^{-1}.

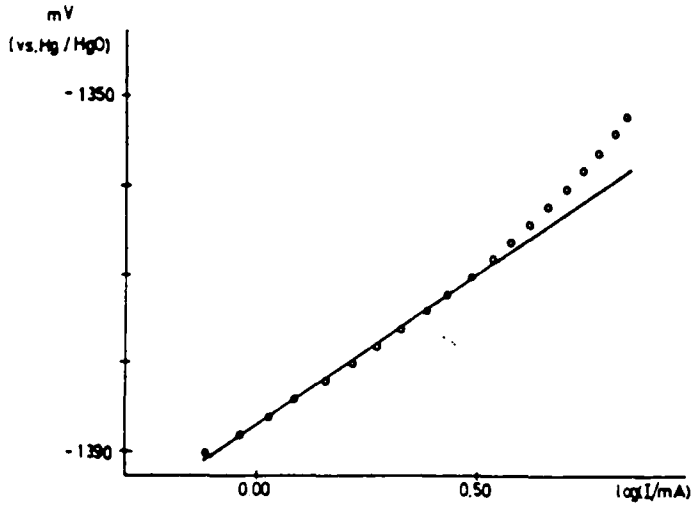

Further information is found from the analysis of the dependence of the potentiodynamic anodic charge on the sweep rate and KOH concentration. The total anodic charge of the anodic sweep is found to decrease with sweep rate increasing. On the other hand, this charge increases with KOH concentration. The same trend is observed when only the anodic charge comprised between the potentials corresponding to I=0 and to the first anodic peak is considered.

Scanning electron micrographs of the electrode surface at different points of the potentiodynamic cycle have also been performed. Fig.4 corresponds to the point M in Fig. 1 and show the important corrosion of the electrode. Before the potentiodynamic oxidation, the surface is relatively flat. At the beginning of the oxidation, several pits appear and grow until the

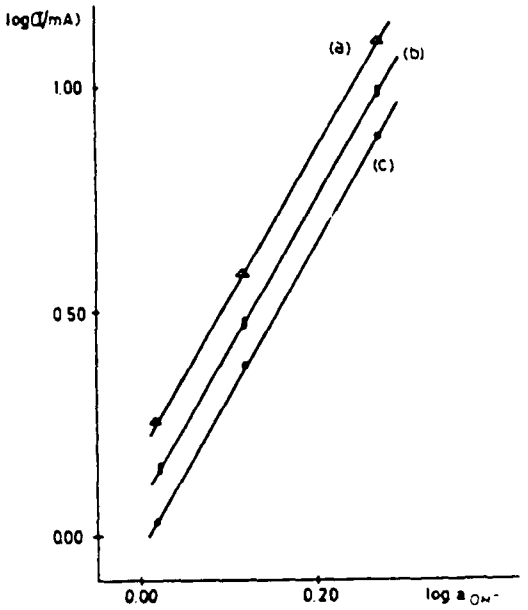

Fig.3.-Sweep rate of 5 $mV.s^{-1}$.(a)-1364; (b)-1368;(c)-1372mV.

asoect of Fig.4 is reached. After the oassivation potential, the electrode surface becomes much more uniform and exhibit more quantity of precipitate. The SEM studies clearly shows that the metal oxidation takes place with the formation of a soluble compound, possibly the $Zn(OH)_4^{2-}$ ion.

The results obtained in this work for the initial stages of the potentiodynamic oxidation of zinc in alkaline media are in agreement with the mechanism already proposed by Bockris et al[2] from the potentiostatic and galvanostatic techniques, being $Zn(OH)_2^- + OH^-$ → $Zn(OH)_3^- + e^-$ the r.d.s.

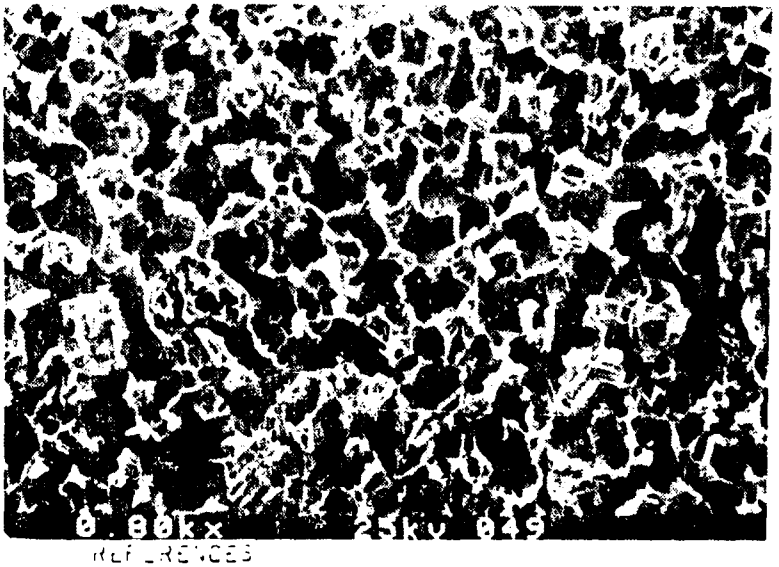

Fig.4.-4.00 M KOH,sweep rate of 5.0 $mV.s^{-1}$.

REFERENCES

1)D.A.Payne and A.J.Bard,J. Electrochem.Soc.,119,1665(1972).
2)J.O'M.Bockris, Z.Nagy and A.Damjanovic, J. Electrochem. Soc., 119,285(1972).
3)J.P.G.Farr and N.A.Hampson,J.Electroanal.Chem.,13,433(1967).
4)Y.C.Chang and G.Prentice,J.Electrochem.Soc.,132,375(1985).
5)J.Hendrikx, A. van der Putten, W.Visscher and E.Barendrect, Electrochim. Acta, 29,81(1984).
6)R.Armstrong and G. Bulman,J.Electroanal.Chem.,25,121(1970).
7)R.W.Powers and M.W.Breiter,J.Electrochem.Soc.,116,719(1969).
8)R.W.Powers, ibid.,118,685(1971).
9)M.C.H.McKubre and D.D.Macdonald, ibid.,128,524(1981).

06120

TAFEL SLOPES FOR Cu(I) AND Cu(II) OXIDE FORMATION IN ALKALINE SOLUTIONS.

F.A. CENTELLAS, J.A. CARRIDO, P.LL. CABOT and E. PEREZ.
Departament de Química Física. Facultat de Química. Universitat de Barcelona
Avda. Diagonal, 647. C8028-Barcelona (Spain).

The study of galvanostatically generated films on copper electrodes in alkaline solutions is carried out from H_2 to O_2 evolution.

The galvanostatic curves show several anodic plateaus associated with monovalent, divalent and trivalent[1] species. During this process, the presence of mono and divalent soluble species and the electrogeneration of another insoluble ones, in different layers, is commonly accepted.

The subject of this work, is the measurement of the Tafel slopes corresponding to the formation of the Cu(I) and Cu(II) species. The results obtained are reviewed from electrochemical and optical data.

The monocompartimental cell used has been described in early works[2]. KOH solutions are 0.1; 0.75; 1.0; 2.0; 3.0; 4.5 and 6.0 mol.dm^{-3} and were prepared with Milli-Q water and deareated by means of N_2 bubbling. Copper mechanized bars of 99.9 % in Cu was used, and the metal area exposed to the solution was 0.484 $\pm$ 0.005 cm^2. The reference electrode is the Hg/HgO/KOH(sln) system and showed a good stability and reproducibility. The potentials obtained in this work are referred to this electrode.

The anodic curves begin at -1330 mV, when a clear release of H_2 on the copper electrode occurs. afterwards, the polarity of the current is inverted and the galvanostatic curves are registered electromechanically.

The electrode potential rises sharply up to -1050 mV followed by a showing down of the rising rate and moving in a nearly linear way up to -330 mV, where a new decrease of the mentioned rate appears. Around -620 mV, a characteristic and repetitive point associated to potential slope decrease change appears.

A second anodic step occurs at -130 mV and is associated with the formation of the Cu(II) species. The O_2 evolution potential, 750 mV, is preceded by another irregularity of the curve at potentials near 640 mV.

When overpotential at t = 0 is plotted versus the logaritm of current density at constant KOH concentration, a good linearity for stirred and unstirred solutions are obtained. This representations are carried out, first, for Cu(I) species (point C) and second, for the Cu(II) species (point D).

The experimental values obtained for these slopes shown in the Tables I and II.

Tafel slopes obtained for C (formation of the Cu(I) species) are practically independent of KOH concentration and stirring rate. This value is near 0.050 mV.dec^{-1}. Tafel slopes corresponding to Cu(II) compounds depend on alkalinity and stirring rates. (0.062 - 0.105 and 0.071 - 0.089).

In view to explain the galvanostatic behaviour of copper in alkaline

TABLE I

KOH* / mol.dm^{-3}	Slope / V.dec^{-1}	
	Point C	Point D
0.1	0.048	0.089
0.75	0.050	0.076
1.0	0.051	0.076
4.5	0.052	0.071

*without solution stirring.

TABLE II

KOH* / mol.dm^{-3}	Slope / V.dec^{-1}	
	Point C	Point D
0.1	0.047	0.105
0.5	0.050	0.085
0.75	0.050	0.085
1.0	0.55	0.063
3.0	0.055	0.062

*stirring rate = 2 ml.s^{-1}.

solutions, we have considered for the transfer coefficient associated to a process which occurs in multiple steps, an equation of the type:

$$\alpha = \frac{\beta\ (\ n - \overleftarrow{n} - \overrightarrow{n}\ ) + \overleftarrow{n}}{\nu}$$

being β the symmetry factor; ν the stechiometric number, n the total number of electrons; $\overleftarrow{n}$ and $\overrightarrow{n}$, the number of electrons before and after the rate determining step.

For Cu(I) oxide formation, Tafel slopes correspond to a transfer coefficient near 0.5. This value, and assuming 0.5 for the symmetry factor, is consistent with several nechanisms:

Mech. 1:

a) $Cu + CH^- \longrightarrow CuCH + e$

b) $CuOH + OH^- \longrightarrow Cu(OH)_2^-$

c) $Cu + Cu(OH)_2^- \longrightarrow Cu_2O + H_2O + e$

a = rate determining step.

Mech. 2:

a) $Cu + OH^- \longrightarrow CuOH + e$

b) $CuOH + Cu + OH^- \longrightarrow Cu_2O + H_2O + e$

a = rate determining step.

Mech. 3:

a) $Cu + 2OH^- \longrightarrow Cu(OH)_2^- + e$

b) $Cu + Cu(OH)^- \longrightarrow Cu_2O + H_2O + e$

a = rate determining step.

The overall reaction in the cases above mentioned are similar:

$$2Cu + 2OH^- \longrightarrow Cu_2O + H_2O + 2e$$

Mech. 2 supposes inexistence of soluble Cu(I) species. The formation of cuprous oxide via discharge of electrolitic OH^- and further nucleation and crystalline growth. This mechanism is supported by experimental data using electrochemical and ellipsometric methods[1-5].

On the other hand, in Mech. 3, the Cu_2O formation takes place by a dissolution precipitation process. The experimental evidence of soluble Cu(I) compound, $Cu(OH)_2^-$ has been carried out by means of the rotating disk electrode technique[5,6].

Both mechanisms are consistent with experimental values of slopes associated with i - t curves (near 0.5). In addition thermodynamic formation of CuCH and/or $Cu(OH)_2^-$ compounds are possible as been proposed in a recent theoretical study[5]. Kinetical considerations seen to imply that the adsorption of a Cu(I) compound, is the rate determining step in the electrogeneration of Cu_2O via soluble or insoluble intermediates.

Tafel slopes corresponding to Cu(II) oxide formation are 0.071 - 0.089 and 0.062 - 0.105 $V.dec^{-1}$ for unstirred and stirred solutions. These values are in agreement with the mechanism:

a) $Cu_2O + 2OH^- \longrightarrow Cu(OH)_2 + 2e$

b) $5Cu_2O + 10OH^- + 5H_2O \longrightarrow 10Cu(OH)^-$

c) $10Cu(OH)_2^- \longrightarrow 5Cu(OH)_2 + 5Cu + 10OH^-$

d) $7Cu(OH)_2 \longrightarrow 7CuO.H_2O$

d) $5Cu + 10OH^- \longrightarrow 5\ CuO.H_2O + 10e$

being d the rate determining step. The overall reaction is:

$$6Cu_2O + 6H_2O + 12OH^- \longrightarrow 12CuO.H_2O + 12e$$

This mechanism is similar for the different KOH concentrations and electrolite stirring rate, corresponding the diferences observed to the extension of the reaction:

$$CuO.H_2O + 2OH^- \longrightarrow Cu(OH)_4^{2-}$$

following the step e.

The intermediates propsed in order to justify the Cu(II) oxide formation are established experimentally by several autors.

REFERENCES

1. J. AMBROSE, R.G.BARRADAS and D.W. SHOESMITH; J. Electroanal. Chem., 47, 47, (1973).
2. F.A. CENTELLAS; J.A. GARRIDO, E. PEREZ and J. VIRGILI; An. Quím., 80A, 317, (1984).
3. M.J. DIGMAN, D.B. GIBBS; Can. J. Chem., 48, 1242, (1970).
4. J.M.M. DROOG, C.A. ALDERLIESTEN, P.T. ALDERLIESTEN, G.A. BOOTSMA; J. Electroanal. Chem., 61, 111, (1979).
5. V.ASHWORTH, D. FARRHURST; J. Electrochem. Soc., 124, 506, (1977).
6. F. ILLAS, J. RUBIO, F.A. CENTELLAS and J. VIRGILI; J. Phys. Chem., (accepted for publication).

TREATMENT OF POTENTIOSTATIC CURVES IN ANODIC OXIDATION OF COPPER IN ALKALINE SOLUTIONS.

F.A. CENTELLAS, P.LL. CABOT, J.L. FERNANDEZ, J.A. GARRIDO and E. PEREZ.
Departament de Química Física. Facultat de Química. Universitat de Barcelona
Avda. Diagonal, 647. 08028-Barcelona (Spain).

Potentiostatic studies on copper, tin and other electrodes in alkaline solutions, show particular morphologies for the i-t curves. When a potential characteristic for oxide formation is applied, the i-t curve show a minimum and posteriorly a maximum. This suggest the existence of different steps for the potentiostatic oxide formation[1].

In the first step, oxide formation is in agreement with a diffusive model[2] but only prevails for a short time. In this work a model based in cationic migration through the oxide film is considered in order to interpret the experimental results. This model was applied succesfully in the potentiostatic formation of aluminium oxides in sulphuric and propanedioic acids[3].

The monocompartimental cell used, was described in a previous work[4]. The solutions were prepared with R.A. quality products and water Milli-Q and were deareated by means of N_2 bubbling. The Cu and Sn anodes are 99.9 and 99.9999. Reference electrode is the Hg/HgO/KOH(sln) system, and showed a good stability and reproducibility. The potentials reported in this work are referred to this electrode.

The potentials studied cover the range from 40 to -120 mV for Cu electrode and from -680 to -820 mV for Sn.

The electrodes are treated electrochemically 1-3 minutes at certain cathodic potential and then, the constant set potential is applied.

Potentiostatic curves obtained for Cu and Sn electrodes are similar and show a characteristic minima and maxima. The differences, obbiously, corresponds to the different characteristics of the electrogenerated oxides.

In order to establish a good treatment for the experimental data corresponding to the formation of the first oxide (before to minimum) a model established for oxide growth by means of ionic migration is applied. In this model, the equation for current density and thin films (< 5 Å), is:

$$i = \frac{1}{2}\left|\frac{\alpha(\beta - 1)}{\kappa}\right|^{\frac{1}{2}} \cdot t^{\frac{1}{2}} \qquad \text{Eq. 1}$$

were α and β are complex equations although constants for a certain set potential. When the oxide films are thicker (> 5 Å) the equation corresponding to the current density is:

$$i = \frac{F\,M}{\kappa\,\Omega}\,t^{-1} \qquad \text{Eq. 2}$$

with Ω = molar volume of oxide and $\kappa = F.E/R.T$.

In this migration model, the electric field through the oxide is supposed independent of this thickness, depending only of the characteristics of the oxide. Equations 1 and 2 justify the experimental values corresponding to other metals[6], and are summarized in the form:

$$i = k.t^{-m} \qquad \text{Eq. 3}$$

where k is a function of the applied potential and the oxide characteristics, and m depending only on the applied potential.

Other autors have proposed for similar models an equation of the type[7,8]:

$$i = \frac{1}{t/B + (1/i)_{t=0}} \qquad \text{Eq. 4}$$

B being a constant. This equation when $B/i_o \ll t$ corresponds to Eq. 3 with $m = 1$. A value of m near 0.5 is in agreement with diffusive control of the process and growth of oxide film by migration at low fields. When m is near 0.66 the rate determining step is associated with metal dissolution by low electric field action. At very high electric fields, Eq. 1 prevails.

When log i - log t plots are made in the formation of the first copper oxide in low alkalinity solutions, the value of the slope obtained is near -1 ($m = 1$), wich is in agreement with a 10^5 $V.cm^{-1}$ electric field, fig 1.

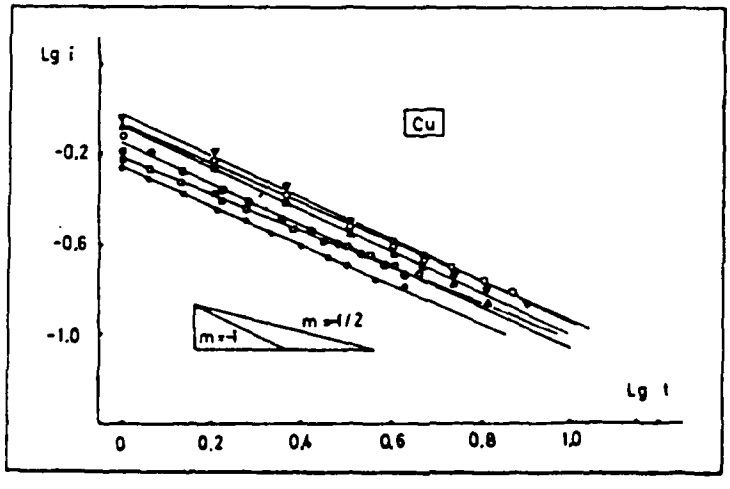

Figure 1: lg i(mA)-lg t(s). ●,□,●, KOH 0.05 mol. dm^{-3} E = -80, -60 y -40 mV. ▽,▲,○, KOH 0.1 mol. dm^{-3} E = -80, -60 y -40 mV. Metal: Copper.

The slopes obtained for Sn potentiostatic oxide formation are -0.70, fig. 2, corresponding with oxide growth from solution and low electric fields. These results are in agreement with those obtained by other workers in reference to the chemical dissolution and inestability of this first oxide film[9].

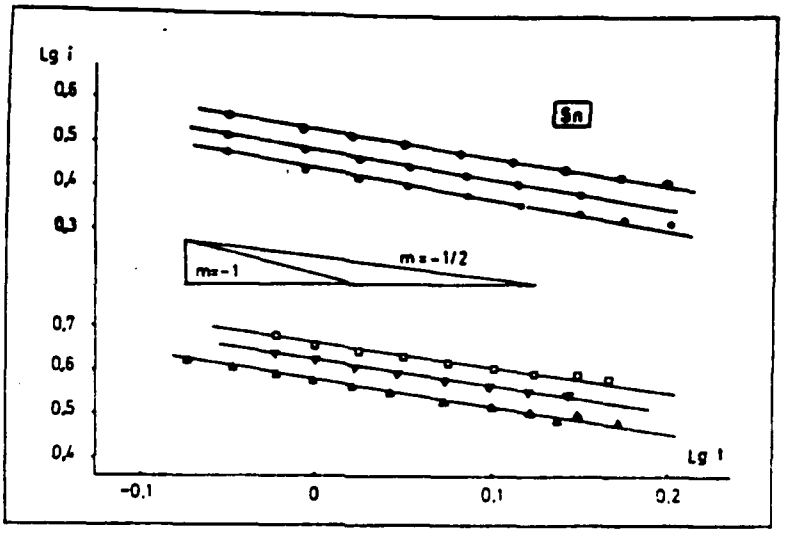

Figure 2: lg i(mA)-lg t(s). ●,○,●, KOH 0.05 mol. dm^{-3} E = -680, -720 y -760 mV. □,▽,▲, KOH 1.0 $mol.dm^{-3}$ E = -650, -760 y -680 mV. Metal: Tin.

REFERENCES

1. C.Y. CHAO, L.F. LIN and D.D. MACDONALD; J. Electrochem. Soc., 128, 1187, (1981).
2. P. DELAHAY; New Instrumental Methods in Electrochemistry. Interscience . New York (1964).
3. P.LL.CABOT, F. CENTELLAS, E. PEREZ and J. VIRGILI; Electrochim. Acta, in press.
4. F.CENTELLAS; J.A. GARRIDO, E. PEREZ and J. VIRGILI; An. Quím., 80A, 317, (1984).
5. D.D. MACDONALD; Transient Techniques in Electrochemistry. Plenun Press. (1977).
6. D.D. MACDONALD and B. ROBERTS; Electrochim. Acta., 23, 557, (1978).
7. S. ASAKURA and Y. NOBE; J. Electrochem. Soc., 118, 536, (1971).
8. N. SATO and M. COHEN; J. Electrochem. Soc., 111, 512, (1964).
9. S.D. KAPUSTA and N. HACKERMAN; Electrochim. Acta., 25, 1625, (1980).

06140

COMPARISON BETWEEN MECHANICAL AND ELECTRICAL DEPASSIVATION OF STAINLESS STEELS IN HOT CHLORIDE MEDIA

M. CID, D. DESJARDINS, M.C. PETIT, M. PUIGGALI
Laboratoire de Mécanique Physique, U.A. CNRS 867, Université de Bordeaux I
351 cours de la Libération, 33405 Talence cedex (France)

To compare mechanical and electrical depassivation we make a study of three alloys : 308 L, 321, 316 L.

	C	Mn	Si	S	P	Ni	Cr	Mo	Cu	Ti
308 L	0.013	1.86	0.135	0.006	0.013	9.85	19.64	0.06	0.075	<0.02
321	0.053	1.24	0.62	9 ppm	0.029	9.18	17.70	0.29	0.19	0.42
316 L	0.013	1.41	0.41	0.005	0.017	12.7	18.67	2.70	0.085	<0.02

Before depassivation studies, polarization curves are drawn for each alloy in a solution of $MgCl_2$ - 30 % - 117°C (fig. 1). The passivity is delimited by E_o (potential for zero current) and E_{dp} (potential of the end of the passivity plateau). For all the alloys the free corrosion potential E_{cor} is situated in the passivity range.

	E_o	E_{dp}	E_{cor}
308 L	- 460	- 350	- 369
321	- 440	- 340	- 368
316 L	- 390	- 280	- 340

Characteristic potentials (mV/ECS)

To follow the mechanical depassivation of these alloys, cylindrical samples (ϕ = 1,5 mm, l = 80 mm) are quickly subjected to a given plastic strain rate (ε = 10 %) with a strain rate $\dot{\varepsilon}$ = 66 % mn^{-1}. This tests are realized under controlled potential E = E_{cor}. Current-time curves are recorded during and after straining (fig. 2). During sample straining the current increases ; when straining is stopped a more or less rapid current decrease is observed. The maximum of the current depends on the alloy composition.

The electrical depassivation study is made on cylindrical samples (lateral surface 5 cm^2) by potential jump (ΔE = 100 mV) from a potential near

E_{dp}. The current evolution is different for each alloy (fig. 3).

The figures 2 and 3 let us the comparison between the current evolution during mechanical and electrical depassivation : a 308 L stainless steel which shows a more important current during mechanical depassivation is also distinguished by a rapid current increase during electrical depassivation. The depassivation of 316 L stainless steel is more difficult in the two types of tests.

The two depassivation test methods are complementary. The electrical depassivation leads to a better understanding of the current evolution during mechanical depassivation.

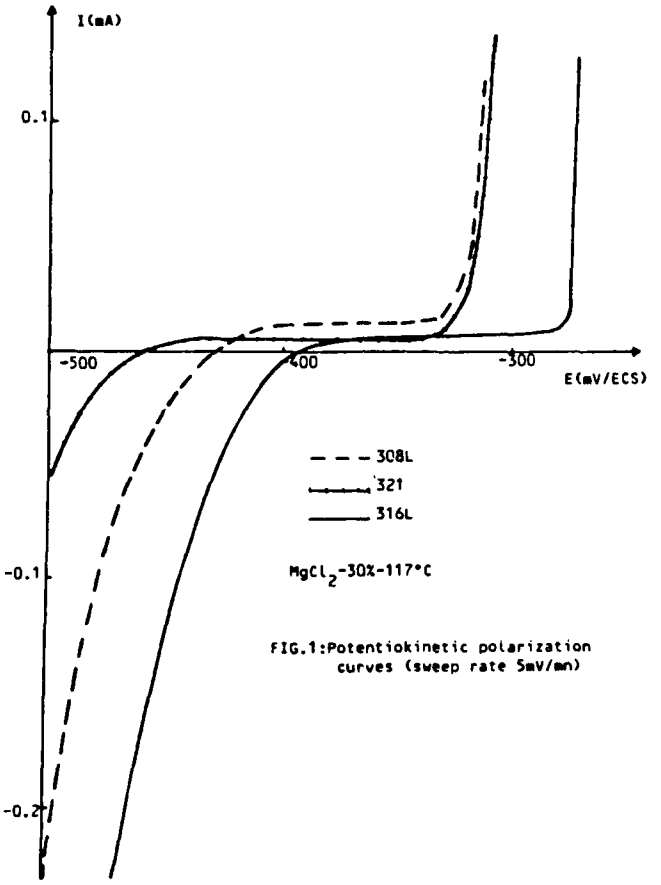

FIG.1:Potentiokinetic polarization curves (sweep rate 5mV/mn)

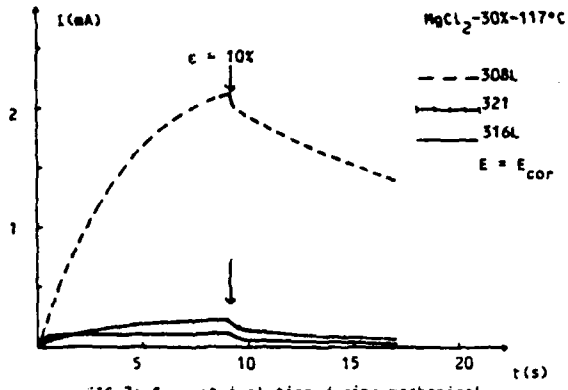

FIG.2: Current évolution during mechanical depassivation $\dot{\varepsilon}$ = 66% /mn

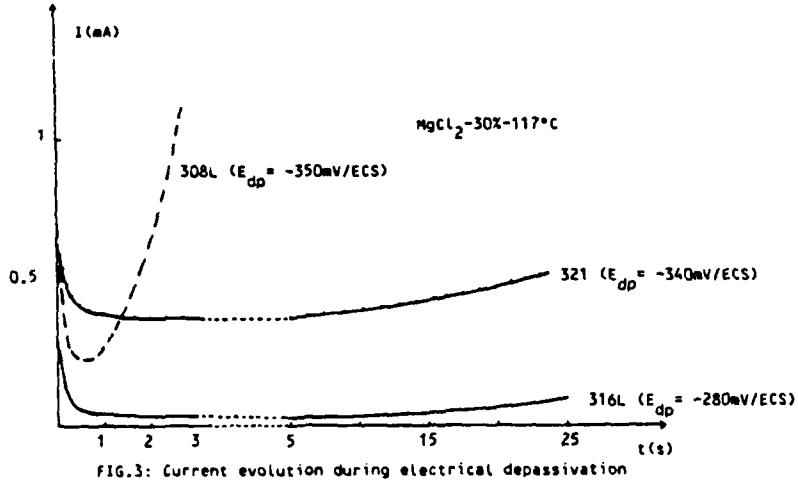

FIG.3: Current evolution during electrical depassivation potential jump : E = E_{dp} + 100mV

06150

THE EFFECT OF SO_4Fe TREATMENT ON COPPER ALLOYS IN POLLUTED SEA WATER

H.DI NEZIO, C. MANFREDI, S. SIMISON and S.R. de SANCHEZ
Instituto en Ciencia y Tecnología de Materiales, Facultad de Ingeniería, Universidad Nacional de Mar del Plata, Mar del Plata, Argentina.

The quality and the behaviour in sulphide contaminated sea water of the lepidocrocite (FeOOH) film growed on different copper alloys (aluminum brass 76:22, aluminum bronze 95:5, and copper-nickel alloys 90:10, 70:30) have been studied.

Corrosion current and pittin susceptibility were determined and optical microscope and SCAN observations were used also to show the effect of sulphide in the film formation.

The lepidocrocite film enhances the polarization of the oxygen reduction and modifies the anodic current making it lower and change the pitting potential in those alloys susceptibles to this form of attack.

Sulphides prevent either the growing of lepidocrocite film if present at the begining of treatment or promote the fisuration and detachment of the previously formed film.

The laboratory test reproduce the plant conditions to permit the applicability of the lab results and the selection of the best material for heat exchanger be used with SO_4Fe treatment in polluted sea water.

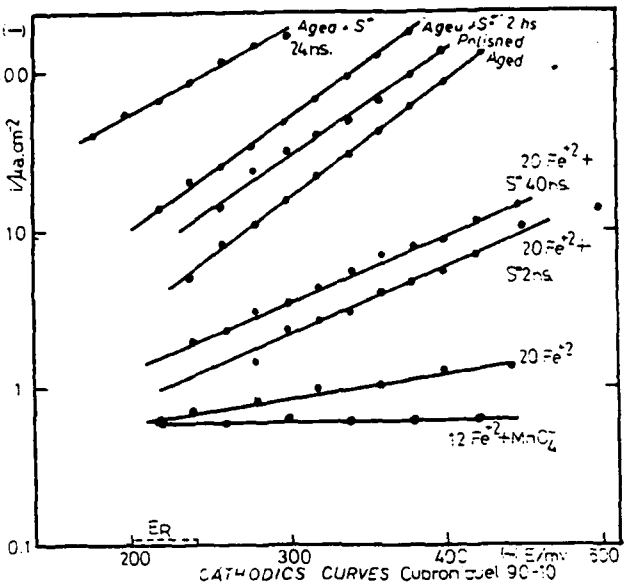
Aged + S=
24hs.
Aged + S= 2 hs
Polished
Aged
20 Fe+2 +
S= 40hs.
20 Fe+2 +
S= 2hs.
20 Fe+2
12 Fe+2 + MnO4-
100
10
1
0.1
i/μa.cm-2
ER
200
300
400
E/mv
CATHODICS CURVES Cupronickel 90-10

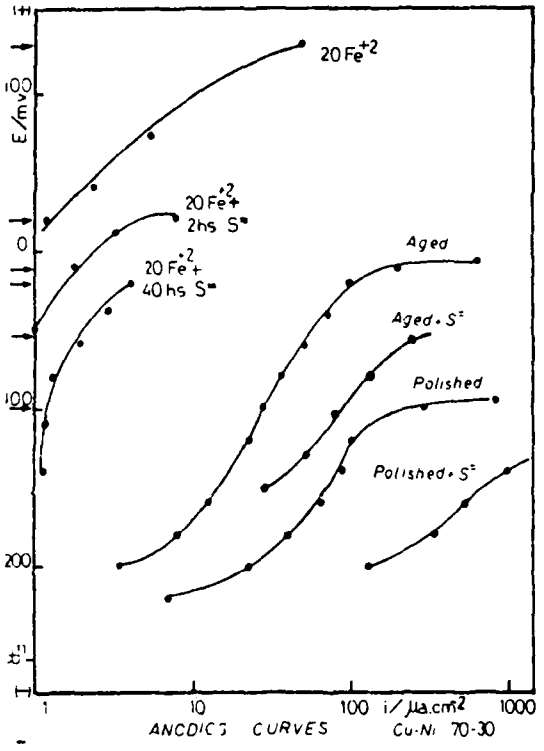
20 Fe+2
20 Fe+2 +
2hs S=
20 Fe+2 +
40 hs S=
Aged
Aged + S=
Polished
Polished + S=
E/mv
0
100
200
1
10
100
i/μa.cm2
1000
ANODICS CURVES Cu-Ni 70-30

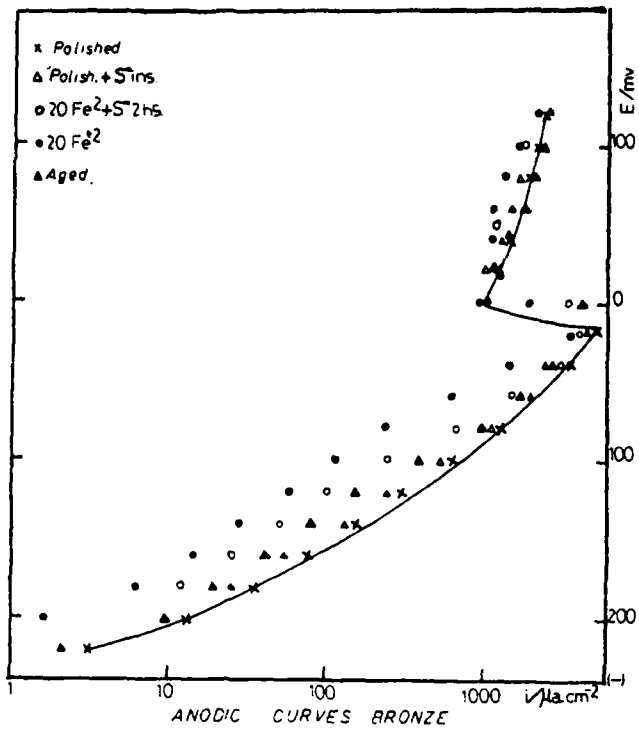

ANODIC CURVES BRONZE

06160

FACTOR CONTROLLING CORROSION RATE IN CONCRETE EMBEDDED REBARS

A. MOLINA*, C. ANDRADE**, M.C. ALONSO** and J.A. GONZALEZ*
* C.E.N.I.M., MADRID, SPAIN
** I.E.T. c.c., MADRID, SPAIN

INTRODUCTION

Usually, the diffusion of the atmospheric oxygen through the concrete, until the rebars, has been considered as the most significant controlling factor of the corrosion rate. However, some experimental data are presented in this paper which seem to show that this do not happen so, unless the concrete has been completely saturated in water, since in aireated concrete, the electrical resistivity seems to be the controlling factor.

MATERIALS AND EXPERIMENTAL TECHNIQUE

Prismatic mortar specimens were fabricated in size 2 x 5,5 x 8 cm. They were made with ordinary Portland Cement with a water/cement ratio of 0,5 and a cement/sand ratio of 1/3. They had embedded two identical steel bars of 6 mm diameter as working electrodes (duplicated experiment) and a central graphite bar as auxiliary. The saturated calomel electrode was used as reference.

The Polarization Resistance technique (Stern and Geary's method) as measurement technique of the corrosion intensity, was employed. A constant B value of 26 mV for the steel in active state and of 52 mV for the passive one, were used.

The specimens were held in a chamber with cyclic variation of the relative humidity: from 40 % RH to 100 % RH and viceversa every cicle lasting 100 days.

RESULTS

Figure 1 shows the evolution with time for the specimens containing 2 % $CaCl_2$ of the corrosion intensity of the rebars (1 a), the resistance measured by the possitive feed-back of the potentiostat (1 b), and the specimen weight variation (1 c) due to the variation of the humidity of the

chamber (the weight in the 40% RH atmosphere has been taken as weight level reference).

Figure 2 shows the same variables for the specimens without admixtures.

According with Gjørv results on the oxygen flux through mortar specimens[1] the limit intensity for the reduction of the oxygen on the rebar surface would be 0,2 $\mu A/cm^2$. This theoretical maximum is overcome in the present results for the $CaCl_2$ containing specimens for, at least, one order of magnitude. Moreover, the results show that the corrosion intensity increases when the humidity increases and if the oxygen diffusion had been the controlling factor, it would happen just the contrary.

By other hand, for specimens containing $CaCl_2$ comparing the trend of the corrosion intensity and the compensated resistance (ohmic drop), they are considered as symmetrical figures, therefore, the electrical resistivity that is, the facility for developping the anodic process control the corrosion rate.

In absence of admixtures (possivated steel) the corrosion intensity is independent of both the conductivity of the mortar and the oxygen diffusion (figure 2).

The very food correlation between corrosion intensity and compensated resistance in shown in figure 3. To explain corrosion intensities about ten times higher than the Gjørv values for the limit oxygen diffusion, either this limit is not of general applicability and serves only for specimens containing passivated reinforcements, or otner cathodic process is developping at the same time. In this last assumption the only possibility would be the reduction of the protons inside the pits.

REFERENCES

1. O. GJØRV, Ø. VENNESLAND, Cement and Concrete Research Institute. The Norwegian Institute of Technology, Report STF F 79069.

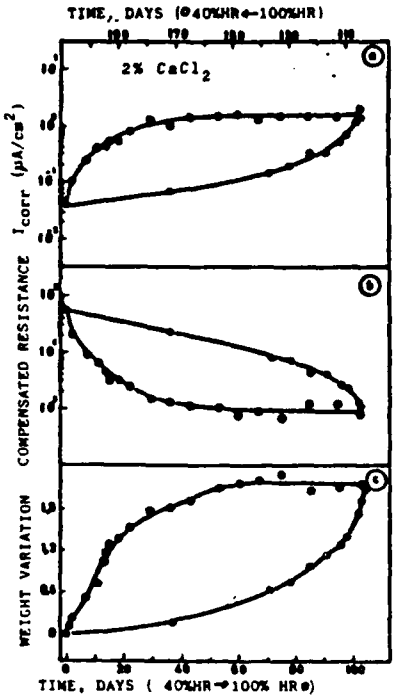

Fig. 1.- Behaviour of the steel embedded in $CaCl_2$ containing mortar following the humidity cycles.

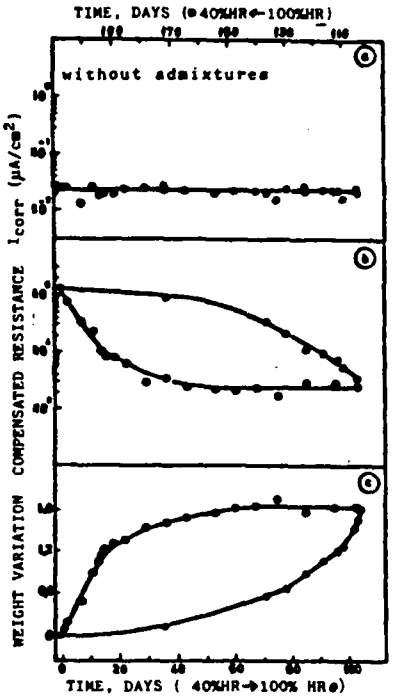

Fig. 2.- Behaviour of the steel embedded in mortar without admixtures following the humidity cycles.

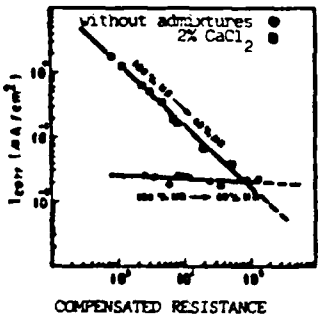

Fig. 3.- Relation between corrosion intensity and compensated resistance (possitive feed-back of the potentiostat) for reinforcements embedded in mortar with $CaCl_2$ and without admixtures.

06170

PITTING AND PROTECTION POTENTIAL OF 18/8 STAINLESS STEEL IN CHLORIDE SOLUTIONS. CATION AND DILUTION EFFECT.

J.J. ROYUELA
Centro Nacional de Investigaciones Metalurgicas. Madrid. Spain.

Nowadays there is a general agreement[1], on considering the pitting potential, E_c, related with susceptibility of stainless steels, to pitting corrosion in chloride environments. Pitting potential is the potential at which a sharp inflexion in the anodic polarization curve is observed.

The object of the present work is to know the critical pitting potentials, pitting and protection potentials, of a commercial 18/8 stainless steel in different chloride solutions.

Measurements were carried out from cyclic potentiodinamic anodic polarization curves, in quasi-stationary conditions, by changing the potential stepwise at a rate of 3 steps of 2 mV each every minute, till a current of about 3 mA $.cm^2$ is reached.

Analysed composition of the stainless steel was: Fe-18.1 Cr - 8.1 Ni - 1.30 Mn - 0,47 Mo - 0,35 Si - 0.050 C - 0.030 P - 0.005 S.

Solutions, 0.1 and 1.0 N, of NH_4^+, Na^+, Ca^{++}, Mg^{++}, K^+, Ni^{++}, Fe^{+++} and Cr^{+++} chlorides were used and test carried out in air saturation condition at 25±1ºC. Tests were performed with agitation of the solution, in the most of the cases, by means of a magnetic stirrer.

The preliminary steps, of the 12 mm diameter disk specimens, were: ground on 320 emery paper, cleaning in benzene and ethanol; mounting of the specimen in a fluorocarbon holder with a circular neoprene toric joint, to avoid leaks, and an adherent electric tape washer for diminishing the crevice corrosion risk, being limited the exposed area to 0.368 cm^2.

Different methods are used to find out the critical pitting potentials[2], but results for pitting potentials are uncertain in many occasions, and the sharp inflexion of the cyclic potentiodinamic anodic polarization curves, in our case, rarely is observed.

In Figs. 1-3 some polarization curves of 18/8 stainless steel in the solutions tested are plotted. In ordinate axis pitting potential, E_c and protection potential, Ep, in NH_4Cl, KCl and $CrCl_3$ 1N and 0.1N solutions are shown. The scan direction is indicated by arrows.

Chloride addition, as studied by Hoar and Jacob[3], has a response in current/time curves in the breakdown of passivity of stainless steel.

This may be the reason by which, in some cases, pitting is not observed after the cyclic polarization test; that is the case of NH_4^+, Na^+, Ca^{++}, and K^+ 1N and NH_4^+, Na^+ and Ca^{++}, 0.1 N chloride solutions.

The sweep rate, at which polarization tests were carried out, 360 mV/h, provide a quasi-stationary condition[4].

Typical hysteresis loop in cyclic potentiodinamic anodic polarization curves can be observed in the middle of the polarization range, between 0.2 and 0.8 volts, same for 1N as for 0.1N chloride solutions. See Fig. 1 to 3.

No hysteresis was observed in stagnant condition with Ca^{++}, Cr^{+++}, Na^+ and Mg^{++}, 1N chloride solutions. Only for 1N $NiCl_2$ solution this phenomenon was noted.

Attack was observed to initiate preferably at the electric tape washer-working electrode interface.

The scatter of the E_c results, from the different test solutions, was quite large: more than 200 mV in the case of 1N $NiCl_2$, same in stagnant as in agitation conditions. No correlation was observed between E_p and resulting corrosion; neither between open circuit potential, E_o, and corrosion effect. E_p has, in all the cases, a lower value than pitting potential. On the contrary a clear relation was noted between E_c-E_o and final corrosion. Smaller differences were observed for the higher localized corrosion (1N $FeCl_3$, $CrCl_3$ and 0.1N $FeCl_3$ solutions). Much more higher differences were observed in stagnant condition.

The higher localized corrosion was noted for the lower E_c-E_p values ($FeCl_3$, $CrCl_3$ and $MgCl_2$ 1N solutions).

At E_c, the values for c.d. was on the range 5 to 85 $\mu A.cm^2$, except in the case of 1N $FeCl_3$ that was higher.

The inverse of polarization resistance Rp^{-1}, gives values of about $10^{-5}\Omega^{-1}$ cm^{-2} for NH_4^+, Mg^{++}, Ca^{++} and K^+ 1N chloride solutions and higher values for Na^+, Ni^{++}, Cr^{+++} and Fe^{+++} ones (2.3×10^{-5}, 1.4×10^{-4}, 9×10^{-4} and $6 \times 10^{-2}\Omega^{-1}$ cm^{-2}, respectively). Lower values are found for stagnant condition and for 0.1N solutions.

References

1 B.E. Wilde and E. Williams. Electrochim. Acta, 16 (1971) 1971.

2 Z. Szklarska-Smialowska. Corros. Sci., 11 (1971) 901.

3 T.P. Hoar and W.R. Jacob. Nature, 216 (1967) 1299.

4 G. Hersleb and W. Schwenk. Corros. Sci., 9 (1969) 615.

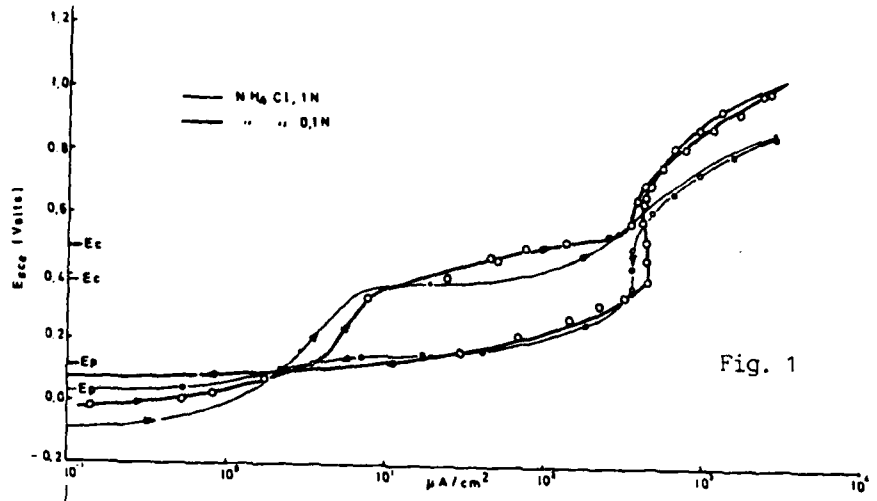

Fig. 1

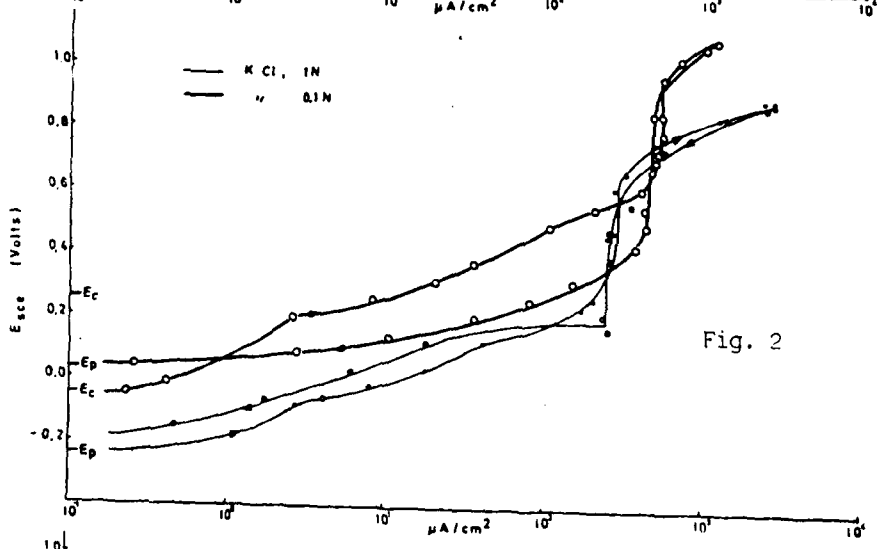

Fig. 2

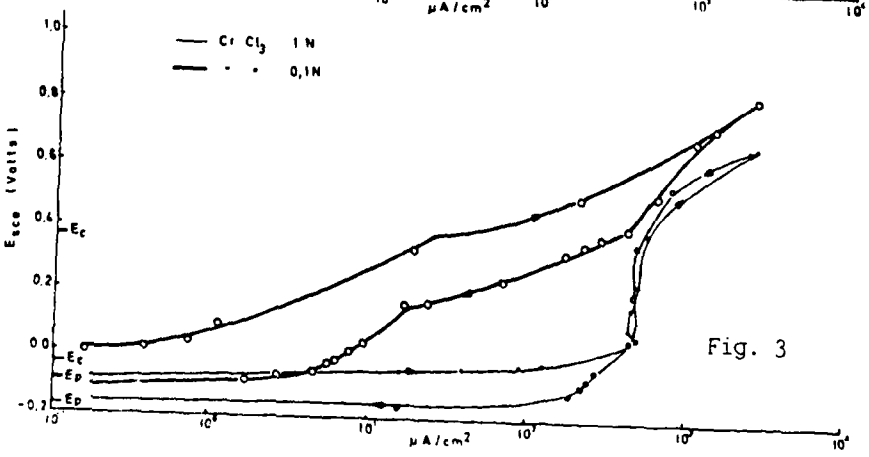

Fig. 3

Cyclic potentiodinamic anodic polarization curves.

06180

INVESTIGATION OF THE PROPERTIES OF OXIDE LAYERS FORMED ON ALUMINIUM AND ACTION OF CITRATE AND CHLORIDE IONS ON THE OXIDE BY THE POTENTIODYNAMIC METHOD

M.ERGUN and S.ONERI

Faculty of Science, Ankara University

Anodic oxide films may be of two types, barrier and porous, depending on the electrolyte in which they are formed. The structure of the oxide formed anodically in any electrolyte, were tried to be determined either,by the use of potential-time curves[1] obtained by the galvanostatic method or current-time curves[2] obtained potentiostatically and electron micrographs[3,4,5]. The current-potential curves were seldom used in the investigation of the structure of the oxide films. These curves were obtained for the investigation of the evolution of hydrogen and oxygen rather than the oxide structure. In our previous investigations[6,7] the structure of the oxide film was investigated between the region ∓ 4.5 V by potentiodynamic method.

The purpose of this study was mainly, the determination of the structure of anodic oxide film by obtaining current-potential curves between corrosion potential and about + 10 V.

The working electrodes were prepared from 1.5x35x0.05 (cm) aluminium sheets with % 99.5 Al (0.40 Fe : 0.25 Si : 0.1 S wt %). Exposed area of the electrodes was about 1.0-2.0 cm^2 and the other parts were lacquered.

The current-potential curves were obtained both in the electrolytes which are known to form barrier film, 0.1 M sodium phosphate, 0.1 M sodium tartarate, 0.1 sodium tetraborate 0.1 M sodium citrate and in the electrolytes known to form porous film, 0.02 M sulfuric acid (pH 2.2), 0.1 M chromic acid (pH 0.9) and 0.1 M sodium sulphate, by the potentiodynamic method at a sweep rate of 300 mV/min. The pH of barrier layer forming electrolytes were adjusted to 9.0 with NaOH.

It can be seen from the potential-current curves illustrated in Fig 1, the type of the oxide film formed on aluminium in any anodizing solution, whether it is porous (Fig.1 a) or barrier (fig.1 b) could be determined from the analysis of these curves. + 1.3 V and about + 7 potential values were

observed as repeating characteristic values on current-potential curves in the formation of aluminium oxide. The first potential (1.3 V) value was independent on the pH value and as this potential is the potential at which oxygen evolution occured, nascent oxygen atoms make the oxide formation and pore initiation easier. The potential value of 7 V seems to be the potential at which the pore diameter and film growth rate has increased. Sulfuric acid has the lowest steady-state growth potential[8] amoung the electrolytes which had the solvent action on the aluminium oxide, namely sulfuric acid, chromic acid and sodium sulphate. The current increase observed at about 2.5 V on the current-potential curve obtained in sulfuric acid, might show that the pore diameter became larger at lower potential values in the sulfuric acid than the chromic acid solution. It was found in this study that $NaHCO_3$ which was not used as anodizing electrolyte till now has supported the growth of barrier film (Fig 1 b-1).

When various amounts of sodium citrate were added to porous film forming electrolytes, 0.1 M Na_2SO_4 (pH 8 and 9) solutions, it was found that the current values decreased as the amounts of sodium citrate increased. In SO_4^{2-} containing electrolytes, the presence of enough citrate ions might cause transition from the porous film growth to barrier film growth. This effect was observed when the $[Cit^{3-}]$ / $[SO_4^{2-}]$ ratio was equal to two for the polarization curves obtained with the electrodes waited in the test solutions and to one for those obtained with the electrodes which were not waited in the test solutions.

Further, the effect of chloride ions in the media containing citrate ion, was investigated. In these media for the fixed values of citrate concentration, varying amounts of Cl^- ions were added. Pitting potential (E_{pp}) and critical pitting potential (E_{cpp}) values were determined from current-potential curves obtained by potentiodynamic method at a sweep rate of 30 mV/min. The following linear relationships were found between E_{pp}, E_{cpp} and Cl^- ions concentration and the $[Cl^-]$ / $[Cit^{3-}]$ ratio.

$$E_{pp} = -0.740 - 0.176 \log[Cl^-]$$

$$E_{cpp} = -0.727 - 0.107 \log[Cl^-]$$

$$E_{pp} = -0.633 - 0.830 \log[Cl^-]/[Cit^{3-}]$$

$$E_{cpp} = -0.632 - 0.089 \log[Cl^-]/[Cit^{3-}]$$

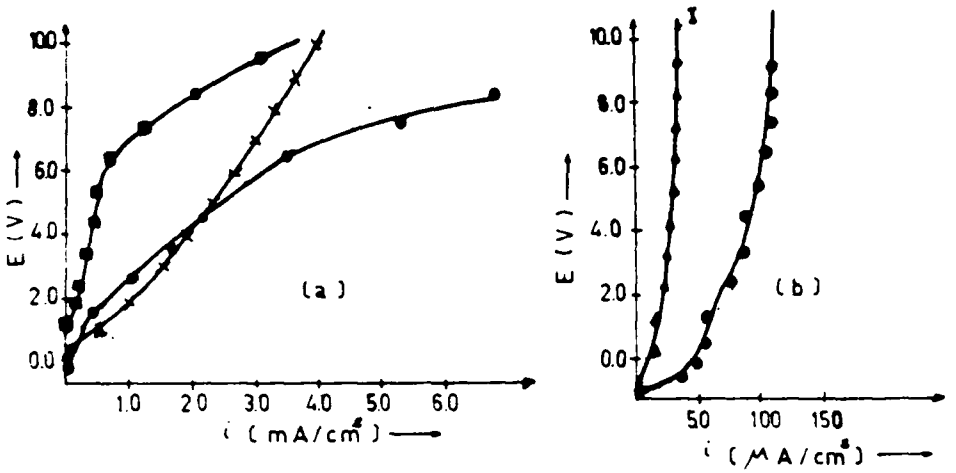

Fig.1. Polarization curves (a) forming the porous film in (■) 0.1 Na_2SO_4, (●) 0.02 M H_2SO_4 and (x) 0.1 M chromic acid and (b) forming barrier film in (▲) 0.1 M $NaHCO_3$ and (●) 0.1 M sodium citrate solutions.

REFERENCES

1. T.P.Hoar and J.Yahalom, J.Elec.Soc. 110, 614, (1963).
2. N.P.Fedot'ev and S.Ya.Grilikes,Electropolishing. Anodizing and Electrolitic Pickling of Metals p.199 Robert Drapes Ltd.Teddington,(1959).
3. M.S.Hunter and P.Fowle, J.Elec.Soc. 101,481, (1954).
4. F.Keller, M.S.Hunter and D.L.Robinson, J.Elec.Soc. 100,411 (1953).
5. J.P.O' Sullivan and G.C.Wood, Proc.Roy. A 317,511 (1970).
6. S.Oneri and M.Erbil, Chim.Acta.Turc. 6,143 (1978).
7. S.Oneri and M.Erbil, Chim.Acta.Turc. 6,199 (1978).
8. Mars Fontana and Roger W.Staehle, Advances in Corrosion Science and Technology Plenum, Press, London (1970).

06190

THE EFFECT OF SO_4^{2-} ON THE KINETICS OF THE ANODIC OXIDATION OF COPPER

Inês T.E. FONSECA and Ana C.S. MARIN
CECUL, R. da Escola Politécnica, 58, 1294 Lisboa Codex (Portugal)

Many studies can be found in the literature on the oxidation of copper in alkaline medium, however very little has been done concerning to the effects of SO_4^{2-}.

Our studies have demonstrated that the electrochemical response of a copper electrode in alkaline medium depends extremely on the conditions of oxidation i.e., electrode pretreatment and potential profile applied. Such effects have also been reported recently by Arvia et col[1,2]. Thus, a standard electrode pretreatment was established and strictly maintained during experiments[3].

The effect of SO_4^{2-} on the electrochemical oxidation of copper in aqueous medium at pHs of 12.8, 9.5, 6.9 and 5.9 was studied mainly by cyclic voltammetry, at different values of sweep rates ($50 < v < 200$ mV s^{-1}) different limits of potentials, and by holding the electrode at certain values of potential, during different time intervals.

Figure 1 shows some of the results obtained for the system Cu/x M Na_2SO_4 at pHs of 5.9, 6.9 and 9.5.

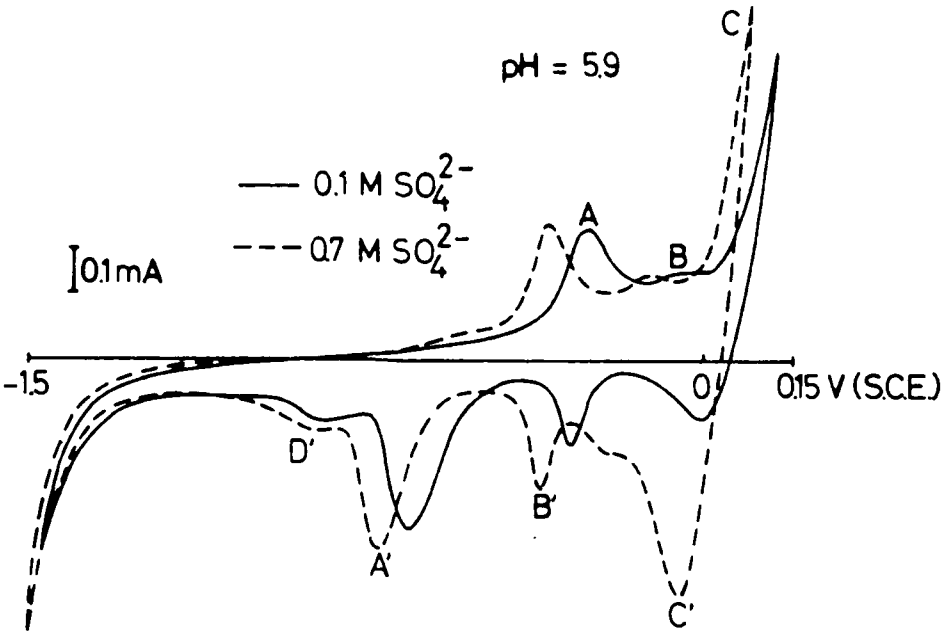

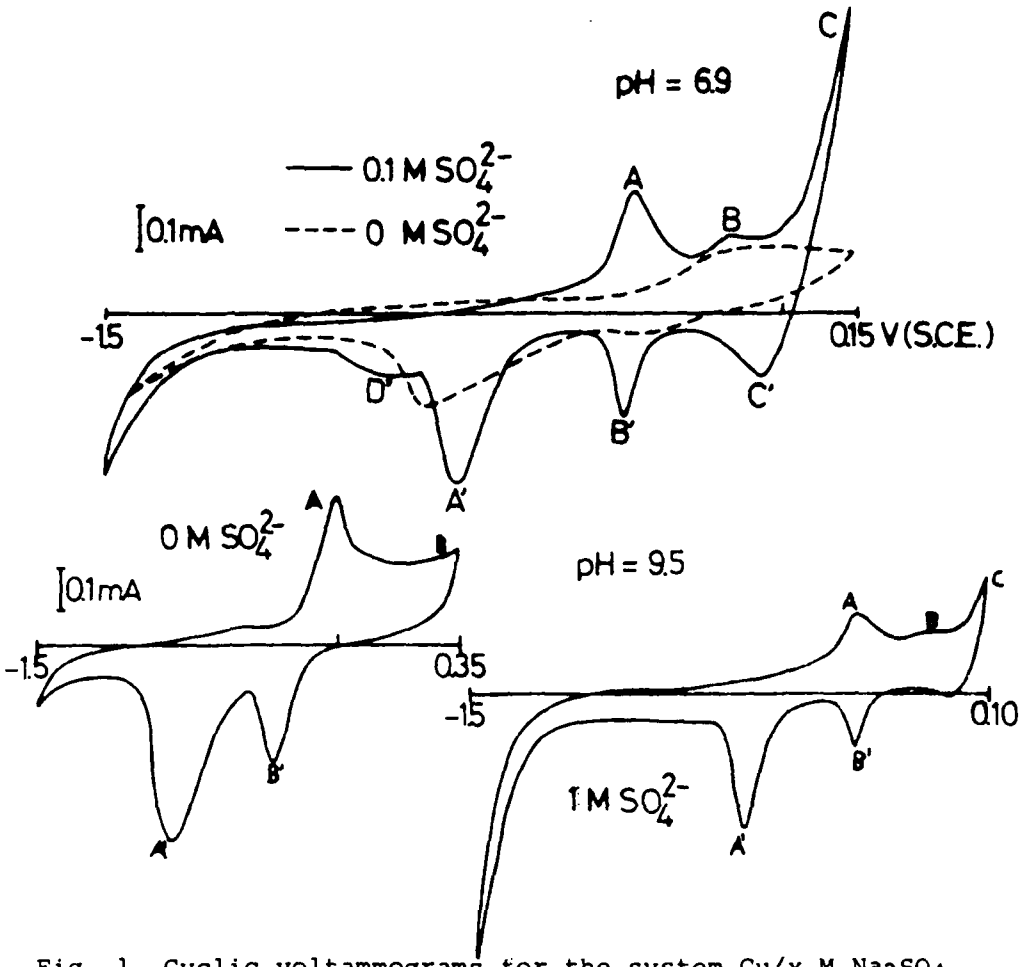

Fig. 1. Cyclic voltammograms for the system Cu/x M Na_2SO_4 at pHs 5.9, 6.9 and 9.5. v = 0.1 V s^{-1}. Ag = 0.264 cm^2.

Results on fig. 1 indicate some special features due to the presence of SO_4^{2-}, e.g.:

i) Promotion of corrosion, both in terms of potential and charges. Moreover, the charge associated to peaks A and B increases when concentration in SO_4^{2-} increases.

ii) The passivity due to the film of $Cu(OH)_2/CuO$ (region B-C) is destroyed at much lower values of potential in the presence of SO_4^{2-}. Consequently, the rate of copper corrosion increases drastically, as shown by the steep increase in current at E ≃ 0 V, followed by the cathodic peak C'.

iii) All reduction peaks are displaced to more negative potentials and an additional peak D' is observed, in the presence of SO_4^{2-}.

The analysis of peak currents, peak potentials and charges as a function of sweep-rate, for each system, was made. The results of such analysis are summarized in table 1.

TABLE 1. Analysis of potential and peak currents as a function of sweep-rate.

pH	E_p^A / V	$\partial \log I_p^A / \partial \log v$	$[SO_4^{2-}]$ / M	E_p^B / V	$\partial \log I_p^B / \partial \log v$
5.9	-0.15 - 0.066 log v	0.55	0.01	-----	0.50
	-0.29	0.72	0.1	-0.09	0.78
	-0.32	0.67	1	-0.12	0.75
6.9	-0.047 - 0.15 log v	0.63	0.01	-----	0.67
	-0.36	0.70	0.1	-0.12	0.75
	-0.32	0.71	1	-0.13	0.71
9.5	-0.032 - 0.13 log v	0.49	0	-----	0.62
	-0.32	0.79	0.1	-0.11	0.71
	-0.31	0.70	1	-0.10	0.73
12.8	-0.36 + 0.033 log v	0.54	0	-0.09+0.033log v -0.05+0.067log v	0.43
	-0.39 + 0.033 log v	0.55	0.1	-0.17+0.033log v	0.52
	-0.36	0.66	1	-0.16	0.80

The relationships obtained between the peak currents and scanning rate indicate that while in the absence of SO_4^{2-} the kinetics of peaks A and B are under diffusion control, in the presence of SO_4^{2-} they change to a mixed control by diffusion ($I_p \alpha v^{1/2}$) and by any surface process ($I_p \alpha v^1$). But, the independence on sweep-rate shown by peak potentials and peak charges, tell us that such controlling surface process is more likely an adsorption process.

Results on table 1 show also that the amount of SO_4^{2-} to produce such changes in kinetics is a function of pH. In fact, while at pH 9.5 $[SO_4^{2-}] < 0.1M$ produce the observed deviations at pH12.8 only $[SO_4^{2-}] > 0.5M$ do so.

The observed results were interpreted as a consequence of the reduction of the activation energy of the electrochemical processes through the sulphate ions, strongly adsorbed on the anodic areas. Quantitative data suggest the direct participation of OH^- and SO_4^{2-} in the elementary steps of the role process.

REFERENCES

1. M.R. Chialvo, S.L. Marchiano, A.J. Arvia, J. Appl. Electrochem. 14 (1984) 165.

2. M.E. Martins and A.J. Arvia, J. of Electroanal. Chem., 165 (1984) 135.

3. I. Fonseca and A. Marin, Port. Electrochim. Acta, (submitted 1984).

06200

PHOTOELECTROCHEMICAL INVESTIGATIONS OF PASSIVE FILMS ON TITANIUM ELECTRODES

K.Leitner, J.W.Schultze
Institute of Physical Chemistry (II)
University of Duesseldorf, 4000 Duesseldorf 1, F.R.G.
and
U.Stimming
Department of Chemical Engineering and Applied Chemistry,
Columbia University, New York, New York 10027, U.S.A.

Introduction

Passive films on metal electrodes are usually formed of the corresponding metal oxides which show semiconducting or insulating properties. For in-situ investigations of the passive film, photoelectrochemical techniques offer the possibility of characterizing the passive film with respect to its solid state properties. In particular, the observation of differences between the behavior of passive films and the corresponding bulk oxides allows for a more detailed analysis. Recent work with amorphous oxides /1/ and model calculations which were carried out for the photoinduced electron transfer in disordered materials /2/ demonstrate that the photoelectrochemical behavior of crystalline and amorphous compounds is quite different in various aspects. For passive films on titanium a change from the amorphous to crystalline state with formation potential of the film was found from electron diffraction /3/. So it seems interesting if such findings can be correlated with photoelectrochemical data. Previous work on photoelectrochemical behavior of passivated titanium electrodes /4,5/ demonstrated TiO_2 properties of thick films, however, breakdown phenomena of the film are also reflected in the results. For very thin films a strong influence of the electric field in the film and a band gap higher than in TiO_2 has been found /4/.

Experiments were carried with passive films of appr. 5-200 nm thickness. Photocurrents were measured as a function of the wavelength of the incident light and the electrode potential. Aging effects on photocurrent spectra and the potential dependence were carried out as well.

Experimental

Passive films were formed in 1M H_2SO_4 at various potentials U_{ox} = 4V to 105 V. The formation time was generally 5 min.; aging was performed at U_{ox}-1V for up to 21h. Photocurrent measurements were carried out in the same electrolyte with a monochromatic light source consisting of a 450 W Xe lamp and a monochromator. Spectra were recorded in the 200-800 nm range; the potential dependence of the photocurrent was measured between U = 0-1.8 V (SHE). Photocurrents were transformed into quantum efficiencies with respect to incident light.

Results and Discussion

Photocurrent spectra are shown in Fig.1 for various formation potentials, U_{ox}, of the passive film. At low U_{ox} a steady increase of the quantum efficiency with the photon energy, hν, is observed. For U_{ox} = 26V a shoulder develops at appr. 4eV which becomes a pronounced peak at 3.8eV for U_{ox} = 56V. For thick films which are represented by the film formed at 105 V this peak

disappears again. The four examples shown in Fig.1 are representative of four different types of behavior. Please note that the curves for 26 and 56 V are enhanced by a factor of five. Over a wide range of hν and especially at higher hν, the quantum efficiency, η, is higher for thin films compared to films of intermediate thickness.

Typical quantum efficiency-potential curves are given in Fig.2 for films formed at 13 and 105 V. Thick films show a limiting current for hν=5.2eV while for lower hν the quantum efficiency still increases with U up to 1.8V, although from U=0.8V on the potential influence is weaker than at low potentials. Thin films have a much stronger potential dependence. The shape for 5.2 eV is similar to that at thicker films for lower photon energies. At 3.2 eV, however, the potential dependence becomes exponential-like indicating a strong influence of the electric field in the passive film.

Aging of the film was done in the electrolyte under potentiostatic control. In general, photocurrents increased upon aging, for longer times also changes of spectral and potential characteristics are observed.

A detailed analysis of the absorption edge shows that band gap energies which were determined from $(\eta \cdot h\nu)^{1/2}$ vs. hν plots has a value of E_g^i of appr. 3.3 eV decreasing slightly to 3.2 eV for thick layers. This band gap value corresponds to indirect transitions in crystalline semiconductors; linearity is also observed with amorphous semiconductors, but reflects rather the density of state function close to the band edges. So-called direct band gaps which are obtained from $(\eta \cdot h\nu)^2$ vs. hν plots can not be observed for films formed at U_{ox}=20 V or less. For high U_{ox}, E_g^d first decreases from 3.7 eV to 3.5 (at U_{ox}=30 V) and then stays constant up to very thick films. This indicates that films formed below 20V are amorphous. This assumption is confirmed by an analysis of the potential dependence of the photocurrent. The strong potential influence found for low hν and thin films (see Fig.2) turns out to follow a Poole-Frenkel behavior which is typical for amorphous semiconductors, as well /1,2/.

The investigations demonstrate that photoelectrochemical measurements are able to determine important solid state properties of passive films under in-situ conditions. At the same time it allows for a distinction between the amorphous and crystalline state of the surface film.

References

/1/ B.Danzfuss and U.Stimming, J.Electroanal.Chem. 164 (1984) 89
/2/ U.Stimming and A.R.Newmark, Proceedings of TELAVI '84 Conference, Telavi U.S.S.R., in press
/3/ L.Assov, M.Froelicher, M.Froment and A.Hugot-Le Goff, J.Chim.Phys. 72, (1975) 275
/4/ J.W.Schultze, U.Stimming and J.Weise, Ber.Bunsenges.Phys.Chem. 86 (1982) 276
/5/ see ref. 24-27 in /4/

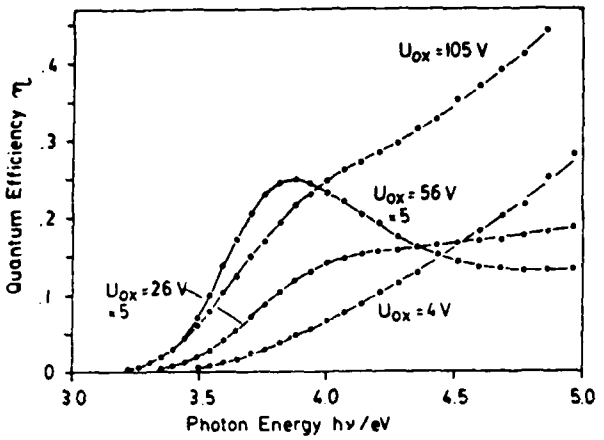

Fig.1 Photocurrent spectra recorded at U = 1.5V for passive films formed at various potentials U_{ox}

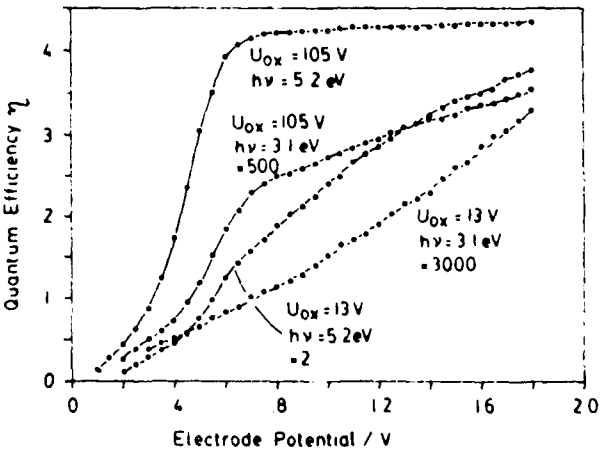

Fig.2 Potential dependence of the quantum efficiency, η, for a thin (U_{ox} = 13V) and a thick (U_{ox} = 105V) film.

06210

APPROXIMATE EQUATIONS FOR THE CONSTANT VOLTAGE STAGE OF THE ANODIC OXIDATION

J.M. ALBELLA, I. MONTERO and O. SANCHEZ-GARRIDO
Instituto de Física del Estado Sólido, CSIC and
Departamento de Física Aplicada, Universidad
Autónoma. Cantoblanco. Madrid 28049 (Spain)

The anodic oxidation of valve-metals, such as Ta, Al, Ti, etc. is usually carried out in a two-stage process in which galvanostatic and potentiostatic conditions are succesively imposed during oxide formation. In the potentiostatic mode there exists a continous decrease of the ionic forming current as a consequence of the film thickness growth. The thickness increase in this stage may amount up to more than 10% of the thickness obtained in the galvanostatic mode. In addition, the constant voltage stage is supposed to be critical in determining the final oxide quality. Despite its technological and fundamental interest, the constant voltage stage of anodization has received little attention in the literature and only scarce data has been published[1].

In this communication approximate relations for the time variation of the anodization ionic current, the thickness growth and the electric field during the constant current stage of anodization will be derived. These relations can be obtained by integration of the differential equation which regulates the potentiostatic process, i.e. the Faraday Law $dx/dt = Ki(t)$, where dx/dt expresses the time derivative of the thickness x, K is a constant which accounts for the charge to mass conversion and $i(t)$ is the instant ionic current density. This last magnitude is given by $i(t) = i_1\{\exp BE(t)\}$ with i_1 and B constants and $E(t)$ the anodization electric field.

Under the condition that the thickness grown in the constant voltage stage (potentiostatic mode), $x(t)$, is a small fraction of the thickness grown at constant current (galvanostatic mode), x_o, that is $x(t)/x_o \ll 1$, it is possible to obtain an approximate solution for the above differential equation. It will be shown that the final equation for the variation of the thickness with time obtained under this approximation is:

$$x(t) = \frac{x_o}{BE_o}\left\{\ln\left(\frac{BE_o t}{t_o} + 1\right)\right\} \qquad (1)$$

In this equation t is time elapsed from the switching to the potentiostatic mode and t_o is the time consummed in the galvanostatic mode.

Similarly, the anodization electric field E(t) and the ionic current density, i(t), are given by the approximate equations:

$$E(t) \approx \frac{E_o}{1 + \{\ln(BE_o t/t_o + 1)\}/BE_o} \qquad (2)$$

$$i(t) \approx \frac{i_o}{BE_o t/t_o + 1} \qquad (3)$$

where E_o and i_o are, respectively, the anodization electric field and the current density imposed during the galvanostatic conditions.

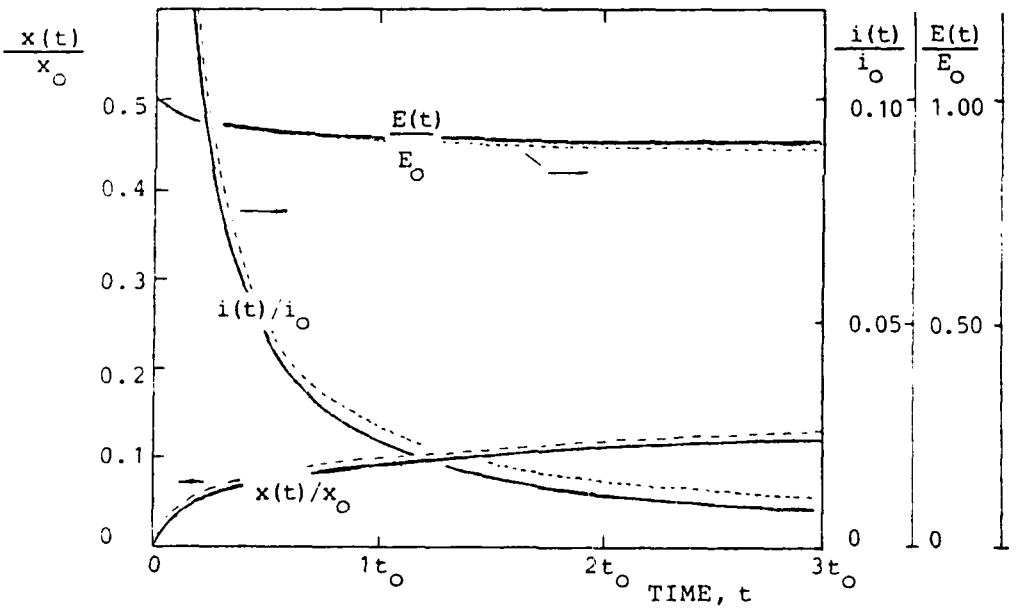

Fig. 1.- Calculated variation of the normalized thickness, x/x_o, ionic current density, i/i_o, and anodization electric field, E/E_o, as a function of the time, for $BE_o = 40$. The broken lines represent the exact values.

From the equations (1-3) it is evident that the normalized values x/x_o, E/E_o and i/i_o only depend on the normalized time t/t_o. This fact allows to calculate theoretically the variation of the above magnitudes for given experimental conditions of anodization. Fig. 1 shows a plot of the normalized thickness, current density and electric field for a value of the product $BE_o = 40$. This is a typical value for tantalum anodization. The broken lines in this figure represent the exact values obtained by numerical methods of integration of the differential equation. It is observed a good agreement between the approximate and the exact values for the thickness and the electric field. Tha calculated error of the total thickness, $x + x_o$, is less than 1% in the range of time $t/t_o < 3$ for the example given above. Due to the exponential dependence of the ionic current density on the anodization electric field the error introduced in the current density by the approximate equation (3) may amount up to 17% for long periods of anodization in the potentiostatic conditions, i.e. for $t/t_o > 3$.

Equation (3) is formally identical to the equation previously obtained by Dreiner[2] using a more restrictive approximation: $x(t) \cong 0$. Obviously, this condition also implies $E(t) \cong E_o$, in contrast to the equations (1) and (2). Furthermore, the use of the normalized variables introduced in this work eliminates the voltage dependence in the current equation given by Dreiner.

References

1. C.J. Dell'Oca, D.L. Pulfrey and L. Young, in "Physics of the Thin Film", pag. 1. Academic Press, N.Y. 1971.

2. R. Dreiner, J. Electrochem. Soc., 111, 1350 (1964).

06220

THE EFFECT OF THE FUNCTIONAL GROUPS IN THE INHIBITOR MOLECULE UPON ITS PROTECTIVE EFFICIENCY

S.Raicheva,E.Sokolova,R.Gulamali
Institute of Chemical Technology, 1156 Sofia,Bulgaria

In a previous paper of ours (1) the effect of the length and the type of the carbon chain in the inhibitor molecule upon its protective efficiency was studied.In the present paper the effect of the functional groups, their type and position in the molecule chain upon the inhibitor protective efficiency is disscussed.

Generally the investigators (2) find a rise in the inhibiting effect with the increase of the number of the functional groups; an explanation of the fact is made assuming these groups to act as adsorption centers.

According to the chemical structure of the functional groups the literature data are as follows: sulpher-containing inhibitors rise the protection,methyl groups lead to its decrease the halogen groups influence it.Atomatic radicals are on the whole more effective than the amine groups, due to the forming of surface complexes with protective efficiency.

The following dependencies according to the place of the functional group in the carbon chain are found.The protective efficiency in the case of branched carbon chain deminishes.The methyl group in o-position has a similar effect.Cis-amines are more effective inhibitors than trans-amines.The last is explained by the changed inhibitor adhesion,due to the different orientatin of its molecule on the metal surface.

Usually when aromatic cycles are get into the molecule the inhibiting effect rises although in some cases the opposite is observed.Benzyl radicals are often more effective than the phenyl radicals.

The inhibiting effect is greater in the case of complex bonds in the functional groups than in the case of simple bonds only.This accounts for the role played by the complex bonds as adsorption centers.The place of the complex bond is of importance as well;the most effective are the compounds with a triple bond at the end of the carbon chain.

The explanations of these experimental facts are usually made on the basis of sterical indrance, of some physical properties of the molecule and of the adsorption layer but mainly - of the chemical structure of the inhibitor, treated as an electron distribution in the molecule chain.

It must be underlined that the experimental data are not sufficient, in some cases even contradictory, which impedes their quantitative interpretation.Moreover the data are often obtained at uncomparable conditions.To this effect it is of interest to compare the protective efficiency of inhibitors distinguished by the number, type and place of the functional groups in the carbon chain keeping all the other experimental conditions constant.

The techniques used and the precise experimental conditions of our study are identical with these in (1)

A comparison is made of the inhibiting effect on steel of two heterocyclic compounds - piperazine (PIP) and morpholine (MOR). The difference in their structure is that in MOR a NH-group is substituted by an oxygen atom.This change decreases the protective efficiency very much - the corrosion current increases from 3.0×10^{-6} A/cm^2 to 5.2×10^{-6} A/cm^2; the corrosion rates estimated as weight loss - from 0.059 g/h.m^2 to 0.062 g/m^2.h .

Again on steel a comparison is made betewen ethyl amine (EA) and ethylendiamine (EDA).After the replacement of the second hydrogen atom by NH_2-group the inhibiting effect slightly slows down.The corrosion current rises respectively from 2.2×10^{-6} A/cm^2.h to 2.5×10^{-6} A/cm^2.h; the corrosion rate rises from 0.010 g/m^2.h to 0.025 g/m^2.h.

The data for EA are compared with these for monoethanol amine (MAA) - both on steel.When a hydrogen atom in the molecule of EA is replaced by a OH-group (in MAA) a decrease in the inhibiting effect is observed.The corrosion current rises from 2.2×10^{-6} to 5.0×10^{-6} A/cm^2.h and the corrosion rate - from 0.010 to 0.044 g/m^2.h.

The data for quinoline (QIN) and 8-hydroxyquinoline (OQI) are compared on copper.The replacement of one of the H-atoms by a OH-group shaply decreases the inhibiting effect.The corrosion current rises from 0.08×10^{-6} A/cm^2 (for QIN) to 7.00×10^{-6} A/cm^2 for OXI. This result is similar to that on steel , on which the replacement of a hydrogen atom by a OH-group also leads to a decrease of the inhibiting effect.

The comparison of OQI and 2-methyl-hydroxyquinoline (MOQ), distinguished by a methyl group only, on copper shows an increase of the inhibiting effect.The corrosion current decreases from 7.0×10^{-6} A/cm^2 to 6.0×10^{-5} A/cm^2.This stands in agreement with the authors (2) who show that with the increase of the number of the substituents the inhibiting effect grows up.There are however papers where the opposite is afirmed.

The results obtained on copper are somewhat in discrepance with the assumption of a compensation of the effect of the methyl-and the OH-group in MOQ on account of which the inhibiting effect is zero, i.e. the corrosion current is the same in solutions with and without inhibitors.This problem needs a further study.

The anodic and cathodic curves on steel are shown in Fig.1 in solution of Na_2SO_4 in the presence of inhibitor -the solid line - and in its absence -dashed line.A typical case is chosen - the protection by EDA.The corresponding curves on copper in KCl and QIN are shown in Fig.2.

Several kinetic parameters for the inhibitors studied on steel and copper are summerized in Tabl.1 and 2 respectively.

For a more detailed discussion of the data obtained for the effect of the length and the type of the chain, as well as the effect of the number,type and place of the functional groups a quantum mechanical treatement is done,which is the object of a next publication of ours.

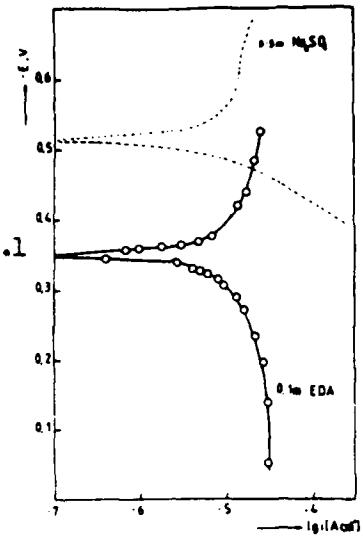

Fig.1

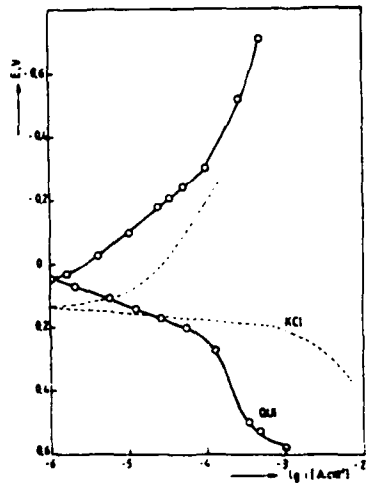

Fig.2

Table 1

Inhibitor	Corrosion current 10^{6} A/cm^2	Corrosion rate g/m^2.h	Tafel constants a_a	b_a	a_c	b_c	Corr. poten. V	Prot. z%
EA	2.2	0.010	0.427	0.075	-	-	-0.350	-
EDA	2.5	0.025	0.310	0.055	-	0.160	-0.350	72
MAA	5.0	0.044	0.428	0.080	-	0.125	-0.325	44
PIP	3.0	0.059	0.755	0.135	-	0.140	-0.360	-
MOR	5.2	0.062	0.575	0.110	-	0.135	-0.355	-
without	10.0	0.069	0.410	0.080	-	0.125	-0.500	

Table 2

Inhibitor	Corrosion current $x10^{6}$, A/cm^2	Corrosion rate g/m^2.h	Tafel constants a_a	b_a	a_c	b_c	Corr. Pot. V	Prot. z %
QUI	0.08	-	-	0.060	2.080	0.260	0.055	-
OQI	7.0	-	-	0.059	2.00	0.310	0.050	-
MOQ	6.0	-	-	0.100	2.30	0.400	-0.040	-
without	6.0	-	-	0.058	1.63	0.210	0.120	-

Literature
1.S.Raicheva,E.Sokolova,R.Gulamali,6thEuropean Symposium on Corrosion Inhibitors,Ferrara 1985.
2.V.Grygoriev,V.Ekilik,Chemical structure and inhibitor effect (1978).

06230

ELECTROCHEMICAL EVALUATION OF THE DEGREE OF SENSITIZATION CAUSED BY HEAT TREATMENTS ON COLD ROLLED AISI 304L

G. RONDELLI[+], T. PASTORE[*], B. VICENTINI [+]

(+) ITM-CNR - Cinisello B. (Italy)
(*) Dipartimento di Chimica Fisica Applicata, Centro di Studio del CNR sui Processi Elettrodici, Politecnico di Milano (Italy)

This work studies the influence of cold plastic deformation and of the possible formation of martensite on the susceptibility to intergranular corrosion (I.G.C.) of austenitic stainless steels.
This work studies the influence of cold plastic deformation and of the possible formation of martensite on the susceptibility to intergranular corrosion (I.G.C.) of austenitic stainless steels. The tests (Modified Strauss test, Oxalic Acid etch), were made on an AISI 304L steel, cold rolled to various reduction ratios at room temperature or at - 196°C and heat treated between 300 and 500°C. Furthermore, the applicability of the electrochemical potentiokinetic reactivation (EPR) test, performed according to Clarke procedure described in a previous paper(*), to determine the susceptibility of cold plastic-deformed materials to intergranular corrosion was verified.

The importance of cold plastic deformation on sensitization was recently brought to light since in practice all steels are somewhat deformed before, during or after heating to sensitizing temperatures. In any of these three cases, the susceptibility to intergranular corrosion may differ from that of undeformed steel.

The effect of cold plastic deformation, performed before or during the sensitizing treatment, can best be explained on the basis of the theory of chromium depletion, commonly accepted for underformed steel. Cold plastic deformation induces structural changes within the austenitic matrix, which help diffusion processes and chiefly chromium diffusion. Room temperature deformation essentially causes dislocation density to increase and deformation bands to form and develop. Consequently, when degree of deformation increases, the chromium-rich carbides nucleate and grow more rapidly and carbide precipitation inside the grain may occurs. Chromium rediffuses more rapidly in those areas that have been depleted by carbides precipitaion.

The deformation at -196°C causes α'- martensite to form. Its presence is not always considered although it also has a similar accelerating effect on the sensitization process due, among other things, to lower carbon solubility.
Some of our results are summarized in Fig. 1, Fig. 2 and Fig. 3. From these results the following conclusion can be drawn:

1. Cold rolling accelerates steel sensitization at temperatures ranging from 500 to 300°C. The effect is more pronounced when α'-martensite is formed.

(*) T. Pastore et al. 9th I.C.M.C. - Toronto, 1984; Volume 1, pp.461-

2. The etching morphology varies for rolled and sensitized test-pieces: etching occurs also or exclusively inside the grain.

3. The EPR test for non-rolled AISI 304L steel shows good correlation with the modified Strauss test; specifically, the sensitization threshold value of the normalized charge P_a = Q/GBA = 2 C/cm^2 (according to Clarke) is confirmed.

4. The EPR test on steel rolled at -196°C (high martensite-content) can also be correlated to the modified Strauss test. In this case, the circulated charge should not be normalized with respect to grain boundary area, since attack mostly occurs inside the grain in correspondence with the martensite or deformation bands, in areas the extension of which only depends on the deformation degree. Microstructural examinations and a comparison with the weight loss measurements during the modified Strauss test show the threshold value of the circulated charge during the EPR tests to be Q/A = 12.5 mC/cm^2. This value should indicate sensitization in materials having undergone a thermo-mechanical treatment similar to that of AISI 304L rolled by 10% at -196°C (martensite content = 26%).

5. The sensitivity of the weight loss measurement during the modified Strauss test on materials rolled at -196°C appears to be greater than that of the same test on non-rolled material, because of possible dropping of parts of grain (P.G.D.).

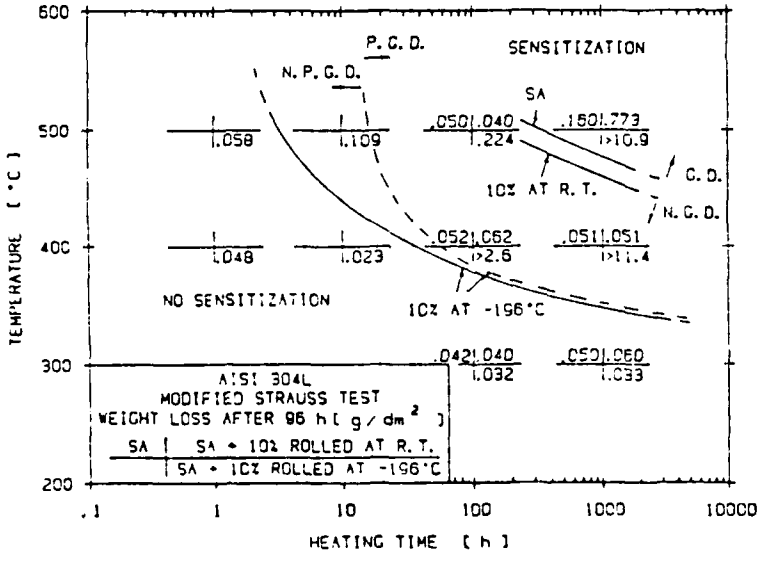

Fig. 1 - TTS curves for AISI 304L stainless steel cold rolled by 10% as a function of cold plastic deformation.

6. The EPR test is significantly affected by rolling mainly in the case of specimens deformed at room temperature and in the absence of sensitization. The circulating charge values obtained in these conditions are unusually high and very scattered. Therefore this fact must be carefully considered in view of the applicability of the EPR test to deformed steels, even starting from rolling ratios as low as 10%.

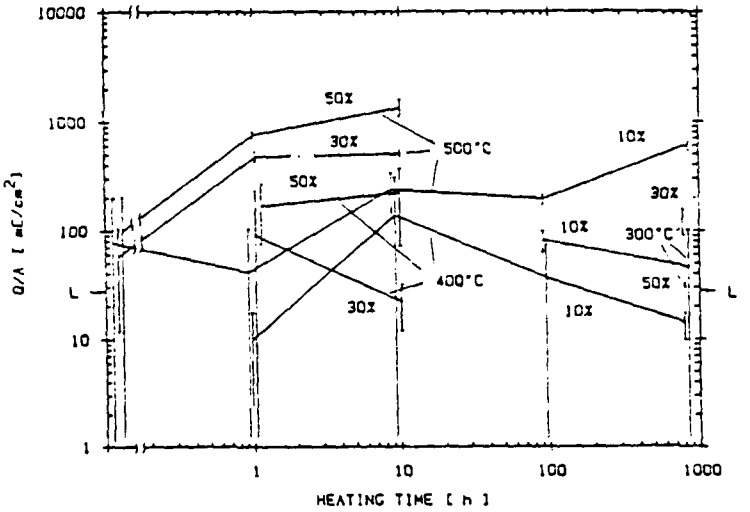

Fig. 2 - EPR test: specific anodic charge for AISI 304L cold rolled at room temperature as a fucntion of heat treatment condition. (L = Sensitization threshold value of specific anodic charge according to Clarke)

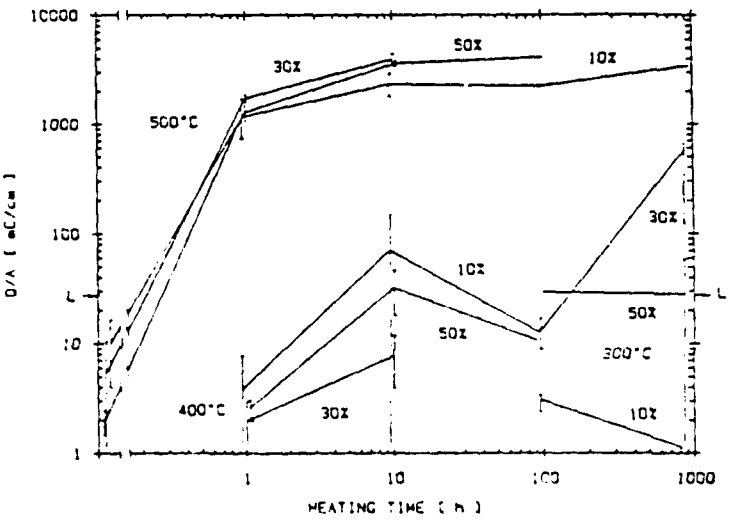

Fig. 3 - EPR test: specific anodic charge for AISI 304L cold rolled at -196°C as a function of heat treatment condition. (L = Sensitization threshold value of specific anodic charge according to Clarke).

06240

CORROSION OF NUCLEAR FUEL (UO_2) UNDER WASTE DISPOSAL VAULT CONDITIONS

D.W. SHOESMITH, S. SUNDER, M.G. BAILEY, G.J. WALLACE and L.H. JOHNSON
Atomic Energy of Canada Limited, Whiteshell Nuclear Research Establishment
Pinawa, Manitoba, Canada ROE 1LO

The rate of radionuclide release from irradiated nuclear fuel under nuclear waste disposal vault conditions will be determined, to a large extent, by the corrosion of the UO_2 matrix, since over 90% of the radionuclide inventory is located within the oxide grains. A large number of factors will exert an influence on the corrosion of UO_2 including redox conditions, groundwater composition, temperature, radiation effects, fuel/container interactions and physical effects such as fuel pellet erosion and break-up.

We have been studying the corrosion of UO_2 using a combination of electrochemical and surface analytical techniques, including X-ray photoelectron spectroscopy (XPS) and scanning electron microscopy (SEM). Our experiments have been performed on UO_2 electrodes fabricated from pieces of unirradiated fuel pellets[1-3]. Experimental and data analysis procedures have also been described previously[2,3].

We have studied both the anodic and cathodic corrosion reactions in some detail. In this communication we will summarize the results of our studies on the anodic reactions occurring on UO_2 under electrochemical conditions, and in the presence of oxidants, such as dissolved O_2 and H_2O_2, likely to be encountered in a nuclear waste vault. Some details on the cathodic processes occurring will also be given.

The following general scheme for the anodic process has been established[4,5]:

$$UO_2 \rightarrow UO_{2+x} \rightarrow UO_{2.33} \rightarrow UO_{2.5} \rightarrow UO_{2.67} \qquad (1)$$
$$UO_2^{2+} + UO_3.zH_2O$$

For neutral and alkaline solutions, the film growth process can be divided into two stages, the first (up to a composition of $UO_{2.33}$) occurring prior to the onset of uranyl-ion dissolution, and the second accompanying the dissolution process. The dissolution process can be represented by the reaction

$$UO_{2.33} + 0.33H^+ \rightarrow UO_2^{2+} + 0.33OH^- + 1.33e \qquad (2)$$

A different mechanism is observed in acid solutions (pH < 5.0), dissolution occurring via a uranyl-containing surface layer of undetermined composition.

In the presence of complexing anions such as carbonate and phosphate, which are likely to be encountered in groundwater, dissolution is accelerated and the phases $UO_{2.33}/UO_{2.67}/UO_3$ are not observed[6]. A precipitate of $UO_3.zH_2O$ is obtained at high anodic potentials ($\gtrsim$ +300 mV. vs. SCE)) under stagnant conditions. The insulating UO_3 layer is only obtained in alkaline solutions (pH $\gtrsim$ 12).

Under natural corrosion conditions in air- or oxygen-saturated solutions, surface oxidation proceeds only to the $UO_{2.33}$ stage. The transformation, $UO_2 \rightarrow UO_{2+x} \rightarrow UO_{2.33}$, occurs slowly at neutral pH values ($4 < pH < 10$), a film of approximately 6 ± 1 nm thickness being formed in ~ 8 hours. After ~ 24 h a steady-state corrosion potential is achieved. Under these conditions steady-state dissolution of UO_2 is occurring via reaction (2). The dependence of the corrosion potential on pH suggests that the corrosion process is controlled by the kinetics of the anodic reaction in solutions with $pH \geq 10$, but by the kinetics of the cathodic reduction of O_2 in the neutral pH range ($4 < pH < 10$).

The rate of the anodic film-formation process, $UO_2 \rightarrow UO_{2+x} \rightarrow UO_{2.33}$, in solutions containing H_2O_2 is ~ 200 times faster than in the presence of comparable concentrations of oxygen. This difference appears to be due to the involvement of hydroxide radicals in the case of H_2O_2 solutions. Under steady-state corrosion conditions the similarity between the corrosion potential of UO_2 and the potential of a Pt electrode in the same solution suggests a similar potential-determining reaction at both electrodes. This supports the claim that OH radicals are involved in the oxidation of UO_2.

Under steady-state conditions, at pH = 9.5, H_2O_2 decomposition appears to predominate over the dissolution of UO_2 for $[H_2O_2] \gtrsim 5 \times 10^{-2}$ mol.dm^{-3}. At higher H_2O_2 concentrations, UO_2 oxidation (to $UO_{2.5}$ and $UO_{2.67}$) and dissolution becomes more important and the hydrogen peroxide decomposition process less important. At more acidic pH values the corrosion potential becomes very positive and UO_2 attack more extensive. The corrosion process appears to be controlled by the kinetics of the anodic reaction over the whole pH range, $4 < pH \lesssim 12$, in contrast to the behaviour observed in dissolved oxygen.

References

1. L.H. Johnson, D.W. Shoesmith, G.E. Lunansky, M.G. Bailey and P.R. Tremaine; Nucl. Tech. 56, 238, 1982.
2. S. Sunder, D.W. Shoesmith, M.G. Bailey, F.W. Stanchell and N.S. McIntyre; J. Electroanal. Chem. 130, 163, 1981.
3. S. Sunder, D.W. Shoesmith, M.G. Bailey and G.J. Wallace; Proc. Int. Conf. Radioactive Waste Management, Winnipeg 1982, Canadian Nuclear Soc., Toronto, 1982, pp 398-405.
4. N.S. McIntyre, S. Sunder, D.W. Shoesmith and F.W. Stanchell; J. Vac. Sci. Technol. 18, 714, 1981.
5. S. Sunder, D.W. Shoesmith, M.G. Bailey and G.J. Wallace; J. Electroanal. Chem. 150, 217, 1983.
6. D.W. Shoesmith, S. Sunder, M.G. Bailey, G.J. Wallace and F.W. Stanchell; Applic. of Surf. Sci. 20, 39, 1984.

06250

"THE CORROSION OF MILD STEEL EVALUATED FROM DATA IN THE PRE-TAFEL AND TAFEL REGIONS"

C.M. Rangel, I.T. Fonseca, M.F. Reis
Laboratório Nacional de Engenharia e Tecnologia Industrial-LNETI- Paço do Lumiar,22
1600 Lisboa, Portugal
Centro de Electroquimica e Cinética das Universidades de Lisboa-CECUL- R. da Escola Politécnica, 56 - Lisboa, Portugal

The corrosion of mild steel in de-aerated acid sulphate solutions in the pH range from 0.3 to 4 was studied using potentiodynamic polarisation in the overpotential range that covers the pre-Tafel and Tafel regions.

Measurements were carried out at a scanning rate of 1 mV/sec. Agitation was introduced at two qualitative levels : Slow(S) and Rapid(R).

Fig 1 shows the polarisation resistance, R_p, of the system mild steel/1.0 N H_2SO_4 as a function of pH. R_p is observed to increase with agitation for values of pH less than 1 with a rapid fall after the maximum. Thereafter R_p appears to be independent of agitation.

Two well defined linear regions were found in the Tafel domain irrespective of pH and agitation, values of the order of 0.080 V were associated to lower overpotentials whilst at higher overpotentials b_a values of 0.030-0.040 V were observed.

Fitting of the polarisation curves in the pre-Tafel region using Mansfeld's method(1) generated theoretical curves that compared well with those obtained experimentally. The b_a values used to produce such result correspond to those found in the lower overpotential region(η =60-100mV). Values of b_a of the same order of magnitude(0.080-0.100 mV) has been associated to higher overpotential regions in the case of ClO_4^- and SO_4^{2-} in the presence of Cl^- or Br^- (2)

At adequately positive potentials(η > 100 mV) the anodic Tafel slope presents values of 0.030-0.040 V according to pH, that can be associated to a Bockris or Heusler type of mechanism(3).

A good correlation between R_p and i_{corr} is shown in Fig 2. The corrosion current density values were obtained using experimental values of b_a(those in the "lower Tafel region) and b_c.

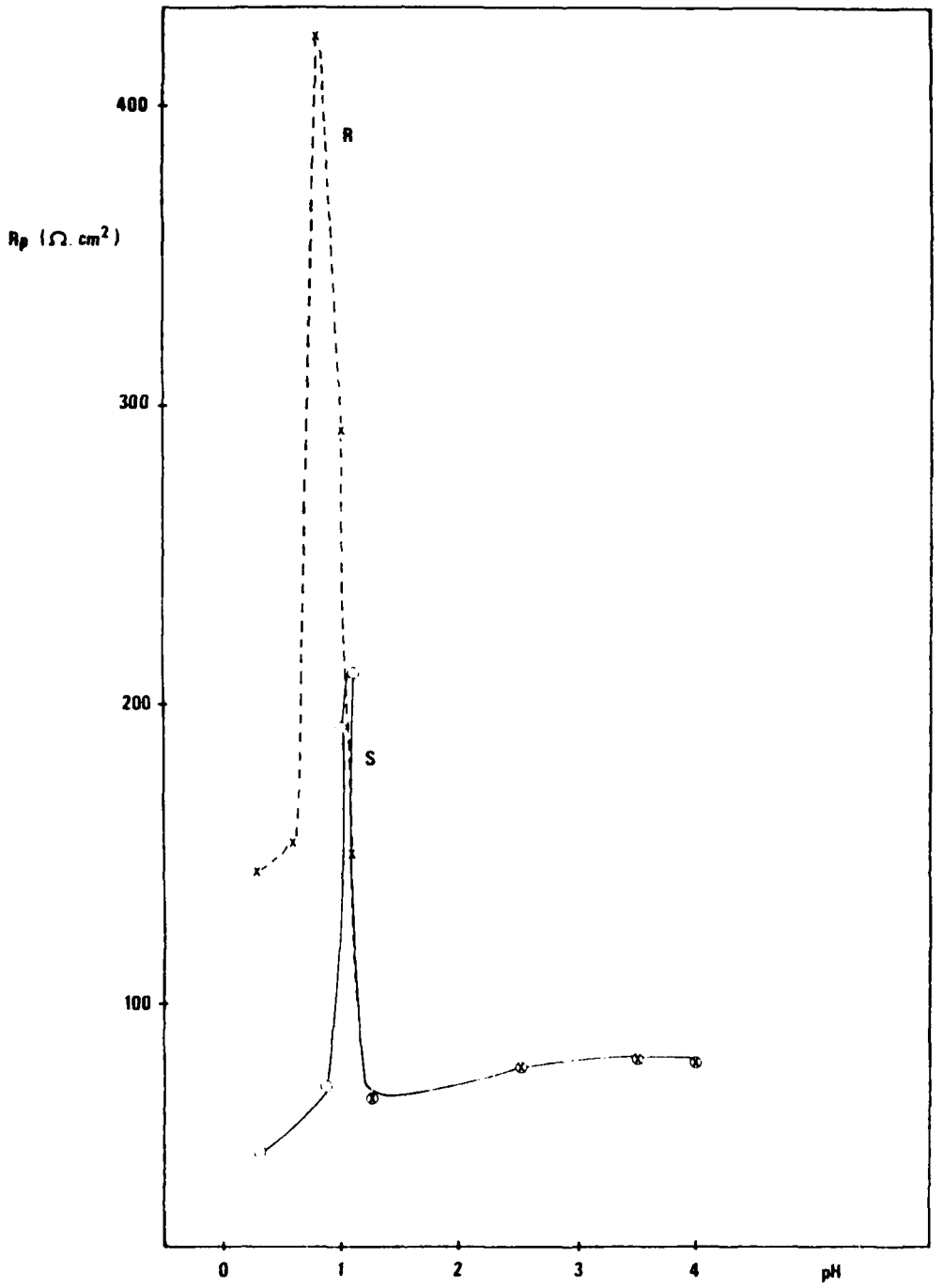

Figura 1 - The effect of pH on the polarisation resistance, Rp, for mild steel in 1.0 N H_2SO_4. Data correspond to Slow (S) and Rapid (R) agitation and 3 hours exposure time

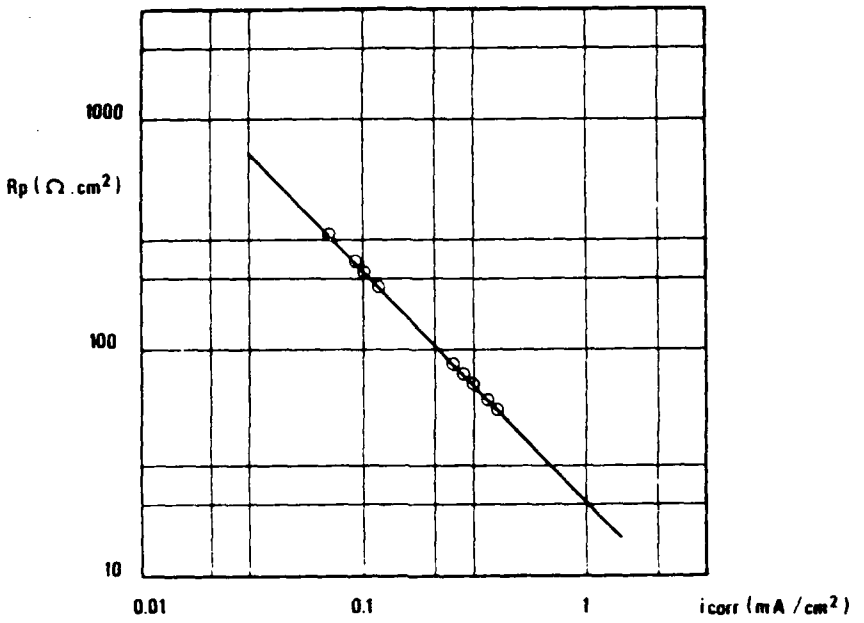

Figura 2 - The polarisation resistance, Rp, and the corrosion current density, icorr, found using ba values from the "lower Tafel region"

The work presented here shows that the anodic dissolution of mild steel in acid sulphate solutions takes place via two separate reactions that are gradually displaced as the potential is increased giving place to a change in mechanism.

It is thought that at lower overpotentials the reduction products of sulphate containing ions (4) participate in the acceleration of the corrosion process and that for pH≤1 an increase in agitation is associated with a decrease of such effect.

Acknowledgement

This work is partially financed by JNICT under Research Contract no. 510.83.87.

References

(1) F. Mansfeld, "The polarisation resistance technique for measuring corrosion currents", Advances in Corrosion Science and Technology, Ed by Fontana and Staehle, vol 6, (1976)

(2) G. Bech-Nielsen, Electrochim. Acta, 23, 425, (1978)

(3) W. Lorenz, F. Hilbert, Y.Mizoshi and G. Eichkorn, J.Electrochem. Soc., 118, 1928, (1971)

(4) H. Bala, Electrochim. Acta, 29, 119, (1984)

AD-A162 434 EXTENDED ABSTRACTS INTERNATIONAL SOCIETY OF 7/12
ELECTROCHEMISTRY (36TH) HELD AT SALAMANCA SPAIN ON
23-28 SEPTEMBER 1985(U) INTERNATIONAL SOCIETY OF
UNCLASSIFIED ELECTROCHEMISTRY 28 SEP 85 F/G 7/4 NL

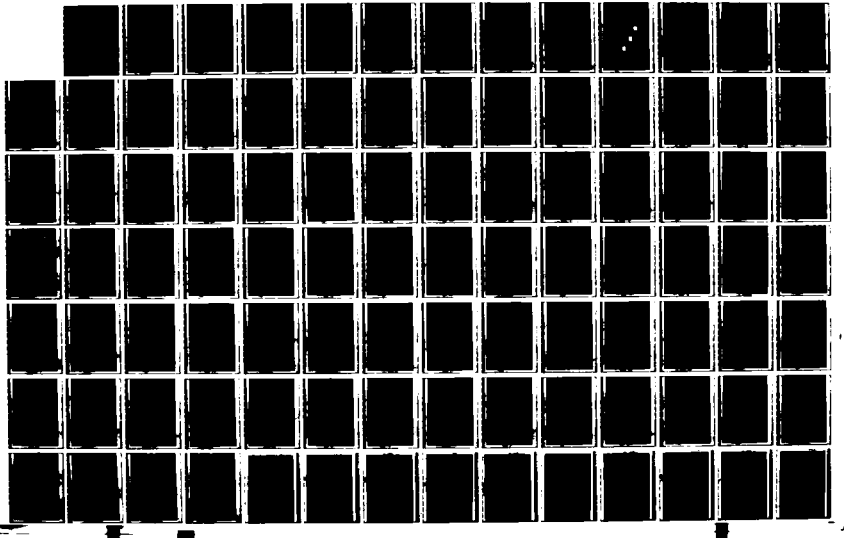

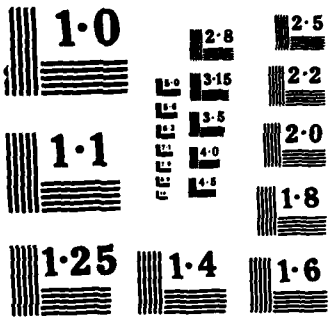

06260

GALVANIC CORROSION OF AL ALLOYS COUPLED TO ADVANCED COMPOSITE MATERIALS

F.BELLUCCI[a],L.NICODEMO[a],A.BONGIOVANNI[a],A.DI MARTINO[a],G.CAPOBIANCO[b]
[a]Dipartimento di Ingegneria dei Materiali e della Produzione-Napoli(Italy)
[b]Dipartimento di Chimica Fisica-Padova(Italy)

There is an increasing use in the transportation industries of advanced composite materials due to the high strenght to weight ratio exibited by these materials compared to those of metallic one's [1-2].A composite material which is actually used in aerospace industries is composed of high strenght high modulus graphite fibers combined with an amine cured polymer epoxy resin(GECM).In such applications the composite come in electrical contact with a metallic material. Owing to the good electrochemical cathodic behaviour of GECM[3],when such a material is coupled to a metallic one there follows on the latter an accelerated dissolution process if the couple is immersed in a corrosive environment.

The increase in dissolution rate of metals when electrically coupled to a more noble one is one of the most common and most severe forms of corrosion. Thus a careful attention must be paid in the choice of metals to couple to GECM in a component design of aircraft.

In order to evaluate the extent of galvanic corrosion the Al alloys generally used in aerospace components i.e. 2024-T3,7075-T6,7075-T73 and 5052,where galvanically coupled to GECM and exposed to an aqueous neutral aerated 3.5% NaCl solution.The galvanic current,which can be easly converted in dissolution rate,has been continuosly measured in a 24 hr test using a potentistat modified to operate as a zero-resistence ammeter.

RESULTS AND DISCUSSION.

Typical galvanic current data obtained in a 24 hr test are shown in fig.1 as a function of time t for the Al alloy/GECM couples investigated.Fig.1 shows a decrease of the galvanic current Ig in the order 5052 > 7075-T6 > 7075-T73 > 2024-T3 and that after an initial period of 6 hours the galvanic current remained more or less constant.Moreover it can be observedthat the galvanic current extrapolated at time t=0 differ significativly from those measured at steady-state for all the Al alloys investigated.The obeserved difference might be attributed to an anodic polarization phenomena due to the extent of galvanic corrosion which is quite high as can be calculated from the average galvanic current density.The study described so far was carried out at an area ratio of A^C/A^A nearly equal to one.From a practical point of view the cathodic to the anodic area ratio is usually different from one,a large area ratio being especially damaging to the anode.This is the most propably case in the aerospace industry.Figs. 2 and 3 show typical galvanic currents plot for different values of A^C/A^A for the 2024-T3 and 5052 type alloys.As can be seen from these figures the galvanic current Ig does not depend on the anodic area A^A(see curves for

A^A=1 and A^A nearly equal to 26).On the other hand Ig is linearly dependent of the cathodic area A^C.In fact a decrease of Ig by about a factor of 25 is measured when the cathodic area is reduced by the same amount.

Based on the galvanic current Ig versus time traces the galvanic current density $\bar{i}_g$ with respect to the aluminium alloy in a galvanic couple has been calculated for the values of the cathodic to anodic area ratio investigated together with the potentials of the galvanic couples measured(v.s. SCE) at the start and at the end of the test.By comparing the potentials of the galvanic couples with those of the uncoupled alloys in the same environment,it is shown that the cathodic process is under diffusion control whilst the anodic one is activation controlled.

1)R.J.Morgan and J.O'Neal.J.Mat.Sci.Chem. A3,275(1969)
2)J.C.Seferis and L.Nicolais."The role of the polymeric Matrix in the Processing and Structural Properties of Composite Materials"Plenum Press.New York and London (1983)
3)F.Bellucci,A.Di Martino and C.Liberti"Electrochemical behaviour of Graphite Epoxy Composite Materials(GECM) in aqueous salt solutions"J.of Applied Electrochemistry,in press.

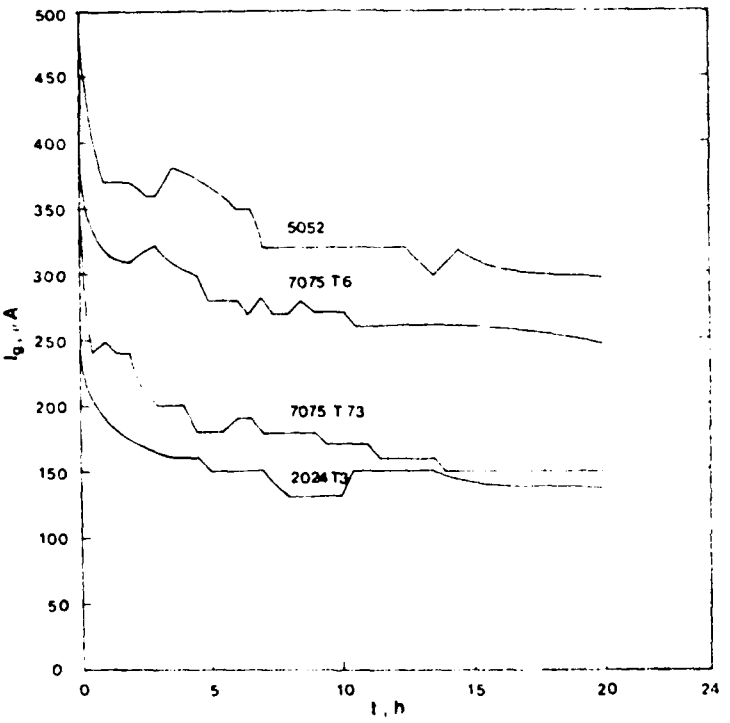

Fig.1:Galvanic current Ig as a function of the time t for Al alloys coupled to GECM in neutral aerated 3.5% NaCl aqueous solution.

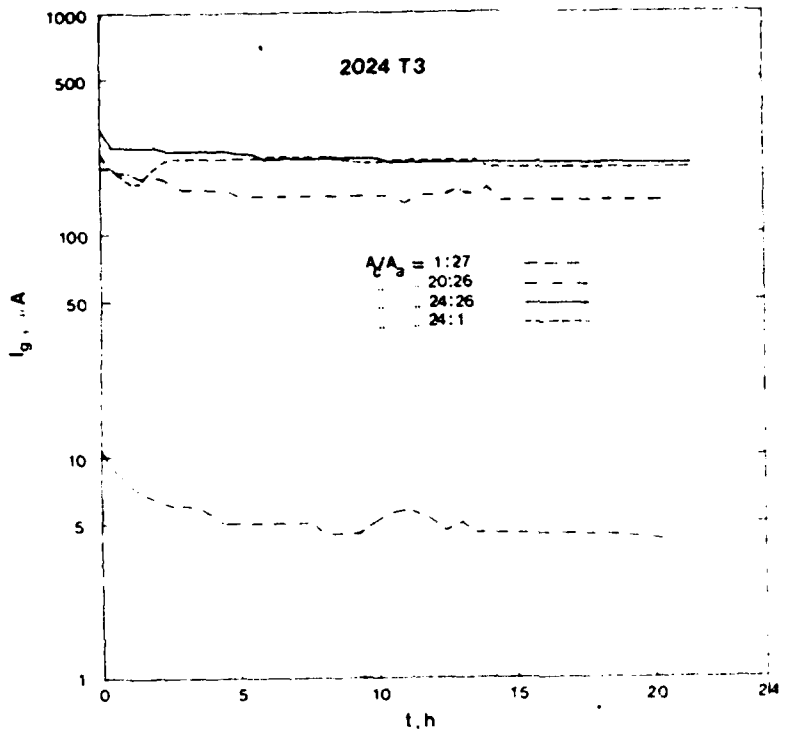

Fig.2
Galvanic current Ig as a function of the time t and of area ratio for the couple 2024-T3/GECM in neutral aerated 3.5% NaCl aqueous solution.

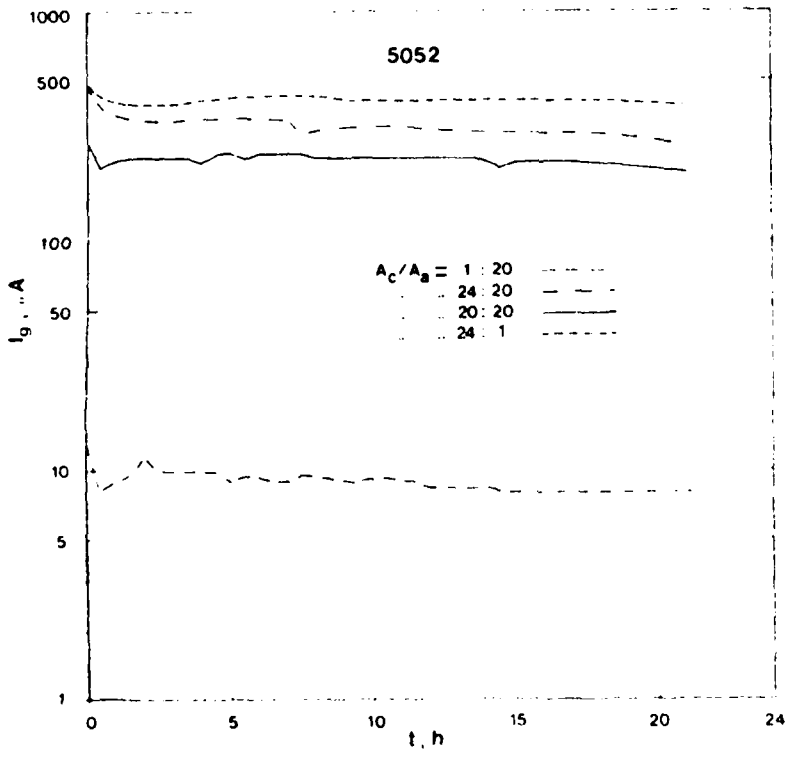

Fig.3
As in Fig.2 for the couple 5052/GECM

06270

INTERGRANULAR CORROSION OF WC/Ni AND WC/Co METAL MATRIX COMPOSITES

D. ZUR MEGEDE and E. HEITZ
Dechema Institut, D-6000 Frankfurt (Germany)

Introduction

Cemented carbides with a nickel or cobalt matrix containing tungsten carbide particles are typical composites. Because of their hardness they are in use as wear resistant components in mechanical seals of pumps. However, they often show intergranular corrosion of the metal matrix /1,2/ with high corrosion rates into the materials. It was the aim of this investigation to explain the high corrosion rates by a suitable model and to interprete the flow depency of the corrosion process. The corrosion systems tested have been the composites WC/6 % Co and WC/9,5 % Ni in aerated aqueous 0,02 and 0,5 mol/l NaCl solutions.

Corrosion model

Composites as discribed above consist of surface regions with high and low metal content. In addition, the surface is penetrated by pores. In regions with high metal content or/and in pores bimetallic corrosion starts. A hole is formed with the wall of which acting as cathode (WC) and the bottom as anode (metal). In the hole a steady state is established controlled by an increasing cathode area (rising corrosion rate) and by oxygen diffusion into the hole (decreasing corrosion rate). Estimates of corrosion rates by assumption of cathodic corrosion control and a hole diameter of 1 µm result in values from 2.5 to 25 mm/y. For the time dependence of the corrosion rate a convective flow influenced initial phase and a purely diffusion controlled end phase is postulated.

Experiments and Results

In Fig. 1 polarisation curves of the components Ni, Co and WC in 0.02 M NaCl as well as Fe and C of the "composite" grey cast iron are shown.

It can be seen that for all systems an "internal" bimetallic corrosion is possible and that WC is the more active cathode (lower overvoltage).

The apparatus for testing the flow dependency of corrosion is a rotating disk in front of a wall and made of high alloyed steel DIN 1.4571 resp. AISI 316. It is integrated in a loop of PVDF and high alloyed steel. The disk has a maximum rotation speed of 10,000 rpm. The corrosion rate (measured as Rp^{-1})

is, as expected, time dependent with high rates in the initial phase and lower in the steady state (Fig. 2). The composite WC/Ni shows a significant influence of the rotation speed at 80°C.

For the composite WC/Co a decrease of the flow dependency within the first 9 hours can be seen. The values of the corrosion rates are 2.5 and 5 mm a^{-1} (WC/Ni) or 2.5 and 25 mm a^{-1} (WC/Co). The corrosion attack is general with the formation of islands. Within the islands the corrosion rate is higher, but from a specific depth the corrosion seems to grow preferently sideway. The formation of islands can be explained by assumption of surface regions with high metal concentration leading to pores with large diameters and few narrow passages.

References

/1/ P.-H. Effertz, W. Fichte; Der Maschinenschaden 54 (1981), 113-123

/2/ M. Lagerquist; World Pumps 1982, 108-112

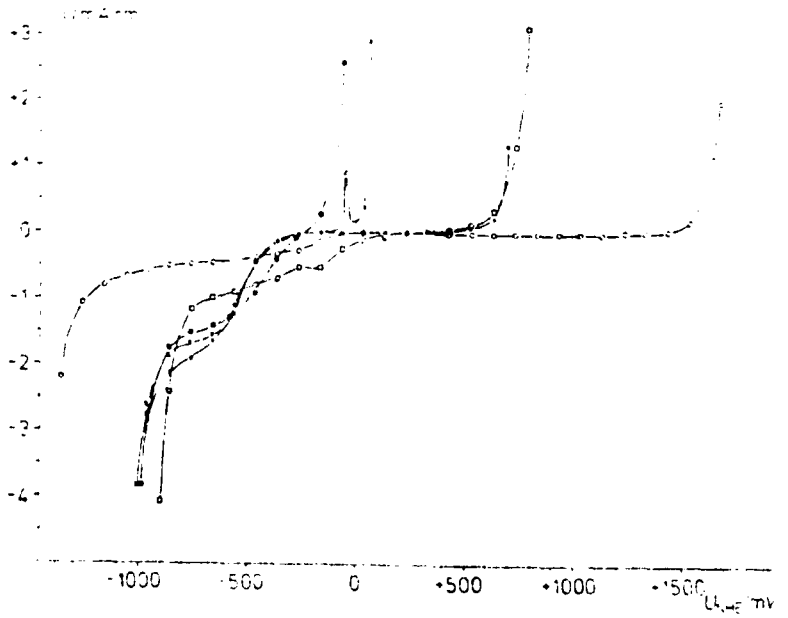

Fig. 1: Polarisation curves of Ni, Co, WC and Fe, C in aerated 0,02 M aqueous NaCl at 22,5°C (■ : Fe, x: Co, ● : Ni, □ : WC, o: C)

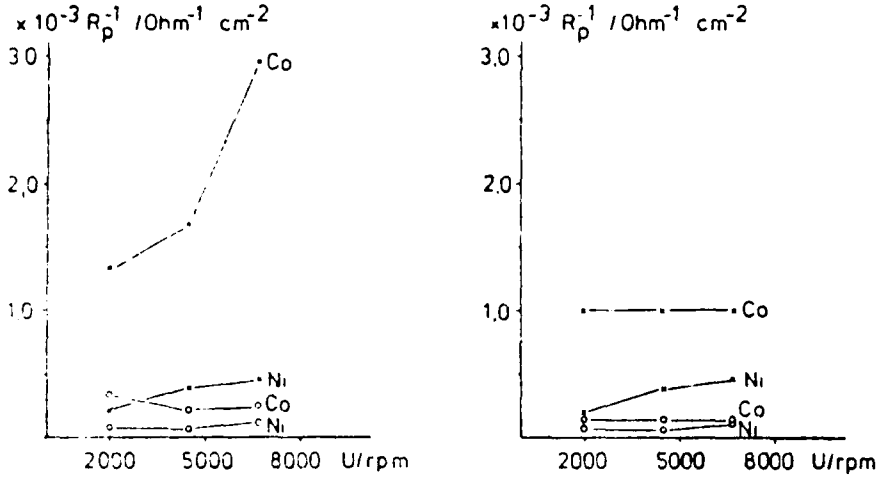

Fig. 2 Corrosion rates (as Rp^{-1}) of the composites WC/Ni and WC/Co in aerated 0.5 M(x) and 0.02 M(o) aqueous NaCl at 80°C. Left: Initial phase; right: after 9 hours corrosion

ACTIVE, PASSIVE AND TRANSPASSIVE CHROMIUM

M. Metikos-Hukovic, M. Ceraj-Ceric*

Institute of Electrochemistry, Faculty of Technology,
University of Zagreb, Yugoslavia
Pliva, Zagreb, Yugoslavia*

Chromium oxide exhibits good corrosion, catalytic and electrocatalytic properties [2,3] making it a competitive material for precious transition metal oxides. Doping TiO_2 photoanodes with Cr_2O_3 snifts their spectral sensitivity to the visible part of the spectrum.

The corrosion resistance, catalytic and electrocatalytic properties of chromium are due to its several oxidation states. Investigation of the semiconducting properties of chromium oxides in situ is therefore of great practical and theoretical importance.

However, many important aspects of the electrochemical behavior of chromium have not yet been clarified such as the mechanism of active anodic dissolution in acidic solutions, transition from the active state to the passive state, the transpassive state and secondary passivity.

This study concerns the electrochemical and photoelectrochemical properties of thermal chromium and polycrystalline chromium oxide electrodes prepared by the direct oxidation of chromium at 800°C. These are then tested in ammonium borate buffer solutions, pH 6.2 and 8.2 at 25°C. The techniques of potential sweep voltametry, impedance, photocurrent and photopotential measurements were employed to characterize the electrode/electrolyte interface. The electrode surface and the distribution of chromium were investigated by means of scanning electron microscopy. The thermically formed Cr oxide was found to consist of Cr_2O_3 (SEM) and to have a thickness of 1-2 μm.

These polarization experiments were performed in the direction of the positive potential, from -2.5 V vs. S.C.E. up to the transpassive potential range.

Chromium dissolves as Cr^{2+} in the active dissolution range. A new mechanism is proposed for the active dissolution of chromium in sulphuric acid solutions, similar to Bokris' mechanism for iron dissolution [5]. The transition to the passive state occurs independently of active dissolution and is related to the formation of

trivalent chromium oxide. The present study has shown that this is a p-type semiconductor (Figure 1), with a forbidden gap with of Eg = 1.6 eV. During the transition from the active state to the passive state, no current peak appears during the linear sweep. In contrast to iron, chromium demonstrates secondary passivity after the transpassive region in a narrow potential range at pH 6.2.

The capacity, resistance, photopotential and photocurrent give much information on the properties of the solid phase during polarization. Sharp changes in these structurally sensitive values indicate transition from lower to higher oxides during the anodic sweep, in situ (Figure 1). The transition photoeffects seen in Figure 1 involve a change in the film structure.

It has been found that the oxidation state of chromium oxide increases continuously with rising electrode potential. The transformation of lower to higher oxides occurs continuously via a solid state mechanism:

$$Cr_2O_3 \text{ (p-type)} \longrightarrow Cr_2O_2/CrO_2 \text{ (transition photoeffects)} \longrightarrow CrO_3 \text{ (n-type)}$$

REFERENCES

1. Wu Yuang, R. Ni and H. Hua, Corros. Sci. 24, 691 (1984).
2. M.Metikoš-Huković, M. Ceraj-Cerić, Extended Abstract, 33rd Meeting of ISE, Lyon, Vol. II (1983).
3. F. Beck and H. Schulz, Electrochim. Acta. 29, 1569 (1984).
4. A. M. Kraichberg, V. Y. Pleskov and Y. S. Mardishev, Electroknimiya, 19, 1435 (1983).
5. M. Okuyama, M. Kawakami and K. Ito, Electrochim. Acta, 30, 767 (1985).

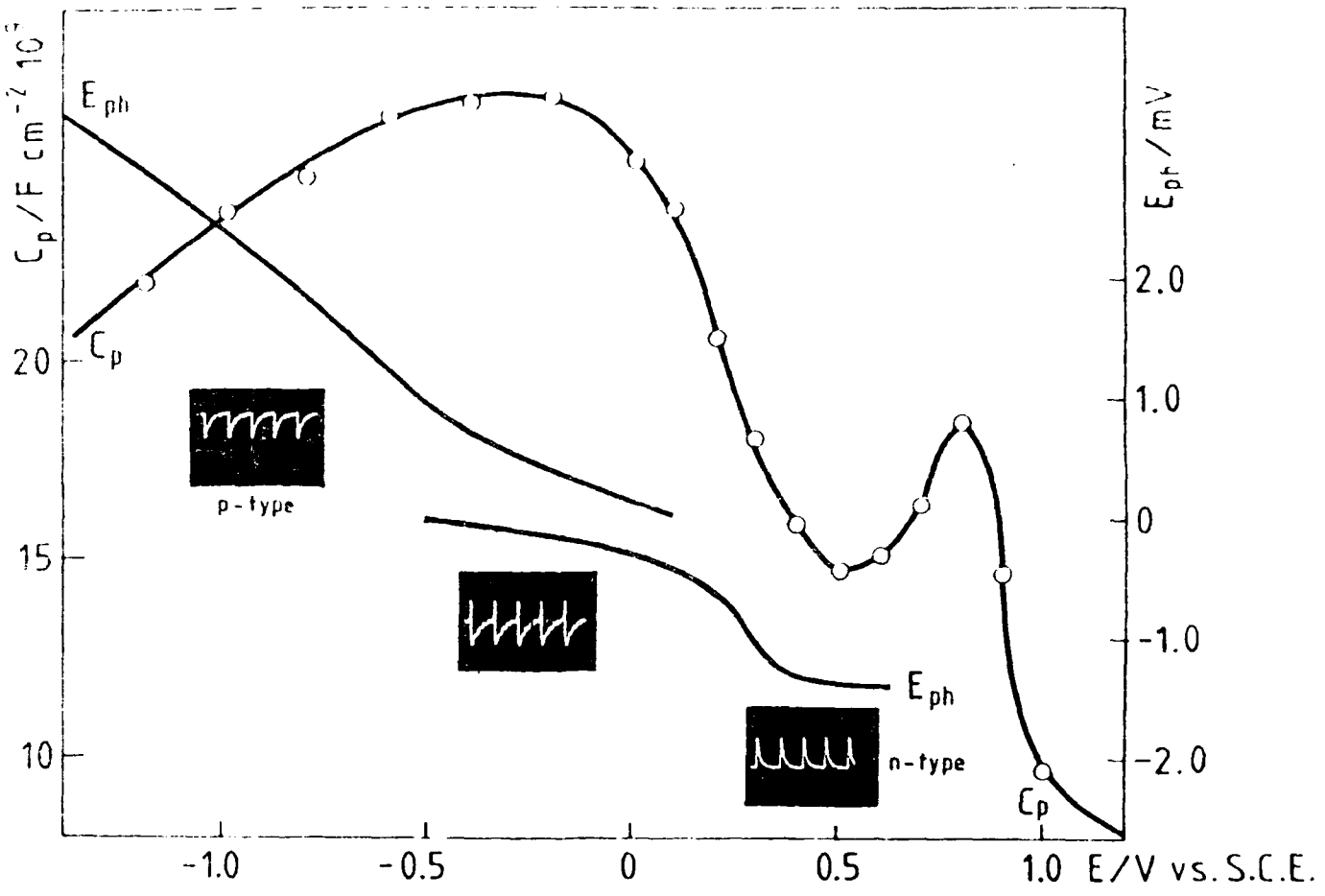

Fig. 1. Capacitance (C_p) at 1 kHz, photopotential vs. potential for the thermal Cr oxide electrode illuminated by 100-W tungsten halogen lamp with short light impulses. t_L = 0.95 ms.

06290

PLATINIZED TITANIUM ANODES IN CATHODIC PROTECTION

A. Rendić, M. Metikoś-Huković, S. Ferina

Institute of Electrochemistry, Faculty of Technology,
University of Zagreb, Yugoslavia

Advances in the construction of bimetal anodes have made possible the use of platinum and its alloys in the form of thin coatings on electrodes constructed of inexpensive materials. Several techniques have been developed for obtaining an active coating of platinum on either titanium or tantalum substrates. In the construction of Ti/Pt-electrodes for use in cathodic protection systems or for electrical applications requiring high electroactivity, selectivity and corrosion stability, coatings of platinum obtained through electrodeposition are the most satisfactory[1].

The primary emphasis of this study was to obtain thin (3 to 5 microns), adherent, nonporcus coatings through the electrodeposition of platinum on a Ti-substrate from aqueous solutions of Pt-salts. Two electrolytes were used: one having a base of $H_2Pt(NO_2)_2SO_4$ and the other a base of H_2PtCl_6. The latter is very quickly exhausted and requires constant monitoring of the bath and considerable practical experience. Adhesion porosity (morin test) and coating thickness (beta radiation reflection) were monitored before and after the electrochemical processes.

In the galvanizing of titanium, great difficulties are encountered due to the exceptionally high affinity of titanium for oxygen and the rapid formation of oxide layers, even in a humid atmosphere [2].

In order to achieve firm adherence of the platinum coating to the titanium, it is necessary to remove the oxide and prevent its regeneration until electrolysis commences. This is both the technological procedure of the production of Ti/Pt-anodes, and determines their final level of quality.

The electrochemical and corrosion behavior of platinized titanium electrodes has been studied using cyclical voltametry in deaerated solutions of 1 mol dm^{-3} $HClO_4$ at 25°C. For electrode rotation, Pine Instrument Company equipment was used, on which 400-10,000 rpm can be achieved.

Some characteristics of electroplated Pt-coatings on Ti-substrates are discussed, including method of preparation, overvoltage, composition surface quality, and platinum thickness [3]. The results of accelerated laboratory tests to define conditions which limit application are presented, and the electrochemical properties are contrasted with bulk platinum and commercially available platinized titanium anodes for cathodic protection (Figures 1 and 2).

REFERENCES

1. L. M. Jakimenko, Elektrodni materiali v prikladnoi elektrohimiji, Izd. Himia, Moscow (1977).

2. M. Metikoš-Huković and M. Ceraj-Cerić, Surf. Technol. 28, 273 (1985).

3. D. M. Novak, B. V. Tilak and B. E. Conway, Modern Aspects of Electrochemistry, No. 14, Edited by J.O'M. Bokris, B.E. Conway and Ralph E. White, Chapter 4, Plenum Publishing Corporation (1982).

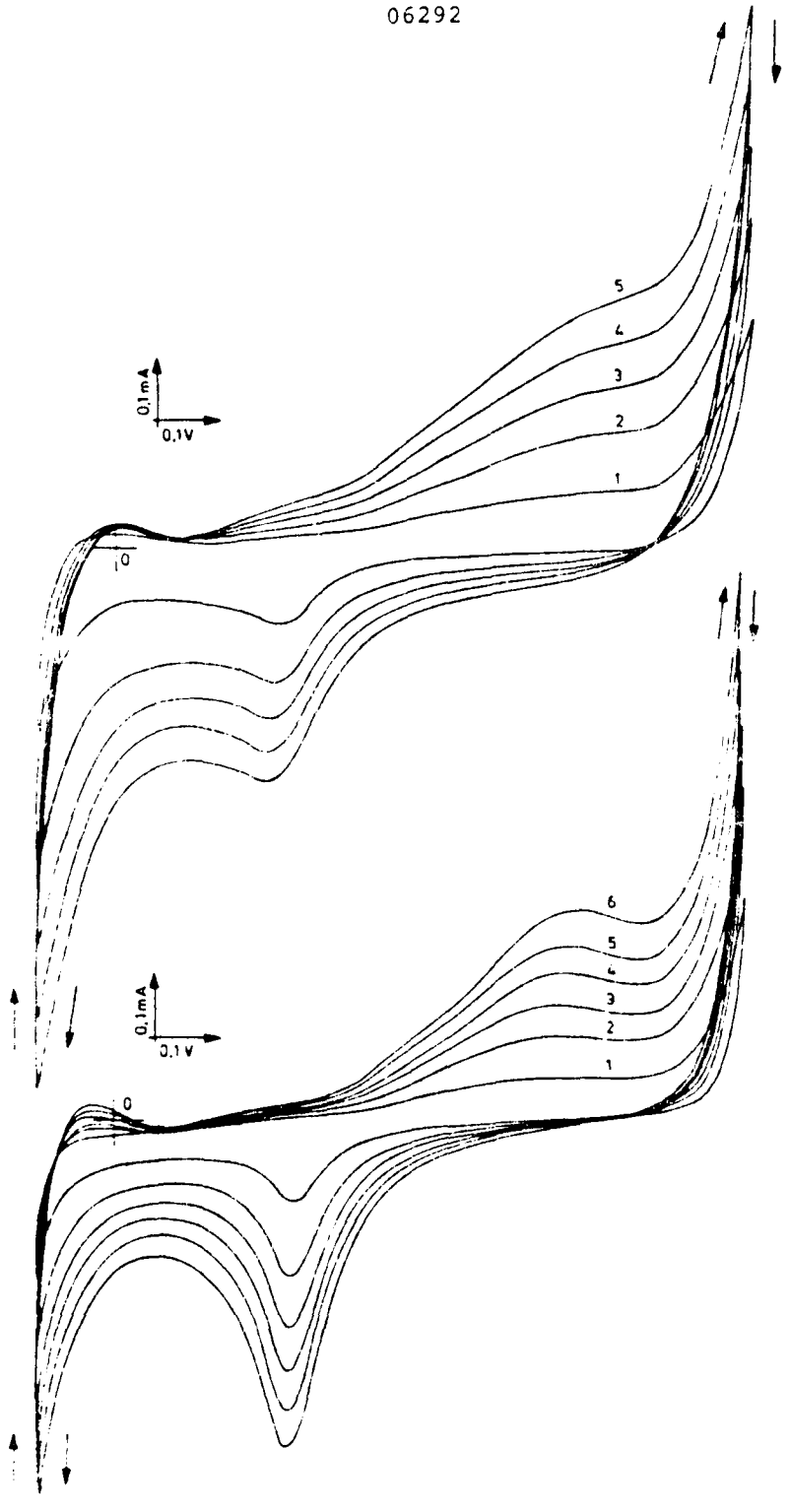

Fig. 1

Fig 2

Fig. 1 Cyclic voltammograms obtained for commercial Ti/Pt anodes intended for use in cathodic protection. Nonmoving electrodes, i.e. 0 rpm. $dE/dt = 50, 100, 150, 200, 250, 300\ mVs^{-1}$

Fig. 2 Cyclic voltammograms obtained for Ti/Pt electrodes manufactured by the authors. Nonmoving electrodes, i.e. 0 rpm. $dE/dt = 50, 100, 150, 200, 250, 300\ mVs^{-1}$

06300

DUAL EFFECT OF ANIONS IN PITTING CORROSION

M. PRAŽÁK

State Research Institute for Material Protection G.V.Akimov
250 97 Praha 9 - Běchovice, CZECHOSLOVAKIA

For the pitting corrosion of Cr18Ni9-type stainless steels in chloride solutions, the inhibiting effect of anions, such as SO_4^{2-}, NO_3^- and OH^-, has been known for a long time. The stimulating effect is typical of some sulphur compounds, similarly as in the process of SCC[1,2].

In this study, the effect of inhibiting or stimulating anions on the breakdown potential E_B and on the repassivation potential E_R was investigated, as well as the different mechanisms of reactions controlling both potentials.

EXPERIMENTAL

The Cr18Ni9Ti-type steel was investigated in solutions of NaCl 0.5 mol.dm^{-3} with other anions additions. The E_B potential was measured potentiodynamically with the scan rate +1 mVs^{-1} at 0.1 $mAcm^{-2}$. The E_R potential was measured intensiostatically at +0.1 $mAcm^{-2}$ after 40 minutes polarization. Results are listed in Table 1.

DISCUSSION

Typically inhibiting anions shifted both E_B and E_R potentials to positive values. Stimulating anions - especially those releasing SH^- ion - shifted the E_R to negative values, but - under certain circumstances - shifted E_B to positive values.

This situation can be explained by different reaction mechanisms at both potentials. At the breakdown potential E_B the passive oxide film is destroyed by the chloride ions. All types of added anions decrease the Cl^- ion activity

according an adsorption mechanism given in [4], inhibiting thus the reaction of the film breakdown.

On the contrary, the repassivation potential E_R is controlled by the active metal corrosion mechanism inside the pit yet created. This mechanism is accelerated by stimulating ions - especially strong by SH^- ions[5]. Thus some anions - e.g. CNS^- - can simmultaneously act stimulating for E_R and inhibiting for E_B.

For the real corrosion behavior, the shift of the only stabile E_R potential is decisive, denoting thus the real inhibiting or stimulating effect of added anions.

Table 1 Values of E_B and E_R for the Cr18Ni9Ti steel in the NaCl solution with accompanying salts added.

Solution: NaCl 0.5 mol dm^{-3} + additions:		E_B /mV, SCE/	E_R
no addition		+ 365	+ 30
$NaNO_3$	0.1 mol dm^{-3}	+ 1145	+ 1260
$NaNO_2$	"	+ 520	+ 75
K_2CrO_4	"	+ 535	+ 55
Na_2SO_4	"	+ 515	+ 60
NaOH	"	+ 610	+ 180
Na_2SO_3	"	+ 530	- 220
$Na_2S_2O_3$	"	+ 55	- 150
KCNS	"	+ 380	- 225
Na_2S	0.02 mol dm^{-3}	+ 35	- 310
Na_2SO_4 + KCNS	0.1 mol dm^{-3} + 0.1 mol dm^{-3}	+ 650	- 190

1. G.Herbsleb, Werkstoffe u.Korr. 33, 334 /1982/.
2. D.V.Vasgues Moll, A.J.Arvia et al., Corros.Sci.24,751 /1984/.
3. G.Cragnolino, D.D. MacDonald, Corrosion 38, 406 /1982/.
4. M. Pražák et al., Zaschita metallov 5, 371 /1969/.
5. Z.O. Iofa, Protection of metals 16, 220 /1980/.

06310

ELECTRODISSOLUTION KINETICS OF PALLADIUM IN ACIDIC CHLORIDE SOLUTIONS

R. DURAN. Dpto. Electroquímica. Sub. de Tecnología de Explotación. División de Corrosión. Instituto Mexicano del Petróleo.
J. GENESCA. Dpto. Metalurgia. Facultad Química. Universidad Nacional Autónoma de México. Ciudad Universitaria. 04510 México.

Mechanistic studies on metallic dissolution in aqueous media have been mainly focused on the effect of pH at constant anion concentration. However, there have few reports which consider the direct participation of anions in metallic dissolution.
In a previous work [1,2] the anodic dissolution of palladium in deoxygenated perchlorate chloride solutions was studied. Electrodissolution behavior was examined at different chloride concentrations. Tafel slopes of 85 mV/decade and a reaction order with respect to the chloride concentration of 2.1 have been obtained. The perchlorate ion was chosen because it is not believed to adsorb strongly on palladium nor it has very strong tendencies to serve as ligand in complex formation.
In this study, the effect of chloride ions at constant pH on the kinetics of palladium dissolution is investigated using steady-state polarization techniques.
The anodic behavior of palladium in sulfuric chloride solutions depends separately on Cl^- and H^+ ion activities. The results obtained with different solutions containing the same Cl^- ion concentration and varying H_2SO_4 concentrations, showed that the active dissolution of palladium depends, as previously reported[3], only on Cl^- concentration.
Anodic polarization plots for palladium in deoxygenated $xNaCl-yH_2SO_4-zNa_2SO_4$ (y= 0.2M, x+y+z= 1M) solutions are shown in Figure 1. The Cl^- concentration was varied between 0.01 and 0.5M. Increasing the Cl^- concentration shifted the polarization plots in the more active direction. This means that the rate of the anodic reaction is increased by the Cl^-. For all the Cl^- concentrations a Tafel slope of approximately 58 mV/decade was obtained. The reaction order with respect to the chloride ion concentration for palladium dissolution can be determined from the polarization curves. Log current density vs log chloride ion concentration in the Tafel region is plotted in Figure 2 and shows that

$$(\partial \log j_a / \partial \log \{Cl^-\})_{pH,E} = 1.1$$

The following mechanism is proposed for palladium dissolution in deoxygenated chloride media

$$Pd + Cl^- \rightleftharpoons PdCl_{ad} + e \qquad (1)$$

$$PdCl_{ad} + Cl^- \xrightarrow{rds} PdCl_2 + e \qquad (2)$$

where reaction (1) represents Cl^- ion discharge with the simultaneous formation of (Pd...Cl) groups of chemisorbed chloride -

on the surface, leading to the weakening of the bond linking -- the Pd atom to the metallic lattice. Subsequent reaction (2) is assumed to be the rate determining step of the process. As a -- consequence, the rate of dissolution for a given potential --- should be proportional to the surface concentration of Cl^-.
This reaction product ($PdCl_2$) dissolves in excess of chloride - ion giving rise to a well defined complex $\{PdCl_4\}^{2-}$. This com - pound is approximately 10^{11} more stable than[4] $\{Pd(H_2O)_4\}^{2+}$.
The formation of $\{PdCl_4\}^{2-}$ has been demonstrated[5] by UV[4] absorp - tion spectroscopy analysis of the solution. This result is in - good agreement with the E - pCl diagram shown in Figure 3.
The kinetic parameters predicted by this mechanism are depen -- dent on the adsorption behavior of the intermediate, $PdCl_{ad}$.
If the adsorbed intermediate follows Temkin adsorption behavior ($0.2 < \theta < 0.8$) and if values of 1/2 for the symmetry factors are considered, the rate expression for palladium dissolution can - be obtained

$$j_a = k_a.\{Cl^-\}^{1.5}.\exp(F\mathcal{E}/RT) \qquad (3)$$

Equation (3) is in reasonable agreement with the empirical rate expression for palladium electrodissolution in 1M (H_2SO_4-Na_2SO_4 NaCl) solutions which is

$$j_a = k_a.\{Cl^-\}^{1.1}.\exp(F\mathcal{E}/RT) \qquad (4)$$

Thus the proposed mechanism predicts values of 60 mV and 1 for the anodic Tafel slope and the reaction order, respectively. These calculated parameters are in good agreement with the expe - rimental data.
One can conclude that chloride ions participate in the dissolu - tion of palladium independently of type of anion (ClO_4^- or SO_4^{2-}) and in both cases, chloride have an accelerating effect.
It should be mentioned that the reaction order of chlorides in ClO_4^- and in SO_4^{2-} solutions are specific for each system. This - difference in their respective reaction order seems to be inter - preted in terms of the competitive adsorption of chloride and - sulfate ions on the palladium surface. This effect is confirmed by the different Tafel slopes. A depolarisation effect is obser - ved in SO_4^{2-}/Cl^- system (58 mV/decade) vs ClO_4^-/Cl^- system (85 mV /decade) which can be attributed to the displacement of chlori - de ions by sulfate. The competitive adsorption of sulfate and - chloride ions on iron was studied by Hackerman and Stephens[6] -- using radiotracer techniques. Their results indicated that smal quantities of chloride ions in a sulfate solution increased sul - fate ion adsorption. On the other hand, larger chloride ion con - centration decreased sulfate ion adsorption. As previously des - cribed, it is evident that the effect of chloride ions on the - dissolution of palladium becomes a more complicated phenomenon by the presence of sulfate ions in the solution.
Although the sulfate ion may not participate directly in the di - ssolution mechanism, its effect on the adsorption of chloride - ions must be considered. Thus, it is difficult to interpret the data obtained for a SO_4^{2-}/Cl^- system because of the indirect par - ticipation of SO_4^{2-} ions.

REFERENCES.

1.- F. Lomenech, J. Genescá and L. Victori, Rev. Metal. CENIM 14 (6) 321 (1978)
2.- J. Genescá and L. Victori, Corrosion NACE, Submitted

3.- Th. Heumann and R. Schurmann, Z. Elektrochem. 67, 601 (1963)
4.- L. Victori, J. Tomás and F. Malgosa, Afinidad 32, 867 (1975)
5.- L. Victori, PhD Thesis, University of Madrid (1975)
6.- N. Hackerman and S.J. Stephens, J. Phys. Chem. 58, 904 (1954).

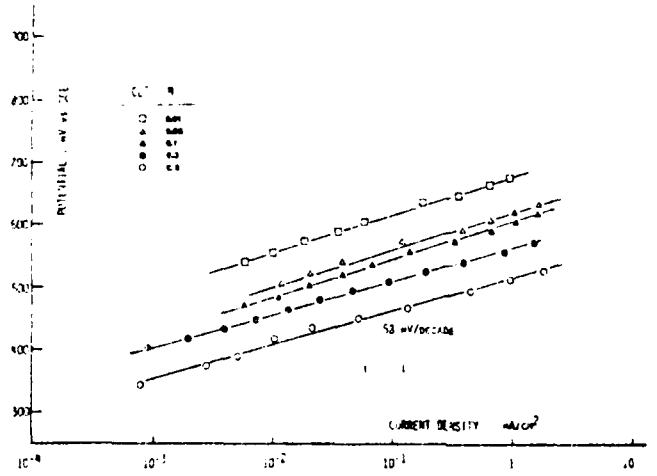

Figure 1.- The effect of chloride concentration at Tafel region. $xNaCl-yH_2SO_4-zNa_2SO_4$ y = 0.2 M. (x+y+z = 1 M)

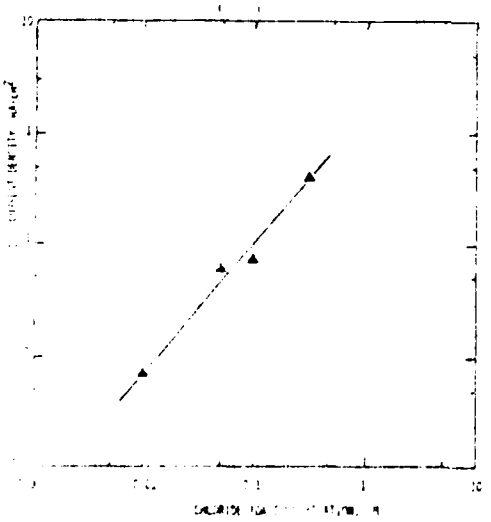

Figure 2.- Reaction order p... with respect to chloride ions for palladium disolution. ... - 540 mV (sce).

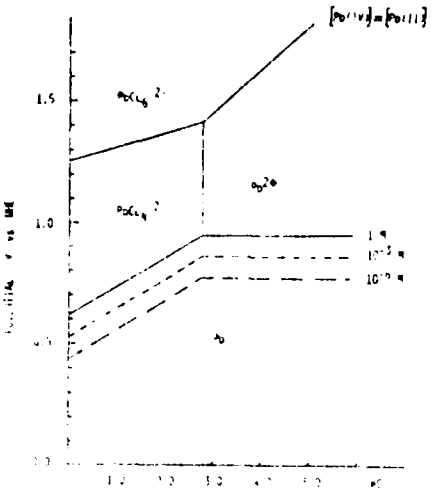

Figure 3.- E - pCl Diagram for Pd at 25°C.

06320

CORROSION OF IRON AND IRON OXIDES IN MOLTEN SODIUM HYDROXIDE

TZVETI TZVETKOV

Higher Instiutte of Chemical Technology, Sofia (Bulgaria)

Rather conflicting data exist about the corrosion resistance of iron and its alloys in a sodium hydroxide melt[1-6]. In the present study, iron and iron oxide corrosion was investigated in a sodium hydroxide melt at 480°C.

The corrosion rate of Fe, FeO, Fe_2O_3 and Fe_3O_4 was found to be strongly influenced by the nitrogen, oxygen and water vapour content of the atmosphere over the melt. Thus, the corrosion rate of iron in a melt with pure oxygen atmosphere proved to be four times as high as with an atmosphere composed of 99% nitrogen and 1% oxygen (Fig. 1).

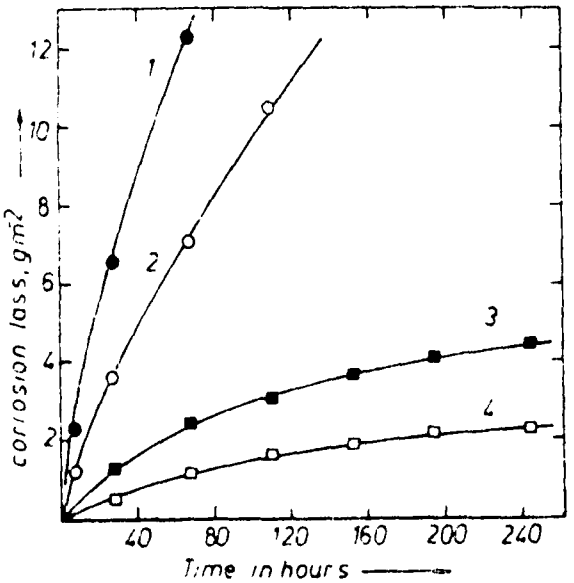

Fig. 1

Influence of the at mosphere over the melt of NaOH(480°C) on the time dependence of iron corrosion:

1,2 - O_2

3,4 - N_2 + 1%O_2

1,3 - Corrosion lass, incl. oxide (passive) film.

2,4 - Corrosion lass, without oxide (passive) film.

In iron corrosion, an adherent oxide film seems to be initially formed. Further action of the sodium hydroxide metl transformed the film in water soluble products and products that partially dissolved in the melt.

The dissolution of corrosion products was further investigated with iron oxides. The corrosion rate of iron oxides was found slightly to decrease with time. The insoluble corrosion products on the specimen surface probably inhibited further chemical action of the melt.

Furthermore, increased water vapour content of the atmosphere proved to inhibit the corrosion rate of iron and iron oxides in the melt. The water vapour content influenced especially the formation of water soluble corrosion products.

REFERENCES

1. E.Curovich, I.Priclad. Chem. 32:817 (1959).

2. D.Willams et.al., I.Amer.Chem.Soc. 78:3150 (1956).

3. A.Rahmel, H.Krüger, Werkstoffe und Korrosion, 18:193 (1967).

4. I.Tzvetkov, S.Stavrev, in: Ext. Abstr. (34.ISE Mtg. Erlangen, BRD, 1983), p. 0629.

5. I.Tzvetkov, in: Ext. Abstr. (35. ISE Mtg. Berkeley, CA, 1984).

6. I. Tzvetkov, R.Raicheff, in: Ext. Abstr. (34. ISE Mtg. Erlangen, BRD, 1983) p. 0628.

06330

CORROSION OF GOLD, SILVER AND PLATINUM IN A SODIUM HYDROXIDE MELT

TZVETI TZVETKOV

Higher Institute of Chemical Technology, Sofia (Bulgaria)

The corrosion of noble metals in a moltenhydroxide is known to depend on the composition of the atmosphere over the melt[1-6]. The corrosion of gold, silver and platinum with a purity grade of 99,9% was studied, using the experience of previous work.

The experiments proved that the rate of noble metal corrosion depended on the oxygen and water vapour content of the atmosphere over the melt. A decisive corrosion factor seemed to be the sodium peroxide content of the sodium hydroxide melt:

$$2NaOH + 1/2O_2 = Na_2O_2 + H_2O \qquad (1)$$

This content depended on the partial pressure of oxygen and water vapour. The rise in the partial pressure of water vapour reduced the concentration of peroxide in the melt, and consequently, the corrosion rate of gold and

$$O_2^{2-} + H_2O = 2OH + 1/2O_2 \qquad (2)$$

platinum.

An increased water vapour content did not inhibit but accelerated silver corrosion. Apparently, the peroxide mechanism of corrosion does not hold for silver (Fig. 1).

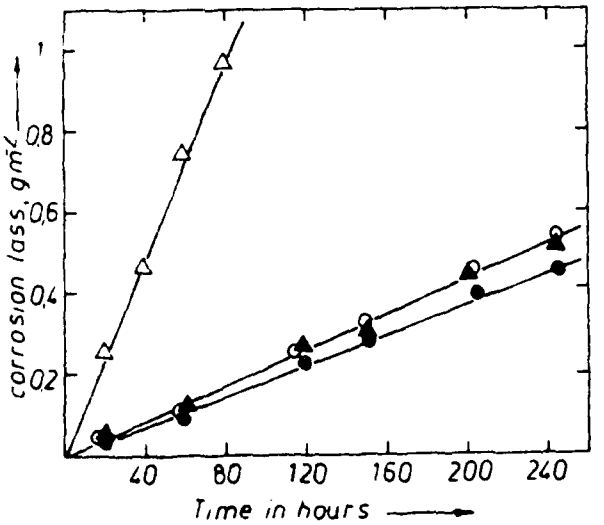

Fig. 1

Influence of the atmosphere over the melt of NaOH (480°C) on the time dependence of silver corrosion;

△ O_2 + 6,5% H_2O

▲ O_2

○ N_2 + 1%O_2 + 6,5%H_2O

● N_2 + 1%O_2

REFERENCES

1. H.Lux et.al., Z. anorg. allg. Chem. 310:305(1961).

2. H.Krüger et.al., Electrochimica Acta, 13:625 (1968).

3. A.Rahmel. H.Krüger, Werkstoffe und Korrosion, 18:193 (1967).

4. T.Tzvetkov, S.Stavrev, in: Ext. Abstr. (34.ISE Mtg. Erlangen, BRD, 1983) p. 0629.

5. T.Tzvetkov, in: Ext.Abstr. (35.ISE Mtg. Berkeley, CA, 1984).

6. T.Tzvetkov, R.Raicheff, in: Ext. Abstr. (34.ISE Mtg. Erlangen, BRD, 1983) p. 0628.

06340

THE CORROSION BEHAVIOR OF IRON- AND COBALT-BASE METALLIC GLASSES

J. PRZYLUSKI, A. KROLIKOWSKI and J. FULARA
Institute of Solid State Technology
Warsaw Technical Uniwersity, Warsaw /Poland/

Recently much attention has been focused on the corrosion properties of glassy metallic alloys. Extensive investigations were carried out on glasses containing Cr[1], Ti[2] or Zr[3]. These materials easily undergo passivation even in highly corrosive media and exhibit better corrosion resistance than traditional corrosion resistant alloys. The superior corrosion resistance of these alloys is attributed more to the presence of the passive film forming elements than to their amorphous structure. Little is known about corrosion properties of glassy alloys without typical film formers. They do not passivate easily and show very diverse corrosion behavior in comparison with their crystalline counterparts. The aim of our present work is to examine the corrosion resistance of Fe-13,5B - - 3,5 Si-2C[+] and Co-4,7 Fe - 15 Si - 10 B[+] amorphous alloys in various media and establish the change of corrosion behavior due to crys - tallization.

Ribbons of the glassy alloys mentioned were prepared by rapid quenching[++]. Some of these alloys were thermally crystallized. The structure of amorphous and recrystallized samples was confirmed by X-ray diffraction. The corrosion behavior of alloys under consideration was characterized using electrochemical and gravimetric methods. Polarization curves were measured potentiodynamically with sweep rate of $1 mV \cdot s^{-1}$. The average corrosion rate of materials studied in test solutions was estimated from the weight loss. All tests were carried out in open to air solutions at ambient temperature.

The potentiodynamic polariation curves for amorphous and crystallized iron-base alloys in 0,1 N HCl are shown in Fig. 1a. The curve for Fe-Armco is also depicted for comparison. All materials dissolve actively in this medium. Anodic branches of the polarization curves are similar. The effect of crystallization is more pronounced in the cathodic region. The crystallized sample shows higher cathodic current densities than those of the as quenched sample. The corrosion potential of the annealed alloys is slightly shifted to more moble values. These findings

[+]The numbers indicate contents of the alloying elements in atomic percent.

[++]The glassy alloys were provided by Institute of Material Science, Warsaw Technical University.

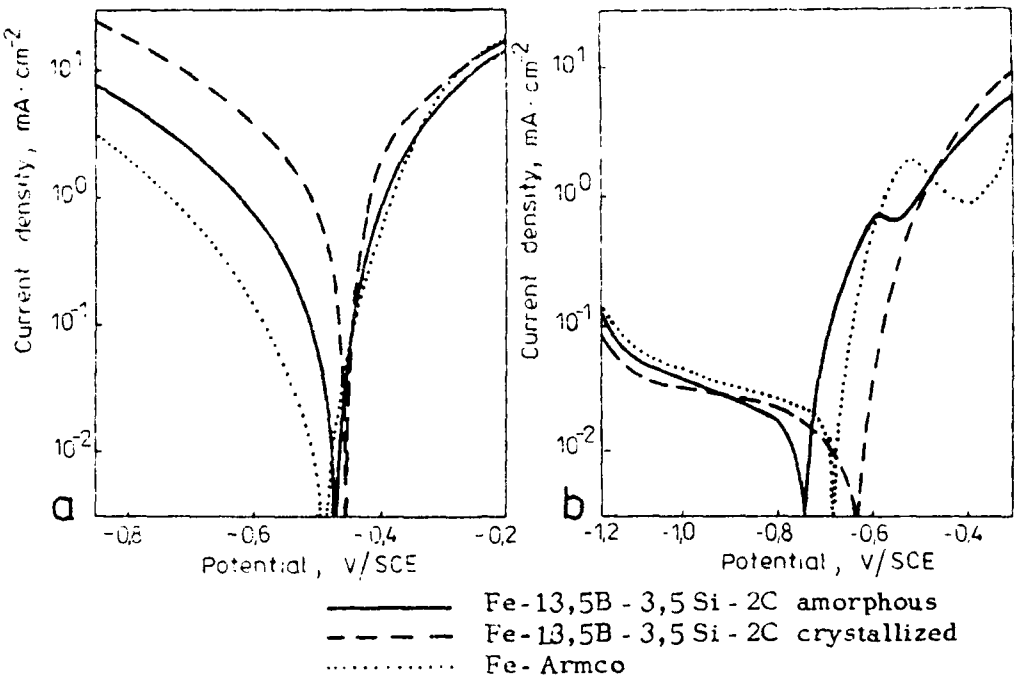

Fig.1. Polarization curves in /a/ 0,1 N HCl and /b/ 0,5 N NaCl.

Table 1. Results of gravimetric tests /110h/.

Material	Corrosion rate $g \cdot m^{-2} \cdot h^{-1}$
0,1 N HCl	
Fe-13,5B-3,5 Si-2C amorphous	0,54
Fe-13,5B-3,5 Si-2C crystallized	20
Fe-Armco	0,14
0.5 N NaCl	
Fe-13,5B-3,5 Si-2C amorphous	0,061
Fe-13,5B-3,5 Si-2C crystallized	0,035
Fe-Armco	0,065

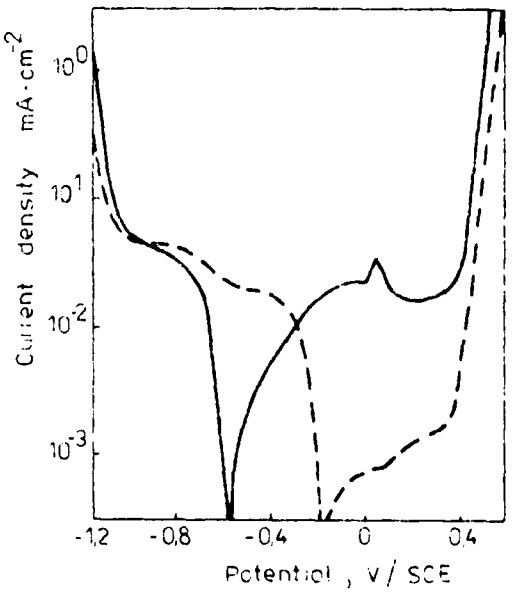

Fig.2. Polarization curves in 1 N NaOH for Co-4,7 Fe-15 Si-10B:
amorphous
crystallized

indicate that crystallization leads to an enhancement of cathodic reaction and gives rise to an increase in the corrosion rate. Apparently the amorphous alloy shows an inhibition of hydrogen evolution in comparison with the recrystallized one. This conclusion was confirmed by results of gravimetric measurements /Table 1/. It is clear that crystallization reduces the corrosion resistance of glassy alloy in acidic medium. The corrosion rate of the Fe-base glass was found to be above one order of magnitude less than that of the crystallized sample. Similar behavior was observed for Fe-B glass[4].

In Fig. 1b polarization curves for Fe-base alloy in as quenched and crystallized states and for Fe-Armco in 0,5 N NaCl are demonstrated. All materials corrode actively and show quite similar polarization behavior. The effect of crystallization is slight. This suggests comparable values of corrosion rate of all materials tested in this medium that was proved in immersion measurements /Table 1/.

The materials studied undergo spontaneous passivation in 1 N NaOH. An amorphous Co-base alloy exhibits more negative corrosion potential and passive current density of about one order of magnitude higher than the recrystallized one /Fig.2/. Thus, the passive film formed on the glass shows significantly poorer protective properties than that formed on the annealed alloy. The existing literature data suggest quite opposite effect. Amorphous alloys when passivated are thought to be more corrosion resistant than their crystalline counterparts. It is related to a rapid formation of highly protective passive film on a homogeneous amorphous substrate[1,2]. Such is not the case in this instance: the heterogeneous multiphase alloy formed due to crystallization shows better passivation than the glass. Similar effect was reported for Fe-B system[5]. Further work is necessary to clarify this point.

In conclusion it should be stressed that the corrosion behavior of glassy alloys is controlled by their structure and composition as well as by features of corrosive environment. Crystallization of Fe-B-Si-C and Co-Fe-Si-B glasses reduces their corrosion resistance in acidic solutions but improves it in alkaline media and has nearly no effect in neutral environments.

This work was done under Program MR-I-21.

References

1. K.Hashimoto, T.Masumoto, Treat. Mater. Sci. Technol.,20,291,1981,
2. R.B.Diegle, N.R.Sorensen, T.Tsuru, R.M.Latanision, Treat. Mater. Sci. Technol., 23,60,1983,
3. J.C.Turn, R.M.Latanision, Corrosion, 39,271,1983,
4. L. Kiss, P. Kovacs, J.Farkas, A.Lovas, Zashch. Met.,18,193,1982.
5. M. Janik-Czachor, Proc.9-th Intern. Cong. Metallic Corrosion, Toronto 1984, Vol. 1,p.234.

06350

THE CORROSION STUDY OF AMORPHOUS AND CRYSTALLINE Co-P FILMS

A. KROLIKOWSKI
Institute of Solid State Technology
Warsaw Technical University, Warsaw /Poland/

Amorphous alloys often exhibit corrosion characteristics quite different from those observed for crystalline materials. Corrosion behavior of metallic glasses is influenced by their specific structure and chemical composition [1,2]. A separation of these two effects is difficult especially in a case of multicomponent alloys. Electrodeposited Co-P films show amorphous or crystalline structure depending on their chemical composition. Thus, this binary alloy seems to be a suitable model system to study the effects of composition and structure on the corrosion behavior.

Co-P films were electrodeposited on copper foil from chloride-phosphite solution [3]. 30-40 μm thick layers with P content ranging from 3 to 23 at.% were obtained. Their structure was examined by X-ray diffraction. Pure Co films were also deposited and subsequently used as comparative samples for corrosion tests. The corrosion behavior of Co-P films was studied with potentiodynamic polarization and impedance techniques. Potentiodynamic runs were carried out using potential sweep of $1mV \cdot s^{-1}$. Impedance measurements were performed at the corrosion potential using a frequency response analyzer Solartron 1172. All experiments were carried out in open to air solutions at 295± 1 K.

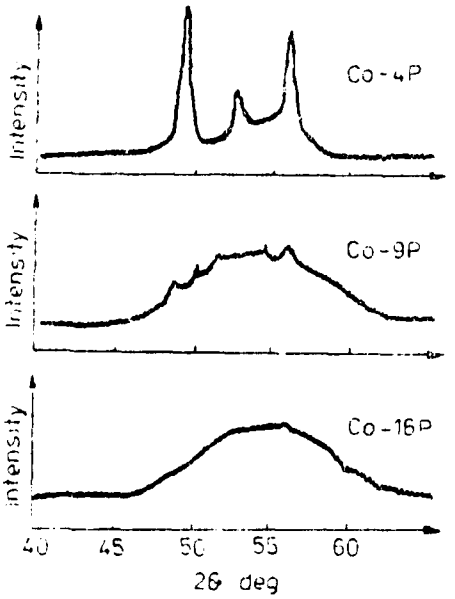

Fig. 1. Representative X-ray diffraction patterns of Co-P films.

In Fig. 1 X-ray diffraction patterns for Co-P with various phosphorus contents are shown. Films containing less than 8 at.% P are crystalline while those with P content above 11 at.% are amorphous. Samples of intermediate composition /8-11 at.%P/ show microcrystalline /amorphous structure.

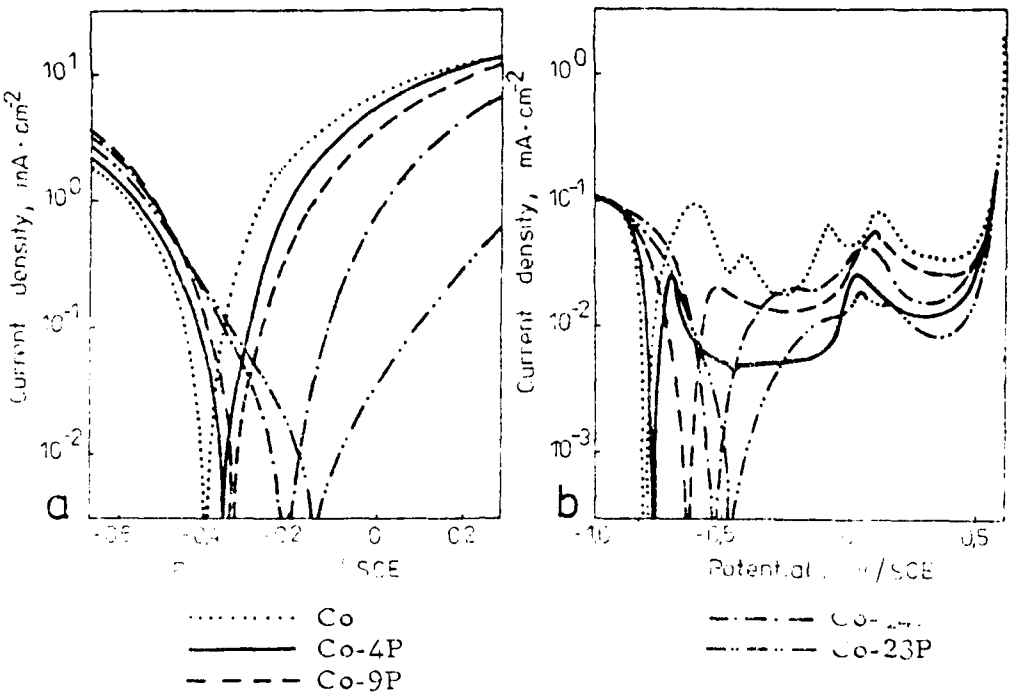

Fig.2. Polarization curves in /a/ 0,1 N H_2SO_4 and /b/ 0,1 N NaOH.

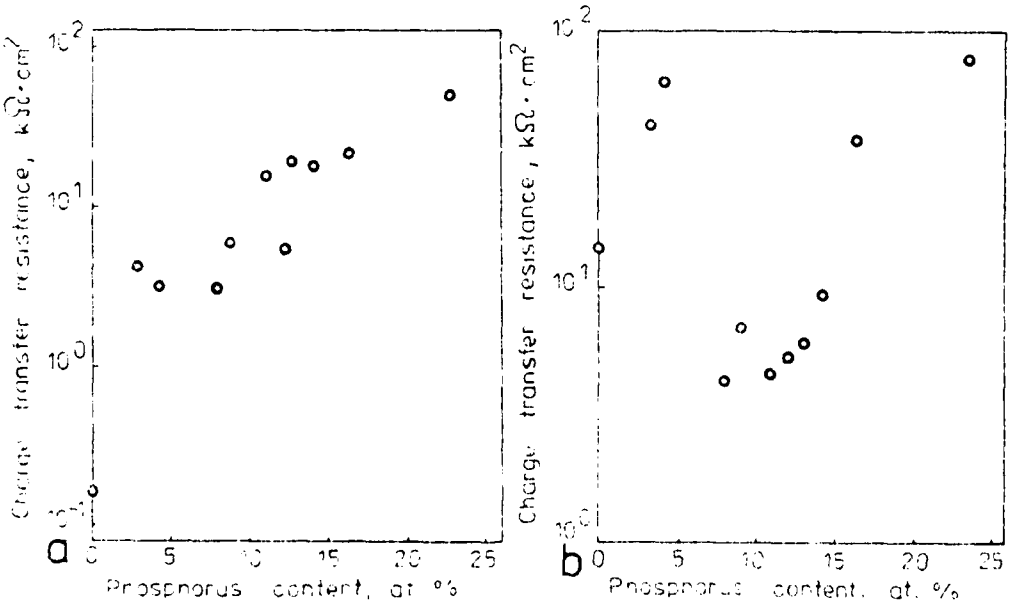

Fig.3. Effect of P content on the charge transfer resistance of Co-P films in /a/ 0,1 N H_2SO_4 and /b/ 0,1 N NaOH.

Polarization curves for pure Co and Co-P films with various P contents in 0,1 N H_2SO_4 are given in Fig.2a. All samples corrode actively and a shape of these curves is relatively similar. However a slope of cathodic and anodic branches decreases with increasing P content indicating an inhibition of hydrogen evolution and oxidation of alloy. Thus, an improvement of the corrosion resistance for P rich alloys can be expected. A relationship between alloy composition and the charge transfer resistance of Co-P in 0,1 N H_2SO_4 /estimated from impedance measurement/ is shown in Fig.3a. A trend of gradual rise of the charge transfer resistance with P content is generally observed. This finding supports the conclusion about better corrosion resistance of P rich alloys. Of interest is that a structural state of Co-P films do not significantly affect their corrosion behavior in H_2SO_4 medium. A composition of the alloy seems to be the primary factor controlling the corrosion properties of Co-P in this environment.

Polarization curves for materials studied in 0,1 N NaOH are shown in Fig.2b. The main difference between these curves appears in their anodic portions. Pure Co and Co-4P exhibit an active-passive transition. However the latter is more corrosion resistant considering a lower current density in active and passive regions. An active loop can be hardly seen for Co-9P and Co-14P samples but they show a higher passive current density in relation to Co-4P. An alloy containing 23 at. % P passivates spontaneously. A sharp drop of the charge transfer resistance of Co-P films in 0,1 N NaOH is observed near the composition range which corresponds to the transition from the crystalline to microcrystalline /amorphous structure /Fig.3b/. This fact indicates a significant reduction of the corrosion resistance of microcrystalline /amorphous films in comparison with that of crystalline ones.

The main conclusions of the present work are as follows. In a case of active corrosion in H_2SO_4 the corrosion behavior of Co-P films is first of all controlled by the alloy composition and the structure has a rather slight effect. However in NaOH when Co-P films undergo passivation their corrosion resistance is strongly influenced by the structural transition from crystalline to microcrystalline/amorphous state.

The author is greathy indebted to Professor Przyluski /Warsaw Technical University/ for his encouragement to perform this work and to Professor Boehni /ETH Zurich/ for making available impedance measurements.

This work was done under Program 05.3.

References

1. K.Hashimoto, T.Masumoto, Treat. Mater. Sci.Technol.,20,291,1981,
2. Y.Waseda, K.T.Aust, J.Mater.Sci., 16,2337,1981,
3. G.S. Cargill III, J.Appl, Phys., 41,12,1970.

06360

SURFACE ENHANCED RAMAN SCATTERING (SERS) INVESTIGATION OF CORROSION INHIBITION OF COPPER

M.M. MUSIANI*, G. MENGOLI*, and M. FLEISCHMANN**

* Istituto di Polarografia ed Elettrochimica Preparativa del CNR, Padova (Italy)

** Chemistry Department, University of Southampton, Southampton (Great Britain)

In recent years both ex situ high vacuum spectroscopies (XPS, AUGER, SIMS, ISS[1]) and in situ techniques (photo-current spectroscopy[2], ellipso- metry) have become popular and powerful tools in the investigation of solid phases on corroding metal surfaces. The spectroscopic study of organic and inorganic adsorbates is currently much less developed, mainly because the in situ identification of mono- and submonolayers requires great sensitivity and selectivity with respect to species in solution.

Surface enhanced Raman scattering (SERS)[3] fulfils these requirements, as the Raman signals of species adsorbed at roughened Ag, Cu or Au electrodes are enhanced by a factor of 10^6. Some papers have been published since 1981 reporting SERS spectra of corrosion inhibitors recorded at Ag[4,5] and Cu[6,7].

We studied the competitive adsorption of corrosive anions and organic corrosion inhibitors on Cu[8,9] by comparing SERS and electrochemical results, in order to evaluate potentialities and limitations of in situ Raman spectroscopy when applied to corrosion inhibition phenomena. The SERS behaviour of all investigated systems falls within one of the following general patterns:

i) only the spectrum of the inhibitor is observed;

ii) both inhibitor and corrosive anion are detected;

iii) SERS signals are lost at open circuit.

i) Stable SERS intensity of the inhibitor alone at the corrosion potential is interpreted as an indication of effective corrosion inhibition. This behaviour is shown by benzotriazole (BTA, 10^{-2} M) in 1M KCl. The Cu-Cl band at 286 cm^{-1}, present in the spectrum of KCl alone, disappears after addition of BTA, which is so strongly adsorbed that the electrode may eventually be transferred to pure 1M KCl and left at open circuit potential without significant intensity loss. In agreement with SERS results, 10^{-2}M BTA was shown to reduce the corrosion rate of copper in 1M KCl by 90%.

ii) Simultaneous detection of spectra due to both inhibitors and corrosive anions points to conditions favourable to localized corrosion. Coadsorption was observed for 1M KCl + 10^{-2}M benzimidazole and for 10^{-3}M KCN + 10^{-2}M BTA in 1M KCl. For the BTA/KCN system, a continuous transition from BTA to cyanide ion spectra

corrosion. Coadsorption was observed for 1M KCl + 10^{-2}M benzimidazole and for 10^{-3}M KCN + 10^{-2}M BTA in 1M KCl. For the BTA/KCN system, a continuous transition from BTA to cyanide ion spectra was observed by progressively increasing the KCN concentration up to 10^{-2}M.

iii) Loss of SERS at open circuit, due to removal of adatoms, may have different causes. It may be ascribed to corrosion. However, corrosion promoted by cyanide ions was shown to occur without destruction (or with regeneration) of SERS-active sites. An alternative explanation for SERS signal loss is the growth of a thick surface film. SERS spectra could, however, be detected at a Cu electrode on which a thick Cu-BTA film had grown.

Other useful experiments may be carried out. For instance, mixtures of inhibitors may be investigated, for further information on relative strength of adsorption, kinetics of displacement and possible synergetic effects.

In conclusion, despite the restricted number of SERS active metals, surface enhanced Raman spectroscopy provides structural information on adsorbed species as a function of potential, concentrations and time, and may contribute to the elucidation of corrosion inhibition mechanisms.

1) H. Leidheiser Jr. in "Passivity of metals", R.P. Frankenthal, J. Kruger (Eds), The Electrochemical Society, Princeton (1978) p. 223.
2) F. Di Quarto, S. Piazza, C. Sunseri; Electrochim. Acta 30, 315 (1985) and references therein.
3) R.K. Chang, T.E. Furtak (Eds) "Surface Enhanced Raman Scattering", Plenum Press, New York (1982).
4) M. Oshawa, H. Matsuda, W. Suetaka; Chem.Phys.Lett. 84, 163 (1981).
5) J.C. Rubim, I.G.R. Gutz, O. Sala; J.Mol.Struct. 101, 1 (1983).
6) J.J. Kester, T.E. Furtak, A.J. Bevolo; J. Electrochem. Soc. 129, 1716 (1982).
7) D. Thierry, C. Leygraf; Electrochem.Soc.Meeting, Cincinnati, May 1984, no. 430.
8) M. Fleischmann, I.R. Hill, G. Mengoli, M.M. Musiani, J. Aknavan; Electrochim. Acta, in press.
9) M. Fleischmann, G. Mengoli, M.M. Musiani, C. Pagura; Electrochim. Acta; in press.

06370

LASER RAMAN SPECTRO-ELECTROCHEMICAL STUDIES ON THE CORROSION AND PASSIVATION BEHAVIOR OF NICKEL IN AQUEOUS SOLUTIONS

K. CARR, S. XU, and C. A. MELENDRES
Materials Science and Technology Division/Chemical Technology Division
Argonne National Laboratory
Argonne, Illinois 60439, U.S.A.

Laser Raman Spectroscopy (LRS) continues to provide useful information on the composition of corrosion films on metals.[1] The ability to examine surface layers "in-situ," under actual environmental conditions, is particularly valuable and of great advantage over other more conventional surface analytical methods which study materials under high vacuum conditions. We have used the technique, in conjunction with cyclic voltammetry, to determine the structure and composition of anodic corrosion films on Ni in acid, base and near-neutral solutions. Results are herein presented.

EXPERIMENTAL

Nickel electrodes were prepared from 0.010-in. thick foils of Marz grade material (99.999% purity) purchased from Materials Research Corporation, Orangeburg, New York. The solutions used were: 0.05 N NaOH (pH = 11.8), 0.15 N sodium borate buffer (pH = 8.4), 0.15 N Na_2SO_4 (pH adjusted to 8.4 by addition of NaOH), and 0.5 M K_2SO_4 + 0.005 M H_2SO_4 (pH = 3.1). Reference electrodes consisting of Hg/HgO, saturated calomel (SCE) and Hg/Hg_2SO_4 were used in basic, borate, and sulfate solutions, respectively. The corrosion specimens were anodized at constant potential in ambient-air using a 3-compartment spectro-electrochemical cell described previously.[2] Measurements at temperatures above ambient were carried out in a single-compartment cell which was heated electrically by wrapping a 'Briskeat' flexible heating tape (Briscoe Manufacturing Co., Columbus, Ohio) around the cell body. The electrochemical and LRS equipment used were the same as before.[2]

RESULTS AND DISCUSSION

Cyclic voltammograms of Ni in 0.15 N sodium borate buffer solution of pH 8.4 are shown in Fig. 1. Consider for the moment the behavior at 25°C. The redox wave at about 0.75 V, represents the formation and reduction of a surface film. Raman spectroscopic identification of the film was carried out "in-situ" while potentiostating the electrode at 0.85 V. A typical result is shown in Fig. 2a; two vibrational bands are observed at 479 and 552 cm^{-1}. In order to establish the composition of the film, standard samples were prepared and their spectra taken. Some of these are shown in Fig. 3. It is evident that the reference spectrum which corresponds most closely to that observed for the electrode is that of $Ni_2O_3 \cdot 2H_2O$. Thus, the anodic corrosion film is composed of a higher valency form of Ni oxide. No Raman bands were observed at less positive potentials where Ni(OH)2 or NiO have been proposed to be present. Presumably, the film thickness corresponding to the amount of these materials present is so thin and thus beyond our detection sensitivity.

The temperature dependence of the rates of film formation processes corresponding to the anodic wave at about 0.75 V (Fig. 1) is also shown. From the observed current maxima, it is evident that the rate increases about 4-times as the temperature is raised from 25 to 100°C. The Raman spectra shows an increase in the intensity of the band at 478 relative to that at 552 cm^{-1} with temperature. In the absence of a definite vibrational band assignment, it is difficult to explain the significance of this result. It presumably reflects a change in the structure of the anodic film.

The electrochemical behavior of Ni in 0.15 N Na_2SO_4 of pH 8.4 is shown in Fig. 4. We were unable to observe any vibrational bands at potentials cathodic of the wave at about 0.3 V. Raman scans following anodization at 0.35 V, however, yielded spectra similar to that in Fig. 2a. This suggests that the composition of the anodic film is the same as that found in borate solution of the same pH.

Essentially the same electrochemical and spectroscopic results are obtained in 0.05 M NaOH (pH ~ 12). In this solution the redox wave occurs at about 0.5 V vs. Hg/HgO and the spectrum obtained following anodization at 0.6 V shows the same bands at 478 and 552 cm^{-1}. In contrast, we were unable to observe any vibrational bands when Ni was anodically corroded in acidified sulfate solution (0.5 M K_2SO_4 + 0.005 M H_2SO_4, pH ~ 3). We find an irreversible anodic wave at about -0.3 V vs. Hg/Hg_2SO_4 in the cyclic voltammogram of Ni in this solution, as Bockris, et al. have observed.[3] However, no Raman spectrum was obtained despite the fact that the charge corresponding to the anodic wave would suggest about the same film thickness as were formed in the near-neutral solutions. It is probable that the structure and composition of the anodic corrosion film formed in acid solution may be different from that formed at pH 8.4.

In conclusion, the present studies have shown the existence of a higher valency oxide of Ni at potentials close to the transpassive region just prior to oxygen evolution. The composition is found to correspond to $Ni_2O_3 \cdot 2H_2O$. This appears to be the first time this compound has been shown to exist as a surface film on Ni. Previous studies have dealt mostly with the lower valent oxide NiO.[4] The present findings appear to be consistent with that predicted by the Pourbaix diagram.[5]

ACKNOWLEDGEMENT

This research work was done under the auspices of the Division of Materials Science, Office of Basic Energy Sciences, U.S. Department of Energy. One of the authors (K. C.), gratefully acknowledges financial support by the Division of Educational Programs, Argonne National Laboratory, under its Student Research Participation Program.

REFERENCES

1. C. A. Melendres, S. Xu, and B. Tani, J. Electroanal. Chem. 162, 343 (1984).
2. C. A. Melendres and F. A. Cafasso, J. Electrochem. Soc. 128, 755 (1981).
3. J. O'M. Bockris, A. K. N. Reddy, and B. Rao, J. Electrochem. Soc. 113, 1133 (1966).
4. B. MacDongall, D. F. Mitchell, and M. J. Graham, J. Electrochem. Soc. 127, 1248 (1980).
5. M. Pourbaix, "Atlas D'Equilibres Electrochimiques" pp. 325, Gauthier-Villars, Paris (1963).

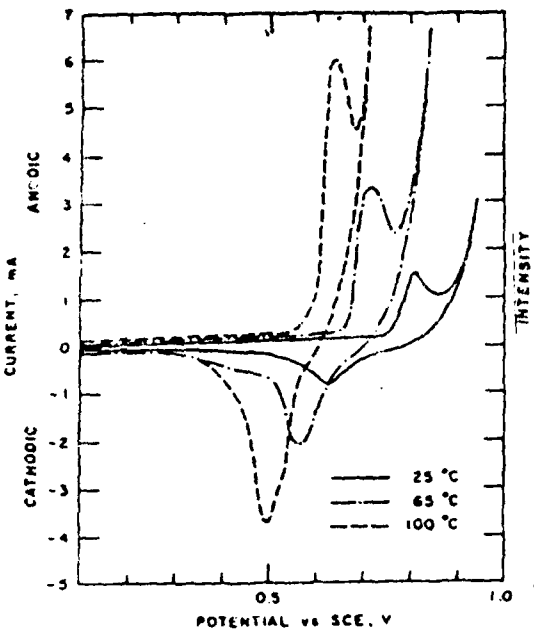

Fig. 1. Cyclic Voltammograms of Ni in Borate Buffer Solution (pH=8.4) at Various Temperatures. Scan Rate = 10 mV/sec.

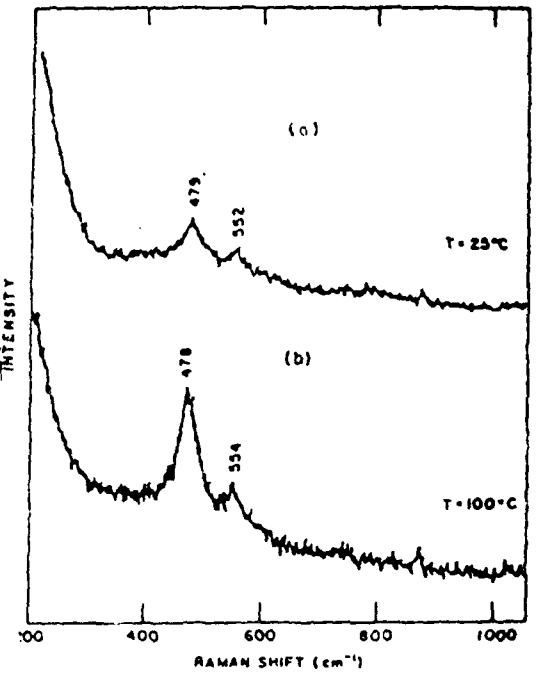

Fig. 2. Laser Raman Spectra of Ni in Borate Buffer Solution, pH=8.4, E=0.85 V vs. SCE
Ar⁺ laser, 5145 Å Exciting Line, 100 mW Laser Power

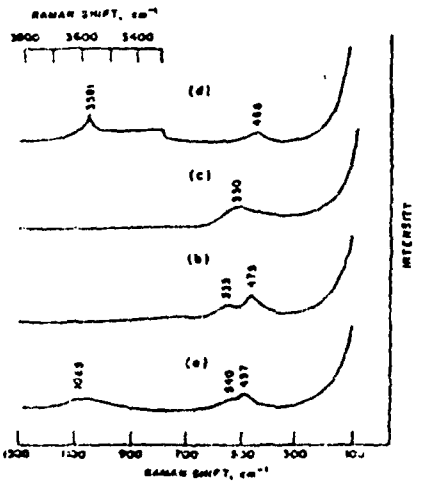

Fig. 3. Laser Raman Spectra of Standard Samples of Ni Compounds (20/80% in KBr pellet);
a) NiO
b) $Ni_2O_3 \cdot 2H_2O$
c) Charged Ni electrode for Ni/Fe battery
d) $Ni(OH)_2$

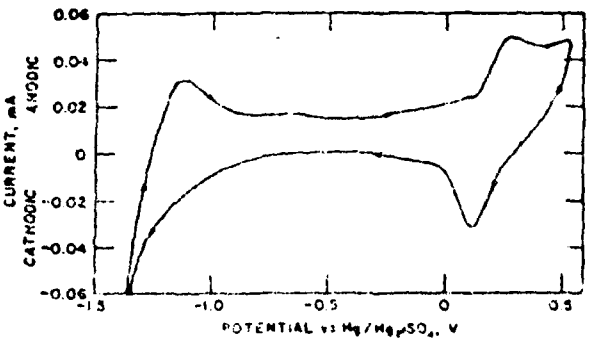

Fig. 4. Cyclic Voltammogram of Ni in 0.15 M Na_2SO_4 Solution, pH=8.4
Scan rate = 10 mV/sec.

06380

EFFECT OF ADDITION OF HALIDE IONS ON THE ANODIC BEHAVIOUR OF TIN IN STANNATE PLATING SOLUTIONS

S.S. ABD EL REHIM and A. EL SAYED
Faculty of Science, Ain Shams University, Cairo /Egypt/

The effect of adding various concentrations ranging from 0.03 upto 1 M of NaCl, NaBr and NaI on the behaviour of speck pure tin anode of 0.5 cm^2 area in an alkaline-stannate bath containing 50 gl^{-1} $Na_2Sn(OH)_6$ +10 gl^{-1} NaOH was studied galvanostatically and potentiostatically using SCE as a reference electrode and Pt wire as a counterelectrode at $30^0 \pm 1^0C$.

A typical galvanostatic potential-time curve for the anodic oxidation of Sn in the alkaline-stannate bath at anodic current density of 60 $mAcm^{-2}$ is given in Fig.1. The anodic potential increases very slowly giving rise to two poorly defined arrests and then jumps suddenly to a steady state potential at the inflexion point C. The first arrest is very short /few seconds/ as compared with the second one. Along the first arrest the potential compares satisfactorly with the equilibrium system $Sn/Sn(OH)_2$, while that of the second arrest compares to the system $Sn/Sn(OH)_4$ at the corresponding pH value. When the anode surface is covered with the passive film, which would be some sort of the reaction product out of $Sn(OH)_2$ and or SnO, and $Sn(OH)_4$ and or SnO_2, the potential jumps suddenly to the inflexion potential C. The time elapsed from the starting until the potential jump is the passivation time τ.

Progressive addition of Cl^- ion into the bath up to a certain critical concentration causes a gradual increase in the passivation time and a shift in the inflexion potential into the more positive directin, indicating aggressive action. Beyond this critical concentration, the passivation time starts to decrease and the inflexion potential increases, indicating inhibitive action. The relation between the passivation time and the molar concentration of Cl^- ion is shown in Fig. 2. The broken line AB represents the passivation time in the absence of halide ion. The results denote that Cl^- ion behaves bifunctionally, causing a breakdown of the passive film at lower concentrations and reestablishing it at higher concentrations. The extent of these two opposing mode of action increases with increasing the Cl^- ion concentration. Apparently the two action must be based on different mechanisms.

Similar results were obtained by using an anodic current density of 120 mA cm^{-2}. The transition in the function of Cl^-

ion occurs at a lower passivation time, the higher is the current density used.

A series of the potential-time curves were conducted at various current densities ranging between 20 to 120 mA cm^{-2} using the stannate solution devoid of or containing either 20 gl^{-1} /aggressive concentration/ or 50 gl^{-1} /inhibitive concentration/ of Cl^- ion. The results show that the passivation time is inversly porportional to the current density. The log j-log τ curves are linear as shown in Fig. 3. These results confirm the aggressive and inhibitive actions of Cl^- ion, since the broken line lies between the two curves for the solutions containing Cl^- ion.

The aggressivity of Cl^- ions is based on their specific adsorption on the surface of the passive film, where under the effect of electrostatic field they penetrate and rupture the passive film. Primary the inhibitive funciton of Cl^- ion may be due to the precipitation of a basic sparingly soluble tin oxychloride which tends to block the pits and seal the pores in the passive film. Thus the inhibitive action is due to a successive formation of a new film forming phase[2].

In contrast, addition of Br^- or I^-, the less aggressive ions /within the concentration range studied/ promots the achievement of passivation as manifested by enoblement of the inflexion potential at C and by a gradual decrease in the passivation time as shown in Fig. 2 where their curves lie below the broken line AB. The inhibitive action of these ions is tentatively understood on the basis of the deposition of basic tin oxyhalides. The inhibitive action of I^- ion is greater than that of Br^- ion.

Fig. 4 shows a typical potentiostatic curve of tin anode in the alkaline-stannate bath. Sweeping started from the rest potential up to + 2000 mV with a scan rate of 20 mV min^{-1}. The polarization curve consists of two dissolution current peaks I and II in active region and a permanent passivation region III followed by a transpassive region IV prior to oxygen evolution. The current peaks I and II could be attributed to the formation of $Sn(OH)_2$ /and or SnO/ and $Sn(OH)_4$ /and or SnO_2/ respectively. The permanent passivation region[4] III extends about 1 V and the very small current density flowing along it is independent on the potential and used to replace the passive film.

Addition of the halide ions causes a gradual decrease in the height of both the current peaks I and II. The behaviour is due to the tendency of the halide ions to adsorb on the metal surface at more negative potentials than those corresponding to the permanent passivation and retards the entry of tin ions into the solution at the anode[3]. Moreover, addition of low concentrations of Cl^- ion enhances slightly the current

density flowing along the permanent passivation region III. Addition of Higher concentrations of Cl^- ion has no appreciable changes on the permanent passivation region. Similarly the addition of Br^- or I^- ion has no significant effect on this region.

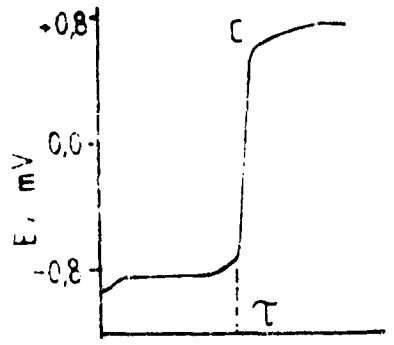

Fig 1.

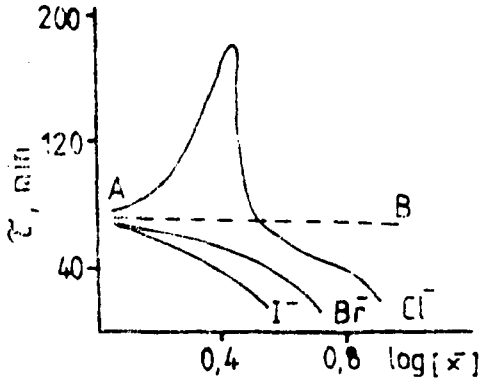

Fig.2

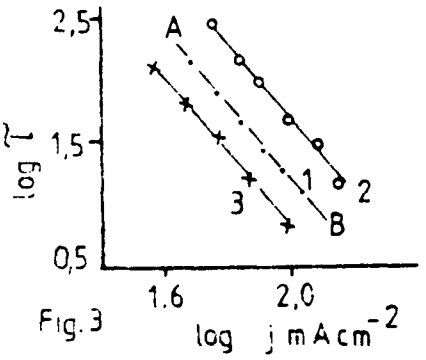

Fig.3

(1) 0,0 ; (2) 20 ; (3) 50 gl^{-1} Cl^-

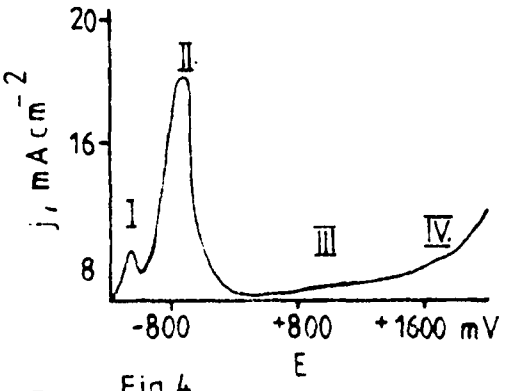

Fig.4

REFERENCES

1. A.M. Azzam, S.S. Abd El Rehim and M.H. Fawzy, J. Appl. Chem. Biotechnol., 23, 563 /1973/

2. F.M. Abd El Wahab, J.M. Abd El Kader, H.A. El Shayeb and A.M. Shams El Din, Corros. Sci., 18, 997 /1978/

3. Ya.M. Kolotyrkin, J. Electrochem. Soc., 108, 209 /1961/

06390

SOME RESULTS OF A.C. AND D.C. TECHNIQUES USED TO MEASURE THE CORROSION RATE OF STEEL AND ZN EMBEDDED IN MORTAR

C. Alonso, A. Macías, P. Santos, C. Andrade

Instituto Eduardo Torroja, Madrid, Spain.

INTRODUCTION

The difficulty of the use of electrochemical techniques in steel embedded in concrete is accounted for the special characteristics of the concrete as electrolyte, for example its high electrical resistivity and its physical heterogeneity.

At the present time, the most studied techniques are the Polarization Resistance (D.C.) (1) and the A.C. Impedance measurements (2). In this work, some results obtained by the use of these two techniques, are presented.

The systems studied have been: bare steel and pure zinc embedded in mortar. Finally, an attempt to compare the results obtained through the two techniques, is explained.

MATERIALS AND EXPERIMENTAL PROCEDURE

Small prismatic mortar specimens (2 x 5,5 x 8 cm in size) were employed. They were fabricated with common Portland cement of fast hardening (P - 450 - ARI). The specimens contained two identical working electrodes (duplicated experiment) of bare steel or Zn. In the mortar specimens containing bare steel, 3% of Na NO_2 as corrosion inhibitor, was added in the mix. These mortar specimens were carbonated by an accelerated method introducing them after a cure period of 28 days, in chamber with an atmosphere almost saturated in CO_2 and with about 60% of R.H. Finally, the specimens were stored in a chamber with cyclic variations of the relative humidity: 100% - 50%, partially inmersed in distilled water.

In specimens containing Zn, different proportions of Ca Cl_2 (2% or 3% by weight of cement), to active corrosion, were added. They were stored in a chamber with 100% of R.H.

RESULTS AND DISCUSSION

Figures 1 and 2 show the evolution of the corrosion intensity (Icorr) versus time, of steel and Zn bars, measured by Rp (D.C.) technique. By the trend of figure 1 it is possible to deduce that the steel is passivated during the cure period and remains so during the rest of the experiment, even during the carbonation process and in the later humidity conservation periods. The presence of 3% Na NO_2 is revealed effective to avoid corrosion of steel in these situations.

The trend of figure 2 shows a similar behaviour for Zn embedded in mortar containing different proportions of Cl^-: although at the begin-

ning of the experiment the Icorr values are high but decrease as the time proceeds. Only 3% Ca Cl_2 maintains the Icorr in high values.

Figures 3 and 4 show Nyquist diagrams obtained by A.C. Impedance measurements. They were simultaneously obtained in the same specimens that in former figures. Figure 3 shows the results on the case of the steel: the variation of the impedance with the frequency gives a more or less vertical line that may be the beginning of big semi-circles. This type of trend is always obtained when steel is passivated; the phase at the lowest frequency tested is higher than 45º. Figure 4 shows the Zn behaviour: without chlorides or with 2% Ca Cl_2 although the Zn is not being corrode, the phase shift at the lowest frequency tested is smaller than in the steel, but in the case of 3% Ca Cl2 the angle at low frequencies is smaller than 45º.

Finally a graphical extrapolation, using a Bode representation has been carried out in order to compare the Rp values obtained by the D.C. technique, with the impedance module value obtained by the A.C.technique. In the case of the steel a good agreement is obtained at 10^{-5} Hz and for the Zn, the agreement is obtained at 10^{-2} Hz - 10^{-3} Hz.

By these results it may be drawn that the D.C. technique is the most useful in order to obtain values of the corrosion rate, but the A.C. technique may give the most useful ones in order to know the morphology of the attack.

REFERENCES

(1) C. Andrade, J.A. González - Werkstoffe und Korrosion, 29 (1978) 515.

(2) D.G. John, P.G. Searson, J.L. Dawson - British Corrosion Journal 16 (1981) 102.

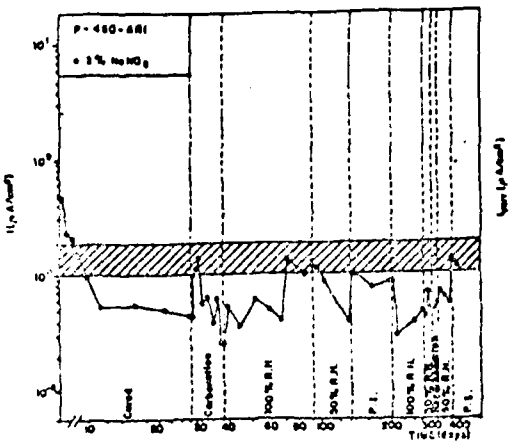
P-450-ARI
+ 3% NaNO2
Cond
Carbonatation
100 % R.H
30 % R.H
P.I.
100 % R.H
23 % R.H
50 % R.H
P.I.

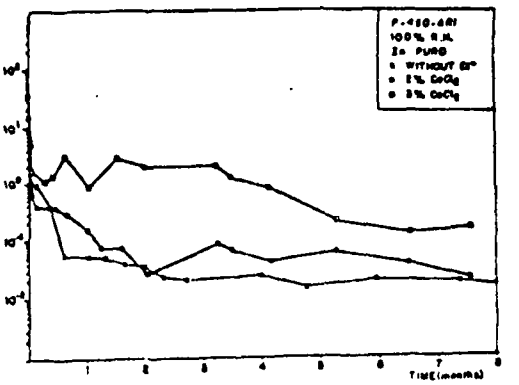
P-450-ARI
100 % R.H.
In PURE
WITHOUT Cl-
3% CaCl2
3% CaCl2

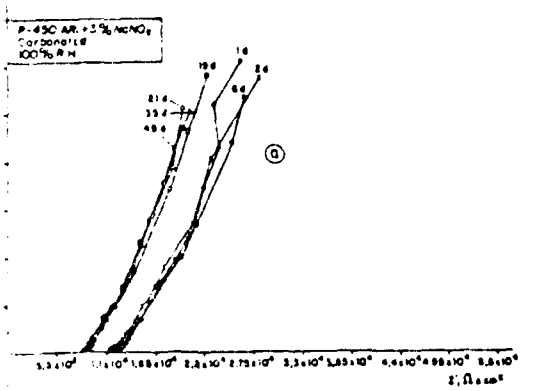
P-450 ARI + 3% NaNO2
Carbonated
100 % R.H
a

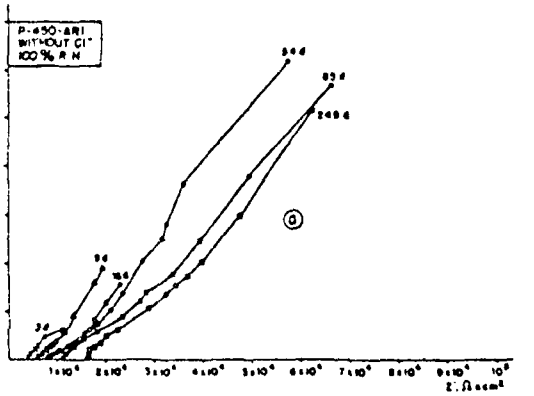
P-450-ARI
WITHOUT Cl-
100 % R.H
a

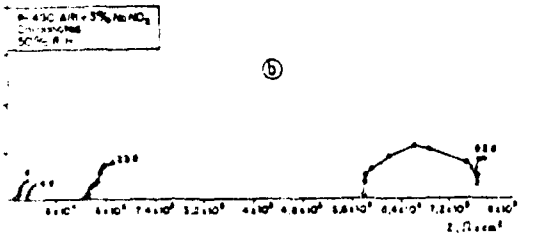
b

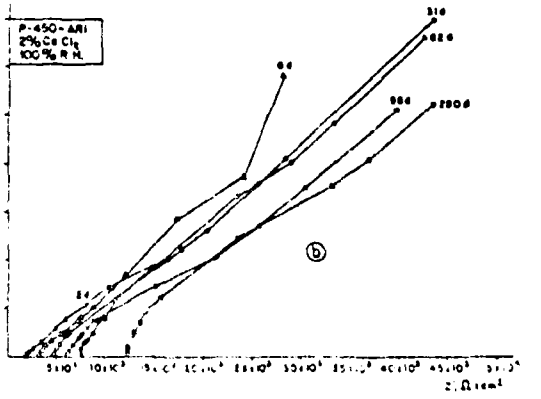
P-450-ARI
3% Ca Cl2
100 % R.H.
b

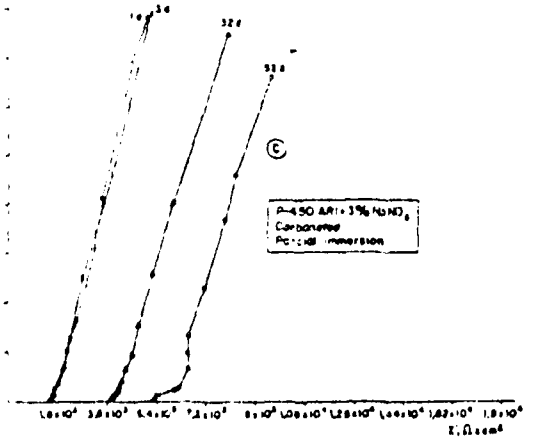
c
P-450 ARI + 3% NaNO2
Carbonated
Partial immersion

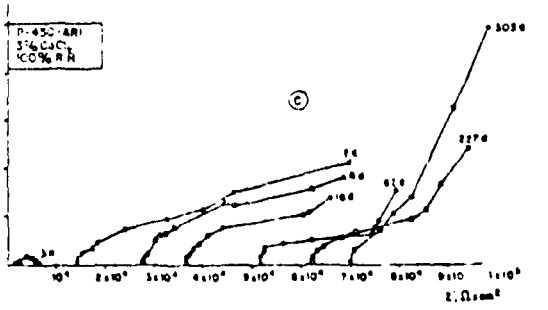
P-450-ARI
3% CaCl2
100 % R.H
c

06400

CORROSION AND STABILIZATION OF n-GaAs IN AQUEOUS IODIDE SOLUTIONS

P. ALLONGUE*, H. CACHET*, P. CLECHET**, M. FROMENT*, J.R. MARTIN** and E. VERNEY**

* Laboratoire de Physique des Liquides et Electrochimie (LP 15 CNRS)
associé à l'Université Pierre et Marie Curie
4, place Jussieu - 75230 Paris Cedex 05, France
**Laboratoire de Physicochimie des Interfaces (UA 404 CNRS)
Ecole Centrale de Lyon
BP 69131 Ecully Cedex, France

Corrosion of photoanodes is one of the factors which limit the use of n type small gap semiconductors in the photoelectrochemical conversion of solar energy. Photoanodes can be stabilized by concentrated reducing redox systems [1,2]. Results will be presented concerning the stabilization of n-GaAs (1,0,0) single crystals by the (I^-/I_2) couple at various pH and at different concentrations of iodide and iodine. The stabilization coefficient is determined by the rotating ring disk technique [3]. The energetic conditions and the transfer kinetics are studied by impedance measurements. Corrosion products in the dark and under illumination are identified thanks to reflexion high energy electron diffraction (RHEED).

Rotating ring disk measurements prove the dependence of stabilization on the reducing agent concentration and the proton activity. The best stability ($\sim$ 100 %) is obtained with highly concentrated iodide medium (7 M) at pH = 0 as measured with the glass electrode. In the 7 M medium we observe, with increasing acidity, that (i) the thickness of the formed oxide layer decreases, and (ii) the surface roughness disappears. Indeed, a cfc As_2O_3 oxide layer is found by RHEED analysis after 4.5 hour illumination at V = + 0.1 V/SCE (I_{ph} = 1 mA/cm^2) in 7M NaI pH = 2 (Fig. 1a) and pH = 0 (Fig. 1b) solutions. The well defined ring pattern obtained in Fig. 1a indicates a thicker layer at pH = 2 than at pH = 0. For lower iodide concentrations the anodic photocorrosion of n-GaAs occurs ; the stabilization efficiency is only 40 % in a 2M NaI pH = 0 solution.

Impedance measurements performed in the dark in I_2 free solutions show that the band edge positions of n-GaAs are independent of the I^- concentration in the range 0.1M - 7M. However, as others [4], we find a positive shift of the band edges with an increasing I_2 concentration. These variations are presented in Fig. 2a for the 7M NaI pH = 0 (as measured with the glass electrode) solution. Note that the spontaneously formed I_2 ($\simeq 10^{-4}$M) in such an acidic medium explains that the flat band potential is - 0.85 V/SCE. This value is slightly positive compared to the V_{fb} found in I_2 free solution (- 0.93 V/SCE). Fig. 2b shows the variations of the flat band potential shift ΔV_{fb} against the saturated current density (proportional to illumination) measured at V = + 1.0 V/SCE in a 7M NaI pH = 0 (•) and a 2M NaI pH = 0 (⋆) solution . The electrode area is 0.25 cm^2. In the highly concentrated medium the limiting value of ΔV_{fb} is only $\sim$ 140 mV while it is $\sim$ 260 mV in the 2M solution. If we consider that the redox potential is + 0.1 and + 0.18 V/SCE, respectively for the 7M and 2M electrolytes, it is

found that the energy diagram of the junction (band edge positions of n-GaAs with respect to the redox potential) remains almost the same in both media. This later remark indicates that the hole trapping at the surface, responsible for the V_{fb} displacement [5], is controlled by both charge transfer kinetics at the interface and corrosion rate. A very good stabilization and a greater transfer kinetics in the 7M electrolyte would then explain the smaller shift ΔV_{fb}.

Preliminary experiments have been performed with Ruthenium treated n-GaAs electrodes. The chemisorption of Ru^{3+} is achieved by dipping the electrode in a 10^{-2}M $RuCl_3$ + 10^{-1}M HNO_3 solution. Fig. 3 presents potentiostatic I-V characteristics of the n-GaAs/7M NaI (pH = 0) junction under illumination with a Ru-treated (curve a) and a bare (curve b) electrode (area 0.25 cm^2). As in the case of Se^{2-} solutions [6], it can be seen that this surface modification increases both fill factor and photopotential of the junction (curve a, Fig. 3). Moreover the band edges remain pinned at - 0.84 V/SCE even under illumination. The former fact indicates, as before [6], that the Ruthenium has a catalytic effect upon the transfer. The later fact confirms that the magnitude of the flat band potential shift is correlated to the transfer kinetics [7].

ACKNOWLEDGMENTS

This work is supported by both CNRS (PIRSEM) and AFME through GRECO 130061 research program .

REFERENCES

1. C.P. Kubiak, L.F. Schneemeyer, M.S. Wrighton
J. Am. Chem. Soc. 129, 1977 (1980).

2. L.F. Schneemeyer, B. Miller
J. Electrochem. Soc. 129, 1977 (1982).

3. E. Verney, J.R. Martin, P. Cléchet
J. Electrochem. Soc. (accepted).

4. J.E.A.M. Van Den Meerakker
Electrochim. Acta 30, 435 (1985).

5. P. Allongue, H. Cachet
J. Electrochem. Soc. 131, 45 (1985).

6. P. Allongue, H. Cachet
J. Electrochem. Soc. 130, 2861 (1984).

7. P. Allongue, H. Cachet
Solid State Comm. (accepted) (1985).

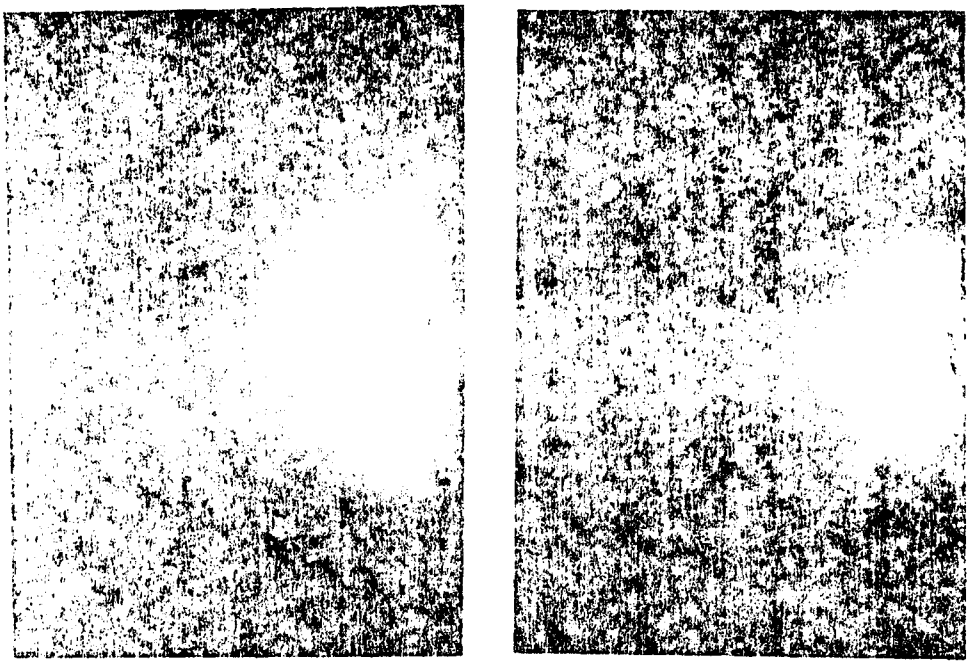

Figure 1

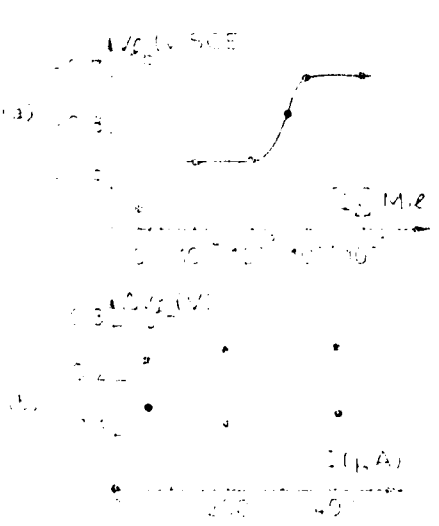

Figure 2

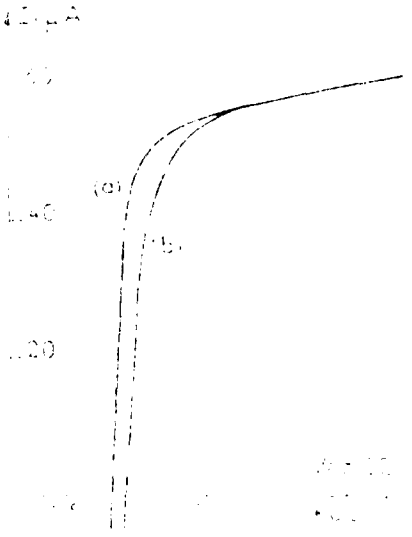

Figure 3

06410

APPLICABILITY OF THE ELECTROCHEMICAL METHODS TO THE STUDY OF THE EXTERNAL CORROSION OF METALLIC TUBES IN BUILDINGS

F. HUETE AND J.J. ROYUELA
CENIM, Madrid (Spain)

Introduction

Since UR Evans' work in the 20's the electrochemical nature of the metallic corrosion was known. Different methods to study the behaviour of metals and metallic alloys in different environments were developed[1]. In general electrochemical methods consist in the application a DC or AC signal to the system and registration of its response. If the imposed magnitude is current the methods are galvanostatic, and if the magnitude is potential the method are potentiostatic or potencidinamic.

The positive results obtained in previous papers on the corrosion of steel and galvanized steel in concrete[2,3], justifies the use of electrochemical methods for the specific case of tubes in buildings, which is a similar environment. The main difference between these environments consist in the low protector character of the "poor" mortar (low cement/sand and high water/cement ratios, and other filler materials (sand, gypsum, rubbish, etc), which are normally in contact with embedded tubes. This circunstance implies high sensibility to the environmental changes: moisture level, pH and high level of corrosive anions (Cl^-, SO_4^{-2}..

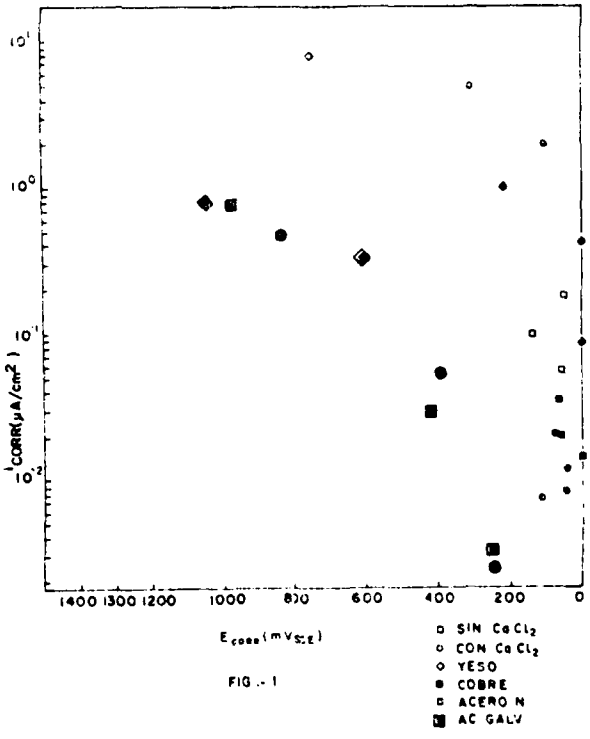

FIG.- 1

Experimental procedure

In this work DC an AC potenciostatic methods were

employed. In the DC metod an overpotential of -10 mV with relation to E_{corr} was applied and the response were recorded in current after 30 second (steady-state). With these values Rp was determinated and employing the Stern-Geary formula, i_{corr} were calculated[4]. The measurements were made with a potentiostat AMEL-55' with positive feedbach. In the AC method a frecuencies sweep between 55 kHz and 1 mHz was realized. The amplitude signal was of 10 mV. The impedance vector was represented in the module/argument form at different frecuencies (Nyquist Diagram) and assuming the validity of the Randles' circuit, the values of Rp and i_{corr} were calculated. The electrochemical interface 1186 with a Frecuency Response Analyser 1250 Solartron was employed.

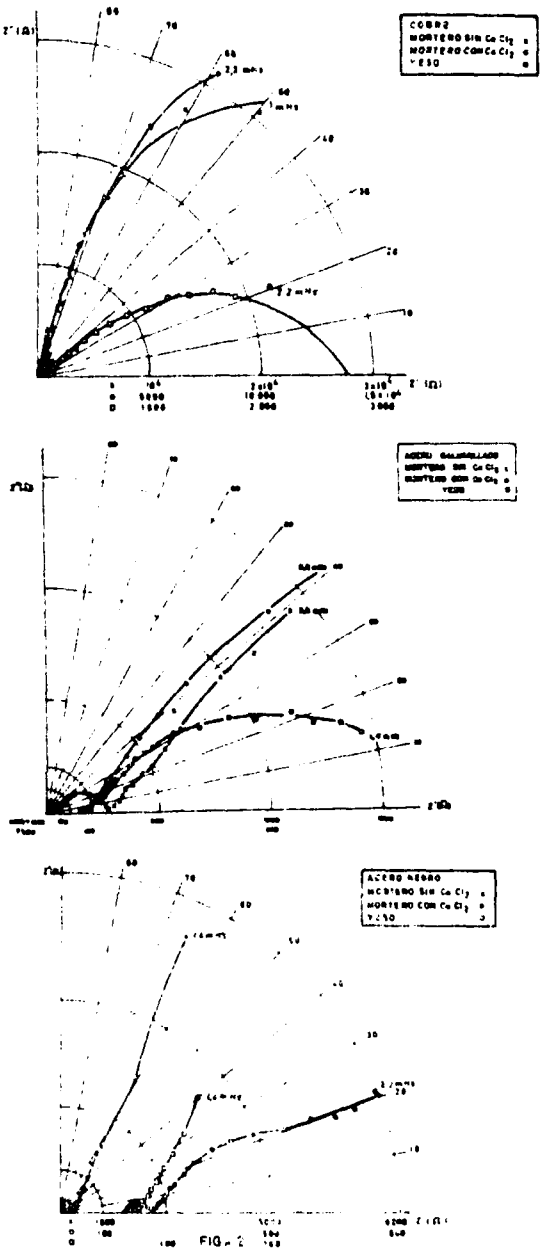

The probes were prepared with normalized tubes of the more common metals used in buildings (steel galvanized steel and copper) in contact with a mortar of cement/sand 1/3 and water/cement 1/1 ratios. The mortar probes were stored in different degrees of humidity: partially submerged in water 100% and 50% of relative moisture. In some cases a 3% in weight of $CaCl_2$ 2 H_2O was added to the cement in order to study the influence of chlorides in the corrosion kinetic. Finally, a group of probes made out of white gypsum

Results and coments

According to the results obtained we can see that the electrochemical methods give acceptable information about the exterior corrosion of tubes embedded in buildings. In the fig. 1 some significant examples of the measurements in the DC method in different conditions were plotted. These values corresponding to the end of the study. In the case of the steel and the galvanized steel in gypsum and stored in 50% RH, due to the drying of this construction material the measurements cannot be made until the finish of the test. We can see that only there is a linear relation between E_{corr} and i_{corr} for the galvanized steel. In the case of the steel and specially in the copper, there are big differences of the values of i_{corr} compared with a very similar values of E_{corr}, this mean that occues changes in the corrosion kinetics in different environments.

Some examples of the impedance diagrams are shows in fig. 2 for the metals and the environments employed in this study. These diagrams indicate the validity of the Randles' equivalent circuit, in the case of the steel without chlorides where the capacitive behaviour may concern to the passive state of the iron.

On the other hand the behaviour of the steel embedded in gypsum perhaps can be explained because when a little half-circunference appear in the diagram is hard to show clearly.

References

1.- Wagner C. und Traud W. Z., Electrochem. n-7 (1983), 391.

2.- González, J.A. y Andrade C., BR. Corr. Jour 17(1982) 21.

3.- González, J.A. y Andrade C., Corr. y Prot. 11, 3(1980) 27.

4.- Stern M. and Geary A., Jour Electrochem. Soc. v. 104 (1957) n-1, 56.

5.- Mladky K, Callow L.M. and Dawson J.L., Br. Corros. Jour v-15 n-1 (1980).

ELECTROCHEMICAL ESTIMATION OF CORROSION RATES ON PAINT COATED METAL SURFACES

S. FELIU, J.M. BASTIDAS and M. MORCILLO
Centro Nacional de Investigaciones Metalúrgicas, Ciudad Universitaria, Madrid, Spain.

Introduction

The determination of the corrosion rates of painted metals by electrochemical measurements presents the problem of the high ohmic resistance across the organic coating. The value of the charge transfer resistance, which under other circumstances can measure the corrosion rate, appears now masked by the high ohmic resistance through the paint coating. Only when this coating is damaged the interference disappears. However, the measurements in these conditions are less interesting.

Electrochemical measurements carried out on a paint coating in relatively good condition give direct information about its insulating power as well as indirect information about its porosity and the probable corrosive activity level existing on the metallic substrate. However, this last information is only qualitative. It is necessary to adopt a new approach to be able to produce quantitative data.

The aim of this communication is to study the possibility of operating below the paint coating using the so called "segmented test piece" (Fig. 1), as previously described (1,2), on which it is possible to analyse the response of the metallic substrate to electric signals without passing these across the paint coating.

Equivalent circuits

The equivalent circuit from Fig. 2(A) is representative of conventional electrochemical testing with a counter electrode external to the paint coating (Fig. 2, sketch on right). In this figure, R_2 is normally of an order of magnitude equal to or higher than R_1. Fig. 2 (B) shows the equivalent circuit using the new measuring technique based on the segmented test piece when the metal/paint interface is contaminated with salt and exhibits ionic conductivity. In this case the current flows in a line parallel to the metallic surface. The resistance R_4 of the thin electrolyte film on the metal/paint interface is, normally, much lower than the resistance R_3 of the faradaic process.

Experimental results and discussion

The contaminated metal/paint interface attains conditions of ionic conductivity in a short time from the start of its exposure to water. This can be seen when comparing the impedance diagrams obtained with the conventional method and the new one (Fig. 3). On initiation exposure period

both diagrams have the same "open arc" shape, with high values of impedance moduli and phase angles. However, whilst the impedance diagrams obtained with conventional testing continue practically without change. "closed curves" with a semicircular shape are obtained in a short period of time when using the segmented test piece. It seems likely that this period of time (permeation time) will depend on how quickly water molecules reach the metal/paint interface by diffusion, and it appears to depend on the thickness of paint film. For example, for 20 mg $NaCl/m^2$ surface contamination, permeation times of 4, 10 and 42 hours have been determined on paint films 44, 1000 and 208 μm thick, respectively.

Provided that the metal/paint interface becomes conductive, the impedance diagrams obtained with the segmented test piece allows an easy evaluation of the corrosion rate (V_C) of the metallic substrate by using the Stern-Geary formule ($V_C=B/R_T$) and assuming that the diameter of the semicircle of the impedance diagram is R_T. It is interesting to note the strong effect of thickness and exposure time on the protection offered by the paint coating. Corrosion rates of the metallic substrate determined after 9-10 hours of exposure to the aggresive medium are almost inversely proportional to coating thickness. Finally, the impedance diagrams obtained suggest that a surface contamination above 20 mg $NaCl/m^2$ has farther little effect on the corrosion rate of the metallic substrate.

References

1. S. Feliu, J.M. Bastidas and M. Morcillo, Rev. Ib. Corrosión y Protección, 14 (1983), 319.

2. S. Feliu, M. Morcillo and J.M. Bastidas, Pitture e Vernici, 7 (1984), 29.

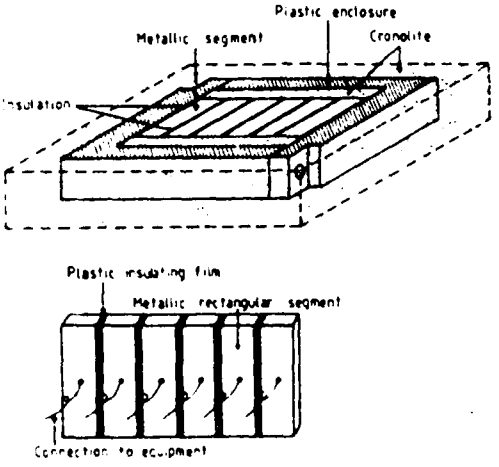

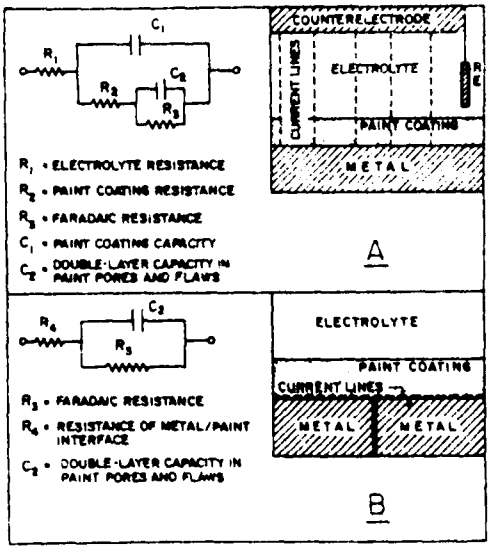

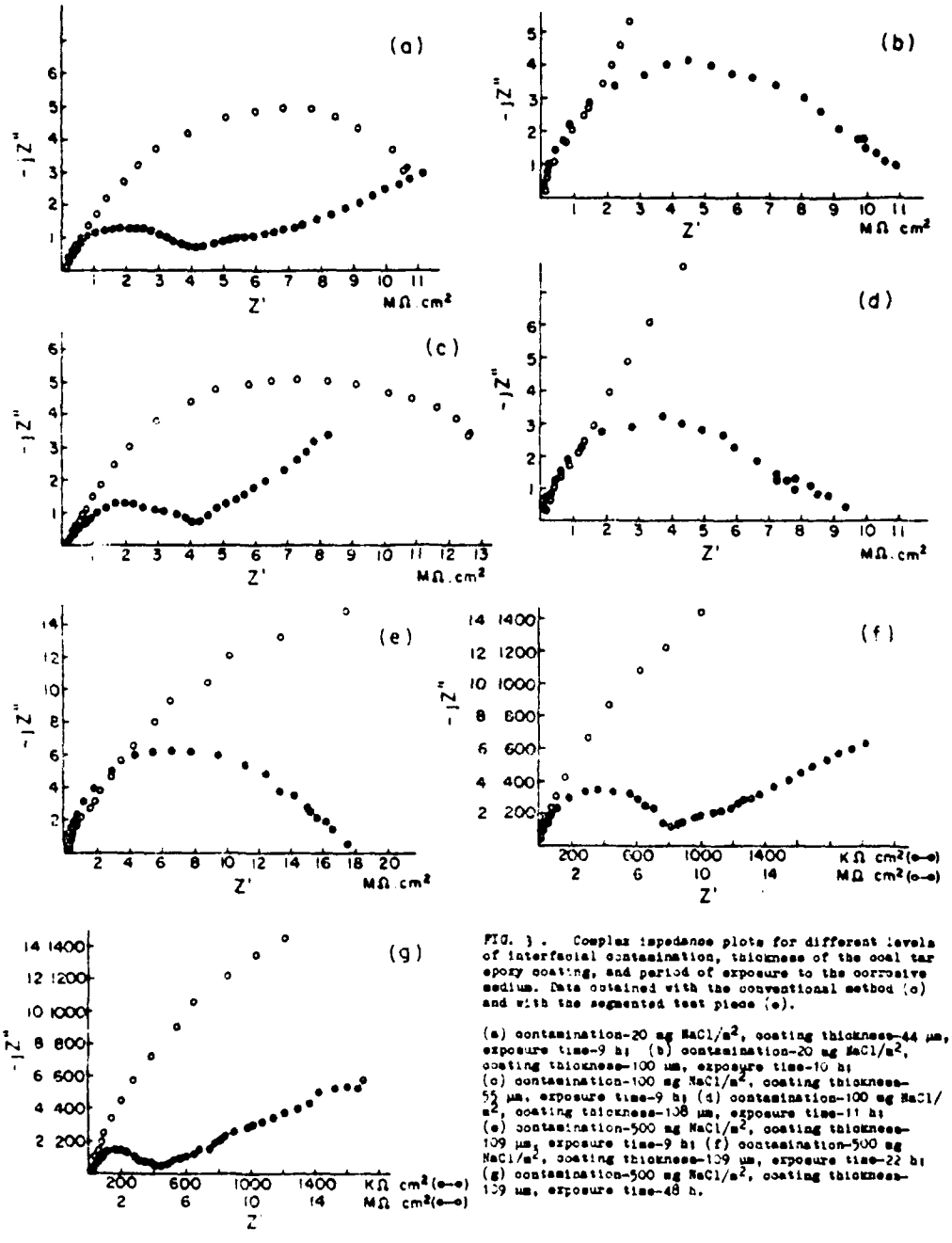

FIG. 1. Complex impedance plots for different levels of interfacial contamination, thickness of the coal tar epoxy coating, and period of exposure to the corrosive medium. Data obtained with the conventional method (a) and with the segmented test piece (e).

(a) contamination-20 mg NaCl/m², coating thickness-44 μm, exposure time-9 h; (b) contamination-20 mg NaCl/m², coating thickness-100 μm, exposure time-10 h; (c) contamination-100 mg NaCl/m², coating thickness-52 μm, exposure time-9 h; (d) contamination-100 mg NaCl/m², coating thickness-108 μm, exposure time-11 h; (e) contamination-500 mg NaCl/m², coating thickness-109 μm, exposure time-9 h; (f) contamination-500 mg NaCl/m², coating thickness-109 μm, exposure time-22 h; (g) contamination-500 mg NaCl/m², coating thickness-109 μm, exposure time-48 h.

06430

ELECTRICAL MODEL FOR STUDYING THE CORRODING STEEL/CONCRETE SYSTEM

S. FELIU and J.A. GONZALEZ
Centro Nacional de Investigaciones Metalúrgicas. Ciudad Universitaria, Madrid, Spain

C. ANDRADE
Instituto de la Construcción y del Cemento, Apartado 19.002, Madrid, Spain

V. FELIU
Universidad Nacional de Educación a Distancia, Madrid, Spain

Introduction

The difficulties to achieve the steady-state conditions when polarization is applied to the steel/concrete system have favored other techniques based on impedance (1) and, sometimes, transient measurements. In order to interpret these measurements it is necessary to assume a model (equivalent circuit) which simulates the behaviour of the steel/concrete system under an electrical signal. If the experimental data are sampled during a quite short period of time after applying the signal, the effect of mass transfer can be ignored.

In practice, the duration of the current-time transient, which results from the application of a potential to the specimens, is longer than the theoretical prediction based on the model of Fig. 1. In the frequency-domain, also, the impedance diagram may show an small and bad-resolved second semicircle at high frequencies instead of drawing an unique semicircle. Thus, doubts are cast about the validity of circuit in Fig. 1 for representing the steel concrete system.

This experimental contradiction may be overcome with other models as shown in Fig 2, where the transient period is longer due to the addition of the resistance R_3 in series with the capacitance C_2.

Response to a potential step of the proposed model

Using the operational calculus, it is not difficult to derive the response functions to different electrical signals for the model shown in Fig. 2. When this signal is a potential step, the response is expressed by:

$$I = \Delta V \left[K_0 + K_1 \exp(x_1 t) + K_2 \exp(x_2 t) \right] \qquad [1]$$

where the values of x_1 and x_2 are the (real and negative) roots of the equation:

$$x^2 + \left(\frac{1}{C_1 R_1} + \frac{1}{C_1 R_2} + \frac{1}{C_1 R_3} + \frac{1}{C_2 R_3} \right) x + \frac{R_1 + R_2}{R_1 R_2 R_3 C_1 C_2} = 0 \rightarrow \begin{matrix} x_1 \\ x_2 \end{matrix} \qquad [2]$$

$$\text{and} \quad K_o = \frac{1}{R_1+R_2}, \quad K_1 = \frac{Ax_1^2 + Bx_1 + C}{x_1(x_1 - x_2)}, \quad K_2 = \frac{Ax_2^2 + Bx_2 + C}{x_2(x_2 - x_1)}$$

$$\text{being } A = \frac{1}{R_1}, \quad B = \frac{R_2C_1 + R_2C_2 + R_3C_2}{R_1R_2R_3C_1C_2}, \quad C = \frac{1}{R_1R_2R_3C_1C_2}$$

In practice, the values for x_1 and x_2 usually differ over one order of magnitude. Immediately after applying the signal the response curve is mainly affected by only one of the two exponential terms of Eq. 2, while the influence of the other exponential term becomes important after periods of time of the order of one or more seconds from the start, when the effect of the first one can be neglected. Therefore, in order to have a complete knowledge of the response function, it is necessary to combine data taken during the first few fractions of a second from the start with data taken throughout a period of various seconds (e.g., between 2 and 10 s). The values of the parameters K_o, K_1, K_2, x_1 and x_2 which best fit the experimental data are obtained with the help of a computer program.

The values of components of the proposed electrical model are readily calculable from the parameters of Eq. 2.

Experimental technique and results

Four series of cement mortar specimens (T_1, T_2, T_3 and T_4 series) were prepared with a water/cement ratio of 1/3. In the T_1 and T_2 series, 2% of $CaCl_2$ by weight was added to the cement. Plain steel bars were used in the T_1 and T_2 series, and corrugated bars were used in the T_3 and T_4 series. The specimens were 2 cm x 5.5 cm x 8 cm size, and the metallic area exposed to corrosion was about 6 cm^2. All the results are referred to this area.

The specimens were held in a chamber at about 100% relative humidity. From time to time pulses of potential were applied to them. Fig. 3 shows the typical response to a 10 mV potential step. An oscilloscope was used to record the response curve during the first fractions of a second from the start, and a graphical plotter, for the period between 0.5 and 10 or more seconds.

Parameters of the proposed model

The numerical data to be used in the calculations were sampled from the response curves. Table I shows the calculated values of parameters K_o, K_1, K_2, x_1 and x_2 for the response curves after 4 months specimen life. From these values the components R_1, R_2, R_3, C_1 and C_2 have been calculated (Table II).

In the model in Fig. 2, the component R_1 represents the ohmic resistance between the working and reference electrodes. It seems reasonable that R_2 corresponds to the resistance of the faradaic process, and C_2 to the double layer capacitance. More doubtful is the physical significance of the other two components, C_1 and R_3.

Determination of the corrosion rate

For determining the corrosion rate, it is not necessary to identify all the components of the equivalent circuit in Fig. 2. Only the value of the resistance R_2 is needed. Accepting that R_2 represents the charge transfer resistance, the corrosion intensity will be calculated using the well-known Stern-Geary equation $I_{corr} = B/R_2$.

An easy way to calculate R_2 come out from the fact that one of the exponential terms of Eq. 2 becomes negligible after a very short time interval. If $t \geqslant 1$ seconds, this equation may be rewritten as $I/\Delta V = K_o + K_1 \exp(x_1 t)$. Advantages of this simplification are (a) the easy way to obtain the experimental data, e.g. from a single graphic record between 1 and 10 seconds, and (b) the easy treatment of these data for calculating the parameters of such an equation. Thus, if R_1 is determined separately or compensated, the value of R_2 can be immediately calculated from the value of parameter K_o expressed by the relationship $K_o = 1/(R_1 + R_2)$.

Reference

(1) D.G. John, P.C. Searson and J.L. Dawson: Br. Corros. J., 16, No. 2 (1981), 102-106.

Table I. Values of parameters for the response equation.

Specimen	K_o	K_1	K_2	x_1	x_2
T_1	$0.380\ 10^{-4}$	$2.949\ 10^{-4}$	$10.299\ 10^{-4}$	-0.643	-18.457
T_2	$1.231\ 10^{-4}$	$7.432\ 10^{-4}$	$9.180\ 10^{-4}$	-0.512	-20.885
T_3	$0.086\ 10^{-4}$	$3.510\ 10^{-4}$	$6.870\ 10^{-4}$	-0.957	-7.802
T_4	$0.055\ 10^{-4}$	$3.589\ 10^{-4}$	$5.216\ 10^{-4}$	-0.869	-10.065

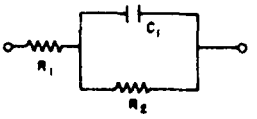

Fig. 1

Table II. Values of components for the proposed model. Corroding interface area, 6 cm^2.

Specimen	R_1	R_2	R_3	C_1	C_2
T_1	734	25532	2728	$9.7\ 10^{-5}$	$4.5\ 10^{-4}$
T_2	560	7563	704	$1.6\ 10^{-4}$	$1.6\ 10^{-3}$
T_3	955	115324	2721	$1.9\ 10^{-4}$	$2.7\ 10^{-4}$
T_4	1129	180690	2192	$1.4\ 10^{-4}$	$3.3\ 10^{-4}$

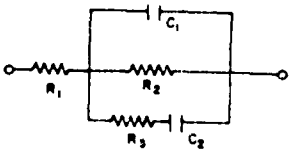

Fig. 2

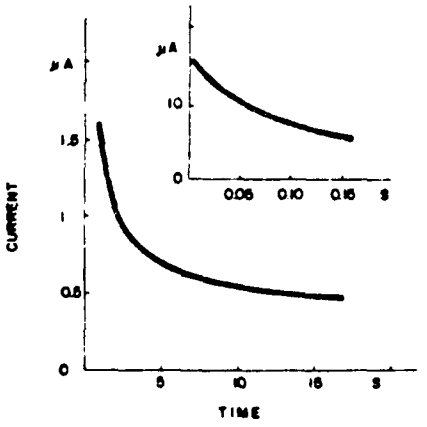

Fig. 3

06440

ANODIC BEHAVIOUR OF A.I.S.I. 446 STAINLESS STEEL IN METHANOLIC ENVIRONMENT

G.CAPOBIANCO[a], G.FARNIA[a], C.A.FARINA[b], F.BELLUCCI[c]

[a]Dipartimento di Chimica Fisica - Padova (Italy)

[b]Istituto G.Donegani - Dipartimento di Corrosione - Novara (Italy)

[c]Dipartimento di Ingegneria dei Materiali e della Produzione - Napoli (Italy)

One of the main difficulties in the corrosion electrochemical testing in organic solvents is the low reproducibility of the experimental measurements strictly related to the surface conditions of the specimen used as electrode and to the possibility of mantaining the testing solution free from oxidation products both of the solvent and electrode.

The need of working with a fresh generated metal surface, free from airborn passivity and in conditions ensuring the constant composition of the solution, required to set-up an experimental procedure allowing measurements in flowing electrolyte.

The polarization cell[1-2] was a cylindrical Pyrex glass tube (Fig. 1); the metal specimen, of cylindrical shape with a surface area of ca.5.5 cm^2, was mounted using a Teflon electrode holder. The electric contact was made by an inner metal rod.

The flow (4-5 ml/min) was obtained by pressurizing a solution reservoir with dessicated nitrogen.

The test and pickling solutions were alternatively pumped from the reservoirs. For the preparation of the metal surface, the usual treatment with emery paper was followed by a cathodic polarization directly within the cell at -0.7V (SCE) for 10 minutes in a $2 \cdot 10^{-3}$M H_2SO_4 methanolic solution. After the pickling treatment the test solution was introduced into the cell.

The anodic behaviour of A.I.S.I. 446 Stainless steel has been investigated in deaerated methanolic solutions. The formation and stability of the passivity film has been evaluated by varying water content (200-5000 ppm_v), chloride and sulphuric acid concentrations ($10^{-4} \div 10^{-2}$M) and temperature (10-40°C). The study has been performed by means of anodic potentiostatic transients. The analysis of corrosion behaviour by means of anodic potentiostatic transients can give more simple and direct information as regards the kinetic aspect of the passivity film formation. The latter aspect is in fact disregarded by potentiodynamic curves which, even at the lowest scan rates, always represent the present situation of the specimen.

Measurements have been carried out using an Amel equipment assembled with a potentiostat mod. 552, a signal generator mod. 567, an interface mod. 560 and a current integrator mod. 721.

In order to increase the conductivity, 0.1M lithium perchlorate was added to the solutions.

Experimental results indicate that A.I.S.I. 446 Stainless Steel is not particularly prone to corrosion phenomena in deaerated methanolic solutions. In fact, even in the presence of relatively high acidity (10^{-3}M H_2SO_4) and/or chlorides (LiCl < 10^{-3}M), stable protective oxide films are built-up if the water content is about 5000 ppm_v (Fig. 2, a,b).

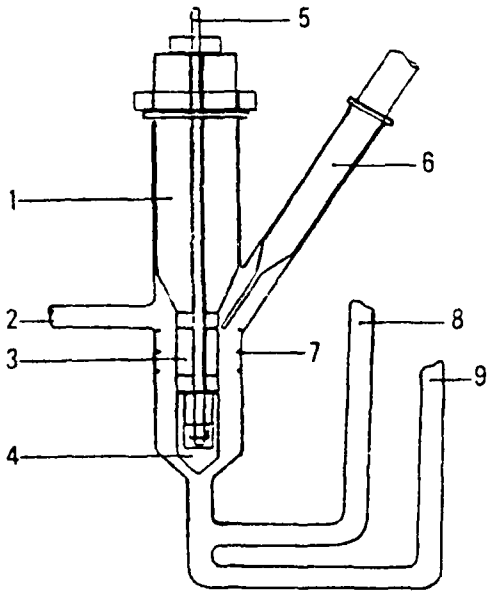

Fig. 1 - Cell for measurements in flowing solution.

1) Teflon electrode holder
2) Solution exit
3) Metal specimen
4) Teflon
5) Electric contact
6) Luggin capillary
7) Platinum counter electrode
8) Solution inlet
9) Nitrogen inlet

Fig. 2 - Typical behaviour of potentiostatic transients at +100 mV for A.I.S.I. 446 Stainless Steel in methanolic solution 10^{-1}M $LiClO_4$. T=20°C.

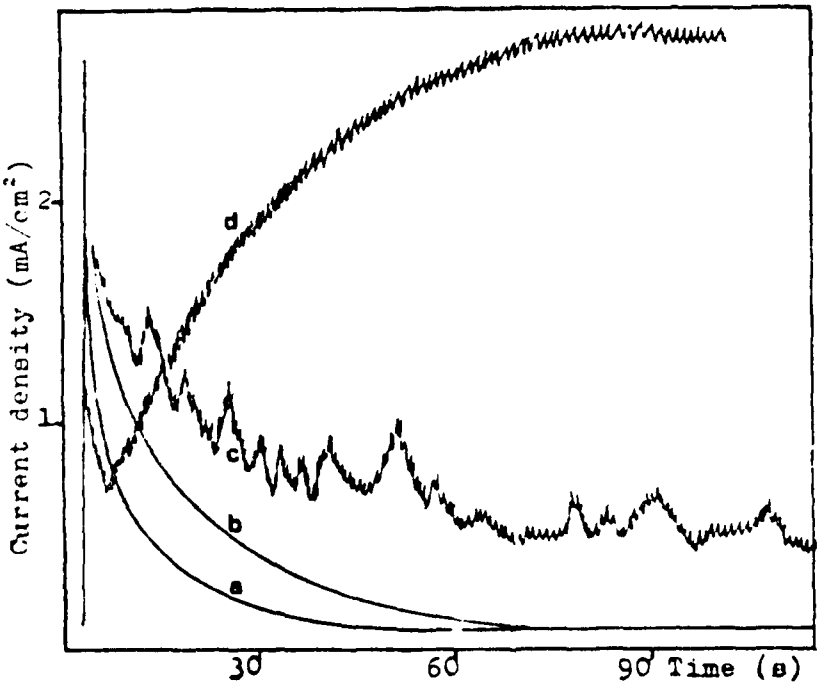

a) 10^{-3}M H_2SO_4 0.5% H_2O
b) 10^{-3}M H_2SO_4 10^{-3}M LiCl 0.5% H_2O
c) 10^{-3}M LiCl 0.02% H_2O
d) 10^{-3}M H_2SO_4 10^{-2}M LiCl 0.5% H_2O

On decreasing the water content, the corrosion resistance of the metal is greatly reduced and the conditions for localized attacks are likely to occur (Fig. 2,c).

The influence on corrosion phenomena of a decreasing of the water content results greater than that corresponding to an increase of acidity and chlorides.

In aggressive environments the passivation current increases with the temperature while a beneficial effect is observed in conditions in which stable passive films are formed.

F.Mazza, S.Torchio, N.Ghislandi, Proceeding of the International Congress on Metallic Corrosion, Toronto, 1, 102 (1984)

G.Capobianco, G.Farnia, G.Faita, C.A.Farina, Proceeding of the International Congress on Metallic Corrosion, Toronto 3 532 (1984).

06450

ELECTRODE PROCESSES AT HAFNIUM IN VARIOUS ELECTROLYTES

J.PIROTH and E.BRAUER
Institut für Physikalische Chemie der Universität
Frankfurt/Main, West-Germany

The knowledge of the behaviour of Hafnium in acidic and basic solutions (H_2SO_4, HNO_3, $HClO_4$, NaCl, NaOH) is of growing interest with respect to the corrosion phenomena of this metal, which is being used more and more in reactor plants. The extremely high corrosion resistance is due to the generation of thin protective oxide layers, the growth of which is shown in Fig. 1 as a function of the applied potential.

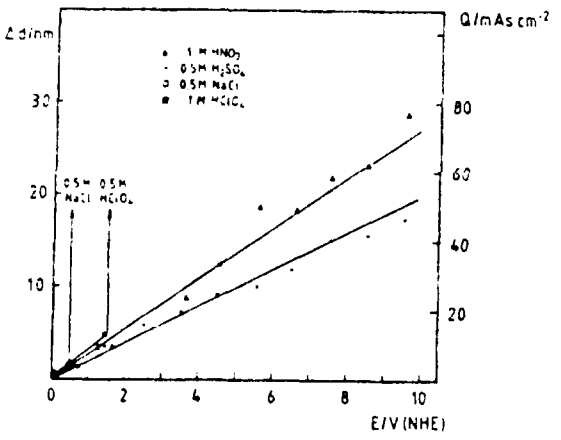

Fig. 1: oxide layer growth as a function of applied anodic polarisation

The oxides were found to be non-uniform according to SIMS on Hf oxide prepared by anodic polarisation with 0.5 mA/cm^2 in 0.5 M H_2SO_4 (Fig. 2).

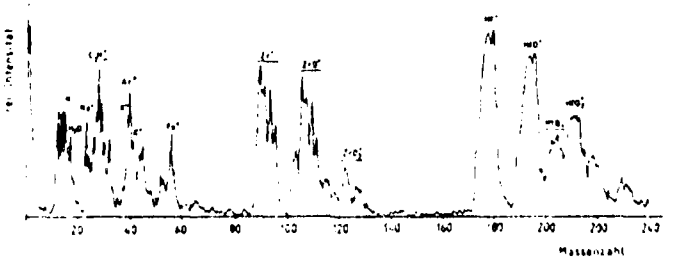

Fig. 2 : SIM spectrum of Hafniumoxid

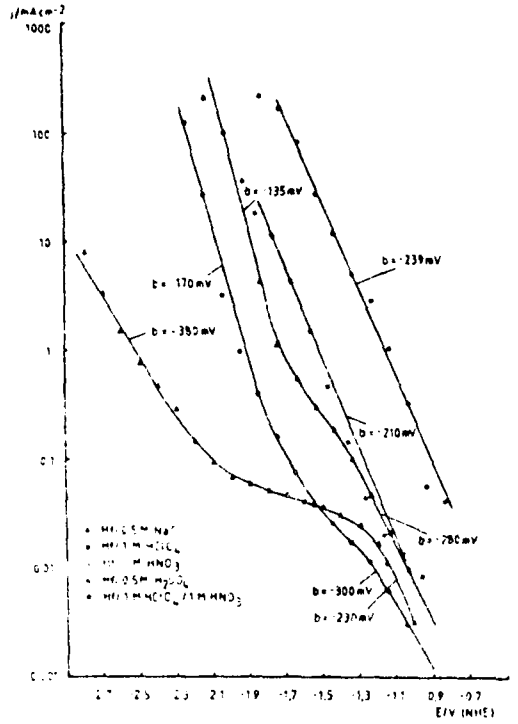

Cathodic Tafel plots of Hf in various electrolytes are given in Fig. 3, the unregularities will be discussed.

Fig. 3: Tafel plots of Hafnium in various electrolytes

Extended impedance measurements were performed to elucidate the electrode processes of *Hafnium*. A *suggestion* by Göhr to use equivalent circuits was followed to interprete the spectra. Fig. 4a presents a series of spectra for Hf in 0.5 M H_2SO_4 after anodic polarisation at: 1 = 0.1 V, 2 = 1.6 V, 3 = 6.6 V, 4 = 8.6 V.

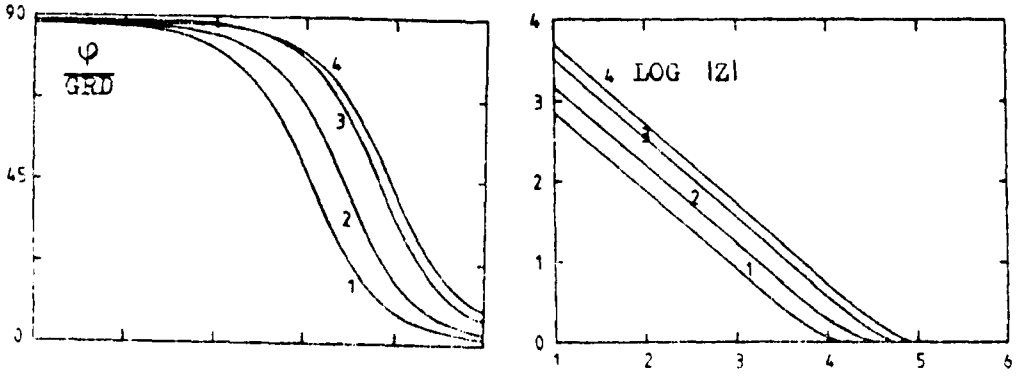

Fig. 4: Impedance spectra of anodic polarisation

The corresponding equivalent circuit is shown in Fig. 4b and the values of the parameters are listed in Table 1.

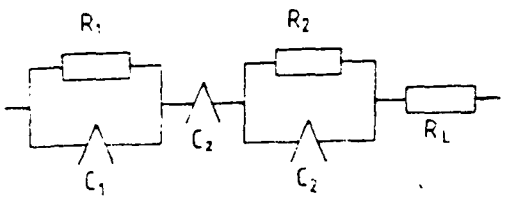

Fig. 4b: Equivalent circuit for simulation the phase angle and impedance spectra of Hf in 0.5 M H_2SO_4.
R = resistance, C = capacity, R_L = electrolyte resistance

E / V	R_1 / kΩ	C_1 / µF	φ	C_2 / µF	φ	R_2 / kΩ	C_2 / µF	φ
0.1	160	49	0	1500	0.62	2.1	34	0.11
1.6	650	21	0	1200	0.68	6.8	17	0.09
6.6	700	8.2	0.01	760	0.73	26	9.4	0.02
8.6	10000	5.6	0.02	630	0.76	58	6.7	0.02

Table 1: Calculated parameter for the elements in Fig. 4b

Impedance spectra of Hafnium after cathodic polarisation differ clearly in shapes for φ and Z from those shown above. The equivalent circuit contains an adsorption parameter.

The results will be discussed and compared to those of Ti and Zr.

06460

INVESTIGATION OF AMORPHOUS TITANIUM ALLOY IN 0.2 N H_2SO_4

M.V.ŠUŠIĆ
Institute of Physical Chemistry, Faculty of Science, Belgrade, Yugoslavia

Titanium, together with its alloys, containing different metals belongs to a group of the most important building materials due to their high corrosion resistance to various agents and high thermal stability. Titanium also belongs to a group of so called "valve" metals which owing to spontaneous or direct electrochemical passivation protect themselves from corrosion. During this process oxide layers, different in thickness and properties which depend on the very nature of metals and formation conditions, are composed.

On the basis of literature data[1-3] and our previously obtained results[4,5] concerning the problem of anodic layers formation on valve metals, we established an equation that describes the decrement of current passivation during time t, i.e.

$$1/i = 1/i_0 + kt/b \quad \text{or}$$

$$-\log i + \log(i - i/i_0) = \log(k/b) + \log t \qquad (1)$$

where i_0 and i is a current passivation at t=0, i.e. at t>0, while k and b are constants. It follows from (dE/dt)=ki relation that a constant k is the measure for the rate of anodic layer formation potential (E) charge at constant current, i.e. the measure of the increment rate of oxide layer resistance, independently from the layer thickness. Therefore, it follows from the above that the more consumed current is for area passivation the less is k, what means that corrosion is greater. The left side of equation (1) marked F written according to log t gives a straight line with the slope 1, the value k/b for log t=0 can be derived from, while the value k can be derived from a particular galvanostatic (chronopotentiometry) experiment. The position of a streight line F vs. log t within a coordinate system, i.e. the value log k/b for different values of a polarization potential demonstrates the resistance to corrosion. The more positive is the value log k/b, i.e. a line is shifted to the right within a coordinate system, the greater the resistance of a sample to corrosion is. This holds for those passivation processes that are not followed by other electrochemical processes.

Both cyclovoltmetric and potentiostatic (cyclochronoampermetry) (PAR-170) investigations of a plain surface (D) and a cross section (C) of a foil of Ti3%Al alloy and a plain surface (B) and a cross section (A) of a ribbon of amorphous alloy 62Ti25Ni9Cu4Si, proved, on the basis of the above mentioned equation (1) that plain surfaces are more resistant to corrosion than the corres-

ponding cross sections. It can be seen from Fig. 1 that the density of current passivation at potential 1.0 V are higher at the cross sections than at plain surfaces, as well as the fact that the quantity of electricity expended in the course of the first passivation cycle from 0.0 to 3.0 V for 6 sec. shows a twin-like behaviour as is presented in the following Table:

Sample	A	B	C	D
Current, mA/cm^2	13.66	2.40	3.24	2.64
Q, mC/cm^2	366.4	60.7	21.4	15.4

The rise in number of cycles is followed by a decrease rate of anodic current at the end of cycles at 3.0 V, that is greater at plain surfases when compared to cross-sections, Table I.

Table I The anodic current depending on the number of cycles at 3.0 V.

Current mA/cm^2 Sample	A	B	C	D	t,sec.
i_1	268.8	42.5	39.6	3.6	6
i_2	165.9	21.6	23.1	1.2	12
i_3	143.0	16.2	19.5	0.9	18
i_4	127.0	13.3	-	0.6	24

The analysis of chronoampergram shows that the current passivation, when all samples are taken into consideration, reaches a constant value after a certain period of time. This analysis gives straight lines, Fig. 2, according to equation (1), with a slope different from one; different values can be found for k/b and the same order is characterized for the values of a constant k as is evident from the following Table:

Sample	A	B	C	D
$\Delta F/\Delta \log t$	0.625	0.847	0.827	0.933
$-\log(k/b)$	3.6	2.57	2.91	1.07
$k,(v.cm^2/mA.s)$	0.0088	0.140	0.075	0.180

All the quoted data, together with Tofel's analysis of polarization curves, save the values of straight lines'slope ($\Delta F/\Delta \log t$ for 0.8 V) indicate a greater corrosion along cross section when compared to plain surfaces. However, the slopes point to the fact that the formation of anodic oxide layer is followed by another anodic process, the product of which has no influence on the oxide layer thickness. The intensity of this process is in the oposite relation to the slope value. Therefore, the analysis of the thickness of anodic oxide layer was carried out by measuring the capacity (C) of the boundary phase of anodized sample/electrolyte cy ac polarography with a phase sensitive detector within frequence field 100-1000 Hz, depending on passivation potential (Table II). The results proved that the relative capacities are greater with cross sections than with plain surfaces and that the same decrease with the rise of formation potential i.e. with the rise of oxide layer thickness. This in fact shows that the cross section of samples are more resistant to corrosion than the plain surfaces are, as they become passivated owing to a thinner oxide layer and are therefore characterized by a greater capacity. Thus, following the mentioned results we can say that a greater current expen-

diture in total anodic process should be attributed to oxygen evolution. It results from the above that the oxygen overpotential is lower at passivated cross section than at passivated plain surfaces. Having compared the amorphous titanium alloy with a crystal alloy, it can be concluded that although they have different quantity of titanium (amorphous alloy contains more titanium) an amorphous alloy is far resistant to corrosion than is the crystal alloy form Ti3%Al. Therefore it can be reasonable to expect that amorphous alloys can be utilized as good anodic materials for oxygen evolution. Table II shows the capacities of the boundary phase anodized samples/electrolyte in dependence of potential of oxide layer formation i.e. of a layer thickness.

Table II.

Sample	A	B	C	D
E, V		C, $\mu F/cm^2$		
1.0	220.0	26.12	48.7	29.3
2.0	112.6	18.04	29.1	18.8
3.0	76.6	15.70	21.6	12.8

Crystallization (devitrification) of amorphous alloy (using DSC method) occurs in three distinct steps, at 736, 774 and 784 K, respectively, the last of which represents the process of crystals' formation to which the enthalpy of $\Delta H = 22.3$ J/g corresponds.

References
1. J.Jahalom, T.P.Hoar, Electrochim. Acta, 15, 677 (1970).
2. K.Ogura, N.Hackerman, Electronchim. Acta, 17, 1717 (1972).
3. R.Dreiner, J.Electrochim. Soc., 111, 1350 (1972).
4. B.Simonović, M.Šušić, Bull. Acad.Serbe Sci Arts. Belgrade, Classe Sci. natu., 56, 13 (1977).
5. M.Šušić, Materials Chem. and Phys., 8, 193 (1983).

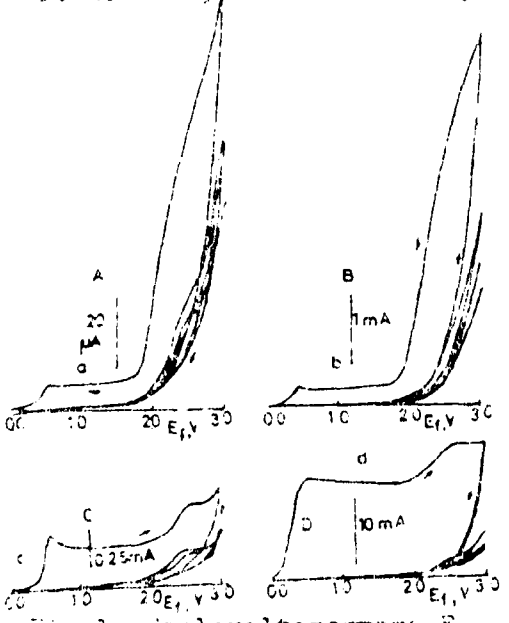

Fig.1. Cyclovoltamograms, E_i = 0.0 V, E_f=3.0 V, 500 mV/s.

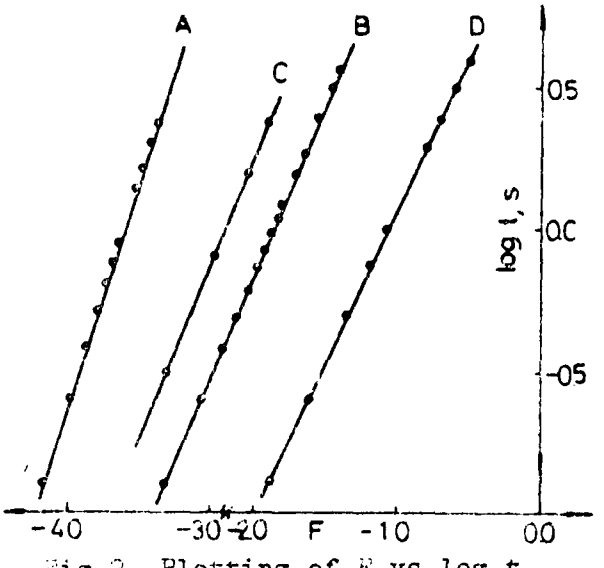

Fig.2. Plotting of F vs. log t for samples A,B,C ad D, E_f=0.8 V.

06470

CORROSION PROTECTION OF TITANIUM ALLOY AND STEELS IN MOLTEN ALKALI CARBONATES

Ozeryanaya I.N., Manukhina T.I., Sannikov V.I., Anfinogenov A.I.

Institute Electrochemistry, Sverdlovsk, USSR, 620219

Aluminium and its alloys are selfpassivated in the alkali carbonate melts. The application of aluminium alloys in the molten carbonate fuel cells are limited by low melting point of these metals. The investigation of passivation of aluminized titanium alloy and steels in the alkali carbonate melt is described in this paper. The diffuse aluminizing of the titanium alloy (VT1) was carried out in the following condition: (mas.%) $BaCl_2-KCl-NaCl$ eutectic - 85; $AlCl_3$ -5; powder $FeAl_3+Al$ - 10 for 5h. at 630°C. The aluminized layer thickness is 20-23 μm Al_3Ti was found on the sample surfaces by x-ray analysis.

The aluminizing of the steels (X18H10T and St 20) was done in the melt (mas.%): $BaCl_2$ -45; KCl -33; $NaCl$ - 11,5; $AlCl_3$ - 3; powder $FeAl_3$ -7,5 at 600°C, for 1-4h Al_5Fe_2 (60 - 140 m thick) for St 20 was found on the sample surfaces by x-ray analysis. $AlFe_2$ and Al_5Cr2 (4-8 μm thick) were found on the sample surfaces of the X18H10T. The passivation of aluminized specimens was investigated in the alkali carbonate melt $Li_2CO_3-Na_2CO_3-Na_2CO_3$(4:3:3) at 600° and 700°C; the cell atmosphere was CO_2 or $CO_2+\frac{1}{2}O_2$. The passivation efficiency of the investigated metals was studied by the patentiostatic anode polarisation relative to the carbonate reference electrode. The analysis of the results shows (Fig.1) that aluminized VT1 is passivated by the evolved oxigen during the anode process: $CO_3^{2-}-2e \rightarrow CO_2+\frac{1}{2}O_2$ (1)

The anode polarization curves of the aluminized VT1 are similar to those of the nonaluminized metal and VT5 alloy. The passivation characteristics of aluminized VT1 are better than those of the initial metal: the passivation current density is 6-7 times lower than that of the initial metal and 2 times lower than that of the VT5, which contained 5% Al. A very thin layer (1 μm) of $\alpha-Al_2O_3$ and aluminates was found on the aluminized surface VT1. The solid solution of oxigen and $\alpha-Ti$ was no formed on the aluminized VT1 samples.

The anodic potentiostatic curves of the aluminized St20 (Fig.2a) differ significantly from the iron curves under the same conditions. The region of the iron active solution at -1÷ -0,6V was not observed on the aluminized St20 curves but it was got on the iron curves. The passivation current density of the aluminized St20 is 5 times lower than that of iron, but the potential region of the passivation is the same. The process of envolving the anode gases ($CO_2+\frac{1}{2}O_2$)

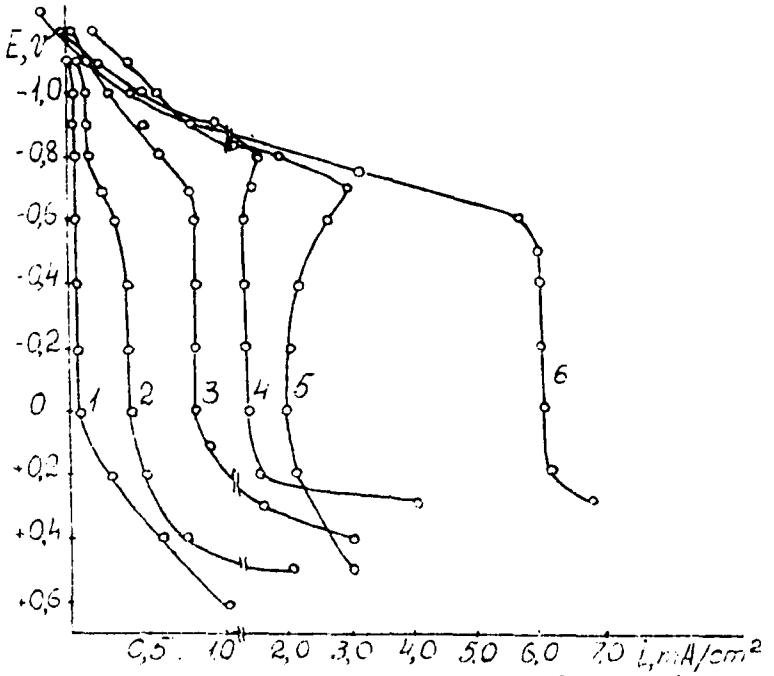

Fig.1. The anodic potentiostatic polarization atmosphere CO_2; VT1 aluminized: 1-600°; 4-700°; VT5: 2-600°; 5-700°; initial VT1: 3-600°: 6-700°

proceeds at the overpotential 0,2 V. The potentiostatic characteristics of the aluminized X18H10T differ from those of the initial steel. The anode polarization cerves of the X18H10T specimens are of a similar character as aluminium (Fig.2b).

α-Al_2O_3 and $LiAlO_2$ were found on the surface layers of the X18H10T specimens, as on aluminium. The dependence of the oxidizing rate of the investigated metals on time may be characterized by the kinetics of the formation of protective films at constant potential. We have observed the decreasing of the current density with time at constant potentials. The values of these passivation region of the aluminized steels (X18H10T and St20) at 600°and 700°. The results obtained showed that the change of the anode current density with time obeyed the parabolic law of the oxide film growth (Table) after 10 min of polarization for the X18H10T anodes and after 3 min - for St20. The oxidation rate constants are increasing with the increase of polarization potentials (St20) and temperature (X18H10T).

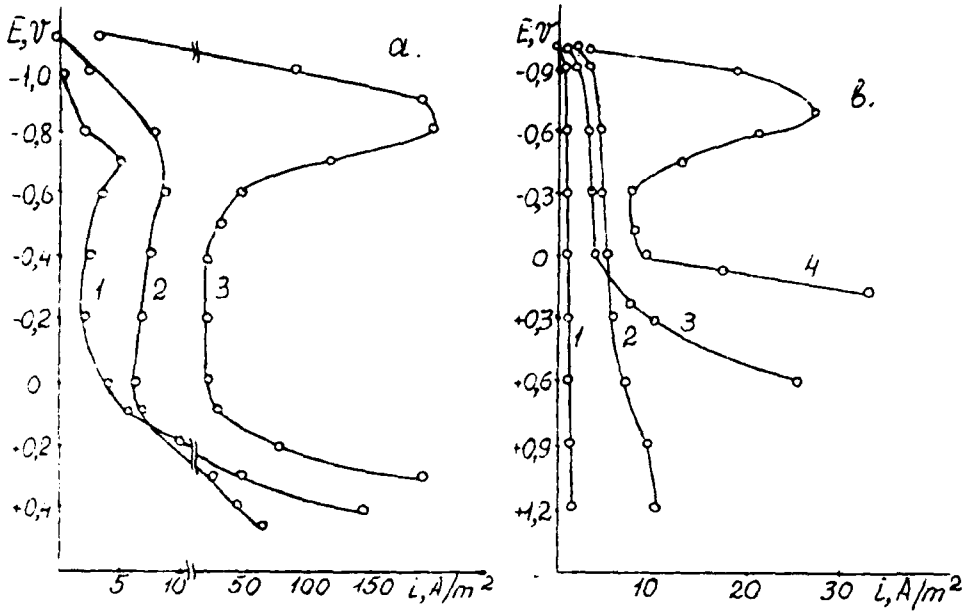

Fig.2. The anodic potentiostatic polarization, atmosphere $CO_2 + \frac{1}{2} O_2$ a) 700°; St20 aluminized for: 1-2h; 2-2h; 3-Fe, 600°, b) 1-Al, 600°; Steel X18H10T, 700°; aluminized for: 2-4h; 3-2h; 4-initial X18H10T, 600°

T a b l e

The dependence of the current density ($A.M^{-2}$) on time during the polarization of the steels

Steel	The time of aluminizing, h	The oxidizing temperature, °C	The polarization potential, V	The change of the anode current density with time, A/M^2
X18H10T	2	600	-0,2	$i=(54,4\pm8,9)\tau^{-0,5}$
	4	"	-0,2	$i=(158,9\pm10,2)\tau^{-0,5}$
	2	700	-0,2	$i=(174,6\pm21,6)\tau^{-0,5}$
St 20	1	600	-0,2	$i=(210,7\pm3,1)\tau^{-0,5}$
	2	"	-0,2	$i=(77,6\pm17,9)\tau^{-0,5}$
	2	"	-0,4	$i=(54,9\pm9,7)\tau^{-0,5}$

Summery

The diffused aluminized layers significally increase the corrosion resistance of the VT1 and Steels (X18H10T and St20) in the molten alkali carbonates at 600° and 700°.

06480

INFLUENCE OF WATER VAPOR PRESSURE ON ALUMINIUM CORROSION IN MOLTEN LITHIUM AND KALIUM CHLORIDES

OZERYANAYA I.N., SHARDAKOV N.T
Institute Electrochemistry, Sverdlovsk, USSR, 620219

$LiCl$-KCl mixture was used as the soldering flux of aluminium and its alloys[1]. The data about the influence of the usual admixtures in this melt may be of importance for improving industrial processes.

We have studied the aluminium corrosion in the molten eutectic mixture of lithium and kalium chlorides at the water vapor pressure from $13,3_2$ to $15,10^5$ Pa at 673-873 K.

A well-known method[2] was used for the $LiCl$ and KCl mixture preparation. But we have determined the humidity of both the chlorine hydride and helium[3]. The aluminium specimens A999 (area- 2 cm^2, thickness - 0,3 mm) were chemically polished. The experiments were carried out both in the hermetic, quartz, 3 electrode electrochemical cell with helium atmosphere[4] and in the optical quartz cell, which is placed into a hightemperature microscope camera KM-456 ("Union"). x 400.

The interaction products were analysed with x-ray (DRON-2), Scanning electron-probe x-ray ("Comebax") and atomic-absorption (spectrometer "Perkin-Elmer") methods. The corrosion current density of aluminium was measured by the weight change of the specimens during their contacts with the melt (from 1 to 50 h) and by anodic galvanostatic polarization curves, which were obtained in realation to the chlorine reference electrode.[3]

We have found[3], that when the water vapor pressure in the cell is lower than $2,6\cdot10^3$ Pa, aluminium interacts with the hydrolysis products of the $LiCl$ melt and admixture-ions (Fe^{2+}, Mg^{2+} and s.o.) throgh the oxide film defects in the following way:

$$LiCl + H_2O = LiOH + HCl \quad (1)$$

$$Al + HCl = AlCl + \tfrac{1}{2} H_2 \quad (2)$$

$$3AlCl = 2Al + AlCl_3 \quad (3)$$

The corrosion current density of aluminium was in the range of 10^{-5} g/$cm^2\cdot$h in these conditions.

The measurements of the aluminium corrosion current density were carried aut in the quaztz ampulas (ampula volume - 30 cm^2; melt volume - 5 cm^3) at the partial water vapor pressure higher than $2,6\cdot10^3$ Pa.

The preliminary prepared $LiCl$-KCl mixture and Al specimen were placed into the ampula.

It was evaquated upto the residual pressure 10^{-1}-10^{-2} Pa.

Then the definite quantity of water wasintroduced into the ampula and it was soldered. It was heated for 10h at

constant temperature. The colded ampula was immersed into the distilled water and broken. The solutionof the eutectic $LiCl-KCl$ after the experiments contained a white powder. The Al^{3+} ion concentration and pH were determined in the filtrate. The white powder contained γ-Al_2O_3 and a small portion of $LiAl_5O_8$. The Al^{3+} ion concentration was negligible in the filtrate. pH of the filtrate was 5,5-6,0 and the same acidity of the $LiCl-KCl$ solution was registered before the experiment To determine the corrosion rate of only with water (without $LiCl-KCl$ melt), the Al sample and a certain quantity of water were sealed into the ampula and heated 10h at constant temperature. The experiment showed that the weight change of the sample was in the limits of the aceuracy of weighting.

The dependence of the Al weightlosses on the water vapor pressure is shown in Fig.

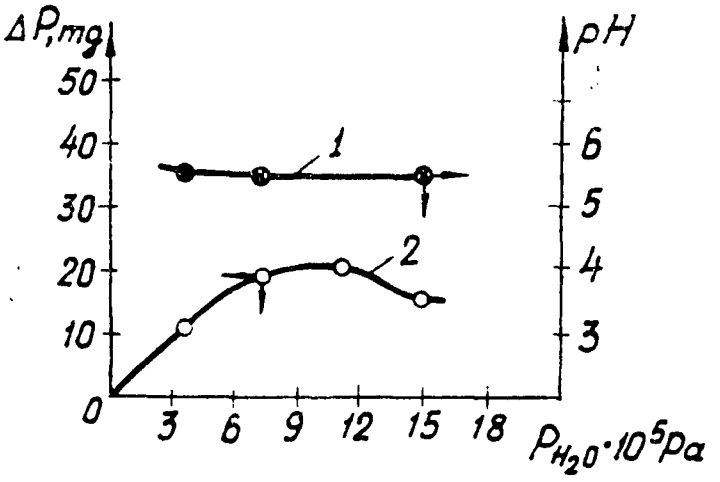

Fig. The dependence of aluminium weightlosses on the water vapor pressure
1-pH; 2-weightloss of the samples, mg.

The analysis of the results showed that the aluminium interacts withe the $LiCl-KCl$ melt at the water vapor pressure higher than $2,6\cdot10^3$ Pa in the following way:

$$LiCl + H_2O = LiOH + HCl \quad (4)$$

$$2Al + 6HCl = 2AlCl_3 + 3H_2 \quad (5)$$

$$2AlCl_3 + 3H_2O = Al_2O_3 + 6HCl \quad (6)$$

$$5Al_2O_3 + 2LiOH = 2LiAl_5O_8 + H_2O \quad (7)$$

Thus, β-Al_2O_3 and $LiAl_5O_8$ are products of the Al interaction with the $LiCl$-KCl melt at the water vapor pressure from $2,6 \cdot 10^3$ to $15 \cdot 10^5$ Pa.

References

1. Storchai E.I. Flusovaya paika aluminiya. M.Metallurgia, 1980.
2. Bek R.Ju, Lifshiz A.S., Burenkov I.M. Metod prigotovleniya besvodnoi evtektiki $LiCl$-KCl zhur. prikl.chim. 1968, 41, 1319-1322.
3. Ozeryanaya I.N., Shardakov H.T. Primenenie visokotemperaturnogo microscopa dlya isucheniya mechanisma aktivazii aluminiya v rasplave $LiCl$-KCl.
   Dokladi 9 Intern. Cong. Cor. Met Toronto 1984 Proc Ottawa, v 4, p.400-403.
4. Smirnov M.V. Elektrodnie potenziali v rasplavlennich chloridach. M. "Nauka", 1973, 36-51.

06490

A GENERALIZATION OF THREE POINT METHOD

GABRIELE ROCCHINI
Italian Electricity Board, Milan (Italy)

A comparison between the values of the corrosion rate of a metal, determined by electrochemical or direct technique, shows that the two determinations can be generally different even if in some case this difference is negligible. On the basis of this experimental evidence one can ask if an approximate evaluation of the corrosion current density is more convenient than the numerical analysis of the polarization curve.

The three point method, suggested by Barnatt and modified by Le Roy, seems to have the previous property when it is utilized with Stern and Geary equation $I_c = 1/[R_p(\alpha+\beta)]$ or $I_c\ 3 \int_{\Delta E_2}^{\Delta E_1} i(\Delta E)\,\Delta E\, d(\Delta E)/ [(\Delta E_2^3 - \Delta E_1^3)(\alpha+\beta)]$.

The polarization resistance, R_p, can be calculated by the equation $R_p = \sum_{j=1}^{n} \Delta E_j^2 / \sum_{j=1}^{n} i_j \Delta E_j$. A useful application is afforded by the screening of the inhibitor effectiveness of some organic components and on-line monitoring of corrosion rate of a metal. In both cases the main goal is to have an idea of the entity of the corrosion process. This point of view is supported also by the theory of error propagation, even if in principle the two methods have been suggested for the purpose of determing the corrosion current density.

In the following paper the author gives a new version of the two method that are based on the equations

$$\frac{i_2}{i_3} = -\exp(2\alpha\Delta E)\left[\frac{i_2}{i_1} - \exp(\alpha\Delta E)\right]^2 \qquad \text{(Barnatt)}$$

and

$$\frac{i_1}{i_3} = -\exp(\alpha\Delta E)\left(\frac{i_2}{i_1} - \exp(\alpha\Delta E)\right) \qquad \text{(Le Roy)}$$

The three points are chosen in the following way: $i_1 = i(\Delta E)$, $i_2 = i(2\Delta E)$ and $i_3 = i(-2\Delta E)$ (Barnatt) and $i_1 = i(\Delta E)$, $i_2(2\Delta E)$ and $i_3 = i(-\Delta E)$ (Le Roy).

The advantage of this formulation is given by the removal of the complex roots that can be present in the original suggestion. It is well-known that the original versions are based on the solution of a second-degree equation.

The inadequancy of the model is given by the following conditions $(\alpha,\beta)<0$ or $(\alpha,\beta)>1$ because α and β are always positive and less than one. It is very important to underline that the missing representation of the polarization curve in the vicinity of the mixed potential can be ascribed to the reciprocal position of the three points and not to the physical law that governs the electrochemical system.

This hypothesis can be verified by the NOLI method, which gives the electrochemical parameters I_c, α e β of the current-voltage characteristic $i=I_c[\exp(\alpha\Delta E)-\exp(-\beta\Delta E)]$ for a system under activation energy control.

The generalization of the two previous equations is given by the functions G and G_1, defined as

$$G=\sum_{j=1}^{n}\left[\left|i_{2_j}/i_{3_j}\right|^{\frac{1}{2}}-\exp(\alpha\Delta E_j)(i_{2_j}/i_{1_j}-\exp(\alpha\Delta E_j)\right]^2 \qquad \text{(Barnartt)}$$

and $$G_1=\sum_{j=1}^{n}\left[\left|i_{1_j}/i_{3_j}\right|-\exp(\alpha\Delta E_j)(i_{2_j}/i_{1_j}-\exp(\alpha\Delta E_j)\right]^2 \qquad \text{(Le Roy)}$$

In this case the value of α is obtained by the search for the minima of G and G_1.

However this new formulation of the three point method has some limits imposed by the shape of the two functions, G and G_1, which are a linear combination of the constituent equations. But when the model is successful, there is a considerable advantage with the NOLI method because in the present case we have only an unknown parameter.

The three point method with Barnatt's selection criterion was applied to the study of the behaviour of ARMCO iron in H_2SO_4 solutions at different pH values and at 25°C. The results obtained are shown in table 1 together with the NOLI analysis. All the polarization curves are of the galvanostatic pulse type and the zero of the function has been determined numerically with the dichotomic method. Table 1 shows that the values of the parameters, b_a, b_c and I_c, *do not change practically with the choice* of the initial value, E.

Furthermore there is a good agreement with the NOLI analysis, which was carried out on the interval [-60,60] mV. All the results are referred to the polarization curves corrected for the ohmic drop. For a correct application of the selection criteria recourse was had to the best-fitting of the experimental point with INTER 1 code. The application of Le Roy's scheme gave the same results. Table 2 shows some results of the application of the function, G, to the same systems. The quantity of the third column I_c has been calculated with the integral formulation of the polarization resistance, R_p, on the interval [-10, 10] mV. The values obtained are quite close to that of table 1. This good agreement is due only to the experimental technique used for carrying out the polarization curves, which in the present case, gives a current-voltage characteristic very near to the ideal one. However, it is not a common characteristic of all the electrochemical systems and in the case of H_2SO_4 1N + RODINE 92A 0.5 cc/l at 75°C we had b_a=196 mV, b_c=281 mV and I_c=116 μAcm^{-2}.For the same system NOLI gave b_a=120mV, b_c=108mV and I_c= 56 μAcm^{-2}.

Another application concerns the system HCl 1N + BORG P16 0.1 cc/l at 75°C. The results of the present method were b_a=189 mV, b_c=540 mV and I_c=134 μAcm^{-2}; on the other hand, NOLI gave b_a=135 mV, b_c=199 mV and I_c=73 μAcm^{-2}. All the calculations were carried out considering the following initial values of ΔE : ΔE = 4 mV, ΔE = 6 mV, ΔE = 8 mV, ΔE = 12 mV and ΔE = 14 mV. Therefore, the values of the electrochemical parameters are referred to 16 experimental points. This is very important because the information provided by the old method is of a local type while its generalization can give a global indication with a suitable choice of the number of experimental points.

Table 1

pH	E(mV)	b_a(mV)	b_c(mV)	I_c(μA cm^{-2})	NOLI		
					b_a(mV)	b_c(mV)	I_c(μA cm^{-2})
0.03	4	87	90	1254	93	103	1382
	8	87	90	1246			
	12	86	90	1244			
0.3	4	77	108	605	76	101	602
	8	78	109	615			
	12	80	110	626			
1	4	72	86	263	68	89	252
	8	73	86	266			
	12	74	87	269			
1.5	4	66	89	272	64	100	279
	8	67	90	274			
	12	67	91	277			

Table 2

pH	b_a(mV)	b_c(mV)	I_c(μA cm^{-2})
0.03	86	89	1236
0.3	80	114	636
1	74	88	271
1.5	68	92	278

06500

HOT-WATER HYDRATION OF POROUS ANODIC OXIDE FILMS ON ALUMINIUM — ANALYSIS OF FILM STRUCTURE BY ANODIC POLARIZATION.

M. Koda, H. Takahashi and M. Nagayama

Faculty of Engineering, Hokkaido University, Sapporo, Japan

When porous anodic oxide films formed in acid solutions are immersed in hot water, they undergo reduction in porosity and show improved corrosion protective abilities. This has been ascribed to plugging of the pores with hydrous oxide produced by the reaction between the oxide and water, and, for this reason, the process is often called 'sealing'. This investigation was undertaken to examine the sealing process by an anodic polarization technique, following the previous analysis with gravimetric[1] and impedance[2] data.

Porous oxide films were formed on pure Al specimens by applying a const.c.d.(i_a) of 10 ma/cm^2 for different periods, t_a, in a 2% oxalic acid solution at 30°C, the anodizing voltage was constant at E_a=41V. The formed films have the pore-diameter (2r) of 36 nm, pore-wall thickness (δ) of 38 nm, and the porosity (α) of 0.10, irrespective of t_a. The total film thickness (H) increases linearly with t_a at a rate of 0.27μm/min. After anodizing, the specimens were hydrated in hot-water at 99.5°C for different periods (t_h), and then transferred into a 0.5M H_3BO_3-0.05M $Na_2B_4O_7$ solution (20°C, pH=7.4) to follow the reanodizing voltage (Vr) at i_r=0.5 ma/cm^2 for different periods (t_r).

Fig. 1 shows V_r-t_r curves obtained for t_a=2 min films hydrated for different t_hs. The curves consist of two straight line portions having slopes of m_{ox} (initial) and m_{hy} (later). The initial portions coincide irrespective of t_h, but the later portions shift downward as the knee point voltage (V_p) decreases with t_h. A straight line with slope m_1 is obtained for specimens without hydration (t_h=0), and a broken straight line with slope m_2 is obtained for specimens from which all oxide film is removed by acid dissolution. Fig. 2 shows V_r-t_r curves measured for specimens formed for different times (t_a=1 to 10 min) and hydrated for t_h=10 min. For t_a=3 to 10 min films, only the initial portions with m_{ox} are observed. The second portion of the curve appears as t_a decreases below 3 min, and for t_a<1.5 min, only the second portion of the curve (slope m_{hy}) is observed.

According to a previous investigation[1], the changes in the film structure by hot water treatment is shown schematically in Fig. 3. Dekker and Middelhoek[3] suggested that, when i_r is applied to anodized but not-hydrated specimens (Fig. 3, a), it

is carried by the movement of Al^{3+} and O^{2-} across the barrier layer to form new oxide at the oxide/solution and oxide/metal interfaces. Thus, pores in the oxide are gradually filled with new oxide. They considered that the increase in the voltage, V_r, reflects the increase in the barrier layer thickness and the knee point appearing in the V_r-t_r curve corresponds to the completion of pore-filling. Based on their theory, the transport number of Al^{3+} in the barrier oxide is expressed by

$$T_{Al^{3+}} = \alpha(1-m_1/m_2) \;/\; (1-\alpha)m_2/m_1 \qquad (1)$$

where α is the porosity of oxide, m_1 and m_2 are the slopes of the V_r-t_r curves for specimens with and without oxide. The value of $T_{Al^{3+}}$ estimated in our previous work is 0.40[3].

Now, when i_r is applied to the hydrated specimen (Fig. 3, b), pore-filling proceeds in two steps; (a) the formation of voids due to dehydration of hydrous oxide and (b) the filling of voids with new oxide[4]. The volume ratio of the voids in the film is considered to be the same as $\alpha = 0.1$. Replacing m_1 with m_{ox}(=0.76 V/sec) in Eq.(1) and using m_2 (=0.24 V/sec), we obtain $T_{Al^{3+}} = 0.24$. (This value is considerably smaller than that obtained with non-hydrated specimens.) The knee point of the V_r-t_r curve corresponds to the completion of pore-filling up to the thickness H_{ox} where the pore-wall is remaining (Fig. 3, b). H_{ox} is calculated using

$$H_{ox} = kVp - \frac{i_r \cdot tp \cdot M_{Al_2O_3}}{nF\delta_{ox}}(1-T_{Al^{3+}})$$

Here, Vp and tp correspond to the knee point, k(=1.3 nm) is the thickness/voltage ratio and δ_{ox}(=2.93) is the density of the formed oxide, n=6 is the number of electrons associated with the formation of Al_2O_3, $M_{Al_2O_3}$ is the molecular weight of Al_2O_3, and $T_{Al^{3+}}$ is 0.24. The first term on the right side of the equation, kVp, is the barrier layer thickness at tp. Subtraction of the second term, the thickness of the barrier layer formed by the O^{2-} migration, gives H_{ox}. H_{ox}-t_h relationships obtained by the polarization method for t_a=2 min films with hydration for different times, t_h, is shown in Fig. 4. The result is in good agreement with that calculated from the gravimetric data reported already[1].

1) M. Koda, H. Takahashi, and M. Nagayama, J. of Metal Finish. Soc. Japan, 33, 242 (1982).
2) M. Koda, H. Takahashi, and M. Nagayama, ibid., 34, 44 (1983), Proc. of the 1983 ISE Meeting, No. 0803 (Erlangen).
3) A. Dekker, and A. Middelhoek, J. Electrochem. Soc., 117, 440 (1970), H. Takahashi, and M. Nagayama, Corr. Sci., 18, 911 (1978).
4) M. Koda, H. Takahashi, and M. Nagayama, J. of Metal Finish. Soc. Japan, 34 (1983).

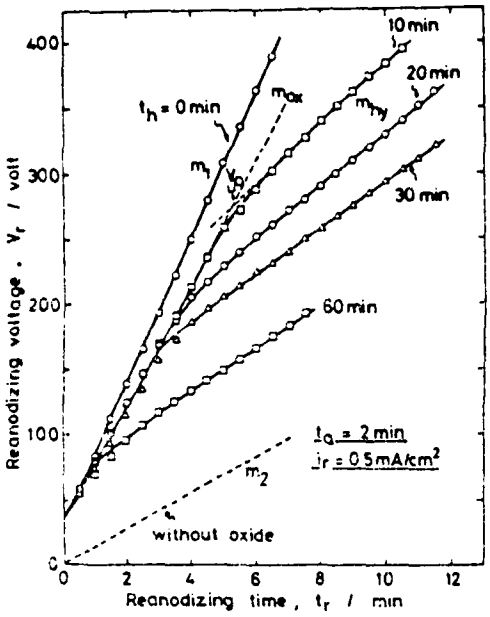

Fig. 1 V_r-t_r curves for t_a=2 min films hydrated for different t_hs.

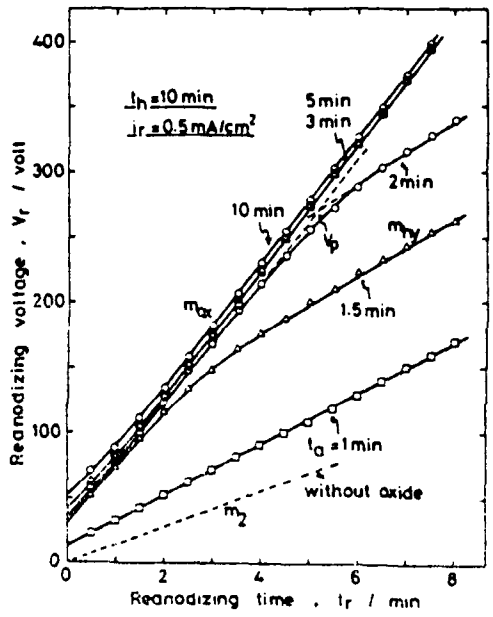

Fig. 2 V_r-t_r curves for films with different t_as and hydrated for t_h=10 min.

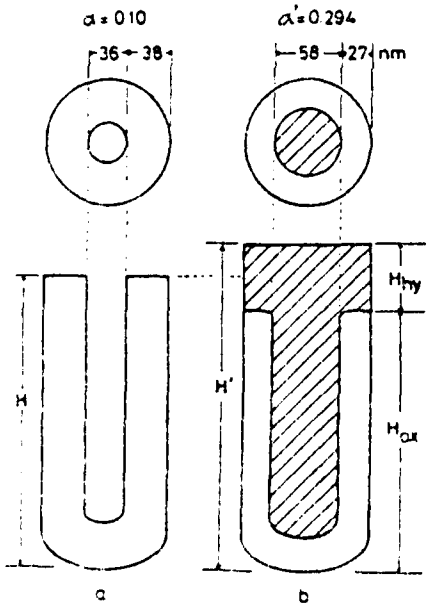

Fig. 3 Model explaining the changes in film structure by hydraion.

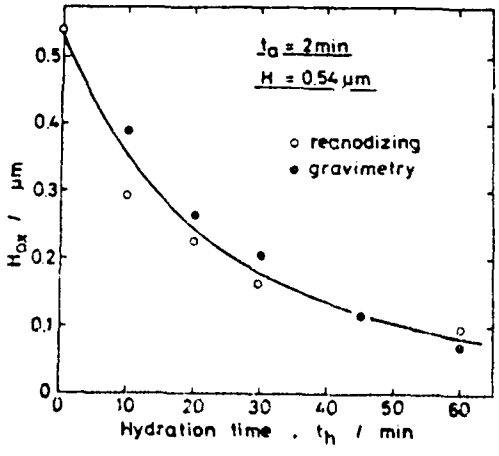

Fig. 4 Changes in H_{ox} with t_h.

06510

EFFECT OF METALLOID ELEMENTS ON THE CORROSION BEHAVIOR OF Fe BASE GLASSY ALLOYS

M. JANIK-CZACHOR

INSTITUTE OF PHYSICAL CHEMISTRY,
POLISH ACADEMY OF SCIENCES,
WARSAW, POLAND

The effect of substituting Si for B in families of the glassy alloys Fe-B and Fe-Ni-B on their electrochemical behavior has been investigated in solutions with pH ranging from 4 up to 8.4. Effect of substituting P for B in an alloy has also been studied. It has been found that: Si, when substituted for B in Fe-B glassy alloys, brings about the following changes in their electrochemical reactivity: improves their ability to passivate, extends the otherwise narrow range of their stable passivity in borate buffer solution thus eliminating localized corrosion, when the Si content attains 12% at., decreases their susceptibility to localized corrosion in chloride or sulphate containing solutions. Si, when substituted for B in Fe-Ni-B glassy alloys, exhibits only a minor effect on their anodic behaviour in buffered aqueous solutions. However, it distinctly improves their resistance against chloride or sulphate attack. XPS analysis suggests that at Si$<$12%, silicates, and at Si $\geq$12%, silicon oxides, are the main components of the passivating film. The oxides efficiently counteract the detrimental effect of boron compounds in the film and provide a much better protection to the metal substrate than the silicates.

P when substituted for B in the Fe-B-Si alloy improves dramatically its ability to passivate; reducing its critical c.d. for passivation and c.d. within the passive region. It is not clear, however, whether the beneficial influence of P in this case is only due to eliminating the detrimental B or also due to improving the protective ability of the film by the presence of P-containing compounds there.

06520

STAINLESS STEELS WITH ALUMINIUM AND SILICON ADDITIONS : PREPARATION, METALLOGRAPHY AND PITTING CORROSION STUDY.

L. GRAILLOT and R. REICH
Laboratoire Physique des Solides, bât. 510, Université Paris-Sud 91405 Orsay
and C. FIAUD
Laboratoire "Corrosion" ENSCP, 11 rue P. et M. Curie, 75005 Paris (France).

Introduction - Chromium is one of the most important alloying elements used in stainless steels. Indeed, it produces an extremely thin (10-100 Å), dense and adherent oxide film (Cr_2O_3) which protect the steel from corrosion. However, chromium is a strategic element and its content lowering in standard austenitic stainless steels (18%Cr+10%Ni) should be suitable as shown by Stephens (1). This paper describes on the one hand the preparation of martensitic steel alloys (where Al and/or Si are added in order to increase the chromium equivalent content) and on the other hand the pitting corrosion resistance of these new synthetic alloy grades.

Alloy steel preparation - Two synthetic alloy grades based on 13%Cr + 10%Ni - 0.06%C martensitic stainless steels (labelled A_{00}) are prepared : the first group by addition of Al or Si and the second group with both elements. These various grades are named A_{ij} (i = %Al and j = %Si) and their chemical analyses are given in the Table I. At the melting point of stainless steels (≈ 1400°C), the liquid Al shows high vapour pressure, light weight and low viscosity. Hence, to avoid its volatilization, a levitation induction melting under pure argon (1 bar pressure) is used. Moreover, a new alloying method is proposed : the bits of Al (or Si) are squeezed in the blind hole of a stainless steel "crucible" blocked up with a screw plug of the same matrix material. To avoid the melted Al throwing up through the thead under the archimedean upthrust, the first melting operation in the case of single element additions (2%Al or 2%Si) is carried out with the screw plug pointed downwards. The electromagnetic forces (H.F. field and eddy-current interactions) provide a stirring in the molten bath. Two or three such levitation meltings, each of them followed by a quenching (alloy contact with the water cooled hearth after H.F. switching off), provide very homogeneous alloys. In the case of a binary addition, 1%Al + 1%Si or 2%Al + 1%Si, the alloying process is different. Its first stage is an induction pre-melting of "sandwiches" of Si and Al bits, set between stainless steel plates. The induction coil is passed along this charge put on a cold horizontal copper crucible. In the second stage, the cut-off rounds from the resulting alloy bar are melted in the above-mentionned levitation crucible to obtain the suitable homogeneity.

Heat treatments - Three typical heat-treatments, labelled I, II and III, include a common stage numbered ① consisting of a 1300°C isothermal annealing followed by a chilled water quenching. It is the heat-treatment "I" which induces homogeneity and retains austenite (Fig.1). In the second treatment II, carbide precipitation and intermetallic compounds occur because of a low rate cooling: 15 hours from 1100°C to room temperature, stage ②. In the third treatment III, an annealing at 1010°C and a tempering at 600°C, each of them followed by a chilled water quenching, stages ③ and ④, there is the redis-

solution of carbides. The carbon content differences for a given alloy grade after the various heat-treatments, varies from 10 to 180 p.p.m.(table 1).

Metallography and pitting corrosion study - The corrosion potential E_c and the pitting potential E_p vs. SCE are determined from anodic polarization curves. The conditions of our potentiodynamic studies are : stirred and deaerated wt 3% NaCl solutions, 25°C, mechanically polished samples on 600 carborandum paper and no cathodic prepolarization. After the working (alloy steel) and the auxiliary electrodes have been connected during 30 minutes to reach the equilibrium, the circuit is open, E_c is measured and then the potential is swept in the anodic direction with a rate of 0.83 mV/s up to the cell current density equal to 10.10^{-6} A.cm^{-2}. The corresponding anode potential defines E_p. Because of the well-known scattering of experimental data, each test must be repeated 15 times and hence a average value of E_p is obtained. The choosen significant parameter characterizing the localized breakdown of the surface oxide film is the potential difference : $\Delta E = E_p - E_c$. The discrepancy resulting from surface heterogeneities equals ± 15 mV. The influence of our different heat-treatments on the potential difference ΔE is schematized in fig.2. After the treatment I, the Al alloys (A_{1j} with j= 1 or 2) and the binary A_{21} show a better corrosion resistance than the Si alloys. Such a phenomenon results from the Al diffusion through the Al (or Al+Si) steel alloys towards its surface and its oxidation during the annealing. The formation of this thick oxide film corresponds to a higher Cr equivalent content with respect to the Si alloy and an ordinary martensitic alloy (A_{00}), see fig. 3. The thermal treatment II resets the ΔE values of all the alloys in the same potential range. Such similar corrosion behaviors show the decrease of Cr eq influence (fig.4). The carbide precipitation and the rejection of more intermetallic compounds reduce the Al, Si and Cr contents in the matrix and hence a less corrosion resistance of 2%Al alloys is observed. On the contrary, the raise of the retained austenite content in the 2%Si alloy gives a corrosion resistance increase. In the binary alloys, these two opposite phenomena counterbalance each other. The last treatment III dissolves the carbides and produces a more or less redissolution of intermetallic compounds. The resulting higher Al and Si contents in solid solution within the matrix observed for the binary alloys (A_{11} and A_{21}) shift the corrosion resistance in the noble direction contrary to the phenomenon observed for the 2%Al alloy (A_{10}) and the matrix A_{00}. Indeed, in these two last grades, the treatment III reduces the retained austenite content which decreases the corrosion resistance.

TABLE 1

Sample	Heat treatment	%Cr	%Ni	%Al	%Si	%C ×10^{-3}
A_{20}	I	11.0	9.0	2.0	-	48.3
	II	12.1	9.0	2.0	-	41.3
	III	12.4	9.0	2.0	-	30.1
A_{02}	I	11.5	9.0	-	1.8	28.4
	II	12.5	9.0	-	2.0	26.5
	III	12.0	9.2	-	1.8	21.7
A_{11}	I	12.0	9.1	0.9	0.9	38.9
	II	12.3	9.1	0.8	1.0	33.4
	III	12.1	9.0	0.9	1.0	30.5
A_{21}	I	11.3	9.1	2.0	1.4	43.6
	III	12.4	9.0	1.9	1.0	30.3

Conclusion - The figure 2 shows that less strategic elements, such as Al and Si elements, can be substituted for part of the Cr (in fact by additions of these elements in martensitic 13%Cr + 10%Ni stainless steel alloys) without degrading the corrosion resistance relative to an ordinary austenitic 18%Cr + 10%Ni alloy (type 304SS), if the special heat treatment III is applied.

(1) J.R. Stephens and C.A. Barret, N.A.S.A. Technical Note D-8459 (1977).

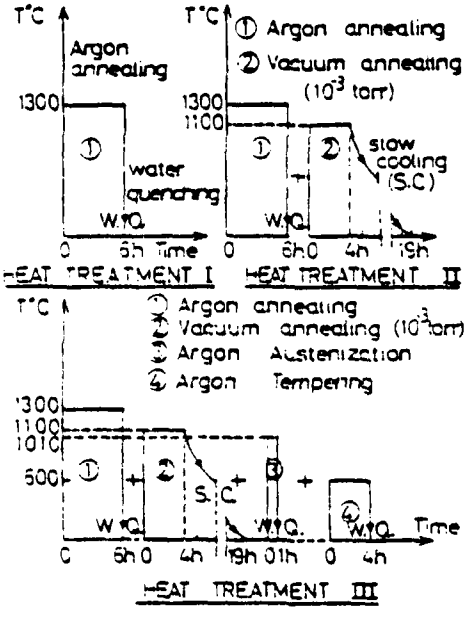

Fig. : Schematic description of the three different heat treatments.

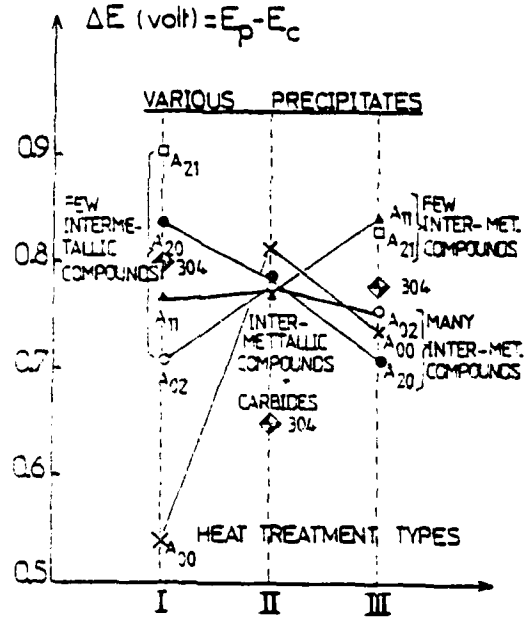

Fig.2 : Influence of the heat treatments on the pitting corrosion parameters ΔE.

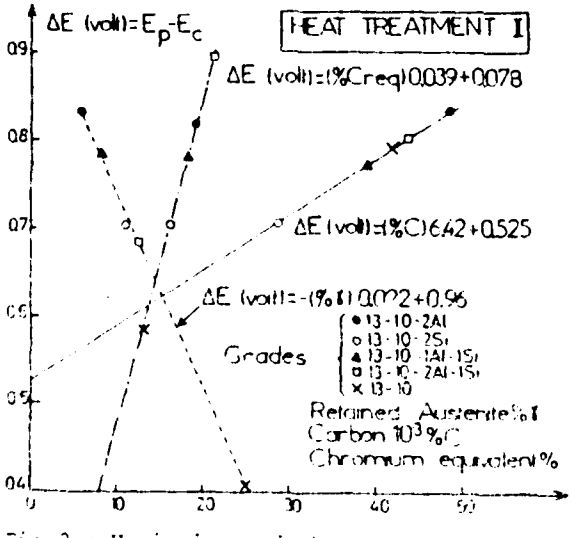

Fig.3 : Variations of the parameters ΔE versus %δ , %C and %Cr eq for the heat treatment I.

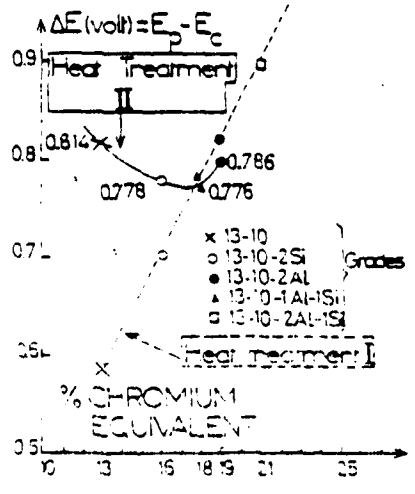

Fig.4 : Variation of the parameter ΔE versus %Cr eq for treatment II.

06530

INFLUENCE OF MINOR ALLOYING ELEMENTS ON PASSIVATION BEHAVIOR OF IRON-CHROMIUM ALLOYS IN HCl

R. Goetz, J. Laurent, D. LANDOLT
Materials Department
Swiss Federal Institute of Technology
CH-1007 Lausanne/Switzerland

INTRODUCTION

The corrosion resistance of stainless steels is intimately related to their passivation behavior. Generally, the higher the chromium content the more passivation is facilitated and chemical stability is improved. Other elements are usually added to modify structure and mechanical properties of the alloys and/or to increase corrosion resistance.

In our laboratory the reaction mechanism by which molybdenum improves the corrosion resistance of iron-chromium alloys in chloride media is being studied by electrochemical and surface analytical techniques [1-3]. In this context it was considered of interest to compare the effect of alloyed molybdenum with that of other metals such as tungsten, vanadium and silicon that might exhibit similar behavior. For that purpose, these elements were alloyed to binary Fe-Cr alloys in equal and relatively high atomic concentration. Indeed, a comparison of the effect of different alloying elements must be done based on equal value of atomic rather than weight percent because large density differences between different alloying elements may otherwise lead to wrong conclusions. The use of a relatively high concentration is indicated to improve the signal to noise ratio of surface analytical measurements.

EXPERIMENTAL

All studies were carried out with rotating disk electrodes of 0.1 cm^2 (diameter 0.357 cm) insulated with a PTFE shrinkable tubing. Experiments were performed at 6000 RPM in 1M HCl at 25 ^{o}C under nitrogen atmosphere.

The V containing electrodes were analysed by Auger depth profiling. For this they were held at a constant potential in the active (a) at -300 mV she, the low passive (pl) at +200 mV or the high passive (ph) potential region at +950 mV, respectively.

RESULTS

Among the pure alloying metals studied only Cr exhibits an active-passive transition, Mo, W, V being spontaneously passive in 1M HCl.

The binary Fe-13Cr alloy in 1M HCl undergoes uniform active dissolution but addition of Mo, W, V or Si leads to an active-passive transition. All alloys exhibit pitting with the pitting potential increasing in the order W<Si<V<Mo. The order of the pitting potentials of the different alloys is independent of the relative magnitude of the passivation current density.

The binary Fe-24Cr alloy exhibits passivation and pitting. Adding approx. 6 at % of Mo, W or V lowers the passivation current density, the effect of V being less pronounced than that of W and Mo. No pitting occurs with these alloys, the range of stable passivity extends up to the potential of transpassive Cr dissolution. Alloying of Si leads to a similar transpassive behavior but in the active and beginning passive potential region measured currents are substantially higher than with the other alloys and the passivation current density exceeds even that of the binary Fe-24Cr alloy.

Auger depth profile analysis shows that in the passive potential region Cr is enriched in the anodic film. With increasing potential this enrichment becomes more pronounced. The same behavior has previously been observed on Mo containing alloys. Because of the unfavorable signal to noise ratio the V Auger profiles are less certain. Active dissolution apparently does not lead to any substantial change in the V surface concentration with respect to the reference contrary to the behavior of Mo and W. In the passive potential region the outermost atomic layers of the oxide film are apparently depleted in V in both the passive low (200 mV (she)) and passive high (950 mV (she)) potential region. The beneficial action of the presence of V on pitting, therefore, cannot be explained by enrichment of the film with this element.

REFERENCES

1. R. Goetz, D. Landolt
Electrochim. Acta 29, 667 (1984)

2. R. Goetz, D. Landolt
Electrochim. Acta 27, 1061 (1982)

3. R. Goetz, C. Boband, D. Landolt
Proc. 8th ICMC Mainz 1981 p. 247

06540

ELECTROCHEMICAL BEHAVIOR OF AlMnFe INTERMETALLICS IN ALKALINE SOLUTION

OTTO LUNDER and KEMAL NISANCIOGLU
Division of Metallurgy and Corrosion Center, SINTEF and Department of Industrial Electrochemistry, Norwegian Institute of Technology, N-7034 Trondheim-NTH, Norway

Iron containing intermetallic phases play a significant role in the pitting and other forms of localized corrosion of aluminum alloys. These phases are normally more noble than the surrounding matrix alloy, and, as a result, they act as the local cathodes in a corrosion process. The fact that AlMn alloys have a good resistance to pitting is related to the presence of intermetallics in the AlMnFe series, which are less effective cathodes than the binary Al_3Fe phase and phases of the AlFeSi series commonly found in commercial aluminum alloys.[1] The amount of information available about the electrochemical properties of the AlMnFe series is very limited.[2] As cathodes in an actual corrosion situation, the surfaces of these phases are expected to be at a somewhat higher pH than the bulk of the solution.[3] It is of interest, therefore, to investigate their electrochemical behavior in alkaline solutions.[4]

As part of an effort to correlate the microstructure, electrochemical behavior and corrosion resistance of AlMn alloys, intermetallic crystals with varying Al, Mn and Fe content were prepared from the pure components by controlled solidification procedures. Compositions of the binary phases were found to agree well with the stoichiometric compositions of Al_3Fe (40.7% Fe) and Al_6Mn (25.3% Mn) (see table 1). The phases $Al_3Fe(Mn)$ and $Al_6Mn(Fe)$ were prepared to study the extent to which small additions of Mn and Fe affect the properties of, respectively, Al_3Fe and Al_6Mn. The electrochemical behavior of these crystals were investigated in 0.1N NaOH solutions with and without the presence of Cl^-.

Exposure of these phases to 0.1N NaOH solution leads to an enrichment of the more noble components Mn and Fe at the surface due to the selective dissolution of aluminum. In the case of the binary phases, a layer of pure Mn or Fe can be formed. The enrichment of ternary phases with Mn and Fe occurs in such a way that the Fe/Mn ratio in the enriched layer appears to remain unchanged relative to the ratio in the bulk of the crystal body as determined by X-ray EDS analysis. In particular, for the $Al_6Mn(Fe)$ phase maintained for 2 h at -1.7 V_{SCE}, the enriched surface layer was found to contain 71% Mn and 11.7% Fe amounting to an enrichment of these components by about a factor of 3. Interpretation of the electrochemical data has to be performed in view of this surface-enrichment phenomenon.

Fig. 1 shows cyclic potentiodynamic data obtained for Al_3Fe and $Al_3Fe(Mn)$ phases in 0.1N NaOH. Analogous data for Al_6Mn and $Al_6Mn(Fe)$ are given in fig. 2. The polarization curves of Al_3Fe and $Al_3Fe(Mn)$ are characterized by several oxidation and reduction peaks as can be visualized clearly for the Al_3Fe phase in fig. 1. The significance of these peaks in describing the selective dissolution mechanism of aluminum and oxidation and reduction kinetics of iron and iron oxides on an Fe-enriched surface has been discussed elsewhere.[4,5] A similar analysis for the Al_6Mn has not yet been carried out. Nevertheless, it is clear from these data that the presence of even a small amount of Mn in Al_3Fe has an appreciable effect in reducing the rates of cathodic and anodic reaction rates in general. Conversely, the presence of a small concentration of Fe in Al_6Mn depolarizes the cathodic reaction to a significant degree; however, its effect on the anodic behavior is much less pronounced. A large reduction peak (Peak A) is observed for $Al_6Mn(Fe)$ during the reverse sweep of potential, whereas the curve for Al_6Mn does not exhibit a similar peak. Iron oxides are expected to have been reduced to metallic iron at potentials appreciably more positive than the potential of Peak A.[5] Therefore, this peak results from a superimposition of current density due to hydrogen evolution, catalyzed by an Fe-enriched surface, and an anodic contribution (Peak B) at a more negative potential due to selective dissolution of aluminum.

The presence of Cl^- in 0.1N NaOH solution appears to reduce the passivity of iron oxides in general on an Fe-enriched Al_3Fe (or $Al_3Fe(Mn)$) surface (fig. 3). In particular, the chloride ion affects the passivity of Fe_3O_4 as indicated by a significant enlargement of Peak 3, which describes the formation of an Fe_3O_4 bulk layer from $Fe(OH)_2$ and metallic iron.[5] The presence of Cl^- does not appear to have such a dramatic effect on the electrochemical behavior of Al_6Mn and $Al_6Mn(Fe)$.

The results demonstrate clearly the detrimental effect of Fe in catalyzing the cathodic reaction on aluminum base intermetallics. The chloride in the environment plays an indirect role by accelerating the enrichment of Fe on these phases. The presence of Mn is instrumental in reducing the rate of cathodic reaction. Manganese also reduces the rate of selective dissolution of aluminum, which is responsible for the enrichment of crystal surfaces with iron.

References

1. M. Zamin, Corrosion, 37, 627 (1981).
2. T. Fukuzuka, K. Shimogori and K. Fujiwara, Boshoku Gijutsu, 28, 323 (1979).
3. K. Nisancioglu, K. Y. Davanger, O. Strandmyr and H. Holtan, J. Electrochem. Soc., 128, 1523 (1981).
4. K. Nisancioglu and M. Metzger, Abstract No. 154, 164th Meeting of The Electrochemical Society, Oct. 9-14, 1983.
5. K. Nisancioglu and M. Metzger, Extended Abstracts, 36th Meeting of ISE, Salamanca, Sept. 23-28, 1985.

Table 1. Composition of intermetallic phases in weight percent as determined by quantitative X-ray EDS analysis.

Phase	Al	Fe	Mn
Al_3Fe	58.8	41.2	-
$Al_3Fe(Mn)$	59.8	39.8	0.4
Al_6Mn	73.5	-	26.5
$Al_6Mn(Fe)$	72.9	3.6	23.6

Fig. 1. Potentiodynamic polarization curves for phases Al_3Fe and $Al_3Fe(Mn)$ in deaerated 0.1N NaOH at 25°C. Sweep rate = 120 mV/min.

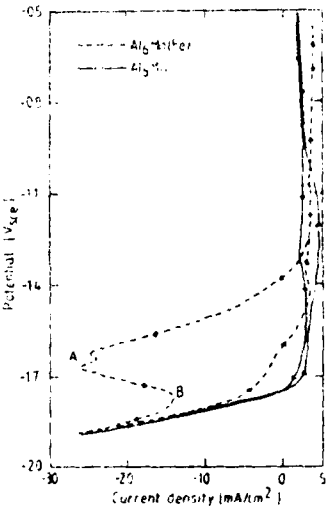

Fig. 2. Potentiodynamic polarization curves for phases Al_6Mn and $Al_6Mn(Fe)$ in deaerated 0.1N NaOH at 25°C. Sweep rate = 120 mV/min.

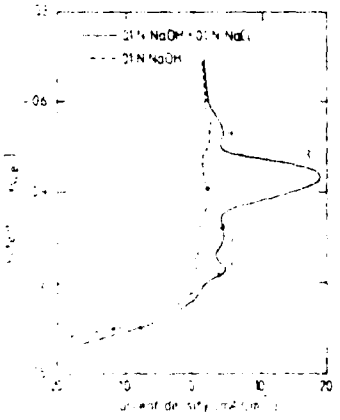

Fig. 3. The effect of presence of 0.1N Cl^- in 0.1N NaOH solution on the polarization behavior of Al_3Fe.

THE EFFECT OF DRAG REDUCERS ON THE INHIBITOR EFFICIENCY AND CORROSION PROTECTION IN NON-AQUEOUS MEDIUM

P.KIRKOV, T.ANOVSKI, J.ARSOVSKI, S.PEJOVSKI, J.NAUMOVSKI, T.GRČEV, Lj.ARSOV, A.PRUSSI

Center for Application of Radioisotopes in Science and Industry, Faculty of Technology, University "Kiril and Metodij", Skopje, Yugoslavia

Introduction

The effect of polymers on drag reduction has ecconomical importance for decreasing the cost of flow transportation especially petroleum products.[1,2]

The nature of polymers drag reducers is subject of many theoretical interpretations, however it is clear that presence of polymers effects solid (metal)-liquid(petroleum white products) interface reducing friction more probable with formation a vary movable inter layer. The presence of surface active inhibitors influence on the structure of the metal-liquid interface and effects charge-mass transfer phenomena (corrosion).

The subject of this work is to contribute for better understanding simultaneous effect of drag reducers and inhibitors for optimal corrosion protection and drag reduction.

Experiment

A rig system presented on figure 1 has been used for semipilot detrmination effect of drag reducers and inhibitors on the corrosion rate in petroleum white products:Gasoline,Kerosin and Naphta, with concentration of moisture (water) from 0-saturation. Drag reducers poly-oxi, oxi-celulose and polyamid have been used in concentration from 0-100 ppm and two types of diamin inhibitors in concentration from 0-250 ppm (water concentration from 0-10 g/l)

The correlation between flow rate and pipeing energy has been used for determination drag reduction efficiency with and without presence of inhibitors. The corrosion rate as a function of flow rate, the concentration of drag reducers, the concentration of inhibitors and moistures have been determined by surface popylation of pits on polished segments of pipes adjusted on linear part of the ring system.(fig.1)

Result and discussion

The corrosion rate of the pipe on the segment of the rig system without drag reducers and inhibitors depends from the moisture (water) concentration. The addition of the drag reducers increases pipeing efficiency and slightly decreases rate corrosion. However, the corrosion rate decreases substantively with increase concentration of inhibitors but does not effect pipeing energy of definite flow. The simultaneous adding of the drag reducers and inhibitors have double effect on reduction of corrosion and friction (fig.2). There is optimal concentration between drag reducers and inhibitors for the corrosion rate protection and friction reduction. This relation depends on structures of polymers and slightly from the nature of inhibitors.The substitution of the inhibitors functional group in the molecul of drag reducers has positive effect on the corrosion reduction (tab.1).

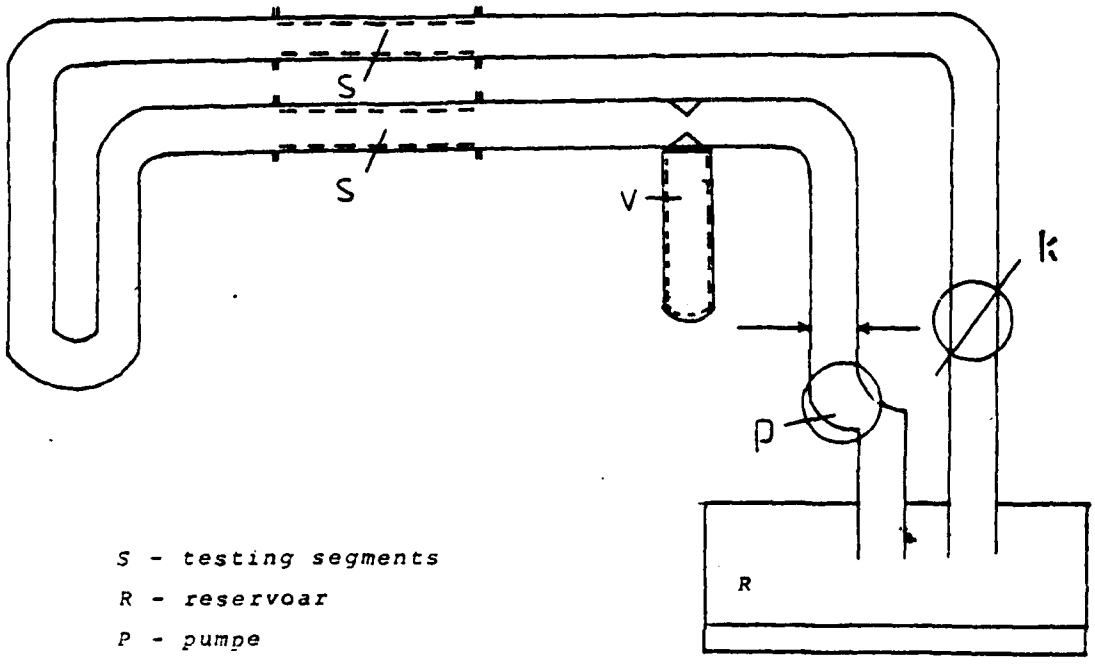

S - testing segments
R - reservoar
P - pumpe
V - flowmeter
K - speed kontrol

Fig. 1 Rig system

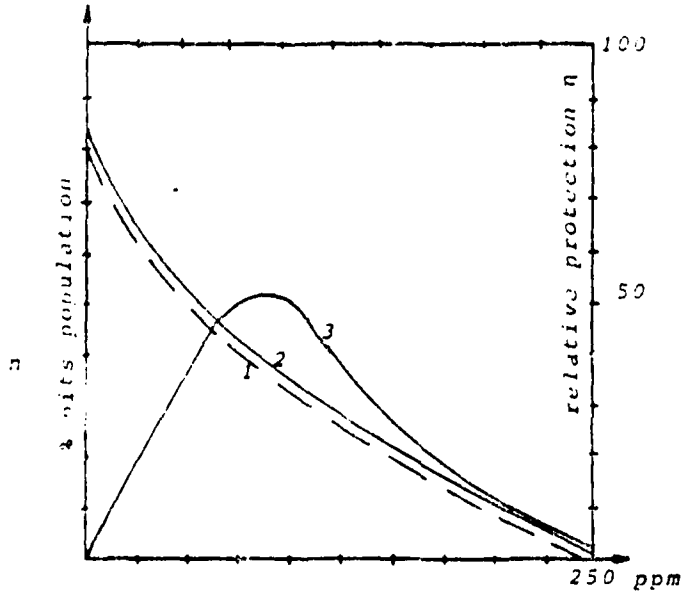

Fig. 2
Influence of inhibitors on corrosion rate in 1.Kerosine, 2.Nafta and 3.relation of reduction of corrosion in different ratio of drag reducers and inhibitors

However, efficiency of drag reducers of such substituated polymers depends of the metod of substitution. The optimal concetration of drag reducers and inhibitors has been used in the pipeline (65 km) for transportation petroleum white products (Naphta and Kerosin). The observation of the rig system and on the pipe line in exploration are comparable. Positive aspect of simultaneous application of polymers and inhibitors of the corrosion rate and friction reduction could be interpreted of stable interface metal/fluid protective layer preventing charge transfer and consequently reduction of metal oxidation.

Table 1

Effect of the substituted polymers on corrosion rate reduction

The type of the substituted polymers	Number of population of substituted functional groups No.of NH_2/ molecule of polymers	Protection efficiency $\eta = \frac{\Delta So - \Delta S}{\Delta So} 100$
Substituted in monomers	500	35
	10000	72
Tretеated polymers	500	5
	1000	12

ΔSo = population of pits without substituents
ΔS = population of pits with substituents

07010

7 ELECTROGENERATED LUMINESCENCE OF TERBIUM COMPLEXES ON AN ALUMINIUM ELECTRODE

J. KANKARE, K. HAAPAKKA, O. PUHAKKA and S. KULMALA
Department of Chemistry, University of Turku, SF-20500 Turku, Finland

Electrogenerated luminescence on aluminium electrodes in electrolyte solutions has been known already for about 100 years. The phenomenon has been a subject of numerous studies during these years but generally this luminescence, sometimes called g... inoluminescence, has been regarded as a scientific curiosity, affected by ill-defined surface defects, and completely without applications. However, a few years ago we showed that cathodic low-voltage electroluminescence is very sensitive to trace constituents in the solution.[1] By using forced convection with a rotating disk electrode (RDE) the electroluminescence (EL) measurements could be made reasonably reproducible, and even quantitative determination of some trace metal ions can be effected[2,3]. A new phase in the development is that also the luminescence of organic compounds can be excited by electrolysis on an aluminium electrode[4]. A special case of this phenomenon is the ligand enhanced luminescence of terbium, which is interesting firstly because very selective and sensitive method for the determination of terbium and/or its ligand can be devised, and secondly because the luminescence system gives some clues on the mechanism of the excitation. Various ligands are known to be effective in the energy transfer from the excited state of the ligand to terbium. For this work Tiron (1,2-dihydroxybenzene-3,5-disulfonic acid sodium salt) was chosen although some preliminary work with dipicolinic acid was also made.

In the experimental arrangement a rotating aluminium electrode was used and the light emission from the electrode surface was measured using an interference filter (546 nm) and photomultiplier with associated electronics[2-5]. A conventional three-electrode cell was used with a Pt counter electrode and an $Ag-Ag_xCl$ reference electrode. Potassium sulfate in water was used as the supporting electrolyte. The solutions contained also potassium peroxydisulfate and they were deaerated with ultrapure nitrogen. Symmetric double step waveform[2-5] was used for the excitation.

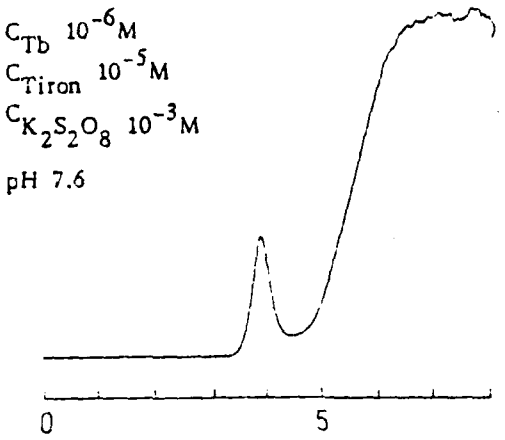

Fig.1. Luminescence intensity vs. pulse amplitude. Rotation rate 1000 rpm, pulse length 8 ms.

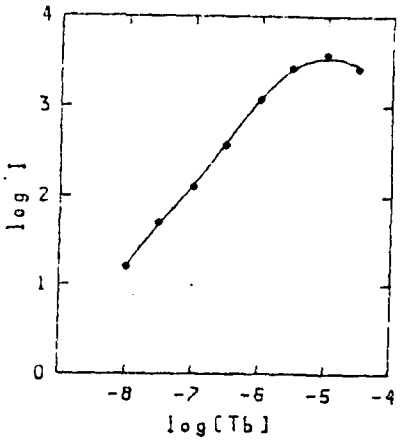

Fig.2. Calibration curve for Tb. Other conditions as in Fig.1.

The general shape of the EL intensity averaged over cathodic light pulses as the pulse amplitude is rapidly swept from 0 to 8 V is shown in Fig.1. A sharp "prepeak" is observed at ca. 4 V with a subsequent more gentle slope. After the first scan the position and height of the prepeak remain fairly constant and reproducible. The pH dependence of the prepeak is very complicated, presumably partly due to the numerous homogeneous and heterogeneous protonation equilibria prevailing in the solution, partly due to the complicated adsorption and desorption kinetics. However, the reproducibility is surprisingly good in spite of the heterogeneous nature of the system.

The calibration curve for terbium (Fig.2.) is obtained by measuring the height of the prepeak and keeping the concentration of Tiron constant. As can be seen, the detection limit for terbium is ca. 10^{-9} M and the linear range is at least three orders of magnitude. It should be noted that this may not be the ultimate limit of the method, because no effort was taken to optimize the conditions. The main limitation is the background luminescence which presumably could be reduced by varying the composition of the solution and the pulse train used for the excitation.

The necessity of peroxydisulfate for the luminescence shows that the phenomenon bears resemblance to the well known EL of gallium arsenide. Presumably adsorbed sulfate monoanion radical is formed from peroxydisulfate during the cathodic pulse. This forms a trapped exciton with an electron from an adsorbed

organic donor molecule or by the Schottky emission from aluminium. The recombination energy of the exciton is transferred to the ligand of the adsorbed terbium complex. The pH dependence of EL and that of the adsorption of Tb-Tiron complexes resemble each other which supports the important role of adsorbed species in the electroluminescence.

REFERENCES

1. J. Kankare, D. Ryan and B. Furst, Can. J. Chem. **55**, 1193 (1977).
2. K. Haapakka, J. Kankare and S. Kulmala, J. Lum. **31&32**, 966 (1984).
3. K. Haapakka, J. Kankare and S. Kulmala, Anal. Chim. Acta, in press.
4. K. Haapakka, J. Kankare and O. Puhakka, 36th Meeting of ISE, Salamanca, 1985.
5. K. Haapakka and J. Kankare, Anal. Chim. Acta, **138**, 253 (1982).

07020

DETERMINATION OF FLUORESCENT COMPOUNDS BY ELECTROLUMINESCENCE

K. HAAPAKKA, J. KANKARE and O. PUHAKKA
Department of Chemistry, Turku (Finland)

The electrolytic reduction of hydrogen peroxide and peroxodisulfate in an aqueous solution at an oxide-covered aluminium electrode generates light, i.e. electroluminescence.[1] As pointed out elsewhere,[2,3] numerous metal ions at trace level catalyze the electroluminescence induced by the reduction of hydrogen peroxide and, furthermore, this catalytic effect can be utilized in the determination of metal ions in an aqueous environment even at the level 10^{-10} M.

According to our preliminary measurements with the peroxodisulfate-induced electroluminescence at the anodized aluminium electrode, trace metals have no appreciable catalytic effect on this electroluminescence, but, interestingly, these measurements showed that numerous organic fluorescent compounds capable of adsorbing onto the surface of aluminium oxide enhanced drastically this luminescence.

The applicability of the peroxodisulfate-induced electroluminescence on the determination of organic fluorescent compounds in aqueous solutions was tested by using salicylic acid as a model compound. The electroluminescence measurements were carried out at a rotating oxide-covered aluminium disc electrode and the symmetric double step waveform shown in Figure 1a was used to generate the electroluminescence. This luminescence in 0.1 M sodium acetate at pH 9.3 in the presence of salicylic acid is presented in Figure 1b. Figure 2 shows the electroluminescence intensity as a function of the pulse amplitude of the symmetric double step potential.

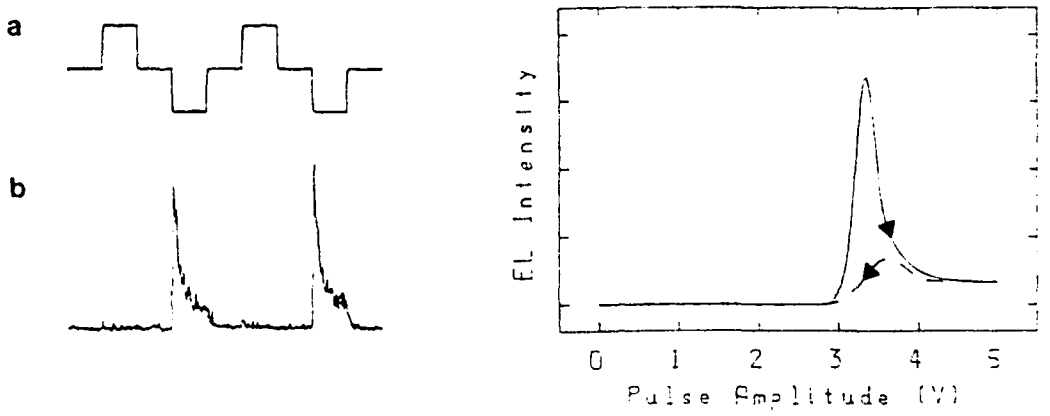

Figure 1. (a) Symmetric double step potential, (b) peroxodisulfate-induced electroluminescence, conditions: 0.1 M sodium acetate, pH 9.3, pulse amplitude 3.3 V, pulse length 12 ms, rotation rate of electrode 1500 rpm, scan rate of pulse amplitude 500 mV s^{-1}, peroxodisulfate concentration $1x10^{-3}$ M, salicylic acid concentration $1x10^{-6}$ M, solution deaerated with nitrogen.

Figure 2. Effect of pulse amplitude of the symmetric double step waveform on the intensity of the peroxodisulfate-induced electroluminescence in the presence of salicylic acid, conditions as in Figure 1.

The pulse amplitude and pulse length of the symmetric double step potential, rotation rate of the electrode, scan rate of the pulse amplitude, pH and peroxodisulfate concentration were optimized for the determination of salicylic acid in aqueous solutions. Under the optimized conditions, the analytical curve, i.e. log electroluminescent intensity vs log concentration, is linear at the concentration range 10^{-8} - 10^{-4} M and eight successive measurements for $5x10^{-6}$ M salicylic acid gave a relative standard deviation of 5 %.

Table 1 lists the relative electroluminescence intensities (I_{el}) of some organic compounds out of 34 tested under

the conditions stated in Figure 1. In addition, the table contains the relative fluorescence intensities (I_{fl}) and percentile adsorptions onto γ-aluminium oxide of these compounds under the same conditions.

Table 1. Effect of some organic compounds on the peroxodisulfate-induced electroluminescence.

Compound	I_{el}	I_{fl}	%-Ads
Blank	1	-	-
Salicylic acid	200	100	30
5-Sulfosalicylic acid	480	115	45
Chromotropic acid	6900	40	85
Calcein	3550	215	70
8-Hydroxyquinoline	870	-	87
Morin	710	-	88
Acridine	-	130	-
Tiron	-	-	89
3-Hydroxybenzoic acid	-	-	-

On the basis of these results it is tempting to suppose that in order to catalyze the peroxodisulfate-induced electroluminescence the organic compound must be fluorescent or capable of forming a fluorescent complex with aluminium and, furthermore, the compound must be readily adsorbed onto the surface of the oxide-covered aluminium electrode.

References:

1. J. Kankare, D. Ryan and B. Furst, Can. J. Chem. 55, 1193 (1977).
2. K. Haapakka, J. Kankare and S. Kulmala, J. Lumin. 31 & 32, 966 (1984).
3. K. Haapakka, J. Kankare and S. Kulmala, Anal. Chim. Acta, in press.

07030

ROTATING RING-DISK ELECTRODE STUDY OF THE COMPETITIVE PHOTOOXIDATION OF I^- AND H_2O AT n-TiO_2 ELECTRODE

P. SALVADOR* and C. GUTIERREZ**
*Instituto de Catálisis, C.S.I.C., **Instituto "Rocasolano", C.S.I.C.
Serrano 119, 28006 MADRID, Spain

Numerous studies have been reported on the photoassisted anodic evolution of oxygen at TiO_2 electrodes. However, the detailed mechanism of this process remains unknown. A mechanism which involves the intermediacy of H_2O_2 has been proposed[1,2]. We have undertaken a rotating ring-disk electrode (RRDE) study of the competitive photooxidation of I^- and H_2O at an n-TiO_2 electrode, in order to obtain more light on this problem. Several studies on this system have appeared[3].

The RRDE had an inner disk of sintered, H_2-reduced polycrystalline TiO_2 electrode, and an outer platinum ring. Details about the inner disk and the experimental set-up are given in Refs. 4 and 1, respectively.

The results obtained in 0.1M KI, 0.5M Na_2SO_4, pH 4.0 at a potential of +1500 mV vs SCE, positive enough to eliminate recombination (i.e. photocurrent transients) are shown in Fig. 1. There it is plotted the efficiency for iodide oxidation, Φ, vs the stationary photocurrent at the disk, I_D, with Φ=ring current/(collection efficiency x disk current). It can be seen that Φ decreases with increasing I_D, which points to a higher reaction order (in a common reactant) for H_2O oxidation than for I^- oxidation. A possible reaction mechanism could be:

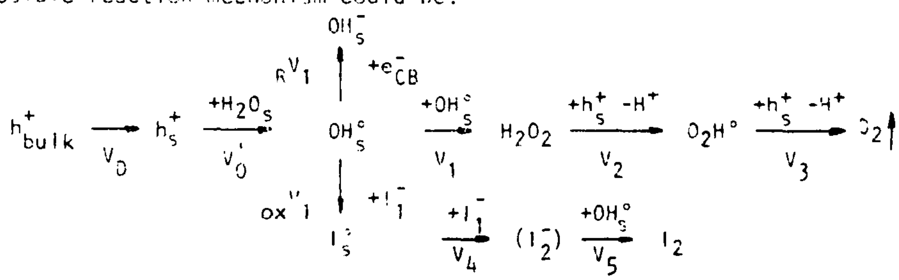

We assume that all reaction steps are irreversible. Then, the relationship between Φ and I_D is completely determined by k_1 and ${}_{ox}k_1$, as is easily shown:

$$\frac{I_D}{q} = \frac{I_{H_2O}}{q} + \frac{I_{I^-}}{q} = 4V_1 + 2\,{}_{ox}V_1 = 4k_1\left[OH^\circ_s\right]^2_{st} + 2\,{}_{ox}k_1\left[OH^\circ_s\right]_{st}\left[I^-_s\right]_{st} \qquad [1]$$

From here we obtain:

$$\left[OH^\circ_s\right]_{st} = \frac{-2\,{}_{ox}k_1\left[I^-_s\right]_{st} + \sqrt{4\,{}_{ox}k_1^2\left[I^-_s\right]^2_{st} + 16k_1\, I_D/q}}{8k_1} \qquad [2]$$

Besides,

$$\phi = \frac{I_{I^-}}{I_{I^-} + I_{H_2O}} = \frac{{}_{ox}k_1 \left[I_s^-\right]_{st}}{{}_{ox}k_1 \left[I_s^-\right]_{st} + 2k_1 \left[OH_s^\circ\right]_{st}} \qquad [3]$$

Substitution of [2] in [3] and rearrangement yields

$$I_D = \frac{q \; {}_{ox}k_1^2 \left[I_s^-\right]_{st}^2}{k_1} \frac{1-\phi}{\phi^2} \qquad [4]$$

Therefore, provided ${}_{ox}k_1 \left[I_s^-\right]_{st}$ and k_1 remain constant, the model predicts that a plot of I_D vs $(1-\phi)/\phi^2$ should give a straight line passing through the origin. When plotted in this way the data of Fig.1 give, instead a smooth curve, convex towards the abscissae axis. Effectively, the agreement between the model (chain line) and the experimental data (full line) is far from perfect. This could be justified if we assume, either that k_1 decreases monotonically with increasing illumination intensity, due to a decrease of the reactivity of the remaining OH_s° surface sites), or that ${}_{ox}k_1$ increases monotonically, due to unpinning of the band edges and improvement in the overlap, or both.

The dependence of ϕ on disk potential at constant illumination has also been included in Fig. 1. Provided k_1 and ${}_{ox}k_1[I^-]$ remain constant, Eq. [4] should also apply. Effectively, when plotting I_D vs $(1-\phi)/\phi^2$ the first four points define a straight line that passes through the origin. The agreement between the model (dotted line) and the experimental points (full line) is rather good. This is surprising, since the agreement was rather poor in the experiments at constant potential.

The dependence of ϕ on iodide concentration at two constant disk currents is shown in Fig. 2. The dependence predicted by the model is obtained from Eq. [4] as:

$$\left[I_s^-\right]_{st} = \frac{1}{{}_{ox}k_1} \sqrt{\frac{k_1 I_D}{q}} \frac{\phi}{\sqrt{1-\phi}} \qquad [5]$$

At constant I_D, a plot of $\left[I_s^-\right]_{st}$ vs $\phi/\sqrt{1-\phi}$ should give a straight line passing through the origin. If the model is obeyed, Eq. [5] allows us to obtain the shape of the I^- adsorption isotherms from experiments at constant I_D, such as those in Fig. 2, by simply plotting $\phi/\sqrt{1-\phi}$ vs $[KI]$. These curves are included in Fig. 2. They have been normalized, and nearly coincide, as they should.

Finally, the influence of pH is shown in Fig. 3. At pH 12 ϕ is independent of the disk current. At this pH the TiO_2 surface is charged negatively, which could repel the I^- ions away from the surface, so that perhaps they cannot accept a hole from an OH_s° radical, but directly from the surface as h_s^+, in a less efficient (lower ϕ) process. This mechanism would explain the observed constancy of ϕ.

It is very interesting that at pH 10 ϕ initially increases and finally merges with the curve obtained at pH 4. Again, this means that I^- photooxidation is less efficient at alkaline pH, and that, due to mass transfer limitation of OH^- ions from the bulk to the surface, the local pH at the surface decreases with increasing disk current from 10 to 4, at which moment

the two curves merge.

REFERENCES

1. P. Salvador and F. Decker, J. Phys. Chem., 88, 6116(1984).
2. P. Salvador and C. Gutiérrez, Surf. Sci., 124, 398(1983).
3. A. Fujishima, T. Inoue and K. Honda, Chem. Lett., 377(1978) and J. Amer. Chem. Soc., 101, 5582(1979); T. Kobayashi, H. Yoneyama and H. Tamura, J. Electroanal. Chem., 122, 133(1981) and 138, 105(1982); S.N. Frank and A.J. Bard, J. Amer. Chem. Soc., 99, 4667(1979).
4. P. Salvador, J. Electrochem. Soc., 128, 1895(1981).

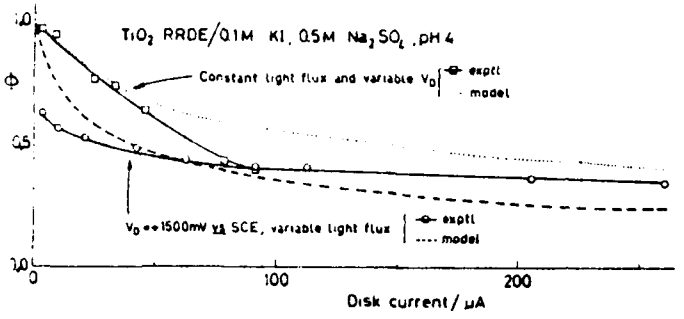

Fig. 1

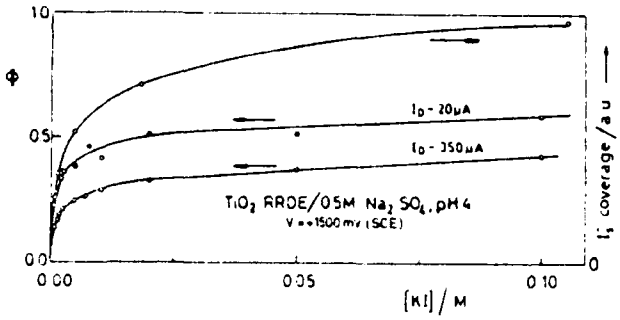

Fig. 2

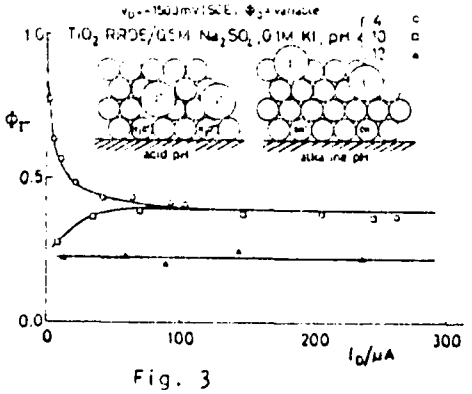

Fig. 3

07040

KINETICS OF THE DISSOLUTION OF SPENT LEAD-BATTERIES WITH THE "G.S." ELECTROCHEMICAL PROCESS

M. MAJA and P. SPINELLI
Dipartimento di Scienza dei Materiali e Ingegneria Chimica
Politecnico di Torino, Italy.
M.V. GINATTA and G. ORSELLO
Elettrochimica Marco Ginatta S.p.A., Torino, Italy.

With the G.S. process (1) the spent batteries after bottom cutting, are loaded on racks to be activated and then placed in the electrolysis tanks as soluble anodes, while pure lead is deposited on the cathodes.

The dissolution of the plates, which is one of the main electrochemical features of the process, was investigated by means of: i) current and potential measurements on especially prepared full-size batteries containing reference electrodes for monitoring of the plates' potential; ii) analytical and weight-loss determinations on plates withdrawn from batteries removed from the tanks after different processing times. Some results are reported in Table I.

From the values of the mean weight of the battery components, the distribution of the dissolved lead was estimated, indicating the following weight ratios 6.4/3.2/0.54 referring to electrolyte/cathode/slime respectively. Due to lead enrichment of the electrolyte, the G.S. process employs electrowinning tanks with insoluble anodes in addition to the dissolution tanks. Table I shows the weight percent dissolution values of positive and negative plates after removing the batteries from the dissolution tanks at different processing times.

Interpretation of the electric measurements was done on the basis of the equivalent electric circuit partially shown in fig. 1. The measured and computed values are compared in figs. 2 and 3. These results indicate that dissolution occurs with current yields controlled by the ohmic losses in the electrolyte.

A better understanding of the positive plates dissolution was possible by determining the variation of the lead-dioxide content during the process. This was done with laboratory tests on short-circuited positive and negative plates of about 1 Ah capacity, by measuring the amount of electric charge flowing from the positive to the negative plate. At the end of the test, the positive plate was immediately extracted from the solution, washed and dried and then analysed for the PbO_2 content. Some results of these tests are shown in Table II. In the same Table II we see that the weight loss of the negative plates agrees very closely to the measured

electric charge, while the positive plates show a weight loss of an order of magnitude higher than that corresponding to the measured charge. This proves that one of the major dissolution mode is the local galvanic coupling metal grid/positive active material. These results agree very well with industrial operating conditions as indicated in table I, where dissolution of positive plates is shown to proceed at higher rate than the negatives at the beginning of the process.

References

1 - Ginatta M.V., U.S. Patent n° 4,098,658.

PROCESSING TIME (h)	0.5		8		24	
	pos	neg	pos	neg	pos	neg
FINAL WEIGHT (g)	103.0	98.8	78.7	42.9	22.0	6.9
WEIGHT LOSS (g)	44.2	19.5	68.5	75.4	125.2	111.4
WEIGHT LOSS %	30.0	16.5	46.5	63.7	85.1	94.2

TABLE I

MEASURED ELECTRIC CHARGE (Ah)	NEGATIVE PLATE WEIGHT LOSS (g)	POSITIVE PLATE WEIGHT LOSS (g)	Δ% PbO_2
0.94	3.66	24.2	11.9
2.05	8.02	92.5	17.6

TABLE II

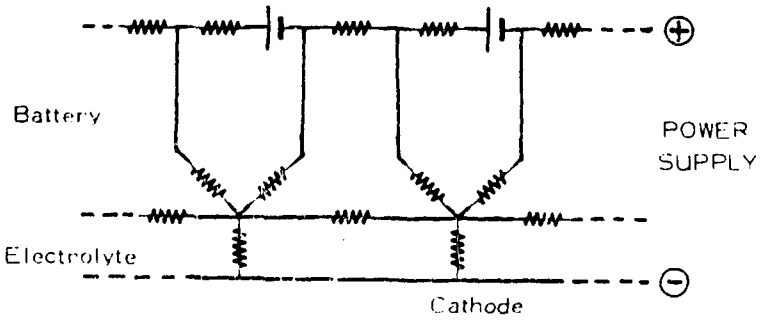

Fig. 1 - Electric circuit equivalent to the system Battery/Electrolyte/Cathode.

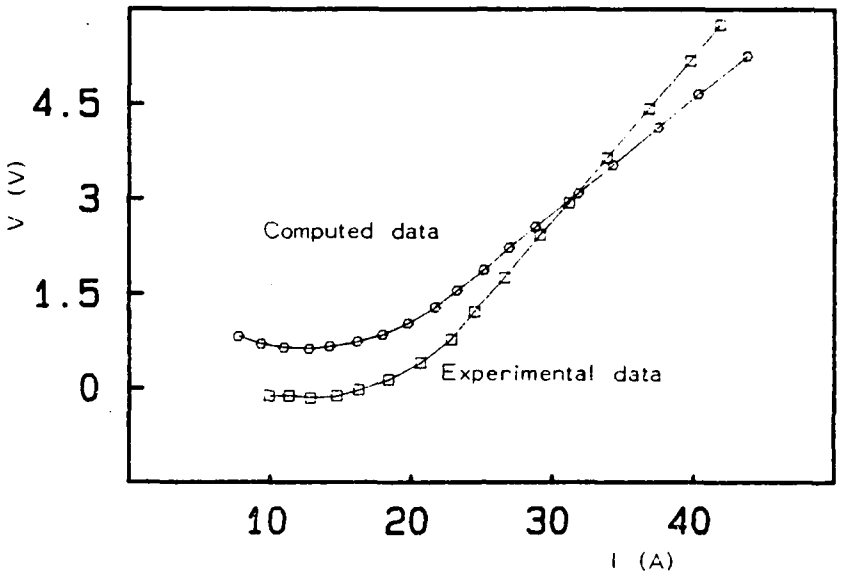

Fig. 2 - Battery voltage as a function of current intensity during the dissolution process.

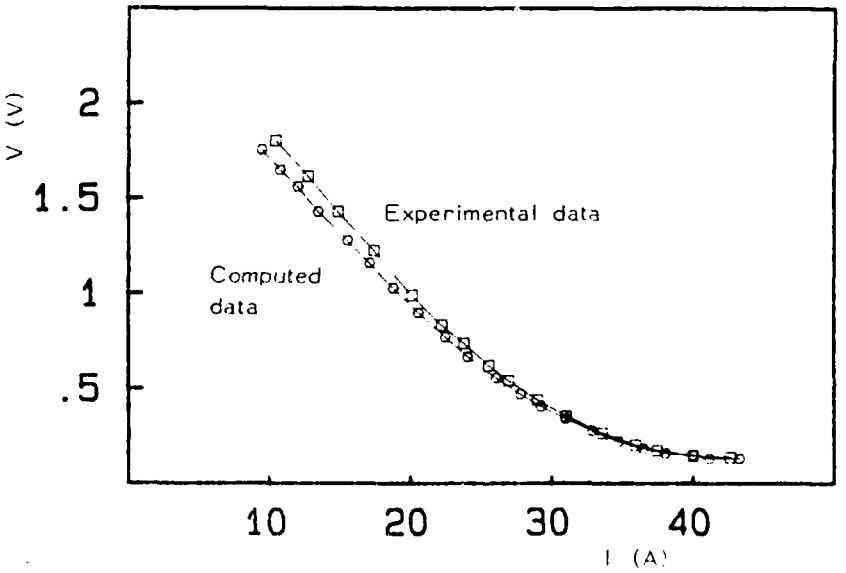

Fig. 3 - Voltage of the positive post vs. a lead reference electrode in the electrolyte, as a function of current intensity during the dissolution process.

07050

SOME NEW EXPERIENCE IN THE OPERATION OF SALINE ALUMINIUM-AIR BATTERIES

A.R. DESPIĆ, K. KRSMANOVIĆ, A. VORKAPIĆ, M. DOBRIĆ and B. VESIĆ
Laboratory for Electrochemical Energy Conversion,
Institute of Electrochemistry ICTM, Belgrade, (Yugoslavia)

Aluminium-air batteries represent a relatively new chemical power source, which is still in the state of developement of models and prototypes of future commercial products. Two lines of work are pursued in the world: that on a high-power density battery with alkaline electrolyte, typically for electric vehicle application and a high-energy density one with neutral saline electrolyte to be used as a common small power source of electricity, as reserve power or even for electric vehicles in a hybrid combination. The saline battery has the advantages of simplicity of the system, of hazardless manipulation and ecological acceptability.

However, a basic shortcoming of the saline electrolyte is that, if stagnant, the reaction product (hydrated aluminium oxide) forms in the form of a gel which tends to solidify the electrolyte already at an early stage and block the operation (brings the voltage down to an impractical level).

Two ways of overcoming this difficulty were developed in our laboratory.

For small power batteries a special construction is developed[1]. The cell consists of two parts: an electrolyte container and an active part consisting of an aluminium anode and an air cathode in a fixed position with respect to each other with an air-pocket providing the air to the cathode through and opening at the top. The active part was made to slide in and out of the electrolyte container in a telescopic arrangement. A wiper-bar is fixed inside the electrolyte container so as to enter between the two electrodes, with rubber wipers pressing against the electrode surfaces. As the active part is pulled up, out of the electrolyte container, or back, the wipers scrub the electrodes. Hence, when the cell is filled with the electrolyte and the active part inserted the cell attains the voltage and is ready to deliver current. When the operation is to be interrupted the active part is pulled up, out of the electrolyte. At the same time the wipers scrub the electrodes free of the product. It was found that is suffices to lift the active part and return it down once in 8 to 16 hrs, for the operation of the cell to run smoothly for days till the exhaustion of the electrolyte. Typical operation at different external loads is shown in fig. 1. for a cell with an aluminium alloy anode and a concentrated NaCl + + Na_2SO_4 electrolyte.

For medium and large power batteries the principle of reciprocation of the electrolyte was introduced[2]. Also, a bipolar cell design was effected with a self-perpetuating wedge anode[3]. The operation was tested with an aluminium alloy anode with pure

AD-A162 434 EXTENDED ABSTRACTS INTERNATIONAL SOCIETY OF ELECTROCHEMISTRY (36TH) HELD AT SALAMANCA SPAIN ON 23-28 SEPTEMBER 1985(U) INTERNATIONAL SOCIETY OF ELECTROCHEMISTRY 28 SEP 85 8/12

UNCLASSIFIED F/G 7/4 NL

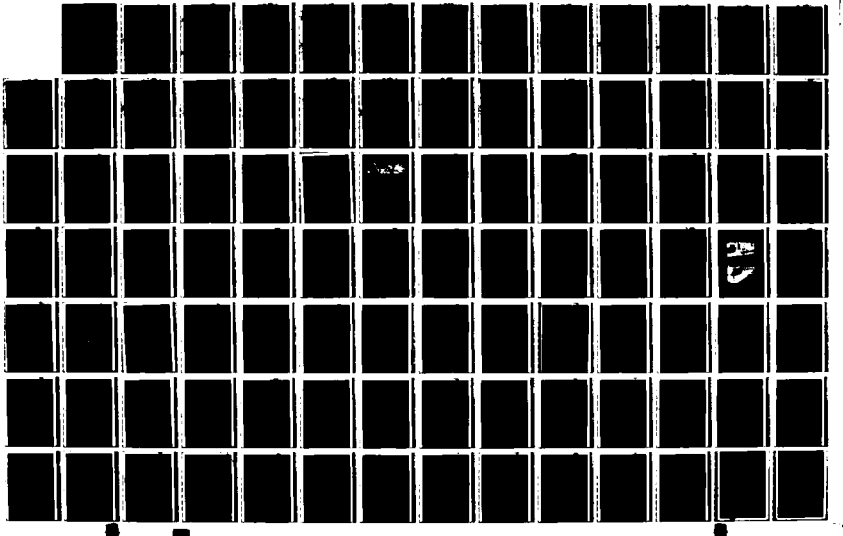

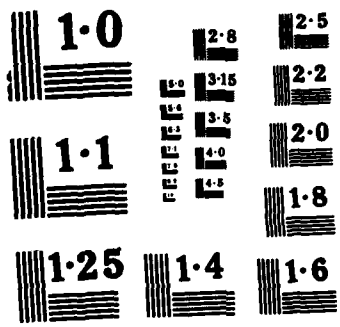

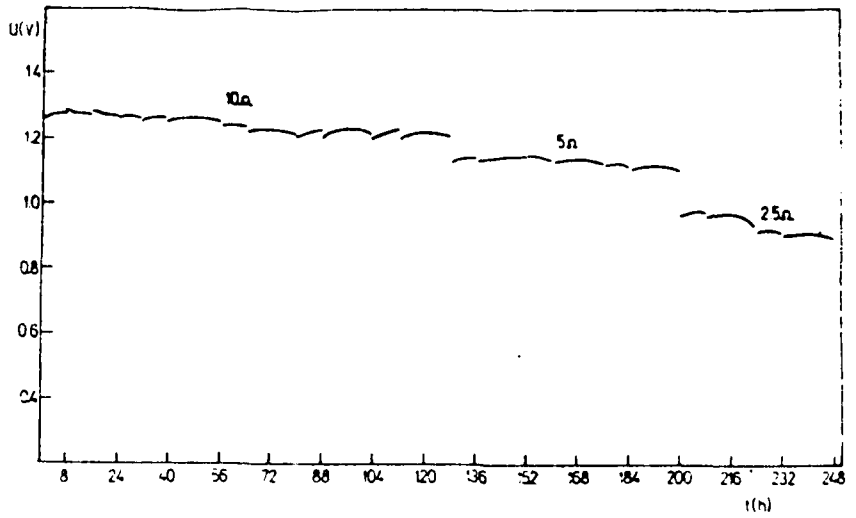

Fig. 1. Operation of the stagnant electrolyte cell on different constant load with scrubbing of the electrodes each 8 and 16 hours.

concentrated sodium chloride (2M) and a mixture of sodium chloride and sodium sulphate. The purpose was to check on the perpetuation of the wedge (shape maintaining) as well as on the functioning of the electric contact between the wedge and the conducting wall between adjacent cells. Problems were encountered with both. The shape was not maintained well, as is experienced with the alkaline electrolyte. After about 50 hrs of operation at 20 mA cm^{-2} the shape changed to the one shown in fig. 2.

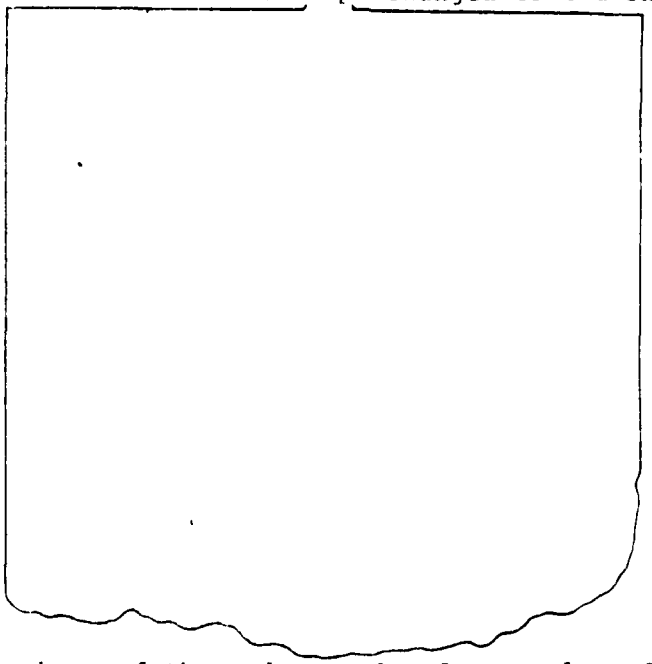

Fig.2. The shape of the wedge-anode after prolonged operation

Also significant voltage drop was found between the anode and the wall. This difficulty was overcome by painting the back of the anode with the conducting laquer.

Further investigations are in progress.

References:

1. K. Krsmanović, A. Despić, Yug. Pat. Appl.

2. A.R. Despić, D.M. Dražić, Bull.Soc.Chim. (Belgrade) 48 (1983) S 299

3. A.R. Despić, J. Applied Electrochem. 15 (1985) 191

07060

OXYGEN REDUCTION ON RUTHENIUM ELECTRODE MODIFIED BY THALLIUM AND LEAD ADSORBATES

N. Anastasijević, Z. Dimitrijević[1] and R. Adžić
Institute of Electrochemistry, ICTM Belgrade, Yugoslavia

Studies of oxygen reduction on Ru electrodes are rare. Nekrasov and Khruscheva[1] have found a series mechanism of O_2 reduction on Ru in alkaline electrolyte. We have recently shown that the reaction proceeds by a parallel mechanism[2]. Both works emphasize the role of the oxidation state of the Ru surface on kinetics of O_2 reduction. In this work the effects of adsorbates of Tl and Pb on O_2 reduction on a partially oxidized Ru electrode have been studied. The adsorbates of Tl and Pb have been obtained by the underpotential deposition and the ionic chemisorption on Ru-oxide.

A pronounced influence of the negative potential limit was found on O_2 reduction. If the negative limit is outside the potential region of the hydrogen adsorption/desorption process, the electrode looses its activity towards O_2 reduction. This is apparently due to a buildup of a thicker oxide layer under these conditions. A presence of the trace quantities (10^{-6}M) of Pb^{2+} and Tl^{+} in the electrolyte, which results in their adsorption on Ru and RuOx surfaces, causes that a full activity for O_2 reduction is obtained (Fig. 1, 2)[3].

The analyses of the disc-ring measurements shows that O_2 reduction is first order with respect to dissolved O_2. Four electrons are exchanged in this reduction. The presence of Tl adsorbates changes the Tafel slope from -180 mV/dek into -125 mV/dek.

The electrochemical reduction of HO_2^- also depends on the oxidation state of the Ru electrode. The reaction is first order with respect to HO_2^-. It goes with the exchange of 2 electrons. A presence of the Tl adsorbate changes the Tafel slope from -240 mV/dek to $\approx$ -110 mV/dek. The catalytic effect of the Pb and Tl adsorbates is seen in the shift of $E_{1/2}$ by 40 mV to more positive potentials and a certain increase of the limiting current density.

---

1 Permanent address: Institute for Chemical Power Sources, Zemun Polje

Fig. 3 gives the plot of I_D/I_R vs. $w^{-1/2}$ obtained from the disc--ring measurements for O_2 reduction on Ru/Pb_{ad}. The plot of slopes vs. intercepts (Fig. 4) obtained from Fig. 3 shows the intercept $J' > 1$, which, according Wroblowa et al.[4], suggests a parallel mechanism of O_2 reduction to OH^-. It may be surprising that a four electron reduction of O_2 is observed on a partially oxidized Ru surface modified by Pb and Tl adsorbates. This can be explained by the ion exchange reaction on the RuOx surface viz.,

$$RuOH + M^+ \longrightarrow RuO\text{-}M + H^+ \qquad (1)$$

This gives essentially a metallic surface facing the O_2 containing electrolyte. On such a surface the interaction of O_2 with two sites may lead to a rupture of the O = O bond, a prerequisite for a parallel mechanism.

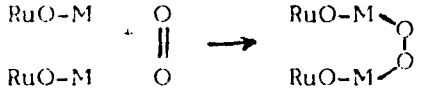

(2)

The Tafel slope of -125 mV/dek suggests a first electron exchange as the rate determining step. These effects may provide useful data on the relation of the state of electrode surface and O_2 electrocatalysis with a considerable applicative potential.

References:

1. L.N.Nekrasov, E.I.Khruscheva., Elektrokhimiya. 3, 166 (1967)
2. N.A.Anastasijević, Z.M.Dimitrijević, R.R.Adžić, J.Electroanal. Chem. in press.
3. R.R.Adžić, N.A.Anastasijević, Z. M. Dimitrijević, J.Electrochem. Soc. 131, 2730 (1984).
4. H.S.Wroblowa, Y.D.Pan, G.Razumney, J.Electroanal.Chem. 60, 195 (1976).

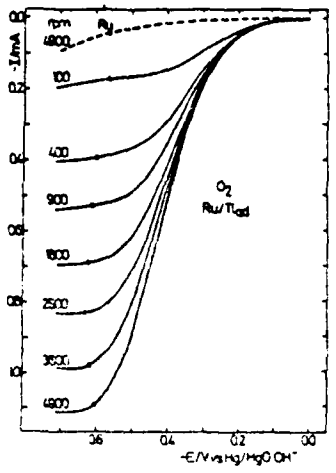

Fig.1. O_2 reduction on Ru and Ru/Tl_{ad} in 0.1M NaOH and 0.1M NaOH+$1x10^{-4}$M Tl^+. Sweep rate 50 mVs^{-1}.

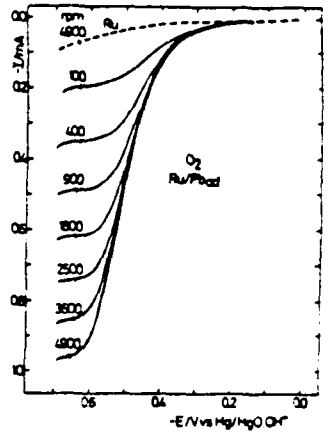

Fig. 2. Same as in Fig. 1 but for $1x10^{-5}$M Pb^{2+} in 0.1 M NaOH.

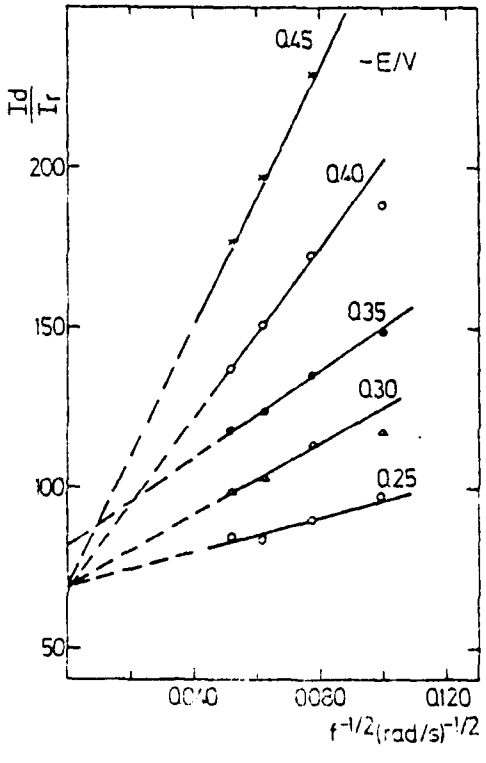

Fig.3. The plot of I_D/I_R vs $\omega^{-1/2}$ for O_2 reduction on Ru/Pb_{ad} in 0.1M NaOH. E_R=0.15V. Collection efficiency N=0.11.

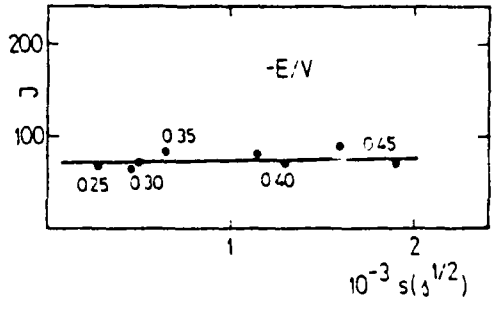

Fig.4. intercept vs.slope plot obtained from Fig.3.

07070

ELECTROCHROMISM OF LUTETIUM DIPHTHALOCYANINE THIN FILMS. ELECTROCHEMICAL INVESTIGATION.

F. CASTANEDA* and V. PLICHON
Laboratoire de Chimie Inorganique et Electrochimie. ESPCI,
10 rue Vauquelin, 75231 PARIS CEDEX 05 (FRANCE).

Lanthanide diphthalocyanines have been proposed as electrochromic materials because they are highly coloured and stables [1,2].

The electro-oxidation of the initial green compound, in contact with aqueous electrolytes at neutral pH, leads to an orange form whilst electroreduction in the same conditions leads to a blue form. Changing the electrolyte does not affect the colours.

$$\underset{\text{blue}}{LuPc_2^-} \overset{+e^-}{\rightleftharpoons} \underset{\text{green}}{LuPc_2} \overset{-e^-}{\rightleftharpoons} \underset{\text{orange}}{LuPc_2^+} \quad \ldots (1)$$

As noted in the literature, the peak potential (E_p) of the first scan exibits a significant overpotential when compared to its position after repetitive cycling [1].

We have shown that both the peak potential and the coulometric yield on the first scan differ from that measured after repetitive cycling (Table 1, fig. 1)

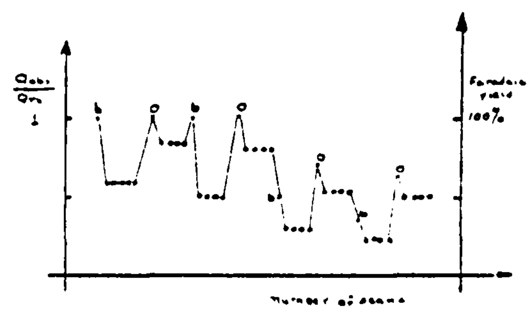

Fig 1 variation of Qobs/Qth or Faradaic yield as a function of the number of scans [illegible] first scan [illegible] first scan

One electron was found for the two redox systems (green-blue, green-orange) in the first or alternative first scan

---

*Scholarship of the Mexican Government (CONACYT)

i.e. in the green-blue first colour transition or in the green-orange first colour transition after cycling several times on the other redox system (Fig. 1). Reactions yield progressively decreases with the number of alternative first scans.

TABLE I

Values of E_{pc} Vs mercurous sulphate electrode of the green-blue couple on first and n^{th} scan for $LuPc_2$ thin film deposited on Pt as a fonction of several electrolytes.

	NaF	NaCl	NaI
1^{st}	-1.20	-1.02	-1.25
n^{th}	-0.91	-0.93	-0.87

Therefore, we have studied the mechanism of the ions incorporation. It is shown that in the reduction process there is no change of E_p with the electrolyte cation nature as expected but there is an unexpected dependence on the anion.

Meanwhile, in the oxidation reaction there is a normal shift of E_p with the electrolyte anion nature (Fig. 2).

REFERENCES

1. G.C.S. COLLINS and D.J. SCHRIFFIN. J. Electroanal. Chem. 139, 1982, 335.

2. J.S. KIRIN and P.N. MOSKALEV, Zhur. Fiz. Khim. 41, 1967, 497, Russ J. Phys. Chem. N°2, 1967.

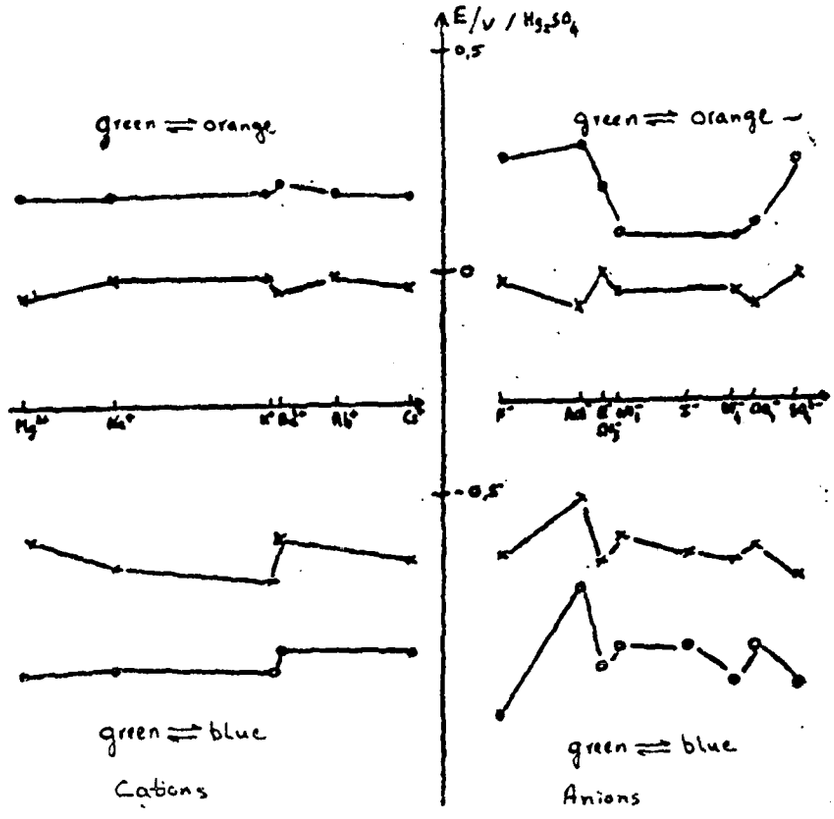

Fig 2. E_p dependence on the anion and cation ionic radii in the reduction and oxidation processes.

07080

"IN SITU" SPECTROSCOPIC STUDIES OF N,N'-DIBENZYL-VIOLOGEN RADICALS ADSORBED ON METALLIC (Pt,Au) OR SEMICONDUCTOR (TiO_2) SURFACES

B. BEDEN, P. CROUIGNEAU, O. ENEA and C. LAMY,
Laboratoire de Chimie I, Electrochimie et Interactions, U.A. au CNRS N°350,
Université de Poitiers, 40, avenue du Recteur Pineau, 86022 POITIERS, France.

The N,N'-dimethyl-4,4'-dipyridinium cation MV^{2+} (methylviologen) and its long chain or aromatic derivatives present a considerable interest as electron relays in various processes for hydrogen generation through the photochemical splitting of water[1]. No simple correlation can be established between the efficiency for hydrogen generation and their respective redox potentials because of a number of secondary reactions like catalytic hydrogenation or dimerization of radicals,...[2]. Besides, their adsorption on semiconductor (TiO_2 ,...) [3] or metallic (Pt, Au) [4] surfaces plays an important role in the trapping of the photoproduced electrons and the subsequent consumption of the negative charge at metallic surfaces.

Recently, we have investigated by cyclic voltammetry coupled with "in situ" UV-visible reflectance spectroscopy [5] and by electron spin resonance spectrometry [6] some viologen radicals adsorbed on Pt electrodes or on TiO_2 colloidal particles. In the present work we use these experimental methods to examine the interfacial behaviour of the N,N'-dibenzyl-4,4'-dipyridinium dication BV^{2+} (benzyl viologen), a compound which has been shown to display very interesting properties as electron carrier [2].

EXPERIMENTAL

Benzyl viologen chloride (synthetized by Dr. A. BRAUN, Ecole Polytechnique Fédérale de Lausanne, Switzerland), was dissolved in deionized-triply distilled water. Final concentrations ($\sim 4.10^{-5}$ M) used in the spectroelectrochemical experiment were prepared with a supporting electrolyte (0.1 M H_2SO_4) adjusted to a suitable pH value ($\sim$ 3.54). Voltammetric and spectroscopic measurements were simultaneously carried out in a three-electrode cell with quartz windows. Smooth platinum or gold discs (area $\sim$ 0.33 cm^2), carefully polished with 0.05 µm alumina, were used alternatively as working electrodes. A mercurous sulphate electrode (MSE) was used as the reference electrode and a platinum gauze as the counter-electrode.

Cyclic voltammetry was carried out with conventional equipment at a sweep rate of 100 $mV.s^{-1}$ or 300 $mV.s^{-1}$ between -1.7 and +0.25 V/MSE. The change in the relative reflectivity $\Delta R/R$ of the surface due to the presence of an absorbing layer, was recorded at a fixed wavelength λ as a function of the electrode potential E, using a Harrick model RSS-C Rapid Scan Spectrometer. These reflectograms were recorded and averaged several times using a Nicolet 1020 A signal averager in order to improve the signal-to-noise ratio.

After a series of experiments at different wavelengths all over the spectral range 350 to 800 nm, the reflectograms were plotted in a tridimensional diagram giving the absorbance $\Delta A = - \Delta R/R$ as a function of E and λ, $\Delta A = f(\lambda,E)$, as in fig. 1. The surface $[A,E,\lambda]$ could thereafter be cut at a constant potential E to redraw the absorption spectrum $\Delta A = f(\lambda)$ of the species adsorbed on the surface of the working électrode (Au or Pt).

The TiO_2 colloidal solution (average radius of particles $\sim$ 50 Å) was prepared by J. MOSER (in Prof. Grätzel's Laboratory, Ecole Polytechnique Fédérale de Lausanne, Switzerland) by hydrolysis and dialysis of purified $TiCl_4$. Photochemical reduction of the benzyl-viologen was achieved with a Cunow 150 W XBO Xenon Lamp, which irradiates the colloidal suspension previously deaerated and contained in a flattened quartz tube inside the resonant cavity of a Varian E_3 spectrometer. The ESR spectra recorded at a low microwave incident power (2 to 5 mW) are shown in Fig. 2.

RESULTS AND DISCUSSION

The three-dimensional diagrams [A,E,λ], (Fig. 1), contain by themselves all the informations needed for identifying the adsorbed species. At potentials close to the upper limit E_a , where the benzyl-viologen dication BV^{2+} predominates, there is practically no change in the absorbance throughout the spectral range used. Conversely, at potentials around the lower limit E_c , where the BV^+ blue radical is formed, the absorbance greatly varies with the wavelength, displaying a rather narrow peak around 400 nm and a wider peak around 540 nm. Comparatively to the steep rise of the relative absorbance intensity, when potentials approach E_c , the decrease is significantly slower, when the potential sweep is reversed. The adsorbed BV^+ radicals still persist a few seconds at potentials much more positive than the half-wave potential $E^\circ_{BV^{2+}/BV^+}$, a result observed also for other viologens (6).

If the absorbance spectra of the BV^+ species adsorbed respectively on Pt and Au are compared, a red-shift of $\sim$30 nm can be observed in the second case. This shift cannot be related directly to the interaction of the BV^+ radicals with the metal : the BV^+ radicals are more strongly adsorbed on Pt than on Au. The red-shift observed is more probably due to interactions between the adsorbed BV^+ radicals themselves, than to interactions with the support.

The absorption spectra of photoreduced BV^+ radicals adsorbed on colloidal TiO_2 particles are very similar to those obtained for the corresponding cations in the bulk when a 5.10^{-4} M BV^{2+} solution was electrochemically reduced in a quartz cell. They present significant differences when compared with spectra of radicals adsorbed on Pt or Au.

The ESR spectra ($2.004 < g < 2.005$) of the BV^+ radicals adsorbed on colloidal TiO_2 particles display a partially resolved hyperfine structure showing a relatively delocalized electron inside the free radical structure. The mutual interactions of the photogenerated radicals spread on TiO_2 particles, having a large surface area, seems to be low and, consequently, the hyperfine structure is not too much disturbed.

ACKNOWLEDGEMENT

The financial support by CNRS and AFME (PIRSEM grant n° 3024) is gratefully acknowledged.

REFERENCES

(1) K. KALYANSUNDARAM and M. GRÄTZEL, Photochem. and Photobiol., 40, 807 (1984)
(2) P. KELLER, A. MORADPOUR, E. AMOUYAL and B. ZIDLER, J. Molec. Catalysis., 12, 261 (1981).
(3) A.N. FURLONG and W.H.F. SASSE, Colloids Surfaces, 7, 29 (1983).
(4) O. ENEA, Electrochim. Acta, 30, 13 (1985).
(5) B. BEDEN, O. ENEA, F. HAIN and C. LAMY, J. Electroanal. Chem., 170, 357 (1984).
(6) P. CROUIGNEAU, O. ENEA and C. LAMY, I.S.E. Extended Abstracts, 35, 503 (1984).

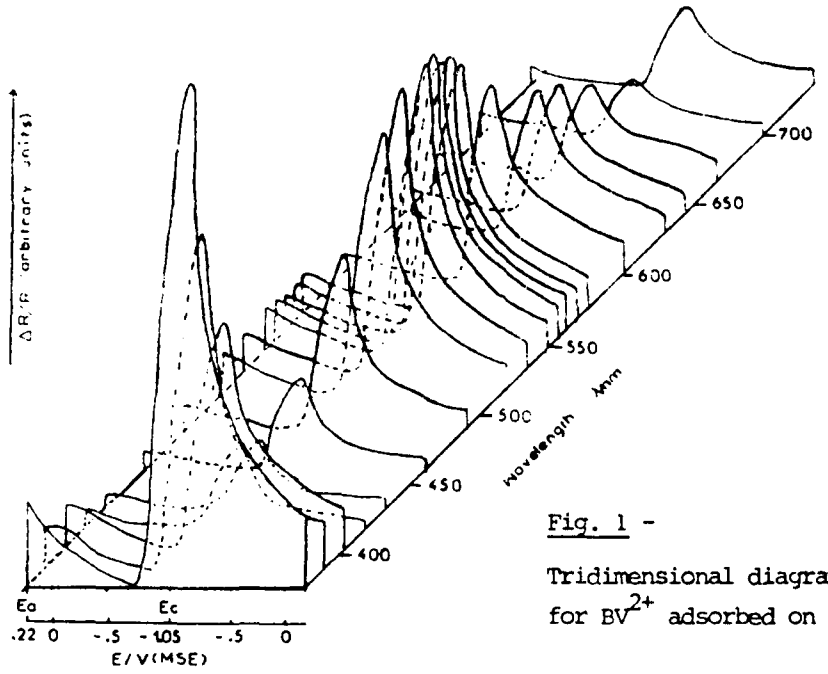

Fig. 1 -

Tridimensional diagram $[-\frac{\Delta R}{R}, E, \lambda]$ for BV^{2+} adsorbed on Pt

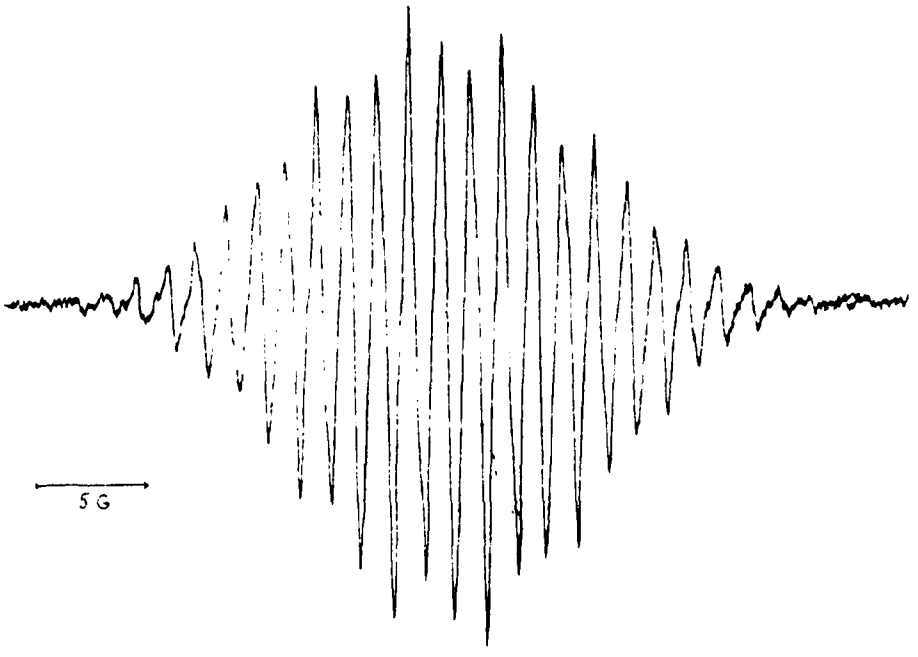

Fig. 2 - ESR spectrum of irradiated BV^{2+} adsorbed on TiO_2 particles

07090

THE EFFECT OF Pt AND RuO_2 DEPOSITS ON THE PHOTOREDUCTION OF METHYLVIOLOGEN ON Ti/TiO_2 ELECTRODES AT OPEN CIRCUIT

O. ENEA and M. GRÄTZEL*

Laboratoire de Chimie I, Electrochimie et Interactions, U.A. au C.N.R.S. n°350
Université de Poitiers, 40 avenue du Recteur Pineau, 86022 POITIERS, France

*Institut de Chimie Physique, Ecole Polytechnique Fédérale de Lausanne, 1015 - ECUBLENS, Suisse

Photoredox reactions occuring at the surface of semiconductor particles suspended in solution can be rationalized in terms of photoelectrochemical concepts. Recently [1], the mechanisms and the majority carrier flow at semiconductor/electrolyte interfaces having very different sizes were examined comparatively on the bases of informations available for dispersed systems and polarized electrodes. Nevertheless, it could be argued that modifications of interfacial properties by external electrical fields [2] makes polarized electrodes less appropriate as models for semiconductor particles than the same electrodes at open circuit. Some aspects of the photo(electro)chemical processes occuring at successively polarized and open circuit electrodes were recently examined [3] by following the kinetic of methylviologen, MV^{2+}, photoreduction at these interfaces.

The present work uses this experimental technique in order to obtain more informations concerning the effects of catalytic deposits (Pt, RuO_2) on the photoactivity of Ti/TiO_2 electrodes at open circuit, investigated as models for the particulate TiO_2 dispersed photocatalysts.

EXPERIMENTAL

TiO_2 (anatase) layers of 10-40 µm thick, deposited by the thermal decomposition of $TiCl_4$ on titanium sheets (7.5 x 7.5 x 1 mm) were finally annealed at 720 K under Ar. All Ti/TiO_2 electrodes were tested and only those having reasonably close onset potentials and photocurrent[illegible] subsequently used to study the photoreduction of methylviologen as a function of its concentration. Some of these Ti/TiO_2 electrodes were platinized under irradiation during various times between 8 and 80 minutes in a solution (pH = 2.43) containing $8.2\ 10^{-3}$ M K_2PtCl_6. Various amounts of RuO_2 were successively deposited on others Ti/TiO_2 electrodes by the thermal decomposition at ~360 K of measured volumes of dilute solutions containing (0.01 - 0.1 g dm^{-3}) RuO_2.

In all irradiation experiments we used a 450 W Xe-Lamp (Oriel) with a 8 cm water filter and a 350 nm cutoff filter to prevent the direct photolysis of methylviologen [4]. Currents and potentials of polarized electrodes were measured versus a saturated calomel electrode (SCE) with a Wenking PGS 73 potentiostat. Production rates of blue methylviologen radicals were determined with a He-Ne laser from their optical absorbance at 632.8 nm (ϵ = 8060 $M^{-1}cm^{-1}$). Alternatively, $\Delta i/\Delta t$ slopes were determined from photocurrents measured as function of time for the reoxidation of $MV^{+\cdot}$ at a gold collector electrode held at 0.2 V/SCE.

RESULTS AND DISCUSSION

The main experimental results are briefly summarized in the following :

1) The shape of $\Delta i/\Delta t$ vs. $C_{MV^{2+}}$ dependences (see fig. 1) measured as slopes of photocurrent vs. time curves for Ti/TiO_2 electrodes at open circuit is similar in shape to the $v_{MV^{+\cdot}}$ vs. $C_{MV^{2+}}$ [illegible] curves [illegible], where

the photoproduction rate, $v_{MV^{+\cdot}}$, of methylviologen radicals was alternatively determined [3] from optical absorbance of $MV^{+\cdot}$ or from i-E curves measured for polarized Ti/TiO_2 electrodes. The increase of both $\Delta i/\Delta t$ or $v_{MV^{+\cdot}}$ quantities at low concentrations of methylviologen (where $e^-_{CB} >> C_{MV^{2+}}$) levels off when methylviologen concentration is raised until $e^-_{CB} << C_{MV^{2+}}$ and their respective limiting values are reached.

All $\Delta i/\Delta t$ values measured with a collector electrode are proportional to the quantities of photoproduced $MV^{+\cdot}$ detected from optical absorbance or calculated from i-E curves [3] of polarized electrodes. The study of the kinetics of MV^{2+} photoreduction in particulate suspensions of TiO_2 (too opaques to allow optical measurements) is therefore possible by means of an inert collector electrode which can be subsequently used in the same experimental conditions to describe the behaviour of Ti/TiO_2 electrodes at open circuit chosen as models for TiO_2 particles.

2) A Ti/TiO_2 electrode having anatase on both illuminated and dark sides produces a higher quantity of $MV^{+\cdot}$ radicals than the same electrode after the insulation of the dark side (see fig. 1). The majority of photoproduced electrons are therefore trapped on the illuminated side when a rather efficient electron trapping agent like methylviologen is used.

3) Small platinum deposits formed during a short time (<8 minutes) photodeposition on the illuminated side of Ti/TiO_2 electrodes do not change significantly $\Delta i/\Delta t$ vs. $C_{MV^{2+}}$ (or V_{MV^+} vs. $C_{MV^{2+}}$) curves, while experiments with polarized electrodes have shown a shift (~60 mV) towards more positive potentials for the reduction of MV^{2+}, a shift considerably smaller with respect to those found for O_2 (~250 mV) and water (570 mV) reductions. The quantity of photoproduced $MV^{+\cdot}$ radicals decreases progressively when larger quantities of Pt are deposited, presumably because of the obscuring of anodic zones on TiO_2 surfaces.

4) The dependence of $\Delta i/\Delta t$ values with the quantity of RuO_2 reaches a maxima at 5.10^{-5} g cm^{-2} RuO_2 and decreases progressively when larger RuO_2 quantities are deposited on anatase surface (see fig. 2). The photoreduction of MV^{2+} is significantly lower for a $Ti/TiO_2/RuO_2$ electrode containing 2.10^{-5} g cm^{-2} RuO_2, especially at higher concentrations of methylviologen. The efficiency of RuO_2 deposits, well known to enhance water oxidation [5], can be less effective when relatively high OH^- concentrations are used (in our experiments pH = 13) than in acidic or neutral solutions [6]. In addition, RuO_2 dispersion on both cathodic and anodic zones of TiO_2 might diminish the activity of cathodic zones for the photoreduction of methylviologen. Combined electron microscopy and X-ray analyses have effectively shown the formation of an almost complete RuO_2 overlayer on anatase surface : this explains the decrease of methylviologen photoreduction when higher quantities of RuO_2 are deposited.

Clearly, only small, appropriate and well arranged Pt and/or RuO_2 deposits appear able to bring valuable catalytic properties without a significant decrease of the own photoactivity of the semiconductor.

REFERENCES

1) G. HODES and M. GRÄTZEL Nouveau J. Chim. 8, 509 (1984).
2) P. CLECHET, C. MARTELET, R. OLIER, J.P. THOMAS and M. FALLAVIER J. Electrochem. Soc. 130, 1795 (1983).
3) M. NEUMANN-SPALLART and O. ENEA J. Electrochem. Soc. 131, 2767 (1984).
4) T.W. EBBESEN, G. LEVEY and L.K. PATTERSON Nature 298, 545 (1982).
5) E. BORGARELLO, J. KIWI, E. PELIZZETTI, M. VISCA and M. GRÄTZEL J. Am. Chem. Soc. 103, 6324 (1981).
6) O. ENEA and A.J. BARD Nouveau J. Chim. in press.

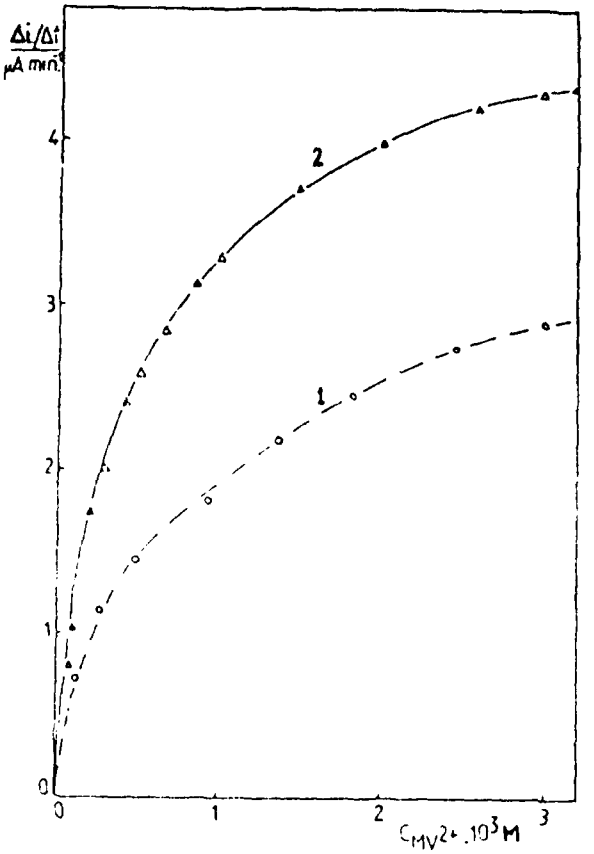

Fig. 1 $\Delta i/\Delta t$ vs. C_{MV}^{2+}

-anatase on both sides (full curve)

- anatase on the illuminated side only (dotted curve)

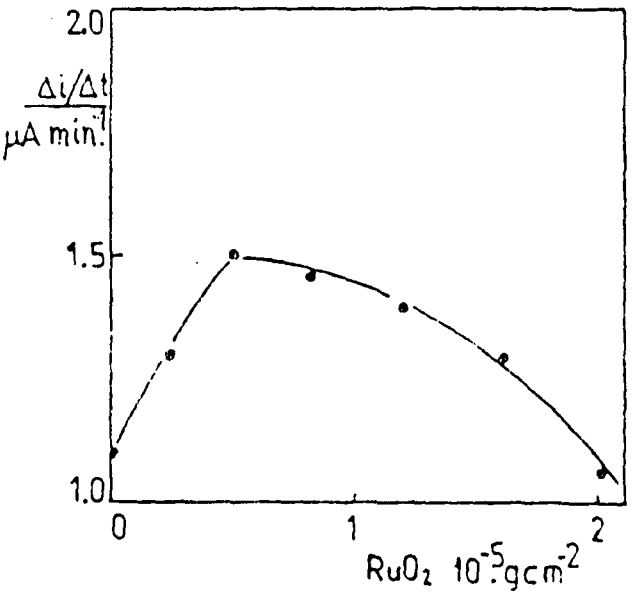

Fig. 2 $\Delta i/\Delta t$ vs. RuO_2

illuminated side

2.5×10^{-4} M MV^{2+}

07100

pH EFFECTS ON THE PHOTOOXIDATION OF SOME SUGARS BY THE IRRADIATED SUSPENSIONS OF TiO_2

O. ENEA and A.J. BARD*
Laboratoire de Chimie I, Electrochimie et Interactions, U.A. au CNRS N° 350, Université de Poitiers, 40 avenue du Recteur Pineau, 86022 POITIERS, France.

*Department of Chemistry, The University of Texas at Austin, Austin, Texas 78712

The conversion of chemical energy of biomass constituents like sugars, polyalcohols and monoalcohols into electricity is actually an important goal for electrochemistry and photocatalysis. Recently, the photodecomposition and the photofermentation of some sugars were investigated [1,2,3] in relation with the photocatalytic activity of various platinized semiconductors. Also, the electrooxidation of D-glucose on Pt electrodes was studied by voltammetric methods [4]. Among these investigations none has described the influence of pH on the photooxidation of sugars.

Our preliminary work on various polyalcohols[5,6,7] has pointed out a significant dependence of photocurrents measured for TiO_2/polyalconol/methylviologen suspensions on the initial pH. In this work, electrochemical and gas chromatography measurements are jointly used to examine the influence of pH on the photooxidation of D-saccharose comparatively to that of its components, D-glucose and D-fructose.

EXPERIMENTAL

The amounts of D-glucose adsorbed on TiO_2 particles were determined by enzymatic analysis. Samples of vigorously stirred (one hour) suspensions containing 0.1 % wt. of D-glucose were centrifuged (30 minutes at 5000 rpm), the supernatant was filtered (0.5 µm size of pores) and subsequently analyzed by using the glucose oxidase procedure.

In some of photoelectrochemical experiments, the suspension of vigorously stirred TiO_2 powder (P 25 Degussa, 2.5 g dm^{-3}) contained 0.1 % wt. of sugar, 0.0325 M K_2SO_4 and 0.001 M methylviologen, the initial pH being adjusted at the desired value. A three-electrode cell with two compartments and a flat window, thermostated at 25°C was used. The anodic photocurrent produced under irradiation with a 450 W lamp at $350 < \lambda < 420$ nm of the previously degassed suspension was measured on a platinum flag (25 x 25 x 0.25 mm) held at 0.2 V/SCE.

In other experiments, TiO_2 suspensions containing 0.5 % wt. of sugar were irradiated with a 1.6 kW Xe lamp and photocurrents were collected at a gold electrode (10.6 cm^2).

The amounts of photogenerated H_2 during the irradiation of different samples (40 cm^3) of Pt/TiO_2 or $TiO_2 + {}^2Pt/SiO_2$ suspensions contained in a 55 cm^3 Pyrex flask were detected by gas chromatography.

RESULTS AND DISCUSSION

The rates of the change of photocurrents with time ($\Delta i/\Delta t$) shown in Fig.1 were determined as initial slopes of the photocurrent vs. time curves recorded for TiO_2/sugar/methylviologen systems at various initial pH values. $\Delta i/\Delta t$ vs. pH curves intercept the pH axes in the acidic range. Such behaviour, already observed for polyalcohols [6,7], can be explained by the preferential adsorption

of sugars or polyalcohols on the surface of TiO_2 particles, and seems to be governed by the chain length and by the number of >CHOH units.

The quantity of adsorbed sugar was found [7] to be 0.6 mM dm^{-3} per gram of TiO_2 particles suspended in dilute (0.1 % wt.) aqueous solutions of D-glucose. If the average radius ($\sim$ 140 Å) and BET area ($\sim$55 m^2g^{-1}) of TiO_2 particles (Degussa P 25) are considered, it results, that only $\sim$15 $Å^2$ of anatase surface is available for each adsorbed molecule of sugar. This area is much smaller than the total surface area of D-glucose (201 $Å^2$) calculated from Van der Waals increments of the constitutive atoms and groups [8]. Presumably, only one hydroxyl group per molecule of D-glucose is dissociatively adsorbed (in the dark) :

$$>CHOH \rightarrow >CHO^- + H^+ \qquad (1)$$

on anatase basic sites. The total number of produced protons ($\sim 6.10^{19}$), deduced from the shift of pH values during the adsorption process is effectively of the same order of magnitude as the total number of adsorbed molecules of D-glucose ($\sim$ 8.4 10^{19}).

According to intercepts on pH axes (Fig.1) the adsorption of D-saccharose on TiO_2 surface appears to be similar to that of D-glucose or of D-fructose. On the contrary, the hole scavenging efficiency of D-saccharose is significantly lower than that of its constitutive sugars, presumably because of a lower ratio of OH groups per C atoms. If this is generally true, we should expect a lower photoactivity of TiO_2 particles in systems containing polysaccharides than in systems containing equivalent amounts of simpler sugars.

The adsorption of polyalcohols or sugars having more than 5 or 6 >CHOH units on TiO_2 particles produces a high concentration of OH groups close to the surface of the semiconductor. The photoproduced holes interact with the alkoxide ions :

$$>CHO^- + h^+ \rightarrow >C=O + H^{\cdot}_{ads} \text{ (or } H^+ + e^-) \qquad (2)$$

and pH values become progressively more acidic during the continuous illumination. The maximum values of photocurrent, i_{max}, reached within 20 to 30 minutes, and $\Delta i/\Delta t$ values are both governed by the initial quantity of OH^- ions in the bulk. The hole scavenging action of sugars is enhanced by the simultaneous consumption of holes by OH^- ions, as previously observed [5,6,7] for different polyalcohols. Protons produced during the photooxidation of sugars decreases the initial quantity of OH^- ions : consequently in the long term experiments i_{max} decreases progressively, unless other quantities of OH^- ions are periodically introduced.

Alternatively, H^+ (and $H^{\cdot}_{ads}$) species can be removed by using an appropriate catalyst for H_2 production to maintain a constant pH value and thus a high photoactivity. Platinum deposits on TiO_2 particles significantly decreased the $\Delta i/\Delta t$ and i_{max} values [9]. The amount of H_2 evolved found by GC was strongly dependent upon the initial concentration of OH^- ions and increased at alkaline pH values (Fig. 2). Photocurrent values decreased also when platinum loaded silica particles were mixed with a suspension of TiO_2 particles and the initial value of pH was almost constant during the long term illuminations. In this case, the quantity of H_2 produced and the rate of its production with time of illumination show maximum values for pH = 2, and strongly decrease in neutral or alkaline mediums. Apparently, the inter-particle transfer involved in the mixed TiO_2 + Pt/SiO_2 suspensions and the catalysed MV^+-proton reaction is enhanced in acid solutions. The formation of larger conglomerates between TiO_2 and Pt/SiO_2 cannot be excluded a priori but is probably of minor importance. Since electron transfer from the TiO_2 particle cannot take place through the silica particle to reach Pt deposits, the mobility of these particles seems to be essential to accomplish successively both electron trapping and water reduction on catalyst surface.

CONCLUSIONS

The ratio of OH groups per C atoms and the length of the molecular chain appear to determine the efficiency of the hole consumption by sugars in irradiated suspensions of TiO_2 . The splitting of natural biomass components (polyoses) into simpler sugars or polyalcohols having only 4 to 6 C atoms and a higher OH content should precede their photochemical conversion into electricity or H_2 by semiconductor particles.

Significant electron transfer between the negatively charged TiO_2 particles after irradiation and platinum deposits on SiO_2 particles occurs, if the proton concentration is sufficiently high to favor the catalytic consumption of these electrons in water reduction. The presence of Pt deposits on the TiO_2 surface greatly improves their electron trapping action and promotes H_2 production at alkaline pH values, where the hole scavenging action of D-glucose is favored.

ACKNOWLEDGEMENTS

The support of this cooperative research by CNRS (AD 15/4/959251) and NSF (CHE 8304666) is gratefully acknowledged.

REFERENCES

1. T. SAKATA and T. KAWAY Nouveau J. Chim. 5, 279 (1981).
2. T. SAKATA, T. KAWAY and K. HASHIMOTO Int. Symp. Univ. Tokyo, Japan, 1983.
3. T. KAWAY Int. Symp. Univ. Tokyo, Japan, 1983.
4. M.F.L. de MELE, H.A. VIDELA and A.J. ARVIA J. Electrochem. Soc. 129, 2207 (1982).
5. O. ENEA Nouveau J. Chim. 9, April (1985).
6. O. ENEA 166th Meeting of Electrochemical Society, New Orleans, USA, 1984.
7. O. ENEA J. Electroanal. Chem., submitted.
8. F. SHAHIDI Ph.D.Thesis McGill University, Montreal, 1976.
9. O. ENEA and A.J. BARD Nouveau J. Chim. in press.

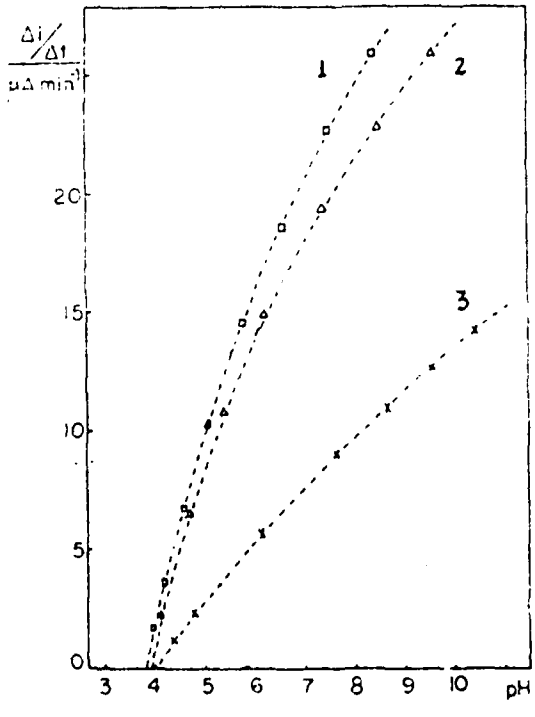

Fig.1 Δi/Δt vs. pH 1) D-fructose, 2) D-glucose, 3) D-saccharose

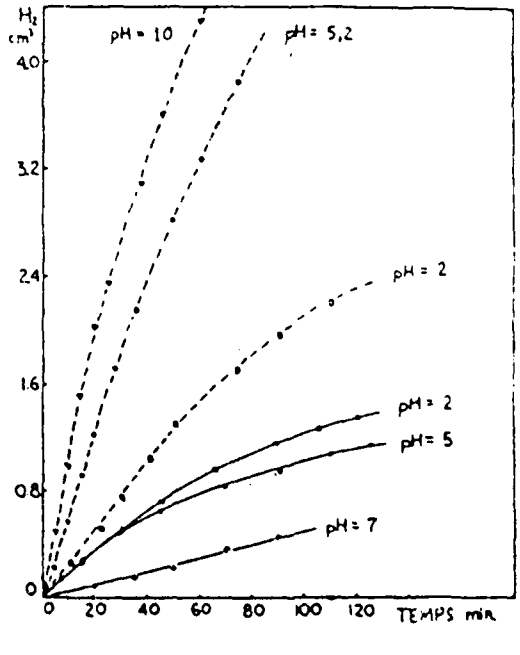

Fig.2 Photoproduced H_2 at various pH Pt/TiO_2 (dotted) ; TiO_2 + Pt/SiO_2 (full)

07110

ELECTROCHEMICAL BEHAVIOUR OF POLYPYRROLE FILMS IN ClO_4Li/PC AS SECONDARY BATTERY ELECTRODES.

F. TRINIDAD; J. ALONSO-LOPEZ and M. NEBOT.
Departamento Investigación TUDOR SA.
Azuqueca Henares, Guadalajara (Spain)

Polypyrrole films (PP) are electrochemically[1] deposited on platinum in an electrolyte of pyrrole 0,1 M and ClO_4Li 0,1 M in propylene carbonate (PC). The film thickness (0,5 - 50 μ) is controlled by applying a constant current density (1 mA/cm^2) for a certain period of time (0,24 C/cm^2 to obtain a $\sim$1μ film). The solution is continuosly degassed with Argon.

Cyclic Voltametries.

After the electrochemical synthesis the polypyrrole films are cycled in ClO_4Li 0,1 M - PC electrolyte. The scan rate (as a function of the film thickness) and the potential interval (- 1,0 and + 0,8 V. vs Ag/ClAg) have been selected to obtain a complete reduction of the polymer within the stability range of the electrolyte.

Figure 1 shows the voltamogram obtained for a polypyrrole film of $\sim$1μ thickness. The reduction peak in the first cycle (-0,8 V) corresponded to the loss of positive charge of the polymer. The quantity of charge obtained was 14 % of that needed to deposit the film. This is an agreement with the previously reported[2] level of doping (33 %) and the elemental analysis data (C : 46,61 %; H : 2,71 %; N : 12,54 %; Cl : 10,11 %) which gives the formula $C_4\ H_{2,80}\ N_{0,92}\ (ClO_4)_{0,29}$.

After the first scan reproducible voltamograms are obtained with an oxidation peak (doping) at -0,1 V and a reduction peak (undoping) at -0,3 V. At positive potentials (between 0 and 0,8 V) a capacitative zone of charge with quasi-constant current density is formed. The equivalent capacitance ($\sim$ 0,02 F/cm^2) is three orders of magnitude greater than that of a metal in this electrolyte and is proportional to the film thickness. This is probably due to the highly porous structure of polypyrrole films[3].

The reduction peak at -0,8 V obtained in the first cycle is displaced to -0,3 V in the following scans. A possible explanation could be the change in the dopant anion that has been observed by other authors[4]. Nevertheless the elemental analysis of cycled films is essentially the same as fresh film (C : 48,54; H : 3,35; N : 12,82; Cl : 10,08 %) indicating that the dopant anion is ClO_4^- in both cases, the interaction with the polymer being different after cycling.

The oxidation and reduction charge in each cycle is the same and does not depend on the scan rate. The peak height is proportional to the scan rate as is expected for a reversible surface process.

Increasing the film thickness the capacity of the electrode is increased but slower scan rates are required to make the reduction of the polypyrrole film possible.

Impedance Analysis.

The impedance of the system Pt/PP ($\sim 1\mu$) / ClO_4Li-PC has been measured in the frequency range of 55 KH_z to 1 mH_z at different potentials. At low frequencies (< 1 H_z) and positive potentials (PP doped) the behaviour is similar to a capacitor with very high capacitance (0,02 F/cm^2). This result agrees with that obtained in cyclic voltametries.

At negative potentials (-1,0 V) in which the PP film is not conducting the capacitance decreased several orders of magnitude, being similar to a platinum electrode partially covered by a porous film (Figure 2).

Battery Experiments.

$LiAl/ClO_4Li$, PC/PP batteries have been constructed with aluminium as negative electrode and platinum as positive electrode in the same electrolyte to deposit the PP films and Li. Figure 3 shows the first charge ("formation") and discharge of this battery.

The capacity in the first discharge is 16 % of that employed in the first charge. In the following cycles, the culombic efficiency is better than 90 % but there is a progressive loss of charge in the system and the shelf-life is poor.

Studies are continuing to improve the capacity, cycle life and shelf-life of polypyrrole films and as a consequence of this to make the utilization of PP as a secondary battery electrode possible.

References:

1. A.F. Diaz, K.K. Kanazawa and G.P. Gardini.
J. Chem. Soc. Chem. Commun. 635, (1979).

2. E.M. Genies and J.M. Pernault.
Synthetic Metals. 10, 117, (1984).

3. R.A. Bull, F.F. Fan and A.J. Bard.
J. Electrochem. Society. 129, 1009, (1982).

4. W.R. Salaneck and others.
Synthetic Metals. 5, 125, (1983).

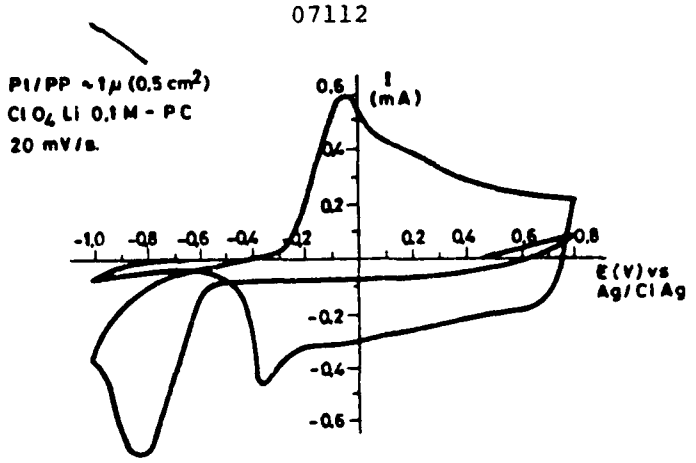

Figure 1: CYCLIC VOLTAMMETRY OF PP IN ClO_4 Li - PC

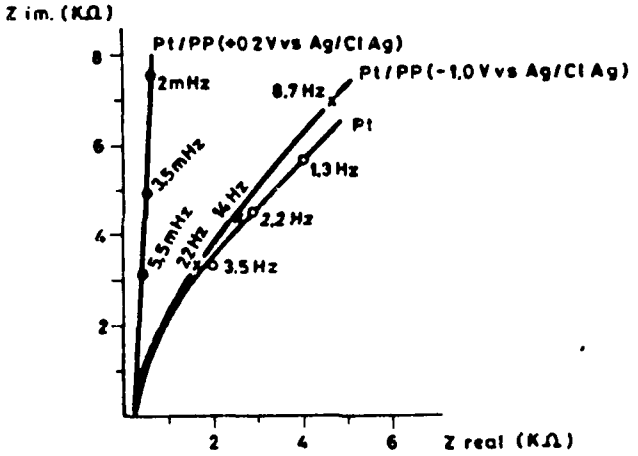

Figure 2: AC IMPEDANCE ANALYSIS OF PP FILMS

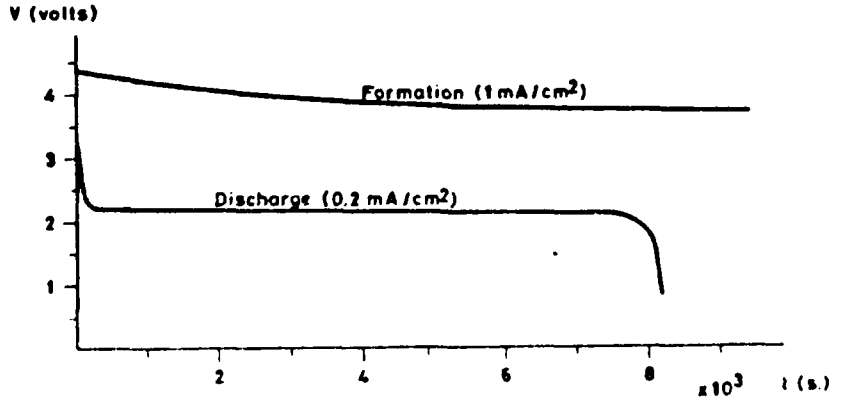

Figure 3: DISCHARGE CURVE OF Li Al / ClO_4 Li - PC / PP BATTERY

07120

REDOX FLOW BATTERY USING Fe^{3+}/Fe^{2+} AND Cr^{3+}/Cr^{2+} COUPLES

P. GARCES, M.A. CLIMENT+, M. LOPEZ SEGURA and A. ALDAZ
Departamento de Química-Física, Universidad de Alicante, Spain.
+ E.U. Ing. Técnica de Obras Públicas, Universidad Politécnica de Valencia, Spain.

The storage of electrical energy in electrochemical redox systems is particularly useful when used with intermittent energy sources (solar, wind, etc.) and for load leveling in electrical energy networks. This redox system is based on the employment of two fully soluble and highly reversible couples such as Fe^{3+}/Fe^{2+} and Cr^{3+}/Cr^{2+}, separated by a selective membrane.

A prototype of a Fe/Cr flow redox storage system (monopolar type), using a filter-press cell has been built on the basis of research work carried out in different centers[1,2,3]. The electrodic materials were bulk non-catalyzed graphite for both couples. Fig. 1 shows the scheme of the cell with the data adquisition system.

The more important reasons for the decrease in efficiency are the low reversibility of the Cr^{3+}/Cr^{2+} couple, and H_2 evolution that starts when 75% of charge is reached. The hysteresis in the open-circuit voltages for charge and discharge processes is attributed to this lack of reversibility, fig. 2.

These reasons mean that the charge and discharge process must be performed in 25-75% state of charge range. Fig. 3 shows that for states of charge higher than 75% or lower than 25% the overpotentials due to the depletion of the active species for both couples begin to contribute remarkably to the cell voltage.

The temperature has an important effect on the system performance. So the voltages for the charge process decrease and the cell voltages for the discharge process increase when the temperature is raised. This happens specially in the higher states of charge, fig. 4.

Table I shows the results obtained in the three centers developping Fe/Cr redox systems (until we know).

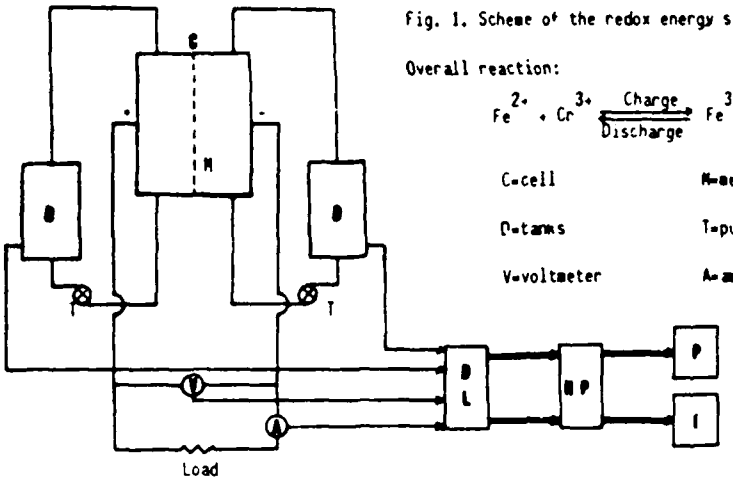

Fig. 1. Scheme of the redox energy storage system.

Overall reaction:

$$Fe^{2+} + Cr^{3+} \underset{\text{Discharge}}{\overset{\text{Charge}}{\rightleftharpoons}} Fe^{3+} + Cr^{2+}$$

C=cell M=membrane

D=tanks T=pumps

V=voltmeter A=ammeter

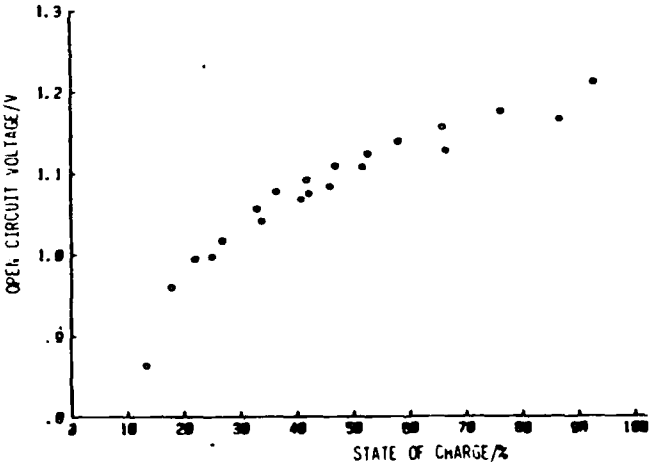

Fig. 2. o= Charge
●= Discharge

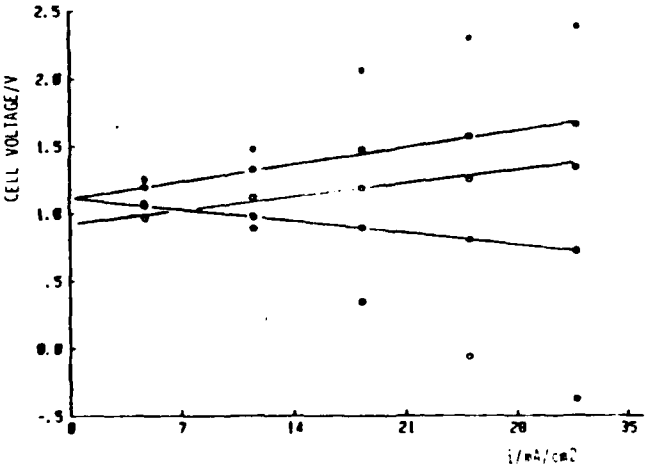

Fig. 3. Polarization curves.
o= 25% state of charge
●= 50% "
■ = 75% "

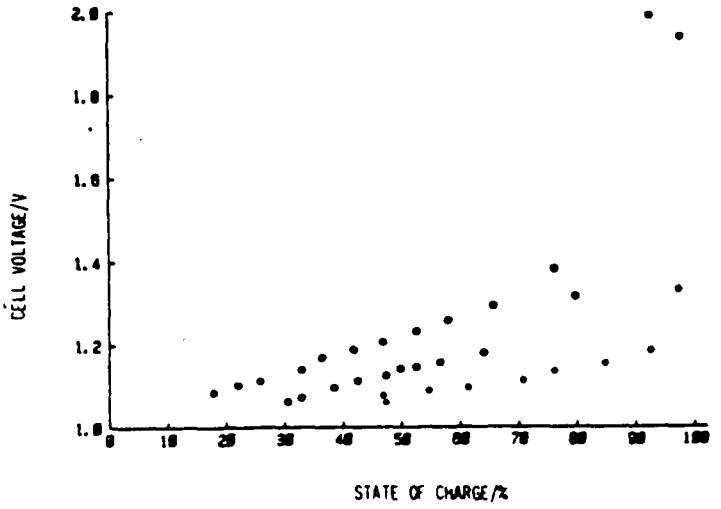

Fig. 4. Effect of temperature on the charge process.
● = 29ºC
○ = 40ºC
▲ = 55ºC

TABLE I

COMPARISON OF THE RESULTS OBTAINED WITH THE REDOX ENERGY STORAGE SYSTEM Fe/Cr BY DIFERENTS CENTERS

CENTER	ELECTRODE: tipe/area cm2	CURRENT DENSITY mA/cm2	η_C (%)	η_V (%)	η_E (%)	ENERGY POWER
NASA	carbon felt 310	64.5	99	73	72	10Kwh-1Kw
Electrotech loboratory JAPAN	graphite felt 432	30	84.8	81.6	69.2	8Kwh-1Kw
Dep. physical chemistry. Univ. Alicante. SPAIN	graphite 400	9	81.2	81.6	66.3	80wh-10w*

η_C=CURRENT EFFICIENCY; η_V=VOLTAGE EFFICIENCY; η_E=ENERGY EFFICIENCY

* only two electrodes. No shunt losses

REFRENCES

1 L.H. THALLER, DOR/NASA/1002-79/4, NASA TM-79186.
2 K. NOZAKI and T. OZAWA, Progress in Batteries and Solar Cells, vol. 5 (1984).
3 P. GARCES, M.A. CLIMENT and A. ALDAZ, An. Quim., Ser. A (in press).

07130

ELECTROCHEMICAL AND PHOTOELECTROCHEMICAL BEHAVIOR OF LANGMUIR-BLODGETT MONOMOLECULAR ASSEMBLIES ON Au AND SnO_2 ELECTRODES

M. FUJIHIRA and K. NISHIYAMA
Department of Chemical Engineering, Tokyo Institute of Technology
Ohokayama, Meguro-ku, Tokyo 152, Japan

Well organized molecular assemblies in lipid membranes play an important role in charge separation in photosynthesis in plants. For designing artificial photosynthetic molecular systems for solar energy conversion, it is of great interest to mimic elaborate arrangement in space of electron donors and acceptors in the charge separation unit of biological systems.

In the present paper, we will describe a novel molecular photodiode which is fabricated by a molecularly ordered film on a gold optically transparent electrode (Au OTE) or an SnO_2 OTE by the Langmuir-Blodgett (L.B.) method. The L.B. film is consists of viologen, pyrene, and ferrocene surfactant derivatives as an electron acceptor (A), a sensitizer (S), and an electron donor (D) component of the photodiode, respectively. Photoelectrochemical properties of the photodiode were investigated by using an electrochemical cell in which a modified Au OTE (or SnO_2 OTE), a gold plate , and a saturated calomel electrode (SCE) were used as a working, a counter, and a reference electrode, respectively. When A, S, and D surfactant layers were deposited in this order on the electrode surface, anodic photocurrents were observed as we would expect. On the other hand, cathodic photocurrents were observed on the electrodes where the surfactants monolayers were deposited in the reversed order. The effects of pH, electrode potentials, and number of layers on the photoelectrochemical responses will be presented together with UV absorption and emission characteristics of the L.B. films.

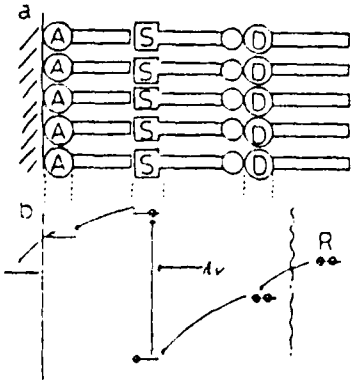

A
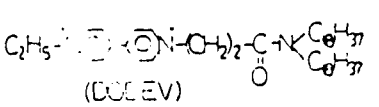
(DOLEV)

S
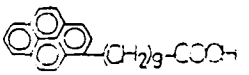
(PyC9COOH)

D
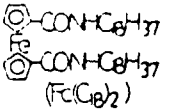
(Fc(C18)2)

07140

DYE SENSITIZATION OF RHODAMINE B AND $Ru(bpy)_3^{2+}$ SURFACTANT DERIVATIVES ON Au AND SnO_2 OTE

M. FUJIHIRA, K. AOKI, S. INOUE,
H. TAKEMURA and S. AOYAGUI
Department of Chemical Engineering, Tokyo Institute of Technology, Ohokayama, Meguro, Tokyo 152 (Japan)

Recently the dye sensitization of semiconductors has become of great interest in the fields of solar energy conversion and photographic science. The research on dye sensitization has a relatively long history, but there remain many fundamental problems still unsolved. These are, for example, the mechanisms and kinetics in terms of the elementary processes and the relation between the quantum efficiency and the basic characters of dyes and semiconductors in terms of geometry in atomic or molecular scale and of their electronic structures. Very recently, however, some of them have been going to be clarified by remarkable development in measuring and in sample preparation techniques such as fast kinetic spectroscopy and molecular architecture, respectively. Presently, as the former practice, laser flush photolyses in nano- and pico-second time scales are readily available, while, for the latter, chemical modification and the Langmuir-Blodgett (L.B.) method are widely used.

In the present work, several surfactant derivatives of rhodamine B and Ru(II) complexes with two long alkyl chains were synthesized. The surfaces of optically transparent SnO_2 and vapor-deposited gold film electrodes were modified with the L.B. films of these surfactants. Photoelectrochemical characteristics of the monolayer-modified electrodes thus prepared (photocurrent(i_p) spectra, i_p-E curves, pH dependence of i_p, etc.) together with the physicochemical properties of L.B. films on the electrodes and on glass plates (UV absorption and emission characteristics) will be discussed in terms of:

i) the surface concentrations of the sensitizer (i.e. the dye) in a mixture of the dye surfactant and arachidate (or other aliphatic acid salts),

ii) the distance of the chromophore(i.e. the dye moiety of the sensitizer surfactant) from the electrode surface,

iii) the orientation of the surfactant in the film, i.e. the direction of the sensitizer head group toward or apart from the electrode surface,

iv) the numoer of the dye surfactant layers or the number of the arachidate layers as a spacer intervening between the dye surfactant and the electrode surface.

THE OXIDATION OF HCOOH AT A Pt ANODE PARTIALLY COVERED BY COPPER

Inês T.E. FONSECA and Ana C.S.S. MARIN
CECUL, Rua da Escola Politécnica, 58, 1294 Lisboa Codex (Portugal)

It is widely accepted that the oxidation of formic acid occurs by the mechanism first proposed by Capon and Parsons[1], i.e.

$$HCOOH \xrightarrow{Pt} Pt\text{-}H + Pt\text{-}COOH \qquad (1)$$

$$Pt\text{-}H - e \xrightarrow{fast} Pt\text{-}H^+ \qquad (2)$$

$$Pt\text{-}COOH - e \xrightarrow{fast} Pt + CO_2 + H^+ \qquad (3)$$

where reaction (1) is the rate controlling step. But, the rate of the reaction can rapidly be reduced due to the formation of surface poisons, by side reactions such as,

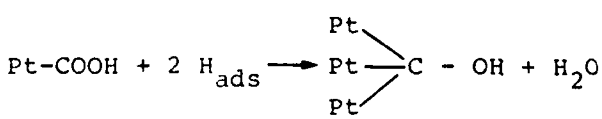

(4)

It has been demonstrated by ourselves[2] and other workers[3,4,5] that the role played by adatoms, i.e., Pb, Bi, Tl and Cd, on the oxidation of HCOOH is due to special structural units created on the Pt surface by such adatoms. The most active surfaces have shown to be the ones having a large number of Pt sites where there are two adjacent Pt atoms (for reaction (1) to occur), but few sites with three adjacent Pt atoms where poisson can form.

Quite recently Scortichini et al.[6] have observed that Cu adatoms form preferentially at certain Pt crystal planes. On the otherhand, Clavilier et col.[7] have shown that the rate of the oxidation of HCOOH is quite different on the various single crystal faces of Pt. The most active plane have shown to be the Pt(100).

In our previous studies with Cu adatoms (10^{-2}M < Cu^{2+} < 10^{-3}M), instead of a catalytic effect a small inhibition was observed for the oxidation of HCOOH in the presence of Cu^{2+} [8]. However, by the time, we were not convinced that the best catalytic surface has been achieved. Thus, we have decided to carry on such studies, using different limits of potential, different time-scales, and different Cu^{2+} concentrations. We have avoid conditions for multilayer formation[8].

Figure 1 shows the results obtained for the oxidation of HCOOH in 1M H_2SO_4 + x M $CuSO_4$ at v = 0.2 V s^{-1}.

TABLE 1. Peak current for the oxidation of 0.1M HCOOH at 0.55 as a function of holding time at 0.25V, in the presence and absence of Cu^{2+}. v = 0.1V s^{-1}.

E_{Ac} = 0.25V		i_p^I / μA cm^{-2}	$I_p^{I'}$ / μA cm^{-2}	$\frac{i_p^I}{i_p^{I'}}$
t/s	θ_{Cu}^{Pt}	0.1M HCOOH + $+1 \times 10^{-5}$ Cu^{2+}	0.1M HCOOH	
0	0.03	659.1	303.9	2.2
10	0.07	181.8	110.5	1.6
20	0.09	136.4	82.9	1.6
30	0.11	119.3	69.1	1.7
60	0.14	102.3	62.2	1.6
120	0.20	82.9	= 0	---

The reason why Cu ad-atoms do not catalyse significantly the oxidation of HCOOH looks most likely to be related to its deposition process. As it has been referred by Bruckenstein[5], at low coverages Cu ad-atoms do not deposit on Pt (100), the plane responsible for most of the oxidation of HCOOH[7].

REFERENCES

1. A. Capon and R. Parsons, J. Electroanal. Chem., 45 (1973), 205.
2. I. Fonseca, J. Lin-Cai and D. Pletcher, J. Electrochem. Soc., 130 (1983), 2187.
3. D. Pletcher and V. Solis, J. Electroanal. Chem., 131 (1982), 309.
4. R.R. Adzic, D.N. Simic, D.M. Drazic and A.R. Despic, J. Electroanal. Chem., 61 (1975), 117; 65 (1975), 587; 80 (1977), 81.
5. M. Shabrang, H. Mizota and S. Bruckenstein, J. Electrochem. Soc., 131 (1984), 306.
6. C.R. Scortichini and C.N. Reilly, J. Electroanal. Chem., 135 (1982), 233.
7. J. Clavilier, R. Parsons, R. Durand and C. Lamy, J. Electroanal. Chem., 139 (1982), 233.
8. I. Fonseca and D. Pletcher, in Extended Abstracts of ISE 35th meeting, Berkeley 1984, pg. 415.

ACKNOWLEDGEMENTS

We are gratefully to Dr. D. Pletcher for useful discussions and to INIC for financial support.

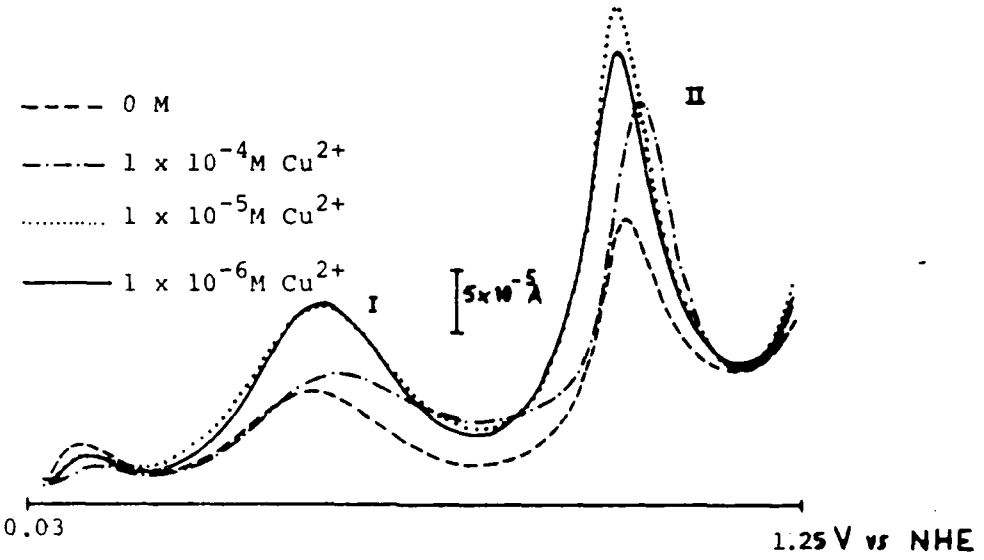

Fig. 1. First anodic cycle for the systems: 1M H_2SO_4 + 0.1M HCOOH + + x M $CuSO_4$/Pt, where x = 0, 10^{-4}, 10^{-5} and 10^{-6}M. Real areas of the Pt electrode 0.310 cm^2.

Results have shown for the first time a catalytic effect on the oxidation of HCOOH, in the presence of small amounts of Cu^{2+} (10^{-4} - 10^{-6}M). An enhancement in the peak current and in the oxidation charge is observed either for peak I (E_p^I = 0.55V) and for peak II ($E_p^{II} \simeq$ 1.0V). The enhancement ratio is of the order of two.

Degrees of coverage of Pt by Cu ad-atoms (θ_{Cu}^{Pt}) were calculated by integration of the stripping peaks for copper desadsorption at 0.8 V vs N.H.E. The degrees of coverage obtained from solutions 10^{-4}, 10^{-5} and 10^{-6}M in Cu^{2+} were calculated from voltammograms run in the same conditions as in fig. 1 and the values are respectively 8%, 3% and 2%. Therefore, it looks likely Cu ad-atoms do enhance the oxidation of HCOOH ($f \simeq 2$), but only at very low coverage.

The effect of holding the electrode at certain cathodic limits, during different times in a solution 1M H_2SO_4 + 0.1M HCOOH in the absence and presence of Cu^{2+} was studied. Some of the results obtained from cyclic voltammograms are summarized in table 1.

Similar results were obtained when the cathodic limit was 0.03, instead of 0.25 V.

07160

DISCHARGE BEHAVIOUR OF A REDOX THERMOGALVANIC AND CONCENTRATION CELL

J.M. HORNUT and A. STORCK
CNRS-ENSIC, 1 rue Grandville
54042 NANCY CEDEX (FRANCE)

A thermogalvanic cell can be defined as a thermoelectrical process allowing the direct conversion of thermal energy into electrical energy [1]. Principle of such a cell consists of performing an oxidoreduction reaction between a hot electrode and a cold electrode; both of them are of the same nature. An electromotive force appears between the electrodes and its value is related to temperature gradient ($T_1 - T_2$) and to specific temperature coefficient ($dE°/dT$) of considered redox reaction.

Besides, a concentration cell directly converts chemical energy into electrical energy and consequent electromotive force is a function of concentration ratio (Ox/Red) for involved redox couple.

Practical processing of such devices is far from easy since several technical constraints must be regarded :

(i) distance between electrodes has to be very small to minimize ohmic drop of potential.

(ii) Temperature or concentration gradient must be kept at a constant value while avoiding short circuit between the electrodes.

(iii) Power losses due to activation overpotential at the electrodes have to be as low as possible.

The present work deals with results of a theoretical and experimental study of a thermogalvanic and concentration cell, whose device is depicted in Fig. 1. The reactor is a parallel plate cell. This one allows the existence of two distinct electrolyte flows along the electrode surfaces. In case of a well established and regular regime, two thermal boundary layers (or concentration boundary layers) with increasing thickness are developped at the contact plan zone of the two fluids, thus lessening the short circuit.

Presented results were obtained with Ferri-/Ferrocyanide redox couple in NaOH aqueous medium; this system was chosen for its very satisfactory electrochemical properties (electrochemical kinetics and specific temperature coefficient). Performance of the device described above was optimally determined from numerous experimental trials. In addition, these results make it possible to deduce the influence of main physical parameters (flow velocity, interelectrode gap, presence of separator or not, physicochemical properties of fluids) on the recovered electrical power and the heat or mass flows exchanged at the interface. Under best experimental conditions, specific powers obtained do not exceed some W/m^2 for a thermal gradient of 40°C or a concentration ratio close to 100.

In absence of a separator, if the existence of a mixing zone between the two laminar flows is assumed, an hydrodynamical model allows a quantitative determination of fluxes exchanged at the interface for both heat and mass transfers. Under the definite conditions, the order of magnitude of the mixing zone thickness may be deduced from experimental results; furthermore, these results point out an excellent analogy between both kinds of transfer.

A cellophane separator considerably hinders heat or mass short circuit without any increase of the total generator resistance, thus implying an important enhancement of the energetic cell performance.

Reference

(1). W. VIELSTICH, "Fuell cells", pp 345-361. Wiley Intersciences, New York (1960).

Figure caption

Figure 1. Scheme of principle of experimental device : thermogalvanic cell and concentration cell.

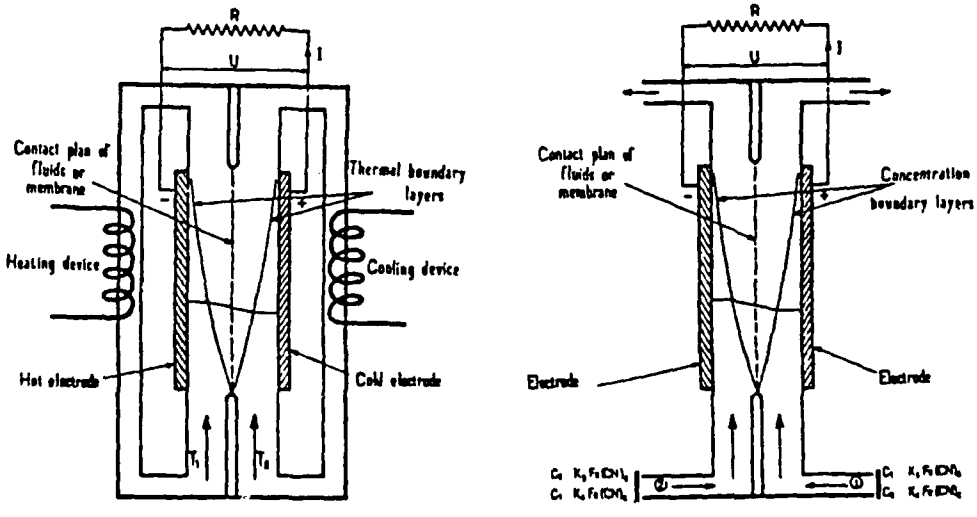

FIGURE 1.

07170

EVOLUTION IN THE POROSITY OF THE LEAD DIOXIDE ACTIVE MASS DURING CYCLING AND PHENOMENA LEADING TO ITS DESTRUCTION

D.PAVLOV and E.BASHTAVELOVA
Central Laboratory of Electrochemical Power Sources
Bulgarian Academy of Sciences, Sofia 1040, Bulgaria

A survey of recent literature (1,2) on the behaviour of the positive active mass (PAM) of the lead-acid battery during cycling shows that there is no general agreement for the causes of its degradation. Recently we advanced a model (3) for the structural organization of PAM, according to which it comprises two levels: microstructure - built up of small PbO_2 crystallites organized in a porous agglomerate and macrostructure or skeleton, where the individual agglomerates are linked in a macroporous skeleton, mechanically supporting the PAM, conducting the electric current, and acting as a memory into which the technology of the PAM preparation is stored. During cycling the agglomerate macrostructure desintegrates to separate crystallites. The contact between them deteriorates and the capacity rapidly decays. Hence, the destruction of the structural organization of PAM determines the life of the plate. It is the aim of this paper to elucidate the phenomena leading to this destruction.

A variety of PAM structures was prepared by using pastes with different phase composition: $PbO.PbSO_4$, tet-PbO, $3PbO.PbSO_4.H_2O$, and $PbO.PbSO_4$. Positive plates with these 4 types of PAM were cycled to a 80% depth of discharge and 50% utilization of PAM. Following cycling we measured the pore volume distribution (Hg porometry), the BET surface area, the apparent density (Hg pycnometry), and the plate thickness in charged and discharged state. Table 1 presents the pore volumes and the apparent densities of charged PAM's of the 4 types of plates at the 5th and 30th cycles. The data reveal that during cycling structural changes occur, resulting in the increase in the pore volume and a decrease in the apparent density of the PAM's.

Table 1

PAM formed from	5th cycle		30th cycle	
	V(ch) $cm^3.g^{-1}$	apparent density $g.cm^{-3}$	V(ch) $cm^3.g^{-1}$	apparent density $g.cm^{-3}$
$3PbOPbSO_4H_2O$	0.115	4.3419	0.137	3.9105
tet-PbO	0.092	4.8240	0.102	4.2892
$PbOPbSO_4$	0.183	3.3300		2.6885
$4PbOPbSO_4$	0.115	4.5013	0.134	3.6789

Table 2 shows the evolution of the average plate thickness measured at several fixed points of the plate in charged state, discharged state and after storage for 16 hrs in the electrolyte at open circuit (OC).

The juxtaposition of the data for the 5th and 30th cycle reveal that the plate thickness grows during cycling. The thickening of the plate depends on the rigidity of the skeletal structure. It is largest for PAM prepared from $PbO.PbSO_4$, which is the least stable and sheds readily. On the other hand, the thickness of the plate prepared from $4PbO.PbSO_4$, is practically constant. This PAM is known as the most stable and plates prepared from it have the longest cycle life (3).

Table 1

PAM formed from	5th cycle			30th cycle			
	char. mm	disch. mm	disch. +OC mm	char. mm	disch. mm	disch. mm	char. mm
$3PbOPbSO_4H_2O$	2.390	2.440	2.410	2.790	3.010	2.820	2.790
tet-PbO	2.380	2.420	2.410	2.580	2.750	2.590	2.590
PbOPbSO	2.580	2.740	2.630	3.260	3.610	3.280	3.260
$4PbOPbSO_4$	2.660	2.690	2.670	2.660	2.860	2.760	2.660

Table 2 presents the change in the plate thickness within one charge-discharge cycle and reveals that the charged plates are thinner than the discharged ones. It is also seen that the thickness of discharged plates stored at OC in the electrolyte decreases. Consequently, the PAM "breaths" during each charge-discharge cycle, whereby during the discharge mechanical stresses are generated within its structure and the plate expands. During storage and charging these stresses are released as a result of the recrystallization processes and the plate contracts.

The SEM observations (Fig.1) of the crystal morphology of PAM after charge, after discharge and after storage at OC in the electrolyte are in accordance with the above findings. Fragments of $PbSO_4$ crystallites which are not well formed (Fig.1b) and are strongly attached to the PAM are observed after discharge. Since, the molar volume of $PbSO_4$ is larger than that of PbO_2, the $PbSO_4$ crystallites, linked to the skeleton, will generate internal stresses during their growth, causing an expansion of the macrostructure. If the skeleton is not rigid enough, it will begin to swell. During storage at OC dissolution of the non-equilibrium $PbSO_4$ crystallites and the subsequent deposition of $PbSO_4$ onto equilibrium crystals occurs. As a consequence, well shaped $PbSO_4$ crystallites are formed (Fig.1-c). Fig.1 reveals that the discharge process comprises the electrochemical reaction of the reduction of PbO_2 to $PbSO_4$ as well as the recrystallization process, where in the Pb^{2+} ions are transferred along the pores and deposited on equilirium $PbSO_4$ crystallites. When the latter process takes place, then the oxidation of the $PbSO_4$ crystallites to PbO_2 during the recharge will be modified accodingly.

Fig. 1

Indeed,as seen from the curves in Fig.2 the recharge of PAM stored at OC in the electrolyte occurs at a higher polarization than in the case when the plate is charged immediately after its discharge.

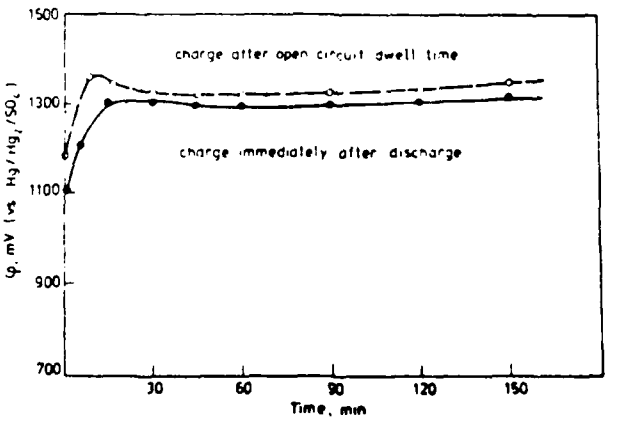

Fig. 2

In the initial cycles, when the skeleton is still rigid enough it can support the mechanical stresses generated during cycling. With the increase of the number of cycles the rigidity of the skeleton decays, the volume changes augment, and, as a consequence, the swelling of the PAM grows. This in turn facilitates the deterioration of the contacts between the agglomerates and leads finally to the ultimate failure of the battery.

References

1. A.C.Simon,S.M.Caulder,J.T.Stemmle,J.Electrochem.Soc.122,461 (1975).
2. S.M.Caulder,J.S.Murday,A.C.Simon,J.Electrochem.Soc.120,1515 (1973).
3. D.Pavlov,E.Bashtavelova,J.Electrochem.Soc.131, 1468 (1984).

07180

STUDY OF CdTe/ELECTROLYTE INTERFACE : FLAT-BAND POTENTIALS, PHOTOCURRENT AND PHOTOCORROSION

O. SOLORZA and G. POILLERAT*
Laboratorio de Energetica Electroquimica
CINVESTAV, A.P. 14-740, 0700 MEXICO DF, MEXICO

The CdTe/electrolyte interface has been extensively studied for its photovoltaïc energy conversion capability. In the present work we present the flat-band potential determination and consequently energy band diagram of n- and p- type CdTe in differents electrolytes (pH = 6.7 and 14) and the I-V curves both in the dark and under illumination. Thus an attempt to explain the behavior of this interface and determine its possibility of solar energy conversion.

Experimental

CdTe monocrystals, n (In doped) and p (As doped) have been used. Samples have been etched with Br_2 - methanol (5 %) solution. We have prepared in the laboratory the Na_2Te solutions almost following the published procedure (1) and preventing the solution from oxygen.

Flat band potential determinations

The flat band potential, V_{f-b} , have been determined using three differents techniques. Impedance diagrams and capacity measurements allow us to draw the Mott Schottky diagrams (2) ; a typical set of results is shown on figure 1. The Rectified Alternating Photocurrent Voltammetry (RAPV) have been used (3). A new promising method : the Light Modulated Induced Electrical Resonance (LMIER) have also been used (4). Typical curves obtained by this last method are shown on figure 2. All the results represent the average obtained from several determinations. The determinations of V_{fb} have been carried out in two differents electrolytes : $NaClO_4$ (0.1 M ; pH = 6.7) and NaOH (5 M) + 0.012 M Na_2Te (pH = 14) . Results can be seen on Table 1.

Table 1 : Flat Band Potentials (V/SCE)

Semiconductor	Mott Schottky		RAPV		LMIER	
	pH = 6.7	pH = 14	pH = 6.7	pH = 14	pH = 6.7	pH = 14
n CdTe	- 1.34	- 2.10	- 1.15	- 1.5	- 1.31	- 1.68
p CdTe	+ 0.06	- 0.60	-	- 0.65	-	- 0.32

*Present adress : Lab. Electrochimie, ULP, B.P. 296, 67008 STRASBOURG CEDEX, FRANCE.

The results obtained by RAPV seem us more difficult to agree with because the difference between the n and p type V_{f-b} is far from the energy gap of CdTe . Generally the RAPV method give the V_{onset} (onset of photocurrent) rather than V_{fb} . Impedance and LMIER determined V_{fb} are also different although the difference between V_{fb} (n type) and V_{fb} (p type) give us the energy gap of CdTe with a good aproximation. There is also some discrepancies between the published results (1,5). We note a variation of V_{fb} with pH which have been discuss in the litterature (1,5) and may be related to etching procedures. LMIER results seem more coherent with litterature but we have not yet explanations for the discrepancy of impedance method. With LMIER results we can draw the Energy Diagram of the n and p CdTe/NaOH + Na_2Te interface (figure 3).

Photocurrent and Photocorrosion current

On the figure 4 we reported the dark and illuminated I-V curves for three systems. If we take into account the possible decomposition of CdTe (5b) which could correspond, at pH = 14 , to

$$E^\circ = -0.54 \text{ V/SCE} \quad \text{for} \quad CdTe + 2\,OH^- + 2\,p^+ \longrightarrow 4\,CdO_2^- + H^+ + Te$$

and $E^\circ = -1.68$ V/SCE for $CdTe + 2\,e^- \longrightarrow Cd + Te^-$

some conclusions can be drawn from these curves. The current we measured in the CdTe/$NaClO_4$ system (Fig. 4c) is only a photocorrosion current. It could be the same phenomenon with all redox couples which have a standard redox potential higher than - 0.5 V.SCE . In the - 0.8 to - 0.2 V range the recombination of electron-hole pairs seems to be very important (6). The current obtained in the CdTe/NaOH + Na_2Te system (fig. 4a) on the contrary is a photocurrent which could be used for photovoltaïc conversion.

Acknowledgments :

- Laboratoire d'Electrochimie, ULP, STRASBOURG (Prof. P. CHARTIER) for experimental facilities and financial support to assist to 36th ISE Meeting.
- Laboratoire PHASE, CRN, STRASBOURG (Prof. SIFFERT) for CdTe samples.

Bibliography

1. A.B. ELLIS, S.W. KAISER, J.M. BOLTZ and M.S. WRIGHTON, J. Am. Chem. Soc., 99, 2839 (1977).
2. J.F. McCANN and S.P.S. BADWAL, J. Electrochem. Soc., 129, 551 (1982).
3. J.F. McCANN and J. PEZY, J. Electrochem. Soc. 128, 1735 (1981).
4. J.P. PETIT, N. ALONSO VANTE and P. CHARTIER, J. Electroanal. Chem., 157, 145 (1983).
5. a) D. LINCOT and J. VEDEL, J. Electroanal. Chem., 175, 207 (1984).
   b) J.L. SCULFORT, R. TRIBOULET and P. LEMASSON, J. Electrochem. Soc., 131, 209 (1984).
   c) A. RAKHSHANI and L.E. LYONS, Aust. J. Chem., 35, 1949 (1982).
6. O. SOLORZA and G. POILLERAT, C.R. Acad. Sc. Paris, 299, 857 (1984).

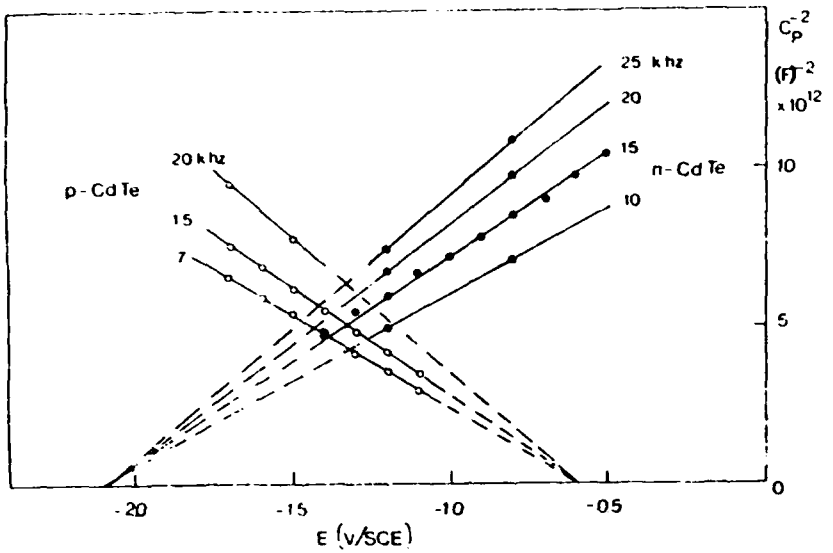

Figure 1 : Mott Schottky diagrams for n- and p- CdTe/NaOH 5 M + Na_2Te 0.012 M

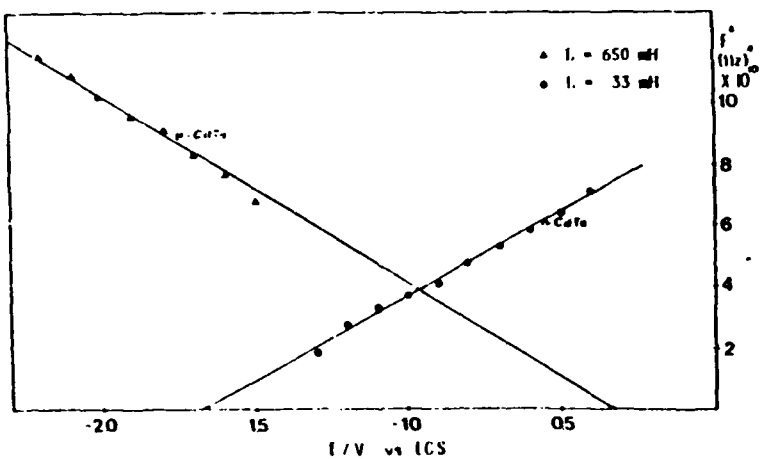

Figure 2 : Resonance frequency, determined by LMIER , vs potential
Electrolyte : NaOH 5 M + 0.012 M Na_2Te

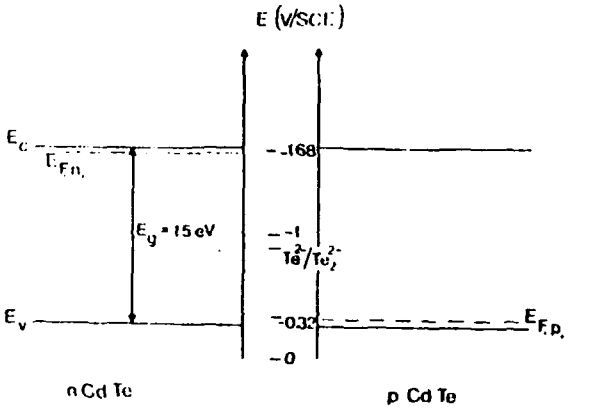

Figure 3 : Energy band diagram of n CdTe and p CdTe / NaOH 5 M + 0.012 M Na_2Te , pH = 14 from LMIER determinations.

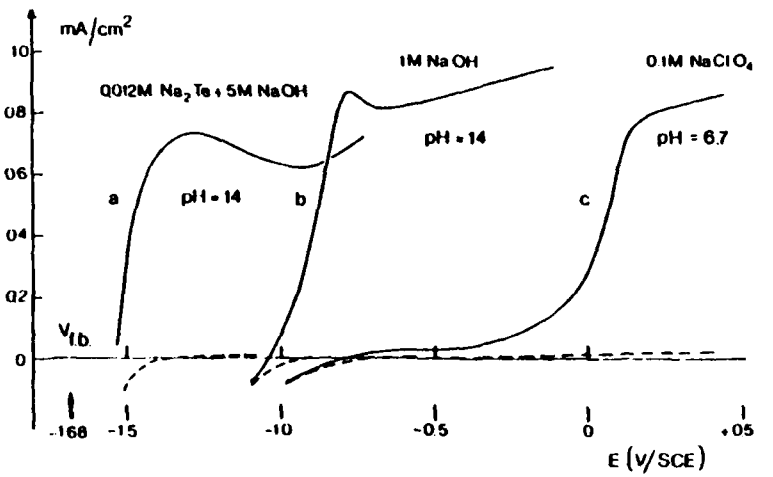

Figure 4 : Dark current (---) and photocurrent (——) vs potential at the n CdTe/electrolyte interface with three differents electrolytes.

07182

07190

OPTIMIZATION OF THE ELECTROCHEMICAL PROCESS TAKING PLACE IN A METHANOL-HYDROGEN PEROXIDE FUEL CELL

SERBAN AGACHI and LIVIU ONICIU
Faculty of Chemical Technology, University of Cluj - Napoca, Romania

In previous studies[1,2], the optimization problem of a 3W laboratory fuel cell was approached from the current density maximization point of view. A following study dealt with the optimization of a 250 W model, by means of a factorial experiment, the fuel cell power being optimized.[3] The results of the experiment were used in the design of a 10 kW fuel cell, whose optimization was economically approached.

A simplified flow-sheet of a methanol-hydrogen peroxide fuel cell plant is shown in fig. 1.

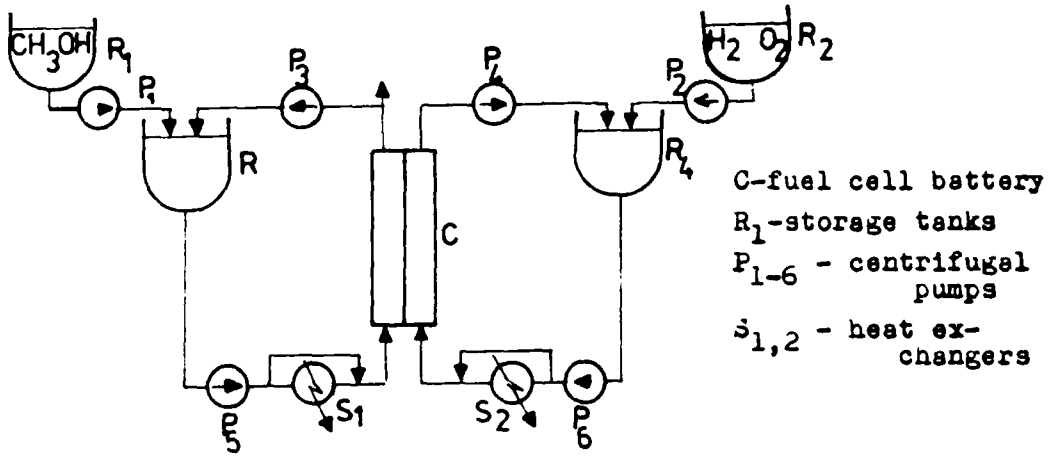

Fig. 1

Because the operational costs of a fuel cell plant are extremely reduced (due to the high efficiency of the cell)[4], the optimization was a task of minimizing the investment effort. The objective function developed

$$y = \frac{\text{cost of fuel cell, storage tanks, heat exchangers, pumps, pipes}}{\text{total delivered energy}} \qquad (1)$$

depends on:

a. fuel concentration in electrolyte (C_c); the relation between fuel and oxidant concentrations is[5]:

$$\frac{C_o}{C_c} = \frac{K_c}{K_o} \cdot \frac{Z_c}{Z_o} \cdot \frac{r_c}{r_o} \qquad (2)$$

b. electrolyte temperature (T_e)

c. electrolyte flow through the battery (F_{el}).

Relation (1) is subjected to the following constraints:

$$0,1 \leq C_c \leq 2,5 \text{ M}$$
$$293 \leq T_{el} \leq 313 \text{ K}$$
$$0,001 \leq F_{el} \leq 0,003 \text{ m}^3/\text{s} \quad (3)$$

These are imposed by the hydrogen peroxide maximum allowed concentration, by the high vapor pressure of methanol at higher electrolyte temperatures and by energy consumption at higher flows.

The components of the objective function are the equipment costs, calculated with the general formula[5]:

$$C = \alpha D^{\beta} \quad (4)$$

Fuel cell battery cost

Fuel cell cost can be considered proportional to the electrode area:

$$C_{bat} = \alpha_{bat} A_{el} \quad (5)$$

α_{bat} was calculated taking into account the cost of raw materials used in the manufacturing of electrodes (Pd Cl_2, Ag, Ni) and the cost of work of manufacturing the cell stack.

The value thus calculated was

$$\alpha_{bat} = 8569 \text{ lei/m}^2$$

The electrode area[3] was expressed by means of the following relation:

$$A_{el} = \frac{P}{U_c \, 0,0022 \, D_T \, Re^{0,875} \, Sc^{0,25} \, \gamma_c \, . \, z \, F \, (C_c/d_e)} \quad (6)$$

Thus, the battery cost became:

$$C_{bat} = 14719 \frac{1}{F_{el}^{0,875} . C_{med}} \quad (7)$$

Storage tanks cost[3]

$$C_{rez\ i} = 124346 \, F_i^{0,44} \quad (8)$$

Centrifugal pumps cost[3]

$$C_{pc\ i} = 8987 \, F_i^{0,7} \quad (9)$$

Pipes cost[3]

$$C_{cond} = 664,8 . F_{el}^{0,4} \quad (10)$$

The cost of piping is referred only to the piping of electrolyte.

Heat exchangers cost[3]

The cost of the two heat exchangers implied in maintaining the temperature at the desired level was calculated with the same general relation (5):

$$C_{sch} = 8323 \, A_{sch}^{0,75} \quad (11)$$

where

$$A_{sch} = \frac{4424602 \, F_{el} \, (T_{el} - 290)}{K_{TT} \, (T_{el} - 280) \, [3,178 - \log (323 - T_{el})]} \quad (12)$$

Optimization

A Newton-type optimization method was used in order to determine the optimal working parameters ($C_{med\ opt}$, $F_{el\ opt}$, $T_{el\ opt}$). The method was that of Davidon-Fletcher-Powell which approximate the hessian matrix on its inverse, using the information from

first-order derivatives. The computing algorithm is

$$x^{(k+1)} = x^{(k)} + \lambda^{(k)} \hat{s}^{(k)} \quad (13)$$

where $x^{(k+1)}$ and $x^{(k)}$ are two vectors calculated in two different successive stages, $\lambda^{(k)}$ the step of searching and $\hat{s}^{(k)}$ the searching direction matrix.

A computer program has been prepared, structured as it follows (fig.2):

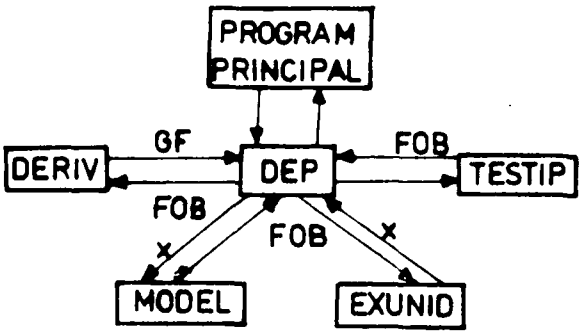

Fig. 2

DFP - Davidon-Fletcher-Powell subroutine
DERIV - subroutine calculating the derivative of object function
MODEL - subroutine calculating the components of object function
EXUNID - subroutine exploring the direction of one parameter
TESTIP - subroutine testing the reaching of optimum

Conclusions

The results show an investment decreasing from 197742 lei/kWh (C_{med} = 2,5M, T_{el} = 313 K, F_{el} = 0,003 m^3/s) to 25070 lei/kWh (C_{med} = 2,05 M, T_{el} = 300 k, F_{el} = 0,001 m^3/s). Due to the savings in using fuel and oxidant (7,6% methanol and 7,7% hydrogen peroxide), the cost of a kWk was reduced from 0,96 lei to 0,91 lei.

Nomenclature

$C_{o,c}$ oxidant and fuel concentration ($kmol/m^3$)
$K_{c,o}$ mass transfer coefficients of oxidant and fuel species(m/s)
$\gamma_{c,o}$ adimensional current densities
T^e electrolyte temperature (^oC)
F_{el} flow of electrolyte (m^3/s)
C_u equipment cost (lei)
α,β cost coefficients specific to each type of equipment
A_{el} electrodes area (m^2)
P_{el} power delivered by the fuel cell battery (kW)
U cell voltage (V)
D_T diffusion coefficient (m^2/s)
Re,Sc criterial numbers
$\mathcal{F}$ Faraday number (C/kmol)
d_e equivalent flowing diameter (m)
K_{TT} heat transfer coefficient (W/m^2K)

References

1. L. Oniciu, S. Agachi - Stud.Univ.Babeş-Bolyai, Ser.Chem.,19, 1974, 76
2. S. Agachi, L. Oniciu - Stud. Univ. Babeş-Bolyai, Ser. Chem, 2o, 1975, 72
3. S. Agachi - Modelarea matematică şi automatizarea proceselor din pilele de combustie, cu produse petroliere şi petrochimice.Teză de doctorat, Institutul de Petrol şi Gaze din Ploieşti, 1984.
4. K.L. Hsueh, D.T. Chin, J. McBreen, S. Srinivasan -Journ.of appl. electrochem., 11, 1981, 51o
5. O.Smigelschi, A.Woinaroschi -Optimizarea proceselor din industria chimică, Ed.Tehn., Bucureşti, 1979
6. D. Himmelblau - Applied nonlinear programming, McGraw-Hill Book Comp., 1972.

07200

BROMINE DOPED POLYDITHIENOTHIOPHENE:CATHODE ACTIVE MATERIAL IN AQUEOUS MEDIUM.

M.BISERNI, P.BUTTOL, A.MARINANGELI, M.MASTRAGOSTINO

Istituto chimico G.Ciamician dell'Universita' di Bologna (Italy)

At present much scientific work[1-3] has been devoted to organic conducting polymers because of the large field of potential applications (as electrods materials of rechargeable batteries or as electro-optic display devices,etc.).The main interest concerns their ability to be switched by chemical or electrochemical doping ,from a neutral (non conducting) state to an oxidized or reduced conducting state.

Recently we have electrosynthesized[4] a new conducting polymer:polydithieno(3,2-b:2,3-d)thiophene (pDTT) with a doping level of 50% (counteranions ClO_4^- ,PF_6^-).This doped polymer was electrochemically prepared at controlled current (0.5 - 1 mA/cm^2) or at controlled potential (1.4 V vs.SCE) on Pt,SnO_2 and glassy carbon electrodes in degassed and anhydrous electrolytic medium formed by CH_2Cl_2 ,the monomer dithieno(3,2-b:2,3-d)thiophene (Fig.1) and tetrabutylammonium salts.

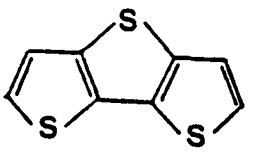

Fig.1.Dithieno(3,2-b:2,3-d)thiophene (DTT)

In CH_2Cl_2 /tetrabutylammonium perchlorate (TBAP) the anodically synthesized doped pDTT can release and store charge equal to 20% of the charge involved in its initial electrochemical preparation[5] .In the same electrolytic medium doped pDTT presents some attractive features relevant to its application as cathode active material in battery technology,e.g.,a high doping level (which corresponds to a capacity of 55 mAh/g with ClO_4^- as counteranion),an initial value of V_{oc} of ca. 1 V vs.SCE ,high values of the charge recovered at constant current up to 0 V vs.SCE with respect to that stored (from a maximum of 95% for I=-0,04 mA/cm^2 to a minimum of 27% for I=-4 mA/cm^2) ,cyclability with no evidence of appreciable degradation and an apparent O_2 stability.On the other hand ,films of doped pDTT preserved in CH_2Cl_2 /TBAP solution have shown the disadvantage of a fast

self-discharge.This phenomenon is not due to polymer degradation but to an uncontrolled redox reaction involving the used electrolytic medium.Work is in progress to investigate the behavior of this material in other nonaqueous solvents and in water.Some results have been obtained in propylene carbonate[6] .

We are corrently examining the possibility of doping neutral pDTT by electrochemical oxidation in aqueous medium involving $ZnBr_2$ as electrolyte in order to test the feasibility of the polymer as cathode active material in a model of a $ZnBr_2$ aqueous battery.

The neutral pDTT electrodes are prepared by exhaustively reducing at 0 V vs.SCE in CH_2Cl_2/TBAP solution the doped pDTT electrosynthesized in CH_2Cl_2/TBAP,DTT.

The electrochemical oxidation at constant current on neutral pDTT/SnO_2 electrode of an aqueous solution is accompanied by an electrode colour change from red to black,attesting to the polymer doping.The same colour change is observed when the neutral pDTT electrode is dipped in Br_3^- -$ZnBr_2$ aqueous solution.VIS and near IR absorption spectra, which evidence the pDTT doping process, will be illustrated.

Fig.2 shows the variation of the potential of a pDTT/Pt electrode during a charge-discharge cycle at constant current in $ZnBr_2$ aqueous solution.Table I summarizes the coulombic efficiencies of several regenerative cycles (discharge made immediately after the charge).

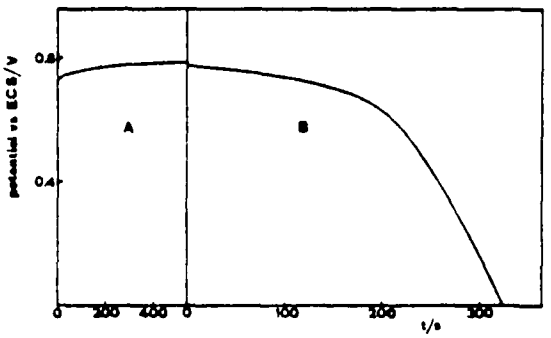

Fig.2 V(t) of a pDTT/Pt electrode during a charge-discharge at I=0.4 mA/cm^2 in $H_2O/ZnBr_2$ 0.2M .A)charge, B)discharge.

Table I. Coulombic efficiency of six charge-discharge regenerative cycles of a pDTT/Pt electrode at I=0.4 mA/cm^2. Qox = 215 mC/cm^2 ,Qred recovered up to 0 V vs.SCE.

Number cycle	Coulombic efficiency (Qred/Qox)
1	0.60
2	0.63
3	0.49
4	0.56
5	0.49
6	0.55

The amount of charge involved in the oxidation process corresponded to 1.5 electron/DTT unit,taking into account the following possible stoichiometry of the doping process:

$$2\ +DTT+\ +\ 3\ Br^- \rightleftharpoons +(2DTT)^+ Br_3^- + \ +\ 3\ e^-$$

to which would correspond a capacity of 127 mAh/g.However,spectroscopical measurements and exhaustive

discharges at 0 V vs.SCE of doped pDTT have shown that this value of capacity can not be achieved.

We also observed a drop in both the potential of the charged electrode and the values of the recovered charge during the exhaustive reduction as a function of the time elapsed from the end of the charge. This self-discharge of the electrode may be explained by the displacement within the doped pDTT of Br_3^- by Br^- and by an undoping reaction or by a degradation of the oxidized pDTT. This problem is still under investigation.

ACKNOWLEDGEMENTS

This work was carried out with the financial support of the CNR Progetto Finalizzato Energetica 2, no.830211759.

REFERENCES

1 - J.C.W.Chien - "Polyacetylene" - Academic Press - (1984).
2 - K.K.Kanazawa, A.F.Diaz, M.T.Trounbi, G.B.Street - Synth.Met. 4, 119 (1981).
3 - G.Tourillon, F.Garnier - J.Electroanal.Chem. 161, 51 (1984).
4 - P.G.Di Marco, M.Mastragostino, C.Taliani - Mol.Cryst.Liq.Cryst., Conf. Proc.ICSM 84; 118, 241 (1985); P.G.Di Marco, M.Mastragostino, C.Taliani - Patent (Italy), no.21430A/84.
5 - M.Biserni, A.Marinangeli, M.Mastragostino - J.Electrochem.Soc. (1985), in press.
6 - M.Mastragostino, B.Scrosati - J.Electrochem.Soc. (1985), in press.

07210

PHOTOCHEMICAL INVESTIGATIONS OF THE METAL/ELECTROLYTE AND THE METAL/METALOXIDE/ELEKTROLYTE INTERFACE USING HIGH POWER LASER PULSES

A. FELSKE, W.J.PLIETH

Freie Universität Berlin, Institut für Physikalische Chemie
Takustr.3, D-1000 Berlin 33 (Dahlem)

In the paper it will be shown, that high power laser pulses can be used to study photoelectrochemical processes on smooth as well as on oxide covered electrodes. Main emphasis is put on the investigation of the passive film of iron.

Experimental: The experimental equipment consisted of a potentiostat with a three electrode cell, a scan generator and a XY-recorder. As the light source, an excimer pulse laser at a wavelength of 248 nm (KrF) was used. The pulse width was 16 ns. The photocurrents were recorded with a digitizing storage oscilloscope.

Photocurrents on platinum. In a prelimanary investigation the behaviour of a platinum electrode in the oxide layer region was studied. Fig. 1 represents the effect of the light pulses on a cyclic voltammogram. At potentials higher than the potential corresponding to the formation of an oxide layer, sharp anodic photocurrent peaks appeared simultaniously with the light pulses and superimposed to the dark current. The oscillogram of the photocurrent showed a short pulse of about 200 us half width which is followed by a slow process of oxide layer regeneration. The reason for this behaviour is an electron-hole pair generation in the semiconducting metaloxide coupled with a photolytic decomposition.

At lower potentials (0 - 800 mV vs NHE), cathodic photocurrents appeared, too fast to be recognized by the XY-recorder. This effect is due to the photoemission of electrons from the metal into the electrolyte and will not be discussed further. In the intermediate potential region between double layer and oxide layer region a cathodic peak is preceding the anodic photocurrent peak.

Photocurrents of iron: With the same method as used for the investigation of the platinum surface, the passive film of iron was investigated in 0.5 M sulfuric acid and in borate electrolyte (0.15 M H_3BO_3/0.0375 M $Na_2B_4O_7$, pH = 8.4). The photocurrent depended on the pH-value and on the potential. In the strong acid electrolyte (Fig. 2) the magnitude of the photocurrent was ten times larger then in weakly alkaline solution (pH 8.4, Fig. 3). In the latter example cathodic and anodic photocurrents are observed. The zero point is approximately equal to the flat band potential. The photocurrent depended also on the laser intensity (Fig. 4). A saturation region was obtained which should be proportional to the thickness of the film. The saturation allowed the determination of the overall quantumefficiency of = 10^{-6}.

A minimum intensity is required for the onset of the photocurrents. This is explained as the amount of surface states and electron traps which have to be filled before a photocurrent can flow. A total number of 10^{-8} surface states and traps is estimated from the determined minimum intensity.

Fig. 1 Cyclic voltammogram of platinum in 0.5 H_2SO_4 under pulsed laser illumination.

Fig. 2 Peak height of the photocurrent pulses vs. potential of iron in 0.5 M H_2SO_4, laser power 27 mJ/cm^2.

Fig. 3 Same as Fig. 3 but in borate buffer, pH = 8.4. The linear plot represents ellipsometric thickness values determined by Sato et. al.

Fig. 4 Dependence of the peak height of the photocurrent vs. the square root of the laser power.

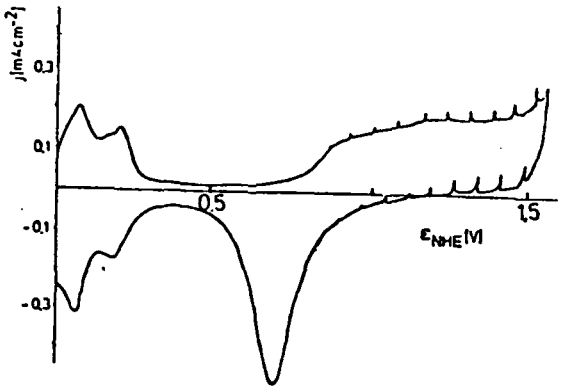

Fig. 1

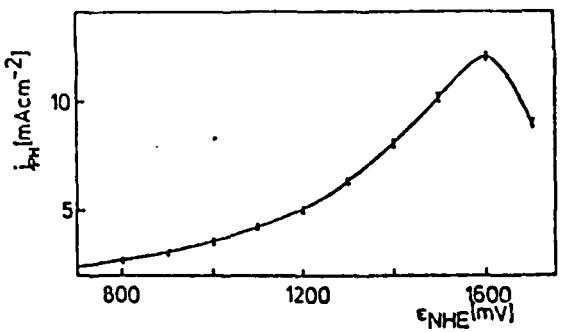

Fig. 2

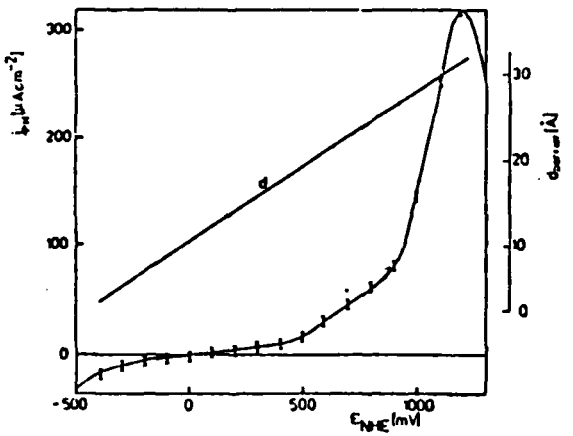

Fig. 3

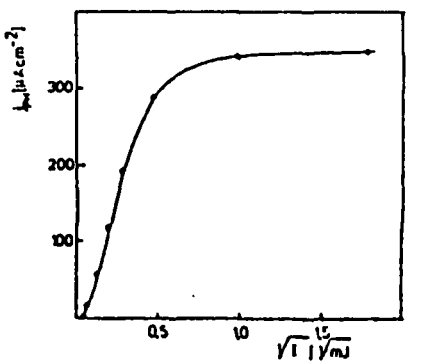

Fig. 4

07212

07220

Impedance of a sodiumpolysulphide electrode during the phase transition molten/solid

R. Knödler
Brown, Boveri & Cie
Central Research Laboratory
Heidelberg (Germany)

Introduction

The molten polysulphide electrode had received some attention because it is used in the sodium sulphur battery /1/, /2/. Depending on the melt composition there are two regions at the operating battery temperature of 350 °C. In the one-phase region Na_2S_x exists with x from about 2.7 to 5. In the two-phase region sulfur and Na_2S_5 exist together. The conductivity of these melts and the polarization of the graphite/melt interface has been studied already /3/, /2/. However, no information is available on the behaviour in the frozen state and in the transition region molten/frozen. This is important because a sodium sulphur battery has to be cooled down from time to time. Depending on the amount of nuclei in the sulphide the melts tend to undercool and to solidify within a very short time.

Experimental

The process of solidification was observed by measuring the impedance of a blocking electrode (molybdenum) in Na_2S_x using a Solartron 1170 frequency response analyzer. A good electric contact between the molybdenum rod and the solid Na_2S_x is provided because Na_2S_x has a higher thermal expansion coefficient than Mo /4/. The polysulphides were chemically prepared from sulfur and anhydrous Na_2S (Cerac) at 450 °C. Experiments with electrochemically prepared Na_2S_x yielded the same results.

Results

The impedance characteristics show beyond about 100 Hz a pure ohmic resistance. At lower frequencies a 45° line is observed, indicating a diffusion controlled process. The diffusion coefficient decreases during cooling and at the transition temperature drops sharply below the measuring limit of about 10^{-8} cm^2 sec^{-1}. By plotting the logarithm of the impedance (at 30 Hz) against the reciprocal temperature straight lines are obtained for the frozen and the molten state, respectively. With Na_2S_4 the resistance difference between these two states is about 3 orders of magnitude, with Na_2S_3 only about 1 order. This means that the resistivity of Na_2S_4 at room

temperature is about 10^8 Ωcm, for Na_2S_3 only 10^5 Ωcm. The activation energies for both sulphides are about 45 kJ mol^{-1}. The transition from the molten to the frozen state and vice versa proceeds in the case of Na_2S_4 within less than 10 °C, in the case of Na_2S_3 this region is extended to about 40 °C. This indicates a glass-like behaviour of Na_2S_3 which was confirmed also by calorimetric measurements.

A further indication for a glassy-amorphous state of Na_2S_3 is the observation that after letting a cell stand for a week at room temperature, the impedance rose during this time by several orders of magnitude, from 10^5 to about 10^8 Ωcm for Na_2S_3. This was due to the slow crystallization of the amorphous Na_2S_3.

References

/1/ N.K. Gupta and R.P. Tischer;
J. Electrochem. Soc. 119 (1972), 1033.

/2/ R.D. Armstrong, T. Dickinson and M. Reid;
Electrochimica Acta 20 (1975), 709.

/3/ B. Cleaver, A.J. Davies and M.D. Hames;
Electrochimica Acta 18 (1973), 719

/4/ R. Knödler, A.R. Nicoll;
J. Mat. Sci. Letters 3 (1984), 911.

07230

THE INFLUENCE OF THE ELECTROLYTE ON THE KINETICS OF CR(III)-REDUCTION

C.RÜSSEL, D. KRAUSS and K.LEDJEFF
Fraunhofer-Institut für Solare Energiesysteme
Freiburg (Germany)

INTRODUCTION

Conventional electrochemical storage systems in which solid state reactions occur are only suitable for solar energy storage to a certain degree. The iron-chromium redox flow cell, in which the energy is stored in the form of metal ion pairs in different oxidation states has technically more favorable prerequisites. [1]
Anode and cathode regions are separated by an anionexchange membrane. The two regions are each connected to a pump and an electrolyte storage tank.

In order to optimize the electrode and the electrolyte composition it is helpful to know the mechanism of electrode reaction - especially that of the chromium (III)-reduction. This reduction mechanism has not been investigated as well as the iron(III)-reduction and is in addition complicated by hydrate isomerization.

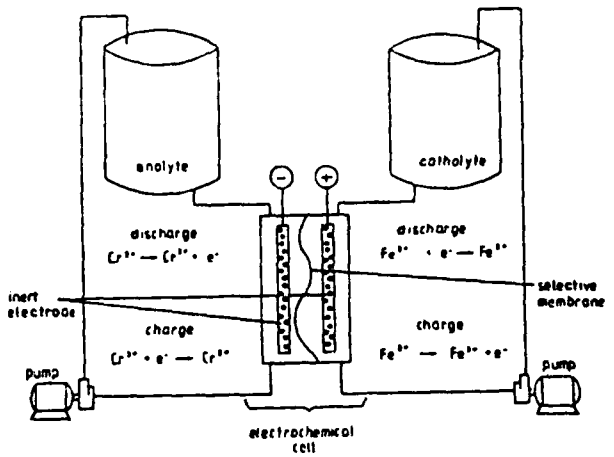

Fig. 1: Redox battery

EXPERIMENTAL

Cyclic voltammograms of a 1 M $CrCl_3$/1M HCl solution (Fig. 2) seem to show a reversible or quaisreversible electrode reaction. The peak current densities increase with increasing scan ν according to $i \sim \nu^{1/2}$ and also with increasing concentration in the relation $i \sim c$. A small amount of $PbCl_2$ was added as a catalyst and to suppress H_2 evolution. If the measurement is repeated at a later period in time the results are similar qualitatively. The peak current densities decline however as a function of time to approx. 10% of the original value. [2]

The follwing reactions occur when $CrCl_3 \cdot 6H_2O$ is dissolved in water:

$$CrCl_3 \cdot 6H_2O + H_2O \rightleftharpoons [CrCl_2(OH_2)_4]^+ + 3H_2O + Cl^-$$
$$[CrCl_2(OH_2)_4]^+ + H_2O \rightleftharpoons [CrCl(OH_2)_5]^{2+} + Cl^-$$
$$[CrCl(OH_2)_5]^{2+} + H_2O \rightleftharpoons [Cr(OH_2)_6]^{3+} + Cl^-$$

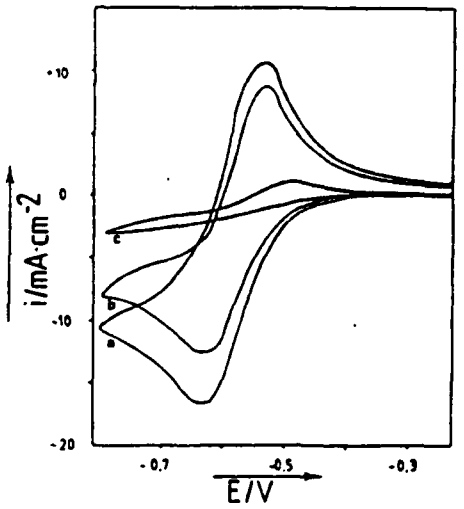

Fig. 2

Cyclic voltammograms of
1 M $CrCl_3$/1 M HCl solutions

a) freshly prepared

b) 5 day old solution

c) 180 day old solution

The color of the chromium (III)-solutions are different depending on which complex is present.

Solutions which contain $[Cr(OH_2)_6]^{3+}$ are blue-grey, $[Cr(OH_2)_5Cl]^{2+}$-solutions are green and $[Cr(OH_2)_4Cl_2]^{+}$-complexes have a light green color. A procedure was developed using anion exchange chromatography with which the complexes in HCl could be separated. Their spectra are shown in figure (3).

The reactions in equation 1 and 2 reach equilibrium only after a considerable amount of time. The spectra of a freshly prepared and aged 1 M $CrCl_3$/1 M HCl-solution are shown in figure (4). A change in the spectra can still be seen after months.

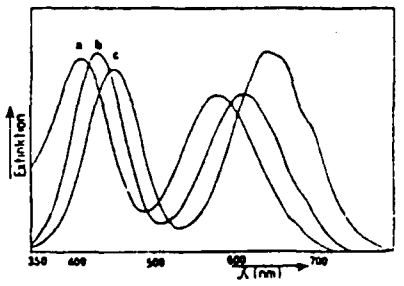

Fig. 3: UV spectra of the isolated complexes; a) $|Cr(OH_2)_4 Cl_2|^{+}$ b) $|Cr(OH_2)_5Cl|^{2+}$ c) $|Cr(OH_2)_6|^{3+}$

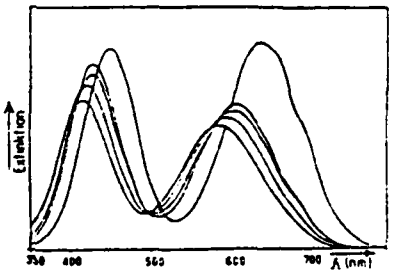

Fig.4: UV spectra of 1 M $CrCl_3$/1M HCl solutions: freshly prepared, 8, 13, 56, 154 day old

In order to explain the electrode reaction better, impedance spectra were measured in a broad frequency region from 10 mHz to 1 MHz (IM5 Zahner Elektrik, Cronach, Germany). These spectra are portrayed in figure (5) as points in log |Z|, vs. log f and |φ| vs. log f diagrams. [3]
This highly specific frequency dependency can be optimized with the equvalent circuit.

The simulated curve can be seen in fig. 5 a solid line. The mean deviation of the experimental phase angle from simulated curve was less than 0,3°.

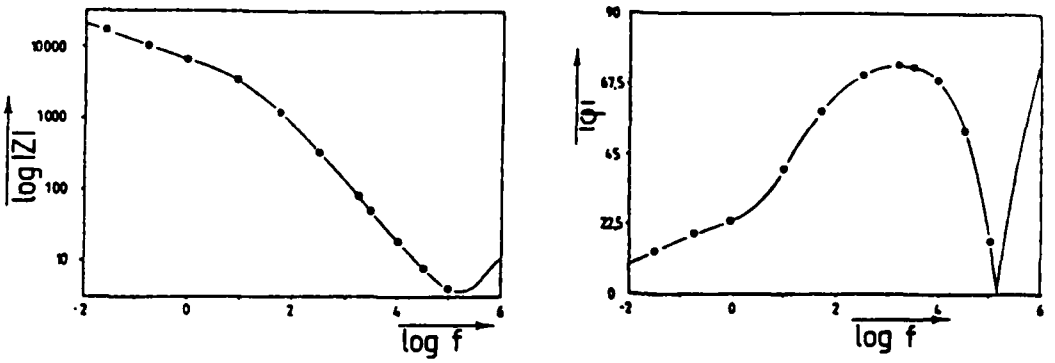

Fig. 5: Impedance spectrum of freshly prepared 1 M $CrCl_3$/1 N HCl solution at -600 mV vs SCE. Dots: experimental values, solid line: simulated curve

DISCUSSION

The equivalent circuit for the chromium(III) reduction agrees with that of the iron(III) reduction except for a further parallel resistance.[4] This eqivalent circuit has already been assigned to an electron transition through an adsorbed state. The reason for the extra circuit element, the parallel resistance, is probably due to the small H_2 evolution which always occurs parallel to chromium(III) reduction.

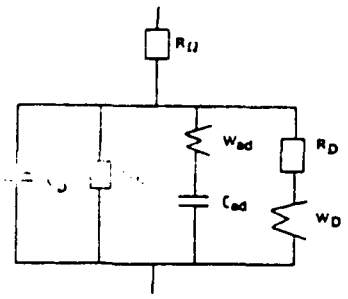

Fig. 6): Equivalent circuit of the impedance spectra in fig. 5

When one looks at the aging of Chromium(III) complexes, an electrochemical disactivation occurs parallel to the band shifts in UV spectra. The spectra of hydrate complexes isolated with anion exchange chromatography show that mainly the tetraaquocomplex is present in a fresh $CrCl_3$ solution; after a few days the pentaaquocomplex which after a few months converts to the electrochemically inactive hexaaquo complex. The higher electrochemical activity of the pentaaquo complex is probably due its ability to form a bridge over the Cl-ligands to the electrode.

1) H. Cnobloch, W.Kellermann, H. Nischik, K. Pantel, A. Siemsen, Siemens Forsch. Entwickl. Ber. 12, 79 (1983)
2) D. Sh. Cheng, A. Reiner, E. Hollax, J.Appl. Electrochem.15, 63 (1985)
3) H. Göhr, Ber. Bunsenges. Phy. Chem. 85, 274 (1981)
4) R. Kaus, Thesis Erlangen 1978

07240

THE BIPOLAR ZINC-BROMINE BATTERY: IMPROVED CARBON-BROMINE ELECTRODES

K. KORDESCH, J. GSELLMANN and M. RESCH
Technische Universität Graz, A-8010, Austria

The use of bipolar electrodes with a circulating electrolyte introduces a new problem not encountered in monopolar stack designs. The conductive pathways formed by electrolyte manifolding promote stray currents, called either parasitic or shunt currents. Parasitic currents waste power, cause charge imbalances within the stack and, more importantly, lead to early stack failures by inducing Zn to grow into the manifolds. A new technique, called "Shunt Current Protection" has been developed to deal with these problems.

The active carbon surface on which the organic bromine complexes are formed in the charging process, or from which the bromide ions are released, in the discharge process, is a specially prepared part of the bipolar plate. It must combine a high resistance to chemical attack by bromine (intercalation) with the properties of an electrochemically active interface. Only if both of these requirements are satisfied, can a long life expectancy (over 1500 deep cycles) at high current densities be achieved. Research on carbon activation and about carbon stabilization is therefore the main objective.

Circulating Zn-Br_2 Batteries

The principal component is the electrochemical module, where the actual electrochemistry takes place. The second component is the circulating electrolyte, an 3.5 molar solution of zinc bromide and a bromine complexing agent, e.g. a quarternary ammonium base like methyl-ethyl-morpholinium (or - - pyrrolidinium) bromide, which is circulated in two streams (divided by a porous separator) through the electrochemical module. The third component is the system of pumps and reservoirs which circulate and store the electrolyte.

During charge, zinc is plated at the negative electrode and bromine is evolved at the positive. As soon as the Br_2 is evolved, it reacts to form a bromine rich phase which is circulated out of the electrochemical module and is separated by gravity in the catholyte reservoir. Charge retention depends on the quality of the separator, but is generally good because the Br_2 is stored remotely from the zinc. 100 % discharge-cycles serve as equalizing steps.

The electrolyte can also be stored outside of the module, preventing self-discharge during very long storage times. A specific feature of the patented Exxon-Bromine complex is its partial water solubility, assuring the bromium availability without the need for special dispersion measures. Zn and Br_2 electrochemically react back to the original zinc bromide solution, liberating the energy absorbed during charging.

Bipolar Stack Design

The conductivity of carbon plastic (1 Ohm.cm) is adequate for thin bipolar electrodes. Therefore, such electrodes offer a distinctively simpler and cheaper stack design. In addition, the higher voltage of bipolar designs can be interfaced economically with high voltage chargers and DC motors.

Shunt Current Protection

The concept of shunt current protection is given in US Pat. No. 4,277,317. The central idea is that shunt currents can be prevented from entering the electrolyte manifolding by passing an auxiliary protective current through a seperated small manifold. The main purpose is the elimination of zinc deposits in the channels, an additional gain is the reduction of energy losses.

Research, Development and Testing of $Zn-Br_2$ Batteries

The present level of $Zn-Br_2$ development is the testing of multi-kW bipolar stacks equipped with shunt current protection. Bipolar electrodes have been successfully upscaled to about 12 dm^2 and can be mass-produced. Typical zinc loadings are in the range from 90 to 120 mAh/cm^2. The cells can be completely discharged and even charged in the opposite direction without damage. This, in addition to the light weight, is the major advantage over lead-acid batteries.

Design Specifications for an 80 V, 20 kWh Stack (Exxon 1983):

Specific Energy:	65 - 85 Wh/kg
Specific Power:	80 -100 W/kg
Energy Efficiency:	75 - 80 %
Life of this 52-cell stack:	650 deep cycles
Projected cost (OEM):	$ 30-50/kWh, mass-produced

Specific modifications allow optimization for maximum energy efficiency (90 % Zinc utilization) energy density (100 Wh/kg) and power density (150 W/kg), of course not all in the same battery.

The cycling of multiple Bromine-Bromine cells to test carbon materials is done at the Technical University Graz. With improved active carbon layers, the life of electrodes has been proven to be over 1500 deep cycles at the 3 hour rate.

Applications:

The technology will be adapted for load levelling, storage of wind- and solar power and electric vehicle propulsion. In all this applications a battery must demonstrate low cost, high efficiency, and voltages compatible with existing electrical systems.

The Zinc-Bromium System is produced by the "Studiengesellschaft für Energiespeicher und Antriebssysteme GmbH, (S.E.A)", in Mürzzuschlag, Austria. **Fig. 1** shows a portable 12 V, 2 kWh Zinc-Bromine Battery on the test stand.

Acknowledgements:

Research on carbon materials suitable for zinc-bromine cells is supported by the Austrian Federal Ministery of Science and Research. The study of a hybrid system Motorgenerator/Battery is sponsored by the Styrian State Government. **Fig. 2** shows our experimental battery-operated electric vehicle with a trailer, containing the motorgenerator (350 cm^3 displacement, 7 kW dc electrical output).

Literature (with more references):

1. P. Grimes, R. Bellows, P. Malachesky (Exxon R&E), 19th Intersociety Energy Conversion Engineering Conference (IECEC) - 1984, Vol.2, paper No. 849444.
2. R.P. Clark, J.L. Chamberlin, H.J.Saxton, P.C. Symons: "The Status of Flow-Batteries in the USA", Power Sources 9, pp. 271-285, Academic Press, 1983.

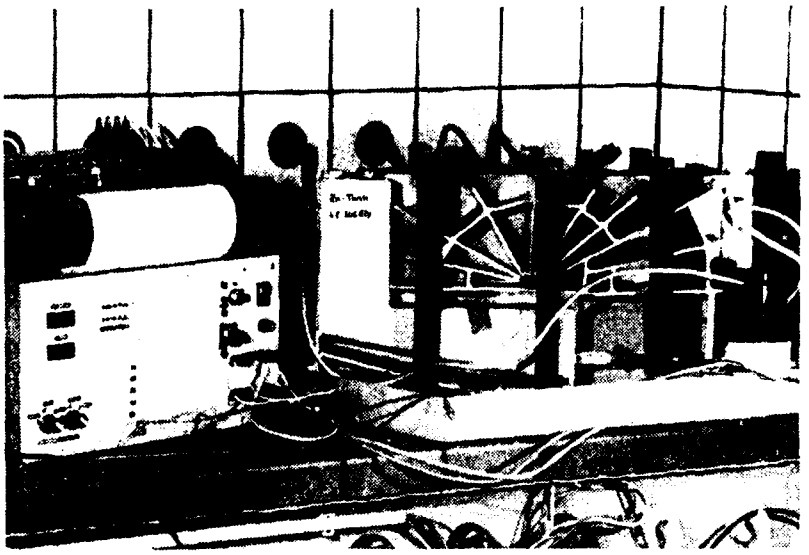

Figure 1: Laboratory Test on a 12 V, 2 KWh Zinc-Bromine Battery. This portable system is built with bipolar carbon-plastic plates and sealed on all sides. (Courtesy of S.E.A., GmbH, Austria).

Figure 2: The Electric Car of the Technical University Graz, used for field testing of Hybrid Systems: The 7.5-kW ac Motorgenerator (a HONDA 350 cm³ watercooled engine plus diodes) is mounted in a trailer. It can be connected to vehicles with different batteries, like lead-acid, zinc-bromine, and fuel cell systems, when available.

07250

ELECTROLYTIC MANGANESE DIOXIDE PRODUCTION IN A FLOWING ELECTROLYTE SYSTEM

W.J. Harer and K. Kordesch
Institut fuer Chemische Technologie Anorganischer
Stoffe der Technischen Universität Graz
A-8010 Graz, Austria

Electrolytic manganese dioxide for high quality Leclanche cells and alkaline batteries is a large scale product[1] . The deposition on lead-, carbon-, or titanium electrodes is well optimized. International Common Samples are available as comparison materials[2] .

In our laboratory we have investigated different types of manganese dioxides in respect to their rechargeability[3] . It turned out that there is no obvious direct relationship between porosity, particle size, surface area or analytical data and the rechargeability of gamma manganese dioxide. However, a strong dependance on physical parameters of the manufactured electrodes was found[4] .

It was found that the way of making the electrolytic manganese dioxide did influence the rechargeability[5] . Among other effects, adding small amounts of titanium salts, especially the sulfide, improved the cycle number[6] .

For that reason it was decided to start a series of experiments in which the manganese dioxide was produced without forming a solid deposit (layer) on an electrode at high temperatures (90 Deg.C) as is the common approach. A change in the deposition mechanismus takes place at lower temperatures, the manganese dioxide is formed according to a disproportionation reaction which was already discribed by Welsh[7] . The current yield of this process is poor, but the manganese dioxide has quite different properties, at low temperatures it forms a fine divided suspension and can be collected by settling out in the lower portion of the electrolysis unit. To make sure that no further changes occur, the collecting vessel is even cooled to room temperature.

The material produced by the electrolysis is removed with electrolyte from the outlet and seperated from the solution. The solution, from which the product is seperated, is returned to the process and reused.

Figure 1 shows the reactor which was used to produce manganese dioxide in a continuous flow system. The temperature can be chosen from room temperature to 90 Deg. C. The reactor can be operated hot, the collector vessel can be cooled. Self casted lead-antimony electrodes and special coated titanium corrugated plate anodes were used in this reactor. Current densities amounded from 0,5 - 30 A/dm^2.

At elevated temperatures the reaction at the anode consists of several steps: an anodic oxidation (electrochemical step), a disproportionation- and a hydrolysis step and then dehydration[8] . The manganese dioxide deposits usually at a coherent solid layer. In order to avoid the layer formation, a turbolent boundary layer stream of electrolyte was necessary. The deposits break up in small particles and can also be continuously collected. The appearence of this manganese dioxide is different from the "low temperature product".

Several charges of electrolytic manganese dioxides were produced, they amount of 100 g to a few kg of materials and serve now as supply materials for analytical tests, determination of surfaces (B.E.T.-method) and pores distribution with a poriosimeter. The final testing is done now about behavior from rechargeability of manganese dioxide in alkaline electrolyte. The results will be reported in another paper.

REFERENCES

1) A. Kozawa, S. Yoshizawa and K. Takahashi, Electrochemistry of Manganese Dioxide, Batteries in Japan, Vol. 1, pp. 57-114, The ECS of Japan, 1971.

2) The I.C.-Sample Office, P.O.B. 45035, Cleveland, OH, 44145, USA

3) R. Chemelli, J. Gsellmann, G. Koerbler, K. Kordesch, 2nd International Manganese Dioxide Symposium, Vol. 2, pp. 150, Tokyo, 1980

4) K. Kordesch, J. Gsellmann, M. Peri, K. Tomantschger, Electrochimica Acta 26, pp. 1495-1504 (1981)

5) W. Harer, Studies for the Dipl.-Ing., Technical University Graz, Austria 1982, continued as Doctor Thesis 1983.

6) J. Gsellmann, W. Harer, K. Holzleithner, K. Kordesch, Proc., Symposium on Manganese Dioxide Electrodes, pp. 567-578, ECS-Meeting, Oct. 1984

7) J.Y. Welsh, Electrochemical Technology 5, No. 11-12 (1967)

8) Eberhard Preisler, "Moderne Verfahren der Großchemie: Braunstein", Serie Chemie in unserer Zeit, Jahrg. 14, pp. 137, GDCh, Oct. 1980, see also:
E. Preisler, Journal of Applied Electrochem. 6, pp. 301-310, (1976).

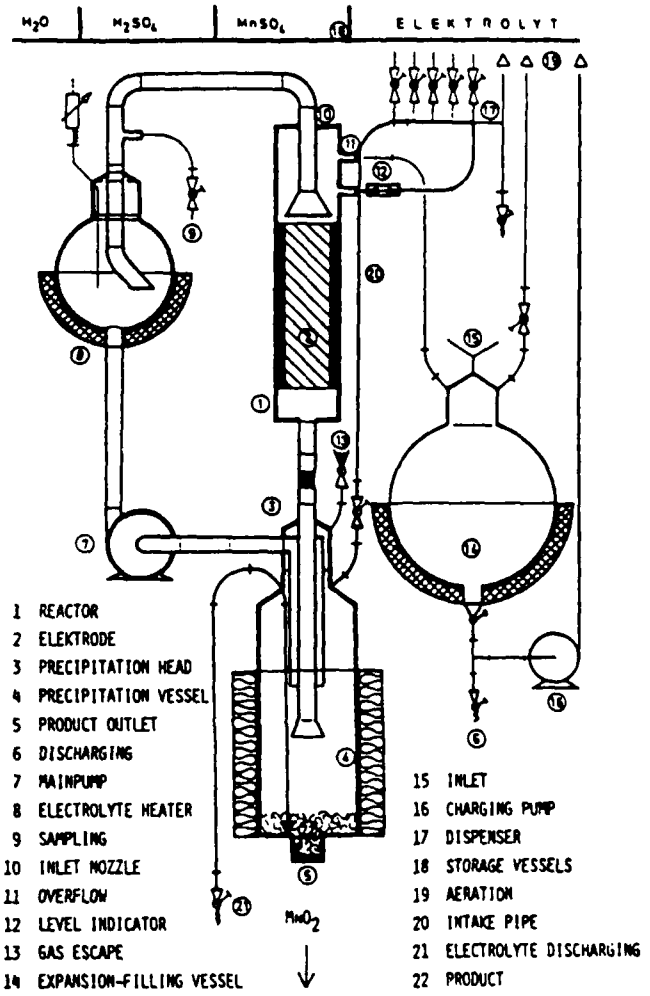

Fig.1: The Production of Manganese Dioxide in a flowing Electrolyte System.
Material for Lead Electrodes Supplied by the Bleiberger Bergwerks Union AG and Special Coated Titanelectrodes Supplied by CONRADTY GmbH & Co Metallelectrodes KG were used in this unit.

07260

IN SITU MONITORING OF SEMICONDUCTOR/LIQUID JUNCTION BY SIMULTANEOUS PHOTOCURRENT AND PHOTOTHERMAL DEFLECTION SPECTROSCOPY

J.P. ROGER, D. FOURNIER, A.C. BOCCARA
R. NOUFI[a] and D. CAHEN[b]
Laboratoire d'Optique Physique, E.S.P.C.I.
10, rue Vauquelin, 75231 PARIS CEDEX 05 - FRANCE
(a) Solar Energy Research Inst., GOLDEN CO. 80401 - U.S.A.
(b) The Weizmann Inst. of Science, REHOVOT 76100 - ISRAEL

In solar cells, and other optoelectronic devices, use of thin polycrystalline or amorphous films is desirable both because of possible cost savings and simplification of manufacture, and because of increased flexibility in choice of materials. The suitability of a film for such purpose will depend to a large extent on its optical properties. Generally these are not measured for the film in the actual device configuration (or part of it), but rather on an optically transparent substrate to allow transmission measurements. It would clearly be preferable to perform such measurements on samples that resemble the device as close as possible, and in such a way that, after measurement, the samples can be used further, to complete device manufacture, for example.

Photothermal deflection spectroscopy (PDS or "Mirage effect") has been used successfully to study optical properties of amorphous silicon thin films[1,2] deposited on silica, glass or silicon substrates. In conjunction with Fourier Transform (FT) PDS becomes a powerful, fast and convenient method to obtain optical absorption spectra[2]. Its suitability for samples with rough surfaces, such as those commonly found for polycrystalline thin films deposited on rough, scattering substrates should extend its use considerably.

Here, we will report on the feasibility of PDS investigations on films of $CuInSe_2$ on Al_2O_3 or on Mo/Al_2O_3 and for comparison on a single crystal of $CuInSe_2$, and on the problems encountered in these studies, so as to enable realistic evaluations of the possibilities and limitations of PDS for the optical characterization of thin polycrystalline films. In addition, we present FT photocurrent spectroscopic results on a semiconductor ($CuInSe_2$)/liquid junction system.

As an example, Fig. 1 shows the FT PD spectra for three films. These data are used to determine the absorption coefficient multiplied by the thickness ℓ (by the thermal length μ for the single crystal) at photon energies close to the bandgap and the optical bandgap value. Films that were rich in Cu_2Se (sample 55) have shown no or very poorly resolved absorption edges. For Cu-poor samples (46) the absorption coefficient fits the relation $\alpha \propto (h\nu - E_g)^{1/2}/h\nu$ which indicates a direct allowed transition. When Mo is present on Al_2O_3 (46B), the strong subbandgap absorption which is obtained can be attributed to Mo. The signal induced by the Mo absorption is a roughly linear function of $h\nu$ in the 1 eV region, thus we can obtain $\alpha\ell$ for the $CuInSe_2$ film proper by simple substraction.

Results obtained on the single crystal sample (Fig. 2a, b) agree well with literature values. In this case, from the variation of the phase angle of the signal with photon energy, it was possible to determine that sub-bandgap absorption originated from the bulk rather than from the surface.

The numerical values obtained are reasonable ones, which is of importance for the further application of this methodology as part of the use of semiconductor/liquid junction systems for semiconductor characterization[3]. There, for the determination of numerical values of effective optoelectronic parameters, the doping density and minority carrier diffusion length, knowledge of α at photon energies close to the bandgap is necessary[4].

Fig. 2 and 3 show the FT PD spectra (and the absorption spectra) and the FT photocurrent (η) spectra for the single crystal and the film 46B respectively. For these experiments, we used an acetonitrile-based redox electrolyte[3]. The significant shift seen in Fig. 2 between the photocurrent and PD spectra is mainly due to the difference between the thermal diffusion length ($\sim$ 100 μm) and the electron diffusion length ($\sim$ 1 μm) which causes different depths of the sample to be probed by the two methods. This difference is much less significant in the case of the film where the thickness ($\sim$ 4 μm) rather than the thermal diffusion length controls the PD signal. None of the two photocurrent spectra fits the expected $(h\nu.\eta)^2$ vs.$h\nu$ behavior as do the absorption coefficients. At least in the case of thin film this could indicate that the expected proportionality between α and η breaks down.

The possibility to obtain quantitative optical data for rough semiconducting films on scattering substrates in addition to the possibility of direct comparison of absorption and quantum yield spectra, should make PDS measurements a valuable addition to methodologies for the characterization of such films on conducting substrates.

ACKNOWLEDGEMENTS :

We thank R.A. Mickelsen (Boeing Engineering Co.) and F.A. Thiel (A.T. and T. Bell Labs.) for thin film and single crystals samples, resp. D.C. thanks the U.S. - Israel Binational Science Foundation, Jerusalem, Israel, for partial support.

REFERENCES

1. W.B. Jackson, N.M. Amer, D. Fournier and A.C. Boccara, Technical Digest, 2nd Int. topical meeting on Photoacoustic Spectroscopy, Berkeley, June 1981, and W.B. Jackson and N.M. Amer, Phys. Rev. B.25 (1982) 5529.
2. D. Fournier, A.C. Boccara and J. Badoz, Appl. Opt. 21 (1982) 74.
3. D. Cahen, Y.W. Chen, P.J. Ireland, R. Noufi, J.A. Turner, K.J. Bachmann and C. Rincon, Proc. 17th IEEE Photovolt. Spec. Conf., IEEE, N.Y. (1984) 786-791 ; Y.W. Chen, D. Cahen, R. Noufi, J.A. Turner, Solar Cells, in press.
4. Cf. Y. Mirovsky, D. Cahen, G. Hodes, R. Tenne, W. Giriat, Solar En. Mater., 4, 169 (1981).

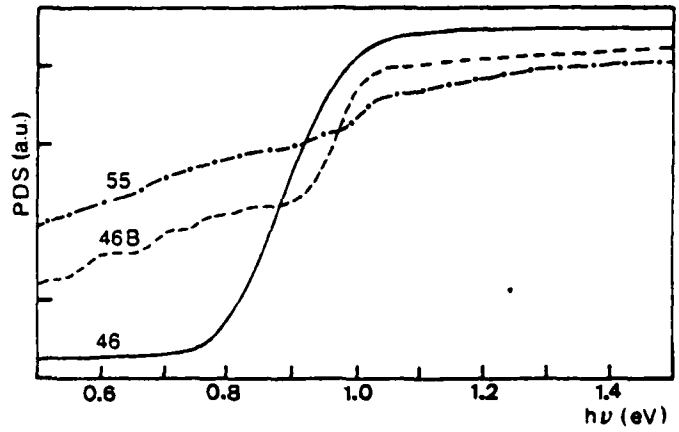

Fig. 1 -Normalized photothermal deflection spectra for three $CuInSe_2$ films. Samples 55 and 46 are on Al_2O_3 ; sample 46B is on Mo/Al_2O_3.

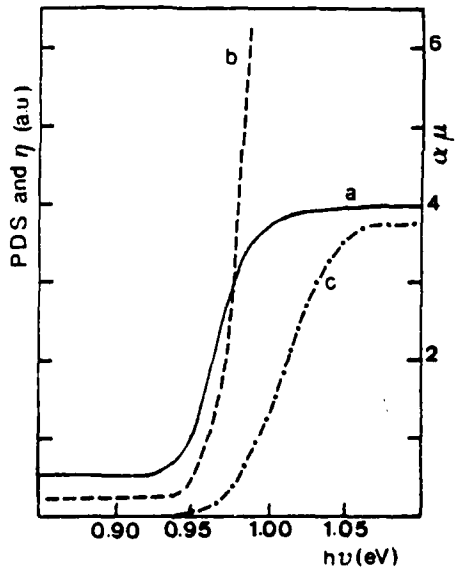

Fig. 2 - $CuInSe_2$ crystal ; (a) normalized amplitude of photothermal deflection spectrum ; (b) $\alpha\mu$ ($\alpha\mu$ = 1 corresponds to $\alpha = 1.3 \times 10^4\ cm^{-1}$) ; (c) normalized photocurrent (η) spectrum.

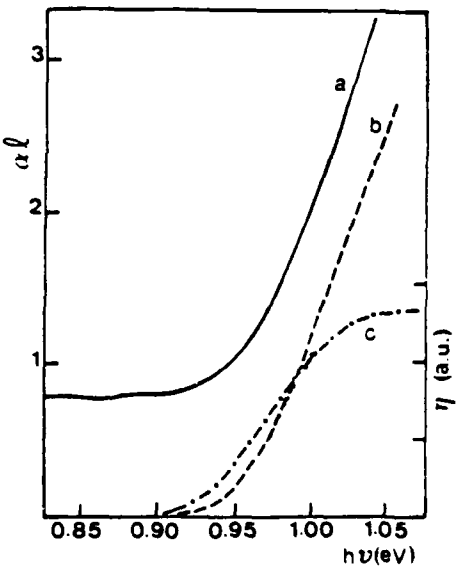

Fig. 3 - $CuInSe_2$ on Mo/Al_2O_3 (46B) : (a) $\alpha\ell$ as a function of photon energy : (b) $\alpha\ell$ after substraction of Mo absorption from curve (a) ; (c) normalized photocurrent (η) spectrum.

07270

ELECTRODEPOSITION OF ZINC USING PULSE-CURRENT.

L. BINDER
Institute for Inorganic Chemical Technology, Techn.University
A-8010 Graz, Austria.

For improving the quality of metal deposits, periodically changing current has been applicated for a relatively long time.

In 1971 Despić and Popov[1] and some years later N. Ibl[2] collected the available informations on this topic, adding their own practical experiences and theoretical considerations.

Reversing current, a.c. superimposed on d.c., and pulsating current were used to overcome the detrimental phenomena due to inhibited diffusion of the depositing substance through a diffusion layer which is steadily extending into the solution under d.c.-conditions of electrolysis.

Reversing current and asymmetric current (a.c. superimposed on d.c.) contain periods with an anodic (dissolving) current flowing. This current should cut off the most active sites of the deposit combining an electropolishing effect upon the surface with the prevention of a too low concentration of metal ions in the diffusion layer. The relaxation periods of the pulsating current should provide an equalization of the concentration of metal ions near the surface of the deposit with the concentration in the bulk solution.

These advantages can be combined by the application of a current consisting of at least three components, a cathodic (depositing) current, an anodic (dissolving) current, and a pause. Such a sequence was proposed by Appelt and Jurewicz for the deposition of zinc[3,4,5]. It was called "three-component impulse current (T.C.I.C.)" and the deposits were regarded as sufficiently porous and adherent to be used as storage battery electrodes.

To generate the required pulse sequence for the following experiments, a simple self-made electronic device was used. This generator controlled a laboratory potentiostat (Wenking, LB 75M) run as galvanostat. The resulting pulse-current was fed into the test-cell. The electrode arrangement can be seen in Fig.1. It consisted of two sheets of separator, an U-shaped frame made from polymethacrylate, carrying the counter electrode made from porous nickel, a spacer (polymethacrylate), and the working electrode. The latter was a copper foil (series F) or a copper wire grid (series G), covered with epoxy-resin (hatched area) so that an exposed geometrical area of 10 cm^2 remained. The components were stuck together using a solution of acetylcellulose in acetone with appropriate viscosity.

When the described cell-stack was inserted into the empty reaction-vessel, the chosen electrolytes were filled in the two compartments: KOH with zincate in the larger working electrode-space and zincate-free KOH in the smaller counter electrode-space. The concentration of zincate-ions was chosen in this way that after a zinc deposition of 0,3 Ah only 15% (series 2) of the initial amount of zinc remained in the solution.

The applied current densities were 2,5,10,15,20, and 30 $mA.cm^{-2}$. All the depositions were made with d.c. and "multi-component pulse-current (m.c.p.-current)" in parallel. The m.c.p.-current consisted of a cathodic pulse of 5 milliseconds, an anodic pulse of 5 milliseconds, and a pause lasting 10 milliseconds. So the whole sequence repeated after 20 milliseconds, that means with a frequency of 50 Hz. The cathodic and anodic amplitudes resulted in effective cathodic current densities according to the applied d.c. values. The ratio of cathodic to anodic amplitudes was 5 to 2. The deposition time varied with the applied current density to provide in any case a maximum Ah-capacity of 0,3 (100% current-efficiency for zinc deposition assumed). After deposition the zinc was redissolved at a constant anodic d.c. and a current density of 15 $mA.cm^{-2}$. The time to the point of exhaustion of the previously prepared zinc electrode was measured and the obtained Ah-capacity was compared with the input of 0,3 Ah for deposition.

The results of series 2, where 85% of the available zinc was deposited and only 15% zinc remained in the electrolyte, can be seen in Fig.2.

Series 2-F (above) with copper foil as substrate yielded significantly better deposits when the charging was done with m.c.p.-current instead of d.c.. But the average current efficiency over the whole range of current densities could not be raised over 60%. At the highest current density of this series (30 $mA.cm^{-2}$) the difference between d.c.- and m.c.p.-charging was about 20%.

A very different picture resulted when copper wire grid was used as substrate (series 2-G, below). The average current efficiency increased and noticeable effects of m.c.p.-charging were evident only between 5 $mA.cm^{-2}$ and 15 $mA.cm^{-2}$.

An additional observation was made when the standard deviations of the parallel measurements were calculated. In series 2-G the reproduceability of the d.c.-measurements was better over the whole range of current densities. Series 2-G was the only one which showed this behaviour.

References.

1 A.R. Despić and K.I. Popov, Mod. Aspects Electrochem., 7(1972)199.
2 N. Ibl, Surface Technology, 10(1980)81.
3 K. Appelt and K. Jurewicz, Electrochimica Acta,24(1979)253.
4 K. Appelt and K. Jurewicz, J.of Power Sources,5(1980)235.
5 K. Appelt and K. Jurewicz, Electrochimica Acta,27(1982)1701.

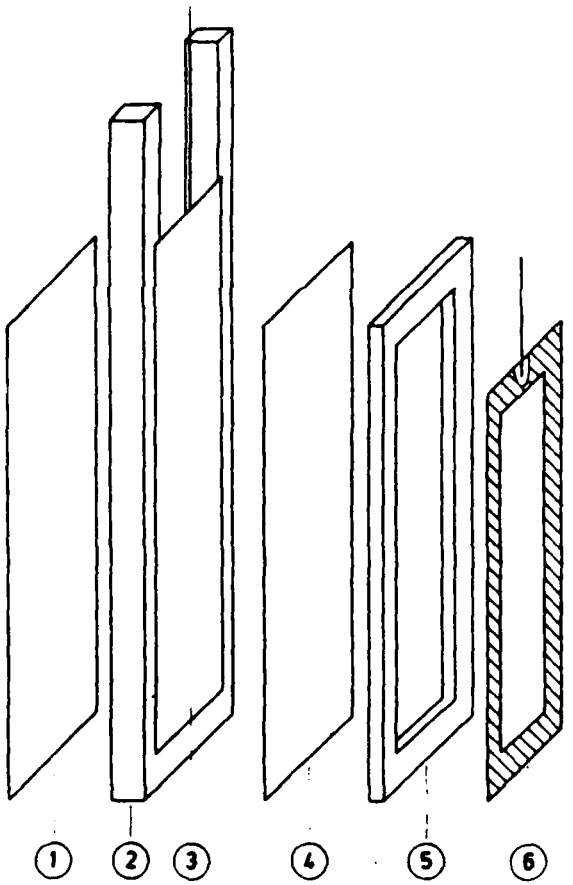

Fig.1. Electrode arrangement for deposition tests. 1-separator, 2-frame, 3-counter electrode, 4-separator, 5-spacer, 6-working electrode.

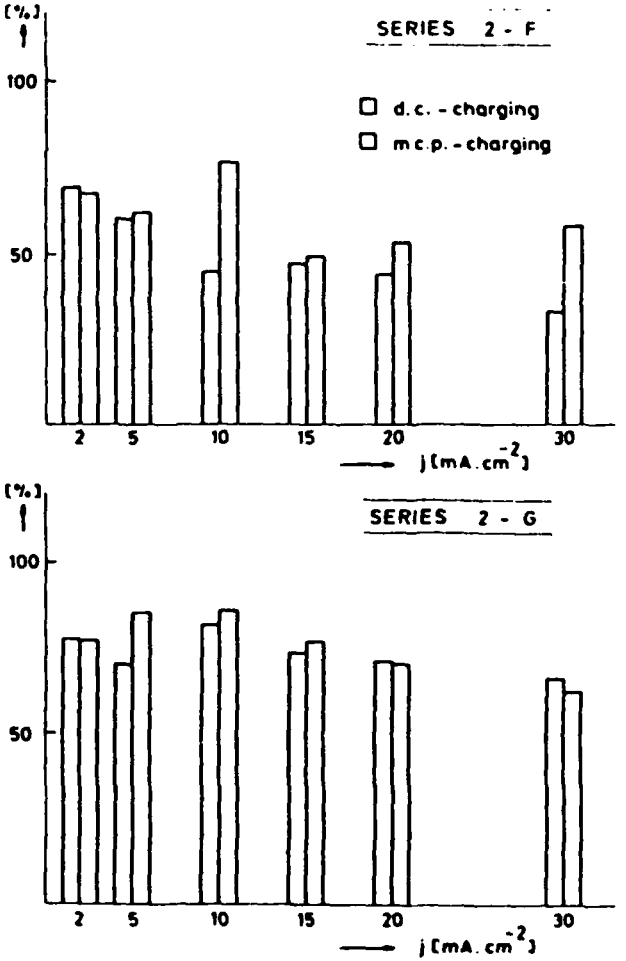

Fig.2. Results of deposition tests.

07272

07280

FOURIER ANALYSIS IN PRESENCE OF NONSTATIONARY APERIODIC NOISE

Z.STOYNOV , B.SAVOVA-STOYNOV
Central Laboratory of Electrochemical Power Sources,
Bul.Acad.Sci.,G.Bonchev Va,1040 Sofia,Bulgaria

The Fourier Analysis has a large scale of application in electrochemistry.According to the specific nonlinear nature of the electrochemical processes the small signal linearization approach allows the application of the linear relationship between the input/output signals and the application of the classical Transfer Function and Spectral Analysis definitions.Thus,in this cases the Fourier Analysis has to be performed in presence of large noises generated by the instrumental environment as well as by the system under investigation itself.

Following the classical frequency domain description of the stochastic processes the additive noise is very often presented by Fourier series with mutually independant zero mean random coefficients.Based on this Rice representation of the noise,many signal processing techniques have been developed and applied in electrochemistry.

However,in many real cases the filtering has to be performed in a finite time and the additive noise(or a part of the noise) is not statistically sufficient or is aperiodic and the Rice representation can not be used.Therefore,the investigation of the estimation properties under these conditions appears a central feature of the Fourier analysis in a finite time.

While the main signal is definite in the frequency domain,the aperiodic additive noise could be presented in the time domain by a power series

$$n_a(t) = \sum_{k=0}^{\infty} a_k t_r^k , \qquad (1)$$

where t_r is the relative time between the two spaces,and a_k are series coefficients having under given conditions the sense of a Taylor or orthogonal Legendre series representation.

$$n_a(t) = \sum_{k=0}^{\infty} \frac{t_r^k}{k!} n_a^{(k)}(t_0) \qquad (2)$$

Thus the noise is presented by its relative Taylor or Legendre spectrum.

The analysis of the errors of the finite time Fourier estimation of the periodic signal y(w) in presence of aperiodic noise $n_a(t)$ shows that in the general case the errors of the estimates can be presented as:

$$\varepsilon_{R(w,N)} = \frac{1}{R_y(w)} \sum_{k=0}^{\infty} L_{k-1} \frac{n_a^k(t_0)}{w^k} \qquad (3)$$

$$\varepsilon_{I}(w,N) = \frac{1}{X_y(w)} \sum_{k=0}^{\infty} L_k \frac{n_a^k(t_0)}{w^k} \quad , \qquad (4)$$

where $R_y(w)$ and $X_y(w)$ are the components of the periodic signal $y(w)$ and L_k forms the coefficient series

$$L_k = \frac{(2\pi N)^{k-1}}{k!} - L_{k-2} \quad ; \; L_0=0, \; L_1=1 \qquad (5)$$

where N is the number of the Fourier analysis estimation periods.

The relation (3),(4) show that in the presence of aperiodic noise the Fourier analysis becames an biased,unconsistent and unefficient estimator.In the practice the errors (3), (4) limit the precision in the low frequency short time analysis and the application of the infra low frequency impedancemetry.

The noise immunity properties of the classical finite time Fourier analysis could be improved.Taking into account the initial phase of the estimation in

$$R(w,N,t_i) = \frac{1}{NT} \int_{t_i}^{t_i+NT} X(t) \cos wt \, dt \qquad (6)$$

$$I(w,N,t_i) = \frac{1}{NT} \int_{t_i}^{t_i+NT} X(t) \sin wt \, dt \qquad (7)$$

where R and I are the estimates of the noisy signal X(t), we can define a Phase definite Fourier Transform(PFT).

The analysis of the estimation properties of the PFT shows that the initial phase t_i plays an important role in (6),(7).In the general case the errors of the PFT are:

$$\varepsilon_{R,I} = \sum_{k=0}^{\infty} f_k(L_k, n_a^{(k)}(t_0), w^k, t_i) \qquad (8)$$

While the classical Fourier Transformation estimator is orthogonal to the first - zero term in (1) or (2) ,the PFT can be designed as orthogonal to the next terms of the noise spectrum (1),(2).Choosing the appropriate values of t_i in(6), (7) the efficient noise rejection can be achieved.

If the noise is presented by a limit $k \leq n$ power series spectrum (1),the estimation procedure has to include m estimates

$$R_i(w,N,t_i) = R_y(w) + \sum_{i=1}^{n} \varepsilon_i \left\{ w,N,t_i,n_a^{(k)}(t_0) \right\} \qquad (9)$$

$$X_j(w,N,t_j) = X_y(w) + \sum_{j=1}^{n} \epsilon_j\left\{w,N,t_j,n_a^{(k)}(t_0)\right\} \qquad (10)$$

which are functions of t_i and the noise spectrum (2).

The solution of the system (9),(10) allows the determination of unbiased estimates $R_y(w)$,$X_y(w)$ as wll as the evaluation of the noise spectrum.

The optimal design of the short time PFT depends on the applications.The analysis of the convergence of the series (3),(4),(8) shows that for a given spectrum (2) of the noise and in a given frequency range $w \geq w_{min}$,the series (3),(4) and (8) are fast convergent.Thus the noise spectrum (2) can be truncated and the system (9),(10) can be easily solved.

The Phase definite Fourier estimator-PFT (6),(7) is an generalization of the finite time Fourier Transform.In presence of an aperiodic noise presented by a finite power series,Taylor or Legendre spectrum,the optimal PFT is unbiased, consistent and efficient estimator.The application of the PFT for low frequency measurements could extend the range of the usable frequencies in the impedancemetry and supply an additional information about the slow processes.

07290

ELECTROLYTE-FREE ELECTROLYTIC HYDROGEN PEROXIDE

K. MUELLER, B. CARCER, R. KOETZ, and S. STUCKI
Brown Boveri Research Center, CH-5400 Baden, Switzerland

Electrochemical cells where the electrolyte is a sheet of ion-exchange polymer (IEP or solid polymer electrolyte) were developed, originally for fuel reactions (GE's hydrogen-oxygen fuel cells), later for the electrolysis of water, hydrochloric acid, and sodium chloride solutions as well as for organic electrosynthesis [1]. The common feature in these applications is bifunctionality of the ion-exchange membrane (separator and ionic conductor).

In recent work at Brown Boveri, an exploratory effort was made to produce electrolyte-free hydrogen peroxide in such cells by oxygen reduction at a cathode/IEP interface:

$$H_2O \rightarrow 2\,H^+(aq) + 2\,e^- + 1/2\,O_2 \qquad \text{anode/IEP interface} \qquad (1)$$

$$O_2 + 2\,H^+(aq) + 2\,e^- \rightarrow H_2O_2(aq) \qquad \text{cathode/IEP interface} \qquad (2)$$

$$1/2\,O_2 + H_2O \rightarrow H_2O_2(aq) \qquad \text{cell reaction} \qquad (3)$$

First results are reported here.

The preparative efforts were preceded by ring-disc experiments. These had the purpose of identifying cathode materials which would cathodically reduce oxygen to hydrogen peroxide in an acidic environment (arbitrarily, 1 N H_2SO_4). Results are shown in Fig. 1 for glassy carbon, which was identified as the most suitable cathode material.

In Fig. 1, the dashed line was obtained in nitrogen-saturated 1 N H_2SO_4; it must correspond to cathodic hydrogen evolution. The dotted lines were obtained in the same electrolyte containing increasing amounts of H_2O_2; they chiefly correspond to hydrogen peroxide reduction. The solid line was obtained in peroxide-free, oxygen-saturated 1 N H_2SO_4; it corresponds, for the most part, to cathodic oxygen reduction. In its plateau, peroxide is produced, as identified by corresponding ring currents.

The intersections between the solid line and the dotted lines in Fig. 1 indicate that by continued oxygen reduction, the hydrogen peroxide concentration in solution can be built up to a certain level. When this is reached, equivalent amounts of the intended product H_2O_2 are formed by cathodic O_2 reduction and destroyed by further reduction, and the current efficiency drops to zero. Below this concentration limit, higher efficiencies can be attained. More than 80 % current efficiency were attained at low product concentrations in the solution. The relationship between current efficiency and product concentration is shown in Fig. 2 (curve $\eta[lim]$-$c[lim]$).

Higher oxygen concentration in solution will raise the currents of oxygen reduction to a proportionately higher level, and for any given operating potential, the intersections (Fig. 1) will then occur at higher current densities and higher product concentrations.

The preparative work was carried out in solid polymer electrolyte cells at an oxygen pressure of about 30 bar. The basic cell design was as described previously [2]. The anode was platinized titanium. The cathode was a porous glassy-carbon structure [3]. The electrodes were separated by Nafion(R) sheet. When (wet) oxygen was passed through the porous cathode, electrolyte-free Hydrogen peroxide solution could be collected. The maximum concentration achieved was 0.7 %. The water in the product was that transported across the Nafion sheet with the migrating protons. The current efficiency, however, was mere fractions of one percent only.

For more rapid removal of product H_2O_2 from the interface region, the Nafion sheet was replaced by a porous Nafion structure (Nafion powder bed or, simply, perforated Nafion sheet), and oxygen was admitted to the cell together with a variable water stream on the anode side, so as to set up a percolating system (filtering diaphragm). The oxygen reached the cathode/electrolyte interface through the pore space in the electrolyte, together with variable amounts of water. Hydrogen ions (see Eq. (2)) still were only transported through the solid electrolyte. Thus, electrolyte-free hydrogen peroxide could be produced as dilute aqueous solutions. In this fashion, current efficiency goes up dramatically. The values of efficiency that can be attained are a strong function of water flow rate. Some results (from experiments with a cell arrangement which was not optimized for reactant flow) are superimposed upon the curve of Fig. 2 (traces labelled 1.9 and 2.5 V: water flow rate increasing from right to left along the trace; trace labelled 150 ml/h: cell voltage increasing from top to bottom along the trace). Current efficiency is seen to be in an inverse relationship with product concentration. The latest ring-disc results show that compromise figures of (simultaneously) 60 to 80 % current efficiency and 3 to 0.5 % hydrogen peroxide concentration, respectively, can be attained in principle.

The strong effect of water flow rate means that, for acceptable efficiency, in any given cell design a fairly high water flow rate should be maintained. A current of proportionate density should then be passed at the cathode if, simultaneously, acceptable product concentrations are to be reached. Higher current densities can be attained at higher cell operating potentials. Here, H_2O_2 concentration was found to go up substantially (solid line, Fig. 3). The current efficiency, however, dropped under the same conditions (solid line, Fig. 4), but not so much as to offset the gains in concentration (and productivity). The loss in current efficiency implies that hydrogen is evolved, and other means must be sought to improve the current density. Several possibilities have been identified from work on oxygen reduction reported in the literature.

[1] K. H. Simmrock, E. Griesenbeck, J. Joerissen, and R. Rodermund, Chem. Ing. Techn., 53 (1) 10 - 25 (1981).
[2] K. Mueller, C. Schueler, and S. Stucki, Rendiconti, 84a Riun. Annu. Assoc. Elettrotec. Elettron. It., Mem. A 39 (1983).
[3] Swiss Patent Appl. 6058-84.

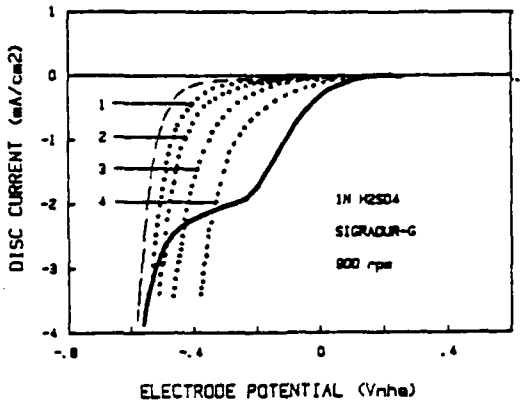

Fig. 1 Reduction currents at glassy carbon (RRDE results). The peroxide concentrations: 0.4 (1), 0.8 (2), 1.5 (3), and 3.0 % (4).

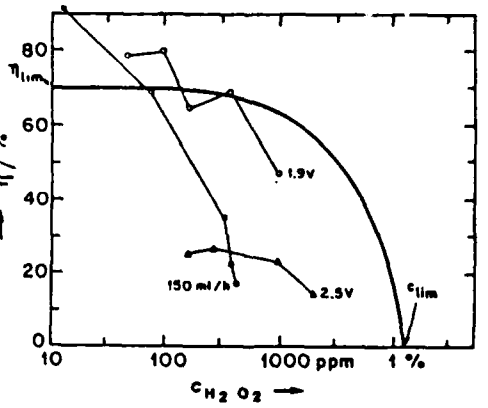

Fig. 2 Experimental current yields and hydrogen peroxide concentrations. The heavy "limiting" line: RRDE results. Other traces: preparative work.

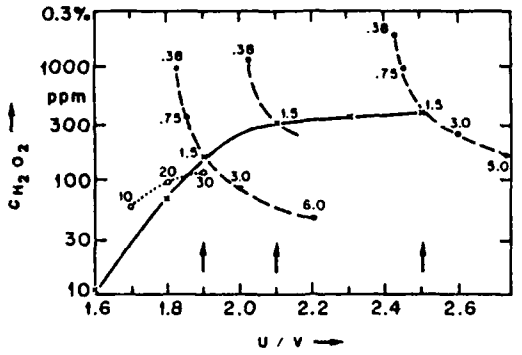

Fig. 3 Hydrogen peroxide concentrations, c, as functions of cell voltage, U (the solid line), water flow rate (dashed lines), and pressure (dotted line).

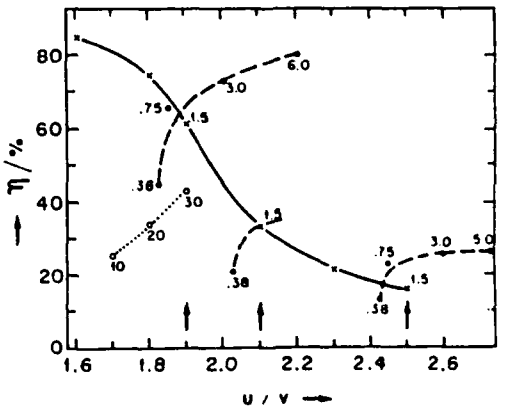

Fig. 4 Current yields, η, as functions of cell voltage, U (the solid line), water flow rate (dashed lines), and pressure (dotted line).

07300

NONLINEAR EFFECTS IN ELECTROCHEMICAL CELLS SUBJECTED TO ALTERNATING CURRENT AND MAGNETIC FIELD

A. SHORYGIN and G. DANIELYAN
Institute of Control Sciences, Moscow (USSR)

The effect of alternating current on electrochemical cells is the subject of many papers. These give most attention, however, to relatively high frequencies such as those applied in conductometry or to very low frequencies used in coulometric experiments. The intermediate range of infrasoninc and low audio frequencies is explored unsufficiently.
In the low infrasonic part of the frequency spectrum new effects in electrochemical cells such as resonance absorption and parametric oscillation could be expected since these cells under certain conditions tend to generate oscillations with frequencies of several Cps or lower. The evidence of such processes are voltage drop alteration across the cell, visualy observed pulsations in the interelectrode gap media and the change of the interferometric image obtained by the authors with visible monochromatic light [3].
The influence of A.C. in the infrasonic frequency range on D.C. current-voltage characteristics and on the phenomena observed in the cell were studied in the current-controlled process. The superposition of A.C. on D.C. was performed by means of the resistive adding network . The usual dependence of D.C. equivalent resistance on the direct current is U-shaped[4] . When the infrasonic A.C. is superimposed on D.C., the right-hand part of the curve drops. At the same time that part of the curve obtains a pronounced first wave maximum. With increasing A.C. amplitude the maxima move toward higher D.C. values, the displacement increases almost directly as the A.C. amplitude. Further studies revealed the existence of threshold and quasi-hysteresis effects with continuous change of both the frequency and amplitude of the superimposed alternating current. With the A.C. amplitude (or frequency) being within the loop parts of the curve no partial hysteresis loops could be obtained. This is the evidence of the auto-oscillating nature of the process. Further experiments using a wide range of the parameter values in the A.C. generator output circuit and in the D.C. circuit showed that the observed phenomena are independent of external network characteristics and so are caused by factors inherent in the cell itself. Microscopic observations of process in the cells showed a conformity of the quasihysteresis electric characteristics and the variation of optical pictures in the interelectrode gap. Small values of D.C. resistance match a zone of low frequency fluctuations observed (below 1 Cps). With the increase of frequency D.C. impedance reachs its largest value when these fluctuations cease abruptly.

These results lead us to conclude that the threshold and quasihysteresis effects found by the authors are due to parametric excitation which arises in the electrochemical system with certain relations of frequencies and amplitudes. The effect of the magnetic field was studied also in the current-controlled process. If the magnetic induction vector is normal to the gravity vector and the cell is in the anode up position, the D.C. impedance R increases with the magnetic field. With the same arrangement, but in anode down position, the change remains within the limits of the measurement error. Thus it could be admited that unlike the case of solid state semiconductors, the magnetoresistive effect in electrolythic cells is caused by combined action of the Lorentz and the Archimedes forces; when these add up the electrochemical convection increases, and the cell resistance falls.
Numerous experiments with the superposition of infrasonic alternating current show that with a constant magnetic field the extrema in the equivalent resistance - D.C. current characteristics become more pronounced. Of the greatest interest is the range of large D.C. and A.C. in which the streamlines and isoconcentrates systems in the interelectrode gap change abruptly and the right-hand part of the characteristic of the cell subjected to a magnetic field (independent of its sign) go up dramatically. The frequency quasihysteresis is seen to disappear.
With the cell in anode up position quasihysteresis in the dependence D.C. impedance on magnetic field induction was found. The effect is proved irreversible: to recover the initial cell state the direct current should be switched off and then switched on again. The plot retains its shape with any direction of the induction vector when this remains normal to the cell longitudinal axis.

References

1. Shorygin A.P., Kazaryan E.V. Gvaramadze I.L. Elektrokhimiya, vol.7, 414-417, (1971).
2. Shorygin A.P., Kazaryan E.V. Elektrokhimiya, vol.9, 1223-1225, (1973).
3. Shorygin A.P., Danielyan G.L. Elektrokhimiya, vol.8, 777-780, (1972).
4. Shorygin A.P., Gvaramadze L.L. Elektrokhimiya, vol.9, 860-864, (1973).

07310

LEAD OXIDES AS CATHODIC MATERIALS FOR VOLTAGE COMPATIBLE LITHIUM CELLS

L. PERALDO BICELLI, F. BONINO and B. RIVOLTA
Department of Applied Physical Chemistry of the Milan Polytechnic
Research Centre on Electrode Processes of the C.N.R., Milan (Italy)

Recently, the attention has been focused on organic electrolyte lithium cells having a working voltage in a range (1.2 - 1.5 V) close to that of conventional systems. These so called "voltage compatible" lithium batteries are thus expected to be interchangeable with conventional primary cells without a remarkable modification of the existing equipment.

Numerous research activities are currently under way on this new class of lithium batteries. The use of lithium as an anode offers many performance advantages over conventional batteries. First, the advantage of a substantial increase in energy density which results in a reduction of the battery size or in an increase of its service life. Of equal importance is the long shelf life of the lithium systems presenting the opportunity for new applications.

Different cathodic materials have been considered, including lead oxides (1,2). PbO and PbO_2 (1) have also been examined; however, a complete investigation was mainly undertaken on the performance of Pb_3O_4 and $Bi_2Pb_2O_5$, only (1,2).

Within a research programme on metal oxides in non aqueous lithium cells (3) and with the aim of going deep into the basic knowledge of lead oxides, yellow PbO and βPbO_2 have been examined as possible alternative materials in "voltage compatible" lithium batteries.

RESULTS AND DISCUSSION

The cathodic pellets of both PbO and PbO_2 were obtained by compressing the powders at 350 MPa on a copper support.

The experiments were performed at ambient temperature in a two-electrode cell of the type:

(-) Li/electrolyte/lead oxide (+) .

Four electrolytes were tested in order to select the one giving the best results, namely: 1 M $LiClO_4$ - propylene carbonate (PC); 0.5 M $LiCF_3SO_3$-PC; 1 M $LiAsF_6$ - γ butirolactone (BL); 1 M $LiCF_3SO_3$-BL.

A great difference in behaviour was observed, the $LiClO_4$-PC electrolyte showing the most satisfactory performance (Fig. 1). Hence, this electrolyte was chosen for the further development of the research.

Typical discharge curves at various current densities are reported in Fig. 2 and 3 for PbO and PbO_2, respectively. The composition parameter in

abscissa refers to lithium equivalents inserted into one mole of the oxide.

The striking feature of the curves is a very long plateau at a voltage around 1.3 V vs. Li/Li^+ (at a current density of 0.5 $mA.cm^{-2}$), suggesting the formation of a new phase.

X-ray analysis of the end products showed that the discharge process mainly consists in a displacement reaction. In fact, lead diffraction peaks completely dominate the X-ray spectrum of the discharged material. This result is also in agreement with the discharge reaction approximately involving two and four Faraday per mole of PbO and PbO_2, respectively.

As already noted for other lead oxides, e.g. Pb_3O_4 (1,2), the discharge process of the Li/PbO_2 couple seems not to occur in steps, namely through a preliminary reduction step to PbO, followed by a subsequent step to lead.

Disappointlingly, PbO_2 shows an initial voltage drop with a very short quasi-plateau for low lithium insertion. Experiments are in due course to find out whether such plateau may be related to the presence of one or more electrochemically reducible impurities.

CONCLUSIONS

From this research, PbO and PbO_2 result to be particularly interesting as possible candidates for voltage compatible lithium cells owing to a very long plateau having the proper voltage value and an appreciable specific capacity and energy: 265 $Ah.kg^{-1}$ and 345 $Wh.kg^{-1}$, respectively for PbO; 370 $Ah.kg^{-1}$ and 475 $Wh.kg^{-1}$ for PbO_2 at a current density of 0.5 $mA.cm^{-2}$ and for a cut-off voltage of 1 V vs. Li/Li^+.

REFERENCES

(1) M. Broussely, Y. Jumel and J.P. Gabano, in J. Thompson (ed); Power Sources 7, Academic Press, London (1979) 637.
(2) M. Broussely, Y. Jumel and J.P. Gabano, J. Power Sources 5 (1980) 83.
(3) F. Bonino, L. Peraldo Bicelli, B. Rivolta, M. Lazzari and F. Festorazzi, Solid State Ionics, in print.

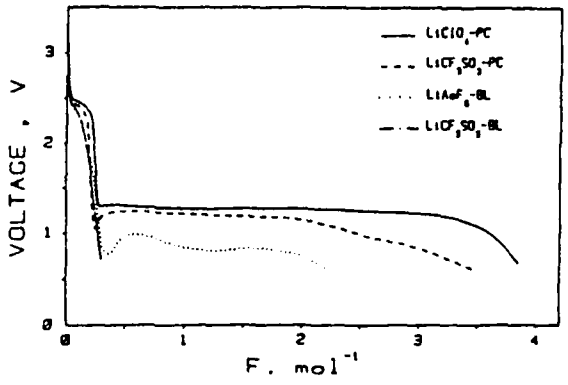

Fig. 1 Typical discharge curve of PbO_2 in four electrolytes and at room temperature.

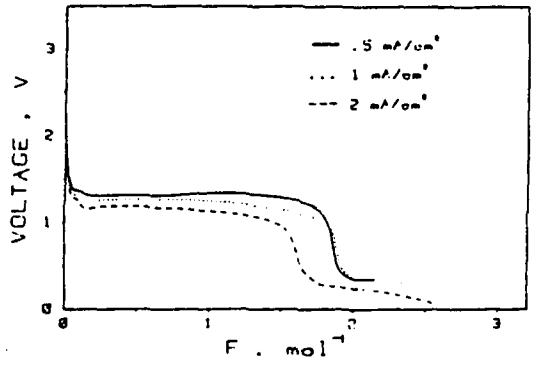

Fig. 2 Typical discharge curve of PbO in 1 M $LiClO_4$-PC at various current densities and at room temperature.

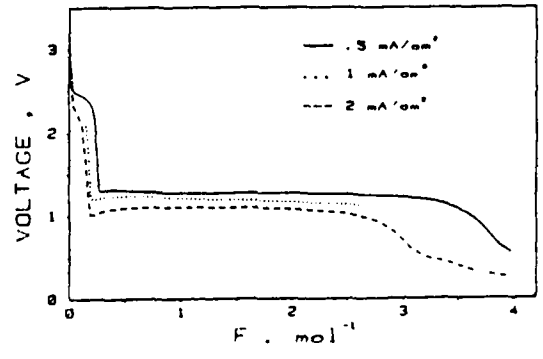

Fig. 3 Typical discharge curve of PbO_2 in 1 M $LiClO_4$-PC at various current densities and at room temperature.

07320

A 12% EFFICIENT PHOTOELECTROCHEMICAL CELL WITH POLYCRYSTALLINE n-$CuInSe_2$ ELECTRODES

G. RAZZINI, L. PERALDO BICELLI, B. SCROSATI[+] and L. ZANOTTI[o]
Department of Applied Physical Chemistry of the Milan Polytechnic,
Research Centre on Electrode Processes of the C.N.R., Milan (Italy)
+ Department of Chemistry, University of Rome "La Sapienza", Rome (Italy)
o MASPEC C.N.R., Parma (Italy)

The development of photoelectrochemical cells has been so far somewhat hindered by the relatively low conversion efficiency and the poor stability offered by the most common semiconductor/electrolyte systems.

Recently, there has been a renewed interest in the field due to the characterization of highly efficient and stable semiconductor electrodes selected among ternary chalcogenides of the chalcopyrite or spinel type.

Undoubtedly, the most promising material of this class is $CuInSe_2$, a direct band gap material having an optimum band gap value (around 1.04 eV). A very promising photoelectrochemical behaviour is therefore expected, as recently observed by Cahen et al. (1-3) and Lewerenz et al. (4-7) on single-crystal electrodes, properly selecting the nature and composition of the electrolyte solution.

Effectively, when a polyiodide electrolyte with suitable additions of Cu^+ and In^{3+} ions and of HI is used (3,5,7) and when the semiconductor surface is protected by an indium oxide film, an efficiency of 11.7% (3) and of 9.5% (5) is achieved.

These results certainly make the $CuInSe_2$ photoelectrochemical cells worth considering for practical applications. However, for successfully attaining this goal one must necessarily consider low-cost polycrystalline electrodes. So far the attempts in this direction have not been encouraging as efficiencies well below 1% have been obtained (4).

Therefore, we carried out a careful synthesis of n-$CuInSe_2$ polycrystalline samples, in order to establish their effective potentialities.

EXPERIMENTAL DETAILS

A direct synthesis from the melt of $CuInSe_2$ using stoichiometric amounts of 6N pure constituents elements in an evacuated (10^{-5} Torr) round bottom quartz ampoule was performed. Since indium reacts exothermally with selenium leading to the generation of unreacted selenium vapour, the ampoule was initially kept at 200°C for about 10 hours and then heated slowly (4-5°C/h) to melting. A complete homogenization was obtained keeping the melt at 1050°C for about 20 hours. Then the furnace was cooled gradually (20°C/h) to avoid ampoule cracking due to the thermal expansion of the melt on solid-

ification.

Following this procedure, we have obtained very homogeneous polycrystalline ingots in which the average grain size was in the 1-2 mm range. The material is of n type and has a resistivity of 2.6 ohm.cm.

Slices of about 1 mm thickness were cut from the ingots, mounted on a teflon holder having a current collector, polished and etched with a Br_2-MeOH (2%) solution. The samples were then polarized at -1 V (vs. SCE) for 5 minutes in an aqueous solution of 1 mM $In_2(SO_2)_3$ and 1 M Na_2SO_4 to electrodeposit an indium film on the surface of the semiconductor. The film was then oxidized by annealing at 130°C for 3 hours. The $CuInSe_2$ electrode so prepared was assembled in the photoelectrochemical cell following a procedure described in details elsewhere (8).

The electrolyte used was an aqueous solution of 2 M KI, 20 mM I_2 (generally indicated as polyiodide), with addition of CuI (20 mM), $In_2(SO_4)_3$ (20 mM) and of HI (2 M). The current-voltage curves of the $CuInSe_2$/polyiodide cell were obtained under a Xenon lamp of 100 $mW.cm^{-2}$ illumination.

RESULTS AND DISCUSSION

Similarly to what found for single-crystal electrodes (3,5,7), the performance of the polycrystalline n-$CuInSe_2$ samples is greatly influenced by surface treatments and electrolyte compositions. Under the best conditions, we observed a conversion efficiency of 12% (Fig. 1), which we believe is the highest value ever obtained with a photoelectrochemical cell based on polycrystalline electrodes. This value appears even more interesting considering that the cell was not optimized in terms of electrode separation and of light reflectivity.

The impressive behaviour shown by the curve of Fig. 1 is the result of various combined effects, which include an accurate synthesis of the polycrystalline samples, a suitable modification of their surface and convenient ion additions in the electrolyte.

In this last respect, particularly relevant is the role of the hydriodic acid (5), since its addition to the electrolyte dramatically improves the performance of the cell, both in terms of efficiency and stability.

Fig. 2 shows the trend of the output photocurrent under continuous illumination for a cell without (curve a) and with (curve b) addition to the polyiodide solution of CuI, $In_2(SO_4)_3$ and HI. In the latter case, the current remained practically unchanged for 60 hours. SEM examination of the electrode surface at the end of the test did not show surface modifications. These results point out the excellent stability of the polycrystalline n-$CuInSe_2$ electrode in the preferred electrolyte solution.

ACKNOWLEDGEMENTS

The authors are grateful to Miss L. Tenti for the experimental measurements. This work was carried out with the financial support of the Consiglio Nazionale delle Ricerche, PFE 2, Sottoprogetto Carbone e Idrogeno.

REFERENCES

(1) Y. Mirovski and D. Cahen, Appl. Phys. Lett. 40, 727 (1982).
(2) Y. Mirovski, G. Demjal and D. Cahen, Nuovo Cimento 2D, 2039 (1983).
(3) D. Cahen and Yih-Wen Chen, Appl. Phys. Lett. 45, 746 (1984).
(4) H.J. Lewerenz, H. Goslowsky and F.A. Thiel, Solar Energy Mat. 9, 160 (1983).
(5) S. Menezes, H.J. Lewerenz and K.J. Bachmann, Nature 305, 615 (1983).
(6) S. Menezes, H.J. Lewerenz, G. Betz, K.J. Bachmann and R. Kötz, J. Electrochem. Soc. 131, 3030 (1984).
(7) K.J. Bachmann, S. Menezes, R. Kötz, M. Fearheil and H.J. Lewerenz, Surface Science 138, 475 (1984).
(8) G. Razzini, M. Lazzari, L. Peraldo Bicelli, F. Lévy, L. De Angelis, F. Galluzzi, E. Scafé, L. Fornarini and B. Scrosati, J. Power Sources 6, 371 (1981)

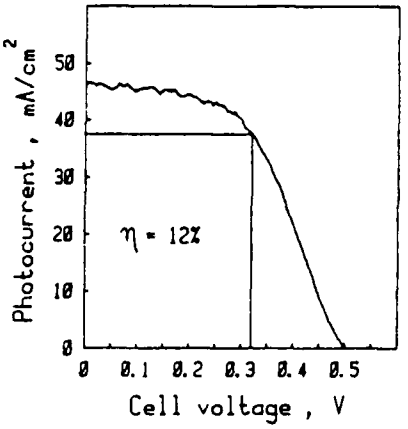

Fig.1 Photocurrent-photovoltage curve for the n-$CuInSe_2$ polycrystalline electrode coated with oxidized indium in 2M I^-, 20 mM I_2, 20 mM Cu^+, 20 mM In^{3+} and 2M HI solution, under nitrogen atmosphere.
Light power density = 100 mW/cm^2.

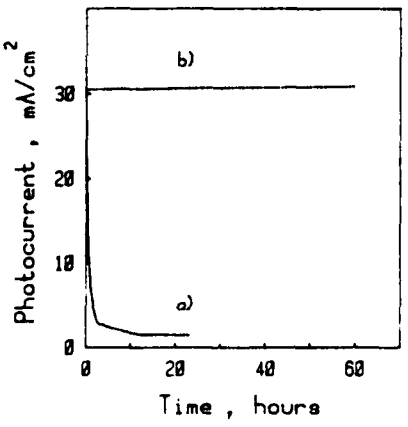

Fig.2 Photocurrent at maximum power output vs. time of the n-$CuInSe_2$ photoelectrochemical cell:

a) bare electrode in the polyiodide solution;

b) electrode coated with oxidized indium in the polyiodide solution with the addition of Cu^+, In^{3+} and HI.

08010

8

THE ELECTROCHEMICAL REDUCTION OF PYRAZINE IN HIGHLY ACIDIC SOLUTIONS. AN ADMITTANCE AND POLAROGRAPHIC STUDY

M. RUEDA[+], M. SLUYTERS-REHBACH and J. H. SLUYTERS
Van't Hoff Laboratory of Physical and Colloid Chemistry, State University, Padualaan 8, 3584CH Utrecht (The Netherlands)

+ Department of Applied Physical-Chemistry, Faculty of Farmacy , c/Tramontana s/n, Sevilla 41012 (Spain)

INTRODUCTION

The electrochemical behaviour of biologically important pyrazine/dihydropyrazine redox couple has been studied by several dc electrochemical techniques[1-6]. It seems well established, at present, that it is a dc reversible system in acid solutions involving the consecutive uptake of two electrons with formation of an intermediate radical cation whose stability strongly depends on pH.

However, there is no information about adsorption processes accompanying the electron transfers, although it is known that pyrazine itself is adsorbed at the mercury-water interface[7]. A small amplitude transient technique as the faradaic impedance measurement has been proved to be more suitable in making adsorption manifest within the faradaic region[8,9]. For this reason, and because it also provides quite complete information about the heterogeneous process and possible coupled homogeneous reactions[10], the application of this technique to organic electrode reactions seems wortwhile.

In this communication a combined impedance and dc polarographic analysis is presented for the reduction of pyrazine at the DME in aqueous solutions of pH 0.5 and 2.8.

RESULTS AND DISCUSSION

At pH 0.5 two overlapping one-electron waves show up and at pH 2.8 one two-electron wave. Under both conditions, the $\log j_F/(j_D-j_F)$ vs. E plots are indicative of a stepwise reversible mechanism.

Ac data also support this conclusion, but, in addition, they clearly show that the electrode process is complicated by adsorption. This is deduced from the facts: 1- The magnitude $C_{rev} = (Y'' - Y')/\omega$ is equal to the C_d value for the supporting electrolyte alone at potentials outside the faradaic region, but is much higher than C_d at potentials near $E_{\frac{1}{2}}$. 2- C_{rev} decreases with increasing frequency. 3- The $\omega^{1/2}/Y'$ vs $\omega^{1/2}$ plots are descendent.

In order to account for this behaviour the theory existing for the admittance in case of a reversible reaction with reactant adsorption[8] is extended to the case of a stepwise mechanism including adsorption of all species.

From the frequency analysis of the admittance the warburg

coefficient, σ and the adsorption parameters were obtained. The σ -E plots for solution of pH 0.5 can only be explained if the product of the second electron transfer is involved in a homogeneous reaction. The fit of experimental points to theoretical equations allows the standard potentials for the two electron transfers and the rate constant for the homogeneous reaction to be obtained. The potential dependence of adsorption parameters leads to the conclusion that the reactant, product and intermediate are adsorbed at the interface.

REFERENCES

1 - L.F. Wiggins and W.S. Wise, J.Chem.Soc. 4780 (1956)
2 - L.N. Klatt and R.L. Rousseff, J.Am.Chem.Soc. 94 (1972) 7295
3 - J. Volke and S. Beran, Coll.Czech.Chem.Comm. 40 (1975) 2232
4 - M. Maruyama and K. Murakami, J.Electroanal. Chem. 102 (1979) 221
5 - J. Swartz and F.C. Anson, J.Electroanal.Chem. 114 (1980) 117
6 - E.D. Moorhead and Britton, Anal. Letters, 1 (1968) 541
7 - a)B.E. Conway and H.P. Dhar, Croat.Chem.Acta 45 (1973) 109; b) B.E. Conway, J.G. Mathieson and H.P. Dhar, J.Phys.Chem. 78(12) (1974) 1226
8 - B. Timmer, M. Sluyters-Rehbach and J.H. Sluyters, J.Electroanal. Chem 18 (1968) 93; 19 (1968) 73
9 - M. Sluyters-Rehbach and J.H. Sluyters, J.Electroanal.Chem. 136 (1982) 39
10- M. Sluyters-Rehbach and J.H. Sluyters in "Comprehensive Treatise of Electrochemistry" vol. 9, J.O'M. Bockris, B.E. Conway and E. Yeager (Editors), Plenum Press, N.Y. 1984

08020

REDUCTION OF PYRIDOXAL 5'-PHOSPHATE IN ETHANOL-WATER SOLUTIONS ON A MERCURY ELECTRODE

R. IZQUIERDO, M. BLAZQUEZ, F. GARCIA-BLANCO AND M. DOMINGUEZ
Departamento de Quimica Fisica, Facultad de Ciencias,
Universidad de Cordoba, 14005 Cordoba (Spain)

INTRODUCTION

Pyridoxal-5'-phosphate (PLP) is a compound of well-known importance in enzimatic catalysis. Its action is a function of its enviroment. PLP is bonds via a Schiff base to an amino group of a polypeptide chain in hidrophobic or hidrophilic surrounding [1-3].

To correlate chemical properties and biological behaviour, different pattern compounds have been studied in which PLP is in Schiff bases with amino acids and amines [4-6]. However, the behaviour of PLP itself is not well-known, especially as regards its electrochemical reduction.

Several electrochemical studies conclude that PLP reduces on DME via a complex mechanism [7,8] Recently, we have reported its electrochemical behaviour in acidic medium in aqueous solutions [9], observing that in some aspects the reduction mechanism of PLP is not different from that of other aromatic aldehydes. Nevertheless, hydration-dehydration reaction of the carbonyl group seems to be subject to intramolecular catalysis [10,11]. This is an important difference from the behaviour of other carbonyl compounds of analogous structure.

The aim of this communication is to study the PLP reduction process in aqueous-ethanol solution in acidic medium in order to check previous results on the hydration-dehydration process in aqueous solutions and to show the influence of the dielectric constant on the overall reduction reaction.

EXPERIMENTAL

LCSV measurements were carried out using a wave generator mod. 305 of Belport a and fast potentiostat mod. 105 of Belport with compensation of the iR drop. Data were collected with a digital oscilloscope mod. Prowler from Norland provided with analog output. A HDME was used.

RESULTS AND DISCUSSION

In aqueous solutions and acid medium (pH<5.5), PLP yields two ill-defined polarographic waves. The overall reaction corresponding to the first wave involves one proton and one electron per molecule, giving rise to a free radical which is liable to dimerize. The second wave is due to a transfer of the one electron and one proton to yield the end reduction product, i.e. the corresponding alcohol [9].

The study of the capillary characteristics in the limiting zone of the total wave allows to state that a chemical reaction prior to the electron transfers controls the rate of the process. Thus, the log i_L vs log t plots are linear, with slopes of approximately 0.25, higher than the theoretical value for a diffusion-controlled process. The chemical reaction involves the dehydration of the carbonyl group of PLP, which is hydrated in aqueous solution . Although this kinetic effect has not been mentioned in the literature, it can be confirmed from the results obtained at low temperature. Thus, at 8°C the log i_L vs log t plot is linear, with a slope of 0.32, this increase indicating that the rate of a chemical reaction prior to the electron transfer has decreased.

With regard to the influence of the ethanol on the reduction process, the total limiting current decreases as the ethanol concentration increases (Figure 1a). Only one wave is observed at ethanol concentration above 30%. The $i_L (\eta/\eta_0)^{\frac{1}{2}}$ vs dielectric constant plot (Figure 1b) shows that the decrease in the current is not due to an increase in the solution viscosity as suggested for other solvents.

We have studied the influence of the capillary characteristics as a function of the ethanol content. The results found demonstrate that an increase in the prekinetic

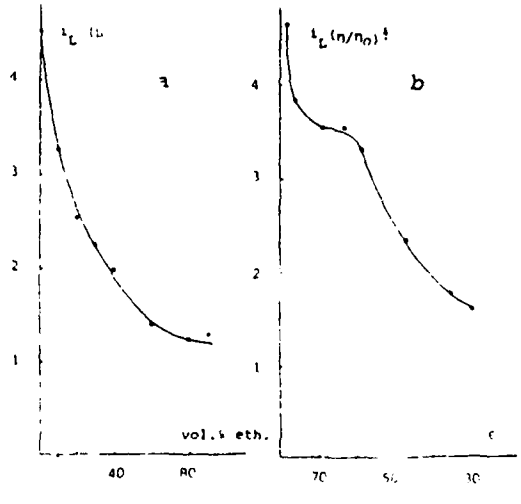

Figure 1

character is observed as the dielectric constant of the solution decreases. The log i_L vs log t plots are linear, with slopes ranging between 0.25-0.59 for ethanol concentrations in the range 0-90%.

The logarithmic analyses of the waves are linear in the etanol concentration range 30-90%. For lower contents, the deviations from linearly observed are due to the occurence of two very close waves. The slopes of the plots are approximately -37 mV/dec., characteristic of an irreversible

two-electron process. This fact is confirmed by the results of the influence of the drop time at potentials corresponding to the foot of the waves, since the slopes of the plots of log i vs log t are close to 0.67.

The study of the i-t curves on the rising portion of polarographic waves has permitted us to use the diagnostic criterion based on the time-independent function recently reported by Camacho[12]. Thus, the only function yielding linear plots is:

$$(i_L/i - 1)\ (i_D/i_L)\ t^{\frac{1}{2}}$$

which corresponds to prekinetic irreversible process.

From the i-E curves, Tafel slopes of -37 mV/dec have been obtained in the whole ethanol concentration range. The C-E curves traced at normal PLP concentrations show that for ethanol concentration above 40%, PLP is not appreciable absorbed on the DME.

The linear sweep cyclic voltammetric measurements yield two very close cathodic peaks at sweep rates lower than 1 V/s. Such peaks correspond to the two waves obtained in DC polarography. Only one cathodic step-shaped wave is observed at higher sweep rates, which is characteristic of a kinetic controlled process.

The results, therefore, are consitent with an irreversible process, partially controlled by a prior dehydration chemical reaction in the limiting zone, the kinetic control increasing with decreasing dielectric constant.

The results seem to indicate that the reported effect of the intramolecular catalysis decreases in a less polar medium.

REFERENCES

1. M.E.Goldberg, S.York and L.Stryer, Bioelectrochemistry, 7(1968)3662.
2. E.E.Snell, Vitamins Hormones, 28(1971)265.
3. S.Shatiel and M.Cortijo, Biochem. Biophys. Res. Commun, 41(1970)594.
4. H.N.Christensen, J.Am.Chem.Soc.,80(1958)99.
5. P.S.Tobias and R.G.Kallen, J.Am.Chem.Soc., 97(1975)6530.
6. C.M.Metzler, A.Cahill and D.E.Metzler, J .Am. Chem. Soc. 102 (1980)6075.
7. O.Manousek and P.Zuman, Collect. Czech. Chem. Commun., 29(1964)1432.
8. J.Llor and M.Cortijo, J.Chem.Soc.Perkin Trans. 2(1977)1715.
9. R.Izquierdo, M.Blazquez, M.Dominguez and F.Garcia-Blanco, Bioelectrochem. and Bioenerg., 12(1984)25.
10. M.L.Arhens, G.Maass, P.Schuster and H.Winkler, J. Am. Chem.Soc., 92(1970)6134.
11. M.Blazquez, M. Dominguez, F. Garcia-Blanco, C. Rubio, J. Donoso and R. Izquierdo, Proceedings of the 9th Ibero-american Symposium on Catalysis, 1(1984)364.
12. L.Camacho, J.Electroanal.Chem., 177(1984)59.

08030

CORROSION IN VIVO OF PROSTHESIS MATERIAL

ESCUDERO, M.L., GONZALEZ, J.A., RUIZ, J.
CENTRO NACIONAL DE INVESTIGACIONES METALURGICAS
Avda. Gregorio del Amo, 8 28040 MADRID SPAIN

The in vivo tests which provide the fullest information are those using electrochemical measurements during the time the test material remains in the animal's body.

These tests are not generally used on account of their difficulty. However tests have been performed on rats[1,2] for instantaneous corrosion determination.

The experimental design described in this report makes it possible to determine in dogs, parameters such as polarization resistance or corrosion potential. Further, it has permitted plotting of polarization curves and determination of breakdown and repassivation potentials. We have not found any records of the latter type of test in scientific references.

An AISI 316L alumina-covered steel was the material tested. The alumina layer was applied by plasma spraying.

The work electrode design was as follows: the ceramic-coated steel specimen was drilled to accommodate a press-fit copper terminal for contact assurance. This externally-threaded terminal has, in turn, an axial drilled hole through which the conductor wire passes and this is welded to the lower end of terminal. The bond was insulated by an epoxi-resin sealed Teflon cover (Fig. 1).

This arrangement was used to prepare both the work electrode and the counter-electrode which were identical. Some reference Ag-ClAg microelectrodes were also prepared (Fig. 2).

The electrodes under study together with the reference electrodes were implanted in the muscle tissue in the legs of dogs.

The described experimental design permitted the following determinations to be made:

- Measurement of corrosion potential vs time
- Rp measurement
- The plotting of anodic polarization curves[3].

The in vivo results obtained make it possible to verify that the 316L alumina-covered stainless steel stays in the passive state, throughout time.

The anodic polarization curves reveal a reduced susceptibility to pitting corrosion, given the great difference between the breakdown and corrosion potentials (Fig. 3).

Following forced rupture by means of externally-applied polarizations, it was proved that the passivating film regenerates itself in a few hour's time. Fig. 4 shows this evolution with time of the potential and corrosion intensity values. It is quite evident that the initial values tend to be recovered.

The developed technique allows determination of corrosion rate in implanted materials and the evolution of the pitting corrosion susceptibility.

All the facts confirm that this material is suitable for the manufacture of implants from the corrosion point of view.

REFERENCES

1.- COLANGELO, V.J., GREENE, N.D., KETTLEKEMP, D.B ALEXANDER, H. and CAMPBELL, C.J. : J. Biomed. Res 1(1967) p. 405.

2.- FONTANA, M.G. and GREENE, N.D.: "Corrosion Engineering". Mc Graw-Hill, (1978) p. 7.

3.- ESCUDERO, M.L.: "Corrosión in vitro e in vivo de las prótesis mixtas acero inoxidable-cerámica". Tesis Doctoral Universidad Autónoma de Madrid, March (1985).

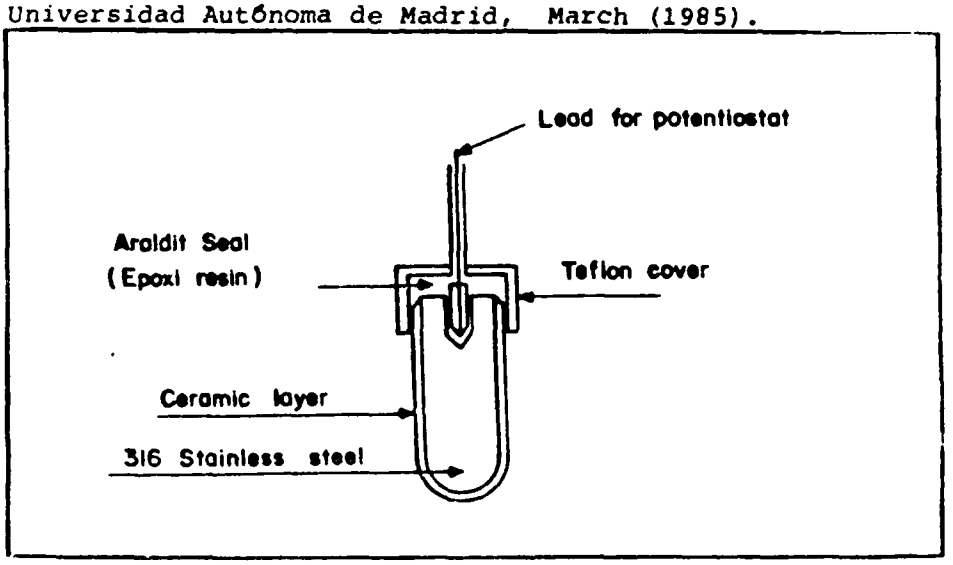

Fig. 1.- Diagram of prosthesis connecting lead connections and insulation of electrodes used in vivo measurements.

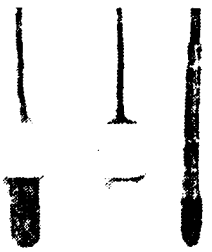

Fig. 2.- In vivo implanted electrodes. One, of grey ceramics, another white and the Ag/ClAg reference electrode.

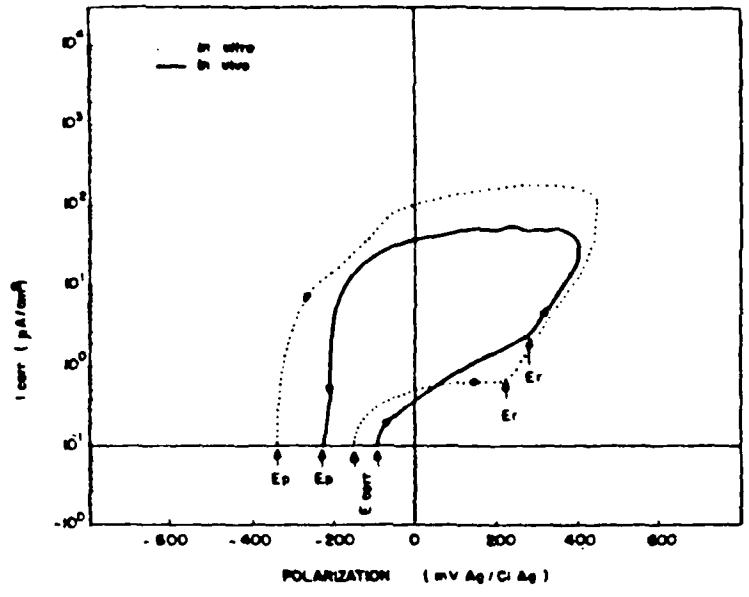

Fig. 3.- Anodic polarization curves of electrodes implanted intramuscularly in dog.

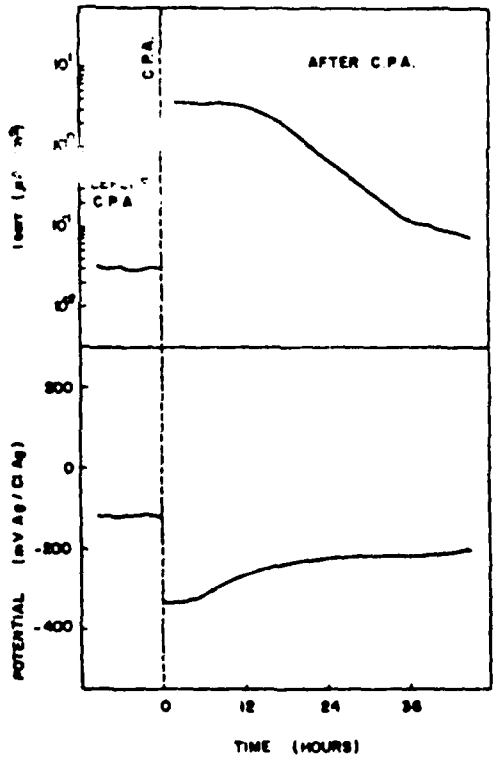

Fig. 4.- Evolution of parameters with the time towards values prior to pitting.

08040

Reversible Formation and Disruption of Micells by Control of the Redox State of the Surfactant Head Group

T. Saji, K. Hoshino, and S. Aoyagui
Tokyo Institute of Technology, Tokyo, Japan

Redox-active surfactant micelles with attached redox probes are of considerable interest since they are expected to play an important role in energy storing photoreactions. However, no studies have so far dealt with the change in the aggregation behaviour of surfactants by control of the redox state of the surfactant molecules. This paper reports that micelles formed by the univalent surfactant $FcCH_2N^+(CH_3)_2C_{12}H_{25}$, I^+, are reversibly disrupted into monomers and re-formed from the monomers by oxidation to the divalent surfactant, I^{2+}, and re-reduction, respectively.

Figure 1 shows the concentration dependence of the diffusion coefficient and half-wave potential of I^+ and I^{2+} in 0.2 M Li_2SO_4 aqueous solution at 25 °C. The values of the diffusion coefficient, D_{app} were determined by potential-step chronoamperometry. The I^{2+} solution was prepared from a solution of I^+ by controlled-potential bulk electrolysis. In Fig. 1 it was found that the CMC of I^+ in the presence of 0.2 M Li_2SO_4 lay near 0.5 mM and the D_{app} value of I^+ below the CMC, i.e. the diffusion coeff. of the I_2^+ monomer D_m, was kept nearly constant at $(5.0 + 0.5)\times10^{-6}$ cm^2 s^{-1}. The D_{app} of I^+ beyond the CMC, $[I^+]$ = 2.0 mM, was $(1.6 \pm 0.2)\times10^{-6}$ cm^2 s^{-1}, whereas that of 2.0 mM I^{2+} generated by controlled potential electrolysis of I^+ or by its chemical oxidation with equimolar amount of $Ce(SO_4)_2$ was $(4.6 \pm 0.5)\times10^{-6}$ cm^2 s^{-1}, which was in good agreement with the D_m value. This finding suggests that the micelles of I^+ be broken up into the monomers by oxidation, probably owing to the enhancement in elecrostatic repulsion among the posotively charged head groups and in their hydrophilic character, and hence the CMC value of the surfactant increased.

In order to apply the above function of I^+ micelle, we have turned to spectral measurements on 1-[(2-methylphenyl)azo]-2-naphthalene, TAN, solubilized in I^+ micelle. Fig. 2 shows visible absorption spectra of the following test solutions: A, 2 mM I^+ + TAN; B, 2mM I^{2+} + TAN; A', 2mM I^+ (background for A); and B', 2 mM I^{2+} (backgound for B) in 0.2 M Li_2SO_4 aqueous solution. The absorbance of TAN at 470 nm (A_{470}) determined from Fig. 2 were 0.294 for the spectrum A and 0.022 for the spectrum B by making background correction. The TAN is only poorly soluble in water and was not oxidized by $Ce(SO_4)_2$ at all. A comparison of these A_{470} values show that 92% of TAN molecules solubilized in I^+

micelles were released immediately after the breaking up of the micelles and precipitated because of its poor solubility in water. In addition, the spectrum A could be reproduced (spectrum c) by adding hydroquinone to the stirred solution exhibiting spectrum B, which suggests that the I^{2+} monomers be reduced to I^{+} to reform micelles solubilizing the TAN.

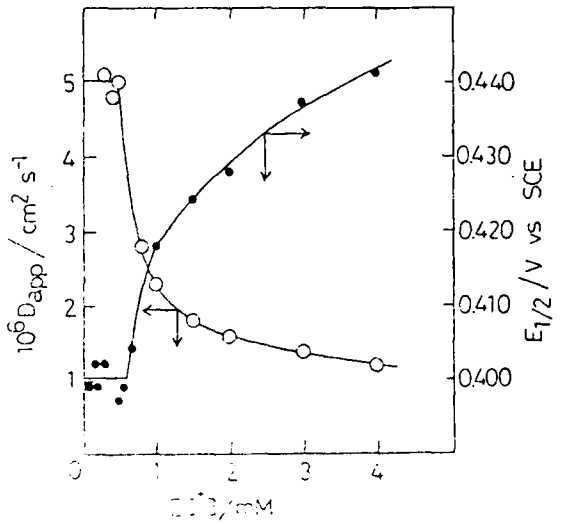

Fig. 1

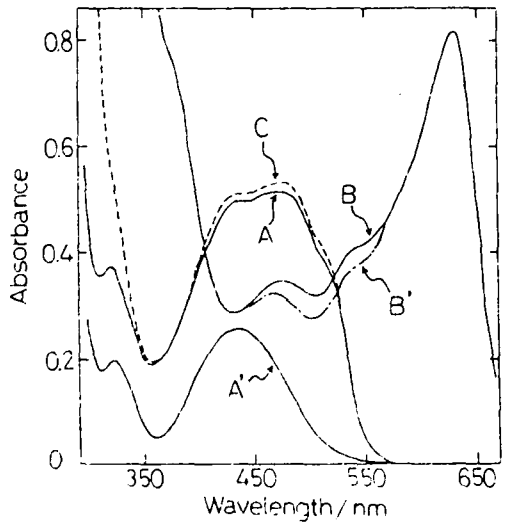

Fig. 2

08050

A SYNTHETIC MODEL OF NADH WORKING CATALYTICALLY IN A BIPHASIC MEDIUM

G. PIERRE, P. CHAUTEMPS and J.L. PIERRE.
Laboratoire de Chimie Organique Analytique (U.A. C.N.R.S. 321) and Laboratoire d'Etudes Dynamiques et Structurales de la Sélectivité (U.A. C.N.R.S. 322).
B.P. 68 - Saint Martin d'Hères (France).

Biomimetic reductions with synthetic models of NADH have been well studied[1-3] and it is of interest to find a technique allowing a recovery of the expansive reducing agent in order to use it several times or at low concentrations. For example, if Ox is an organic species, the reaction could be written as follows :

$$NADH + Ox \rightarrow NAD^+ + Red. \quad (1)$$
$$NAD^+ \rightarrow NADH \quad (2)$$

The reaction (2) has been studied using chemical reducing agents like sodium dithionite ($Na_2S_2O_4$). But a test of regeneration of NADH led to an accumulation of the sulfite formed and the reaction stop after 5 cycles.

An electrochemical regeneration of the product by electrolysis is developped in this paper in order to avoid the problem of the accumulation of an undesirable chemical product. But it was necessary to find a reversible system analog to the NAD^+/NADH system.

The studied system deals with N-phenyl carbamoyl pyridinium salt NPA^+ which is known to be reduced into the dihydro 1,4 pyridine derivative (or N-phenyldihydronicotinamide PNAH) without other isomers which would give by products[5].

The electrochemical behaviour of the N-phenyl carbamoyl-3 pyridinium chloride in an aqueous pH 7 solution is shown on the figure, curve 1. On mercury, two waves are observed at - 0.8 and - 1.8 V vs SCE corresponding to the reactions.

$$PNA^+ + e \rightarrow PNA^\cdot$$
$$PNA^\cdot + e + H^+ \rightarrow PNAH$$

A reduction at - 1.2 V, that is on the current plateau of the first wave gives directly the N-phenyl dihydro 1,4 nicotinamid resulting from a disporportionation reaction[6,7].

$$2\ PNA^\cdot \rightarrow (PNA)_2$$
$$(PNA)_2 + H^+ \rightarrow PNA^+ + PNAH$$

The substrat Ox chosen to study the reducing properties of PNAH (reaction 1) was the hexachloroaceton. Following the results of ROMER et al[8], this ketone is reducible in neutral solution as soon as OV. but the reduction current is very low, about 150 times lower than for the monochloroaceton. In fact, a reduction of $(CCl_3)_2$ CO on a mercury pool did not lead to the formation of the alcool derivative.

At the opposite of the pyridinium salt, the ketone and PNAH are poorly soluble in water but soluble in some organic solvents. So the electrolysis has been performed in a cell containing a biphasic mixture H_2O + CH_2Cl_2 (see the scheme below)

PNA^+ is reduced at - 1.2 V on mercury in the aqueous medium and gives an insoluble yellow precipitate which falls down at the bottom of the cell containing CH_2Cl_2 and $(CCl_3)_2$ CO. The chemical reduction of the ketone takes place (with a slow rate, θ = 40°, 48 h.) giving the acohol derivative, detected by ^1H NMR, and the pyridinium salt for another cycle. Four cycles of the PNA^+/PNAH have been performed.

The study of more sophisticated systems is in progress.

References :

1. VAN-TAMELEN edit., Bioorganic Chemistry, vol. IV, Academic Press (1978).

2. R.M. KELLOG, Topics in Current Chemistry, 101, 126 (1982).

3. J.L. PIERRE, l'Actualité Chimique, 6, 33 (1984).

4. K. NAKAMURA, A. OHNO, S. YASUI and B. OKA, Tetrah. Lett., 4815 (1978).

5. P.J. ELVING, W.T. BRESNAHAN, J. MOIROUX and Z. SAMEC, Bioelectrochem. Bioenerg., 9, 365 (1982).

6. Y. OHNISHI, Y. KIKUCHI and M. KITAMI, Tetrah. Lett., 3005 (1979).

7. W.T. BRESNAHAN and P.J. ELVING, Biochem. Biophys. Acta, 678, 151 (1981)

8. M.M. ROMER and P. ZUMAN, J. Electroanal. Chem., 64, 258 (1975).

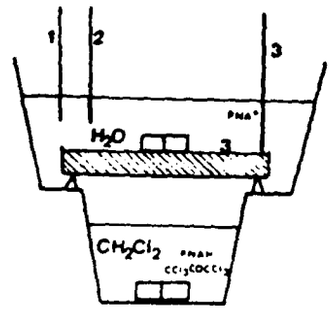

Fig.1: Biphasic system cell.

1 auxiliary electrode
2 reference electrode
3 mercury pool working electrode

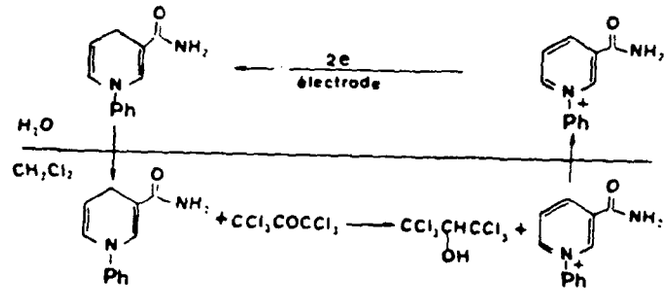

Fig.2: General scheme of the studied system.

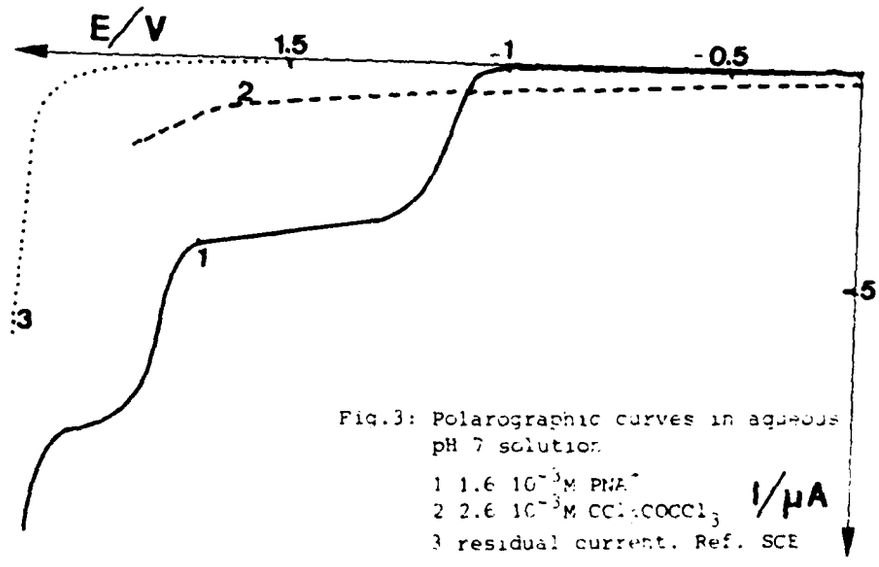

Fig.3: Polarographic curves in aqueous pH 7 solution

1 1.6 10^{-3}M PNA^+
2 2.6 10^{-3}M CCl_3COCCl_3
3 residual current. Ref. SCE

09010

9 EFFETS DE LA DOUBLE COUCHE D'HELMOLTZ SUR LA DISTRIBUTION DU POTENTIEL ET LE COMPORTEMENT CAPACITIF DE L'INTERFACE SEMICONDUCTEUR OU SEMIMETAL / ELECTROLYTE

G. BARRAL, J.P. DIARD, C. MONTELLA

Ecole Nationale Supérieure d'Electrochimie et d'Electrométallurgie de Grenoble - Laboratoire d'Energétique Electrochimique - LA associé au CNRS n° 265 - BP 75 - Domaine Universitaire - 38402 SAINT MARTIN D'HERES - FRANCE

Le modèle de l'interface semiconducteur/électrolyte conduit aux relations :

(1) $C^{-1} = C_{CE}^{-1} + C_H^{-1}$

(2) $V - V^{BP} = \Delta\phi_{CE} + \Delta\phi_H = \Delta\phi_{CE} + (q_{CE}.C_H^{-1})$

qui permettent d'estimer les contributions des capacités différentielles des couches de charge d'espace C_{CE} et d'Helmoltz C_H et des variations $\Delta\phi_{CE}$ et $\Delta\phi_H$ des ddp d'origine non dipolaire aux bornes de ces couches à : (1) la capacité différentielle C et (2) la variation de la ddp interfaciales [1-3].

Pour des phases semiconductrices non dégénérées, les valeurs de la charge d'espace q_{CE} et de C_{CE} calculées à partir de l'équation de Poisson-Boltzmann et une valeur de C_H comparable à celle que l'on mesure aux interfaces idéalement polarisables métal/électrolyte concentré, ménent aux inégalités :

(3) $C_{CE} << C_H$ et $|\Delta\phi_{CE}| >> |q_{CE}|.C_H^{-1}$

Les variations de C avec la tension d'électrode V de ces matériaux usuels sont analogues à celles de C_{CE} avec $\Delta\phi_{CE}$ [1-3].

Une exception est théoriquement attendue pour certaines phases extrinsèques de grande énergie d'activation qui possèdent une constante diélectrique relative ε_r élevée [4]. La détermination de la tension de bande plate V^{BP} par extrapolation à $C^{-2} = 0$ de la représentation Mott-Schottky nécessite la connaissance de la valeur de C_H^4 . Celle-ci pourrait être obtenue par simulation de la courbe expérimentale au moyen des relations (1) et (2) [5].

En fait, le rôle de la couche d'Helmoltz devient plus important pour des phases dégénérées en raison d'une énergie d'activation faible, d'un doppage important et/ou d'une polarisation appropriée. Différents cas seront envisagés.

Le carbone pyrolytique hautement orienté (HOPG) est présenté ici à titre d'exemple. Ce semimétal intrinsèque a une énergie d'activation négative [6].

Les variations expérimentales de sa charge [7] et de sa capacité différentielle [8] ont été reproduites sur les figures 1 et 2. Sur ces mêmes figures, nous avons représenté les variations théoriques calculées à partir des relations (1) et (2) en supposant que les densités d'états énergétiques du HOPG sont paraboliques. q_{CE} et C_{CE} ont été obtenues à partir de l'équation de Poisson-Fermi [1-3,9]. Nous attribuons les bons résultats obtenus par cette méthode au fait qu'elle conduit dans certains cas [10] à des valeurs de q_{CE} en assez bon accord avec celles calculées par une méthode approchée de résolution simultanée des équations de Poisson et de Schrödinger.

Le pourcentage de la variation de la ddp qui est localisée aux bornes de la couche d'Helmoltz a été reporté sur la figure 3.

1 - H. GERISCHER in "Advances in Electrochemistry and Electrochemical Engineering", Vol. 1, p 139-232, ed. by P. Delahay, Interscience Plublischers (1961).

2 - V.A.MYAMLIN, Y.V. PLESKOV, "Electrochemistry of semiconductors", Plenum Press (1967).

3 - M. GREEN in "Modern Aspects of Electrochemistry", Vol. 2, Butterworth's Scientific Plublications (1959).

4 - B. PETTINGER, H.-R. SCHÖPPEL, T. YOKOYAMA, H. GERISCHER, Ber. Bunsenges. Physik. Chem., 78 (1974) 1024.

5 - [illegible] OSAKI, H. KITA, J. Electrochem. Soc., 130 (1983) 895.

6 - A.W. MOORE in "Chemistry and Physics of carbon" Vol. 17, p. 233-286, ed. by P.L. Walker, Jr. and P.A. Thrower, Marcel Dekker (1981).

7 - I. MORCOS, J. Phys. Chem., 76 (1972) 2750.

8 - J.P. RANDIN, E. YEAGER, J. Electroanal. Chem., 36 (1972) 257.

9 - R. SEIWARTZ, M. GREEN, J. Appl. Physics., 29 (1958) 1034.

10 - Ch. M. HARDALOV, E.P. VALCHEVA, K.G. GERMANOVA, Surface Science, 147 (1984) 329.

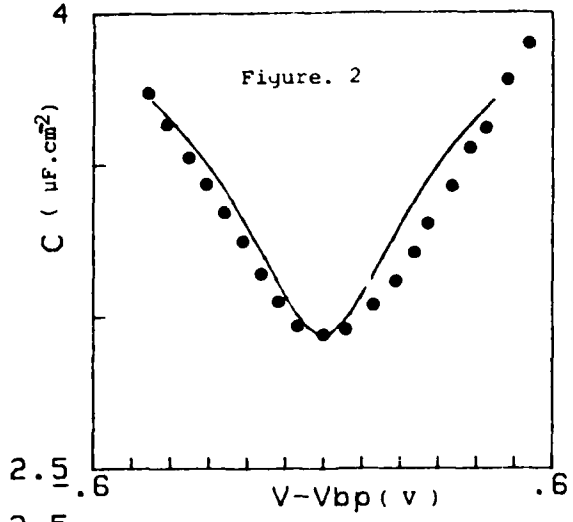

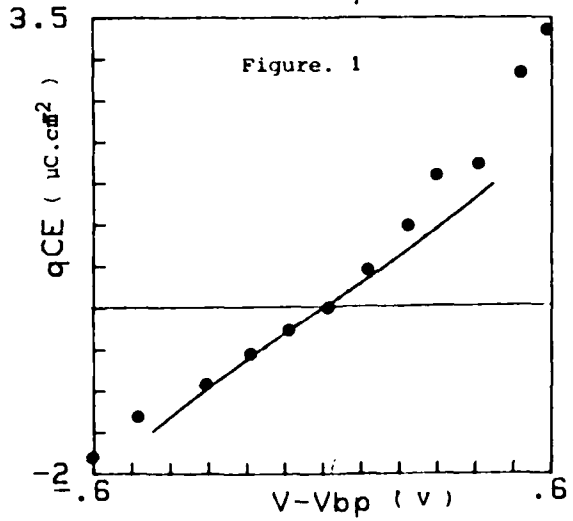

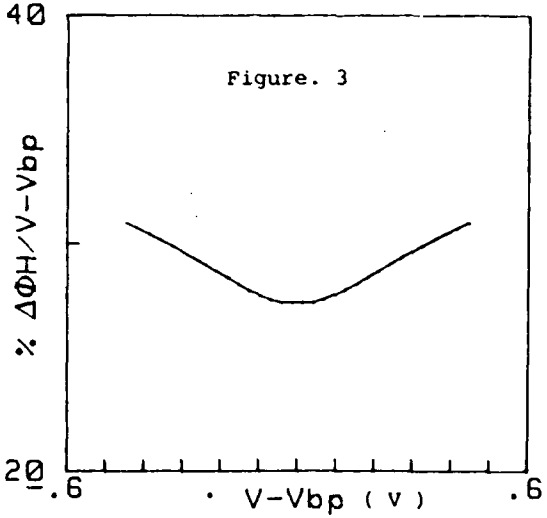

Graphite pyrolytique hautement orienté intrinsèque :

Valeurs calculées (———)+ et expérimentales [7,8] (● ; Vbp= 0 V/ENH)

Figure. 1 -Charge d'espace (LiCl 1 mol.l^{-1})

Figure. 2 -Capacité différentielle de charge d'espace (NaF 0.5 mol.l^{-1} ; pH=6 ; T= 25°C)

Figure. 3 - % de la variation de la ddp interfaciale localisée aux bornes de la couche d'Helmoltz

+ énergie d'activation (-30,8 meV)
densité effective d'etats (5.10^{18} cm^{-3})
ε_r=3,5 ; C_H = 10,8 µF.cm^{-2}.

09012

09020

ADSORPTION OF THE ETHYLENEDITHIOLDIACETIC ACID AND THIOGLYCOLIC ACID AT THE MERCURY SOLUTION INTERFACE

M. ERCEG and D. SUZNJEVIĆ

Faculty of Science, Institute of Physical Chemistry, Univ. of Belgrade, Belgrade, Yugoslavia

A series of differential capacity vs. potentials curves have been obtained from aqueous buffered (Britton-Robinson univ. buffer) KNO_3, and nitric acid-nitrate solutions, covering the wide pH range from 0.65 to 9.8. The concentration of ethylenedithioldiacetic acid (H_2Z) and thioglycolic acid (TGA) in these experiments was $1 \cdot 10^{-3}$ mol/dm^3. The capacity curves were also recorded upon varrying conc. of acids in the presence of B.R. buffer conc. which was 0.1 mol/dm^3. The characteristic C-E curves at different pH are represented at Fig. 1 and Fig. 2 for H_2Z and TGA respectively.

From Fig. 1 it was assumed that the neutral molecule of H_2Z adsorbs at the electrode surface causing the double layer capacity lowering around e.c.m. By increasing the pH the capacity rises to a certain extent aproaching the first dissociation constant, pK_1 = 3.2. Above that value the capacity increases sharply to the second dissociation constant pK_2 = 4.1 and then the capacity line shows a tendancy to follow the supporting electrolyte one. It means that the dissociation products of H_2Z do not adsorb at the mercury surface. Adsorption/desorption capacity peaks, as it was noticed from Fig. 1 may only be observed at the negative side of the e.c.m. They have good simmetry and oval form which suggests that corresponding attractive constant, a, is less than one. The peak simmetry potential moves towards negative values by increasing of pH, showing clearly the two inflections at the characteristic value, i.e. pK_1 and pK_2.

Fig. 1. C-E curves for H_2Z at different pH.
The e.c.m. of the supporting electrolyte is about -0.45 V vs SCE

At the positive side of e.c.m. the faradaic process, takes place[1] at he poten-

tial of H_2Z desorption producing pseudocapacity increase so that adsorption/desorption capacity peak in this potential region could not be possible to observe.

At the constant pH the capacity depression around e.c.m. becomes more intensive by increasing of H_2Z conc. From the graph constructed using surface coverage vs equilibrium conc. of neutral form, H_2Z, the adsorption izotherm of the Langmuir type was obtained.

The C-E curves at different pH for TGA (Fig. 2) show capacity depression in a relatively wide range of potentials around e.c.m. only at higher acidity and that range becomes rather narow at pH above 3. The relation between capacity.

At constant potential and pH applied the constructed graph gave evidence of the first dissociation constant of TGA (pK_1 = 3.4). The pK_2 was not possible to obtain because the pseudocapacities presented from the corresponding faradaic processes covered the potential region examined. In the whole potential range at the positive side of e.c.m. the adsorption/desorption capacity peaks were not possible to resulute from the pseudocapacities presented. At the negative side of the e.c.m. the [illegible] are very small and distorted so they are not common for analysing.

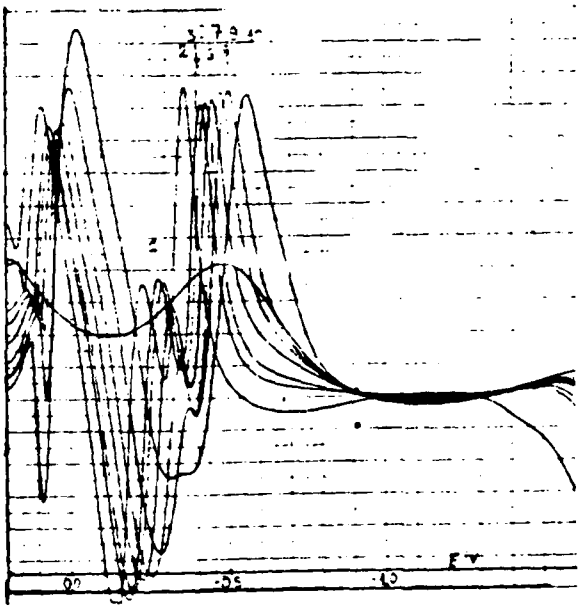

Fig. 2. C-E curves for TGA at different pH (all other stated as in Fig. 1)

Fig. 3. represents the C-E curves of TGA obtained for different acid conc. covering region between $2 \cdot 10^{-5}$ to $5 \cdot 10^{-2}$ mol/dm^3. At pH = 2.10 (B.R. buffer + KNO_3). From the pretty wide potential region, which was not disturbed by the pseudocapacities, it was posible to follow the electrode surface coverage in function of equilibrium conc. of TGA. The obtained adsorption izotherm, from such analysis, gives evidence of two plateaus indicating that the reorientation of adsorbed TGA

probably occurs at higher TGA conc. as a result of stronger interaction betwe-en adsorbed molecules and mercury. The number of adsorbed TGA molecules which corresponds to the second plateau becomes about two time greater than the one calculated from the furst plateau.

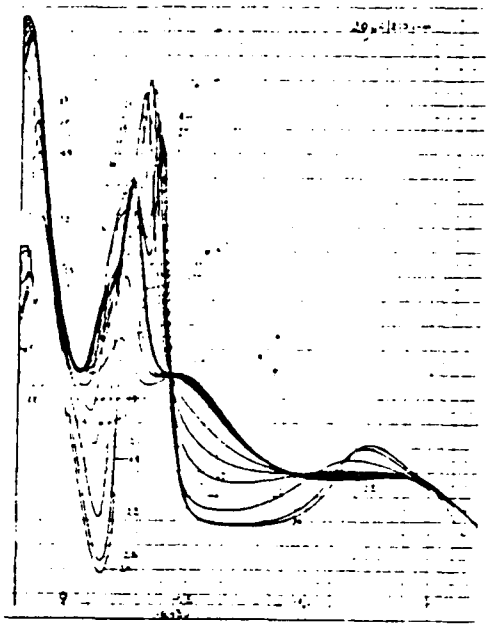

Fig. 3. C-E curves for TGA at different acid conc. from $1 \cdot 10^{-4}$ to $5 \cdot 10^{-2}$ mol/dm^3 (all other stated as in Fig.1)

On the basis of differential capacity studies it was possible to expla-in the compley mechanism of Me-ion reduction from H_2Z[1] as well as anodic beha-viour of TGA in d-c. polarography. In both cases the adsorption of neutral molecules has a big influence on the electrode kinetics in these system.

REFERENCESE

1. D.Sužnjević, Thesis, Univ. Belgrade, Belgrade 1975
2. M. Erceg, Thesis, Univ. Belgrade, Belgrade 1984

09030

DIFFERENTIAL CAPACITANCE AND SURFACE CONDUCTANCE OF GOLD IN THE PRESENCE OF ADSORBED AMYL ALCOHOL

R.I. Tucceri and D. Posadas
Instituto de Investigaciones Fisicoquímicas Teóricas y Aplicadas - (INIFTA)
Casilla de Correo 16, Sucursal 4, (1900) La Plata, ARGENTINA

INTRODUCTION

Recently the measurement of the surface conductance (SC) as a tool to study adsorption at electrodes has received growing attention[1,2]. In order to study the effect of adsorption on SC we choose amyl alcohol as a probe molecule. Since this requires the knowledge of the degree of coverage as a function of the electrode potential, we carried out a capacitance study for the adsorption of pentane-1-ol on the thin film gold electrodes together with the resistance measurements.

EXPERIMENTAL

Measurements were carried out using the same techniques and experimental setup as previously reported for capacitance and SC measurements. The surface characteristics of the electrode were the same as those employed before. Five concentrations in the range $5\times10^{-2} < C < 0.15$ M of amyl alcohol at 25°C were studied.

RESULTS AND DISCUSSION

The analysis of capacitance data allows to fit Frumkin adsorption isotherm with parameters very similar to those found by previous workers for the adsorption of ethyl ether on single gold crystals[3]. The isotherm is congruent with $(E-E_m)^2$ where E is the potential and m refers to the maximum of adsorption. The relevant parameters of adsorption are compared with those on mercury and (110) single gold crystal in table 1. The meaning of the symbols is the usual one[3]. From them it is inferred that amyl alcohol adsorbs weakly on gold. The change with potential of the coverage, θ, for different concentrations of the alcohol is shown in Fig. 1. The relative change of resistence, $\Delta R/R$ as a function of potential, is shown in Fig. 2. It is observed that the $\Delta R/R$ decreases as the potential increases until that at a potential near the minimum of the capacitance curve for the corresponding alcohol concentration, it increases again. Comparison of Figs. 1 and 2 shows no direct correlation between $\Delta R/R$ and θ. In the base electrolyte alone no field effect[1,2] is found. The field effect is the $\Delta R/R$ change brought about by the change in the surface charge, σ, on the electrode, $\Delta R/R = k\sigma$. Thus, we infer that the field effect could be masked by the effect of the re-orientation of the solvent on the electrode resistance as σ changes. As the alcohol adsorbs, due to its weak adsorption energy, the main effect on ΔR would be to displace the solvent mole-

AD-A162 434 EXTENDED ABSTRACTS INTERNATIONAL SOCIETY OF 9/12
ELECTROCHEMISTRY (36TH) HELD AT SALAMANCA SPAIN ON
23-28 SEPTEMBER 1985(U) INTERNATIONAL SOCIETY OF
UNCLASSIFIED ELECTROCHEMISTRY 28 SEP 85 F/G 7/4 NL

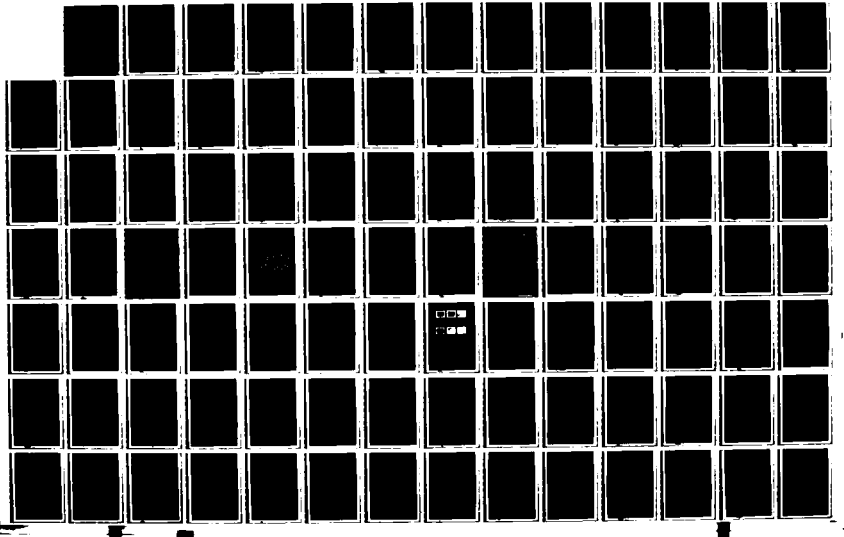

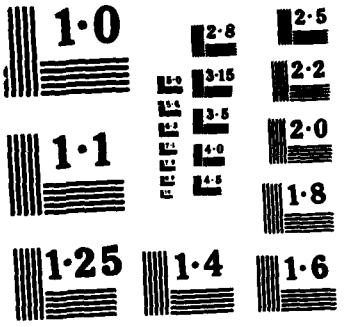

cules. In this way the field effect would increase causing a decrease in $\Delta R/R$.

REFERENCES

1. D.L. Rath, J.Electroanal.Chem., 150 (1983) 521.
2. R.I. Tucceri and D. Posadas, J.Electroanal.Chem. (in press).
3. J. Lipkowski, C.N. Van Huong, C. Hinnen and R. Parsons, J. Electroanal.Chem., 143 (1983) 375.
4. B.B. Damaskin, O.A. Petrii and V.V. Batrakov, Adsorption of Organic Compounds on Electrodes, Plenum Press, London, 1978.

ACKNOWLEDGEMENT

INIFTA is a Research Institute jointly established by the Universidad Nacional de La Plata, the Consejo Nacional de Investigaciones Científicas y Técnicas and the Comisión de Investigaciones Científicas de la Provincia de Buenos Aires.

TABLE 1

Adsorption parameters of amyl alcohol on mercury and gold and diethyl ether on (110) single gold crystals.

Parameters	this work	amyl alcohol on mercury[4]	diethyl ether on Au[3] (110) single crystal
E_m/V	-0.03	-	-0.52
E_H/V	0.02	0.2	-0.45
$\sigma_m/10^{-6}$ C cm^{-2}	0.4	-	-2.0
$C^1/10^{-6}$ F cm^{-2}	9.77	4.20	12.0
$C_o/10^{-6}$ F cm^{-2}	37.4	-	44.0
Γ_m/molec n m^{-2}	2.1	2.9	2.7
β_m/dm^3 mol^{-1}	4.05	-	1.1
$-\Delta G$/kJ mol^{-1}	13.41	19.14	10.0
a	1.63	1.48	1.35
b/V^{-2}	7.6	-	14.0

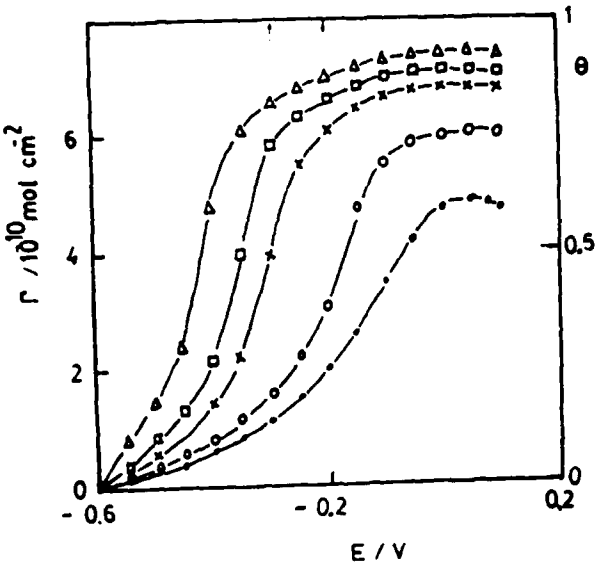

Fig. 1.- Coverage of amyl alcohol, θ, as a function of potential vs. CSE, E. (---) 0.04 F, (o-o-) $5x10^{-2}$, (x-x-) $2.0x10^{-2}$, (□-□-) $1.1x10^{-1}$, (Δ-Δ-) $1.5x10^{-1}$ M amyl alcohol.

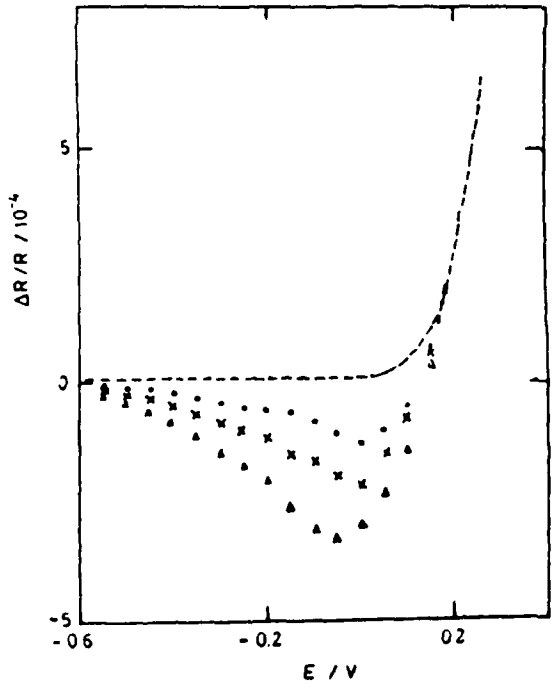

Fig. 2.- Relative resistance change, ΔR/R, vs. potential, E. The meaning of the symbols is as in Fig. 1.

09040

IONIC COMPONENTS OF CHARGE AT THE MERCURY/KI + KCl AQUEOUS SOLUTION INTERPHASE

G.J. Gordillo* and D. Posadas
Instituto de Investigaciones Fisicoquímicas Teóricas y Aplicadas - (INIFTA)
Casilla de Correo 16, Sucursal 4, (1900) La Plata, ARGENTINA

The study of the ionic components of charge at the metal/solution interphase has been mostly restricted to pure salts and to mixtures with KF and KPF_6 at constant ionic strength where the F^- and PF_6^- ions are assumed not to be specifically adsorbed.

In mixtures with F^- ions an anamolous behaviour of the specifically adsorbed charge has been observed for anions such as PF_6^-, NO_3^-, ClO_4^-, $H_2PO_4^-$ and Br^- which has been attributed, in some cases, to the specific adsorption of the F^- ion at high anodic charges. This was inferred, in the work at constant ionic strength, from a crossing point in the charge of the specifically adsorbed anion at high positive charges. If this were so, a mixture of two anions, such as Cl^- and I^- should show a similar behaviour in that both, a crossing point for the charge of the specifically adsorbed I^- together with an increase in the specific adsorbed charge of Cl^- should be found.

To this end the differential capacity of 63 solutions of varying composition were measured employing the experimental set up described previously[1]. The concentration variable selected was the chemical potentials of the salts. Nine concentrations of KI ($7\times10^{-3} < C_{KI} < 0.1$ m) at constant activity of KCl and seven concentrations of KCl ($9\times10^{-3} < C_{KCl} < 0.38$ m) at constant activity of KI were made. The potentials of zero charge were determined by the streaming mercury electrode and by the back integration method[2].

The ionic components of charge for iodide ion, σ_{I^-} and chloride ion, σ_{Cl^-} were determined, following the thermodynamic analysis given in (2), from Parsons' function and employing Gouy Chapman theory at a sufficiently negative charge to ensure that neither I^- nor Cl^- ions were specifically adsorbed. They are shown in Fig. 1. The main feature of Fig. 1 is the appearance of a crossing point in σ_{I^-} and the absence of adsorption of Cl^- ion. We conclude, therefore, that the appearance of a crossing point is not necessarily related to the specific adsorption of the anion of the supporting electrolyte. It is seen in Fig. 1 at high negative charge that for the most dilute solutions σ_{I^-} increases with $-\sigma$. This behaviour has been previously observed in dilute solutions for different anions: SO_4^-, OH^-, ClO_4^-, Cl^- and I^-. In our opinion this behaviour is consistent with an adsorption of the anion at the diffuse layer at high cationic charges due to oscillations of the potential with the distance.

---

*Present address: Departamento de Química Física, FCEN, UBA, Ciudad Universitaria, Pabellón 2, Buenos Aires, ARGENTINA.

This effect for the I^- ion should be more noticeable at high concentrations of KCl and low concentration of KI. Since the condition for the occurrence of the adsorption of I^- at the diffuse layer is a high cation charge in the diffuse layer, this phenomena would also occur at high positive charges where σ_{K^+} is high. Therefore, σ_{I^-} have a contribution due to adsorption at the diffuse layer which is more important at the lower concentrations of KI. This would explain why a crossing point is observed.

REFERENCES

1. M.I. Sosa, D. Posadas and A.J. Arvia, J.Electroanal.Chem., 137 (1982) 307.
2. G. Gordillo and D. Posadas, J.Electroanal.Chem., 159 (1983) 217.

ACKNOWLEDGEMENT

INIFTA is a Research Institute jointly established by the Universidad Nacional de La Plata, the Consejo Nacional de Investigaciones Científicas y Técnicas and the Comisión de Investigaciones Científicas de la Provincia de Buenos Aires.

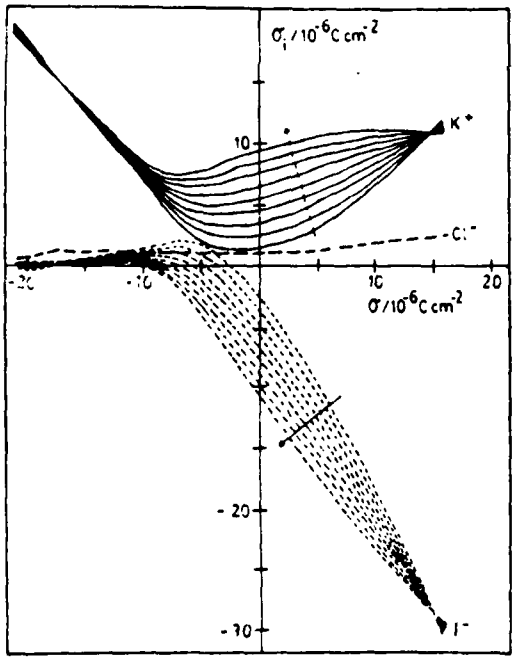

Fig. 1.- Ionic components of charge, σ_i, as a function of the charge on the metal, σ at 25°C. The arrows indicate increasing concentrations of KI: 0.002, 0.0034, 0.0054, 0.0086, 0.0136, 0.0213, 0.0328, 0.0494 and 0.0726 m at constant activity of KCl, a_{KCl} = 0.0774 m.

09050

PROPERTIES OF THE INTERFACE STEEL - THERMALLY FORMED OXIDE/ELECTROLYTE

J. MALINA and B. LOVREČEK*

Faculty of Metallurgy Sisak, University of Zagreb (Yugoslavia)

Oxide layers thermally grown on steel are practically and theoretically of considerable interest. The investigation of their properties can be applied in a number of uses, from hydrometallurgy to energy conversion. In this work, the iron oxide - solution interface has been investigated by studying the electrochemical aspects of it. The aim is to derive the informations about the interaction at this interface from double layer characteristics.

Potentiometric titration and streaming potential methods were applied. The oxide was thermally formed on steel filings (DIN St 12, 0.3 to 0.4 mm size) at 773 K in an oxygen atmosphere for one hour, then cooled down for 15 minutes in the same atmosphere. Metallographic and X-Ray diffraction analyses indicated that oxide scale on steel consists of two layers: the inner layer Fe_3O_4 ($\sim$90 %) is covered with thin outer layer of α -Fe_2O_3.

Supporting electrolyte was 0.15 M H_3BO_3 or 10^{-3} M KNO_3. Acidity was adjusted by means of 0.075 M $Na_2B_4O_7$ (borate buffer) and by means of 10^{-2} M KOH or HNO_3.

From the experiments in borate buffer solutions derived zeta-potential vs pH dependance revealed a linear relation (Fig. 1.). This indicates that H^+ and OH^- ions are potential-determining at oxide layer/electrolyte interface as shown schematically for hydrated surface[1]:

$$\left[\geqslant Fe(H_2O)_2(OH)\right]^+ \underset{OH^-}{\overset{H^+}{\rightleftharpoons}} \left[\geqslant Fe(H_2O)(OH)_2\right] \underset{H^+}{\overset{OH^-}{\rightleftharpoons}} \left[\geqslant Fe(H_2O)(OOH)\right]^-$$

Such interface can be interpreted in terms of a classic double layer structure with simple equilibrium relationships.

*B.L. - Nalješkovićeva 29, Zagreb, Yugoslavia

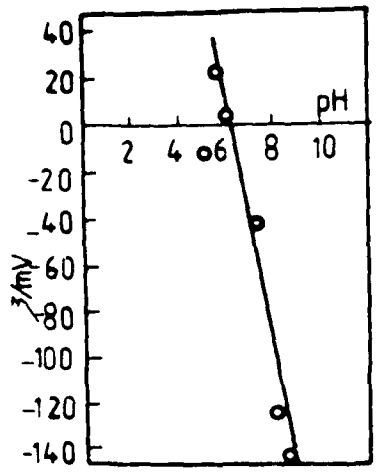

Fig. 1. Zeta-potential vs pH in borate solutions

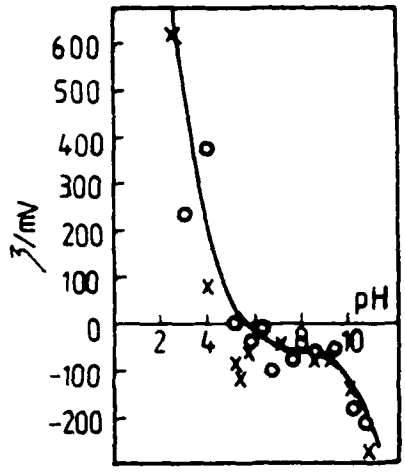

Fig. 2. Zeta-potential vs pH in nitrate solutions: x-conditioned by contact with filings, o-unconditioned

In KNO_3 solution the situation is rather different, and the values of zeta-potential, formally calculated seems to high at extreme points. As indicated in Fig. 2, through experimental points an S - shaped curve can be drawn. It is interesting that this shape appears to be alike to the q = f(pH) curve derived from potentiometric measurements (Fig. 3), but the difference in zero charge - point is cca one pH unit. Surface charge density values can be used for calculation of zeta potential, as well as for the diferential capacity and interfacial energy curves. These calculations are based on some assumptions which represent a certain formal standpoint. As an example, by calculating zeta - potential depending on pH very high, even unrealistically high values are derived. By graphical integration of the charge density plot in Fig. 3, the changes in the interfacial energy are obtained (Fig. 4).

The measurements performed and the analysis of results show that applied methods can give the useful informations about the system investigated, as well as they reveal a complex nature of it. The differences which appear by changing electrolyte and pH in a given range show that system is composition depending. The buffering effect of borat electrolyte, the kind of ionic species present, particularlily anionic - this are the factors that influence the system, without mentioning the solubility that must be taken into accont at more detailed analysis. In this stage of work, the interaction with anions is the most interesting aspect.

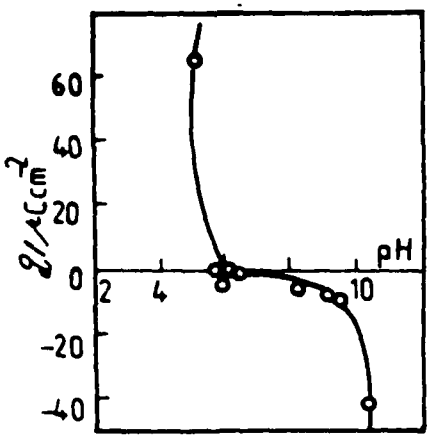

Fig. 3. Surface charge vs pH in nitrate solutions

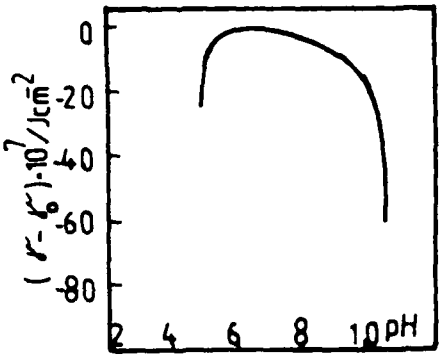

Fig. 4. Interfacial energy variation in nitrate solutions

This interaction can be manifested in different ways, even by incorporation resp. exchange of the surface OH groups[2]:

$$\left[\geqslant Fe(H_2O)(OH)_2\right] \underset{OH^-}{\overset{H^+,A^-}{\rightleftharpoons}} \left[\geqslant Fe(H_2O)_2^{+2}A^-\right]^+ + OH^-$$

The system investigated, in which hydrated layer is in contact with the solution, such an interaction could also participate. This interaction has dual effect: first, it changes the nature of layer (specially at surface), and secondly it gives rise to experimentally determined q. In this sense our results are discussed.

References:

1. S.M. Ahmed, in "Oxides and Oxide-Films", (ed. J.W. Diggle) Vol. I, Marcel Dekker, New York, 1971, pp. 319-517.

2. S.M. Ahmed, AIChE Symp. Ser., 71 (1975) 24.

09060

INVESTIGATION OF SULFUR ADSORPTION ON NOBLE METALS BY CYCLIC VOLTAMMETRY

J. BARBIER, E. LAMY-PITARA
Laboratoire de Chimie en Catalyse Organique U.A. CNRS 350
POITIERS - FRANCE

The deactivation of metal catalysts by sulfur compounds is a major problem in heterogeneous catalysis. Transient electrochemical methods can give interesting informations about the nature of adsorbed sulfur species on the surface of metals, such as platinum and iridium, used in particular as reforming catalysts.

The adsorption of H_2S is carried out in an acid solution and in the potential region of double layer (0,5V/ERH) on platinum and in the potential of minimum current (0,4 V/ERH) on iridium. This operation is followed by a positive non-stationary current indicating the oxidation of the sulfide species on both metals. The degree of coverage of the sulfidized electrode is measured by some voltammetric cycles in the hydrogen region. When the anodic limit of potential is extended to the region of formation of oxides (1,5V/ERH for the platinum and 1,4V/ERH for the iridium), the adsorbed sulfur species are oxidized and desorbed as sulfates, but several cycles are needed to oxidize all the adsorbed sulfur. All these qualitative remarks are the same for the platinum [1,2,3] and for the iridium electrodes. A balance between the number of electrons involved during the adsorption of sulfur species and during their oxidation, reported to the number of occupied metal atoms, allows the determination of the adsorption valency and of the adsorption stoichiometry of these species [3]. Several platinum electrodes have been studied in function of the degree of coverage by the adsorbed sulfur species. The adsorption valency, X_s, depends on the degree of coverage, θ_s (fig 1) : it is negative for low degrees of coverage ($\theta_s < 0,25$) and close to zero for high θ_s. An effect of the surface roughness is also observed : the adsorption valency is not the same for electrodes of different degree of roughness and in some cases (high degree of roughness) it can be positive (for $0,25 < \theta_s$). The adsorption stoichiometry, $n_{Pt/s}$, depends also on the degree of coverage (fig 2): it changes from about $n_{Pt/s} = 2$ for low sulfur coverages ($\theta_s < 0,25$), to near $n_{Pt/s} = 1$ for high θ_s. The effect of the degree of coverage on the adsorption valency is qualitatively the same for the system S/Ir (fig 3). But the adsorption stoichiometry $n_{Ir/s}$ is higher than that of the system S/Pt (fig 4) : it is greater than five for $\theta_s < 0,20$ and $n_{Ir/s} = 2$-3 for $\theta_s > 0,25$. Indeed, it is very difficult to obtain a low θ_s on Ir (lower than 0,15), because the first fraction of adsorbed sulfur inhibits the hydrogen adsorption on a large number of iridium atoms.

This experimental method has been checked with the help of the system S/Au. Indeed, on the gold, the adsorption of the sulfur can be studied on a wide potential region ; another advantage is that the oxidation of adsorbed sulfur species in sulfate is complete during one voltammetric cycle.

The behaviour of the adsorption valency X_s in function of the degree of coverage is the same as in the case of platinum and iridium. Thus, it can be deduced that the bond of sulfur with metals of group VIII and IB is partially ionic in low degrees of coverage, $\theta_s < 0,25$), becoming mostly covalent for higher θ_s.

References
1) T. LOUCKA, J. Electroan. Chem., 31, (1971), 319.
2) A.Q. CONTRACTOR and HIRA LAL, J. Electroan . Chem. 96, (1979), 175
3) E. LAMY-PITARA, L. BENCHARIF and J. BARBIER, Electrochimica Acta, in press

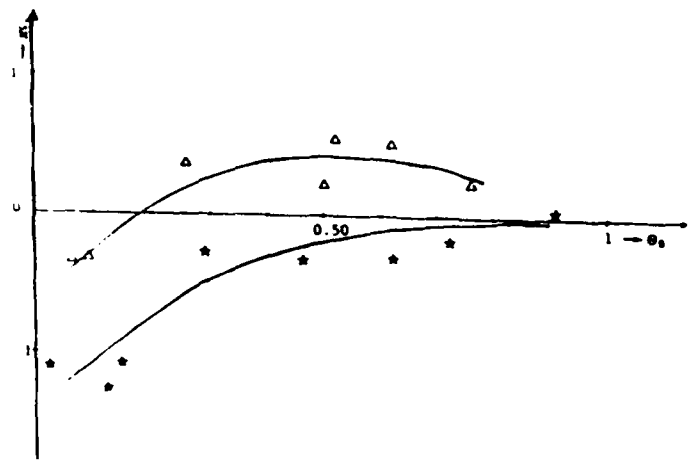

Fig 1 : Dependence of the adsorption valency of sulfur on platinum on the degree of coverage by sulfur
△ roughness factor r=100
★ roughness factor r=20

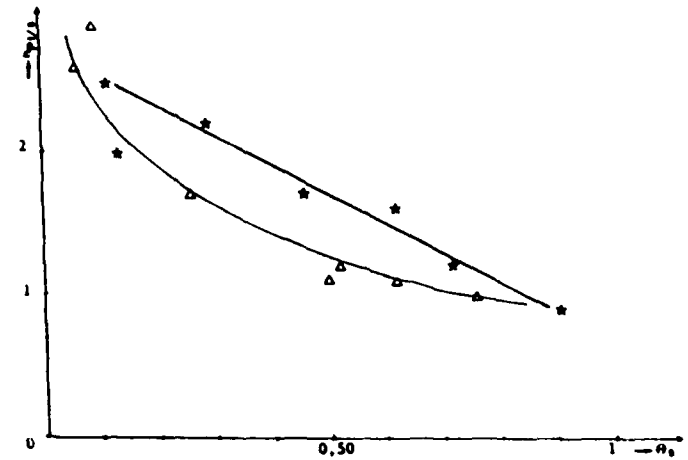

Fig 2. : Dependence of the adsorption stoichiometry of sulfur on platinum on the degree of coverage by sulphur
△ roughness factor r = 100, ★ roughness factor r = 20

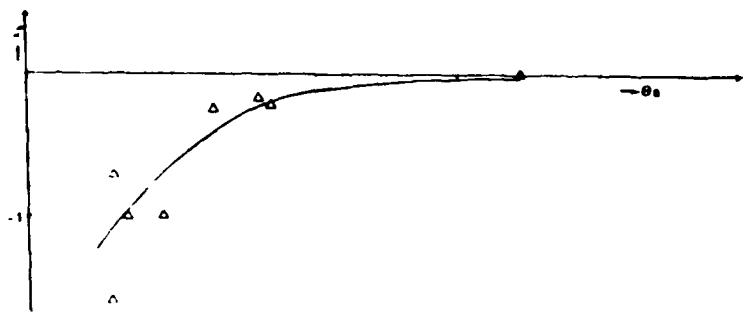

Fig 3 : Dependence of the adsorption valency of sulfur on iridium on the degree of coverage by sulfur.

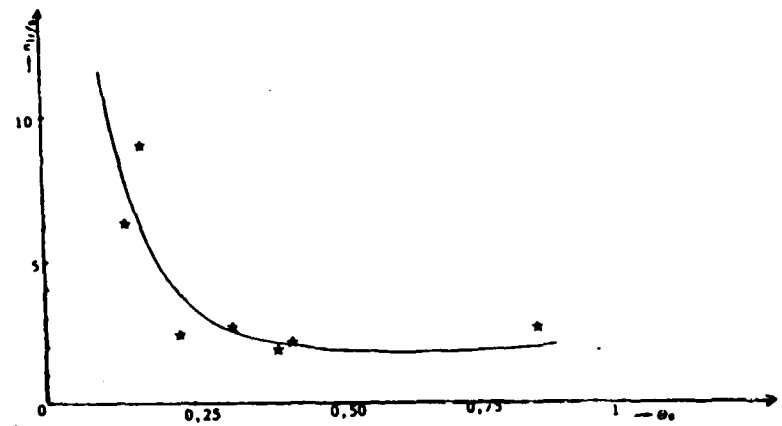

Fig 4. : Dependence of the adsorption stoichiometry of sulfur on iridium on the degree of coverage by sulfur

T9060

09070

ADSORPTION OF ASCORBATE IONS ON MERCURY ELECTRODE IN PRESENCE OF POTASSIUM PERCHLORATE.

Ma.M.GOMEZ and E.ALDA
Departamento de Electroquímica. Universidad Autónoma de Madrid.
28049 MADRID. Spain.

INTRODUCTION

The ascorbate ion (AH^-) is a monovalent ion of the L-ascorbic acid (Vitamin C). The acid itself and the monovalent ion consist of roughly planar γ-lactone ring with side-chain in a more or less staggered conformation. The acidity of the compounds is associated with the proton at O(3) because of the conjugated O(1)=C(1)-C(2)=C(3)-O(3) system in the ring.

The aim of the present study was to determine the structure of the mercury solution interface for AH^- and to analyze how the desprotonitation at O(3) affects the adsorption process by comparing the results with those obtained for L-ascorbic acid[1] (LAA). Potassium perchlorate was used as support electrolyte and the pH of the solution was mantained equal to 7 with KOH, in order to study the adsorption of the monovalent anion.

EXPERIMENTAL

Electrocapillary and capacity measurements were carried out in aqueous solutions of 10^{-2}M $KClO_4$ at seven different concentrations of LAA ($5x10^{-4}$-$7x10^{-3}$). A pH of 7 was mantained for each solution by adding KOH. Measurements were taken at 25°C. and all solutions were previously deoxygenated by bubbling nitrogen during 1h.

The double layer capacity was determined using an impedance bridge. REsults were independent of drop time. Measurements were ussually made at a frequency of 937 Hz, they were independent of frequency within the range 0.2-1.4 KHz. A satured calomel electrode was used as the reference electrode. The measurements of the zero-charge potential was carried out using a streaming electrode. The maximum interfacial tension was obtained by using a classical electrometer.

RESULTS AND ANALYSIS

The capacity hump occurs in the anodic region of p.z.c. and increases in height with a shift towards negative potentials as the bulk concentration of the electrolyte increases. It is observed that at concentrations greater than $2.5x10^{-3}$M of ascorbate ion the minimum in the capacity curve disappears.

Integration of the capacity curves provides the corresponding curves for electrode charge, σ^M, against the potential which

coincide at $\sigma^M \approx -3\mu C.cm^{-2}$. By integration of these curves the electrocapillary curves were obtained.

In the present system, the electrocapillary equation is:

$$d\xi_+ = E_+ d\sigma^M - \Gamma_{C10_4^-} d\mu_{KC10_4} - \Gamma_{AH^-} d\mu_{KAH} \qquad (1)$$

In order to determine the adsorption of the perchlorate ($C10_4^-$) and ascorbate anions, measurements at constant mole ration of $C10_4^-$ were also analyzed using the method described by Lakshmanan and Rangarajan[2].

Having evaluated the total suface excesses of two anions, the surface excess of K^+ was found from: $\sigma^M = -F(\Gamma_+ + \Gamma_-)$. Assuming that all Γ_+ are in the diffuse layer, it was possible to obtaine the total diffuse layer excesses due to anions as well as their individual contribuion $\Gamma^{2-s}_{C10_4^-}$ and $\Gamma^{2-s}_{AH^-}$ with the help of diffuse layer theory. The specifically adsorbed excess due to the individual anions $\Gamma^1_{C10_4^-}$ and $\Gamma^1_{AH^-}$ were then obtained. Values of Γ^{2-s}_+ and $\Gamma^1_{AH^-}$ increase markedly as σ^M becomes more positive, the plots of $\sigma^1_{AH^-}$ vs σ^M are approximatly linear and parallel. Values of $\Gamma^1_{C10_4^-}$ are negatives at concentrations of potassium ascorbate greater than 10^{-3}M. Then it is reasonable to assume that specifically adsorbed perchlorate is absent at concentrations of potassium ascorbate greater than 10^{-3}M.

The surface pressure for anionic adsorption at constant charge was derived according to Parsons expression[3]: $\phi = \xi^\circ_+ - \xi_+ + I$ where ξ°_+ is the value for 10^{-2}M $KClO_4$ solution in absence of potassium ascorbate, and I is the contribution of the diffuse layer to the surface pressure:

$$I = -\int_{\mu 1}^{\mu 2} \Gamma_-^{2-s} \, d\mu \qquad (2)$$

where 1 and 2 stand the lowest concentration studied and any other higher concentration respectively.

The adsorption isotherm was analized by superimposing the surface pressure vs $\ln a_{\pm AH^-}$, at constant charge. The composite surface pressure curve fits well to the Frumkin isotherm with an interaction parameter of -2.4 and $\Gamma_s = 2.2 \times 10^{-10} mol.cm^{-2}$.

The standard free energy of adsorption, ΔG°, calculated by the Parsons method, at $\sigma^M = 0$ is -20.25 $KJ.mol^{-1}$. It was observed that the standard free energy displays a linear dependence on the charge.

The rational potential drop across the inner layer, $\Delta\phi^{M-2}$, was calculated from the measured potential by sustracting the potential for the m.e.c. in absence of specific adsorption and the diffuse layer potential drop given by the Gouy-Chapman theory. The change in $\Delta\phi^{M-2}$ at constant charge shows a linear dependence on the specifically adsorbed charge due to the ascorbate anions, these lines are parallel which correspond a linear

dependence of $\Delta G°$ on σ^M in view of the approximate relationship:

$$\left(\frac{\partial\ \phi^{M-2}}{\partial\ \sigma^1_{AH^-}}\right)_{\sigma^M} = \frac{RT}{F}\ \frac{\partial\ \ln\beta}{\partial\ \sigma^M} \qquad (3)$$

where β is the adsorption coefficient.

The term of the left-hand side of (3) is equal to the reciprocal of one component of the inner layer $_{\sigma_1}C^i$ which can be replaced by the corresponding integral capacity $_{\sigma_1}K^i$.

The total inner layer capacity C^i was calculated from:

$$\frac{1}{C} = \frac{1}{C^i} + \frac{1}{C^d}\left(\left(\frac{\partial\ \sigma^1}{\partial\ \sigma^M}\right)_\mu + 1\right) \qquad (4)$$

The components of the inner layer capacity were then calculated from the identity:

$$\frac{1}{C^i} = \frac{1}{{}_{\sigma^M}C^i} + \frac{1}{{}_{\sigma_1}K^i}\left(\frac{\partial\ \sigma^1}{\partial\ \sigma M}\right)_\mu \qquad (5)$$

where $_{\sigma^M}C^i$ is the capacity measured at constant amount adsorbed the integral capacity $_{\sigma^M}K^i$ was obtained from the change of $\Delta\phi^{M-2}$ with σ^M at constant $\sigma^1_{AH^-}$. From the ratio $_{\sigma^M}K^i/_{\sigma_1}K^i$ was evaluated the ratio $(x_2-x_1)/x_2$ where x_2 and x_1 are the distances from OHP and IHP planes to the metal respectively.

REFERENCES

1. Ma.M.Gómez, E.Díez, E.Alda and A.Aldaz; J.Electroanl.Chem., 165(1984)207.

2. S.Lakshmanan and S.K.Rangarajan; J.Electroanl.Chem., 27(1970) 127.

3. R.Parsons; Trans.Faraday Soc., 51(1955)1518.

09080

STUDY AND COMPARISON OF ANOMALIES OBSERVED ON IMPEDANCE DIAGRAMS OF NICKEL IN THE PRESENCE OF F^- AND HSO_4^- ANIONS

M. CID and M.C. PETIT
Laboratoire de Mécanique Physique, U.A. CNRS 867, Université de Bordeaux I
351 cours de la Libération, 33405 Talence cedex (France)

We present a comparison between the study of nickel polarization characteristics and the evolution of impedance diagrams in function of potential. We analysed nickel response into two very different acidid media : hydrofluoric and sulphuric solutions.

1 - Study of I(E) curves

Polarization curves are shown from corrosion potential to oxygen escape. In N H_2SO_4 solutions, I(E) curve shows three separated maxima : two in the active range, one in the transpassive range. In a solution of 0.01N HF/0.5N NaF, the I(E) curve shows only one maximum, the potential of which changes with the F^- anion concentration (figure 1).

2 - Impedance diagrams

Impedance diagrams are drawn, after stabilization of current, from 10^4Hz to 10^{-3}Hz. We observe three types of diagrams.

(a) At potentials corresponding to positive slopes of I(E) characteristics, impedance diagrams present capacitive and inductive loops and turn, with respect to decreasing frequency, in the direction of watch hands and close to a R_p positive polarization resistance (type 1).

(b) At potentials corresponding to negative slopes of I(E) characteristics impedance diagrams turn in the opposite direction of watch hands, at decreasing frequency, and close to a R_p negative polarization resistance (type 2).

(c) In some cases, before current maxima (positive slopes of I(E)), impedance diagrams present a anomaly, they turn in the opposite direction of watch hands, but always close to a Rp positive polarization resistance and in these conditions they cross over the four quadrants of the complex plan (R,-jG) (type 3).

3 - Study of nickel behaviour in the presence of F^- and HSO_4^- ions

From electric response point of view, we can separate the different current maxima.
In the case of sulphuric solutions, type 3 impedance diagrams (anomaly) are only observed in a range of potential before the third maximum. In the active range impedance diagrams are always like types 1 and 2.
In the case of hydrofluorhydric solutions, type 3 impedance diagrams are also observed before the current maximum.

In all cases near the current maximum, we found classical impedance diagrams (types 1 and 2).

4 - Conclusion

There is not a straight correlation between the I(E) characteristics and the evolution of impedance diagrams with potential ; in effect, anormal impedance diagrams, type 3, does not always correspond to a current maximum and are not a signature of an active-passive transition.
Therefore impedance diagrams of type 3 must be connected with a particular configuration of the adsorbed intermediates at nickel interface which depend simultaneously on the nature of anions and potential.

References

M. CID, M.C. PETIT and F. VARAILHON DE LA FILOLIE - J. Chim. Phys., 75, 612 (1978).
A. SARABY-REINTJES - Electrochim. Acta, 30, 387 (1985).
A. SARABY-REINTJES - Electrochim. Acta, 30, 403 (1985).

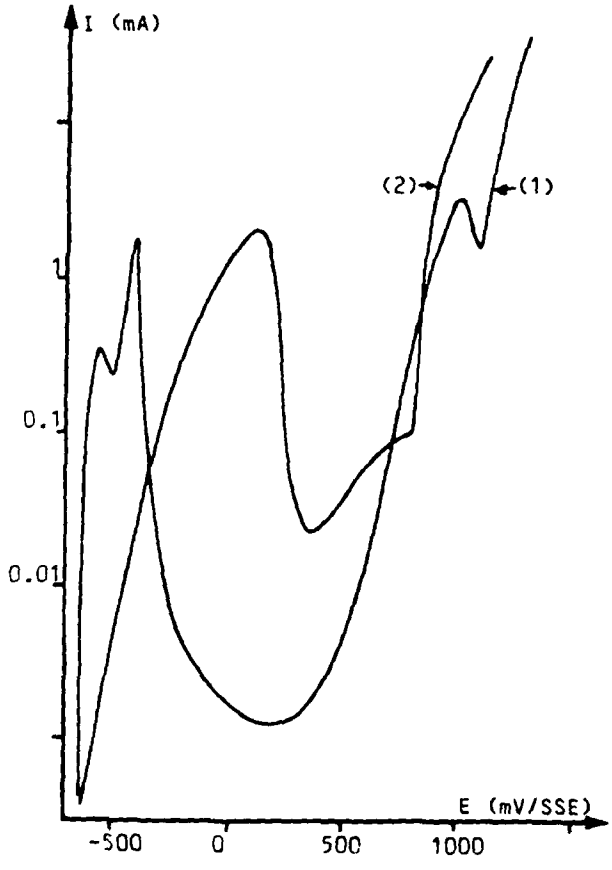

Fig.1- Characteristics of nickel in : (1) sulphuric acid
(2) hydrofluoric solution

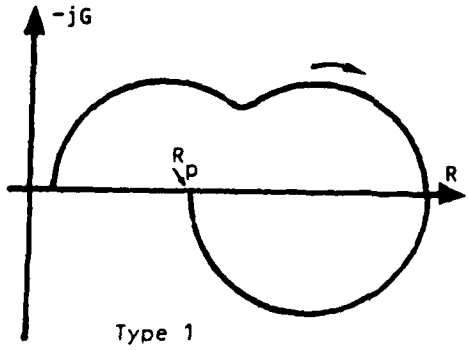

Type 1

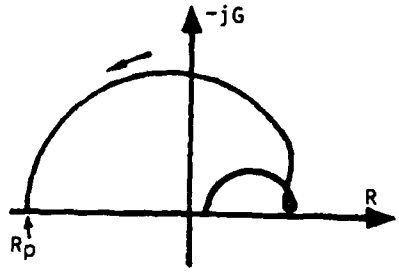

Type 2

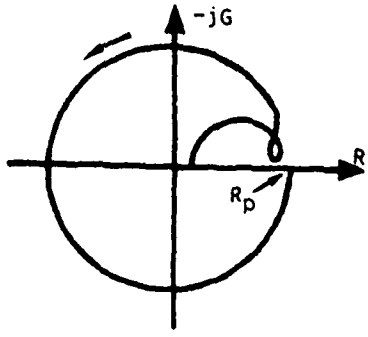

Type 3

09090

STUDY ON THE ADSORPTION OF Zn(II) IN PYRIDINE-$NaClO_4$ MEDIA

M.Pérez Sanchez, M. Barrera, S.González and A.Arévalo
Department of Physical Chemistry. University of La Laguna.
La Laguna. Tenerife. (Spain).

This report is comprised within a more general study on the inducing effect of adsorption of metal cations in the presence of organic bases, specially heterocyclics, on mercury electrode and the adsorption patterns which are followed. We present here the adsorptive behaviour of Zn(II) in $NaClO_4$ 1 M varying the pyridine and Zn(II) concentrations.

The double step chronocoulometric [1,2,3] and the cyclic voltammetric techniques on the H.M.D.E. have been used in order to determine the surface excesses of the Zn(II) species, which is reduced on the mercury electrode and to ascertain the adsorptive behaviour of this electrodic process. The concentrations of Zn(II) were: 0.5, 1.0 and 1.5 mM and the pyridine concentrations were: 0.02, 0.05, 0.1, 0.2, 0.4 and 0.6 M; the ionic strength was maintained at 1.0 with $NaClO_4$ and the pH was adjusted to 7.8 to prevent the presence of the pyridinium ions.

The increase of cathodic peak currents as the scan rate in L.S.V. increased clearly shows the adsorptive character of the electrode process. On the other hand, the variation of the i_{pa} / i_{pc} ratio as the scan rate increased shows a progressive decrease which is characteristic of a process with an adsorption control in addition to diffusion control of the charge transfer.

In previous papers [4,5] the formation of complex species of Zn(II)-pyridine has been pointed out. Likewise, the characteristic adsorptive behaviour of pyridine on Hg electrode in KCl and other ionic media has been studied.[6,7,8] One of these features is the different orientation of pyridine molecules on the surface of Hg electrode in both branches of electrocapillary curves. In the present study the initial potential values are within the -0.4 to -0.7 V vs. SSCE range and this fact indicates that the more favoured adsorption is towards more cathodic potentials, together with the existence of

positive charge of Zn(II)-pyridine species which is adsorbed and reduced on Hg electrode.

At potentials of anodic branches of electrocapillary curves the flat orientation of the pyridine molecules adsorbed on Hg electrode is preventing the bridge ligand mechanism from being carried out. On the contrary, this was surely more favoured in the cathodic branches. This is the opposite behaviour to that observed in the cases of the adosrption of Zn(II) in SCN^- and N_3^- media[9,10]. An adsorption increase was observed from $n\bar{F}\Gamma$ vs. potential data as the cathodic potentials and Zn(II) concentration increased at pyridine concentrations comprised between 0.02 and 0.2 M. At pyridine concentrations 0.4 and 0.6 M, the initial tendency is progressively attenuated and even a depression is present in these curves $n\bar{F}\Gamma$ vs. E_i at higher Zn(II) concentrations. This is probably due to the maximun recovering of surface electrode. Moreover it is not characteristic of all pyridine concentrations studied that the increase of Zn(II) concentration gives rise to an increase of the amount of adsorption.

The scheme:

$$[Zn(II)(pyr)_n]^{2+}_{sol} \rightleftharpoons [Zn(II)(pyr)_n^{2+}]_{ads}$$

is fundamentally proposed at the more anodic of the potentials studied whereas at the more cathodic potentials a ligand bridge mechanism is more favoured, although it is not yet clear at all which of the two mechanisms predominates at these potentials.

Figure 1 shows the dependence of $n\bar{F}\Gamma$ vs. E_i in the presence of (⊙),0.5; (×), 1.0; (△). 1.5mM Zn(II), 0.02M pyridine. Figure 2 shows the variation of $n\bar{F}\Gamma$ vs. pyridine concentration for:(⊙), -0.5; (×), -0.6; (△), -0.7V.

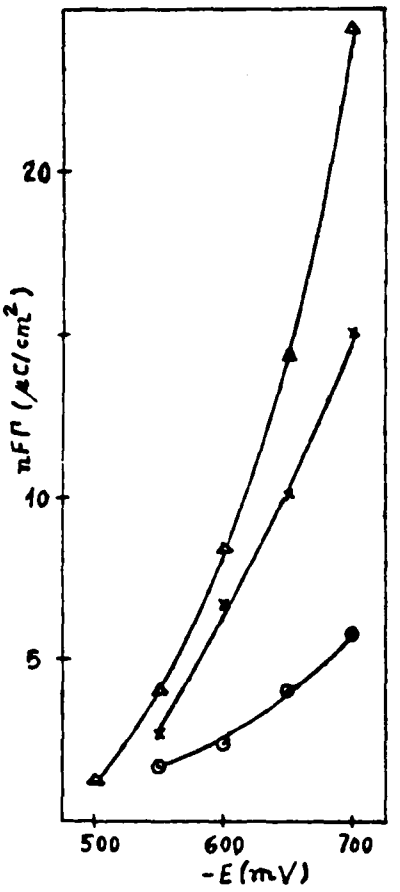

Figure 1

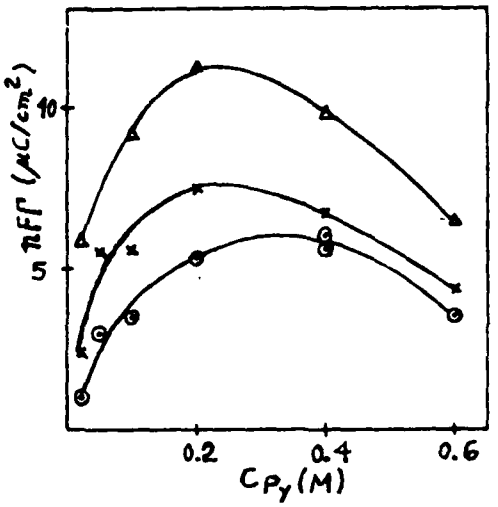

Figure 2

References

1. F.C.ANSON, J.H.CHRISTIE and R.A.OSTERYOUNG. J.Electroanal Chem. 13, 343, (1967).
2. J.H.CHRISTIE, R.A.OSTERYOUNG and F.C.ANSON. J.Electroanal Chem. 13, 236, (1967).
3. G.LAUER, R.ABEL and F.C.ANSON. Anal.Chem. 39, 765, (1967)
4. J.N.GAUR. J.Electroanal. Chem. 9, 321, (1965).
5. D.R.CROW and N.C.ZANOPOULOS. J.Electroanal.Chem. 109, 231, (1980).
6. R.G.BARRADAS, P.G.HAMILTON and B.E.CONWAY. Coll.Czech. Chem.Commun. 32, 1790, (1967).
7. B.E.CONWAY, R.G.BARRADAS, P.G.HAMILTON and J.M.PARRY. J.Electroanal.Chem. 10, 485, (1965).
8. B.B.DAMASKIN. Electrochim. Acta. 9, 231, (1954).
9. G.LAUER and R.A.OSTERYOUNG. Anal. Chem. 41, 1822, (1969).
10. Z.KOWALSKI and F.C.ANSON. J.Electrochem. Soc. 116, 1208, (1969).

09100

EVALUATION OF OHMIC POTENTIAL DROP AND DOUBLE LAYER CAPACITANCE OF THE INTERFACE BETWEEN TWO IMMISCIBLE ELECTROLYTE SOLUTIONS FROM GALVANOSTATIC PULSE MEASUREMENTS

Zdeněk Samec and Vladimír Mareček

J. Heyrovský Institute of Physical Chemistry and Electrochemistry, Czechoslovak Academy of Sciences,
U továren 254, 102 00 Prague 10 (Czechoslovakia)

The progress was made in the performance of the galvanostatic pulse technique which was shown to yield reliable information on the ohmic potential drop and capacitance of the interface between two immiscible electrolyte solutions[1]. Through the reduction of the resistance inside the reference electrode connected to the organic solvent phase and through the introduction of the computer control, the whole procedure was made much faster than before. Prior to the initialization of the current pulse, the interface was polarized by a small current, the magnitude and the direction of which was changed by means of the microcomputer until a pre-programmed potential value was reached. The measurement and the storage of about 30 galvanostatic transients at different initial potentials over the whole potential range available took approximately 20 seconds. The comparison was made with an ac impedance technique.

From the fast galvanostatic pulse measurements at 25°C the capacitance of the water/nitrobenzene interface was evaluated as a function of the interfacial potential difference $\Delta_o^w\varphi$ for system consisting of NaBr, LiCl or $MgSO_4$ in water and tetrabutylammonium tetraphenylborate, tetraphenylarsonium tetraphenylborate or tetraphenylarsonium dicarbollylcobaltate in nitrobenzene[2]. The modified Verwey-Niessen model, in which an inner layer of solvent

molecules separates two space-charge regions (the diffuse double layer), describes the structure of the water/nitrobenzene interface well at electrolyte concentrations above ca. 0.02 mol dm^{-3}, provided that the ions are allowed to penetrate into the inner layer over some distance. For all the systems studied the zero-charge potential difference was found at $\Delta_o^w \varphi_{pzc} \approx 0$ on the basis of the standard potential difference $\Delta_o^w \varphi^o_{TMA^+} = 0.035$ V for tetramethylammonium cation which was used as a reference ion. At zero surface charge the comparison was made with the theoretical capacitance calculated using the mean spherical approximation for a model consisting of two ion and dipole mixtures facing each other. The effect of ion penetration on the interfacial capacitance was estimated from the solution of the linearized Poisson-Boltzmann equation for a triple dielectric model with a continuous distribution of the point ions. The concentration-independent inner layer potential difference and capacitance can only be inferred from the capacitance data if the ion size effect is taken into account. A non-iterative procedure based on the hypernetted-chain equation was used for the evaluation of the potential drop across the diffuse double layer. The extent of the penetration into the inner layer appears to be a function of ion solvation, e.g. the more hydrated ion the less extensive ion penetration is likely.

1 V.Mareček and Z.Samec, J. Electroanal. Chem. 185 (1985) 263-271

2 Z.Samec, V.Mareček and D.Homolka, J. Electroanal. Chem., in press

09110

TEMPERATURE EFFECT AT GOLD SINGLE CRYSTALS/AQUEOUS SOLUTION INTERFACES

A.HAMELIN and L.STOICOVICIU, LEI, CNRS Meudon, 92195 (France)
F.A.SILVA and M.J.SOTTOMAYOR, University of Porto (Portugal)

It was clearly shown for several high melting sp metals that there is an influence of the atomic arrangement of the electrode surface on the double layer properties[1]. Up to now only two communications deal with the influence of the temperature on the structure and composition of the dl at solid sp metal faces[2,3].

For mercury the variations of the capacity minimum and its potential with temperature are linear : a few tenths of a millivolt per degree for the PZC.

For solid faces the published values of the PZC are not given more precisely than $\pm$ 10 mV. Precise observations are more difficult on solid faces because they cannot be renewed, therefore the interface has to remain clean for several hours for observation of the influence of the temperature.

Several faces of gold were studied in perchloric acid solutions. The changes of the temperature at the interface were followed recording -for a given temperature- a cyclic voltammogram including the formation of a monolayer of oxidized compounds and their reduction.

Differential capacity-potential curves (C(E)) were recorded for different concentrations at different temperatures ranging from 1 to 60°C. For dilute solutions, with temperature, the PZC varies linearly and positively and the capacity at the minimum varies linearly and negatively (figure 1).

C(E) were integrated taking the PZC at the capacity minimum. Obviously there are two charge domains on the C(σ) curves (σ : charge density) where the temperature coefficients have different signs (figure 2).

For concentrated solutions there are also two charge domains on the C(σ) curves where the temperature coefficients have different signs ; a temperature invariant capacity is also observed but less precisely.

Residual excess entropies S^* (see[4]) are obtained as a function of the charge density at the gold faces.

The degree of solvent orientation at the interfaces is discussed.

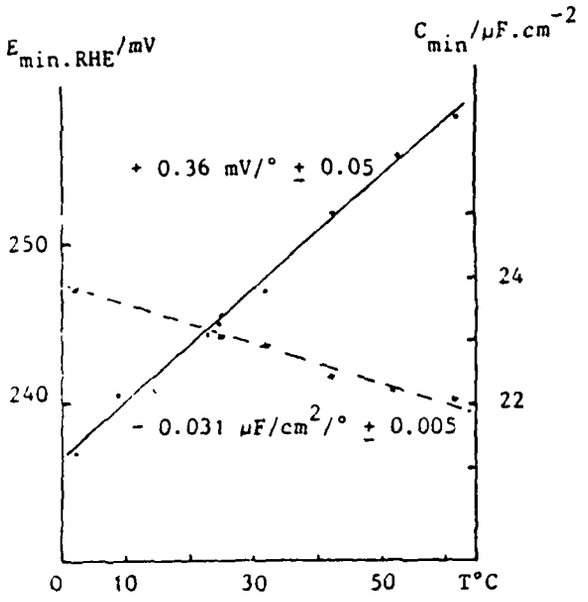

Fig.1 : For Au(210) in 10 mM $HClO_4$, variations of E_{min} (.) and C_{min} (x) as a function of temperature[3].

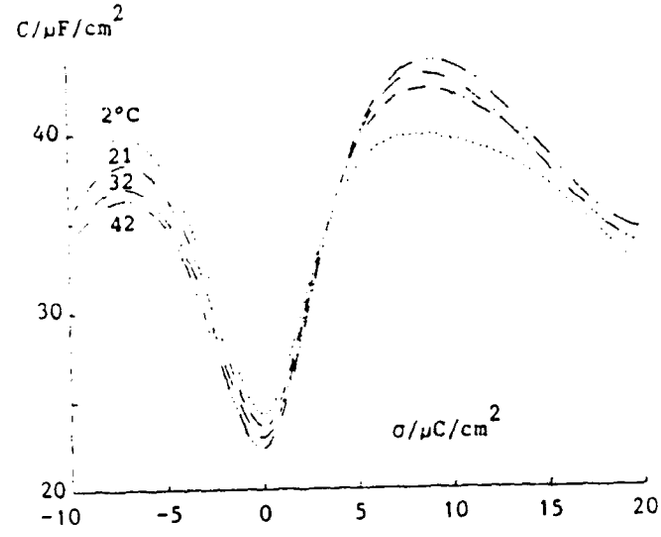

Fig.2 : C(σ) curves for Au(210) in 10 mM $HClO_4$[3].

1. A.HAMELIN, T.VITANOV, E.SEVASTYANOV and A.POPOV, J.Electroanal. Chem., 145 (1983) 225.
2. F.A.SILVA, A.HAMELIN and R.PARSONS, 34th ISE Meeting, 1983, Erlangen (Germany).
3. A.HAMELIN, L.STOICOVICIU and F.A.SILVA, Electrochim.Soc., Spring Meeting, 1985, Toronto (Canada).
4. G.HILLS and F.A.SILVA, Can.J.Chem., 59, n°13 (1981) 1835.

09120

ADSORPTION OF Tl(I) ON MERCURY IN AZIDE MEDIA

S.GONZALEZ, P.CARRO and A.AREVALO
Department of Physical Chemistry. University of La Laguna, Tenerife (Spain).

In a previous work[1] we pointed out that the adsorptive behaviour of Tl(I) on the Hg electrode in NaSCN media did not follow the model proposed by Anson and Barclay[2], i.e., SCN^- anions adsorbed are not involved in the adsorption mechanism, nor does the model of anion induced adsorption adequately explain the adsorption of Tl(I) halides[3]. In order to determine if this is a specific behaviour of Tl(I), we have carried out a new study of its adsorption in azide media. The N_3^- anion is adsorbed specifically on the mercury electrode and gives rise to one weak complex species[4] with the Tl(I) cation. Nevertheless, this anion N_3^- induces the adsorption of Cd(II) and Zn(II) cations on the Hg electrode by a bridge mechanism[5]. These features appear to point to the Tl(I) cation as the agent responsible for this adsorptive pattern.

The Tl(I) surface excess in azide media on the H.M.D.E. has been determined using the double-potential step chronocoulometric technique[6, 7, 8]. The concentration of Tl(I) were: 0.5, 1.0 and 1.5mM. The concentration in NaN_3 were: 0.4, 0.6, 0.8 and 1.0M. The ionic strength of all solutions was maintained at 1.0 with $NaClO_4$. We observe the adsorption increases with increasing cathodical potential and increasing azide concentrations. Moreover, an increase in the adsorption amount was observed as the Tl(I) concentration increased. As some authors[9] suggest, the charge on the metal, q_m, is an indepent variable prefereable to the potential in adsorption studies, so we have use it. Thus at constant charge the electrode-particle interactions should be approximately constant. Figure 1 shows the Tl(I) adsorption amount vs. the electrode charge, q_m, at a concentration of Tl(I) = 1.0 mM and various corresponding NaN_3 concentrations. The adsorption decreases as the anodic potential shifts, unlike the adsorptive behaviour of the N_3^- anion[10]. These facts appear to indicate that the $Tl(I)-N_3^-$ complex species is occupying the vacant sites left by the anions in their desorption process, as the cathodic potential increases. That is, the N_3^- anion adsorbed is not involved in the adsorption process. The adsorption mechanism proposed by us follows the next scheme:

$$\left[Tl(I)-N_3^-\right]_{sol} \rightleftharpoons \left[Tl(I)-N_3^-\right]_{ads}$$

differing from the mechanism reported by Anson et al.[2], which is characterized by a direct involvement of the adsorbed N_3^-.

The adsorption mechanism which takes into account the proven facts of direct binding of the $Tl(I)-N_3^-$ species to the surface electrode is also shown in figure 2, where the surface excess of Tl(I) is plotted against the azide surface excess. The $\Gamma_{N_3^-}$ values were obtained from data reported by Parsons[10] We observed a Tl(I) adsorption decrease as the N_3^- adsorption increased, and we think that there must be a competition between the $Tl(I)-N_3^-$ and the N_3^- adsorption processes. Neither of the cases observed shows a saturation state of the surface electrode, perhaps due to the small solubility range of Tl(I) in azide media.

The q_m variation, Δq_m, has been calculated in order to determine the changes in the electrode charge caused by the adsorbed species. Δq_m is given by the difference of the electrode charge in the presence and absence of Tl(I), respectively. The Δq_m values obtained are very small, indicating that the Tl(I) adsorption scarcely changes the charge on the electrode. This is the expected behaviour since the only complex species existing in the solution is TlN_3, whose adsorption does not modify the electrode charge and does not eject the anions already adsorbed, the complex species occupying the sites left vacant by the azide anions in their desorption process.

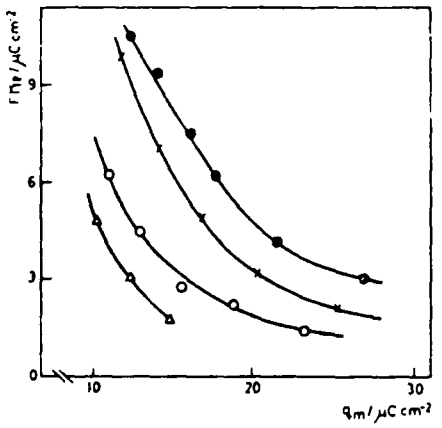

Figure 1

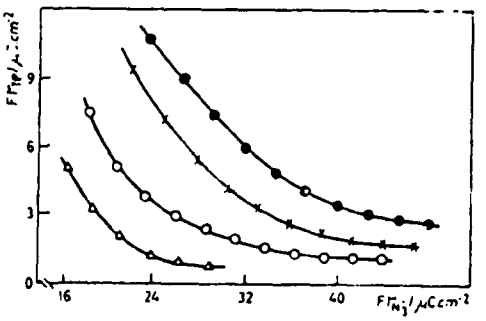

Figure 2

References:

1. S.GONZALEZ, P.CARRO and A.AREVALO. Electrochim. Acta, 30, 811, (1985).
2. F.C.ANSON and D.J.BARCLAY. Anal. Chem., 40, 1791, (1968).
3. C.M.ELLIOT and R.W.MURRAY. Anal.Chem.,48, 259, (1976).
4. V.S.K.NAIR and G.H.NANCOLLAS. J.Chem.Soc., 318, (1957).
5. Z.KOWALSKI and F.C.ANSON. J.Electrochem.Soc., 116, 1208, (1969).
6. F.C.ANSON, J.H.CHRISTIE and R.A.OSTERYOUNG., J.Electroanal Chem., 13, 343, (1967).
7. J.H.CHRISTIE, R.A.OSTERYOUNG and F.C.ANSON. J.Electroanal Chem., 13, 236, (1967).
8. G.LAUER, R.ABEL and F.C.ANSON. Anal.Chem., 39, 765, (1967)
9. R.PARSONS. J. Electroanal. Chem., 7, 136, (1964).
10. C.V.D'ALKAINE, E.R.GONZALEZ and R.PARSONS. J.Electroanal. Chem. 32, 57, (1971).

09130

OBSERVING THE COMPONENTS OF THE IDEALLY POLARIZABLE DOUBLE LAYER USING INFRARED SPECTROSCOPY

GALEN J. HANSEN* and WILFORD N. HANSEN*
Department of Physics
Utah State University
Logan, Utah 84322

James F. Andrew
Los Alamos National Laboratory
Los Alamos, New Mexico 87545

The work of Hansen, Kolb, and co-workers has shown that over an extended potential range, the working electrode can be emersed hydrophobically (i.e. visually, the electrode is completely dry and the contact angle is non-zero), with the tenuous double layer intact[1-6]. This is possible because of the required charge neutrality within the double layer, i.e. one type of charge on the electrode and the opposite charge on the ionic side, and also because of the huge fields between the opposite charges of the double layer (on the order of 10^7 V/cm). Emersed, the components of the tenuous double layer can now be observed using infrared spectroscopy without interference from the bulk solution. The spectra are clear, and the information concerns only the electrochemical interphase.

By continuous rotation, the electrode can be emersed continuously and the double layer observed within seconds after emersion[4,6]. Any part of the emersed double layer is electrostatically isolated from the solution and from the rest of the double layer on the emersed part of the electrode. As the electrode is rotating, the electrode potential can be cycled. In such a case, the potential drop across the emersed double layer will vary continuously from one side of the electrode to the other, each part corresponding to the electrode potential as that part of the electrode was emersing[6].

In this study, infrared spectra of gold electrode surfaces were taken at various electrode potentials as the electrode rotated and emersed. The spectra at the various potentials were ratioed to reveal changes in the emersed double layer due to potential changes. Ions such as perchlorate and fluoride were used to avoid specific adsorption, allowing the double layer to be ideally polarizable. The vibrational spectra of ions and water within the interphase were observed as a function of potential, ion concentration, length of time in situ and ex situ, as well as other conditions. Figure 1 is an example of infrared spectra of a gold-coated electrode emersed from 0.10 M perchloric acid. The broad downward peak at approximately 1110 cm^{-1} is due to the perchlorate

* presently working at Los Alamos National Laboratory, Los Alamos, NM 87545

ion within the emersed double layer. The upward peak at 1710 cm^{-1} is probably the hydronium ion of the acid solution. The downward peak at 1380 cm^{-1} could be due to adsorbed water. The sharp gaseous water bands are present because of small changes in the amount of water vapor within the cell and spectrometer. Note the 100X expansion of I/I_o%.

REFERENCES

1. D.M. Kolb and W.N. Hansen, Surf. Sci., 79 (1979) 205.

2. W.N. Hansen and D.M. Kolb, J. Electroanal. Chem., 100 (1979) 493.

3. W.N. Hansen, D.M. Kolb, D.L. Rath and R. Willie, J. Electroanal. Chem., 110 (1980) 369.

4. D.L. Rath and D.M. Kolb, Surf. Sci., 109 (1981) 641.

5. W.N. Hansen, J. Electroanal. Chem., 150 (1983) 133.

6. G.J. Hansen and W.N. Hansen, J. Electroanal. Chem., 150 (1983) 193.

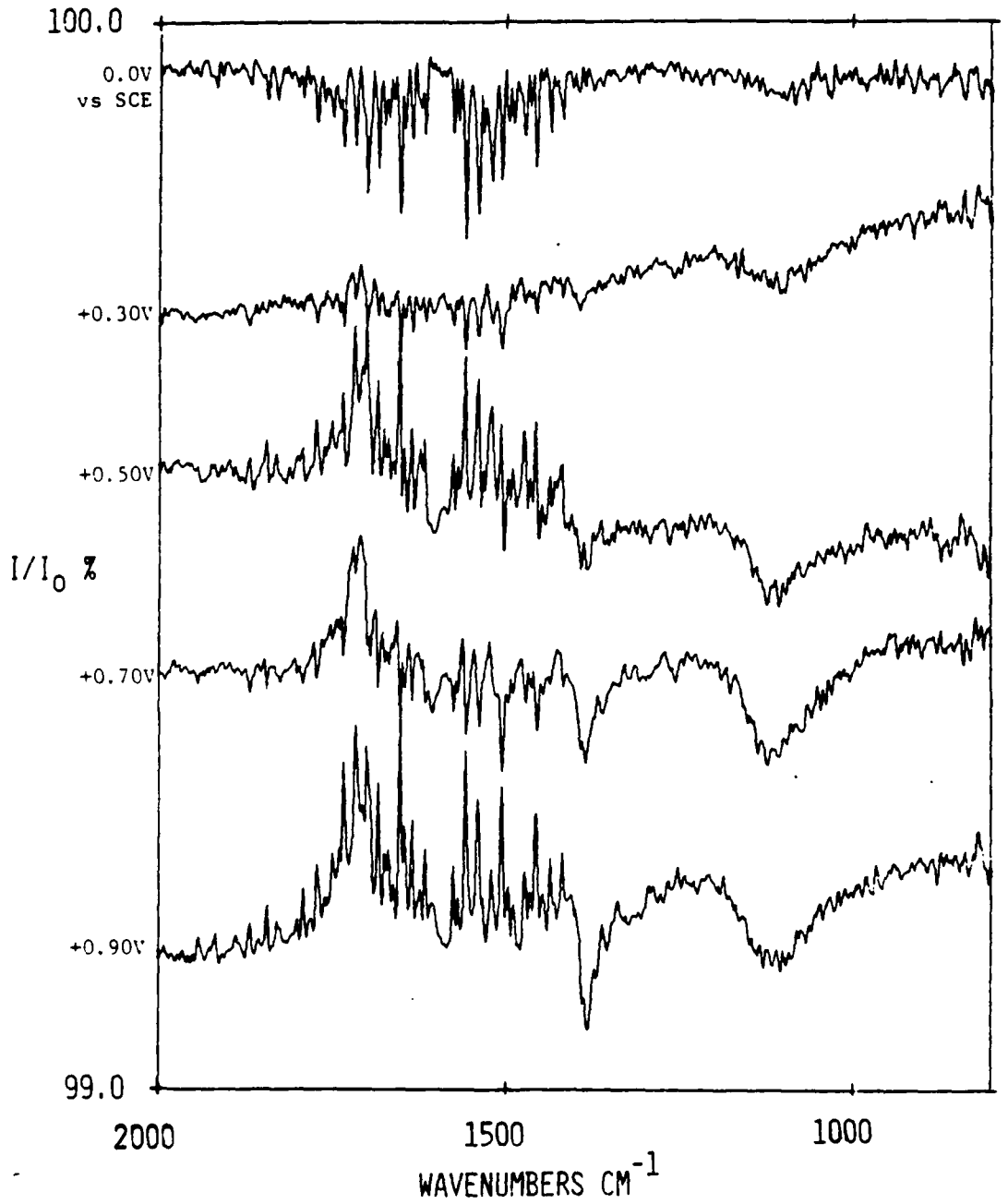

Figure 1. Series of infrared spectra taken as gold-coated electrode continuously emersed at various electrode potentials. Spectra are ratioed to spectrum at -0.30 V vs SCE. Approximately 1000 A Au evaporated on plate glass. Electrolyte was 0.10 M $HClO_4$. Electrode was rotated at 30 sec/rev.

09140

INTERFACE CONSTRUCTION TO INFORMATIZATION OF ELECTROCHEMICAL PROCESSES

L. Victori, W. Bek, L. Núñez, R. Fortuny

Analytical Department. Instituto Químico de Sarriá. BARCELONA

Introduction

In the Chemical Analysis area, the possibilities of the microcomputer applications in investigation have become very interesting.

The objective of the present work is the construction of an interface in order to implement a microcomputer into the electrochemical processes which are the object of study.

The apparatus permits the intensity or voltage data acquisition and the potential function generation to be applied in general electrochemical experiences.

Experimental

The interface has been designed for an informatic system established by an 8-bit microcomputer (Z-80 microprocessor) with an external memory (cassette or diskette), a monitor and a register (X/t or X/Y Plotter).

The microcomputer used in this work is a VIDEO GENIE SYSTEM EG 3003, which operates in conjunction with a conventional electrochemical system.

This system can be applied to processes with potential or intensity control.

Results and Discussion

A system for the application of any voltage function to an electrochemical cell has been developed. The potential function values must be between -10 and +10 volts. The experiences have to longer than a minimal duration. In the case of the cyclic voltammetry, with a periodic triangular voltage function, the minimal duration is 24.8 seconds per cycle.

The interface also permits the voltage or intensity data acquisition with a maximal sampling frequency of 8700 data per second.The acquired values must be in the range of -4 to +4 volts for the voltage or $\pm$10 A to $\pm$300 mA for the intensity.

The voltammogram showed in Figure I has been obtained with a 0.1 M Fe(II)/ 0.1 M Fe(III) system in 4 M H_2SO_4 solution with a Platinum electrode. The voltage function applied is a periodic triangle between -0.580 and 0.800 volt (Hg/Hg_2SO_4 Reference electrode), with

a scanning rate of 100 mV/s. The same voltammetry is showed in Figure *II*, but the function voltage was generated by the microcomputer. The comparison of both does not show any important differences. Figure III is the offline graphic representation of the acquired potential data of the voltammetry showed in Figure II. A little noise signal can be observed overlapping on the cell signal, in comparison with Figures I and II. This background might be produced, in part, by noise captations from AC Power Supply in great impedance points of the system. This kind of avoided signals decreases notably in intensity with an adequate blindage. The other cause of the signal perturbations is the discretization of a continuous signal in order to be digitalized; under the working conditions, it is not possible to reduce it.

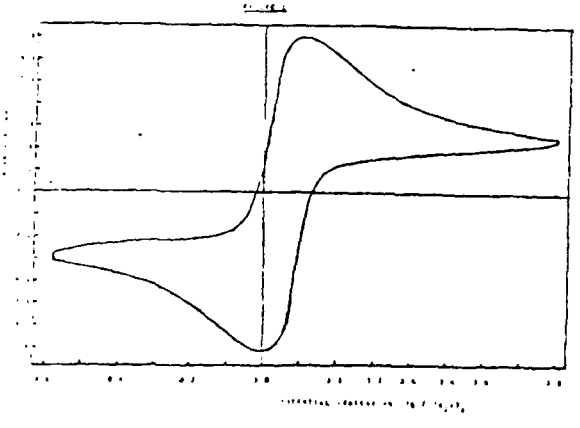

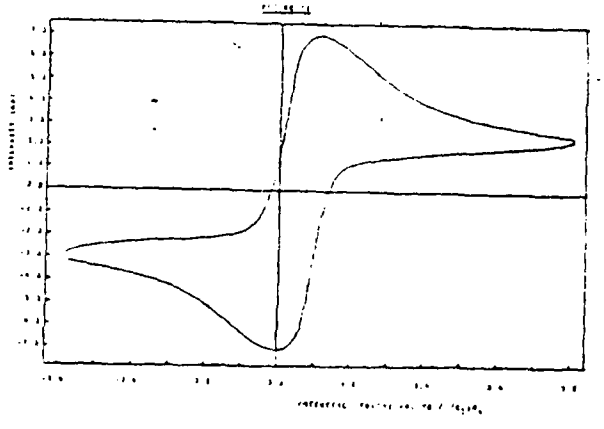

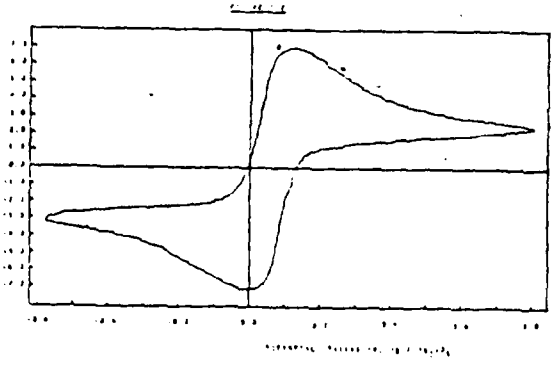

09150

ADSORPTION OF α, β-UNSATURATED ALDEHYDES AT THE MERCURY-WATER INTERFACE

D. GONZALEZ-ARJONA and M. RUEDA
Department of Applied Physical-Chemistry, Faculty of Farmacy, c/Tramontana s/n, Sevilla 41012 (Spain)

INTRODUCTION

α, β-unsaturated aldehydes have been shown to present different reduction behaviour on a mercury electrode depending on the type of substituent on the ethilenic bond[1-3]. An aryl substituent seems to facilitate the reduction of the ethilenic bond whereas an alkyl group that of the carbonyl. As it is known that aromatic and aliphatic compouds behave also differently at the Hg/electrolyte solution interface[4], it appears possible that the disposition of the molecule on the electrode could determine the reduction process.

Bearing this in mind, a study has been made of the adsorption behaviour of α, β-unsaturated aldehydes, cinnamaldehyde (CA) and crotonaldehyde (CRA), at mercury/water interface.

Differential capacity, zero charge potential and maximun surface tension measurements were carried out for 1M KCl solutions with different organic compound concentrations.

RESULTS AND DISCUSSION

Phenomenologically the two aldehydes present quite different behaviour at the interface. Differential capacity curves for CRA show an anodic adsorption-desorption peak whereas CA is adsorbed even at -100mV. The σ-E curves have a commun intersection point at σ_{max}= -.1 μC cm^{-2} and E_{max} = -520mV, for CA adsorption. On the contrary, for CRA only the curves for lower concentrations (C_{org} ≤0.1M) intersect at σ= - 3 μC cm^{-2} and E= -608mV. Potentials of zero charge shift positively when adsorbate concentration increases. The shift is small for CA and quite pronounced for CRA.

Congruence with respect to either charge and potential was detected for CA adsorption but this was not the case for CRA adsorption. The parameters of a Frumkin isotherm were obtained by the analysis of the $\ln\theta/C_{org}(1-\theta)$ vs. θ and φ vs. Γ plots, at each potential. The experimental precission allows us to deduced only two parameters of the α, Γ_s and n set. Potential-independent α = 2.4 and Γ_s = 3.5 10^{-10} mol cm^{-2} values were found for CA adsorption. On the contrary, in the case of CRA, α is better described by a quadratic function of potential and Γ_s adopts values close to 8. 10^{-10} mol cm^{-2}.

It seems that cinnamaldehyde is orientated flat on the electrode and crotonaldehyde takes on a vertical orientation. However a carefully exam of $\Delta\phi_2^M$ vs. Γ plots suggests the idea of a changing molecular orientation of CRA depending on charge and coverage.

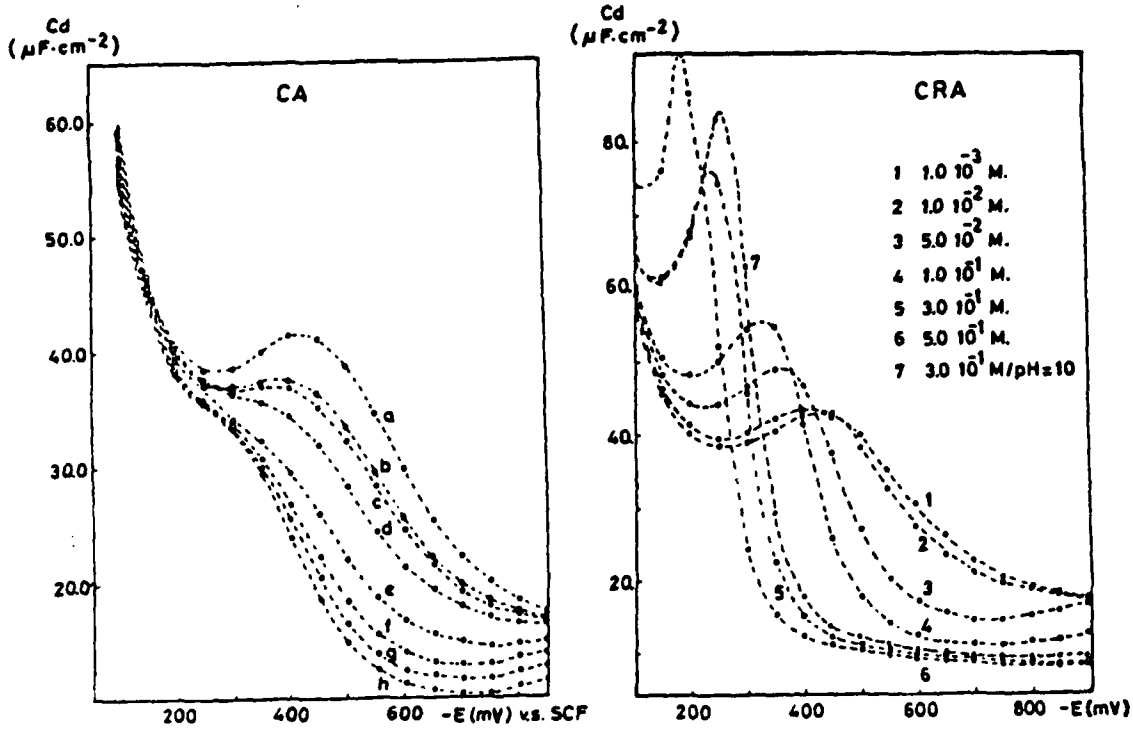

The contribution of dipole moment calculated according to Parsons' formulation[5] of Esin-Markov effect gives an autoconsistent picture of interactions with the electric field. In both cases the molecular dipole moment would orientate in order to attain a better interaction with the electric field. However, whereas small oscilations of the molecular plane could explain the change in normal dipole component with charge for CA, in the case of CRA that would be accompanied by appreciable changes in orientation and intermolecular interactions, which could justify non-congruence.

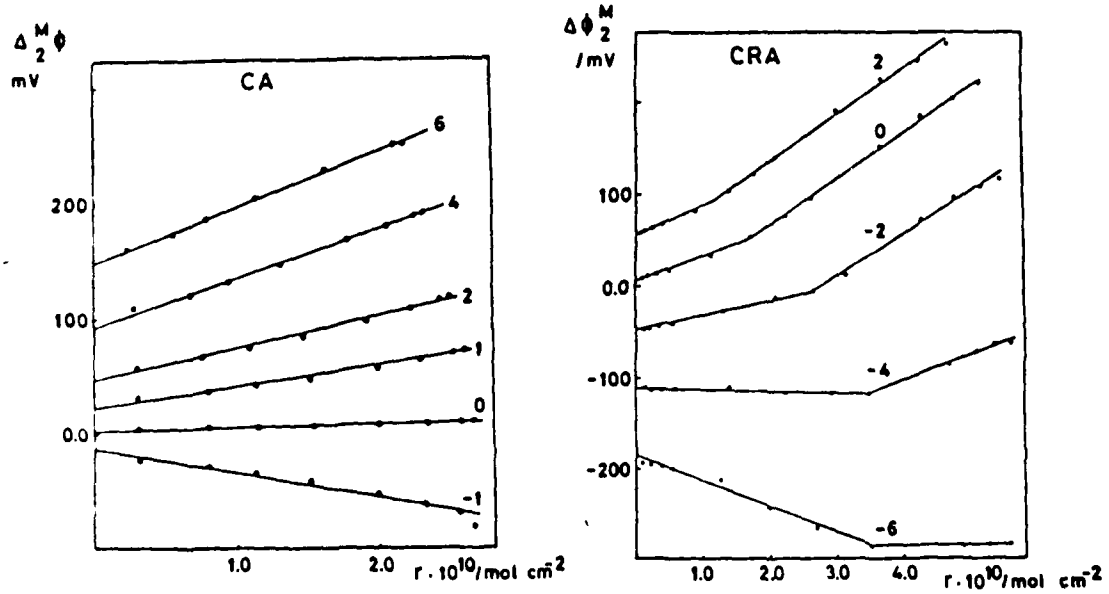

The interpretation of non-congruence as a results of differences in polarizability of adsorbate and solvent[6] does not account for the experimental CRA results.

The flat orientation, independent of potential and the higher value of $|\Delta G_{ad}|$ (34.4 kJ mol^{-1} for CA, 14. $kJmol^{-1}$ for CRA) found in adsorption of CA indicate stronger interactions at the interface, probably π-electron interactions with the metal. However, they cannot be described unambigously by the partial charge transfer between the electrode and the adsorbate.

REFERENCES

1 - D. Barnes and P. Zuman, Trans. Faraday Soc., 65(1969) 1668; 65(1969)1681 and J. Chem.Soc., B (1971)1118.
2 - L. Spritzer and P. Zuman, J. Electroanal. Chem. 126(1981)21.
3 - D. Gonzalez-Arjona and M. Rueda; An. Quim.;78(1982)170.
4 - B.D. Damaskin, V.V. Batratov and O. Petrii; "Adsorption of Organic Compounds on Electrodes", Plenum Press, N.Y. 1971.
5 - R. Parsons, R. Peat and R. M. Reeves, J.Electroanal.Chem.62 (1975)151.
6 - M.V. Sangaranarayanan and S.K. Rangarayan, J.Electroanal.Chem 176(1984)1-118.

09160

FLUORIDE AND BROMIDE COADSORPTION AT THE Hg ELECTRODE

H.D. HURWITZ, A. JENARD and B. BICAMUMPAKA
Faculté des Sciences, C.P. 160, Université Libre de Bruxelles,
50, av. F.D. Roosevelt, 1050 Brussels, Belgium.

The dependence of the electrocapillary behaviour with respect to specifically adsorbed ions at the Hg ideally polarized electrode has been established in the case of almost all inorganic anions. Many results have been obtained from differencial capacity measurements in solutions of mixed electrolytes MX-MF kept at constant ionic strength. However, in spite of the numerous studies made so far with this method, several problems related to the coadsorption in the Nernst layer of the counter-ion M^+ or the reference co-ion F^- remain still unsettled. A detailed analysis of the problem of the cationic concomitant adsorption with halide ions has been made by Damaskin et al.[1] and U. Palm et al.[2]. It has thus already been emphasized that the adsorption of Br^- ions at the Hg/N.M.F. interface may involve coadsorption with K^+ ions in the inner layer. On the other hand, the very weak specific adsorption of the F^- ion at the Hg/H_2O interface severely restricts the applicability of most electrocapillary methods in view of the determination of the amount of F^- specifically adsorbed. Yet the problem has been tackled by several authors[3-5], and D. Schiffrin[6] has derived some values of the surface excess of $\Gamma_{i\ F^-}$ in the inner layer at 15°C.

Specific coadsorption of F^- ions from mixed electrolyte solutions MX-MF might have some important consequences especially in the case of X^- ions which are weakly adsorbed.

We endeavour, in this study, to investigate such effects of coadsorption of both the counter- and co-ion at the Hg electrode with Br^- ions in presence of mixed NaF and NaBr aqueous electrolyte systems at 25°C. In the present approach we have adopted the method proposed by Damaskin[1] for the determination of the inner layer surface excess of Na^+, $\Gamma_{i\ Na^+}$ and the quasi-thermodynamical treatment suggested by Lakshmanan and Rangarajan[7] for the evaluation of the inner layer surface excess of F^-, $\Gamma_{i\ F^-}$. The latter method, published in 1970, has scarcely been employed for the analysis of anionic coadsorption on Hg[8-10].

Although the NaF-NaBr aqueous system has already been investigated several times, a careful reconsideration of this system seems opportune in view of the coadsorption effects mentioned above.

For this system, the virial adsorption isotherm corrected for the O.H.P. potential ϕ_2

$$F_1 = \ln \left(\frac{\Gamma_{i\ Br^-}}{m_{Br^-}\ q}\right) - \frac{F\phi_2}{RT} = \ln \beta - 2\ B\ F\ \Gamma_{i\ Br^-} \qquad (1)$$

is plotted in Fig. 1. This plot indicates that the slope B changes from positive (lateral attraction) to negative (lateral repulsion) values in the region of double layer recharging, hence about the values of the electrode charge densities $q \simeq -F\Gamma_{i\ Br^-}$. A similar distinctive behaviour is observed in the Christie plot giving the potential drop ϕ^{M-2} across the inner layer at constant q as a function of $\Gamma_{i\ Br^-}$ (Fig. 2). The results recorded in Fig. 1 and 2 have been obtained with solutions at constant $J = m_{Br^-} + m_{F^-} =$

0.1 mole.kg^{-1}. The treatment suggested by Damaskin consists in determining virtual adsorption energies ln β_{virt} and virtual virial coefficients B_{virt} from the relationship :

$$F_{virt} = \ln \left(\frac{\Gamma_{i\ Br^-}}{m_{NaBr}}\right)_q = \ln \beta_{virt} - 2\ B_{virt}\ F\ \Gamma_{i\ Br^-} \qquad (2)$$

extrapolated to $\Gamma_{i\ Br^-} = 0$. The Gouy-Chapman theory gives at $\Gamma_{i\ Br^-} \to 0$:

$$\ln \beta = \ln \beta_{virt} - 2 \sinh^{-1} \frac{q}{2A\sqrt{J}} \qquad (3)$$

$$B = B_{virt} - (q^2 + 4\ A^2 J)^{-1/2} \qquad (4)$$

This theoretical determination of ln β and B is used to compute F_1 which allows the calculation of ϕ_2 and consequently of $\Gamma_{i\ Br^-}$ according to the relations :

$$\phi_2 = \frac{RT}{F}\ (F_{virt} - F_1) \qquad (5)$$

and

$$F\ \Gamma_{i\ Na^+} = F\Gamma_{i\ Br^-} \mp 2A\sqrt{J}\ \sinh \frac{F\phi_2}{2RT} - q \qquad (6)$$

The specific adsorption isotherms of Na^+ coadsorbed with Br^- as a function of $\Gamma_{i\ Br^-}$ are recorded in Fig. 3. The determination of $\Gamma_{i\ F^-}$ is based on the usual cross differentiation of terms in the Gibbs equation, respectively under condition of constant J and of constant ratio $\alpha = m_{Br^-}/m_{F^-}$. These treatments lead to the following expressions :

$$-\frac{F}{kT} \int_{q_o}^{q} \left(\frac{\partial E^+}{\partial \ln m_{Br^-}}\right)_{qJ} dq = F\Gamma_{i\ Br^-} - \alpha\ F\ \Gamma_{i\ F^-} \qquad (7)$$

$$-\frac{1}{2}\frac{F}{RT} \int_{q_o}^{q} \left(\frac{\partial E^+}{\partial \ln J}\right)_{q\alpha} dq = F\Gamma_i + A\sqrt{J}\ Y_D \qquad (8)$$

where $\Gamma_i = \Gamma_{i\ Br^-} + \Gamma_{i\ F^-}$ and

$$Y_D = (|y| + \sqrt{y^2+1})^{\mp 1} - (|y_o| + \sqrt{y^2 + 1})^{-1} \qquad (9)$$

with the exponent of the first term equal to +1 and -1 respectively for $y = (q - F\Gamma_i)/2A\sqrt{J} > 0$ and $y < 0$. The subscript o corresponds to the initial integration boundary at -1.5V vs S.C.E.. Both partial derivatives in eq. (7) and (8) are made at values of α, m_{Br^-} and J related by the condition $J = m_{Br^-}\ (1 + 1/\alpha) = 0.1$ mole.kg^{-1}.

The adsorption isotherms of F^- coadsorbed with Br^- are sketched out in Fig. 4. From this figure, it appears that the Br^- specific adsorption seems to impede the F^- specific adsorption to such an extent that the latter remains restricted to small values of m_{Br^-} and to $F\Gamma_{i\ Br^-} < q$.

However, the amount of F^- in the inner layer may reach relatively important values and therefore affect the shape of both the virial adsorption isotherm and the Christie plot, as they are recorded in Fig. 1 and 2.
This is illustrated in Fig. 5 which shows the potential drop ϕ^{M-2} as a function of Γ_i (continuous line) after correction for F^- coadsorption. These plots demonstrate furthermore the influence of the Na^+ coadsorption. The dashed lines have been drawn across the experimental points after recalculation by taking into account both the Na^+ and F^- specific adsorption.

Closer examination of these experimental results raises some questions about the validity of the double layer model.

References

1. B.B. Damaskin, U. Palm and M. Väärtnov, J. Electroanal. Chem. 70 103 (1976).
2. U. Palm , M. Väärtnov and M. Salve, J. Electroanal. Chem. 35 86 (1978).
3. A.W.M. Verkoost, M. Sluyters-Rehbach and J.H. Sluyters, J. Electroanal. Chem. 24 1 (1970).
4. G.J. Hills and R.M. Reeves, J. Electroanal. Chem. 31 264 (1971).
5. G.J. Hills and R.M. Reeves, J. Electroanal. Chem. 42 355 (1973).
6. D.J. Schiffrin, Trans. Farad. Soc. 67 3318 (1971).
7. S. Lakshmanan and J.K. Rangarajan, J. Electroanal. Chem. 27 170 (1970).
8. L.M. Bough and R. Parsons, J. Electroanal. Chem. 58 224 (1975).
9. M. Hamdi, R. Bennes, D. Schuman and P. Vanel, J. Electroanal. Chem. 108 255 (1980).
10. L.A. Avaca, E.R. Gonzales and R.C. Filho, J. Electroanal. Chem. 147 345 (1983)

fig. 1

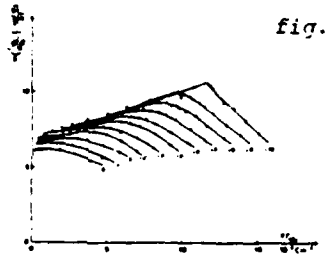

fig. 2

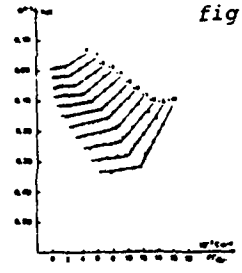

fig. 3

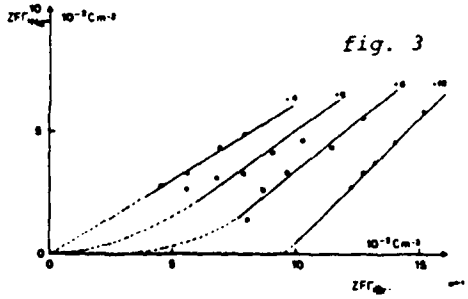

fig. 4

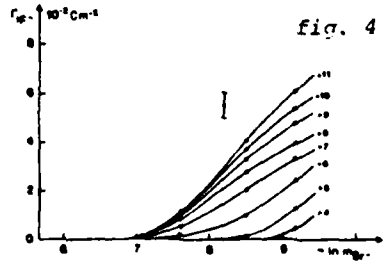

fig. 5

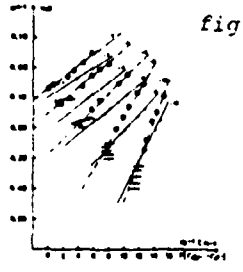

09170

ADSORPTION ON DIFFERENT FACES OF Ag SINGLE CRYSTAL ELECTRODES

M. BACCHETTA and S. TRASATTI
Department of Physical Chemistry and Electrochemistry
University of Milan (Italy)

A. HAMELIN and L. DOUBOVA*
Laboratoire d'Electrochimie Interfaciale
CNRS, Meudon (France)

Detailed measurements of the capacitance of Ag single crystal faces has been carried out by Hamelin and Valette[1], by Valette[2] and by Vitanov et al.[3]. The surface is activated by a cyanide-based electropolishing procedure in the first two cases and by in-situ electrolytic growth in a Teflon capillary in the last case. It has recently been shown that cyanide-based polishing can also give well structured surfaces as it appears from the LEED analysis[4].

In this work we have investigated the interfacial behavour of the (110) face of silver by making use of an alternative chemical polishing procedure based on chromates. The differential capacity was measured by a E-310 Brucker polarograph equipped with a lock-in amplifier. The method involved measuring the in-phase and out-of-phase ac component. Fig. 1 shows the capacity curve of the (110) face in 0.04 mol dm^{-3} NaF solution. The previous data of Valette and Hamelin, and Valette are also reported for comparison.

The potential of zero charge of the (110) face has been found to shift with the F^- concentration slightly. Fig. 2 shows that the present data are in excellent agreement with those obtained by Valette. Thus, there exists a definite evidence for F^- specific adsorption. Quantitative study of this aspect has been performed by Valette for the (100) face[5] but not for the (110) face. Therefore, the specific adsorption of F^- on the (110) face was investigated by using the mixed electrolyte method. The capacity has been measured for 8 solutions of variable composition according to the formula x NaF + (0.04 - x) KPF_6 with x = 0.001, 0.002, 0.005, 0.01, 0.02, 0.03, 0.04 mol dm^{-3}. Fig. 3 shows that the anodic peak increases with NaF concentration testifying to the specific adsorption of F^-. The shift of the capacity minimum is thus partly due to the behaviour of the anodic peak. A better determination of the potential of zero charge was carried out by back integration of the capacity curves from the negative branch. Thus, $E_{\sigma=0}$ has been found to shift of only a few mV as the NaF concentration varies from 0 to 0.04 mol dm^{-3}. Therefore, the adsorption is vanishingly small at the potential of zero charge and can be neglected.

The adsorption of F^- has been found to be well described by a virial isotherm as well as by a square root isotherm[6]. In any case, the free energy of adsorption varies linearly with the electric field and becomes probably slightly positive at $E_{\sigma=0}$. Fig. 4 shows the dependence of specific adsorption of F^- on charge and concentration. Adsorption is remarkably higher than on Hg,

---

* L. D. is grateful to the Department of Physical Chemistry and Electrochemistry of the University of Milan for supporting her staying in Meudon.

in agreement with what has been found[7] for Cl^- and organic substance adsorption[8].

Preliminary experiments have shown that the temperature coefficient of the potential of zero charge of the (110) face is very small or even negative. The shape of the capacity curve appears not to be appreciably affected by the temperature. These observations are very useful for the understanding of the origin of the high inner layer capacity of silver single crystal faces[9,10].

Capacity measurements have also been carried out with the (311) and the (331) faces never investigated before. The value of the potential at the capacity minimum in dilute NaF solutions is about -0.68 to -0.69 V(SHE) in the former case and -0.67±0.01 V in the latter case. These values fall in the expected range according to the stereographic triangle of FCC metals[11]. F^- ions adsorb specifically also on these faces. Quantitative determinations are in progress for the (311) face.

REFERENCES

1) G. Valette and A. Hamelin, J. Electroanal. Chem., 45(1973)301.
2) G. Valette, J. Electroanal. Chem., 122(1981)285.
3) T. Vitanov, A. Popov and E.S. Sevastyanov, J. Electroanal. Chem., 142 (1982)289.
4) R.R. Adzic, M.E. Hanson and E.B. Yeager, J. Electrochem. Soc., 131(1984) 1730.
5) G. Valette, J. Electroanal. Chem., 138(1982)37.
6) R. Parsons, Trans. Faraday Soc., 51(1955)1518.
7) G. Valette, A. Hamelin and R. Parsons, Z. Phys. Chem. N. F., 113(1978) 71.
8) S. Trasatti, Electrochim. Acta, 28(1983)1083.
9) S. Trasatti, J. Electroanal. Chem., 138(1982)449.
10) S. Trasatti, J. Electroanal. Chem., 172(1984)27.
11) A. Hamelin, Surface Sci., 52(1976)771.

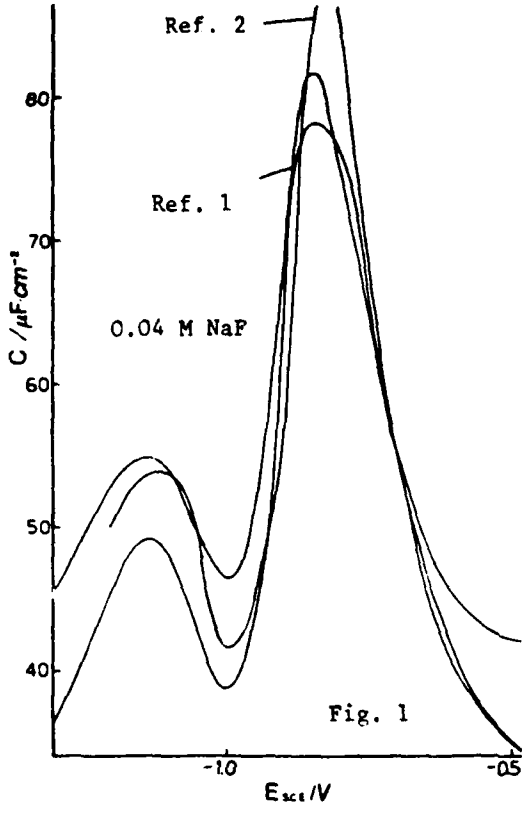

Fig. 1

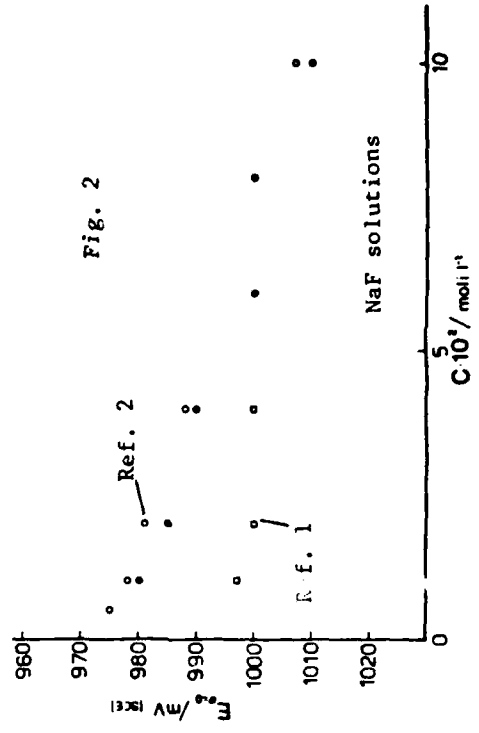

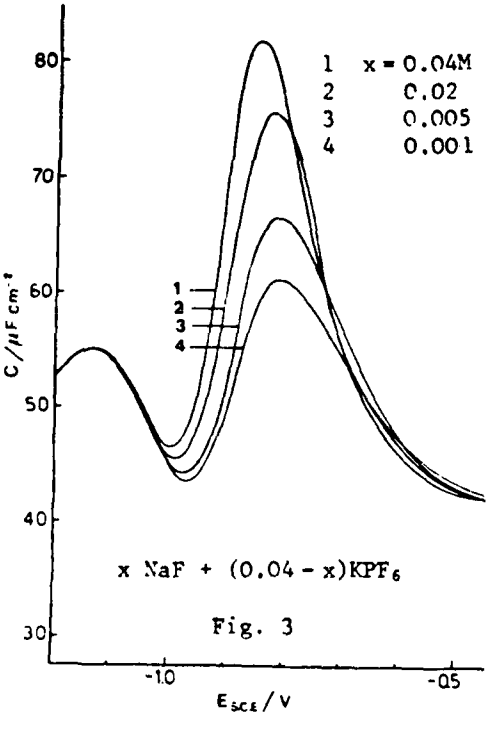

x NaF + (0.04 - x)KPF_6

Fig. 3

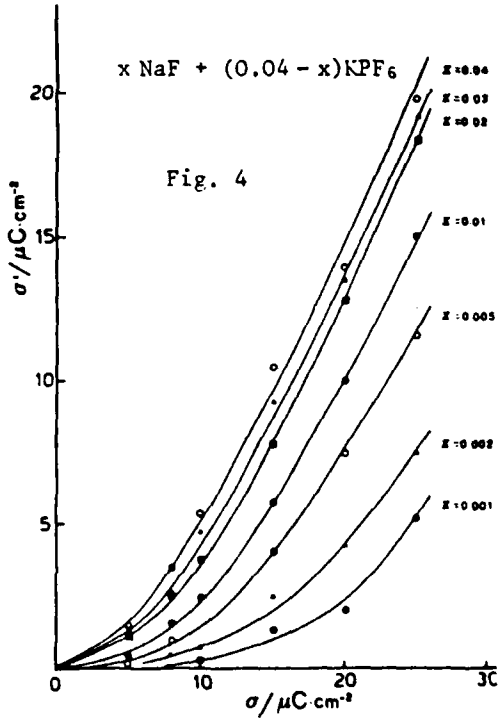

Fig. 4

09180

ADSORPTION OF ETHERS OF ETHYLENE GLYCOL AT THE AIR/SOLUTION AND THE Hg/SOLUTION INTERFACE

A. DAGHETTI and S. TRASATTI
Department of Physical Chemistry and Electrochemistry
University of Milan (Italy)

I. ZAGORSKA and Z. KOCZOROWSKI
Department of Chemistry, University of Warsaw (Poland)

Previous studies[1,2] have shown that the comparison of the adsorption behaviour of an organic substance at the air/solution and the Hg/solution interface is a powerful tool to elucidate the structural details of the adsorption layer. In particular, the free energy of adsorption at the electrode surface is very sensitive to dipole-metal interactions which are strongly dependent on the position of the adsorbate at the interface.

Ethylene glycol (EG) is a non-aqueous solvent which has been widely used for interfacial studies[3-6]. Its adsorption from aqueous solution onto the Hg electrode has been investigated[7] and the parameters of adsorption have been used to derive information on the state of water at the electrode interface. It is however still unclear whether this substance is really suitable to such purpose. Since the permittivity of the inner layer is not greatly modified by the adsorption of EG, the conclusions which can be derived from the application of models are not unambiguous. In this context, it has been decided to investigate the adsorption behaviour of homologous series of derivatives of EG. In particular, in this paper we report on the adsorption behaviour of monoethers of EG with the general formula $R\text{-}O\text{-}CH_2\text{-}CH_2OH$ where R is a linear aliphatic substituent.

The following ethers were investigated: monomethyl (MEG), monoethyl (EEG) and monobutyl (BEG). The monopropyl ether is not available commercially. The interfacial tension at the Hg/solution boundary was measured by means of a capillary electrometer. The surface tension at the air/solution interface was measured by means of the method of the maximum pressure in a bubble. The adsorption potential shift was determined by the dynamic condenser method[8].

In this work, the adsorption at the air/solution interface is compared with the behaviour at the uncharged surface of Hg (potential of zero charge). Fig. 1 shows the decrease in interfacial and surface tension upon adsorption of the monoethers. It can be seen that the differences between the two interfaces become more significant with increasing chain length of the substituent. In particular, adsorption is stronger at the air/solution interface for MEG but stronger at the Hg/solution interface for BEG. If the ratio of concentrations at $\Delta\gamma = 3$ mN m^{-1} is calculated, Traube's rule is found to be obeyed at the air/solution interface, but the coefficient is higher at the Hg/solution interface where, therefore, adsorbability is not simply governed by the expulsion of the organic substance from the bulk of the solution.

The different behaviour of the adsorbates at the two interfaces shows up much more clearly in terms of adsorption isotherm. Surface excesses have been derived by graphical differentiation of surface pressure-log x curves.

Fig. 2 shows, as an example, the adsorption isotherms of MEG at the free surface of water and at the Hg/solution interface. In all cases no S-shaped isotherm is observed which means that lateral interactions are very weak or repulsive. This is a very intriguing result, since for most of the other substances (including nitriles[1]), for the aliphatic alcohols in particular[9], the lateral interaction term corresponds to strong attraction.

In order to quantify the above quanlitative observations, the experimental points have been fitted to different kind of isotherms. In particular, since lateral repulsion is involved, the virial and the square root[10] isotherms have also been tested.

The adsorption potential shifts to more positive values at both interfaces which suggests that, formally, the adsorbates are oriented with the positive end of the molecular dipole pointing away from the solution. If ΔE is plotted as a function of the surface excess of adsorbate, the curves for the three ethers at the air/solution interface overlap quite nicely.

In conclusion, aliphatic monoethers of ethylene glycol adsorb at the Hg/solution interface in a way which differs structurally and energetically from the situation at the air/solution interface. The unability of the hydrocarbon tail to protrude from the liquid phase as the solid wall is present is probably responsible for this. The generally negative value of the interaction parameters may be interpreted in terms of a high solubility of the adsorbates in the interfacial layer due to the hydrophilic groups being probably capable of hydrogen bonding to neighbouring water molecules. The orientation of the ethanol moiety at the air/water interface is probably the same for all ethers investigated, while it is variable at the Hg/solution interface.

REFERENCES

1) A. Daghetti, S. Trasatti, I. Zagorska, Z. Koczorowski, J. Electroanal. Chem. 129(1981)253.
2) S. Mingozzi, A. Daghetti, S. Trasatti, I. Zagorska, Z. Koczorowski, J. Chem. Soc. Faraday Trans. I 79(1983)2801.
3) V.A. Chagelishvili, M.G. Vyaértnyu, U.V. Palm, J.I. Japaridze, Elektrokhimiya 14(1978)890.
4) J.I. Japaridze, Sh.S. Japaridze, B.B. Damaskin, Elektrokhimiya 7(1971) 1305.
5) J.I. Japaridze, V.A. Chagelishvili, J. Electroanal. Chem., submitted.
6) J.I. Japaridze, N.A. Abuladze, Sh.S. Japaridze, A. De Battisti, S. Trasatti, Electrochim. Acta, submitted.
7) S. Trasatti, J. Electroanal. Chem. 28(1970)257.
8) S. Minc, I. Zagorska, Z. Koczorowski, Rocz. Chem. 41(1967)1983.
9) B. Damskin, A. Frumkin, A. Chizov, J. Electroanal. Chem. 28(1970)93.
10) R. Parsons, Trans. Faraday Soc. 51(1955)1518.

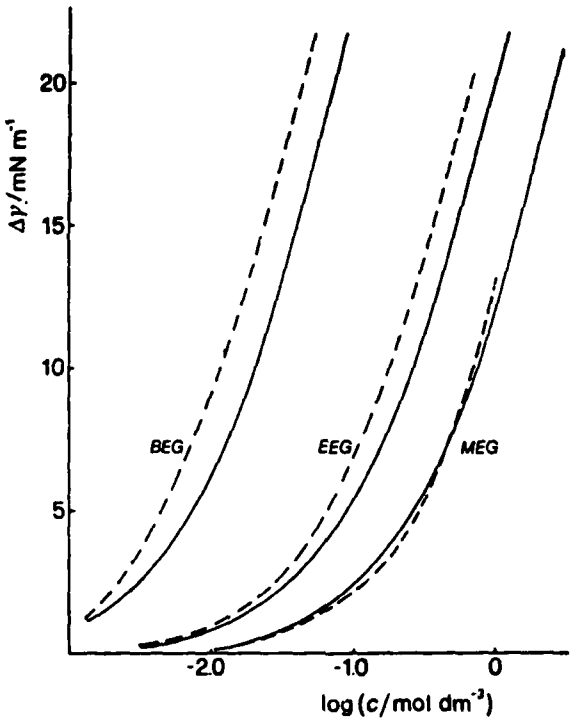

Fig. 1 - Surface pressure due to adsorption of methoxy- (MEG), ethoxy- (EEG), and buthoxyethanol (BEG) at the air/solution (——) and the Hg/solution (----) interface.

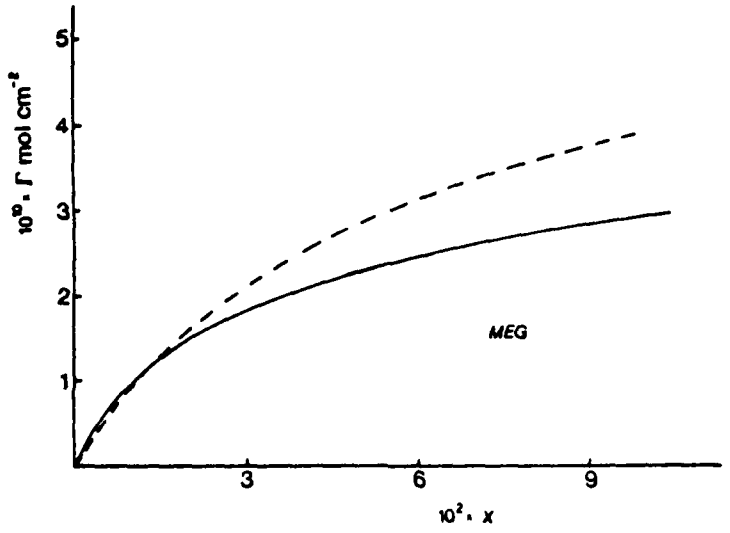

Fig. 2 - Adsorption isotherm of methoxyethanol at the air/solution (——) and the Hg/solution (----) interface.

IONIC ADSORPTION FROM MIXED ELECTROLYTE SOLUTION AT CONSTANT CATIONIC STRENGTH

E.DUTKIEWICZ and P.SKOŁUDA
Department of Electrochemistry, Faculty of Chemistry,
A.Mickiewicz University, Grunwaldzka 6, Poznań /Poland/

The problem of adsorption of ion from mixed electrolyte solution of different types of symmetry with a common nonadsorbing cation or anion is still open both from theoretical and experimental point of view. The aim of this work is to propose an approximation method of studying the adsorption process of ion from a binary mixture of two salts of 1:1 KA + 1:2 K_2B symetry in which only a divalent anion B is specifically adsorbed, while the other electrolyte components being present in the diffuse layer and in the bulk.

The method proposed is, in particulary, convenient in studying the adsorption process on solide electrode.

Let us consider the solution of electrolytes of constant cationic strength but with variable concentration of aions and of total composition:

$$(m_T - 2\,m_{K_2B})\,KA + m_{K_2B}\,K_2B$$

where $m_T = m_{KA} + 2\,m_{K_2B}$ are the total molar concentrations of salts 1:1 and 1:2.

Electrocapillary curve for that mixed electrolytes and for the constant T and p, takes the following form.

$$-d\gamma = \sigma^M dE^{\pm} + \Gamma_B d\mu_{K_2B} + \Gamma_A d\mu_{KA} \qquad (1)$$

where γ is the interfacial tension, μ_{K_2B} and μ_{KA} chemical potentials of salts K_2B and KA, Γ_B and Γ_A the surface excess concentration of the anions under consideration, σ^M is the surface charge per unit area on the electrode, $E^{\pm}$ is the potential of the electrode measured with respect to a reference electrode reversible to cation or anion in the working solution. Changes in chemical potentials of individual salts can be expressed through the changes in their concentrations :

$$d\mu_{K_2B} = RT\,d\ln(m_{K_2B}) \qquad (2)$$

$$d\mu_{KA} = RT\,d\ln(m_T - 2\,m_{K_2B}) \qquad (3)$$

Substituting eqns. (2) and (3) into eqn. (1) we obtain :

$$-d\gamma = \sigma^M dE^{\pm} + \left(\Gamma_B - 2\Gamma_A \frac{m_{K_2B}}{m_T - 2m_{K_2B}}\right) RT d\ln(m_{K_2B}) \qquad (4)$$

A simplification may be obtained in the special case of a very dilute solution of one salt, K_2B, in an excess of the ether, KA, i.e. $\frac{m_{K_2B}}{m_T - 2m_{K_2B}} \rightarrow 0$. Eqn. (4) then reduces to

$$-d\gamma = \sigma^M dE^{\pm} + \Gamma_B RT d\ln(m_{K_2B}) \qquad (5)$$

Assuming that $\Gamma_B = \Gamma_B^1 + \Gamma_B^d$ where Γ_B^1 is the surface excess of ion B in the inner layer and Γ_B^d is the surface excess of ion B in the diffuse layer we can write :

$$-\frac{1}{RT}\left(\frac{\delta\gamma}{\delta\ln m_{K_2B}}\right)_{T,P,E} = \Gamma_B^1 + \Gamma_B^d \qquad (6)$$

As a first apprcximation we treat this system as different ionic strength one. The error introduced by this approximation should not be significent.
On the other hand that method has several advantages :

1. Permit to use in experiment on electrolyte with negligible specific adsorption e.g. NaF. This is of particular admantage since divalent anions are usualy adsorbed on mercury electrode and in particulary on solid electrodes in the amounts which cannot be neglected.
2. Using the higher conductivity of the base solution by application of nonadsorbing electrolyte KA as compare to the single salt solution the potentiodynamic method of capacity measurement are easier and more accurate.
3. At constant catienic strength potential of electrode studied is directly expressed in the thermodynamic scale if the reference electrode is reversible to the cation.
4. Activity coefficients in mixed electrolyte solution are almost constant or slightly change.
5. At the extremely negative potential when all anions are desorbed the capacity curves for the range of not to high concentration studied coincide and the back-integration method to integrate the differential capacity curves can be applied.

09200

ADSORPTION OF SULFONATE IONS ON MERCURY ELECTRODE FROM SOLUTION AT CONSTANT IONIC STRENGTH

R.DUTKIEWICZ and J.STUCZYŃSKA
Department of Electrochemistry, Faculty of Chemistry,
A.Mickiewicz University, Grunwaldzka 6, Poznań /Poland/

Up to the works of Parry and Parsons[1,2] the detailed study of the specific adsorption of ions at the mercury electrode has been confined to the simple monoatomic halide ions. In their papers they get through the analysis of adsorption process for such sulfonates ions like p-toluenesulfonate (p-PTS) and m-benzenedisulfonate (BMDS). Later, Dutkiewicz[3] studied the adsorption of benzenesulfonate ion (BS) from aqueous solutions at constant ionic strength.

In this paper the effect of the number of ionic groups compared with the size of aromatic system, the effect of position of substituents in aromatic ring and the influence of π electrons on adsorption process have been studied.

The study were carried out using : sodium salts of α naftalenesulfonate (α NaNS), β naftalenesulfonate (β NaNS), 1,5 naftalene disulfonate (1,5 DNS), benzenesulfonate (NaBS) and cyklohexanesulfonate (CHS) at constant ionic strength of solutions. The interfacial tension between mercury and solutions was measured using capillary electrometer with MBP method[4]. The double layer capacity of the interphase was measured with an a.c. bridge. All measurements were carried out in an air thermostat at 298 $\pm$ 0,2K. The potentials of the ideal polarized electrode were measured with respect to mercurous sulfate electrode. The capacity curves were integrated numerically. The integration constants were obtained from the electrocapillary curves. All solutions were prepared volumetrically from tarice distilled water. For all these systems except 1,5 DNS we used NaF as the base electrolyte. For 1,5 DNS, Na_2SO_4 was used as the base electrolyte.

The capacity curves obtained for α NaNS, β NaNS and CHS ions show similar concentration effect on double layer capacity. At the lower concentrations, the capacity curves show a marked peak. However, as the concentration of ions increases this peak loweres and appears is replaced by a minimum, while a higher and narrower peak appears at more negative potentials. This effect is similar to that obtained by Parry and Parsons for p-PTS ions for which they suggest that at low bulk concentrations of p-PTS ions are lying flat on the mercury surface while at higher concentrations reorientation to allow closer packing of ions.

The capacity curves obtained for 1,5 DNS are similar to that of BMDS ion[2]. It leads to the preasumption that the number of aromatic rings does not play a dominating role in the influence of the concentration effect on the shape of capacity curves. It is rather associated more with number of ionic groups than compared with the size of the aromatic system, although we cannot omit its influence on the process of adsorption.

For all these systems we note the changes is slope of the lines of Φ^{M-2} vs Q at constant charge of the metal which is connected with fact that the standard free energy of adsorption as a function of charge is non linear. This is quite different than for BMDS ion where this dependence were linear [2]. From the analysis of adsorption process the following series of increasing adsorbability may be proposed [1]: 1,5 DNS < BS < PTS < CHS $< \alpha$ NaNS $< \beta$ NaNS. From this series it may be concluded that the adsorbability of the considered ions depends on the electrical and geometrical properties.

References
1.J.M.Parry,R.Parsons J.Electrochem.Soc.113,1966 992
2.J.M.Parry,R.Parsons Trans.Faraday Soc.59,1963 241
3.E.Dutkiewicz J.Electroanal.Chem. 50,1974 221-234
4.D.J.Schiffrin J.Electroanal.Chem. 23,1969 168

09210

SOLVENT EFFECTS ON THE DOUBLE LAYER AT THE ELECTRODE/SOLUTION INTERFACE

Z. BORKOWSKA
Institute of Physical Chemistry, Polish Academy of Sciences, Warsaw (Poland)

The influence of the common organic solvents on the double layer capacity and entropy curves has been analysed for the mercury/electrolyte solution interface without detectable specific adsorption.

The coordinates of capacity minimum and maximum at 25°C are summarized below:

solution		minimum		maximum	
		C_i/Fm^{-2}	$/Cm^{-2}$	C_i/Fm^{-2}	$/Cm^{-2}$
Methanol (MeOH)	KF	0,095	-0,05	-	-
	$NaClO_4$	0,095	-0,05	0,359	0,06
	$LiBF_4$	0,095	-0,05	0,315	-
	KPF_6	0,095	-0,05	-	-
Dimethylformamide (DMF)					
	$NaClO_4$	0,070	-0,110	0,558	0,20
	KPF_6	0,070	-0,110	-	-
	$LiBF_4$	0,072	-0,100	0,51	0,20
Propylene carbonate (PC)					
	$NaClO_4$	0,065	-0,13	0,385	0,15
	KPF_6	0,062	-0,13	0,28	0,14
Acetone (AC)	$NaClO_4$	0,068	-0,10	0,47	0,08
	KPF_6	0,068	-0,10	0,33	0,09
n-methylformamide (NMF)					
	$NaClO_4$	0,150	-0,014	0,20	-0,095
	KPF_6	0,150	-0,012	0,20	-0,095

It can be noted that the coordinates of the capacity minimum and the charge density at the capacity maximum are solvent dependent and independent of the electrolyte. The latter increases in the following order:

MeOH < AC < NMF < PC < DMF

Similarily increases the free energy of adsorption of the organic solvents from aqueous solutions[1]: MeOH < AC < NMF, and the dipole moment of the solvents. This may indicate the predominant role of the electrostatic, non- specific dipole - image dipole interfactions between the solvent molecule and the electrode. Such interactions would priviledged on orientation in which the solvent dipole is parallel to the electrode surface.

The comparison of the capacity and entropy curves for investigated solvents indicate two typical interfacial behaviour:

(i) The entropy curve followes the capacity curve - protic solvents such as MeOH and NMF.

(ii) The entropy curve has maximum at negative charge density where the capacity is small and almost charge independent - aprotic solvents such as DMF, PC, AC.

1. Z. Borkowska, J. Electroanal. Chem., 146 (1983) 385.

10010

THEORETICAL ANALYSIS OF THE MEANS OF IMPROVING THE SENSITIVITY OF ELECTROANALYTICAL TECHNIQUES.

10

J. CHEVALET, N. FATOUROS, R. REEVES.

Laboratoire d'Electrochimie, Universite Pierre et Marie CURIE, 4 place Jussieu, 75230 Paris Cedex 05. FRANCE.

A set of general solutions has been derived which verifies the theoretical analysis for controlled potential step perturbation techniques, for both reversible and irreversible electrochemical systems. The solutions allow both renewed and non-renewed electrode surfaces to be employed as well as a wide range of perturbation waveforms.

The generality of the solution is such that a full analysis of the influence of the various parameters can be made for any type of electrochemical method in which the potential perturbation can be approximated by a staircase function, allowing the theoretical optimisation of these factors to generate the maximal response.

From this study, a new technique which lies midway between differential pulse polarography (DPP) and square wave voltammetry has been found to have an optimal sensivity around two orders of magnitude greater than DPP.

Initially the electrode is maintained at a suitable potential. A certain number of potential perturbations is then imposed to create what has been termed a "crenellated" waveform. This wave name implies that the perturbation amplitudes are constant. The

voltacoulommetric response wave, which has the classical bell shape, is obtained by a series of measurements of the differential charge response at different potentials, i.e. a response which is the difference between the charge response to the applied perturbation and the corresponding underlying polarographic component. This is the same technique as employed in integrated differential pulse polarography (IDPP) where only one potential step is considered.

The fractions of the charge recovered during the odd and even periods converge rapidly towards the same absolute limit which represents around 70% of the first current integral. Two operating modes are suggested, A and B, depending on the way in which the successive responses are combined.

In mode A the charges are summed ignoring their signs, the response being given by:

$$Q = 1.4\ C^{te}\ M\ Q_1$$

where M is the number of periods and Q_1 the charge corresponding to the first potential step, i.e.the IDPP response. C^{te} contains the usual parameters, diffusion coefficients and the initial concentration of electroreducible species.

In mode B, the charge responses are summed including their signs and the following approximate solution applies,

$$Q = C^{te}\ (R\ M\ v)^{1/2}$$

where R=v/(v+u), v and u being the odd and even period lengths.

This formula shows clearly that the charge response varies as the square root of the number of periods and yields a sensitivity increase around 10, when compared with IDPP on the

same timescale . This approach is practically an extension of the double potential step method proposed by F.Anson.

In mode A the current integration period is limited by the time t necessary for the decay of the capacitative current, while in mode B, capacitative compensation is achieved for an even number of perturbations.

It can be shown by calculation that optimal response in mode A is achieved when the odd and even perturbations are of equal duration v and for a ratio t/v close to .22. Practicaly t is limited to around a few ms. and the impulse durations are close to those used in classical IDPP. On the other hand, in mode B, a totally dissymetrical waveform is optimal with a ratio between the odd and even half periods as large as possible. In practice a value of 9 is sufficient. In both modes the peak potential of the response curve follows the laws as found in IDPP.

References:

N. Fatouros, J. Chevalet, R. Reeves, J. Electroanal. Chem., 182 (1985) 235.

C. Mauduit, N. Fatouros, J. Chevalet, R. Reeves, J.Electroanal. Chem. 184 (1985) 221.

DETERMINATION OF METALS AT TRACE LEVEL BY SECOND HARMONIC ALTERNATING CURRENT ANODIC STRIPPING VOLTAMMETRY

CLINIO LOCATELLI, FRANCESCO FAGIOLI, CORRADO BIGHI

Laboratory for Analytical Chemistry, Department of Chemistry, University of Ferrara, Via L. Borsari 46, 44100 FERRARA (Italy)

The half-wave potentials of the reduction of lead(II) and thallium(I) as well as antimony(III) and bismuth(III) respectively are very close to one another in the commonly electrolytes which hinders their simultaneous polarographic determination.
Several authors employed various organic complexing agents or special solutions as the supporting electrolyte to determine these elements. This contrivance can be avoided employing the second harmonic alternating current voltammetry technique, which, unfortunately, is very selective, but not sufficiently sensitive. Since the concentrations of the metal in samples of special interest, as inorganic and organic-biologic matrixes, are often at trace level, the possibility to combine the second harmonic alternating current voltammetry, extremely selective, with the anodic stripping method, which allows to achieve a very high analytical sensitivity, was studied[1,2].
This paper describes the determination, by second harmonic alternating current anodic stripping voltammetry, of lead and thallium, bismuth and antimony in 1 mol/l HCl, where the half-wave potentials are respectively only 40 and 60 millivolts apart.
A conventional three-electrode arrangement was utilized.
The working electrode was the long-lasting sessile-drop mercury electrode (LLSDME) with a drop time of 240-300 seconds: this electrode permits a longer electrolysis time and rest time, slower potential scan rates and consequently a higher current response. A saturated calomel electrode (SCE) and a platinum electrode were respectively employed as reference and auxiliary electrodes.
Established the experimental conditions for the determination of lead, thallium, bismuth and antimony, the calibration curves were determined by second harmonic alternating current voltammetry with the stripping method: the peak current was calculated on the cathodic peak for thallium and antimony and on the anodic peak for lead and bismuth.

Subsequently the problem of the analytical determination of each element in the respective mixtures was studied.
Fixed the best experimental conditions, the simultaneous determination, by second harmonic alternating current anodic stripping voltammetry, of lead and thallium, antimony and bismuth in the mixtures was possible in the range of concentration ratios:

$$7:1 \leqslant C_{Pb}:C_{Tl} \leqslant 1:36$$

$$45:1 \leqslant C_{Sb}:C_{Bi} \leqslant 1:35$$

where C is the metal concentration (mol/l).
However it was interesting to observe that, when the concentration ratio was unfavourable, the determination of the elements was equally possible; in fact it was sufficient to bring again the concentration ratio inside the above-mentioned range through suitable additions of metal standard solution to determine again both elements.
The experimental data were processed by monovariate and bivariate analysis.
The monovariate analysis neglects the presence of the interfering element, while the bivariate analysis takes into account the contribution of the interfering element as well.
It was very interesting to mark that the slope coefficient of the bivariate analysis, for both elements of each mixture, was practically equal to the slope coefficients of the calibration curves and the monovariate analysis.
This fact proved that, in the considered range of concentration ratios, the mutual interferences of lead-thallium and bismuth-antimony in the respective mixtures were negligible.
The detection limit, in the used experimental conditions, was about 10^{-8} mol/l for all the understudied elements in the respective mixtures.
For this method, the precision of the analytical procedure, expressed by the residual standard deviation (s_r), was of the order of 3-4 %, and the accuracy, expressed as relative error (e), was of the order of 2-3 %.

References

1) Determination of metals by second harmonic alternating current voltammetry with a semistationary mercury electrode.
C. Locatelli, F. Fagioli, T. Garai, C. Bighi
Accepted for pubblication (Talanta).

2) Trace metals determination by second harmonic alternating current anodic stripping voltammetry.
C. Locatelli, F. Fagioli, C. Bighi, T. Garai
Accepted for pubblication (Analytical Letters).

THE EFFECTS OF ADSORPTION OF THE ION ASSOCIATES IN ELECTROANALYSIS

I.D.GRAMA, I.I.VATAMAN and Yu.M.LOSHKAREV
Institute of Chemistry of the M.S.S.R. Academy of Sciences
Kishinev (USSR)
Dnepropetrovsk State University, Dnepropetrovsk (USSR)

The electroreduction and adsorption regularities of the reactant particles in the Bi(III) - chloride ion - quinoline, Sb(III) - chloride ion - quinoline and Sb(III) - oxalate ion-β-quinoline systems at various pH were investigated by chronovoltammetric, tensammetric methods and electrocapillary curves measurements.

The cathodic chronovoltammograms of Bi(III) and Sb(III) in the presence of quinoline with chloride as supporting electrolyte and Sb(III) in the presence of β-quinoline with oxalate as supporting electrolyte have the form of isosceles triangular, characteristic for the processes, complicated by the adsorption of depolarizer. Diagnostical criteria based on the dependance of the cathodic (I_p^c) and anodic (I_p^a) peak currents on scan rate(V), $\lg I_p^c/S - \lg V$, $I_p^c/V^{1/2} - 1/2 \lg V$, $I_p^a/I_p^c - 1/2 \lg V$ also testify of the adsorption of the reacting electroactive particles. The dependance of I_p^c of Bi(III) and Sb(III) on the concentration (C) of quinoline(Quin) in the presence of chloride ions passes through its maximum at quinoline concentrations equal to 0,25 M. Peak currents of Bi(III) and Sb(III) at C_{Quin} = 0,25 M increase with the increase of the chloride ions concentration in solution and reach their maximum value at chloride ion concentration equal to 0,5 M for Bi(III) and 1,5 M for Sb(III), and with further growth of chloride ion concentration remain unchanged.

The comparison of the these data with the results of the for average charge ($\bar{z}$) calculations of the chloride complexes of Bi(III) and Sb(III) in the bulk of the solution shows that peak current sharply increases with the growth of negative value of $\bar{z}$ as it is seen from Fig.1. I_p^c of Bi(III) and Sb(III) reduction begin to increase at small values of average $\bar{z} < 1$, when anion complexes of Bi(III) and Sb(III) appear in solution and reach maximum value at $\bar{z}=-2$ for Bi(III) and $\bar{z}=-1$ for Sb(III). This testifyes about the advantageous adsorption of anion complexes $[BiCl_5]^{-2}$ and $[SbCl_4]^-$. Values of surface concentration(Γ) of the electroactive complexes of Bi(III), calculated from the triangular peak form area, reach under these conditions the value of 1,1-1,5 10^{-10} moles cm^{-2}, and the area, occupied by one particle of the depolarizer, is approximately 120 A^2, correspondingly (proceeding from the complete filling of

surface by the monolayer of the adsorbed particles). Values of Γ found are close to those, usually observed for the adsorption of the organic substances. It is characteristic that the area, determined from Stuart-Briglem model, occupied by the quinoline molecule, is twice smaller and is equal to 60 $Å^2$. The latter makes it possible to assume, that the adsorbed electroactive particle uncludes two quinoline molecules.

While studying the nature of electroactive complexes it is necessary to take into account that in the interval of pH investigated quinoline is present in protonated form and draws the anions of $[BiCl_5]^{-2}$ or $[SbCl_4]^-$ into the adsorption layer, increasing their surface concentration. Under these conditions the formation of ion associates of metal anion complexes with protonated quinoline molecules is very likely, electroactive particles $\{[BiCl_5];2QuinH\}$, which occupy the area, twice exceeding the corresponding value for the quinoline molecule, in particular. The similar ion associates are formed in acidic media in solutions, containing Bi(III), quinoline and iodide ions, Bi(III), dipyridil and chloride ions.

The similar effects are observed during the electroreduction of oxalate complexes of Sb(III) in the presence of β-quinoline as well, which is manifestated in the increase of peak currents and values of Semerano criteria.

The comparison of electrocapillary and tensammetric curves (Fig.2) indicates at sharp increase of the Sb(III) oxalate complex adsorbed in the presence of β-quinoline cations, wich displays in the decrease of values of mercury border tension and double layer capacity at potentials more positive - 0,4 V (*vs Ag/AgCl*).

Thus, the electroreduction processes of Bi(III) and Sb(III) anion complexes in the presence of protonated quinolines can be expressed by the following scheme:

$$[MeA_n]^{(3-nz)-} + mRH^+_{ads} \dashrightarrow \{[MeA_n]^{(3-nz)-};mRH^+\}_{ads} \xrightarrow{+3\bar{e}} \dashrightarrow Me(Hg) + mRH^+ + nA$$

Here Me - Bi(III), Sb(III); A- Cl^-, $C_2O_4^{-2}$; R- Quin, β-Quin.

At high concentrations of Bi(III) and Sb(III) the simultaneous discharge of metal anion complexes, diffusing from the solution, is possible, which manifestates in splitting of chronovoltammogram peak.

The possibility of the anion complex formation of Bi(III) and Sb(III) with chloride ions and, consequently, ther associates with protonated quinolines depends on pH value. It is found that changing of pH within the range of 0,3 - 3 pH does not influence the electroreduction of Bi(III) in hydrochloric acid solution of quinoline. At pH> 3 the decrease of the cathodic peak, connected with Bi(III) hydrolysis, is observed. For Sb(III) changing of pH withing the same range considerably influence I_p Sb(III). This difference is stipulated for the fact that Sb(III) complexation with chloride ions at iow concentrations of hydrogen ions is complicated because of the firmnes of Sb-O bond. It can be assumed that in the interval 0,5<pH< 2

mixed hydroxochloride cationic complexes, which do not adsorbed no the electrod surface, predominate. At pH< 0,5 anionic $[SbCl_4]^-$ complexes became to predominate, which form associates with protonated quinoline molecules.

Using the effects of pH and chloride ion concentration influence, it is possible to select conditions, when Bi(III) electroreduction in hydrochloric acid solutions is taking place from the adsorbed state, and Sb(III) electroreduction process is controlled by diffusion. This made it possible to increase the sensivity and selectivity of the determination of Bi(III) in the presense of 200-fold excess of Sb(III) and 400-fold excess of Sn(IV) with 0,5 M KCl + 0.25 M quinoline as basic electrolyte at 1 < pH < 2 and to carry out the chronovoltammetric method of high sensivity of Bi(III) determination in copper alloys.

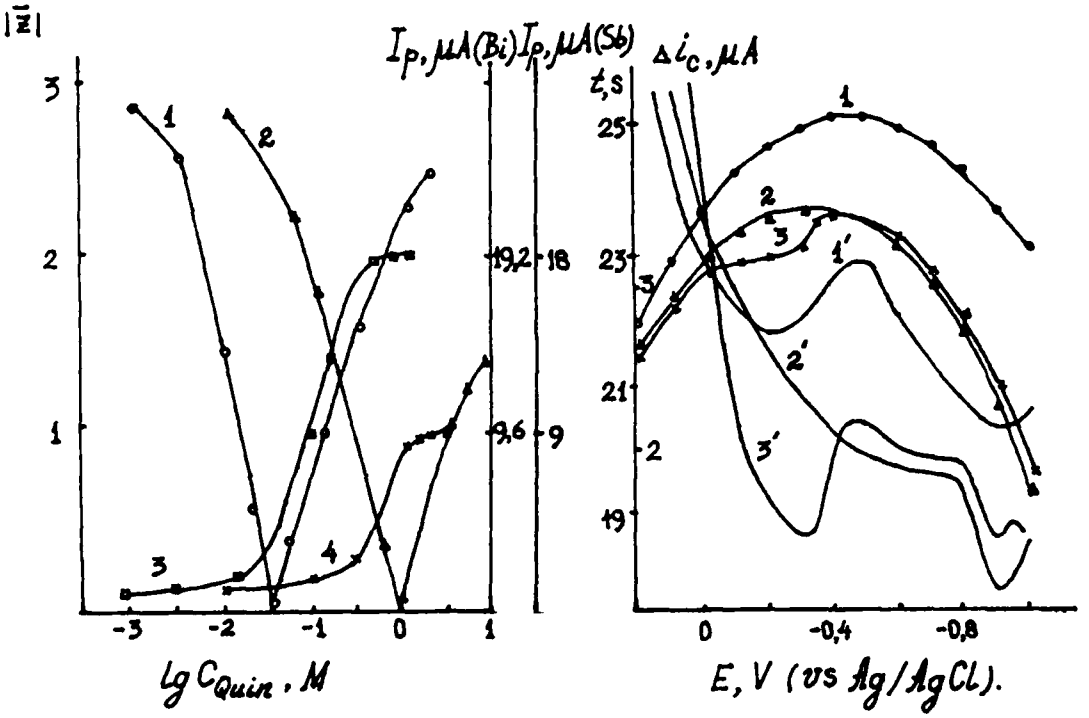

Fig.1 Average charge value of chloride complexes(1,2) and I_p^c(3,4) of Bi(III)(1,3) and Sb(III)(2,4) vs chloride ion concentration.

Fig,2 Electrocapillary(1,2,3) and tensammetric(1',2',3') curves: 1,1' - 0,4 M $H_2C_2O_4$; 2,2' - 1,1'+0,05 M β-Quin; 3,3' - 2,2'+1,6 10^{-4} M Sb(III).

POTENTIOMETRIC BEHAVIOUR OF THE Ce(IV)/Ce(III) COUPLE AT PLATINUM AND CARBON PASTE ELECTRODES

G. López Cueto and A.F. Cueto Rejón

Department of Analytical Chemistry, Faculty of Science
University of Alicante, Alicante, Spain

Kinetics of the iodide-catalyzed cerium(IV)-arsenic(III) reaction[1] has been widely applied to iodide determination at trace level. UV-V spectrophotometry has been mainly used in monitoring reaction rate.

In this paper, possibility of potentiometric monitoring is studied with analitycal purposes.

The equilibrium potential of the Ce(IV)/Ce(III) couple according to Nernst's equation is:

$$E = E^{\circ\prime} + \frac{RT}{nF} \ln \frac{[Ce(IV)]}{[Ce(III)]} \qquad (1)$$

In the presence of an excess of Ce(III), its concentration is closely constant along the reaction, and therefore

$$E = E^{\circ\prime} - \frac{RT}{nF} \ln [Ce(III)]_o + \frac{RT}{nF} \ln [Ce(IV)] \qquad (2)$$

Reaction kinetics is pseudofirst-order when arsenic(III) is in a large excess over cerium(IV)[2]. Then:

$$\ln [Ce(IV)] = \ln [Ce(IV)]_o - kt \qquad (3)$$

From this, equation (2) may be writen as:

$$E = E^* - \frac{RT}{nF} kt \qquad (4)$$

According to this equation, the equilibrium potential should vary with time linearly, and so, the rate constant for the catalized reaction, k (proportional to the iodide concentration), may be calculated from the slope of the potential-time straight line.

EXPERIMENTAL

For the potentiometric measurement, a Crison 501 digital potentiometer and a Metrohm E 516 potentiograph with platinum wire or carbon paste as indicators electrodes, and Ag/AgCl as reference electrode were used.

Current-voltage curves were obtained with a Metrohm E 506 polarograph. Platinum wire or carbon paste as indicators electrodes, platinum wire as auxiliar electrode and Ag/AgCl as reference electrode were used. Solution was stirred magnetically. Temperature was mantained constant at 25±0.1°C.

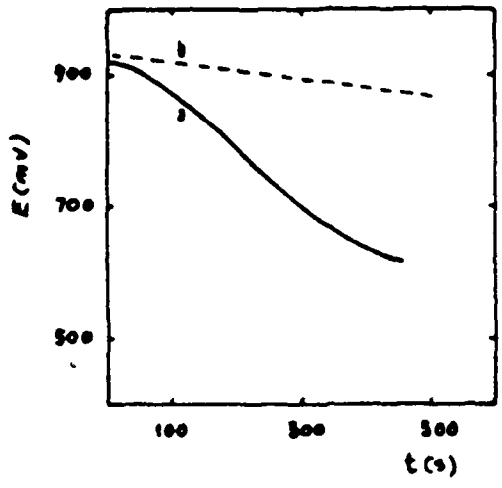

Fig 1.- Potential-time curve with platinum electrode. Ce(IV),$2x10^{-4}$; Ce(III),$5x10^{-3}$M; As(III),10^{-2}M; H_2SO_4 0.2M; I,51ng.mL^{-1}; temp.,25°C. a) experimental curve, b) straight line with theoretical slope.

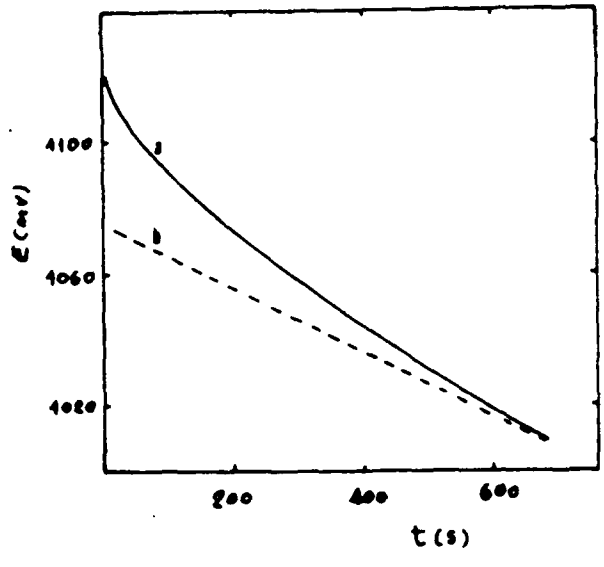

Fig 2.- Potential-time curve with carbon paste electrode. Ce(IV),$2x10^{-4}$M; Ce(III),$6x10^{-3}$M; As(III),$2x10^{-3}$M; H_2SO_4,0.4M; I,43.5ng.mL^{-1}; temp.,25°C. a) experimental curve, b) theoretical curve.

RESULTS AND DISCUSSION

Platinum indicator electrode:

Potential-time curves obtained with a platinum indicator electrode along the I^--catalyzed Ce(IV)-As(III) reaction have a very different shape from the theoretical ones, both in the presence and in the absence of Ce(III), (Fig 1).

The current-voltage curves of a Ce(IV) and Ce(III) solution at a platinum electrode show an irreversible behaviour in 0.5M H_2SO_4 medium but reversibility increases in more acidic medium. So, in 12M H_2SO_4, a single cathodic-anodic wave is obtained. However, As(III) gives an anodic current which overlaps with those from the Ce(IV)/Ce(III) couple, owing to which a mixed potential is measured with platinum electrode, even on reversibility conditions.

Carbon paste indicator electrode:

From the current-voltage curves, the Ce(IV)/Ce(III) couple appears to be reversible at a carbon paste electrode. Little effect has been found from acidity on the reversibility. It is interesting, moreover, that As(III) does not show its anodic wave before the oxigen evolution, and therefore no interference from As(III) must be expected on the potential measurement.

Fig 2 show the variation of electrode potential along the reaction time in an excess of Ce(III). Experimental values approach to the theoretical ones only at large time values. If electrode potential is plotted versus log [Ce(IV)]/ [Ce(III)] a non-nernstian response may be deduced.

Although a better agreement is found between experimental and nernstian curve at lower values of the [Ce(IV)]/ [Ce(III)] ratio, experimental measurements are not equilibrium, but mixed potentials.

Potential-time curves are nearly linear even in the absence of Ce(III) and its slope is linearly related to the iodide concentration at least up to 48 $ng.mL^{-1}$ with a relative standard deviation of 5.8% (ten determinations), and a detection limit of about 4 $ng.mL^{-1}$.

A lower detection limit may be attained if the potential decay at 60 min. is plotted against the iodide concentration. The calibration plot is linear at least in the range from 0.1 to 14 $ng.mL^{-1}$, and the relative standard deviation is 8%.

REFERENCES

(1) I.M. Kolthoff and E.B. Sandell, Mikrochim. Acta 1,(1934),1426
(2) P.A. Rodriguez and H.L. Pardue, Anal. Chem. 41,(1969),1369

Contributions to the Etching of ABS plastics for the chemical copper plating.

A.M. Martínez; J.L. Polo* y R. Guzmán. Dto. de Química Física. Facultad de Químicas y Matemáticas. Universidad de Murcia. Spain.

Plastics have a wide field of application, one of the most interesting being that of superficial copper plating (1), wich provides them with properties very similar to those of metals, i.e., electricals conductors, being more interesting than metals, as they are free to corrosion. At the same time they allow the electroplating of other metals.

On the other side, we are studyng the processes of chemical copper plating on differents plastics, presenting in this communication the studies realized on the ABS type (acrilonitrile-butadiene-styrene), as it is the most widely used in this field and that presenting the best conditions for the chemical plating.

The most important processes may be classified in four steps:

1º).- Chemical treatment with a sulphochromic solution in order to obtain a microfisurated surface.
2º).- Sensibilization by the $SnCl_2$ action.
3º).- Activation by $AgNO_3$.
4º).- Chemical copper plating in isself.(2).

And lately it may be subject of an electrochemical treatment, as the electroplating of another metal.

This study has been made as a function of the following parameters: temperature, minimum time required for the action of sulphochromic solution and dichromate concentration.

With that object, we have made two graphs:

a).- Dichromate concentration vs. minimum time (Graph 1).
b).- Temperature vs. minimum time (Graph 2).

It is possible to observe from both graphs, that so the reactive concentration as the temperature, influence mainly on the superficial copper plating of ABS plastics.

It has not been possible its study at high temperature because have appeared softening phenomena in the polymer.

The kinetics of the processes show the aparition of very interesting phenomena, as some inflection points in each one of the processes submitted to the plastic, being always in the same range of temperature (45-55 °C), but at dichromate concentrations lower than $2,3.10^{-4}$ M.

These inflection points appear later when the dichromate concentration is lower.

We think that it is an inductive-kinetic phenomena

---

*) Dto. de Química Analítica. Facultad de Químicas y Matemáticas. Universidad de Murcia. Spain.

being actually widely studied.

This communication is enlarged with exposition and observation of the photographs at microscope (900x) of the mentioned surfaces.

Once seen then, it is possible to observe the micro fisurization due the sulphochromic solution is more intensive as the temperature and the dichromate concentration a higher, which are in accordance with our graphs.

Graphs 3 shows two series of microphotos of the facts above mentioned.

So, it is easy to find the optimun working conditions for each practical case, as could be the preparation of integrated electrical microcircuits, no being rejectable its use in other fields of industry an research.

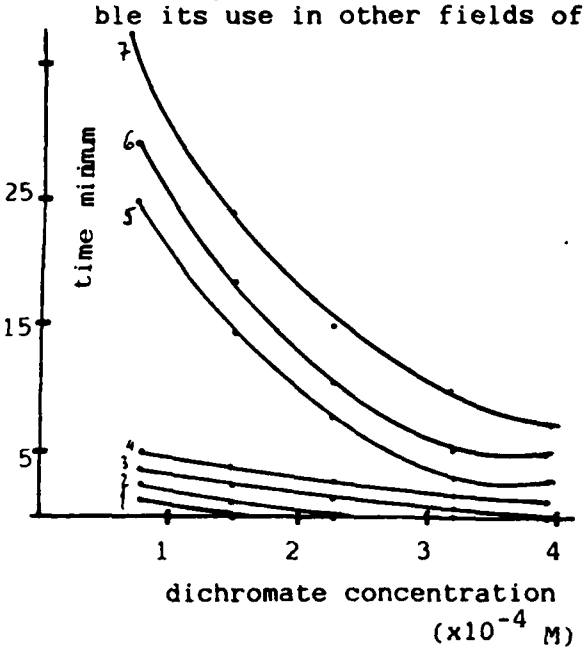

Graph 1

1) 20 °C.
2) 30 °C
3) 40 °C
4) 50 °C
5) 60 °C
6) 70 °C
7) 80 °C.

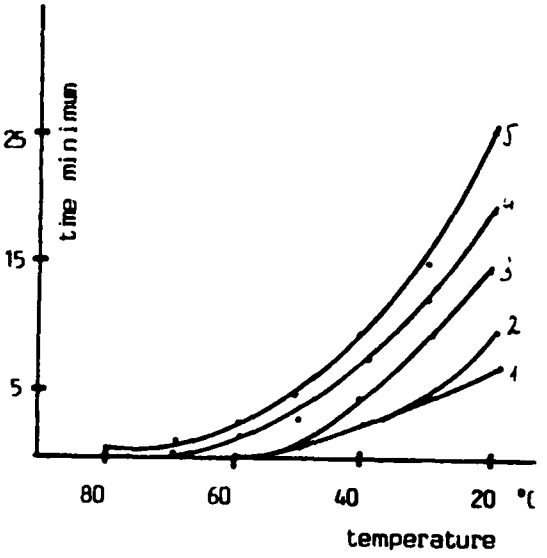

Graph 2
Dichromate concentration

1) $3,94.10^{-4}$ M
2) $3,18.10^{-4}$ M
3) $2,31.10^{-4}$ M
4) $1,48.10^{-4}$ M
5) $0,84.10^{-4}$ M.

Surface without attack | Surface attacked | Surface copper plated.

Conditions: $[Cr_2O_7K_2]$ = $0{,}84.10^{-4}$ M, $[SO_4H_2]$ = 3,34 M T^a = 40 °C

Time 10 min.

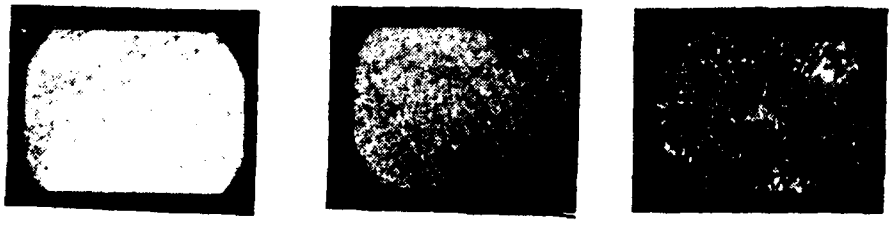

Surface without attack | Surface attacked | Surface copper plated

Conditions: $[Cr_2O_7K_2]$ = $2{,}31.10^{-4}$ M, $[SO_4H_2]$ = 8,53 M. T^a = 80 °C

Time 3 min.

REFERENCES.-

1).- "Plating on plastics". G. Müller and D.W. Baudraud. Ed. Robert Draper. 1.971.

2).- Apports au ètude de la cinetique du cuivrage chimique des plastiques. Journées D'electrochimie. Firenze. Italia. May 1985.

THE APPLICATION OF REVERSE NORMAL PULSE POLAROGRAPHY TO THE CATHODIC STRIPPING DETERMINATION OF SUBSTANCES OF BIOLOGICAL INTEREST.

J. M. LOPEZ FONSECA, J.C. GARCIA MONTEAGUDO, A. RIVEIRO y A. OTERO
Departamento de Físico-Química Aplicada. Facultad de Farmacia.
Universidad de Galicia. Santiago de Compostela. Spain.

INTRODUCTION

Reverse pulse polarography ("scan-reversal pulse polarography") is a variant of normal pulse polarography in which the initial voltage is set to a value at which the electrode reaction being studied takes place. This technique can be used on commercially available instruments, and Osteryoung and Kirowa-Eisner[1] have demonstrated its potential for the characterization of electrode reactions, including the analysis of their polarographic reversibility[2] and the identification and quantitative determination of their intermediate and final products. Analytically, the amperometric mode of the method has been employed for the determination of a variety of species using solid electrodes as flow detectors[3,4]. The present communication describes the use of reverse pulse polarography for the determination of substances that take part in the electrochemical formation of insoluble films of mercury compounds on the electrode surface. The technique presented is a form of cathodic stripping voltammetry, and shares the latter's inherent sensitivity.

THEORY

Any species A that forms insoluble compounds with mercury ions produces a polarographic anodic wave due to the oxidation of the mercury of the electrode:

$$z\,A + Hg \rightleftharpoons (A_z - Hg)_{el} + ne^- \qquad (1)$$

where the subscript el indicates the surface of the electrode. If the concentration of A is such that the maximum surface concentration of the compound $A_z - Hg$ is attained, this wave may be followed by a second at more positive potentials.

When reverse normal pulse polarography is employed with an initial voltage corresponding to the limiting current of the anodic wave, the above electrode reaction takes place during the time t_1 that elapses between the moment in which the electrode drop begins to form and the moment in which the voltage pulse is applied. An analysis of the phenomenon similar to that published by Koryta[5] shows the number N of moles of product formed in conditions in which the surface is not saturated to be given by

$$N = 0{,}85\, m^{2/3}\, t_1^{2/3}\, \Gamma = 0{,}627.10^{-3}\, C_A\, D_A^{\frac{1}{2}}\, m^{2/3}\, t_1^{7/6}\, z^{-1} \qquad (2)$$

where m is the mercury flow rate, Γ the surface concentration of $A_z - Hg$, C_A the molar concentration of A and D_A its coefficient of diffusion.

Applying a sufficiently large negative voltage pulse drives reaction (1) backwards, reducing the compound concentrated on the electrode surface. The mechanism is thus similar to that of normal pulse polarography in electrode reactions in which the reagent is adsorbed[6,7], and the current-voltage curves present a characteristic peak shape.

When the negative pulse is applied, the compound $(A_z - Hg)_{el}$ is stripped

from the cathode to form A, whose concentration in the proximity of the electrode depends on the voltage of the pulse. Following the application of the pulse, $(A_z - Hg)_{el}$ continues to be reduced until the whole film deposited has been eliminated, since its re-dissolution from the cathode acts to maintain the concentration of A at the electrode surface and so compensate for the diffusion of A away from the electrode. Thus the current recorded at a fixed time t_p after the application of the pulse increases with negative potential as a result of the increasing concentration of A at the electrode surface (which increases its diffusion rate), until a point is reached at which it begins to decrease with further increments in -E because the film deposited is exhausted before current begins to be recorded. For a fixed voltage, current increases as t_p is reduced, because the rate of diffusion of A increases due to the relationship between t_p and the concentration gradient of A. Since reducing t_p furthermore means that the film deposited may not be totally consumed, it may be expected that for short t_p the peak current recorded, which is proportional to the quantity of $(A_z - Hg)$ deposited on the electrode, will be greater than in techniques in which peak current is related to the diffusion of A.

RESULTS AND DISCUSSION

The analytical possibilities of the technique sketched above have been investigated using two thiolic compounds of biological interest, cysteine and penicillamine. At low concentrations ($\simeq 5\times10^{-5}$M) in 0,06M sodium tetraborate (pH 9.2), both these compounds produce anodic waves in normal pulse polarography. Reverse pulse polarography with an initial voltage E_i corresponding to the limiting current of the n.p. wave yields a well-defined peak whose potential E_p is close to the anode wave's $E_{\frac{1}{2}}$. Varying E_i between -0.1 and -0.4 V has no significant effect upon the peak current i_p, which is however very sensitive to changes between 1.0 and 9.9s in the droptime of the electrode, t_d, and hence to t_1. For 5×10^{-6}M penicillamine the graph of log i_p against log t_1 is a straight line of gradient 1.17, which by equ.(2) confirms that i_p is proportional to the quantity of mercury compound deposited on the electrode. Similarly, i_p is also very sensitive to varying t_p between 10 and 80ms, exhibiting an exponential rise as t_p is decreased, so that the values of i_p for t_p = 20ms and t_p = 80ms are approximately 60% and 20% respectively of its value for t_p = 10ms.

Under optimal instrumental conditions (t_d = 9.9s; t_p = 10ms), reverse normal pulse polarography (r.p.p.) proves to be a better analytical tool for the determination of the compounds used than either normal pulse polarography (n.p.p.) or differential pulse polarography (d.p.p.). With respect to n.p.p., for 5×10^{-6}M penicillamine i_p(r.p.p.)/i_p(n.p.p.) $\simeq$ 5, with r.p.p. offering the additional advantage of providing peaked curves instead of waves. With respect to d.p.p., i_p(r.p.p.)/i_p(d.p.p.) $\simeq$ 8 for the same instrumental sensitivity even though the peak d.p.p. currents are multiplied by a factor of 10, and the r.p.p. peaks are furthermore better defined, with half-peak amplitudes $W_{\frac{1}{2}}$ of 55mV in r.p.p. as against 135mV in d.p.p. Finally, in r.p.p. i_p is proportional to the concentration of the thiolic compound over the range of concentrations tested ($2\text{-}10\times10^{-6}$M); and in the presence of excess Cu(II) r.p.p. allows penicillamine to be determined in the range $5\times10^{-8}\text{-}1\times10^{-6}$M by using the peak due to the reduction of its complex with copper.

REFERENCES

1) OSTERYOUNG J. and KIROWA-EISNER E., Anal. Chem., 52, 62 (1980).
2) OLDHAM K.B. and PARRY E.P., Anal. Chem., 42, 229 (1970)
3) MAIZOTA P. and JOHNSON D.C., Anal. Chim. Acta, 118, 233 (1980).
4) WANG J. and DEWALD H.D., Talanta, 29, 901 (1982)
5) KORYTA J., Collect. Czech. Chem. Commun., 18, 206 (1953).

6) FLANAGAN J.B., TAKAHASHI K. and ANSON F.C., J. Electroanal. Chem., 85, 257 (1977).
7) LOVRIC M., J. Electroanal. Chem., 170, 143 (1984).

PHASE SELECTIVE ALTERNATING CURRENT POLAROGRAPHIC BEHAVIOUR OF MESNA.ANALYTICAL APPLICATIONS*

M.J. GARCIA GUTIERREZ, P. TUÑON BLANCO, A. COSTA GARCIA
and S. ARRIBAS JIMENO
Department of Analytical Chemistry
University of Oviedo.Asturias.Spain

Sodium 2-mercapto-ethanesulfonate (mesna) is a molecule which has a proved ability to bind and detoxify the urotoxic metabolites of oxazaphosphorine / cytostatics[1,2]. Frequently,actual dosage formulations of mesna in pharmaceutical preparations are suministered to patients under oxazaphosphorine cytostatic treatments.

The absence of specific analytical methods for mesna prompted us to look / for and carry out electroanalytical methods for its determination. Further / improvements of the investigation of mesna pharmacokinetics by polarographic methods are to be expected.

EXPERIMENTAL

DC, AC, and DPP signals for mesna were recorded by using a Metrohm Polarecord E506 in conjunction with an E506 polarography stand equipped with a mechanical droptimer.Mesna was kindly facilitated by Asta Werke Labs. (W.G.)

RESULTS AND DISCUSSION

As previously reported[3], mesna suffers a complex oxidation process on DME which can be used for analytical purposes.The nature of the process is - -/ better observed if a DPP or AC signal is recorded. All criteria of reversibility checked by using DC,AC and DPP techniques show the process to be reversible.The electrochemical reaction proposed is :

$$2\ HS\text{-}CH_2\text{-}CH_2\text{-}SO_3Na \longrightarrow \begin{matrix} NaSO_3\text{-}CH_2\text{-}CH_2\text{-}S \\ | \\ NaSO_3\text{-}CH_2\text{-}CH_2\text{-}S \end{matrix} + 2\,e^- + 2\,H^+$$

which is in agreement with the number of electrons coulometrically analyzed or deduced by the Tomes plot on the DC wave[4]. This fact was also examined by addition of dimesna to the electrolytic cell and recording DC polarogram. At pH 6 the catho-anodic wave observed seems to be reversible with a $E_{1/2}$ value of -0.360 V (vs SCE).

The electrode mechanism is seriously influenced both by the concentration of mesna or by the pH medium. In fact when the mesna concentration changes, one or two peaks can be observed if a DPP signal is recorded. Figure 1 shows the dependence of the current observed for both peaks on the mesna concentration. This means that an adsorption step (1^{st} peak) may become more or less meaningfull depending on mesna concentration.

The influence of the pH is greater in the case of the AC signal than in / the case of the DPP signal as is shown in figure 2. From the $E_{1/2}$ versus pH plots, a polarographic pK value of 9.2 is obtained.

*This work was funded by the Spanish Commission for Research and Technology (CAICYT). Project No. 1182/81

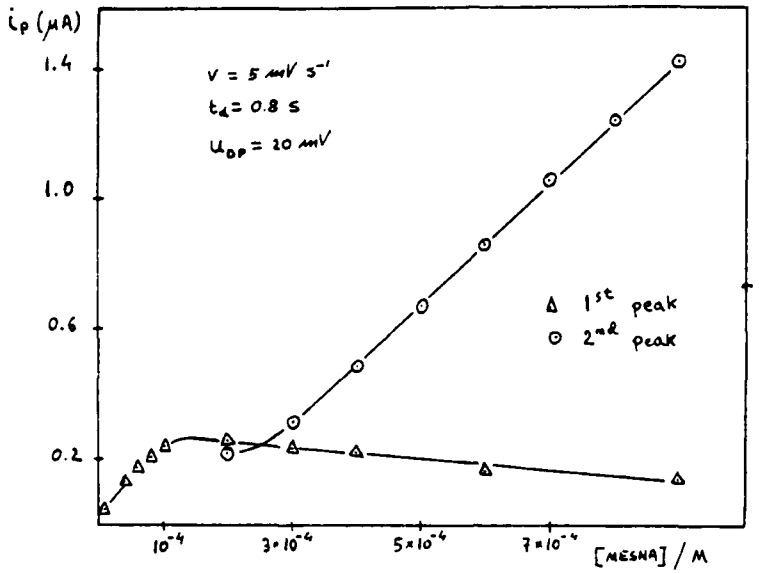

Figure 1

ANALYTICAL APPLICATIONS

DC responses are not useful for analytical purposes because wave distorsion is always found.The best medium for DPP calibration of aqueous solu-/ tions of mesna is $HClO_4$ 0.1 M.In this medium linear calibration graphs between 4 X 10^{-7} M and 8 X 10^{-5} M are obtained. Greater sensibility is found when AC signals are used for analytical purposes. In fact calibration plots are found covering three exponetial order of magnitude (from 10^{-7} to 10^{-4} M).

Urine samples

Mesna can be analized in urine by usinga very simple method. The sample -/ is defrosted , centrifugated and mixed with Ac/AcH buffer (pH 5) in the proportion 1 : 1. After that the DPP or AC signal is recorder.Either calibration or standard addition method may be followed.

In a urine pool comprising a mixture of at least 40 individual samples -/ the detection limit found for AC is less than 10^{-7} M and linear calibration graphs close to three exponetial order of magnitude were found.Although AC blank signal is not so clean as DP one's is.

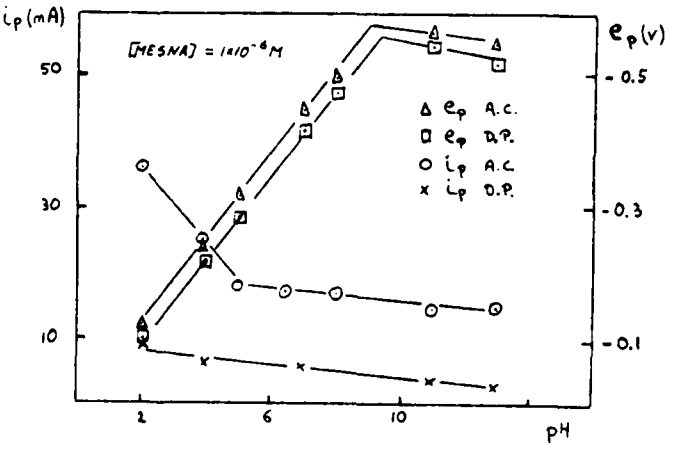

Figure 2

REFERENCES

1 T.A. *Connors*,Europ. J. Cancer, 2(1966)293
2 M. Ishidate et col. , Gann, 44(1953)386
3 Work presented to the "XX Reunión Bienal de la R.S.E.Q." 1984 Castellón Spain.
4 J. Tomes, Coll. Czech. Chem. Comm., 9(1937)150

OXIDATIVE AMPEROMETRIC DETECTION IN HPLC DETERMINATION OF ANTICANCER DRUG METHOTREXATE *

MIRANDA ORDIERES,A.J.,TUÑON BLANCO,P.,COSTA GARCIA,A., GARCIA FERNANDEZ,M.A.,ARRIBAS JIMENO,S.

Department of Analytical Chemistry.University of Oviedo. Asturias.Spain.

INTRODUCTION.-

The anticancer drug Methotrexate yields anodic processes at glassy carbon electrodes,useful for amperometric measurements in flowing systems.A carefully selection of mobile phase composition and pH can overcome problems arising from large possitive applied potentials and electrode fouling by electrochemical reaction products.

EXPERIMENTAL.-

Anodic behaviour of MTX at glassy carbon electrode was examined by cyclic voltametry in aqueous (Britton Robinson buffer) and aqueous-methanolic (Phosphate buffer) media.A wall-jet cell was used as amperometric detector.Reverse phase chromatography (C_{18} column) with isocratic elution provides MTX separation from naturally occurring serum components.

RESULTS AND DISCUSSION.-

Cyclic voltammetric curves show an anodic peak in the pH range 1-10 at slow scan rates.No cathodic peaks corresponding to this process were observed on the available potential range at scan rates up to 500 mVs^{-1}. Dependences of peak potential and peak current with pH are shown in Figure1.

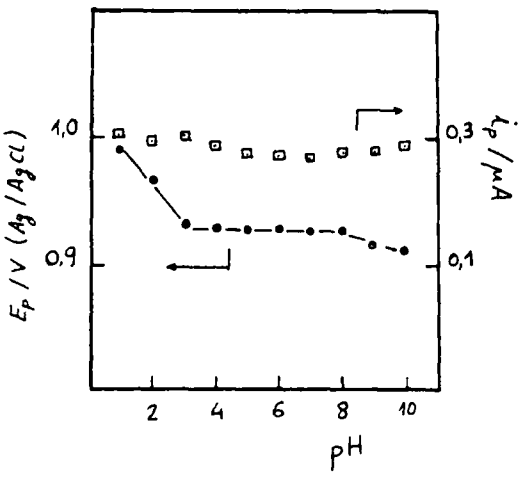

Severe electrode fouling caused by reaction product adsorption was indicated by decrease of both peak current and $n\alpha$ values with sucessive scans.Electrode activation by polishing with Alox powder and immersion in pure methanol yields an acceptable reproductibility of CV curves.

As expected addition of increasing amounts of organic solvent to background electrolyte reduces electrode fouling problems.In pH=3,0 phosphate buffer, a 25 % v/v of added methanol allows self-cleaning of electrode surface if solution is stirred for 3 minutes between sucessive scans, yielding excellent reproductibility of C.V. curves. In this background electrolyte, be-

* This work was funded by Spanish Commission for Research and Technology (CAICYT) Project No 1182/81.

haviour of anodic peak (E_p = + 1,01 V vs. Ag/AgCl/sat.KCl at 20 mVs^{-1}, $n\alpha$ =0,8) indicates an irreversible,diffusion-controlled process.

MTX is strongly retained in C_{18} columns.Retention time increases as mobile phase pH decreases.So,more acidic mobile phase allows the use of higher contents of organic solvent,permiting k' values to remain adequate in order to chromatographic separation.Oxidation of background electrolyte occurs at more possitive potentials as pH decreases,whereas MTX peak potential and peak current remain almost constant in the pH range 3,5 - 10 .Accordingly the use of a mobile phase with pH close to 3,5 enables the application of more possitive potentials,as well as a higher content of organic solvent, the latter enhancing the electrode self cleaning effect.

Experimental results indicates that in 0,025 M phosphate buffer pH=3,0 containing 28 % methanol,working electrode activity remains constant for more than 40 hours of continuous operation under an applied potential of + 1,15 V (Ag/AgCl/sat KCl).Conversely at pH=5 and 20 % methanol,applied potentials higher than 1,00 V origines a rapid decrease in peak heigth for sucessive inyections of fixed amounts of MTX.

Obviously,final selection of mobile phase composition and pH must be a compromise between separation and detection requirements.A good separation of MTX from matrix components was obtained with 0,025 M phosphate buffer pH=3,0 containing 25 % of methanol,at a flow rate of 0,8 ml min^{-1} and 30°C, and detection at + 1,10 V.A calibration plof obtained in this conditions was linear between 0,45 and 226 ng of MTX inyected.Detection limit for MTX assay in human serum was found to be $5x10^{-8}$ M.

10090

PHASE SELECTIVE ALTERNATING CURRENT POLAROGRAPHIC DETERMINATION OF METHOTREXATE IN BIOLOGICAL MATRICES*

A.J. MIRANDA ORDIERES, P. TUÑON BLANCO, A. COSTA GARCIA
and S. ARRIBAS JIMENO
Department of Analytical Chemistry
University of Oviedo.Asturias.Spain

Prevention of toxic side effects in high-dose Methotrexate (MTX) therapy of a widw variety of tumors requires drug monitorization of serum concentration at submicromolar level. Present paper examines the performance of AC polarographic methods applied to resolve this problem.

EXPERIMENTAL

AC polarography was carried out by using a Metrohm E-506 polarograph operating at fixed frequency (75 Hz). MTX electroreduction was examined also in DC and DP polarography and cyclic voltammetry at HMDE.

RESULTS AND DISCUSSION

MTX originates up to three reduction processes at DME, the first of them being a two electron reduction with an EC mechanism[1]. This process gives rise to an AC polarographic peak whose potential as a pH function is expressed by the following equations (potentials measured vs. SCE),

(1) e_p = -0.211 - 0.070 pH 1 pH 3.4
(2) e_p = -0.259 - 0.056 pH 3.4 pH 7.5
(3) e_p = -0.162 - 0.069 pH 7.5 pH 12

AC peak potential values show great coincidence with DC half wave potentials on the whole pH range.

DC polarograms at the concentration level of 5 X 10^{-5} M in MTX exhibit a prewave at pH higher than 3.1 which gradually disappears with increasing pH, becoming unappreciable at pH 6. At pH 7 a postwave starts to develop.Its -/ height increases and its halfwave potentials shifts to more positive values with increasing pH. These results, indicating reactant and product adsorption, were confirmed by cyclic voltammetric experiments. At MTX concentrations lower than 5 X 10^{-6} M CV curves shape is completely simmetrical,appearing both anodic and cathodic peaks at the same potential. Ratio of anodic to cathodic peak current is close to 1, and the current of both peaks increases linearly with electrode-solution contact time.

pH range 2.2- 3.5 was found to be suitable for analytical purposes in AC polarography.Peak currents reach their maximum value in this range. At pH 3.5 (e_p = -0.460 V) and 5 X 10-6 M in MTX , peak width at its half height is 65 mV (90/n for a reversible process).Plot of i_p versus drop time power to 7/6 is linear with an intercept near 0. e_p being independent of drop time. Linear dependences of i_p upon $h^{-1/2}$, MTX concentration and e were also established. These results are in agreement with theoretical predictions[2] / for a quasi reversible charge transfer coupled with both reactant and product adsorption under Langmuir isotherm conditions.

Calibration plot of i_p vs. bulk MTX concentration presents a linear dinamic range from 1.00 X 10^{-8} M to 1.05 X 10^{-5} M (r= 0.999). Measurements /

*This work was funded by the Spanish Commission for Research and Technology (CAICYT). Project No. 1182/81

were made in the sampled current mode with an amplitude modulation of 30 mV and a drop time of 0.8 s. These conditions were found to be suitable for analytical determination of MTX in human serum. Due to strong interferences caused by serum proteins, a sample clean-up procedure must be used. MTX extraction from serum samples with reversed -phase C_{18} cartridges (Sep-Pak, Waters), after protein precipitation with $HClO_4$, yields a mean recovery value of 42 %. Addition of known amounts of MTX to a solution containing the extract of 2 ml of human pooled serum dissolved in 6 ml of Britton-Robinson buffer (pH 2.2), yields a linear calibration plot. The detection limit found was of 27 ng of MTX. Standard additions method is recommended for MTX quantitation in serum samples.

A comparison of AC and DP polarograms of serum blanks and samples shows that AC method produces cleaner blanks and superior sensitivity. In fact sensitivity of AC measurement is essentially limited by capacitive current, whereas DP polarograms show interferences from matrix components undergoing reduction processes at potentials close to that of MTX peak.

REFERENCES

1 R.C. Gurira and L.D. Bowers, J. Electroanal. Chem., 146(1983)109
2 E. Laviron, J. Electroanal. Chem., 97(1979)135

VOLTAMMETRIC TECHNIQUES APPLIED TO THE STUDY OF THE HYDROLISIS OF S-ADENOSIL L- METHIONINE*

J.L. MUÑIZ ALVAREZ, A.J. MIRANDA ORDIERES
P. TUÑON BLANCO, A. COSTA GARCIA and S. ARRIBAS JIMENO
Department of Analytical Chemistry
University of Oviedo.Asturias.(Spain)

S-adenosil methionine is a molecule of great biological importance.It was first formulated in 1952 by G.L.Cantoni[1] and the ordinary and natural via of synthesis consists in the combination of methionine and ATP-derived adenosin.

The biological importance of S-adenosil methionine (SAMe) is attributed to the fact that it participates actively in innumerable biological processes/ that take place via transmetilation.This unique fact explains the great clinical and biochemical interest in pharmaceuticals containing SAMe in a wide spectrum of therapeutical uses ranging from liver diseases to mental disorders.

According to R.T.Borchardt[2],SAMe suffers a strong hydrolisis reaction in/ strong alkaline media ($OH^- > 0.05$ M) with the production of adenine and pentosilmethionine exclusively whereas if a weaker alkaline medium is used, there is a further and competitive hydrolisis reaction which leads to the formation of homocysteine lactone and methylthioadenosine.

EXPERIMENTAL

As mentioned in a previous study[3] , SAMe originates anodic and cathodic / processes in a stationary mercury electrode which are strongly influenced by the pH of the medium; these processes have been studied by means of cyclic/ voltammetric techniques.

Both cyclic voltammetry and and cathodic stripping voltammetry were used/ to study the evolution of SAMe hydrolisis reactions ; the formation of the cathodic peak was observed in both cases.

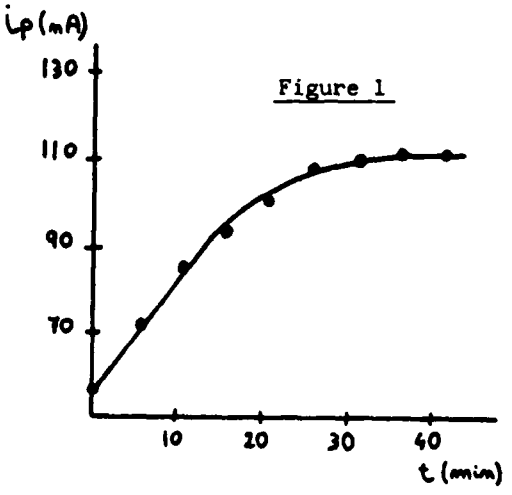

Figure 1

RESULTS AND DISCUSSIONS

From pH up to a concentration of NaOH 0.1 M, SAMe originates cathodic stripping processes which clearly show the evolution of the SAMe solution as a function of time. The fact that these processes are not seen at smaller pH values --/ shows that the hydrolisis either/ does not take place or that the / kinetics is extremely slow.Finally, it is possible that the hydrolisis of SAMe under stronger alkaline / conditions originates products in-

*This work was funded by the Spanish Commission for Research and Technology (CAICYT).Project No.1182/81.

capable of experimenting cathodic stripping.

In a Britton-Robinson pH 12 buffer, the stripping peak reamains stabilized three and a half hours after the initial solution preparation. In NaOH 0.01 M, the SAMe solution evolves at a faster rate and / peak stabilization takes place after 25 minutes. (Figure 1). This study was carried out on a 10^{-5} M solution of SAMe and if this concentration is submitted to a cyclic scan at a rate of 20 mV s^{-1} the voltagram shown in Figure 2 is obtained. As shown in the figure, cathodic and anodic peaks appear when the potentials are -/ close to -0.2 V. The time needed for stabiling the solution is reduced when the concentrations of NaOH exceed 0.01 M ; a concentration of 0.05 M or higher - / causes the peak current to be stabilized instantaneously.

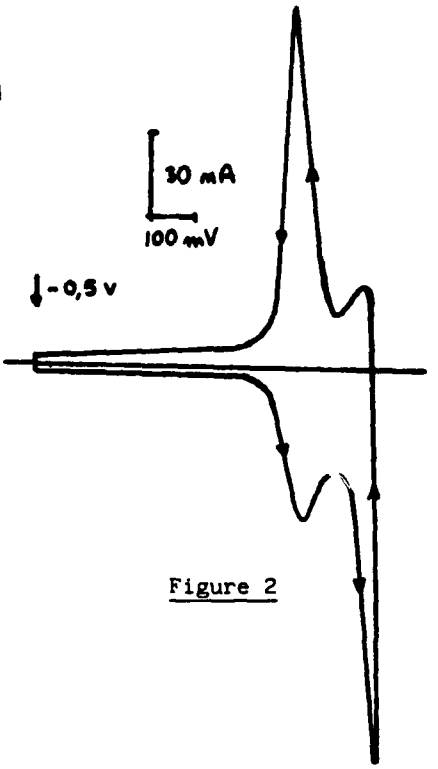

Figure 2

ANALYTICAL APPLICATIONS

The cathodic stripping peak can be -/ used for analytical purposes and sensitivity may be improved by pulse scanning.

In aqueous solutions of SAMe, a deposition time of 1 minute at a potential - of -0.02 V and a pulse amplitude of 25 mV originate a detection limit of 10^{-8} M. At the same time, linear calibrations -/ from 10^{-8} to 7.0 X 10^{-7} M for SAMe concentrations are found.

The method can also be used for the determination of SAMe in serum provided / that the sample is previously cleaned by passing it through a Sep-Pak C_{18} cartridge with a H_3PO_4/NH_3 pH 8 buffer and eluting with H_3PO_4 0.025 M.

Recovery is found to be 60.5 % with a detection limit of 10^{-7} M and linear calibrations may be obtained from 10^{-7} to 2.5 X 10^{-6} M.

REFERENCES

1 G.L. Cantoni, J.Amer.Chem.Soc., 74(1952)2942.
2 R.T. Borchardt, J.Amer.Chem.Soc., 101(1979)458.
3 Work presented to the "XX Reunión Bienal de la R.S.E.Q." 1984 Castellón. Spain.

DETERMINATION OF BIOLOGICALLY INTERESTING MOLECULES BY PULSE VOLTAMMETRY

J. OSTERYOUNG, M. WOJCIECHOWSKI, A. WEBBER AND E. TAKEUCHI
Department of Chemistry, State University of New York at Buffalo,
Buffalo, New York (U.S.A.)

Pulse voltammetry comprizes a suite of techniques based on current-sampled chronoamperometry, the most important of which are normal pulse, differential pulse, staircase, and square wave voltammetry. These techniques are described in Figure 1.[1] These techniques provide many possibilities for

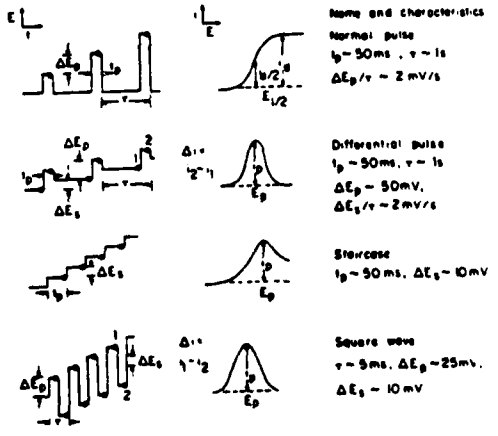

Fig. 1. Potential-time sequence and resulting current-time response in pulse voltammetry.

analytical and mechanistic studies of biologically interesting molecules. The examples described here include mechanistic and analytical studies of an antibacterial agent, 1,2-dibromo-2,4-dicyanobutane (DBDCB),[2] of reduced nicotinamide adenine dinucleotide (NADH) and related compounds[3,4] and of a proposed intracellular intermediate in nitrate-induced vasodilatation, N-acetyl penicillamine thionitrite (RSNO).[5] These examples illustrate a range of mechanisms, compound types, techniques, and electrodes.

The Compound DBDCB.[2] In general organic halides undergo irrversible cathodic reduction with formation of halide ions and organic product on products. Vicinal dihalides usually loose halides in a single two-electron step which yields an olefin. Because the cyanide group is strongly electron-withdrawing, halogenated alkyl nitriles are reduced at more positive potentials than corresponding alkyl halides. It is widely observed that mercury electrodes participate chemically in the reduction process. Cyclic staircase voltammetry (Figure 2) shows the strong catalytic effect of the mercury

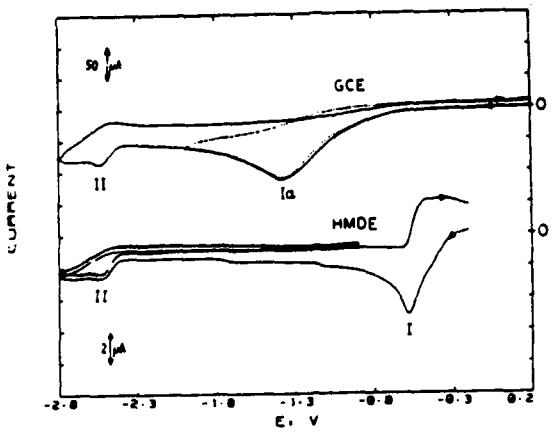

Figure 2. Cyclic voltammetry of DBDCB on glassy carbon electrode (GCE) and on hanging mercury dropping electrode (HMDE) in acetonitrile). The solution was 0.5 mM in DBDCB and 0.1 M in TEAP. The scan rate was 0.63 V s^{-1}.

electrode on the first reduction process which corresponds to the reaction

$$H_2C(Br) - C(CN)(Br) - CH_2CH_2CN + 2e^- \rightarrow C_6N_2H_6 + 2Br^- \quad (1)$$

in which $C_6N_2H_6$ is most probably 2,4-dicyano-1-butene. The solubility of DBDCB in water was determined by reverse pulse polarography[6] as 0.16±0.01%.

The compound NADH.[3] The compound NADH can be converted to and held for a period of hours in its hydrated form which results from adding water across the 5,6-double bond of the nicotinamide ring. This compound adsorbs on mercury surfaces under diffusion-control and gives rise to a cathodic stripping current proportional to concentration in solution. The technique of choice for determination is square wave voltammetry, although staircase voltammetry can be used as well. The detection limit is less than 7 nM, and the range of linear response covers 2-3 orders of magnitude change in concentration of NADH. Nicotinamide adenine dinculeotide (NAD+) and related compounds exhibit very similar electrochemical response, which is due to a 4H+-4e- totally irreversible reduction of the adsorbed adenine moiety.[4]

The Compound RSNO.[5] Thionitrites are proposed intracellular intermediates in organic nitrate-induced mammalian vasodilatation. Although these intermediates have been demonstrated indirectly no sensitive quantitative methods for direct determination have been developed previously. On mercury electrodes a reversible pH-dependent wave appears which is the same as that for the parent penicillamine and probably corresponds to the reaction

$$RSNO + Hg + H_2O \rightarrow RSHg + HONO + H^+ + e^- \quad (2)$$

An irreversible wave appears at more negative potentials at both mercury and glassy carbon electrodes which appears to be due to the reaction

$$RSNO + H^+ + e^- \rightarrow RSH + NO \quad (3)$$

This reaction can be used for analytical purposes employing square wave voltammetry as shown in Figure 3 with resulting detection limits ca 40 μM and

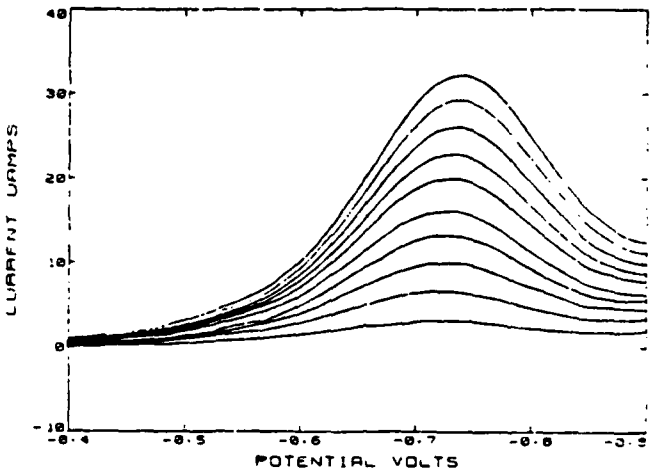

Figure 3. Square wave voltammetry of N-acetyl penicillamine thionitrite from 0.1 mM to 1 mM in steps of 0.1 mM, 0.1, M HCl/KCl, pH 2.0. Step height = 5 mV, amplitude = 25 mV, frequency = 10 Hz.

linear range up to 1.5 mM.

Acknowledgments.

The authors thank John O'Dea, Mumtaz Shah, and Ho-Leung Fung for their assistance. This work was supported by the National Science Foundation of the U.S.A. under Grant Numbers CHE-7917543 and CHE-8305748.

REFERENCES

1. Janet Osteryoung, J. Chem. Ed. 60, 296 (1983).

2. M. Wojciechowski and Janet Osteryoung, Anal. Chem. 57, 927 (1985).

3. A. Webber, M. Shah and Janet Osteryoung, Anal. Chim. Acta 157, 1 (1984).

4. A. Webber and Janet Osteryoung, Anal. Chim. Acta 157, 17 (1984).

5. E. S. Takeuchi, Janet Osteryoung and H.-L. Fung, Anal. Chim. Acta, in press.

6. Janet Osteryoung and E. Kirowa-Eisner, Anal. Chem. 52, 62 (1980).

POLAROGRAPHIC AND VOLTAMMETRIC STUDY OF 2-MERCAPTOETHANOL AND ITS COMPLEXES WITH CADMIUM (II) ION

E. Casassas, C. Ariño and M. Esteban

Department Química Analítica. Fac. Química. Univ. Barcelona
Av. Diagonal, 647. 08028-Barcelona (Spain)

A polarographic study of 2-mercaptoethanol (RSH) and its Cd(II)-complexes at different pH and RSH concentrations by DC, DP, AC_1 and AC_2 polarography is described. A comparative study by cyclic voltammetry at HMDE has been made.
In the electrocapillary curves of Hg in Cd(II)-ion solutions an important deformation appears at more positive potentials than -0.7 v, depending on the pH, when RSH is present in the solution (Fig. 1). These deformed curves are very similar to those obtained in Cd(II)-free RSH solutions.

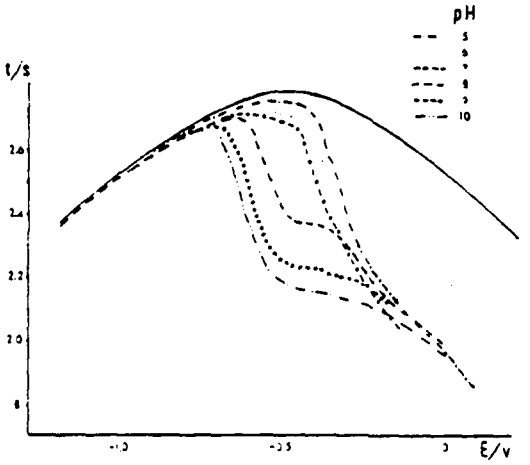

Fig. 1.- Electrocapillary curves of Hg in a solution of $8\ 10^{-6}$ mole dm^{-3} Cd(II), $6.5\ 10^{-3}$ mole dm^{-3} RSH, 0.5 mole dm^{-3} $NaClO_4$ at different pH. Continuous line: Cd(II)-$NaClO_4$ solution.

As a consequence, if the morphology of the Cd(II)-ion reduction polarograms is greatly affected by the presence of RSH, especially by AC techniques. Lack of reversibility is shown by the fact that the potential shifts produced in the polarograms by the addition of RSH into the Cd(II) solutions are dependent on the employed technique (1). The reduction of Cd(II) ion in the presence of RSH is not diffusion-controlled, as the dependence of i_d vs t_{drop} shows.

Cyclic voltammograms of Cd(II)-ion reduction in the presence of RSH do not meet the usual criteria of reversibility (2). The reversibility deviation is also shown by the morphology of the voltammograms. The potential shifts produced by the addition of RSH in Cd(II)-ion solutions, as measured by cyclic voltammetry, are always higher than those measured by polarography at the same experimental conditions.

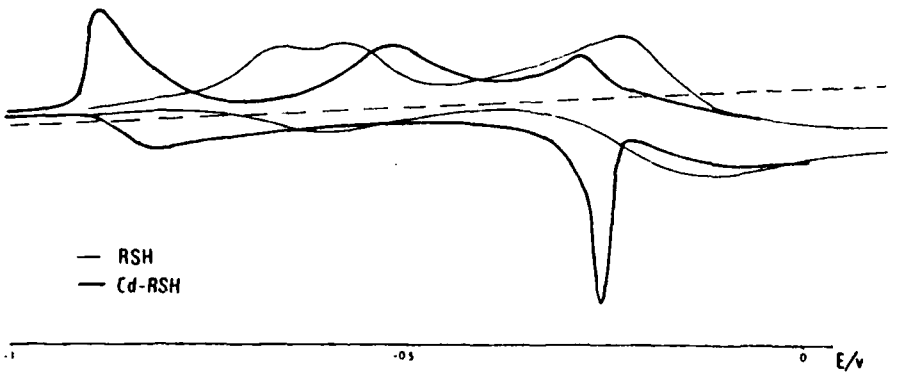

Fig. 2.- Cyclic voltammograms of RSH and Cd(II)-RSH. 1 10^{-4} mole dm^{-3} Cd(II) and 6,5 10^{-4} mole dm^{-3} RSH. pH 6,5.

The anodic scan of RSH shows two polarographic waves: an adsorption pre-wave at -0.55 v and a diffusion wave at -0.3 v, due to mercury oxidation with mercaptide formation (3). A cyclic voltammetric scan shows a wave at -0.21 v, and another one at -0.51 v (these potential values are the cathodic peak potentials). The second one shows overlaped peak at -0.59 v. Neither diffusion nor reversible criteria are verified. It is observed an influence of the pH on the waves. If Cd(II) ion is present the morphology of RSH voltammograms changes as Fig. 2 shows. It is observed a shift from the -0.21 v wave to -0.31 v. The value of $E_{cat}-E_{an}$ changes from 100 mv to 20 mv, as the figure shows. Studies of cathodic peak current and peak potential vs scan rate at different pH and RSH concentrations are also described.

Mercury mercaptide formation on the electrode allowed to develop a CSV-method for RSH determination (4).

REFERENCES

(1) A.M.Bond and G.Hefter, J. Electroanal. Chem. 68, 203 (1976)

(2) R.S.Nicholson and I. Shain, Anal. Chem., 36, 706 (1964)

(3) R.L.Birke and M. Mazorra, Anal. Chim. Acta, 118(2), 257 (1980)

(4) E.Casassas, C.Ariño and M.Esteban, Anal. Chim. Acta (Submitted for publication).

POLAROGRAPHIC STUDY OF THE ANODIC OXIDATION OF MERCURY IN THE PRESENCE OF THIOETHER CARBOXYLIC ACIDS.

E. Casassas , M. Esteban and C. Ariño

Depart. Química Analítica, Fac. Química, Univ. Barcelona.
Av. Diagonal 647 08028-Barcelona (SPAIN)

The anodic oxidation of mercury in the presence of mercapto compounds and ligands that contain mercapto and carboxylic groups has been largely studied. On the contrary, the study in the presence of thioether compounds has been very limited (1, 2).

The thioether carboxylic acids studied in this work have been: methylthioacetic, CH_3-S-CH_2-COOH (mta); 2,2'-thiobisacetic, $S(CH_2-COOH)_2$ (tba); 3,3'-thiobispropanoic, (tbp) $S(CH_2-CH_2-COOH)_2$; 2,2'-[1,1-methandiylbis(thio)] bisacetic, $H_2C(S-CH_2-COOH)_2$ (mdbt) and 2,2'-[1,2-ethandiylbis(thio)] bisacetic, $(H_2C-S-CH_2-COOH)_2$ (edbt).

A systematic study of the influence of general and instrumental parameters in the anodic oxidation of mercury in the presence of these thioether carboxylic acids has been made by DC(rapid), DP, AC_1 and AC_2 polarography, cyclic voltammetry and coulometric measurements at constant potential.

The electrocapillary curves show the very small tendency of thioether group towards adsorption in DME, in accordance with the expected results (3).

Poorly developed, for mta, and better developed, for tba and tbp, anodic DC waves are obtained. At pH>3 the DC curves show two anodic waves, the second one being a current spike typical of the change in the electrode surface covering (4).

The DP and AC polarographic curves show two anodic peaks, in the pH range 2-11, for mdbt, and one anodic peak, in the

pH range 2-7, for edbt.

The dependence of $E_{1/2}$ and E_p vs pH shows a behaviour depending on the pH range with respect pK_a values. Table 1 shows the mean slope values observed in each case by four polarographic techniques.

Table 1 : Mean slope values of the dependences of $E_{1/2}$ and E_p vs pH by four polarographic techniques.

Compound	$pH < pK_1$	$pK_1 < pH < pK_2$	$pH > pK_2$
mta	59	0.5 (at pH pK_1)	-
tba	120	60	0.75
tbp	120	60	0.75
mdbt	60	30	0.50
edbt	59	30	0.50

In each case, $E_{1/2}$ and E_p of the main wave and peak shows a linear variation with the logarithm of concentration with a slope value of ca. 30 mV, except for mta at concentrations lower than 0.5 mM and pH<3 that is independent of concentration. Relationships of I_p or I_d vs concentration are linear in each case. For mta two kinds of linearity occurs, the first one at low concentrations with slope value double of the corresponding at high concentrations. For mta, tba and tbp the plots of E vs $\log\left[(I_d-I)^2/I\right]$ are straight lines with slope values of ca. 29 mV. The main waves are diffusion-controlled.

The study of mdbt and edbt shows analogous results and similar kind of behaviour.

The coulometric oxidation of mercury at constant potential in the presence of the thioethers shows the transfer of one (mta and edbt) and two (the rest) electrons per molecule.

During each coulometic experiment the formation of an insoluble brown compound which quickly turns black is observed. Elemental analysis shows that these compounds are not pure, and that their composition varies with time. These facts show that in the coulometric processes Hg(I) compounds are formed which undergoes disproportionation. IR spectra show the carboxylate bidentate coordination and the Hg-S bands.

Typical cyclic voltammograms of thioethers are similar to the shown in Fig 1. The main anodic peak has the characteristics of diffusion-controlled process. The ΔE_p values increase

with increasing scan rates, as corresponds to a not fully reversible process.

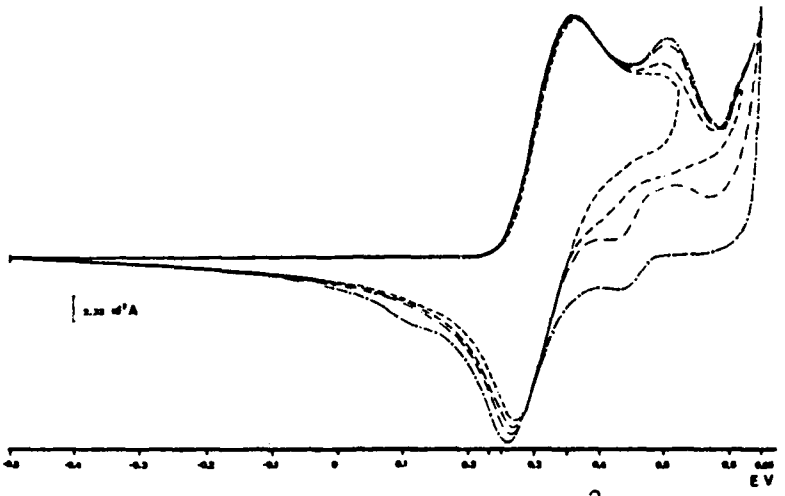

Fig 1 : Cyclic voltammogram of a 1.294 10^{-2} M mta solution.

The results are coherent with the following overall processes: a) For mta, the 1:2 Hg^{I}-mta complex formation which undergoes disproportionation to the Hg^{II}- complex; b) For tba and tbp, the 1:2 Hg^{I}-L complex formation which undergoes to the stable HgL_2^{2-} complex (5). In the coulometric conditions the $HgL.8H_2O$ formation is very probably (5); c) For mdbt, the 1:1 Hg^{II}-mdbt complex formation; d) For edbt, the HgZ_2^{2-} complex formation, in accordance with the results of Suznjevic et al. (1).

REFERENCES

(1): D. Suznjevic, J. Dolezal and M. Kopanica, J. Electroanal. Chem. 20 (1969) 279

(2): J. Kotek, H. Klierova, J. Dolezal and M. Kopanica J. Electroanal. Chem. 31 (1971) 451

(3): B.A. Parkinson and F.C. Anson, Anal. Chem. 50 (1978) 1886

(4): M.T. Stankovich and A.J. Bard, J. Electroanal. Chem. 75 (1977) 487

(5): O. Prochazkova, J. Podlahova and J. Podlaha, Collect. Czech. Chem. Commun. 38 (1973) 1128

POLAROGRAPHIC DETERMINATION OF TITANIUM AT TRACE LEVEL

Y. CASTRILLEJO, E. BARRADO, R. PARDO and P. SANCHEZ BATANERO
Department of Analytical Chemistry, Faculty of Sciences,
Valladolid, Spain

The titanium(IV) can be determined at trace level by using a combination of two reactions, the first being an amplification one between titanium(IV) and 12-molybdophosphoric acid (12-MoPA) to give a ternary heteropolymolibdic acid with a 11:1:1 stoichiometry, i.e. 11-molybdophosphotitanic acid (11-MoPTiA)[1]:

$$PMo_{12}O_{40}^{3-} + TiO^{2+} + H_2O \rightleftharpoons PTiMo_{11}O_{40}^{5-} + HMoO_3^{+} + 3\,H^{+} \quad (1)$$

This reaction is combined with a polarographic reduction based on the catalytic effect produced by the molybdenum(VI) on the reduction of the hydrogen peroxide, according to the mechanism proposed by Kolthoff and Parry[2]:

$$MoO_4^{2-} + H_2O_2 \rightleftharpoons MoO_5^{2-} + 2\,H^{-} + 2e^{-} \rightleftharpoons MoO_4^{2-} + H_2O \quad (2)$$

(MoO_5^{2-} regenerated by H_2O_2)

The analytical procedure implies: a) the formation of the 11-MoPTiA, b) elimination of the excess of 12-MoPA by extraction with an organic solvent, c) extraction of 11-MoPTiA, d) stripping of the 11-MoPTiA to aqueous medium and e) determination of the molybdenum(VI) bonded to titanium(IV) by the polarographic reaction. The 11:1 amplification provided by the reaction (1) and the high sensitivity of (2), permits the accure determination of titanium(IV) in the ppb range.

Indicator reaction

Altough the polarographic reductions of both, hydrogen peroxide or molybdenum(VI) does not have analytical applications, when the two species coexist in an acid solution, a catalytic current is obtained, which is proportional to the concentrations of both reagents. In the adequate conditions, that current can be used as a basis for the molybdenum(VI) determination. (Figure 1 shows the obtained polarograms). The optimal conditions for the development of the current are: $/H_2SO_4/$=0.2 M and $/H_2O_2/$=0.02 M. The molybdenum(VI) is then determined by measuring the height of the wave at 0.2 V (vs. SCE), in the concentration range comprised between $5.0.10^{-7}$ and $1.2.10^{-5}$ M. The presence of phosphate and/or titanium(IV) does not affect neither the shape nor the height of the polarograms.

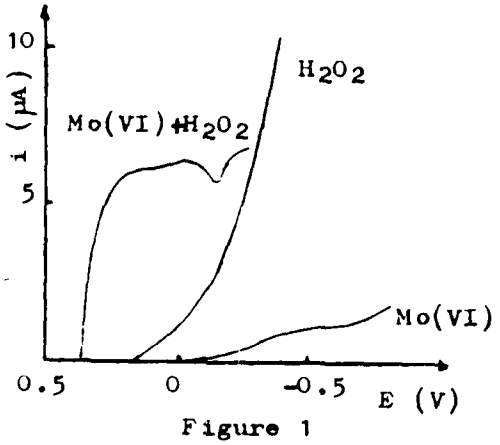

Figure 1

Amplification reaction

The 11-MoPTia is produced in acid media from titanium(IV) and 12-MoPA, being necessary an excess of the last to form quantitatively the ternary. Due to this excess and also to the inspecifity of the indicator reaction, which detects all the molybdic species and not only the ternary one, it is necessary to isolate the 11-MoPTiA before to carry out the polarographic reaction, as was outlined previously. Some parameters implied in the analytical procedure are known from previous works[3,4], i.e. the corresponding to the steps b), d) and e), so were fixed at their optimum values (See Table 1). The parameters corresponding to the formation and extraction of the 11-MoPTiA (steps a) and c)), were optimized by using the Super Modified Simplex method (S.M.S)[5]. This method permits to reach the optimal values of the parameters (amounts of 12-MoPA and perchloric acid in the a) step, and the amount of perchloric acid of the c) step) with a smaller number of experiments than a classical parameter-to-parameter approach. The optimal values along with the rest of the procedure are given in Table 1.

Table 1

Step	Reagent	Amount
11-MoPTiA Formation	10^{-2} M 12-MoPA 2 M $HClO_4$ Ti sample	0.55 ml 1.00 ml carry to 25 ml
12-MoPA Elimination	Ethyl acetate	two 25 ml-portions
11-MoPTiA Extraction	10 M $HClO_4$ MIBK	3.00 ml 10 ml
Mo(VI) Stripping	1 M NaOH	25 ml
Mo(VI) Determination	4 M H_2SO_4 0,2 M H_2O_2	5.00 ml 10.00 ml carry to 100 ml

By using the proposed procedure, titanium(IV) can be determined between $1.0.10^{-7}$ M (4.79 µg/l) and $1.4.10^{-6}$ M (67.06 µg/l). The calculated detection limit is 4.09 µg/l.

The effect of other elements which can also give heteromolybdic species was also studied. Their maximum molar ratio Element: :titanium(IV) allowed were: Silicon (300:1), Arsenic (200:1), Germanium (25:1), Thorium (3:1), Vanadium (0.3:1), Zirconium (0.3:1). Therefore only the two last elements produce a serious interference and must be previously eliminated.

The method has been applied to certified aluminium samples with good results.

References

1.- G.F.Kirkbright, A.M.Smith, T.S.West and R.Wood, Analyst, 1969,94,754
2.- I.M.Kolthoff and E.P.Parry, J.Am.Chem.Soc.,1951,73,5315
3.- R.Pardo, E.Barrado, Y.Castrillejo and P.Sanchez Batanero, Talanta,1983,30,655
4.- Y.Castrillejo, R.Pardo, E.Barrado and P.Sanchez Batanero, Talanta,1985,32,407
5.- M.W.Routh, P.A.Swartz and M.B.Denton,Anal.Chem.,1977,49,1422

DETERMINATION OF ARSENIC AND GERMANIUM BY MEANS OF AN INDIRECT POLAROGRAPHIC METHOD

M. BARAJAS, E. del REAL, R. PARDO, Y. CASTRILLEJO, E. BARRADO and P. SANCHEZ BATANERO
Department of Analytical Chemistry. Valladolid. (Spain)

Arsenic, Germanium, Phosphorus and Silicon react with Mo(VI) to form binary heteropolyacids. The two later have been determined using this reaction and detecting the Mo(VI) bonded with them [1,2]. In this paper a similar procedure for Ge(IV) and As(V) is proposed.

The Mo(VI) is determined by measurement of the hydrogen peroxide catalytic wave in the presence of Mo(VI). The mechanism of this reaction was proposed by Kolthoff and Parry[3], and in the optimal conditions[1], $|H_2SO_4| = 0.2$ M and $|H_2O_2| = 0.02$ M, the Mo(VI) can be determined between $5.0.10^{-7}$M and $1.2.10^{-5}$M. By combining the amplification 12:1 provided by the binary heteropolyacid formation with this sensible signal, arsenic and germanium can be determined at trace level. Moreover, the presence of As(V) and Ge(IV) in the measurement medium affect neither the shape nor the height of the polarograms.

Amplification reactions

The amplification reactions occur according to

$$H_3AsO_4 + 12\ HMoO_3^+ + 15\ H_2O \quad ========== \quad AsMo_{12}O_{40}^{4-} + 15\ H_3O^+$$

$$GeO_2.H_2O + 12\ HMoO_3^+ + 17\ H_2O \quad ========== \quad GeMo_{12}O_{40}^{4-} + 16\ H_3O^+$$

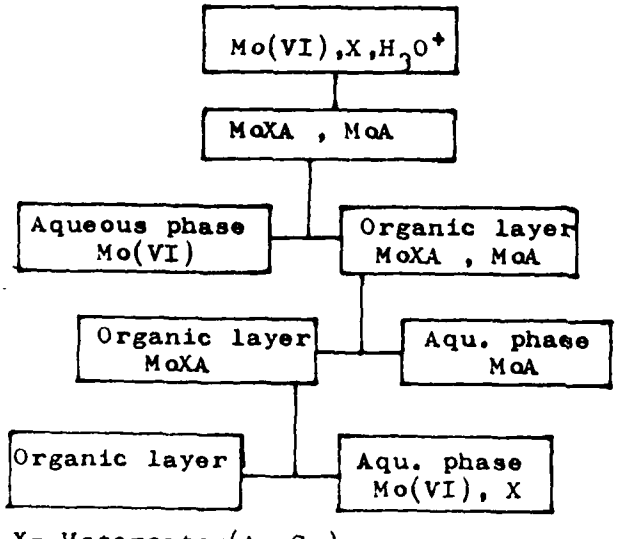

X= Heteroatom(As,Ge)

Fig. 1

The steps involved in the procedure, shown in Figure 1, are : a) formation of binary heteropolyacids (MoAsA and MoGeA), b) isolation of the Mo(VI) excess necessary for a quantitative formation, by means of extraction with an organic solvent, c) washings of the organic layer and e) stripping of the heteropolyacids to aqueous medium.

a) Formation

Figure 2 shows the yield of the heteropolyacids formation versus acid concentration. The adequate pH is obtained with 0.15 M and 0.40 M H_2SO_4 solutions,

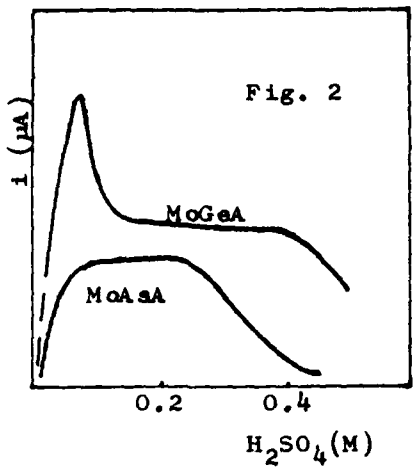

Fig. 2

respectively, for As and Ge. The solution contains also an excess of Mo(VI), necessary for a quantitative reaction. The optimun MoO_4^{2-} concentration is 2 ml of 2% ammonium paramolybdate for As and 1ml for Ge, and 15 minutes of reaction are enough.

b) Extraction

Due to Mo(VI) excess, it is necessary to carry out a selective extraction of 12-MoAsA and 12-MoGeA with an organic solvent, since the indicator reaction will detect all Mo(VI) present in the solution and not only that arising from heteropolyacids. The use of Esters, selective extractants of phosphorus, and the mixture diethylether-n-pentanol, used for silicon, were rejected. Intead, n-butanol for arsenic and methyl-isobuthylketone (MIBK) for Ge happened to be the most efficient.

c) Washing

H_2SO_4 was used to wash the organic layer. The pH range is not critical and a concentration of 0.8 M is choosen. Two 10-ml portions are enough to decrease the signal of the blanks.

c)Stipping

The heteropolyacids were stripped out to an aqueous solution with NaOH according to :

$$H_4AsMo_{12}O_{40} + 27\ OH^- \quad ========== \quad 12\ MoO_4^{2-} + AsO_4^{3-} + 15\ H_2O$$

$$H_4GeMo_{12}O_{40} + 25\ OH^- \quad ========== \quad 12\ MoO_4^{2-} + GeO(OH)_3^- + 13\ H_2O$$

The pH of these extracts was then adjusted to about 4 with sulphuric acid, which gives the correct conditions for the indicator reaction.

TABLE 1

STEP	REAGENT	As	Ge
Formation	2% $(NH_4)_2Mo_7O_{24}$	2 ml	1 ml
	5 M H_2SO_4	0.75 ml	2 ml
Extraction	n-Butanol	10 ml	-
	MIBK	-	10 ml
Washings	0.8 M H_2SO_4	10 ml	10 ml
	Operations	2	2
Stripped out	1 M NaOH	25 ml	25 ml
Detection	Initial pH	4	4
	4 M H_2SO_4	5 ml	5 ml
	0.2 M H_2O_2	10 ml	10 ml

Table 1 shows the optimal values of all variables involved in the experimental procedure. In the Table 2 we present the parameters of the calibration lines whereas Table 3 shows the interfering action produced by some elements along their maximum ratio element/determinant allowed.

TABLE 2

Parameters of calibration lines

	As	Ge
Interval (M)	$1.0.10^{-7}$-$1.2.10^{-6}$	$1.0.10^{-7}$-$1.0.10^{-6}$
Intercept (μA)	-0.09	0.23
Slope(μAmol^{-1}l)	$0.895.10^{7}$	$1.26.10^{6}$
R	0.993	0.999
Detection limits ($\mu g\ l^{-1}$)	2.5	3.92

TABLE 3

Interference of some elements

	Molar ratio, assuming a mean concentration of determinand of 5.10^{-7} M	
Element	Interf./As	Interf./Ge
P	0.15/1	1.25/1
Si	30/1	2.5/1
Ge	0.4/1	-
As	-	67/1

References :
1.-R. Pardo, E. Barrado, Y. Castrillejo and P. Sánchez Batanero, Talanta,1983,30,655
2.-E. Barrado, R. Pardo, J.A. García, Y. Castrillejo and P. Sánchez Batanero, Analusis, in press
3.- I.M. Kolthoff and E.P. Parry, J.Am.Chem.Soc.,1951,73,5315

STUDY OF THE ELECTROCHEMICAL BEHAVIOUR OF MINERAL SOLID SUBSTANCES USING A HOME-MADE CARBON PASTE ELECTRODE

M. EGUREN; M.L. TASCON; M.D. VAZQUEZ and P.SANCHEZ BATANERO
Department of Analytical Chemistry, Valladolid (Spain).

INTRODUCTION

The electrochemical behaviour of the casiterite has been studied by cyclic voltammetry. For it we have used a carbon paste electrode, whose main utility is the analysis of mineral compounds with small solubility, such as oxides of iron[1,2], manganesum[3,4] or sulfides of copper[5], iron[6], lead[7].....

From the current-voltage curves obtained, it is possible a identification of the chemical species present in the sample, as well as their oxidation states and their red-ox mechanism. In some cases, quantitative determination can be also carried out.

EXPERIMENTAL

The working electrode used in the work is a carbon paste electrode obtained by mixing powdered grphite, a electrolytic binder and the sample to be studied. The construction and performance of a such electrode is described in several papers[8,9].

In our case the amounts used were: 80 mg of U.P.C. graphite II grade, an amount of casiterite comprised between 0.5 and 12 mg, and the binder: 40 ml of 1.8 M sulphuric acid. The mixed paste is put into a J-shape glass tube, and a platinum wire ensures the electric contac.

The working electrode, as well as a refernce electrode (satured calomel electrode) and a platinum counter-electrode are immersed in a measuring cell which contains a solution whose composition is the same than the electrolyte used a binder, i.e. 1.8 M sulphuric acid.

The record the voltammetric curves we used a 551 AMEL potentiostat, in combination with an 560-A AMEL interface unit, a 556 AMEL function generator and LY 1700 LINSEIS X-Y register.

RESULTS AND DISCUSSION

A previous study was carried out to choose the optimal concentration of both the background electrolyte and binder which must have the same composition. Several acids and concentrations were tested, and the best results were obtained with 1.8 M sulphuric acid, which was used in all posterior studies. A voltage scan rate of 0.5 mV/s, was used giving voltammetric curves with a good definition.

1.- Voltammetry of the casiterite. Elucidation of the peaks.

When a 2.0 mg sample of casiterite is scanned from the potential of null-intensity (0.2 V) to 1.2 V, no anodic peaks are obtained. If the first scan is carried out from 0.20 to -0.30 V, the voltammetric curves presents two cathodic peaks (c_1 and c_1' in Figure 1). The subsequent anodic scan shows an only peak at 0.015 V (A in Figure 1). A new cathodic scan produces an only cathodic peak at -0.065 V (c_2 in the Figure 1).

The cyclic voltammetry (between +0.60 to -0.30 V) shows than the peaks A and C are related, whereas c_1 and c_1' are transformes in C. The peaks A and C can be assigned to the electrochemical reaction:

$$Sn^{+4} + 2\,e^- \rightleftharpoons Sn^{+2}$$

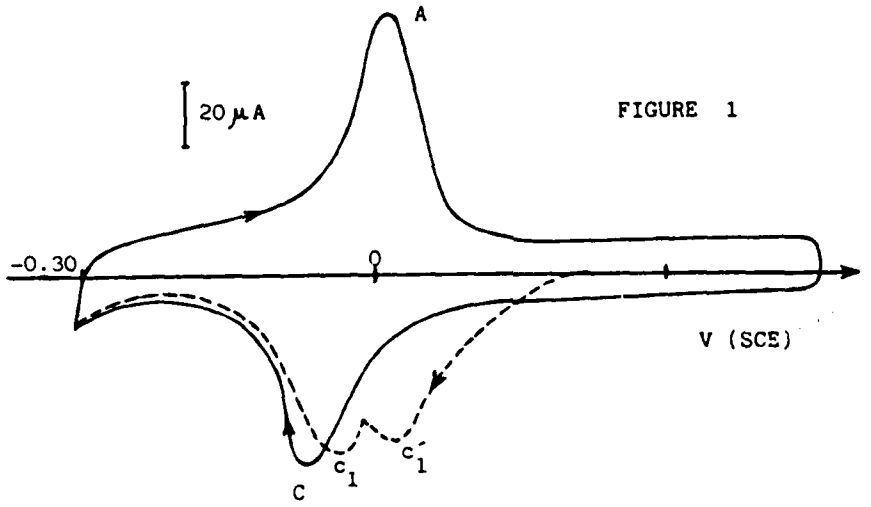

FIGURE 1

The peaks c_1 and c_1', which only appear in the first cathodic scan, can be related to the reduction of SnO_2 in its two α and β forms, according to:

$$(\alpha \text{ or } \beta)\ SnO_2 + 4\ H^+ + 2\ e^- \longrightarrow Sn^{+2} + 2\ H_2O$$

2.- Electrolysis of the casiterite

After the elucidation of the current peaks, we have carried out an attempt to determine quantitatively the SnO_2. The potential of the working electrode is fixed at a value of -0.30 V sufficient to reduce to Sn^{+4} *without any interfering effect* proceeding from the reduction of the medium. If cyclic scans are made after the electrolysis, the height of the obtained peaks increase in each sucessive scan. Notwithstanding, if the electrolysis time is higher than 45 minutes, not variation of the height peaks is found in the different scans. In these conditions there is a linear relation between the SnO_2 amount in the carbon paste and the peak area.

REFERENCES

1.- J.M. LECUIRE, Analusis 2, 489 (1973)
2.- R.D. ALLEN and N.A. HAMPSON, J.Electroanal.Chem. 99,299 (1979)
3.- F. CHUAIB, O. CAUQUIL and M. LAMACHE, Electrochim. Acta 26,325 (1981)
4.- J. Mc. BREEN, Electrochim. Acta 20, 221 (1975)
5.- M. LAMACHE, D. KENDE and D. BAUER, Nouv. J. Chem. 1, 377 (1977)
6.- C. IWAKURA, N. ISOBE and H. TAMURA, Electrochim. Acta 28, 277 (1983)
7.- M. LAMACHE, D. BAUER and J. PEGOURET, Electrochim. Acta 26,1845 (1981)
8.- M. LAMACHE and D. BAUER, Analyt. Chem. 51, 1320 (1979)
9.- M. LAMACHE, Electrochim. Acta 24, 79 (1979)

ANALYSIS OF THE OXIDATIVE SULFONATION OF AROMATIC COMPOUNDS

U.NICKEL, M. SCHNEIDER and W. JAENICKE

Institute for Physical Chemistry, Erlangen (W. Germany)

Sulphite is often used as an antioxidant in chemical processes, especially in photographic developers. Sometimes the oxidation products are only reduced by this antioxidant, sometimes, however, they are sulfonated. By this second reaction the most important developing substance in black-white photography, hydroquinone, is transformed into hydroquinonemonosulfonic acid, which reduces silver halogenid even better than hydroquinone itself. Thus superadditivity may occur, especially in presence of some other reducing agents. Reactions of this type were studied intensively some time ago in electrochemical investigations (1,2).

In colour photography the most important developing substances are N,N-dialkyl substituted p-phenylenediamines. But since their oxidation products, p-quinonediimines, are needed for the formation of the colour by coupling with an adequate organic compound, any reaction with sulphite will decrease the desired colour. Therefore in colour developing solutions sulphite cannot be present in great concentration, and it is necessary to know exactly its reaction with p-quinonediimine in concurrence to the colour forming coupling reactions. Some of the possible reactions are collected in scheme 1.

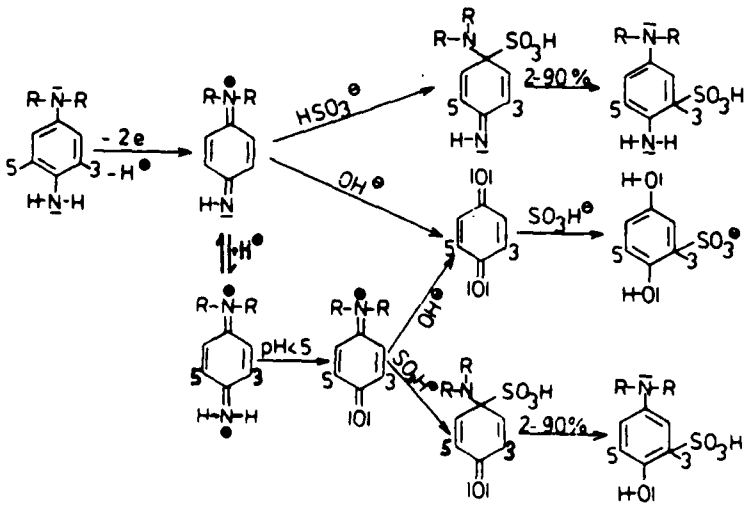

scheme 1

Homogeneous investigations in a stopped flow apparatus indicated that sulfonation cannot occur, if the positions 3 and (or) 5 are occupied by alkyl groups. In this case the chinoidic intermediate with the NR_2 -and SO_3H -group in position 1, which exhibit characteristic absorption at 270 and 420 nm, will be remarkably stable at pH < 7, whereas at higher pH deamination to the respective quinone takes place. Acid deamination, which is possible in the stop bath of the photographic development, yields N-substituted p-quinone-monoimines (3). In weak acid solution these compounds also form stable quinoidic intermediates with sulphite. At higher pH, however, they are deaminated to the respective quinones as well. Most of these reactions can easily be observed in a stopped flow apparatus using optical detection. Some reactions, however, can be better observed with electrochemical methods, because the use of homogeneous oxidants sometimes causes a lot of difficulties. Some of the results obtained by cyclic voltammograms at a stationary gold electrode (0.12 cm^2) are given in figs. 1 - 4.

Fig. 1 shows that the addition of sulphite to aqueous N.N-diethyl-p-phenylenediamine shifts the cv-wave and increases the current. This is due to an adsorption of sulphite and to a catalytic current as observed during the oxidative sulfonation of hydroquinone (2). Even rather small amounts of sulphite prevent a cathodic current. This result is in agreement with those obtained by homogeneous oxidative sulfonation yielding sulphonated p-phenylenediamines in a rather fast consecutive reaction.

Fig. 2 shows that nearly the same results as in fig 1 are obtained with N.N-diethyl-3,5-dimethyl-p-aminophenol. Homogeneous measurements, however, indicate that there occurs no sulfonation but only the formation of the quinoidic intermediate (see scheme 1), because the positions 3 and 5 are occupied by methyl-groups. Therefore this intermediate seems to be electrochemically inactive.

Fig. 3 shows that the quinoidic intermediate is electrochemically inactive indeed, because after the addition of sulphite to homogeneously oxidized N.N-diethyl-3,5-dimethyl-p-phenylenediamine or the respective quinonemonoimine no cyclic voltammogram can be obtained. After addition of OH^-, however, an electrochemically active compound is formed by deamination. It should be 3,5-dimethyl-p-quinone (4).

This can be proved by the cyclic voltammogram of 3,5-dimethylquinone, which was prepared in homogeneous solution by oxidative deamination. As demonstrated in fig. 4 it is very similar to that obtained in fig. 3 after deamination of the sulfonated intermediate. Addition of excess sulphite, however, again produces an electrochemically inactive substance. Therefore it is not sure that substituted quinones are sulfonated as indicated. Perhaps quinoidic compounds are formed similar to those in scheme 1.

Thus by combination of optical and electrochemical methods the mechanism and the kinetics of the oxidative sulphonation of substituted p-phenylenediamines, p-aminophenols and similar compounds can be determined rather accurately.

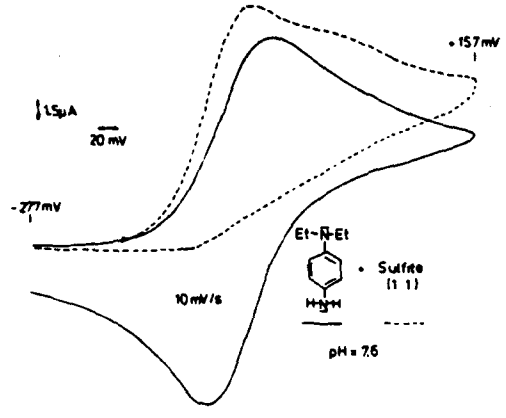

fig.1

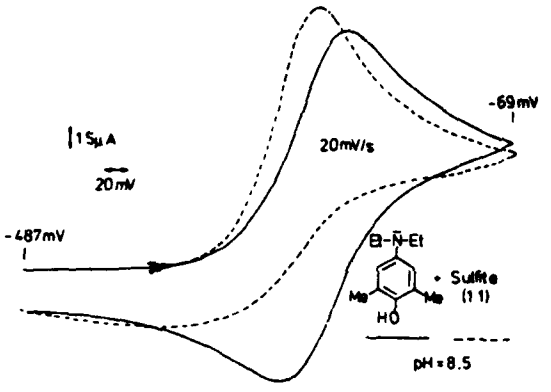

fig. 2

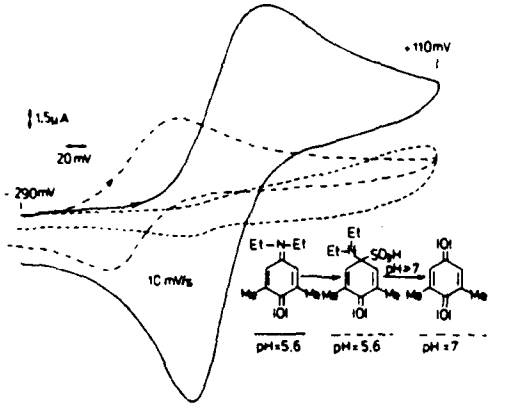

fig. 3

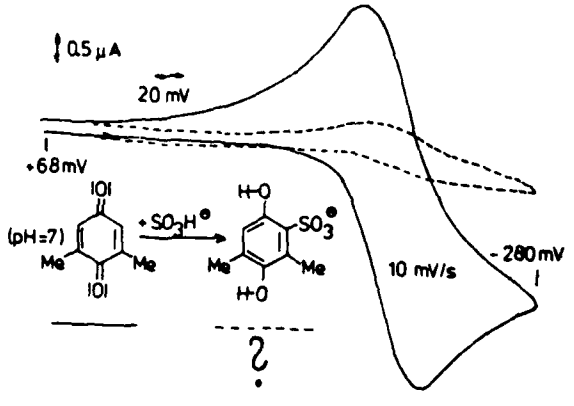

fig. 4

1) W. Jaenicke and H. Kobayashi, 31 st ISE-Meeting Venice 1980, 159-161
2) W. Jaenicke and H. Kobayashi, J. Phot. Sci. 31, 69-74 (1983)
3) U. Nickel, K. Kemnitz and W. Jaenicke, J.Chem.Soc.Perkin II 1978, 1188-1193
4) U. Nickel and W. Jaenicke, J.Chem.Soc.Perkin II 1980, 1601-1605

DETERMINATION OF PHOSPHOLIPIDS IN DRUGS AND BIOLOGICAL LIQUIDS

L. Campanella*, M. Mascini**, G. Palleschi**, M. Tomassetti*.

(*) (Dipartimento di Chimica, Università di Roma "La Sapienza")
(**)(Dipartimento di Scienze e Tecnol.Chim.,II Univ. di Roma)

Phosphatydilcholine is one of the most important constituting compounds of many commercial drugs commonly employed in the biliar and hepathic affections such as hepatitis, cirrhosis, gallstones, in the dislipidemies, hypercholesterolemies, arteriosclerosis and for the therapy of the brain metabolism disfunctions. Lecithin is occasionally contained, even if at low concentration levels, in syrups and other pharmaceutical formulations, where it plays different roles; lastly it is also part of many dietetic products since long time very diffuse in the commerce. It is well know also that phosphatydilcholine is contained in some fluids and tissues of animals and vegetables (bile, serum, some seeds, encephalic tissue). The quantitative determination of lecithin in drugs and in the above mentioned matrixes is often requested for different reasons: quality control from the manufactures or from public offices ad hoc appointed, determination of merceological, bioclinical or forensic interest. The determination of lecithin can be performed by different chromatographic methods, during last years especially by HPLC; all these methods nevertheless require long time, pretreatment of the sample and complicated apparatus. For all these reasons simple and rapid methods are looked for and, when individuated, they are experimented for many of the described analytical problems.

Lately we developed a simple method of determination of lecithin that employs an enzymatic supersensor and the enzyme phospholypase D in homogeneous phase. The supersensor was obtained by immobilizing the cholineoxydase on a nylon net and by fixing this one on a Clark electrode indicating oxygen concentration. Lecithin is hydrolized by phospholipase to choline and phosphatydic acid. By this method we determined lecithin both in some human biliar samples and in some control sera and in some commercial drugs produced in different confections: phials, caps, grams. The analysis was performed with a flow system by which a good reproducibility (SD%=1.5% in choline standard solutions and = 1.1% in lecithin standard solutions) and a linearity concentration range (2.5×10^{-5} + 2.0×10^{-4}) mol/l were obtained. In the Fig. the response of the enzyme sensor at increasing choline concentration is reported.

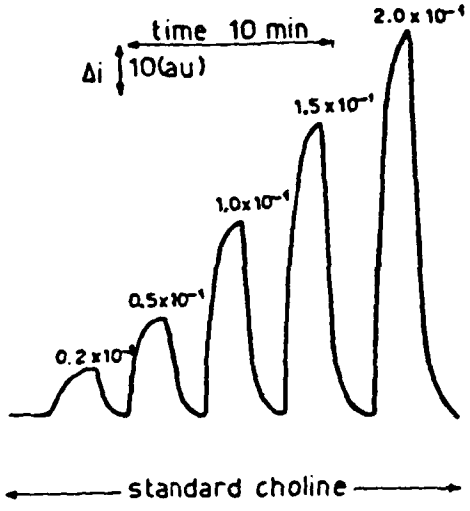

A comparison between nominal and experimental value of lecithin levels was performed; the comparison was extended to the values obtained on the same drugs by an enzymatic spectrophotometric method. The values obtained by the new method we developed resulted generally in a good agreement with the nominal ones. More differently from the spectrophotometric methods our method is free from any chromatic or turbid interference following the alcoholic extraction of the examined drugs.

REFERENCES

1) L. Campanella, M. Mascini, G. Palleschi, M. Tomassetti: "The CAN-AM. Chemical Congress" (Montreal) 3-6-1984.

2) L. Campanella, M. Mascini, G. Palleschi, M. Tomassetti: "XV Congr. Naz. Soc. Chim. Ital". (Grado) 16-9-1984.

3) L. Campanella, M. Mascini, G. Palleschi, M. Tomassetti: Clin. Chim. Acta (submitted).

APPLICATION OF A FIA SYSTEM WITH AMPEROMETRIC DETECTION TO THE DETERMINATION OF FOLMALDEHYDE.

Lucas Hernandez, Jose-Maria Pinilla and Jesús R. Procopio.

Department of Analytical Chemistry, Autonoma University of Madrid, 28049 Madrid, Spain.

A flow injection analysis system with amperometric detection was performed for determination of formaldehyde in aqueous solutions (Fig. 1). The detector was a wall-jet tipe cell equiped with a gold disk electrode. The influence of flow rate, coil length and internal diameter and injection volume on the sensitivity was established, being their optima values for determination 3.75 ml/min, 55 cm, 0.5 mm and 100 ul, respectively. The carrier was a 0.1 M NaOH solution. The electrode potential was 0.0 V. vs. S.C.E.. The working range of concentrations was 0.06-1 mM HCHO and the limit of determination 0.016 mM. The FIA-gramm obtained for various stock solutions of formaldehyde is showed in Fig. 2. The maximun sampling frecuency was about 110 samples per hour. No deaeration of samples and carrier was necesary, because in the working electrode potential the reduction of solved oxigen is neglectable.

AD-A162 434 EXTENDED ABSTRACTS INTERNATIONAL SOCIETY OF ELECTROCHEMISTRY (36TH) HELD AT SALAMANCA SPAIN ON 23-28 SEPTEMBER 1985(U) INTERNATIONAL SOCIETY OF ELECTROCHEMISTRY 28 SEP 85 10/12

UNCLASSIFIED F/G 7/4 NL

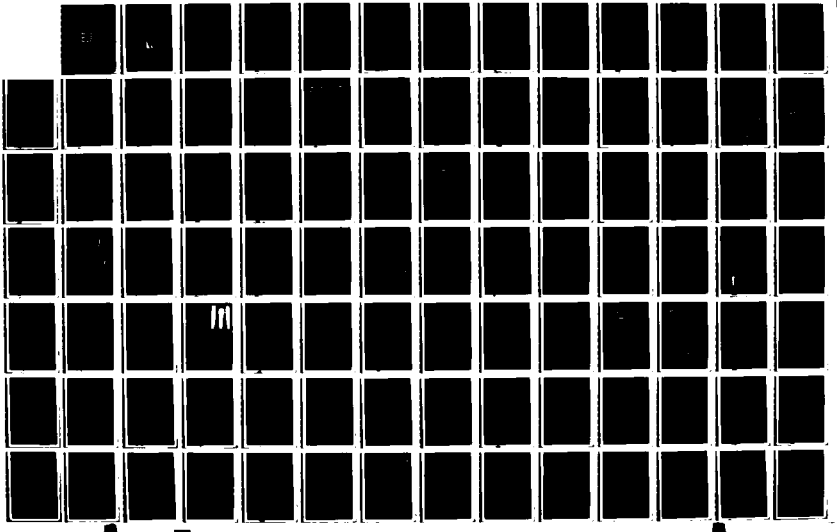

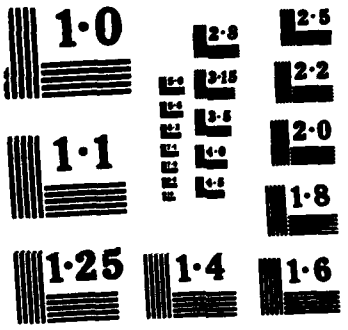

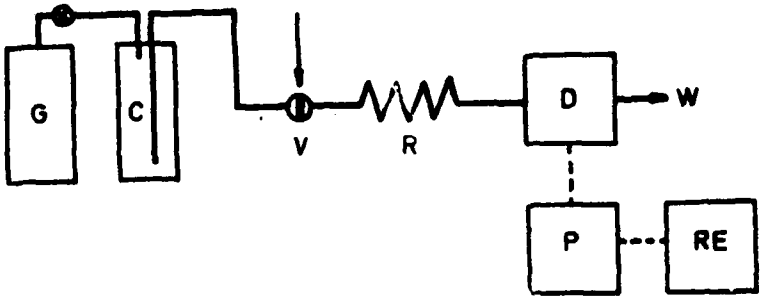

Fig 1. Flow Injection System: G, gas pressure; C, carrier solution; V, valve with an external loop; R, reactor; D, Amperometric detector; P, polarograph; RE, register.

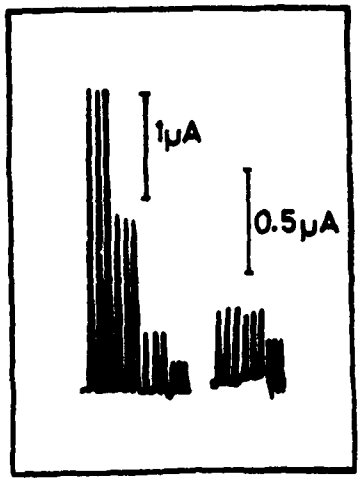

Fig 2. Calibration runs for formaldehyde standards. 1.32, 0.794, 0.265 and 0.132 mM and 0.132, 0.079 and 0.027 mM.

10200

ANODIC STRIPPING VOLTAMMETRY ANALYSIS OF CLOZAPINE ON A GLASSY CARBON ELECTRODE.

Elisa González Romero and Lucas Hernández Hernández.

Dpto. Química Analítica. Universidad Autónoma de Madrid.

INTRODUCTION.

In this work, we have studied the determination of an antidepressive drug: 8-chloro-11(4-methyl-1-piperazinyl)-5H-dibenzo-b,e-1,4-diazepin (CLOZAPINE).

Kauffmann and Patriarche [1,2] have studied the electrochemical behaviour of clozapine by means dc, ac, dp and cyclic voltammetry at the glassy carbon electrode (G.C.E.). They suggest the existence of an adsorption phenomenon on the electrode surface, which could be used to the analysis of clozapine by anodic stripping voltammetry on G.C.E.

RESULTS.

It was necessary, in order to obtein reproducible results, to clean the glassy carbon electrode surface before each measurement. The electrode was pulished mechanically with alumina prior to each set of experiments, follow by cycling the electrode repeatedly between -0.1V and +0.9V vs S.C.E. and applying +1.5V vs S.C.E. until the current reached a steady level prior to each anodic stripping trials.

From an analytical point of view, the linear dependence of the peak heights on the concentration of the clozapine analyzed is most important. Calibration graphs showed linearility in the concentration ranges 10^{-5} - 2.10^{-6} M. and 8.10^{-7} - 10^{-7} M. clozapine at stationary electrode.

Another important factors are the deposition time and the deposition potential.These influences are illustrated in Figure 1 and 2, respectively.

Other important factors connected with the deposition process are the value of pH,nature and concentration of the supporting electrolyte.The experimental results have shown that optimum medium were phosphate buffer solution 0.1 M. at pH 3.2.The constante stirring necessary for the deposition step was attained by means of magnetic stirrer and held at 500 r.p.m.

The heiht of the peaks is more affected by variation of the scan rate.It has been observed that the amount of material deposited increases linearly with increasing scan rates [3,4].Scan rate of 20 mVs^{-1} was employed for this analytical work.

The accuracy and precision of the method was checked on five series of clozapine sample.The relative error in determining 0.03 - 0.3 p.p.m. of clozapine does not exceed 3% and the relative standard deviation was 1%.The detection limit can be estimated at 8.2 10^{-9} M.,corresponding to 2.7 µg/l of clozapine when a phosphate buffer solution at pH 3.2 is used.

REFERENCES.

1- J.M. Kauffmann, G.J. Patriarche and G.D. Christian. ANAL. LETT, 12(B11), 1217 (1979).

2- J.M. Kauffmann, G.J. Patriarche and M. Genies. ELECTROCHIM. ACTA, 27(6), 721 (1982).

3- T.M. Florence. J. ELECTROANAL. CHEM. 27, 273 (1970).

4- M. Kopanica and F.J. Vydra. ELECTROANAL. CHEM. 24, 379 (1970).

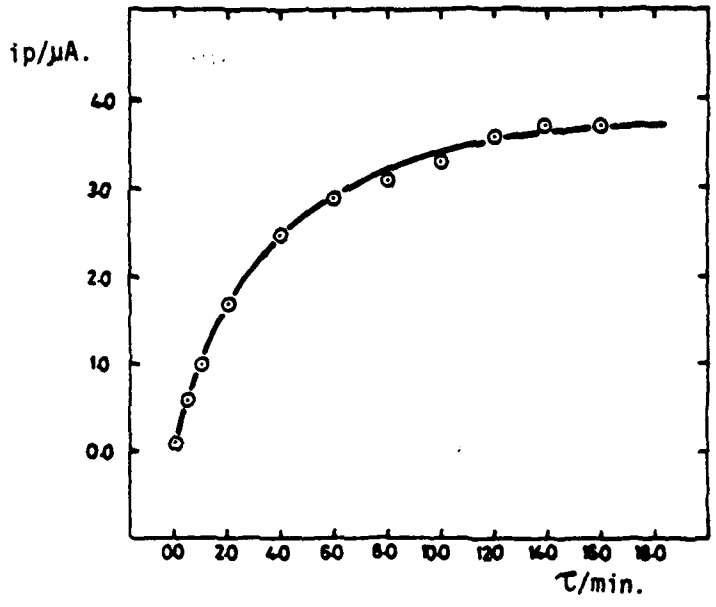

Fig. 1: Relationship beween clozapine peak currents as a function of deposition time.

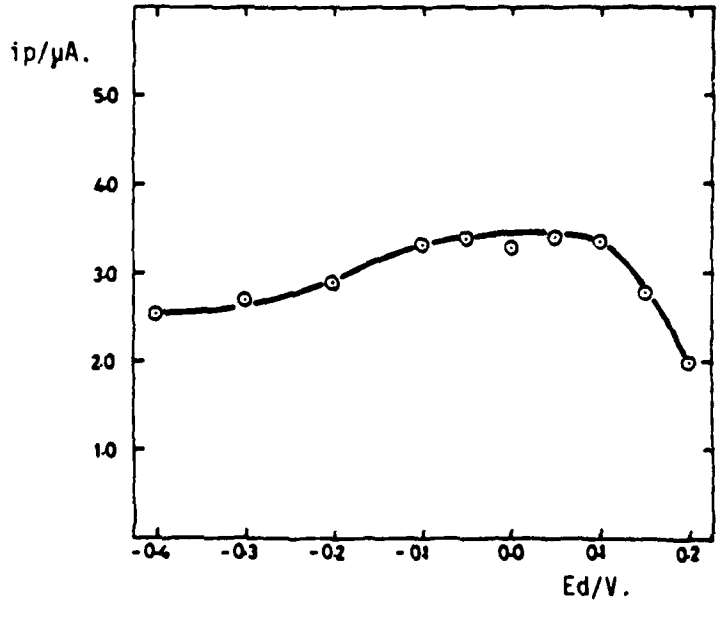

Fig. 2: Relationship between clozapine peak currents as a function of deposition potential.

POLAROGRAPHIC REDUCTION OF NAPHTHOL YELLOW S

L.I. DE LA CRUZ YAGUEZ, J.M. PINGARRON CARRAZON and L.M. POLO DIEZ.
Department of Analytical Chemistry, Faculty of Chemistry, Complutense University of Madrid, 28040 Madrid, Spain.

INTRODUCTION

Naphthol Yellow S (disodium salt of 8-hydroxy-5,7-dinitro-2-naphtalensulfonic acid) is a water soluble nitro-dye, widely used in cosmetics and pharmaceutical products[1], with the following structure:

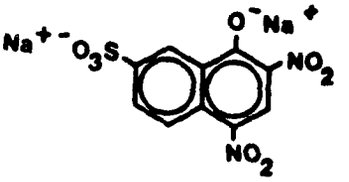

The aim of this work is to study the polarographic and voltammetric behaviour of Naphthol Yellow S in order to establish its electrochemical characteristics and to develop analytical methods for its determination in different samples.

METHODOLOGY

The electrochemical study of Naphthol Yellow S was carried out in a Britton-Robinson buffer, each acid having a concentration of 0.1M, at three different pH values: 3.5, 7 and 9. The following polarographic techniques were used: normal direct current polarography (dc), tast polarography, differential pulse polarography (dpp) and first harmonic alternating current polarography (ac_1). All potential values were measured with respect to the Ag/AgCl electrode.

RESULTS AND DISCUSSION

Naphthol Yellow S shows a dc polarographic reduction wave at pH values lower than 6; between pH 6 and pH 10 two cathodic waves appear, whose separation depends strongly on pH. The plot of half-wave potential as a function of pH is shown in Figure 1. As can be seen, the half-wave potential shifts towards more negative values when pH increases, indicating that protons are involved in the dye reduction process.

In the pH 6-10 range, in which two polarographic waves appear, the difference between $E_{1/2}$ values of both waves becomes greater with increasing pH.

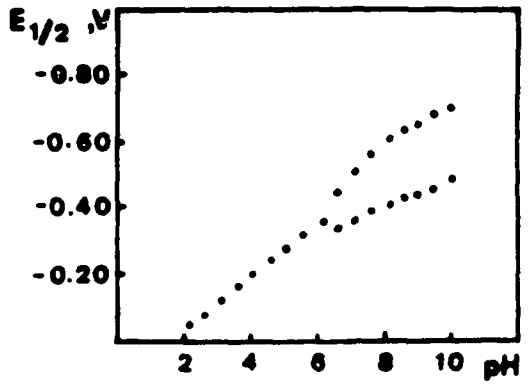

Figure 1.- pH influence on $E_{1/2}$ in normal dc polarography. Naphthol Yellow S 1.0×10^{-4}M.

On the other hand, limiting current remains practically constant up to pH 6 (Figure 2). The heights of the two waves which appear at pH higher than 6 are quite similar, being approximately half that obtained at pH lower than 6.

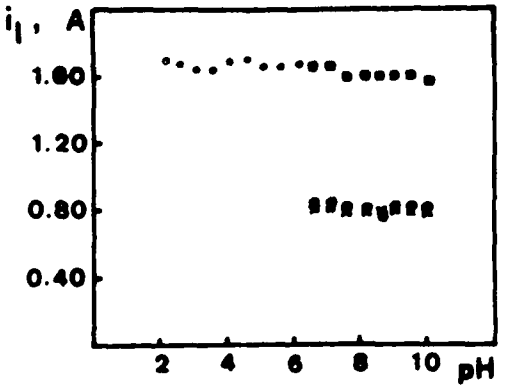

Figure 2.- pH influence on i_1 in normal dc polarography. Naphthol Yellow S 1.0×10^{-4}M. •,only one wave; o, first wave; x, second wave; ▫ addition of first and second wave.

From the results obtained in this study, working pH conditions of 3.5, 7 and 9 were chosen for further studies.

In order to determine the characteristics of the electrodic process the following studies were carried out:
-Effect on limiting current of the height of mercury reservoir, temperature and electroactive species concentration[2].
-Qualitative examination of the i-t curves at different potentials[2].

From the results obtained, it can be concluded that

the Naphthol Yellow S reduction process is diffusion-controlled in the three studied media.

Reversibility of the polarographic process was studied by applying the following criteria:

-Logarithmic analysis of the polarograms obtained by normal dc, tast[2] and ac_1[3] polarography.

- Analysis of $E_{3/4}-E_{1/4}$[2].
- Effect of the pulse amplitude on peak potential (E_p), peak current (i_p) and half-peak width ($w_{1/2}$) in dpp[4].
- Comparison of $E_{1/2}$ in dc and E_p in ac_1[3].
- Analysis of $w_{1/2}$ in ac_1[3].
- Relationship between I_p and the height of the mercury reservoir in ac_1[3].
- Analysis of the relation between dropping time and E_p in ac_1[3].

The results obtained by applying these criteria and techniques showed the irreversibility of the Naphthol Yellow S reduction process in the three studied media.

The number of electrons involved in the reduction process was estimated from the Ilkovic equation, assuming a diffusion coefficient value within the range given in the literature for this kind of compounds. A 12 electron exchange seems to occur, which will be further confirmed by controlled-potential coulometry in future work.

Standar criteria were applied to determine kinetic parameters of the polarographic reduction process[2]. The values obtained for the electron transfer coefficient α and for the rate constant $k^o_{f,h}$ confirm the irreversibility of the reduction wave(s) in the three studied media.

Calibration graphs showed proportionality between dye concentration and diffusion current, for the different polarographic techniques used. The linear ranges in normal dc and tast polarography are between 1.0×10^{-4} and 1.0×10^{-5}M, while the quantitative determination of Naphthol Yellow S by dp polarography should be carried out in the 1.0×10^{-4} - 3.0×10^{-7} M concentration range.

REFERENCES

1.- D.M. MARMION, Handbook of U.S. Colorants for Foods, Drugs, and Cosmetics, John Willey and Sons., N.Y., 1979.

2.- L. MEITES, Polarographic Techniques, 2nd edn, Interscience Publishers, John Willey and Sons, N.Y., 1967.

3.- A.M. BOND, Modern Polarographic Methods in Analytical Chemistry, Elsevier Ed., London, 1980.

4.- A.J. BARD and L.R. FAULKNER, Electrochemical Methods, John Willey and Sons, Inc., N.Y., 1980.

APPLICATION OF SEVERAL REVERSIBILITY CRITERIA TO THE POLAROGRAPHIC REDUCTION OF METHYLENE BLUE IN A BRITTON-ROBINSON BUFFER.

G.TOMAINO BELTRAMI, J.M.PINGARRON CARRAZON and L.M.POLO DIEZ
Department of Analytical Chemistry, Faculty of Chemistry, Complutense University of Madrid, 28040 Madrid, Spain.

In general, electrochemical reactions may be classified, according to their rate, in two groups: reversible and irreversible reactions. A large variety of criteria to determine the reversibility of these reactions using different polarographic techniques are available[2,3].

In this work we evaluate the reversibility of the methylene blue (MB) polarographic reduction by applying several criteria using different polarographic techniques:

1.- Logarithmic analysis of the polarograms obtained by normal dc polarography[1].

The behaviour of the electrode potential as a function of the current for a reversible cathodic wave at 25°C is described by the following equation:

$$E = E_{1/2} - \frac{0.059}{n} \log (i/i_d - i)$$

consequently, the E versus log $(i/i_d - i)$ plot for a diffusion

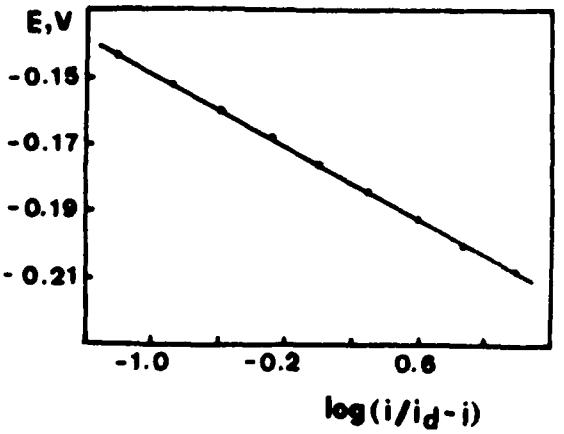

Figure 1.- Normal dc polarography: logarithmic plot of methylene blue. MB 5.0×10^{-4} M, Britton-Robinson buffer 0.1M in each acid; pH 6.55; E vs. Ag/AgCl.

-controlled reversible process at 25°C will produce a straight line whose slope is -0.059/n V.

The polarogram obtained from a MB solution at pH 6.55 gives rise to the logarithmic plot shown in Figure 1.

In this case, a linear plot is obtained, whose slope is -0.0268 V. Taking into account that there are two electrons involved in the electrodic reduction of methylene blue, determined by controlled-potential microcoulometry (theoretical slope -0.0295 V), it may be deduced that the electrodic process involved is reversible in this technique.

2.- Logarithmic analysis of the polarograms obtained by alternating current polarography, first harmonic $(ac_1)^2$.

The equation which describes the relation between peak potential and peak current for a reversible process, in alternating current polarography, is given as follows:

$$E_{dc} = E^r_{1/2} \pm 2\left(\frac{2.303\ RT}{nF}\right) \log \left[\left(\frac{I_p}{I}\right)^{1/2} \pm \left(\frac{I_p - I}{I}\right)^{1/2}\right]$$

therefore, the E_{dc} versus $\log \left[(I_p/I)^{1/2} \pm (I_p - I/I)^{1/2}\right]$ plot for a reversible process will give a straight line of slope 2(2.303 RT/nF).

The polarogram obtained from a MB solution at pH 6.50 gives rise to the logarithmic plot shown in Figure 2.

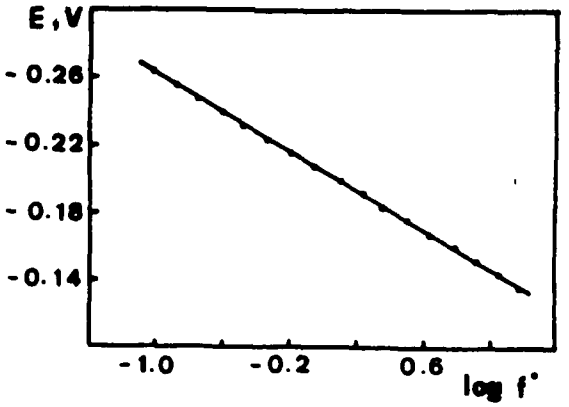

Figure 2.- ac_1 polarography: logarithmic plot of methylene blue. MB 1.31×10^{-4}M, Britton-Robinson buffer 0.1 M in each acid; pH 6.50; E vs. Ag/AgCl. $f^\circ = \left[(I_p/I)^{1/2} \pm (I_p - I/I)^{1/2}\right]$.

As can be deduced from this graph, a straight line is obtained, whose slope is -0.0573 V. This value agrees well with the theoretical value (-0.0591 V) for a reversible process when n = 2. Thus, using this technique, similar conclusions may be drawn regarding the reversibility of the electrodic process, to those obtained from the first criterium

applied.

3.- Effect of pulse amplitude on peak current (i_p), in differential pulse polarography (dpp)[2].

The equation defining the peak current behaviour in differential pulse polarography is the following:

$$i_p = (\Delta i)_{max} = nFAC(D/\pi t_m)^{1/2} (\sigma - 1/\sigma + 1)$$

where $\sigma = \exp(\frac{nF}{RT} \frac{\Delta E}{2})$, ΔE being the pulse amplitude. Therefore the i_p vs. $(\sigma^2 - 1/\sigma + 1)$ plot will yield a straight line for a reversible reduction process at 25°C.

The results obtained for methylene blue at pH 6.50 are shown in Table I.

Table I.- Pulse amplitude influence on the i_p values. MB 2.5 x 10^{-4}M; Britton-Robinson buffer 0.1 M, pH 6.50

/ΔE/,mV	σ	$(\sigma - 1/\sigma + 1)$	$i_p \pm 0.004\ \mu A$
5	0.8231	0.0970	0.080
10	0.6776	0.1922	0.158
20	0.4591	0.3707	0.300
30	0.3111	0.5255	0.418
40	0.2108	0.6518	0.520
50	0.1428	0.7501	0.616

After adjusting the values by the least square method, values of 0.0004 μA for the ordinate at the origin; 0.808 μA^{-1} for the slope and 0.9995 for the regression coefficient were obtained. These results confirm the reversibility of the methylene blue reduction process.

Similarly, the following reversibility criteria were applied:

4.- Analysis of $E_{3/4} - E_{1/4}$[1].

5.- Effect of pulse amplitude on peak potential (E_p) and half-peak width ($w_{1/2}$) in dpp[2].

6.- Comparison of $E_{1/2}$ in dc and E_p in ac[2].

7.- Analysis of $w_{1/2}$ in ac[2].

8.- Relationship between I_p and the height of the mercury reservoir in ac[2].

9.- Analysis of the relation between dropping time and E_p in ac[2].

The results obtaineo confirm the reversibility of the electrodic process involved.

REFERENCES

1.- L. MEITES, Polarographic Techniques, 2nd edn, Interscience Publishers, John Willey and Sons, N.Y., 1967.

2.- A.M. BOND, Modern Polarographic Techniques in Analytical Chemistry, Elsevier Ed., London, 1980.

3.- A.J. BARD and L.R. FAULKNER, Electrochemical Methods, John Willey and Sons, Inc., N.Y., 1980.

AMPEROMETRIC DETERMINATION OF ETHANOL IN BLOOD BY FLOW INJECTION ANALYSIS

M. VALCÁRCEL, M.D. LUQUE DE CASTRO and A. FERNÁNDEZ
Department of Analytical Chemistry, Faculty of Sciences,
University of Córdoba, Spain

Despite the large variety of methods for the quantitative determination of ethanol in blood described so far, it is necessary to note that these are based on slow methodologies, are not very precise or require expensive instrumentation. In this paper we aim to demonstrate the suitability of Flow Injection Analysis FIA, for the determination of alcoholemia in blood as well as the viability of its amperometric detection by a simple and inexpensive method excelling all techniques previously described.

The proposed method is based on the oxidation of ethanol to acetaldehyde through the action of alcohol dehydrogenase (ADH) in the presence of the coenzyme NAD^+:

$$CH_3CH_2OH + NAD^+ \xrightarrow{ADH} CH_3CHO + NADH + H^+$$

The amperometrically controlled species is the reduced form of the coenzyme, which can also be monitored photometrically or fluorimetrically. The presence of a trapping agent for acetaldehyde formed (thiosemicarbazide, hydrazine, etc.), which favours the completion of the reaction cannot be used with the electrochemical control, because the reducing character of these species interferes in the determination.

The FIA configuration used is shown in Fig. 1. It consists of a peristaltic pump (P), a low-pressure injection valve (IV), a reactor (R) (length 150 cm and diameter 0.5 mm) and a 5 µL flow-through electrochemical microcell (MC) whose auxiliary and working electrodes are glassy carbon, while the reference electrode is an Ag/AgCl one, using a voltammetric detector (D).

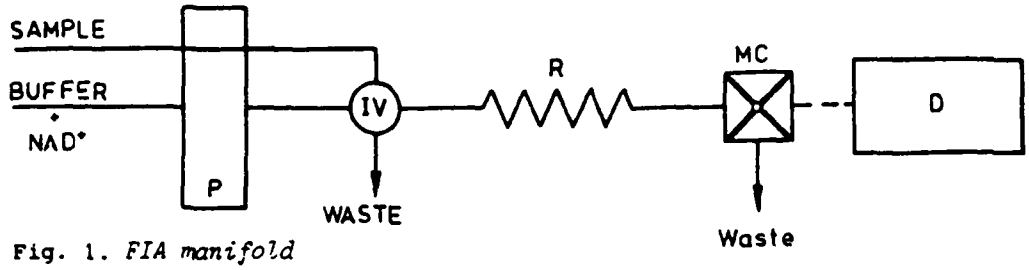

Fig. 1. *FIA manifold*

A systematic study has been performed to optimize the different variables influencing the determination in order to obtain the maximum sensitivity and precision. In Table I are shown the optimum values found.

Table I. OPTIMIZATION OF VARIABLES

	VARIABLES		OPTIMUM VALUE
CHEMICAL	concentration of	ADH	40 $U.mL^{-1}$
		NAD^+	0.8 $mg.mL^{-1}$
	pH		9.0
FIA	reactor length		150 cm
	injected volume		172 µL
	flow rate		1.25 $mL.min^{-1}$
Temperature			37° C

It has been shown that the prior mixing of the enzyme solution with the sample results in higher sensitivity and, in addition, spares enzyme.

The blood sample needs no pretreatment. A 1:100 dilution with pyrophosphate buffer pH 9 is enough. The continuous flow system allows a permanent wash of the electrode surfaces; moreover, the residence time of the sample plug inside the cell is very short.

Samples for running the calibration curve are prepared by placing 50 µL of whole blood (from normal adults), 2 mL of 100 $U.mL^{-1}$ enzyme solution and variable volumes of an aqueous solution of 2500 ppm of ethanol in a 5-mL volumetric flask made up to volume with pyrophosphate buffer of pH 9. A linear range is obtained between 5 - 300 $mg.L^{-1}$ of ethanol (regression coefficient 0.995). The statistical study of the reproducibility performed on

samples with 10 $mg.L^{-1}$ of ethanol yields a relative standard deviation of ±0.90%. The sampling frequency is 50 h^{-1}.

The suggested method has the following features:

a) Unnecessary sample pretreatment.

b) Small sample volume.

c) Determination range suitable for controlling alcoholemia according to the legislation.

d) Good reproducibility.

e) Rapidity, simplicity and low cost.

POLAROGRAPHIC DETERMINATION OF PARATHION AND PARAOXON. INDUCTION OF PARATHION HYDROLYSIS BY Pd(II)

J.HERNANDEZ MENDEZ, R.CARABIAS MARTINEZ
and J.SANCHEZ MARTIN
Department of Analytical Chemistry. Faculty of Chemistry. University of Salamanca. Spain.

The difficulty involved in the simultaneous determination of parathion and its metabolite, paraoxon, lies in the fact that they both have the same electroactive group and that the rest of their molecule does not differ significantly in size or polarity.

This communication reports on a polarographic method (DPP) for the simultaneous determination of parathion and paraoxon based on their different hydrolysis rates in the presence of Pd(II). This cation shows a selective affinity for the thiophosphate group[1,2], inducing the hydrolysis of parathion but not of paraoxon.

Other metallic ions of known catalytic activity in the hydrolysis of organophosphorous pesticides [3,4] were assayed, though the best results were obtained with Pd(II).

RESULTS AND DISCUSSION

Reaction of parathion and paraoxon with Pd(II), Cu(II) and Hg(II)

In 50% (v/v)MeOH/H_2O, 0.1 M HAc/0.1 M NaAc medium parathion shows a well-defined reduction peak at -0.376 V (v.s. S.C.E.). The addition of Pd(II) to the solution causes a progressive decrease with time in the parathion peak and the appearance of three new peaks at -0.480, -0.590 and -1.340 V. After 20 min, the parathion peak can not be observed and those obtained at -0.590 and -1.340 acquire a constant value. However, the peak corresponding to -0.480 V increases progressively with time. It was proved that the -0.590 and -1.340 V peaks are due to the reduction of p-nitrophenol and that of -0.480 V to the reduction of a Pd(II)-O0'diethylthiophosphate complex.

If the Pd(II) concentration is greater than that of parathion, a precipitate of metallic Pd appears with time, due to the reduction of the free metallic ion by the methanol of the medium. In Pd(II)-complexing media, such as 0.1 M HCl and 0.1 M HAc/NaAc/EDTA, the precipitate is not formed, but in these conditions the parathion is not hydrolyzed. In 30% (v/v)MeOH/H_2O medium and Britton-Robinson buffer the solutions of Pd(II) are stable and cause the hydrolysis of parathion. In the same medium, paraoxon is reduced at -0.370 V and the presence of Pd(II) does not induce its hydrolysis,at least before 72 h.

Similar studies were carried out with Cu(II) and Hg(II). With the former, parathion is not hydrolyzed, at least over the first three hours. With Hg(II) hydrolysis does take place; though slower than in the presence of Pd(II).

Hydrolysis reaction of parathion in the presence of Pd(II)

According to the studies carried out, the polarographic determination of parathion in the presence of paraoxon is possible by inducing the hydrolysis of the former with Pd(II) and measuring the p-nitrophenol formed.

The hydrolysis reaction of parathion becomes slower as pH increases, suggesting that it is advantageous to work in acid media. However, the difference between the peak potentials of paraoxon and p-nitrophenol is greater for pH > 8. On the other hand, the difference between the peak potentials of paraoxon and the Pd(II)-O,O'diethylthiophosphate increase at pH lower than 8.

The reaction presents an induction period dependent on pH, temperature and the Pd(II) concentration, and is not autocatalytic. The induction period is apparently caused by the formation of an unstable complex of Pd(II) with the pesticide.

Determination of parathion and paraoxon

The following procedure is proposed for the simultaneous determination of parathion and paraoxon:

Palladium (10^{-4}M) is added to a solution containing both pesticides in 30% (v/v) MeOH/H_2O medium, 0.12 M Britton-Robinson buffer, pH=8. After 120 min, the paraoxon is determined by measurement of its own peak (E_p=-0.540 V) and parathion by the peak of the p-nitrophenol formed. An alternative method for carrying out the indirect measurements of parathion with better precision consists in alkalinizing the solution to pH 9.25, after hydrolysis has taken place; under such conditions the p-nitrophenol peak obtained is better defined (Figure 1).

Simultaneous determinations of the both pesticides are possible with acceptable accuracy, if the ratios of their concentrations are lower than 40. For higher ratios the method is only recommendable for the determination of the pesticide at higher concentration.

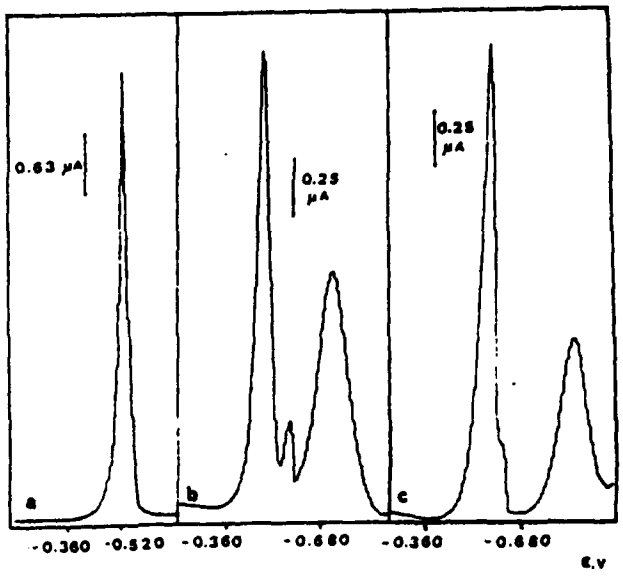

Figure 1

Polarograms (DPP) of parathion and paraoxon

a) parathion $1.14.10^{-4}$M; paraoxon $1.16.10^{-4}$ M; pH 8.0
b) solution a + Pd(II) $1.0.10^{-4}$M (after 120 min)
c) solution b at pH 9.25

REFERENCES

1. O.Antoine, G.Mees, J.Chromatog.,58(1971)247.
2. T.F. Bidleman, R.W.Frei, Talanta,20(1973)103.
3. M.Sanchez Camazano, M.J.Sánchez Martín, Soil.Sci.,136 (1983)89.
4. K.B.Agustinsson, G.Heimbürger, Acta Chem.Scand.,9(1955) 383.

DETERMINATION OF CLOBAZAM AND NORCLOBAZAM BY DIFFERENTIAL PULSE POLAROGRAPHY

J.HERNANDEZ MENDEZ, C.GONZALEZ PEREZ, M.I.GONZALEZ MARTIN and M.J.ARIAS RODRIGUEZ
Department of Analytical Chemistry. Faculty of Chemistry. University of Salamanca. Spain

Clobazam is a psychotropic drug which belongs to the 1,5-benzodiazepine group; norclobazam is its major metabolite. Several methods have been proposed for its determination[1], most of them

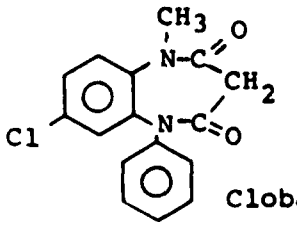

Clobazam

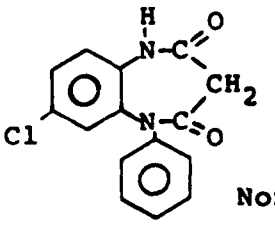

Nor-clobazam

are carried out by chromatography, fluorometry and RIA. The present work describes the polarographic (D.P.P.) behaviour of clobazam and nor-clobazam. The characterization of the electrode processes includes an examination of the degree of reversibility, electrocapillary curves, influence of surfactant agents and the effect on the peak current of pulse amplitude, ionic strength, drop time, temperature and concentration of electroactive species. Methods for the polarographic determination of clobazam and nor-clobazam are proposed.

Results

Different types of peaks were obtained depending on the pH. Clobazam, in Britton-Robinson buffer exhibits an anodic peak at 0.05 V, well defined for pH values in the 2-7 range, and another cathodic peak at -1.41 V, observed at pH values above 5. Nor-clobazam shows only an anodic peak at -0.05 V and its intensity reaches maximum values for pH lower than 4. The influence of ionic strength was studied by adjusting with the buffer itself. It was observed that intensity reached maximum and practically constant values between 0.05-0.1 M (clobazam), 0.02-0.1 M (nor-clobazam), and decreased for higher concentrations.

The effect of pulse amplitude was studied for both benzodiazepines, in the ±100 mV range. For values less than ±40 mV there was a linear peak height dependence, in agreement with the theoretical predictions[2]. The influence of temperature was studied between 10-60°C. The peak height/temperature coefficients for all the peaks have negative values. Such behaviour suggests the existence of an adsorption processes. Furthermore, the peak height does not vary linearly with $t^{2/3}$.

The peak currents exhibit a dependence on the clobazam and nor-clobazam concentrations which resembles a Langmuir adsorption isotherm; a linear relationship was obtained for values lower than 4.0×10^{-4} M (clobazam) and 1.0×10^{-4} M (nor-clobazam). In order to confirm the existence of adsorption phenomena, the electrocapillary curves for the different species in solution were obtained. The results show that the curves corresponding to the solutions of benzodiazepine are modified with respect to the background curve, with a decrease in the electrocapillary maximum and a shift towards more positive potentials.

The reversibility of the electrodic processes was studied using the criteria of Birke et al.[3]. From the results obtained it may be concluded that the electrodic processes involving clobazam and nor-clobazam are quasi-reversible. The same conclusion is reached when working with conventional polarography, $\log i/i_l - i$ vs E. In view of the linearity between peak intensities and benzodiazepine concentrations it is posible to determine clobazam and nor-clobazam by differential pulse polarography.

The presence of a cathodic peak at -1.41 V corresponding to clobazam and the absence of such a peak for nor-clobazam means that in principle it is possible to determine clobazam in the presence of its metabolite. Furthermore, the differences observed in the behaviour of both benzodiazepines against pH can be used for the same purpose, since in very acid media the intensity of the anodic peak of clobazam reaches a maximum and that of the peak corresponding to its metabolite a minimum.

References

1. SCHUTZ,H., "Benzodiazepines", Springer-Verlag, Berlin(1982).

2. BARD,A.J. and FAULKNER,L.R. "Electrochemical Methods", John Wiley. New York (1980).

3. BIRKE,R.L., MYUNG-HOON,K. and STRASSFELD,M., Anal.Chem., 53,852 (1981).

POLAROGRAPHY OF CIMETIDINE AND RANITIDINE

J.HERNANDEZ MENDEZ, A.SANCHEZ PEREZ
and M.DELGADO ZAMARREÑO
Department of Analytical Chemistry, Faculty of Chemistry,
University of Salamanca (Spain)

Cimetidine(I) and ranitidine(II) are the two effective H_2-receptors antagonists of histamine that are now largely prescribed in the treatment of gastric and duodenal ulcer patients.

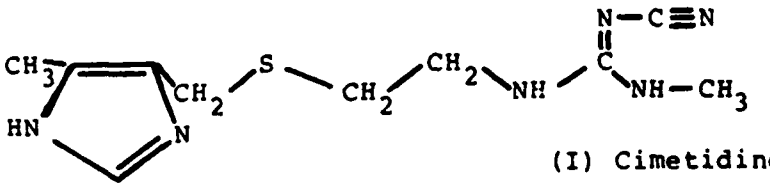

(I) Cimetidine

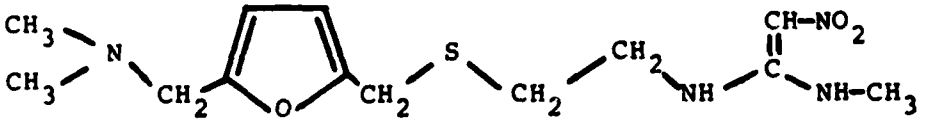

(II) Ranitidine

Polarographic Behaviour of Cimetidine

The test proposed by Feigl[1] for the identification of N-Cyano compounds, based on the chemical reduction of the cyanoimino group by Zn in a strong acid, suggested the possibility of the polarographic reduction of cimetidine. We first investigated the polarographic behaviour of cimetidine to establish the optimal conditions for analysis of this compound[2]. However, our efforts to clarify the polarographic process were unnecessary considering the recent publication by Webber et al.[3]. These authors studied the reduction of cimetidine in 0.1 M HCl by square-wave and cyclic voltammetry and indicated that direct current (dc), normal pulse and differential pulse polarography were not useful for analytical purposes; this is not surprising in view of the 0.1 M HCl solution used as supporting electrolyte. They proposed that the reduction of cimetidine involves a $4e^-$ $4H^+$ (2-step) reduction of the cyano group to the corresponding methylamine, in contrast to the chemical reduction of N-cyano compounds which leads to the release of hydrogen cyanide. We found no evidence of HCN formation in the coulometric reduction of cimetidine.

Our results show that when the supporting electrolyte is a strong acid, such HCl, $HClO_4$, H_2SO_4 or H_3PO_4, in ade-

quate concentration, the wave obtained in the dc polarographic reduction of cimetidine is defined. The acid concentration influences the $E_{1/2}$, I_{lim} and morphology of the wave; only in the 0.5-1.0 M HCl concentration range the wave is well-defined. The diffusional characteristics of the reduction wave of cimetidine in 1M HCl ($E_{1/2}$=-0.80 V, vs SCE) have been investigated. Results show that the polarographic process in controlled by the rate of diffusion of cimetidine toward the electrode surface.

Instead of conventional dc polarographic wave first derivative curve may be obtained and the corresponding peak current advantageously used for analytical purposes. A method for the polarographic determination of cimetidine in the 4-80 µg/ml range with a coefficient of variation of 1.3% has been developed and further applied to the determination of cimetidine in tablets. The results obtained by the dc polarographic method agree with those obtained by an aqueous potentiometric titration of cimetidine with $HClO_4$ using the Gran graphic method to estimate the end point.

Polarographic Behaviour of Ranitidine

In the polarographic reduction of ranitidine three waves may be observed whose $E_{1/2}$ and I_{lim} are strongly dependent on the pH of the solution (Table 1).

Table 1

Influence of pH on the polarographic reduction of ranitidine

Wave	pH range	$E_{1/2}$ -pH dependence
1st	0.8 < pH < 2.7	$E_{1/2}$ =-0.195 - 0.095 pH
2nd	1.5 < pH < 11	$E_{1/2}$ =-0.57 - 0.067 pH
3rd	4.1 < pH < 7.0	$E_{1/2}$ =-1.09 - 0.052 pH

First and second wave are due to the reduction of the protonate, $=CH-NO_2H^+$, and unprotonated, $=CH-NO_2$, nitroethene group of ranitidine, pKa=2.3 [4]. The origin of the third wave is unknow.

The characteristics of the second and third waves are studied in acetic acid-sodium acetate medium (first wave does not appear); results pointing to the existence of adsorption phenomena in the reduction of the nitro group, the diffusive characteristics of the third wave and the irreversible nature of both. Coulometry is used to determine the number of electrons involves in the nitro group reduction.

The analytical usefulness of the polarographic reduction of ranitidine in acetic acid-sodium acetate medium ($E_{1/2}$ =-0.90 V vs Ag/AgCl) is evidenced by appliying it to the determination of this compound by d.c. (2.5×10^{-5}-5×10^{-4}M range) and d.p.p. (2.6×10^{-7} - 2×10^{-5} M range). For a standard solution of ranitidine 8.75×10^{-6} M the R.S.D. of the method is 2.7%.

References

1.-Feigl,F. and Anger,V.(1975) Spot-test in Organic Analysis, Elsevier Scientific Publishing Co., Amsterdam, The Netherlands, p.268.

2.-Sánchez Pérez,A., Hernández Méndez,J. and Fuentes de Frutos,J.E., J.Assoc.Off.Anal.Chem. (Accepted March 15, 1985, to be published vol.68, n°5, 1985).

3.-Webber,A., Shah,M. and Osteryoung,J. (1983) Anal.Chim.Acta, 154,105.

4.-Cholerton,T.J., Hunt,J.H., Klinker,G. and Martin-Smith,M., J.Chem.Soc., Perkin Trans.,II(1984) 1761.

ELECTROANALYTICAL STUDIES OF PESTICIDES. DETERMINATION OF GUTHION

J.HERNANDEZ MENDEZ, R.CARABIAS MARTINEZ
and E.RODRIGUEZ GONZALO
Department of Analytical Chemistry. Faculty of Chemistry. University of Salamanca. Spain.

The determination of Guthion, S-(3,4-dihydro-4-oxobenzo [d] -(1,2,3)-triazin-3yl-methyl)0,0'-dimethyl phosphorodithioate was proposed by Bates[1] using cathode ray polarography for the analysis of this pesticide in apples, pears, cucumbers and tomatoes using a supporting electrolyte of 0.05 M KCl/0.01 M CH_3COOH/60% acetone, pH 3.8. In this medium guthion produced a wave at-0.83 V (v.s. S.C.E.). The limit of detection was quoted to be 0.1 µg/ml. This author suggested that the wave must be due to the reduction of the carbonyl group.

This communication reports on polarographic studies (DC and DPP) of guthion reduction in 20% (v/v) MeOH/H_2O, Britton-Robinson buffer; the results showed that the pesticide gives rise to two reduction waves. The electrochemical behaviour of the guthion was interpreted according to the polarographic data and with the aid of other techniques (coulometry, spectrophotometry).

RESULTS AND DISCUSSION

The first wave (I_1) appears in acid media, pH=1, while the second one (I_2) appears at pH 2.4. The height of I_1 is constant and independent of time up to pH=9; the half-wave potential is shifted to more negative values at pH$<$9, the $E_{1/2}$-pH relationship was found to be $E_{1/2}$=-0.432-0.058 pH.

The I_2 wave exhibits a maximum in DC and a minimum in DPP, its intensity being constant and independent of time; the half-wave potential is pH-independent. At pH values above 9 the shift of the I_1 to more cathodic potentials leadsto a wave overlap, thereby a wave sum of I_1 I_2 is obtained.

In 0.1 M NaOH medium the height of the wave sum decreases with time due to hydrolysis of the pesticide. After 3 hours, an anodic wave (DC) appears due to the dithiophosphate produced, together with two poorly-defined cathodic waves of weak intensity; the more cathodic one is due to the formaldehyde generated during hydrolysis.

The further polarographic studies were carried out at a pH close to 5. In this medium, an increase in the MeOH concentration produces a shift in the half-wave potential of I_2 to more cathodic values and the maximum disappears.

An increase in temperature enhances the I_2 wave maximum, its temperature coefficient, in presence of Triton X-100,

being 0.98%. Under same conditions, the I_1 wave has a coefficient of 1.66%.

The results obtained upon va·ying drop time (Table I) and the base pulse show that only the first wave is diffusion controlled.

Table I

	I_1	I_2
DC, log i/log t	0.172	0.254
DPP, log i_p/log t	0.668	0.348

Owing to the poor definition of I_2 in the absence of Triton X-100, logarithmic analysis was only carried out for I_1; it was found that the reduction process is irreversible; the value of $n\alpha$ is 1.35 and the number of protons exchanged in the controlling electrode reaction is one.

The relationship between the wave heights and guthion concentration was determined for different drop times in both the presence and absence of Triton X-100. For I_1, the relationship was linear both in DC and DPP. For I_2, linear relationship are found, both in the presence and absence of the tensoactive agent, only for concentrations lower than $3.0.10^{-4}$M. For higher concentrations I_2 tends to a constant value. The detection limits (3s) using DPP are $1.3.10^{-7}$M for I_1 and $3.4.10^{-6}$M for I_2.

In order to determine the mechanisms of the electrodic reactions a coulometric study was carried out at potentials of the limiting currents of I_1 and I_2 for different pesticide concentrations. The change of wave heights and of the UV absorption spectra for the pesticide and for the species generated during the electrolysis was followed. When the electrolysis was carried out at the potential of the limiting current of I_1 the decrease of wave I_2 was parallel to that I_1. Simultaneously, two anodic waves appear . If these products are left in contact with the air, the two reduction waves are regenerated and only one anodic wave remains; on the other hand the formation of a black layer over the mercury pool was also observed.

The possible mechanism of the electrode reactions is postulated and a new method for the determination of the pesticide is proposed.

REFERENCE

1. J.A.R.Bates, The Analyst, 87(1962)786.

11 ALUMINIUM ELECTRODEPOSITION FROM $AlCl_3$-NaCl AND $AlCl_3$-KCl MELTS ON PLATINUM, GOLD AND VITREOUS CARBON ELECTRODES

J.N.JOVIĆEVIĆ* and V.D.JOVIĆ
Institute of Technical Sciences Serbian Academy of Science and Arts, Knez Mihajlova 35, 11000 Beograd, Yugoslavia

Aluminium deposition on platinum and gold policrystalline electrodes and vitreous carbon electrode from $AlCl_3$-NaCl and $AlCl_3$-KCl melts was investigated using linear sweep voltammetry (LSV) and potential step techniques, as a function of melt composition (ranging from 50.0 to 52.0 molar % of $AlCl_3$) and temperature applied (200-300°C).

The cell arrangement and method of preelectrolysis of melt was explained elsewhere[1].

LSV results obtained at 264°C from equimolar $AlCl_3$-NaCl and $AlCl_3$-KCl melts on three electrodes used are presented in Fig.1., (a) and (b). Generally speaking voltammogram features obtained for one and the same electrode material under the same experimental conditions in both electrolytes used are almost identical, except for the current densities which are somewhat smaller in the case of $AlCl_3$-KCl melt. It appears that gold and platinum electrodes are being easelly alloyed by aluminium already in UPD region (starting at 0.5V vs. Al) which is identified by several cathodic and anodic waves[1,2]. Observable difference appears in the aluminium overpotential region on vitreous carbon electrode in $AlCl_3$-NaCl melt, where cathodic currents exhibit sings of two successive processes. First, most probably, is aluminium deposition from $Al_2Cl_7^-$ species (whose concentration depends strongly on $AlCl_3$:NaCl(KCl) ratio) and the second aluminium deposition from $AlCl_4^-$ species[3].

Fig.2., (a) and (b), represents j-t transients due to single potential step applied to the same three electrodes in both melts, under the same experimental conditions as presented in Fig.1. It appears quite evident that Al with Pt and Au forms several types of alloys both in UPD and OPD region, before bulk Al starts depositing. Reduction of Al^{z+} species in the UPD region is easelly observed in the form of cathodic j-t transients as a responce to

* Materials Research and Development Institute, Energoinvest, Sarajevo, Yugoslavia

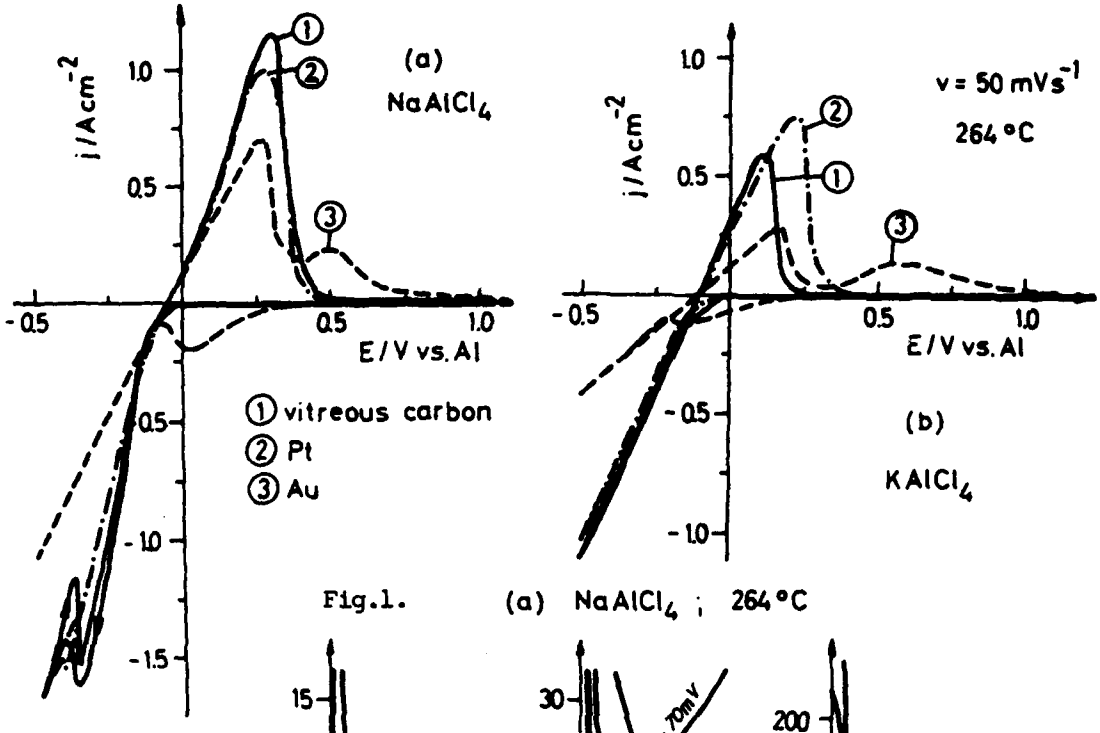

Fig.1. (a) $NaAlCl_4$; 264 °C

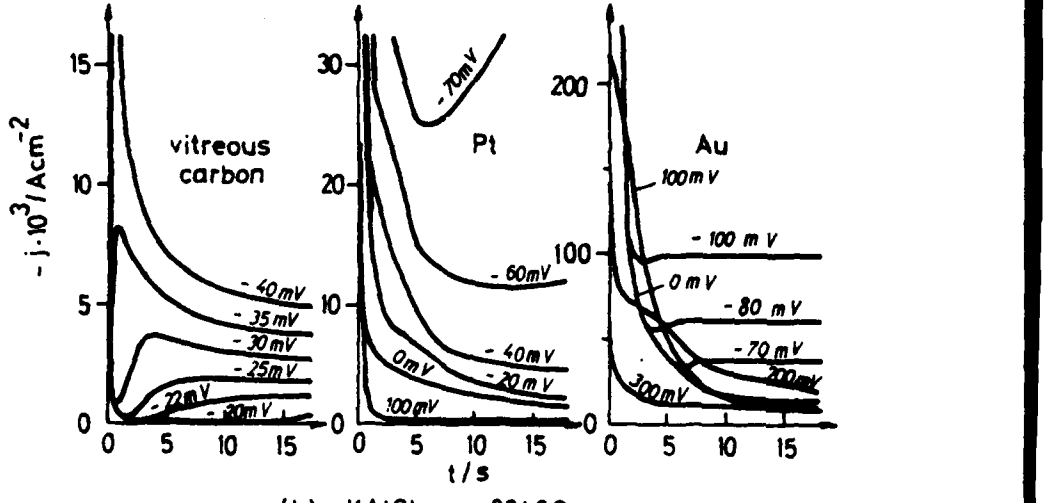

(b) $KAlCl_4$; 264 °C

Fig.2.

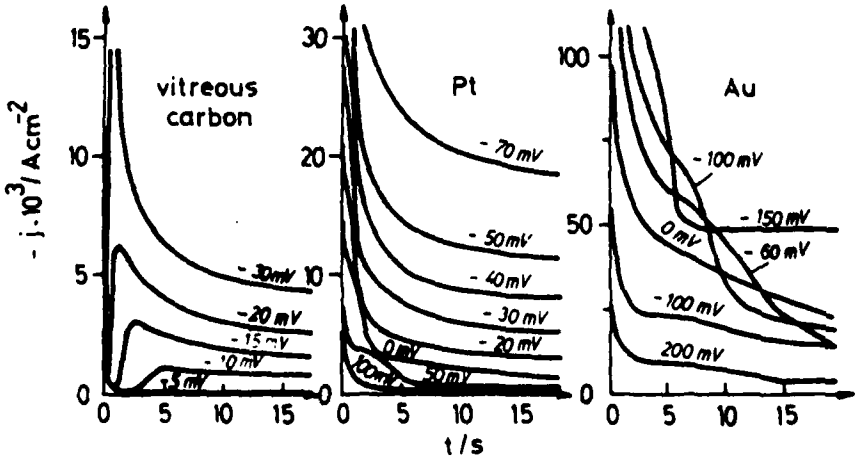

potential steps whose amplitude is as much as 300 mV more positive then the "reversible potential" of bulk aluminium in the same melt. In the case of vitreous carbon electrode cathodic rising j-t transients are observed only in the overpotential Al deposition region. It is not difficult to recognize two sort of those transients: one which reaches what appears to be a diffusion control behaviour at averpotentials higher then -40 mV vs.Al, and second one which reaches diffusion control only above -900 mV vs. Al. First type of j-t transients most probably reflect aluminium deposition from $Al_2Cl_7^-$ species, and detailed analysis of its initial rising portion shows $j\text{-}t^3$ relationship, which would sujjest progressive 3D nucleation and growth controled by crystal lattice building step.

Fig.3. shows typical LSV and potential step results obtained on vitreous carbon electrode in $AlCl_3$-NaCl melt of composition 52 mol % $AlCl_3$ - 48 mol % NaCl at 200°C. Above mentioned observations are readily recognized.

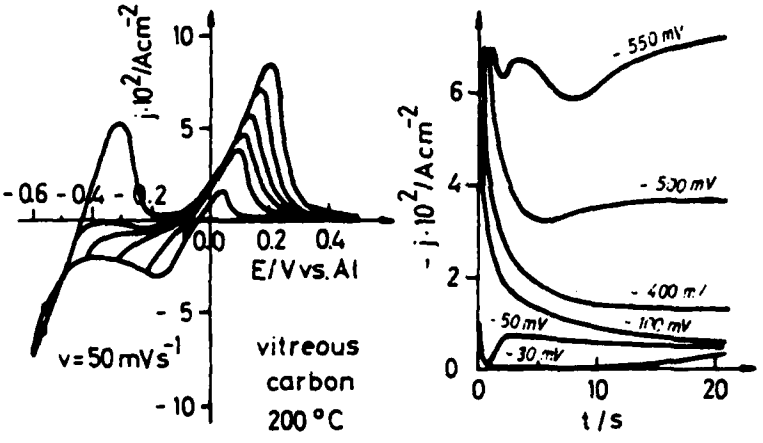

Fig.3.

References:

1. V.D.Jović, J.N.Jovićević, L.Ž.Vorkapić, 8. Yugoslav Meeting of Electrochemistry, Extended Abstracts, p.244., Dubrovnik (1983).
2. J.N.Jovićević, V.D.Jović, 9. Yugoslav Meeting of Electrochemistry, Extended Abstracts, Dubrovnik (1985), in press.
3. P.Rolland, G.Mamantov, J.Electrochem.Soc., 123(1976)1299.

SALT FORMATION DURING THE ANODIC DISSOLUTION OF IRON IN AQUEOUS $(NH_4)_2SO_4$ AT pH = 2

C. Moina and D. Posadas*
INTI, Sector Electroquímica. Parque Tecnológico Miguelete, Miguelete, Provincia de Buenos Aires, ARGENTINA.

* Instituto de Investigaciones Fisicoquímicas Teóricas y Aplicadas, INIFTA, División Electroquímica. Casilla de Correo 16, Sucursal 4, (1900) La Plata, ARGENTINA.

INTRODUCTION

During the anodic dissolution of metals in different media, salt formation on the surface of the electrode occurs. Although this phenomenon is known since a long time ago its mechanism has not been completely elucidated yet. The purpose of this work is to investigate the salt formation and dissolution processes under stationary and transient conditions of non-noble metals such as iron in $(NH_4)_2SO_4$ at pH = 2.

EXPERIMENTAL

The stationary polarization curves of a rotating disk electrode show a constant current region, I_L, between -0.4 and 0.2 V vs SCE which depends on the rotation speed, ω. This current was measured as a function of ω, the concentration of $FeSO_4$ and $(NH_4)_2SO_4$ in solution at different temperatures, T, in the range $273\ K < T < 318\ K$.

The process of salt formation was investigated through the current and potential responses to a potential or current step, respectively, from the rest potential to a region corresponding to the constant current in the polarization curve.

Auxiliary techniques such as scanning electron microscopy, SEM, EDAX and X-Ray diffraction, were employed in an attempt to identify the salt film formed.

RESULTS AND DISCUSSION

The current density, i_L, depends linearly on $\omega^{1/2}$. The slope decreases with $C_{(NH_4)_2SO_4}$ and with C_{FeSO_4}. The latter dependence, assuming that the current is determined by the dissolution of the salt, allows to determine by extrapolation to $i_L = 0$, the saturation concentration, C_s, of the salt and the diffusion coefficient of the Fe(II) ion. The temperature dependence of C_s allows the heat of solution to be estimated. These data and the information obtained with the auxiliary techniques suggest the salt present on the electrode is $FeSO_4.7H_2O$.

The potential-time response shows the appearance of a transition time. The SEM pictures show that a salt film is forming during the transient. However at the end of the transient, when the potential goes to very positive values, structures suggesting the presence of γ-FeOOH appear.

The shape of both potentiostatic and galvanostatic transients can be interpreted with a model of heterogeneous nucleation and growth from the solution. By fitting the model to the experimental data the oversaturation can be evaluated. The Tafel plots obtained from the fit ranging between 0.14 and 0.16 V/decade without ohmic correction.

The present results therefore support the mechanism of nucleation and growth controlled by diffusion for the precipitation of salt films on non-noble dissolving metals.

ACKNOWLEDGMENT

INIFTA is a Research Institute jointly established by the Universidad Nacional de La Plata, the Consejo Nacional de Investigaciones Científicas y Técnicas and the Comisión de Investigaciones Científicas de la Provincia de Buenos Aires.

KINETICS OF THE POLYCRYSTALLINE IRON ELECTRODE IN CARBONATE-BICARBONATE SOLUTIONS IN THE 0-75°C RANGE

C.R. Valentini[1], C.A. Moina[1], E.B. Castro[2], J.R. Vilche[2] and A.J. Arvia[2]

(1) Instituto Nacional de Tecnología Industrial (INTI), Sector Electroquímica Aplicada, C.C. 157, 1650 San Martín, ARGENTINA.

(2) Instituto de Investigaciones Fisicoquímica Teóricas y Aplicadas (INIFTA), C.C. 16, Suc. 4, 1900 La Plata, ARGENTINA.

INTRODUCTION

The corrosion and passivation of iron in aqueous solutions containing carbonate is of importance in relation to the behaviour of the metal in contact with aqueous system absorbing carbon dioxide. The publications on the subject concern mainly with static iron samples[1,2] and the influence of the hydrodynamic conditions[3,4]. Iron samples in solution containing carbonate ions undergo different processes which also affect the susceptibility to an enhanced attack under corrosion fatigue or stress corrosion cracking conditions[5,6]. Apparently, the active to passive transition of iron in carbonate-bicarbonate electrolytes implies the competitive formation of a prepassive hydrous iron oxide and a salt layer[7].

This paper refer to the phenomenology of the dissolution, prepassivation and passivation of iron in carbonate-bicarbonate solutions at different temperatures, ionic strenght and pH, paying particular attention to mass transport contribution to the overall anodic process.

EXPERIMENTAL

Runs were made with polycrystalline iron (Specpure, Johnson Matthey Chem. Ltd.) rotating disc electrodes. The experimental setup was the same described in previous publications[7]. The composition of the electrolyte solutions was x M $KHCO_3$ + y M K_2CO_3, $0.005 \leq x \leq 2.5$ and $0.005 \leq y \leq 2.5$. Solutions were prepared from analytical grade chemicals and bidistilled water, previously boiled to remove CO_2. Voltammetric runs were made at potential sweep rates (v) in the 0.001 to 0.25 V/s range. The rotation speed of the rde (w) was varied in the 0 to 2580 rpm range. Potentials in the text are given in the NHE scale. SEM observations, EDAX and electron-probe microanalysis were performed.

RESULTS

Voltammograms run at 25°C between -0.98 V and 0.23 V at 0.025 V/s in quiscent solution of pH 8.9 exhibit three anodic peaks (I, II and III) in the -0.65 to 0.15 V range and the cathodic peaks, one poorly defined at ca. -0.4 V (peak IV) and another one at ca. -0.8 V (peak V), which preceds the hydrogen

evolution reaction. In the active to passive transition, both the charge and hight of peak II increase considerably with w, but those of peak I appears independent of w.

In the 0-75°C range, the height of peak II ($i_{p,II}$) increases linearly with $w^{\frac{1}{2}}$ in the whole range of v covered in this work. At constant v, T and pH, a linear $i_{p,II}$ vs. $w^{\frac{1}{2}}$ relationship is observed, the slopes of the straighlines increase accordingly to the ionic strength. The lines, however, do not intercept the origin of coordinates as peak II is recorded also in still solutions. At constant pH, v and w, the height of peak II increases linearly with $KHCO_3$ (or K_2CO_3) concentration in solution. On the other hand, at a constant v, the charge ($Q_{p,II}$) related to peak II increases linearly with $w^{\frac{1}{2}}$, but at a constant w, it increases linearly with v^{-1}. For the latter, the value $Q_{p,II}$ extrapolated to $v \rightarrow \infty$ (0.7 mC/cm^2) can be assigned to the formation of the first passivating layer.

At constant w, both $i_{p,II}$ and $Q_{p,II}$ fit linear relationships with the ionic strength, being the slopes close to one. At constant ionic strength, both $i_{p,II}$ and $Q_{p,II}$ are independent on pH.

Specimens previously held during 60 min in the potential range of peak II reveal the presence of carbonate species in the film.

DISCUSSION

The active to passive transition of iron in carbonate-bicarbonate solutions involves at least two stages. The first one, associated with peak I, occurs in the potential range where only Fe(II) species are expected as reaction products. The small charge involved in peak I, can be assigned to the prepassive layer, probably, a hydrous ferrous hydroxide layer.

The second stage, related to peak II, implies a mass transport from the solution coupled to the proper electrochemical reaction. The iron electrodissolution through the prepassive layer increases both the thickness of film and the concentration of Fe^{2+} and anions at the interface. At least three processes occur simultaneously within the potential range of peak II, the grow of the $Fe(OH)_2$ layer, the precipitation of $FeCO_3$ and the partial removal of $FeCO_3$ from the surface by a chemical reaction. The latter is controlled by the concentration of protons at the interface. The latter is determined by the metal dissolution yielding $Fe(OH)_2$ and the various equilibria related to Fe^{2+}, HCO_3^- and CO_3^{2-} ions.

REFERENCES

1. J.G.N. Thomas and J.D. Davies, Br.Corros.J., 12, 108 (1977).
2. W. Schwenk, Werkst.Korros., 34, 287 (1983).
3. R.D. Armstrong and A.C. Coates, J.Electroanal.Chem., 50, 303 (1974).
4. D.H. Davies and G.T. Burstein, Corrosion, 36, 416 (1980).
5. R.H. Ricci, L.B. Berardo, L.M. Gassa and J.R. Vilche, Proc. 9th Intern.Congr.Metall Corros., Vol. 3, Toronto, pp. 161-168 (1984).
6. R.N. Parkins, C.S. O'Dell and R.R. Fessler, Corros.Sci., 24, 343 (1984).

7. C.R. Valentini, C.A. Moina, J.R. Vilche and A.J. Arvia, Anal. Asoc.Quím.Arg., 71, 555 (1983); Corros.Sci., in press.

ACKNOWLEDGEMENT

INIFTA is a Research Institute jointly established by the Universidad Nacional de La Plata, Consejo Nacional de Investigaciones Científicas y Técnicas and the Comisión de Investigaciones Científicas de la Provincia de Buenos Aires.

THE ELECTRODEPOSITION OF SILVER AT THE SUBMONOLAYER AND MULTILAYER LEVELS ON POLYCRYSTALLINE RHODIUM IN ACID ELECTROLYTES

B. Parajón Costa, M.C. Giordano and A.J. Arvia
Instituto de Investigaciones Fisicoquímicas Teóricas y Aplicadas - (INIFTA)
Casilla de Correo 16, Sucursal 4, (1900) La Plata, ARGENTINA

The electrodeposition of foreign atoms in the monolayer and submonolayer level on noble metals has been extensively investigated in relation to electrocatalysis, heterogeneous catalysis and galvanic processes. Polycrystalline Rh in acidic solutions has been also examined as catalyst for organic fuel combustion due to its dehydrogenation ability, but, in this case, only a relatively small attention was paid to the behaviour of adatoms.

This work refers to the electrochemical behaviour of Rh electrodes in 1 M H_2SO_4 in the presence of Ag electrodeposited under different preset potentials at temperatures in the 0°C and 65°C range. Polycrystalline rhodium wires (Johnson Matthey and Co) of 0.59 cm^2 geometrical area were used as working electrode. Silver electrodeposition was made either under a slow potential sweep or at a constant potential, E_τ, for different periods of time, τ. Values of E_τ were set either more positive or more negative than the reversible Ag/Ag^+ (x M, y°C) electrode, E_r, to investigate both UPD and the early stage of bulk Ag electrodeposition. Base electrolyte was 1 M H_2SO_4 added to Ag_2SO_4 in the range of 10^{-6} to 10^{-4} M. Most of the experiments, however, were performed with 10^{-5} M Ag_2SO_4. As E_r for Ag/Ag^+ 10^{-5} M at 25°C is 0.534 V vs RHE, the UPD of Ag on Rh electrodes occurs very closely to the beginning of the OH-electroadsorption on Rh. To investigate the influence of the oxidized surface on Ag electrodeposition runs on prereduced Rh and on partially oxidized Rh were performed. The Ag-Rh interactions were followed voltammetrically. Combined linear sweeps and potential steps were applied to study: i) H-adatom electrodesorption in the presence of different amounts of electrodeposited Ag; ii) bulk phase formation Ag at $E_\tau < E_r$; iii) UPD Ag electrooxidation after adsorption on a previously reduced or partially oxidized Rh surface; iv) the influence of the remaining oxide after Ag electrodeposition; and v) the total oxide electroreduction charge after Ag electrooxidation.

The results can be summarized as follows:

1. Ag electrodeposition on Rh can produce either a submonolayer or a bulk phase accordingly to E_τ and τ values.
2. UPD Ag on Rh is characterized by two anodic stripping current peaks (peaks I and II) appearing in the potential range of O-electroadsorption.
3. After relatively long electrodeposition times, peak I becomes a shoulder of peak II.
4. As it is already known for Pt, the Ag UPD on Rh inhibits the electroadsorption of H-adatoms.

5. Silver UPD on a Rh surface containing O-adatoms, the H-adatom electroadsorption charge decreases and simultaneously, the H-adatom electrodesorption potential appears at lower potentials.
6. When peak II and that of bulk Ag stripping are recorded, the O-electrodesorption charge increases ca. 20 percent and the corresponding voltammetric peak becomes wider.
7. On previously reduced Rh, peak I is firstly formed, whereas peak II appears at longer times.
8. On a Rh surface partially covered by O-adatoms, peak II appears as overlapping the O-electroadsorption on the remaining bare Rh surface. In this case, peak II is observed at times shorter than that corresponding to 3.
9. The increase in temperature causes a greater separation of the potentials of stripping peaks I and II, due to the shift of peak II towards more positive potentials as T is raised.
10. As the temperature decreases the overlapping of peaks I and II is observed, so that a single wide voltammetric peak is recorded.

The analysis of these results yields information about the silver deposition on rhodium under non-equilibrium conditions in the presence and in the absence of rhodium oxides species in the surface.

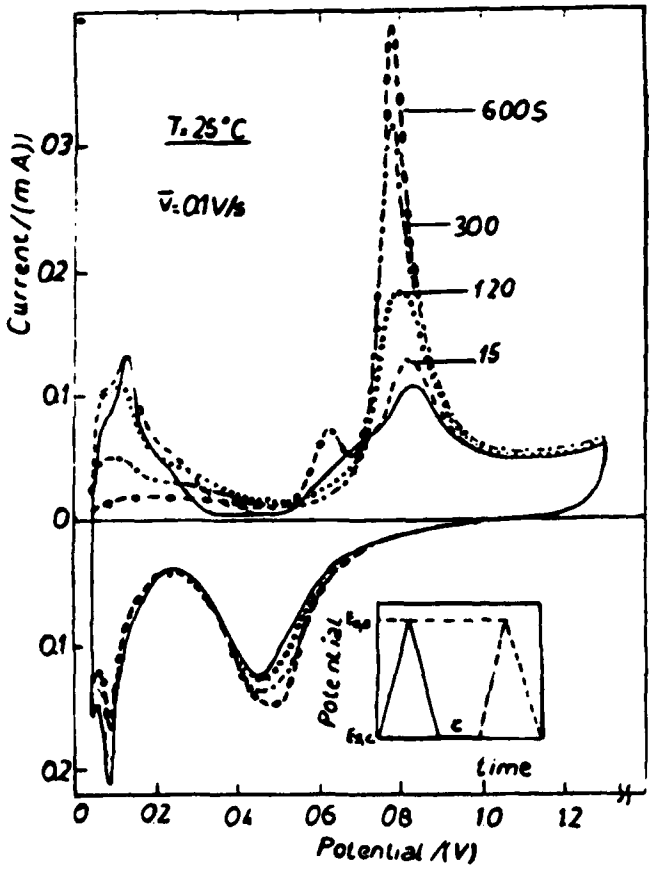

Fig. 1.- Voltammograms in 1 M H_2SO_4 after Ag^+ deposition on Rh at 0,03 V different τ. 10^{-5} M Ag_2SO_4, 0.1 V/s, 25°C.

ACKNOWLEDGEMENT.- INIFTA is a Research Institute jointly established by the UNLP, CONICET and CIC de la Provincia de Buenos Aires.

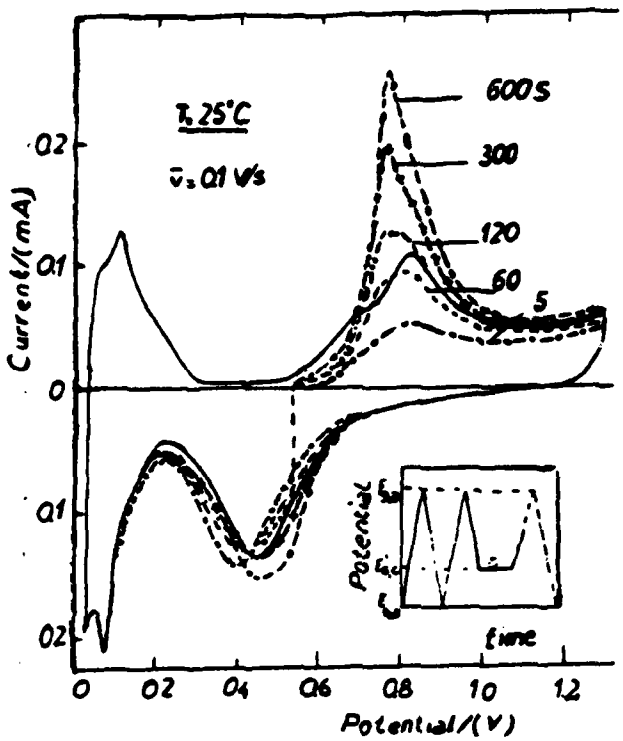

Fig. 2.- Voltammograms in 1 M H_2SO_4 after Ag^+ deposition on a partially oxidized Rh surface. E_τ = 0.58 V, 10^{-5} M Ag_2SO_4, 0.1 V/s 25°C.

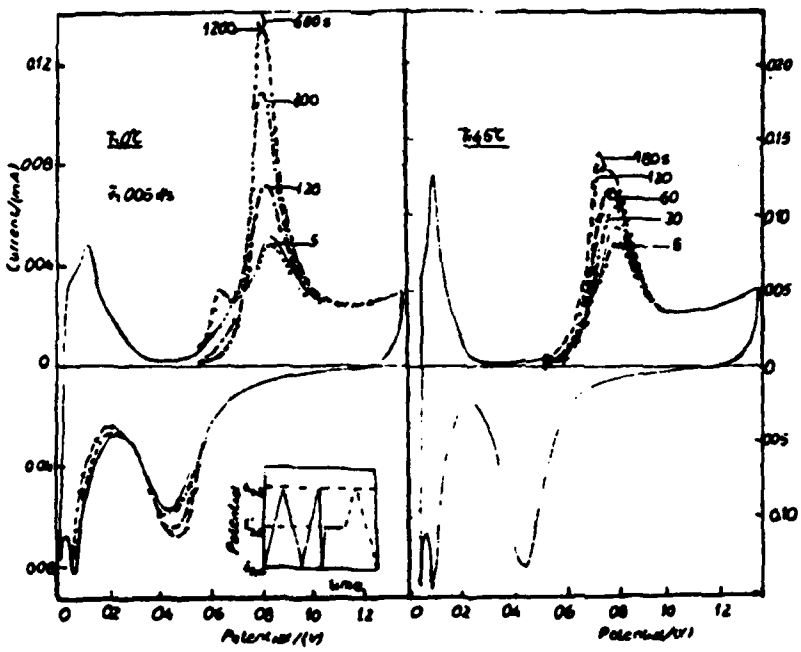

Fig. 3.- Voltammograms of upd Ag on Rh in 1 M H_2SO_4 at different temperatures. 10^{-5} M Ag_2SO_4. 0.05 V/s. a) 0°C, b) 45°C.

ELECTRODEPOSITION OF COPPER FROM SOLUTIONS CONTAINING NITRATES

R.E. SIODA
Industrial Chemistry Research Institute, PL-01-793 Warszawa, Poland

In solutions analyzed for trace metal elements nitrates are frequently present, as nitric acid is added to stabilize the solutions. Nitrates are electro-active, and thus can influence electroanalytical determinations of heavy metal ions. If electrolysis is prolonged, the concentration of nitrates, as well as pH, can change, and new species can form, like nitrites, nitric oxides, ammonium cation, and ammonia. These secondary products can act as oxidants, reductants, and complexing agents for heavy metal ions and atoms present respectively in solution, and on the electrode. Thus, nitrates are not chemically neutral in electroanalytical determinations. Their interfering role will increase, the longer is electrolysis time, and the smaller is the concentration of a metal trace to be determined.

In several recent analytical papers a controversy arose concerning a low concentration limit in trace metal electrodepositions and preconcentrations. It was experimentally found that, despite of long electrolysis time, a small concentration of the metal ion remains in solution. This residual concentration is several orders of magnitude higher, than would follow from the Nernst equation of equilibrium potentials. A model was published according to which, in presence of deposit covered electrode, the solution will contain an equilibrium concentration of depositing metal ions:

$$c_{eq}=k_2/k_1 \qquad (1)$$

where k_1 is a specific rate constant of electrodeposition (cms^{-1}), and k_2 is a specific rate of deposited metal dissolution ($molcm^{-2}s^{-1}$). By measuring independently c_{eq}, k_1, and k_2, it is possible to confirm equation (1).[1]

EXPERIMENTAL

Standard solution: 0.10 M Na_2SO_4 (Merck, Suprapur of max. $1x10^{-6}$% Cu) in distilled water, acidified to pH=2 by nitric acid (pro analysis).
Electrolysis: constant current, in beakers with 150 ml solution mixed by magnetic stirrer. Copper foil of active surface area 12.0 cm^2 was cathode, platinum wire - anode.
Analysis: electrolytic solution samples were analyzed for Cu using Perkin-Elmer 503 Flame and Pye-SP9 Furnace AAS Instruments at 324.8 nm. Deuterium lamp background correction was applied. Copper foil dissolution experiments were monitored by square-wave voltammetry on IBM EC225a Voltammetric Analyzer and PARC Model 303 Static Mercury Drop Electrode, and were confirmed by ICP-AES.

RESULTS AND DISCUSSION

It was reported earlier that during cathodic polarization of copper foil, Cu(II) equilibrium concentration was generated in solution[1]. This experiment has been now repeated with better analytical control of the solution. The measured equilibrium concentrations fall in the range: 40 ÷ 80 μg Cu l^{-1}, i.e. 0.6 ÷ 1.2 μM, as is shown in Table 1. Cathodic current density (c.d.) of 8 and 33 $mA.cm^{-2}$ has been applied, and the respective copper cathode potentials were: -1.02 and -1.40 V vs. SCE. A change of c.d. from 8 to 33 $mA.cm^{-2}$ had no apparent effect on the level of the measured equilibrium concentrations.

TABLE 1

Cu(II) equilibrium concentrations in aerated standard solution during electrolysis with copper cathode (c.d.=33 $mA.cm^{-2}$). Concentrations determined by Furnace AAS, each value is a mean of three determinations. Average RSD (relative standard deviation) is a pooled value for all determinations.

Electrolysis time/hr	Cu(II) concentration/μg Cu l^{-1}	RSD%
1	46.8	28.2
2	77.2	9.5
3	49.0	24.7
4	65.8	18.5
5 (outlayer)	491.9 (?)	4.8
6	42.6	3.2
average (without outlayer)	56.3	18.0

The equilibrium concentrations of Table 1 fluctuate with time. A special statistical calculation was performed to decide, if the observed differences are significant, or are just manifestations of a random error of the determination method. Formally speaking, at confidence level of 95%, the calculated statistically significant difference is 18.2 μg Cu l^{-1}, or more. Thus, the concentration values of 77.2 and 65.8 may be significantly different from 46.8 and 42.6 (outlayer has been excluded). The fluctuations have a standard relative deviation of 26%.

k_1 and k_2 magnitudes and c_{eq} values, all measured under standardized conditions, are required for the experimental confirmation of equation (1). Both k_1 and k_2 depend on solution mixing rate (m.r.); c_{eq} may not depend on m.r., if m.r. effects mutually cancel in k_2 and k_1 ratio of equation (1). In the present work an arbitrary m.r. was applied, and k_1 was approximately determined as 3×10^{-3} cms^{-1} from kinetics of Cu(II) electrolysis at 35°C.

The dissolution of copper foil immersed in aerated standard solution gave $k_2 = 3.0 \times 10^{-11}$ $molcm^{-2}s^{-1}$ at 21°C. It was also found that k_2 is strongly temperature dependent, and increases on average 20% per °C in the range of 6.5 to 45.5°C. On the other hand, k_2 decreases substantially, when solution is de-aerated, thus indicating that oxygen plays a significant role in copper dissolution. For the de-aerated standard solution, $k_2 = 3.5 \times 10^{-12}$ $molcm^{-2}s^{-1}$ has been determined at 25°C.

The constant current electrolyses have been conducted with a considerable surplus of c.d. concerning such reducible species as Cu(II) ions and the dissolved molecular oxygen. Hence, it is reasonable to as-

sume that in the aerated solution electrolyses, the concentration of oxygen in the diffusion layer was virtually zero. Then, it will be logical to substitute into equation (1) k_2 measured for the de-aerated standard solution.

Ideally, all the variables of equation (1) should be measured at the same temperature. Both c_{eq} and k_1 were measured at 35°C, however, k_2 for the de-aerated standard solution was measured at 25°C. Thus, k_2 should be corrected for the +10°C temperature difference, which probably would mean doubling k_2 value. As the following calculation is approximate, this correction is neglected. Substituting into equation (1) the values of k_1 and k_2 (for the de-aerated standard solution), a following estimate of the equilibrium concentration is obtained:

$$c_{eq} \approx \frac{3.5\times10^{-12}\ \text{molcm}^{-2}\text{s}^{-1}}{3\times10^{-3}\ \text{cms}^{-1}} = 1.2\times10^{-9}\ \text{molcm}^{-3} \qquad (2)$$

The average measured value, given at the bottom of Table 1, is

$$c_{eq} = (0.89 \pm 0.09)\times10^{-9}\ \text{molcm}^{-3} \qquad (3)$$

where the confidence limits correspond to 95% confidence level, and to the total number of determinations N=15.

Thus, there is a reasonable agreement between c_{eq} values, the first of which was calculated according to equation (1), and the second was measured experimentally. The important assumption leading to the agreement is that of using in the calculation k_2 determined for the de-aerated standard solution. If k_2 determined for the aerated solution is used instead, the calculated c_{eq} is one order of magnitude higher, than the experimentally determined value. This disagreement is due to a considerable enhancement of copper dissolution rate caused by the dissolved molecular oxygen.

CONCLUSIONS

It has been shown that during constant current cathodic polarization of copper electrode in a standard solution of pH=2 an equilibrium concentration of Cu(II) ions in solution is formed of arqund 1 μM. This concentration is invariant, if c.d. of 8 or 33 mA.cm^{-2} is applied. Further, the equilibrium concentration can be simply related, according to equation (1), to the experimental: specific rate constant of Cu(II) electrodeposition, and specific rate of Cu dissolution in de-aerated solution.

The equilibrium concentration fluctuates with time, which possibly means, in view of equation (1), that the rates of Cu deposition and dissolution are not stabile, but fluctuate with time too.

REFERENCES

1. R.E. Sioda, Talanta, 31, 135 (1984).
2. R.E. Sioda, Monatsh. Chem., 116, 49 (1985).

ACKNOWLEDGEMENT

The experimental help of P.E. Sturrock and D. Owens is greatly appreciated.

ELECTRODEPOSITION AND DISSOLUTION OF NICKEL ON AND FROM TRANSITION METALS SUBSTRATES WITH VACANT OR PARTLY FILLED d-ORBITALS

D. SUŽNJEVIĆ, D. ŠPAGNUT*, Č. LAČNJEVAC*** and M. JAKŠIĆ**
University of Belgrade:
Faculty of Science, *Faculty of Trafic, **Faculty of Agriculture,
***Air Deport "Moma Stanojlović", Batajnica near Belgrade,
Belgrade, Yugoslavia

On the basis of the Brewer valence bond theory[1] and genaralized Lewis acid-base reaction[2] for bonding in metals, alloys and intermetallic phases there has been pointed aut[3] that whenever metals of the left-half of the transitions series that have empty or half filled vacant d-orbitals are alloyed with metals of the right-half of the transition series that have internally paired d-electrons not available for bonding in the pure metal, there arises well pronounced synergism in electrocatalysis for the hydrogen evoluation reaction (h.e.r.), which often exceeds individual effects of noble metals and each other (the synergism condition) and approaches the reversible behaviour at almost equilibrium potential within the wide range of current density. The Brewer theory[1,2] predicts that such intermetallic phases behave extraordinary stability features because of improved interorbital bonding and mutual sharing of internally paired electrons. Such state of the art has suggested the investigation of potential sweep cycles (cyclic voltammetry, c.v.) for deposition and dissolution of transition metals with empty or half filled d-orbitals upon d-metals with internally paired d-electrons, and vice versa. Unfortunately, the deposition of transition metals with vacant d-orbitals is possible only from fused salts. On other hand, d-metals with less than five d-electrons characterises a rather strong bonding of oxygen and usually a pronounced hydration and therefore it is not easy to provide their clean metallic surface for deposition of other adatoms. Such electrodepositions of transition metals with internally paired d-electrons upon the ones with vacant d-orbitals so far has rather scarcely been investigated and appears interesting from many points of view, first of all for electrocatalysis.

The basic system in the present paper has been the deposition of Ni upon transition metals with vacant d-orbitals (Nb, Hf, Ti, Ta). According to the bonding effectivness, the Breqr theory[1,2] predicts the underpotential deposition for such d-metal pairs[3].

The c.v. curves were recorded in the potential region between +0.5 to -1.5 V. The sweep rate varried from 1 to 500 mVs^{-1}.

Fig. 1 represents the c.v. curves of the Ni deposition-dissolution process at the Ni electrode from blank soln. (constituents of the Watts solution without Ni salts) curve 1,and from Watts soln curve 2. In the first case the c.v. curve shows hydrogene-oxygene reaction limits in between of which the anodic dissolution peak of Ni, A_1, exists at -0.28 V. In the second case the cathodic current arised at the characteristic value for the Ni/Ni(II) potential. When the Ni working electrode (w.e.) was replaced by Nb, the obtained c.v. curve was free of anodic peak in the blank solution (Fig. 2, curve 1). When the Watts soln. was applied the cathodic current, which corresponds to the Ni deposition,starts from somewhat more negative potential in relation to the Ni/Ni(II) value. When cathodic potentials becomes more negative the current after potential reversion shows tendency to reach the Ni/Ni(II) potential making the loop on the c.v. curves. Only the first A_1 peak from the two, A_1 and A_2, significantly changes in height by the change of the cathodic limit towards more negative potentials. The peak A_2, at the somewhat more positive potential in relation to the peak A_1 is bed developed and cancels completly in some experimental condition. Its peak current was desturbed by some gaseous product, probably oxygen,which evolves at somewhat negative potentials.

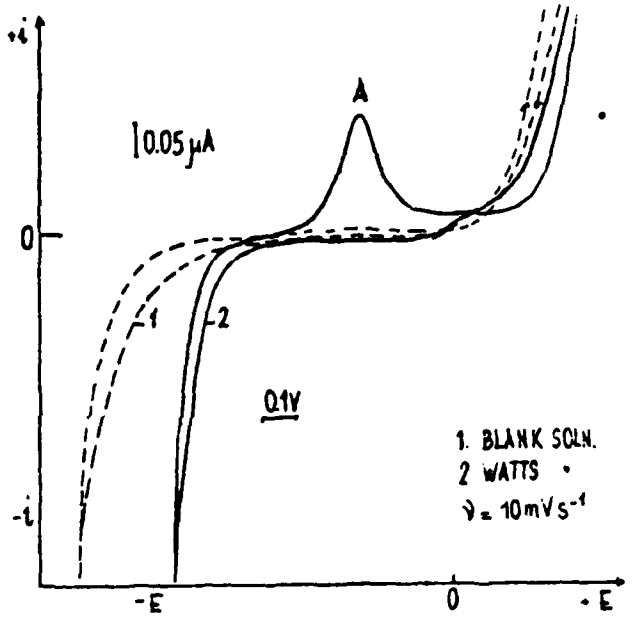

Fig. 1. C.v. curves of reduction/dissolution of Ni at Ni electrode from the Watts and from Watts soln, without Ni salts (blank)

The other Me investigated have similar behaviour as Nb. Fig. 3 represent the corresponding c.v. curves for Hf, Ta and Ti respectively. As it was noticed in the cathodic part of Ni deposition the potential does not vary significantly with the Me studied, and only the current after potential reversion from cathodic limit shows different tendency towards reaching the Ni/Ni(II) reversitble deposition potential. The Ni dissolution peaks, A_1 and A_2 appear at the same

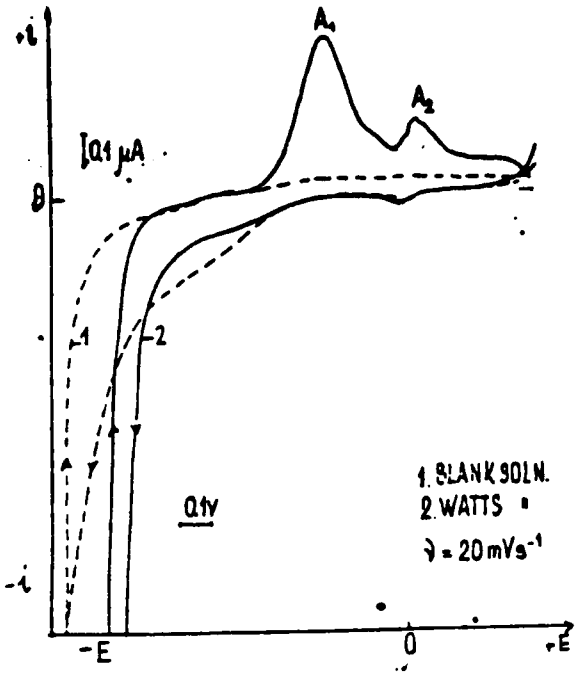

Fig. 2. C.V. curves of reduction/dissolution of Ni at Nb electrode from watts soln. and from Watts soln. without Ni salts (blank)

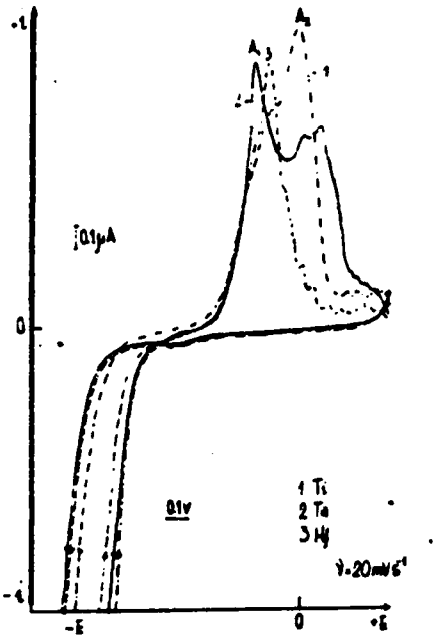

Fig. 3. C.v. curves of reduction/dissolution of Ni at Ti, Ta and Hf electrode from Watts solution

potentials in all investigated systems but the oxygen evolution has more significant influence on the peak A_2 in the case of Hf.

As the conclussion there could be assumed that the Ni deposit at at the various Me substrates shows two different states, suggested by the dissolution peaks A_1 and A_2. First of thise peaks represents the dissolution of Ni from the multilayer and the second from submonolayer deposti. The oxygen evolution in the presence of this later is somewhat negative in respect to the corresponding potential at the pure Me. Two different Ni states were not possible to observe in the cathodic current region because of the rather small sensitivity and very high Ni(II) ion conc. in the Watts solution.

REFERENCES

1. L. Brewer, Science, 161, 115 (1968)
2. L. Brewer and P.R. Wengert, Metall. Trans..4, 83 (1973)
3. M. Jakšić, Electrochim. Acta, 29 (11) 1539 (1984)

TITANIUM ANODES FOR THE CHROMIUM PLATING

M.G.Pavlović, V.D.Jović*, J.N.Jovićević**

Institute of Electrochemistry, ICTM, Beograd, Yugoslavia
Institute of Technical Sciences of the Serbian Academy of Science and Arts, Beograd, Yugoslavia

It is well known that the current efficiency for the hard chromium plating is very low (8-12%), because of codeposition of hydrogen. Also, mechanism of the electrodeposition of chromium from the chromium plating baths is still undefined, having in mind that deposited chromium is in fact an alloy of chromium, hydrogen and oxygen (0.25 - 0.50 wt. % of O_2)[1,2].

In this paper are presented results of the investigation of the influence of different anode materials on energy consumption and current efficiency during the process of hard chromium plating.

EXPERIMENTAL

All experiments were carried out in standard electrochemical cell. The characteristics of three different anode materials (Pb+5% Sb, Ti(RuO_2) and Ti(Pt-IrO_2)) were investigated by linear sweep voltammetry (LSV) and stationary potentiostatic techniques in the electrolyte containing 250 g dm^{-3} CrO_3 and 2.5 g dm^{-3} H_2SO_4. Ti(RuO_2) and Ti (Pt-IrO_2) anodes were made by baking rough titanium plates, which were coated by the solution of Ru, or Pt-Ir chlorides in an electric furnace on the temperature of 500°C.

RESULTS AND DISCUSSION

Typical LSV for the three investigated electrodes in the electrolyte used are presented in Fig. 1. (a) and (b). It is seen that the Ti(RuO_2) and Ti(Pt-IrO_2) electrodes catalysed both, reaction of hydrogen reduction and oxygen evolution, and that Ti(Pt-IrO_2) electrode is somewhat better for the evolution of oxygen in the range of higher current densities (Fig. 1(b)). It is also

** Materials Research Institute, Energoinvest, Sarajevo, Yugoslavia

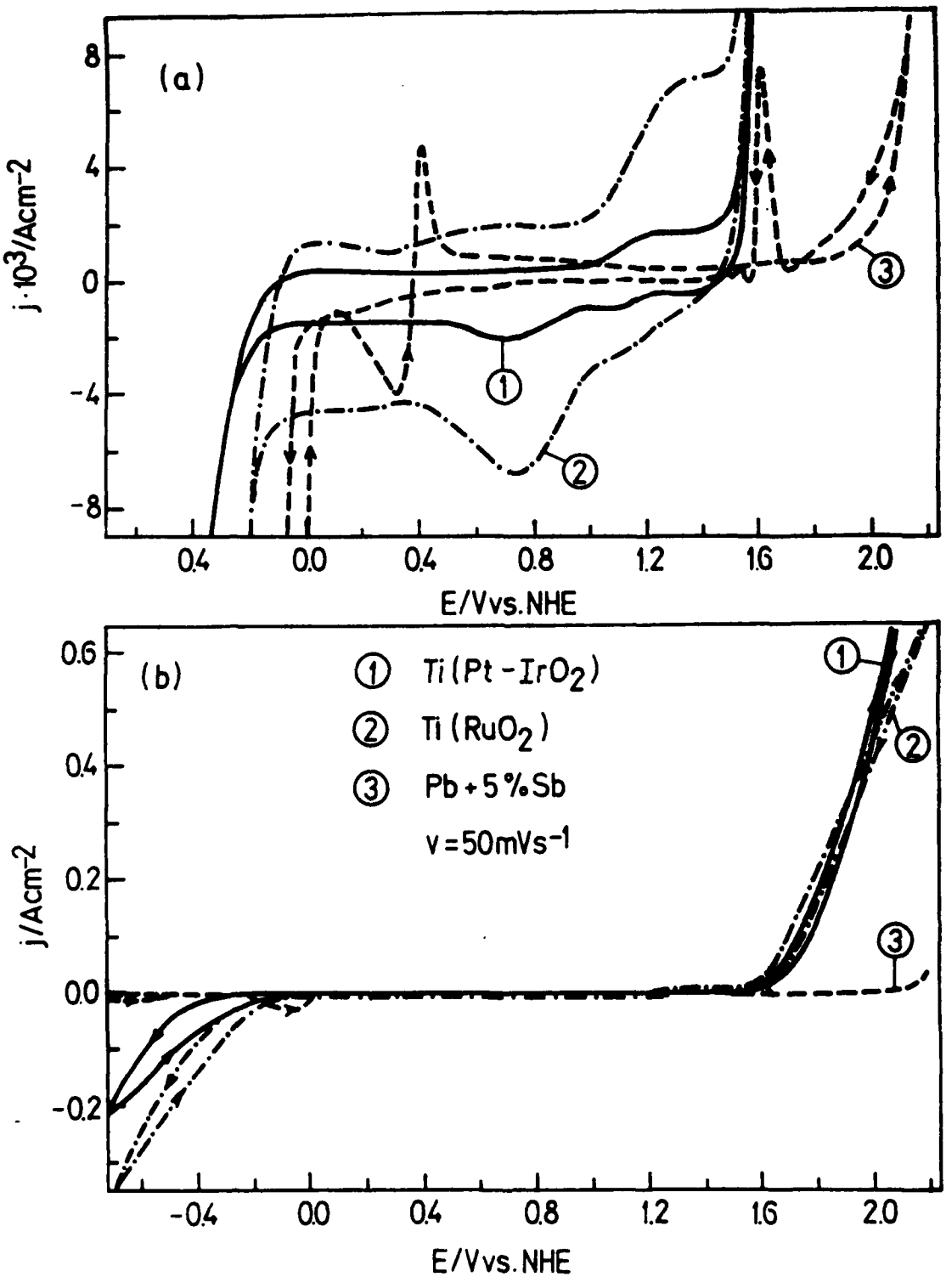

Fig. 1. LSV for the three different electrodes in chromium plating electrolyte

seen that voltammogram of Pb + 5% Sb electrode has very complex structure in the range of potential from 0.0 to 2,2 (V) vs. NHE, which is probably due to formation of different chemical compounds of lead with the components of solution and oxygen[3].

Polarization characteristics of three anodes used are presented in Fig. 2. It is seen that Ti(RuO_2) and Ti(Pt-IrO_2) anodes have much lower polarization in whole range of current densities and that this effect is more pronounced for high current densities, which is in good agreement with the LSV results. Under the long polarization Ti(RuO_2) anode become unstable and loses its good performances.

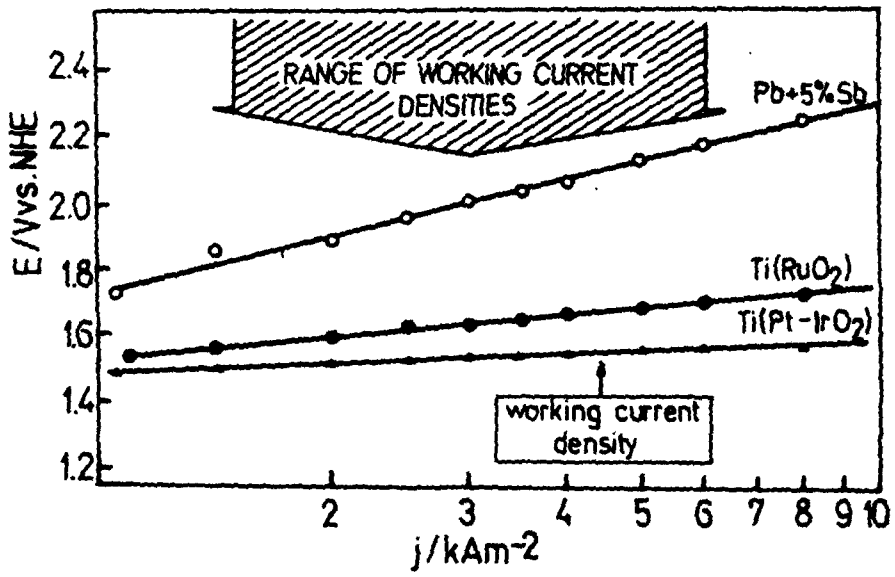

Fig.2. Polarization characteristics of three different anodes

Current efficiency of chromium plating also depends on the anode materials as it is seen in Table I.

Table I: Current efficiency of Cr plating, $j = 4.5\ kAm^{-2}$, $t=52^{\circ}C$

	Anode materials		
	Pb+5%Sb	Ti(RuO_2)	Ti(Pt-IrO_2)
Current efficiency	11.8%	12.0%	18.4%

References:

1. "Modern Electroplating", (edited by F.A.Lowenheim), Chapman and Hall, London(1974).
2. "Canning Handbook of Electroplating", E.and F.N.Son, London, 22nd Edition, (1978).
3. T.M.H.Saber, A.M.Shams El Din, "Electrochimica Acta", 13, 937(1968).

ELECTRODEPOSITION OF PLATINUM-RUTHENIUM ALLOYS

M.A.QUIROZ, I.GONZALEZ AND Y.MEAS.
Universidad Autónoma metropolitana-Izt. Dpto. Química
P.O.Box 55-534, MEXICO 09340 D.F.

The cathodic codeposition of various elements with the formation of metallic alloys or compounds, from aqueous electrolytic solutions has been the subjet of several studies, and has been known for several years[1]. The deposition potential is generally shifted to more positive values, with respect to the less noble metal, due to interactions between the components in the deposit, and this has been called "induced codeposition"[2]. The termodinamic fundaments of codeposition and the nature of the species which determine the potential have been studied in detail by Kröger[3].

In order to analyze the chemical species in the solution which determine the alloy codeposition potential, is necessary to take into account the electrochemical reaction represented by equation (1):

$$rM^{m+} + sN + rme^{-} \longrightarrow MrNs \ , \qquad (1)$$

where M^{m+} represents the less noble electroactive component of the system, and the potential for M/M^{m+} is expressed as:

$$E'_M = E^{\circ}_M + \frac{RT}{nF} Ln(a_M{}^{m+}) - \frac{\Delta G^{\circ}_{MrNs}}{rmF} \ , \qquad (2)$$

where $a_M{}^{m+}$ is the activity for M^{m+}, and ΔG°_{MrNs} is the free energy of formation for the MrNs alloys.

To produce the codeposition of the N^{n+} and M^{m+} ions to give the MrNs alloy, it must be accomplished that:

$$\frac{RT}{F} Ln|(a_M{}^{m+})^{1/m}/(a_N{}^{n+})^{1/n}| = (E^{\circ}_N - E^{\circ}_M) + \frac{\Delta G^{\circ}_{MrNs}}{rmF} \ . \qquad (3)$$

Being that $(E^{\circ}_N - E^{\circ}_M) > |\Delta G^{\circ}_{MrNs}/rmF|$, then the alloy will be formed only if $a_M{}^{m+} >> a_N{}^{n+}$. Thus, the deposition potential must be greater than E_M and lower than E_N. Therefore the activity of the M^{m+} metallic ion is determinant of the potential needed to produce the alloy.

In this work, we have studied the formation of Pt-Ru alloys using transient techniques. The analysis of the depositions and codepositions of Ru, Pt, and Pt-Ru was carried by means of sweep voltammetry, chronoamperometry, chronocoulometry, and the "quasi rest potential" variation.

Some of the experimental results obtained are shown in figures 1 and 2, and in table 1. The comparison between the i=f(t) and Q=f(t) curves, which are drawn at various potentials for solutions of Pt, Ru, and Pt-Ru, points out that both metals are forming an alloy. This may be justified by:

- The fact that the slopes of the Q vs $t^{1/2}$ curves (table 1) for the Pt-Ru systems are greater than those of Ru systems. This is indicative of a simultaneous deposition of Pt and Ru, thus Pt and Ru are forming an alloy, and this allows the former to deposit at potentials where the deposit of Pt does not occur.

- At more negative values of potential, where both metals are allowed to deposit, and at higher concentrations of Ru, the ratios of the Q vs $t^{1/2}$ slopes change, and this indicates that the characteristics of the alloy are dictated by the ratio of the Pt(IV) and Ru(III) activities at the interface[4].

REFERENCE

1.- A.Brenner, "Electrodeposition of Alloys", Vol.,1 and 2, Academic Press, New York, 1963

2.- A.Brenner, "Electrodeposition of Alloys", Vol.1,p78, Vol.2, p345, Academic Press, New York, 1963

3.- F.A.Kröger, J. Electrochem. Soc., 125, 2028 (1978)

4.- M.A.Quiroz, Tesis Doctoral

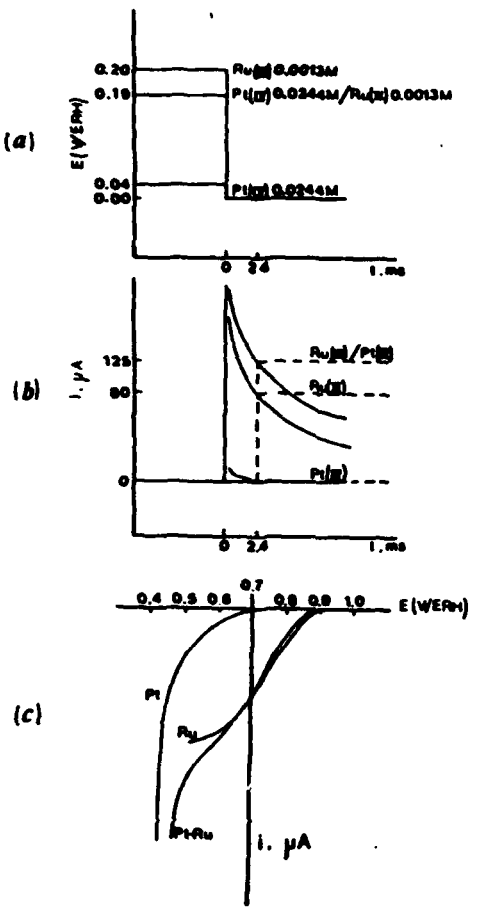

FIGURE 1

TABLE 1

SISTEM	Ein V/ERH	M4 0.70V	M7 0.55V	M8 0.50V
Ru(III) 1.3mM	0.900	5.39	15.78	15.31
Ru(III) 1.3mM/Pt(IV) 24.1mM	0.890	8.36	20.56	21.93
Ru(III) 2.6mM	0.900	9.73	17.61	18.41
Ru(III) 2.6mM/Pt(IV) 23.1mM	0.895	11.87	18.45	20.05
Ru(III) 3.9mM	0.900	10.71	23.12	23.09
Ru(III) 3.9mM/Pt(IV) 21.8mM	0.898	11.86	20.46	24.08
Ru(III) 5.2mM	0.900	17.07	35.21	37.77
Ru(III) 5.2mM/Pt(IV) 20.5mM	0.900	25.00	28.88	29.57

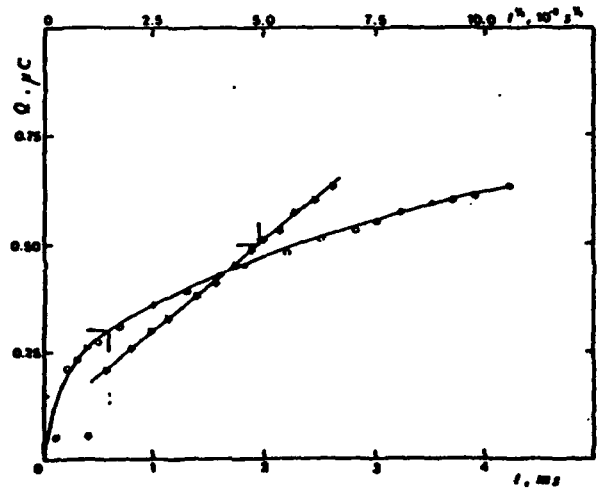

FIGURE 2

11082

ELECTROCHEMICAL REDUCTION OF CHROMIUM (VI) IN PRESENCE OF FLUORINE COMPOUNDS

B. POPOV, D. SLAVKOV and D. DRAŽIĆ*
Faculty of Technology and Metallurgy, University "Kiril and Metodij" Skopje
*Faculty of Technology and Metallurgy, 11001 Belgrade, Yugoslavia

The deposition of black chrome is generally done with conventional chroming bath free from sulphates, to which "catalyst" such as acetic acid, sodium nitrate, amonium methavanadate or fluorine compounds is added[1-5]. The exact mechanism by which the catalyst ions enable chromium reduction is still open to conjecture.

The purpose of the present work is to study the electrochemical reduction of chromic acid in the presence of fluorine compounds and to determine the electroplating conditions for obtaining selective absorbing surface.

All c.v. experiments were performed in a special plastic cell, because of the presence of fluorine ions. Working electrodes of Pt sealed into a glass tube with a geometric area $6{,}2 \cdot 10^{-3}$ cm^2 and a Pt mounted in a teflon holder with geometric area of $1{,}76 \cdot 10^{-3}$ cm^2 were used. The working electrodes were mechanically polished after each measurement. SCE was used as a reference electrode. Black chrome was electrodeposited from a solution containing 4,2 M CrO_3 and 0,05 M $BaCO_3$, in presence of fluorine ions. The fluorine compounds were added in the cathode compartment during the course of the run.

Rest potentials observed on Pt cathodes in chromic acid solution with fluorine ions additions are listed in Table(1). The rest potentials probably are mixed potential of the reduction of dichromate ion and oxidation of Pt. PtO are further reduced when the cathode is polarized at negative potentials.

Table(1)
Rest potential values obtained on Pt electrode in chromate solutions catalyzed by F^- ions, with respect to SCE

Solution	F^- Conc. (M)	E (V)
	0,024	1,043
	0,048	1,020
	0,078	1,025
$H_2Cr_3O_{10}$ 4M	0,115	1,015
	0,166	0,998
	0,261	1,010
	0,357	1,015

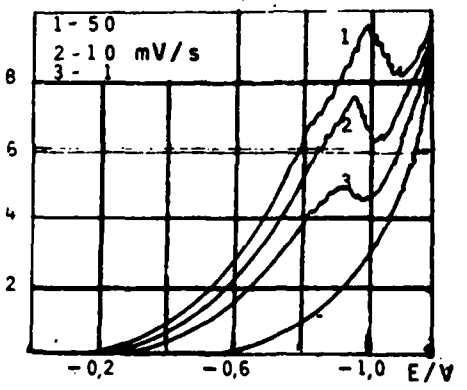

Fig(1) Typical c.v. curves

Fig(1) shows typical c.v. curves for electrodeposition of black chrome from pure chromic acid (4,2 M) in which only 0,05 M $BaCO_3$ was added. The curves were obtained at different sweep rates. $BaCO_3$ was added in order to precipitate $SO_4^=$ ions, present as impurities. The curves show the cathodic maximum at -0,98 V vs SCE, with strong evolution of hydrogen

at this potential. The peak current was found to increase with increasing the sweep rate, but this dependence was not found to be a linear function of the square root of the sweep rate, which suggest that this process is not diffusion controlled.

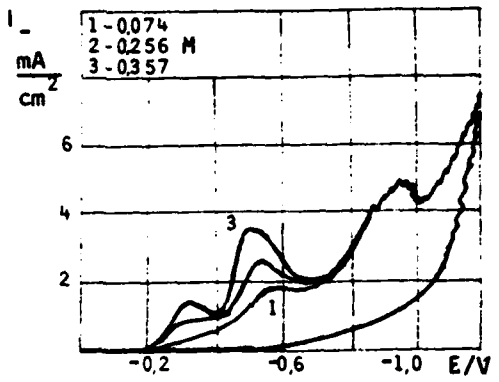

Fig(2) Cyclic voltammograms at different concentrations of fluorine ions

Fig(2) shows cyclic voltammograms at 0,02 V/s for electrochemical reduction of chromic acid at different concentrations of fluorine ions (from 0,074 to 0,357 M). In the presence of catalyst ions two more peaks appear for the reduction of chromic acid at -0,35 V and at -0,5 V vs SCE. It has been found that the peak at -0,35 V does not depend upon the concentration of fluorine ions, but it appears only at concentrations higher than 0,35 M. The cathodic peak current at -0,5 V vs SCE was found to depend on the concentration of fluorine ions (Fig 3), but is not a linear function of the square root of the sweep rate.

In table(2) are shown cathodic charges (C/cm^2) calculated by integrating the surfaces under the cathodic peaks at -0,5 V. The charges increase from $10,07 \cdot 10^{-3}$ C/cm^2 to $95,22 \cdot 10^{-3}$ C/cm^2. From the results obtained one can conclude that the catalyst ions have an accentuated influence only on the second reduction step of chromic acid. It was also found that in presence of fluorine ions the evolution of hydrogen decreases remarquably.

No deposit was found when chromic acid was potentiostatically electrolysed at -0,35 V and at -0,5 V. Black deposit was observed only at higher applied potentials (-1,1 V vs SCE) and the amount of the deposited material was found to depend on the concentration of fluorine ions.

Table(2)
Cathodic charges (C/cm^2) calculated by integrating surfaces under the peaks as a function of F^- ion concentration

C_{F^-} (M)	Q (C/cm^2)$\cdot 10^3$	Solution
0,024	10,07	
0,048	23,13	
0,072	23,13	
0,096	40,13	$H_2Cr_3O_{10}$ 4M
0,110	47,69	
0,144	70,35	
0,168	88,93	
0,192	95,22	

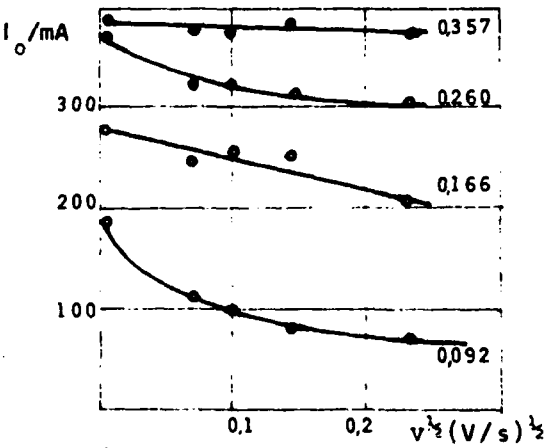

Fig(3) Variation of I_o with square root of the sweep rate

In order to determine the optimum operating conditions under which black chrome surfaces appear, spectral reflectance of spectrally selective surface of black chrome on nickel plated cooper have been studied as a function of deposition time. The following standard experimental conditions were used in preparing the samples for reflectancemeasurements: agitation of the electrolyte with nytrogen, temperature 295 K, current density 10 to 12 A/dm^2, cathode to anode ratio 1:1. A computer program for PDP-11 computer was used for calculation of the normal thermal emittance and the hemispherical absorptance from specular normal and hemispherical reflectivities in order to determine the selective properties of the electroplated black chrome coatings. Fig(4) shows the variation of the spectral reflectance. For the deposit obtained for 120 s $\hat{a}_S$ = 0,928 with $\hat{e}_T$(40 °C) = 0,1 and $\hat{a}_S/\hat{e}_T$(40 °C) = 9,28. For the deposit prepared at 50 s $\hat{a}_S$ = 0,80, $\hat{e}_T$ (40 °C) = 0,018 with $\hat{a}_S/\hat{e}_T$ (40 °C) = 4,4.

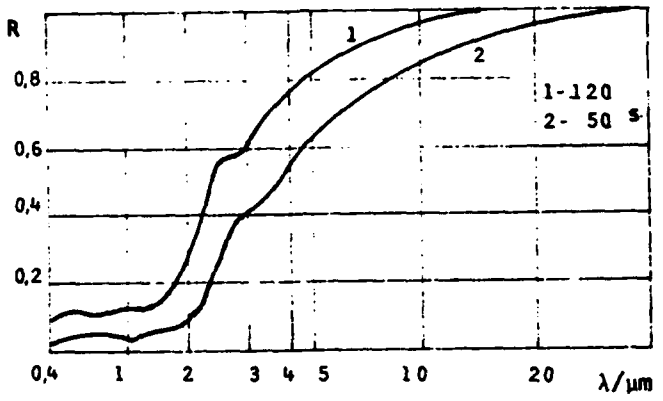

Fig(4) Spectral reflectance of black chrome coatings

References:
1. L.Sivaswamy, S.Gowry, B.A.Shenoi, Metal Finibing 72 (1974) 48
2. B.A.Shenoi, S.Gowry, Metal Finishing 71 (1973) 139
3. A.Ungeloenk, US Patent 1.975.239 (1934)
4. M.F.Quaely, US Patent 2.824.829 (1958)
5. G.E.McDonald, Solar Energy 17 (1975) 119

ELECTROCHEMICAL REDUCTION OF INDIUM (III) IN MOLTEN LITHIUM CHLORIDE-POTASSIUM CHLORIDE MELT

B. POPOV, D. SLAVKOV and H. A. LAITINEN*

Faculty of Technology and Metallurgy, University "Kiril and Metodij", YU

*Department of Chemistry, University of Florida, Gainesville Florida, USA

The instrumentation and equipment used in this study have been previously described [1-5].

Partial thermodynamic values in molten LiCl-KCl have been determined from 693 K to 813 K in the In concentration range of 0,016 M to 0,5 M. The study was made with cells of the type:

$$In|InCl_3,LiCl\text{-}KCl||LiCl\text{-}KCl,PtCl_2|Pt$$

In Fig(1) are ploted indium electrode potentials vs log concentration of indium (III) for five temperatures. The dependence is linear and the slopes determined are compared in Table(1) with the slopes calculated from the Nernst equation, assuming n=3.

Using the equation,

$$E_{Pt|PtCl_2||Cl^-|Cl_2} = -0,3223 + 0,00034(t - 450),$$

determined by Laitinen and Pankey[6], indium electrode potentials with respect to the platinum reference are normalized to the chlorine electrode, and obtained values are numerically the same as the potential difference for the cell $In|InCl_3,LiCl\text{-}KCl||LiCl\text{-}KCl|Cl_2$. The reaction corresponding to this cell is the formation of indium(III) chloride in solution. Partial thermodynamic quantities for the formation of $InCl_3$ in molten LiCl-KCl have been calculated and are listed in Table(2). The potential of indium electrode was ploted against temperature for fixed concentrations and values of $(\partial E/\partial T)_p$ were found for each concentration. Using these values the partial molar entropy was calculated, as shown in Table(2).

$InCl_3$-LiCl-KCl System - Chronopotentiograms of In(III) in molten LiCl-KCl were found to depend on the concentration of In(III). Qualitatively, a single chronopotentiometric wave occurs at a quarter wave potential of -0,81 V vs the Pt(II)|Pt reference electrode. The Sand equation was tested at five different In(III) concentrations. The transition time constant is independent

of 1, indicating that electrode process is diffusion controlled over the time interval investigated. The average value of the transition time constant is 545,48 $A \cdot s^{\frac{1}{2}} \cdot cm^3 \cdot mol^{-1}$. Based on analytical data n=3, the diffusion coefficient was calculated to be $1,81 \cdot 10^{-5}$ $cm^2 \cdot s^{-1}$. Only one product was observed for the reduction of In(III) at -0,81 V. The reduction product was analysed by standard procedures and was found to be pure indium.

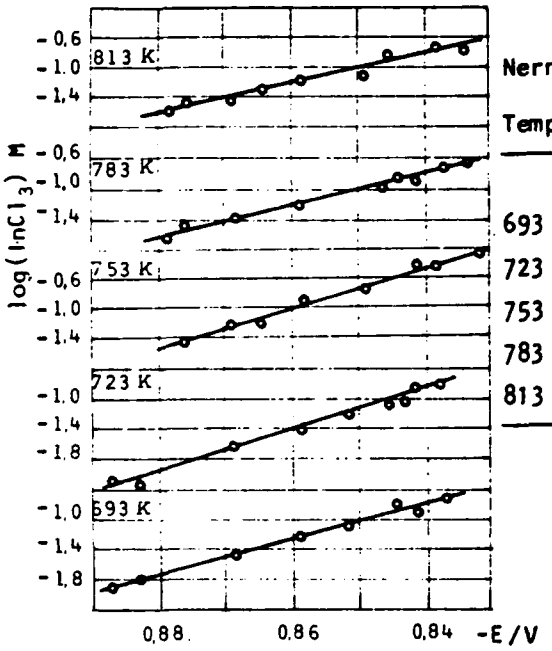

Fig(1) Potential of indium electrode with respect to Pt reference electrode

Table(1)

Nernst behaviour of the indium electrode

Temp. (K)	$(\partial E/\partial \log In^{3+})_T$ (V)	
	Calculated	Observed
693	0,0458	0,0490
723	0,0477	0,0450
753	0,0497	0,0468
783	0,0517	0,0481
813	0,0537	0,0522

In_2O_3-LiCl-KCl System - A single chronopotentiometric wave occurs at a quarter wave potential of -0,7 V vs the Pt(II)|Pt reference electrode. The transition time constant in the Sand equation has been calculated and was found to depend on I (Fig 2). There is a decrease in $I_0\tau^{\frac{1}{2}}/C$ with increasing current density which is generally a sign of a slow chemical reaction preciding charge transfer.

It was observed during the chronopotentiometric measurements that a volatile product evaporates from the melt, indicating that there is an acid-base reaction going on between In_2O_3 and chloride melt. In a non protonic solvent such as alkali halide melt, acid-base reactions can be conveniently considered in terms of the Lewis acid-base concept. Since alcaly metal ions have a relatively small ability to accept electrons, they will not ordinarily enter into acid-base reactions. On the other hand be-

cause halide ions can donate a pair of electrons, they act as a leveling base upon most heavy cations, forming metal halide complexes.

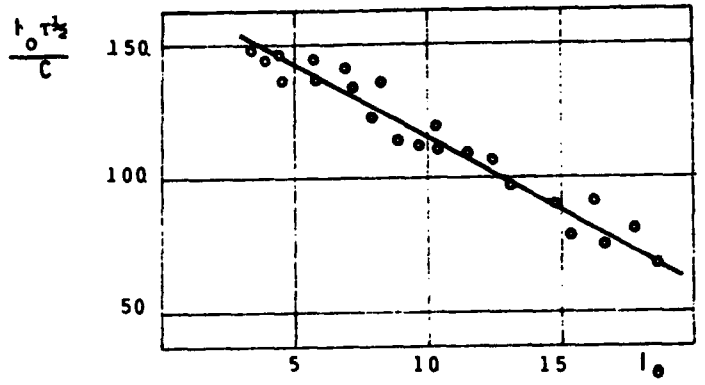

Fig(2) Variation of $I_0\tau^{1/2}/C$ with I_0 for the reduction of In_2O_3

In order to account for the observed chronopotentiometric and coulometric results for In_2O_3 reduction, the following acid-base reactions were considered between In_2O_3 and chloride melt preceding charge transfer:

$$In_2O_3 + 2Cl^- \rightleftarrows In_2O_2Cl_2 + O^{2-}$$

$$In_2O_3 + 4Cl^- \rightleftarrows In_2OCl_4 + 2O^{2-}$$

$$In_2O_3 + 6Cl^- \rightleftarrows 2InCl_3 + 3O^{2-}$$

Table(2)

Partial thermodynamic quantities for the formation of $InCl_3$ in molten LiCl-KCl

Conc. (M)	ΔG (J/mol)	ΔS (J/K)	ΔH (J/mol)
0,0165	-349.716	95,53	418.784
0,0405	-344.505	83,95	405.720
0,0645	-342.189	78,16	398.698
0,1650	-336.399	46,32	369.888
0,5020	-330.030	28,95	350.960

Samples of the electrode deposit were prepared by constant current electrolysis. The reduction product reacts with platinum cathode.

References:
1. B.Popov, H.A.Laitinen, J.Electrochem.Soc., 117 (1970), 482
2. B.Popov, H.A.Laitinen, J.Electrochem.Soc., 120 (1973), 1346
3. B.Popov, H.A.Laitinen, J.Electrochem.Soc., 122 (1975), 1616
4. B.Popov, Kem.Ind. 32(2) (1983), 65
5. B.Popov, H.A.Laitinen, ISE 33th Meeting, 1 (1982), 442
6. H.A.Laitinen and J.W.Pankey, J.Am.Chem.Soc., 81 (1959), 1053

APPLICATION OF CYLINDRIC SYSTEM WITH A ROTATING ELECTRODE FOR INVESTIGATION OF THE SILVER TRANSPORT PHENOMENA DURING COPPER ELECTROREFINING

J. HOTLOŚ and M. JASKUŁA
Department of Physical Chemistry and Electrochemistry
Jagiellonian University, Cracow (Poland)

A simple theoretical model describing quantitative transport of silver ions to the cathode during copper electrorefining was proposed in the previous paper.[1] The influence of such parameters as electrolyte composition, overvoltage, current density and electrolyse time on silver contents in bath and in cathodic deposit was taken into account.

This model was used to describing of electrolysis results obtained in the system of two vertical copper electrodes without stirring of electrolyte.[2] The high initial concentrations of silver ions (0.5-12ppm) used in experiments correspond to case of their reduction not only on the cathode but also on the anode, and to decrease their concentration in bath. The model foresees also the possibility of increase of Ag^+ ions concentration in the electrolyte however, the execute of this case requires very low initial Ag^+ concentrations or high overvoltages. Then it is possible to obtain information concerning the dissolution of silver contained in anodes. According to the paper[2] application of a system with forced convection having the better defined transport conditions should improve accordance of the obtained results with the theoretical model.

EXPERIMENTAL

In this work the system of coaxial cylinders was used to investigation of silver transport. The rotating inner cylinder made from synthetic copper-silver alloy (silver contents 0.1-0.7 weight%) or from industrial black copper (0.27%Ag) was an anode. The external motionless cylinder from stainless steel was cathode (Fig.1).

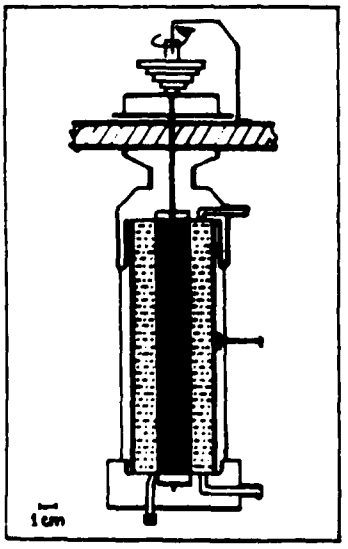

Fig.1.

Schematic representation of the concentric cylinder reactor.

The constants of transport rate of silver ions $k=D/\delta$ to cathode as well as to anode described as the functions of rotation speed for this system, were determined in other investigations. For rotation speed v=545 1/min used in silver transfer measurements they are: $k^a=2.94*10^{-3}$ cm/s and $k^c=1.47*10^{-3}$ cm/s respectively. It should be noticed that the transport rate towards the cathode was higher due to greater cathode surface ($S^c=212$ cm^2, $S^a=76$ cm^2).

The 230 ccm of electrolyte containing 100 g/l of H_2SO_4 and 50 g/l of Cu^{2+} was used for each experiment. The electrolyte was previously carefully desilvered by shaking with copper powder. The electrolysis were carried out at the room temperature and at constant charge of 10800 C (current 1-10 A). This charge provided minimal amount of cathodic deposit necessary to analyse and on the other hand the amount of slime forming on the anode was negligible.

The silver contents in cathodic deposit and in the electrolyte were measured by AAS method.

RESULTS AND THEIR INTERPRETATION

The average silver contents in electrolyte after shaking with copper powder were about 0.1 ppm and have not changed (in the limit of error) during electrolysis. The equilibrium concentration of silver ions in the used bath in contact with metallic copper was 0.0015ppm. Therefore it is assumed that most analytically determined in electrolyte silver is the metallic silver (subtle suspension, slime?) formed during cementation, and the ionic silver takes its equilibrium concentration.

The obtained cathodic deposit was divided into 12 parts from which 6 were independently analysed. In the emphatic majority of analysed probes the silver contents were below the limit of sensitiveness of the AAS method (0.06ppm) that allowed to assess that the silver contents in cathode are no greater then about 4.8ppm. In a few cases the greater amount of deposit was analysed and it was determined that silver contents in the cathode occured in the range from 1.9 to 4.8 ppm.

Assumed the higher value of silver contents (4.8ppm) and that all silver founded in the cathode is coming from the reaction of reduction of silver ions which takes place at limiting current, it was calculated that the average concentration of Ag^+ ions in bath during electrolysis must be no greater then 0.005 ppm for longest electrolysis (10800 s) and no greater then 0.03 ppm for shortest electrolysis (1350 s).

It should be stressed that the value of 0.005 is relatively close to the equilibrium concentration and for this case it is possible to estimate what the upper limit of amount of silver in the ionic form transferred from anode into solution is.

Assuming that the only source of ionic silver is anode (and neglecting the possibility of the cementation reaction in the bulk), according to the previously described mathematical model the results for longest electrolysis (10800 s) were interpreted: for average silver ions concentration in the bulk obtained $c^b=0.0065$ppm, and for surface concentration at the anode $c^{sa}=0.012$ppm (that corresponds to overvoltage of $\eta_a=53$ mV). This is illustrated on Fig.2.

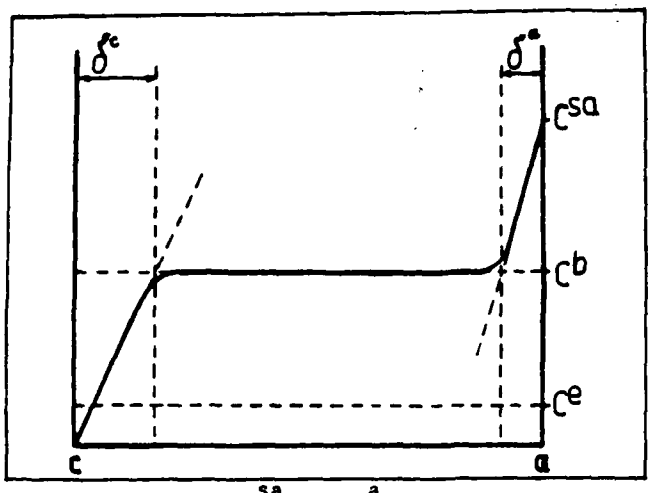

Fig.2.

Schematic diagram of Ag^+ ions concentration distribution in the reactor (profile at time t=10800 s)

From values c^{sa} and k^a estimated the upper limit of the flux of ionic silver from anode as no greater as $8.1*10^{-6}$ μg Ag/cm²s (~0.29 mg Ag/m²h). For electrolysis at higher current densities the greater sources may be expected and for current of 7A, the value of 1.8 mg Ag/m²h was obtained. These results demonstrate that the flux of ionic silver from an anode into the bulk is insignificant. It is also independent on the kind of used anode and its silver contents. It leads to the conclusion, that the considerable silver contents in cathodes observed in an industrial practice are due to transfer slime rich in silver.

If even a short-lived anode passivation occures then this situation changes radically. The silver contents increase then many times and may range 2 ppm in bulk and more then 200 ppm in cathode. Our observations show that the contribution of slime-transport is in this case significant.

REFERENCES:

1. J. Hotloś and M. Jaskuła, Ext.Abstr.31.ISE, Venice 1980, G24, pp.849 - 851.
2. J. Hotloś and M. Jaskuła, Ext.Abstr.32.ISE, Dubrovnik 1981, pp.1097-1100.
3. J. Hotloś and M. Jaskuła, J.Appl.Electrochem., 13,173 (1983).

ON THE ELECTRODEPOSITION OF CARBON FROM $NaF-AlF_3$ MELTS SATURATED WITH ALUMINIUM CARBIDE.

R. ØDEGARD, A. STERTEN AND J. THONSTAD

Laboratories of Industrial Electrochemistry, and SINTEF,
The Foundation of Scientific and Industrial Research
at the Norwegian Institute of Technology,
N-7034 Trondheim-NTH, Norway.

Two subjects related to solutions of aluminium carbide in $NaF-AlF_3$ melts were studied:

1) The equilibrium concentration of dissolved aluminium carbide in $NaF-AlF_3$ melts.

2) The electrodeposition of carbon from aluminium carbide saturated melts.

Solubility. In the solubility experiments a graphite crucible with a close fitting graphite lid, containing 140g of molten salt and 25g of aluminium, was placed in the isothermal zone of a vertical Kanthal furnace with argon atmosphere. During a holding time of 5-6 hrs at temperature, aluminium carbide was formed by reaction between aluminium and the graphite crucible, saturating the melt. After removal of the lid a melt sample (3g) was taken with a steel ladle that was lowered from the cold part of the furnace. The aluminium carbide content of the sample was determined from the volume of $CH_4(g)$ evolved by treatment with a 10% HCl solution. The hydrolysis apparatus was similar to that described by Rogers et al.[1].

Fig. 1. shows the concentration of dissolved aluminium carbide as a function of the NaF/AlF_3 molar ratio (CR) at 1020°C. The full line represents the best fit for a model based on the equation

$$Al_4C_3(s) + 5AlF_3(diss) + 9NaF(l) = 3Al_3CF_8^{3-} + 9Na^+ \quad (1)$$

Activity data for AlF_3 and NaF given by Sterten and Mæland[2] were used in the calculations.

Dewing[3] has previously measured the solubility of aluminium carbide in $NaF-AlF_3$ melts for $1.6<CR<4.5$, as shown in Fig.1. The present data, although higher in carbide concentration, are in fair agreement with those of Dewing. Because Dewing's measurements were not extended to low CR's, the concentration peak shown in Fig.1 was not detected. The broken line in the figure is our representation of Dewing's data.

Electrodeposition of carbon. It was found that carbon could be electrodeposited by electrochemical oxidation of dissolved aluminium carbide. Voluminous deposits were obtained on electrodes made of graphite, vitreous carbon, iron, tungsten and platinum. The carbon deposit was found to be amorphous by x-ray diffraction analysis.Based on the weight loss when burning the carbon deposite the number of electrons exchanged pr mole of deposit was calculated to be ~4 when assuming 100% current efficiency for the deposition reactions.

Fig. 2 depicts carbon deposits on iron, vitreous carbon and tungsten electrodes. Similar anodic deposits were obtained by Morris and Harry[4] in LiCl-$CaCl_2$ melts containing dissolved CaC_2.

In Fig.3 is shown an example of potential decay curves recorded in carbon deposition experiments. A constant current of 5A (~0.5 A/cm^2) was disconneted at time zero. The potential difference between an aluminium electrode and a vitreous carbon electrode with carbon deposits on it was recorded. The potential plateau which is clearly visible in the figure, corresponds to an aluminium carbide formation cell. The semi-stable potential was +127 mV versus the aluminium electrode. This gives $\Delta G^o(Al_4C_3)$ = - 35.108 kcal/mol at the temperature of the experiment (1013°C). The interpolated JANAF[5] data is $\Delta G^o(Al_4C_3)$ = - 34.166 kcal/mol at that temperature. The difference is within the limits of error indicated in JANAF.

References:

1: Rogers, P.S., Bevan, D.J.M. and Tomlinson, J.W., Microchim. Acta 12, 1839 (1956).

2: Sterten, A. and Mæland, I., Acta Chem. Scand., A39 (1985). In print.

3: Dewing, E.W., Trans. Met.Soc. AIME 245, 2181 (1969).

4: Morris, D.R. and Harry, J.R., Proceeding of the Int. Conf. Ind. Carbon and Graphite (Society of Chemical Industry) London, 1965, p.36.

5: JANAF Thermochemical Tables, 2.ed., Dow Chemical Co., Midland, Michigan, 1971.

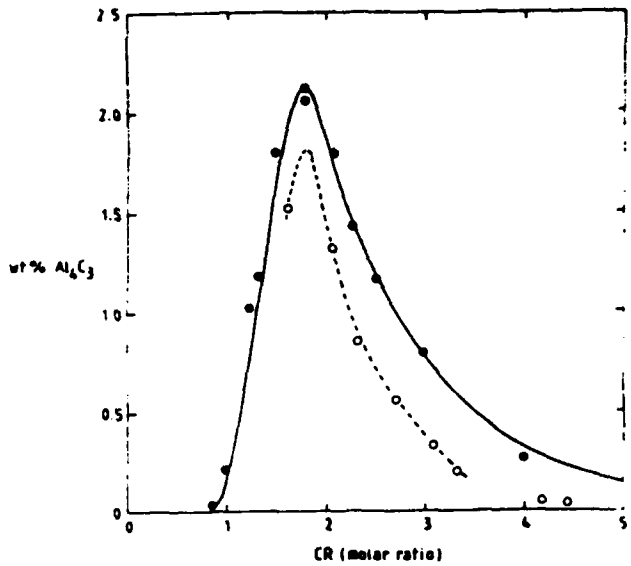

Fig.1.
Concentration of dissolved aluminium carbide as a function of the NaF/AlF_3 molar ratio (CR) at 1020°C.
● - present work;
○ - Dewing[3]. The full line represents the model given by equation (1).

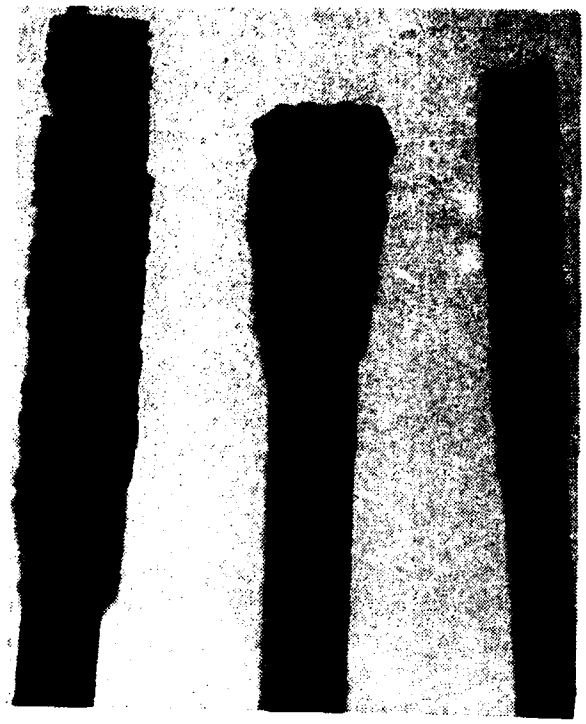

Fig.2.
Electrodeposited carbon on electrodes of:
1: iron, 2: vitreous carbon and 3: tungsten.
Melt composition:
CR = 1.50,
temperature: 1000°C,
total current: 1-5 A.

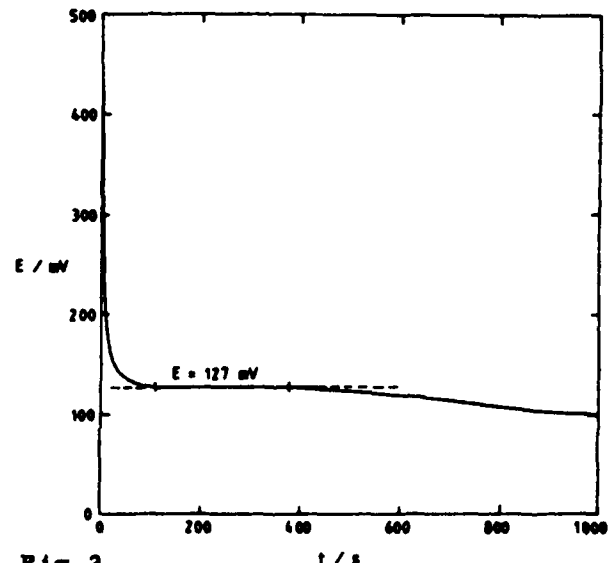

Fig.3.
Potential decay curve in a carbon deposition experiment. The potential of a vitreous carbon electrode with carbon deposit was measured versus an aluminium electrode. At t<0, I = 5A (0.5 A/cm^2).
Temperature: 1013°C, CR = 1.50.

A SIMPLE LINEAR THERMODYNAMIC MODEL OF ZINKOXIDE CHARGING AND DARK DISSOLUTION

O.FRUHWIRTH, G.W. HERZOG,
Institute of Inorganic Chemical Technology, Technical University of Graz, Austria
J.POULIOS, present adress:
Laboratory of Physical Chemistry, Aristotelian University of Thessaloniki, Greece

The dissolution rate of ZnO and the flatband potential display a linear pH dependence. The aim of this work was to find a simple model, which could explain phenomenologically this behavior, first observed by Lohmann[1] and Hauffe et al.[2], but not yet interpreted on a common basis. Furthermore this model should give an explanation of the linear pH dependence of the photocurrent, when ZnO is illuminated with 365 nm light (bandgap) and is decomposed by holes.

The model is based on irreversible thermodynamics originally developed by Prigogine[3] and on splitting the electrochemical energy term into an electrical energy part connected with double layer charging and the chemical potential which is connected with H^+ or OH^- concentration.

The common electrochemical model for dark dissolution rates of oxides in acidic solution, given by Engell[4] and improved by Vermilyea[5], is based on transfer control of the lattice ions of the dissolving oxide. For the rate of dissolution of hydroxides or oxides this gives a power law of the form (1).

(1) $$v = n_+\vec{k}_+\left(\frac{n_-\vec{k}_-c_{H^+}}{n_+\vec{k}_+}\right)^{\frac{\alpha_+z_+}{\alpha_-z_- - \alpha_+z_+}}$$.

By simplification through $\alpha_+ = \alpha_-$ and $z_+ = z_- = 2$ a proportionality of the rate v with $(c_{H^+})^{\frac{1}{3}}$ result.

For the dissolution of oxides Vermilyea discussed some cases with different first step of reaction leading to

$v \sim (c_{H^+})^{\frac{1}{3}}$, **first** step: hydration of ZnO or adsorption of H^+ with saturated sites n_{OH^-} at the interface

$v \sim (c_{H^+})^{\frac{1}{2}}$, **first** step: reaktion of O_2^- with a proton to OH^- and then in a fast step with a second proton to H_2O.

$v \sim c_{H^+}$, first step: two protons react with O_2^- to water or the adsorption of H^+ with nearly empty $n_{OH^-} \sim c_{H^+}$.

Only the last two cases show the practically measured dependence on pH with the above mentioned restrictions but without an explanation for the linear potential - pH dependence.

From Prigogine's law of irreversible thermodynamics follow directly linear relations of the dissolution rate on pH and potential. These laws hold for reactions near equilibrium, or if a chain of reactions is composed of single steps beeing in a quasi stationary state and each of them not far from equilibrium. If the overall reaction for the dissolution of ZnO in the dark is thought to be composed of the following successive steps (3) the linear irreversible thermodynamics gives for the reaction rate the electric current for charged species.

(2) $ZnO + 2\,H^+ \longrightarrow Zn^{++} + H_2O$

(3) $ZnO_s + H^+ \longrightarrow ZnO.H^+_{ads} \longrightarrow Zn^{++} + OH^-$

(4) $$v = -\vec{v}\frac{\Delta G}{RT} \quad \text{or} \quad i = -\vec{i}_0\frac{\Delta\eta}{RT}$$

By splitting $\Delta\eta$ into the chemical energy $\Delta\mu$ and the electrical part $zF\Delta\gamma$ and after insertion of the concentration dependence of μ and of the dissolution current (5), taking the charge with z=1 for the first step in (3), we yield the measured linear relation (6):

(5) $$i_0 = -zF\left(\frac{dn}{dt}\right)_0 = zF\cdot\vec{k}\cdot(c_{H^+})_0$$

(6) $i = -\frac{F}{RT}\vec{k}\,(c_{H^+})_0\,[F\Delta\Psi + \Delta\mu^0_{ads} + 2{,}3RT\ pH]$

$\vec{k}$: forward rate constant under pure kinetic control

$(c_{H^+})_0$: equilibrium proton concentration with a constant surface coverage of H^+ assuming constant activity of the surface

An analogous treatment of the second step in (3) leads to a similiar equation but with a Zn^{++} dependent term:

(7) $i = -\frac{F}{RT}\vec{k'}\,[F\Delta\Psi + \Delta\mu^0_{des} - 2{,}3RT\ (pOH - pZn)]$

If we postulate in (6) one limiting case for an insoluble oxide with i = 0 the equation (8) with the pH independent terms collected in A follows.

(8) $\Delta\Psi = A - \frac{2{,}3RT}{F}\,pH$

This means that if all charges contribute to the oxide/solution interface the potential difference between oxide and solution is proportional to pH. This first was observed by Lohmann[1] for ZnO single cristals when he measured the flatband potential by capacity measurements under pH variation.

The other limiting case of (6) demands an unpolarisable oxide where all charge is transfered and contributes to dissolution. In equation (9) the slope corresponds to the chemical rate konstant and the proton concentration at equilibrium. This case seems to be predominant in Hauffe's[2] dissolution experiments with small polarisation of the ZnO crystal.

(9) $i = B - 2{,}3\,(c_{H^+})_0 \cdot \vec{k} \cdot pH$

In praxis most cases will be found between these extremes, that means, charging of the oxide interface to some extent of potential where the dissolution of the lattice decomposition get dominant, when no potentiostat is applied.

Under illumination the anodic photocurrent of ZnO shows a linear dependence on pH too, though another mechanism of dissolution has been postulated by Gerischer[6] working with photogenerated holes and by Morrison[7] a water oxidation reaction via holes has been introduced.

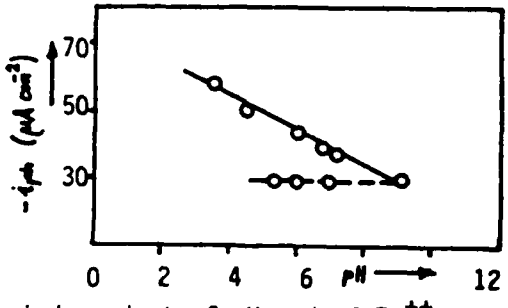

In figure 1 the pH dependence of the photocurrent of a Zn doped ZnO single crystal is shown without and with Zn^{++} saturation in the elektrolyte.[8] Because of the restricted dissolution when saturation of Zn^{++} is provided, we assume that the photocurrent in this case must belong to water oxidation.

(10) $H_2O + p^+ \longrightarrow 1/2\ H_2O_2 + H^+$

With saturation the photocurrent is independent of pH and of Zn^{++} and contributes to a ground level in the other case. When Zn^{++} concentration in the elektrolyte is far from saturation and no transport limitations are observed at the RDE the observed total photocurrent is linearly pH dependent. The additive photocurrent should belong to the ZnO lattice decomposition via holes and proved to be proportional to the incident light intensity.[9]

(11) $ZnO + p^+ + H^+ \longrightarrow 1/2\ H_2O_2 + Zn^{++}$

For this overall reaction the first step in the thermodynamic model of (3) is postulated to govern the other steps and therefore this model should hold, resulting in a linear i_{ph}/pH dependence, which is shown in fig.1 or in a linear dissolution rate expressed through equation (6) or (9) but with a somewhat different equilibrium term $(c_{H^+})_0$.

The photocurrent is independent of Zn^{++} concentration at each pH of investigation though it is different in value and higher than the basic current

with saturation of the Zn^{++} cation. This behavior is shown in fig.2 and can only be the case if the concentration dependent step in (3) is not dominant.

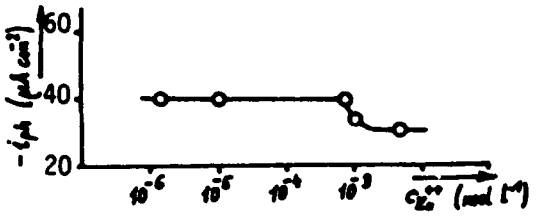

The dissolution rate control by Zn^{++} or OH^- desorption would give a dependence of the form of equation (7) but has not been observed hitherto. In buffered solutions, where no H^+ or OH^- diffusion limitation takes place, the Zn^{++} dependence would cause a decreasing rate with time because of enrichment of the dissolving cation in the solution.

Conclusion: Below the isoelectric point at pH≈ 9 in dark for ZnO the surface get charged positively by adsorbing protons when the oxide is immersed into the aqueous solvent. If thereby the pH of the solution changes, the flatband potential changes too.

If on the other hand the pH is fixed by buffer solution or the external potential difference is fixed by potentiostat, the adsorbing protons will raise the dissolution rate. Both cases may be qualitatively described as limits of the equation (6), which has been derived by irreversible thermodynamics.

The illuminated ZnO surface ($h\nu > E_g$) will be decomposed by holes faster than in the dark. The rate of this photodecomposition depends linearly on pH when the generation of holes is sufficient. The absence of an influence of the Zn^{++} concentration below the IEP favors a mechanism the first step of which can be described by the thermodynamic modell too.

This is not the case for the water oxidation by holes on the illuminated ZnO surface which proceed in the whole pH region up to the iep and is controlled by the photon flux too, but not by H^+ or Zn^{++} concentration.

Acknowledgement

This work was supported by the Fonds zur Förderung der wissenschaftlichen Forschung in Österreich.

References

1) F.Lohmann, Ber.Bunsenges.physik.Chem. 70(1966)428
2) H.Erbse,K.Hauffe,J.Range, Z.phys.Chem.NF 74(1971)248
K.Hauffe,J.Range,K.Volenik, Ber.Bunsenges.physik.Chem. 74(1970)286
3) I.Prigogine, Introduction to Thermodynamics of Irreversible Processes, Interscience Publ., N.Y.,1967
4) H.J.Engell, Z.phys.Chem.NF 7(1956)158
5) D.A.Vermilyea, J.Electrochem.Soc. 113(1966)1067
6) H.Gerischer, J.Electroanal.Chem. 82(1977)133
7) S.R.Morrison, The chemical Physics of Surfaces, Plenum N.Y.,1977
8) J.Poulios, Thesis: Technical University Graz, 1982
9) O.Fruhwirth,G.W.Herzog,J.Poulios, Surf.Technol., 24(1985)1063

ELECTROLESS DEPOSITION OF Ni-P THIN FILMS ON CERAMIC SUBSTRATES

M. FERNANDEZ, J.M. MARTINEZ-DUART and J.M. ALBELLA
Instituto de Física del Estado Sólido, CSIC and
Departamento de Física Aplicada. Universidad
Autónoma, Cantoblanco. Madrid 28049 (Spain)

Electroless deposition of nickel films has been widely used for different purposes. Specifically, the deposition methods based on the chemical reduction of a nickel salt by sodium hypophosphite has attracted a great interest for the preparation of electrical resistors as well as for other electronic devices[1,2]. This fact is due to the phosphorous incorporation into the nickel films coming from the electroless bath. It has been shown[2] that the phosphorous concentration in the deposited film has a strong influence in some of their physical properties, such as in the electrical resistivity or in the contact resistance of the metal/semiconductor interfaces. In the present work, we have investigated the deposition conditions of the electroless nickel films grown onto ceramic substrates from a typical hypophosphite solution in order to obtain good quality thin film resistors.

The basic electrochemical reactions taking place during electroless Ni deposition from a hypophosphite solution are:

$$Ni^{2+} + H_2PO_2^- + H_2O \rightarrow Ni + 2H^+ + HPO_3^- \qquad (1)$$

and

$$H_2PO_2^- + H_2O \rightarrow H_2PO_3^- + H_2 \qquad (2)$$

both reactions occurring simultaneously. The reaction (1) gives rise to the nickel reduction and to the formation of H^+ ions. The presence of these H^+ ions during the chemical reaction diminishes the nickel deposition rate[3], which becomes practically zero when the solution pH falls below a value about 3. In order to keep constant the deposition rate alkaline reagents as well as other stabilizing compounds were added to the electroless solution. The final composition of the solution was: nickel sulfate, sodium hypophosphite, ammonium chloride, sodium citrate, acetic acid and fixed amounts of ammonia to control the solution pH to a predetermined value.

Table I reports the results concerning the effect of the pH and temperature of the solution on the deposition rate of the nickel deposits onto the ceramic esteatite substrates. From this data, it can be observed that for a given temperature, the deposition rate increases with the solution pH. Within the considered pH range, the deposition rate follows an exponential law according to the equation: $v = a \exp(b(pH))$, with $a = 0.64 gr\ cm^{-2}\ min^{-1}$ and $b = 0.22$.

TABLE I

DEPOSITION RATE FOR SEVERAL TEMPERATURES AND pH OF THE ELECTROLESS BATH

Temperature (°C)	pH	Deposition rate (gr cm^{-2} min^{-1})
20	8.2	40.0
20	7.0	21.8
20	6.2	11.7
20	5.0	6.4
20	4.0	3.3
20	3.4	1.8
44	5.0	43.0
60	4.0	52.4
60	3.4	27.3

Due to this effect, the deposition rate becomes very slow in the low pH ranges. However, as it can be appreciated from table I an increase in the temperature up to 40° or 60° C may partially compensate the decrease in the deposition rate, making it possible to work with acid solutions. Thus, by means of an apropiate selection of both controlling parameters, pH and temperature of the solution, a wide range of film characteristics can be obtained.

We have made use of these posibilities in order to deposit films in a wide range of the resistance values and with a very low temperature coefficient of the resistance (TCR).

Samples with a constant film thickness has been prepared varying the solution pH between 3.4 and 8.6 at different temperatures. The phosphorous content of the films has been analysed by colorimetric methods dissolving the films in nitric acid and complexing the phosphorous with the Duval B reagent. It has been observed that the phosphorous concentration of the films decreases almost linearly from 11% to 5% when the pH of the solution increases in the above mentioned range. Simultaneously the measured TCR of these films decreases from 800 to 100 ppm $°C^{-1}$. These results confirm the strong correlation existing between the phosphorous content and the TCR of the resistive films. A discussion of the conduction mechanism and the influence of the structural characteristics of the film deposits will be also presented.

References

1. J. Dearden, Electrocomp. Sic. Techn. 3, 103 (1976).
2. B.K. Singh and R.N. Mitra, J. Electrochem. Soc. 127, 2578(1980)
3. P. Parikh and A. Subrahmanyam. Res. Ind. New Delhi 15, 157 (1970).

THROWING POWER AND CATHODE EFFICIENCY STUDIES OF GOLD PLATING ELECTROLYTES USED IN PRINTED CIRCUITS AND ELECTRONICS

E. JULVE
Departement of Physical Chemistry.Faculty of Sciences.
Universidad Autônoma de Barcelona(Bellaterra). Spain.

INTRODUCTION

Although alkaline-cyanide electroplating gold baths have a good cathode efficiency and produce good gold coatings,unfortunately they attack both the laminate and adhesives used in copper foil bonding of printed circuits.So,it is necessary to provide a plating system that does no attack these matherials and give uniform distribution of gold deposits on basis,with a suitable thickness and desirable brightness.The acid gold plating systems are able to accomplish these conditions.So,in the present work we have studied several acid gold electrolytes and comparisons have been made between them after adding several organic compounds to improve the uniform distribution of gold deposit and its quality.In order to achieve perfect distribution a suitable way can be to create a certain conditions on the gold plating solutions so that the cathode efficiency falls with increasing current density.Thus, if at 0.001 A/cm^2 the cathode efficiency is,for instance,30% and at 0.003 A/cm^2 the cathode efficiency is,for instance,10% ,then,providing that the cathode efficiency/current density relationship is non linear, uniform gold thickness can be obtained when plating between these limits of current density. In this work attention has been paid to the phenomenon of throwing power and gold coating distribution.To this end comparisons were made between various types of gold plating systems,using Hull cell tests.Haring-Blum cell tests and cathode efficiency measurements.

EXPERIMENTAL

a) Electrolytes : The acid electrolytes studied were prepared from a gold salt: potassium cyan-aurate(I), to which a phosphate-citrate buffer plus a metal complex and several organic compounds(as brighteners) were added.These compounds were incorpored to the electroplating bath in order to increase the bulk density of the electrolyte,modifie the buffering power and modifie,also,polarization characteristics.The gold in the bath was controlled by periodic analysis,replenishing it with the gold salt $K[Au(CN)_2]$ when necessary.The compounds of different types added to the electroplating aqueous basic solution were the following:

Bath(1): Cobalt complex(CoK_2EDTA)(0,5-10 g/l) as brightener grain refiner.

Bath(2): Nickel complex(NiK_2EDTA)(0,5-10 g/l) for the same purpose.

Bath(3): organic brightener class 1: tetraethylenepentamine(1-10 g/l).
Bath(4): CoK_2EDTA (0,5-10 g/l)+ tetraethylenepentamine(1-10 g/l).
Bath(5): NiK_2EDTA (0,5-10 g/l)+ tetraethylenepentamine(1-10 g/l).
Bath(6): NiK_2EDTA (0,5-10 g/l)+ organic brightener class 2: a condensation product of potassium ethyl-xanthate reaction with the acrolein (0,5-10 g/l) and finally neutralisation of bath to the operating pH with KOH.

b) Hull cell Measurements : The cell volume was 267 cm^3, the anode was a platinised titanium sheet and the cathode(panel) size was:10×5,7 cm(total)(área submerged: 50 cm^2).Rod agitation(2 m/min) in front of cathode was used.The measurements were made under the following conditions : current: 1 A ,temperature: 30°C(or as stipuled in the experiment),pH: 4.5 (or as stipuled in the experiment).Gold electrodeposited thickness was measured with a "Coulometre C-120"(Electrofinish-France) instrument based on the anodic dissolution method.

c) Haring-Blum cell Measurements : The Haring-Blum cell used had the dimensions of 25×6 cm and the platinised titanium mesh anode and the two cathodes(panels) had an 43.5×5 cm area.The anode was situated 4 cm from one end in order to give a ratio of cathode distance of 5:1. A small stirrer,situated in the middle of the cell,was used to circulate the solution slowly around the two compartments of the cell.A current density of 0.01 A/cm^2 was applied to both cathodes,which were weighed before and after electroplating.An analytical assay balance "Sartorious" monoplate was used.

d) Efficiency Measurements : Cathode efficiency was measured for each electrolyte(carrying the respective additive) at different current densities to show changes in the efficiency-current density curve and to obtain an electroplating bath which gave efficiency-current density curves with a negative slope.A copper coulometer was run in series during each test and temperature and pH values were as stipulated for each experiment.Agitation was rocking cathode movement at 2 m/min. All measurements were made simultaneously in series,electroplating onto brass panels of appropiate area.

RESULTS AND DISCUSSION

a) Electrolyte : As result of this investigation we have found that the best electroplating acid gold bath(with uniform deposit distribution,good throwing power and suitable brightness) to use in printed circuits and electronics has been the following:

Gold(as $K[Au(CN)_2]$):10 g/l ; Potassium dihydrogen phosphate:10 g/l; Potassium citrate: 40 g/l; Citric acid: 40 g/l; Nickel(as NiK_2EDTA): 2 g/l; organic brightener class 2 (condensation product of potassium ethyl-xanthate reaction with acrolein): 1,5 g/l. The density of aqueous baths is: 12-13 °Bé. The operation conditions are: Temperature: 30-32 °C pH: 4,0-5,0(adjusted with KOH); current density: 0,01-0,02 A/cm^2; anode/cathode ratio: 1/1 ; continuous filtration ; agitation by cathode oscillation(4 m/min speed).

b) Efficiency : As Fig. 1 shows, only in bath(6) (with high density and improved buffering power and carrying a metal complex and an organic brightener class 2) the efficiency falls with increasing current density.

c) Hull cell : As we can see in Fig.2(that shows distribution of gold deposits obtained from various acid gold baths on a 1 Amp.Hull cell panel) the deposit thicknesses tend to increase continously with increasing current density in the cases of baths 1,2,3,4 and 5. Only in the case of bath 6 there is a significant fall in thickness at high current density.

d) Haring-Blum cell: The formula used for calculating the throwing power T(%) was not the original given by Haring and Blum, but the formula proposed by Field: $T(\%) = \frac{K - M}{K + M - 2} \times 100$, where K is the cathode distance ratio(K=5) and M is the ratio of the weights of gold deposited on the near and far cathodes. The results have been the following(to 0.01 A/cm^2 average): bath(1):13% , bath(2):14% , bath(3):18% , bath(4):20% , bath (5):21% and bath(6):44%.

CONCLUSIONS

The bath(6), proposed, has shown to have a negative efficiency/current density slope and, from the Hull cell data at 0.03 A/cm^2, we can see that the slope of the thickness-current density curve is much less than at 0.01 A/cm^2. Also, at 0.01 A/cm^2 the slope of the thickness-current density curve for bath(6) is less than that for the other experienced baths. Hence, the throwing power and distribution of deposit is better when we electroplating with bath(6) than when plating with any of the other acid gold baths.

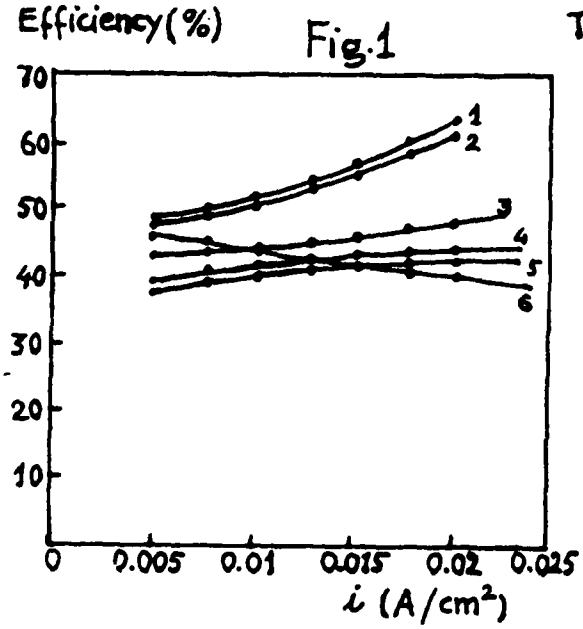

Fig.1

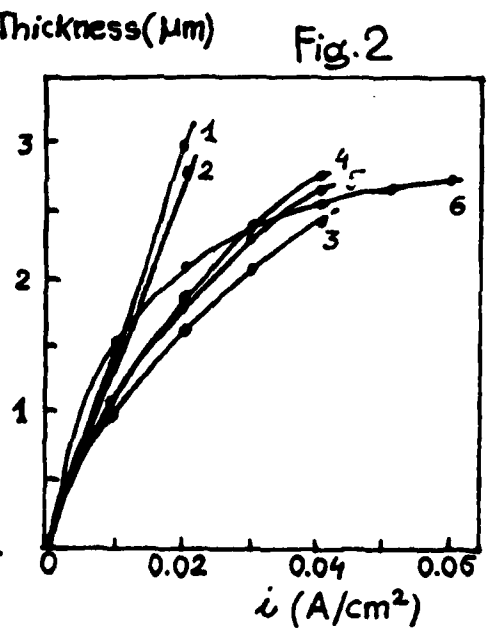

Fig.2

Pt ANODES: INTERRELATION OF CORROSION, ELECTROCATALYTIC AND ADSORPTION CHARACTERISTICS.

Ya.M.Kolotyrkin, A.N.Chemodanov, I.I.Asheulova
L.Ya.Karpov Institute of Physical Chemistry, Moscow (USSR)

The paper presents experimental results on the kinetics of the smooth Pt anodic dissolution at potentials of O_2 evolution. As is known, these processes accompany as side reactions many practically important electrochemical processes realized on Pt anodes in aqueous media. Pt dissolution rate was determined by radiotracer technique.

The experimental data indicate kinetic similarity of both reactions[1]. In H_2SO_4, HNO_3, NaOH and AcNa+AcH solutions the steadystate dissolution of Pt at measurable rates ($\geq 10^{-9}$ A/cm^2) may be monitored only after reaching potentials at which steadystate O_2 evolution starts. Under potential (or current density i) variation the reaction rates i_{Pt} and i_{O_2} change, in many cases, roughly proportionally to each other;2 in the absence of other electrode reactions this is manifested in that the current efficiency of Pt dissolution $CE_{Pt} = i_{Pt}/i$ as a function of i is practically constant (Fig.1). Sometimes CE_{Pt} remains constant also under varied electrolyte concentration (Fig.2) and pH.

Such a parallelism of Pt dissolution and O_2 evolution kinetics can be explained presuming that both reactions proceed through intermediate stages of chemisorbed metal-oxygen compounds' formation[1]. Many experimental data prove the existence of an interrelation between the Pt anode's corrosion behaviour and its surface coverage by chemisorbed oxygen, θ_O. Thus, for some systems there has been established a correlation between θ_O decrease observed in the presence of other adsorbed particles (θ_O was determined by fast voltammetry technique), and anode dissolution inhibition (Fig.3).

Based on the developed concepts and experimental data we may out forward some considerations as to the conditions for the appearance of the above mentioned parallelism.

For acidic electrolytes with nonsurfaceactive anions, which do not undergo anodic oxidation, the CE_{Pt} constancy should be expected, first of all, in the potential region where practically all the current is used for water molecules discharge with O_2 formation. Pt dissolution rate in this region depends little on the anion' nature; the differences in CE_{Pt} values observed for different acids are conditioned mostly by the differences in O_2 evolution kinetics.

The effect of potential on CE_{Pt} may occur at higher potentials when, besides water discharge, the anions' discharge becomes also possible. If the latter reaction does not involve the appearance on the Pt surface of particles facilitating metal dissolution, then CE_{Pt} would decrease with increasing polarization. Whether, in this case, the current efficiency of Pt dissolution related to the partial O_2 evolution rate $CE'_{Pt} = i_{Pt}/i_{O_2}$ remains constant will depend on the composition of final electrolysis products. If the anion discharge accompanied by formation of new products, the parallelism between Pt dissolution and O_2 evolution would remain; this case is reali-

zed under anodic oxidation of chloride and chlorate[2]. If the resulting radical intermediates at further chemical stages react with water forming O_2 and regenerating the parent anions, then the i_{Pt}/i_{O_2} ratio would decrease; an example may be 1M(HNO_3+$NaNO_3$)[2]solution electrolysis with the only final anodic product, at any potential, being O_2 (Fig.4).

In the cases when surface particles formed during anions discharge may, along with surface oxygen particles, directly participate in Pt dissolution reaction, a shift from water discharge potentials to preferential anion discharge potentials might be accompanied by the increase of i_{Pt}/i_{O_2} ratio. At that, generally speaking, CE_{Pt} may decrease or increase as well. The former case seems to be realized in the system Pt-acetate electrolyte. The latter case might be expected in conditions when anion discharge sharply acceleratesanode dissolution. Further potential increase in anion discharge region may cause CE_{Pt} stabilisation on a new level.

The described parallelism effects seem to be of rather general character and were observed, besides Pt, for some other noble metals anodes (Ru, Ir at low polarization) and metaloxide anodes (RuO_2, DSA).

The prospects for practical application of the existing interrelation of noble metal-based anodes dissolution and anodic O_2 evolution are, first of all,associated with possible development of relatively simple techniques to control and predict corrosion behaviour of such anodes, basing on measurements of the accompanying O_2 evolution reaction rates.

REFERENCES.

1. Chemodanov A.N., Kolotyrkin Ya.M., Dembrovsky M.A., Kudryavina T.V., Dokl.AN SSSR, v.171, No.6, p.1384 (1966).
2. Uzbekov A.A., Losev V.V., Nosova K.I., Electrokhimia, v.8, No.12, p.1868 (1972).

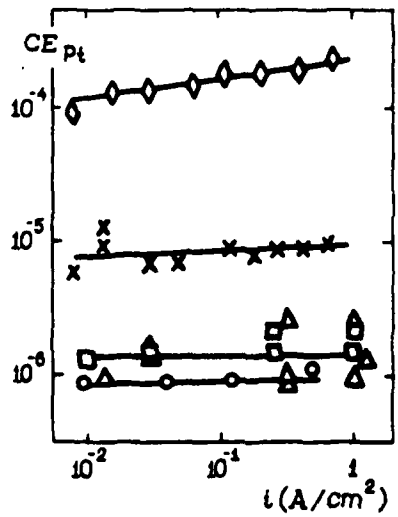

Fig.1. Current efficiency of Pt dissolution as a function of current density

◊ 4M KF, pH 10
× 4M K_3PO_4
□ 0,5M H_2SO_4
△ 1M $HClO_4$
○ 5M NaOH, 50°C

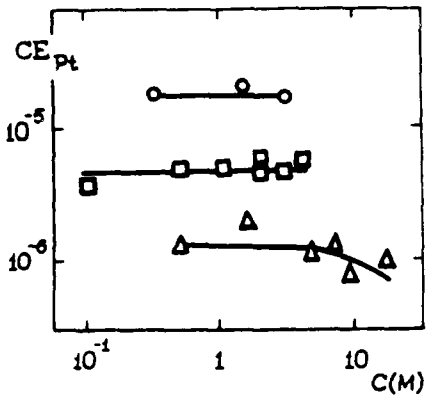

Fig.2. Current efficiency of Pt dissolution as a function of solution concentration

○ AcNa + AcH (1:1), φ = 2,84 V (n.h.e.)

□ K_3PO_4, φ = 2,2 V (n.h.e.)

△ H_2SO_4, $i \simeq 0,1$ A/cm^2

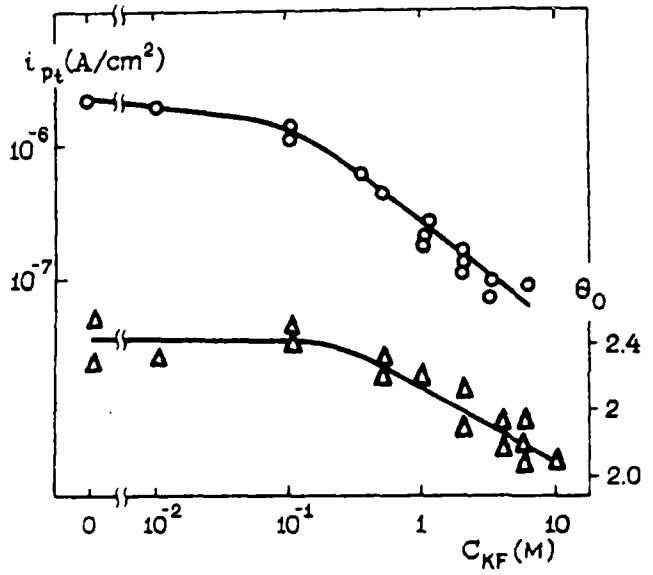

Fig.3. Pt dissolution rate in KF solution, pH 13,5 (○) and surface coverage by chemisorbed oxygen (△) as a function of solution concentration. φ = 2,2 V (n.h.e.)

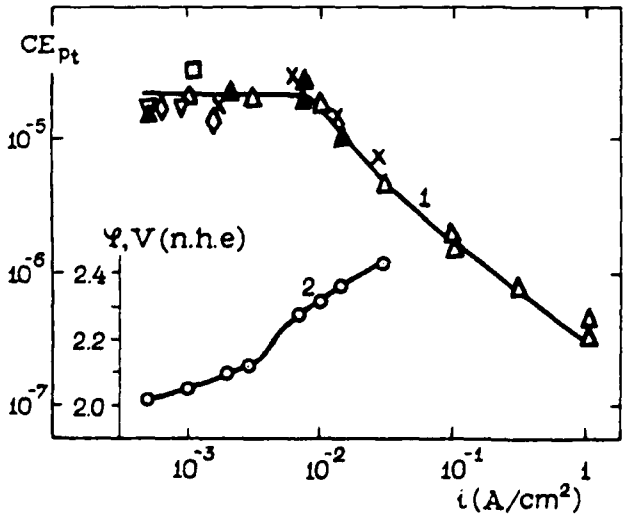

Fig.4. Curve 1 - current efficiency of Pt dissolution in 1M (HNO_3+$NaNO_3$) as a function of current density.

pH values: △ - 0,1

▽ - 0,6

◇ - 1,1

× - 1,5

□ - 2,0

Curve 2 - steadystate polarisation curve for Pt in 1M HNO_3.

KINETICS OF THE INITIAL STAGES OF GALVANOSTATIC ELECTRODEPOSITION

A.N.BARABOSHKIN, V.A.ISAEV
Institute of Electrochemistry, Sverdlovsk, USSR

Under galvanostatic conditions of nucleation and growth of the new phase supersaturation varies substantially during electrodeposition. An important feature of this process is the interdependence between the nucleation kinetics and the nucleus growth one. The transfer of the substance to the electrode is effected in this case under non-stationary conditions. The emergence of nuclei leads to a redistribution of the current at the electrode.

For the description of this process the computer simulation method has been used. With this method the nuclei are introduced into numerical memory of the computer and their evolution is monitored.

The current balance equation for a given instant of time is as follows

$$I = CS\frac{d\eta}{dt} + I_a + \Sigma I_q \quad ,$$

where I is the external current, C is the double-layer capacity, S is the electrode surface area, η is the overpotential, I_a is the current used to form adatoms, I_q is the current used for the nucleus growth. The summation is over all the nuclei existing at the given instant of time. The nuclei are introduced into the numerical memory of the computer at a frequency determined by the Volmer rate of nucleation

$$J = K_1 \exp\left(-\frac{K_2}{\eta^2}\right) \quad ,$$

where K_1 and K_2 are nucleation constants.

For adatoms concentration Γ we have

$$i_a = zF\frac{d\Gamma}{dt} \quad .$$

The concentration of ions being deposited near the flat surface of the electrode (not occupied by nuclei) is equal to

$$c_s = c_0 - \frac{1}{zF\sqrt{\pi D}}\int_0^t \frac{i_a(\tau)d\tau}{\sqrt{t-\tau}} \quad ,$$

where c_0 is the concentration of ions being deposited in the electrolyte, D is the diffusion coefficient of the ions being deposited. The value of I_q is preset depending on the nucleus mechanism.

In the calculations use has been made of experimental values of the parameters of electrodeposition of silver on platinum in nitrate melts[1]. The analysis of calculated data has made it possible to reveal the main regularities of galvanostatic formation and growth of the new phase[2]. Following the switching on of current the double layer charges up, the adatom concentration grows and the overpotential rises. After a certain interval of time the first nucleus emerges. Beginning from

this moment a part of the current is used up for the growth of this nucleus. The adatom concentration at which the first nucleus evolves is several percent (1-5) of the concentration of fully filled silver monolayer. If the nucleus growth current does not exceed the external current, the overpotential centinues to grow and the next nuclei are formed.

At $i > i_{max}$ the total nucleus growth current exceeds the external current, while the adatom concentration and overpotential decrease. At this stage of deposition a predominant transter of adatoms occurs from the electrode into the bulk of the electrolyte. Because of this process the total nucleus growth current can exceed the external current.

At low current densities (10^{-3} -10^{-4} A/sm^2) only one nucleus forms at the electrode. The nucleation process is rather symmetrical relative to i_{max} and t_{max} . According to estimates made the exchange current density at the electrolyte-nuclei interface is at least 500 A/sm^2

At the final stages of the process at small overpotentials only the growth of nuclei occurs without the emergence of new nuclei. An overpotential rise at the growth stage is possible in case of mass crystallization, when the growing nuclei start to overlap. In the theoretical model[3] a chaotic distribution of nuclei over the electrode surface is assumed. The nuclei are considered to be semispherical, emerged instantaneously in the region of maximum overpotential.

Let us examine the case when the deposit growth proceeds by diffusion of the ions being deposited to the surface of the deposit. The following dependence of overpotential on electrodeposition parameters has been established

$$\eta = \frac{2\sigma V}{zFr} - \frac{RT}{zF} \ln\left[1 - \frac{i}{2zFc_0 D w(x)\sqrt{\pi n}}\right] ,$$

where σ is the surface energy of the electrolyte - deposit interface, V is the molar volume of the deposit, r is the nucleus radius, n is the number of nuclei per unit area of the electrode, $x = r\sqrt{\pi n}$, $w(x)$ is the Dawson integral

$$w(x) = \exp(-x^2)\int_0^x \exp\xi^2 d\xi .$$

The η, t - curve from the instant of formation of nuclei has a U-shape. The overpotentical attains a minimum value at the degree of filling of electrode by the deposit $\theta = 0{,}57$.

References

1. A.N.Baraboshkin. Electrocrystallization of Metals from Molten Salts. Moscow, Nauka, (1976).
2. A.N.Baraboshkin, V.A.Isaev, V.N.Chebotin. Electrokhimia, 17, 483 (1981).
3. A.N.Baraboshkin, V.A.Isaev. Electrokhimia, 19, 806 (1983).

THE ANODIC FORMATION OF MERCUROUS OXALATE IN $HClO_4$ AQUEOUS SOLUTIONS

M. SARRET, J. CLARET and M. MULLER
Dep. Química-física. Fac. Química. U. Barcelona
Diagonal 647. 08023 Barcelona.

The formation of mercurous oxalate by anodic oxidation of mercury electrode has been showed by Armstrong and col. in a previous work[1]. The purpose of this work is to study the electrocrystallization of this compound in $HClO_4$ aqueous solutions by potential and current perturbations, in order to establish the mechanism and kinetics of its formation.

1. Voltammetry

A typical voltammogram is shown in the figure. Integration of the

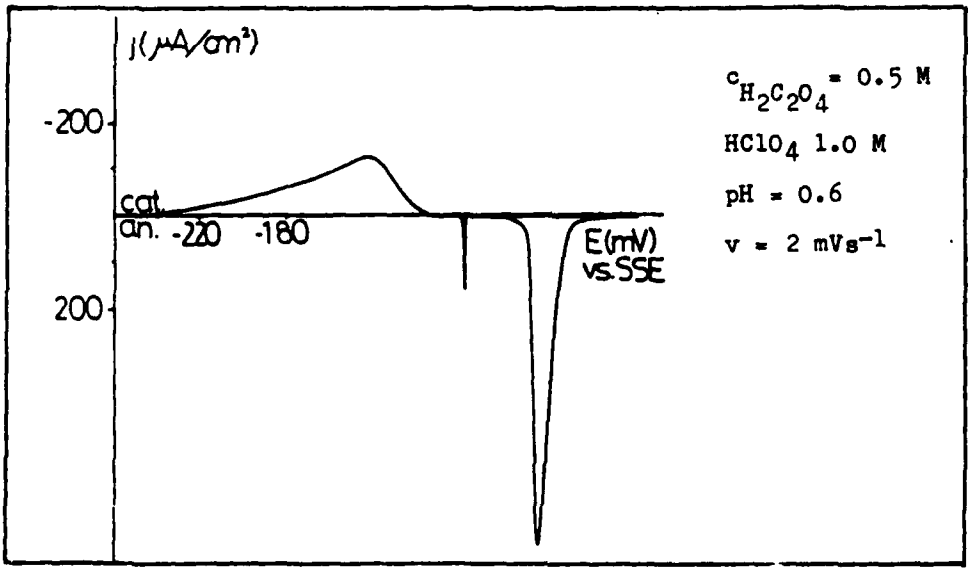

first anodic peak gave a charge of 73±5 μCcm^{-2} and a more detailed study showed the characteristic feature of nucleation[2] : an anodic peak in the cathodic scan. The cross-over potential is poorly defined and two maxima are observed in the reverse scan (-97.0 mV and -98.0 mV), proving a complex behaviour of the deposit. This complexity can be seen holding the potential at -91.0 mV : only a reduction peak is observed at -98.0 mV with a charge of 86±7 μCcm^{-2}. These two cathodic peaks seem to correspond to two possible deposit structures. The form of the peak and the value

of $\theta_p = 0.62$ agree with the calculated for a 2D progressive nucleation and growth mechanism[3].

The second anodic peak exhibits the feature of nucleation, also. When the peak is allowed to grow slowly at -70.0 mV, a only reduction peak is observed whose charge depends on the growing time. This second peak seems to be the three dimensional growth of the deposit.

2. Potentiostatic transients

The potentiostatic transients corresponding to different first peak overpotentials show a general shape characteristic of a nucleation and growth process with a charge of 70±5 μCcm^{-2}. The experimental data at low overpotentials (3-4 mV) follow closely the response predicted for a 2D progressive nucleation (i/i_m vs t/t_m, i vs t^2, $i_m t_m$)[4]. In the overpotential range of 5-7 mV the transients evolution to an instantaneous nucleation and at higher overpotentials ohmic control appears. The slopes of the potential dependences of i_m and t_m involve an extreme dependence of k^2A on the overpotential. The experimental data have been tested also with a theory in terms of coverage [5] and the conclusions have been the same.

At overpotentials higher than 20 mV a second peak is observed in the current-time transients. At low overpotentials this peak seems to correspond to a 3D growth with mixed control, and at higher overpotentials is a three dimensional growth with diffusion control[6].

3. Galvanostatic transients

Two galvanostatic steps with the characteristic potential maxima of a nucleation process can be observed on the transients. The first step corresponds to a 2D nucleation and growth of a monolayer (charge between the potential peaks of 72±6 μCcm^{-2}) and the second step is a 3D growth. The coverage θ_{min} for the monolayer corresponds very closely to the value of 0.39 predicted for the instantaneous nucleation of two dimensional centers[7]. (This different behaviour under potentiostatic and galvanostatic conditions has alredy been analyzed[7]). An analysis of experimental data ($\partial \log \beta_i / \partial \eta$, $\partial \log i_g / \partial \eta$) allow us to compare the experimental transients with the potential response predicted and the agreement is satisfactory. The same agreement is obtained in terms of coverages[5]. The reversible potentials of the layers are measured with the open circuit technique.

4. Impedance measurements

The comparation of the C vs E curve with the voltammogram show the absence of adsorption in the capacitative range.

References

1. R.D. ARMSTRONG, M. FLEISCHMANN, Z. Phys. Chem. (Neue Folge) 52, 131-143 (1967)

2. S. FLETCHER, C.S. HALLIDAY, D. GATES, M. WESCOTT, T. LWIN, G. NELSON, J. Electroanal. Chem. 159, 267-285 (1983)

3. R.G. BARRADAS, F.C. BENSON, S. FLETCHER, Electrochim. Acta 22, 1197-1200 (1977)

4. M. FLEISCHMANN, H.R. THIRSK (P. Delahay Ed.) Advances in Electrochemistry and Electrochemical Engineering. Vol. 3, Wiley, New York 1963

5. R.G. BARRADAS, J.D. PORTER, J. Electroanal. Chem. 110, 159-180 (1980)

6. B.R. SCHARIFKER, G. HILLS, Electrochim. Acta 28, 879-889 (1983)

7. G.J. HILLS, L.M. PETER, B.R. SCHARIFKER, M.I. DA SILVA PEREIRA, J. Electroanal. Chem. 124, 247, 262 (1981)

11190

AUTOCATALYTIC TIN DEPOSITION

A. MOLENAAR and B.C.M. MEENDERINK

Philips Research Laboratories Eindhoven, The Netherlands

Tin is deposited on other metals (e.g. copper) to produce a corrosion resistent or solderable coating. Such layers are usually made by immersion plating, electrodeposition or dip-soldering. Immersion plating, which involves a displacement of the substrate metal by tin, is restricted to layers with a limited thickness; deposition ceases when the substrate is completely covered. Autocatalytic plating gives the possibility of selective deposition of metals to unlimited thickness.

The Wagner and Traud theory of mixed potentials for corrosion systems[1] can also be used for autocatalytic deposition. The polarization curves for independent anodic and cathodic processes may be combined to predict the overall rate (fig. 1). Generally the electrons for autocatalytic metal deposition are supplied by reducing agents such as hypophosphite, formaldehyde and borohydride. Catalytic oxidation of these reducing agents does not occur on a tin surface. We found that tin deposition can be obtained by an unusual autocatalytic process[2]. The metallization takes place by a disproportionation reaction in which a tin(II)compound supplies electrons according to the reaction

$$Sn^{2+}\ \text{compound} \longrightarrow Sn^{4+}\ \text{compound} + 2e.$$

Analyses confirmed that tin is deposited by a disproportionation mechanism

$$2Sn^{2+}\ \text{compound} \longrightarrow Sn^{4+}\ \text{compound} + Sn\ \text{metal}.$$

The mixed potential of the partial reactions in fig. 1 is the plating potential of the autocatalytic tin solution. We measured the plating potential over a long period and found a value of about 1022 mV against Hg/HgO reference electrode. In fig. 2 a cyclic voltammogram is given with an activated copper surface as electrode measured in an autocatalytic tin solution after three hours continuous scanning. Curve AB in fig. 2 corresponds to curve a in fig. 1 (E_{MP} = 1021 mV). At point B the current decreases because all the deposited tin is dissolved.

With a solution containing 0.33 mol/l tin (II)chloride, 2.5 mol/l sodium hydroxide, 0.66 mol/l sodium citrate at a temperature of 75°C we found a deposition rate of 2.3 μm/hour/cm^2, which corresponds to a metallization current (i_m) of 0.76 mA/cm^2 (fig. 2). Both a metallization solution made with tin (II)chloride and a solution without chloride ions made by oxidation of metallic tin gave the same deposition rate on a catalytic surface. Both solutions also gave the same NMR spectrum. So, the disproportionating agent does not consist of a chloride complex. It is likely that a tin(II)hydroxy compound is the active species on the tin metal surface. Because the solutions are stable for days the disproportionating agent must be formed from an inactive tin(II)complex in the solution to give an active compound on the growing tin surface. A possible reaction mechanism for the disproportionation is

$$Sn\overset{\overset{3}{|}}{\underset{|}{}}O - Sn - OH + H_2O + 2e \longrightarrow Sn + 2OH^- + Sn\overset{\overset{2}{|}}{\underset{|}{}}OH$$
$$Sn\overset{\overset{2}{|}}{\underset{|}{}}O - Sn - OH + 4OH^- \longrightarrow SnO_3^{2-} + 2H_2O + 2e + Sn\overset{\overset{3}{|}}{\underset{|}{}}OH$$

$$2Sn\overset{\overset{3}{|}}{\underset{|}{}}O - Sn - OH + 2OH^- \longrightarrow Sn + SnO_3^{2-} + H_2O + 2Sn\overset{\overset{2}{|}}{\underset{|}{}}OH$$

$Sn\overset{\overset{3}{|}}{\underset{|}{}}O - Sn - OH$ can be formed from the solution

$$(Sn\overset{\overset{2}{|}}{\underset{|}{}}OH + HSnO_2^- \rightleftharpoons Sn\overset{\overset{3}{|}}{\underset{|}{}}O - Sn - OH + OH^-)_2$$

As overall reaction we therefore find

$$2HSnO_2^- \longrightarrow SnO_3^{2-} + Sn + H_2O$$

We tried to identify the disproportionating agent by Conversion Electron Mössbauer Spectroscopy with a moving disk electrode as described by Kordesch[3].

References

1. C. Wagner and W. Traud. Z. Electrochemie 44, 391 (1938).
2. A. Molenaar and J.J.C. Coumans. Surface Technology 16, 265 (1982).
3. M.E. Kordesch, J. Eldridge, D. Scherson and R.W. Hoffman, J. Electroanal. Chem. 164, 393 (1984).

Fig. 1. Schematic anodic and cathodic processes for autocatalytic metal deposition and metal corrosion.

Fig. 2. Cyclic voltammogram using an active copper surface as electrode measured in an autocatalytic tin solution after three hours continuous scanning.

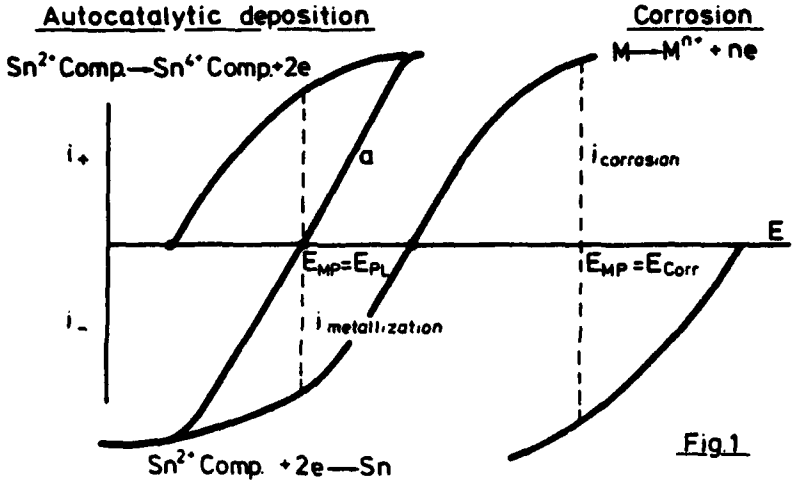
Autocatalytic deposition
Corrosion
Sn^{2+} Comp.—Sn^{4+} Comp.+2e
M—M^{n+} + ne
i_+
a
$i_{corrosion}$
E
$E_{MP}=E_{PL}$
$E_{MP}=E_{Corr}$
i_-
$i_{metallization}$
Sn^{2+} Comp. +2e—Sn

Fig.1

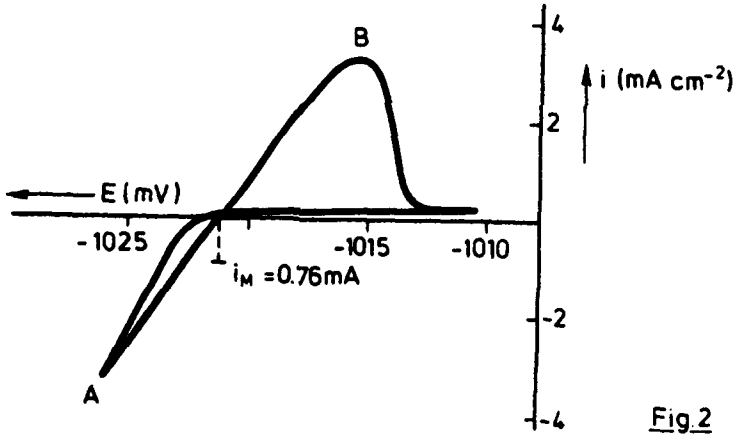
B
4
i (mA cm^{-2})
2
E (mV)
-1025
-1015
-1010
i_M =0.76mA
-2
A
-4

Fig.2

EFFECT OF UV-ILLUMINATION ON THE DISSOLUTION OF ZnO POWDER AQUEOUS SOLUTIONS.

A. Prieto, J. Doménech and C. Franco.
Departament de Química Física. Universitat Autónoma de Barcelona
Bellaterra(Spain).

The stability of semiconductor powder suspensions were investigated under UV-irradiation. The decomposition of ZnO was determined by measuring polarographically the resulting Zn(II) concentration in solution at different irradiation times, pH, and mass of semiconductor.

The effect of adding different hole scavangers was also investigated. Finally, some electrochemical measurements were carried out with the aim to determine the energy levels of electrons in the semiconductor particles under illumination.

Some dissolution of the ZnO aqueous powder (0,25 g/30 ml water, pH=6,5) was noted after stirring for several minutos in the dark, yielding an equilibrium concentration of 0,05 mM, which indicates that ZnO suffers a slow chemical attack. Under illumination, the ZnO decomposition increases in agreement with the negative E_D^o(standard potential of decomposition) respect to the water oxidation. This photodecomposition increases linearly with time(Zn(II) =0,082 mM at 30 min.). At pH of 9,7, the amount of ZnO decomposed is the same as in the dark ($Zn(II)_{eq}$ =0,015 mM). At pH<5, the ZnO dissolution is complete in the dark.

On the other hand, it has been observed the formation of H_2O_2 which can be produced from the reduction of O_2 present in the solution by the conduction band electrons or by water oxidation by the valence band holes created by illumination. The presence of H_2O_2 is not observed when O_2 is removed by bubling the suspension with N_2. Under these conditions, it has been obtained the same amount of Zn(II), that when O_2 is present. This fact indicates that H_2O_2 is formed by the O_2 reduction and not by water oxidation, e.g. water does not competes efficiently with ZnO decomposition for hole capture.

It has been observed that an increase of the mass of ZnO increases the amount of semiconductor decomposed. However, the initial decomposition rate for different mass of ZnO, are the same. This behaviour is consistent with the fact that the ZnO decomposed is lower when the suspension is not stirred.

The decomposition of ZnO particles in presence of O_2, was determined by adding I^-, Br^-, Cl^- and AcO^- ions acting as hole scavangers, at different concentrations and irradiation times. It has been observed that the stability of ZnO decreases in the order, $I^- > Br^- > AcO^- > H_2O > Cl^-$. Further, the stability increases with the salt concentration for I^-, AcO^- and Br^-, while decreases with concentration increasing for Cl^-. The results for halide ions are in agreement with the thermodynamics requirements, according with the location of the energy levels (see figure). The AcO^- ion is

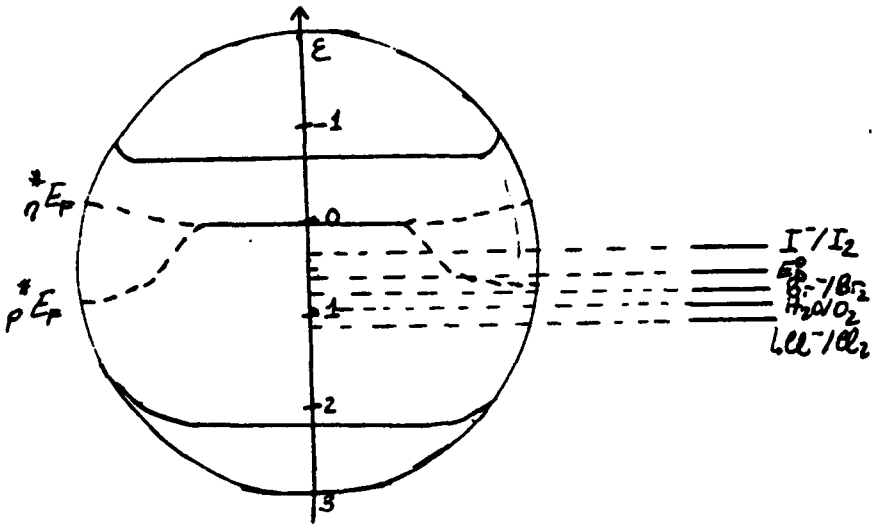

a well known hole scavanger largely used which goes to irreversible oxidation by the valence band holes, to produce probably methane and CO_2.

The energy levels of the electrons in the semiconductor particle under irradiation in presence of 0,1 M of I^-, Br^-, Cl^- and AcO^- ions, have been determined by electrochemical measurements by means a three electrode systems , where the working electrode was an slurry electrode. . The measured photocurrent was compensated for the photoreponse of the Pt collector electrode. The energy levels of the electrons in the semiconductor particles under irradiation, in presence of the ions above mentioned and referred to SCE decreases as follows, Cl^- (+0,4 v)> AcO^- (-0,2 v.)$\geq$ Br^- > I^- (-0,1 v),(experimental conditions: 0,10 g ZnO/25 ml solution, N_2 purged).

Further, it has been observed a photocurrent enhancement on introducing $Fe(CN)_6^{3-}$ ion into the different solutions. This fact is consistent with the reduction of $Fe(CN)_6^{3-}$ by the photogenerated electrons in the particles and the posterior oxidation of $Fe(CN)_6^{4-}$ in the Pt collector electrode held at +0,4 v. The photorreduction of $Fe(CN)_6^{3-}$ is possible because the measured potential of photoelectrons in the ZnO is negative respect to the redox potential for $Fe(CN)_6^{3-}$ (E=0,11 v) in all cases.

Due to the great surface/volume relation in the semiconductor powders, the photoelectrochemical process will be governed by the interface features and particularly by the existence of surface states. The ion adsortion on the particle creates surface states which behave as acceptors or donors of electrons. Under illumination a redistribution of the electron occupancy in these surface states, and a variation of the band bending, is produced, leading to a rapid flux of electrons from the surface states to the conduction band (donor surface states) or viceversa (acceptor surface states) Hence, the quasi-Fermi levels on the particle surface are shifted with respect to the position which it would have in the absence of surface states. Then, the greater or lesser overlap of the surface states with the redox levels in solution, will control the oxidation kinetics of the anions with the valence band holes. A very low overlap, favoures e-h recombination or the semiconductor photocorrosion.

The existence of donor surface states, increases the energy of the electrons in the particle leading to a greater value for the difference between E_f in the dark and under illumination, than in the case of the existence of acceptor surface states. These differences, $E_f^{dark} - E_f^{ill}$, have been obtained experimentally by measuring the difference between the potential of the collector electrode and that of the reference electrode in the dark and under illumination, in shortcircuit[3]. These differences decreases in the order: $Cl^- > AcO^- > Br^- > I^-$, which coincides with the order established for the electron energy levels in the particle under irradiation. Furthermore, the $E_f^{dark} - E_f^{ill}$-values are positive in all cases, except for I^- ion which is practically zero. Consequently it can be concluded that Cl^-, AcO^- and Br^- induce the formation of donor surface states in the particle, whilst for I^- ion the acceptor surface states play an important role.

REFERENCES

1- B. Kraeutler and A.J. Bard, J.Am.Chem.Soc., 100, 5985(1978).
2- M. Fujii, et al., Chem.Phys.Lett., 106, 517(1984).
3- W. Dunn et al., J.Am.Chem.Soc., 103, 3456(1981).

INVESTIGATION OF THE ELECTROCHEMISTRY OF IRON ON IN-SITU GENERATED SURFACES IN ALKALINE SOLUTION

KEMAL NISANCIOGLU
Division of Metallurgy and Corrosion Center, SINTEF and Department of Industrial Electrochemistry, Norwegian Institute of Technology, N-7034 Trondheim-NTH, Norway

M. METZGER
Department of Metallurgy and Mining Engineering and Materials Research Laboratory, University of Illinois at Urbana-Champaign, Urbana, IL 61801, USA

The passive behavior of iron in moderately alkaline solutions has been extensively studied. Various chemical, electrochemical and mechanical techniques are employed for activating the electrode, and these are followed by the application of fast transient techniques for determining the electrochemical behavior.[1-3] An unexpected result of an investigation of the electrochemical behavior of the intermetallic phase Al_3Fe in alkaline solution was that sufficiently active iron surfaces could be generated in situ by selective dissolution of the Al component at potentials well below the reversible potential for oxidation of iron.[4] As a result, oxidation and reduction phenomena could readily be detected without resorting to fast transient techniques.

The Al_3Fe phase was prepared from pure Al and Fe by a controlled solidification procedure. The phases were separated from the surrounding aluminum matrix and recast in epoxy to produce multicrystalline Al_3Fe electrodes. After polishing metallographically through 0.05 μm alumina, the electrodes were immersed in deaerated 0.1N NaOH solution, maintained at 25°C, for polarization tests. The latter consisted mainly of cyclic sweeps between various potential limits at a rate of 100 mV/min.

Fig. 1 depicts typical voltammograms which can be obtained by this technique. The oxidation peak 1 is associated with the selective dissolution of aluminum leading to an enrichment of the crystal surface with a layer of pure iron. This has been confirmed presently by microanalytical investigation of surfaces generated by potentiostating the specimens at potentials more negative than the peak 1 potential. Prolonged exposure of the crystal in this manner leads to exfoliation of flakes of iron at the surface. These flakes were observed to exhibit a highly porous structure. The apparent activity of the surface as an anode can thus be related to a large effective electrode area due to the porosity of Fe layer.

A passivation process is initiated at -1.175 V* corresponding to the current maximum at peak 1. This potential is found to be reproducible within only a few millivolts. During reverse potential sweep, the current starts rising towards peak 1 at about the same characteristic potential indicating a nearly reversible reduction of the passivating oxide and resumption of selective dissolution of aluminum. Based on the work of Burstein and Ashley,[3] the passivation process is attributed to the formation of an adsorbed monolayer of FeOH on the Fe layer.

As the potential is increased in the positive direction, the adsorbed layer and metallic iron oxidize to form the divalent bulk oxide $Fe(OH)_2$. This process is responsible for peak 2 observed at -1.06 V, which is about 50 mV more positive than the reversible potential calculated for the formation of a bulk $Fe(OH)_2$ from metallic iron.[3] Based again on the thermodynamic[3] and kinetic data[4] available for iron in alkaline solutions, we believe that peak 3 at -0.90 V corresponds to the formation of Fe_3O_4 by oxidation of $Fe(OH)_2$ and metallic iron.

The steady-state condition of the Al_3Fe surface in the potential range between peaks 1 and 4 can be described as essentially passive. Application of a constant potential to a passivated specimen in the vicinity of peak 4, however, leads to an increase of current with time. At an applied potential of -0.75 V, the current stabilizes at about 2 mA/cm^2 after 30 min indicating the presence of a transpassive condition. Another evidence for this condition is the fact that, like peak 1, the oxidation peak 4 is observed independent of the sweep direction, while peaks 2 and 3 are only observed during potential sweep in the positive direction. The transpassive condition of the surface is further verified by the observation that specimens potentiostated at about -0.75 V form exfoliating layers of rust on their surfaces. In view of the foregoing, we believe that peak 4 is a result of selective dissolution of aluminum (peak 4a) followed by the oxidation of metallic iron into γFe_2O_3 (peak 4b at -0.66 V). Lower valence oxides formed up to this point are also expected to oxidize further into γFe_2O_3. After the potential sweep is reversed, the first oxidation peak observed (4a) is again due to selective dissolution of aluminum. This is followed by the oxidation of fresh Fe generated at the surface (peak 4c) into an oxide having the most favorable oxidation kinetics at about -0.85 V. Fe_3O_4 can be formed; however, since this is a slow reaction,[4] the formation of $Fe(OH)_2$ is more probable.

Peak 4c is followed immediately by reduction processes characterized successively by peaks 4' and 2', respectively, at -1.03 V and -1.18 V. These reduction processes can be correlated with the oxidation processes described by peaks

---

*) All potentials are reported with respect to SCE.

4b and 2, respectively, by reversing the potential sweep after each oxidation peak as demonstrated in fig. 1. A reduction peak corresponding to peak 3 can be obtained only if the potential sweep is reversed in the negative direction immediately after resolving peak 3. The reduction peak then observed (peak 3') lies at a more negative potential than peak 2' indicating that the reduction of Fe_3O_4 is a relatively slow process. Thus, peak 4' is attributed to reduction of γFe_2O_3 to $Fe(OH)_2$, and peak 2' is associated with the reduction of $Fe(OH)_2$ to metallic iron.

The numerical values of potentials cited above for the oxidation and reduction peaks related to the formation and reduction of bulk oxides on Al_3Fe crystals agree very well with the fast-scan voltammetry data reported by Geana et al.[2] for pure iron at pH 13, with the possible exception of peak 2', which is presently superimposed on the anodic peak 1. However, our interpretation of these data are more in line with the work of McDonald and Owen,[1] especially concerning the significance of peaks 2 and 3.

References

1. D. D. Mac Donald and D. Owen, J. Electrochem Soc., 120, 317 (1973).
2. D. Geana, A. A. El Miligy and W. Lorenz, J. Appl. Electrochem., 4, 337 (1974).
3. G. T. Burstein and G. W. Ashley, Corrosion, 39, 241 (1983).
4. K. Nisancioglu and M. Metzger, Abstract No. 154, Extended Abstracts, 83-2, 240, 164th Meeting of The Electrochemical Society, Oct. 9-14, 1983.
5. D. C. Silverman, Corrosion, 38, 453 (1982).

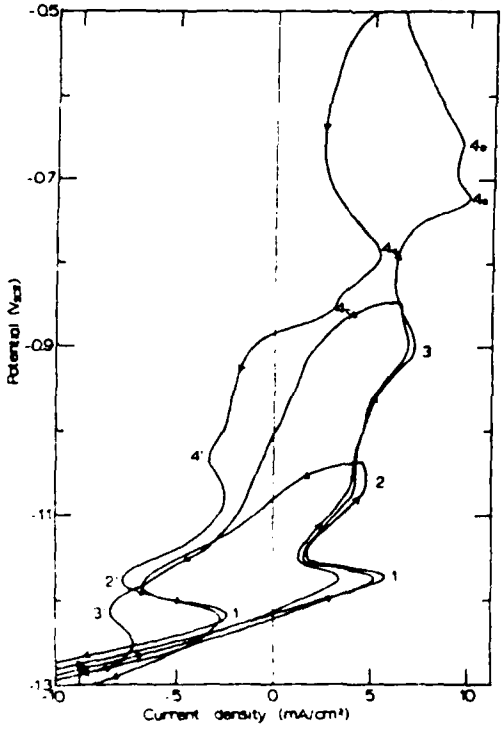

Fig. 1. Typical cyclic polarization curves for the Al_3Fe phase in 0.1N NaOH with sweep reversal at three different potentials. The negative limit for each cycle is -1.5 V.

ANODIC DISSOLUTION OF GADOLINIUM IN PERCHLORATES AND CHLORIDES IN AQUEOUS AND NON AQUEOUS SOLVENTS

R. REICH, S.M. MAYANNA[+] and M. MALDY
Laboratoire de Physique des Solides, Bâtiment 510, Université Paris-Sud
91405 Orsay Cedex (France)

Introduction : Previous current-potentiel curves (1) relative to gadolinium anodic dissolution in methanolic lithium perchlorate solutions at -76°C show the viscosity increase (2-propanol+MeOH) as the dielectric constant decrease (THF + MeOH) raise the transpassive potential E_{max} (upper limit of passivity range) and reduce both the passive and active current densities (fig.1). At this low temperature, the H_2O influence (fig.2) and the solute concentration role are explained by the high viscosity increase. The potentiodynamic curves at -76°C with various potential scan rates (vs Ag/AgCl) exhibit active, passive and transpassive ranges which correspond nearly to corrosion, pitting and electropolishing (2). The significant parameter which quantitatively characterizes the anodic dissolution process is the faradaic efficiency, ρ, defined as the ratio of the weight loss actually measured, W_{ex}, to the weight loss, W_{th}, predicted by Faraday's law assuming a normal oxidation state, n, for the metal ions in solution, i.e. n=3 for Gd. The apparent valence of dissolution, Ne, is calculated using the relation : $Ne=AQ/W_{ex}F$, where A=molecular weight of Gd, Q=electric charge passed, F=Faraday, and hence $\rho=n/Ne$. A constant valence value Ne=1.4-1.5 is observed at -76°C in anhydrous MeOH and its mixtures with THF, 2-propanol and H_2O, which is independent of perchlorate cations, (Li or alkaline earths), if the cell potential or the current density is high enough (1)(2). Moreover, a same value of Ne is found (2) in MeOH containing 0.115M $LiClO_4$ + 0.115M LiCl (fig.3) contrary to Ne$\sim$3 in 0.23M LiCl+MeOH. If dissolution would involve formation of transitory monovalent Gd^+ (very powerful reducing agent) which subsequently could react chemically in the electrolyte, Ne for dissolution should be the same for $LiClO_4$ and LiCl, since homogeneous chemical reactions following the charge transfer step at the interface do not affect the weight loss.

Perchlorate reduction: Our preceeding investigations reveal the important role of Cl^- in the anodic dissolution of Gd. Hence, the quantitative chemical analysis of Cl is carried out after the electrolysis by Mohr's method because of reduction of perchlorate to chloride. The fig.4 is relative to the variation of Ne and the Cl^- amount, m_{Cl^-}, (for a given charge passed Q=300C) with the current density, i, from 0.005 to 0.68 $A.cm^{-2}$ at - 40°C in anhydrous 0.23M $LiClO_4$-MeOH solution. A quantitative relation between the amount of Cl^- liberated and the Ne value is noticed at any current density. Moreover, the Ne plateau corresponds to a bright Gd surface: electropolishing conditions, i.e. transpassive range. If we assume a Gd dissolution process at the anode such as : Gd° (metal) $\rightarrow Gd^{3+}(CH_3OH)_z + 3e^-$ [1], with the Nerst potential of -2.40 V (in aqueous systems), we must suppose the ClO_4^- reduction at the bright Pt cathode according to the reaction: $ClO_4^- + 8e^- \rightarrow Cl^- + 4O^{2-}$ [2]. The O^{2-} anions may combine with the Li^+ ions giving lithium oxide (neutral species). So, the balance of the two electrochemical reactions [1] and [2] corresponds to an apparent valence of Gd lower than n=3. Such a hypothesis seems to be confirmed by the pH increase during the anodic dissolution, the non-formation of formaldehyde and the constancy of the "corrected" valence, N_{corr}, after taking into account the equivalent charge, Q_{Cl^-}, corresponding to m_{Cl^-}. Indeed, N_{corr}, is calculated using the relation: $N_{corr} = (Q + Q_{Cl^-}).A/W_{ex}.F \equiv Ne + N_{Cl^-}$ [3], where $N_{Cl^-} = A\ Q_{Cl^-}/W_{ex}F$.

Influence of temperature in anhydrous MeOH solutions: Before each experiment, the H_2O content in $LiClO_4$ + MeOH is determined (144 µg/ml) by Karl Fischer coulometer (Acquavit-Tacussel). After the dissolution, the analysis indicates no increase of H_2O concentration (146 µg/ml). The fig. 5 shows the variation of Ne and N_{corr} versus i at various temperatures (-76°C to 20°C). The very important fact is the constancy of N_{corr} values ($N_{corr} \simeq 3.0$) over a wide range of current density at every temperature, contrary to the exponential decrease and attaining a limiting value of Ne. Indeed, the plateau corresponds to a bright surface (transpassive domain-electropolishing conditions), contrary to the Ne falling range relative to a more or less darkening of the gadolinium (transpassive to active region). The current density of getting plateau decreases with temperature.

Influence of temperature in water-methanol mixtures: The faradaic efficiency under galvanostatic conditions is systematically investigated in (1-y)MeOH + y H_2O with $LiClO_4$ (0.23M). The significant result at -76°C (fig. 6) is the similar constancy of Ne over a wide range of H_2O content ($0 \leqslant y \leqslant 0.42$ where y=0.42 corresponds to the solution freezing limit). N_{corr} decreases slightly from 3.0 to 2.8 with increase in H_2O content. So, the water content has no influence on the faradaic efficiency during anodic dissolution at low temperature, which is in agreement with the previous potentiostatic studies (2). This implies that H_2O does not play any role in the electrodic processes and ionic mechanisms, despite the high increase of viscosity and dielectric constant of the medium. At room temperature, a similar investigation is made with all range of H_2O mole fraction : $0 \leqslant y \leqslant 1$. An increase in the apparent valence Ne=1.43 for y=0.013 to Ne=2.8 for y=1 (pure water) is observed. Such a behavior is in good agreement with a potentiostatic study carried out at 20°C with two different cell potentials 20 and 60 V, which shows a continuous variation of Ne with y from 0 to 1. Such a variation of faradaic efficiency with H_2O content results from a change in the Gd dissolution process. Indeed, even at 20°C, the electrode surface is bright in anhydrous MeOH because of prevailing of electropolishing conditions (transpassive range), but it is not the case in presence of appreciable amount of H_2O (y>0.013). In this last case, a considerable overgrowth of yellowish-black anodic product on Gd surface occurs with increase of H_2O content rendering the anode surface towards passive and active regions. This is further reflected by the drastic decrease of Cl^- liberated ($m_{Cl^-} \to 0$) with H_2O content increase.

Influence of pH:During the anodic dissolution in $LiClO_4$ + MeOH at any current density, the pH of the medium raises from 4 to 8.5. The influence of initial pH on Ne is investigated by adding appropriate amounts of $HClO_4$ or LiOH at -76°C. With addition of $HClO_4$(pH=2), the behaviors of Ne and N_{corr} are the same as in pure ClO_4^- solutions. On the contrary, the added LiOH (pH=9) gives an important rise of Ne and N_{corr}, particularly in the high current density range ($Ne \to 17$ and $N_{corr} \to 60$). This low faradaic efficiency in basic solutions may be due to the blocking of active sites of Gd surface by OH^- ions.

Conclusions:The existence of a plateau for Ne (Ne=1.4-1.5) cannot be taken into account by using the surface desintegration model ("chunk effect"). The strong difference in Ne values in ClO_4^- (Ne=1.4-1.5) and Cl^- ($Ne \simeq 3.0$) is against the existence of a monovalent transitory ion. Observed results may be explained by simultaneous electrochemical reactions with a normal valence of Gd for anodic dissolution, i.e. Ne=n=3. Such a fact is in agreement with the absence of lower valence state for Gd, this lanthanide with a single oxidation state.

+permanent address:Deprt.Chemistry,Central College, University Bengalore,India.

(1) R. Reich & C. François,Meeting Electro.Soc.USA,Seattle,78-1(1978)p.1376-78.
(2) R.Reich & M. Maldy,Ext.Abstr.35th ISE Meeting, Berkeley,USA,B3-24(1984)p.658

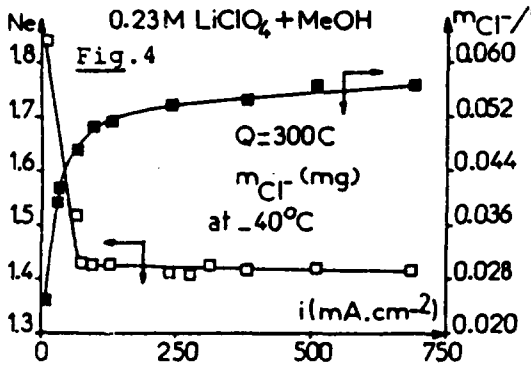
0.23 M LiClO4 + MeOH
Fig. 4
Ne
mCl-/Q
Q=300C
mCl- (mg)
at -40°C
i(mA.cm-2)

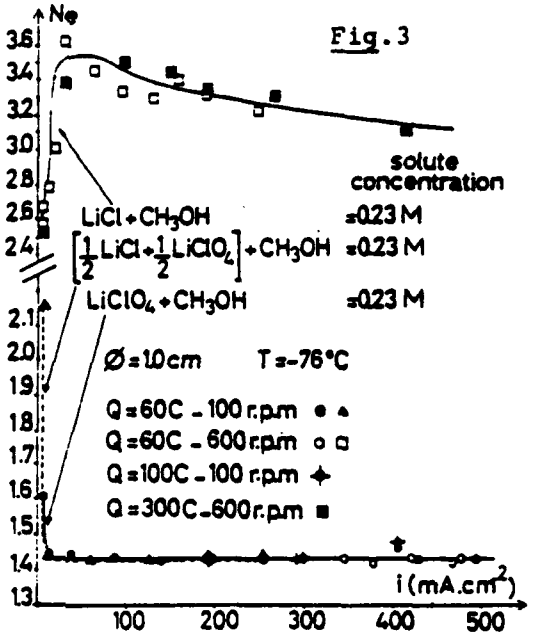
Fig. 3
Ne
solute concentration
LiCl + CH3OH =0.23 M
[1/2 LiCl + 1/2 LiClO4] + CH3OH =0.23 M
LiClO4 + CH3OH =0.23 M
Ø = 1.0 cm T = -76°C
Q = 60C - 100 r.p.m
Q = 60C - 600 r.p.m
Q = 100C - 100 r.p.m
Q = 300C - 600 r.p.m
i (mA.cm2)

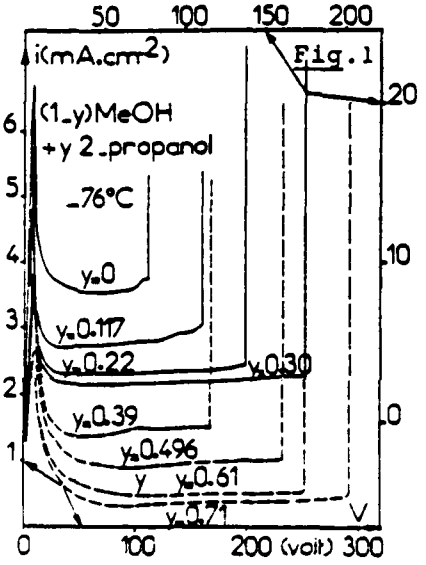
Fig. 1
i(mA.cm-2)
(1-y)MeOH
+ y 2-propanol
-76°C
y=0
y=0.117
y=0.22
y=0.30
y=0.39
y=0.496
y=0.61
y=0.71
V
(volt)

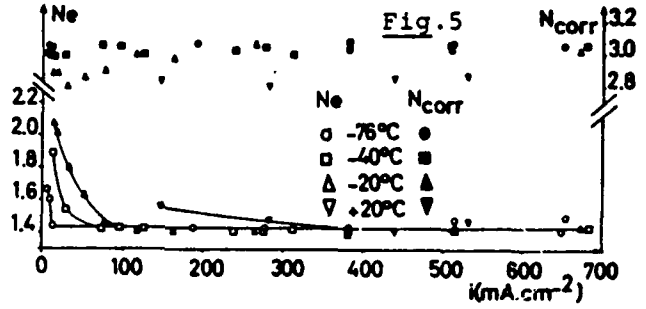
Fig. 5
Ne
Ncorr
Ne Ncorr
-76°C
-40°C
-20°C
+20°C
i(mA.cm-2)

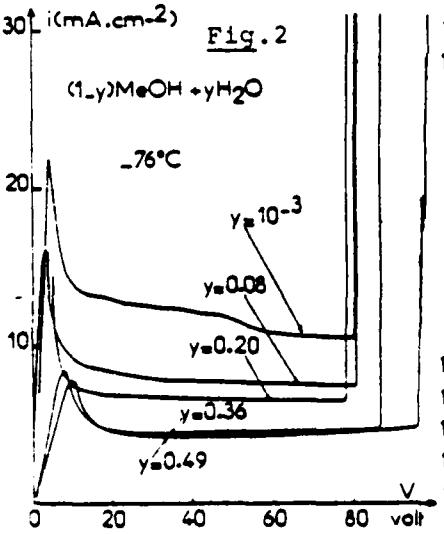
Fig. 2
i(mA.cm-2)
(1-y)MeOH + yH2O
-76°C
y=10-3
y=0.08
y=0.20
y=0.36
y=0.49
V
volt

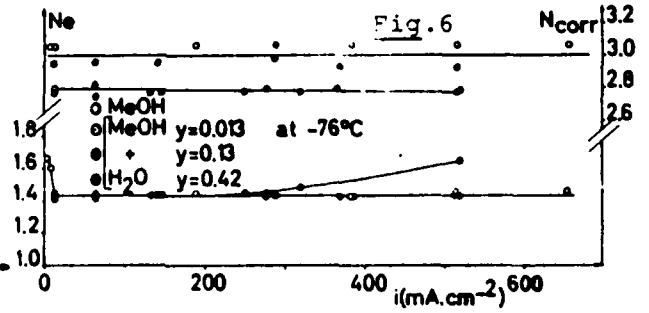
Fig. 6
Ne
Ncorr
MeOH
MeOH y=0.013 at -76°C
y=0.13
H2O y=0.42
i(mA.cm-2)

PREPASSIVE DISSOLUTION AND PASSIVATION OF Zn IN ALKALINE MEDIA

J. Sabater and L. Victori

Electrochemistry Section, Instituto Químico de Sarria. BARCELONA

In previous works(1) , we have concluded that the mechanism of dissolution of Zn in alkaline media is diffusionally controlled by $Zn(OH)_4^{-2}$ ion, on its separation from the interface, and that passivation occurs through a dissolution-precipitation mechanism. These conclusions agree with other works(2,3), but it seems to be in clear disagreement as to which is the prepassive dissolution mechanism. The resume of the works about this subject can be detailled as; first possibility, dossolution to $Zn(OH)_4^{-2}$ ion,through $Zn(OH)_2$ as intermediate, or second possibility, dissolution to $Zn(OH)_4^{-2}$ ion through ionic species, as Bockris proposed, in the form of an active dissolution in the presence of $Zn(OH)_2$ on the metal. This $Zn(OH)_2$ is not an intermediate, it would come as a consequence of the precipitation of $Zn(OH)_2$ from the dissolution. Due to his porous structure its presence on the surface should nrt produce any restrictions in the normal way of dissolution.

Another important thing is the large overvoltage accompanying the formation of ZnO and that its formation seems to be catalized by the presence of $Zn(OH)_2$ on the surface of the metal.

RESULTS AND DISCUSSION

In a previous work carried out by Powers et al.(4), who followed the passivation process through a microscopical observation and inferred the existance of two oxides in the passivation process. They named them as ZnO type I and ZnO type II, and they observed too, that when the solution is stirred,then the first oxide seems not to appear.

In our work, working with a solution in completely repose or using a disk electrode rotating at 2800 rpm and immersed in an ultrasonic bath, we have observed differences of 1500mvolts between the passivation potencials of these two situations. It would imply an overvoltage

of 2000mvolts for the formation of the ZnO oxide.

On the other hand, when an electrode is just passivated in resting conditions, and is suddenly subjected to ultrasonic agitation, the metal becomes active again and returns to its theoretic situation in the I/E curve.

The study carried out by Modulated Electroreflectance Spectroscopy seems to confirm that on the surface of the metal there is a compound which can not be zinc oxide on account of the energy associated to the maximum of the electroreflectance band and for the same reason the zinc oxide does not appear at potencials near the passivation point.

We intend to take the dissolution and passivation processes of Zn in alkaline media as the next topic; which will involved the explanation of our experimental results.

PATH I

(active dissolution)

$Zn + OH^- \text{ --- } Zn(OH) + e^-$

$Zn(OH) + OH^- \text{ --- } Zn(OH)_2^-$

$Zn(OH)_2^- + OH^- \text{ -- } Zn(OH)_3^- + e^-$

$Zn(OH)_3^- + OH^- \text{ -- } Zn(OH)_4^{-2}$

PATH II

(prepassive dissolution)

$Zn + OH^- \text{ --- } Zn(OH) + e^-$

$Zn(OH) + OH^- \text{ --- } Zn(OH)_2^-$

$Zn(OH)_2^- + OH^- \text{ --- } Zn(OH)_3^- + e^-$

$Zn(OH)_3^- + OH^- \text{ --- } Zn(OH)_4^{-2}$

$Zn(OH)_4^{-2} \text{ ==== } Zn(OH)_{2(s)}$ (on the electrode)

PATH III

(passivation)

$Zn(OH)_4^{-2} \text{ === } Zn(OH)_{2(s)}$ (on the electrode)

$Zn + OH^- \text{ --- } Zn(OH)^+ + 2e^-$

$Zn(OH)^+ + OH^- \text{ --- } Zn(OH)_{2(s)}$

PATH IV

(oxide growth)

$Zn + OH^- \text{ --- } Zn(OH)^+ + 2e^-$

$Zn(OH)^+ + OH^- \text{ --- } ZnO + H_2O$

BIBLIOGRAPHY

(1) X. Marti, J. Sabater, E. Soler and L. Victori, "Mecanismo de pasivación del Zn en medios alcalinos". Instituto Químico de Sarria.

(2) Ming-Biann Liu, G.M.Cook, N.P.Yao, J. Electrochem. Soc.,128,1663(1981

(3) K. Ogura, Electrochimica Acta, 25,335(1980)

(4) R.W.Powers, M.W.Breiter, J.Electrochem Soc. 116,719(1969)

12010

12

POLYMER COATED SEMICONDUCTOR AS A CALCIUM SELECTIVE ELECTRODE

M. SYRJÄMÄ and J. KANKARE
Department of Chemistry, University of Turku
SF-20500 Turku 50, Finland

Coated wire electrodes (CWE's) refer to a type of ion-selective electrode (ISE) in which an electroactive species is incorporated in a thin polymeric film coated directly on a metallic conductor. Leaching of the sensor material has precluded the use of ultrathin coatings in the ion-selective electrodes, although it would decrease the diffusion and response time. By covalent binding leaching can be prevented but selectivity may become a problem.

In the present work we have constructed a calcium selective ultrathin coated plate electrode (UTCPE) based on simple design principle.

The host polymer (Figure 1) is formed from propylene oxide and allyl glycidyl ether via coordination polymerization catalyst, an organotin alkyl phosphate condensate catalyst[1]. The sensor material is a suitable calcium salt such as calcium bis(diallylphosphate) (Figure 2) which is grafted to the host polymer via reactive allyl groups by controlled thermopolymerization.

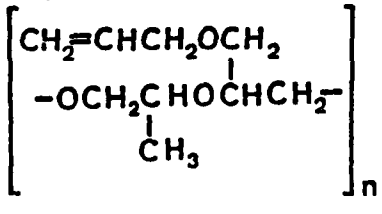

Figure 1.

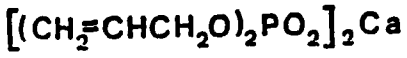

Figure 2.

One of the main advantages of the electrode production is the ease of fabrication. Because of the non-leachable character of the sensor it is possible to spincoat or electrospray 100 - 300 nm thin membrane coatings on a semiconducting substrate (In_2O_3 - SnO_2 coated glass plate). After the coating procedure the electrode is baked at 100 - 150 ^{o}C in oxygen atmosphere to cross-link the sensor compound into the host polymer backbone. The presence of calcium in the grafting step increases the selectivity presumably by the template effect.

In order to get the best physical and electrochemical properties the extent of cross-linking of the membrane is controlled primarily by the amount of propylene oxide and allyl glycidyl ether present in the host polymer and by the curing

time and temperature.

The electrodes produced by this simple technique have the linear response in the range 10^{-1} - 10^{-5} M with a slope of 27 mV per decade (Figure 3).

Because of the thinness of the membrane the response times are generally very short, with dynamic times being in the region of 1 s for the range 10^{-1} - 10^{-5} M Ca^{2+}. When the extent of cross-linking is too high the response times become much longer.

The lifetime of this type of electrode is longer than the lifetime of polymer entrapped liquid ion exchanger electrodes. Well cross-linked membranes lasted more than 2 months.

Selectivity studies were performed by mixed solutions method. The potentiometric selectivity coefficients towards monovalent cations were reasonable good. The response curves are presented in Figure 3, when the interferent level is maintained at 10^{-1} M.

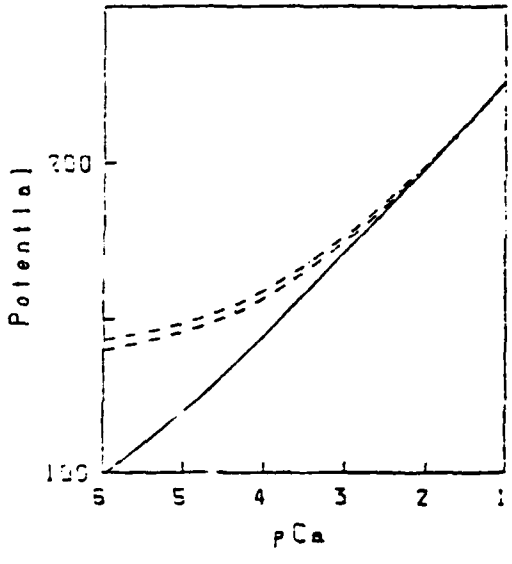

Figure 3. Calibration graph for a calcium-UTCPE (————). The interferent effect of Na^+ (— — —) and Li^+ (—·—·—·) solutions (0.1 M) are also shown.

References

1. Tetsuya Nakata, "Coordination Polymerization" (C.C. Price and E.J. Vandenberg Ed.) Plenum, New York, 1983, p. 55.

POLAROGRAPHIC BEHAVIOUR OF Cd(II) CATION IN ETHYLENE GLYCOL-WATER MIXTURES WITH LITHIUM PERCHLORATE AS BACKGROUND ELECTROLYTE.

E. BRILLAS*, J. DOMENECH**, J.A. GARRIDO* and R.M. RODRIGUEZ*.
*Departament de Química Física. Facultat de Química. Universitat de Barcelona. Avda. Diagonal, 647. 08028-Barcelona (Spain).
**Departament de Química Física. Facultat de Ciències. Universitat Autònoma de Barcelona. Bellaterra (Spain).

INTRODUCTION

Ethylene glycol (EG)-water mixtures are interesting because both solvents are highly structured and, therefore, important changes in the solvent structure can be expected when they are mixed.

In this paper, we have studied the polarographic reduction of Cd(II) ion in aqueous and aqueous EG solutions containing different concentrations of $LiClO_4$ as background electrolyte. From the polarographic data, the standard free energy of transfer and the Walden product for Cd(II) ion in these media have been determined and further discussed in terms of ionic solvation and solvent structure.

EXPERIMENTAL

Ethylene glycol and Lithium perchlorate were Fluka, A.R. grade. Cadmium sulphate and Ferrocene were Merck, A.R. grade. All solutions were prepared by weight with water obtained using a Millipore Milli Q system.

The polarographic measurements were made with an Amel 471 multipolarograph. The cyclic voltammetric measurements were carried out with conventional instrumentation consisting of an Amel 551 potentiostat, a P.A.R. 175 universal programmer and a Philips 8043 X-Y recorder. A saturated calomel electrode (SCE), with aqueous solution of NaCl, was used as reference electrode and a Pt wire as counter-electrode.

Solutions of Cd(II) ($5.0 \cdot 10^{-4}$ M) in water and EG-water mixtures of EG mole fraction between 0.10 and 0.70, containing concentrations $2.5 \cdot 10^{-2}$, $5.0 \cdot 10^{-2}$ and $1.00 \cdot 10^{-1}$ M of $LiClO_4$ as background electrolyte, were studied.

RESULTS AND DISCUSSION

The Cd(II) ion displayed a single well defined polarographic reduction wave in all the studied solutions. The wave is diffusion controlled because the plots of log of the limiting current, I_l, vs. log of t were always linears with slopes close to 0.17. In each solution the half-wave potential, $E_{1/2}$, was found to be independent of the drop time. Moreover, good linear correlations between E (applied potential) and log of $((I_l - I)/I)$, with slopes of about 30 mV per decade, were always obtained. These results indicate that in all solutions Cd(II) ion reduction is a two-electron reversible process[1].

The half-wave potential shifts to more positive values when either the EG mole fraction or the $LiClO_4$ concentration increases. The value of the diffusion-current constant, I_d, gradually decreases as the EG content in the solvent increases.

Cyclic voltammetric curves of saturated solutions of ferrocene in the EG-water media were also recorded, showing a redox couple corresponding to the ferricinium ion/ferrocene system (Fic^+/Foc), with a difference between the anodic and cathodic peak potentials, $E_p^a - E_p^c$, of about 60 mV, as expected for a one-electron reversible process[1].

Then, the variation of $E_{1/2}$ for this system is ascribed to the change in the liquid junction potential and the half-wave potentials of Cd(II) ion were expressed with respect to the half-wave potentials of ferrocene, $E_{1/2,Foc}$. The difference ${}^{w}\Delta^{x}E^{\circ}$ between the standard potentials of the Cd(II)/Cd(Hg) system in mixed solvent, x, and water solution, w, both with equal concentration of $LiClO_4$, was calculated using the equation[2,3]:

$$ {}^{w}\Delta^{x}E^{\circ} = {}^{w}\Delta^{x}E_{1/2,Foc} + \frac{RT}{nF} \ln \frac{(\gamma_{ox})_w (D_{ox})_x^{1/2}}{(\gamma_{ox})_x (D_{ox})_w^{1/2}} $$

where γ_{ox} and D_{ox} are the activity and diffusion coefficients of Cd(II) ion in each solution, respectively. Activity coefficients were estimated according to Arévalo et al[4].

The ${}^{w}\Delta^{x}E^{\circ}$ values thus obtained were independent of the $LiClO_4$ concentration in the solvent and this allows the standard free energies of transfer of one mole of Cd(II) ions from water to mixed solvents, ΔG_t°, to be calculated according to the following expression:

$$ \Delta G_t^{\circ} = 2 F {}^{w}\Delta^{x}E^{\circ} $$

The results obtained are given in table I. The ΔG_t° values are negative in all the range of solvent compositions studied, increasing with EG content in the solvent. This fact indicates that the transfer of Cd(II) ion from water to mixed solvents is thermodynamically favoured and, also, that the process becomes more spontaneous with adding EG to the mixed solvent.

TABLE I. Values of ΔG_t° and $\Delta G_{t,ch}^{\circ}$ for Cd(II) ion in EG-water mixtures, at 25.0°C.

x_{EG}	ΔG_t° /kJ.mol^{-1}	$\Delta G_{t,ch}^{\circ}$/kJ.mol^{-1}
0.00	0	0
0.10	-1.73	- 5.98
0.20	-5.02	-12.16
0.30	-7.53	-17.83
0.40	-10.04	-24.05
0.50	-12.93	-30.35
0.60	-15.25	-35.90
0.70	-18.34	-42.08

The ΔG_t° can be splitted into two contributions: i) an electrostatic one, $\Delta G_{t,el}^{\circ}$, which arises from the change in the dielectric constant of the solvent, and ii) a chemical one, $\Delta G_{t,ch}^{\circ}$, which depends on the solvation and other specific ion-solvent interactions.

The $\Delta G_{t,ch}^{\circ}$ values calculated by means of the Born equation[5] are listed in Table I. These values are more negative as long as the EG content in the solvent increases (see Fig. 1). This can be explained by taking into account the existence of specific acid-base interactions between Cd(II) ion and solvent molecules. Thus, the mixtures are more basic than water, increasing its basicity with adding EG to the solvent and hence, producing stronger ion-solvent interactions.

On the other hand, the decrease in D_{ox} when the EG content in the solvent increases is mainly due to the increase in viscosity of the solution.

The Walden product, $D_{ox}\eta$, for Cd(II) ion changed with solvent composi-

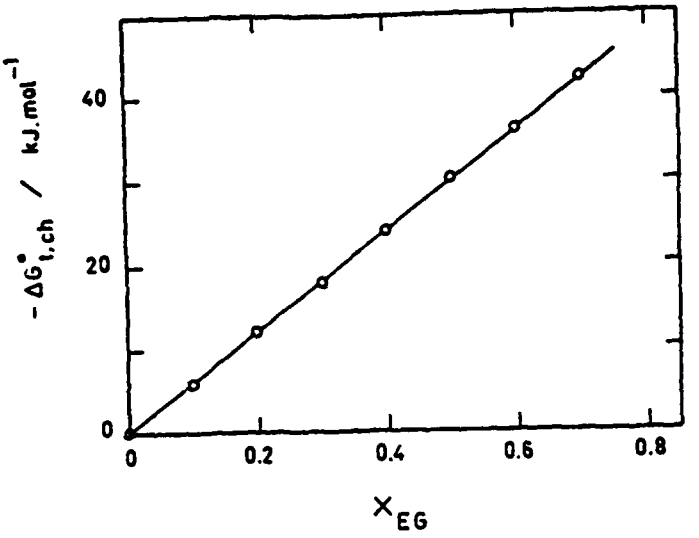

Fig. 1: Dependence of the $\Delta G^{\circ}_{t,ch}$ for Cd(II) ion on EG mole fraction. Temperature 25.0°C.

tion, although remained practically constant with $LiClO_4$ concentration (see fig. 2). This parameter reaches a maximum value approximately at $x_{EG} = 0.2$, indicating that in the water-rich region, the Cd(II) ion becomes more structure-breaking. At $x_{EG} > 0.2$ addition of EG to mixed solvent causes a decrease in solvent structure and hence, a loss in mobility of the Cd(II) ion, as well as an increase in the solvated radius of this ion due to the substitution of the more voluminous EG molecules by water ones.

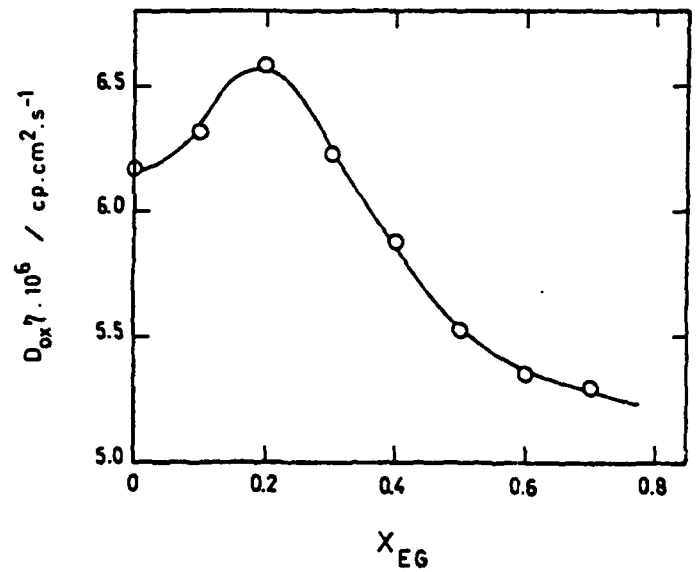

Fig. 2: Variation of the Walden product for Cd(II) ion with EG mole fraction at a 0.100 M $LiClO_4$ concentration. Temperature 25.0°C.

REFERENCES

1. Z. Galus, Fundamentals of Electrochemical Analysis, Chap. 7, Harwood, Chichester, 1976.
2. J.J. Lingane, J.Amer. Chem. Soc., 61, 2099 (1939).
3. D.D. DeFord and D.L. Andersen, J. Amer. Chem. Soc., 72, 3918 (1950).
4. A. Arévalo, A. Vivo and E. Tejera, An. Quím., 70, 318, (1974).
5. M. Born, Z. Physik, 1, 45 (1920).

ELECTROCHEMICAL MEASUREMENTS IN AQUEOUS-MIXTURES WITH HIGH CONTENTS OF ETHANOL. TRANSFERENCE NUMBERS FOR NaCl AT 25°C.

M.A. ESTESO, M.M. LEMUS, D.M. GRANDOSO, A.R. RUANO and O.M. GONZALEZ
Dept. of Physical Chemistry. University of La Laguna. Tenerife (Spain)

INTRODUCTION

The study of the structure and properties of solutions of electrolytes by using mixed aqueous-organic solvents is a common practice in electrochemical laboratories, since the physical properties of the system, in these mixed media, can readily be manipulated according to the requirements of each particular case.

Our laboratory has been engaged on this work for the past few years, presenting transference number values for the ions of KCl[1] and of NaCl[2] in some ethanol-water mixtures, analyzing the influence on this parameter of the ethanol content of the medium. However, only the analysis of mixtures with a low ethanol content (up to 30 wt% of ethanol) was reported in those papers, on account of the very remarkable variations that took place in such zones of composition. The convenience of extending these studies to the regions in which the mixture becomes richer in ethanol seems evident, in order to obtain data along the entire composition range of the said mixtures.

The determination of the transference number, $T_{\pm}$, in ethanol-rich media, presents great experimental difficulties due to the great increase in resistance of the solutions employed and to the decrease in solubility of some of the electrolytes. The paucity of conductance data for the following electrolytes employed, in those ethanol-water mixtures, presents a further problem and implies resorting to arduous procedures in the search for an appropriate concentration of the following electrolyte which will allow the formation of a stable moving boundary that moves at a constant rate.

In this paper, data are presented for the Na^+ and Cl^- ions at several concentrations of NaCl in ethanol-water mixtures with 40 and 60 wt% of ethanol. The results obtained at the different concentrations of NaCl have been extrapolated to zero concentration by using theoretical equations. Such extrapolated values are analyzed as a function of the ethanol content of the medium, together with the data previously obtained[2].

EXPERIMENTAL RESULTS AND DISCUSSION

The experimental method used to determine this ionic parameter is the direct moving-boundary technique, already described in previous communications by this laboratory. Both falling and rising sheared moving-boundary cells were used, although the main block of results here presented was obtained by using a falling-type cell, the accuracy of which proved to be much greater in this case than that of the other type.

The following electrolytes used were: $NaIO_3$ (rising) and $NaOOCC_6H_5$ (falling) for the anion runs and $CdCl_2$ (rising) and $(C_4H_9)_4NI$ (falling) for the cation runs. The salts were purified by the usual methods in all cases. The electrodes used in all the experiments were of Ag (anode) and AgCl (cathode), keeping closed, to serve as reference of the movement, the electrode compart-

ment which contained the NaCl leading solution. The volume increase occured in the said reference compartment on passing a current of 1 Faraday through the cell, employed to calculate the volume correction, was given by:

$$\Delta V_{\pm} = \pm [\bar{V}(Ag) - \bar{V}(AgCl) + T_{+}(NaCl)\,\Phi\,(NaCl)]$$

The corrected transference number values, after volume and solvent corrections applied, T_{cor}, are collected in Table I. Because the sum of both cation

Table I. Transference numbers for NaCl in ethanol-water mixtures at 25°C

40 wt%				60 wt%			
C(NaCl) ($eq \cdot dm^{-3}$)	$(T_+)_{cor}$	$(T_-)_{cor}$	$(T_+)_b$	C(NaCl) ($eq \cdot dm^{-3}$)	$(T_+)_{cor}$	$(T_-)_{cor}$	$(T_+)_b$
0.02000	0.4284	0.5691	0.4294	0.01998	0.4316	0.5695	0.4311
0.02998	0.4280	0.5713	0.4283	0.03000	0.4310	0.5698	0.4306
0.04002	0.4271	0.5724	0.4274	0.03500	0.4304	0.5695	0.4305
				0.03999	0.4305	0.5700	0.4303

and anion transference numbers at each concentration of the leading solution must be equal one and accepting that the discrepancy observed with respect to this unit value is due to little errors that affect in the same manner to both cation and anion transference numbers, "best" values of these parameters can be obtained by dividing each corrected value by the sum of both cation and anion corrected ones at each concentration of NaCl. Such "best" values are also presented in Table I, but only for the cation.

The extrapolation of the T_{best} values to zero concentration was made by using different theoretical equations[1], being the 1957 Fuoss-Onsager one[3] which leads to the most adequate results. These results are:

$$T^{\circ}_{+} = 0.4346 \quad \text{with} \quad a = 2.5\ \text{Å} \quad \text{(for 40 wt\%)}$$

and

$$T^{\circ}_{+} = 0.4362 \quad \text{with} \quad a = 6.3\ \text{Å} \quad \text{(for 60 wt\%)}$$

where "a" is the distance of the closest approach cation-anion obtained from the use of those equations.

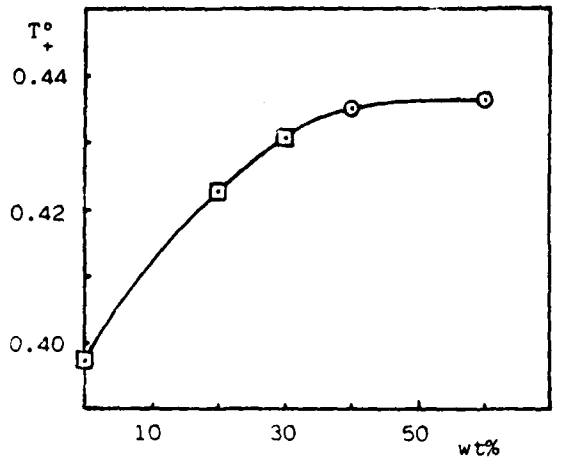

Fig. 1. Plott of T°_{+} vs wt% of ethanol. o, present work; □, ref. 2.

The values for T°_{+} thus obtained are plotted against the ethanol content of the mixture in Figure 1, together with the ones found in others mixtures with low ethanol content[2], previously studied.

The fast initial increase of the parameter T°_{+} with the first additions of ethanol to the medium, suggests us the possibility of some dehydration of the cation as a consequence of a competition between the ethanol and water molecules to penetrate into the solvation sphere of the ion. The result of such dehydration would be a reduction of the efective size of the ion which could easier move through the solvent.

When the ethanol content in the medium increases, the entrance of molecules of this solvent in the solvation sphere of the ions should be favoured and the size of these ions will increase. This effect of size combined to the increase in the viscosity of the solvent, have to be the causers of the brake in that initial increment of T^{o}_{+}.

REFERENCES

(1) Esteso, M.A. and Grandoso, D.M. *J. Chem. Eng. Data* **1980**, *25*, 398-400

(2) Esteso, M.A. and Lemus, M.M. *Resumenes IV Reunión Grupo de Electroquímica. Puerto de la Cruz - Spain* **1981**, *A-5*, 62-3

(3) Fuoss, R.M. and Onsager, L. *J. Phys. Chem.*, **1957**, *61*, 668-82

AD-A162 434 EXTENDED ABSTRACTS INTERNATIONAL SOCIETY OF ELECTROCHEMISTRY (36TH) HELD AT SALAMANCA SPAIN ON 23-28 SEPTEMBER 1985(U) INTERNATIONAL SOCIETY OF ELECTROCHEMISTRY 28 SEP 85 11/12

UNCLASSIFIED F/G 7/4 NL

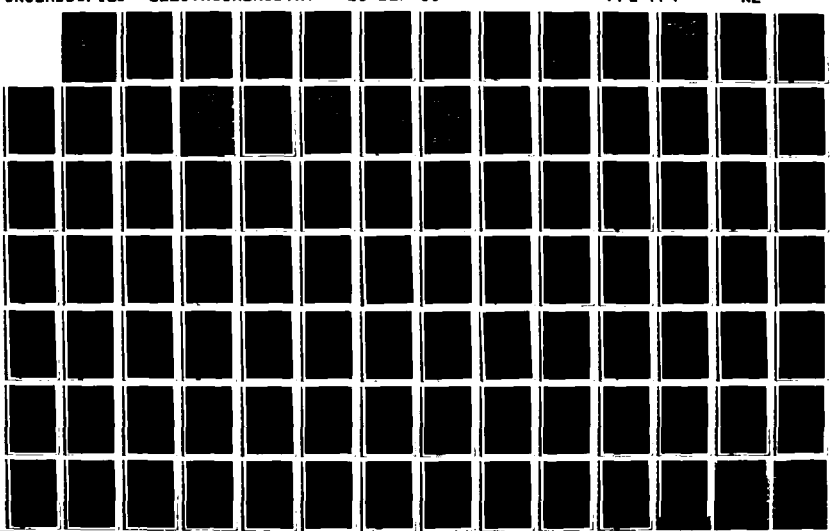

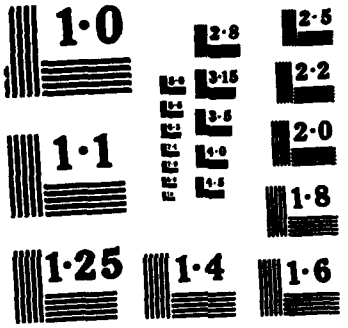

NATIONAL BUREAU OF STANDARDS
MICROCOPY RESOLUTION TEST CHART

ON THE STRUCTURE OF AQUEOUS AND HYDROCHLORIC SOLUTIONS OF $MnCl_2$. THE EFFECT OF CHANGES IN THE COMPOSITION ON THE STRUCTURE

E.BERECZ and T.TÖRÖK
Dept.of General and Physical Chemistry
Technical University for Heavy Industry,Miskolc /Hungary/

The effect of changes in the composition on the structure of the solutions of $MnCl_2$-H_2O and $MnCl_2$-HCl-H_2O are often discussed in terms of stepwise equilibria of complex formation and hydration phenomena of the possible species in the given system. As the concentration of $MnCl_2$ and HCl are increased in the solution more and more Mn-Cl complexes of different types are formed[1,2,3]. In the highly concentrated $MnCl_2$-HCl-H_2O solutions, besides the weak complexes of $Mn/H_2O/_{6-n}Cl_n^{2-n}$ /n=0,1,2/, which are predominant in the aqueous manganese chloride solution, the anionic octahedral complexes type $MnCl_3/H_2O/_3^-$; and $MnCl_4/H_2O/_2^{2-}$, as well as $MnCl_6^{4-}$, and at very high concentration also the tetrahedral complexes $MnCl_n/H_2O/_{4-n}^{2-n}$ /n=1,2,3,4/ are supposed to exist[1].

We measured the density and conductance of the above system at 25 °C. Though, generally, the volumetric properties and the conductance are not considered to be the most sensitive properties, we expected to observe some marked structural changes in the function of concentration, when a very wide concentration range of HCl at also a considerably high concentration of $MnCl_2$ /Fig.1/ are to be studied.

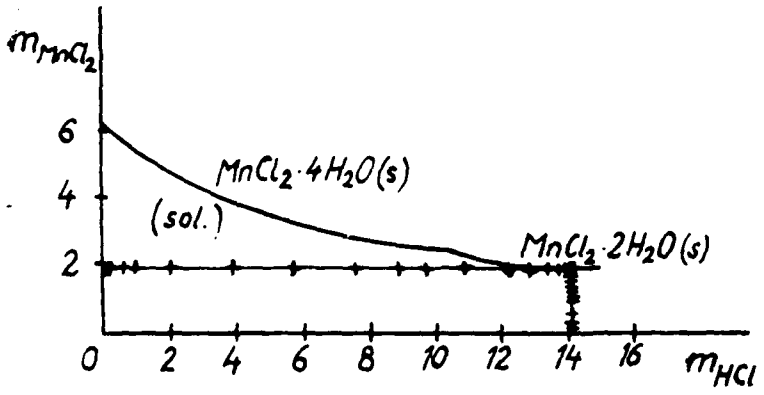

Fig.1. Solubility isotherm[4] and molalities of solutions investigated /+/

The concentration dependence of the conductivities are shown in Fig.2. The additivity rule[5] holds as good as in

some other MCl_x-HCl-H_2O /x=1,2/ type systems of alkali and alkaline-earth metal chlorides and $LaCl_3$ in hydrochloric acid, investigated earlier also in our laboratory /see K/add/ in Fig.2/.

The partial molal volumes of HCl and that of $MnCl_2$ were calculated /Fig.3/, where the recent density data of Rard and Miller[6] for the aqueous solutions of $MnCl_2$ were also used. The small changes in the curvature on the plot of V_{MnCl_2} at about m=2 and m=4 can be attributed to the higher degree of association of Mn^{2+} and Cl^- ions in the solution and probably to the formation of complexes $MnCl/H_2O/_5^+$ and $MnCl_2/H_2O/_4$ in these concentrated solutions.

In the series of ternary solutions at constant $MnCl_2$ molality /m_{MnCl_2}=1.848/ even a striking colour change was observed with increasing concentration of HCl from pink to brownish yellow, starting at around m_{HCl}= 8, which has also been accepted as evidence for the formation of chloro-complexes of manganese/II/. The curvature of V_{HCl} vs. m_{HCl} at constant $MnCl_2$ molality also shows some change at around m_{HCl}=7 and probably also at around m_{HCl}=13. At this very high HCl concentration the formation of tetrahedral anionic complexes is quite plausible.

Although the curve V_{MnCl_2} vs. m_{MnCl_2} does not show anomalous curvature /i.e. there are no break points/ with increasing concentrations of $MnCl_2$ up to saturation, nevertheless, the shape of the curve may be interpreted by the shifting of the stepwise equilibria of the complexation to the direction of formation of tetrahedral complexes containing more and more chlorides in the first coordination shells of manganese/II/ ions.

[1]Gmelin Handbuch der anorganischen Chemie, Mangan, Teil C5. Verlag Chemie, Weinheim, 1978. pp.60-63, 75-76 and see the references therein.

[2]Kublanovsky, V.S.: Zhurn. Neorg. Khim. 22 735-8 /1977/

[3]Libuś, Z.: Polish J. Chem. 53 1971-83 /1979/

[4]Balarew, Chr., Spassow, D., Simeonova, B.: Zschr. anorg. allg. Chem. 451 181-8 /1979/

[5]Berecz, E.: Acta Chim. Hung. 87/4/ 371-83 /1975/

[6]Rard, J.A., Miller, D.G.: J. Chem. Eng. Data 29 151-6 /1984/

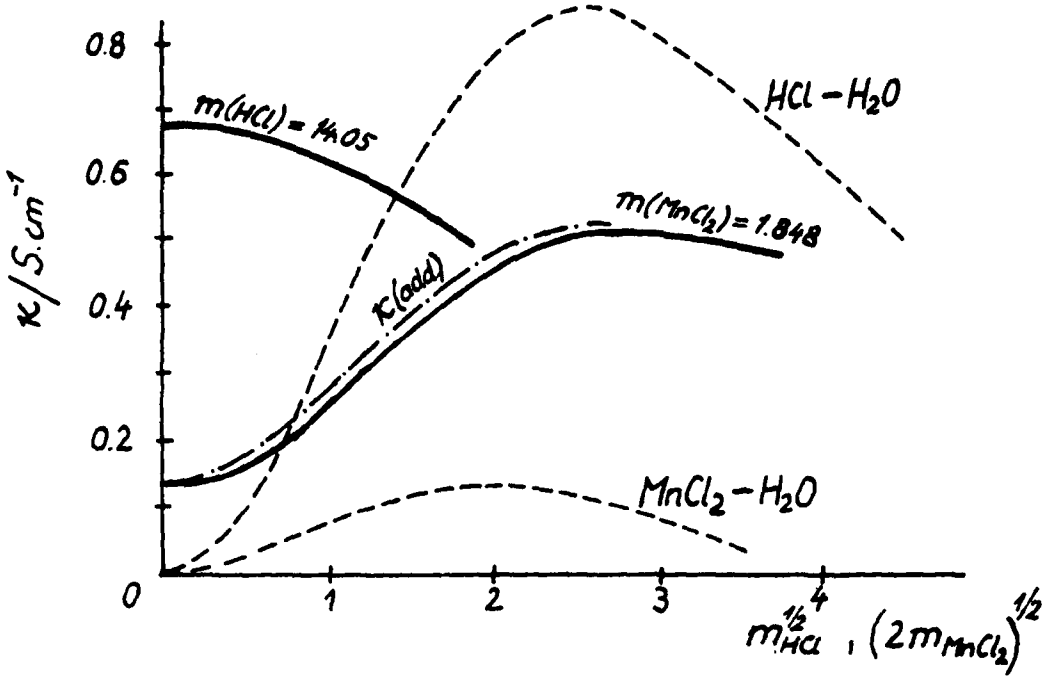

Fig.2. Electrical conductivities of binary (- - -) and ternary (———) $MnCl_2$-HCl-H_2O solutions investigated at 25 °C.

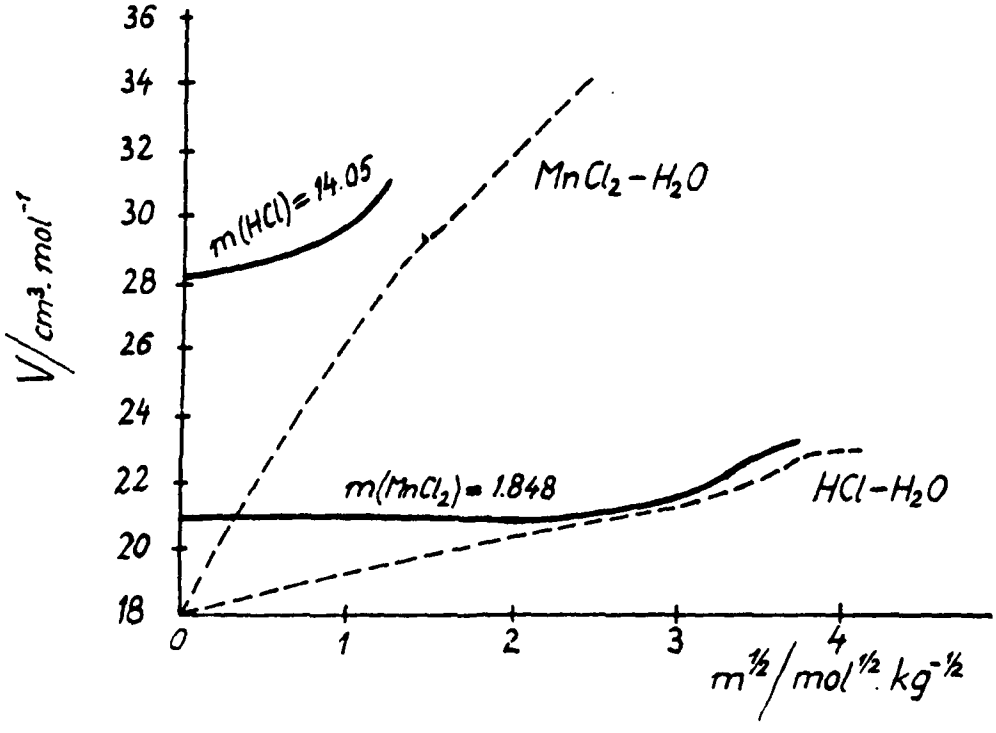

Fig.3. Partial molal volumes of binary (- - -) and ternary (———) $MnCl_2$-HCl-H_2O solutions investigated at 25 °C.

ELECTRODE-POTENTIAL / TEMPERATURE EQUILIBRIUM DIAGRAMS AND SOME OF THEIR APPLICATIONS[*]

by

Marcel POURBAIX
Belgian Center for Corrosion Study CEBELCOR, Brussels
(Belgium)

Equilibrium diagrams of the types E = f(T) and log p = f(1/T) will be presented for the 17 following systems :

Oxydation Equilibria :
- O
- O-Al
- O-C
- O-Fe
- O-H
- O-S
- O-Si
- O-Zn
- O-C-Fe
- O-C-Si
- O-C-Zn
- O-H-Fe
- O-S-Al
- O-S-Fe

Sulphidation Equilibria :
- S
- S-Al
- S-Fe

Applications of these diagrams are given concerning the following phenomena :

- the thermal dissociation of gaseous O_2, CO_2, H_2O, SO_3 and SO_2,
- the thermal decomposition of molten Al_2O_3 and *FeO*, and of solid ZnO,
- the thermal production of metallic zinc and silicon by carboreduction of their oxide,
- the corrosion and protection of iron in high-temperature water,
- the surface treatment of annealed carbon steel before phosphatization,
- the production of iron carbonyl, and the production of pure iron by thermal decomposition of iron carbonyl,
- the catalytic oxidation of SO_2 to SO_3,
- the high temperature corrosion of metals in atmospheres containing oxygen-and sulphur derivates,
- the formation of iron sulphides tenorite and pyrrhotite in meteorites and in the earth crust.

POLAROGRAPHIC STUDY OF THE COORDINATED SYSTEM Cd(II)-LEUCINATE.

G. RUIZ CABRERA, C. QUINTANA PERERA, J.C. RODRIGUEZ PLACERES, A. AREVALO.
Department of Physical Chemistry, University of La Laguna, Tenerife, Canary Islands, Spain.

The importance of knowledge of the systems with simples molecules[1-6] in the study of complex biological macromolecules has prompted us to undertake a series of works on metallic ion--aminoacid coordination[7-9].

The polarographic analysis of the coordinated system Cd(II)-Leucinate in aqueous medium is reported here. To the best of our knowledge, this system has only been studied on one occasion[10], by the potentiometric method, the metal values obtained under the two conditions assayed being: $\beta_1 = 1 \times 10^4$ and $\beta_2 = 2.9 \times 10^7$, and no trace being detected of the presence in the medium of complexes with a greater number of ligands.

EXPERIMENTAL

Each of the i-E curves was plotted with a Metrohm E506 polarograph with an E505 polarographic stand, Pt (EA285) and Ag/AgCl/NaCl sat. Metrohm EA427 electrodes were used as counter and reference electrodes, respectively, and the working one was a D.M.E. The temperature in the cell was 25± 0.05°C. Ionic strenght was adjusted to $\mu = 1.0$ with $NaClO_4$. Measurements of pH were carried out with a pHM84 digital potentiometer with a GK2401C Radiometer combined electrode. The concentration of metal ion was maintained constant at 2×10^{-5}M in all recordings. Drop-time was controlled at 3.0 s.

The sodium perchlorate and cadmium sulfate were Merck products of p.a. quality, the L-leucine was from Sigma and the sodium Hidroxide used for adjusting the pH was also of p.a. quality from May and Baker. The values of pK have been taken from D.D. Perrin[11] and are: $pK_1 = 2.37$ and $pK_2 = 9.62$.

RESULTS

Leucine in aqueous solution will give place to an equilibrium between its protonated forms, neutral and leucinate ion, governed by the acidity constants. At a sufficiently high pH, the complexes with leucinate will predominate, since its concentration will be significative and the corresponding stability constants are much higher than those of the possible species

coordinated with the neutral leucine.

The two studies were carried out varying the pH of an initial solution, and, therefore the concentrations of the different forms of leucine, between the limits 10.34×10^{-2}M and 10.21×10^{-2}M.

From the plots of $\log[(\bar{i}_d - \bar{i})/\bar{i}]$ vs E the reduction was shown to have taken place through a reversible bielectronic process. The halfwave potentials were also obtained from these plots.

The analysis of equilibrium was carried out following the method of De Ford and Hume[12], accepting as the value of β_1 that proposed by Data et al.[10]. The good linear dependence found for F_2 vs [Leucinate], fig. 1, points to the existence in the medium of complexes with two and three leucinate ligands. This is the first experimental evidence of the formation of the species $[CdL_3]^-$.

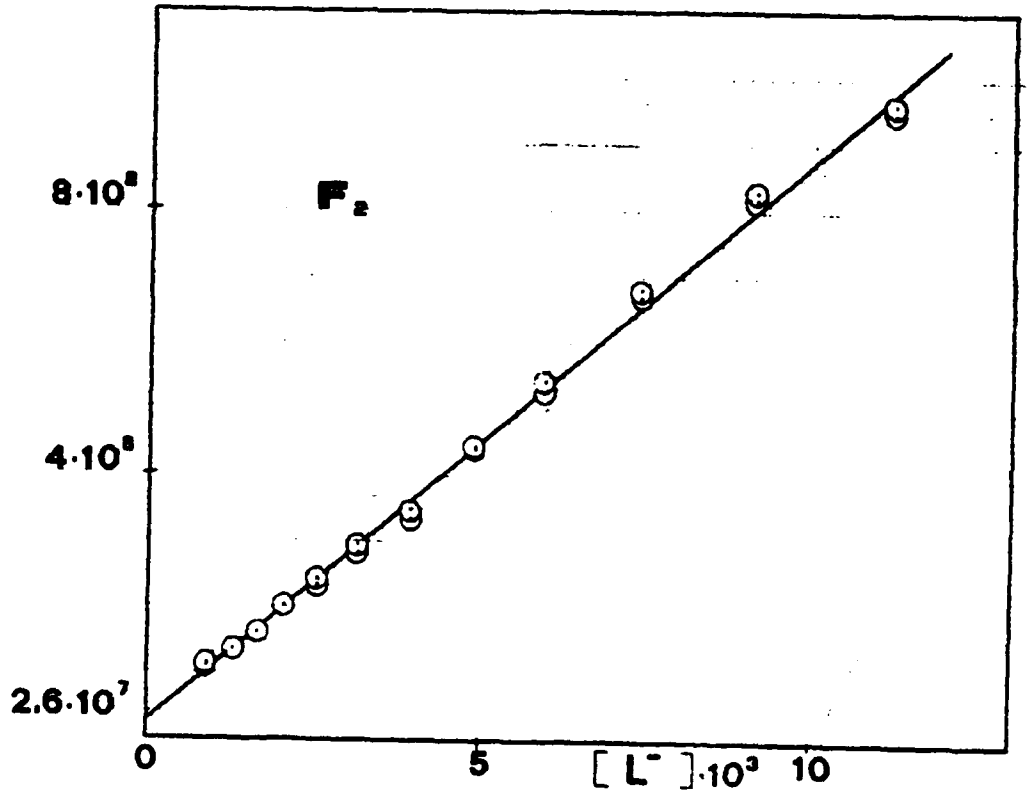

FIGURE 1

The values for the stability constants were obtained by square minima method and are given in Table 1:

TABLE 1

Studies	β_1	β_2
1	3.5×10^7	7.9×10^{10}
2	2.6×10^7	8.5×10^{10}

Their acceptable general concordance allows us to propose the followings constants of the coordinated species $[CdL_2]$ and $[CdL_3]^-$: $\beta_2 = 3 \times 10^7$; $\beta_3 = 8.2 \times 10^{10}$. The value of β_2 is in perfect agreement with that reported in the literature: $\beta_2 = 2.9 \times 10^7$ (see reference 10).

REFERENCES

1 FREEMAN H.C.,von EICHHORNS G.E.,Ed. "Inorganic Biochemistry", Elsevier,Amsterdam,pages 121-126.

2 GIORDANO R.S. and BEREMAN R.D.,Am. Chem. Soc. 96,1015 (1974).

3 LEVITZKI A.,PECHT I.,ANBAR M.,Nature 207,1386 (1965).

4 SHARMA V.S.,SCHUBERT J., J. Am. Chem. Soc.,91,6291 (1969).

5 SHARMA V.S.,SCHUBERT J.,BROOKS H.B. and SICILIO F., J. Am. Chem. Soc.,92,822 (1970).

6 SIEGEL H.,Angew Chem.,81,161 (1969).

7 RODRIGUEZ PLACERES J.C.,PASTOR G.,SANCHEZ J.A.,AREVALO A. Quím. Anal. (in press).

8 RODRIGUEZ PLACERES J.C.,RAMOS STEFFENS F.,PASTOR G. and AREVALO A., Anal. Quím. (in press).

9 RODRIGUEZ PLACERES J.C.,SANZ ALAEJOS M.T.,GARCIA MONTELONGO F.,Anal. Quím. (to be published).

10 DATTA S.P.,LEBERMAN R.,RABIN B.R.,Trans. Faraday Soc.,55, 1982 (1959).

11 PERRIN D.D.,J. Chem. Soc.,3125 (1958).

12 DE FORD D.D. and HUME D.N., J. Am. Chem. Soc.,73,5321 (1951).

POLAROGRAPHIC STUDY OF THE COORDINATED SYSTEM Cd(II)-OXALATE-NITRATE.

G. RUIZ CARRERA, G. PASTOR, J.C. RODRIGUEZ PLACERES and A. AREVALO.
Department of Physical Chemistry, University of La Laguna, Teneriffe, Canary Islands, Spain.

We have shown recently[1] that the constants of metal-ligand coordinated complexes, obtained when weakly complexing electrolytes are used to adjust the ionic strength, are not in fact true stability constants and really correspond to an arrangement of formation constants of simple and mixed species existing in the medium.

In this work we report the analysis of the coordinated system Cd(II)-oxalate-nitrate in aqueous medium and ionic strength 1.0. The simple Cd(II)-oxalate equilibria have been sufficiently studied but the ionic strength generally being adjusted with nitrates in such studies, invalidating the results obtained.

With respect to the mixed complexes, we have been unable to find any reference to then study and have therefore applied a method developed by us[2], which will provide new prospects in this area of research.

RESULTS AND DISCUSSION

System Cd(II)-oxalate-perchlorate.

Two studies were carried out.

Fig. 1 show the application of the De Ford and Hume method[3] to this coordinated system.

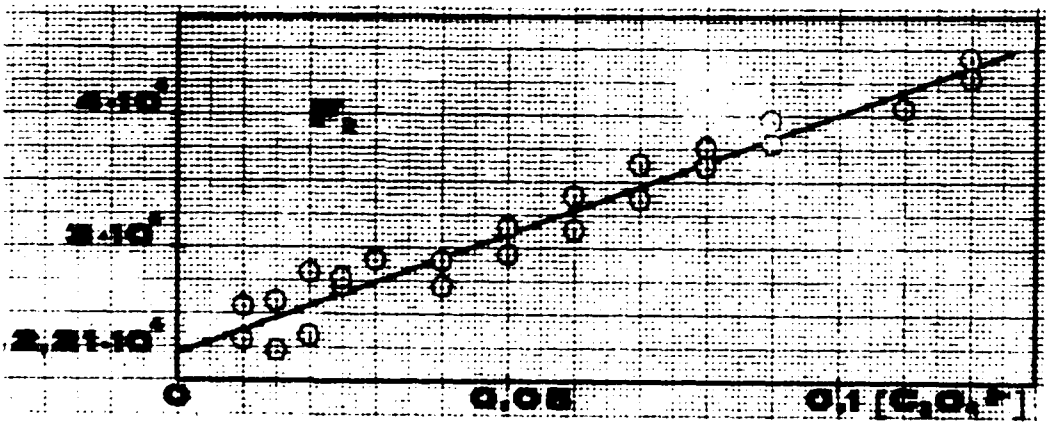

If can be observed that the dependence of F_2 vs. [ox] is a straight line, indicating the stabilization of the complexes $[Cd(ox)]$, $[Cd(ox)_2]^{2-}$ and $[Cd(ox)_3]^{4-}$. The fitting of the function: $F_1=\beta_{10}+\beta_{20}[ox]+\beta_{30}[ox]^2$ led to the values presented in Table 1.

TABLE 1

Study	β_{10}	$\beta_{20}\cdot10^{-4}$	$\beta_{30}\cdot10^{-5}$
I	452	2.21	1.80
II	466	2.00	1.85

The good general agreement allows the following to be proposed as the best data among the formation constants:

$\beta_{10}= 460$; $\beta_{20} = 2.1\cdot10^4$ and $\beta_{30} = 1.82\cdot10^5$

System Cd(II)-oxalate-nitrate.

The system Cd(II)-nitrate was studied previously under experimental conditions identical with those used in this work[4], the presence of the complexes $[Cd(NO_3)]^+$ and $[Cd(NO_3)_2]$ being determined in the medium, with stability constants: $\beta_{01} = 0.38$ and $\beta_{02} = 0.21$

Similarly, a mean value of 1.64 was obtained for the F_0 function corresponding to the 1.0M concentration of nitrate, in good agreement with that of 1.59 determined from the above-mentioned formation constants.

The stabilization of three complexes with the oxalate ion and two with nitrate allows us to propose the following expression for the function R_0, defined by Rodriguez Placeres et al[1].

$$R_0 = 1 + \frac{-3\beta_{01}-6\beta_{02}+\beta_{10}+\beta_{11}+\beta_{12}}{1+\beta_{01}+\beta_{02}}[OX] + \frac{9\beta_{02}-3\beta_{11}-6\beta_{12}+\beta_{20}+\beta_{21}}{1+\beta_{01}+\beta_{02}}[OX]^2 + \frac{9\beta_{12}-3\beta_{21}+\beta_{30}}{1+\beta_{01}+\beta_{02}}[OX]^3 \quad (1)$$

The function R_2 plotted in Fig. 2 ratify the dependence foreseen in equation (1):

$$R_0 = 1 + B[ox] + C[ox]^2 + D[ox]^3$$

The fit made following the least-squeres method gave the coeefficient values: $B = 372$; $C = 1.29\cdot10^4$ and $D = 1.1\cdot10^5$

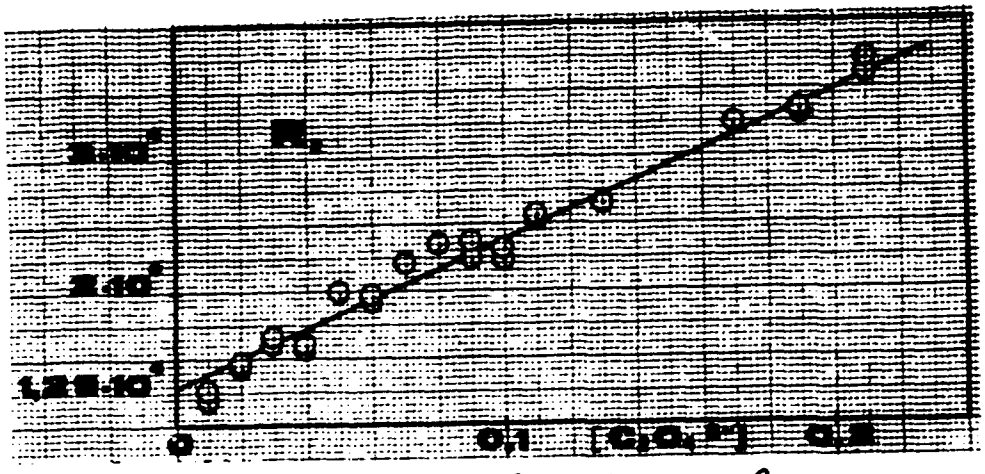

An approximate evaluation of β_{11}, β_{12} and β_{21} is necessary prior to the correct use of the above values for the determination - on the basis of expression (1) - of the constants of the mixed complexes. This calculation will be based as usual on the Watters equations[5]. given: $\beta_{11} = 133$; $\beta_{12} = 8.2$ and $\beta_{21} = 2120$ allowing us to foreses the impossibility of determining the values of β_{12} and β_{21}, considering the negligible value of the former as componed to β_{11} in the definition of the B coefficient and of both with regard to β_{20} and β_{30} in C and D.

The stability constant of the complex $\left[Cd(ox)(NO_3)\right]^-$ can be calculated from the value of B. A value of $\beta_{11} = 131$ is obtained in perfect agreement with that determined by means of the Watters equations.

The goodness of our data can be verified by comparing the experimentally obtained values of C and D with those deduced theoretically from the mathematical expressions of C and D. Substitutions in these expressions give: $B = 1.30 \cdot 10^4$; $C = 1.14 \cdot 10^5$ in total accordance with the experimental values: $B = 1.29 \cdot 10^4$; $C = 1.1 \cdot 10^5$.

REFERENCES

1 J.C. RODRIGUEZ PLACERES, M. BARRERA, R.M. FERNANDEZ and A. AREVALO. J.Electroanal. Chem., 69,169 (1984).

2 J.C. RODRIGUEZ PLACERES, G. RUIZ CABRERA, J.A. SANCHEZ and A. AREVALO., J.Electroanal. Chem. (to be published).

3 D.D. DE FORD and D.N. HUME., J. Am. Chem. Soc. 73,5321 (1951).

4 J.A. SANCHEZ. Thesis, University of La Laguna, Teneriffe, Spain, (1981).

5 J.I. WATTERS and R. LEWITT., J. Am. Chem. Soc. 82,1333 (1960).

12080

ACTIVITY COEFFICIENTS IN CONCENTRATED POTASSIUM HYDROXIDE - POTASSIUM ZINCATE ELECTROLYTES

M.J. ISAACSON, E.J. CAIRNS and F.R. MCLARNON
Applied Science Division
Lawrence Berkeley Laboratory
Department of Chemical Engineering
University of California
Berkeley, California 94720
U.S.A.

INTRODUCTION

Concentrated potassium hydroxide-potassium zincate electrolyte has been the favored electrolyte for secondary zinc/air and zinc/nickel oxide batteries. Despite the large amount of research done on rechargeable zinc cells over the past two decades, the electrolyte activity and osmotic coefficients have not been published. Several authors (1,2) have published activity coefficients calculated from zinc potential measurements. However, these calculations assume that the zincate ion does not specifically affect the hydroxide activity. The purpose of this work is to calculate the activity coefficients without relying on this assumption. There are three components, so two independent activity measurements must be made. The Zn/HgO cell potential is one activity measurement, and the alpha-Pd/HgO cell potential is being investigated as the other measurement. Macdonald (3) has demonstrated that H_2(Pt)/HgO cell potentials may also be used. The activity and osmotic coefficients are calculated from the potentials by numerically integrating the Gibbs-Duhem equation.

EXPERIMENTAL

Zinc potential measurements are performed in an H-shaped cell constructed from 3/8" Teflon tubing and tubing fittings. The Hg/HgO electrode occupies one side of the cell, and the zinc electrode occupies the other side. A Teflon plug physically separates the two half cells, but allows electrical contact to be maintained. Orifices drilled into the tubing fittings serve as openings for the Zn and HgO electrode connections, a thermocouple, and nitrogen-purge and vent lines. The zinc electrode is a 1.0-mm-diameter zinc wire that is sheathed with heat-shrinkable Teflon tubing, except for the end which is immersed in the electrolyte. Purge nitrogen is presaturated by bubbling it through a saturated salt solution of approximately the same water activity as the electrolyte. Electrolyte is injected into the cell with a syringe. The potential of the cell is monitored with a high-impedance electrometer and recorded on a strip-chart recorder until it has stabilized. Some measurements were performed in a glass cell of similar design.

Alpha-Palladium electrode potentials are measured in a similar manner, except that a counter-electrode and electrolyte compartment are added so that the Pd may be cathodized. The palladium electrode assembly is similar to that of Macdonald's (4). A 0.25-mm Pd wire is spot welded to a 0.25-mm Pt wire. This wire is then sandwiched between two

pieces of heat-shrinkable Teflon tubing with a Teflon rod in the center. After electrolyte is injected into the cell, the Pd electrode is cathodized against the counter electrode. The potential is then measured versus the HgO reference electrode.

RESULTS

Figure 1 shows the dependence of the Zn/HgO cell potential on the logarithm of the zincate ion molality at 7.666 molal KOH. A slope of 25 mV/decade is obtained. This slope may be compared to an ideal slope of 29.6 mV/decade.

Equation (1) indicates that the zinc potential should not depend on the hydroxide concentration in ZnO-saturated electrolytes

$$Zn + HgO = ZnO + Hg \qquad (1),$$

and the experimental verification of this prediction is shown in Figure 2. The error bars indicate the potential "drift" during a two-hour time period.

REFERENCES

1. J. Hendryks, A. VanderPutten, W. Visscher and E. Barendrecht, Electrochim. Acta 29, 81 (1984).

2. D.P. Boden, R.B. Wylie and V.J. Spera, J. Electrochem. Soc. 118, 1298 (1971).

3. W.B. Johnson, G.S. St. Pierre, D.D. Macdonald and M.K. Malhotra, "An Experimental Evaluation of the Thermodynamic Properties of Concentrated Aqueous Potassium Hydroxide Solutions," Lawrence Berkeley Laboratory Report No. LBL-19146 (February 1985).

4. D.D. Macdonald, P.R. Wentrcek and A.C. Scott, J. Electrochem. Soc. 127, 1745 (1980).

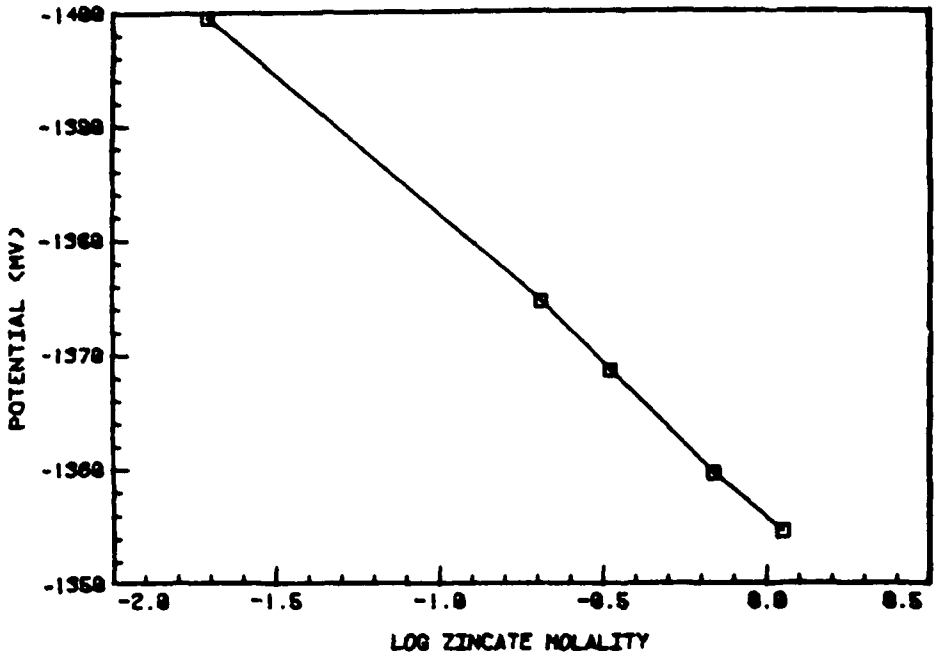

POT'L OF ZN ELECTRODE VS. HGO ELECTRODE @ 7.866 MOLAL HYDROXIDE

Figure 1

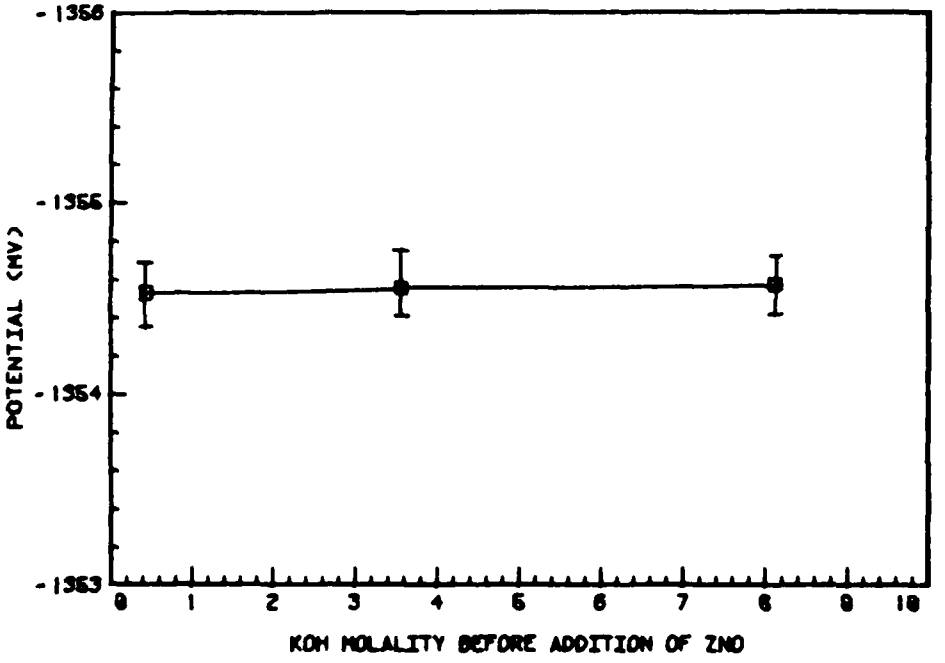

POT'L OF ZN ELECTRODE VS. HGO ELECTRODE FOR ZNO SAT'D ELECTROLYTE

Figure 2

THERMODYNAMICS OF THE COMPLEXES OF Cd(II) AND Pb(II) WITH GLYOXYLATE IONS.

K.K.CHOUDHARY+,S.C.BAGHEL* AND J.N.GAUR
Department of Chemistry,University of Rajasthan,Jaipur 302004(Ind)
Engineering College,Kota(India).

Shift in half-wave potential of metal ions by addition of sodium salt of glyoxylic acid shows complex formation with Cd(II) and Pb(II). The present studies are in succession to our study on In-glyoxylate[1].The values of overall formation constants and thermodynamic parameters of glyoxylate complexes of Cd(II) and Pb(II) at 303K and 313K are reported.

Experimental : The sodium salt of glyoxylic acid was used for complexation with Cd(II) and Pb(II) at u=1.0 in $NaClO_4$ at pH 6.5±0.2.The characterstics of capillary used were m=2.0 mg/sec and t=5.0sec in open circuit.0.005% gelatin was used to supress maxmia in all the Pb(II) solution.All the solutions were polarogramed in a H type cell in nitrogen atmosphere and potentials were measured w.r.t. S.C.E. The observations were made at two temperature 303K and 313K.Ligand concentration was varied from 0.05 to 0.50M.

Result and Discussion : The process of reduction in complexing media was found reversible and diffusion controlled as the slopes of the plots of log i/i_d-i vs Ede is 32± 0.1mv and i_d vs $h^{\frac{1}{2}}$ is straight line.The values of overall formation constants of the complexes were determined by DeFord and Humes method by plotting $F_j(x)$ v.s C_x(ligand concentration).The corresponding values of B_0, B_1,B_2,B_3 are obtined by extrapolating $Fo(x)$,$F_1(x)$,$F_2(X)$ and $F_3(x)$ to zero ligand concentration.Three complex species of the following composition $M(CHO.COO)^+$,$M(CHO.COO)_2$,$M(CHO.COO)_3$ are noticed with both the metal ions at 303K and 313K and the values of stability constants are given below.

System	Temp.	B_1	B_2	B_3
Cd-Glyoxylate	303K	40	50	1060
	313K	40	100	760
Pb-Glyoxylate	303K	500	3000	32250
	313K	500	3000	4650

+Address for Correspondance
Laxmi Udyog,Sitaram Bazar,Kaisergang,Ajmer 305001(India).

Thus it is evedient that the stability of the complexes of the bivalent metal ions with glyoxylate ions follows the following order Cu>Pb>Cd. Thus confirming the results of Meller and coworkers[2],on the basis of above results the nature of binding may be shown as below

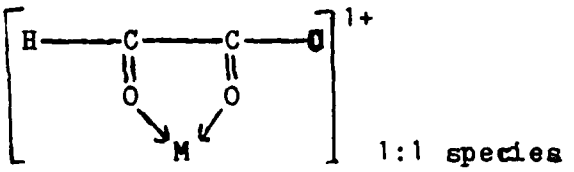

1:1 species

indating bidentate nature of glyoxylic acid,also shown by Rossoti[3] by N.M.R. signals of number of carboxylic acid in water.

By rise of temperature,the stability of the metal complex decreases and diffusion current increases and $E_{\frac{1}{2}}$ shifts to more +ve side as compared to 303K.The thermodynamic functions for 1:3 complexes were calculated from the values of overall formation constants at 303K and 313K,shown below

Complex species	ΔF° K Cals/mole	ΔH° K Cals/mole	ΔS° Cals/mole
Pb-Glyoxylate	-6.29	-36.50	-99.70
Cd-Glyoxylate	-4.22	-6.3	-6.9

As seen from the above table that the enthalpy change is more negative in Pb-glyoxylate complexes as compared to Cd-glyoxylate complexes further confirming our results that the complexes of lead are more stronger than Cadmium.The percentage distribution of various complex species of lead and cadmium in varius forms are calculated and plotted against -log Cx.are

Reference:1.K.K.Choudhary and J.N.Gaur, Indian Journal of chemistry,Vol.14A,pp 596-598(1978).
2. Mellor D.P. and Malvel; Nature 159,370(1947);161,463(1948)
3. Dillon K.B. and Rosmoti F.J.,Chem.Commun.,21,768(1966).
4. Day and selbin,Theoretical Inorganic Chemistry(East West Student Edition) 314(1967)

13 KINETICS OF COMPETING REACTIONS OF ACRYLONITRILE ELECTROREDUCTION TO ADIPONITRILE AND PROPIONITRILE

L. ONICIU[+], I. A. SILBERG[++], I. BALDEA[+], FLORENTINA CIOMOS[++]

MARIA JITARU[++], D. A. LOWY[++], O. H. OPREA[+] and LILIANA RADU[+]

[+]University of Cluj-Napoca, Dept. of Physical Chemistry
[++]ICECHIM - Institute of Chemical and Biochemical Energetics, Cluj-Napoca Research Group, Cluj-Napoca, Romania.

Cathodic reduction of acrylonitrile (ACN) in neutral phosphate buffer media on lead electrodes yields adiponitrile (ADN) by hydrodimerization and propionitrile (PN) by hydrogenation of the homogeneous double bond. As a consequence of chemical and electrochemical processes, the formation of several minor by-products was also observed; the "hydrotrimer" 1,3,6-tricyanohexane (T) is to be noted among these, due to its occurrence along the main line of the mechanistic steps entailed by the electrosynthesis of ACN. Excellent selectivities of ADN formation are ensured by adding submicellar concentrations of a cationic surfactant to the electrolyte.

It is the purpose of this paper to report kinetic investigations on the electrohydrodimerization of ACN to ADN, aiming at determining optimal preparative conditions by refining knowledge about the reaction mechanism, the part played by the quaternary ammonium salts (QAS), and the influence of the temperature upon the selectivity of the electroreduction.

A survey of literature data[1] and critical evaluation of recent papers (e.g.[2]) made us to favor the following reaction sequence as embodying the main pathway leading from ACN to ADN, PN, and T:

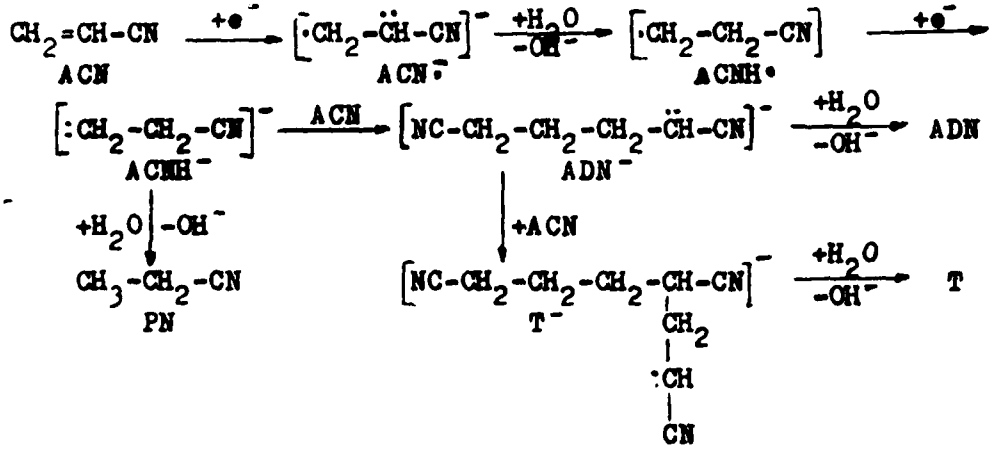

We assume that the first step consists of the electro-

nation of ACN yielding a highly reactive anion-radical, capable of extracting a proton from a water molecule even in the comparatively hydrophobic environment created by the QAS adsorption on the cathode. Since the radicals are characterized by a strong electrophilicity, we also consider that the first three steps (an ECE sequence) take place in the adsorbed state and only the carbanion ($ACNH^-$) becomes a free moving reaction species. It is at this stage that the competing reactions occurs, leading to PN by protonation or to ADN, via the second carbanion ADN^-, in a Michael addition, amounting to a cyanoethylation of $ACNH^-$.

Unlike previous considerations in the literature, focusing only on the partial exclusion of water from the pericathodic region by the cationic surfactants, we think that the phase-transfer catalytic activity of the QAS is at least as important. In our opinion, the observed product ratios ADN >> T > PN can be accounted for only by accepting that $ACNH^-$ is transferred from the aqueous environment to the ACN-rich organic phase droplets by the QAS coating of the latter, the rate of ADN^- formation thus considerably exceeding that of PN. In ADN^-, the location of the unshared electron pair of the carbanion next to the -CN group leads to mesomeric forms in which the basicity clearly surpasses the nucleophilicity,

$$-\overset{\ominus}{\ddot{C}}H-C\equiv N: \longleftrightarrow -CH=C=\overset{\ominus}{\ddot{N}}:$$

whereas for $ACNH^-$ the reverse is obviously true. Thus, unlike $ACNH^-$, the protonation is favored in the case of ADN^- over the reaction with ACN and the trimer is only a by-product.

The high reactivity of the intermediates and the catalytic effects involved are the premises for using the steady-state approximation and the following kinetic model emerges:

Process	Rate expression
$ACN + e^- \longrightarrow ACN^{\cdot -}$	$1/2\,\mathcal{F}$
$ACN + H_2O \xrightarrow{k_e} ACNH\cdot + OH^-$	$k_e[ACN^{\cdot -}][H_2O]$
$ACNH\cdot + e^- \longrightarrow ACNH^-$	$1/2\,\mathcal{F}$
$ACNH^- + H_2O \xrightarrow{k_1} PN + OH^-$	$\delta k_1[ACNH^-][H_2O]$
$ACNH^- + ACN \xrightarrow{k_2} ADN^-$	$\delta k_2[ACNH^-][ACN]$
$ADN^- + H_2O \xrightarrow{k_2'} ADN + OH^-$	$\delta k_2'[ADN^-][H_2O]$
$ADN + ACN \xrightarrow{k_3} T^-$	$\delta k_3[ADN^-][ACN]$
$T^- + H_2O \xrightarrow{k_3'} T + OH^-$	$\delta k_3'[T^-][H_2O]$

Here δ stands for the width of the reaction layer and i for the overall current density; since no other way for the consumption of $ACN^{\cdot -}$ is considered, it can be taken that the

contributions of the two electromation steps to $\underline{i}$ are equal, (i/2). In agreement with experimental observations, no hydrogen evolution is to be taken into account.

In the experiments herewith reported, attention was focused on the determination of PN/ADN ratios at different temperatures. The kinetic model leads to

$$\frac{C_{PN}}{C_{ADN}} = \frac{k_1 \left(k_2' [H_2O] + k_3 [ACN] \right)}{k_2 \, k_2' [ACN]}$$

As both PN and T represent minor products, $k_1 k_3 [ACN] \ll k_1 k_2' [H_2O]$ and with a good approximation,

$$\frac{C_{PN}}{C_{ADN}} = \frac{k_1'}{k_2 [ACN]}$$

where $k_1 [H_2O] = k_1'$.

Thus, increased ACN disponibility for the reaction, by improved mass transfer, efficient phase-transfer catalysis and optimized ACN/aqueous support electrolyte ratio significantly improve the selectivity of ADN *vs.* PN formation, with only tolerable increase of [T] in the crude electrosynthesis product.

In our experimental conditions the C_{PN}/C_{ADN} ratios at 15°, 25°, and 35°C were 1.331, 0.336, and 0.300, respectively, yielding for the overall activation energies the values $E^{\neq}_{PN}$ = 63.1 kJ/mole and $E^{\neq}_{ADN}$ = 69.0 kJ/mole, suggesting that there is an additional slight preference for ADN formation when working at, or above ambient temperature, and that energy consumming cooling operations are not necessary.

Work is now in progress investigating the possibility of promoting a one-step formation of an ADN radical by an concerted low-energy electromation-protonation of an $(ACN)_2$ π-complex on the electrode surface in a QAS matrix, without PN-, and with negligible T formation.

References.

1. L. ONICIU, I. A. SILBERG and FLORENTINA CIOMOS, Rev. Chim. 36, 406, (1985).

2. A. N. HAINES, I. F. McCONVEY and K. SCOTT, Electrochim. Acta 30, 291, (1985).

KINETICS AND MECHANISM OF p,p'-DIAMINODIBENZYL ELECTROSYNTHESIS

L. ONICIU[+] I. A. SILBERG,[++] VIRGINIA DANCIU,[++] MARIA OLEA[+] and SIMONA BRAN[+]

[+]University of Cluj-Napoca, Dept. of Physical Chemistry
[++]ICECHIM- Institute of Chemical and Biochemical Energetics, Cluj-Napoca Research Group, Cluj-Napoca, Romania.

In contrast with other aromatic nitroderivatives, there are very few data in the literature concerning the electroreduction of p,p'-dinitrodibenzyl (DNDB) to the corresponding diamine (DADB), an important intermediar in the manufacturing of polyurethanes. The reported polarographic (on Hg)[1] and cyclic voltammetry[2,3] investigations were carried out in non-aqueous media and are of little avail to preparative work. A recently patented procedure of van TILBERG[4] only mentions the cathodic reduction of DNDB.

With a view to elaborating a useful preparative electrosynthesis of DADB, the present paper reports an investigation of the reduction of DNDB under potentiostatic and galvanostatic conditions. A thermostated electrolysis cell with a microporous Modilene membrane, diluted aqueous H_2SO_4 as anolyte, lead as anode, and a stirred $8.2\ 10^{-4}$ M solution of DNDB in aqueous ethanol as catholyte was used. The absorbance at 283 nm served for monitoring the DNDB concentration during the electroreduction.

The Guggenheim method yielded the rate constants, determined from the slope of the $\log(E_t - E_\infty)$ *vs.* time straight line where E_t and E_∞ stand for the absorbances at a time t after the start, respectively after completion of the electrolysis. The measurements were carried out at 42°, 50.5° and 62° and at various cathode overvoltages (η_c), maintained with a Wenking HP-72 potentiostat; a saturated calomel electrode served as a reference. By means of Arrhenius plots, overall activation energies were determined, on tin and copper cathodes (Table 1). At the same overvoltages, on tin and lead cathodes, after 30 min. (the half-life time of DNDB in the process) faradaic yields (r_p) and conversions (x) were calculated (Table 2). The results in Table 3 display the parameters of galvanostatic experiments on tin at 62° and various current densities.

The values of E demonstrate, in agreement with observations made under somewhat similar conditions on nitrobenzene and p-nitrotoluene,[5] that the diffusion is the rate-controlling process, stressing the importance of activated mass transfer and of increasing the solubility of DNDB by means of cosolvents. Tin is by far the best cathode material, and a

Table 1

Cathode	η_c V	E^+ kJ/mole
Tin	e.1ee	18.4
	e.15e	16.2
	e.2ee	21.5
	e.25e	25.9
Copper	e.1ee	59.8
	e.2ee	25.6

Table 2

Cathode	η_c V	r_F %	x %
Tin	e.1ee	84.4	8e.3
	e.15e	36.9	85.e
	e.2ee	26.1	82.1
	e.25e	22.5	92.5
Lead	e.1ee	68.6	39.3
	e.15e	68.2	44.5
	e.2ee	6e.2	46.8
	e.25e	59.6	48.6

Table 3

i, $mAcm^{-2}$	22.2	33.3	44.4	66.6	88.8
k, $1e^{-4}s^{-1}$	4.71	5.77	7.44	6.25	3.31

corroboration of data in Tables 1 and 2 lead to the conclusion that e.1ee V is the optimal compromise value for cathode overvoltage. Under these conditions, the DADB is formed mainly by a chemical process, mediated by the Sn^0/Sn^{2+} couple, the electrochemical contribution consisting almost exclusively of the regeneration of tin metal. When higher overvoltages are imposed, the activation energy increases, denoting a decrease in importance of the chemical reduction, direct electrochemical conversion of DNDB into DADB coming in the forefront. The fact that on copper cathodes the activation energies are 2-3 times larger than on tin, indicates that on copper the direct electrochemical reduction is predominant, in agreement with the well-known lack of reductive properties in the case of copper, unlike that of tin.

Under galvanostatic conditions, the reduction rate reaches a maximum around 45 $mAcm^{-2}$; over this value of current density, at the DNDB concentrations used, there is increasing hydrogen evolution, a process which hampers the diffusion of DNDB molecules towards the cathode, and diminishes the rate.

The electrosynthesis of DADB on tin in hydrochloric acid-ethanol media is remarkably selective, only traces of 3-chloro-4,4'-diamino-dibenzyl being formed by a transposition at the hydroxylamine stage, as shown by chromatographic separations coupled with mass-spectrometric structure checks.

The herewith reported results open the route to a preparative electrosynthesis of DADB and are now subject of scale-up investigations.

References.

1. J. G. LAWLESS, D. E. BARTOK, J. Am. Chem. Soc. 91, 7121,(1969)
2. F. ANNUAR, J. B. SAVEAUT, J. Electroanal. Chem. Interfacial Electrochem. 47, 111, (1973).
3. M. MAHBOOB, Electrochim. Acta 22, 487, (1977).
4. W. J. TILBERG, Eur. Pat. Appl. 28,43o; C. A. 95, 69965x (1981)
5. S. V. GORBACHEV, C. F. BELEVSKII, Zh. Fiz. Khim. 32, 13o4, (1958).

13030

ADSORPTION OF ANODICALLY GENERATED RADICALS AT CARBON AND PT-ELECTRODES AND ITS ROLE IN ELECTROORGANIC SYNTHESIS

Hartmut WENDT, Vojtech PLZAK, Wolfgang JENSEIT
Institut f. Chem. Technologie, TH Darmstadt
Petersenstr. 20, D-6100 Darmstadt, Fed.Rep.Ger.

Anodic addition of radicals (generated from different anions) to olefins is an interesting means to produce 1.2-bisubstituted (monomeric (eq.5)) and 1.4-bisubstituted (dimeric (eq.4)) products[1].

(1) $X^- - e^- \longrightarrow X^\cdot$, (2) $2\,X^\cdot \xrightarrow{k_1} X_2$

(3) $X^\cdot + \diagup C = C \diagdown \xrightarrow{k_{add}} X - \overset{|}{C} - \overset{|}{C}\,\cdot$

(4) $2\,X - \overset{|}{C} - \overset{|}{C}\,\cdot \xrightarrow{k_2}$ dimer

(5) $X^\cdot + X - \overset{|}{C} - \overset{|}{C}\,\cdot \xrightarrow{k_3} X - \overset{|}{C} - \overset{|}{C} - X$

The outcome of the electrosynthesis-reaction depends strongly on the reactivities of produced radicals and olefin-scavengers: high reactivities of both species favour dimer formation according to reaction sequence (1), (3),(4) and low reactivities of both favours the annihilation reaction (2).
Additionally the relative yields of the different products,e.g. the selectivity,is strongly influenced by the choice of the electrode-material:
At carbon anodes the yield of X_2 is greatly enhanced at the expense of 1,2-substituted products and the yield of 1,4-disubstituted products is decreased even more
For $X^- = N_3^-$ the reaction was investigated voltammetrically and measured current voltage curves are evaluated based on the Nernst-formula with respect to rate constants k_1 and k_{add}.

The kinetic analysis reveals that if platinum electrodes are used, all consecutive reactions following the initiating charge transfer (eq.(1)) are essentially homogeneous reactions proceding in the narrow reaction layer in front of the electrode. Seperately determined rate constants for k_{add} allow

to predict dependence of yields on current ensity and olefin-concentration according to a homogeneous-reaction model and the predictions are well verified by preparative data.
At carbon anodes all consecutive reactions proceed essentially heterogeneously and are heterogeneously catalyzed. Especially the (often undesired) radical-annihilation reaction (eq. 2) is strongly accelerated. The reason are established saturation-concentration of styrene at carbon electrodes already at relatively modest styrene concentrations (1 molar) and pronounced adsorption of the azide-radicals on carbon anodes.[2.3.4.]

Measurements of electrode-impedances of carbon anodes and platinum anodes at which azide radicals are being oxidized reveals distinctively different adsorption patterns of azide anions/radicals at these two different electrode materials:

At Pt-anodes, which are covered by Pt-oxide in the potential-range, where N_3^--anions are oxidized, one observes expressed pseudocapacitance - maxima due to insertion of N_3^- into Pt-O. Therefore the discharge associated with this process must not be associated with the formation of $N_3^{\cdot}$-radicals.

At carbon anodes an adsorption-pseudocapacitance cannot be detected - very likely because the stationary concentrations of $N_3^{\cdot}$-radicals are very low. Those stationary surface concentration of $N_3^{\cdot}$-radicals on carbon-anodes already were supposed from the kinetic data to be of the order of magnitude 10^{-14} to 10^{-13} mole/cm² ($\theta \approx 10^{-5}$ to 10^{-4}).[5]

/1/ H. Schäfer, A. Alzarak, Angew. Chem. 80 (1968) 485;
/2/ V. Plzák, H. Wendt, Ber. Bunsenges. Physik. Chem. 83 (1979) 481;
/3/ H. Wendt, V. Plzák, J. electroanal. Chem. 154 (1983) 13;
/4/ V. Plzák, H. Wendt, J. electroanal. Chem. 154 (1983) 29;
/5/ v. Plzák, H. Wendt, J. electroanal. Chem. 180 (1984) 185

CARBON-CARBON BOND FORMATION BY REACTION OF ELECTROCHEMICALLY GENERATED ARYL RADICALS WITH NUCLEOPHILES

C. AMATORE[1,3], C. COMBELLAS[2], M.A. OTURAN[1]
J. PINSON[1], J.M. SAVEANT[1] and A. THIEBAULT[2].

[1]Laboratoire d'électrochimie, Université Paris 7, 2 Place Jussieu, 75251 Paris Cedex 05, France.

[2]Laboratoire de Chimie Analytique des Milieux Réactionnels, ESPCI, 75231, Paris Cedex 05, France.

[3]Present adress : Laboratoire de Chimie : Ecole Normale Supérieure, 24 rue Lhomond, 75005 Paris.

$S_{RN}1$ reactions constitute a powerful method for the aromatic nucleophilic substitution of non activated substrates. It proceeds along the following mechanism

$$ArX + 1e \rightleftarrows ArX^{\cdot -} \quad (1)$$

$$ArX^{\cdot -} \rightleftarrows Ar^{\cdot} + X^{-} \quad (2)$$

$$Ar^{\cdot} + Nu^{-} \rightleftarrows ArNu^{\cdot -} \quad (3)$$

$$ArNu^{\cdot -} - 1e \rightleftarrows ArNu \quad (4)$$

$$\text{or } ArNu^{\cdot -} + ArX \rightleftarrows ArX^{\cdot -} + ArNu \quad (5)$$

$$\text{but also } ArNu^{\cdot -} \rightarrow \text{Further reaction products} \quad (6)$$

Electrochemistry affords an easy way for triggering the above sequence via a quantitative formation of aryl radicals from haloaromatics (equ.1). The method is successfully applied to various carbon nucleophiles to obtain carbon carbon bond formation.

Nucleophile	substrate	Product	Solvent	Yield	Mechanism
Ketone enolate $^{-}CH_2-\underset{\underset{O}{\|}}{C}-CH_3$		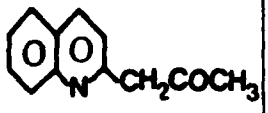	NH_3		Reactions 1-5
Propionitrile anion $CH_3-\underline{C}H-CN$	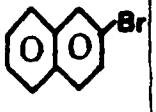	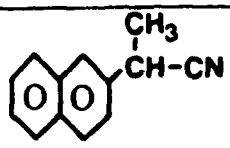	NH_3	90	1-5
Cyanide CN^-		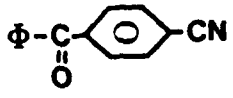	ACN NH_3	95	1-5
2.Nitropropanate $CH_3-\overset{\overset{NO_2}{\|}}{C}-CH_3$	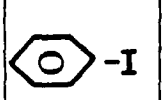 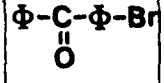	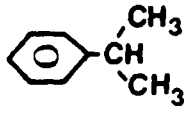 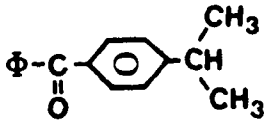	DMSO DMSO NH_3	30 43	1-3 + 6 1-3 + 6
Oximate $CH_3-\overset{\overset{N}{\|}{\|}O}{C}-CH_3$	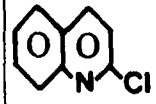	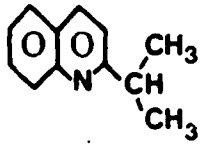	H_2O	≈20	1-3 + 6
Phenate 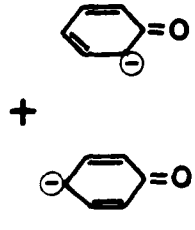	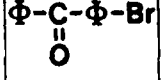	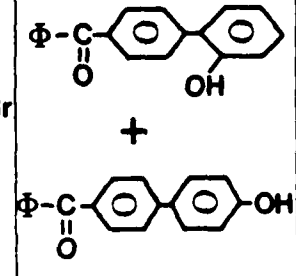	NH_3 DMSO	55	1-5

References

1) J.M. SAVEANT, Acc. Chem. Res., 13, 323,(1980).

2) J. PINSON and J.M. SAVEANT, J. Am. Chem. Soc., 100, 1506, (1978).

3) C. AMATORE, J. CHAUSSARD, J. PINSON, J.M. SAVEANT and A. THIEBAULT, J. Am. Chem. Soc., 101, 6012, (1979).

4) C. AMATORE, J. PINSON, J.M. SAVEANT and A. THIEBAULT, J. Am. Chem. Soc., 104, 817, (1982).

ELECTROCHEMICAL BEHAVIOUR OF 1-METHYL-2,4-DICYANOPYRIDINIUM ION IN DIPOLAR APROTIC SOLVENTS.

ITALO CARELLI[a], ANTONIO CASINI[b] and FRANCO LOMBARDO.
a: Centro di Studio per la Elettrochimica e la Chimica Fisica delle Interfasi del CNR, Via del Castro Laurenziano, 7 - ROMA, Italy. b: Cattedra di Chimica Farmaceutica Applicata - Università "La Sapienza" - ROMA.

Electrochemical reduction patterns of 1-methylcyanopyridinium ions were extensively investigated in our laboratories for mechanistic, as well as synthetic purposes[1,2,3].

We report now on the electrochemical behaviour of 1-methyl-2,4-dicyanopyridinium tosylate 1 in aprotic dipolar solvent, such as dimethylformamide (DMF) or acetonitrile. Then, cyclic voltammetry measurements performed on HMDE or GCE, showed the presence of two cathodic-anodic one-electron, well resolved, processes, the first one at about -0.2 V vs SCE and the second one at about -1.1 V vs SCE (Fig. 1,a and Table I).

As already reported in a previous communication[4], the first cathodic process corresponds to the formation of a stable pyridinyl radical,which can reversibly be reoxidized to the starting ion. This radical, obtained also by electrolysis of 1 at potential values more negative than the first cathodic peak was unambiguously identified by e.s.r. and u.v. spectroscopy as 1-methyl-2,4-dicyano-4-pyridinyl radical, identical to that obtained by chemical reduction of 1 [5].

The second cathodic process can also be rationalised as one-electron process, consistent with the evidence from voltammetric (Table I) and coulometric (n=2) data. The reversibility of the second step is lower than that of the first one; however, the value i_{pa}/i_{pc} of the former indicates a certain degree of stability of the product, reasonably a dihydropyridinyl anion.

When the CV is performed in the presence of a small excess of weak protonating agents such as 3,4-xylenol or water, a remarkable decrease of the second anodic peak can be observed (Fig. 1,b and Table II), due probably to the coupling of the anion with the proton. Therefore, it seem likely that the reduction of 1 at potential values more negative than the second cathodic peak, in the presence of protonating agents affords dihydropyridine species. In fact, the u.v. spectrum of the electrolyzed solution, taken immediately after the end of the electrolysis, displays absorption maxima at 328 and 365 nm, strongly suggestive of dihydropyridines. 1-methyl-2,4-dicyano-1,4-dihydropyridine 2 and 1-methyl-2,4-dicyano-1,2-dihydropyridine 3, prepared via an in-

dependent route, actually display absorption maxima at 328 and 365 nm, respectively.

SCHEME

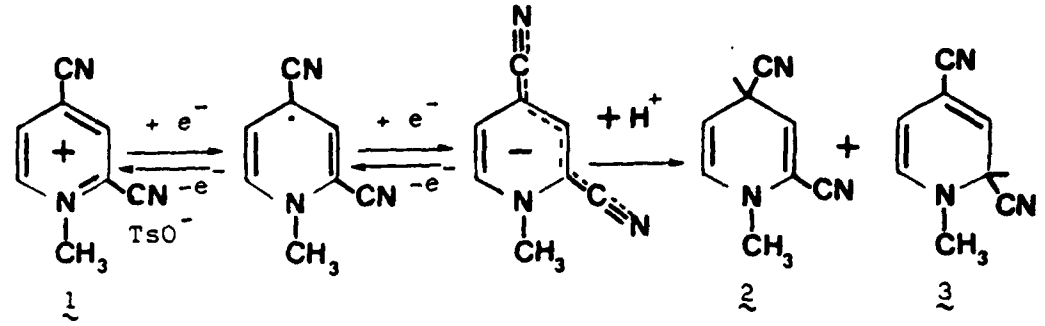

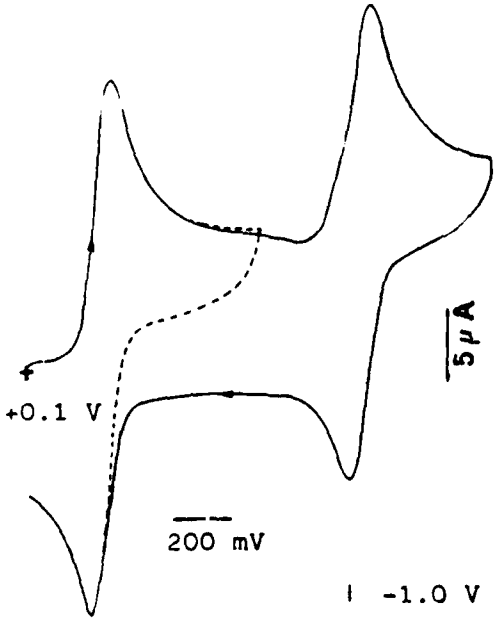

Fig. 1, a

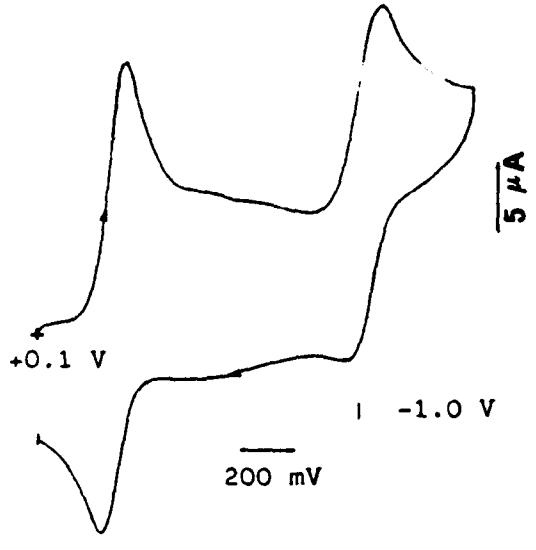

Fig. 1, b

Fig. 1, a: Cyclic voltammogramm of 1 (1.0×10^{-3} M) in DMF and 0.1 M TEAP on GCE. Scan rate: 0.20 V/s. Dotted line: Voltammogramm limited to the first process.
Fig. 1, b: Cyclic voltammogramm of 1 (1.0×10^{-3} M) in DMF and 0.1 M TEAP on GCE in the presence of 3,4-xylenol (5.0×10^{-3} M). Scan rate 0.20 V/s.
Potential values are referred to the S.C.E.

TABLE I. Voltammetric data of a solution of 1 (1.0×10^{-3} M) in DMF and 0.1 M TEAP on GCE. Potential values are referred to the S.C.E. (see Fig. 1,a).

Scan rate	$-E_{pC}$	i_{pC}	$i_p/v^{0.5}$	$-E_{pA}$	i_{pA}	$i_p/v^{0.5}$	i_{pA}/i_{pC}
V/s	V	μA		V	μA		
Peak I							
0.05	0.21	9.60	43.04	0.13	9.60	43.04	1.00
0.10	0.21	13.20	41.77	0.12	13.80	43.67	1.04
0.20	0.21	19.00	40.71	0.12	19.60	43.84	1.03
Peak II							
0.05	1.10	7.80	34.97	1.02	5.20	23.31	0.67
0.10	1.10	11.00	34.81	1.01	8.60	27.21	0.78
0.20	1.10	16.20	36.24	1.01	13.20	29.53	0.81

TABLE II. Voltammetric data of a solution of 1 (1.0×10^{-3} M) in DMF and 0.1 M TEAP in the presence of 3,4-xylenol (5.0×10^{-3} M). Potential values are referred to the S.C.E. (See Fig. 1,b).

Scan rate	$-E_{pC}$	i_{pC}	$i_p/v^{0.5}$	$-E_{pA}$	i_{pA}	$i_p/v^{0.5}$	i_{pA}/i_{pC}
V/s	V	μA		V	μA		
Peak I							
0.05	0.20	9.00	40.35	0.12	9.00	40.35	1.00
0.10	0.20	12.80	40.50	0.12	12.80	40.50	1.00
0.20	0.20	17.80	39.82	0.12	18.60	41.16	1.04
Peak II							
0.05	1.10	8.40	37.66	0.96	3.80	17.00	0.45
0.10	1.10	10.80	34.17	0.96	5.20	16.45	0.48
0.20	1.10	14.40	32.21	0.96	8.20	18.30	0.56

References

1. I.Carelli, M.E. Cardinali, A.Casini and A. Arnone, (1976), J.Org.Chem., 41, 3967-3969.
2. I.Carelli, M.E.Cardinali and A.Casini, (1979), J.Electroanal. Chem., 105, 205-215.
3. I.Carelli and M.E.Cardinali, (1981), J.Electroanal.Chem., 124, 147-153.
4. I.Carelli and A.Casini, Atti del XV Congresso Nazionale della Società Chimica Italiana, Div. Elettrochimica, Grado, 17-21 settembre 1984 (Italy).
5. L.Greci, A.Alberti, I.Carelli, A.Trazza and A.Casini, (1984), J.Chem.Soc.Perkin II, 2013-2018.

13060

ON THE OXIDATION MECHANISM OF NITROXIDE RADICALS IN APROTIC MEDIA

A. TRAZZA, R. ANDRUZZI and G. MARROSU
Dipartimento Ingegneria Chimica - Università "La Sapienza"
and Centro di Elettrochimica e Chimica Fisica delle Interfasi
del C.N.R. - Via del Castro Laurenziano, 7 - 00161 ROMA - Italy

As a continuation of our previous researches on the reactivity of radicals we are studying the chemical (with cerium ammonium nitrate) and electrochemical (at a platinum electrode) oxidation of 1,2-dihydro-2,2-diphenyl-3-aryliminoindolin-1-oxyls (nitroxide radicals) 1a-e in acetonitrile in both the presence and the absence of nucleophilic agents of various strengths.

In the range of concentration used (1.10^{-4}-5.10^{-3}mol dm^{-3}) nitroxide radicals 1a-e in MeCN (with Et_4NClO_4 as supporting electrolyte) exhibit at a pulsed platinum electrode an oxidation step at potentials between 0.6 - 0.7V (vs. $Ag/AgClO_4$ in MeCN). The oxidation process turns out to be mono-electronic, reversible, diffusion-controlled (in the dc sense) and yields the corresponding oxoammonium cations 2a-e. The cyclic voltammetric experiments at a stationary platinum electrode show that the oxoammonium cations are stable during the time of the measuraments; i.e., the cyclic voltamperograms of 1a-e exhibit an anodic-cathodic system ($ip_a/ip_c = 1$) even at sweep-rates as slow as 50mV s^{-1}. On addition of increasing amounts of water (molar ratio water/reactant, 0 - 300) to the solutions of nitroxide radicals 1a-e in MeCN-Et_4NClO_4 the oxidation step increases until its height becomes approximately three times higher (i.e., the electrode process tends to become three-electronic) than the original step. The corresponding cyclic voltammetry shows that in MeCN-H_2O the oxidation process of 1a-e becomes completely irreversible, kinetic in character and involves two to three electrons. In fact, i) the original anodic peak increases its height, ii) the corresponding complementary cathodic peak is replaced by another cathodic peak at about zero potential and related to the follow-up chemical reaction of their primary oxidation product, iii) on increase of the sweep-rate, the current function ($ip_a/\sqrt{v}$) decreases and the oxidation peak potential (Ep) shifts towards more positive values.

During the controlled-potential electrolysis(at 0.9V) of nitroxide radicals 1a-e in pure MeCN-Et_4NClO_4, the current decayes slowly to values in accordance with n_{app} = ca.3. Cyclic voltamperograms indicate that the original anodic-cathodic system is gradually replaced by two reduction peaks, the first at approximately zero potential and the second at ca. -0.6 V, which correspond to reduction of protons and quinoneimine N-oxides, respectively.

Macroscale electrolyses (at 0.9V) of 1a-e in MeCN-$LiClO_4$ with a large excess of water show that the current decays rapidly to the background current with n_{app}= 3. From the electrolysed solutions are isolated the corresponding 5- (3a-e) and 7- (4a-e) quinoneimine N-oxides in percent yields 80-90 and 15-7, respectively.

To explain the above findings, we suggest for the oxidation mechanism of nitroxide radicals 1a-e the scheme 1.

SCHEME 1

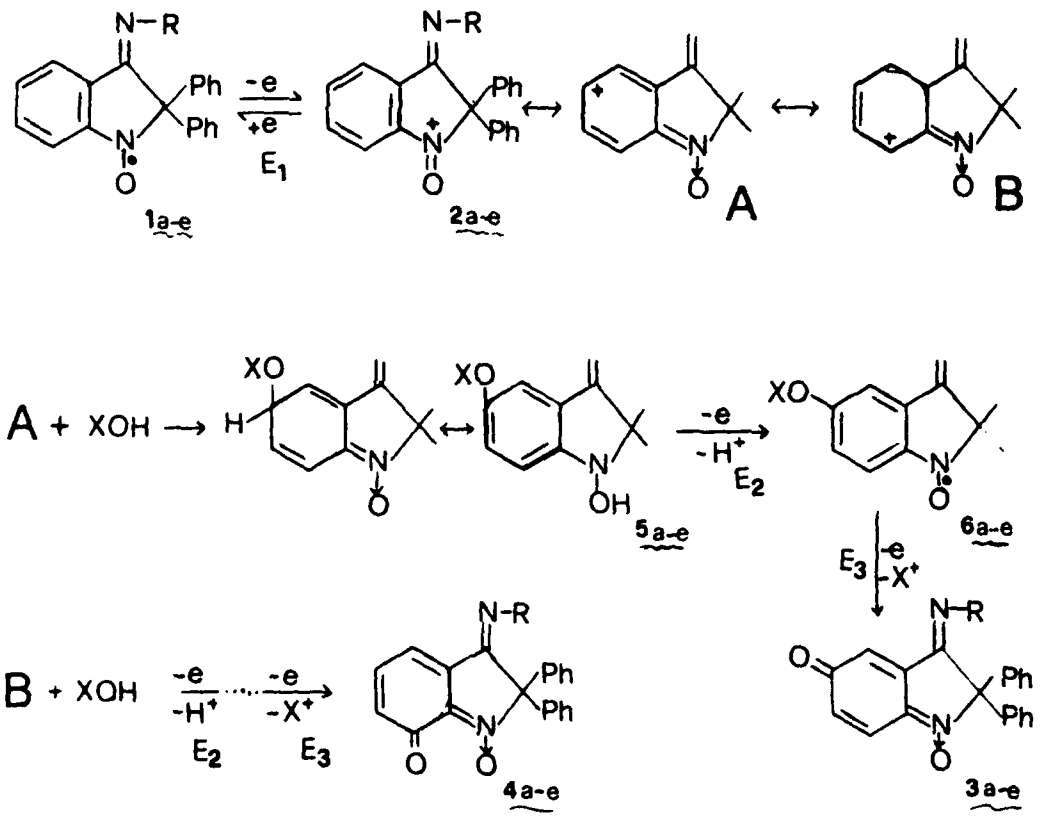

a) R = C_6H_5; b) R = C_6H_4-OMe(p); c) R = C_6H_4-Me(p); d) R = C_6H_4-Cl (p); e) R = C_6H_4-Br (p).

$E_1 > E_2 \approx E_3$

XOH refers to nucleophilic agent like H_2O, MeOH, etc.

Thus the electrode process of nitroxide radicals 1a-e in MeCN begins with a reversible one electron step yielding the corresponding oxoammonium cation 2a-e. These cations in pure MeCN are stable at the electrode during the time of the voltammetric measurements but during the electrolysis they undergo in the solution a nucleophilic attack at C-5 (or at C-7) yielding the C-5 (or C-7) monosubstituted hydroxylamino derivatives 5a-e (or 7a-e). These derivatives can be further oxidized at the same potential of 1a-e to give the corresponding 5- (or 7-) substituted nitroxide radicals 6a-e (or 8a-e). Finally, the oxidation of these radicals yields the 5-(3a-e) or 7-(4a-e) quinoneimine N-oxides. When the oxidation of 1a-e is carried out in MeCN containing H_2O (or MeOH the oxoammonium cation can undergo the nucleophilic attack at C-5 (or C-7) even at the electrode , therefore the anodic step involves three electrons.

13070

ANODIC CHLORINE EVOLUTION AND CHLORINATION OF c-HEXENE IN NITROMETHANE SOLUTION

CS.VISY and M.NOVÁK
Institute of General and Physical Chemistry,
University of Szeged,
H-6701 Szeged, P.O.Box 105, Hungary

Previous studies on the electrochemical chlorination of c-hexene (CH) on a Pt electrode in nitromethane (NM) solution revealed that the process yields not only dichloro -c-hexane and 2-chloro-c-hexanol, but also 2-chloro-c-hexanone. Formation of the latter can be detected only in the early period of electrolysis and is inversely connected to the water content of the solution[1]. The relative formation of this ketone derivative at the beginning of electrolysis increases with the potential applied[2].

On the basis of data obtained by galvanostatic and convolution potential sweep voltammetric methods, chlorine evolution in the absence of CH could be described by a recombination-controlled mechanism. This extends the validity of the conclusions claimed in 3.

As shown earlier, the addition of CH to the solution led to a homogeneous reaction, with the formation of dichloro and chlorohydroxy derivatives. The formation of chloroketone appeared to be a heterogeneous reaction. Thus, if CH is present, it should adsorb on the electrode in NM solution. The faster rate of change in the current under potentiostatic conditions during electrolysis of a solution containing both CH and Cl^- indicates the adsorption. Similarly, the currents obtained during the linear potential sweeps reveal the effect of this phenomenon.

The increase in the limiting current with the increase of CH concentration shows saturation, indicating that the effect of the olefin present arises not in the homogeneous, but rather via heterogeneous route.

On the basis of the product distribution one might assume that the current excess is due to the ketone formation, the rate of which might be characterized by an expression containing the coverage of CH.

References:
1. M.Novák and Cs.Visy
   Electrochim.Acta, 28, 511 (1983).
2. M.Novák and Cs.Visy
   Electrochim.Acta, 28, 507 (1983)
3. B.E.Conway and D.M.Novak
   J.Electroanal.Chem., 99, 133 (1979).

POLYMER FILM FORMATION ON A STEEL CATHODE BY ELECTROCHEMICALLY INITIATED COPOLYMERIZATION OF ACRYLONITRILE AND ACRYLAMIDE IN AQUEOUS SOLUTIONS

M.Cvetkovska,T.Grčev,Lj.Arsov

Cyril and Methodius University,Faculty of Technology and Metallurgy,Skopje,Yu

Introduction:Electrochemical obtantion of polymer films on metal surfaces with given caractheristics arouse a great interest due to many positive aspects which include a possibility of producing very thin films having specific and very highly praised properties such as electroinsulation,thermostability,anticorrosion and biocompatibility.

Experimental:Polymer and copolymer films of acrylamide(AA) and acrylonitrile(AN) on steel cathode(316 AISI) are obtained by electrochemically initiated polymerization(EIP) from aqueous solutions at a constant current and/or constant potential at 30° C in a standard electrochemical cell.A working electrode was a steel cylinder,mounted on teflon holder,(exposed area 5 cm^2);auxilliary electrode was a platinum foil(20 cm^2),and as a reference electrode a saturated calomel electrode was used.

The kinetics of polymer and copolymer film formation was followed,in-situ,by ellipsometry(Rudolph Research Ellipsometer 43603-200),in optical cell at angle of incidence of 70° and wavelength of 546,1 nm.

Results and Discussion:EIP of AA on metal surfaces from aqueous solutions of AA in presence of $ZnCl_2$ is a known process in the literature and it was also subject of some our previous research(1).Polyacrylamide(PAA) has,however,some specific properties and,thus,a specific and limited application.Properties of the polymer film are modified,by copolymerization of AA and AN, so that the fields of its application are also enlarged;(AA and AN are monomers similar by its reactivity and polarity which can be seen by values of Q and e in the Alfrey and Price scheme:Q_{AA}=1,18;e_{AA}=1,3;Q_{AN}=0,6;e_{AN}=1,2;AA is somewhat more reactive than AN, thus,it is expected that copolymer contains more AA which is result of r_{AA} and r_{AN} values,namely,r_{AA}=1,727, r_{AN}=0,573 or $r_1.r_2$=0,99 which is characteristical for a free radical copolymerization and a statistical copolymer).

Chronopotentiometric experiments of electrochemically initiated copolymerization of AA and AN in aqueous medium in presence of $ZnCl_2$(0,15 M $ZnCl_2$;j=2-5 mA/cm^2;pH=4,2-5,2),figure 1,indicate that the process of copolymerization takes place at the potential of reduction of Zn^{2+} ions or Zn^{2+}-AA;$ZnOH^+$-AA;Zn^{2+}-AN and $ZnOH^+$-AN complexes(-1,20 to -1,50 V/sce).The formation of polymer or copolymer film leads to a reduction and a significant anodic shift of the process of electrochemical dissolution of deposited Zn,fig.1.On the other hand,the presence of monomers(AA and AN) in the solution leads to significant shortening of transition time,occurence of new reduction process

at about -2,oV(hydrogen evolution from water present in the film) and cathodic shift of the quarter-wave potential.In aqueous solution of $ZnCl_2$ containing AN(1,5 M) and AA(2-5 M) at constant current,3-5 mA/cm^2,for 1-3 min. copolymer films(determined by IR-spectroscopy)with a thickness of 2-lo μm and exellent electroinsulating properties(ρ = 2-4.lo^{lo} S^{-1} cm)are produced.Polymerization,in this cases,is carried out by a free radical mechanism,and the active radicals are formed by a direct reduction of Zn^{2+} or $ZnOH^+$-AA and AN complexes.

During above mentioned experiments,zinc deposition and copolymer film formation on electrode's surface take place simultaneously.Deposited zinc has some advantages,but however,its presence is considered undesirable and,therefore,copolymerization process was also performed in more acid solutions (o,o25 M H_2SO_4) without $ZnCl_2$.

In this case,the kinetics of polymer film formation on steel cathode depends on cathodic potential,i.e.cathodic current density.The EI copolymerization of AA and AN even at relatively low cathodic potentials,simultaneously with the reaction of hydrogen evolution(more cathodic than -1,lo V) or rather more anodic than reduction potentials of AN and AA(-1,87 and -1,95 V) is an additional proof for assumed mechanism of initiation of polymerization of vinyl monomers in acid aqueous solutions via hydrogen radicals,i.e. H_{ads} ($H^+ + e = H_{ads}$ and $H_{ads} + M = H\text{-}M^{\bullet}$).

The kinetics of polymer or copolymer film formation in acid solutions(H_2SO_4),figures 2 and 3,indicates existence of an induction period of 7-9 minutes,and a rather slower development of processes compared with systems containing $ZnCl_2$,figure 3. This is,most probably,due to a interrelationship between the rate of hydrogen evolution and the initiation of polymerization.
The obtained films(PAN and PAN+PAA),with a thickness of 3-5 μm, have a good electroinsulating and anticorrosive properties.

Literature

1. M.Cvetkovska,T.Grčev,Lj.Arsov and Gj.Petrov,Chemistry in Industry,34(5),243,1985

2. F.S.Teng,R.Mahalingam, J.Appl.Polym.Sci.,23,101,1979

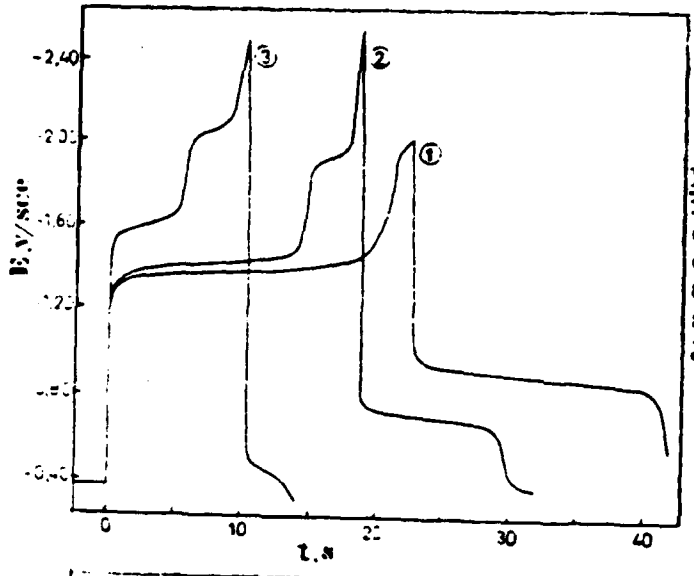

Fig.1:Chronopotentiometry of aqueous solutions of 1,5M $ZnCl_2$,pH=4,8(1); containing 1,5M AN(2) and 1,5M AN+4M AA(3)on steel electrode at $j=30$ mA/cm^2.

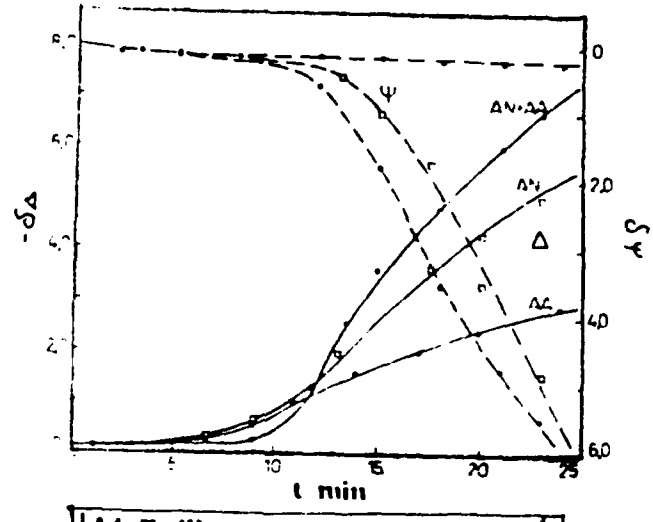

Fig.2:Ellipsometric changes during constant current electrolysis(20mA/cm^2 of acid aqueous solutions (0,025M H_2SO_4)of AA(1,5M); AN(1,5M)and AA+AN(1,5M each)on steel cathode.

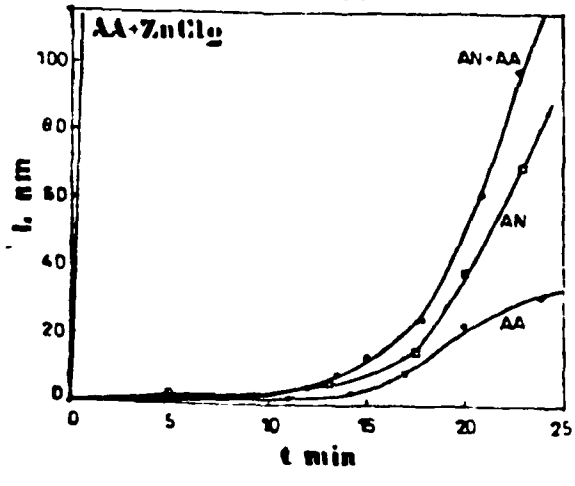

Fig.3:Kinetics of polymer and copolymer film formation determined by ellipsometry(Fig.2) and by weighing method for the AA+$ZnCl_2$ system(0,15M $ZnCl_2$+ 5M AA,pH=4,8;$j=5$ mA/cm^2)on steel cathode.

13090

EFEECT OF CONTACTING PATTERNS ON SOME ELECTROLYSES IN TWO PHASE ELECTROLYTS

Z.IBRIŠAGIĆ and D.PLETCHER
Faculty of Chemical Engineering,"Djuro Pucar Stari" University,78ooo Banja Luka, Yugoslavia.

Department of Chemistry,the University,Southampton, SO9 5NH,England.

Earlier work[1,2,3] has shown the influence of zinc chloride on the chlorination of naphtalene by electrolysis in a water/ methylene chloride emulsion and using tetrabutylammonium ion as a phase transfer catalyst.The addition of $ZnCl_2$ to the electrolyte increases the selectivity for 1-chloronaphtalene mostly from a decrease in the consumption of naphthalene and therefore from a slower formation of di- and polychlorinated products[3].

Both a hith selectivity and a high current yield are dependent on balancing the flux of cation radical away from the anode surface with the flux of nucleophile to the surface, which is essentially controlled by the flux of $ZnCl_4^{2-}$ or the bulk concentration of tetrabutylammonium ion[3].

Hence, one could expect that the contacting pattern would have an influence on the reaction path and products distribution.

Experiments were performed in an undivided and divided stirred tanc reactors and emulsions were formed with a rapidly rotating magnetic stirrer.In the undivided cell,electrodes were perpendicularly dipped in the electrolyte,having ca. 3 cm the interelectrode gap.However,they were parallel with a magnetic bar stirrer in the divided cell and mutually separated by glass frit.

In the flow cells emulsions were formed by the intensive pumping of the two phase electrolyte within the flow system with undivided cells.In the flow through electrodes cell the emulsion was flowing through electrode grids located over the entire crossection of a cell with the inter electrode gap ca. 4 cm, while was passing trough the rectangular channel in the flow along electrodes cell the interelectrode gap was ca.5 mm and the wall - electrode gap ca 7 mm.

Results clearly shows that the selectivity for 1-chloro naphthalene is higher in the divided stirred tanc reactor (Fig.2) than in the undivided cell (Fig.1) but the larger effect is on conversion of naphthalene and hence current efficiency.

However, the concentration profile against F mol^{-1} in the flow through electrodes cell (Fig.3) is quite comparable to the data obtained for an undivided stirred tanc reactor (Fig.1),but the selectivity,particularly at lower F mol^{-1} fits better to the behaviour of the divided cell (Fig.2).

It seems that in the divided stirred tanc reactor besides the fact that an eventual harmful interaction of the reaction product with the counter electrode is avoided, the increase in the conversion and the selectivity could also be due to the electrode-electrolyte contacing pattern. Bearing in mind that a layer of a circulated emulsion is parallel to the electrode surface, one could visualize a possible formation of an uniform layer of cation radicals which could have a good chance to react with nucleophile before being swept away to the bulk of the emulsion. The similar situation arose from the flow through cell (Fig.3). The direct contact of unreacted naphthalene with the electrode surface may produce a high concentration of radical cations in the fluid leaving the anodic surface for the reaction for surrounding nucleophile before being mixed with neutral molecules of naphthaline. Consequently a high selectivity for 1-chloronaphthalene is seen at low F mol^{-1} (Fig.3) Table 1.

In the flow along electrodes cell a severe drop in the conversion of naphthalene and the selectivity for 1-chloro naphthalene was observed (Fig.4). If we assume that plug flow prevailed in the system most of naphthalene flowing molecules would not reach the anodic surface and therefore conversion would fall. However, cation radicals formed, would easily be mixed in the bulk of emulsion, what may cause the decrease in the selectivity for 1-chloronaphthalene.

Table 1.

STIRRED TANC REACTORS					FLOW CELLS								
UNDIVIDED		DIVIDED		THROUGH ELECTRODES				ALONG ELECTRODES				
F mol^{-1}	1.1	2.1	1.0	2.6	0.4	0.64	0.83	1.15	0.4	0.8	1.0	2.0	2.4
X,%	56	41	46	70	14	20	28	38	12	28	22	36	42
S,%	71	57	86	90	87	93	82	79	36	27	51	37	32

X - conversion of naphthalene, S - selectivity for $C_{10}H_7Cl$

Nevertheless the electrochemical oxidation of dimethyldithio carbamate (NaDTC) to tetramethylthiuram disulfide (TMT) in aqueous saturated NaCl/solvent emulsion, at ruthenized titanium electrode, at constant current density ($i = 16$ A dm^{-2}) being terminated to 1 F mol^{-1} NaDTC does not depend on the interfacial contact of the electrode - electrolyte system.

Besides a high conductivity of the electrolyte and a good mass transfer, only a good product solubility in the solvent used is required to obtain a very high product yield and current efficiency, as it is shown in the experiment with chloroform (Fig.5). If this condition is not met, like in the experiment with benzene (Fig.6), the product yield and current efficiency remain at much lower value[4,5].

The part of this work is supported by ICI plc, The Heath, Runcorn, Chesire WA7 4QE, England, to whom we are greatly acknowledged.

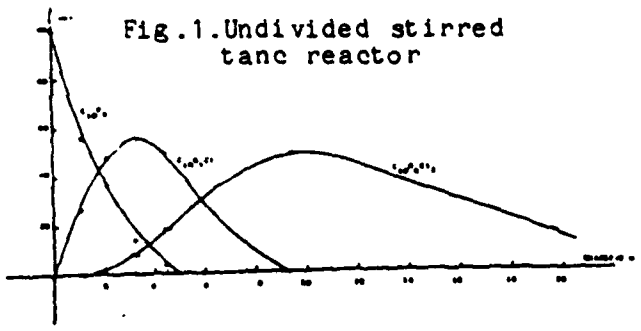

Fig.1.Undivided stirred tanc reactor

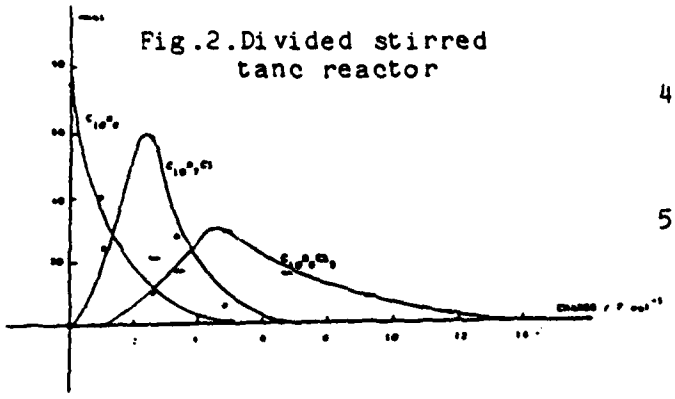

Fig.2.Divided stirred tanc reactor

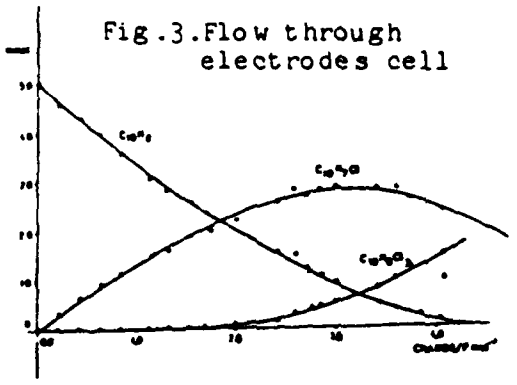

Fig.3.Flow through electrodes cell

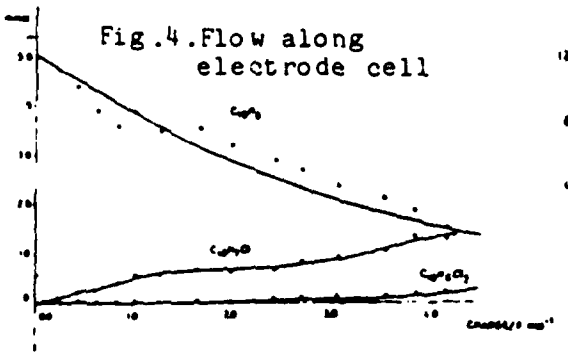

Fig.4.Flow along electrode cell

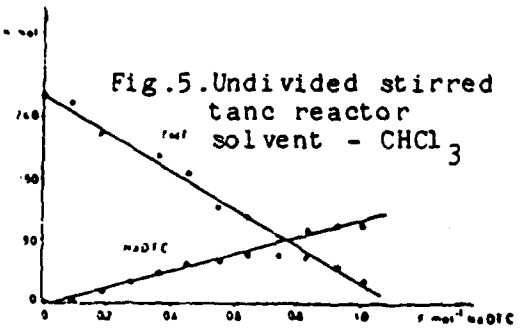

Fig.5.Undivided stirred tanc reactor solvent - $CHCl_3$

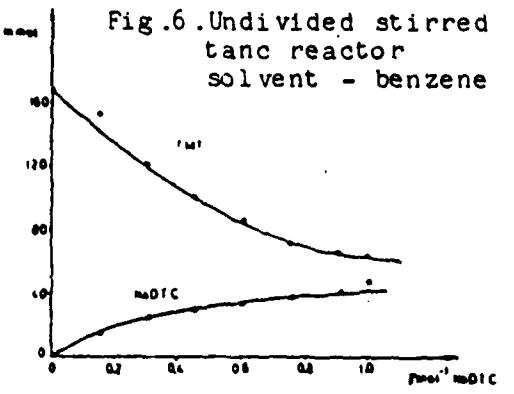

Fig.6.Undivided stirred tanc reactor solvent - benzene

References

1. S.R.Ellis,D.Pletcher, W.N.Brooks,K.P.Healey, J.Appl.Electrochem.,13 (1983) 1984.
2. W.N.Brooks,K.P.Healey, Z.Ibrišagić,D.Pletcher, The Electrochem.Soc. Meeting,Cincinatti,Ohio, U.S.A.,May 1984.
3. Z.Ibrišagić,D.Pletcher, W.N.Brooks,K.P.Healey, J.Appl.Electrochem., (to be published).
4. Z.Ibrišagić,V.Mišović, I.Tabaković, I.Šantić, Yugoslav Pat.,2528/82, Nov.,1982.
5. Z.Ibrišagić,V.Mišović, I.Tabaković,I.Šantić, J.Appl.Electrochem., (in print).

ELECTROCHEMICAL REDUCTION OF 2-BROMO-CARBOXAMIDES. SELF-PROTONATION AND PARTICIPATION OF THE SOLVENT

F. MARAN,[a] E. VIANELLO,[a] G. CAVICCHIONI,[b] and F. D'ANGELI[b]

[a]Dipartimento di Chimica Fisica, Padova (Italy)

[b]Laboratorio di Chimica Organica, Facoltà di Farmacia, Ferrara (Italy)

Previous investigation on base-promoted reactions of 2-halogeno-carboxamides [1] prompted us to take into consideration the general electrochemical features and product distribution in the cathodic reduction of the title compounds. The anionic intermediates arising upon electroreduction of these substrates in dipolar aprotic solvents were expected to abstract protons from the parent molecule through a self-protonation mechanism.[2,3]

We report here results concerning the reduction of representative 2-bromo-2-methyl-propanamides, $BrCMe_2CONR^1R^2$ (R^1= H, R^2= Ph, Bz, t-Bu, c-hexyl; R^1= Me, R^2= Ph, Bz),[4] and preliminary results obtained with 2-bromo-acetamides, $BrCH_2CONHR^2$ (R^2= Bz, c-hexyl).

The electrochemical reduction of the substrates was carried out at Hg cathodes in anhydrous DMF or MeCN containing Et_4NClO_4 or Bu_4NBr. The voltammetric pattern exhibits two cathodic peaks; in some cases, the second peak is only detectable under suitable conditions, dictated by the sweep rate and the nature of both the substrate and the electrolyte.

Controlled potential electrolyses were carried out at potentials of the first wave, typically in the range -1.4 to -1.9 V vs. s.c.e. Exhaustive reduction required 1 F/mol for each substrate. Product analysis (^{1}H-n.m.r., IR, MS, and HPLC in comparison with authentic samples) indicated that the corresponding amides with H in place of Br were formed in ca. 50% yield, the nature of the main coproduct being strongly dependent on: i) the protic (R^1= H) or aprotic (R^1= Me) character of the starting material; ii) the solvent; iii) the 3° or 1° character of the bromine function. The coproduct distribution can be summarized as follows:

a) Methacrylamides arise upon electroreduction of aprotic 2-bromo-2-methyl-propanamides, independently of the solvent.
b) In DMF, protic 2-bromo-2-methyl-propanamides afford a cyclocondensation product with the solvent itself.
c) In MeCN, the coproduct distribution depends upon the substituent on the nitrogen. Whereas in some cases α,β-unsaturated amides are formed in consistent yields, in other cases a fragmentation path affords acetone and the pertinent isocyanide.
d) Protic 2-bromo-acetamides afford a self-condensation coproduct, i.e. a head-to-tail cyclic dimer.

Accordingly, the macro-electrolysis results can be depicted as follows:

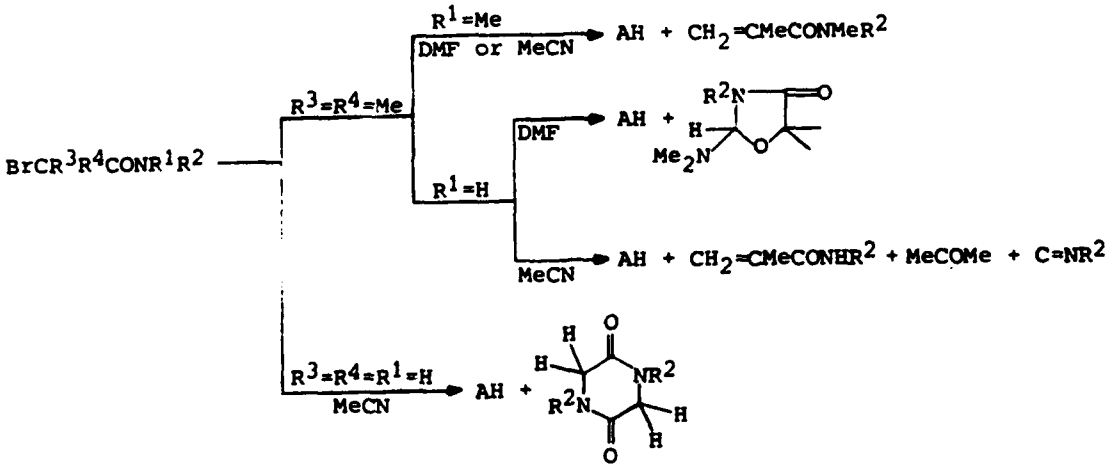

(AH indicates the debrominated product $HCR^3R^4CONR^1R^2$)

The finding that some coproducts are identical with some products from the base-promoted reactions, together with the coulometric results, suggested the occurrence of a self-protonation mechanism, in which an electrogenerated base undergoes proton transfer with a parent molecule. Further evidence was gained by testing the effect of adding a strong base or an acid into the electrochemical cell.

The above results and the consistency of the voltammetric analysis with a recently proposed mathematical treatment on self-protonation nuances,[3] lead to the following conclusions:

a) The process taking place at the first peak is a 2-electron reduction with C-Br bond cleavage.

b) The carbanion electrogenerated from an aprotic 2-bromo-2-methyl-propanamide promotes a 1,2-elimination from a parent molecule, through a self-protonation step. As a consequence, the reduction product AH and the α,β-unsaturated amide (reducible at the second peak) are formed.

c) The carbanion electrogenerated from a protic 2-bromo-2-methyl-propanamide is expected to undergo isomerization according to the acidity of the N-H bond. Also in this case, the electrogenerated base is protonated by a parent molecule, and the reduction product AH is formed along with a bromo-anion, i.e. the conjugated base of the parent 2-bromo-amide. This anionic intermediate can live enough to be reduced at the second peak with C-Br bond cleavage. Cyclocondensation, elimination, or fragmentation products are eventually formed upon decay of the bromo-anion itself.

The reduction scheme of protic 2-bromo-2-methyl-propanamides can be depicted as follows:

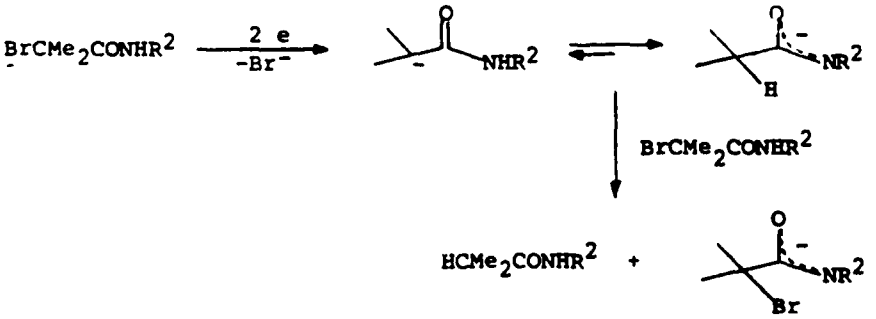

The chemical pathways of bromo-anion decay look controlled by the R^2 substituent on the nitrogen atom and/or the solvent. The observed chemoselectivity may reflect the relative energies of possible intermediates and transition states, as will be discussed on the ground of current studies, including ab initio calculations, stereochemical effects, and electrochemical kinetic analysis.

References

1 (a) G. Cavicchioni, P. Scrimin, A.C. Veronese, G. Balboni, and F. D'Angeli, J. Chem. Soc. Perkin Trans. 1, (1982) 2969; (b) P. Scrimin, F. D'Angeli, V. Baioni, and G. Cavicchioni, J. Chem. Res., (1983) (S) 248, (M) 2237; (c) P. Scrimin, F. D'Angeli, A.C. Veronese, and V. Baioni, Tetrahedron Lett., (1983) 4473.
2 C. Amatore, G. Capobianco, G. Farnia, G. Sandonà, J.M. Savèant, M.G. Severin, and E. Vianello, J. Am. Chem. Soc., 107 (1985) 1815.
3 C. Arevalo, G. Farnia, M.G. Severin, and E. Vianello, in the press.
4 F. Maran, E. Vianello, G. Cavicchioni, and F. D'Angeli, J. Chem. Soc. Chem. Commun., (1985) 660.

ELECTROCHEMICAL CARBOXYLATION OF STYRENE

G.FILARDO*, S.GAMBINO*, A.GENNARO**, G.SILVESTRI*, E.VIANELLO**

*Istituto di Ingegneria Chimica, Palermo (Italia)
**Dipartimento di Chimica Fisica, Padova (Italia)

The electrochemical carboxylation of olefins having very negative reduction potential, i.e. in the same range as carbon dioxide, presents some intriguing problems in the interpretation of the reaction mechanism and is, at present, under investigation in our laboratories. From the synthetic point of view, the electrocarboxylation of some of these olefins is very interesting since substituted succinic acids can be obtained in some cases with excellent yields. This is the case of Styrene (Sty), which is transformed into monophenyl-succinic acid, percursor of several interesting co-monomers for the production of modified polyesters and polyamides.

In strictly anhydrous conditions (i.e. in the presence of dry Al_2O_3) Sty shows only an irreversible cathodic peak in cyclic voltammetry (CV) at low v values, but, at v=20 $V \cdot s^{-1}$, a cathodic/anodic peak system is obtained, corresponding to a reversible one-electron process, with $E^\circ = -2.58$ V vs SCE (1). The reduction potential of Sty lies in between the two values of the reduction potentials of CO_2: the $E^\circ = -2.21$ V (2) and $E_p = -2.8$ V; therefore the Sty anion radical produced cathodically could act as reductant towards molecular carbon dioxide:

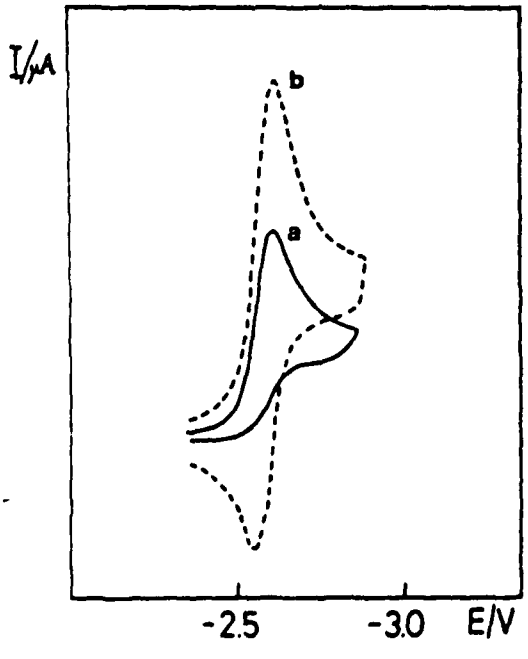

Fig. 1 - CV of Sty in anhydrous DMF: (a) v = 0.1 $V \cdot s^{-1}$; (b) v = 20 $V \cdot s^{-1}$

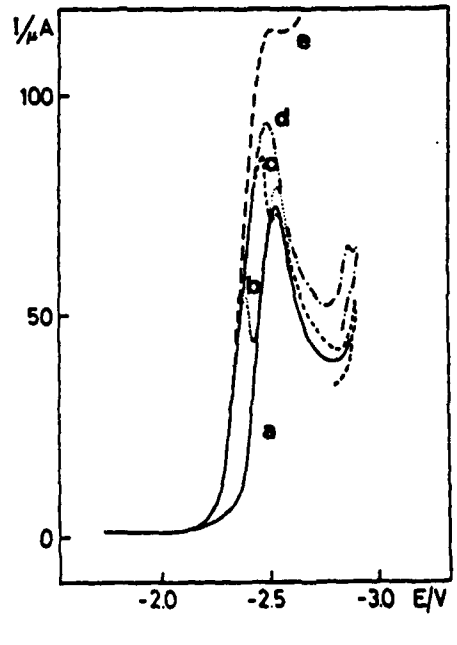

Fig. 2 - CV of Sty in the presence of CO_2: (a) 10^{-2}M Sty; (b-e) effect of increasing amounts of CO_2; v = 0.1 $V.s^{-1}$.

$$Sty + e^- \rightleftharpoons Sty^{\cdot-}$$
$$Sty^{\cdot-} + CO_2 \longrightarrow StyCO_2^{\cdot-}$$
$$Sty^{\cdot-} + CO_2 \rightleftharpoons Sty + CO_2^{\cdot-} \longrightarrow StyCO_2^{\cdot-}$$

Electrocarboxylation by macroscale electrolysis, of Sty in aprotic conditions is a simple and straightforward process in which yields up to 85% in the dicarboxylated derivative are attained. The cathodic material has decisive influence on the behaviour of the electrochemical system: the best yields of electrocarboxylation are obtained with compact grafite (CG), whereas with metallic cathodes (Hg, Cu, Zn) the main cathodic process involves the electropolymerization of the olefin. With vitreous grafite (VG) the dimeric 3,4-dipehnyladipic acid has been produced with yields up to 10%.

The anodic process involves oxidation of sacrificial Al anodes which allows the syntheses to be performed in diaphragm-less cells and the carboxylated product to be recovered as Al salt.

Depending upon experimental conditions, several electrochemical patterns have been observed:

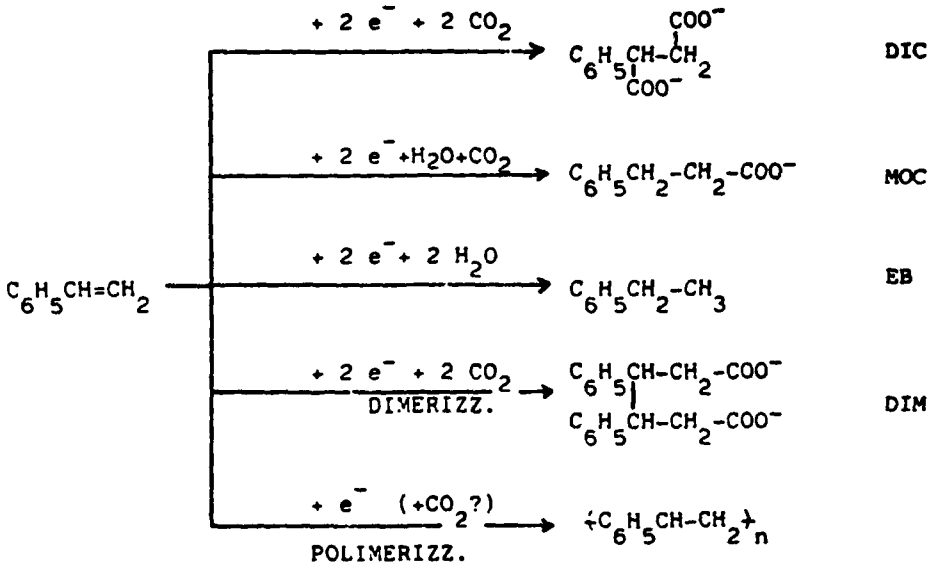

The presence of protic agents generally induces the formation of monocarboxylation derivatives, with the protonation taking place always on the carbon atom adjacent to the activating group. The results of some experimental runs are summarized in Table 1.

For H_2O in the range $10^{-3} \div 1.5$ M, the following relationships among the products yield and water concentration were found:

$$EB\ (\%) = 0.85 + 4.6[H_2O]$$
$$DIC\ (\%) = 18.4 - 22.9 \log[H_2O]$$
$$MOC\ (\%) = 58.6 + 19.3 \log[H_2O]$$

When acetic acid is employed, under strictly anhydrous conditions, we obtain only the dicarboxylated derivative and, as cathodic coproduct,

hydrogen gas. This is presumably to be attributed to acetic acid reduction hindering proton transfer to the adduct between Sty and CO_2.

The carboxylation can be performed at substantially lower potentials through homogeneous redox catalysis, the anion radical of benzonitrile being used as reductant (see Table 2). The voltammetric analysis of the system Benzonitrile/Sty/CO_2 provides useful information as to the reaction mechanism 1 .

TABLE 1. ELECTROCHEMICAL CARBOXYLATION OF STYRENE

Cathode	Protic Agent (M)	E (V)	Sty Conversion[a]	Charge passed[c]	Current yield	Product yields DIC	MOC	EB	DIM
CG	H_2O 10^{-3}	-2	91	2.2	65	85	1	Traces	
VG	H_2O 10^{-3}	-2.7	87	2.3	66	40	35	Traces	5-10
CG	AcH .67	-1.1	80	4.6	36	83	Traces	Traces	
CG	H_2O .23	-1.6	90	2.4	72	40	44	2	
CG	H_2O .61	-1.6	92	2.4	72	23	58	4	
CG	H_2O 3.33	-1.3	97	3.0	47	2	69	16	

a) referred to initial Sty; b) in % referred to Sty converted; c) in mol electrons per mole of Sty.

TABLE 2. ELECTROCARBOXYLATION THROUGH REDOX CATALYSIS.

Moles of Sty	Moles of Ø-CN	Charge passed[d]	E (V)	Sty Conversion[a]	Product yields[b] DIC	MOC
0	$2.3 \cdot 10^{-3}$	$6.9 \cdot 10^{-2}$	-2.15	-	70[c]	-
$2.5 \cdot 10^{-2}$	0	$5.2 \cdot 10^{-2}$	-2.45	60	60	29
$1.9 \cdot 10^{-2}$	$3.4 \cdot 10^{-3}$	$4.0 \cdot 10^{-2}$	-2.15	85	52	22

a) referred to initial Sty; b) in % referred to Sty converted; c) oxalic acid, the yield is referred to the charge passed; d) in mol electrons.

References

1) G.Filardo, S.Gambino, G.Silvestri, A.Gennaro and E.Vianello, J.Electroanal. Chem., 177 (1984) 303.

2) E.Lamy, L.Nadjo and J.M.Savéant, J.Electroanal.Chem., 78 (1977) 403.

ESR STUDY OF SEVERAL METHYLBENZOATES RADICAL ANIONS OBTAINED BY IN SITU ELECTROCHEMICAL METHOD

A.SANCHEZ, P.CALLE and C.SIEIRO*
Dptos.Electroquímica y Q.Física*.U.AM. 28049-MADRID(Spain)

Introduction

The methylbenzoic acids are compounds which are studied in Spanish laboratories using different experimental techniques (visible and U.V and NMR spectroscopies, X-Ray difraction, etc)[1]. The main conclusion of these studies was the observation of a torsion of the carboxylic group when the ortho- positions hinder it. Different values of the torsional angle were reported depending on the experimental techniques used.

We thus consider very interesting to obtain additional information about the torsional angle in analyzing the ESR spectra of the corresponding radical anions. Furthermore, we complete the spectroscopic study of these acids.

Due to the difficulty in the generation of the ϕ-COO$^{\cdot-}$ and ϕ-COO.$CH_3^{\cdot-}$ radical anions by chemical methods, we generate them using electrochemical methods.

The radical ϕ-COO$^{\cdot-}$ are very unstable in protic and in aprotic media, whereas ϕ-COOCH$_3^{\cdot-}$ is sufficiently long lived in aprotic media and this therefore permits its detection in adecuate experimental conditions. Moreover it is well known that the presence of electron donating groups inhibits the electrochemical reduction of the carboxylic acids[2] . However, the aromatic esthers in aprotic solvents[3-4] give rise in the polarographic reduction to two waves the first of them corresponding to the radical anions ϕ-COOR'$^{\cdot-}$ formation. For these reasons, we previously estherified the methylbenzoic acids and we carried out the electrochemical generation of the corresponding benzoates radical anions.

The compounds studied can be seen in Diagram 1.

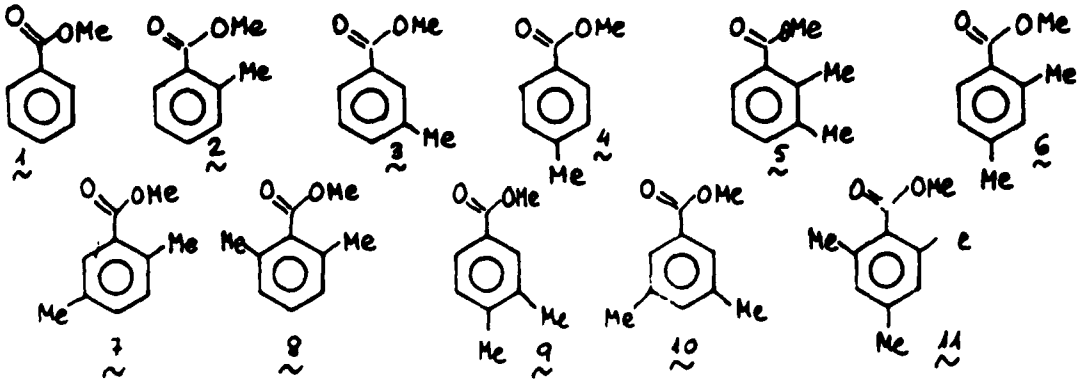

Diagram 1

Experimental

The electrolysis was carried out in a flat cell pla ed in the microwave cavity of the ESR spectrometer.
The following experimental conditions were used: so vent = Acethonitrile distilled in vacuum in presence of Phosphor c pentoxide; supporting electrolyte = tetreethylammonium tetrafl orborate(100 mM); electrodes = Au,Pt or Hg pool depending of the compounds studied; to obtain ESR spectra with high resolution we prepared dilute solutions of the compounds studied (1mM) and w used very low microwave power (2-5mW). The solution were prev ously degassed for to avoid the effect of the dissolved oxygen. Du ing the electrolysis an inert atmosphere was maintained.
The g factor was obtained by means of a glass capil ary filled with the standard peroxylamine dissulphonate, fresh prepared in a sodium carbonate (5mM) aqueous solution. We did n t use a three electrodes electrolysis because the radical generat on in our case can be performed using a constant intensity current. The intensity current used was about .5 - 1 mA.

Results and Discussion

In Table 1 can be shown the hyperfine coupling cons ants and g factor of the radical anions studied.
a)The equivalence of the methyl protons indicates a free rotation of the methyl groups even in the more hindered cases.
b)the hccs for all the radicals indicate that $a(H)_p > a(H)_o > a(H)_m$ in an approximate relation of 4:2:1.
This electron spin distribution agrees with the most stable canonical structures.Fig.1
c)In methoxyl protons we obtain practically the same hccs for all the compounds studied except the very hindered radical, i.e. 2,6-dimethyl- and 2,4,6-trimethyl-. Due to the independency of the methoxyl proton hccs with the torsion angle, we can not obtain any information about this angle.
The radical anions obtained by electrolysis of the esther group were very well resolved but in several esthers we need to try several electrodes in order to obtain a high resolution of the ESR spectra.
This method is extremely useful for obtaining radicals but presents the inconvenience that within few minutes the spin-spin interactions provoke the lines broadening and finally a fast decrease in the radical concentration. This effect is inherent to this type of generation and it is not very easy to avoid the acumulative concentration of radical ions along the working electrode.

Fig.1

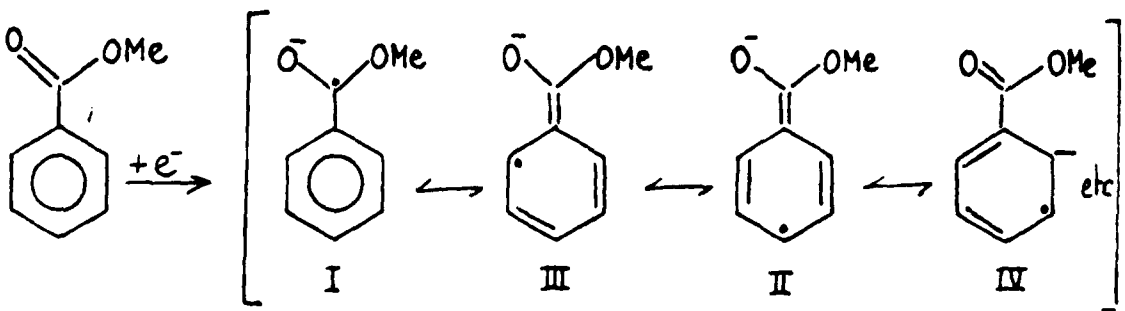

Table 1

MAGNETIC PARAMETER OF THE METHYLBENZOATES RADICAL ANIONS

Comp.	Hyperfine coupling constants						g
	H(2)	H(3)	H(4)	H(5)	H(6)	H(OMe)	
1[a]	4.20	0.94	7.50	0.94	4.20	0.94	2.00363
2[a]	4.25(Me)	0.85	7.70	0.85	4.25	0.85	2.00339
3[a]	4.05	0.95(Me)	7.25	0.95	4.40	0.95	2.00331
4[a]	4.40	1.00	7.90(Me)	1.00	4.40	1.00	2.00315
5[b]	4.40(Me)	1.00(Me)	7.60	1.00	4.20	1.00	2.00312
6[a]	4.50(Me)	0.40	8.30(Me)	0.95	4.00	0.95	2.00322
7[b]	4.40(Me)	0.90	7.60	0.90(Me)	3.80	0.90	2.00324
8[c]	4.50(Me)	0.75	8.40	0.75	4.50(Me)	0.75	2.00334
9[a]	4.52	0.97(Me)	8.15(Me)	0.97	4.52	0.97	2.00327
10[c]	4.00	0.89(Me)	6.90	0.94(Me)	4.00	0.89	2.00309
11[c]	4.50(Me)	1.00	8.00(Me)	1.00	4.50(Me)	0.50	2.00366

a) Pt-Pt electrodes
b) Au-Au electrodes
c) Pt-Hg pool electrodes

References

1. S.GARCIA-BLANCO et al., Acta Cryst.26(1970)972;ibid.,27(1970) 2255;ibid.,23(1967)1010.b)R.PEREZ-OSSORIO et al., An.Quim., 56(1960)379;ibid.,58(1962)423. c)M.COLOMINA et al.,An.Quim., 57(1961)655;ibid.,57(1961)565. d) E.DIEZ et al.,An.Quim.,67 (1971)91;ibid.,72(1976)35;An.Quim.,73(1977)355;Org.Mag.Res.22 (1984)140;Y.G.SMEYERS et al., An.Quim.67(1971)353;Theoret.Chim. Acta 28(1973)355

2. J.H.WAFENKNECHT, J.Org.Chem. 37(1972)1513
3. A.V.ILYASOV,YU.M.KARGIN,YA.A.LEVIN,I.D.MOROSOVA,N.N.SOTNIKOVA, V.KHIRANOVA and R.T.SAFIN, Izv.Akad.Nauk.SSSR,Ser.Khim.(1968) 736
4. D.H.GESKE and H.MAKI, J.Am.Chem.Soc.,82(1960)2671

ELECTROCHEMICAL STUDY OF ETHYLENE BIS SALICYLIDENEIMINATO COBALT COMPLEX. APPLICAITON TO THE ELECTROCATALYSIS OF ORGANIC HALIDES REDUCTION.

J.M. DUPRILOT*, F. BEDIOUI*, J. DEVYNCK*, J.C. FOLEST** and C. BIED-CHARRETON***.

*Laboratoire d'Electrochimie Analytique et Appliquée - ENSCP, 11, rue Pierre et Marie Curie, 75231 - PARIS Cedex 05 (France).

**LECSO, Laboratoires CNRS - THIAIS (France).

***Laboratoire de Chimie de Coordination Bioorganique (UA 255 du CNRS), Université Paris-Sud, 91405 - ORSAY (France).

Electrocatalyzed reduction of organic halides with ethylene bis-salicylideneiminato Cobalt (Co Salen) is studied in THF-HMPT (40-60%) medium at 25°C. The electrocatalytic process can be described by the following scheme :

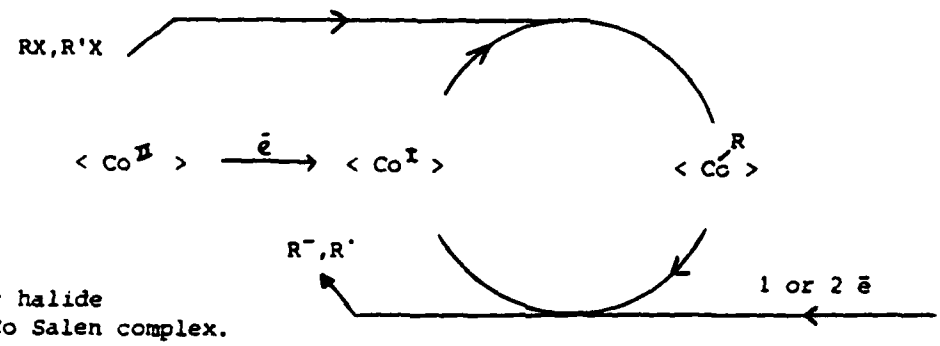

RX = organic halide
< Co^{II} > = Co Salen complex.

The kinetic of formation and rupture of the cobalt-carbon bond have been calulated, for different kind of RX, by analysis of cyclic voltammograms obtained with Co Salen and RX at different scan potantial rates

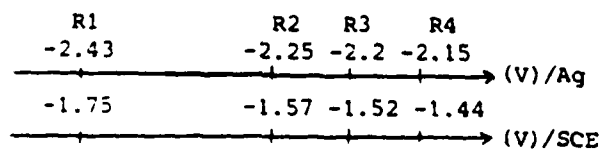

$E_{1/2}$: RCo(III)Salen/RCo(II)Salen$^-$

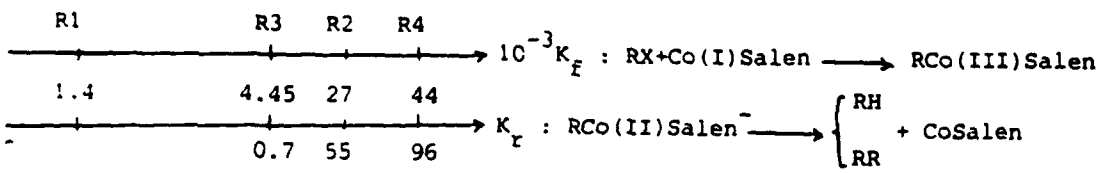

R_1 = n-C_4H_9Br ; R_2 = CH_3CH = $CHCH_2Cl$; R_3 = $C_6H_5CH_2Cl$; R_4 = C_6H_5CH = $CHCH_2Cl$

Quantitative reductions at controlled potential on a mercury pool are performed with RX of various types in presence of Co Salen. The yield of the synthetized products is determined and conditions of the C-C bond formation by homocoupling (RR formation) are precised[1]. The selectivity of the catalytic process depends on the nature of the solvent and the R group (Table 1).

RX	RX/Co (Salen)	Medium	Electrolysis Potential (V/SCE)	Products (%) RH	RR	Yield (%)
$nC_7H_{15}Br$	8	THF/HMPT+0,3M $LiClO_4$ n.d.	-1,72	10	30	40
$C_6H_5CH=CHBr$	10	DMSO+0,1M NBu_4BF_4 n.d.	-1,52	60	0	60
$CH_3CH=CHCH_2Cl$	10	THF/HMPT+0,3M $LiClO_4$ n.d.	-1,82	30	5	35
$C_6H_5CH=CHCH_2Cl$	12	DMSO+0,3M $LiClO_4$ n.d.	-1,52	50	20	70
$C_6H_5CH_2Cl$	10	THF/HMPT+0,3M $LiClO_4$ n.d.	-1,82	41	14	55
$C_6H_5CH_2Cl$	20	THF/HMPT+0,3M $LiClO_4$ d.	-1,82	10	80	90

1

CoSalen : 10^{-2}M
d : dehydrated
n.d : non dehydrated

Application to heterocoupling reactions[1] and carboxylation[2] are reported in tables 2 and 3.

2

[illegible]	[illegible]	[illegible]	[illegible]	[illegible]	[illegible]	[illegible]	[illegible]	[illegible]
$C_6H_5CH_2Cl$ [illegible]	$n-C_4H_9MgBr$ [illegible]	[illegible] (n.d.)	[illegible]	-	[illegible]	[illegible]	[illegible]	[illegible]
$C_6H_5CH_2Cl$ [illegible]	$n-C_4H_9MgBr$ [illegible]	[illegible] (n.d.)	[illegible]	-	[illegible]	[illegible]	[illegible]	[illegible]
$C_6H_5CH_2Cl$ [illegible]	$n-C_4H_9MgBr$ [illegible]	[illegible] (d.)	[illegible]	[illegible]	[illegible]	[illegible]	[illegible]	[illegible]
[illegible]	$C_6H_5CH_2Cl$ [illegible]	[illegible] (d.)	[illegible]	[illegible]	[illegible]	[illegible]	[illegible]	[illegible]
[illegible]	$n-C_4H_9MgBr$ [illegible]	[illegible] (n.d.)	[illegible]	-	[illegible]	[illegible]	[illegible]	[illegible]
[illegible]	$n-C_4H_9MgBr$ [illegible]	[illegible] (d.)	[illegible]	-	[illegible]	[illegible]	[illegible]	[illegible]
$n-C_4H_9MgBr$ [illegible]	[illegible]	[illegible] (d.)	-	[illegible]	[illegible]	[illegible]	[illegible]	[illegible]
[illegible]	[illegible]	[illegible] (d.)	[illegible]	[illegible]	[illegible]	[illegible]	[illegible]	[illegible]

3

ArX	ArX/Co(Salen)	media	P_{CO_2} (atm)	E [1]	RCOOH%
$C_6H_5CH_2Cl$	10	$LiClO_4$ n.d.	1	-2,3	50
$C_6H_5CH_2Cl$	20	$LiClO_4$ d.	2	-2,3	65
$C_6H_5CHClCH_3$	20	$LiClO_4$ d.	2	-2,1	60
$C_6H_5CH=CHCH_2Cl$	20	$LiClO_4$ d.	2	-2,3	90

Solvent : THF + HMPT (60-40%)

(1) Electrolysis potential, ref. : Ag/Ag^+

CoSalen:10^{-2}M;medium:THF-HMPT(40-60%);

This study shows that RR coupling reactions are efficient in well dehydrated solvents, and good yields in heterocoupling necessitate comparative kinetics for the formation and rupture of cobalt-carbon bond. Elsewhere, carboxylation reactions occur in good yield on benzylic compounds and are the first example for carboxylation catalyzed by cobalt base Schiff complexes.

Modified electrodes by fixation of different complexes on electrode surface have been also studied : different methods can be used and these modified electrodes are studied by electrochemical (cyclic voltammetry, chronoamperometry) and optical methods (spectroscopy and electroreflectance). Different types of electrodes are reported :

Type 1 : polystyrene attached cobalt Schiff base[3] and zeolithe modified manganese porphyrin[4] (Mn(III)TMPyP) are pasted with graphite and studied by electrochemical methods.

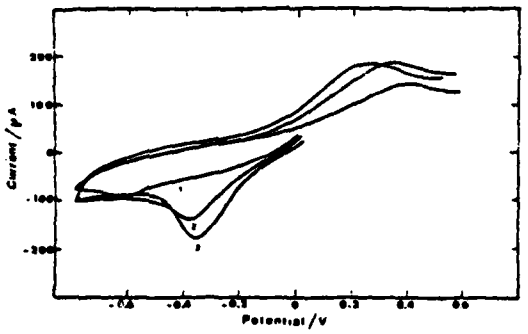

Fig. 4. Cyclic voltammograms at a GPE of poly SalPT Co(II): poly SalPT Co(III)/poly SalPT Co(II) system. Potential sweep rate: 1 mV s^{-1}. (1) Without ohmic compensation; (2) with partial ohmic compensation, R = 700 Ω. (3) with partial ohmic compensation, R = 1150 Ω.

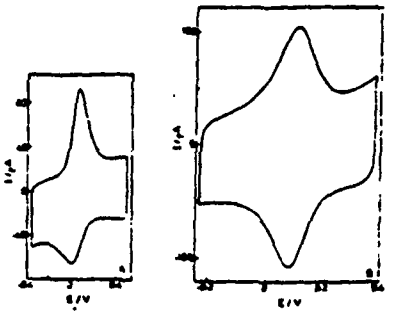

Type 2 : Thin layer of a polymerised base Schiff can be deposited on gold electrodes by evaporation, and anionic porphyrins or cobalt base Schiff complexes can be incorporated in polypyrrole films by electrochemical polymerisation. These electrodes are characterized by optical an electrochemical methods.

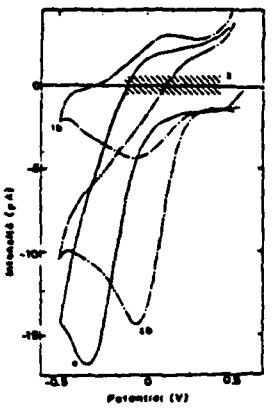

Electrocatalysis reduction of O_2 in H_2SO_4 0.1M

a) Gold electrode
b) Gold/Polypyrrole/TCPPCo(III) electrode
   1.with Argon
   2.with *Oxygen*
3) Potential region where TCPPCo(III)/Co(II) redox system is detected by electro - reflectance technique (Gold/Polypyrrole/ TCPPCo electrode).

Electrodes polypyrrole of type 2 are shown to be efficient in O_2 reduction[5]. Zeolithe-manganese porphyrin electrode (type 1) can be used as a catalyst in phenol oxidation by molecular oxygen.

References.

1 J.M. Duprilot, F. Bedioui, J. Devynck, J.C. Folest, C. Bied-Charreton, J. organomet. Chem.., 1985, 286, 77.

2 J.M. Duprilot, J.C. Folest, J. Perrichon, Y. Robin, J. Devynck, Tetrahed. lett., 1985 (under press).

3 J. Asseraf, F. Bedioui, O. Reyes, y; Robin, J. Devynck, C. Bied-Charreton, J. Electroanal. Chem., 1984, 170, 255-263.

4 B. De Vismes, F. Bedioui, J. Devynck, C. Bied-Charreton, J. Electroanal. Chem., 1985, 187, 197-202.

5 F. Bedioui, C. Bongars, J. Devynck, C. Hinnen, C. Bied-Charreton, Bull. Soc. Chim. Fr, 1985 (submitted to publication).

KINETIC AND THERMODYNAMIC PARAMETERS IN THE REDUCTION OF ALKYLARYLSULPHIDES IN APROTIC MEDIUM

M.C.AREVALO[a], G.FARNIA[b], M.G.SEVERIN[b], E.VIANELLO[b]
[a]Departamento de Quimica Fisica, La Laguna (Spain)
[b]Dipartimento di Chimica Fisica, Padova (Italy)

The electrochemical reduction of organic sulphides of general formula ArSR has been the object of little investigation in the last years[1,2].

The kinetic and thermodynamic characterization of the reduction mechanism of some p-nitrosubstituted arylalkyl sulphides was recently discussed[3,4].

In this communication we report an analysis of the reduction mechanism, in anhydrous dimethylformamide, of the following sulphides: triphenylmethyl-($Ø_3CSØ$), diphenylmethyl-($Ø_2CHSØ$), and phenylmethyl-phenylsulphide ($ØCH_2SØ$).

Cyclic voltammetric measurements and controlled potential electrolyses reveal that the reduction involves the cleavage of a C-S bond (see Fig.1) Product yields and coulometric coefficients (table I) in macroscale electrolysis also indicate that an overall two-electron process is operating for $Ø_3CSØ$ and $ØCH_2SØ$, while an apparent one-electron reduction takes place with $Ø_2CHSØ$.

TABLE I Products (mol %) and coulometric yield

Sulphides	ØSH	$Ø_nCH_{(4-n)}$	R-S-Ø	n
$Ø_3CSØ$	84	95	-	2.0
$Ø_2CHSØ$	58	46	42	1.08
$ØCH_2SØ$	90	75	-	1.94

In the former cases the stoichiometry can be rationalized by the sequence:

$$R\text{-}S\text{-}Ø + e \xrightarrow{E^\circ_1} [R\text{-}S\text{-}Ø]^{\cdot -}$$

$$[R\text{-}S\text{-}Ø]^{\cdot -} \xrightarrow{k} R^\cdot + SØ^-$$

$$R^\cdot + e \xrightarrow{E^\circ_2} \text{and/or } R^\cdot + [R\text{-}S\text{-}Ø]^{\cdot -} \longrightarrow R^- + R\text{-}S\text{-}Ø$$

$$R^- + SH \longrightarrow RH + S^-$$

where E°_2 is much greater than the reduction potential of the substrate itself, at least in the case of $Ø_3CSØ$[4].

Diphenylmethyl phenylsulphide, owing to its acidic properties, can act as a proton donor towards the electrogenerated anionic species, specifically R^-, and the last step is replaced by:

$$Ø_2CH^- + Ø_2CHSØ \xrightarrow{k_p} Ø_2CH_2 + [Ø_2CSØ]^-$$

causing the overall reaction to result an one-electron process.

The voltammetric analysis also shows that the first electron transfer is always the rate determining step.

The reduction has also been carried out by means of convenient sets of redox reagents, with similar coulometric and product yield. This result

allowed us to use the method of homogeneous redox catalysis[5] in order to determine useful kinetic and thermodynamic properties of the process. From these studies we could obtain such parameters as the standard potential, E°_1, of the first electron transfer, the standard rate constant for the homogeneous electron transfer, k°_s, and the rate constant, k, for the homogeneous decay of the primary radical anion (Table II). This latter result actually bears evidence of the existence of a chemical step following the charge transfer and thus of the anion radical as a reduction intermediate.

By taking advantage of the knowledge of the standard potential, the voltammetric data could be analyzed for the kinetic characterization of the heterogeneous electron transfer. Both the transfer coefficient, α , and the standard rate constant, k°_{el}, are obtained for the charge transfer process on a mercury electrode (Table II). The values are determined by making use of various approaches, obtaining comparable results.

The analysis of diphenylmethyl phenylsulphide was complicated by the presence of the self-protonation step. This latter presents the usual treatments of the experimental data to be made. We have therefore performed the mathematical analysis of the mechanism proposed for this sulphide.

The fitting of the experimental data with the theoretical behavior allowed to confirm our qualitative indication and to obtain, also for this compound, the kinetic parameters of the heterogeneous electron transfer, as well as the rate constant, k_p, of the self-protonation reaction (table II).

The reduction mechanism for the three sulphides was confirmed by carrying out of the process on different electrode materials (Pt and vitreous carbon). Over these electrodes the voltammetric behavior is similar to the one shown on Hg and also the kinetic parameters of the electron transfer are the same order to magnitude. These results therefore, evidence the independence, of the reduction mechanism of the electrode material, and in particular the lack of interaction of the sulphides with mercury.

Fig. 1 - Cyclic voltammogram of $Ø_3CSØ$ 2 mM in DMF + TBAP 0.1 M. $v = 40\ Vs^{-1}$ T = 25°C

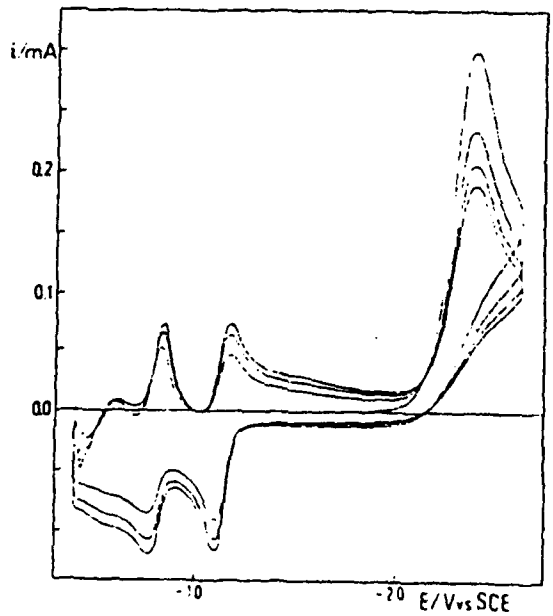

TABLE II	$\phi_3CS\phi$	$\phi_2CHS\phi$	$\phi CH_2S\phi$
E_1^a(V)	-1.991	-2.341	-2.565
$k_s^a(M^{-1}s^{-1})$	1.9×10^{-5}	2.2×10^{5}	8.7×10^{5}
$k_{s,ex}^a(M^{-1}s^{-1})$	1.9×10^{1}	2.8×10^{1}	4.5×10^{2}
$k(s^{-1})$	5×10^{7}	9×10^{7}	2×10^{8}
α_{ap}	0.42	0.47	0.56
$k_{el,ap}^o$(cm s^{-1})	3.0×10^{-4}	8.4×10^{-4}	1.5×10^{-3}
α	0.43	0.48	0.57
k_{el}^o(cm s^{-1})	2.4×10^{-3}	9.7×10^{-3}	3.0×10^{-2}
$k_p(M^{-1}s^{-1})$		5×10^{4}	

References

1) R.Gerdil, J.Chem.Soc. B, 1071 (1966)
2) G.Farnia, A.Ceccon, P.Cesselli, J.Chem.Soc., Perkin Trans. 2, 1016(1972)
3) G.Farnia, M.G.Severin, G.Capobianco, E.Vianello, J.Chem.Soc.Perkin Trans. 2, 1 (1978).
4) G.Capobianco, G.Farnia, M.G.Severin, E.Vianello, J.Electroanal.Chem. 165, 251 (1984).
5) C.P.Andrieux, C.Blocman, J.M.Dumas-Bouchiat, F.M'Halla, J.M.Saveant, J.Am.Chem.Soc., 102, 3806 (1980) and references therein.

HOMOGENEOUS REDOX CATALYSIS OF ELECTROCHEMICAL REACTIONS. CATALYTIC REDUCTION OF SOME SULFILIMINE

L.GRIGGIO and M.G.SEVERIN
Dipartimento di Chimica Fisica, Padova (Italy)

The electrochemical reduction of some sulfonyl derivatives of sulfiliminesmines was recently investigated in DMF, on a mercury electrode[1]. The process was found corresponding to an irreversible two-electron uptake, with cleavage of the sulfiliminic S-N bond as the main pathway.

Neither quantitative data on kinetic and thermodynamic characteristcs of the electron transfer, nor pieces of information on the actual reaction mechanism could be obtained by study on the heterogeneous reactions. The hypothesis of an ECE or EC Disp sequence, with the cleavage taking place at the level of the primary radical anion, was suggested by analogy with similar irreversible two-electron reductions. Even the presence of an electron-withdrawing substituent, such as CN, in the para position of the sulphonyl moiety, cannot give direct evidence of the formation of a primary one-electron reduction product[1].

This intermediate was observed only in conjunction with NO_2 susbtitution[2], owing to its well known radical stabilization property. In the other cases, one can anticipate that if the anion radical exists, it should have a lifetime less than ca. 10^{-5}s.

Recently the method of homogeneous redox catalysis has been theoretically described for a reduction mechanism similar to that assumed[3]. The method, based on the reductive process taking place homogeneously by suitable redox couples (catalyst couples), was shown to allow the determination of the lifetime of very short-living reaction intermediates[4], when their chemical decay (usually a bond cleavage) becomes partially rate-controlling. In different conditions, the method can be used, in conjunction with classical treatments of solution reactions and with the theories on electron transfer reactions, to obtain thermodynamic and/or kinetic parameters of the homogeneous electron transfer[5], when the latter is the rate determining step.

We report in this communication our results on the homogeneous reduction studied by means of homogeneous redox catalysis, as well as on the electrode reduction, for three sulfilimines: S,S-diphenyl-(Sulf I) and S,S-diethyl-N-p-tosylsulfilimine (Sulf II) and S,S-diphenyl-N-p-cyanobenzene sulfonylsulfilimine (Sulf III).

The choice was made with the purpose of clarifying if possible, the effect of different substituents on each side of the sulfilimine, from the point of view of i) stability of the primary anion radical, if it exists; ii) kinetic and thermodynamic easiness to accept one (or more) electron.

A relevant difference among the three compounds, is already evident in the electrode reaction. The heterogeneous reduction of Sulf III is shown, from the voltammetric peak potential behaviour, to be controlled by the first-order step following the charge transfer, while, either a mixed control by the chemical reaction and the electron uptake, or perhaps a definitively slow charge transfer (with a transfer coefficient $\alpha = 0.66$) is observed for Sulf II. The latter situation is also valid for the first sulfilimine ($\alpha = 0.5$). The different behaviourcan be ascribed either to

a faster charge transfer to the CN derivative or to a faster decay of the supposed anion radical intermediate in the CH_3 substituted sulfilimines.

As regards the homogeneous reduction by electrogenerated charge transfer reagents (the stable anion radicals of suitable organic molecules, R), it appears always controlled by the electron transfer step:

$$R^{\cdot-} + \text{Sulf} \underset{k_2}{\overset{k_1}{\rightleftharpoons}} R + [\text{Sulf}]^{\cdot-} \qquad (1)$$
$$\downarrow \text{Products}$$

where the actual formation of the $[\text{Sulf}]^{\cdot-}$ intermediate has been assumed only for simplicity of discussion: the electron transfer can even imply the direct passage from substrate to subsequent products (concerted reaction).

Several redox couples, have been used with each sulfilimine. The rate constants k_1, for the electron exchange (1) have been obtained. For a given sulfilimine they depend on the catalyst standard potential, specifically they decrease as the potential becomes more positive in agreement with the qualitative expectation of electron transfer theories.

The dependence of the log of k_1 on E°_R for Sulf I and partially for Sulf II, is not linear. However a straight line can be approximated at the more positive potentials. A linear relationship is also observed in the case of Sulf III.

According to the usual scheme for solution charge transfer reactions, the rate constant could obey in this region to the simplified equation:

$$\lg k_1 = \lg k_d - \frac{F}{RT\ln 10}\,(E^\circ_R - E^\circ_{\text{Sulf}}) \qquad (2)$$

where k_d is the value of the rate constant for a bimolecular reaction controlled by the reagent diffusion to form the encounter complex.

The approximate expression (2) for electron transfer rate constants corresponds to a thermodynamically unfavoured reaction, whose reverse step is diffusion controlled. By assuming a typical value for k_d in DMF, the fitting of experimental data with equation (2) allows one to determine the standard potentials for the three sulfilimines.

For Sulf I and II, this knowledge also makes possible to analyze the electrode reaction data. If the heterogeneous charge transfer is assumed as rate determining for both compounds, as it seems likely on the basis of the very fast following reaction (vide infra), in addition to the transfer coefficients also the standard electron transfer rate constants can be evaluated[6].

The values for the two compounds are rather similar to each other and of the order of 10^{-1} cm s^{-1}. Indeed the fastness of radical decay must play a preminent role in determining the electrode process as controlled by the charge transfer step.

As regards Sulf III, the knowledge of its standard potential, in conjunction with the electrode behaviour of the compound, directly makes possible the evaluation of the life time of the anion radical[4], which results of the order of 10^{-6} s.

No information can be obtained, on the rate constants of anion radical decay for the other two substrates, either from the electrode process or from the heterogeneous reduction, which is never under partial control of the step following the charge transfer. This fact points out that such chemical reactions are extremely fast, greater than ca. 10^8 s^{-1}.

Such a large value obviously raises some doubt on the very existence of the radical anion intermediate. In any case it indicates that the replacement of ethyl with phenyl groups in the sulfiliminic moiety does not seem to greatly influence the stability of the reduced form, in contrast

with the sensible effect of a CN group in the other side of the molecule.

References

1) L.Griggio and G.Capobianco, J.Electroanal.Chem. 94 (1978) 67.

2) L.Griggio, Electrochim.Acta 27 (1982) 749.

3) C.P.Andrieux, C.Blocman, J.M.Dumas-Bouchiat, F.M'Halla and J.M.Savéant, J.Electroanal.Chem. 113 (1980) 19.

4) C.P.Andrieux, C.Blocman, J.M.Dumas-Bouchiat, F.M'Halla and J.M.Savéant, J.Am.Chem.Soc. 102 (1980) 3806.

5) C.P.Andrieux, C.Blocman, J.M.Dumas-Bouchiat, and J.M.Savéant, J.Am.Chem. Chem.Soc. 101 (1979) 3431.

6) L.Nadjo and J.M.Savéant, J.Electroanal.Chem. 48 (1973) 113.

13160

ELECTROCHEMICAL REDUCTION OF CEFUROXIME

J.E. COSANO, J.L. AVILA, L. CAMACHO, A.M. HERAS
and F. GARCIA-BLANCO
Department of Physical Chemistry, Faculty of Sciences,
University of Córdoba (Spain)

In this work we have carried out a study on the electrochemical behaviour of cefuroxime (I), an antibiotic belonging in the family of cephalosporines C, which exhibits a major antibacterial activity. Such a study has been performed in buffered aqueous solutions over the pH range 2-12. The concentration was 20 p.p.m. except, obviously, for those experiments involving the study of the effect of this variable; the influence of the concentration was analyzed between 5-70 p.p.m.

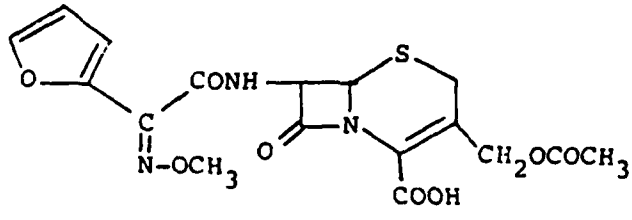

(I)

The study has been carried out mainly by DC polarography and differential pulse polarography. This last technique, on account of its sensitivity and selectivity, has been used earlier for the analysis of this type of compounds (1-6).

The limiting current of the main wave observed by DC polarography is virtually pH-independent. We must indicate, however, that above a pH of approximately 6 the i_L values obtained are not very reliable since the wave partly overlaps with the discharge of the supporting electrolyte.

We have made a study of the stability of dissolved cefuroxime, finding that, for a period of at least 2 h, the limiting current does not appreciably decrease over time at any of the pH values investigated.

The peak current remains constant with the pH and shows its largest value at very acidic pH, progressively decreasing with increasing pH, until reaching a value of 50 nanoamperes at about pH 6. A subsequent new increase in the peak current is observed at more basic pH. We should note that these variations in the peak current are accompanied by a chenge in peak width (the smaller the intensity, the broader the peak).

In the figure is illustrated the variation of the peak potential with the pH. As can be seen, such a variation is rather complex and involves four different segments: a first one with a slope of -50 mV/pH, between pH 0-4; a second one with a slope of -180 mV/pH between pH 4-6.5; a third one with a very steep slope (-245 mV/pH) between pH 6.5-8.5 and, finally, a fourth one starting at pH 8.5, above which the peak potential is pH-independent.

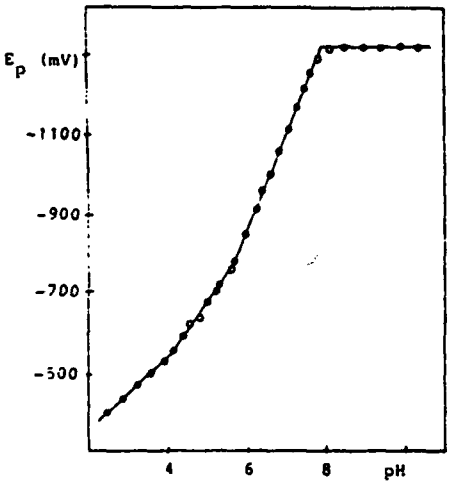

We have studied the effect of the concentration on the peak current at pH 3, 5 and 7, finding a linear variation which allows the analytical determination of cefuroxime by differential pulse polarography, at least within the concentration range investigated.

The data from the i-t curves obtained at potentials corresponding to the limiting current of the DC polarographic curve were plotted as log i vs log t. The plot obtained were linear in every case, with slopes between 0.17-0.20, which shows that, at such potentials, the reduction process is

controlled by the depolarizer diffusion.

We have carried out the logarithmic analysis of the wave between pH 2-6, finding that, in every case, the plot of log $|i/(i_L-i)|$ vs E shows more than one segment, the slope of the first of these increasing with the pH from -50 to -70 mV, and the data obtained at larger overpotentials conforming to steeper slopes at every pH.

The electrochemical behaviour of cefuroxime is indicative of the complexity of its reduction mechanism, the kinetics of which are probably affected by adsorption phenomena.

REFERENCES

(1) G. Dusinsky and P. Antolik, Cesk. Farm., 16 (1967) 120 and 461.

(2) I.F. Jones, J.E. Page and C.T. Rhodes, J. Pharm. Pharmacol. 20 (1968) 455.

(3) M. Ochiai, O. Aki, A. Morimoto, T. Okada, K. Shinozaki and Y. Asahi, Tetrahedron Lett. (1972) 2341 and J. Chem. Soc. (1974) 258.

(4) A.G. Fogg, N.M. Fayad, C. Burgess and A. McGlynn, Anal. Chim. Acta, 108 (1979) 205.

(5) A.G. Fogg, N.M. Fayad and C. Burgess, Anal. Chim. Acta, 110 (1979) 107.

(6) A.G. Fogg and M.J. Martin, Analyst, 106 (1981) 1213.

13170

ELECTROCHEMICAL REDUCTION OF 4,4-DIMETHYL-1-PHENYL-1-PENTEN-3-ONE

M.A. ALMIRON, L. CAMACHO, A.M. HERAS, J.L. AVILA
and F. GARCIA-BLANCO
Department of Physical Chemistry, Faculty of Sciences,
University of Córdoba (Spain)

We have carried out a study on the electrochemical reduction of 4,4-dimethyl-1-phenyl-1-penten-3-one (I), at a 5×10^{-5} M concentration in a Britton-Robinson medium.

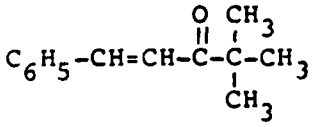

(I)

This compound shows one or two DC polarographic reduction waves, depending on the pH of the medium. At acidic pH appear two reduction waves (a) and (b), the limiting current of which, as well as their height ratio, is pH-independent. These waves are diffusion-controlled at potentials corresponding to the limiting current, as is evident from the linear variation of log i_l with log t, with a slope of 0.19. This has allowed the chronoamperometric determination of the number of the electrons involved in the overall process, finding that the reduction process corresponding to these waves are both one-electron.

Both waves overlap above pH 7 due to the faster shift of the more anodic wave (a) as the pH increases. The height of this third, composite wave, is approximately equal to the sum of the heights of waves (a) and (b). The variation of the half-wave potential with the pH for the three waves is shown in Fig. 1. The slope of the linear variation of $E_{\frac{1}{2}}$ vs pH for wave (a) is approximately -60 mV/pH, whereas for wave (c), such a

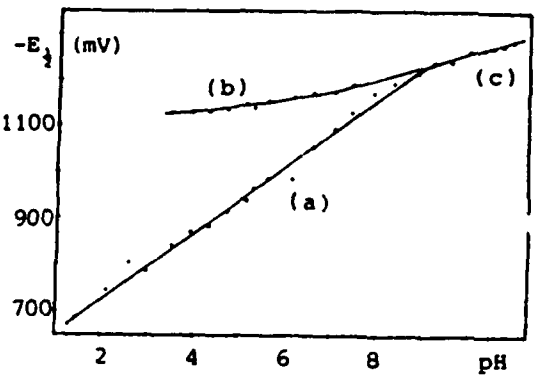

variation is -25 mV/pH. As regards wave (b), and as can be seen, its $E_{\frac{1}{2}}$ is practically pH-independent at more acidic pH, at which the processes corresponding to waves (a) and (b) appear at sufficiently distant potentials. Conversely, when both processes occur at very close potentials, $E_{\frac{1}{2}}$ varies somewhat with the pH, and this apparent variation is due, to our mind, to the difficulty in measuring such close waves at these pH.

As regards the logarithmic analysis, wave (a) yields a linear variation of log $|i^{1/2}/(i_L-i)|$ vs E, with a slope close to -60 mV, which suggests the occurrence of a determining stage involving a heterogeneous radical-radical dimerization (1). At high temperatures or for high ethanol contents in the medium, the logarithmic analysis is linear for a plot of $\log|i^{2/3}/(i_L-i)|$ vs E, which indicates that, under these conditions, the dimerization takes place in the reaction layer, since the intermediate radical is not retained over the surface of the electrode.

Wave (b) yields a linear plot of log $|i/(i_L-i)^{3/2}|$ vs E, with a slope of -60 mV, which would be in agreement with the competition between the incorporation of the second electron and the above-mentioned radical-radical dimerization which, at these potentials, would take place in the reaction layer due to the intermediate desorption.

The logarithmic analysis for wave (c), in the form of log $|i/(i_L-i)|$ vs E, is linear with a slope of -40 mV.

As regards the analysis of kinetic parameters at potentials corresponding to the foot of the wave, we have determined the values of the Tafel slope and reaction orders with respect to (I) and the H^+ ion for waves (a) and (c), finding a values of -30 mV for the Tafel slope for wave (a) and -10 mV for wave (b). This last yielded a reaction order of 1 and 0.6 in (I) and H^+, respectively, whereas wave (a) provided a

value of 2 for both orders.

We have recorded differential cpacity-potential curves point by point with a hanging electrode, both in the presence and in the absence of depolarizer. Owing to the low working concentration, the capacity only estabilizes after 20 sec, which shows the adsorption to be diffusion-controlled. The capacity in the presence of depolarizer is always less than that of the supporting electrolyte at any t value. This, together with the fact that the kinetic aprameters agree with the theoretical ones to be expected in the absence of adsorption, allows us to neglect the effect of the adsorption in formulating the mechanism.

According to our results, we propose the following mechanism for the first reduction wave, (a):

|1| $A + e^- \rightleftharpoons A^{\cdot -}$

|2| $A^{\cdot -} + H^+ \rightleftharpoons AH^{\cdot}$

|3| $2AH^{\cdot} \longrightarrow D$

whereas for wave (b) the process takes place via stages |1| and |2| plus stage |4|, which would compete with step |3|:

|4| $AH^{\cdot} + e^- \rightleftharpoons AH^-$

Finally, the process corresponding to wave (c) would take place trough stages |1|, |2| and |4|, where, in this case, step |4| is an irreversible transfer and step |2| is a protonation in the reaction layer (2), which accounts for the semi-integer order in the H^+ ion.

REFERENCES

(1) L. Camacho, J. Electroanal. Chem., 177 (1984) 59.

(2) J.M. Rodríguez-Mellado, L. Camacho, R. Rodríguez-Amaro and J.J. Ruiz, J. Electroanal. Chem., 177 (1984) 69.

REDOX PROPERTIES OF MESO-TETRAALKYL PORPHYRINS

CHRISTOPHER M.A. BRETT and ANA MARIA C.F. OLIVEIRA BRETT
Departamento de Química, Universidade de Coimbra
3049 Coimbra, Portugal

There is considerable interest in the chemistry of the porphyrins owing to their ubiquity in nature, in photosynthesis and in respiration[1]. They function as part of the biological electron transfer chain, their complexes being bound, in general, to proteins. Much about these compounds can be learned from the study of the porphyrin molecules themselves, and in particular their electrochemical properties.

Most of the porphyrins without a central metal ion are not water soluble and consequently have been studied in non-aqueous media such as N,N-dimethylformamide (DMF) or acetonitrile (ACN) with tetraalkylammonium salts as supporting electrolytes. Variations in solvent, supporting electrolyte and so forth mean that there are often differences in results between authors. Most of the work has involved use of the mercury electrode [2-4] partly because of its large negative potential range. thus enabling the study of the relation between the porphyrin (H_2P) and its phlorin/chlorin (H_4P) reduction products, and partly because of the ease of renewing and having a reproducible electrode surface, obviating unwanted surface adsorption complications. The study of the metal complexes has been directed towards correlating half-wave potentials with the change in electronic properties caused by the central metal ion. Oxidation of porphyrins cannot be investigated at mercury electrodes: some work has been performed at platinum rotating electrodes[5].

As part of a project to investigate further the redox properties of a number of different porphyrins with and without central metal ions, we report here results obtained for some meso-tetraalkyl porphyrins. These compounds have not been investigated in the past due to very low synthetic yields; however modifications in the synthesis have allowed their preparation[6]. DMF solvent was used with supporting electrolytes of tetraethyl ammonium bromide (TEAB), tetrabutylammonium bromide (TBAB), and tetrabutyl ammonium perchlorate (TBAP). Standard procedures were used to ensure the purity of all chemical compounds. Electrodes were of glassy carbon, which in DMF has a potential range of approximately -2.7V to +1.7V vs SCE, enabling both oxidation and reduction to be investigated. Cyclic voltammetry and the rotating disc technique were employed.

The porphyrin molecules is a tetrapyrrolic ring as shown overleaf where X- represents the positions for meso- substitution. In this work X is an alkyl group. If we designate the porphyrin molecule H_2P then the oxidation - reduction scheme can be written as

$$H_2P^{2+} \underset{}{\overset{-e}{\rightleftharpoons}} H_2P^{\cdot+} \overset{-e}{\rightleftharpoons} H_2P \overset{+e}{\rightleftharpoons} H_2P^{\cdot-} \overset{+e}{\rightleftharpoons} H_2P^{2-} \longrightarrow \cdots$$

$$E_{1/2}(2,ox) \qquad E_{1/2}(1,ox) \qquad E_{1/2}(1,red) \qquad E_{1/2}(2,red)$$

The two reduction steps shown are nearly always reversible and the first is often used to characterise the porphyrin. Further reduction steps (not shown) do occur leading to the phlorin or chlorin and involve proton abstraction from the solvent. The studies performed by us in this work involve mainly the electron transfers shown in the above scheme on the previous page.

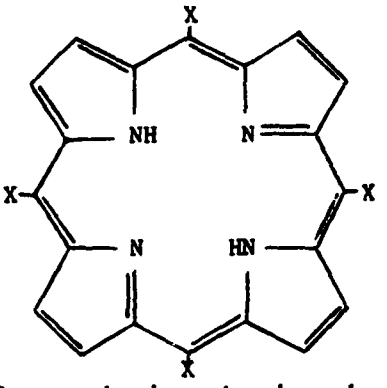

A typical cyclic voltammogram for porphyrin reduction, in this case tetra-n-propyl porphyrin (TnPrP) in TEAB supporting electrolyte is shown in the figure, which demonstrates the reversible nature of the first

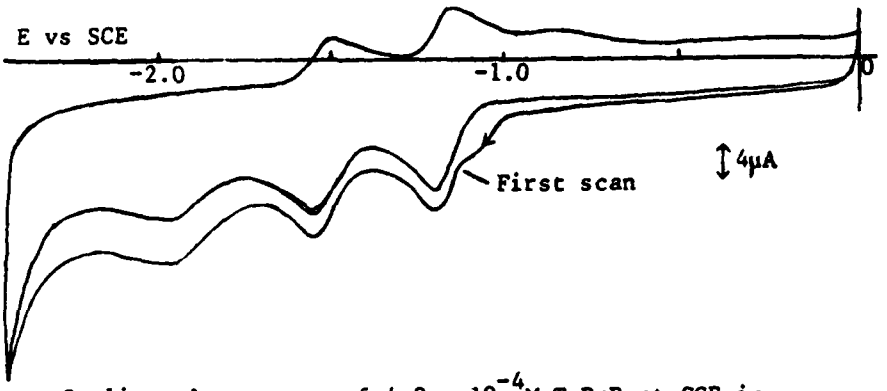

Cyclic voltammogram of 4.0×10^{-4}M TnPrP at GCE in 0.1M TEAB/DMF. Scan 50mV s^{-1}.

two reduction steps. Note that the first cathodic scan is different from the following scans, in particular in the region of ~-1.1V. This behaviour is observable only with bromide containing supporting electrolytes. Rotating disc experiments confirm the above observations. Conclusions can be drawn about the effect of supporting electrolyte on the electrode surface. Pretreatment of the glassy carbon is also very important in determining the electrode response. Results for other meso-tetraalkyl porphyrins will be presented; the conclusions are broadly similar. Electrochemical oxidation studies of these porphyrins at glassy carbon will also be shown.

Finally comparison is made with results obtained at mercury electrodes and with results obtained with meso-tetraphenyl porphyrin.

References

1. D. Dolphin ed., The Porphyrins, Academic Press, New York, 1978.
2. D.W. Clack and N.S. Hush, J. Am. Chem. Soc., 1965, 87, 4238.
3. G. Peychal- Heiling and G.S. Wilson, Anal. Chem., 1971, 43, 550.
4. P. Worthington et al., J. Inorg. Biochem., 1980, 12, 281.
5. A. Stanienda and G. Biebl, Z. Phys. Chem., 1967, 52, 254.
6. A.M. Rocha Gonçalves and M.M. Pereira, in press.

HOMOGENEOUS REDOX CATALYSIS. COMPETITION BETWEEN ELECTRON EXCHANGE AND PROTON EXCHANGE.

A. INESI[o] and E. ZEULI[oo]

[o]Dipartimento ICMMPM, Sezione Chimica Università degli Studi di Roma "La Sapienza" Via del Castro Laurenziano 7 -00161 Rome - I.

[oo]Dipartimento di Chimica, Università degli Studi di Roma "La Sapienza" Piazzale Aldo Moro 5 -00185 Rome - I.

It has been evaluated that proton exchange (reactions 10 and 13, Scheme 2) and nucleophilic substitution (reaction 14, Scheme 2) reactions can become competitive with electron exchange reactions (reaction 3, Scheme 1) in homogeneous redox catalysis processes due to the indirect reduction (Scheme 1) of bromoesters.

Scheme 1:

$$BrCH_2(CH_2)_nCH_2CO_2Et + e \longrightarrow (BrCH_2(CH_2)_nCH_2CO_2Et)^{\cdot-} \quad E_1 \quad (1)$$

$$A + e \longrightarrow A^{\cdot-} \quad E_2 \quad (E_2 > E_1) \quad (2)$$

$$BrCH_2(CH_2)_nCH_2CO_2Et + A^{\cdot-} \longrightarrow (BrCH_2(CH_2)_nCH_2CO_2Et)^{\cdot-} + A \quad (3)$$

$$(BrCH_2(CH_2)_nCH_2CO_2Et)^{\cdot-} \longrightarrow Br^- + {}^{\cdot}CH_2(CH_2)_nCH_2CO_2Et \quad (4)$$

$${}^{\cdot}CH_2(CH_2)_nCH_2CO_2Et + A^{\cdot-} \longrightarrow {}^{-}CH_2(CH_2)_nCH_2CO_2Et + A \quad (5)$$

$${}^{\cdot}CH_2(CH_2)_nCH_2CO_2Et + e \longrightarrow {}^{-}CH_2(CH_2)_nCH_2CO_2Et \quad E_3 \quad (E_3 > E_1) \quad (6)$$

$${}^{-}CH_2(CH_2)_nCH_2CO_2Et + BrCH_2(CH_2)_nCH_2CO_2Et \longrightarrow$$

$$\longrightarrow CH_3(CH_2)_nCH_2CO_2Et + BrCH_2(CH_2)_n\bar{C}HCO_2Et \quad (7)$$

$$BrCH_2(CH_2)_n\bar{C}HCO_2Et \longrightarrow Br^- + \overline{CH_2(CH_2)_n}CHCO_2Et \quad (8)$$

$${}^{-}CH_2(CH_2)_nCH_2CO_2Et + BrCH_2(CH_2)_nCH_2CO_2Et \longrightarrow$$

$$\longrightarrow Br^- + (CH_2(CH_2)_nCH_2CO_2Et)_2 \quad (9)$$

(n= 0,1,2. A: catalyst, 9,10 diphenylanthracene)

Electrochemical data have been correlated with the results of the analyses carried out in solution during and at the end of the catalytic reduction processes.

Thus, the conditions at which the indirect reduction of bromoesters (RX) occurs as a pure catalysis process, i.e. with no consumption of the catalyst, can be deduced from the curves of Figure 1.

Scheme 2:

$$A^{\cdot-} + BrCH_2(CH_2)_nCH_2CO_2Et \longrightarrow {}^{\cdot}AH + BrCH_2(CH_2)_n\bar{C}HCO_2Et \quad (10)$$

$${}^{\cdot}AH + e \longrightarrow AH^- \quad (11)$$

$${}^{\cdot}AH + A^{\cdot-} \longrightarrow AH^- + A \quad (12)$$

$$AH^- + BrCH_2(CH_2)_nCH_2CO_2Et \longrightarrow AH_2 + BrCH_2(CH_2)_n\bar{C}HCO_2Et \quad (13)$$

$$A^{\cdot-} + BrCH_2(CH_2)_nCH_2CO_2Et \longrightarrow {}^{\cdot}ACH_2(CH_2)_nCH_2CO_2Et + Br^- \quad (14)$$

$${}^{\cdot}ACH_2(CH_2)_nCH_2CO_2Et + e \longrightarrow {}^-ACH_2(CH_2)_nCH_2CO_2Et \quad (15)$$

$${}^{\cdot}ACH_2(CH_2)_nCH_2CO_2Et + A^{\cdot-} \longrightarrow {}^-ACH_2(CH_2)_nCH_2CO_2Et + A \quad (16)$$

$${}^-ACH_2(CH_2)_nCH_2CO_2Et + BrCH_2(CH_2)_nCH_2CO_2Et \longrightarrow$$

$$\longrightarrow AHCH_2(CH_2)_nCH_2CO_2Et + BrCH_2(CH_2)_n\bar{C}HCO_2Et \quad (17)$$

(n= 0,1,2. A: catalyst, 9,10 diphenylanthracene)

It results that for $C_o \geq 5.0 \times 10^{-3}$ M and $C_I > 5.0 \times 10^{-3}$ M, $\gamma_I > 1.0$, for $C_{II} > 7.8 \times 10^{-3}$ M, $\gamma_{II} > 1.56$, and for $C_{III} > 8.25 \times 10^{-3}$ M, $\gamma_{III} > 1.65$.

For γ values lower than the above ones, the reduction of RX goes with a decrease of the catalyst concentration, thus occurring as an incomplete catalysis. These results show that the reduction of RX is affected by both the catalyst and the substrate concentration. Indeed, the decrease in the substrate concentration allows the proton exchange (10) and the substitution (14) reactions to compete with the electron exchange one (3).

The hypothesis that the catalyst (9,10 diphenylanthracene) is dihydrogenated by the substrate according to a $DISP_2$ mechanism is in agreement with the experiments.

Scheme 3:

$$A + e \longrightarrow A^{\cdot-}$$

$$A^{\cdot-} + HS \longrightarrow AH^{\cdot} + S^- \qquad DISP_1$$

$$AH^{\cdot} + A^{\cdot-} \longrightarrow AH^- + A \qquad DISP_2$$

$$AH^- + HS \longrightarrow AH_2 + S^- \qquad DISP_3$$

$$AH^{\cdot} + e \longrightarrow AH^- \qquad ECE$$

REFERENCES

1. C.P.Andrieux,G.Bloeman,J.M.Dumas-Bouchiat, F.M'Halla and J.M. Savèant, J. Electroanal.Chem., 113 (1980) 19, and references therein.
2. A.Inesi,E.Zeuli,J.Electroanal.Chem. 149 (1983) 167, and references therein.
3. A.Inesi,A.Zeppa,E.Zeuli,J.Electroanal.Chem. 126 (1981) 175.

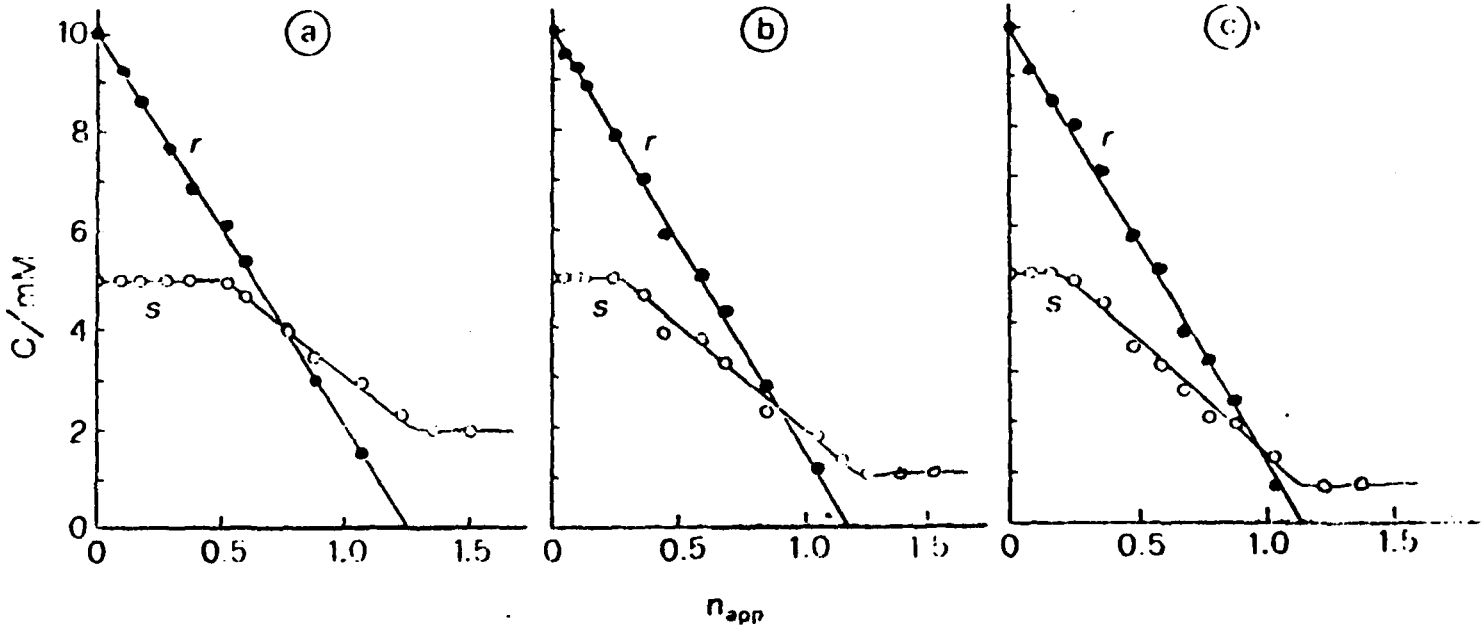

Figure 1: Indirect reduction of ethyl β-bromopropionate (a), ethyl γ-bromobutyrate (b), and ethyl δ-bromovalerate (c) mediated by 9,10-diphenylanthracene. Change in the concentration of ester (r) and catalyst (s) as a function of n_{app}. (n_{app}= Faraday number, measured coulometrically at -1.85 V, x moles of ester initially present in solution.)

CATHODIC REDUCTION OF DIHALOKETONES IN DMF-$LiClO_4$

F.BARBA,M.D.VELASCO,A.GUIRADO and N.MORENO
Department of Organic Chemistry,University of Murcia
Murcia,Spain

The electrochemical cleavage of carbon-halogen bonds in vicinal and geminal polihalides compounds generally proceeds in a two-electron stepwise mechanism. The reduction of vicinal polihalides affords the corresponding olefinic products whose formation has been rationalized through a concerted or an ionic mechanism[1].

When cathodic reduction of geminal polihalides are effected in aprotic solvents, monomeric and dimeric products are obtained[2]. These products can be explained as derived from anionic intermediates though evidences were obtained of carbenes and/or radical anions in the reduction of gem-halides [3-5].

We have previously reported the electrochemical reduction of α-haloketones in dry dimethylformamide [6,7] and methanol[8]. In this communication we report the cathodic reduction of dihaloketones in aprotic medium.

We have carried out the reduction of α-β-dibromo-β-phenylpropiophenone (1) in dry dimethylformamide using controlled potential electrolysis of -0.8 V vs SCE and a mercury pool cathode. The charge consumed was 2 $F.mol^{-1}$ and the product obtained was benzalacetophenone (2). These results suggest that the electrochemical behaviour of this dihaloketone is similar to the one of the others vicinal dihalides.

$$\underset{(1)}{Ph\text{-}CO\text{-}CHBr\text{-}CHBr\text{-}Ph} \xrightarrow[DMF]{+\ 2e^-} \underset{(2)}{Ph\text{-}CO\text{-}CH{=}CH\text{-}Ph}$$

On the other hand, we report the cathodic reduction of a geminal dihalide what shows a different electrochemical behaviour.

The electrolysis of dibenzoyldibromomethane (3) was carried out in dry dimethylformamide using a mercury pool as the cathode and with a controlled potential of 0.0 V vsSCE. A white solid was isolated from the catholyte and it was characterized as the dibenzoylbromomethane (4).

$$\underset{(3)}{Ph\text{-}CO\text{-}CBr_2\text{-}CO\text{-}Ph} \xrightarrow[2)\ H_2O]{1)\text{Electrolysis in DMF}} \underset{(4)}{Ph\text{-}CO\text{-}CHBr\text{-}CO\text{-}Ph}$$

The electron consumption (1 F. mol^{-1}) and the nature of the electrolytic product involve a radical mechanism.

REFERENCES

1.- J.Y. Berker in "The Chemistry of functional groups" Supplement D, S. Patai and Z. Rappoport Ed. John and Wiley, 251, 255, 256 (1983)

2.- F.M. Triebe,K.J. Borhani and M.D. Hawley; J. Electroanal. Chem. Interfacial Electrochem. 107 (2), 375 (1980).

3.- T.L. Gilchrist and G. W. Rees, "Carbenes, Nitrenes and Arynes", Ed. Nelson and Sons Ltd, 1969, cap. 6

4.- J. March, "Advanced Organic Chemistry" Mc Graw-Hill 1977, cap. 5

5.- F. A. Carey, R. J. Sundbery "Advanced Organic Chemistry" part B, Plenum, Rosetta, 1977, cap 8.

6.- F. Barba, M.D. Velasco and A. Guirado; Synthesis 625,(1981)

7.- F. Barba, M.D. Velasco, A. Guirado and I. Barba,Electrochimica Acta, in press

8.- F. Barba, M.D. Velasco and A. Guirado; Electrochimica Acta, 28 (2), 259, (1983).

SYNTHESIS OF 3,6-DIARYLPYRIDAZINES FROM PHENACYL BROMIDES

F. BARBA, M.D. VELASCO , A. GUIRADO and N. MORENO
Department of Organic Chemistry, University of Murcia
Murcia, Spain

Aryl substituted pyridazines can be obtained by cyclization from unsaturated or saturated 1,4-diketones and hydrazine[1,2]. Semicarbazide, thiosemicarbazide and aminoguanidine have been used instead of hydrazine[3].

We report a facile method for the synthesis of 3,6-diarylpyridazines starting from more simple and available materials than unsaturated or saturated 1,4-diketones.

The cathodic reduction of phenacyl bromides semicarbazones in dry dimethylformamide lead to the 1,4-diaryl-1,4-butanedione disemicarbazones in quantitative yields. The heating of the electrolytic products give the 3,6-diarylpyridazines in high yields.

REFERENCES

1.M.Trisle and B. Stanovnik in "Advances in Heterocyclic Chemistry",ed. byA.R. Katrizky and A.J. Boulton; Academic Press ,vol. 9,London 1968, p. 226

2. ibid. ,vol 24, London 1979, p. 364

3. H. Beyer ,T. Pyl, C.E. Völcker; Ann. Chem. 150, 638,1960

ANODIC OXIDATION OF (-)-α-PINENE

V.MONTIEL, M.LOPEZ-SEGURA and A. ALDAZ
Departamento de Química Física. Universidad de Alicante. España
and
F. BARBA
Departamento de Química Orgánica. Universidad de Murcia. España

(-)-α-pinene, (-)1, $(\alpha)_D^{20} = -40$ (c=1.13,$CHCl_3$) was anodically oxidized at constant current (i=119 A/m^2) on graphite paste electrode in a non-divided thermostatized cell (23 ºC) with magnetic sitirring.

Electrolysis was carried with different solvent-supporting electrolyte system (SSE). The solution was electrolyzed until a charge of 2F/mol starting product, was sent through.

For the SSE THF:H_2O:$HClO_4$ 60% (175:80:1 weight) the oxidation products were: (±)pinol,2; (±)cis carveol,3; (±)trans carveol,4; and (±) trans sobrerol,5, with material yield of 16,5,15 and 12% respectively.

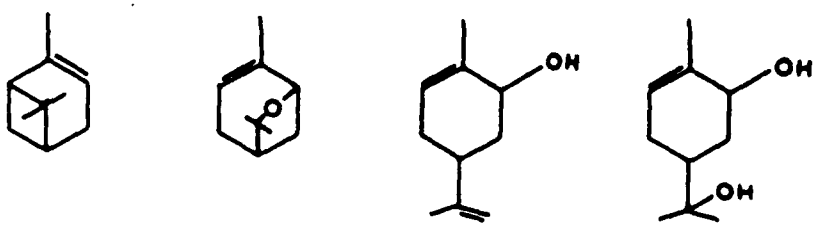

α-pinene pinol carveol sobrerol

For the SSE THF:H_2O:$NaClO_4$(130:5:2 weight) the products obtained, in the same experimental conditions,were the same as before but the yields changed lightly 16,4,12 and 13% respectively. When the SSE was THF:NaOH 5% (8:1 weight) the yields were 10,3,7 and 8%.

All the products were identified by their spectra of IR, NMR, MS and by its rotatory power, these were the same as those described in the bibliography [1,2,3,4].

A logical reaction route would be the one described in schemes 1-3. This route is based on the previous routes described in the bibliography [2,5,6] and on the products obtained.

Pinene is thus oxidized to give a cation radical 6 which by breaking and rearrangement gives 7. Scheme 1.

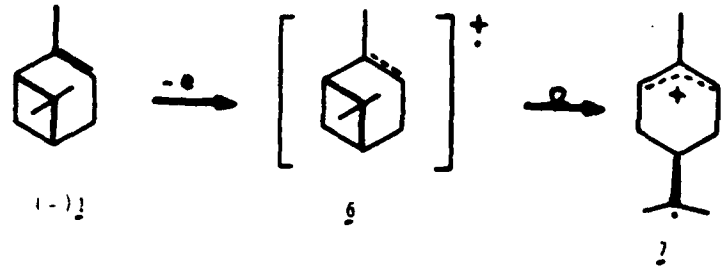

(-)1 6 7

Scheme 1

7, after being attacked by H_2O and having lost a H_3O^+ is oxidized to 8a and 9a. This compound gives (+)4 and (-)5. The formation of (+)4 is explained by deprotonation of 9a and the formation of (-)5 by attack of H_2O and the loss of H_3O^+. 8a gives (+)3 and (-)2 in the proportion 1:3 (cis carveol/trans carveol). This proportion can be explained by the cis structure of the groupes hydroxil and isopropyl.

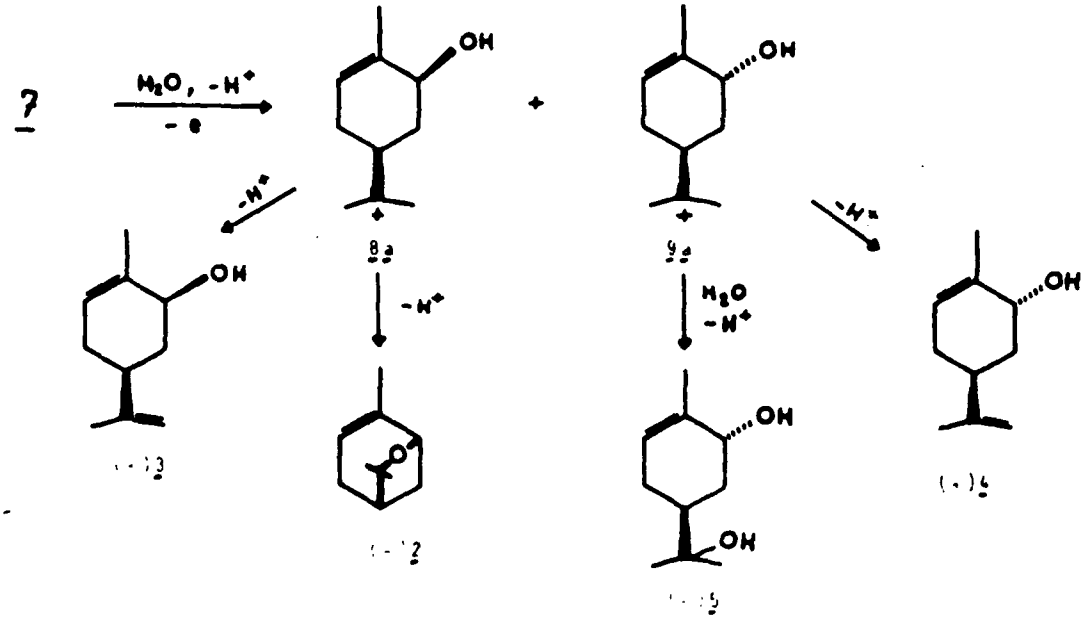

(-)3 (-)2 (-)5 (+)4

7 can also give the enantiomers 8b and 9b which in the same way as before give the enantiomers (-)4,(+)2,(-)3 and (+)5.

All these facts can explain the obtention of racemic products (±)4, (±)2,(±)3 and (±)5.

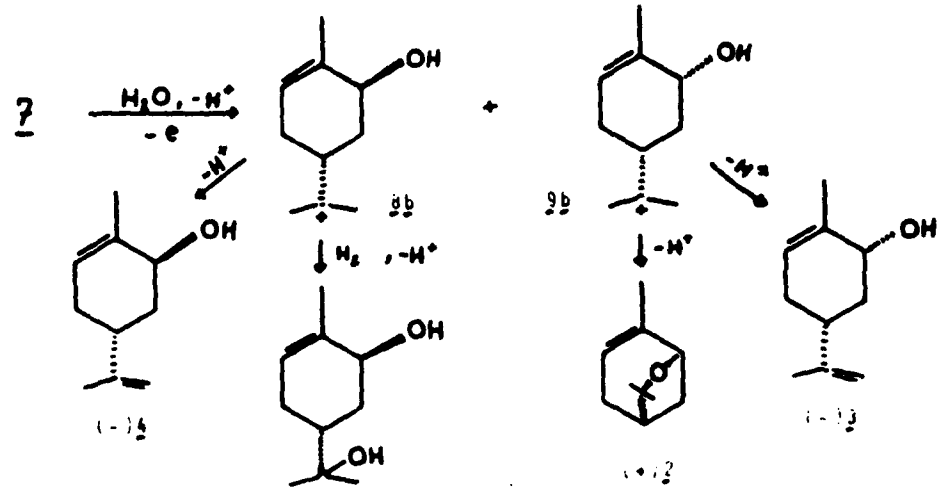

Scheme 3

REFERENCES

1 J.WOLINSKY,R.O.HUTCHINS,J.H.THORSTENSON. Tetrahedron. Vol.27,p.753 (1971)
2 R.LOMBARD,G.HEYWANG. Bul.Soc.Chim.France. 1210 (1954)
3 S.H.SCHROETER,E.L.EBEL. J.Org.Chem.,30,N.1 (1965)
4 J.PASCUAL TERESA,I.SANCHEZ,J.F.SANTOS. An.Quim. V.72,560 (1976)
5 T.SHONO,A. IKEDA,J.HAYASHI,J.HAKOZAKI. J.Am.Chem.Soc.97,4261 (1975)
6 V.MONTIEL,M.LOPEZ-SEGURA,A.ALDAZ,M.GRANDE,F.BARBA.Electrochimica Acta Vol.29,No.8,pp.1123-1126,1984.

ELECTRODIMERIZATION OF BENZOPHENONE ON MERCURY ELECTRODE

MANUEL BLAZQUEZ, JOSE. M. RODRIGUEZ-MELLADO and JUAN J. RUIZ
Departamento de Quimica Fisica, Facultad de Ciencias,
Universidad de Cordoba, 14005 Cordoba (SPAIN)

INTRODUCTION

The reduction mechanisms corresponding to the first reduction wave of aromatic carbonyl compounds have been extensively studied and are assumed to occur through the following scheme:

$$R\text{-}CO\text{-}R' + H^+.e \longrightarrow R\text{-}\dot{C}OH\text{-}R' \longrightarrow \frac{1}{2}\, R_2COH\text{-}COHR'_2$$

To the elucidation of this mechanism has greatly contributed the derivation of explicit theoretical expressions for the waves carried out by Mairanovskii[1] and Laviron[2] on the basis of the reaction layer theory. These equations have been applied to several carbonyl compounds. However, these studies have not yet been applied to the reduction process of benzophenone.

On the other hand, Mairanovskii and Laviron indicate that the deviations from the general behaviour observed by Suzuki and Elving[3] in the case of benzophenone are due to the use of unappropiate experimental conditions and to analysis criteria unaplicable under these experimental conditions. These comments lead us to think it advisable to reinvestigate the electrodimerization process of this compound following the suggestions of these authors on the experimental conditions to employ.

RESULTS AND DISCUSSION

The effect of pH, benzophenone concentration, drop time and ethanol content on the polarographic and kinetic parameters of the first wave is studied. In the zone where the ethanol content is low (0-10%) and the benzophenone concentration is very low ($<6.10^{-5}$M), the experimental data seem to conform equation (1) roughly:

$$E = E'_o + \frac{RT}{F} \ln \frac{i_D - i}{i^{\frac{1}{2}}} + \frac{RT}{2F} \ln \frac{k_3 c\, c_H^2}{K_1^2 i_D} \sqrt{\frac{3\pi t}{7D}} \qquad (1)$$

derived for a electrodimerization at the interface.

Thus, the $E_{\frac{1}{4}}$ vs. log c plots are linear, with slopes (30-40 mV), (close to the theoretical value (30 mV)) and the logarithmic analyses, i.e. the E vs. log $(i^{\frac{1}{2}}/(i_L - i))$ plots are

linear, with a slope of -65 mV, (also close to the theoretical value (-59 mV)). However, the slope of the linear $E_{\frac{1}{2}}$ vs. log t plot, 42 mV, is much greater than the theoretical value (15 mV). This divergence could be due to the fact that equation (1) has been derived by assuming that the depolarizer is not adsorbed on the mercury electrode, whereas the C-E curves indicate that when the ethanol content is very low, benzophenone is indeed adsorbed on the electrode surface.

On the other hand, when the ethanol content is greater than 50%, the experimental data conform equation (2) perfectly:

$$E = E'_o + \frac{RT}{F} \ln \frac{i_D - i}{i^{2/3}} + \frac{RT}{3F} \ln \frac{3\pi k_3 tc\, c_H^3}{7 i_D K_1^3} \qquad (2)$$

derived for a electrodimerization in the reaction layer.

Thus, the $E_{\frac{1}{2}}$ vs. log c and log t plots are linear, with slopes of 18-20 mV, which coincide with the theoretical value (20 mV). Moreover, the E vs. log $(i^{2/3}/(i_L - i))$ plots are linear, with slopes of -58 mV.

These data, together with the C-E curves which show that for ethanol contents greater than 50% the adsorption of benzophenone is negligible, indicate that the reduction process takes place in the homogeneous phase.

Finally, when the ethanol content is low and the benzophenone concentration is greater than 10^{-4}M, the experimental results show an anomalous behaviour. Thus, the $E_{\frac{1}{2}}$ vs. log c and log t plots are linear up to a certain value, over which a discontinuity can be observed. Likewise, the logarithmic analyses are not linear. These facts were observed by Laviron in the reduction of some aromatic aldehydes and attributed by this author to the formation of an insoluble film layer of pinacol at the electrode surface in the curse of the reduction process. This possibility was also considered by Suzuky and Elving in the reduction of benzophenone on a dme. This insoluble film layer exerts an inhibiting effect on the process by decreasing the available surface of the electrode. When the ethanol content increases, the critical values of c or t also increase due to the increasing solubility of benzopinacol. Thus, the "transition concentrations" are 5.10^{-5}, $1.3.10^{-4}$ and $>8.10^{-4}$M for ethanol contents of 0, 10 and 80% respectively. Likewise, when the benzophenone concentration is 6.10^{-5}M, the "transition drop times" are 5 and >6.3 s for ethanol contents of 10 and 80% respectively, whereas for a benzophenone concentration of 2.10^{-4}M, the corresponding time values are 1.6 and >6.3 s, respectively.

On the other hand, the anomalous shape of the i-t curves obtained when the ethanol content is very low, together with the characteristics of the C-E curves, indicate that, under these experimental conditions, the electroreduction process occurs in heterogeneous phase.

The experimental values of the kinetic parameters

determined at potentials corresponding to the foot of the wave confirm the conclusions drawn from the polarographic data, that is, they are in agreement with the above theoretical expressions. Thus, the value of Tafel slopes shifts from -30 to -39 mV as the ethanol content increases from 0 to 50%. These limiting values concide with the theoretical ones. Likewise, the reaction orders with respect to benzophenone and H^+ ion shift from 2.0 to 1.5 over the same ethanol percentage range, in agreement with those theoretically predicted.

From all aforementioned results we can conclude that the electroreduction process corresponding to the first reduction wave of benzophenone occurs via the following reaction kinetic pathway:

$$\phi\text{-CO-}\phi \overset{H^+}{\rightleftharpoons} \phi\text{-}\dot{C}\text{OH-}\phi \overset{e}{\rightleftharpoons} \phi\text{-}\dot{C}\text{OH-}\phi \longrightarrow \frac{1}{2}\,\phi_2\text{-COH-COH-}\phi_2$$

When the ethanol content is very low, this process takes place on the electrode surface and the step

$$|\phi\text{-CO-}\phi|_{sol} \rightleftharpoons |\phi\text{-CO-}\phi|_{ads}$$

must be formulated as the previous one. Moreov · if the benzophenone concentration is high enough, benzopinacol can form an insoluble film layer, thus partialy inhibiting the electrode process.

On the other hand when the ethanol content is greater than 50%, its molecules completely cover the electrode surface preventing the adsorption of benzophenone. Likewise, the solubility of benzopinacol in these media hinders the formation of the film layer at the electrode surface and for these reasons, the electroreduction process must be considered as homogeneous.

REFERENCES

1. S.G. Mairanovskii: Izv. Akad. Nauk. SSSR Otd. Khim. Nauk., 12(1961)2140
2. E. Laviron: Coll. Czech. Chem. Comm., 30(1965)4219
3. M. Suzuki and P.J. Elving: J. Phys. Chem., 65(1961)391

A VOLTAMMETRIC STUDY ON THE OXIDATION OF 2,4-DIBROMO-6-METHYLANILINE IN ACID MEDIA

S. Arias*, E. Brillas** and J.M. Costa*
* Laboratory of General Chemistry. Faculty of Chemistry. University of Barcelona. Spain.
** Department of Physical Chemistry. Faculty of Chemistry. University of Barcelona. Spain

INTRODUCTION

In previous papers [1-3] the electrochemical oxidation of 2,4,6-tribromoaniline and 2,4-dibromoaniline in aqueous sulphuric acid solutions, at a platinum electrode, has been studied by rotating disk electrode (RDE), cyclic voltammetry (CV) and controlled-potential electrolysis. These products undergo two consecutive oxidation processes. The first one always leads to the formation of the corresponding p-benzoquinone derivative, although for 2,4,6-tribromoaniline, a meta dimer was also obtained as final product.

To gain a better understanding of the electrochemical oxidation of p-bromoanilines in acid medium, we now report results on the voltammetric behaviour of 2,4-dibromo-6-methylaniline solutions in different aqueous sulphuric acid media, at a platinum electrode, using RDE and CV.

EXPERIMENTAL

The 2,4-dibromo-6-methylaniline was synthesized by bromination of 2-methylaniline (Merck) in glacial acetic acid. All solutions were prepared with water obtained from a Millipore Milli Q system.

The employed instrument was a standard equipment consisting of an Amel 551 potentiostat, a P.A.R. 175 universal programmer and a Philips PM 8043 X-Y recorder. Voltammetric experiments were carried out in a Tacussel XLRC cell under nitrogen. The temperature was kept at 25.0°C. A Hg/Hg_2SO_4 (aqueous saturated K_2SO_4) was used as reference electrode and a Pt wire as auxiliar electrode. The Pt working electrode was a Tacussel EDI, and its rotating speed, ω, was regulated by a Controvit from Tacussel.

Solutions of aniline (1.0 mM) in sulphuric acid media, at an acid concentration range between 4.0 and 12.0 M, were studied.

RESULTS AND DISCUSSION

Figure 1 shows the RDE voltammograms corresponding to the oxidation of 1.0 mM 2,4-dibromo-6-methylaniline solutions at several sulphuric acid concentrations. Two different oxidation waves can be observed depending on the acid concentration. In solutions of $c_{acid} < 6.0$ M, only one single wave (I) was found. At higher acid concentrations, a second oxidation wave (II) appeared at higher potential values. This wave shifted with increasing acid concentration to less positive potentials. Table 1 summarizes RDE results obtained at a ω value of 16 rps. The first wave was always diffusion controlled with a half-wave potential, $E_{1/2}$, value comprised between 0.92 and 0.95 V vs SCE under all experimental conditions. The second wave is also

TABLE 1

RDE oxidation results of 1.0 mM 2,4-dibromo-6-methylaniline solutions in sulphuric acid at different concentrations, ω = 16 rps, v = 5 mV.s^{-1}.

$c_{H_2SO_4}$/M	η	Wave	$E_{1/2}$/V	$I_{l,a}$/μA	$I_{l,a}\cdot\eta^{1/2}$	αn
4.0	2.11	I	0.92	13.6	19.7	1.14
5.0	2.46	I	0.93	12.2	19.1	1.10
6.0	2.98	I	0.93	11.0	19.0	1.03
		II	1.26	9.2	15.9	0.86
7.0	3.71	I	0.94	9.3	17.9	1.14
		II	1.25	8.2	15.8	0.88
8.0	4.63	I	0.93	8.0	17.2	0.97
		II	1.23	7.9	17.0	0.91
9.0	5.70	I	0.95	5.9	14.1	1.07
		II	1.21	5.3	12.7	1.02
10.0	7.01	I	0.95	5.0	13.2	0.93
		II	1.20	3.5	9.1	0.95
11.0	8.81	I	0.95	4.3	12.8	0.94
		II	1.19	3.2	8.5	0.92

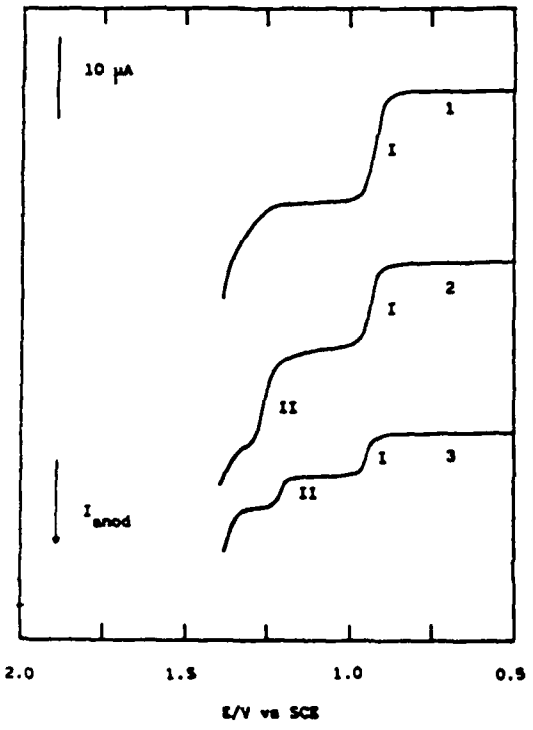

Fig.1.- RDE voltammograms corresponding to the oxidation of 1.0 mM 2,4-dibromo--6-methylaniline solutions in sulphuric acid at concentration: 1) 4.0 M; 2) 6.0 M; 3) 10.0 M, ω = 16 rps, v = 5 mV.s^{-1}.

diffusion controlled up to 11.0 M sulphuric acid, whereas it is kinetically controlled at higher acid concentrations when $\omega > 36$ rps. Corrections for viscosity are also presented in table 1 and their values indicate that most of the observed decrease in anodic limiting current of all waves is due to an increase in viscosity of the reaction medium. Under diffusion control αn products for waves I and II were always close to unity.

In a given solution cyclic voltammograms of 2,4-dibromo-6-methylaniline exhibit one peak for each oxidation process (O_1, O_2) observed in RDE voltammetry. Peak potentials of all anodic peaks shifted to more positive values when v increased. This fact suggests that, under diffusion control, both oxidation processes are irreversible. Two additional redox pairs (O_4/R_4, O_5/R_5) were observed in the cyclic voltammograms made up to

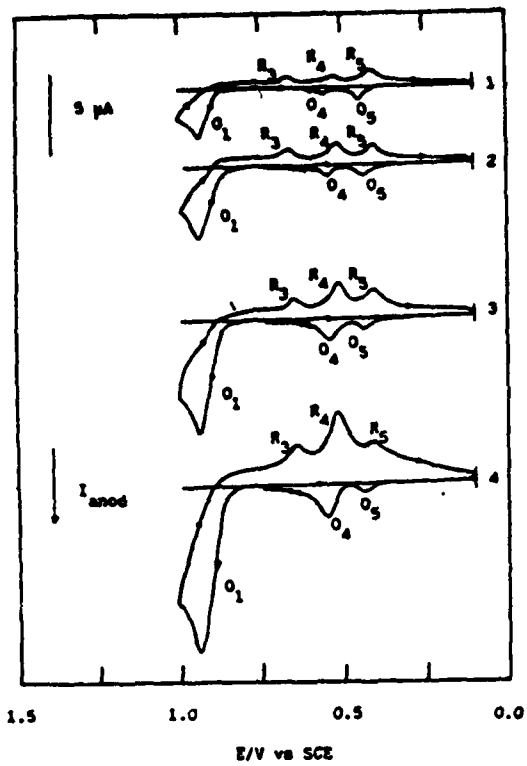

Fig.2.- Cyclic voltammograms corresponding to the oxidation of 1.0 mM 2,4-dibromo-6-methylaniline solution in 11.0 M sulphuric acid at different v values: 1) 10; 2) 20; 3) 50 and 4) 100 $mV.s^{-1}$. Starting potential 0.1 V; first reversal potential 1.0 V and second reversal potential 0.1 V.

peak O_1, as can be seen in fig. 2. Peak potentials of O_4, R_4, O_5 and R_5 were always of 0.54, 0.51, 0.43 and 0.40 V vs SCE respectively. The O_4/R_4 pair predominated over the O_5/R_5 one as long as either acid concentration or v increased. This indicates that the product formed in the peak O_1 and reduced in peak R_4 is hydrolysed to give the compound reduced in peak R_5, decreasing its hydrolysis rate when the acid concentration or v rises. Then the O_4/R_4 pair can be attributed to a p-benzoquinoneimine/p-aminophenol system, whereas the O_5/R_5 to a p-benzoquinone/hydroquinone system. In addition, another reduction peak, R_3, was also found (see fig.2). Its potential peak shifted with increasing acid concentration to less positive values. This peak can be ascribed to the reduction of the bromine formed by oxidation of the bromide anion ejected from the p-benzoquinoneimine formation.

According to the experimental results, the protonated form of the initial compound is the electroactive species. Assuming $\alpha = 0.5$, this species is initially oxidized in a two-electron tranfer to give a trication. This reaction is the rate-determining step of the first process. The resulting trication is hydrolysed to form the p-benzoquinoneimine losing a bromide ion which is further oxidized to bromine. The hydrolysis of this last compound leads to the formation of p-benzoquinone derivative. The loss of protons from the benzenic ring of the trication initially electrogenerated originates the electroactive species of the second process. This last species undergoes an initial two-electron oxidation, this reaction being the rate determining step of the second oxidation process under diffusion control.

REFERENCES

1. E. Brillas, J.M. Costa and E. Pastor, J. Electroanal. Chem.,160(1984)185.
2. E. Brillas, J.M. Costa and E. Pastor, An. Quím., 79A (1983) 211.
3. S. Arias and E. Brillas, Electrochim. Acta, in press.

ELECTRODE BEHAVIOUR OF 2,6-DIHALO-4-BROMOANILINES IN AQUEOUS SULPHURIC ACID SOLUTIONS

E. Brillas**, J.M. Costa* and E. Pastor*
* Laboratory of General Chemistry. Faculty of Chemistry. University of Barcelona. Spain.
** Department of Physical Chemistry. Faculty of Chemistry. University of Barcelona. Spain.

INTRODUCTION

The electrochemical oxidation of haloanilines in sulphuric acid medium leads to the formation of a variety of products [1-3]. Hand and Nelson [1] have shown that for orto- and meta-anilines, the corresponding quinone derivative is the main reaction product. In previous works [2-3], we have studied the electrochemical oxidation of 2,4,6-tribromoaniline, 2-bromo-4,6-dichloroaniline and 2,6-dibromo-4-chloroaniline solutions in several aqueous sulphuric acid media, at platinum electrode, using rotating disk electrode (RDE) and cyclic voltammetry (CV). The first oxidation process of all these compounds is found to be irreversible, leading to the corresponding p-benzoquinone as resulting product.

This communication reports on the oxidation voltammetric behaviour of 2,4-dibromo-6-chloroaniline and 4-bromo-2,6-dichloroaniline in aqueous solutions containing sulphuric acid at concentration higher than 4.0 M. The reaction mechanisms of both compounds are proposed on the basis of the RDE and CV results obtained.

EXPERIMENTAL

The 2,4-dibromo-6-chloroaniline and 4-bromo-2,6-dichloroaniline were synthesized by bromination of 2-chloroaniline (Merck) and 2,6-dichloroaniline (Merck) respectively. All solutions were prepared with concentrated sulphuric acid (Merck, A.R. grade) and water obtained using a Millipore Milli Q system. The voltammetric measurements were carried out with an Amel 551 potentiostat, a P.A.R. 175 universal programmer and a Philips PM8043 X-Y recorder. The experiments were conducted in a three-electrode cell. A SCE was used as reference electrode and a Pt wire as auxiliar electrode. The platinum working electrode was a Tacussel EDI.

Solutions of anilines (1.0 mM) in sulphuric acid media, at an acid concentration range between 5.0 and 15.0 M, were studied. The temperature was kept at 25.0°C.

RESULTS AND DISCUSSION

RDE voltammograms recorded for the two studied anilines display even two consecutive oxidation waves, depending on the medium used (see fig.1). At acid concentration lower than 9.0 M, only one single wave (I) was found, whereas at higher acid concentration, a second oxidation wave (II) was also observed at more positive potentials. RDE results obtained for 4-bromo-2,6-dichloroaniline solutions at a rotating speed, ω, of 16 rps are summarized in table 1. The first wave of both anilines was always diffusion controlled

TABLE 1

RDE oxidation results of 1.0 mM 4-bromo-2,6-dichloroaniline solutions in sulphuric acid at different concentrations, ω = 16 rps, v = 5 mV.s^{-1}.

$c_{H_2SO_4}$/M	η	Wave	$E_{1/2}$/V	$I_{l,a}$/μA	$I_{l,a}\cdot\eta^{1/2}$	αn
5.0	2.46	I	1.01	9.4	15.0	0.94
6.0	2.98	I	1.01	9.1	16.4	0.96
7.0	3.71	I	1.02	8.3	15.8	1.03
8.0	4.63	I	1.03	7.1	15.0	1.01
9.0	5.70	I	1.03	6.1	14.7	0.98
		II	1.46	6.7	16.1	0.76
10.0	7.01	I	1.05	5.6	15.1	1.05
		II	1.45	6.2	16.7	0.78
11.0	8.81	I	1.04	5.1	15.8	1.04
		II	1.44	5.5	17.1	0.81
12.0	11.75	I	1.06	3.5	11.9	1.01
		II	1.42	3.1	12.3	0.94
13.0	15.70	I	1.04	3.1	12.3	1.03
		II	1.40	2.4	9.6	1.01
14.0	19.55	I	1.06	2.8	12.1	1.04
		II	1.39	1.7	7.3	1.02
15.0	23.40	I	1.05	2.4	11.5	0.92
		II	1.36	1.3	6.2	1.03

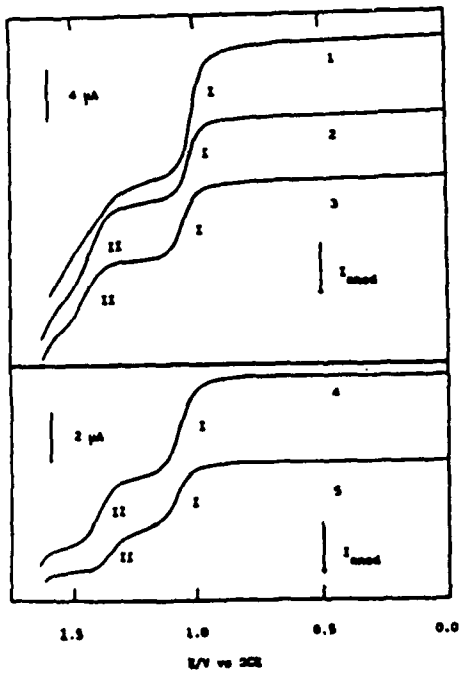

Fig.1.- RDE voltammograms corresponding to the oxidation of 1.0 mM 4-bromo-2,6-dichloroaniline solutions in sulphuric acid concentration: 1) 5.0 M; 2) 9.0 M; 3) 11.0 M; 4) 13.0 M; 5) 15.0 M, ω = 16 rps, v = 5 mV.s^{-1}.

with a half-wave potential, $E_{1/2}$, values comprised between 1.01 and 1.06 V vs SCE under all experimental conditions. The second one is shifted to less positive potentials with increasing acid concentration. The gradual decrease in limiting current, $I_{l,a}$, with rising acid concentration (see table 1) is primordiarly due to the progressive increase in viscosity of the reaction medium, η.

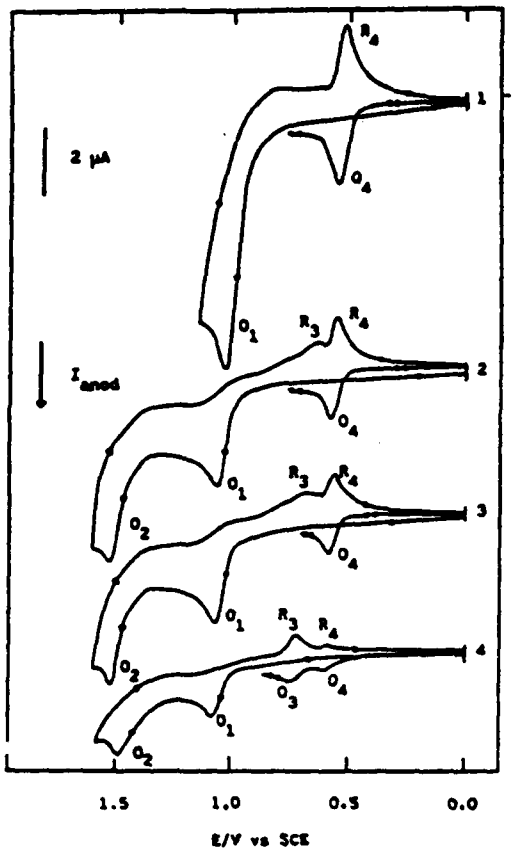

Fig.2.- Cyclic voltammograms corresponding to the oxidation of 1.0 mM 4-bromo-2,6-dichloroaniline solutions in sulphuric acid at concentration: 1) 6.0 M; 2) 9.0 M; 3) 11.0 M and 4) 14.0 M, v = 10 mV.s^{-1}. Starting potential 0 V; first reversal potential 1.10 V for (1) and 1.55 V for (2), (3) and (4); second reversal potential 0 V.

Cyclic voltammograms exhibit two anodic peaks (O_1,O_2) corresponding to the waves observed in the RDE voltammetry. The current function of all anodic peaks progressively decreased when v increased, whereas the anodic peak potential is gradually shifted to more positive potential as long as v rised. These facts suggest that, under diffusion control, the first and second oxidation processes of both anilines are irreversible. The αn product determined from the RDE voltammograms always takes a value practically equal to 1 (see table 1). Two additional couples (O_3/R_3,O_4/R_4) were observed in the cyclic voltammograms made up to peak O_1, as can be seen in fig.2. Peak potentials of O_3, R_3, O_4 and R_4 were always of 0.69, 0.66, 0.57 and 0.52 V vs SCE respectively. The O_3/R_3 couple predominated over the O_4/R_4 one as long as either acid concentration or v increased. This indicates that the product formed in peak O_1 and reduced in peak R_3 is hydrolysed to give the compound reduced in peak R_4. According to Hand and Nelson[1], the O_4/R_4 couple can be attributed to a p-benzoquinone/hydroquinone system, whereas the O_3/R_3 one to a p-benzoquinoneimine/p-aminophenol system.

Because the half-wave potential of the first oxidation process remains independent of the reaction medium, it seems reasonable to consider the protonated forms of both anilines as their electroactive species. Assuming α = 0.5, and initial two-electron transfer of this species takes place, being the rate-determining step of the first process. The resulting trication can undergo a further hydrolysis in para-position with a lost of a bromide ion, generating the corresponding 2,6-dihalo-p-benzoquinoneimine (O_3/R_3 couple). The hydrolysis of this product leads to the formation of the 2,6-dihalo-p-benzoquinone (O_4/R_4 couple).

REFERENCES

1. R.L. Hand and R.F. Nelson, J. Electrochem. Soc., 125 (1978) 1059.
2. E. Brillas, J.M. Costa and E. Pastor, J. Electroanal. Chem., 160(1984)185.
3. E. Brillas, J.M. Costa and E. Pastor, Journées D'Électrochimie '85, Florence, 1985.

REDUCTION MECHANISM OF PARABANIC ACID ON A DME

E. ROLDAN, D. GONZALEZ-ARJONA AND M. DOMINGUEZ
Departamento de Fisicoquímica aplicada, Facultad de Farmacia,
Universidad de Sevilla, Sevilla (Spain)

INTRODUCCION

Parabanic acid (Imidazolidinetrione) is an important product in relation to the enzimatic activity of many biologically significant purines. Although several papers have been reported about its electrochemical behaviour, the detailed reduction mechanism has not been unequivocally established. Thus, Hladik[1] has postulated that parabanic acid is reduced at mercury electrodes in a two-electron, two-proton reaction to 5-hydroxyhydantoin. Struck and Elving[2] concluded that the postwave observed in buffer solutions which contained phosphate was probably due to the reduction of a phosphate conplex of parabanic acid. Dryhurst et al.[3] postulated the reduction overall reaction of parabanic acid and its mono- and di-methyl derivatives using d.c. polarography, coulometry, macroscale electrolysis, thin layer chromatography and mass spectra. They suggested that, particularly at low pH, the overall reaction is reversible although cyclic voltammetry at pyrolitic graphite and mercury electrodes did not give any anodic peaks characteristic of a reversible process at any pH.

In the course of an investigation about enediol-carbonyl systems we have recently studied the electrochemical behaviour and reduction mechanism of alloxan[4] . We have observed that parabanic acid, obtained from homogeneous decomposition of alloxan, could be responsible of a polarographic wave at more negative potentials which had been ascribed to salloxan.

In this sense, the aim of this study is to clarify the reduction mechanism of parabanic acid and the reversibility of the reduction process.

EXPERIMENTAL

LSCV measurements were made by using a single-shot triangular wave generator and a fast potentiostat with a built-in compensator for the iR drop. The voltamograms were recorded on a microprocessor based data acquisition system provided with fast A/D converters. The microcomputer used for acquisition and analysis of data was a 48K-Apple II.

RESULTS AND DISCUSSION

Parabanic acid is reduced on the dropping mercury electrode producing one two-electron polarographic and voltammetric curve in acid media. Logarithmic analysis in the form of E vs. log (i/i_L-i) is linear in HCl 1M. The slope

of the plot. is approximately -30 mV/dec., characteristic of a reversible two-electron process. However, when the pH increases the slope increases appearing two segments in the logarithmic analysis. In 0.1M HCl the slope of the first segment is -40 mV/dec. approximately. At higher pH again one only linear segment with slope of -43 mV/dec. appears.

We have studied the influence of the capillary characteristics as a function of the potential. Log i vs. log t plots are linear on the rising portion on the polarographic wave. Nevertheles, at potentials corresponding to the foot of the wave the slope of the log i vs. log t plots are approximately 0.67 and in the limiting zone 0.19. This result indicates that in the limiting zone the process is diffusion-controlled. However, from the results at potentials corresponding to the foot of the wave can be deduced that the control is by the electron transfer or by a chemical reaction following the tranfer.

Linear sweep cyclic voltammetry confirm the postkinetic nature of the process in acid media. Thus, at low scan rates, only a cathodic peak appears not being observed the corresponding anodic peak as can be observed in Figure 1a. However, at scan rates higher than 5 V/s an anodic peak appears whose peak current increases when the scan rate is increased.

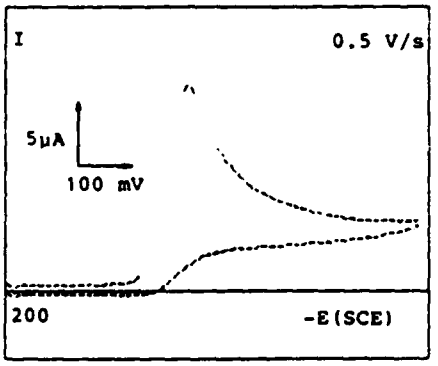

Figure 1a

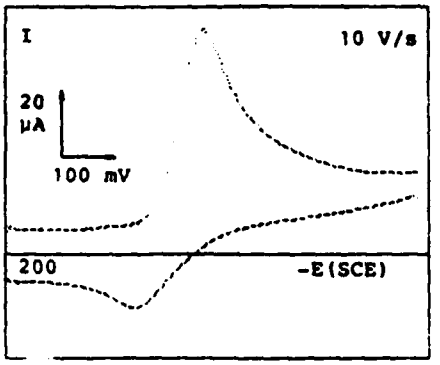

Figure 1b

In Figure 1b the current-potential curve at scan rate of 10 V/s is shown. At this scan rate the difference between anodic and cathodic peak potentials is higher than 60/n mV which indicates a decrease in the rate of the charge transfer reaction.

The variation of cathodic peak potential with the pH is in agreement with two protons exchanged in the overall reaction. Mechanisms are proposed in different acidity conditions.

REFERENCES

1. V.Hladik, Sb. Mezinar. Polarog. Sjezdu, 1st Congr., Pt, 1(1951)686.
2. W.A.Struck and P.J.Elving, Anal. Chem., 36(1964)1374.
3. G.Dryhurst, B.Hansen and E.B.Harkins, J. Electroanal. Chem., 27(1970)375.
4. L.Moreno, M.Blazquez, M.Dominguez and E.Roldan, J. Electroanal. Chem., 185(1985)119.

ANODIC ELECTROPOLYMERIZATION OF THE ACRYLAMIDE IN $NaNO_3$ AQUEOUS SOLUTION: CONVERSION AND MOLECULAR WEIGHT MODIFICATION.

T.F.Otero, Mª A.Mugarza and Y.Jimenez.
Facultad de Ciencias Químicas. Dep. de Química-Física
Apdo. 1072. San Sebastián. Spain.

We are interested in the study of the electrochemical behaviour of the activated iridium electrode in different electrolytes in absence and in presence of acrylic monomers (1-3). The anodic polarization of the electrode in 1M $NaNO_3$ with acrylamide promotes the monomer polimerization into the solution. We presént here the results obtained for the monomer conversion as a function of several kinetic variables, as well as the influence of those variables in the viscosimetric average molecular weight.

An iridium sheet of 0,5 cm^2 of apparent area was used as working electrode. A thick layer of surface oxides with reversible redox behaviour was developed, by consecutive cycles of potential, in 0,5 M H_2SO_4 previously to the electropolymerization process. The experiments were made at constant potential or current density and under N_2 bubbling.

When the monomer concentration increases, the results shown on the table 1 were obtained.

Table 1: slopes of the conversion lines, polimerization rate and middle viscosimetric weight at different acrylamide concentratrion. j= 10 $mA.cm^{-2}$, T= 35ºC, $[NaNO_3]$ = 1M, constant electrode activation.

$[AA]$ $mol.l^{-1}$	slopes of the conversion straight lines. s^{-1}	$R_p.10^5$ $mol.l^{-1}.s^{-1}$	$\overline{Mw}.10^{-4}$
1	0,136	2,26	22,20
2	0,1212	4,04	29,79
3	0,0996	4,98	63,02
4	0,1096	7,30	64,09

The straight lines were obtained for conversion lower than 25% at current flow times lower than 150 min.

The slopes of the conversion straight lines increas when the $NaNO_3$ concentration increases. When the $NaNO_3$ concentration was 4M we attained a limit conversion toward 150 min of current flow. The polymerization rate (Rp) was obtained from the straight section of the conversion curves.

We modified the current density, keeping the other ones electrochemical and chemical parameters constants. The conversion curve obtained presents three different regions. At lower current densities than 15 $mA.cm^{-2}$ the conversion increased linearly with the current density. Between 15 and 30 $mA.\ cm^{-2}$ the conversion remained almost constant. The monomer conversion decreases quickly at current densities higher than 30 $mA.\ cm^{-2}$. At the same time the viscosimetric molecular weight decreases with the current density increase.

Those processes could be explained by means of mixed reactions on the electrode. The NO_3^- discharge with production of $NO_3^{\cdot}$ seems to coexist on the electrode surface with the monomer discharge and the water discharge, at high enough current densities, with oxygen production.

The formation of the primary radicals $NO_3^{\cdot}$ and its desorption from the electrode surface, promotes the begining of the polymerization process. The monomer molecules discharge does not seem to participate directly in the polymerization process. They have an indirect participation by comsumption of the current flow and of the active surface centers; indering the NO_3^- discharge.

This last fact was the responsible for the slope decrease when the monomer concentration increased from 1M to 3M. The polymerization rate, nevertheless, increases continuously. At 4M acrylamide concentration, the influence of the polymerization rate increase is higher than the decreasing in generation of initiating radicals. The continuous increase of

the viscosimetric molecular weight, with the increase of the monomer concentration, was caused by the rise of the polymerization rate.

When the nitrate concentration was modified keping all other kinetic and electrochemistry parameters constans, there was a strong rise of the monomer conversion. This fact seems related with the rise of production of primary radicals, by competitive transfer reaction on the electrode; as the viscosimetric molecular weight was kept constant.

Water discharge, with oxygen production, begins at current densities higher than 15 $mA.cm^{-2}$ on the electrode surface. The presence of three different competitive reactions on the electrode promotes a decrease of primary radicals production. The presence of the oxygen promotes the partial disappearance of the primary radicals produced. Both those efects promote the decrease of the conversion.

At the same time, the oxygen presence produce the decrease of the half live of the polymeric radicals and the decrease of the average molecular weight, such as was showed by viscosimetric measurements.

The results obtained points toward the possibility of controling the monomer conversion as well as the molecular weight distribution by control of the electrochemistry and chimistry parameters. This fac is very important from the view point of the polymer properties.

BIBLIOGRAPHY

1.- T.Fernández, Mª S.Larrocha and M.S.Cruz, Rev.Iberoam. de Corr. y Protec. Pag 85 (1983).

2.- T.Fernández. Makromol. Chem, Rapid Com. 5, 125, (1984).

3.- T.Fernández and Mª S.Larrocha, Pit. e Vernicci, 7, 93, (1984).

KINETIC OF THE ACRYLAMIDE ELECTROPOLYMERIZATION IN NO_3^- AQUEOUS SOLUTION.

T.F.Otero and Mª A.Mugarza.
F. de C. Químicas, Dep. de Química-Física. Apdo.1072.
San Sebastián. Spain.

From the study made in our laboratory about the electrochemistry behaviour of an activated iridium electrode, in presence of acrylamide aqueous solution, using as electrolytes: $NaNO_3$, KOH, H_2SO_4, HCl, phosphate buffer solution, $NaSO_4$ and NaCl; only with $NaNO_3$ the polymer was formed into the solution and separate, when the current was switched off, by precipitation in methanol.

The electrochemical behaviour of the $NaNO_3$ (without acrylamide) is different to the other ones, by transformation of the electrolyte with the current flow, appearing an acidification of the solution, into the anolyte, equivalent to the applied current.

This fact points toward a $NO_3^{\cdot}$ radical generation by charge transfer, capable to take a $H^{\cdot}$ from a water molecule. When the acrylamide was present, some $H^{\cdot}$ were taken from the monomer molecule and some monomer radicals, capables to initiate the polymerization, were obtained in the solution.

But, the NO_3^- discharge on the electrode began over a potential near to the monomer oxidation and water discharge, although the last one, in presence of acrylamide was only significative at higher overpotentials.

Almost all our experiments were made using lows overpotentials (1300 mV) or current densities (10 $mA.cm^{-2}$). In this way, we taked into account only the competitive discharge of NO_3^- and monomer on the electrode surface.

When the monomer concentration was increased from 1M to 3M we found a decrease in the polymer production and an increase in it's average molecular weight. This fact points

toward a non direc participation of the monomer discharge in the initiation of the polymerization. But there is an indirect participation by lowering of the NO_3^- discharge and decreasing the initiation rate.

On this way, the electrode process, could be:

(1a) $NO_3^- + C_L \overset{K_1}{\rightleftharpoons} (NO_3^-)_{ad}$

(1b) $(NO_3^-)_{ad} \xrightarrow{k_{1b}} (NO_3^{\cdot})_{ad} + e^-$

(1c) $(NO_3^{\cdot})_{ad} \longrightarrow (NO_3^{\cdot})_{sol.}$

(2a) $M + C_L \overset{K_2}{\rightleftharpoons} (M)_{ad}$

(2b) $(M)_{ad} \xrightarrow{k_{2b}} (M^{\cdot})_{ad} + e^-$

(2c) $(M^{\cdot})_{ad} \longrightarrow$ Products

With those condictions, all the current crossing the electrode was consumed in both (1b and 1c) transfer reactions:

$$\frac{i}{n\,F} = v_1 + v_2 = k_1\, C_L\, [NO_3^-] + k_2\, C_L\, [AA] \qquad \text{and}$$

$$C_L = \frac{i/nF}{k_1\,[NO_3^-] + k_2\,[AA]}$$

The primary radicals may go by two ways into the solution:

(3) $(NO_3^{\cdot})_{sol} + M \longrightarrow M^{\cdot} +$ Products

(4) $(NO_3^{\cdot}) + H_2O \longrightarrow HNO_3 + OH^{\cdot}$

The $M^{\cdot}$ formation explains the initiation of the polymerization:

$$(5) \qquad M^{\cdot} + M \xrightarrow{k_p} M_2^{\cdot}$$

$$(6) \qquad M_n^{\cdot} + M \xrightarrow{k_p} M_{n+1}^{\cdot}$$

The step (4) could explain the postpolymerization by chemical reaction, once the electric current was switched off:

$$(7) \qquad HNO_3 + M \longrightarrow M^{\cdot} + \text{Products}$$

With respect to the termination step, the experimental results seem to point toward a lineal termination:

$$(8) \qquad M_n \xrightarrow{k_{to}} \text{Polymer}$$

The mutual termination or dismutation was not significative. The termination by combination between polymeric radicals and primary radicals does not seems to be important either.

At high current densities or overpotentials, the water discharge disturbs all the other surface transferences, and, principaly, the termination step of the polymerization process. The oxygen reacts with the polymer-radicals and promotes the decreasing of the molecular weight.

All this discussion drives us toward a polymerization rate, obtained by application of the stady state:

$$R_p = \frac{k_p \; k_i}{k_{to}} \; C_L \; [AA] \; [NaNO_3]$$

in good agreement with the experimental results.

PROGRESS OF THE SPE ELECTROLYZER TO ORGANIC ELECTROCHEMISTRY

Z. TAKEHARA AND Z. OGUMI
Department of Industrial Chemistry, Faculty of Engineering
Kyoto University, Kyoto (Japan)

An SPE composite electrode, which was composed of an ion exchange membrane and a porous metal bound on the former, was applied in a area of electro-organic syntheses. Ion exchange membranes, especially very stable one "Nafion" was utilized as an SPE materials. Porous metal was deposited on the membrane by an electroless plating method using hydrazine or sodium hydroborate as a reductant. In this method, metal ion, reductant, or catalyst permeate through a membrane and a deposited metal layer. Reversing the side after deposition on one side (one-side SPE composite electrode), metal is deposited on the other side (both-sides SPE composite electrode) when needed. Platinum is the easyest in deposition and very stable (Pt-SPE).

Charactristics and advantages of the SPE method can be summarized as follows: 1. Because no supporting electrolyte is needed, the solvent and the reactant concentration can be selected with wide variation and the separation of product is ease. 2. Because of narrow and uniform electrodes gap, high current density electrolysis can be operated with low cell voltage. 3. Polymer coated electrode with high catalytic activity can be used. In this research, following three different types of electrolysis cells were used. 1. One compartment cell with a both-side SPE composite electrode, not as a separator (type A). 2. Two compartments cell with a both-side SPE composite electrode, as a separator (Type B). 3. Two compartments cell with a one-side SPE composite electrode, as a separator and a conventional counter electrode (type C).

1. Kolbe type reactions and reactivity of Pt-SPE

As platinum of Pt-SPE looks like platinum black, a high reactivity is expected from its large surface area. A Kolbe reaction on one-side Pt-SPE in neat acetic acid revealed a large effective surface area, a big roughness factor of 6.

2. Hydrogenation of olefinic double bonds and active site of following chemical reactions

Following chemical reactions are known to be a key step in an electrochemical hydrogenation of olefinic double bonds on a Pt electrode. As described in Table 1, composite electrodes outside of which was covered with gold, an inactive metal in the catalytic hydrogenation, Au-SPE and Au-Pt-SPE, were not active, while Pt-SPE and Pt-Au-SPE were active. The fact indicates that the active site is the outer surface of the deposited Pt for the following chemical reaction as illustrated in Fig.1, a.

3. Reduction of nitrobenzene and an active site of a charge transfer reaction

Nitrobenzene is known to be reduced by a mechanism of direct

Table 1. Electrochemical reduction on different SPE composite electrode (Current: 3.75mA cm^{-2})

Starting material (mol dm^{-3})	Solvent	Current efficiency (%)			
		Pt-SPE	Au-SPE	Au-Pt-SPE	Pt-Au-SPE
α-Mst	n-hexane	11	0	2	25
(0.05)	ethanol	33	0	8	65
DEM	n-hexane	12	0	0	39
(0.05)	ethanol	30	2	2	45
p-BQ	DEE	38	41	42	—
(0.01)	ethanol	50	42	29	—

α-Mst: α-methylstyrene, DEM: diethyl maleate, p-BQ: p-benzoquinone, DEE: diethyl ether

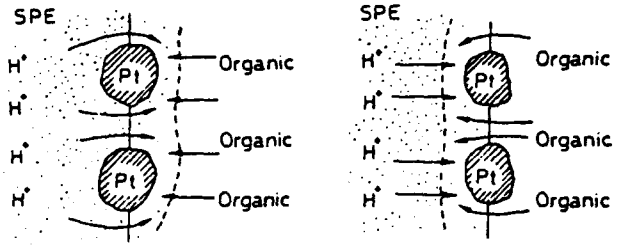

Fig.1 Schematic model of the electrochemical hydrogenation of olefinic compounds on SPE composite

charge transfer on a cathode at fairly negative potential. Pt is not a good electrode material for the reduction. Electrolytic deposition of Cu on the inner surface of Pt-SPE improved the reduction efficiency, while the deposition on the outer surface was not effective. The results explicitly show the importance of the inner surface and lead to the conclusion that the reduction takes place on the inner surface of Pt-SPE as shown in Fig.1,b. It is worth noting that little p-aminophenol was produced regardless that the circumstances of the reaction site favours for its production. This suggests the positive effect of Nafion coating on the reaction selectivity.

4. Halogen mediatory systems

Simple redox mediatory systems such as halogen could play its role by addition of it into a substrate solution. A bromine mediatory system was examined in the methoxylation of furan as shown in Fig.2, and an iodine system was also examined.

5. Fixation of mediatory systems in SPE composite electrodes

Cations can be fixed in Nafion by the difference of exchange affinities (electrostatic interaction). The PTFE backbone of Nafion is usefull to fix some hydrophobic mediators by a hydrophobic interaction. Metal cations, viologens, metal phthalocyanines, phenanthroline complexes, etc. were fixed and

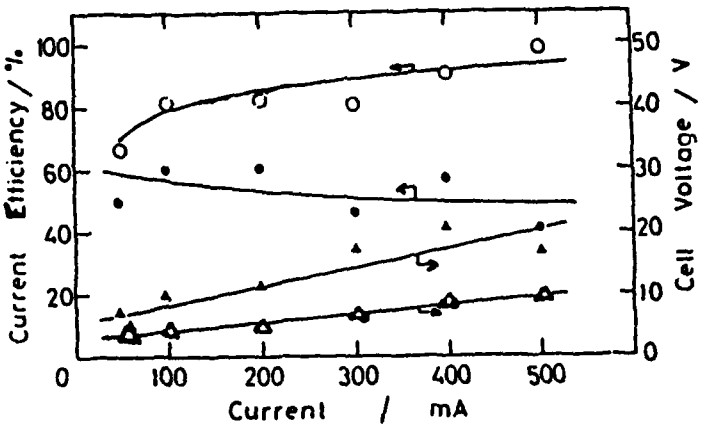

Fig.2 Dependence of the current efficiency of 2,5-dimethoxy-2,5-dihydrofuran and cell voltage on current in furan 20%, methanol 80%, and 0.01M Br_2(o,Δ), and furan 10%, and methanol 90%(●,▲)without Br_2.

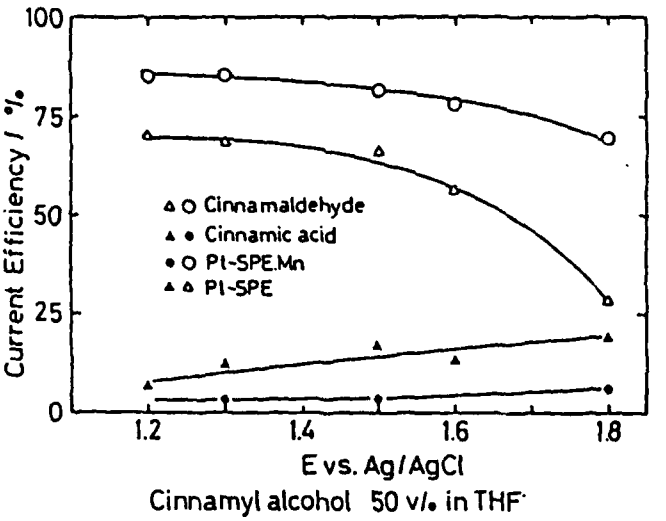

Fig.3 Current efficiencies of cinnamaldehyde and cinnamic acid under potentiosatic electrolysis conditions in 50% cinnamyl alcohol in THF in a working electrode compartment and 0.025M H_2SO_4 in a counter electrode compartment on Pt-SPE, Mn and Pt-SPE.

exhibited a redox behaviour in SPE composite electrodes. A manganese redox system (Mn^{2+}/MnO_2) fixed in Pt-SPE effectively mediated an selective oxidation of cinnamic acid to cinnamaldehyde as described in Fig.3. No contamination by manganese was observed in products. Fixing of mediatory systems remarkably decreased the cell voltage and increased the life of composite electrodes.

H ATOM TRANSFER REACTIONS FROM ALCOHOLS IN ORGANIC ELECTROCHEMISTRY.

C.P. ANDRIEUX[1], J. BADOZ-LAMBLING[2], C. COMBELLAS[2], D. LACOMBE[2], J.M. SAVEANT[1], A. THIEBAULT[2], D. ZANN[1].

1. Université de Paris VII. Laboratoire d'électrochimie, 2 Place Jussieu, 75231 PARIS CEDEX 05, FRANCE.

2. ESPCI. Laboratoire de Chimie Analytique des Milieux Réactionnels, 10 rue Vauquelin, 75231 PARIS CEDEX 05, FRANCE.

The behaviour of primary and secondary alcohols as H atom donors towards aryl radicals generated by the reductive cleavage of aromatic halides is investigated. The study of the process, realised in the alcohol itself and in liquid ammonia makes possible the knowledge of the mechanism, which consists mainly in the competition between the reduction and the deprotonation of the hydroxylated radical generated by the alcohol after H atom transfer.

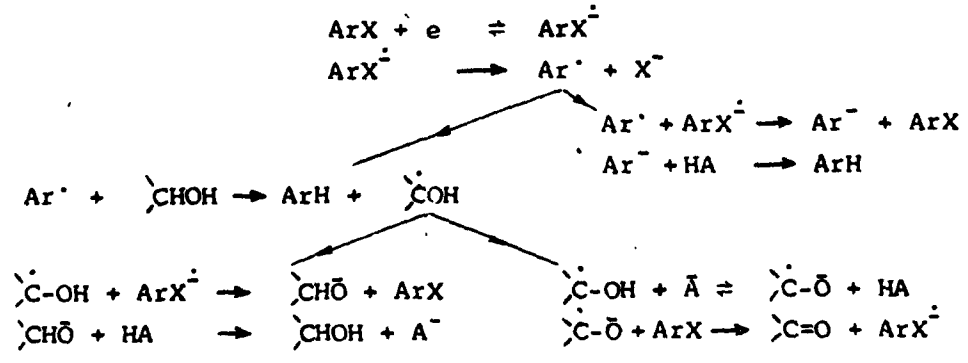

This behaviour can be demonstrated by the electrochemical reduction of 4-bromobenzophenone in pure isopropanol and in liquid ammonia with various amounts of isopropanol.

In pure isopropanol, the balance of electrolysis is equal to one electron per mole of starting product and the formation of ketone can be quantitatively detected by VPC.

In liquid ammonia, the addition of either isopropanol or ethanol, or methanol leads to a decrease of the substrate reduction peak.

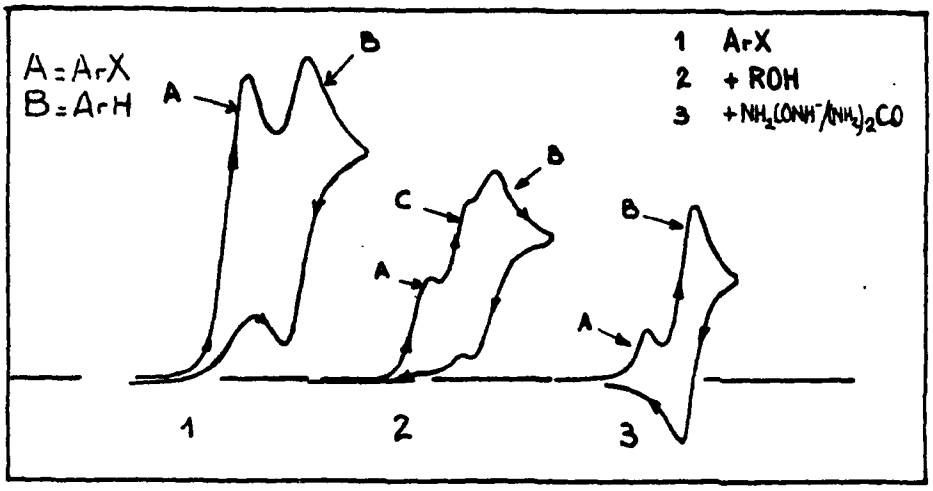

The deprotonation of the hydroxyl radical is clearly demonstrated by the specific reduction peak of benzophenone in the presence of protons (peak C). In the presence of a weak base ($KNH\text{-}CONH_2$) the deprotonation is sufficient to lead to a catalytic system similar to the $S_{RN}1$ mechanism.

REFERENCES

1. C. AMATORE, J. CHAUSSARD, J. PINSON, J.M. SAVEANT, A. THIEBAULT, J. Amer. Chem. Soc., 1979, 101, p. 6012.

2. C. AMATORE, J. BADOZ-LAMBLING, C. HUYGHE-BONNEL, J. PINSON, J.M. SAVEANT et A. THIEBAULT, J. Amer. Chem. Soc., 1982, 104, p. 1979.

AD-A162 434 EXTENDED ABSTRACTS INTERNATIONAL SOCIETY OF ELECTROCHEMISTRY (36TH) HELD AT SALAMANCA SPAIN ON 23-28 SEPTEMBER 1985(U) INTERNATIONAL SOCIETY OF ELECTROCHEMISTRY 28 SEP 85 12/12

UNCLASSIFIED F/G 7/4 NL

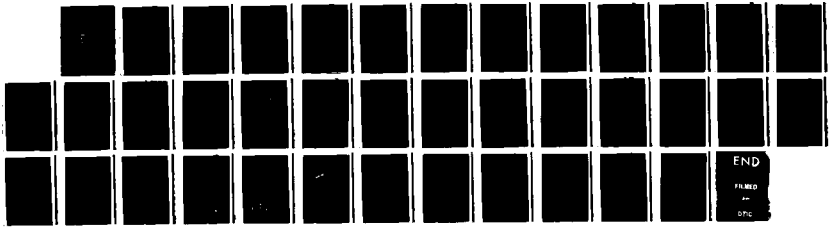

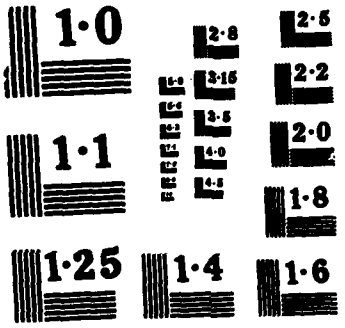

ELECTROCHEMICAL DETERMINATION OF ARYL RADICALS REACTIVITY VS NUCLEOPHILES IN AROMATIC NUCLEOPHILIC SUBSTITUTIONS $S_{RN}1$.

C. AMATORE[1], C. COMBELLAS[2], M. A. OTURAN[2], J. PINSON[3], J.M. SAVEANT[3], A. THIEBAULT[2].

1. ENS. Laboratoire de Chimie, 24 rue Lhomond, 75231 PARIS CEDEX 05, FRANCE.

2. ESPCI. Laboratoire de Chimie Analytique des Milieux Réactionnels, 10 rue Vauquelin, 75231 PARIS CEDEX 05, FRANCE.

3. Université de Paris VII, Laboratoire d'Electrochimie, 2 Place Jussieu, 75231 PARIS CEDEX 05, FRANCE.

$S_{RN}1$ reactions proceed via the following catalytic cycle :

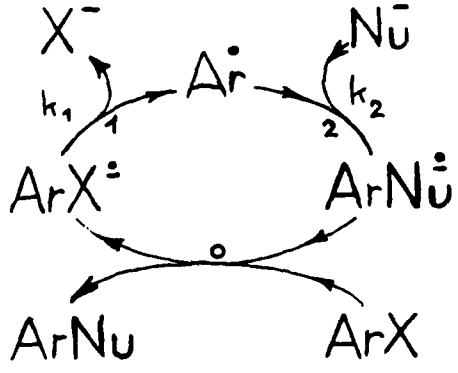

Electrochemistry offers an excellent opportunity for initiating the above cycle through the easy production of $ArX^{\cdot-}$, by reduction of the starting aromatic halide. On the other hand transient electrochemistry, such as e.g. linear sweep voltammetry, allows the determination of the kinetics in the key reaction (2), i.e. the determination of the reactivity of aryl radicals vs various nucleophiles. So far the reactivity of ca 30 different radical/nucleophile couples has been investigated in liquid NH_3.

Three techniques are presented :

a) Direct investigation of the competition of Ar· reduction vs the nucleophilic attack.

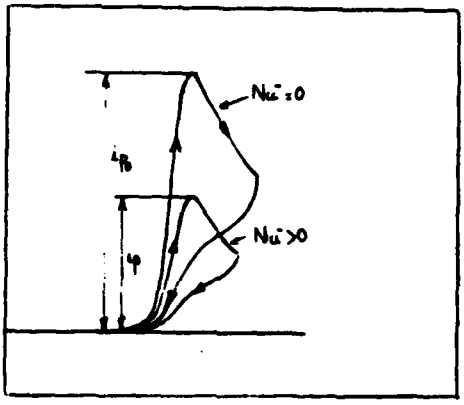

k_2 is obtained from the decrease of the substrate wave in the presence of the nucleophile.

b) Perturbation of redox catalysis by the nucleophilic attack.

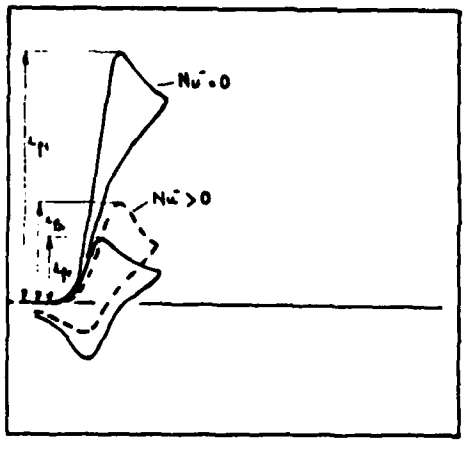

k_2 is obtained from the decrease of the catalyst wave in the presence of the nucleophile.

c) Direct comparison of two nucleophiles on the same radical.

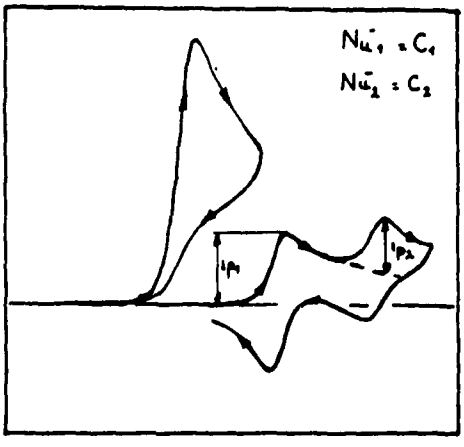

The relative reactivity $k_2^1|Nu_1^-|/k_2^2|Nu_2^-|$ is obtained from the ratio of the two current peaks of the substitution products.

By applying the pertinent method for each substrate-nucleophile system, the following results are obtained :

TABLE I

Values of K according to $K = 10^{-8} k_2$

$Ar^{\cdot} + Nu^{-} \xrightarrow{k_2} ArNu^{\cdot -}$

Ar· \ Nu⁻	PhS^-	$(EtO)_2PO^-$	$CH_3COCH_2^-$	CN^-
phenyl	0.26	3.8		
2-pyridyl	1	>> 1		
3-pyridyl	100	70	160	
4-benzoylphenyl				0.47
2-cyanophenyl	140	80	240	9.6
3-cyanophenyl	150	75	90	
4-cyanophenyl	34	14	26	0.33
1-naphtyl	200	320	420	
2-quinolyl	0.14	0.26	1	0.02
3-quinolyl	19	7.6	38	
4-quinolyl	32	16	54	0.6

REFERENCES

1. C. AMATORE, J. PINSON, J.M. SAVEANT, A. THIEBAULT, J. Amer. Chem. Soc. 1982, 104, p. 817.

2. C. AMATORE, M. A. OTURAN, J. PINSON, J.M. SAVEANT, A. THIEBAULT, J. Amer. Chem. Soc. 1984, 106, p. 6318.

3. C. AMATORE, M. A. OTURAN, J. PINSON, J.M. SAVEANT, A. THIEBAULT, J. Amer. Chem. Soc. 1985, 107, 0000.

4. C. AMATORE, C. COMBELLAS, M.A. OTURAN, J. PINSON, S. ROBVEILLE, J.M. SAVEANT, A. THIEBAULT, J. Amer. Chem. Soc. 1985, 107, 0000.

VOLTAMMETRIC AND SPECTROELECTROCHEMICAL BEHAVIOR OF 2,2'-DIQUINOXALYL AND ITS DERIVATIVES

M. LAPKOWSKI and I. BARANOWSKA
Institut of Inorganic Chemistry and Technology, Institut of Analytical and General Chemistry, Silesian Technical University, 44-101 Gliwice, Poland

Simultaneous spectral observations and electrochemical measurements give better understanding of the process, hence, more detailed information of the reaction studied. Due to the high rate of the electrode processes it is necessary to perform the measurements by means of rapid spectrophotometers and computer acquisition as well as processing of the spectra [1].

Among a number of organic substances studied by spectroelectrochemical methods there is a big group of heterocyclic compounds containing nitrogen atoms [2]. Our previous study [3] has shown that 2,2'-diquinoxalyl (DQx) undergoes a two-stage reduction in DMF solution and both products of reduction are colourful. In acidic solution it is a one-stage process and the reaction product is also colourful. Based on these results we decided to perform spectroelectrochemical study of DQx and its derivatives.

Experimental

Electrochemical apparatus, reagents and their purification were described in [3,4], spectroelectrochemical apparatus and the computer program controlling the spectroelectrochemical system in [1]. Optically transparent electrodes obtained by depositing of platinum layer of 550 Å thick on glass were used. All potentials reported were measured vs. Ag/AgCl. DQx, thieno[2,3-b:4,5-b']diquinoxalyl (TDQx), and 2,2'-dipyrazyl (DP) was prepared as in [5].

Results in neutral solution

Cyclic voltammetric curves of the DQx reduction on the platinum electrode in neutral DMF solution are presented in Fig. 1a.

There are two reduction peaks at E_{RED1}=-0.94 V and E_{RED2}=-1.55 V and one oxidation peak at E_{OX}=-0.84 V. The spectra of electroreduction of DQx in this solution during linear changes of the Pt electrode potential are presented in Fig. 2. In this figure three distinct bands can be observed: λ_1= 440 nm, λ_2= 500 nm, and λ_3= 610 nm. Voltabsorptiometric curves at λ_2= 500 nm (b) and λ_3= 610 nm (c) are presented in Fig. 1. It can be seen from both figures that after reversing the direction of potential changes the colour of both the compounds disappears. The electrochemical and ESR investigations of DQx showed, that the first reduction product in DMF solutions is the anion-radical. The ESR signal is strong, appears at once and is stable for about 5 min after the voltage has been switched off. On the basis of these results the mechanism of reduction process were proposed. The reduction mechanism of TDQx is similar to that and the mechanism of DP reduction is quite different.

Results in acidic solution

The cyclic voltammetric curve for TDQx in DMF with 0.15 M of perchloric acid as supporting electrolyte is presented in Fig. 3. It can be seen from this figure that the process is redox type. The potential value for the reduction peak is equal to E_{RED}=-115 mV, for oxidation peak is equal to E_{OX}=-15 mV. The correspondent spectroelectrochemical measurement is shown in Fig. 4. In this figure there is an absorption band at λ_{max}= 490 nm, which increasses with the decrease of the potential of the optically transparent working electrode. Similar results were obtained for DQx. Basing of the electrochemical and spectroelectrochemical results the reduction mechanism in acidic solution was presented.

References

1. J.Krawczyk, M. Lapkowski and J.Strojek, Anal.Chim.Acta, 152, 458 (1983)
2. W.R.Heineman, Anal.Chem., 50, 390A (1978)
3. I.Baranowska and M.LAPKOWSKI, J.Electroanal.Chem., 179, 209(1983)
4. M.Lapkowski, J.Zak, and J.Strojek, ibid., 145, 173 (1983)
5. R.Baranowski, Zesz.Nauk.Politech.Sl.Chemia, 79 (1976)

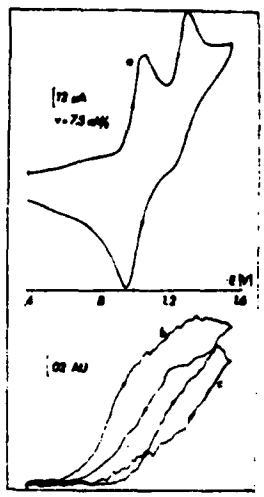

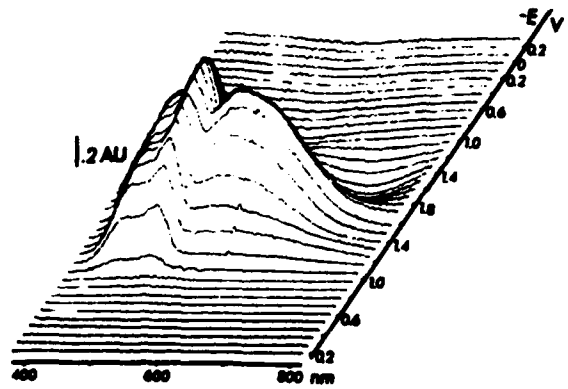

Fig.1. Voltammetric curve of DQx in DMF on the Pt electrode (a) and simultaneous recording of absorbance changes (b) at λ_2 = 500 nm and (c) at λ_3 = 610 nm.

Fig.2. Spectral response of the DQx reduction products in DMF on Pt electrode during linear change of potential. The spectra were recorded every 10 sec.

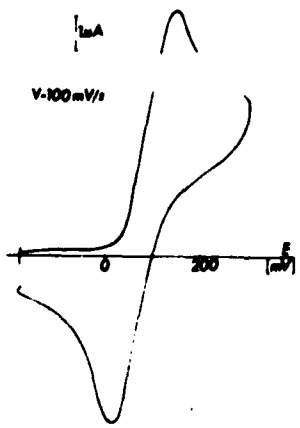

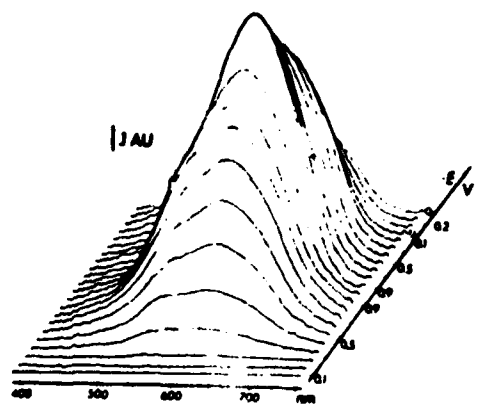

Fig.3. Voltammetric curve of TDQx in DMF with 0.15 M perchloric acid on the Pt electrode.

Fig.4. Spectral response of the TDQx reduction product in DMF with 0.15 M perchloric acid on Pt electrode during linear changes of potential. The spectra were recorded as in Fig.2.

MASS SPECTROMETRIC ANALYSIS OF ELECTROCHEMICAL REACTANTS BY ION FORMATION WITH THERMOSPRAY

G. HAMBITZER and J. HEITBAUM
Institute for Physical Chemistry, Wegelerstr. 12, 5300 Bonn,FRG

1. Introduction

Electrochemists are highly interested in experimental methods that can tell what products are formed within an electrode process. Since mass spectroscopy is a very sensitive technique, it could be used to this end as soon as an on line connection between the electrochemical cell and the mass spec is established. In the case of volatile products and aqueous solutions, Differential Electrochemical Mass Spectroscopy /1/ has proven its feasibility for this kind of studies. Herewith, we report a totally new approach using the thermospray ionization method /2/ to on line detect the product distribution as function of the applied electrode potential. Principally, volatile and non volatile, basic and acidic species can directly be measured from aqueous and non aqueous solutions.

2. Experimental

In the thermospray ionization /2/ method a jet of statistically charged droplets is produced by evaporating the liquid out of a capillary tube. Spontaneous ion emission occurs out of these droplets by ion attachment to neutral molecules which can thus be identified. Before entering the capillary tube, the solution is passed along a coiled Pt-wire that acts as the working electrode and which is forced into a Teflon tube. Thus, a collection efficiency near 1 of the electrochemical products is guaranteed.

Fig.1 displays the electrochemical cell. The counter electrode is simply situated upstream the electrolyte flow, and a Teflon tube acts as the Luggin capillary connecting the main cell chamber with a high pressure calomel reference electrode. A HPLC pump supplies a constant flow of the solution at a rate of normally 1 ml per minute with a pressure of up to 2 MPa.

3. Example: oxidation of N,N-dimethylaniline (DMA)

To demonstrate the feasibility of the above method with respect to electrochemical processes, the electrooxidation of DMA in 0.1 m NH_4Ac was studied. The following mechanism is proposed in the literature /3/:

$$2\ \mathrm{DMA} \underset{0.6\ \mathrm{V}}{\overset{-2e^-}{\rightleftharpoons}} 2\ \mathrm{DMA}^{+\cdot} \xrightarrow[\text{fast}]{-2H^+} \mathrm{TMB} \underset{0.4\ \mathrm{V}}{\overset{-2e^-}{\rightleftharpoons}} \mathrm{TMB}^{++}$$

Trimerization is assumed to occur in an consecutive chemical step, the trimer being electrochemically active as well:

$$DMA + TMB^{+} \longrightarrow \text{trimer} \underset{0.2\ V_{SCE}}{\overset{-\ 2e^{-}}{\rightleftharpoons}} \text{trimer OX}$$

The following abbreviations have been used to symbolize the mechanism:
TMB = N, N, N', N' - tetramethylbenzedine; TMB^{++} = quinone of TMB; TMB^{+} = semiquinone of TMB

Fig.2 proves this mechanism to be principally valid. The spectrum was obtained within 25 s during continuously scanning the potential between - 0.4 and 1.0 V_{SCE} with 0.5 V s^{-1}. The mass peaks beyond 200 amu clearly show the formation of dimers such as TMB and trimers and prove the feasibility of the method as an analytical tool.

As long as the thermospray ionization is stable, the time between the electrochemical generation of a species and its mass spectroscopic detection is given by the so-called dead time necessary for the flow to pass the capillary tube, the time behaviour of the working electrode and eventual consecutive chemical reactions. This is visualized in Fig.3 where the mass intensity of TMB is shown during a square wave potential pulse applied to the working electrode. It impressively features the true time dependent generation of TMB while the faradaic current is at first masked by capacitive effects. It can be taken from Fig.3 that the dead time amounts 9 s for the experimental set up used, but we believe that it can be improved to be less than a second.

The dead time is already small enough to allow mass intensity potential curves to be measured which was previously called Mass Spectroscopic Cyclic Voltammetry (MSCV) /1/. Fig.4 shows such diagrams for DMA, TMB and the trimer. Evidently DMA is shielded from reaching the mass spec as soon as its oxidation starts at about 0.52 V_{SCE}. In parallel, the mass intensities of TMB and the trimer both rise, which proves that they are formed due to the electrochemical process occuring.

4. Conclusions

A new on line method is presented which allows
1. the volatile and non volatile, basic and acidic products of an electrochemical reaction to be identified by mass spectrometry directly out of the electrolyte;
2. electrode processes to be characterized as function of the varying potential (MSCV);
3. consecutive chemical reactions to be studied by varying the dead time.

Since the thermospray ionization method only requires the existence of stable ions in the solution, no restriction exists with respect to its electrochemical application. Any organic or aquous electrolyte can be used together with any solid electrode material. We therefore believe that our method is a valuable complement to the techniques existing so far and can be widely used for the study of the kinetics of electrochemical reactions.

/1/ O. Wolter and J. Heitbaum, Ber. Bunsenges. Phys. Chem. 88 (1984) 2
/2/ M.L. Vestal in "Ion Formation from Organic Solids", A. Benninghoven ed., Springer Ser. Chem. Phys. 25, p. 246, Springer Verlag, Berlin, Heidelberg 1983
/3/ E.T. Seo, R.F. Nelson, J.M. Fritsch, L.S. Marcoux, D.W. Leedy, R.N. Adams, J. Am. Chem. Soc. 88, (1966) 3498

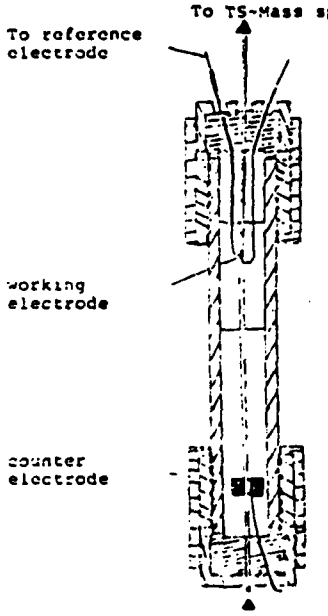

Fig.1: High pressure electrochemical cell

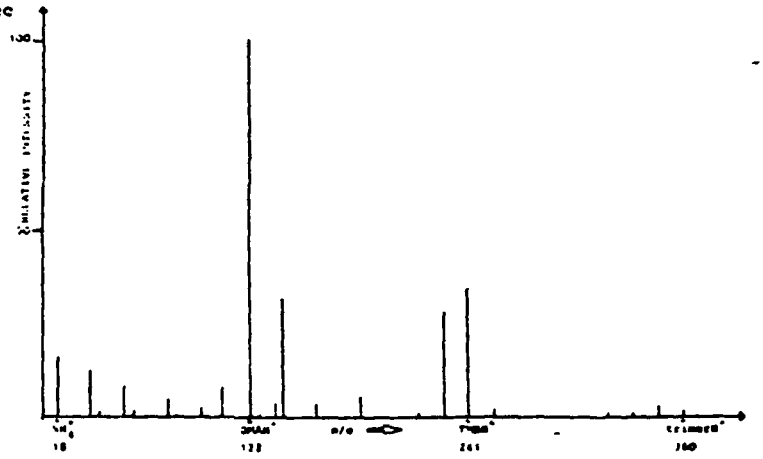

Fig.2: Mass spectrum of DMA and products

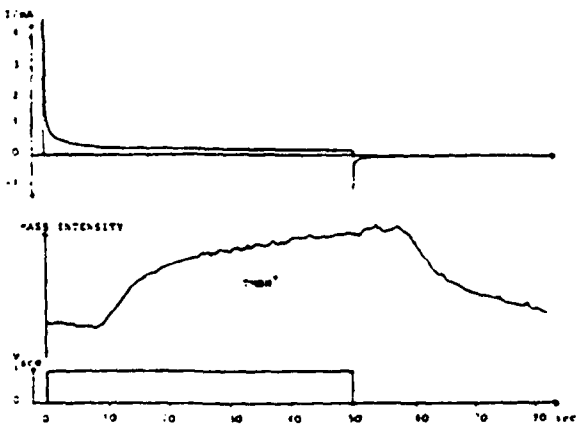

Fig.3: Mass intensity of TMB during a square wave potential pulse

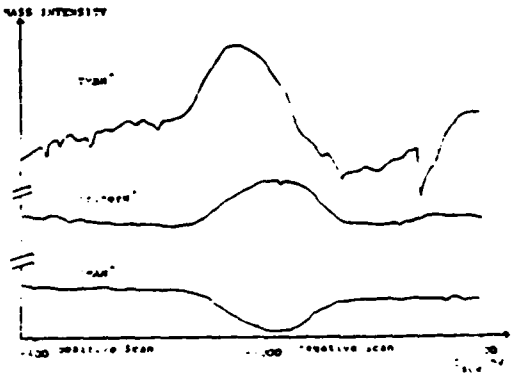

Fig.4: MSCV of DMA, TMB and trimer

MECHANISM AND STEREOCHEMISTRY OF THE ELECTROCHEMICAL REDUCTION OF PHENYL-SUBSTITUTED INDENES

G.FARNIA[a], F.MARCUZZI[b], G.MELLONI[c] and G.SANDONA'[a]

[a]Dipartimento di Chimica Fisica, Padova (Italy)
[b]Dipartimento di Chimica Organica, Padova (Italy)
[c]Istituto di Chimica Organica, Sassari (Italy)

The electrochemical reduction at Hg electrode in DMF/TBAP 0.1 M of some phenyl-substituted indenes (**1-6**) has been investigated with the aim to find out possible relationships between mechanism and stereochemistry of the two-electron two-proton reduction occurring at the double bond of the pentatomic cycle, and affording the corresponding indans of various configurations:

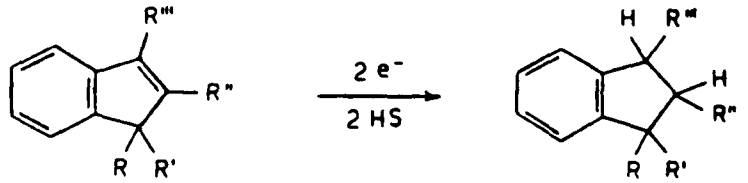

1, R = Me; R' = R'' = R''' = Ph **2**, R = R' = Me; R'' = R''' = Ph
3, R = H; R' = R'' = R''' = Ph **4**, R = R''' = H; R' = R'' = Ph
5, R = R' = H; R'' = R''' = Ph , **6**, R = H; R'' = Me; R' = R''' = Ph

where HS represents the proton donors, such as H_2O, PhOH or the indenes **3-6** (self-protonation) .

In a carefully dried solution the electrochemical reduction of indenes **1** and **2** (Ind) takes place *via* two reversible one-electron transfer processes, corresponding to the formation of the radical anion and the dianion.

Addition of water (in excess) makes the second reduction peak completely irreversible due to the fast protonation of the dianion, and affects also the reversibility of the first peak which increases in height with respect to the second one. This behaviour has been explained, on the basis of voltammetric and homogeneous kinetic experiments, in terms of the disproportionation reaction of the radical anions[1,2]:

$$Ind + e \rightleftharpoons Ind^{\cdot-} \qquad (1)$$

$$2\ Ind^{\cdot-} \rightleftharpoons Ind^{=} + Ind \qquad (2)$$

$$Ind^{=} \xrightarrow{H_2O} IndH^{-} \qquad (3)$$

$$IndH^{-} \xrightarrow{H_2O} IndH_2 \qquad (4)$$

$$Ind + 2e \xrightarrow{2H_2O} IndH_2$$

The voltammetric behaviour of indenes **1** and **2** in dried solution is also observed for indene **3** at low temperatures (< 30°C) or for high sweep rates ($v > 100\ Vs^{-1}$), while in the same experimental conditions the second reduction peak of **4** and **5** is chemically irreversible.

Furthermore, for indenes **3-5** the ratio between the height of the second and the first reduction peak decreases with decreasing the sweep rate, in agreement with a fast protonation of the dianion by the indene itself (IndH),

which transforms into the conjugated base (Ind^-), not reducible within the available potential range.

At lower sweep rates also the reversibility of the first peak is affected, and a single irreversible reduction peak corresponding to a (2/3) electron per molecule can be detected. As regards indene **6**, for which only the first reduction wave is detectable within the available potential range, the same voltammetric pattern is observed. In these conditions, a self-protonation reaction involving directly the radical anion takes place, according to the mechanism:

$$IndH + e \rightleftharpoons IndH^{\cdot-} \quad (1)$$

$$IndH^{\cdot-} + IndH \rightleftharpoons IndH_2^{\cdot} + Ind^- \quad (5)$$

$$IndH_2^{\cdot} + IndH^{\cdot-} \longrightarrow IndH_2^- + IndH \quad (6) \quad \text{and/or} \quad IndH_2^{\cdot} + e \rightleftharpoons IndH_2^- \quad (6')$$

$$IndH_2^- + IndH \longrightarrow IndH_3 + Ind^- \quad (7)$$

$$IndH + (2/3)e \longrightarrow (1/3)IndH_3 + (2/3)Ind^-$$

Voltammetric measurements have been carried out in order to discriminate if the second electron transfer occurs at the electrode (eq (6'), ECE pathway) or in solution (eq (6), DISP pathway) and, in the latter case, if the rate determining step is the first protonation reaction (eq (5), DISP 1 pathway) or the following solution electron transfer (eq (6), DISP 2 pathway).

The experimental values of i_{pa}/i_{pc} for indenes **3-6** and of E_{pc} for indene **6**, detected at various scan rates and indene concentrations, fit well the theoretical working curves calculated for a DISP 1 situation[3]. The values of k_s obtained are reported in Table I.

As regards indene **3**, however, a contribution of a direct disproportionation reaction (eq 2) with protonation by IndH could be operating in part.

In the presence of phenol, all the indenes considered show an irreversible two-electron behaviour, in agreement with a fast protonation of the radical anion by the proton donor. The shift of the peak potential with the sweep rate and phenol concentration, 29 mV at 20°C, is in agreement with the following mechanism:

$$IndH + e \rightleftharpoons IndH^{\cdot-} \quad (1)$$

$$IndH^{\cdot-} \xrightarrow{PhOH} IndH_2^{\cdot} \quad (8)$$

$$IndH_2^{\cdot} + IndH^{\cdot-} \longrightarrow IndH_2^- + IndH \quad (6) \quad \text{and/or} \quad IndH_2^{\cdot} + e \rightleftharpoons IndH_2^- \quad (6')$$

$$IndH_2^- \xrightarrow{PhOH} IndH_3 \quad (9)$$

$$IndH + 2e \xrightarrow{2PhOH} IndH_3$$

with the possible occurrence of both the DISP 1 and ECE_{irr} limiting cases.

Our data suggest the occurrence of DISP 1 mechanism in the case of indenes **1**, **2**, **3**, **5**, of ECE_{irr} in the case of **6**, and of both mechanisms in the case of **4**. The values of k_s are reported in Table I.

The results of macroscale electrolyses reported in Table II indicate two different stereochemical courses, according to the proton donor used. Only the reduction of **1** and **2** in the presence of water affords the indans of most stable configuration, presumably due to the fast isomerization process taking place under the electrolysis conditions. In the presence of phenol or of a self-protonating indene, which do not allow isomerization processes, prevailing *syn*-addition of hydrogen to the carbon-carbon double bond is observed, with the formation of the thermodynamically less stable isomers.

In this case, steric effects must play an important role in the protonation steps of intermediates, due to the high steric hindrance of indenes and phenol. The formation of hydrogen bonded complexes between radical anion and phenol prior to the proton transfer can be invoked to explain the higher stereoselectivity observed when the smaller proton donor (phenol) is used instead of indene.

TABLE I. Protonation rate constant (l mol^{-1} s^{-1})

Indene	3	4	5	6
k_5	$0.6 \cdot 10^2$	$1.2 \cdot 10^3$	$1.7 \cdot 10^3$	$3.5 \cdot 10^5$
k_8	$1.1 \cdot 10^4$	$2 \cdot 10^6$	$8.1 \cdot 10^4$	$1.3 \cdot 10^7$

TABLE II. Results of macroscale potentiostatic electrolyses (T = 20°C)

Indene[a]	Proton donor[b]	Indans isomers yields,%			
		(Z,Z)	*(E,Z)*	*(Z,E)*	*(E,E)*
1	H_2O	-	-	72	28
1	PhOH	57	12	17	14
		(Z)		*(E)*	
2	H_2O	70		30	
2	PhOH	-		100	
		(Z,Z)	*(E,Z)* ≡ *(Z,E)*		*(E,E)*
3	-	70	10		20
3	PhOH	100	-		-
		(Z)		*(E)*	
4[c]	PhOH	73		27	
5	-	62		38	
5	PhOH	71		29	
		(Z,Z)	*(E,Z)* ≡ *(Z,E)*		*(E,E)*
6	-	46	20		34
6	PhOH	60	20		20

[a] 0.1 M. [b] 0.5 M. [c] Fast isomerization of **4** into **5** takes place under self-protonation electrolysis conditions.

References

1) G.Farnia, F.Maran, G.Sandonà and M.G.Severin, J.Chem.Soc. Perkin Trans. II, 1153 (1982).

2) G.Farnia, F.Marcuzzi, G.Melloni and G.Sandonà, J.Am.Chem.Soc., *106*, 6503 (1984).

3) C.Amatore, G.Capobianco, G.Farnia, G.Sandonà, J.M.Savéant, M.G.Severin and E.Vianello, J.Am.Chem.Soc., *107*, 1815 (1985).

ETUDE CINETIQUE DES INTERACTIONS ENTRE UNE CYLCODEXTRINE ET LES ESPECES I^- et I_2

E. SAINT-AMAN et D. SERVE
Laboratoire L.E.D.S.S. 5 (Photochimie), U.S.M.G., B.P. 68
38402 Saint Martin d'Hères (France)

Les cyclodextrines α, β, γ sont des oligomères cycliques possèdant respectivement 6, 7, 8 unités de D- glucose. Elles présentent une cavité torique dont le diamètre compris entre 5 et 9Å autorise la formation de composés d'inclusion [1] non covalents, caractérisés par des interactions faibles du type forces de Van der Walls ou interactions hydrophobes. La stabilité [2] du complexe formé dépend alors essentiellement du bon accord spatial entre la cavité de la cyclodextrine et l'espèce chimique hôte.

Une étude précédente [3] nous a permis de confirmer ce résultat par la mesure potentiométrique des constantes d'association des composés d'inclusion formés par les cyclodextrines α, β, γ et les espèces I^-, I_2 et I_3^- (tableau 1). La stoechiométrie [1,3,4] de ces complexes est du type 1:1. L'ordre de stabilité a alors été déterminé : α > β > γ et I_3^- > I_2 > I^-.

L'importance de ces interactions peut être également illustrée en suivant l'évolution des courbes courant-potentiel (fig. 1,2,3) d'une électrode à disque tournant de platine dans des solutions contenant I^- ou I_2 et une cyclodextrine dont on fait varier la concentration totale. La formation de I_3^- ou les phénomènes d'adsorption à l'électrode ont pu être négligés en travaillant à des concentrations faibles en réactifs ($<10^{-3}$M). Nous mettons en évidence une diminution du courant limite, un déplacement de la courbe vers les potentiels négatifs et une tendance à l'irréversibilité du mécanisme global. Ces variations sont d'autant plus importantes que le complexe considéré est plus stable. Ces résultats permettent de proposer un mécanisme théorique du type C.E.C. :

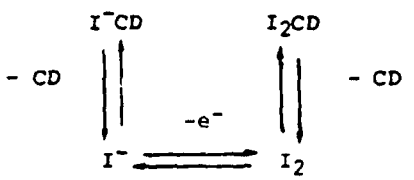

En effet, l'étape chimique précédant le transfert de charge permet d'interpréter la diminution du courant limite car en complexant préalablement l'espèce électroactive, celle ci n'est plus totalement disponible pour maintenir un courant limite maximal. L'étape chimique postérieure au transfert de charge consomme le produit de la réaction électrochimique et la déplace dans le sens de l'irréversibilité. La plus grande stabilité du composé d'inclusion formé par l'espèce oxydante, l'iode (tableau 1), doit induire un déplacement de la courbe i(v) vers les potentiels négatifs. Ce mécanisme peut alors être simplifié. Par exemple, dans le cas où la réaction chimique est lente (cas des systèmes I^- - CD ou I_2 - γ), le contrôle du courant est

du type thermodynamique [5] et il conduit à un faisceau de courbes théoriques comme celui représenté sur la figure 4. Au contraire, lorsque le composé d'inclusion est très stable (cas des systèmes I_2 - α ou I_2 - β), la réaction chimique est considérée comme totalement irréversible.

1. J. SZEJTLI,
   cyclodextrins and their inclusion complexes,
   Akadémiai Kiado, Budapest, 1982.
2. W. SAENGER,
   Angew. Chem. Int. Ed. Engl.,
   19 (1980) 344-362.
3. J.-P. DIARD, E. SAINT-AMAN et D. SERVE,
   J. Electroanal. Chem.,
   sous presse.
4. I. SANEMASA, T. KOBAYASHI et T. DEGUCHI,
   Bull. Chem. Soc. Jpn.,
   58 (1985) 1033-1036.
5. E. VIEIL,
   Thèse, Grenoble, 1979.

Tableau 1:Constante d'association (K_{ass} / M^{-1}) des complexes formés par les cyclodextrines α, β, γ et les espèces I^- ,I_3^- , I_2 à 25°C

K_{ass} / M^{-1}	I^-	I_3^-	I_2
α	8 ± 1	3,3 ± 0,3 x 10^5	2 ± 1 x 10^4
β	10 ± 5	5 ± 1 x 10^3	1,5 ± 0,5 x 10^3
γ	1,3 ± 0,2	5 ± 1 x 10^2	3,5 ± 0,5 x 10^2

CONDITIONS DE TRAVAIL POUR LES FIGURES N° 1 à 4 :
N = 600 rpm ; S = 0,03 cm^2
Electrolyte : Na_2SO_4 5.10^{-2}M à pH3

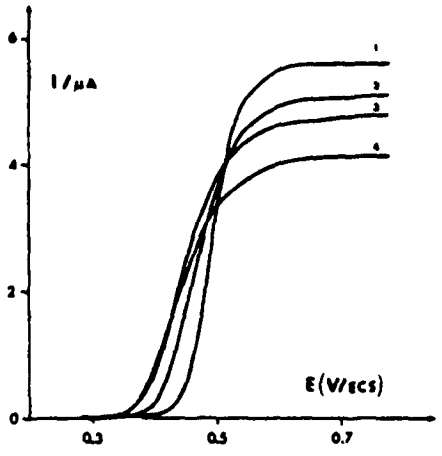

fig. 1 : $(I^-)=2,5.10^{-4}$; $(\alpha)=0$ (1) 5.10^{-4} (2) 2.10^{-3} (3) 2.10^{-2} (4) M

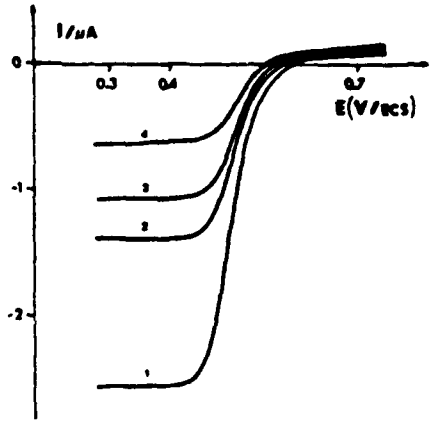

fig. 2 : $(I^-)=5.10^{-6}$; $(I_2)=1,1.10^{-4}$; $(\beta)=0$ (1) 5.10^{-3} (2) 10^{-3} (3) 4.10^{-3} (3) M

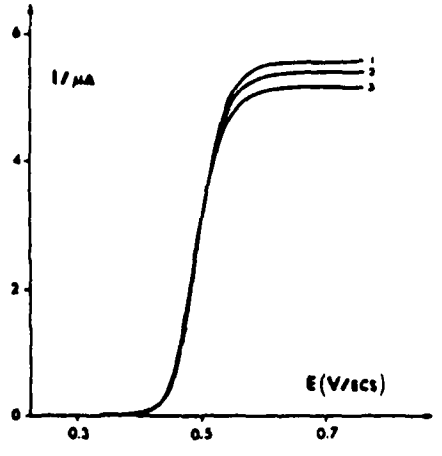

fig. 3 : $(I^-)=2,5.10^{-4}$; $(\gamma)=0$ (1) 4.10^{-3} (2), 10^{-2} (3) M

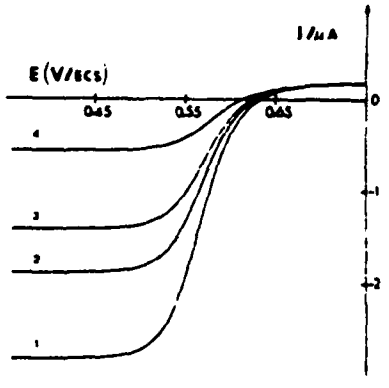

fig. 4 : Brans ert Vanstien ; $(I^-)=7.10^{-6}$; $(I_2)=10^{-4}$; $(CD)=0$ (1) 5.10^{-3} (2) 10^{-3} (3) $4\ 10^{-3}$ (4) M, $D_{I^-}=2,1.10^{-5}$ cm^2/s ; $D_{I_2}=8.10^{-6}$ cm^2/s $\nu=9.10^{-3}$ cm^2/s

ELECTROLYSIS OF HALOBENZENES IN DIMETHYLFORMAMIDE

J.CASADO and I.GALLARDO
Departamento de Química-Física, Autonomous University of Barcelona
Bellaterra, Barcelona (Spain)

INTRODUCTION

The electrolysis at constant potential of iodobenzene (PhI) and Bromobenzene (PhBr) have been carried out in order to determine the products and the number of electrons involved in the process.
In previous works[1,2], electrolysis under constant current of this compounds in presence of CO_2 have been reported, yielding benzene, benzoic acid and benzaldehide. Sease and Reed[3] reported 100% formation of benzene for the reduction of bromobenzene in DMF with Hg cathode.

EXPERIMENTAL AND RESULTS

PhI. After preelectrolysis at -1.70V vs. Ag/AgI, 3.04g(15 mmol) of PhI were added to a deoxygenated solution of TEAP 0.1M in DMF(77ml). The electrolysis was carried out over a stirred Hg pool cathode at -1.50V in a refrigerated cell. After 4 h. the current dropped to 1.7mA and the electrolysis was terminated. From the integration of the I-t curve a number of 1.8 electrons/molecule was obtained.
10 ml of the catholyte were disolved in water and extracted with hexane. The UV spectrum of this solution revealed the presence of benzene (87%). The remaining DMF solution was evaporated under reduced pressure. The residue was extracted with ether. The TEAP, removed by filtration, was 1.4 mmol less than the initial, which indicates that it partially decomposes during the electrolysis. A sample of the crude obtained by removing the ether was analysed by G.C. coupled with mass spectrometry, giving small amounts of $PhCON(CH_3)_2$ and $PhCHOHN(CH_3)_2$ and traces of triethylamine, benzaldehyde, phenol, alcohol benzylic, iodobenzene, diphenyl, PhCOCOPh, PhHgPh and $PhHgCON(CH_3)_2$. Traces of other products were also founded but not identified. Afterwords, the remaining crude was cromatographed through silica-gel, 0.06 g. of PhHgPh (3%) being eluted with hexane.

PhBr. After preelectrolysis at -2.15V, 1.56g(10 mmol) of PhBr were added to a solution of TEAP 0.15M in DMF(74ml). Then , the potential was fixed at -2.10V. After 5h15m, the current dropped to 2.2mA(plateau). A number of 1,9 electrons/molecule was obtained.
The working-up was similar to that described for PhI. The yield of benzene, determined from UV spectra, was 84%. After removing benzene, alcohol bencilic and a small amount of benzaldehyde were also identified from a new UV spectrum. The DMF was practically removed under vacuum and the residue was extracted with chloroform. The amount of the remaining electrolyte was 3.6 mmol less than the initial. Therefore, it decomposes during the reaction. The chloroform was removed and the residue was chromatographed through silica-gel, 0.05 g of a white solid being eluted with hexane-ethyl acetate 80/20. This solid was identified tobe a mixture 30/70 of meso and d,l-1,2-diphenyl-1,2-ethanediol(5%) respectively, using NMR and mass spectroscopy.
Other products analogous to those obtained in the PhI electrolysis were also detected. PhHgPh was not found since it is reduced at -1.7V vs.Ag/AgI.

DISCUSSION

The experimental data can be rationalized according to the following pathway:

(I) $PhX + e^- \rightleftharpoons PhX^{\cdot-} \longrightarrow Ph^{\cdot} + X^-$

(II) $Ph^{\cdot} + DMF \longrightarrow PhH + {}^{\cdot}CONMe_2$ (Me = CH_3)

(III) $Ph^{\cdot} + e^- \rightleftharpoons Ph^-$

(IV) $Ph^- + N(CH_2CH_3)_4^+ \longrightarrow N(CH_2CH_3)_3 + CH_2CH_2 + PhH$ (ref.4)

(V) $Ph^{\cdot} + Hg \longrightarrow PhHg^{\cdot}$

(VI) $2PhHg^{\cdot} \longrightarrow PhHgPh + Hg$ } (ref.5)

(VII) $Ph^{\cdot} + {}^{\cdot}CONMe_2 \longrightarrow PhCONMe_2$

(VIII) $PhCONMe_2 + 2H^+ + 2e^- \longrightarrow PhCHOHNMe_2$ and/or

(IX) $Ph^- + DMF + H^+ \longrightarrow PhCHOHNMe_2$ } (ref.6)

(X) $Ph^- + DMF + H^+ \longrightarrow PhCHO + HNMe_2$ and/or

(XI) $Ph^{\cdot} + DMF \longrightarrow PhCHO + {}^{\cdot}NMe_2$

(XII) $PhCOH + e^- \longrightarrow PhCOH^{\cdot-}$

(XIII) $PhCOH^{\cdot-} + H^+ \longrightarrow PhCHOH^{\cdot}$

(XIV) $2PhCHOH^{\cdot} \longrightarrow PhCHOHCHOHPh$ } (ref.7,8)

(XV) $PhCHOH^{\cdot} + e^- + H^+ \longrightarrow PhCH_2OH$ and/or

(XVI) $PhCHOH^{\cdot} + DMF \longrightarrow PhCH_2OH + {}^{\cdot}CONMe_2$

(XVII) $Ph^{\cdot} + OH^- \longrightarrow PhOH + e^-$

(XVIII) $2Ph^{\cdot} \longrightarrow PhPh$ and/or

(XIX) $2PhHg^{\cdot} \longrightarrow PhPh + 2Hg$ (ref.5)

(XX) $PhHg^{\cdot} + {}^{\cdot}CONMe_2 \longrightarrow PhHgCONMe_2$

The proposed steps or reactions are supported by the cited references, which treat upon similar compounds.

Reaction I is evidenced by the irreversibility of the unique wave in cyclic voltammetry and by the presence of halide ions in the electrolyzed solution.

The relatively small amount of decomposed TEAP suggests the minor importance of IV with respect to II, specially for PhI reduction.

The traces of phenol are due to the small amount (about 0.1%) of residual water in the solvent.For this compound, reaction XVII is more likely than direct combination of $Ph^{\cdot}$ and $OH^{\cdot}$, because it is well known that the homolitic cleavage of water O-H bond is very difficult and it has been shown[9] that nucleophilic attack on neutral aromatic radicals is more favorable than direct radical combination.

The traces of PhCOCOPh may be due to the oxidation of PhCHOHCHOHPh in presence of O_2 during the working-up.However, there is not further experimental evidence for this oxidation.

Reaction XVI is more likely than XV for PhI reduction, since the second reduction wave for benzaldehyde appears at -1.8V vs. Ag/AgI.

The high yield of 1,2-diphenyl-1,2-ethanediol in the PhBr reduction can be explained in terms of the higher concentration of Ph^- than in the PhI reduction, because of the PhHgPh reduction, leading to a major contribution of reactions X,XII,XIII and XIV. On the other hand, the diferent potential determines the adsorption of the substances and it was shown that benzaldehyde reduction occurs in an adsorbed state. Probably the radical dimerization also takes place on the electrode surface[7].

REFERENCES

1.S.Wawzonek and J.H.Wagenknecht, preprint of "Polarographic studies in acetonitrile and dimethylformamide. X The behavior of triphenylphosphine and related compounds".
2.F.Barba,A.Guirado and A.Zapata, Electrochimica Acta, 27:9,1335(1982)
3.J.W.Sease and R.C.Reed, Electrochemical Society Meeting, New York, May 4-9, 1969.
4.A.J. and R.C.Reed, J.Amer.Chem.Soc.,94,8475(1972)
5.M.R.Rifi,"Organic Electrochemistry"(Edited by M.M.Baizer),p.288-293. Marcel Dekker,New York (1963).
6.B.J.Wakefield, "The chemistry of organolithium compounds", p.140 Pergamon Press. Oxford(1974).
7. Reference 5,p.374
8.M.J.Allen, J.Org.Chem.,15,435(1950)
9.J.Pinson and J.M.Saveant,J.Chem Soc.,Chem.Commun.,933(1974).

POLAROGRAPHIC BEHAVIOUR OF o-DIBROMOBENZENE IN PSEUDOAPROTIC MEDIA

J.CASADO and I.GALLARDO
Departament of Physical Chemistry, Autonomous University of Barcelona
Bellaterra, Barcelona (Spain)

INTRODUCTION

The polarographic reduction of o-dibromobenzene (I) in dimethylformamide (DMF) and acetonitrile (AN) was studied by Wawzonek and Wagenknecht[1]. They reported a maximum for the unique observed wave, which still persisted at a concentration of $2,6.10^{-4}$M , and also postulated the formation of benzyne as intermediate. Rifi[2] proposed a concerted mechanism for this reaction, while Barba et al.[3] assumed an ionic pathway.

In this paper we study the polarographic behaviour of I in DMF and AN with several supporting electrolytes, and also with different concentrations of added phenol.

RESULTS

In DMF/TEAP 0,1M , I shows an unique four-electron wave, in contrast to the other studied dihalobenzenes which exhibite two waves. A current peak raising from the bottom of the diffusion wave is observed (fig. 1). The results are reported in table 1.

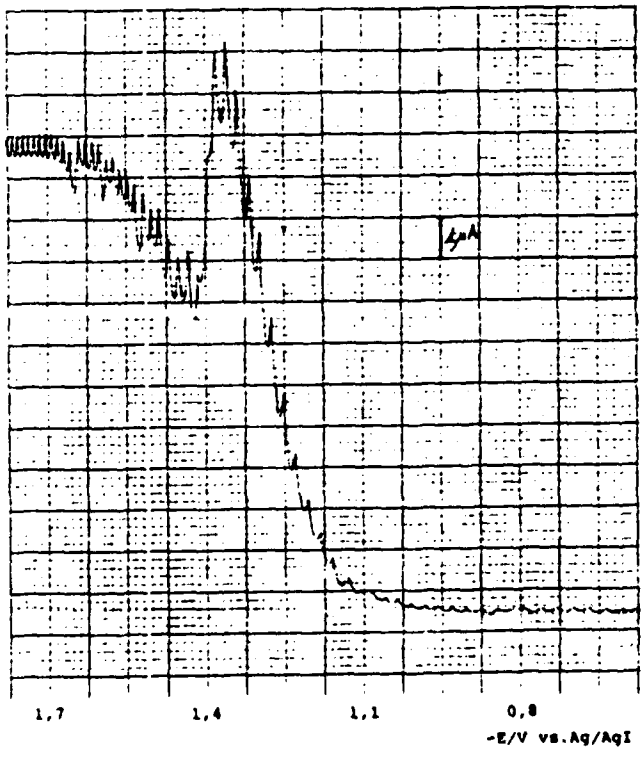

Fig.1. Polarogram of o-dibromobenzene $1,0.10^{-3}$M in DMF/ TEAP 0,1M.

TABLE 1

Polarographic results of 0-dibromobenzene in DMF/TEAP 0,1M.T=25°C; Hg height=35cm; t(-1,8V)=1,68s;m=1,30 mg/s;E vs. Ag/AgI.

$c_{(I)}$/mM	c_{PhOH}/mM	$-E_{1/2}$/V	I_d	$-E_p$/V*	I_p/μA*
0,02	-	1,16	12	-	-
0,04	-	1,18	8,1	-	-
0,10	-	1,21	7,2	-	-
0,20	-	1,29	8,4	1,31	1,2
0,50	-	1,33	8,3	1,32	4,3
0,50	4,5	1,32	10,5	1,32	5,4
1,00	-	1,35	8,5	1,35	12
1,93	-	1,36	8,5	1,36	26

* E_p is the peak potential; I_p is the peak current

It is well known that the height of the polarographic maxima depends on the Hg height.However, I_p does not depend on Hg height. In addition, surfactants, such as methyl red and methylene blue, are unable to suppress this peak.$E_{1/2}$ and E_p depend on the concentration of I (see Table 1).This is consistent with adsorption phenomena for an irreversible process (αn=0,6).Nevertheless, the process is not adsorption controlled.On the other hand, I_p is proportional to $c^{1,4}_{(I)}$.
In DMF/TBAI 0,1M the peak also appears (E_p=-1,49V ; I_p=7 A; I_l=8 A and αn=0,77, for $c_{(I)}$=1,0mM and Hg height=25 cm).As well as in TEAP 0,1M, the maximum suppressors have no effect.

In DMF/$LiClO_4$ 0,1M the peak is not observed.Howewver, when phenol is added in concentration greater than 1.10^{-3}M, the peak appears, reaching a maximum height at 1.10^{-2}M. For higher concentrations the peak current remains constant.At phenol concentrations below 1.10^{-3}M, the peak is adsorption controlled.

$E_{1/2}$ is about 80mV more cathodic than in TEAP o,1M. I_d (5,9) is minor in $LiClO_4$ than in TEAP.The latter result may be due to the major viscosity and/or the absence of proton donors in the solution.

In AN/TEAP 0,1M the behaviour of I is analogous to the corresponding in DMF. The peak currents are more important in this more acidic solvent, and are only observed for concentrations over 4.10^{-5}M.

DISCUSSION

Our results point to an ionic stepwise mechanism for the reduction of I, and they are consistent with the existence of an associated catalytic process leading to hidrogen evolution,i.e. :

$$I + e^- \longrightarrow PhBr_2^{\cdot -} \qquad (1)$$

$$PhBr_2^{\cdot -} + H^+ \longrightarrow PhBr_2H^{\cdot}\,(II) \qquad (2)$$

$$2PhBr_2H^{\cdot} \xrightarrow[rds]{k} 2PhBr_2 + H_2 \qquad (3)$$

An analogous protonation step of the intermediate anion radical (2) has been proposed by Heinze and Schwart for the reductive dehalogenation of anthracene halides[4].

In the presence of a large excess of proton donor (tetraalkylammonium salts or phenol) and at low concentrations of catalyst(I), the peak current can be given by:

$$I_p = AFk^{1/2}D^{1/2}c_{(IIs)}^{3/2}$$

Where A is the average area of the Hg drop, D is the diffusion coefficient of I and $c_{(IIs)}$ is the surface concentration of II, which is proportional to $c_{(I)}^{3/2}$. Therefore, I_p must be proportional to $c_{(I)}^{3/2}$.

This ECC mechanism seems not to be specific for I. Actually, a similar behaviour for ortho- and meta-bromoclorobenzene, metaiodobenzene and iodobenzene has been found[6].

For all the compounds displaying this behaviour, the peak potentials are less cathodic than -1,50V vs. Ag/AgI. This limiting potential may be related to the desorption of the species involved in the catalytic process, in such a way that this process is prevented. On the other hand, it seems likely that a stronger electric field can accelerate the cleavage of the carbon-halogen bond with a similar result.

REFERENCES

1-S.Wawzonek and J.H.Wagenknecht, Journal Electrochemical Soc.110,420 (1963)
2-M.R.Rifi, Organic Electrochemistry (Edited by M.M.Baizer) p.294. Marcel Dekker, New York (1963)
3-F.Barba,A.Guirado,A.Zapata, Electrochimica Acta, 27,1335(1982)
4-J.Heinze and J.Schwart, J.Electroanal.Chem., 126,283(1981)
5-Mairanovskii,S.G, Catalytic and Kinetic Waves in Polarography,p.245 Plenum Press,New York (1968)
6-J.Casado and I.Gallardo, unpublished results.

SYNTHETIC APPLICATIONS OF INDIRECT ELECTRODE REACTIONS: ROLE OF ELECTROCHEMICAL GENERATED REAGENTS

KAMALA ZUTSHI, RAVI RASTOGI and GIRISH DIXIT
Department of Chemistry, University of Rajasthan
Jaipur 302004, India.

Indirect electrode reactions involve electrogenerated reagents acting as catalysts. The present investigations describe some basic electrochemical and synthetic applications of indirect electrode reactions : anodic and cathodic, utilizing the electrochemical generated reagents at constant current, offering excellent possibilities for selective oxidation-reduction, hydrogenation and cyclization reactions which have not already been tried extensively.

The methodology presents the possibility of controlling a wider range of the activity of the reagent, the behaviour of electrons by proper choice of the electrodes, electrode potential and use of various solvents. The transfer of electrons can occur at ordinary temperature atmospheric pressure and at a chosen pH with minimum number of steps and side reactions involved thus facilitating pure products.

Keeping in view the convenience of experimental conditions vis a vis the formation of useful synthetic products, the following model reactions have been described.

The electrolytic hydrogenation of aminobenzoic acids and subsequent cyclization of the intermediate products in situ gave fair yield of bicyclic lactams and ester under normal conditions of temperature and pressure thus claiming superiority over the conventional catalytic hydrogenation[1].

The electrocatalytic hydrogenation of organic substances has been reviewed by many workers[2,3]. At electrodes of low hydrogen over potentials such as platinum, reaction (2) follows reaction (1) and is rate controlling. The conversion of adsorbed hydrogen atom (2) to molecular hydrogen is slow allowing thereby the electrode furface to be covered with absorbed atomic hydrogen which causes the hydrogenation.

$$H^+ + e^- \rightleftharpoons H_{(ads)} \quad (1) \; ; \quad 2H_{(ads)} \rightleftharpoons H_2 \quad (2)$$

The electrogenation of H atom in 2N perchloric acid containing tetra-n-butyl ammonium perchlorate on platinum cathode (working area 0.75 cm^2) is experimented for the reduction and subsiquent cyclization of amino benzoic acids (1-4). Maximum yield was obtained when the current density was 1.33×10^5 $mAcm^{-2}$, yielding the products (5,6,7).

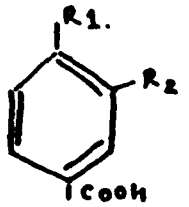

(1) $R_1 = NH_2$; $R_2 = H$
(2) $R_1 = H$; $R_2 = NH_2$
(3) $R_1 = R_2 = NH_2$
(4) $R_1 = NH_2$; $R_2 = OH$

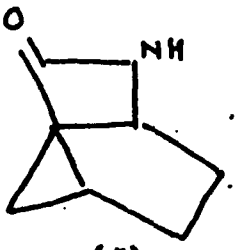

(5)

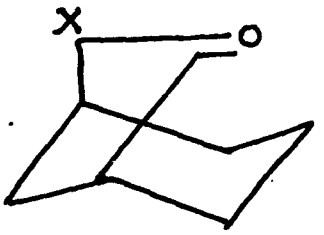

(6) X = NH
(7) X = O

The indirect process of electrochemical reduction of aromatic nucleus via solvated electrons has been reviewed by Lund[4] and Alpatova and Krishtalih[5].

The direct electron transfer from cathode to aromatic nucleus does not take place as such. The reduction of aromatic compounds away from the electrode in the bulk of the solution is caused by introducing the solvated electrons in the solution. However, at sufficiently negative potential, an electron may get released from the electrode and when is not caught by the acceptor, it may end up in a potential energy "trap" introduced by its own polarization field giving rise to solvated electrons[6,7].

$$e^-_{cathode} + S \rightleftharpoons e^-_S \qquad (1)$$

where S is aprotic solvent.

The reduction of the aromatic ring by electrogenerated electrons has been well documented in ethanol containing hexamethylphosphoramide $(CH)_2N_3P{=}O$, (HMPA).

Aniline(s) and p-cresol(2) are reduced by electrochemical generated solvated electrons to cyclohexylamine (3) (43.8-48.5%) and 4-Methylcyclohexanol (4) (34.3-37.2%) respectively. The maximum yield obtained when the current density was 19.61 $mA.cm^{-2}$. The cathode potential which indicates the reduction was -2.20 - 2.3 V vs sce respectively. Lithium chloride was used as supporting electrolyte on aluminium cathode.

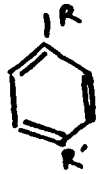

$\xrightarrow[\text{HMPA-}C_2H_5OH\ \text{LiCl}]{+\ 6e^-}$

(1) $R = NH_2$; $R' = H$
(2) $R = OH$; $R' = CH_3$

(3) $R = NH_2$; $R' = H$
(4) $R = OH$; $R' = CH_3$

The blue solution of alkali metals in HMPA 8,9 was observed during electrolysis with substrate present, confirming the presence of solvated electron[10, 11, 12].

The identification of the above products was confirmed on the basis of boiling points, elemental analyses, supported by Infrared and H-nuclear magnetic resonance data.

1. R.L. AUGUSTINE AND L.A. VAG J. ORG. CHEM 40, 1074 (1975).
2. G.A. BOGDANOWSKII, G.A. BASKOVA, V.S. TEMNOV AND G.D. VOVCHENKO KATALITICH REAKESII U. ZHIDIKPAZE P. 232-237 (1974).
3. L.L. MILLER AND L. CHRISTENSEN J. ORG CHEM 43, 2059 (1978).
4. H. LUND IN "ORGANIC ELECTROCHEMISTRY" (M.M. BAIZER ed.) MARCEL DEKKER, NEW YRORK , P. 839-849 (1970).
5. N.M. ALPATOVA AND L.I. KRISHTALIK, ITOGI NAUKI TEKH. ELECTROKHIM. 15, 132 (1979).
6. E.J. HART and M. ANBAR "THE HYDRATED ELECTRON" WILEY INTERSCIENCE, NEW YORK (1970); E.J. HART ACCOUNTS CHEM RES.2, 261 (1969).
7. U. SCHINDEWOLF, ANGEW CHEM, 80, 165 (1968); J.L. DYE ACCOUNTS CHEM RES, 1, 306 (1968).
8. T. CUUIGNY, J. NORMANT AND H.NORMANT, COMPT REND 258 (1964) 3502.
9. G. FRENKEL, S.H. ELLIS AND D.T. DOX, J. AM. CHEM SOC. 87 (1965) 1406.
10. W. GROSS AND U. SCHINDEWOLF, J. PHYS. CHEM 84 (1980) 1266.
11. H.W. STERNBERG, R.E. MARKBY I. WENDER AND D.M. MOHILNER J. AM. CHEM SOC. 91 (1969) 4191.
12. J.M. BROOKS AND RER. DEWALD, J. PHYS CHEM 72 (1968) 2655.

STUDIES ON MIXED LIGAND COMPLEXES OF CADMIUM WITH PYRIDOXINE (VITAMIN B_6) AND SOME AMINO ACIDS

(MISS) RAJANI, C.P.S. CHANDEL AND C.M. GUPTA
Department of Chemistry, University of Rajasthan
Jaipur-302004 (India).

The mixed-ligand complexes of cadmium with pyridoxine and some amino acids (glycine, alanine, valine and serine) were studied polarographically at pH 8.50 and the constant ionic strength (1 μ). The temperature was maintained constant at 303 ± 1 K. All the systems were studied by keeping the concentration of weaker ligand (Pyridoxine) constant while varying that of amino acids. The plots of E_{de} vs log $i/(i_d-i)$ were linear with a slope of 30 ± 2 mV, showing that the two electron reduction is reversible and diffusion controlled. The free ligand concentration is calculated from pH and pK values Cd(II) forms three mixed-ligand species viz., Cd(pyridoxine)(aminoacids), Cd(pyridoxine)(aminoacids)$_2$ and Cd(pyridoxine)$_2$(aminoacids).

The formation constants of simple systems were calculated by the Deford and Hume[1] method, and the values of stability constants of mixed-ligand complexes were determined by the method of Schaap & McMasters[2]. The overall stability constants were evaluated with the help of Leden[3]'s graphical extrapolation method. The over all stability constants log β_{11}, log β_{12} and log β_{21} of all the systems are presented in the Table 1.

Table 1

Systems	log β_{11}	log β_{12}	log β_{21}
Cd-Pyridox-Gly	5.20	6.26	8.35
Cd-Pyridox-Ala	5.30	6.33	8.25
Cd-Pyridox-Val	5.00	5.95	7.70
Cd-Pyridox-Ser	5.05	6.00	7.98

The tendency of formation of simple and mixed complexes can be easily expressed by calculating the disproportionation constant K^D for the equilibria.

$$2\text{Cd(pyridoxine)(aminoacid)} \rightleftharpoons \text{Cd(pyridoxine)}_2 + \text{Cd(aminoacid)}_2$$

The value of log K^D is -0.6 statistically[4] but the observed values are found to be -0.96, -0.86, -1.26 and -0.66 for the cadmium-pyridoxinate-glycinate, cadmium-pyridoxinate, alaninate, cadmium-pyridoxinate-valinate and cadmium-pyridoxinate-serinate systems respectively. The high negative values of log K^D for each equilibria account for the stability of the mixed ligand complexes.

References

1. D.D. Deford and D.N. Hume, J. Am. Chem. Soc., 73, 5321 (1951).

2. W.B. Schaap and D.L. McMasters, J. Am. Chem. Soc., 83, 4699 (1961).

3. I. Leden, Z. Phys. Chem., 188, 160 (1941).

4. D.D. Perrin and V.S. Sharma, J. Chem. Soc., 17, 2060 (1969).

THE SOLVENT EFFECT ON THE KINETICS OF THE ELECTROOXIDATION OF PHENOTHIAZINE

M.OPALLO and A.KAPTURKIEWICZ
Institute of Physical Chemistry, Polish Academy of Sciences
01-224 Warszawa, Kasprzaka 44/52, Poland

One-electron electrooxidation of phenothiazine /PNT/ to the corresponding radical cation PNT :

$$PNT - e \rightleftharpoons PNT \qquad (1)$$

at Pt electrode was choosen as a model system for studies the solvent effect on the heterogeneous electron transfer kinetics because the mechanism of reaction 1 is solvent independent[1].

The standard rate constants /k_S/ were estimated on the basis of the data obtained by cyclic voltammetry experiments.

The apparent values of k_S has been found nearly independent of the supporting electrolyte concentration in given solvent. This suggests that they can be regarded as "true" values, not influenced by the potential drop across the diffuse layer.

The k_S values has been found considerably dependent on the solvent. No simple correlation between k_S and polarity parameter $(\varepsilon_\infty^{-1} - \varepsilon_S^{-1})^+$ as well as donor number of given solvent has been found. Thus the changes of k_S with the solvent cannot be explained by the outer- /Marcus theory[2]/ or the inner-solvation shell effects.

On the other hand the nearly linear relationship between k_S and the reciprocal of the longitudinal dielectric relaxation time $(\tau_L^{-1})^{++}$ of a given solvent has been found in the case of aprotic solvents. Similar correlations were also found in the case of the electroreduction and electrooxidation of transistion metals salene complexes[3], metallocenes[4] and electroreduction of nitromesitilene[5].

Thus the solvent relaxation dynamics[6] play important role in kinetics of reaction 1.

We tried to interprete our results on the basis of the encounter preequilibrium model involving solvent relaxation dynamics[4]:

$$k_S = \varkappa \delta \tau_L^{-1} (\lambda_0/16\pi RT)^{1/2} \exp(-\lambda_0/4RT) \qquad (2)$$

where $\varkappa$ - electron tunneling probability, δ - effective thickness of reaction zone and λ_0 is the reorganization energy of the solvent .

+ ε_∞ and ε_S are the optical and static dielectric permittivity of the solvent.

++ $\tau_L = \tau_d \varepsilon_\infty / \varepsilon_S$ where τ_d is the dielectric relaxation time of the solvent.

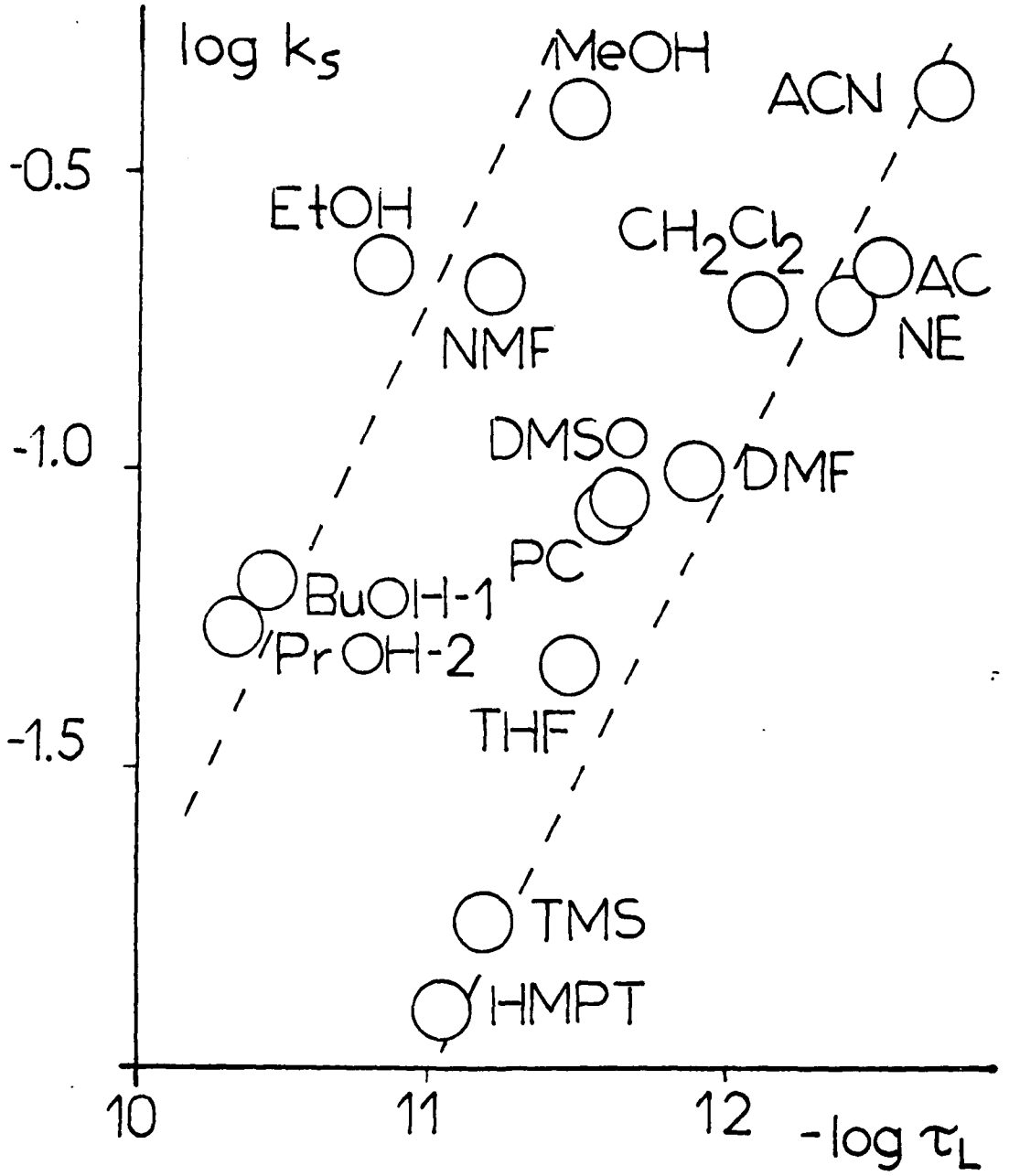

Fig. 1. Standard rate constants of the electrooxidation of PNT k_s as a function of reciprocal of the longitudinal dielectric relaxation time τ_L of a given solvent.

We calculate k_S according eq 2 assuming the reaction 1 adiabatic /$\varkappa\delta$ = 60 pm/ at the closest approach of the reactant to the electrode surface. For all distances of reaction place from electrode surface the sequence of k_S values agrees well with found experimentally but the calculated values are higher than experimental. This can be attributed to the neglection of inner reorganization energy or to the nonadiabacity of reaction 1: $\varkappa \ll \lambda$ hence $\varkappa\delta \ll 60$ pm.

The interpretation of kinetic data in the case of hydrogen bonded solvents is more complicated because in these solvents more than one dielectric dispersion region is observed[8]. Taking into considerations only the slowest value of τ_L one may observ nearly linear relationship between k_S and τ_L^{-1} but the reaction is faster than it could be expected by comparison with the experimental data in the case of aprotic solvents /see fig. 1/.

This difference can be caused by: three reasons:

The neglection of faster dielectric relaxation processes which may also influence the rate of electron transfer.

The polarization diffusion mechanism[9] of the solvent relaxation which can be intrinsic for the solvents with relatively long τ_L.

The difference between $\varkappa\delta$ parameter for both groups of solvents.

1. B.Paduszek, M.K.Kalinowski, Electrochim.Acta, 28/1983/639.
2. R.A.Marcus, J.Chem,Phys., 43/1965/679.
3. A.Kapturkiewicz, B.Behr, J.Electroanal.Chem., 179/1984/187.
4. M.J.Weaver, T.Gennett, Chem.Phys.Lett. 113/1985/213.
5. A.Kapturkiewicz, M.Opałło, J.Electroanal.Chem. 185/1985/15.
6. D.F.Calef, P.G.Wolynes, J.Phys.Chem. 87/1983/3387.
7. J.T.Hupp, M.J.Weaver, J.Phys.Chem. 88/1984/1463.
8. C.J.F.Böttcher, P.Bordevijk, "Theory of Electric Polarization" Elsevier 1978.
9. G.van der Zwan, J.T.Hynes, Chem.Phys.Lett., 101/1983/367.

SPECTROELECTROCHEMICAL STUDY OF POLARON AND BIPOLARON IN POLYPYRROLE STRUCTURAL CHANGES UPON CYCLING

E.M. GENIES AND J.-M. PERNAUT
Laboratoire d'Electrochimie Organique et Analytique, UA CNRS n°321, Laboratoires de Chimie, Département de Recherche Fondamentale, Centre d'Etudes Nucléaires de Grenoble, 85x, F.38041 GRENOBLE CEDEX, France.

Conductive organic polymers can be described as semiconductors with a band model related to the level of doping (1). We present here some results which will contribute to increase the understanding in this area. This study is made in CH3CN (0.5M LiClO4) by the spectroelectrochemistry of polypyrrole film deposited on an optically transparent electrode of indium oxide on glass.

I ELECTROCHEMICAL INTERPRETATION OF REDOX SYSTEME OF PPY

The redox mechanism of polypyrrole is described by the following scheme, where PP represents the neutral species (6 pyrrole units), PP°+, the radical cation (or polaron) and PP++ the dication (possible bipolaron).

PP	⟶	PP°+ + 1e-	E1	1
PP°+	⟶	PP++ + 1e-	E2	2
2 PP°+	⟷	PP + PP++	K	3

The limiting step of the kinetics of charge transfer has been determined to be the diffusion of anion (ClO4-) for oxidation and cation for reduction during first scans of cyclic voltammetry (2).
The figure 1 presents the cyclic voltammetry of a PPy film (0.24um) at 0.05 Vs-1. At lower scan rates we observe sometimes two peaks in reduction which can be assigned to the exixtence of two electronic transfers (reactions 1 and 2).
The figure 1 also presents the concentration profiles for the species, the sum of PP°+ + PP++ and the charge (...) for the polymer versus assigned potential according to reactions 1 and 2 following an ideal Nernstian model with E1 = E2 = - 0.15 V.

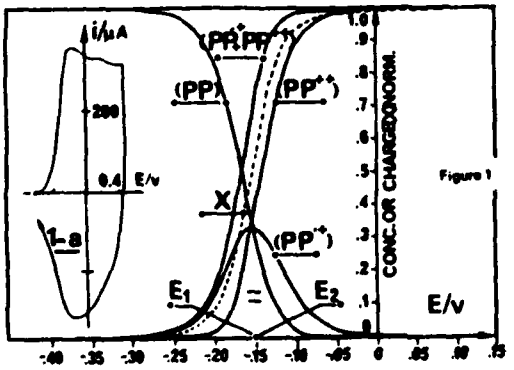

Figure 1

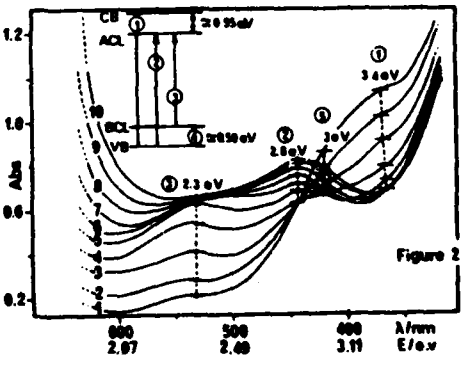

Figure 2

II OPTICAL ABSORTION OF PPY AND NATURE OF TRANSITIONS

The figure 2 shows the absorbance diagram of PPy film (0.24um) at increasing level of doping ranging from -0.5V-1- to +0.4V-10- by increment of 0.1V. The single headed vertical arrows on the energy level diagram indicates allowed optical transitions. VB = Valence band , BCL/ACL = Bonding/antibonding polaron level, CB = Conduction band. The transition 4 cannot be seen because of the limitation of the transmission cell.
We observe that from reduced to oxidized film the absorbance decrease in the area of 3.4 eV and increase under 2.9 eV with a quasi isobestic point. According to the ideal concentration of species determined in § 1, it is possible to determine the absorption molecular coefficient of PP°+ and PP++ for particular wavelengths. For instance at 2.8 eV it is respectively : 850 and 5475 1M-1cm2 .

III TRANSIENT ABSORBANCE MESUREMENTS - POLARON BIPOLARON EVIDENCE

It is very convenient to work at constant wavelength to follow the transfer from a species to an other one. Depending on the conditions of preparation of the film, we achieve two types of polymer :

A/ Slow charge transfer polymer film

The figure 3-a represents the chronoabsorptometric plots of PPy film for a double potential step from -0.5 V to 0 V-1- and to +0.4 V-2- at 410 nm. The stars correspond to the points where the system is relaxed (cut off of the circuit). When the upper limit of the potential is 0 V (3-a-1) we observe a plateau of absorbance because only polaron are created. For higher potential limit, 0.4V (3-a-2) the radical cation is oxidized to dication which is more absorbant at this wavelenght. The difference of absorbance (red-ox) increases then decreases and stabilizes when the dication reaches the maximal concentration.

B/ Fast charge transfer film

The figure 3-b is obtained for potential steps ranging from -0.5 to -0.4 V-1- to -0.5 to +0.4 V-9- by increment of 0.1 V at 400 nm. The interpretation is the same that in fig.3-a, but with fast charge transfer. D = 3.5 10-10 cm2 s-1.

The figure 4-a and b present the evolution of absorbance and potential versus time for relaxation of the system after an oxidation step ,2, an a reduction step ,1, during a double step potential from -0.5 to +0.4V.

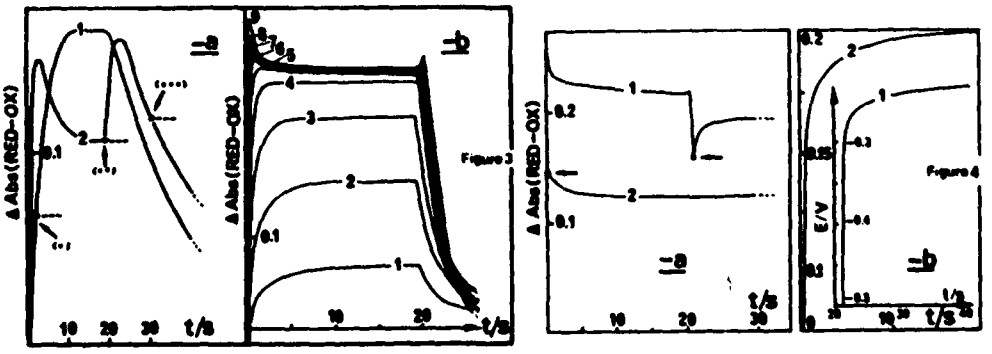

Curves 1 are explained by the reaction 3 occuring to the left because in this case E2 > E1. On the contrary, curves 2 must be explained by the reaction 3 occuring to the right with E2 < E1. This behavior is only observable for largly cycled film.

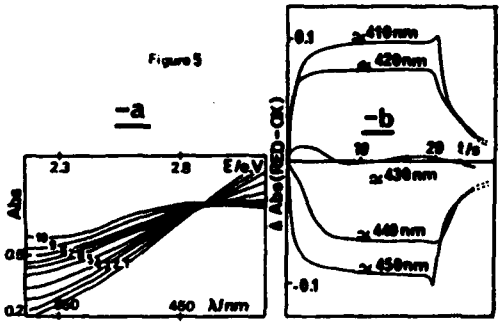

IV EVOLUTION OF PPY FILM UPON ELECTROCHEMICAL CYCLING

The figure 5-a shows the becoming of the absorbance diagram of PPy after 30 cycles of potential sweeping, between -0.5 to +0.4 V at 0.05 Vs-1. The absorbance near 400 nm is really an isobestic point and must be compare to the figure 2.

The figure 5-b is the chronoabsorptometric plots of the film of the same cycled film for double potential (-0.5,+0.4V) step at different wavelengths around the isobestic point.

V CONCLUSION

The oxidation of polypyrrole involves the formation of radical cation PP.+ and dication PP++ sites which corresponds to the creation in the band gap of two bonding-antibonding levels. The kinetic of transfers between radical cation and dication and the absorbance coefficient are evaluated.

The results strongly depend on the condition of the polymer. For fresh new film E2 appears in the range of -0.1 V (Ag/Ag+) and E1 of -0.2 V. After cycling E2 becomes lower than E1 and the electronic structure of the film is irreversibly altered. The experiments of step potential with relaxation are explained with the reactions of disproportionation and the inverse ,3, according to relative position of potential E1 and E2. After cycling the dication formation is favorable and it corresponds best to the bipolaron concept.

The simple Nernstian model is not completly satisfactory and suggests that the active species are subject to large electrostatic interactions .

REFERENCES

1 J.C. Scot t, J.L. Bredas, K. Yakushi, P. Pfluger and G.B. Street, Synth. Met., 9 (1984) 165 .

2 E.M. Genies and J.M. Pernaut, Synth. Met., 10 (1984) 117 .

13420

"ELECTROCHEMICAL REDUCTION OF α-AZIDO CHALCONES"

V.SURYA NARAYANA RAO and DIERK KNITTEL
Institut für Physikalische Chemie, Universität Hamburg,
D-2000 Hamburg 13, FRG.

The electrochemical reduction of α-azido chalcones (2-azido-1,3-diarylpropenones) is investigated in acetonitrile medium in the presence of acetic anhydride and/or protons. The polarographic studies with 1-(4-chlorophenyl-)-2-azido-(4-tolyl-)-propene-2-one-1 (1b) reveal two waves corresponding to a 2-electron and 1-electron reduction respectively. The CV shwos two peaks at -1.31V and -1.65V vs. SCE (100 $mV.s^{-1}$), the second one being reversible. On addition of Ac_2O or AcOH both reduction currents increase, the peak shape being unchanged.

Ac_2O or H^+-donors are used as scavengers for anionic intermediates to prevent polymer formation at the electrode. Controlled potential electrolyses of the azidochalcones at the first reduction wave are carried out in order to check the synthetic utility of this reaction type and to get insight into the reduction path of the enazido function.

The data relating to electrolysis potential, charge consumed, products and yields are presented in the following table. A reaction scheme for cathodic reduction of the azidochalcones is given too.

Preparative electrolysis only with Ac_2O as additive results in untractable mixtures of substances. CV of independently prepared N,N-diacetylamino-propenones reveal that these compounds and the starting azides have almost the same reduction potentials so that any diacetylamino compound formed will be reduced further yielding fragmentation products.

Substrate	E_{p1}[a]	E_{p2}[a]	method	E_{el}[b]	charge per mole	products (yield,%)	E_p[c]
1a	-1,21	-1,5	A	-1,25	2,5	4a (85)	-1,48
			B	-1,30	2	5a (40)	-1,41
						6a (30)	-1,41
1b	-1,33	-1,70[f]	A	-1,40	2,5	4b (85)	-1,72
		-1,68	B	-1,41	2,5	5b (40)	-1,68
						6b (30)	-1,68
1c	-1,50	-1,76	A	-1,55	2	4c (85)[d]	(-1,45)[e]
1d	-1,25	-1,69	A	-1,32	2,5	8d (70)	-1,75
1e	-1,35	-1,60	A	-1,38	2	4e (70)[d]	(-1,58)[e]
1f	-1,05	-1,35	A	-1,12	2,2	4f (88)[f]	-1,63

[a]Peakpotential in CV, 50mV.s^{-1} on Hg vs. SCE; [b]potential of electrolysis; [c]peakpotential for reduction of products; [d]isolated after acetylation; [e]peakpotential of the acetylderivative; [f]in DMF; [r]quasireversible. Method A: electrolysis with addition of AcOH; method B: stöchiometric addition of azide, Ac_2O and AcOH.

Reaction Conditions and Products of Electrolysis of Azidochalcones

As can be seen from this table, electrolysis of the azidochalcones in the presence of protons give rise to only one product in excellent yields.

A mildly acetylation method is developed in order to prepare N-monoacetyl derivatives, since some of the aminopropenones are rather unstable. Addition of a stoichiometric mixture of azidochalcone and AcOH to the electrolysis mixture results in high yields of the E- and Z-isomers of 2-acetylamino-1,3-diarylpropenones from pure Z-azidochalcones.

The reversible second wave in CV following an irreversible one as in the case of 1b is taken as an EECCE-mechanism. Probably there is electron transfer, release of N_2 and protonation on the olefinic carbon (due to residual water or the tetraalkylammonium cation used). If there results an α-ketimine-like structure like 7 a reversible reduction will follow. With the sterically hindered compound 1d the bulky substituents favour this reaction path. Detailed studies on this phenomenon are still in progress.

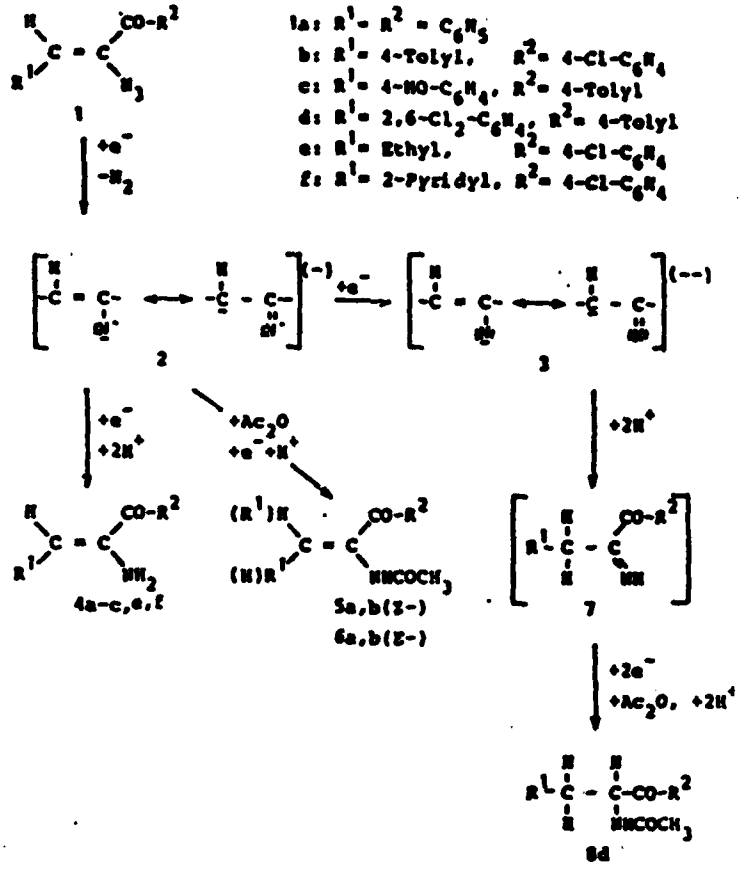

Reaction Scheme for the Cathodic Reduction of Azidochalcones

However the cathodic reduction of simple azidochalcones represents an efficient and selective synthesis of enamino ketones, whereas chemical reduction will affect other functional groups of the starting compounds.

References:

D.Knittel, A.Henning, Monatsh. Chem.,115, 391 (1984).

D.Knittel, Monatsh. Chem.,115, 1335 (1984).

D.Knittel, Monatsh. Chem., in press.

D.Knittel, V.S.N.Rao, Monatsh. Chem., in press.

13430

"ELECTROREDUCTION OF α-AZIDOCINNAMIC ESTERS AND RELATED COMPOUNDS"

DIERK KNITTEL
Institut für Physikalische Chemie, Universität Hamburg,
D-2000 Hamburg 13, FRG.

Cathodic reduction of α-azidocinnamic esters under aprotic conditions can be directed to high yields of N,N-diacylated *dehydroaminoacid* derivatives (i.e. addition of acetic anhydride) or to almost quantitative yields of α-aminocinnamic esters in very pure form by careful addition of H^+-donors. The dehydroamino compounds in turn can be further reduced to the corresponding saturated compounds by subsequent proton addition and application of more negative potential of electrolysis.

Reduction of the azido function in all compounds occurs totally irreversibly (up to $50V.s^{-1}$ in CV). A consumption of $2F.mole^{-1}$ and quantitative evolution of nitrogen is only achieved if scavengers for anionic intermediates are present in excess. Otherwise severe formation of insulating polymers by nucleophilic attack of intermediates on the azido group of the starting materials prevents useful electrolysis.

The versatility of the electrochemical way to dehydroaminocid derivatives has been proved by application to several substituted azidocinnamic and ß-heterocyclic substituted α-azidoacrylic esters.

Examples of this cathodic synthesis are given in the following figures.

1a: Ar= 4-Tolyl-
b: Ar= 4-tert.Butoxylphenyl-
c: Ar= 4-Chlorphenyl-
d: Ar= 2,6-Dichlorphenyl-
e: Ar= 2-Furyl-
f: Ar= 2-Thienyl-
g: Ar= 3-(N-Benzyl-)-indolyl-
h: Ar= 4-Hydroxyphenyl-

2a-g: $R^1 = R^2 = COCH_3$
h: $R^1 = R^2 = COCH_3$, Ar= 4-Acetoxyphenyl-

3a-c,g: $R^1 = H$, $R^2 = COCH_3$

4a-h: $R^1 = R^2 = H$

5d: $R^1 = H$, $R_2 = CO(CH_3)_3$

Substrat	Elektrolyt[a]	Potentiale[b]	isolierte Produkte Ausb. in % d.Th. (chromatogr. Ausb.) N,N-Diacyl-	N-Acyl-	Amino-
1a	A	-1,60	2a: 35 (44)	3a: (2)	4a: (2)
	B	-1,55	-	-	50 (82)
	C	-1,57	-	5d: 35 (39)	4a: (60)
1b	A	-1,60	2b: 25 (56)	3b: 7 (25)	4b: (9)
	B	-1,60[g]	-	-	78 (98)
1c	A	-1,55	2c: 70 (86)	3c: (4)	4c: (2)
	B	-1,66[g]	-	-	35 (60)
1d	A	-1,60	2d: 70 (86)	3d: n.b[c]	4d: (14)
	B	-1,63	-	-	40 (53)
1e	A	-1,60	2e: 40 (58)	3e: n.b[c]	4e: (2)
	B	-1,45	-	-	65 (78)
1f	A	-1,65	2f: 41 (50)	3f: n.b[c]	4f: (2)
	B	-1,50[g]	-	-	48 (75)
1g	A	-1,75	-	3g: 34	4g: (2)[d]
	B	-1,60	-	-	65 (76)
1h	A	-1,55	2h: 50 (73)	3h: n.b[c]	4h: (2)
	B	-1,55[g]	-	-	0 (80)[e]

[a] A: 20 cm^3 AN +5 cm^3 Ac_2O, B: 17 cm^3 AN +3 cm^3 AcOH, C: Pivalinsäureanhydrid, je 0,1M TEAB, 6-8 mM Umsatz. [b] Elektrolysepotential vs. GKE; [c] Ausbeute nicht bestimmt; [d] nur 2 mM Umsatz; [e] Strukturbeweis durch Peracetylierung zu 2h und dessen Ausbeute; [g] nur Schulter auf der Stromspannungskurve.

Table of electrolysis conditions and products.

Since some of the enaminoesters are rather unstable to work up procedures, the diacylation procedure is recommended.

In diacetylation synthesis during the first parts of reaction almost only the enamines are seen (probably due to protonation by residual water in the supporting electrolyte), the enamine formation will cease after a conversion of about 2-10mmoles, so that on prolonged electrolysis yields of about 80% of N,N-diacetylenaminoesters are accessible. The concentration of diacetylenamino products in the catholyte must not exceed 0.02m since otherwise some reduction of those products may start (reduction potential about 200-300mV more negative than that of starting materials). Dehydroaminocinnamic esters are stable to reduction up to -2.1V.

Extension of this cathodic procedure to dienazidoesters yielding useful synthons for Diels-Alder reactions is given in the next scheme. Chemical yields of up to 75% of dienamino-derivatives have been obtained up to now.

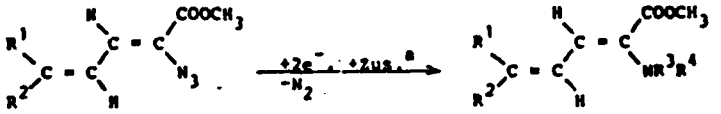

1a: R^1 = H, R^2 = Phenyl

1b: R^1 = R^2 = Phenyl

2a: R^1 = H, R^2 = C_6H_5, R^3 = R^4 = H

2b: R^1 = H, R^2 = C_6H_5, R^3 = H, R^4 = COC_6H_5

2c: R^1 = R^2 = C_6H_5, R^3 = R^4 = H

2d: R^1 = R^2 = C_6H_5, R^3 = R^4 = $COCH_3$

[a] Zus. = AcOH, $AcNH_2$, Ac_2O, $(C_6H_5CO)_2O$

Using nitro substituents in the aromatic part of the azidocinnamic derivatives selectively hydroxylamino-azidocinnamic esters or N,O-acylated diacylamino-esters are accessible. So the cathodic reduction of enazidoesters represents an easy and selective route to a variety of dehydroaminoester derivatives.

References: D.Knittel, Monatsh. Chem. 115, 1335 (1984);

END

FILMED

2-86

DTIC